

Proceedings of the 2001 WJTA American Waterjet Conference

August 18-21, 2001

Hyatt Regency Minneapolis
on Nicollet Mall

Minneapolis, Minnesota

*The 2001 WJTA American Waterjet
Conference is sponsored by the*



Artwork cut in marble using abrasive-waterjet

Courtesy of Hydrodesign S.r.l. of Italy

The design of the cover is made by M. Hashish, assisted by Judith Fulmer

Preface

More than twenty years ago, the first US Waterjet Symposium was held in Golden Colorado. This marked the beginning of what we know today as the WJTA Conferences. Twenty-five papers, presented in five sessions, were published in the *Proceedings* of that Conference. Then, there were no papers addressing such topics as precision, abrasive–waterjets, suspension jets, micro jets, 3-D sculpting, or many of the topics contained in this *Proceedings*.

The papers in this *Proceedings* are contained in two volumes. As in previous conferences, the first volume is related to research, while the second is related to applications although this distinction is sometimes a bit blurry. This distinction, however, helps divide the volume of papers into two manageable book sizes. A CD-ROM is provided to electronically access papers and make searching for topics more effective. I am predicting that soon, there will be no paper proceedings, not even a CD-ROM because all the proceedings will be easily accessible on the Web.

The papers are further grouped into sessions addressing similar subjects. This *Proceedings* contains 15 sessions. An additional session on Safety in Job Shops and Factories was held during the Conference. An outline of a potential recommended safety practices is given in an appendix.

The success of this Conference is mainly attributed to the authors who submitted their work for publication, presented their work, and responded to questions. Equally critical to the success of the Conference are the exhibitors and the technical tour hosts. Without them, the Conference would not be the same. The efforts of the Conference Chairman, Dr. George Savanick, in hosting the conference - in his, the beautiful city of Minneapolis, Minnesota - and facilitating the tours has been most critical to the success of this Conference. The paper review committee: Dr. Thomas Kim, Dr. Lydia Frenzel, and Dr. Andy Conn provided scholarly and timely reviews of the papers. Birenbaum and Associates continue to provide excellent administrative support to WJTA. They are especially recognized for organizing the Conference and managing the publication of this *Proceedings*. Many thanks to Dr. Mark Birenbaum, Ken Carroll, LeAnn Hampton and Lois Schwoebel. Special thanks to Jan Tubbs for her editorial work, logging abstracts and papers, sending review requests, notifying authors, and communicating with numerous national and international authors in a most pleasant and professional way.

Finally, I would like to thank my mother, who is always praying for me and my father, who is rooting for me in the heavens. Thanks to Nadia - my beautiful wife - for her continued understanding, help, and support; and to my two sons - Ameer and Rami - for their help, discussions, continued patience, and their ever fascination with waterjets.

I hope that this *Proceedings* will be a valuable contribution to waterjet technology and will significantly enhance our knowledge.

— Mohamed Hashish, Ph.D.
Editor

Foreword

The WaterJet Technology Association (WJTA) exists to disseminate information concerning waterjet technology. WJTA is very successful in this mission because it has found a way for waterjet practitioners from the many diverse branches of waterjet technology to share insights and information so that the members of the entire waterjet community can learn from each other.

Membership in WJTA is open to all interested parties so that the state-of-the-art of waterjet technology is aided by the combined efforts of workers with widely differing perspectives on the applications of waterjets to technical problems. Job shops, cleaning contractors, medical researchers, miners, equipment manufacturers and academics, among many others, share their ideas on the useful applications of waterjets.

Many examples of this idea-sharing occurred during the 2001 WJTA Conference. Pre-conference courses taught by experts in the field presented students with a view of the present state-of-the-art of waterjet technology. During the conference 61 papers ranging from micro-abrasive machining to underground mining were presented and discussed. Copies of these papers are included in this book.

The WJTA Safety Committee met in open session to gather advice from the membership regarding the content of the prospective safety publication, *“Recommended Practices for the Factory Use of High Pressure Waterjetting Equipment.”* A video version of the widely used safety publication, *“Recommended Practices for the Use of Manually Operated High Pressure Waterjetting Equipment,”* was released. The conference ended with a live demonstration of waterjet equipment presented by nine companies at the facilities of Jet Edge, Inc. in St. Michael, Minnesota.

Widespread interaction among workers from the many parts of the waterjet industry has lead to a successful 2001 WJTA Conference.

— George A. Savanick, Ph.D.
President

To work at pushing back the limits of knowledge is a noble human endeavor. To share this new knowledge is also honorable and rewarding. The WJTA Conferences are an efficient and effective means of assisting in the transfer of knowledge regarding fluid jet technology. These written proceedings further amplify and preserve the new discoveries being made in our industry. They will have long lasting benefits for each of us, our profession, and humankind in general.

My sincere thanks goes out to all the authors represented in these proceedings. They have willingly devoted time and energy to documenting their work and sharing it with the rest of us. Their endeavors provide the very foundation for our association.

— John Wolgamott
Chairman of the Board,
WaterJet Technology Association

WaterJet Technology Association

The WaterJet Technology Association (WJTA) was created in 1983 at the 2nd U.S. Water Jet Conference, held on the campus of the University of Missouri-Rolla, by members of the waterjet industry acting in concert with university and government officials. The major impetus to the creation of the Association was to provide a means of service and communication within the industry, as epitomized by the biennial waterjet conferences.

Formal objectives of the Association have been adopted as follows:

- To provide a means of cooperation between government, industry, university, and research institutions on all matters of fluid jets, including waterjets and abrasive jets for jet cutting, industrial cleaning, and other uses in the manufacturing, mining, construction, and process industries.
- To foster domestic and international trade in jet cutting and jet cleaning, products and services.
- To promote in general the interests of the jet application industry in all branches, including establishment of recommended practices.
- To promote the mutual improvement of its members, and the study and advancement of the arts and sciences connected with jet cutting and industrial cleaning.

In regard to the third objective, it should be noted that at the 3rd U.S. Water Jet Conference held on the campus of the University of Pittsburgh in May of 1985, the Association adopted the first ***Recommended Practices for the Use of Manually Operated High Pressure Water Jetting Equipment***.

The *Recommended Practices* are revised and updated periodically, the most recent revision being published in April 1999.

2001 WJTA Conference Committee

George A. Savanick, Ph.D.

Chairman
Apple Valley, Minnesota

Mohamed Hashish, Ph.D.

Proceedings Editor
Flow International Corporation
Kent, Washington

Andrew F. Conn, Ph.D.

Conn Consulting, Inc.
Baltimore, Maryland

Lydia M. Frenzel, Ph.D.

Advisory Council
San Marcos, Texas

Thomas J. Kim, Ph.D.

University Of Rhode Island
Kingston, Rhode Island

WJTA Administration

John Wolgamott

Chairman of the Board
StoneAge, Inc.
Durango, Colorado

Andrew F. Conn, Ph.D.

Secretary
Conn Consulting, Inc.
Baltimore, Maryland

George A. Savanick, Ph.D.

President
Apple Valley, Minnesota

Larry Loper

Treasurer
High Pressure Equipment Co.
Erie, Pennsylvania

Lydia M. Frenzel, Ph.D.

Vice President
Advisory Council
San Marcos, Texas

International Advisors

Michael Hood, PhD, Australia

Luis Eugenio Ortega Trotter, Brazil

Leo Kosowan, Canada

Jaroslav Vasek, PhD, DrSc, Czech Republic

Pekka Patjas, Finland

Daniel Weber, France

Hartmut Louis, Germany

Minoo F. Engineer, India

Matt Cotterell, Ireland

Giancarlo Francini, Italy

Ryoji Kobayashi, PhD, Japan

Gerard Verberne, Netherlands

Greg Coulter, New Zealand

Gensheng Li, PR China

Antoni Kalukiewicz, DSc, Poland

Won Ho Kang, Republic of Korea

Christian Öjmertz, PhD, Sweden

Ursula Meyer, Switzerland

Joe Harrington, United Kingdom

Pedro Tello, Venezuela



WaterJet Technology Association

917 Locust Street • Suite 1100

St. Louis, MO 63101-1419

Telephone: (314)241-1445 • Fax: (314)241-1449

Email: wjta@wjta.org • Web Site: www.wjta.org

TABLE OF CONTENTS

Proceedings of the 2001 WJTA American Waterjet Conference

Session R1: Surface and Kerf Characteristics

1. "Optical Method for Surface Analyses and Their Utilization for Abrasive Liquid Jet Automation,"
J. Valíček, M. Držík, M. Ohlídal, V. Mádr and L.M. Hlaváč
2. "Modeling and Simulation of Abrasive Water Jet Cut Surface Topography," *N.R. Babu and G. Vikram*
3. "Influences on Structure Formation at the Cutting Edge with Abrasive Waterjets," *A. Henning, R. Friedrich, T. Ditzinger, T. Kübler, E. Westkämper and G. Radons*
4. "Macro Characteristics of AWJ Turned Surfaces," *M. Hashish*

Session R2: Abrasive Suspension and Polymer Jets

5. "Micro Abrasive Waterjet Cutting," *D.S. Miller*
6. "Cutting of Hollow Structures with Polymer Supported Abrasive Water Suspension Jets,"
H. Louis and Ch. von Rad
7. "Cutting of Reinforced Concrete Using Abrasive Suspension Jet," *A. Bortolussi, R. Ciccu and B. Grosso*
8. "Reducing Abrasive Consumption by Using SUPER-WATER® for Venturi Abrasivejet Cutting,"
W.G. Howells and V.L. Imlay

Session R3: Environment and Safety Studies

9. "Environmental Evaluation and Management of AWJ Process," *J. Urbánek*
10. "Abrasive Cutting Comparisons," *R.D. Fossey, D.A. Summers, M. Johnson, D. Burch, J.W. Newkirk and G. Galecki*
11. "Electrostatic Charge Generation in Waterjet Systems," *P.L. Miller*
12. "Abrasive Waterjet Cutting a Comparative Study Between Open Catcher Tank and Water Catcher Tank," *I. Kain and J. Munoz*

Session R4: Nozzle Systems

13. **"Using Porous Lubricated Nozzles to Prevent Nozzle Wear in Abrasive Water Suspension Jets (AWSJ),"** *U. Anand and J. Katz*
14. **"Investigation of a New Cutting Head Concept Based on an Annular Driving Jet,"** *U. Suchy*
15. **"Results of Comparative Nozzle Testing Using Abrasive Waterjet Cutting,"** *D.A. Summers, R.D. Fossey, J.W. Newkirk, G. Galecki, M. Johnson, D. Burch and G. Olson*
16. **"The Hydro-Cannon Nozzle Optimization,"** *G. Atanov*

Session R5: Fluid Flow and Cavitation Modeling

17. **"Numerical Simulation of Abrasive Water Jet,"** *D.H. Ahmed, E. Siores, J. Naser and F.L. Chen*
18. **"Study on the Flow Characteristics of Free Water Jet Based on Hyperbola Flow Line Structure,"** *S. Jiang and M. Fang*
19. **"Numerical Study of the Turbulent Flow Inside a Pure Waterjet,"** *K. Babets and E.S. Geskin*
20. **"Numerical Investigation of Chaotic Motion for Cavitation Bubble in Oscillating Pressure Field,"** *F. Zhang, Z. Liao, C. Tang and L. Yang*
21. **"Experimental Studies of Jet Cavitation Noise Spectrums in Oil Well Casing,"** *G. Li, Z. Huang, D. Zhang and J. Niu*

Session R6: Machining Studies

22. **"Testing of Mineral Types of Abrasives for Abrasive Water Jet Cutting,"** *J. Foldyna, P. Martinec and L. Sitek*
23. **"AWJ To Machine Free Form Profiles in Natural Stone,"** *L. Carrino, M. Monno, W. Polini and S. Turchetta*
24. **"Abrasive Waterjet Machining of Aluminum with Local Abrasives,"** *O.V.K. Chetty and M.K. Babu*

Session R7: Innovative Processes

25. **"Ultra High Pressure Waterjet Peening - Part I: Surface Texture,"** *S. Kunaporn, M. Ramulu, M. Hashish and J. Hopkins*
26. **"Ultra High Pressure Waterjet Peening - Part II: High Cycle Fatigue Performance,"** *S. Kunaporn, M. Ramulu, M. Hashish and J. Hopkins*
27. **"Development of a Technology for Fabrication of Ice Abrasives,"** *D.V. Shishkin, E.S. Geskin and B. Goldenberg*
28. **"Laboratory Research for Water Jet Material Surfaces Cleaning,"** *S. Radu, N. Ilias, A. Magyari and A.A. Magyari*

Session R8: Jet-Material Interaction

- 29. **"Investigation of Metal Piercing Using High-Speed Water Slugs,"** *O. Petrenko, E.S. Geskin, B. Goldenberg and G.A. Atanov*
- 30. **"Abrasive Waterjet & Metal Material Interaction Dynamics,"** *J.F. Urbánek*
- 31. **"Impact Initiation Mechanisms of High Explosive Materials During Waterjet Demilitarization,"** *P.L. Miller*

Session A1: Rock Cutting

- 32. **"Waterjet Use in Sculpting Large and Small Objects,"** *D.A. Summers, J.G. Blaine and L.J. Tyler*
- 33. **"Performance of Water Jet Cutting System in Dimension Stone,"** *C.T. Lauand, G.R. Martin C., W.T. Hennies and M. Agus*
- 34. **"Disintegration of Rocks Exposed to Laser Beam by Waterjet,"** *L.M. Hlaváč, P. Martinec and A. Jančárek*
- 35. **"Limitations to the Use of Waterjets in Concrete Substrate Preparation,"** *G. Galecki, N. Maerz, A. Nanni and J. Myers*

Session A2: Pulsed and Modulated Jets

- 36. **"Development and Design of Self-Rotating Forced Pulsed Waterjet: Basic Study and Applications,"** *M.M. Vijay, W. Yan, A. Tieu and C. Bai*
- 37. **"The Use of the Theory of Sonics for Producing High Pressure Pulsatory Water Jets,"** *A. Magyari, N. Ilias, Gh. Roman and S. Radu*
- 38. **"Modulated vs. Continuous Jets: Performance Comparison,"** *J. Foldyna and L. Sitek*
- 39. **"Hydrodynamic Generator for Ultrasonic Modulation of the Jet: Basic Study,"** *L. Sitek, Z. Říha, J. Foldyna and L. Lhotáková*

Session A3: Cleaning and Coating Removal

- 40. **"Waterjet Cleaning of Truck-Mounted Concrete Mixing Tanks,"** *A.L. Miller, G.W. King and G.A. Savanick*
- 41. **"The Removal of Hardened Grease Deposits from Steam Dryers in a Paper Mill First Successful Contract Application of Forced Pulsed Waterjet,"** *M.M. Vijay, W. Yan, A. Tieu, C. Bai and J. Szemeczko*
- 42. **"Removal of Non-Skid Coatings From Aircraft Carrier Decks,"** *T. Kupscznk and J. Van Dam*
- 43. **"Difference and Similarity of Glue Removal for Airport Concrete Runway and Bitumen Runway,"** *S. Xue, Y. Fan, H. Peng, W. Huang, Z. Chen, T. Jiang and L. Wang*

Session A4: Mining and Excavation

44. "High Pressure Water Jet for Mining Red Sea Egyptian Phosphate," *A.A. El-Saie*
45. "Research of Waterjet Interaction with Submerged Rock Materials," *L. M. Hlaváč, I.M. Hlaváčová, M. Kušnerová and V. Mádr*
46. "The Study on the Breaker of Self-Excited Oscillation Pulsed Jet to Scour the Hard Clay and Rocky Beds Under Water," *C. Tang, F. Zhang, L. Yang and Z. Liao*
47. "Empirio-Analytical Method a Good Means of Water Jetting Technology Investigations," *B.V. Radjko*
48. "Experimental Studies on Swirling Jet for Hole Drilling," *Y. Yang, Z. Shen, R. Wang and W. Zhou*

Session A5: Waterjet Blasting I

49. "Optimizing Water Blast Power," *D. Wright, G. Zink and J. Wolgamott*
50. "Waterjet Technology Challenge to Meet New Expectation," *J. Russell*
51. "The Electro-Aerosol Jet Cleaning the Grease and Impurity on the Metal Surface," *Z. Liao, C. Tang, F. Zhang, S. Zhang and X. Deng*
52. "Advanced High-Pressure Waterjet Cleaning Systems for Investment Casting Foundries," *J. Tebbe*
53. "Field Experiments of a City Street Fence Water Jet Cleaner," *J. Wang, L. Yang, S. Jing and W. Liu*

Session A6: Safety in Job Shops and Factories

OPEN FORUM DISCUSSION

Session A7: Waterjet Blasting II

54. "Development of the PREMAJET Derusting Machine," *Z. Dongsu, L. Benli, J. Beihua and L. Lihong*
55. "Advanced Waterblast Tools Pay for Themselves," *J. Wolgamott, D. Wright and M. House*
56. "Turning a Liability Into an Asset! The Story of an Old Power Plant," *R. Dupuy, R. Ashworth and L. Frenzel*
57. "Comparison of Surface Preparation Using Different Methods," *L.E.O. Trotter*
58. "Development of a Generic Procedure for Modeling of the Waterjet Cleaning," *K. Babets and E.S. Geskin*

Session A8: High Pressure Systems and Components

59. "The Development of Improved High Pressure Valves," *G.G. Yie*
60. "Hydro-Balanced Packing System for High Pressure Pumps," *M.T. Gracey*
61. "800 MPa Pure Waterjet and Abrasive Waterjet Cutting - What's Next," *F. Trieb and K. Zamazal*

AUTHOR INDEX

Proceedings of the 2001 WJTA American Waterjet Conference

A

AGUS, M.

"Performance of Water Jet Cutting System in Dimension Stone"

AHMED, D.H.

"Numerical Simulation of Abrasive Water Jet"

ANAND, U.

"Using Porous Lubricated Nozzles to Prevent Nozzle Wear in Abrasive Water Suspension Jets (AWSJ)"

ASHWORTH, R.

"Turning a Liability Into an Asset! The Story of an Old Power Plant"

ATANOV, G.

"The Hydro-Cannon Nozzle Optimization"

"Investigation of Metal Piercing Using High-Speed Water Slugs"

B

BABETS, K.

"Development of a Generic Procedure for Modeling of the Waterjet Cleaning"

"Numerical Study of the Turbulent Flow Inside a Pure Waterjet"

BABU, M.K.

"Abrasive Waterjet Machining of Aluminum with Local Abrasives"

BABU, N.R.

"Modeling and Simulation of Abrasive Water Jet Cut Surface Topography"

BAI, C.

"Development and Design of Self-Rotating Forced Pulsed Waterjet: Basic Study and Applications"

"The Removal of Hardened Grease Deposits from Steam Dryers in a Paper Mill First Successful Contract Application of Forced Pulsed Waterjet"

BEIHUA, J.

"Development of the PREMAJET Derusting Machine"

BENLI, L.

"Development of the PREMAJET Derusting Machine"

BLAINE, J.G.

"Waterjet Use in Sculpting Large and Small Objects"

BORTOLUSSI, A.

"Cutting of Reinforced Concrete Using Abrasive Suspension Jet"

BURCH, D.

"Abrasive Cutting Comparisons"

"Results of Comparative Nozzle Testing Using Abrasive Waterjet Cutting"

C

CARRINO, L.

"AWJ To Machine Free Form Profiles in Natural Stone "

CHEN, F.L.

"Numerical Simulation of Abrasive Water Jet"

CHEN, Z.

"Difference and Similarity of Glue Removal for Airport Concrete Runway and Bitumen Runway"

CHETTY, O.V.K.

"Abrasive Waterjet Machining of Aluminum with Local Abrasives"

CICCU, R.

"Cutting of Reinforced Concrete Using Abrasive Suspension Jet"

D

DENG, X.

"The Electro-Aerosol Jet Cleaning the Grease and Impurity on the Metal Surface"

DITZINGER, T.

"Influences on Structure Formation at the Cutting Edge with Abrasive Waterjets"

DONGSU, Z.

"Development of the PREMAJET Derusting Machine"

DRŽÍK, M.

"Optical Method for Surface Analyses and Their Utilization for Abrasive Liquid Jet Automation"

DUPUY, R.

"Turning a Liability Into an Asset! The Story of an Old Power Plant"

E

EL-SAIE, A. A.

"High Pressure Water Jet for Mining Red Sea Egyptian Phosphate"

F

FAN, Y.

"Difference and Similarity of Glue Removal for Airport Concrete Runway and Bitumen Runway"

FANG, M.

"Study on the Flow Characteristics of Free Water Jet Based on Hyperbola Flow Line Structure"

FOLDYNA, J.

"Hydrodynamic Generator for Ultrasonic Modulation of the Jet: Basic Study"

"Modulated vs. Continuous Jets: Performance Comparison"

"Testing of Mineral Types of Abrasives for Abrasive Water Jet Cutting"

FOSSEY, R.D.

"Abrasive Cutting Comparisons"

"Results of Comparative Nozzle Testing Using Abrasive Waterjet Cutting"

FRENZEL, L.

"Turning a Liability Into an Asset! The Story of an Old Power Plant"

FRIEDRICH, R.

"Influences on Structure Formation at the Cutting Edge with Abrasive Waterjets"

G

GALECKI, G.

"Abrasive Cutting Comparisons"

"Limitations to the Use of Waterjets in Concrete Substrate Preparation"

"Results of Comparative Nozzle Testing Using Abrasive Waterjet Cutting"

GESKIN, E.S.

"Development of a Generic Procedure for Modeling of the Waterjet Cleaning"

"Development of a Technology for Fabrication of Ice Abrasives"

"Investigation of Metal Piercing Using High-Speed Water Slugs"

"Numerical Study of the Turbulent Flow Inside a Pure Waterjet"

GOLDENBERG, B.

"Development of a Technology for Fabrication of Ice Abrasives"

"Investigation of Metal Piercing Using High-Speed Water Slugs "

GRACEY, M.T.

"Hydro-Balanced Packing System for High Pressure Pumps"

GROSSO, B.

"Cutting of Reinforced Concrete Using Abrasive Suspension Jet"

H

HASHISH, M.

"Macro Characteristics of AWJ Turned Surfaces"

"Ultra High Pressure Waterjet Peening - Part I: Surface Texture"

"Ultra High Pressure Waterjet Peening - Part II: High Cycle Fatigue Performance"

HENNIES, W.T.

"Performance of Water Jet Cutting System in Dimension Stone"

HENNING, A.

"Influences on Structure Formation at the Cutting Edge with Abrasive Waterjets"

HLAVÁČ, L.M.

"Disintegration of Rocks Exposed by Laser Beam by Waterjet"

"Optical Method for Surface Analyses and Their Utilization for Abrasive Liquid Jet Automation"

"Research of Waterjet Interaction with Submerged Rock Materials"

HLAVÁČOVÁ, I.M.

"Research of Waterjet Interaction with Submerged Rock Materials"

HOPKINS, J.

"Ultra High Pressure Waterjet Peening - Part I: Surface Texture"

"Ultra High Pressure Waterjet Peening - Part II: High Cycle Fatigue Performance"

HOUSE, M.

"Advanced Waterblast Tools Pay for Themselves"

HOWELLS, W.G.

"Reducing Abrasive Consumption by Using SUPERWATER® for Venturi Abrasivejet Cutting"

HUANG, W.

"Difference and Similarity of Glue Removal for Airport Concrete Runway and Bitumen Runway"

HUANG, Z.

"Experimental Studies of Jet Cavitation Noise Spectrums in Oil Well Casing"

I

ILIAS, N.

"Laboratory Research for Water Jet Material Surfaces Cleaning"

"The Use of the Theory of Sonics for Producing High Pressure Pulsatory Water Jets"

IMLAY, V.L.

"Reducing Abrasive Consumption by Using SUPERWATER® for Venturi Abrasivejet Cutting"

J

JANČÁREK, A.

"Disintegration of Rocks Exposed by Laser Beam by Waterjet"

JIANG, S.

"Study on the Flow Characteristics of Free Water Jet Based on Hyperbola Flow Line Structure"

JIANG, T.

"Difference and Similarity of Glue Removal for Airport Concrete Runway and Bitumen Runway"

JING, S.

"Field Experiments of a City Street Fence Water Jet Cleaner "

JOHNSON, M.

"Abrasive Cutting Comparisons"

"Results of Comparative Nozzle Testing Using Abrasive Waterjet Cutting"

K

KAIN, I.

"Abrasive Waterjet Cutting a Comparative Study Between Open Catcher Tank and Water Catcher Tank"

KATZ, J.

"Using Porous Lubricated Nozzles to Prevent Nozzle Wear in Abrasive Water Suspension Jets (AWSJ)"

KING, G.W.

"Waterjet Cleaning of Truck-Mounted Concrete Mixing Tanks"

KÜBLER, T.

"Influences on Structure Formation at the Cutting Edge with Abrasive Waterjets"

KUNAPORN, S.

"Ultra High Pressure Waterjet Peening - Part I: Surface Texture"

"Ultra High Pressure Waterjet Peening - Part II: High Cycle Fatigue Performance"

KUŠNEROVÁ, M.

"Research of Waterjet Interaction with Submerged Rock Materials"

KUPSCZNIK, T.

"Removal of Non-Skid Coatings From Aircraft Carrier Decks"

L

LAUAND, C.T.

"Performance of Water Jet Cutting System in Dimension Stone"

LHOTÁKOVÁ, L.

"Hydrodynamic Generator for Ultrasonic Modulation of the Jet: Basic Study"

LI, G.

"Experimental Studies of Jet Cavitation Noise Spectrums in Oil Well Casing"

LIAO, Z.

"Numerical Investigation of Chaotic Motion for Cavitation Bubble in Oscillating Pressure Field"

"The Electro-Aerosol Jet Cleaning the Grease and Impurity on the Metal Surface"

"The Study on the Breaker of Self-Excited Oscillation Pulsed Jet to Scour the Hard Clay and Rocky Beds Under Water"

LIHONG, L.

"Development of the PREMAJET Derusting Machine"

LIU, W.

"Field Experiments of a City Street Fence Water Jet Cleaner"

LOUIS, H.

"Cutting of Hollow Structures with Polymer Supported Abrasive Water Suspension Jets"

M

MÁDR, V.

"Optical Method for Surface Analyses and Their Utilization for Abrasive Liquid Jet Automation"

"Research of Waterjet Interaction with Submerged Rock Materials"

MAERZ, N.

"Limitations to the Use of Waterjets in Concrete Substrate Preparation"

MAGYARI, A.

"Laboratory Research for Water Jet Material Surfaces Cleaning"

MAGYARI, A.A.

"Laboratory Research for Water Jet Material Surfaces Cleaning"

"The Use of the Theory of Sonics for Producing High Pressure Pulsatory Water Jets"

MARTIN C., G.R.

"Performance of Water Jet Cutting System in Dimension Stone"

MARTINEC, P.

"Disintegration of Rocks Exposed by Laser Beam by Waterjet "

"Testing of Mineral Types of Abrasives for Abrasive Water Jet Cutting"

MILLER, A.L.

"Waterjet Cleaning of Truck-Mounted Concrete Mixing Tanks"

MILLER, D.S.

"Micro Abrasive Waterjet Cutting"

MILLER, P.L.

"Electrostatic Charge Generation in Waterjet Systems"

"Impact Initiation Mechanisms of High Explosive Materials During Waterjet Demilitarization"

MONNO, M.

"AWJ To Machine Free Form Profiles in Natural Stone "

MUNOZ, J.

"Abrasive Waterjet Cutting a Comparative Study Between Open Catcher Tank and Water Catcher Tank"

MYERS, J.

"Limitations to the Use of Waterjets in Concrete Substrate Preparation"

N

NANNI, A.

"Limitations to the Use of Waterjets in Concrete Substrate Preparation"

NASER, J.

"Numerical Simulation of Abrasive Water Jet"

NEWKIRK, J.W.

"Abrasive Cutting Comparisons"

"Results of Comparative Nozzle Testing Using Abrasive Waterjet Cutting"

NIU, J.

"Experimental Studies of Jet Cavitation Noise Spectrums in Oil Well Casing"

O

OHLÍDAL, M.

"Optical Method for Surface Analyses and Their Utilization for Abrasive Liquid Jet Automation"

OLSON, G.

"Results of Comparative Nozzle Testing Using Abrasive Waterjet Cutting"

P

PENG, H.

"Difference and Similarity of Glue Removal for Airport Concrete Runway and Bitumen Runway"

PETRENKO, O.

"Investigation of Metal Piercing Using High-Speed Water Slugs"

POLINI, W.

"AWJ To Machine Free Form Profiles in Natural Stone "

R

RADJKO, B.V.

"Empirio-Analytical Method a Good Means of Water Jetting Technology Investigations"

RADONS, G.

"Influences on Structure Formation at the Cutting Edge with Abrasive Waterjets"

RADU, S.

"Laboratory Research for Water Jet Material Surfaces Cleaning"

"The Use of the Theory of Sonics for Producing High Pressure Pulsatory Water Jets"

RAMULU, M.

"Ultra High Pressure Waterjet Peening - Part I: Surface Texture"

"Ultra High Pressure Waterjet Peening - Part II: High Cycle Fatigue Performance"

ŘÍHA, Z.

"Hydrodynamic Generator for Ultrasonic Modulation of the Jet: Basic Study"

ROMAN, GH.

"The Use of the Theory of Sonics for Producing High Pressure Pulsatory Water Jets"

RUSSELL, J.

"Waterjet Technology Challenge to Meet New Expectation"

S

SAVANICK, G.A.

"Waterjet Cleaning of Truck-Mounted Concrete Mixing Tanks"

SHEN, Z.

"Experimental Studies of Swirling Jet for Hole Drilling"

SHISHKIN, D.V.

"Development of a Technology for Fabrication of Ice Abrasives"

SIORES, E.

"Numerical Simulation of Abrasive Water Jet"

SITEK, L.

"Hydrodynamic Generator for Ultrasonic Modulation of the Jet: Basic Study"

"Modulated vs. Continuous Jets: Performance Comparison"

"Testing of Mineral Types of Abrasives for Abrasive Water Jet Cutting"

SUCHY, U.

"Investigation of a New Cutting Head Concept Based on an Annular Driving Jet"

SUMMERS, D.A.

"Abrasive Cutting Comparisons"

"Waterjet Use in Sculpting Large and Small Objects"

"Results of Comparative Nozzle Testing Using Abrasive Waterjet Cutting"

SZEMECZKO, J.

"The Removal of Hardened Grease Deposits from Steam Dryers in a Paper Mill First Successful Contract Application of Forced Pulsed Waterjet"

T

TANG, C.

"Numerical Investigation of Chaotic Motion for Cavitation Bubble in Oscillating Pressure Field"

"The Electro-Aerosol Jet Cleaning the Grease and Impurity on the Metal Surface"

"The Study on the Breaker of Self-Excited Oscillation Pulsed Jet to Scour the Hard Clay and Rocky Beds Under Water"

TEBBE, J.

"Advanced High-Pressure Waterjet Cleaning Systems for Investment Casting Foundries"

TIEU, A.

"Development and Design of Self-Rotating Forced Pulsed Waterjet: Basic Study and Applications"

"The Removal of Hardened Grease Deposits from Steam Dryers in a Paper Mill First Successful Contract Application of Forced Pulsed Waterjet"

TRIEB, F.

"800 MPa Pure Waterjet and Abrasive Waterjet Cutting - What's Next"

TROTTER, L.E.O.

"Comparison of Surface Preparation Using Different Methods"

TURCHETTA, S.

"AWJ To Machine Free Form Profiles in Natural Stone"

TYLER, L.J.

"Waterjet Use in Sculpting Large and Small Objects"

U

URBÁNEK, J.F.

"Abrasive Waterjet & Metal Material Interaction Dynamics"

"Environmental Evaluation and Management of AWJ Process"

V

VALÍČEK, J.

"Optical Method for Surface Analyses and Their Utilization for Abrasive Liquid Jet Automation"

VAN DAM, J.

"Removal of Non-Skid Coatings From Aircraft Carrier Decks"

VIJAY, M. M.

"Development and Design of Self-Rotating Forced Pulsed Waterjet: Basic Study and Applications"

"The Removal of Hardened Grease Deposits from Steam Dryers in a Paper Mill First Successful Contract Application of Forced Pulsed Waterjet"

VIKRAM, G.

"Modeling and Simulation of Abrasive Water Jet Cut Surface Topography"

VON RAD, CH.

"Cutting of Hollow Structures with Polymer Supported Abrasive Water Suspension Jets"

W

WANG, J.

"Field Experiments of a City Street Fence Water Jet Cleaner"

WANG, L.

"Difference and Similarity of Glue Removal for Airport Concrete Runway and Bitumen Runway"

WANG, R.

"Experimental Studies of Swirling Jet for Hole Drilling"

WESTKÄMPER, E.

"Influences on Structure Formation at the Cutting Edge with Abrasive Waterjets"

WOLGAMOTT, J.

"Advanced Waterblast Tools Pay for Themselves"

"Optimizing Water Blast Power"

WRIGHT, D.

"Advanced Waterblast Tools Pay for Themselves"

"Optimizing Water Blast Power"

X

XUE, S.

"Difference and Similarity of Glue Removal for Airport Concrete Runway and Bitumen Runway"

Y

YAN, W.

"Development and Design of Self-Rotating Forced Pulsed Waterjet: Basic Study and Applications"

"The Removal of Hardened Grease Deposits from Steam Dryers in a Paper Mill First Successful Contract Application of Forced Pulsed Waterjet"

YANG, L.

"Field Experiments of a City Street Fence Water Jet Cleaner"

"Numerical Investigation of Chaotic Motion for Cavitation Bubble in Oscillating Pressure Field"

"The Study on the Breaker of Self-Excited Oscillation Pulsed Jet to Scour the Hard Clay and Rocky Beds Under Water"

YANG, Y.

"Experimental Studies of Swirling Jet for Hole Drilling"

YIE, G.G.

"The Development of Improved High Pressure Valves"

Z

ZAMAZAL, K.

"800 MPa Pure Waterjet and Abrasive Waterjet Cutting - What's Next"

ZHANG, D.

"Experimental Studies of Jet Cavitation Noise Spectrums in Oil Well Casing"

ZHANG, F.

"Numerical Investigation of Chaotic Motion for Cavitation Bubble in Oscillating Pressure Field"

"The Electro-Aerosol Jet Cleaning the Grease and Impurity on the Metal Surface"

"The Study on the Breaker of Self-Excited Oscillation Pulsed Jet to Scour the Hard Clay and Rocky Beds Under Water"

ZHANG, S.

"The Electro-Aerosol Jet Cleaning the Grease and Impurity on the Metal Surface"

ZHOU, W.

"Experimental Studies of Swirling Jet for Hole Drilling"

ZINK, G.

"Optimizing Water Blast Power"

OPTICAL METHOD FOR SURFACE ANALYSES AND THEIR UTILIZATION FOR ABRASIVE LIQUID JET AUTOMATION

J. Valíček, V. Mádr and L.M. Hlaváč
VŠB - Technical University Ostrava
Ostrava, Czech Republic

M. Držík
Institute of Construction and Architecture, Slovak Academy of Sciences
Bratislava, Slovak Republic

M. Ohlídal
Technical University Brno
Brno, Czech Republic

ABSTRACT

The knowledge of the surface roughness is a very important parameter for automation of machining techniques. The direct detection of surface quality is a problem of waterjet technology, especially if used for turning, milling or grinding, where the surface is opened for detection. The topic of the paper is a theoretical and experimental investigation of an optical method and its utilization for surface quality analyses. The method is based on scanning of the surface by defocused laser beam. The method is theoretically described and the most important theoretical results are discussed. The experimental data are analyzed from the point of utilization of the methods for determination of roughness and waviness of surfaces prepared by abrasive water jets. The correlation between theoretical and experimental results and the algorithm of the optical surface measurements are also discussed.

1. INTRODUCTION

New and very perspective technology for material machining has been developed within the period of the last twenty years. This technology is mostly called water jetting or abrasive water jetting nowadays. The term water jetting is usually appropriate for jet formed by water without any ingredients. On the contrary, the term abrasive water jet is used for water jets containing particles of solid matter (grains of rock materials, metals, glass, slag, etc.) added into them for increasing of their efficiency. There are two possible methods for abrasive water jet generation. The first one is based on two steps generation. Primarily the pure water jet is generated making the hypotension in a special chamber. As a consequence of it, the air with dry abrasive material particles is sucked into this chamber and mixed there with water jet. Therefore, the chamber is called the mixing chamber. The abrasive water jets generated in this manner are called injection jets. The slurry resulting from the mixing process is guided by so-called mixing tube made of an extreme wear resistant material. The second method of the abrasive water jet generation is based on the direct outflow of the highly pressurized slurry made of water and abrasive material particles in a special tank. This slurry outflows from the nozzle made again of an extreme wear resistant material generating so-called suspension jet.

The most important differences are the following ones: the injection water jets are active for high water pressure in the pump and the energy losses during the generation process often reach 80% and more whilst the suspension jet is efficient even for low water pressure in the pump and energy losses within generation are usually less than 20%. Nevertheless, both jets irrespective of the method of their generation make surfaces with characteristic pattern depending only on parameters of jet (pressure, abrasive material type and grain size, traverse rate, etc.), target material and type of machining.

2. SURFACE CHARACTERISTICS

The surface prepared by abrasive water jet during cutting, drilling, turning, milling, planning, slotting, shaping and grinding (with respect to correlation of the abrasive water jet technology and the classical ones in spite of the specific features) is characterized by typical pattern. There are microscopic pits (craters) on the surface prepared by abrasive water jet created by grains of abrasive material and cavitation. Abrasive particles contained by water jet remove the appropriate small parts of material according to their energy and momentum, size, stress and strain characteristics, angle of impact and other parameters or engrain itself into the surface. The cavitation effects caused by rapid water flowing over the local surface roughness are also contributing to it. Moreover, the further microscopic and even macroscopic patterns are induced by abrasive water jet impact and interaction processes – striation and waviness (see Fig. 1 and 2). These last two one patterns are created as a consequence of the jet and target material vibrations, water flow instabilities, material non-homogeneities, abrasive suction and flow rate instabilities, changes in character of an abrasive particle - target material interaction depending on the angle of impact, etc. Many of the specific phenomena mentioned above were studied, described and discussed by specialists on water jetting from all over the world, e.g. Hashish (1984, 1989), Zeng and Kim (1990), Capello et al. (1994), Guo (1994), Fukunishi et al. (1995), Hlaváč (1994, 1996).

The measurement of surfaces generated by abrasive water jets is quite difficult. It is caused by specific surface structure. Contrary to the classical ones the surface prepared by abrasive water jet is slightly diffusion. Therefore, there are certain difficulties using classical optical methods and the proper method regarding the specific optical properties of the surface is to be used (Držík, 1996). Nevertheless, the effort of many research teams all over the world was concentrated on determination of the quality of walls in cuts by optical methods. Our work is aimed at development of methods usable for an interactive measurement of the surface quality during processes with opened surfaces feasible using abrasive water jet (in terms of a classical material machining it means turning, planning, slotting, shaping and/or grinding). The current state-of-the-art in realization of our intentions can be described as a judgement of the appropriate optical methods. Our first aim is to prepare the method yielding the outputs corresponding with the main surface parameters and characteristics by course of engineering standards ČSN and ISO.

3. VISUALISATION OF THE ROUGHNESS BY OBLIQUE ANGLE ILLUMINATION

Testing few optical methods used for studies of surface characteristics on several samples prepared by abrasive water jet we decided to prepare a new one. It is specially dedicated to measurements on surfaces with diffusion structure. The scheme of the laboratory investigation is presented in Figure 3.

The method is based on the speculation graphically demonstrated in Fig. 4. The optical effect caused by light impinging the surface at an oblique angle is used for visualisation of the geometrical shapes being present at the sample surface. The shapes can be so displayed in a simulated optical plane. The intensity of laser light scattered by surface treated in this manner contains the information about frequency and height of geometrical shapes present at the surface. The principle can be described by equation 1 useful for evaluation of the shape height which is in a close relation with parameters of roughness R_a and R_q .

$$h = \frac{v}{M f} \sin \alpha \quad (1)$$

where v is the traverse rate of the sample [m.s^{-1}]

f is the frequency of the roughness [Hz]

M is the mounting [-]

The angle α was selected from the interval $<10;15>$ degrees. The lens speed of the objective was 1:1.4 and focused the image of the shadowed visualized roughness to the plane of the slot type shutter of the photodiode. The aperture was 0.1 x 0.3 mm. The reflected laser beam is converted to the electric signal in the photodiode. The analogue electric signal is a function of time $U(t)$. This signal is converted to the digital form and downloaded into the computer with programme for signal analysis. The FFT (fast Fourier transformation) converts the time depending signal to its amplitude-frequency image $U(f)$. The function $U(f)$ is the base for calculation of the main roughness parameters R_a and R_q – the arithmetical average of the absolute values of the height deviations of the profile and the average quadratic deviation respectively. The cut off value of the tested optical configuration can

be calculated, according to Ohlídal (1999), from the equation $A_c = l \cdot \lambda \cdot w^{-1}$. Our parameters were as follows: the aperture width $w = 0.1$ mm, stand-off distance $l = 0.2$ m, laser beam wavelength $\lambda = 532$ nm. The cut off value calculated for our investigation is $A_c = 0.1$ mm.

4. RESULTS AND DISCUSSION

Up-to-date three samples were measured using both optical and contact methods. They were square samples prepared from hard steel, mild steel and aluminium alloy cut from the plates 8 mm thick. Each side of the samples was cut using another traverse rate. Each sidewall was passed by both optical signal (a laser beam) and a mechanical tip in zones situated round the lines perpendicular to the sample height in distances 2, 4 and 6 mm from the top (according to the direction of the abrasive water jet flow). The record of the time dependant optical signal is presented in Figure 5. Its FFT is shown in Figure 6.

Graph in Figure 7 shows the record of the same trace as it is shown in Figure 5. The signal is obtained from the contact profilometer HOMMEL TESTER T8000. The initial tested length was 15 mm with cut off 2.5 mm. The signal was processed by filter RC DIN4768 and the resulting length corresponding to the record shown in Figure 7 is 12.5 mm. The presented record starts at about 3.75 mm from the side edge of the measured sample wall. Taking into account the cut off and the position of signal start we can determine the absolute position of the very typical peak situated at approximately 7.15 mm in the graph. The 0.00 mm point (zero position of the unprocessed signal) lies in the distance one half of the cut off from the side edge of the tested wall. Simultaneously, the processed signal begins in the distance 2.5 mm from that point. This deduction and calculation tend to the conclusion that the absolute position of the peak is 8.4 mm from the side edge of the wall. Nevertheless, the typical peak, we have discussed, can be determined also in Figure 5 at position about 5.6 ms. Considering the fact that optical signal starts at the side edge of the wall and the traverse rate is $1.5 \text{ m} \cdot \text{s}^{-1}$ we can calculate the absolute position of the peak. It is again 8.4 mm. We can see analogical behaviour of both signals in Figures 5 and 7 provided the position of the discussed peak is known.

The characteristic frequency f was determined for each data record. The values of the heights of unlevelness h were calculated from the equation 1. The unlevelness h can be considered to be the value R_{max} , i.e. the maximum roughness of the surface by course of its determination by contact profilometer. The correlation of values obtained from the optical signal with the ones specified by the contact profilometer is presented in Table 1. We tried to establish some conversion coefficients to be able to calculate the values R_a and R_q from the value R_{max} determined from an optical signal. The coefficients c_a and c_q were determined as the ratio of values R_a and R_{max} or R_q and R_{max} specified by contact profilometer respectively. The values R_a and R_q were determined from optical measurements by equation 2.

$$R_x = c_x h \quad x = a \vee q \quad (2)$$

All parameters are presented in Table 1 as well as the deviation in percents of values calculated from the optical signal and the ones obtained by contact profilometer. Resulting average deviations of the up-to-date limited set of data circulate round 10%. Nevertheless, it is supposed that further development of the optical method could yield more precise results. The intrinsic intention, however, is to prepare optical method for testing open surfaces during their machining by abrasive water jet. Therefore, the next step just succeeding to the method checkout should be testing it on the wet samples because this method should serve as one of the feedbacks for automation of the machining process with abrasive water jet.

5. CONCLUSIONS

The up-to-now results allow us to summarize the following conclusions:

- optical method yields a signal of sufficient amplitude for further processing;
- signal obtained from the optical method is in a good correlation with the signal obtained by commercial contact profilometer;
- optical method can be stamped and used for determination of the surface parameters.

6. ACKNOWLEDGEMENTS

The authors are grateful to the Grant Agency of the Czech Republic and to the Ministry of Industry and Trade supporting the work presented in the paper by projects No. 106/98/1354 and FB-C3/05 respectively.

7. REFERENCES

- Capello, E., Monno, M., Semeraro, Q., "On the characterization of the surfaces obtained by abrasive water jet machining," *Proceedings of the 12th International Conference on Jet Cutting Technology*, N.G.Allen (ed.), pp.177-193, Mech. Eng. Pub. Ltd., London, 1994.
- Držík, M., "The metallic surfaces microstructure determination by measuring of scattered light," *Journal of Fine Mechanics and Optics*, No.7-8, pp.208-211, 1996.
- Fukunishi, Y., Kobayashi, R., Uchida, K., "Numerical Simulation Of Striation Formations On Water Jet Cutting Surface," *Proceedings of the 8th American Water Jet Conference*, T.J.Labus (ed.), pp.657-670, Houston, Texas, U.S.A., 1995.
- Guo, N.S., "Cutting process and cutting quality by AWJ cutting," *VDI Verlag*, 1994. (in German)
- Hashish, M., "A Modeling Study of Metal Cutting With Abrasive Waterjets," *Transactions of the ASME, Journal of Eng. Mat. & Tech.*, Vol. 106, No.1, pp.88-100, 1984.

- Hashish, M., "Pressure Effects in Abrasive-Waterjet (AWJ) Machining," *Transactions of the ASME, Journal of Eng. Mat. & Tech.*, Vol. 111, No.7, pp.221-228, 1989.
- Hlaváč, L., "Physical model of jet - Abrasive interaction," *Geomechanics '93*, Rakowski (ed.), pp.301-304, Balkema, Rotterdam, 1994.
- Hlaváč, L.M., "Interaction of grains with water jet - the base of the physical derivation of complex equation for jet cutting of rock materials," *Jetting Technology*, C.Gee (ed.), pp.471-485, Mech. Eng. Pub. Ltd., Bury St Edmunds & London, 1996.
- Ohlídal, M., Ohlídal, I., Tykal, M., Pražák, D., Unčovský, M., "Measuring the surface roughness by selected methods of coherent optics in engineering," *Journal of Fine Mechanics and Optics*, No.9, pp.269-267, 1999. (in Czech)
- Zeng, J., Kim, T.J., "A study of brittle erosion mechanism applied to abrasive waterjet processes," *Proceedings of the 10th International Symposium on Jet Cutting Technology*, paper B1, BHRA, England, 1990.

8. NOMENCLATURE

α	the angle between the laser beam axis and the sample surface plane ...[°]
c_a	conversion coefficient for determination of parameter R_a from optical signal ...[-]
c_q	conversion coefficient for determination of parameter R_q from optical signal ...[-]
f	the characteristic frequency of the roughness ...[Hz]
h	the height of the unlevelness ...[μm]
λ	laser beam wavelength ...[nm]
Λ_c	the cut-off value for the optical configuration ...[mm]
l	stand-off distance (laser to surface) ...[m]
M	the mounting - the norm coefficient ...[-]
R_a	mean arithmetic value of the height deviations ...[μm]
R_{max}	maximum value of the height deviation inside measured length ...[μm]
R_q	mean square value of the height deviations ...[μm]
v	traverse rate of the sample ...[m.s ⁻¹]
w	the aperture width ...[mm]

9. TABLES

Table 1. Comparison of data obtained from contact profilometer and optical method.

Sample	R_{maxp}	f_p	f_o	R_{maxo}	Δf	ΔR_{max}	R_{ap}	R_{ao}	ΔR_a	R_{qp}	R_{qo}	ΔR_q
No.	[μm]	[Hz]	[Hz]	[μm]	[%]	[%]	[μm]	[μm]	[%]	[μm]	[μm]	[%]
1	33.90	1070	1120	32.40	4.6	4.4	4.08	4.41	8.1	5.20	5.58	7.4
2	36.79	986	1020	35.58	3.4	3.3	5.12	4.84	5.4	6.39	6.13	4.0
3	27.23	1333	1330	27.28	0.2	0.2	3.78	3.71	1.7	4.82	4.70	2.4
4	33.12	1096	1090	33.29	0.5	0.5	5.51	4.53	17.8	6.80	5.74	15.6
5	37.38	971	1240	29.26	27.7	21.7	3.48	3.98	14.5	4.60	5.04	9.6
6	27.62	1314	1400	25.92	6.6	6.2	4.21	3.53	16.2	5.33	4.47	16.2
7	24.55	1478	1500	24.19	1.5	1.5	2.98	3.29	10.5	3.87	4.17	7.7
8	23.12	1570	1520	23.87	3.2	3.3	3.18	3.25	2.2	4.07	4.11	1.1
9	25.42	1428	1440	25.20	0.9	0.9	3.37	3.43	1.8	4.34	4.34	0.1
Average values of deviations					5.4	4.7			8.7			7.1

Legend:

- f_o characteristic frequency determined from the optical signal
- f_p characteristic frequency calculated from value R_{maxp} (equation 1)
- R_{ao} parameter R_a determined from optical signal using conversion coefficient calculated from data measured by contact profilometer (equation 2)
- R_{ap} parameter R_a determined by contact profilometer
- R_{maxo} parameter R_{max} calculated from characteristic frequency of the optical signal (equation 1)
- R_{maxp} parameter R_{max} determined by contact profilometer
- R_{qo} parameter R_q determined from optical signal using conversion coefficient calculated from data measured by contact profilometer (equation 2)
- R_{qp} parameter R_q determined by contact profilometer

10. FIGURES

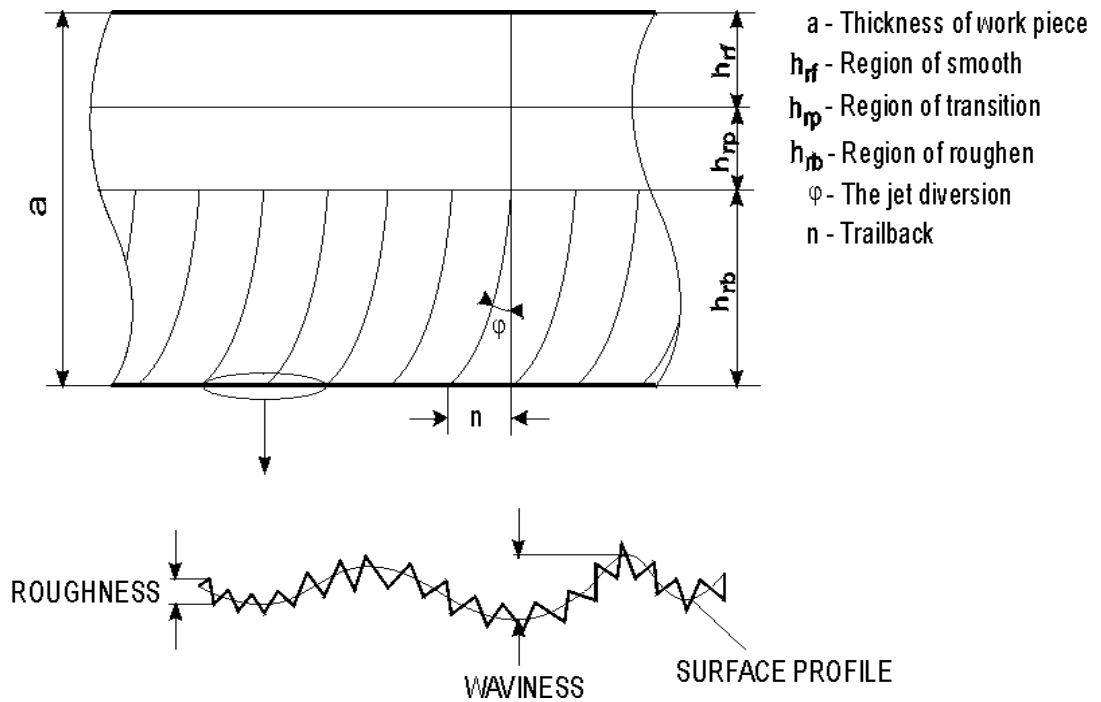


Figure 1. Drawing of the most typical patterns on the walls inside the slot cut by abrasive water jet.



Figure 2. The character of the walls made by abrasive water jet in the slot.

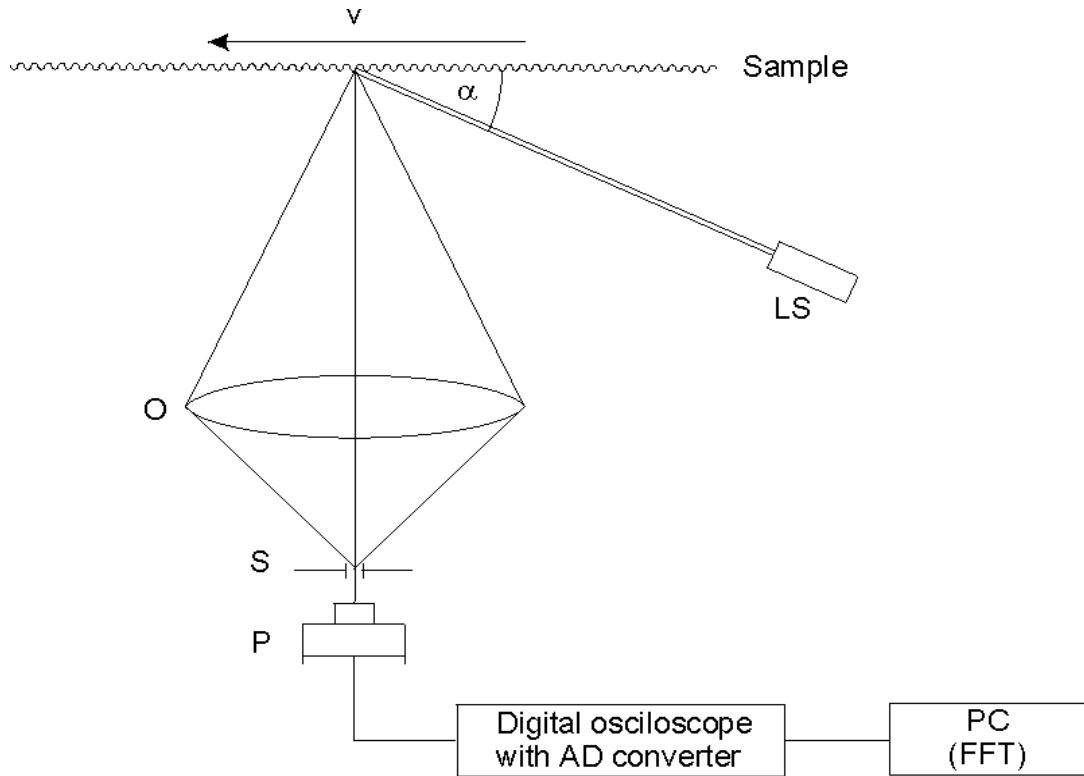


Figure 3. The scheme of the laboratory investigation of our method used for surface quality measurement: LS – laser, O – the objective, S – the aperture, P - photodetector (photo-diode), PC – computer with FFT, v – the traverse rate, α – the angle.

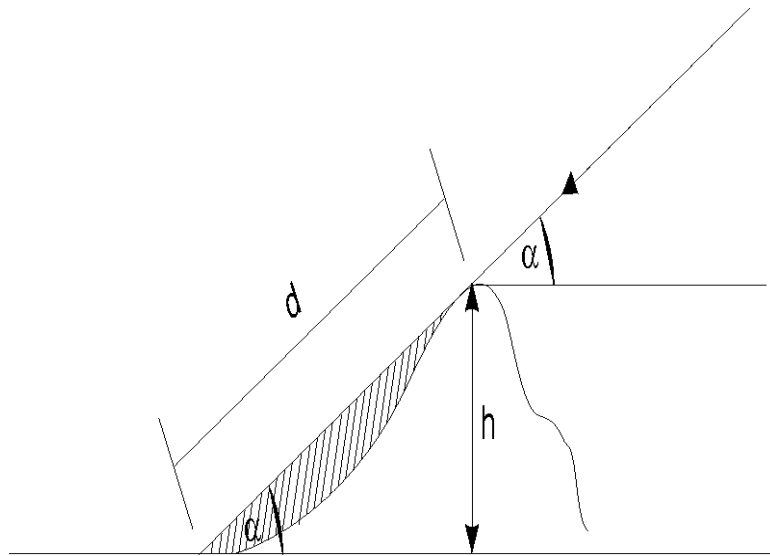


Figure 4. The principle of the surface roughness shadowing: d – the length of the shadow, h – the height of the unlevelness, α – the complementary angle to the laser beam incidence angle.

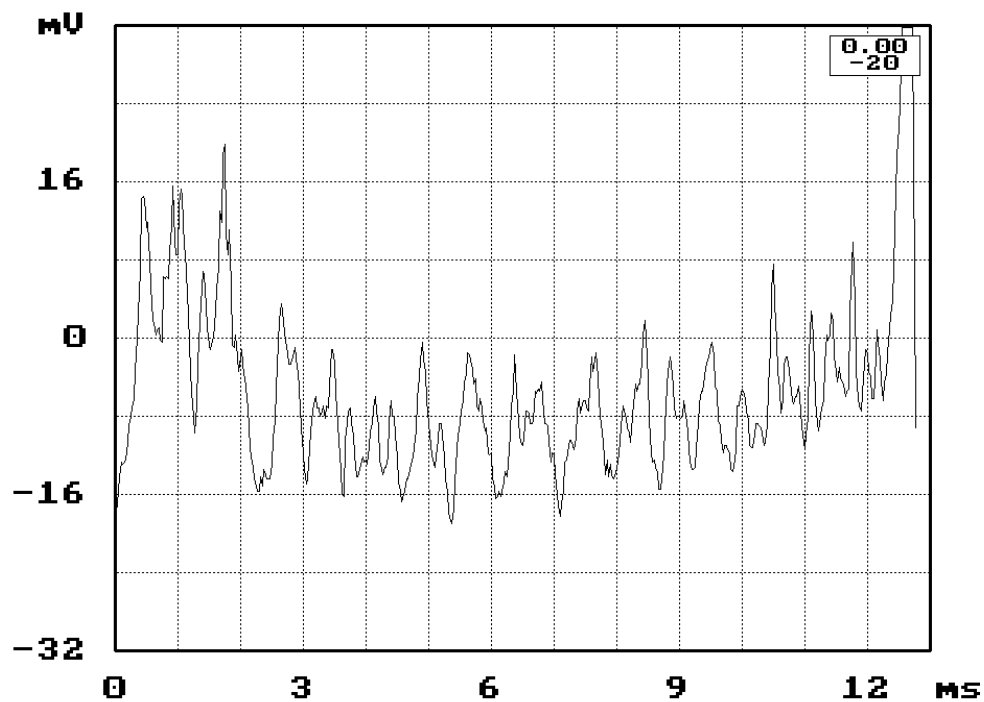


Figure 5. The record of the optical signal scattered by surface of the sample 1, sidewall 1.

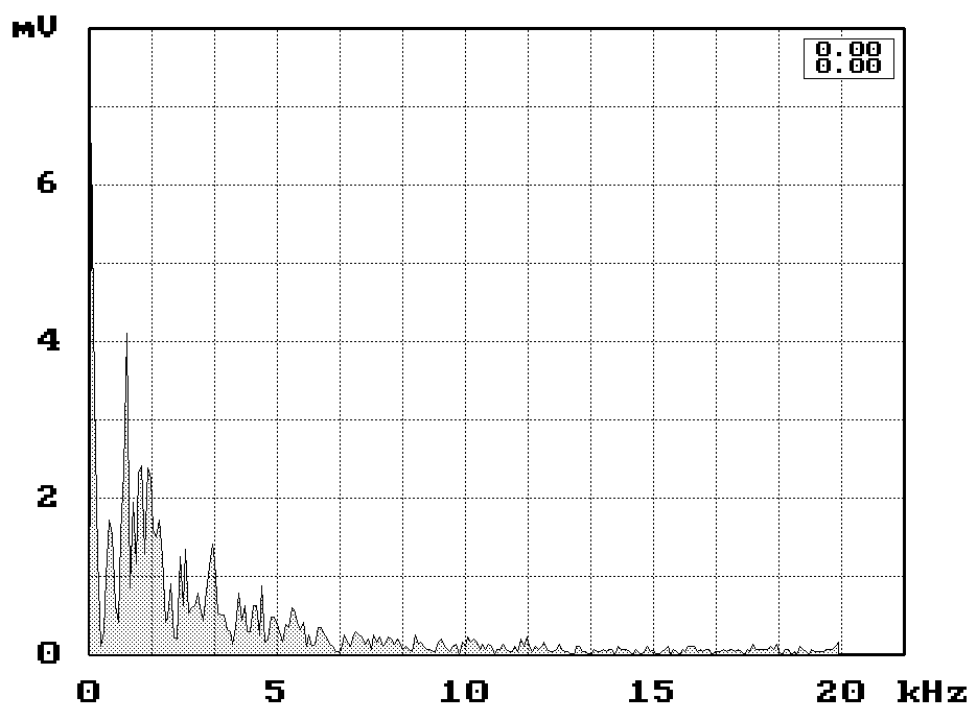


Figure 6. Frequency spectrum obtained by FFT from the time dependent signal shown in Fig. 5.

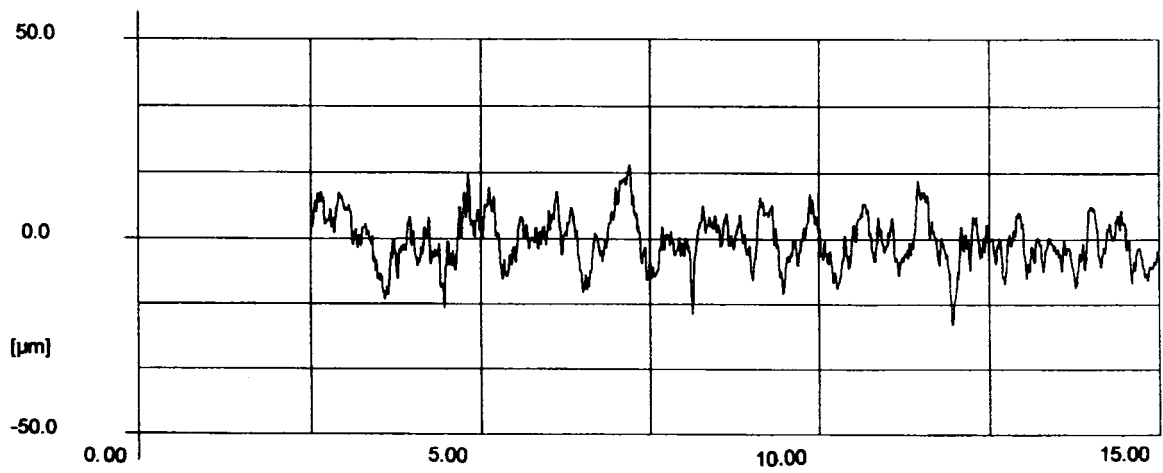


Figure 7. The record of the signal from the contact profilometer HOMMEL TESTER T8000.

MODELING AND SIMULATION OF ABRASIVE WATER JET CUT SURFACE TOPOGRAPHY

G. Vikram and N. Ramesh Babu
Manufacturing Engineering Section
Department of Mechanical Engineering
Indian Institute of Technology Madras
Chennai, India

ABSTRACT

The present work proposes a new approach for modeling the abrasive water jet (AWJ) cut surface topography. It makes use of the trajectory of jet, predicted from the theory of ballistics and Bitter's theory of erosion for material removal, for numerically simulating the cutting front. The surface topography is generated by considering the trajectories on the cutting front and the abrasive particles impacting the walls of the cut surface randomly. For more realistic generation of topography on the cut surface, several instantaneous profiles generated in each region of cut are superimposed. Results obtained with the proposed model are validated with the experimental results.

1. INTRODUCTION

Abrasive water jet (AWJ) cutting makes use of high velocity water entrained with abrasive particles to cut different materials ranging from soft, ductile to hard and brittle materials. It is a non-contact, inertia-less process that offers several advantages like narrow kerf width, negligible heat affected zone, apart from its flexibility in processing a range of materials in different ways. Though it is capable of cutting different materials of different thickness, the extent of penetration of the jet into the material depends on various process parameters and material properties. The penetration of jet into the material was explained by means of different mechanisms of material removal. They are basically identified as cutting wear mode and deformation wear mode of material removal which play an important role in generating a unique topography on the cut surface.

In the past, researchers have attempted to model the abrasive water jet cutting process by experimental and theoretical means (Momber and Kovacevic, 1998). These attempts are elaborated in the works of Hashish (1984, 1989), Momber (1995), Zeng and Kim (1992). Some of the efforts to characterize the AWJ cut surface include visualization studies and semi analytical models (Hashish (1988, 1992), Guo et al., 1992), empirical and semi-empirical models using regression techniques (Blickwedel et al., 1990, Kovacevic, 1991). Very few attempts have been made to numerically simulate the cutting process and determine the surface topography using this simulation (Fukunishi et al., 1995, Sawamura et al., 1997). In their work for simulation of AWJ cutting process, the physical background as well as the entire simulation process were not sufficiently described.

The present work attempts to focus on the generation of cut surface topography from cutting front generation. The cutting front is derived from the trajectory of jet penetrating into the material. This particular trajectory was obtained using Bitter's theory of erosion and considering the jet as a high-speed projectile penetrating into the material.

2. METHODOLOGY

Different steps involved in generating abrasive water jet cut surface topography include:

1. Generation of trajectory of the jet into the material, employing the theory of ballistics and Bitter's theory of erosion for material removal
2. Simulation of the cutting front from the trajectory of the jet
3. Generation of surface topography in different regions of cut.

2.1 Trajectory of Jet

In order to generate the trajectory of jet, the theory of ballistics that determines the velocity of the jet in the material and Bitter's theory of erosion that determines the volume of material removed with abrasive water jet are used. The theory of ballistics basically predicts the velocity of jet in the material with the assumption that the jet is a high speed projectile penetrating into the material. This theory considers the retardation of jet in the material as a function of the

change in momentum and kinetic energy of the jet. Hence, the retardation of the jet can be expressed as (Srivathsa and Ramakrishnan, 1998, Vijay Krishna and Ramesh Babu, 2000)

$$VdV/dy \propto V^{3/2} \quad (1)$$

$$VdV/dy = -K V^{3/2} \quad (2)$$

where K is a constant that is dependent on process parameters used as well as the material properties. By integrating the relation, the velocity of jet at any given depth can be obtained as

$$\int_{V_o}^{V_y} (V/ V^{3/2}) dV = - \int_0^y K dy$$

$$2[(V_o)^{1/2} - (V_y)^{1/2}] = Ky \quad (3)$$

By rearranging the terms, V_y is expressed as

$$V_y = ay^2 + by + c \quad (4)$$

where $a = K^2/4$, $b = -KV_o^{1/2}$, $c = V_o$

The value of K is determined experimentally, as its relation with the process parameters and the material properties is not known. To determine this, the jet with a particular energy is allowed to penetrate through the material to the maximum extent. At this depth, the jet coming out of the material possesses a critical velocity, which is just enough to erode the material. By relating the flexural strength, in case of brittle materials to the stagnation pressure, V_c can be obtained as

$$V_c = (2 \sigma / \rho)^{1/2} \quad (5)$$

By substituting V_c for V_y and maximum depth h_{max} for y in the equation (3), the relation becomes

$$2[(V_o)^{1/2} - (V_c)^{1/2}] = K h_{max} \quad (6)$$

By knowing h_{max} from the experiments, and $V_o = \gamma \sqrt{2P/\rho}$ where $\gamma = 0.88$ (Momber and Kovacevic, 1998), the value of K can be determined. Using the equation (4), the velocity of jet at any depth in the material is obtained.

As the above theory can only give the variation in the velocity of jet in the material, it cannot predict the trajectory of the jet in the material by itself. Thus, the present work makes use of Bitter's theory for material removal to obtain the trajectory of the jet. Figure 1 shows a schematic representation of the trajectory of jet in the material by combining the two theories. By employing Bitter's theory of erosion for material removal, the mass of material removed through deformation wear and cutting wear is given by the expressions (Bitter, 1963).

$$M_D = m [V \sin \alpha - V_c]^2 / 2 \epsilon \quad (7)$$

$$M_C = m [V^2 \cos^2 \alpha] / 2 \beta \quad (8)$$

As the role of V_c in removing the material is negligible, this term is neglected. Thus, the equation (7) becomes

$$M_D = m [V^2 \sin^2 \alpha] / 2 \epsilon \quad (9)$$

By adding the mass of material removed by deformation wear and cutting wear mode, the total mass of material removed is obtained as

$$M = m V^2 [(\sin^2 \alpha) / 2 \epsilon + (\cos^2 \alpha) / 2 \beta] \quad (10)$$

In Figure 1, the trajectory of jet is represented as an arbitrary curve ABC. Bitter's theory predicts the mass of material removed by the jet as it moves from A to C as

$$M_{AC} = m V_o^2 [(\sin^2 \alpha_o) / 2 \epsilon + (\cos^2 \alpha_o) / 2 \beta] \quad (11)$$

At any arbitrary point B on the trajectory at any depth y , the velocity and angle of impact with the horizontal can be represented as V_y and θ . From Bitter's theory, the mass of material removed by the jet when it moves from B to C is given by

$$M_{BC} = m V_y^2 [(\sin^2 \theta) / 2 \epsilon + (\cos^2 \theta) / 2 \beta] \quad (12)$$

From the above, the material removed by the jet while penetrating to a depth y from A to B is determined as

$$M_{AB} = M_{AC} - M_{BC}$$

$$M_{AB} = m V_o^2 [(\sin^2 \alpha_o) / 2 \epsilon + (\cos^2 \alpha_o) / 2 \beta] - m V_y^2 [(\sin^2 \theta) / 2 \epsilon + (\cos^2 \theta) / 2 \beta] \quad (13)$$

By substituting y^1 for $\tan \alpha$ and rearranging the terms

$$M_{AB} = m V_o^2 (y_o'^2 / \epsilon + 1 / \beta) / [2 (1 + y_o'^2)] - m V_y^2 (y'^2 / \epsilon + 1 / \beta) / [2 (1 + y'^2)] \quad (13)$$

But the mass of material removed can also be determined from

$$M_{AB} = (\text{density of material}) * (\text{cross section of the jet}) * (\text{arc length of AB})$$

$$M_{AB} = (\rho_m) (\pi (d_j^2 / 4)) \int_0^x (\sqrt{ 1 + y'^2 }) dx \quad (14)$$

By substituting M_{AB} in the equation (13) and differentiating both the sides with respect to x , the equation transforms to

$$\rho_m \pi (d_j^2 / 4) \sqrt{ 1 + y'^2 } = - m [y' y'' (a y^2 + b y + c)^2 / (1 + y'^2) + (y'^2 / \epsilon + 1 / \beta) \{ (1 + y'^2) (a y^2 + b y + c) (2 a y + b) - y y' (a y^2 + b y + c)^2 \} / (1 + y'^2)^2] \quad (15)$$

This particular differential equation is solved by means of second order Rungae-Kutta-Nystrom iteration method.

2.2 Numerical Simulation of Cutting Front

Figure 2 shows the abrasive particles in the jet striking the surface at an angle, ranging between $(90-\phi)$ and $(90+\phi)$. For a jet diameter of d_j and stand off distance of h ,

$$\phi = \arctan (d_j / 2h)$$

In order to generate the cutting front by numerical simulation, it is assumed that the abrasive particles striking the surface beyond an angle of 90° tend to get oriented towards the trajectory of jet produced already. This assumption is made based on the observation that the jet deflects in the direction of the least resistance path i.e. region where the material is already removed (Hashish, 1988). Thus, the cutting front is simulated by considering the jet striking the surface with impact angles ranging between $(90-\phi)$ and 90 . While generating the cutting front, it is further assumed that several abrasive particles in the jet can be considered as a single ballistic particle striking the surface with the above range of impact angles.

For generating the cutting front by numerical simulation, the jet is assumed to impinge on the surface at equidistant points with initial impact angles between $(90-\phi)$ and 90 and the penetration at these points i.e. jet trajectories are superimposed. The distance between these points is chosen based on the jet traverse rate. Figure 6 shows the cutting front profile generated with different trajectories of jet that are produced when the jet strikes the surface of the work piece with different initial impact angles. The initial orientation of jet is obtained by randomly generating the impact angles between $(90-\phi)$ and 90 .

The geometry of cutting front at any instant is the outer envelope of the trajectory generated till that point. This can be seen as the curve T2-P-T1 in Figure 3.

2.3 Generation of Surface Topography

The cutting front generated, using the procedure outlined in the above section, is in turn used to generate the surface topography. In AWJ cutting, some abrasive particles directly contribute to the material removal and some striking the walls of cut surface contribute to the generation of surface irregularities. For generating the surface topography in different regions of the cut surface, the instantaneous penetration of jet is considered and is assumed to be a circle moving along the trajectory. Figure 4 is a schematic representation showing the instantaneous penetration of jet at different instants along the direction of cut in a particular region. As seen in this figure, the magnitude of overlap of jet is different in different regions. This is more or less uniform in the upper region compared to other regions of cut. When this overlap is more, the interaction of the jet with the material in that region is more. By assuming the instantaneous interaction of jet to be due to a large number of abrasive particles striking the walls of the cut surface with random velocities and random orientations, the jet produces irregularities on the surface. It is expected that these irregularities increase with increasing interaction of the jet with

material i.e. increased overlap at any region of cut. In order to predict this irregularity at any point, the irregularity caused by each particle is found. To obtain the irregularity caused by each particle striking the walls of cut surface at a particular velocity with a particular orientation, the entire material removed during the penetration of jet is considered. If there are n number of abrasive particles that strike the walls for every instantaneous penetration of the jet, the average irregularity caused by these abrasive particles is given by (n depends on the size of abrasive particle and the diameter of the jet)

$$\chi_a = \text{Vol}_m / (n_a A_a) \quad (16)$$

where Vol_m is the material removed by the jet in a cycle and is estimated as

$$\text{Vol}_m = \pi d_j^2 / 4 \int_0^h \sqrt{1 + 1/y^2} dy \quad (17)$$

n_a is given by

$$n_a = (t_j m_f) / (\rho_a \text{Vol}_a)$$

As the irregularity given by the equation (16) is the average irregularity, the irregularities produced due to different abrasive particles are generated using a random generation procedure. Since the abrasive particles are random in nature, this procedure generates irregularities assuming a gaussian distribution with mean as χ_a and standard deviation as 1. To generate the surface topography at any depth, the irregularities produced due to the abrasive particles in a given region are superimposed.

The surface topography generated, using the above procedure, is the instantaneous surface topography generated. It assumes that the abrasive particles in the jet are steady state in nature i.e. the orientation and velocity of the abrasive particles coming out of the nozzle do not change with time. However this does not happen in reality. To account for the stochastic nature of the process, a number of instantaneous surface profiles generated for a given depth are superimposed to get the effective surface profile. This is analogous to the simulation of grinding process wherein a number of section profiles are superimposed to generate the effective surface profile.

3. RESULTS AND DISCUSSION

The model proposed in this work, is validated by comparing the computed results with experimental results. The proposed methodology, generates the surface topography from the cutting front, which, in turn, is simulated from the trajectory of jet. To determine the trajectory of jet employing the proposed method, it is necessary to determine the value of the constant K from experiments. For this purpose, experiments were conducted on black granite by employing a jet pressure of 200 MPa, abrasive flow rate of 0.05 kg/min and jet traverse rate of 30 mm/min. The density and flexural strength of black granite are 2500 kg/m³ and 60.5 MPa respectively. Abrasives with mesh size of 80 and density of 3850 kg/m³ were used. The jet diameter and the stand off distance used were 0.8 mm and 3 mm respectively.

From the experiments, the maximum depth of cut was found to be 36.97 mm. For this situation, critical velocity and input velocity of the jet were estimated as 157.3 m/s and 463.7 m/s respectively. The value of K , using the equation (3), is obtained as 495.96. This particular value was used to generate the trajectories of jet. Figure 5 shows the jet trajectory generated for different initial impact angles of jet in the material.

For the jet diameter and stand off distance chosen, the initial angles of impact were estimated to range between 84 and 90 degrees. Figure 6 presents the cutting front generated using the procedure outlined for numerical simulation of cutting front. It can be seen that the trajectories in the cutting front profile intersect with each other. In fact, the progressive cutting front geometry is the outer envelope of all the trajectories generated till that point. Due to the intersection of these trajectories, the cutting front geometry has shown a sudden change in the slope, which can be observed as a step. This confirms the observations made by Hashish in his visualization experiments (Hashish, 1988). The step formation is attributed to random nature of the abrasive particles striking the material. If the abrasive particles were distributed uniformly and had the same velocity and orientation, the trajectories will be parallel to each other and no step will be formed.

From this simulated cutting front, the surface topography is predicted by means of generating the instantaneous and the effective surface profiles at various depths. Figure 7 shows the instantaneous surface profiles generated at different depths. From this, it can be noticed that the profile changes from random to periodic with increasing depth. This periodicity in the bottom region almost resembles the periodicity generally observed with striations on the cut surface. This trend was observed on the cut surface produced by AWJ cutting. Figure 8 shows the effective surface profiles generated by superimposing several instantaneous surface profiles. Using these effective surface profiles, the width of cut was estimated to be 2.1mm which is in good agreement with the experimentally determined kerf width of 2mm. Table 1 presents the average surface roughness (R_a) values at different depths estimated by using effective surface profiles and the experimentally determined R_a values. These results confirm the capability of the proposed model in predicting the surface topography.

4. CONCLUSIONS

The model proposed to predict the AWJ surface topography is based on the model for predicting the trajectory of jet and the cutting front simulated using the trajectory of jet. By means of the theory of ballistics for predicting the velocity of jet in the material, Bitter's theory of erosion for material removal and the random nature of abrasive particles striking the material, the trajectory of jet predicted was seen to be different in different regions. This is found to be responsible for step formation and striation formation on the cut surface, which are also observed from the numerical simulation of cutting front and the surface profiles generated. Surface topography, generated by impact of abrasive particles on the walls of cut surface, produced the surface topography that is similar to the cut surface topography obtained from experiments. However, the exact topography of AWJ cut surface is generated by assuming the superimposition of several instantaneous profiles. This is analogous to the grinding process where several section profiles contribute to the finish on the work surface. The results computed with this model have

confirmed the experimental results in terms of surface roughness and kerf width. Future work focuses on detailed investigations to examine the influence of several process parameters in generating the AWJ cut surface topography.

5. ACKNOWLEDGMENTS

The authors wish to acknowledge the participation of Mr. G. Baskar in technical discussions during the initial phases of work.

6. REFERENCES

- Bitter, J. G. A., "A study of erosion phenomena," Part 1, *Wear*, Vol.6, pp. 5-21, 1963.
- Bitter, J. G. A., "A study of erosion phenomena," Part 2, *Wear*, Vol.6, pp. 169-190, 1963.
- Blickwedel, H., Guo, N. S., Haferkamp, H. and Louis, H., "Prediction of Abrasive Jet Cutting Performance and Quality," *Proceedings of the 10th International Symposium on Jet Cutting Technology*, pp. 163-179, BHRA, Amsterdam, Holland, 1990.
- Fukunishi, Y., Kobayashi, R., and Uchida, K., "Numerical Simulation of Striation Formation on Water Jet Cutting Surface," *Proceedings of the 8th American Water jet Conference*, pp. 657- 670, Houston, Texas, 1995.
- Guo, N. S., Louis, H. and Meier, G., "Surface Structure and Kerf Geometry in Abrasive Water Jet Cutting: Formation and Optimization," *Proceedings of 7th American Water Jet Conference*, pp. 115-133, Amsterdam, Holland, 1992.
- Hashish, M., "A Modeling Study of Metal Cutting With Abrasive Water Jets," *ASME Journal of Engineering and Technology*, Vol.106, No1, pp. 88-10, 1984.
- Hashish, M., "Visualization of the Abrasive Water Jet Cutting Process," *Experimental Mechanics*, Vol.28, pp. 159-169, 1988.
- Hashish, M., "A Model for Abrasive-Waterjet (AWJ) Machining," *ASME Journal of Engineering Materials and Technology*, Vol.111, pp. 154-162, 1989.
- Hashish, M., "On the Modeling of Surface Waviness Produced by Abrasive-Waterjets," *Proceedings of 11th International Symposium on Jet cutting Technology*, pp. 17-34, BHRA, St Andrews, Scotland, 1992.
- Kovacevic, R., "Surface Texture in Abrasive Water Jet Cutting," *Journal of Manufacturing Systems*, Vol.10, pp. 32-40, 1991.

- Momber, A. W., "A Generalized Abrasive Water Jet Cutting model," *Proceedings of 8th American Water Jet Conference*, pp. 359-376, Houston, Texas, 1995.
- Momber, A.W. and Kovacevic, R., "Principles of Abrasive Water Jet Machining," Springer Verlag, London, 1998.
- Sawamura, T., Fukunishi, Y. and Kobayashi, R., "Three Dimensional Model for Water Jet Cutting Simulation," *Proceedings of 9th American Water Jet Conference*, Vol.1, pp. 15-28, Dearborn, Michigan, 1997.
- Srivathsa, B. and Ramakrishnan, N., "A Ballistic Performance Index for Thick Metal Armour," *Computer Modeling and Simulation in Engineering*, Vol.3, No.1, pp. 33-40, 1998.
- Vijay Krishna, M. and Ramesh Babu, N., "A Model for Prediction of Striation Free Depth in Abrasive Water Jet Cutting," *Proceedings of 1st National Conference on Precision Engineering*, pp. 211-221, Indian Institute of Technology Madras, Chennai, 2000.
- Zeng, J. and Kim, T. J., "Development of Abrasive Water Jet Kerf Cutting Model for Brittle Materials," *Proceedings of 10th International Conference on Jet cutting Technology*, pp.115-133, Amsterdam, Holland, 1992.

7. NOMENCLATURE

A_a	area of cross section of an abrasive particle (m^2)
d_j	jet diameter (m)
h	stand off distance (m)
h_{max}	maximum depth of cut (m)
K	material and process constant
m	mass of abrasive particles
m_f	abrasive mass flow rate (kg/s)
M_C	mass of material removed by cutting wear mode (kg)
M_D	mass of material removed by deformation wear mode (kg)
n_a	number of abrasive particles striking the work piece in the dwell time
P	jet pressure (Pa)
t_j	jet dwell time (s)
V	velocity of any particle (m/s)
V_c	critical velocity of jet (m/s)
V_o	initial velocity of jet (m/s)
V_y	velocity of jet at a depth y (m/s)
Vol_a	volume of an abrasive particle (m^3)
Vol_m	volume of material removed by the jet in one cycle (m^3)
x	distance moved the jet along the traverse direction (m)
y	depth of penetration measured from the top surface (m)
y'	derivative (slope) of the trajectory at a depth y

σ	flexural strength of material (N/m^2)
ρ_a	density of the abrasives (kg/m^3)
ρ_m	density of the material (kg/m^3)
α	angle made by abrasive particle with horizontal (radians)
α_o	initial angle of the jet with horizontal (radians)
θ	angle made by the jet with horizontal at any depth y (radians)
ε	deformation wear constant
β	cutting wear constant
γ	momentum transfer efficiency
χ_a	irregularity created by an abrasive particle (m)
ϕ	maximum angle of impact of an abrasive particle with vertical (radians)

8. TABLES

Table 1. Computational and experimental R_a values at various depths

Depth (mm)	5	10	15	20
Computational R_a (Microns)	18.15	20.68	28.02	34.96
Experimental R_a (Microns)	15.46	17.28	23.2	28.6

9. FIGURES

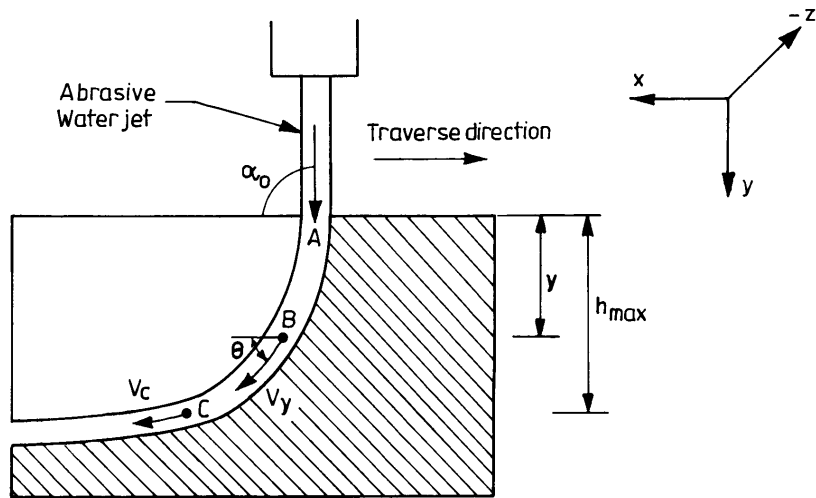


Figure 1. Schematic representation of the trajectory of jet in the material

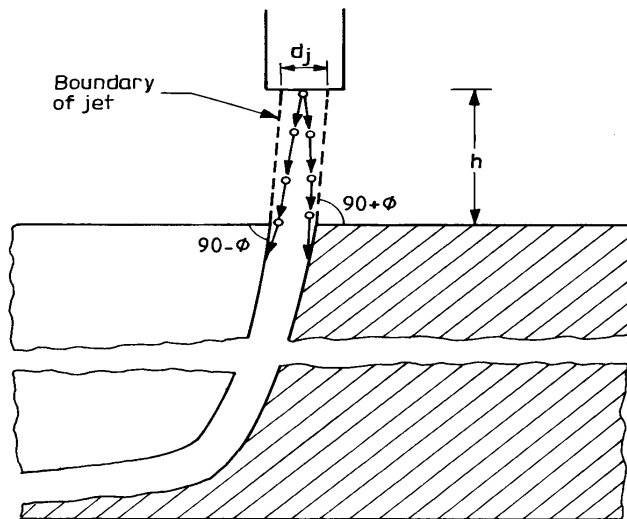


Figure 2. Schematic diagram showing the impact of jet on the material

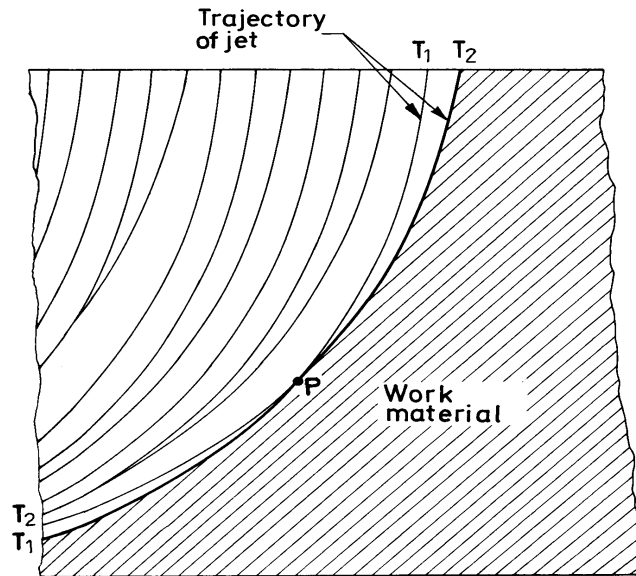


Figure 3. Geometry of cutting front at a particular instant showing the step formation

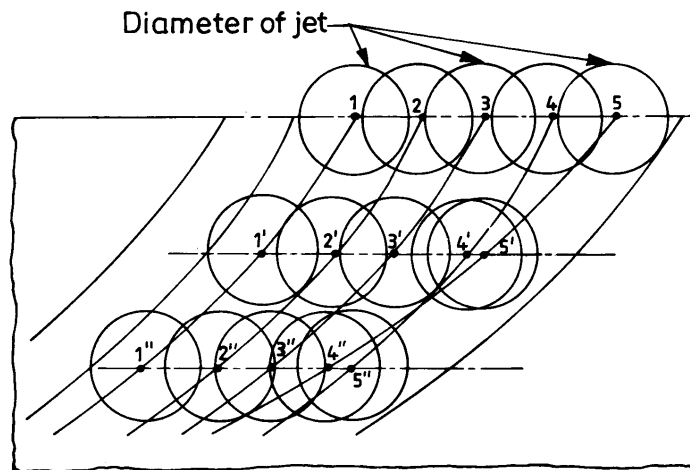


Figure 4. Schematic diagram showing the generation of surface topography in different regions of cut surface by the interaction of jet with the walls of cut surface

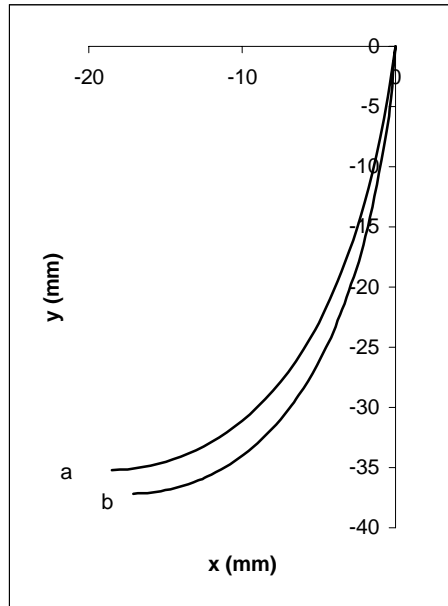


Figure 5. Trajectory of jet predicted inside the material for different initial angles of impact (a) 84° (b) 88°

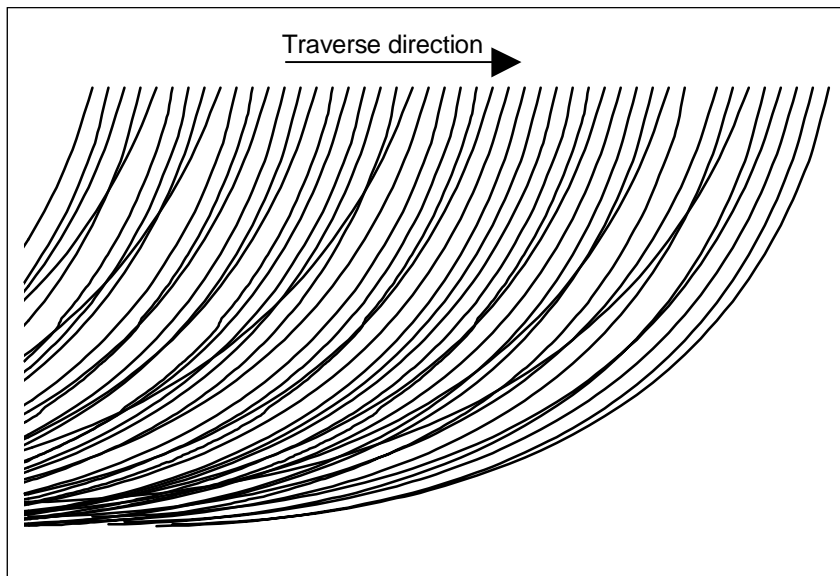


Figure 6. Numerically simulated cutting front

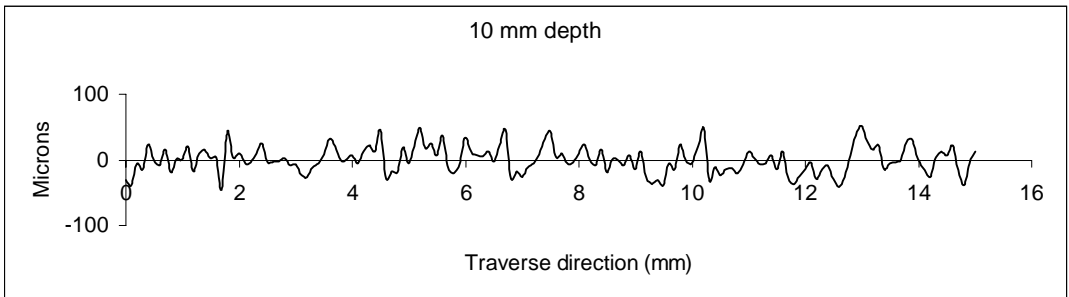
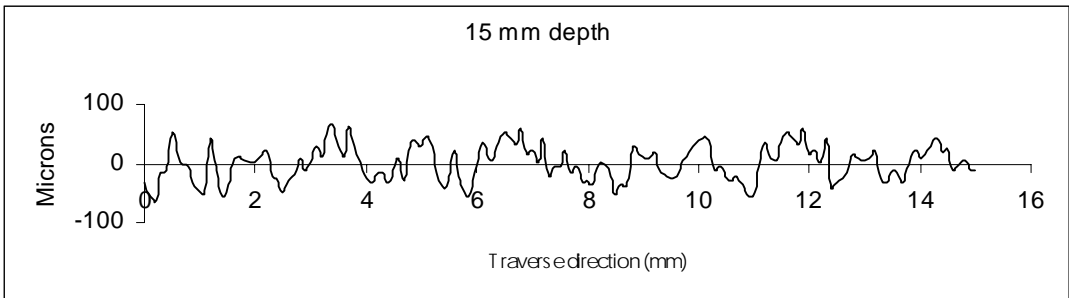
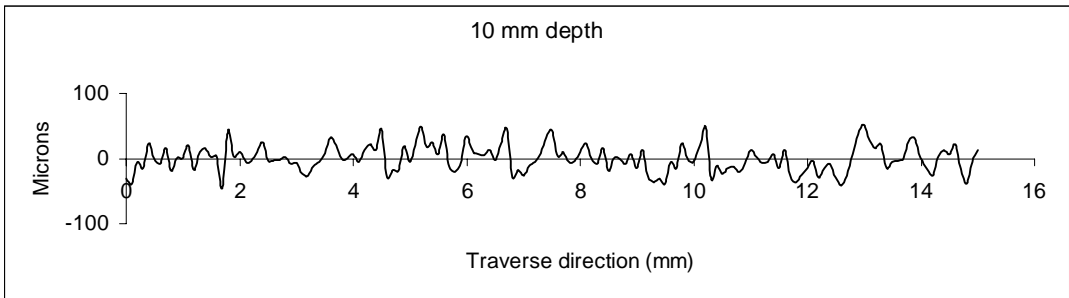
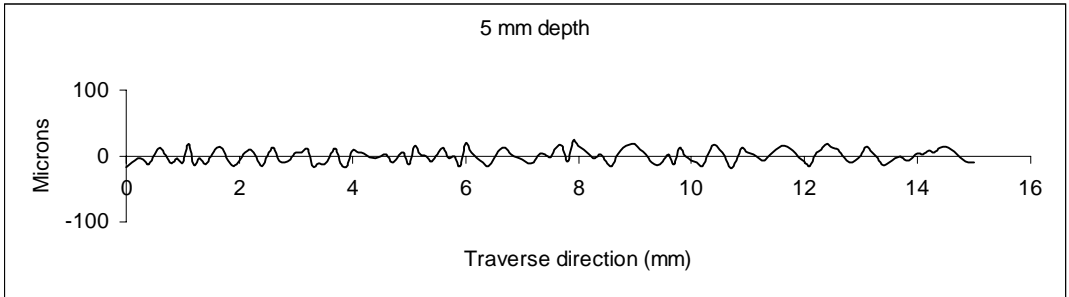


Figure 7. Instantaneous surface profile generated at various depths on the cut surface

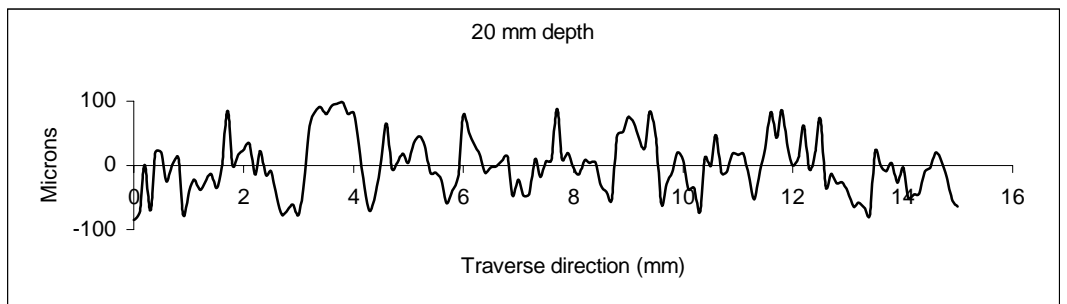
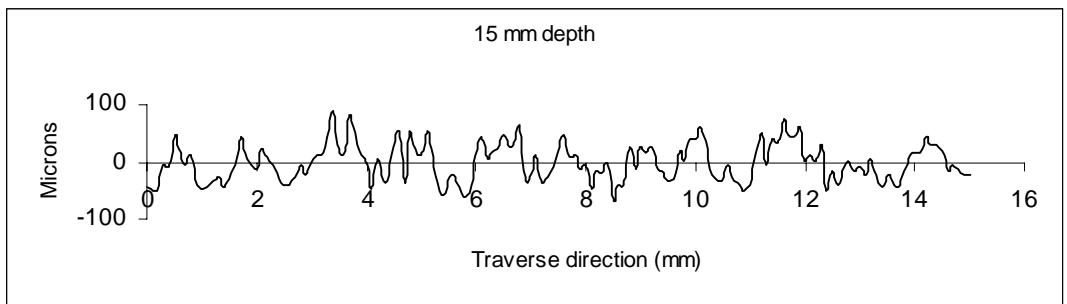
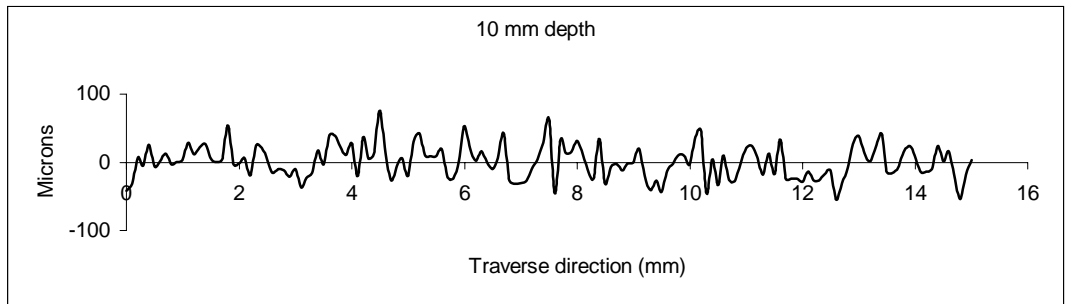
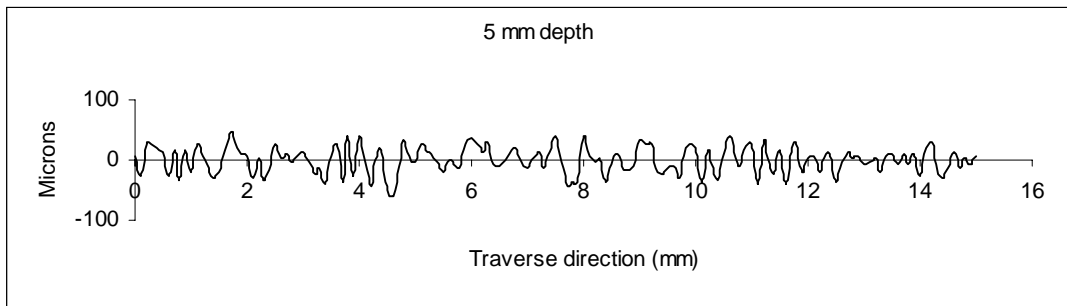


Figure 8. Effective surface profile generated at various depths on the cut surface

INFLUENCES ON STRUCTURE FORMATION AT THE CUTTING EDGE WITH ABRASIVE WATERJETS

A. Henning, E. Westkämper
Fraunhofer Institute for Production Engineering and Automation
Stuttgart, Germany

R. Friedrich, T. Ditzinger, T. Kübler
Institute for Theoretical Physics III
University of Stuttgart, Germany

G. Radons
Institute for Physics
Technical University Chemnitz, Germany

ABSTRACT

Abrasive waterjets have become a most recent tool in mechanical machining. With its great advantages the technology is spreading more and more among industry. Thorough understanding of the relevant processes is essential for achieving the demanded high quality output. With the approach of nonlinear modeling a new sight on the very influences of the process could be gained. In this paper new approaches to modifying the typical structures at the cutting edge utilizing external periodic forces are presented. Suitable process models could so deliver new approaches to improving both quality and performance of the machining outcome.

1. INTRODUCTION

New developments in industry as well as new materials set high requirements for machining processes. With conventional processes these innovative materials are often difficult to machine due to high sensitivity regarding mechanical and thermal stress or to specific material properties. To meet these specific requirements, new machining technologies are necessary. Here abrasive waterjets have become a most recent tool in mechanical machining. Due to its geometrical and material flexibility and its ability of cutting hard-to-machine materials, this technology is spreading more and more for two and three dimensional cutting applications. Applications of waterjet technology can be found in many different fields like the automotive or aerospace industry or for the generation of prototypes (Henning, 1997).

In this paper a new approach to process modeling is presented. With the usage of nonlinear dynamic models influences on the cutting process could be identified that could not be pictured in former models.

2. NONLINEAR PROCESS MODELING APPROACHES

For optimal utilization the understanding of the basic processes that are involved in machining is essential. In Westkämper et.al. (2000) it was shown that the primary impact on the cutting kerf can be well approximated by a gaussian bell function. A first attempt to model the evolution of the kerf formed by the primary impact could simply assume that the gain of depth is proportional to the particle distribution $J(x,y)$. The temporal change of S is the volume removal rate

$$\frac{\partial S(\mathbf{r},t)}{\partial t} = J(\mathbf{r}) \cdot F - u \frac{\partial S(\mathbf{r},t)}{\partial x} \quad (1)$$

This partial differential equation (PDE) models the evolution of the kerf in a workpiece that is moved below the jet in x-direction with feed rate u . The effect of the jet is amplified by F which is constant in this linear approach. This approach leads to a solution $S(r,t)$ which tends to a stationary kerf geometry as it is shown in Figure 1a. The particles flow continuously after the first impact along the cutting front. Secondary impacts most likely have no visible effect and do not change the stationary motion of the cutting front.

Yet in reality non-stationary processes are observed. In phenomenal studies (e.g. Hashish, 1988) it was shown that the cutting process shows cyclic behavior with step formation (Figure 1b). At the steps the particles take off from the cutting front, so that with a shadowing effect on the left/bottom side of the step and an amplified volume removal at the top the step propagates along the cutting front. In Figure 1c the formation of grooves that are formed at the bottom of the kerf is sketched. The particles are focussed into the groove. This groove grows until the next process cycle starts by forming the next step at the top of the cutting front.

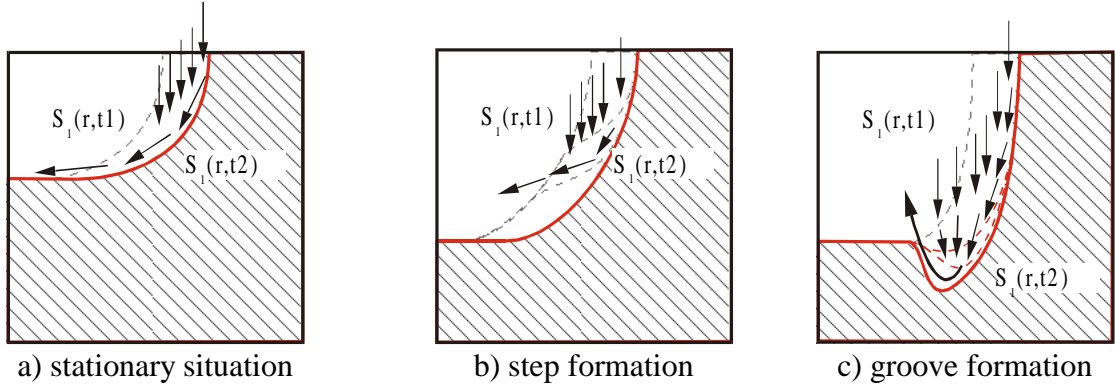


Figure 1: Particle movement at different situations of the cutting front

The fact that modeling on the basis of a first order PDE cannot explain instabilities and therefore pattern formation has been recognized already by Finnie and Habi (1965) in a similar context. In that work it is also argued that higher order derivatives have to be included. From the experimental and also from the theoretical side not much is known about e.g. curvature dependent properties of cutting or wear processes.

In Friedrich (2000) the volume removal rate of the first impact of the jet parallel to the tool axis is assumed not to be proportional to $J(r)$. The factor F is replaced with a function $F = F(|\nabla S(\mathbf{r},t)|, \Delta S(\mathbf{r},t), \Delta^2 S(\mathbf{r},t), \dots)$ which represents the dependence on the impact angle $|\nabla S|$, the curvature of the probe ΔS and higher order spatial derivatives ($\Delta^2 S, \dots$). The resulting equation (2) is of Kuramoto-Sivashinsky type, which was first introduced to characterize e.g. moving flame fronts. In this approach the occurrence of instable modes is possible (Ditzinger, 1999).

$$\frac{\partial S(\mathbf{r},t)}{\partial t} = J(\mathbf{r}) \cdot \left[\frac{1}{1 + (\nabla S(\mathbf{r},t))^2} + \alpha \Delta S(\mathbf{r},t) + \beta \Delta^2 S(\mathbf{r},t) \right] - u \frac{\partial S(\mathbf{r},t)}{\partial x} \quad (2)$$

With this equation the development of the cutting front was simulated at four different feed rates. The results are shown in Figure 2. At high feed rates $u > u_c$ a stable stationary front is established near the jet for large times. For smaller u the cutting front shows a very different behavior although only the feed rate was reduced. A periodic growth of ripples in the jet region can be found, which asymptotically leads to a left travelling wave behind the jet. In the laboratory frame, i.e. on the workpiece, this corresponds with a spatially periodic structure formed by the primary impact zone. These instabilities may be considered a initial condition for step- and structure formation within the cutting process.

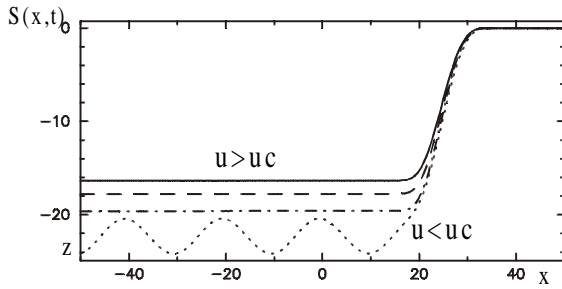


Figure 2: Cutting front $S(x,t)$ simulated at different feed rates u

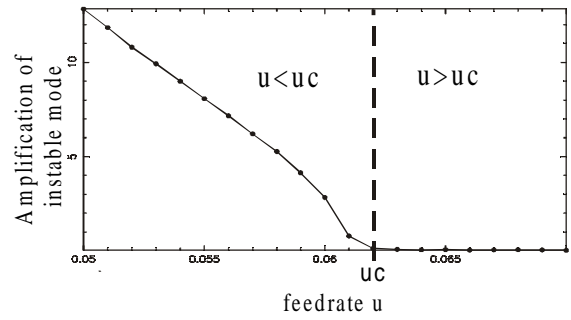


Figure 3: Amplitude of the spatio-temporal modulation as a function of feed rate showing a Hopf-Bifurcation

From the simulation plots the amplitude of the possibly generated structures can also be read off. The results of a systematic investigation of the dependence of the oscillation amplitudes on the feed rate u are shown in Figure 3. It can be observed that the traveling wave solution bifurcates from the stable stationary front solution. The occurrence of the bifurcation has been validated by a linear stability analysis of the stationary front solution (Friedrich, 2000b) which shows that as for a Hopf bifurcation a conjugate complex pair of eigenvalues crosses the imaginary axis. This stabilizing influence of high feed rates is also known from experiments in the field of waterjet cutting (Friedrich, 2000).

3. IMPACT ZONE MODEL

In many modeling approaches the optical appearance of the cutting edge is used to describe up to five different process zones (e.g. Zeng and Kim, 1995). The relevant factor for differentiation in these cases is the quality of the cut surface (smooth-transient-rough etc.). To gain better understanding of the process here a the impacting situation of the particles in the process zone is differentiated (Henning, 2000). In this "Impact Zone Model" two different zones of impact situation are described: Primary and secondary impact zone. The differentiation between those zones is the impacting situation of the very particles. This gives important information for new modeling approaches, because the different impact situations are differentiated.

In the "Primary Impact Zone" the particle impacts on the material for the first time. Being accelerated in the focussing tube the particles achieve a high velocity (up to 400m/s) and thus high kinetic energy. The particles all hit the probe from above parallel to the z -axis (Figure 8).

At the event of impact the particles transfer a portion of their energy to the material, causing material removal or material fracture and reflect from the impact location. Depending on the reflection direction and the left energy, the particles can have consecutive impacts on the material and cause more material removal. This "Secondary Impact Zone" is formed by consecutive impacts of the particles. Here the particles hit the material several times within the cutting front. Depending on the choice of parameters lateral structure formation can also occur here (Guo, 1994).

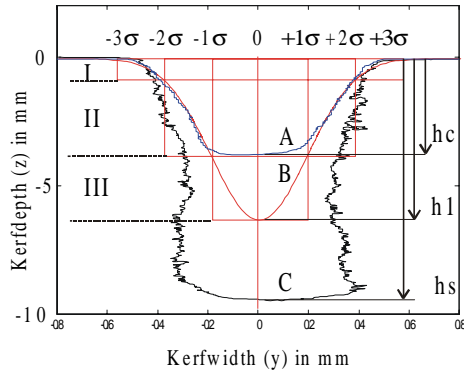


Figure 4: Profiles of cutting and kerfing

- A:** measured profile of kerf
- B:** calculated profile of kerf
- C:** measured profile of cut

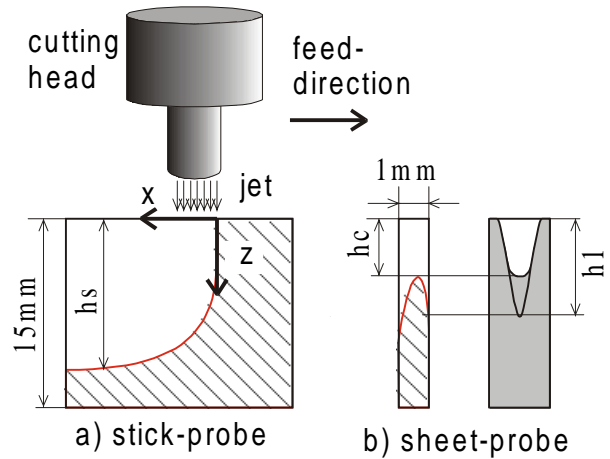


Figure 5: Experimental setup for differentiating the primary and secondary impact zone

In the theoretical approach that is described earlier in this paper a bifurcation effect was found. At a low cutting speed $u < u_c$ instabilities do develop in the primary kerf. To gain information about those active mechanisms an experimental setup was chosen, that could picture the different phases of the process independently (Figure 5). In normal cutting both phases do occur at the same time, though. So in cutting processes a differentiation of the two different processes is not possible. In the chosen setup of kerfing of very thin sheet metal probes the secondary impact phase could be avoided and information about the primary impact could be gained. The primary kerf (Figure 4- graph B) was compared with the profile of a normal cut (graph C).

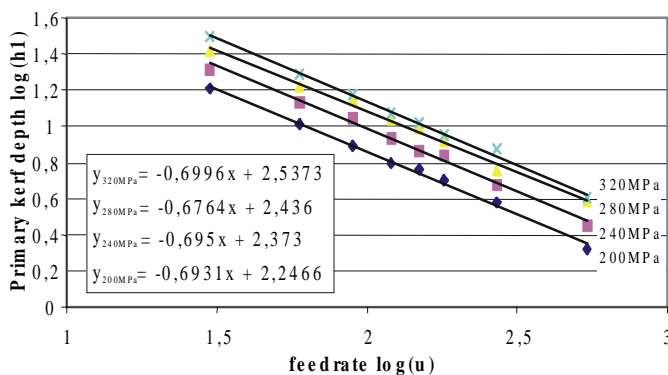


Figure 6: Depth of primary profile
($mp=400g/min$, $u=var.$, $p=var.$, $s=2mm$)

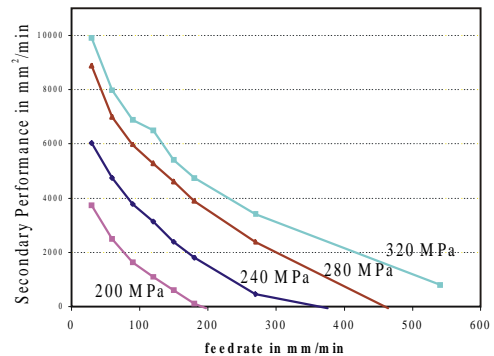


Figure 7: Secondary Performance
($P_2=(hs-hl)*u$) vs. feedrate at $s=2mm$

The depth of the primary profile h_1 showed clear dependence from the feed rate and the other parameters. In Figure 6 the depth of the primary profile is shown in double-logarithmic scale over the feed rate. A relationship of $h_1 \propto u^{-0.7}$ could be assumed from this setup for the depth of

the primary profile. The cutting performance $P_s = h_s \cdot u$ has been reported as being constant in literature (e.g. Zeng 1995, Hashish 1988) up to a lower limit of feed rate. This behavior could also be found in the experiment for the profile of the cut. According to the modeling approach the total cutting depth consists of the depth of the primary profile plus the depth of the effect. In Figure 9 the average cutting performance (P_s^*) is compared with the kerfing performance $P_1 = h_1 \cdot u$ of the primary impact profile. With this the portion of the effect of the primary and the secondary impact can be visualized. At low feed rate the secondary impact shows very dominant behavior. With increasing feed rate the proportion of the primary impact effect increases significantly up to even reaching to the cutting performance. The total cutting performance is therefore (with $h_s = h_1 + h_2$) $P_s = u \cdot (h_1 + h_2) = P_1 + P_2$ which leads to $P_2 = (h_s - h_1) \cdot u$ (Figure 9).

The effect of the secondary impact decreases with higher feed rates significantly. Also water pressure and standoff distance show high qualitative effects on the proportion of primary and secondary effects. The effect of the primary impact is higher at higher feed rate, lower water pressure and larger standoff distance. Especially the dependence from feed rate is very interesting. The higher the feed rate the smaller is the effect of the secondary impact zone. These effects that cannot be explained with linear approaches that have been used so far. As predicted in the theoretical approach also in practical experiments a certain critical feed rate u_c could be identified at which a change within the process may be detected. From the experiments it can be stated that for feed rates $u < u_c$ the effect of the secondary impact rises and becomes dominant for low feed rates (Henning, 2000).

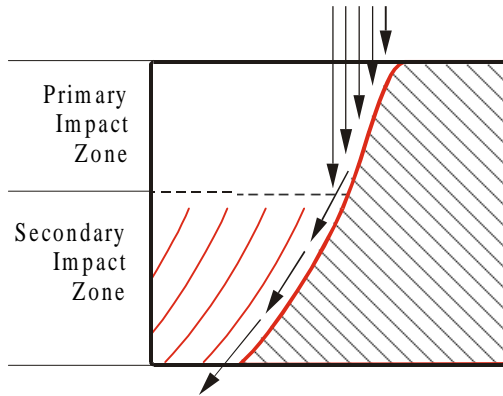


Figure 8: Particle movements in primary and secondary impact zone

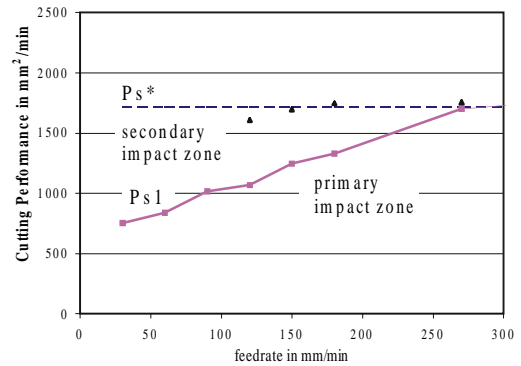


Figure 9: Cutting (P_s^*) and kerfing (P_1) performance ($s=2$, $p=240\text{Mpa}$, $mp=350\text{g/min}$)

There must be a mechanism that causes the secondary impacts to play the dominant role within the process. In comparison with the theoretical modeling which shows a bifurcation like behavior at a critical feed rate this could be the generation of instabilities that lead to the spatio-temporal behavior and thus to the creation of steps at the cutting front. Influences on these processes will be discussed in the next chapter.

4. FREQUENCY COUPLING

In conventional approaches to modeling of the process of the abrasive waterjet many parameters and their effect on relevant factors like cutting depth were examined. The analysis of structure formation has so far not reached to a point of understanding the relevant mechanisms. Many influences on the unwanted ripple formation have been stated in more qualitative than quantitative approaches. The frequency of the plunger oscillation in the intensifier has also been taken into consideration. So far it could not be identified as a relevant factor, though (e.g. Guo, 1994).

In the theoretical approach with the PDE of Kuramoto-Shivashinsky type (eq.2) external periodic modulations are known to have significant influence on process outcome. Here the relationship Q between the external modulation ω_p and the intrinsic frequency of the process ω_0 plays the important role:

$$Q = \omega_p / \omega_0 = \lambda_0 / \lambda_p \quad (3)$$

In the analysis of the parameter situation within a normal conventional cutting process it could be found that with $\omega_0 = 2\pi \cdot f_0 = 2\pi \frac{u}{\lambda_0}$, $\omega_p = 2\pi \cdot f_p$, and $\lambda_0 = \text{const}$ the quotient develops to:

$$Q = \omega_p / \omega_0 = \frac{f_p \cdot \lambda_0}{u} \quad (4)$$

That means that Q rises with higher pumping frequency and lower feed rate. With the pumping frequency being proportional to the water mass flow ($f_p \propto \dot{m}_w$), and the hydraulic power being $P_{hydr} = p \cdot \dot{m}_w$ (p : water pressure) which is proportional to the cutting performance ($P_{hydr} \propto P_s = k_{MAX} \cdot u$) with k_{MAX} being the maximum cutting depth at a specific cutting condition one can state:

$$Q \propto \frac{k_{max} \cdot \lambda_0}{p} \quad (5)$$

That means that at all conventional cutting experiments that have been carried out with the same high pressure intensifier at different cutting parameters the relationship between pumping frequency and the intrinsic process frequency remained the same. The relationship between the pumping frequency and the intrinsic process frequency at structure formation does only depend on the maximum cutting depth, which again does depend on material properties and cutting parameters. An influence of the Quotient Q could therefore not be observed at comparable cutting conditions before.

The goal of the experiment was to analyze the effect of Q at comparable cutting conditions. Therefore an experimental setup was chosen that can alter the frequency of the pump without changing any other cutting parameter. For this a second orifice is implemented as a bypass with

no effect on the cutting process. This orifice does not influence the cutting process but is only used to increase the volume flow at the pump and therefore the pumping frequency (e.g. probe 2025 stands for cutting orifice: 0,2mm, bypass orifice: 0.25mm). With this setup the quotient Q can be varied in a wide range at the same cutting conditions. So the influence of Q can be pictured clearly.

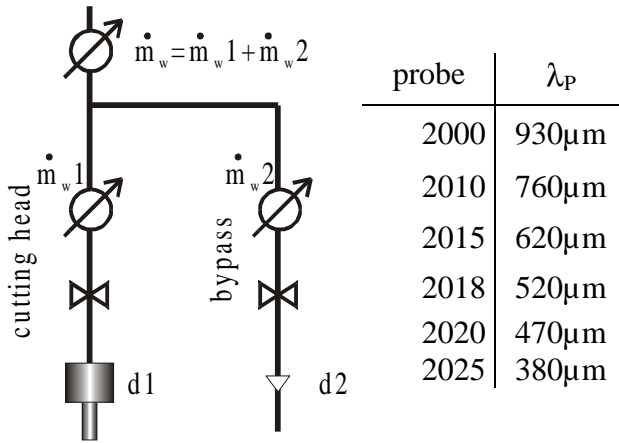


Figure 10: Experimental setup for modulation of pumping frequency

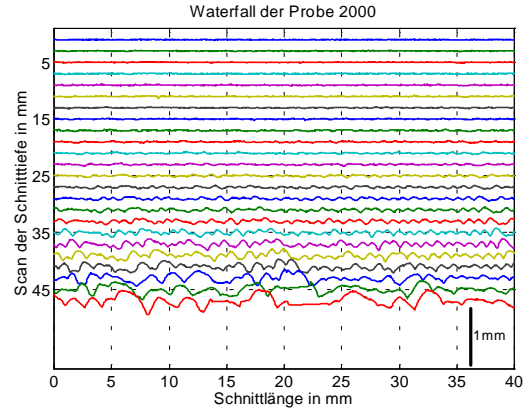


Figure 11: Scan data of cutting edge at different cutting depths (probe 2000)

The qualitative outcome of structures at the cutting edge did not change severely at different pumping frequencies and therefore different Q at the first sight. Also analysis with conventional Fourier methods for each scan gave no significant information as it has been previously reported e.g. by Guo (1994). In Figure 11 the probe 2000 with its scans at different cutting depths with a distance of $\Delta k = 2\text{mm}$ between them are shown. This data is considered raw data for the following evaluation and analysis.

A new methodology was chosen to analyze the qualitative appearance of ripple structures at the cutting edge. The auto-correlation coefficient is known to suppress white noise at time series in order to evaluate significant signals. In Figure 12 the auto-correlation coefficient is shown for six different probes. At every probe the cutting conditions remained the same ($d_o=200\mu\text{m}$, $p=300\text{Mpa}$, $u=19\text{mm/min}$). Only the pumping frequency was changed. The wavelength of the pumping frequency at the probe is shown as grid lines within the graphs. With this method very significant structures became visible. The dominant wavelength of ripples at the cutting edge λ_R was analyzed.

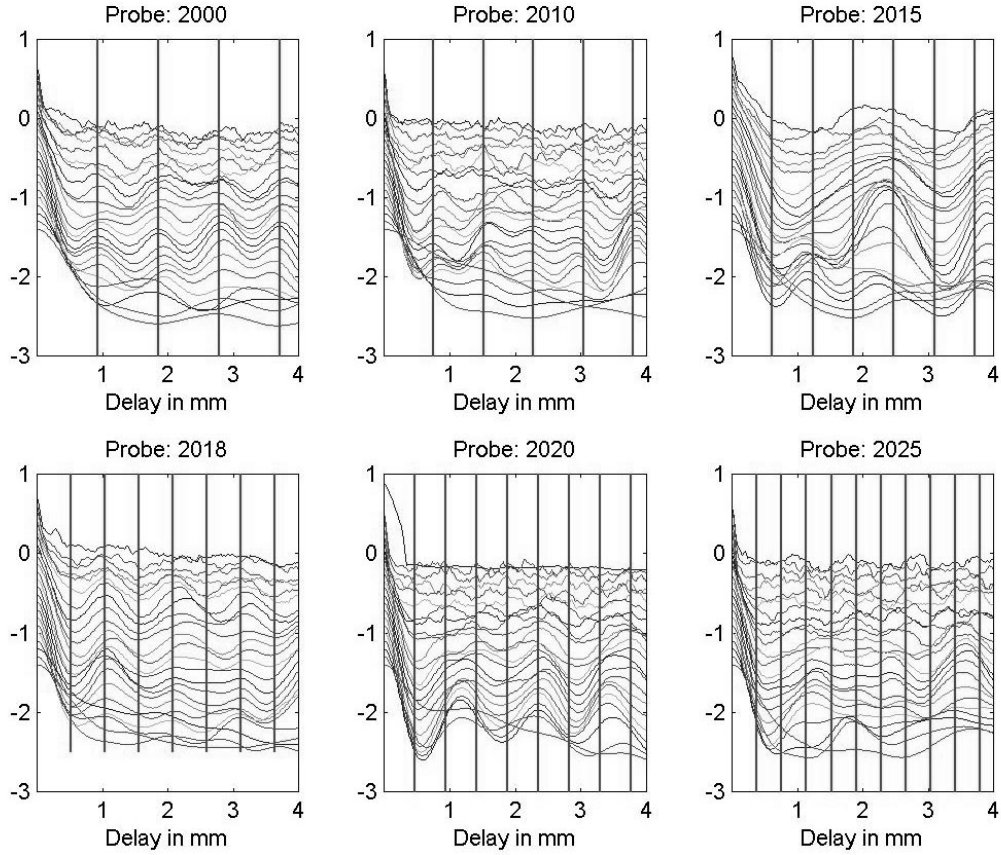


Figure 12: Auto-correlation coefficient of the cutting edge for different pumping frequencies vs. delay distance at different cutting depths (red lines indicate multiples of the pumping wavelength λ_p)

In the probe 2000 the pumping wavelength λ_p could be found as a dominant wavelength λ_R which leads to a coefficient $q = \lambda_R / \lambda_p = 1$. At probe 2010 similar structures can be found. They are not as dominant as in probe 2000, though. At probe 2018 dominant structures at approximately double pumping wavelength can be seen. At the other probes no single dominant wavelength can be identified by visual examination of the auto-correlation coefficient directly. Therefore the mean value of the dominant ripple wavelength λ_R was calculated for each scan of the whole probe. The wavelength of the significant structures was gained as a mean value of wavelength found in the auto-correlation coefficient (Figure 13 and Figure 14). In the upper part of the probe ($z < 20\text{mm}$) where no striation structures are formed as we know from experiments no significant value could be found. In the middle section the wavelength locks into a certain significant value up to a critical cutting depth. In Figure 14 the resulting wavelengths of the ripples at the cutting edge are divided by the pumping wavelength λ_p at the cutting edge and plotted versus cutting depth z . As can be clearly seen for small depths the coefficient $q = \lambda_R / \lambda_p$ increases continuously for all experiments until a critical depth is reached in the threshold region of $z < 20\text{mm}$, dependent from the experiment. For z -values above this threshold the phenomenon of nonlinear frequency locking occurs. As can be seen in Figure 14 the results for the different

pumping frequencies produce wavelengths λ_R which are multiples of the pumping wavelength. This means that sub-harmonic oscillations $\lambda_R = q \cdot \lambda_p$ with integer $q=1,2,3..$ occur. This is a typical property of nonlinear self-oscillatory systems with an external periodic force.

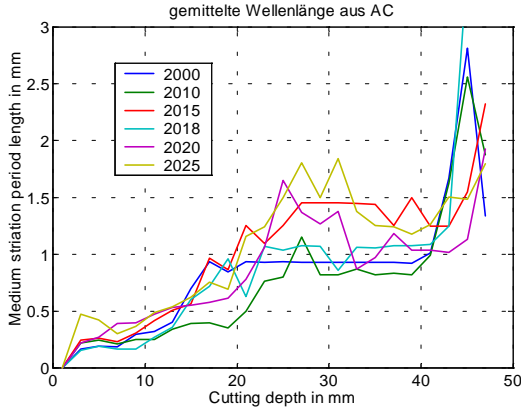


Figure 13: Mean dominant ripple wavelength λ_R vs. cutting depth

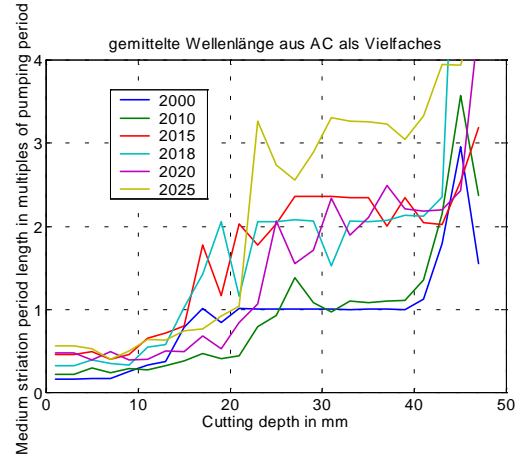


Figure 14: Mean dominant ripple wavelength in multiples of pumping wavelength ($q = \lambda_R / \lambda_p$)

In Figure 15 the significant dominant ripple wavelength λ_R is sketched vs. the wavelength of the pumping frequency. It appears to lock into rational values of q . This shows a behavior like it can be found at nonlinear phenomena known as “devils staircase” (Agyris, 1994).

At some probes the wavelength of the significant structure at the auto-correlation coefficient is not very clear and regular. So further analysis of the signals is necessary. The quotients can be examined as a function of depth in more detail by means of an additional Fourier-analysis of the auto-correlation functions of Figure 12, as it is done at probe 2015 in Figure 16. As can be seen in Figure 16 a detailed fine structure of the spectra becomes visible. As indicated by the vertical lines, the system oscillates- dependent from depth z - with different dominant wavelengths λ_R . At probe 2015 the information of the Fourier power spectrum is very significant. Two different significant peaks can be identified. The first one is at double pumping wavelength ($\lambda_R = 2 \cdot \lambda_p$) and the second is at $\lambda_R = 2mm$ which can be interpreted as double intrinsic frequency of the process ($\lambda_R = 2 \cdot \lambda_0$).

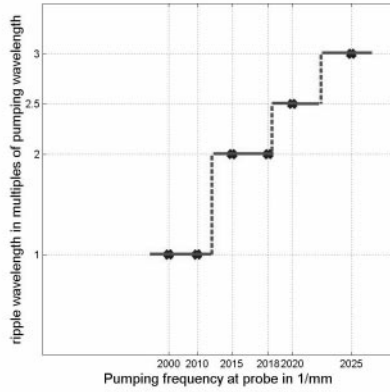


Figure 15: Significant ripple wavelength in multiples of pumping wavelength ($q = \lambda_R / \lambda_P$)

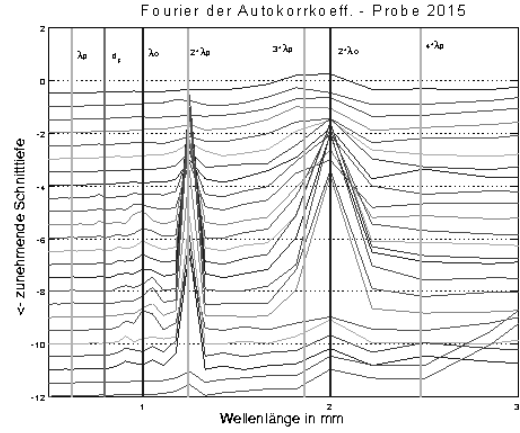


Figure 16: Fourier Powerspectrum of the Auto-correlation coefficient of probe 2015 for different cutting depths vs. wavelength

5. DESCRIPTION OF RIPPLE STRUCTURES

In industrial applications the formation of ripple structures at the cutting edge is the limiting factor for achievable cutting performance and cutting quality. Due to unregular structure formation the analysis of ripple appearance is very difficult with conventional methods (compare Figure 11). The method of calculating the auto- and cross-correlation coefficient suppresses white noise and identifies significant structures. In this approach the cross-correlation coefficient between each two neighboring scans at different cutting depths was calculated. In Figure 17 all cross-correlation coefficient for the probe 2020 are displayed and analyzed (maxima of the graph are marked with '+' minima are marked 'o'). The first maximum of the cross-correlation coefficient (first '+' on each graph in Figure 17) pictures the delay between significant structures (i.e. ripples) between those two scans. With this method the medium form of the ripples can be calculated. It appears (Figure 18) that until a specific cutting depth no significant spatial shift could be found, since in this area no significant ripple formation occurs. After a specific cutting depth k_C ripples occur. The spatial shift shows in all probes linear behavior after that point k_C (Figure 18). This linear behavior of the spatial shift graph leads when being integrated over the cutting depth to a second order parabolic form of the ripples. This also agrees with former studies at curved probes (e.g. Henning 1997,1998).

When analyzing the ripple depth at the probe in terms of standard deviation of the raw surface scan (Figure 11) it also could be found that above that specific cutting depth $z < k_C$ the standard deviation remains on a level that can be described as surface roughness (Figure 18). After that point the depth of the ripples increases in a parabolic manner. Therefore this specific point k_C can be described as being the starting point of ripple formation as a result of secondary impacts. The area above that point can be considered as being subject to primary impacts only.

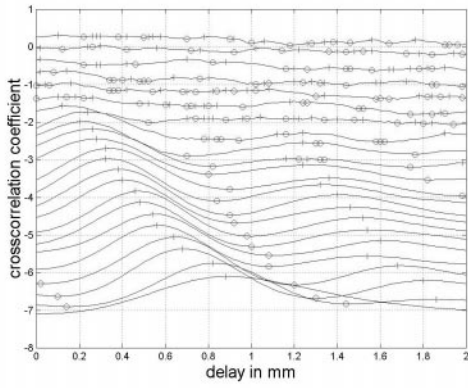


Figure 17: Cross-correlation coefficient between two consecutive scans at probe 2020

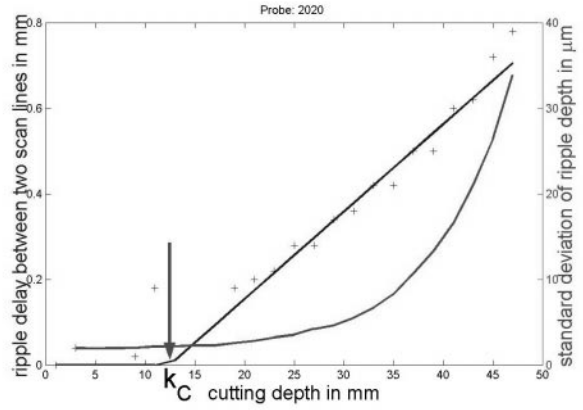


Figure 18: ripple spatial shift in mm and standard deviation in μm vs. cutting depth at probe 2020

6. GEOMETRICAL OSCILLATIONS

As a second external force on the structure formation process a geometrical oscillation was chosen. The normal jet position $x(t)$ at steady movement $x(t) = x(0) + u \cdot t$ was superimposed with a sinus-oscillation resulting in a jet position of

$$x(t) = x_0 + u \cdot t + A \cdot \sin(2\pi \cdot f_G \cdot t) \quad (1)$$

With this movement the average feed rate u and therefore the jet intensity (power per area unit) remains constant. Only the temporal intensity is periodically varied with the feed rate. The resulting geometrical wavelength is $\lambda_G = u / f_G$.

These experiments were carried out at same cutting conditions with variation of oscillation frequency and amplitude of oscillation. It appeared that the occurrence of structure formation (secondary ripples) could be influenced very well. Also frequency couplings at integer multiples between internal, pumping and oscillation frequencies could be found.

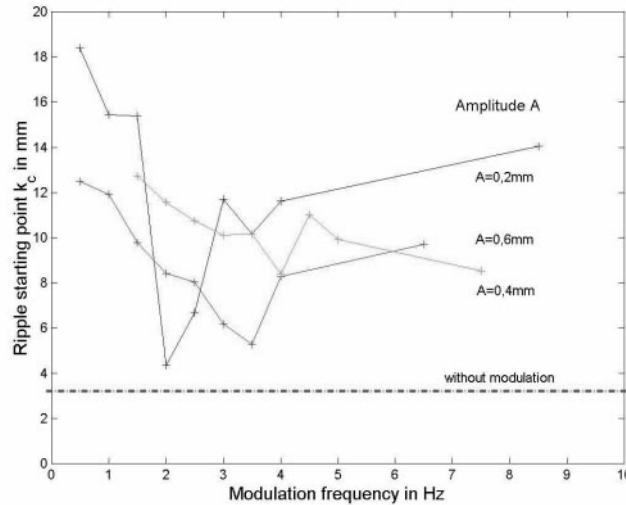


Figure 19: Ripple starting point k_c at different oscillation frequencies and amplitudes

In Figure 19 the starting point of secondary structure formation k_c (see chapter 5) is shown for different oscillation frequencies and at different amplitudes of oscillation. The starting point at the equivalent cut without modulation by geometric oscillation is displayed as a dash-dotted line in the graph. It appears that the zone without curved ripples can be influenced strongly with this kind of external force and a large scale jet lag can be avoided. Due to frequency locking phenomena in some probes straight ripples could be found even in the upper part of the probe. Also the depth of the secondary ripples was increased by using geometrical oscillations. Here further work is necessary in order to gain more understanding about the relevant processes and significant influences.

7. CONCLUSION

Structure formation at the cutting edge plays a vital role when evaluating the quality of a machining operation and often also serves a limiting factor for the cutting performance. In this paper a comprehensive approach to description, influences and theoretical background of structure formation is presented. Both theoretical modeling as well as experimental findings show that periodic external forces play a major role in the structure formation process. According to experiments at the cutting process primary and secondary impact zones can be differentiated. In the primary impacting zone the abrasive particles hit the workpiece in the process zone directly after being accelerated by the jet. After that primary impact the particles flow along the cutting front (secondary impact zone) forming curved ripples in the bottom part of the probe. According to experiment and numerical modeling the effect of this secondary impact zone is larger for low feed rates and most likely only occurs below a critical feed rate.

The Kuramoto-Shivashinsky kind of equation that describes the process is known to be sensible to external forces. Therefore different kinds of external forces were applied. In the first set of experiments the pumping frequency was varied without changing the cutting parameters. It ap-

peared that in the process of structure formation at the cutting edge at least two frequencies play a significant role. First of all an intrinsic “eigenfrequency” could be identified that most likely depends on process parameters (esp. diameter of the focussing tube). The ripple formation does strongly depend on the wavelength λ_0 of this eigenfrequency at the cutting edge. As it has been reported in many previous studies the ripple wavelength always remains in the same range around the “eigenwavelength”. In further analysis this variation was shown to be part of a non-linear oscillatory locking phenomena with the wavelength of the pumping frequency at the cutting edge. So as a second significant frequency for the process of structure formation the pumping frequency can be identified. If those two frequencies (or the multiples of them) are very close together the ripple frequency locks into an integer multitude of the pumping frequency. In between those integer multiples areas both frequencies can be seen (e.g. probe 2015) or even transient chaotic behavior may be observed. Also with geometrical modulation of the cutting process strong influences on the cutting process and especially on the formation of structures could be found. Here the starting point of curved ripple formation and thus the proportion between primary and secondary effects could be influenced in a large scale.

In this new experimental approach the influence of sub- and super-harmonic frequencies was observed. It can therefore be stated that as predicted in the theoretical approach the process is sensible to external periodic forces. These can be pressure fluctuations in form of pumping frequency or any other periodic influence. For industrial usage of these mechanisms the quantitative influences of the different parameters and oscillations has to be studied more thoroughly. With this work to introduce novel kinds of descriptions and understanding of the mechanisms of structure formation at the cutting edge new approaches to optimizing both quality and performance of abrasive waterjet cutting can be elaborated, qualifying this brilliant technique for even more innovative applications.

8. ACKNOWLEDGEMENTS

We gratefully acknowledge the support of the Volkswagen Foundation in this project, We thank T. Dunker for the valuable contributions to this project.

9. REFERENCES

- Agyris, J., Faust, G., Haase, M. (1994) "Die Erforschung des Chaos", Braunschweig, Vieweg Verlag, 1994.
- Ditzinger, T.; Friedrich, R.; Henning, A.; Radons, G. (1999): Non-Linear Dynamics in Modeling of Cutting Edge Geometry. In: Hashish, Mohamed (Hrsg.); *Proceedings of the 10th American Waterjet Conference* - Vol. I : August 14-17, 1999, Houston, USA, S. 15-32.
- Finnie, I. and Hail, Y.H. (1965) *Wear* 8, 60.
- Friedrich, R. , Ditzinger, T. and Merkel, S. (2000b) in preparation.

- Friedrich, R., Radons, G., Ditzinger, T., Henning, A. (2000). "Ripple formation through a convective instability from moving and erosion sources", *Physical review letters*.
- Friedrich, R.; Ditzinger, T.; Henning, A.; Radons, G. (2000): Mechanisms of the Evolution of Spatio-Temporal Instabilities in Abrasive Water Jet Cutting. In: *Proceedings of the 6th Pacific Rim International Conference*, 9-11 October, 2000, Sydney, Australia, S. 83-87.
- Guo, N.S. (1994), Schneidprozeß und Schnittqualität beim Wasserabrasivstrahlschneiden. VDI-Fortschritt-Berichte, Reihe 2, Nr. 328.
- Hashish, M. (1988), "Visualization of the abrasive waterjet cutting processes," *Experimental mechanics* 45, 159 (1988), pp. 159-169.
- Henning, A. (1997). "Computer aided manufacturing for three-dimensional abrasive waterjet machining," in *Proceedings of the 9th American Waterjet Conference*.
- Henning, A.; Anders, S. (1998): Cutting-edge quality improvements through geometrical modeling. In: Papers presented at the 14th International Conference on Jetting Technology, Brugge, Belgium, 21-23 September 1998, S. 321-328.
- Henning, A.; Westkämper, E. (2000): Modeling of contour generation in abrasive water-jet cutting. In: *Jetting Technology : Papers presented at the 15th International Conference on Jetting Technology*, Ronneby, Sweden, 6-8 September 2000, S. 309-320.
- Westkämper, E.; Henning, A.; Radons, G.; Friedrich, R.; Ditzinger, T. (2000): "Cutting Edge Quality through Process Modeling of the Abrasive Waterjet" In: Teti, Roberto (Hrsg.); CIRP; University of Naples Federico II: *Intelligent Computation in Manufacturing Engineering - 2 : Proceedings of 2nd CIRP International, Seminar*, June 21-23, 2000, Capri, Italy. Neapel, I, 2000, S. 179-188.
- Westkämper, E.; Henning, A.; Radons, G.; Friedrich, R.; Ditzinger, T. (1999): Non-linear dynamic modeling of the abrasive waterjet process. In: *Investigation of Nonlinear Dynamic Effects in Production Systems : 2nd International Symposium*, 25.-26. February 1999, Aachen, S. 1-15.
- Zeng, J. and Kim, T. (1992), "Development of an abrasive waterjet kerf cutting model for brittle materials," in *Proceedings of the 11th International Conference on Jet Cutting Technology*.

MACRO CHARACTERISTICS OF AWJ TURNED SURFACES

Mohamed Hashish
Flow International Corporation
Kent, WA

ABSTRACT

The macro-characteristics of AWJ-turned surfaces are presented in this paper. These effects are results of trailback and jet deflection during turning. Machine effects such as vibration and accuracy of motion are other “external” factors that affect the turned surfaces.

Two basic turning operations were studied; these are face turning and diameter turning. It was found that turned faces might have two zones of very distinct characteristics. It is clear at this point, of why such zones exist and under what conditions. Other surface effects such as straightness was analyzed. The parameters that affect diameter turning such as federate, depth of cut and dwell time were studied. The effects of these parameters on macro surface characteristics such as waviness, and undercut were quantified.

1. INTRODUCTION

AWJ cut surfaces have several geometrical and integrity characteristics. The following characteristics are associated with linearly cut surfaces:

- Taper: Cut walls may not be parallel and with either convergent or divergent taper
- Straightness: Cut walls may not be straight but slightly curves
- Undercut: This happens around corners at the bottom of the cut
- Surface waviness: A surface may be wavier at the bottom of the cut than at the top.
- Surface roughness: Highly dependent of abrasive particle size
- To edge rounding: More evident as stand off distance increases
- Bur: Occurs at the bottom of a cut and is more evident for ductile materials
- Delamination: Laminated material may locally separate when cutting or piercing
- Cracking: Brittle materials such as glass may crack, more likely during piercing
- Chipping: Brittle materials and coatings may chip during piercing or cutting
- Embedding: Abrasive particles or their fragments may embed into surfaces

Turned Surfaces may have the same integrity (qualitative) effects but the effects of trail back and jet deflection manifest themselves in a different set of geometrical characteristics.

There have been several studies on AWJ turning but rather limited commercial applications. This is perhaps due to lack of knowledge about AWJ turning, limited marketing of this process, and the initial high cost of custom AWJ systems. However, AWJ turning has several advantages:

- An AWJ can turn almost any material
- Not sensitive to original shape. For example a square can be turned
- Low forces and thus rods with large l/d can be turned
- Relatively high volume removal rate especially for hard to machine materials
- The same tool may perform cutting and drilling on the same turning setup

Hashish (1987) performed a study on the effect of turning parameters on surface waviness and surface roughness. Ansari, Hashish, and Ohadi (1992) performed an extensive investigation into visualizing the turning process using high-speed camera. They showed the complexities of the process due to either radial or axial jet deflection. Ansari and Hashish (1992) developed a simplified physical model of turning while Zeng et. al. (1994) developed a mathematical model. Henning (1999) presented an empirical approach for AWJ turning. None of the above work addressed such effects as undercutting, and precise features. This paper focuses on describing, either qualitatively or quantitatively, the macro surface effects obtained by AWJ turning.

2. TURNING OPERATIONS

Two basic turning operations are discussed here. These are:

- Face turning (slotting)

- Diameter turning

In the following sections, we describe these operations and the resulting surface effects.

2.1 Face Turning (slotting)

In this case, the jet may be driven into the workpiece in a direction perpendicular to the axis of rotation or kept stationery at certain radial position or at the top dead center for complete parting off. Figure 1 shows these two cases.

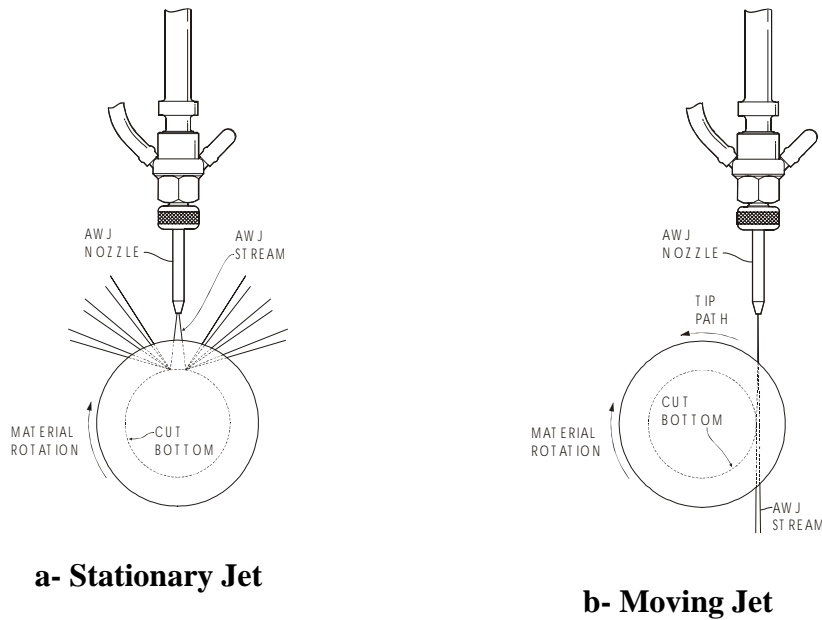


Figure 1: AWJ lathe face turning

2.1.1 Face Turning with Stationary Jets

Facing with stationary jets is illustrated in Figure 1a. In this case, the jet will be kept stationary at certain radial position. To part the workpiece, the jet will be located at the top dead center of the part for complete parting off. Figure 2 shows a sequence of stationary face turning in glass.

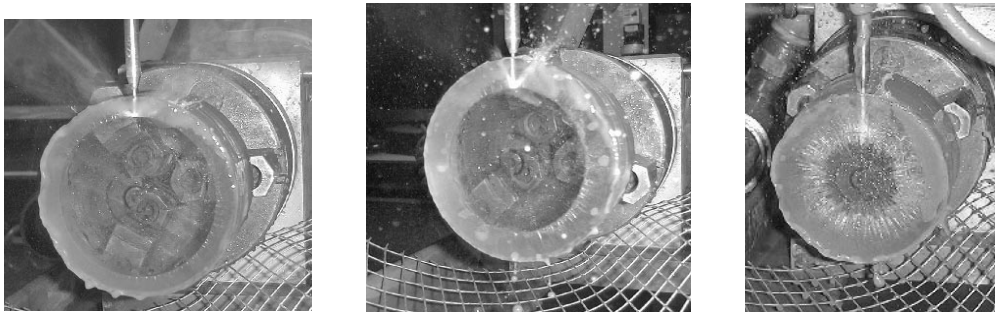


Figure 2: Face turning with stationary jet in glass

It is obvious that, in this case, the stand off distance is continually increasing. This will typically reduce the volume removal rate. The rate of change in diameter can simply be derived to be $dr/dt = C/r$, Where $C = (\pi dm/2) dv/dt$. It is obvious from this equation that the rate of change in diameter increases as the diameter decreases if the volume removal rate remains unchanged. With reduced volume rate, as stand off distance decreases, the rate of change in diameter may have minima or may progress at a reduced rate. This impacts the produced surface straightness. More jet dwell at certain radial location may cause the rebound jet to alter wall straightness and surface finish.

Experiments were performed to part 250-mm diameter bars of Inconel. Figure 3 shows pictures of turned faces. The picture on the left side shows radial waviness, which becomes irregular towards the center of the part, similar to the glass piece shown in Figure 2 above and Figure 3 in the middle. Also, similar to linear cutting, this waviness is less evident near the outside diameter of the part. The waviness can be eliminated by using jets that are more powerful and optimizing the rotational speed. For the Inconel sample above, a 50-rpm rotation was found to be effective in producing waviness-free surface as shown in the right side of Figure 3.

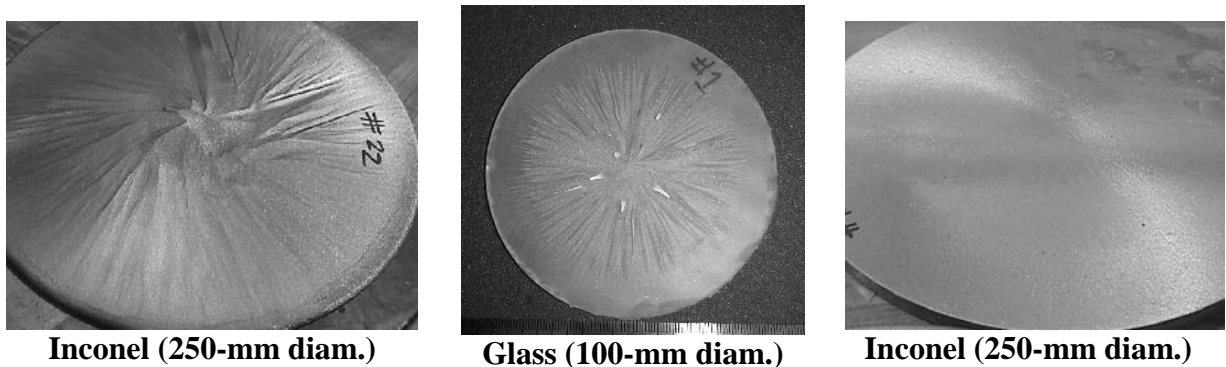


Figure 3: Stationary jet faced Surfaces

The parted-off surfaces are typically tapered. The taper increases at a relatively high rate towards the center of the part. This is attributed to loss of jet energy due to spreading and friction against the walls of the cut. Figure 4 shows a tapered turned surface. Observe the rate of change of taper near the center.

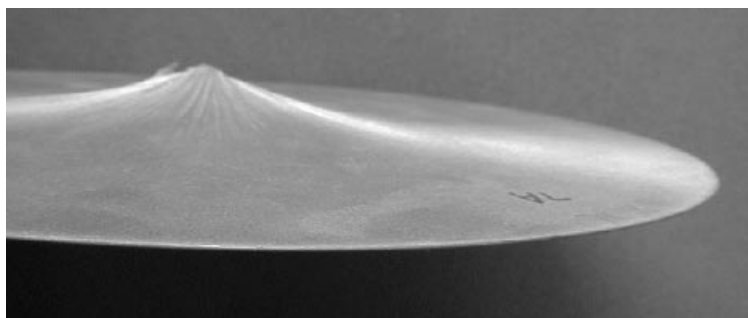


Figure 4: Wall taper of 250-mm diameter turned Inconel

It was found that letting the jet dwell after complete parting off could not easily control the taper of the cut as shown in Figure 4. In this case, the jet will be glancing on the face of the cut and unconstrained in the lateral direction. The jet deflects away causing little taper correction.

However, to eliminate or minimize taper, varying the jet dynamic variables such as pressure, rotational speed, and abrasive flow rate while turning will be a promising approach. For example, at the beginning of facing, the stand off distance is small but the volume swept is relatively large. The rotational speed may be slowed down as to reduce the volume sweep rate. As facing progresses, the standoff distance increases and the rotational speed may be increased to maintain the same volume sweep rate, but the abrasive flow rate may be increased. This work is suggested for future studies or graduate thesis.

One of the most interesting observations on stationary face turning is the formation of two morphologically distinct surface zones. Figure 5 shows two pictures for Silicon and Aluminum. The silicon part is about 75-mm diameter while the Titanium part is about 250-mm diameter. There may be several reasons for this phenomenon. One is that the jet may have a slight angle to the face to be cut which causes it to deflect into the opposite face rather than just in a radial plane. The effect will terminate when the cut causes the jet to be in a radial plane. Another reason is that the jet penetration mode changes as the volume sweep rates drops below certain critical value. This area is recommended for further investigations to both determine the exact cause of this phenomenon and to quantify it.

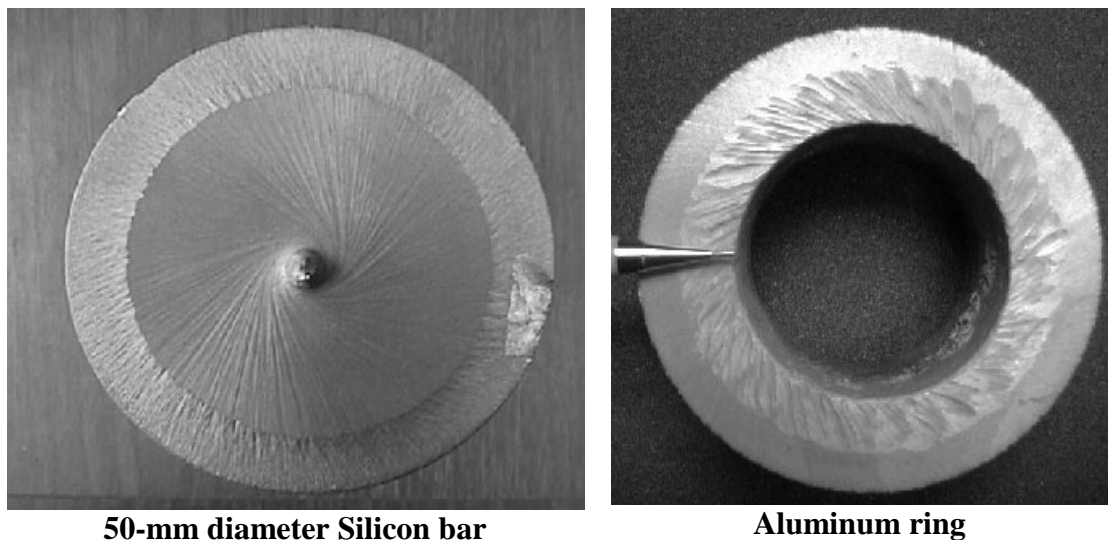


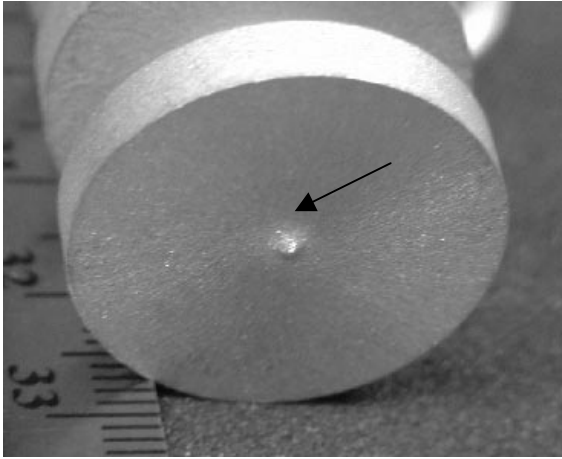
Figure 5: Two surface zones in AWJ-turned faces

2.1.2 Face Turning with moving jet:

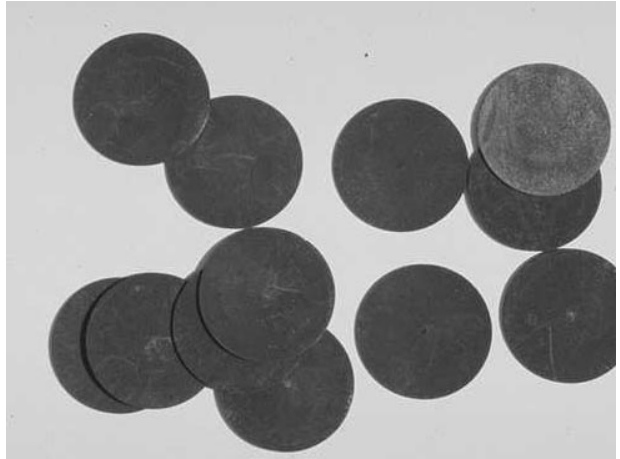
Because of the round part profile (or rotation), the nozzle has to move either in the radial direction only, or in both the radial and vertical (z-axis) direction in order to maintain a constant standoff distance at the outer diameter. The schematic of Figure 1-b illustrates the facing operation. It should be clarified here that the actual stand off distance keeps on increasing as the

turning progresses, similar to the previous case. The angle of jet impact is the main variable that changes by this process in comparison to stationary facing.

Figure 6-a shows an Aluminum face, which was turned while the jet was traveling. Observe the middle uncut part. This is attributed to the fact that the jet is round. The jet leading edge will part off the part before the jet centerline reaches the part centerline. In order to remove this protrusion, the jet must be traversed across center while the other side of the cut is kept in place. Figure 6-b shows wafers cut from 25-mm diameter carbon rods using this strategy. Observe that there are no protrusions in these wafers. The flatness of the wafers was in the range of 0.025~0.03 mm.



a- Aluminum (25-mm diameter)



b- Carbon wafer (25-mm diameter)

Figure 6: AWJ-machined wafers:

To control wall straightness, two variables may be synchronized. These are the surface speed and jet radial traverse rate. Surface speed is controlled by the rotational speed, which can be changed by continually increasing it as the diameter reduces. The jet traverse speed is selected to maintain constant overlap.

When partially facing a part, the jet feed rate and its dwell time at the end of feed will affect the geometry of the faced part. These parameters control the taper of the kerf, thus controlling the perpendicularity of the faced surface. We expect that jet trailback increase with feed rate, degrading the surface finish and accuracy. A long dwell at the end of the cut should allow the jet to straighten before shutting off. This should improve diameter control and perpendicularity. An excessively long dwell allows the jet to flare, creating a “dish” (concave) on the faced surface, followed by a positive taper (convex) as the cutting area moves from the top of the part to the bottom. Figure 7 shows an example ample for measuring kerf taper.

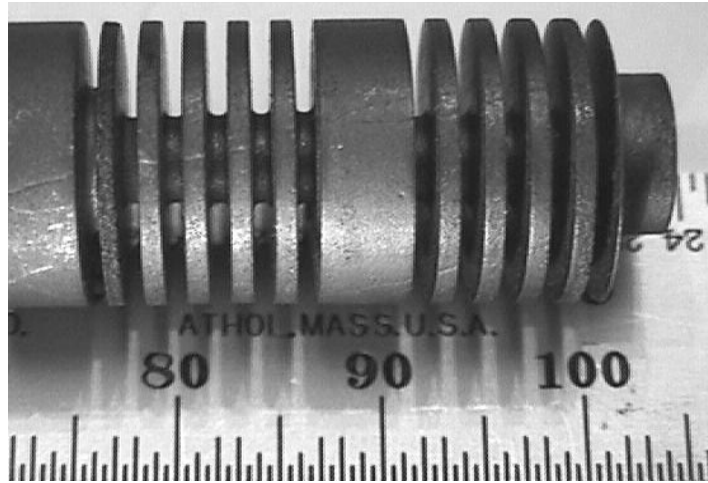


Figure 7: Sample of partially faced Surfaces for measuring taper

Experimental results (Hashish 2000) of the face turning test correlate well to the intuitive predictions mentioned earlier. Figure 8 shows the correlation between dwell, feedrate, and the final diameter of the notched section.

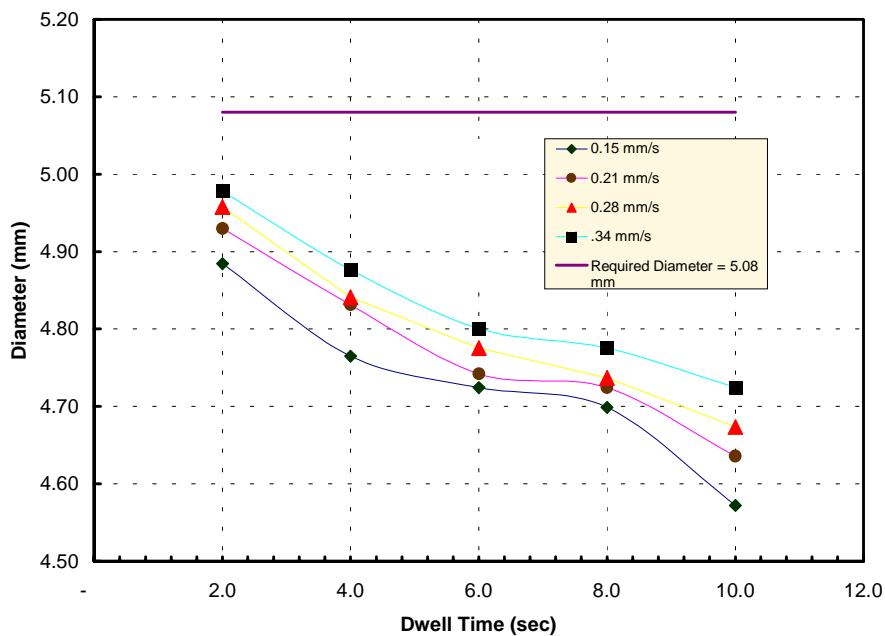


Figure 8: Diameter versus dwell and feedrate

The final diameter of the part is a strong function of the dwell time, no matter what the feedrate is into the cut. The perpendicularity of the cut face to the axis of rotation is an important surface effect. This feature is reflected in the variation of the kerf width. Figure 7 shows a sample used to measure taper. An optical comparator was used to measure the width of cut at the outside and inside diameters of the slot. Figure 9 shows the change in kerf width from the edge of the part to the radius at the end of the cut.

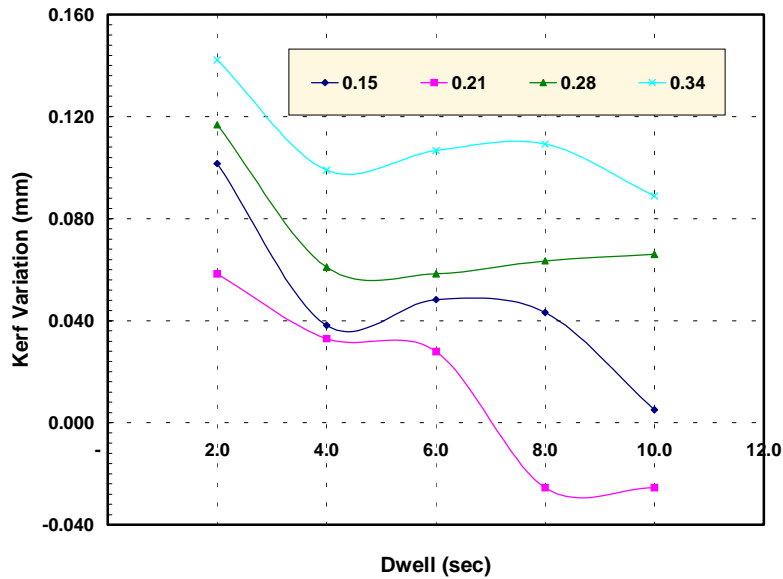


Figure 9: Kerf variation versus dwell and feedrate. Feedrates are shown in mm/s

The variation in kerf is a strong function of both feedrate and dwell time. As intuition would suggest, the taper at high feedrates is larger than at low feedrates (Hashish 2000). Also, increasing the dwell time can help to reduce the taper produced by a high feedrate. Even at a low feedrate, if the dwell is too short, there can be a substantial taper. Figure 9 shows the negative taper produced during the 0.21 mm/s feedrate test. This may be caused by AWJ flare moving the cutting zone towards the middle of the workpiece.

Figure 10 shows another effect of face-turned parts. In this case, the cut face shows spiral lay. The jet rebound from one face to the other may have caused this effect. A slight jet angle may have also been the reason for this rebound effect. It is not certain yet of why this effect will result considering the part was rotating at about 50-rpm, which should average the surface morphology.

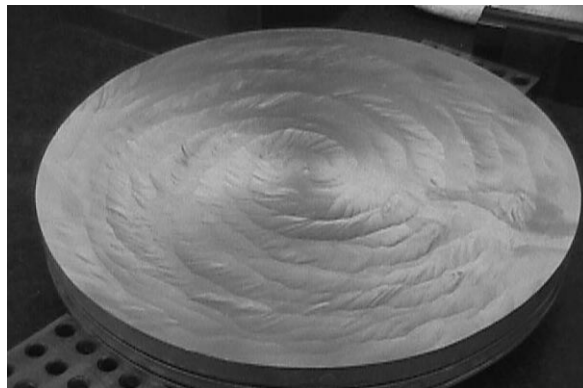


Figure 10: Spiral Lay Pattern for face turning on 250-mm diameter Titanium

2.2 Diameter Turning Tests

In turning the diameter of a part with the AWJ lathe, the jet is fed into the part parallel to the axis of rotation (x-axis). The distance between the jet and the rotational axis controls the diameter of the part. Figure 11 illustrates the lathe turning a diameter.

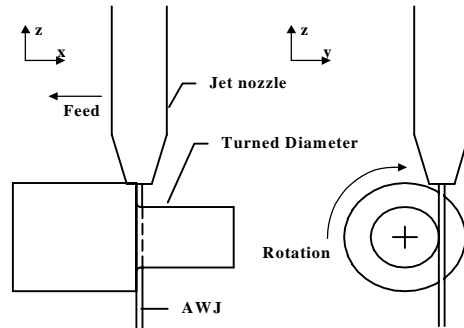


Figure 11: AWJ lathe diameter turning

In this case, nozzle height changes (z-axis) may or may not be required. When turning a fixed diameter, the standoff distance is held constant.

Figure 12-a shows three sample of 25-mm Aluminum turned to produce different diameters in one pass. Clearly, when increasing the depth of cut and thus the volume sweep rate, the surface waviness will be affected. The larger the volume sweep rate, the larger the waviness and surface irregularities. To further investigate this effect for precision turning, Hashish and Stewart (2000) performed a systematic study on turning of gamma Titanium Aluminide. The samples shown in Figure 12-b were turned starting from a diameter of 13-mm to diameters of 5.08, 6.99, 8.89, 10.8, and 12.7-mm. Each test specimen was turned in a single. At the end of each diameter section, a dwell time of 10 sec was added to allow the jet to straighten before shutting off and repositioning for the next diameter section. Figure 13 compares the profiles of the parts made at 0.42 mm/s and 0.017 mm/s.

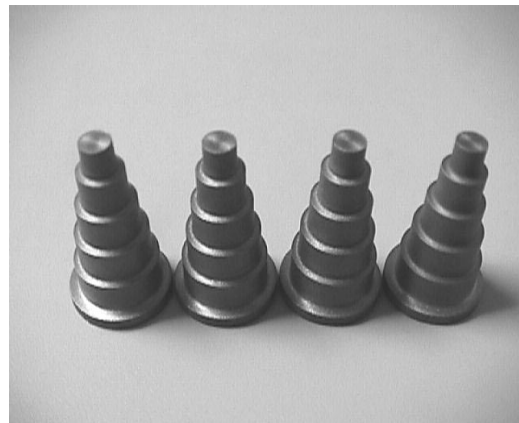
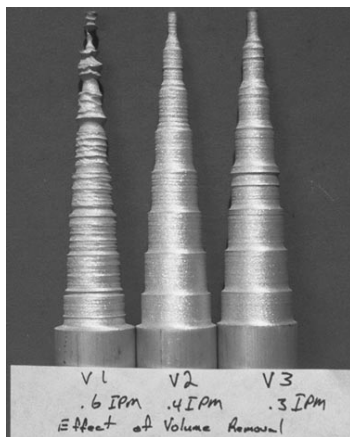


Figure 12: Turning of stepped samples at different feed rates

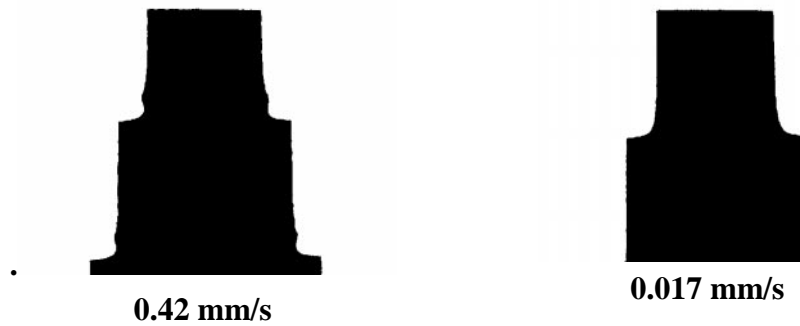


Figure 13: Comparison of high feedrate and low feedrate part profiles

The higher feedrate part has a rougher surface, jet striation marks, poorer roundness, and a less-consistent diameter. This is caused primarily by the increasing trailback and decreasing jet stability when cutting at higher material removal rates.

The bulge near the shoulder of the part is a result of jet trailback, and not a feature of steady-state turning. This bulge is created when the nozzle stops at the end of the cut. The jet itself is still trailing back from the nozzle, cutting the remainder of the diameter. A dwell time was provided to allow the jet to return to vertical before shutting off. At low feedrates, this leaves a smooth radius on the part. However, at higher feed rates, the jet “jumps” over the last bit of material, leaving a characteristic bulge and undercut feature. Typically, the undercut and bulge are larger than the steady state turned diameter, although a low feedrate and long dwell can lead to an undercut of the steady-state diameter. These features are identified in Figure 14-a. Experiments showed that the size of the trailback artifact increases with increasing material removal rate, as diameter decreases and feedrate increases, the artifact grows. Figure 14-b shows an AWJ-turned part showing these effects. Figure 15 illustrates the relationship between diameter, feedrate, and artifact size.

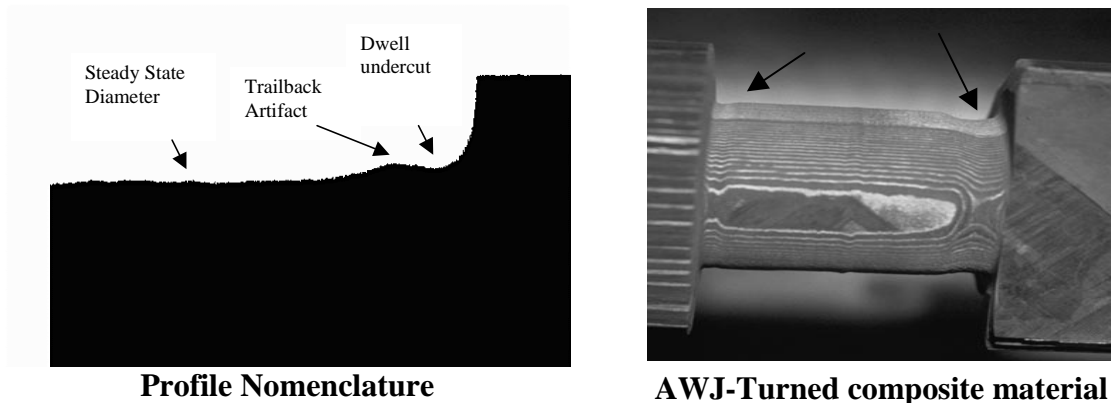


Figure 14: Corner profile features

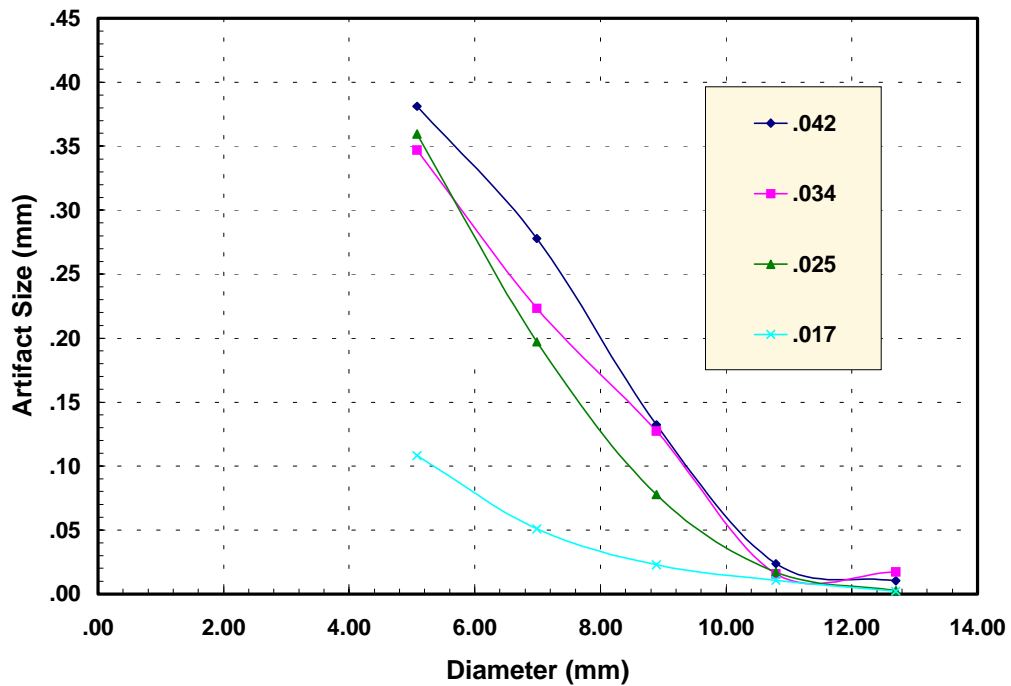


Figure 15: Trailback artifact versus original diameter and feedrate

Like the trailback artifact, surface waviness is also a function of cutting depth and feedrate. This is shown in Figure 16 below.

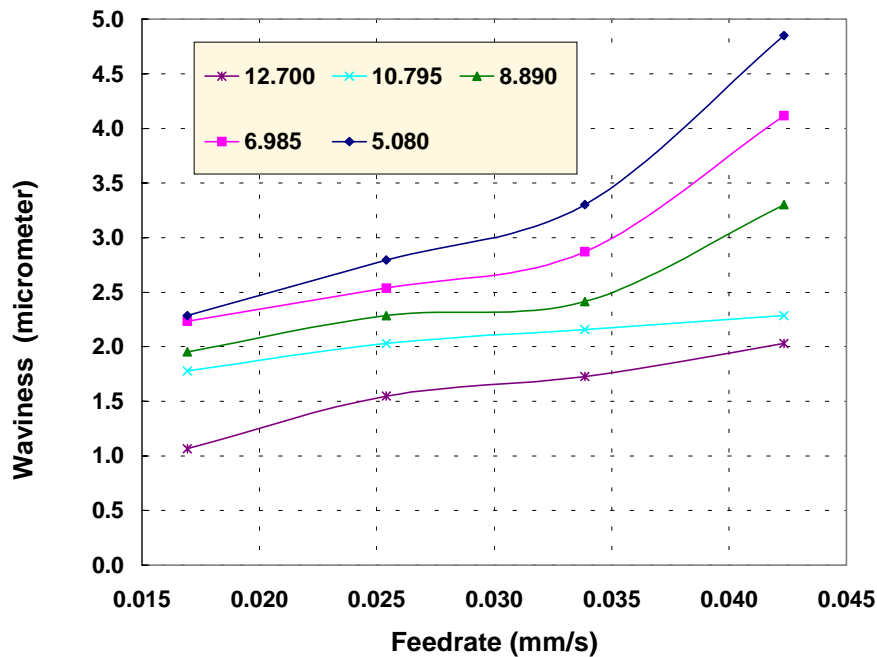
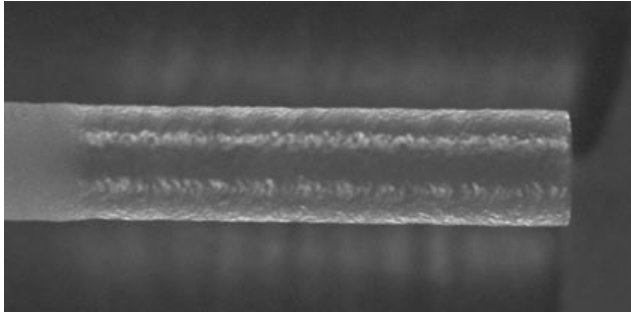


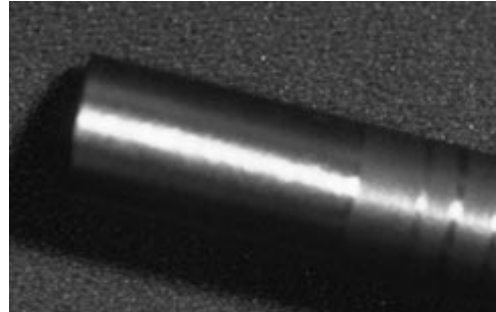
Figure 16: Waviness versus Feedrate and Diameter

From the waviness chart, it is clear that a slower removal rate (lower feedrate and larger diameter) generally improve the surface finish of the part. Visual inspection of the parts indicated that this trend was due more to reduced jet striation rather than improved micro finish.

To improve the surface finish, smaller abrasive particles must be used. Figure 17 shows glass and boron carbide samples with significantly improve surface finish. However, the waviness, especially on the glass sample still evident.



Glass



Boron Carbide

Figure 17: Turned sample with improved surface roughness

The turned diameter could be different than the swept diameter. The error in the diameter (diameter deficit or surplus) of the parts is presented in Figure 18.

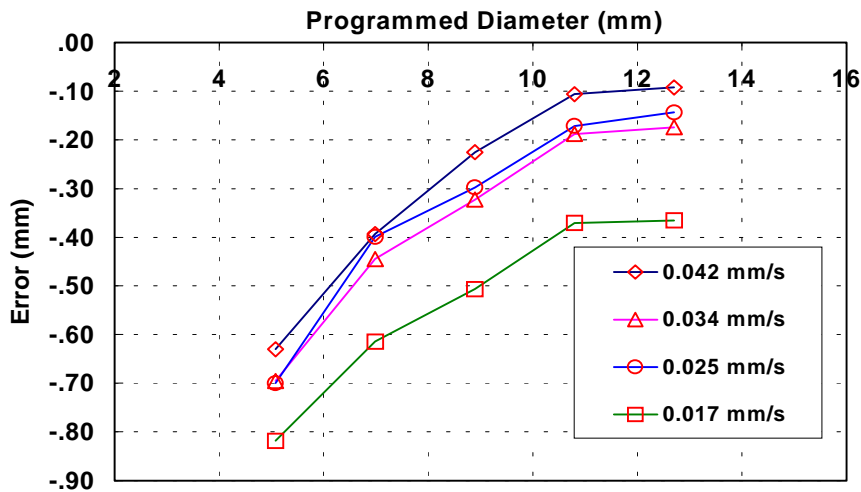
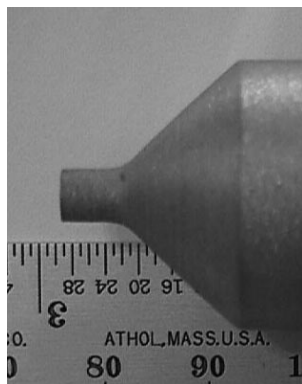


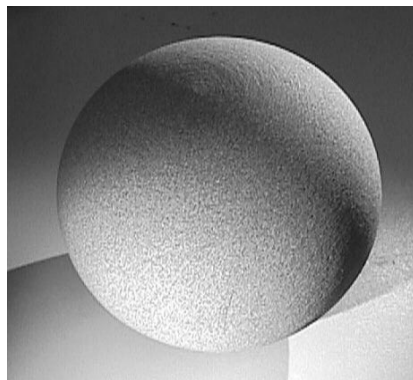
Figure 18: Programmed diameter versus error at different feedrates

In complex shape turning, the jet is traveling in the x, y, and z directions along the required shape starting from round or other workpiece shapes. If the feed rate is kept unchanged, then the required material removal rate will be changing in proportional to the square of the diameter. In case of cone turning, the volume removal is linearly varying along the axial direction. This will yield a surface that is varying in surface finish and error from the required shape unless the feedrate is relatively low. To overcome this problem, the jet feedrate can be controlled to vary

axially such that the volume sweep rate is fixed. Figure 19 shows sample cone and sphere parts part turned with this method. Although the turned surface is of high quality and is free from striations, there was still an error in the cone shape. About 0.04-mm deviation from linearity of the cone surface slope was measured. This could be attributed to jet deflection and its interference with the volume removal process. However, the use of constant volume sweep rate as criteria for feedrate appears to be promising. Figure 19-b and 19-c show other examples.



A - Cone



b- Sphere



c-Complex shape

Figure 19: AWJ-turned surfaces using varying feedrate

The synchronization of jet axial feed rate and workpiece rotational speed can be used to machine threads and spirals. On a round workpiece, the jet axial motion may not be associated with varying standoff distance. Figure 20 shows two pictures of AWJ-turned aluminum spiral and a thread machined in a glass rod. Based on the diameter of the workpiece, the jet feed rate can be estimated. This will determine the rotational speed of the part, which is typically low. Rotating at relatively low rotational speeds (~ 1 rpm) must be accurate as small changes in rotational speed will be of relatively high percentage. Figure 20 shows examples of spirals and threads.

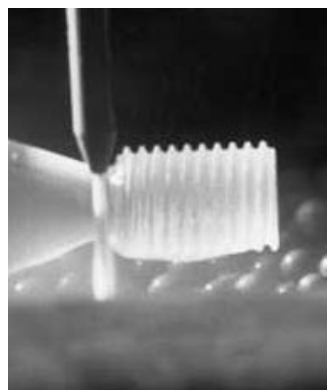
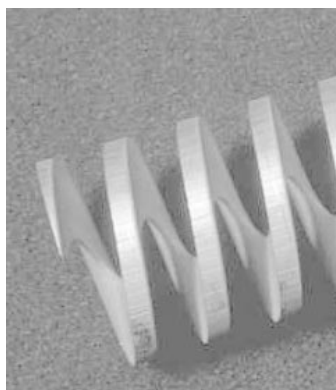


Figure 20: AWJ-turned spiral and thread

3. CONCLUSIONS

The following conclusions can be drawn from this study:

- There are several surface effects as a result of AWJ turning. These effects correlate to those in linear cutting
- Trail back and jet deflection contribute the majority of surface effects.
- The dwell time at the end of a face turning process has a significant effect on the dimension of the final diameter.
- The kerf taper and trailback artifact are strong functions of feedrate and dwell time.
- AWJ can be used to precisely turn parts with minimal waviness.
- To improve the surface finish by reducing abrasive particle size, turned parts must be free from waviness.
- AWJ was used to turn a wide range of shapes such as cones and spheres. Feedrate control is critical in obtaining accurate parts.

4. REFERENCES

1. Hashish, M., (1987) "Turning with Abrasive-Waterjets - A First Investigation," ASME Transactions, Journal of Engineering for Industry, Volume 109, No. 4, pp. 281-296.
2. Hashish, M., and J. Stewart (2000) "Observation on Precision Turning with Abrasive-Waterjets," Proceedings of the 15th International Conference on Waterjetting Technology, Sponsored by BHR group, Ronneby, Sweden, September 6-8, pp. 367-380.
3. Ansari, A., Hashish, M., and Ohadi, M., (1992) "Flow Visualization Study on Macro Mechanics of Abrasive-Waterjet Turning," Journal of Experimental Mechanics. December.
4. Ansari, A., and Hashish, M. "On the Modeling of Abrasive-Waterjet Turning," Jet Cutting Technology, edited by A. Lichtarowicz, Published by Kluwer Academic Publishers, Dordrecht, Netherlands, pp.555-576, 1992.
5. Ansari, A., and Hashish, M., (1995) "Effect of Abrasive-Waterjet Parameters on Volume Removal Trends in Turning" ASME Transactions, Journal of Engineering for Industry, Vol. 117, No. 1., pp. (in press)
6. Zeng, J., Samuel, W., Thomas, K., (1994) "Development of Parameter Prediction Model for Abrasive Waterjet Turning," Jet Cutting Technology: Applications and Opportunities edited by N. G. Allen, Proceedings of the 12th International Conference on Jet Cutting Technology, Rouen, France Published by BHR group, pp.601-617.
7. Henning, A., (1999) "Modeling of Turning Operation for Abrasive Waterjet," Proceedings of the 10th American Waterjet Conference, edited by M. Hashish, published by WJTA, Houston, TX, pp. 795.

MICRO ABRASIVE WATERJET CUTTING

D. S. Miller
Miller Innovations
Harrold, Bedford, UK

ABSTRACT

Micro abrasive waterjets have jet diameters less than 100 μ m but they cut the same materials as conventional abrasive waterjets. They extend the capabilities of abrasive waterjets into micro machining and the profiling of thin materials. Micro abrasive waterjets have a particular application in the machining of glasses and other brittle materials under 0.5mm thick that are difficult to profile and drill by other methods. Systems to produce micro abrasive waterjets are described and details given of their cutting and profiling abilities.

1. INTRODUCTION

New micro machining techniques are required to meet the growing demands for minaturised products and processes. Abrasive waterjets are an ideal candidate for micro machining but they need to be adapted to operate with jet diameters less than 100 μm . Fine abrasive waterjets are also needed to profile thin materials that distort or shatter when cut by conventional abrasive waterjets.

The minimum diameter for conventional abrasive waterjets is about 400 μm . Jet diameters down to 10 μm are possible by changing the jet formation process from entraining abrasive particles into a high velocity waterjet, as used by conventional abrasive waterjets, to passing abrasive particles in pressurised water through a nozzle. Passing abrasive particles in pressurised water through a nozzle is a very efficient process compared to entraining abrasive into a high velocity waterjet. A micro abrasive waterjet operating at 700 bar has the same jet cutting energy density as a conventional abrasive waterjet operating at about 3000 bar.

The benefits that micro abrasive waterjets gain from lower operating pressures, relative to conventional abrasive waterjets, have to be set against handling abrasive particles at high pressures, rather than at the near atmospheric pressures that abrasives are handled in conventional abrasive waterjet equipment. If a significant pressure differential occurs within equipment that contains abrasive particles, high velocities will occur and the cutting capabilities of abrasive flows will be released within the equipment. There are a number of situations that could lead to significant pressure differentials in the flow circuits of micro abrasive waterjets. Preventing situations where significant pressure differentials arise requires careful flow circuit and component design along with good control over flow conditions in the circuits.

After four years of development work, the conditions for reliable operation of micro abrasive waterjets have been established. Prototypes for the first generation of micro abrasive waterjet systems have been designed and built. Trials to accumulate reliability and operability experience are well advanced.

Methods of producing micro abrasive waterjets are described in Section 2. In Section 3 the development of systems to feed 30 to 60 μm diameter jets is described and in Section 4 details are given of their cutting capabilities. Market opportunities for micro abrasive waterjets are outlined in Section 5, and future developments are discussed in Section 6.

2. GENERATION OF MICRO ABRASIVE WATERJETS

Micro abrasive waterjets are generated by passing a pressurised suspension of abrasive particles in water through a cutting nozzle. Abrasive suspensions can be pre-mixed at the concentration required at the cutting nozzle, or abrasive particles can be metered from a bed of abrasive particles and suspended in pressurised water flowing to a cutting nozzle.

Pre-mixed suspensions involve mixing abrasive particles and a suspending additive with water. A cartridge is filled with the suspension and loaded into an abrasive storage vessel. Pressurised water from a pump displaces the suspension out of the cartridge to a cutting nozzle. The use of

pre-mixed suspensions becomes the preferred option at smaller jet diameters. A cartridge with a volume of half a litre contains sufficient suspension to cut for about an hour with a 25µm diameter jet.

When abrasive particles are metered from an abrasive bed, the abrasive is first mixed with water and, if needed, an anti de-watering additive or suspending additive. A cartridge is then filled with the mixture and loaded into an abrasive storage vessel. A percentage of the water flow from a pump is directed to the top of the cartridge. The flow into the top of the cartridge displaces abrasive and water out of the bottom of the cartridge and into water flowing directly to the cutting nozzle. A quarter litre cartridge, containing 70 percent abrasive by weight, can feed a 50µm diameter jet with a 10 percent abrasive concentration for about an hour. Water consumption is 2.5l/hr for a 50µm diameter jet.

The basic flow circuit for micro abrasive waterjet systems is shown in Figure 1. The circuit can operate with pre mixed suspensions, through to settled abrasive beds in the abrasive storage vessel. Filtered water is pressurised by a pump and fed to a control unit. The control unit either directs all the water to the nozzle, or it diverts part or all of the flow to the top of an abrasive storage vessel to displace abrasive and water out of the vessel to mix with any water flowing directly to the nozzle. A valve is provided to depressurise the abrasive storage vessel and a valve can be used in the connection to the nozzle to stop discharge from the nozzle.

3. EQUIPMENT TO PRODUCE MICRO ABRASIVE WATERJETS

3.1 General

Proven technologies are available for the pumps, valves and other components in the water only part of the flow circuits of Figure 1. For the first generation of micro abrasive waterjets the design strategy has been to confine abrasive to the abrasive storage vessel and to short passageways between the abrasive storage vessel and the cutting nozzle. Minimising the parts of the flow circuit subject to abrasive flows has been achieved by positioning the abrasive storage vessel immediately above the cutting nozzle as shown in Figure 2.

3.2 Abrasives

Garnet is the most widely used abrasive for abrasive waterjets and it is available in the particle size ranges needed for micro abrasive waterjets. Garnet abrasive has been adopted as the reference abrasive for development work. Because of the small nozzle diameters it is essential to prevent contamination of the abrasive once it is prepared for use. This is achieved by loading abrasive into cartridges.

Trials are also being carried out with aluminium oxide, which is a more expensive abrasive than garnet. It is also more aggressive so nozzle wear rates are higher. Trials to date indicate that aluminium oxide could be the preferred abrasive when very hard materials, such as ceramics, need to be profiled. Higher abrasive cost and the costs associated with more rapid nozzle wear can be offset by higher profiling rates.

3.3 Water supply

Typically the water requirement for a micro abrasive waterjet is a few litres per hour. This can be supplied directly from the water mains or from a pressurised container that is filled as required. An inline disposable filter is used to protect the pumps.

3.4 Pumps

The pumping duty for a 50 μ m diameter jet is 2.5 l/hr of water at 700 bar. Intensifier plunger pumps, driven by compressed air, are a cost effective way of meeting the pumping duty. A 2kW, single-phase electric motor driven compressor provides an adequate supply of air to drive the pumps and for operating valves. Figure 3 shows a pair of intensifier pumps based on proprietary pneumatic cylinders. The barrels of the plunger pumps are centered within the cylinders making for a compact arrangement. Servo valves, under the control of a programmable logic controller, synchronise the operation of the two plunger pumps to minimise water pressure fluctuations.

3.5 Control Unit

The control unit, in conjunction with restrictors in the flow circuits, is used to either send all the incoming water flow to the nozzle, or to send part or all of the incoming water flow to the top of the abrasive storage vessel. Depending on the duty, the controller may take the form of a valve and a jet pump or two valves.

3.6 Abrasive Storage Vessel

The abrasive storage vessel, shown in Figure 2, is designed to accommodate cartridges of abrasive. The vessel has an interrupted thread between the base and barrel that allows the barrel to be removed by rotating it through an eighth of a turn and lifting it off the base. With the barrel removed the abrasive cartridge contents can be inspected and the cartridge changed. Figure 4 shows the barrel removed with a part-used abrasive cartridge in the vessel base.

3.7 Nozzles

Cutting nozzles with bore diameters between 40 and 60 μ m have been produced in a number of wear resistance ceramics and in diamond materials. Trials are ongoing to develop the best manufacturing method and to establish nozzle life and operating economics.

3.8 Profiling Tables

Proprietary linear motion actuators with the required positional accuracy and repeatability are readily available for moving abrasive storage vessels, or jet catcher tanks with built in work piece supports. This means there is considerable flexibility in deciding how X-Y motion systems are configured for a particular machining duty. During the development programme the following configurations have been used successfully:

- Moving the abrasive storage vessel and nozzle in the X direction and work piece support in the Y direction over a fixed catcher.

- Moving the abrasive storage vessel and nozzle in the X direction and work piece support and integral catcher in the Y direction.
- Moving a catcher tank and work piece support in the X-Y directions under a fixed abrasive storage vessel and nozzle.

The accuracy and repeatability of the motion system has to be selected to achieve the objectives for specific machining operations. A 50µm diameter jet can reproduce micron size features but only if the motion system can position the cutting nozzle with the required accuracy and repeatability.

4. CUTTING AND PROFILING

The cutting behaviour of micro abrasive waterjets is similar to conventional abrasive waterjets but on a smaller scale. In the case of composite materials, the characteristics of the material would have to be scaled to achieve similar cutting behaviour. In practice this is unlikely to be the case, so composite materials that can be cut by conventional abrasive waterjets may not be satisfactorily cut by micro abrasive waterjets. An example is a metal matrix composite of ceramic particles in an aluminium matrix. A conventional abrasive waterjet cuts the material by destroying the matrix and washing out the ceramic particles. If, however, the particles are sufficiently large, relative to the diameter of a micro abrasive waterjet, the jet may be deflected by the particles and little cutting takes place.

A test piece with a dragon motif has been used for profiling trials, Figure 5. It can be seen from the figure that when the test piece is machined from thin springy material, it forms a paperclip. The dragon motif involves some 1600 straight line moves, and as Figure 6 demonstrate the motif provides a good indication of the level of detail that can be reproduced by a micro abrasive waterjet.

By measuring the width of the semi-circular slot in the test piece the diameter of the jet can be determined. The cut edge quality can be assessed by inspecting the outer diameter of the test piece.

Figure 7 shows test pieces that have been profiled from 6 different materials:

1. Stainless steel, 300µm thick
2. Plastic cut from a CD disc
3. Plywood, 3mm thick
4. Titanium, 2mm thick
5. Glass, 300µm thick
6. Aluminium, 1mm thick

Because the same cutting mechanisms are involved in micro abrasive waterjet cutting as conventional abrasive waterjet cutting, the software optimisation procedures developed for conventional abrasive waterjets can be adapted for micro abrasive waterjets. These optimisation procedures include cut edge quality, speed variation for radii and corner cutting, material type and thickness.

Test piece 4 in Figure 7 shows the importance of optimising the cutting speed relative to the detail being cut. Test piece 4 was profiled at a constant 25mm/min and as inspection of the photograph shows the dragon was not completely cut out. Failure to cut through occurred where the jet had to undergo a rapid change in direction. The outside circular cut edge at 25mm/s on test piece 4 was of a high quality. The completely cut out dragon above the titanium test piece 4 was cut at 15mm/min.

Miller et al give a procedure for predicting the cut surface area generation per minute by suspension jets operating at pressures up to 1000 bar. Based on straight line cutting of stainless steel 304L, the cut surface area generated per minute is given by:

$$CSA = 3 \times D \times P \times MF \times QF \times ACF$$

Where:

- CSA is the cut surface area generated per minute, mm²/min
- D is the jet diameter, mm
- P is the water pressure, bar
- MF is the machine ability factor, 1 for stainless steel 304L
- QF is the quality factor, 1 for a good edge quality
- ACF is the abrasive concentration factor, 1 for 10 percent abrasive by weight

The prediction method is based on suspension jets with diameters between 0.5mm and 2mm. Because of scale effects, the prediction method over predicts the cutting performance of micro abrasive waterjets. For a 50 µm diameter jet operating at 700 bar, with a 10 percent abrasive concentration, producing a good quality cut surface on stainless steel 304L, the formula predicts a cut surface area generation of 105 mm²/min. This is equivalent to cutting 1 mm thick stainless steel at 105 mm/ min. Indications are that the cut surface area generation rate is about 60 percent of this figure.

It has been found that a 50 µm diameter jet will cut through about 10mm of metal. Based on a linear relationship between jet diameter and the maximum thickness of material that can be cut, a 10mm thickness cutting capability is less than would be expected based on larger diameter jets. Again a correction factor of about 60 percent is indicated.

5. MARKET POTENTIAL

Micro machining is a multibillion-dollar market that is growing rapidly. The market needs new machining technologies and it particularly needs the proven capabilities of abrasive waterjets to machine high quality profiles from a wide range of materials.

Techniques for micro machining include: lasers; electron beams; electrical discharge machining; chemical etching; high speed routers; fine pressing; diamond tooling, ultrasonic abrasive machining. Each technique has advantages and limitations compared to alternative techniques. The advantages that abrasive waterjet based machine tools bring to micro machining include:

- Easily programmed to profile a wider range of materials than any other technique

- Good cut edge quality, free of heat affected zones and edge distortion
- Ability to profile thin, brittle materials, such as thin glasses for use in electronics
- Low capital cost compared to lasers, allowing application in small workshops, such as jewellery manufacture
- Complementary to micro machining lasers in a job shop environment
- Allow existing abrasive waterjet job shops to extend the machining capabilities that they can provide without the need for major capital expenditure.

Because of these advantages and the fact that micro abrasive waterjet machine tools may not be perceived as a major capital expenditure, the market potential for micro abrasive waterjets is substantial.

6. DEVELOPMENT STRATEGY

It is now established that there are applications for micro abrasive waterjets in micro machining and in profiling and drilling of thin materials. Exploitation of the technology requires that micro abrasive waterjet equipment becomes dependable in terms of usability, reliability, maintainability, serviceability, safety, compliance with legislation and availability.

Currently all development work is aimed at achieving dependability for the first generation systems based on 40 to 60µm diameter jets. Particular areas of development include:

- Abrasive preparation to avoid contaminants blocking nozzles
- Nozzle bore shapes and mounting of nozzles
- Sequencing of control valve operations
- Manufacturing methods for valves and other components.

Future developments will include operation with smaller jet diameters, feeding nozzles remote from the abrasive storage vessel and developing a flow circuit for milling operations. Considerable work is required on work piece holding and support, particularly when cutting parts that may be less than a millimetre in diameter.

7. CONCLUSIONS

- Micro abrasive waterjets act like minaturised versions of conventional abrasive waterjets.
- Micro machining is a growing multibillion-dollar market that needs the proven machining capabilities of abrasive waterjets.
- All of the machine tool technologies to exploit micro abrasive waterjets are available.
- Exploitation is dependent on easy to use and reliable micro abrasive waterjet systems being available.
- A design for the first generation of micro abrasive waterjets has been developed that is easy to use and a strategy is being followed in building up system reliability.

8. REFERENCES

Miller, D. S., Claffey, E., Grove, T., “Technology Package for Abrasive Waterjets” BHR Group Limited, 1996.

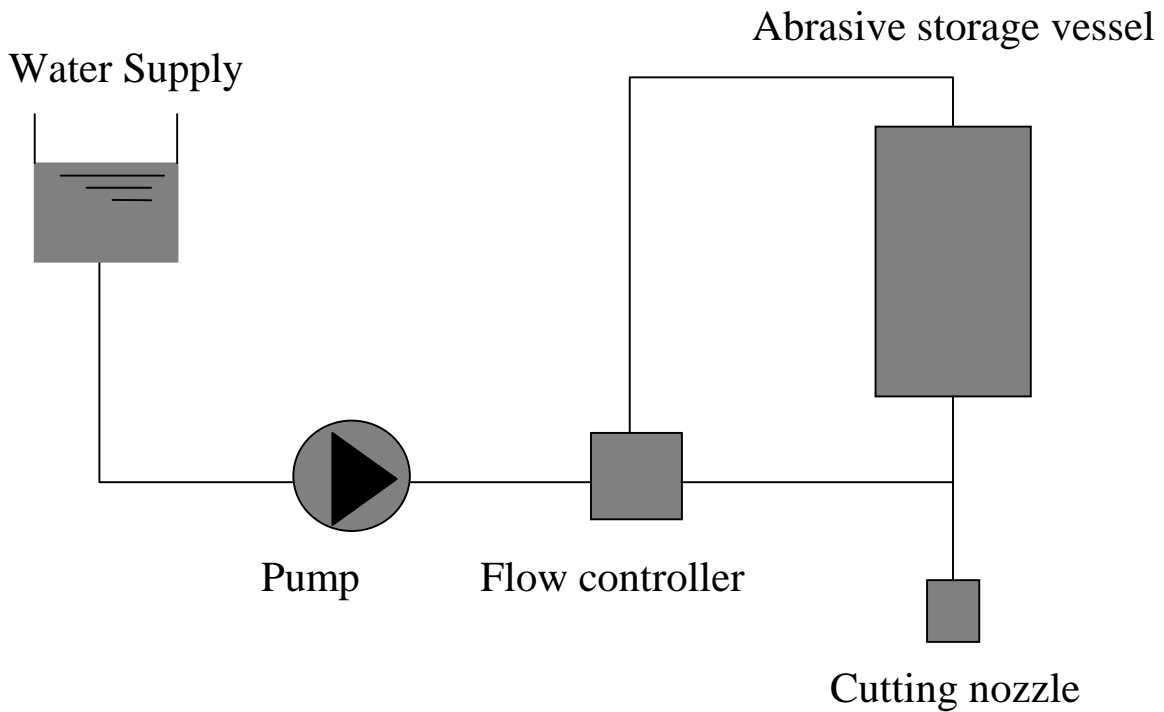


Figure 1. Micro Abrasive Waterjet Flow Circuit

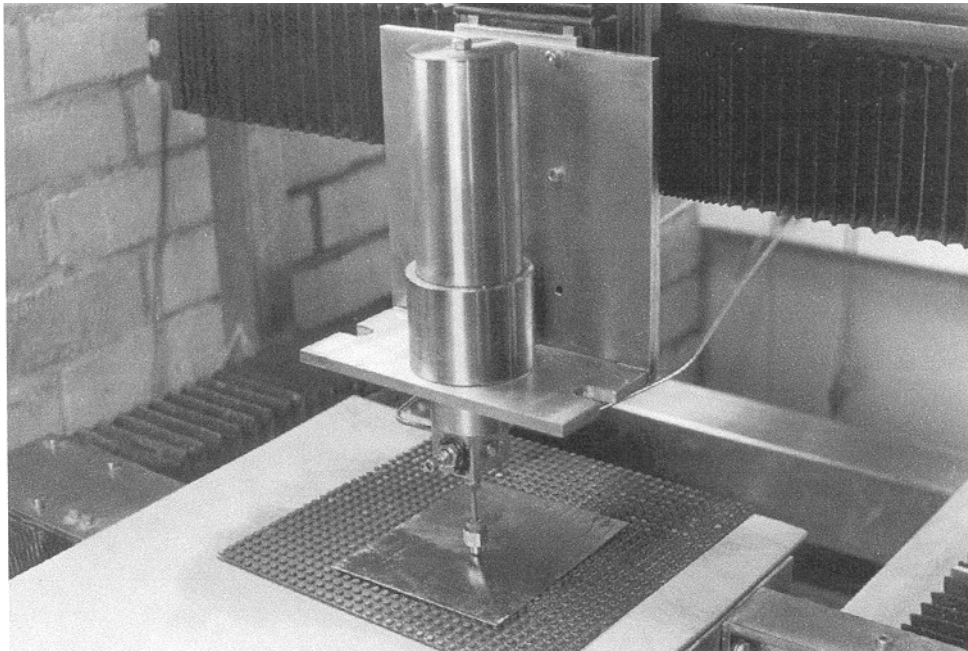


Figure 2. Abrasive Storage Vessel and Cutting Nozzle

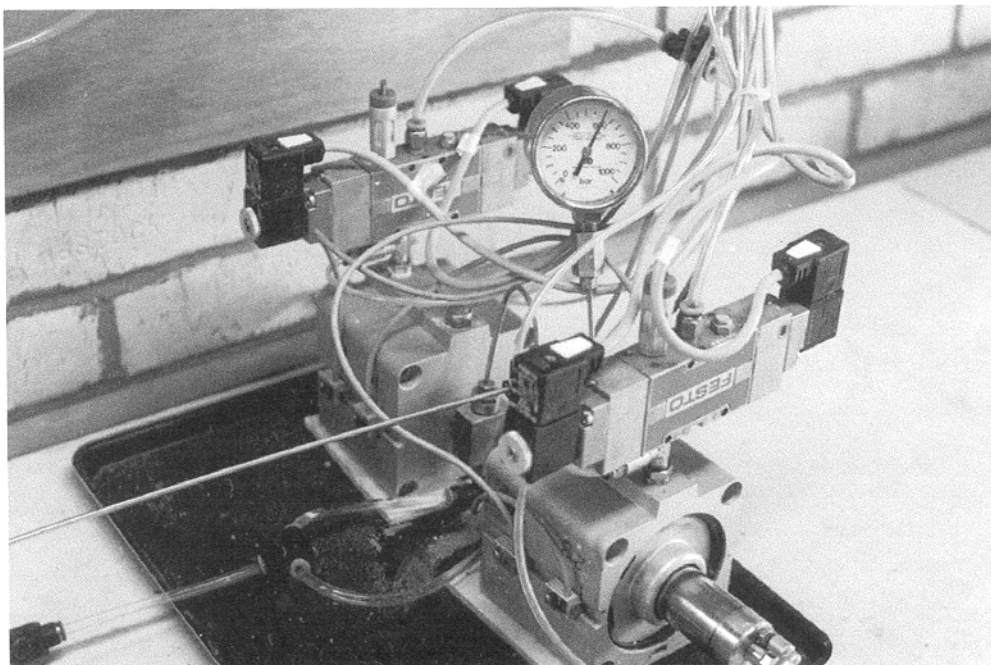


Figure 3. Pumping Unit

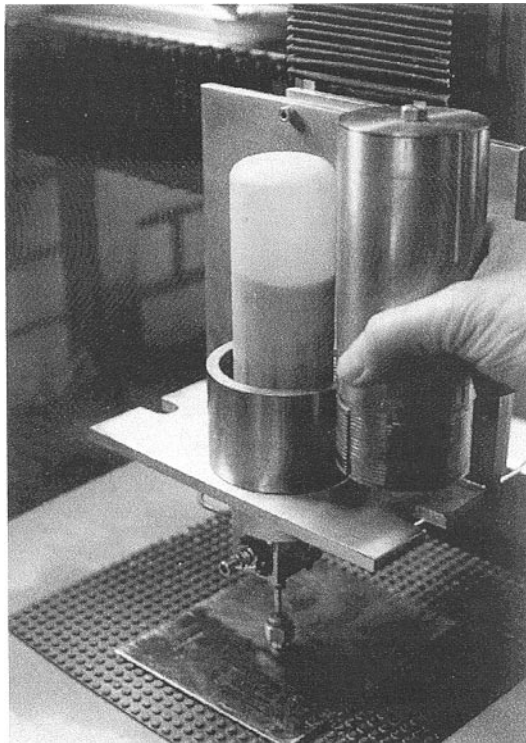


Figure 4. Abrasive Storage Vessel with Barrel Removed

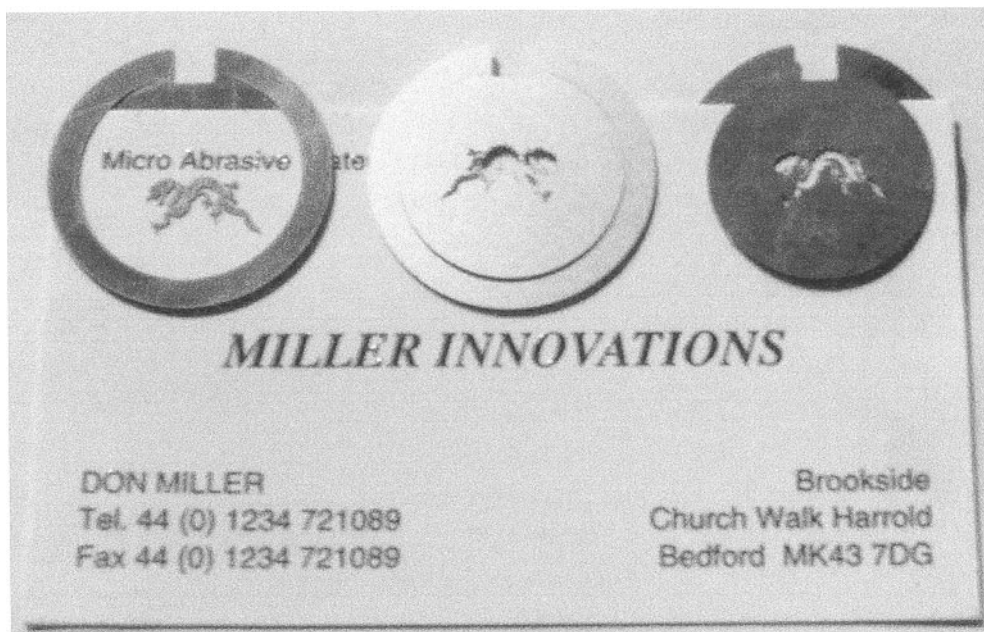


Figure 5. Dragon Test Piece



Figure 6. Test Piece Cut Out

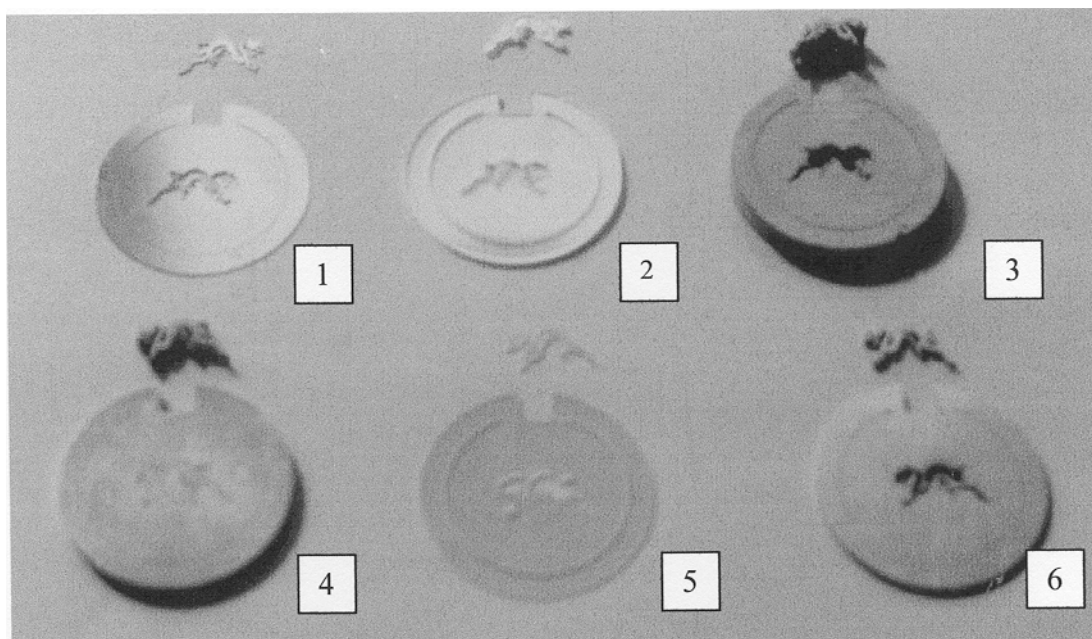


Figure 7. Test pieces in different material (4, 5 and 6 shown from the jet exit side)

CUTTING OF HOLLOW STRUCTURES WITH POLYMER SUPPORTED ABRASIVE WATER SUSPENSION JETS

H. Louis and Ch. von Rad
Institute of Materials Science
University of Hannover, Germany

ABSTRACT

Abrasive Water Suspension Jets have been successfully established for dismantling and decommissioning purposes. Due to the fact, that practically any material can be cut, this technique is superior to most others.

However when cutting hollow structures consisting of solid material and air the cutting efficiency and cutting quality decreases rapidly after passing the hollow part. This is caused by the fact, that the jet spreads after leaving the solid material. The cut in the upper part of the structure acts as a “bad” nozzle. A possibility to minimise this effect is cutting under water. This however also leads to a loss of cutting efficiency. Another solution is the addition of polymers to Abrasive Water Suspension Jets. This leads to an increase of jet coherence and the cutting efficiency. This effect especially can be observed when cutting hollow structures.

The effect of different polymers and relevant parameters on the cutting quality and cutting efficiency has been studied and will be presented in the following paper.

1. INTRODUCTION

Abrasive waterjets are a multifunctional tool, which allows to process practically all technical materials including metals, ceramics and compound materials (Brandt et al., 2001). The abrasive waterjets are not only a tool used for cutting. It is also used for removal, milling, turning or drilling (Brandt et al., 2001). Therefore there are wide application fields for this technology. Abrasive waterjets are contactless cutting method leading to low reaction forces, on the other hand this leads to disadvantages when cutting hollow structures, because the jet loses coherence and efficiency (Louis et al., 2000).

One very promising approach to increase not only the efficiency of abrasive waterjets but also its stability is the addition of long chained polymers to the water. They have been successfully used in the 70s in order to improve the jet coherence and the cutting efficiency of pure waterjets (Franz, 1972; Howells, 1983). Additionally these polymers lead to a reduction of pipe friction in tubes and hoses (Howells, 1983; Howells, 1990) and to a reduced sedimentation of abrasive particles in the tubing system. The effect of these polymers on abrasive water suspension jets – especially in the case of cutting hollow structures is presented in this paper.

2. POLYMERS IN WATERJET TECHNOLOGY

In the 70s jet cutting activities were limited to pure waterjets. Therefore the range of materials to be cut and the cutting efficiency were also limited. In order to enhance the cutting efficiency (i.e. to increase cutting speed) and to extend the range of target materials, long chained polymers were added to the water. These approaches were very successful. Three mechanisms leading to these improvements have been investigated (Franz, 1972; Howells, 1983).

1. Drag reduction: The interaction of long chained polymer molecules with the eddies of the pipe flow reduces the degree of turbulence and decreases the friction in a hose or pipe.
2. Increase of jet coherence: The improved jet stability leads to an increase of the density of the hydraulic power – especially at large standoff distances.
3. Macromolecular bombardment: Agglomerates of large molecules with bonded water molecules hit the surface with supersonic speed, which enhances the material removal.

A large number of applications of additives was polymerblasting for cleaning and removal processes like cleaning of hydro-processing reactors, cleaning of heat exchangers or removal of coke. But also the cutting process was significantly enhanced by the use of additives. This allows the reduction of pressure, an increase of traverse rate and improvements of cutting quality (Howells, 1990).

The transfer of these approaches has been made very consequently. Polymers have been used to enhance the performance of abrasive water injection jets (AWIJ) and to create an abrasive water suspension jet (AWSJ) in the principle of direct pumping (Hashish, 1991). However the potential

of polymers for the efficiency and jet coherence of AWSJs in the bypass principle, which are used for many challenging cutting tasks in decommissioning and dismantling applications has been investigated quite recently (Louis et al., 2001).

3. GENERATION OF POLYMER SUPPORTED AWSJs

Abrasive water suspension jets (AWSJs) are the latest development of abrasive waterjets. Their major application fields are dismantling and civil engineering as well as decommissioning offshore and subsea, where thick and complex structures are very common.

AWSJs are mainly generated by leading a bypass of the pressurised water through a high pressure storage vessel filled with abrasive material. By impulse interaction between the bypass flow and the storage vessel an abrasive slurry is carried out, which recombines with the main flow forming the cutting suspension. This finally is accelerated in the suspension nozzle and can be used to cut (Figure 1).

The use of polymers instead of water for the generation of AWSJs is simple. The pump used works in the bypass principle. The water container, which normally is filled with water, is filled with a polymer solution instead. The solution is pre-pressurised by a centrifugal pump, and then set under working pressure by the plunger pump. Part of the flow, which is not used for the jet is lead back into the container (Figure 1).

The selection of polymers to be used for the experimental investigations was determined by two criteria.

1. Results of small scale experiments during a pre-selection phase
2. To cover a wide range of different chemical and rheological properties

The polymers used are listed in Table 1.

The polymers form a solution in water, each polymer molecule binds a certain number of water molecules, which leads to an increase of viscosity and viscoelasticity. Since the polymers are delivered as a powder or granulate or as an emulsion, they have to be dissolved in water. This hydration process requires several minutes for building up the structures between the polymer and the water molecules.

The polymer molecules however are, sensitive to shear stresses, which can lead to their degradation. This leads to a loss of their efficiency. Since the shear stresses in the centrifugal pump and in the plunger pump (Figure 1) are not negligible and part of the solution due to the bypass principle of the pump even is exposed several times to the stress, the results obtained with the system can be considered as worst case studies. Therefore any system avoiding one of these disadvantages, can be expected to lead to even better results.

This method of polymer addition is simple to apply, but not very effective. Therefore recently a system of direct additive injection under working pressure, which avoids this disadvantage has been developed (Bortolussi et al, 2001).

4. CUTTING EFFICIENCY IN COMPACT MATERIAL

Cutting experiments investigating the influence of polymers on the cutting efficiency of abrasive water suspension jets have been carried out like in (Louis et al., 2001). All experimental parameters were kept constant except the type of additive and the additive concentration. The experimental parameters are given in the list below:

pressure:	$p = 65 \text{ MPa}$
abrasive flow rate:	$\dot{m}_p = 2 \text{ kg/min}$
traverse rate:	$v_f = 400 \text{ mm/min}$
nozzle diameter:	$d_{SD} = 1 \text{ mm}$
abrasive material:	Barton Garnet HP 80
sample material:	AlMgSi0,5

The results of the experiments are given in Figure 2.

The addition of all polymers used lead to a significant increase of cutting efficiency. However two main phenomena could be observed. On one hand the positive effect on the cutting efficiency of the polymer depends on the type of polymer, on the other hand the effect depends on its concentration.

The increase of cutting efficiency can be explained by two different effects. From non-abrasive waterjets it is known, that polymers in aqueous solution can lead to a significant increase of jet coherence (Franz, 1972; Howells, 1983). This increase of jet coherence leads for AWSJs to an increase of the density of the hydraulic and abrasive load and therefore to an increase of efficiency. On the other hand polymer solutions have different rheological properties from water, for example an increased viscosity. This leads to a stronger interaction between the fluid and the abrasive particles during the acceleration process in the suspension nozzle. The improved acceleration process increases the velocity of the abrasive particles, which strongly influences their removal potential.

In order to limit the experiments of cutting hollow structures to a sensible amount. An optimal polymer concentration was selected for the further experiments. The selection was determined by three criteria.

1. Cutting efficiency
2. Polymer consumption (costs)
3. Limitation of the pump (processable viscosity)

The additive concentrations selected are given in Table 2.

5. CUTTING EFFICIENCY IN HOLLOW STRUCTURES

In order to investigate the influence of polymers for the cutting of hollow and complex structures with AWSJs, a simulated hollow structure was build up. It consists of an upper plate, a hollow

distance and a sample underneath (Figure 3). The jet structure and efficiency can be evaluated by the damage profile in the sample. The experimental setup allows to vary the upper plate thickness and material, the hollow distance, the medium in the gap (air or water) and the sample itself.

The main target of the investigations is the effect of polymers when cutting hollow structures with AWSJs. Therefore most cutting and sample parameters were kept constant.

pressure:	$p = 70 \text{ MPa}$
abrasive flow rate:	$\dot{m}_p = 2 \text{ kg/min}$
traverse rate:	$v_f = 250 \text{ mm/min}$
nozzle diameter:	$d_{SD} = 1 \text{ mm}$
abrasive material:	Barton Garnet HP 80

upper plate thickness:	$d_{up} = 10 \text{ mm}$
sample material:	AlMgSi0,5

The parameters varied were:

polymer:	Polyox 0,5%, Praestol 0,3%, Bermocoll 0,4%, Super-Water® 0,3%
hollow distance:	$h = 0 \dots 30 \text{ mm}$
medium:	air, water

The results of the cutting experiments in air are given in Figure 4, where the separated material thickness (upper plate thickness + depth of kerf in the sample) are plotted against the hollow distance for the different fluids used.

As to be expected the separated material thickness decreases with increasing hollow distance. This can be explained by the fact, that the lower edge of the upper plate acts as a bad nozzle. The jet loses coherence and efficiency (Louis et al., 2000).

However in general the cutting efficiency could significantly be improved by the addition of polymers to the jet. Still there are significant differences in the cutting efficiency of the different polymers used. The highest increase of cutting efficiency is achieved by Polyox followed by Praestol, Bermocoll and Super-Water®. Compared to water in compact material the separated material thickness is increased by 68% with the use of Polyox. In hollow structures with a gap of 30 mm air the effect is even stronger. The use of Polyox increases the cutting efficiency by 80% in comparison to pure water.

The same experiments were carried out under submerged conditions. This has the effect, that especially in the gap the jet has to interact with the gap medium water. The polymer influence on the cutting efficiency is shown in Figure 5.

Compared to the decrease of cutting performance of air-filled hollow structures the decrease under submerged conditions is significantly stronger. This is due to the fact, that the jet has to interact with the medium 800 times denser than air (Louis et al., 2000).

As in air all polymers used lead to an increase of the cutting performance in compact material as well as in hollow structures. The increase in comparison to water is even stronger than in air-filled hollow structures. At a gap of 30 mm water the use of Polyox increases the separated material thickness by 111%. Again Polyox leads to the strongest increase followed by Praestol, Bermocoll and Super-Water®.

6. JET COHERENCE IN HOLLOW STRUCTURES

Polymers increasing the rheological properties like viscosity and viscoelasticity not only are expected to increase the efficiency but also the coherence and stability of waterjets and abrasive waterjets. This is of high importance not only for cutting hollow and complex structures, but also for applications, where a high standard of cutting quality and accuracy are required (e.g. for machining).

On the other hand the results on the jet coherence can give a statement about the mechanisms of increasing the cutting efficiency – due to improved jet coherence and/or due to improved particle acceleration. If the polymer does not increase the jet coherence in comparison to water, the efficiency increase is determined by the improved particle acceleration.

The increase of jet coherence can be determined by measuring the width of kerf in the sample below the hollow distance. Figure 6 shows the influence of an air-filled gap on the cutting width of the lower sample (see Figure 3) for different fluids.

A general increase of the cutting width with increasing hollow distance can be observed. The reason for this is the natural divergence of the jet, which is caused by the lower edge of the upper plate acting as a bad nozzle (Louis et al., 2000).

All polymers used lead to a decrease of the cutting width (i.e. an increase of jet coherence). However there is a strong influence of the driving fluid on the coherence of AWSJs. In a 30 mm air-filled gap an AWSJ driven by water diverges 2,2 mm. Under the same conditions a Super-Water® driven jet diverges 2,0 mm, but a Polyox driven jet diverges only 0,45 mm. Obviously the jet coherence of Polyox is significantly higher than of the other additives used.

7. CONCLUSIONS

The cutting results are summarised in Figure 7. It shows the ratio between the cutting performance of additive supported AWSJs and conventional AWSJs for cutting compact material, for hollow structures with a 30 mm air-filled gap and for one with a 30 mm water-filled gap with the experimental parameters as above.

Generally all polymers used lead to a significant efficiency increase at all conditions tested. In all cases the highest efficiency is achieved by Polyox followed by Praestol, Bermocoll and Super-Water®.

Supporting AWSJs by polymers there are two mechanisms enhancing the efficiency:

1. Improved acceleration process of the abrasive particles
2. increased jet coherence

The highest increase of jet coherence was achieved with Polyox, shown by a very small increase of cutting width. This is of advantage especially under submerged conditions, where the jet interacts with a surrounding medium of high density.

The other polymers used also lead to an increase of jet coherence, however their improved cutting efficiency is based to a large extent on an improved acceleration process of the abrasive particles in the nozzle.

Due to the strongest effect on the jet stability Polyox is the polymer leading to the best results for cutting applications – especially for cutting hollow structures.

8. SUMMARY

The paper shows the influence of polymers supporting AWSJs when cutting hollow structures – consisting of two plates with a gap filled with air or water. The following observations were made.

- Polymers increase the cutting performance in compact material up to 68% and in hollow structures up to 111%.
- The upper plate of the hollow structure acts as a bad nozzle, therefore the gap leads to a loss of cutting efficiency.
- Due to the interaction between the jet and the gap medium, the efficiency loss under submerged conditions is stronger than in air.
- The efficiency increase caused by the use of polymers is based on two effects:
 - a) improved particle acceleration in the nozzle
 - b) increased jet coherence
- Especially when cutting hollow structures under submerged conditions the effect of increased jet coherence is of importance. The best results were achieved with Polyox. This corresponds to the results of the cutting width, which were – compared to all other fluids tested - the smallest.

9. ACKNOWLEDGEMENT

The authors are part of the Waterjet Laboratory Hannover (WLH) and members of the German Working Group of Waterjet Technology (AWT).

10. REFERENCES

- Bortolussi, A., Ciccu, R., Louis, H., von Rad, Ch., "Additives improve efficiency of abrasive water suspension jets," *Proceedings of the 7th European Conference on Advanced Materials and Processes*, The Federation of European Materials Societies, 2001.
- Brandt, S., Louis, H., Milchers, W., Mohamed, M., Pude, F., von Rad, Ch., "Abrasive waterjets – a multifunctional tool for advanced materials," *Proceedings of the 7th European Conference on Advanced Materials and Processes*, The Federation of European Materials Societies, 2001.
- Franz, N. C., "Fluid additives for improving high velocity jet cutting," *Proceedings of the 1st International Conference on Jetting Technology*, pp. A7/93-A7/104, BHRA Fluid Engineering, Cranfield, England, 1972.
- Hashish, M., "Cutting with high-pressure abrasive suspension jets," *Proceedings of the 6th American Waterjet Conference*, pp. 439-455, Water Jet Technology Association, St. Louis, Missouri, 1991.
- Howells, W. G., "Polymerblasting – a chemist's point of view," *Proceedings of the 2nd US Waterjet Conference*, pp. 443-447. University of Missouri-Rolla, Rolla, Missouri, 1983.
- Howells, W. G., "Polymerblasting with Super-Water from 1974 to 1989: a Review," *International Journal of Water Jet Technology*, Vol. 1, pp. 1-16, 1990.
- Louis, H., von Rad, Ch., "Cutting of hollow structures with abrasive water suspension jets," *Proceedings of the 15th International Conference on Jetting Technology*, pp. 59-65, BHRA Fluid Engineering, Cranfield, England, 2000.
- Louis, H., von Rad, Ch., "Additives improve efficiency of abrasive water suspension jets," *Proceedings of the 7th European Conference on Advanced Materials and Processes*, The Federation of European Materials Societies, 2001.

11. TABLES

Table 1: Polymers used and their chemical properties

Name	Chemical substance	electric charge	molecular mass	degree of ramification
Praestol 2540	Polyacrylamide with some arcrylate monomer	anionic	$14 \cdot 10^6$	weakly ramified
Bermocoll E481G	Ethylhydroxyethylcellulose	no electric charge	670 000	voluminous structure
Polyox Coagulant	Polyethyleneoxide	no electric charge	$5 \cdot 10^6$	linear molecule
Super-Water®	Polyacrylamide with some arcrylate monomer	no electric charge	$16-18 \cdot 10^6$	weakly ramified

Table 2: Optimal polymer concentrations

Additive	Optimal concentration
Polyox	0,5 %
Praestol	0,3 %
Bermocoll	0,4 %
Super-Water®	0,3 %

12. FIGURES

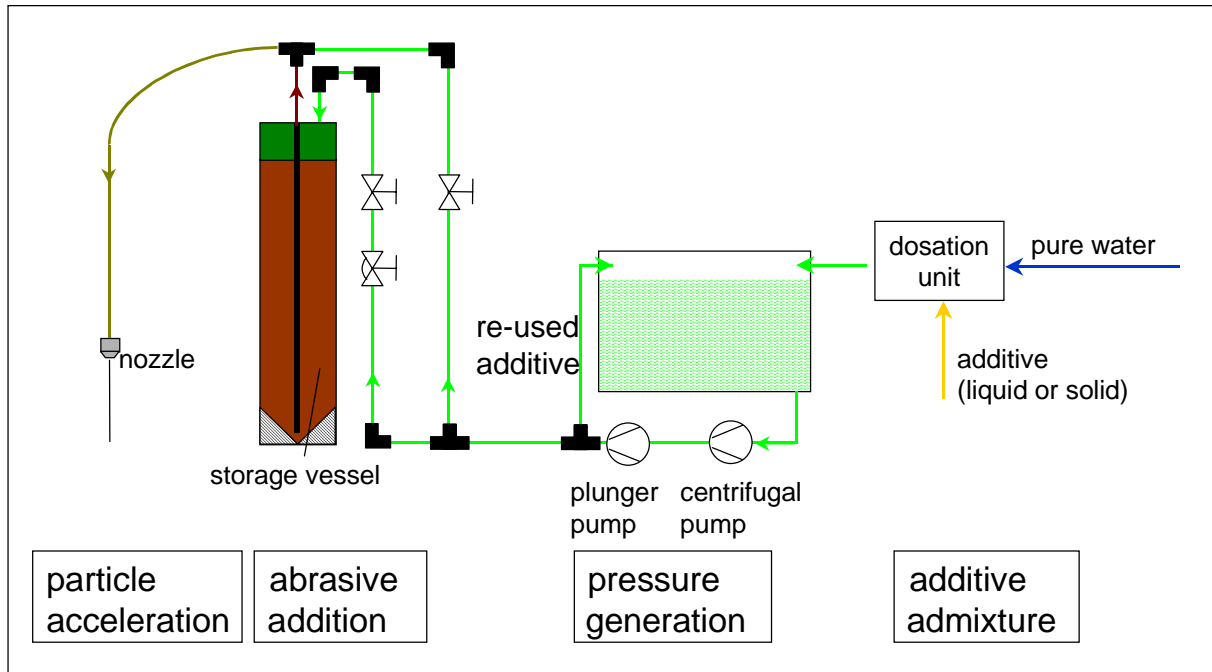


Figure 1: Generation of polymer supported AWSJs

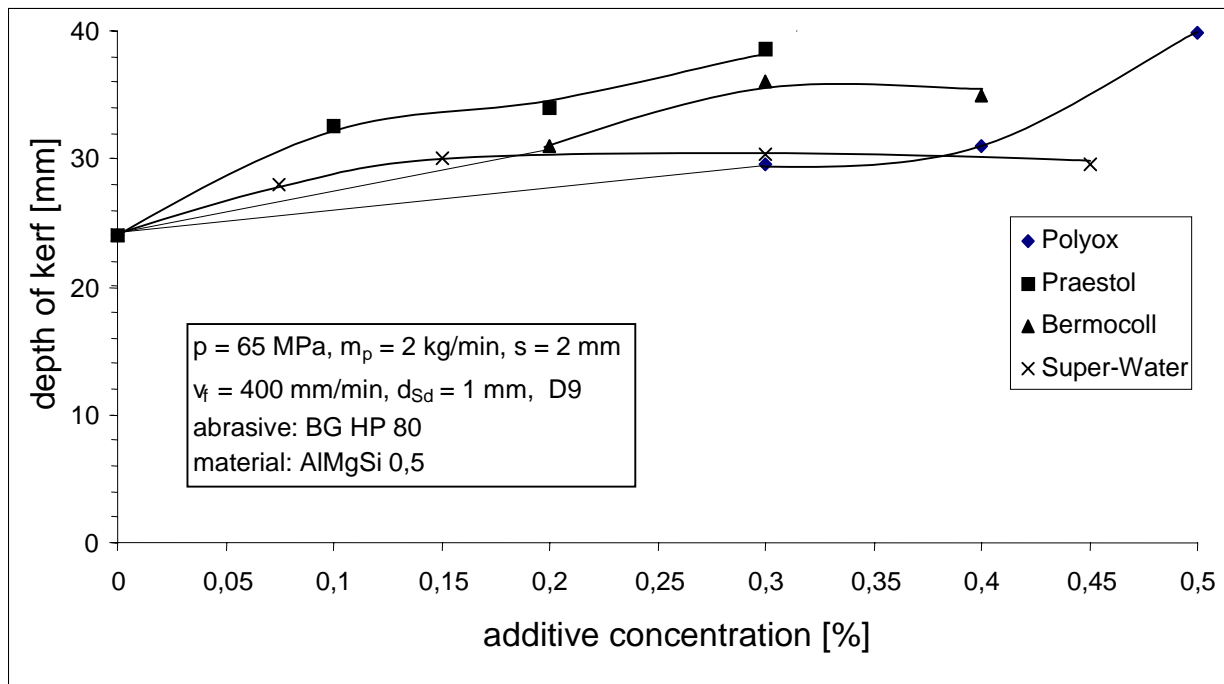


Figure 2: Influence of polymers on the cutting efficiency of AWSJs in compact material

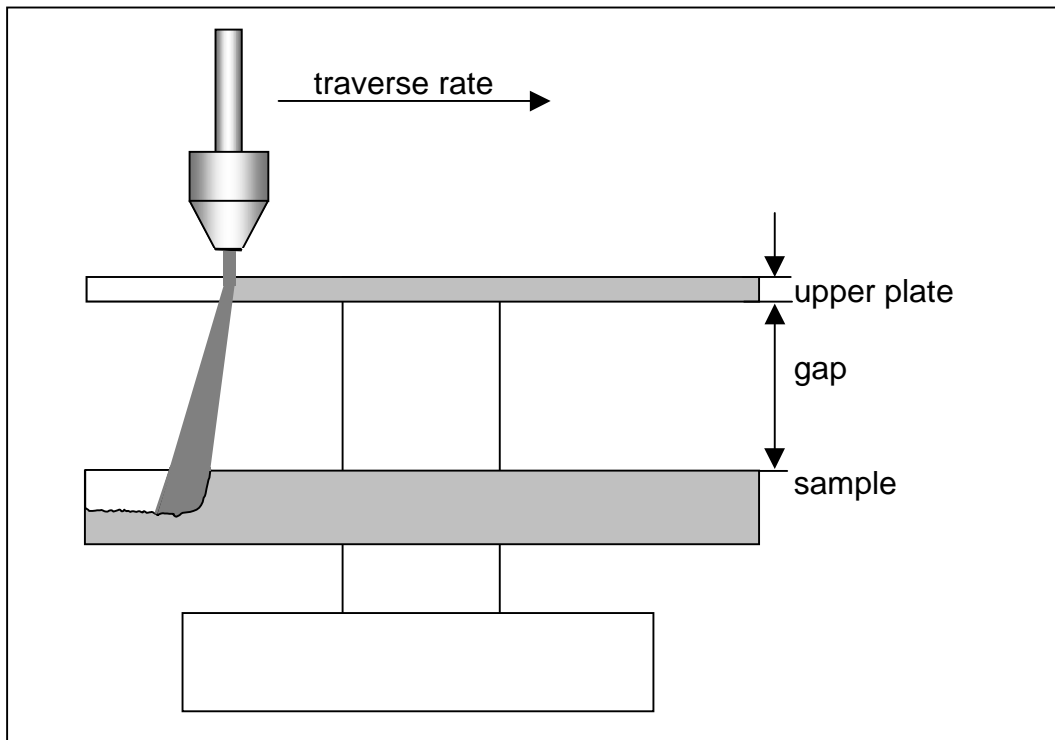


Figure 3: Experimental setup for cutting hollow structures

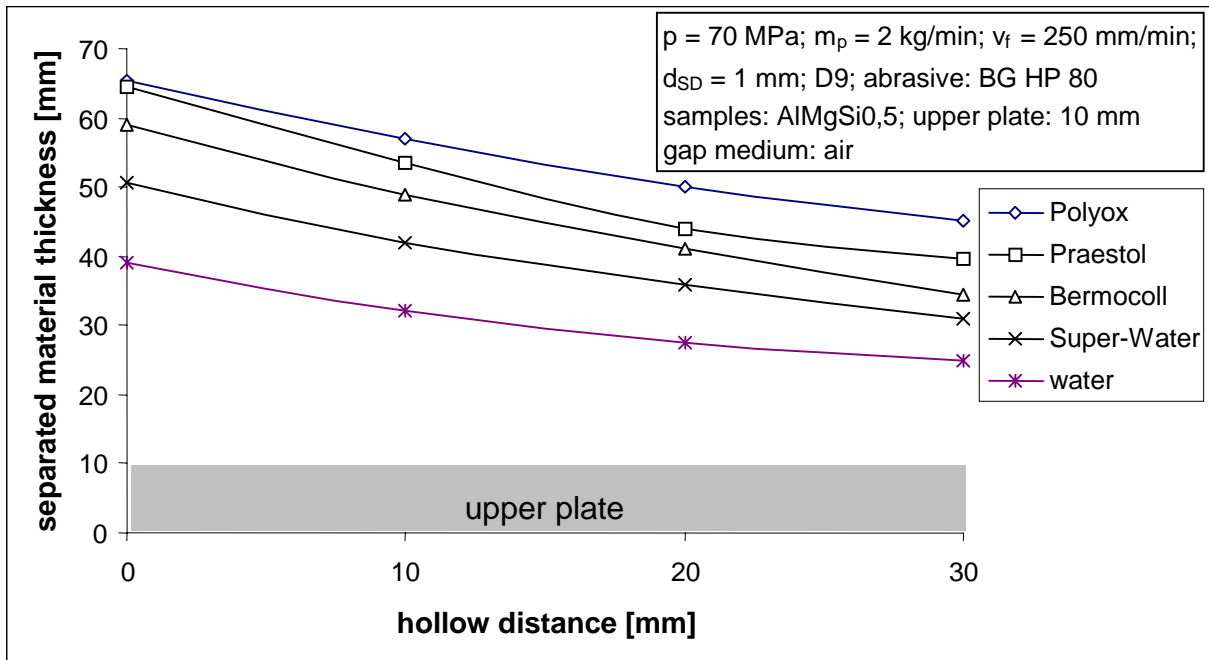


Figure 4: Cutting efficiency of polymer supported AWSJs in hollow structures (air)

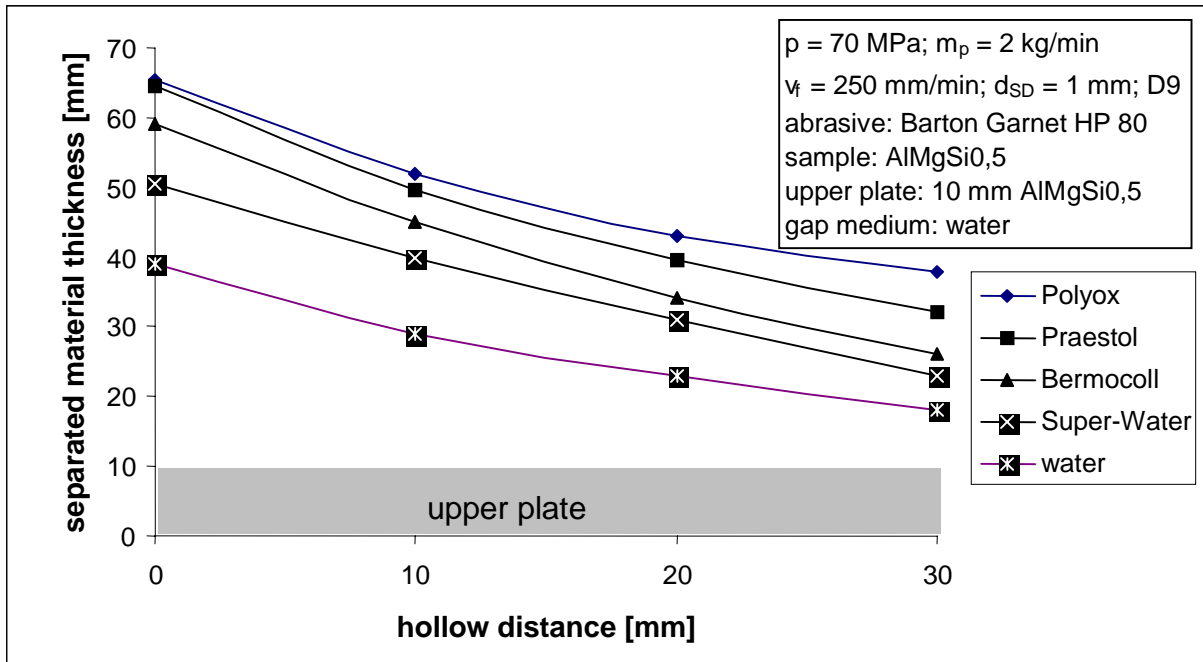


Figure 5: Cutting efficiency of polymer supported AWSJs in hollow structures (water)

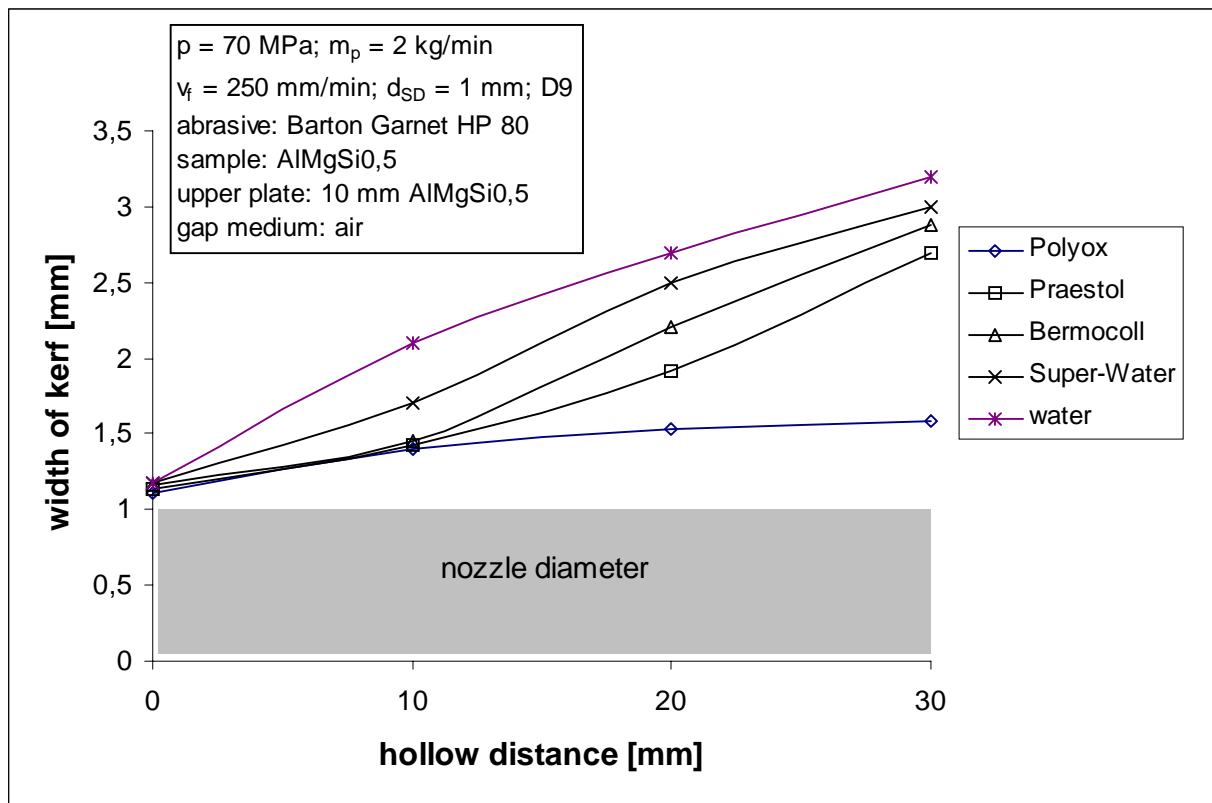


Figure 6: Jet coherence of polymer supported AWSJs in hollow structures (air)

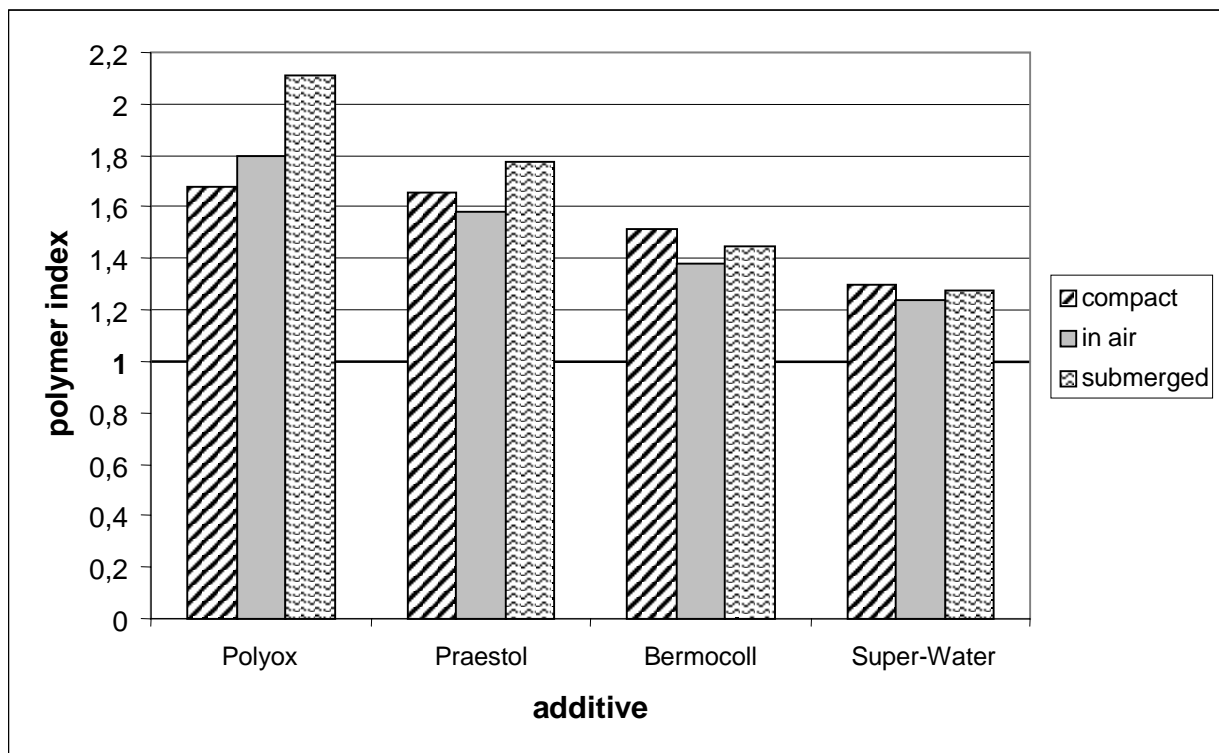


Figure 7: Polymer index for cutting compact material and hollow structures

CUTTING OF REINFORCED CONCRETE USING ABRASIVE SUSPENSION JET

A. Bortolussi, R. Ciccu, B. Grosso

DIGITA, Department of Geoengineering and Environmental Technologies
CSGM, Mineral Science Study Centre of CNR
University of Cagliari, Italy

ABSTRACT

Interest is growing in the world for finding a suitable technology capable of cutting concrete structures safely and economically. Such a technology would enable buildings to be partially or totally dismantled according to a sort of “cut-and-draw” method with minor interference with the surroundings. For this purpose the choice is practically restricted to diamond wire and to abrasive suspension jet.

Accurate cuts can be made with DW irrespective of the thickness of the concrete element, with low noise and no dirt spreading around the place. However the system is relatively burdensome and requires a long installation time and a close control of the operation.

On the other side ASJ demands large amounts of abrasive that must be dealt with properly using a catcher, but it is easier to install and to operate safely from distance.

In order to compare the performance of the two competitor technologies a number of cutting tests have been made on reinforced concrete beams under variable experimental conditions (rope tension and push-down force with DW; pressure, nozzle diameter, abrasive mass flowrate and traverse velocity with DIAJet).

Results are compared in terms of cutting rate as well as of unit cost of cutting in order to identify the most promising field of application and the optimum operational conditions for each technology.

1. INTRODUCTION

Demolition aimed at recovering the space occupied by obsolete or crumbling structures is today a common practice in the frame of new urban upgrading plans.

In addition to this, the high price and the scarce availability of the surface, especially in the city centres and business districts, suggest the erection of new towering buildings in order to take the best advantage of the area, replacing traditional low storeyed civil constructions.

On the other hand, this urban renovation process is somewhat slackened by the interest in safeguarding the historical sites and the architectural issues of the past, while special problems may arise due to the proximity of nearby structures, the presence of technological networks to be kept unharmed and the interference with the normal activity in the immediate surroundings.

In the case of factories swallowed by urban expansion, the demolition becomes mandatory unless the structure is converted to a public fruition in all cases when relevant values of industrial archaeology are recognised. In this latter case the building only requires a thorough surface renovation that can be carried out in a faster and cheaper way and with very good results by using high pressure plain waterjet (hydrodemolition).

Finally demolition can be addressed to a variety of public works and infrastructures such as motorways and railroads, bridges, tunnels, reservoirs, storage silos, cisterns, pipelines, electric lines, dams and so on, if they are no longer adequate to the ever growing traffic needs and to the higher level of service demand.

In face of the great diversity of the structures to be demolished, related to their shape and size as well as to the nature and complexity of the materials employed (concrete, bricks, steel, composites), suitable solutions can be found using a number of methods, the choice among which is made on technical and economic grounds, under safety and environment restrictions, taking into account the specific conditions of the site.

In particular, the decision is influenced by the characteristics of the demolition products which also depend on the method and technologies employed, especially on the selectivity features of each of them. In fact, the problem can only find optimum solution provided that adequate care is taken in the design and the development of all the different interconnected steps: dismounting, loading, transportation and disposal or reuse of the debris.

2. DEMOLITION METHODS AND TECHNOLOGIES

In order to evaluate the potential of high pressure abrasive suspension jet for demolition purposes it seems useful to anticipate a short review of the various technologies, pointing out for each of them the advantages and drawbacks encountered and the respective field of application.

For this purpose, demolition methods can be classified into three main categories based on the development of the operations which essentially depends on the form of energy applied and on the possibility of its control.

2.1 Techniques of mass disintegration

They make use of explosives with a more or less disruptive action which provokes the sudden collapse by gravity of the entire structure rendered unstable through the rupture of the hyperstatic bonds in suitably selected pillars and beams.

This implies a careful study of the structure and the evaluation of the kind and quality of the constituent materials in order to select the critical points where adequate charges should be placed. The outcome depends on the correct design of the blasting plan with scanty possibility of remedy to any possible errors.

The implosion debris form a huge heap, the mucking of which generally takes a long time and requires a further breaking of larger elements using other technologies.

For a rapid destruction of tall buildings having considerable elevation, a big implosion can represent the only viable solution. This is also the case of monolithic concrete items such as chimneys and stacks, towers, walls, pillars and thick beams, for which blasting is the first step followed by splitting and severing stages of the toppled-down sections. It becomes unrivalled in all instances where the access of machines is hindered, difficult or unsafe. In the case of smaller structures other purpose-tailored competitor methods are likely to become preferable.

The demolition cost based on explosive blasting can be relatively low only if resulting debris are easily mucked away and disposed of.

2.2 Techniques of controlled dismantling

Based on the use of mechanical equipment they lend themselves to the demolition of structures having a relatively small elevation within the reach of the active tool.

For the higher parts of the structure the use of impacting heavy bodies with swinging movement is often the simplest solution. For the lower parts it is more convenient to employ earth moving machines, like crawler tractors with pull rope or back-hoe excavators equipped with hydraulic hammer supported by the articulated boom, standing on the floor at safety distance.

The work is efficiently carried out in the case of light structures possibly weakened by explosive charges at selected points. The operation is controlled very well by the machine operator.

2.3 Techniques of cutting and disassembly

Material selectivity can be optimised by applying demolition methods based on cutting operations which also produce a lesser impact on the environment.

Instead of destroying the entire structure or progressively dismantling it with mechanical tools, the constituent elements are individually severed and withdrawn according to a process of ordered disassembly from top to bottom. Each element can be reused as such or treated for alternate uses.

With this “cut-and-draw” method, the formation of debris stockpiles is avoided since each element is put to ground by means of a crane and directly loaded onto the truck platform, thus overcoming the problem of dealing with heterogeneous materials often entangled and difficult to handle.

The disturbances (dust, noise, vibration) are substantially avoided and safety conditions in the working area acceptable (absence of projections, better control of structural failures).

The overall time required is generally very long depending on the size and complexity of the structure, although it can be shortened by multiplying the resources employed since there is a perfect compatibility of many machines working within the same area.

Not taking into account the simple manual tools (diamond blade for shallow cuts, oxyhydrogen flame for thermal cutting of metals, shearing of cables and re-bars) the cutting technologies available for the job are restricted to diamond wire and to abrasive suspension jet.

In order to compare the performance of these competitor technologies a plan of cutting tests has been carried out at the DIGITA Laboratories on samples of reinforced concrete having the following characteristics:

- Cross section: $0.3 \times 0.3 \text{ m}^2$
- Density: $2,350 \text{ kg/m}^3$
- Re-bars: Two sets of three steel elements 10 mm in diameter (see fig. 2)
- Top size of aggregate: 20 mm
- Aggregate composition: mixed (limestone and granite)

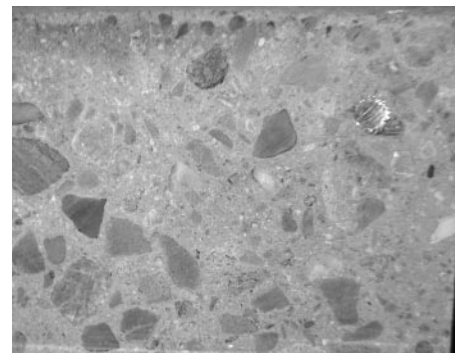
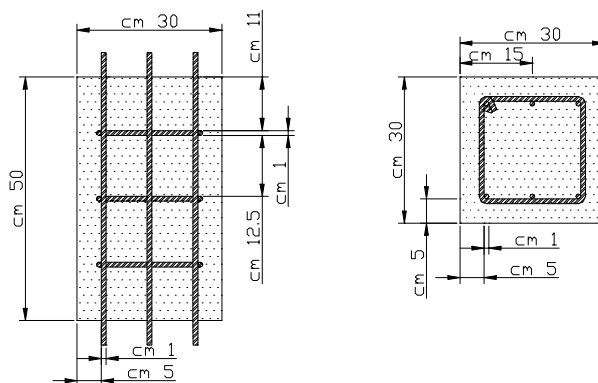


Figure 1. Size of the test sample and close view of the cross section cut with diamond blade

3. CUTTING WITH DIAMOND WIRE

Diamond wire, widely employed in the extraction of dimensional stone blocks (marble, granite) from the quarry face as well as in some further stage of stone processing, has recently been proposed for demolition purposes. Successful results can be achieved especially in those cases where only a part of the structure must be removed, while leaving the rest intact.

The cut is made by embracing the perimeter of the section to be cut and applying a pull-back force to the machine (loop cutting) or by pushing the wire with the help of a pair of driving pulleys against the leading edge of the cut (penetration cutting). The wire is moved at a relatively high peripheral speed (20 - 30 m/s) by means of a flywheel of adequate power (some tens of kW). The tool is cooled by injecting water into the slot. The surface obtained is very smooth and cutting rate is substantially independent of the shape and size of the cut section.

In order to reduce the length of wire and for a better visual control of the process the machine and the operator should stay at close distance from the cutting area with all the consequent implications.

3.1 Experimental tests

3.1.1 Equipment

Cutting tests with diamond wire have been done using a tool for granite consisting of a steel rope wrapped by a protective plastic sheath to which the beads (40 per metre) are fastened.



Figure 2. Overall view (left) and a detail (right) of the Diamond Wire cutting frame

The wire is wound in closed loop around the flywheel driven by an electric motor and a tail sheave at the opposite ends of a beam moving vertically along a pair of columns. The idler pulley can be displaced sideways by means of a pneumatic piston enabling to adjust the tension of the rope.

The lower section of the wire is pushed downwards against the sample with a known force imparted to the beam by a pair of electric motors through screw-volute couplings. The sample is placed onto the base platform and kept fast with a holding fixture.

The equipment used for the tests at the DIGITA Laboratories is shown in Figure 2.

3.1.2 Experimental plan

In order to single out the optimum conditions for cutting reinforced concrete, the chief setting parameters have been varied as follows:

- Pull-back force on the tail sheave: 1,000 and 2,000 N
- Downwards penetration (drop) velocity of the wire: 2, 3, 4 and 5 cm/min

Peripheral velocity of the wire was kept constant (around 20 m/s).

After each test the diameter of the control beads was measured in order to assess the rate of wear that is a capital factor concerning the unit cost of cutting. Wear was expressed in terms of volume lost per metre of wire length U_v from which the wear coefficient C_u was calculated as:

$$C_u = U_v L/A \text{ [cm}^3/\text{m}^2\text{]}$$

where L is the overall length of wire loop and A is the cut area in each test (equal to 0.09 m^2).

Knowing the final diameter of the worn-out bead (9.0 mm against an initial diameter of 10.5 mm) it was possible to calculate the wire yield (or productivity), i.e. the total area that can be cut per metre of wire under the different experimental conditions.

Cutting rate [m^2/h] is given by $C_a = (60 \cdot 10^{-4}) W \times P$ where W is the sample width (30 cm) and P is the penetration velocity of the wire (cm/min).

3.2 Results

3.2.1 Technical performance

The fundamental relationship found between cutting rate and wire yield is represented in Figure 3.

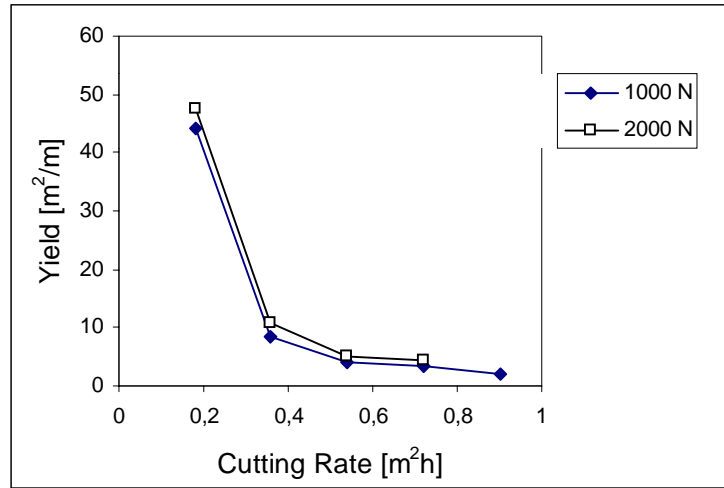


Figure 3. Cutting rate versus wire yield for 1,000 N and 2,000 N pull-back force

It appears that a higher rope tension is slightly better (the corresponding curve lies below), owing to a smaller curvature of the leading front of the cut and thence a more favourable distribution of the bead/rock contact force which strongly influences the wear process.

3.2.2 Cut quality

Cut quality with diamond wire is very smooth for all the experimental conditions, irrespective of the area and shape of the cut surface. Re-bars are also easily cut although at the expense of a small increase of the power required.

3.3 Cost evaluation

In the cost splitting, tool wear takes the prevailing share followed by manpower, machine depreciation, energy and other minor items (lubricants, maintenance and spare parts).

As a function of cutting rate the unit cost of cutting [US\$/m²] has a typical trend showing a minimum point for a cutting rate beyond which the progressively increasing contribution of wear outbalances the reduced significance of the other cost items.

In the case of concrete, the cost analysis suggests that cutting rate should stay within the range from 0.4 to 0.7 m²/h (the corresponding wire productivity being 10 and 5 m²/m). Given the high purchase price of a metre of wire (about 190 US\$) the unit cost of cutting is not far from 73 US\$/m², tool wear accounting for about 60% of the entire cost.

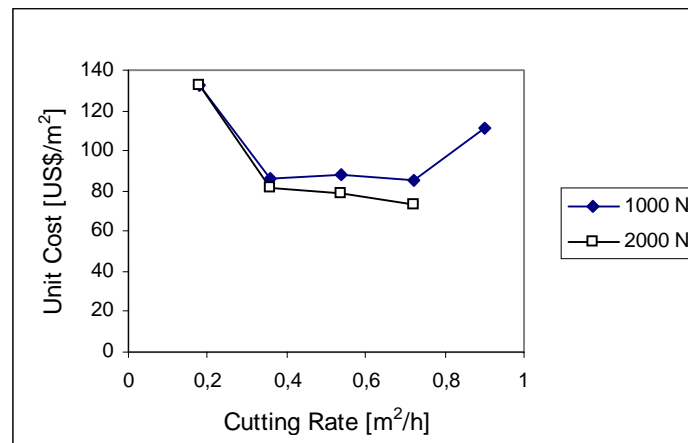


Figure 4. Unit cost cost of cutting with diamond wire as a function of cutting rate

4. CUTTING WITH ABRASIVE SUSPENSION JET

With the ASJ method abrasive particles are premixed with water into a pressurised bottle and delivered to the nozzle through a flexible hose, rendering the system particularly suitable for field operations and in particular for demolition purposes.

In fact:

- An abrasive suspension (or pre-mixed) jet consists of two components only (water and abrasive);
- radial dispersion of solid particles is smaller and it can be further reduced by adding suitable chemicals (soluble polymers);
- the possibility of using coarser abrasive particles that possess a higher erosive power is enhanced;
- the abrasive load is quite large (up to 10 kg/min), allowing deeper cuts to be achieved with higher cutting rate compared to the suction method AWJ;
- the pump is operated at relatively low pressure (up to 70 MPa in the present commercial machines), although systems working beyond 200 MPa are being developed in the attempt to reduce the abrasive mass flowrate;
- the nozzle can be oriented in every directions, under appropriate safety requirements;
- owing to the small size of the cutting head, difficult-to-reach points become accessible making the tool manipulation in restricted room easier;
- the abrasive is amenable to circulation back to the system provided that a suitable catching system is added;
- the remote control of the cutting operation is feasible even from far distances;
- ASJ can be employed in submerged environment or in a flammable atmosphere and it is suitable for cutting through explosive substances.

These features make the system applicable in the field for performing cuts through a variety of materials for the solution of problem such as:

- Dismantling of nuclear power stations (cutting of reactor elements);
- demilitarisation of weapons (cut of missile heads for the safe removal of the explosive);
- decommissioning of off-shore oil rigs (cutting of steel legs at sea depths);
- cleaning of oil tanks (cutting of access windows);
- recovery of oil wells (cutting and removal of damaged casing sections);
- cutting of concrete beams, pillars and platforms;
- piercing of water drainage pipes and so on.

Therefore premixed abrasive jet is very interesting for demolition according to the “cut-and-draw” method as an alternative to diamond wire. The periodic interruption of cutting for bottle refilling is not a major drawback in this kind of operation.

4.1 Experimental tests

4.1.1. Equipment

The equipment used for the tests on concrete is composed of:

- Hammelmann plunger pump
- DIAJet slurry forming unit
- Cutting vessel with the lance manipulation device (Figure 5).

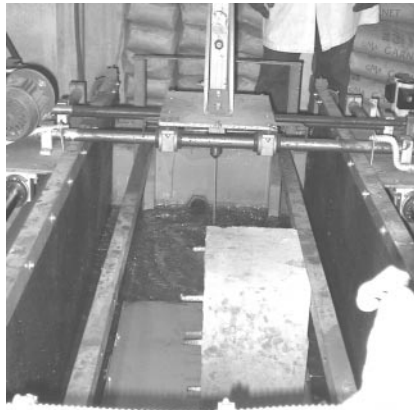


Figure 5. Cutting vessel used in the tests with concrete at the DIGITA waterjet laboratory

4.1.2 Experimental plan

The experimental plan was aimed at understanding the influence of the relevant operational variables on cutting performance and on cost. The following variables have been considered:

- Pressure at the pump: 35 and 65 MPa
- Nozzle diameter: 1.6 and 2.0 mm
- Traverse velocity: variable from 3 to 80 cm/min
- Number of passes until achieving a separation cut: variable from 1 to 20
- Kind of abrasive: Garnet HP80 and copper slag
- Abrasive mass flowrate: 2.5 and 5 kg/min

Since the result at 35 MPa with the 2 mm nozzle was poor, all the other tests have been made at 65 MPa, the maximum allowed by the DIAJet 700 system, using the 1.6 mm nozzle.

4.2 Results

4.2.1 Technical performance

Results are reported in Table 1 grouped into three sets, the first two with garnet and the third with copper slag. For the various experimental conditions a different number of passes was necessary for achieving a separation cut of the test sample through concrete.

However, while the upper re-bars were always easily cut, it was not so for intermediate and especially the lower re-bars for which additional passes are required.

Table 1-a. Garnet HP 80. Low number of passes

Characteristics	Cut 1	Cut 2	Cut 5	Cut 6	Cut 11
Pressure [MPa]	35	65	65	65	65
Nozzle Diameter [mm]	2	1,6	1.6	1.6	1,6
Water flowrate [l/min]	52	52	52	52	52
Abrasive mass flowrate [kg/min]	5	5	2,5	5	2.5
Traverse velocity [cm/min]	8.82	9	3.16	3.16	8.82
Number of passes	4	3	1	1	2
Cutting rate [m ² /h]	0.397	0.529	0.568	0.568	0.788
Upper re-bars	Yes	Yes	Yes	Yes	Yes
Intermediate re-bars	Partial	Yes	No	No	**
Lower re-bars	No	No	No	No	No

Table 1-b. Garnet HP 80. High number of passes

Characteristics	Cut 3	Cut 4	Cut 12	Cut 13
Pressure [MPa]	65	65	65	65
Nozzle Diameter [mm]	1.6	1.6	1.6	1.6
Water flowrate [l/min]	52	52	52	52
Abrasive mass flowrate [kg/min]	2.5	2.5	2.5	2.5
Traverse velocity [cm/min]	8.82	77.42	77.42	35.71
Number of passes	5	21	14	8
Cutting rate [m ² /h]	0.318	0.995	0.995	0.804
Upper re-bars		Yes	Yes	Yes
Intermediate re-bars		Yes	**	**
Lower re-bars		No	No	No

Table 1-c. Copper slag

Characteristics	Cut 7	Cut 8	Cut 9	Cut 10
Pressure [MPa]	65	65	65	65
Nozzle Diameter [mm]	1.6	1.6	1.6	1.6
Water flowrate [l/min]	52	52	52	52
Abrasive mass flowrate [kg/min]	2.5	5	2.5	2.5
Traverse velocity [cm/min]	3.16	3.16	8.82	77.42
Number of passes	1	1	2	21
Cutting rate [m ² /h]	0.568	0.568	0.794	0.664
Upper re-bars	Yes	Yes	Yes	Yes
Intermediate re-bars	Partial	Partial	No	No
Lower re-bars	No	No	No	No

** Cutting from opposite directions according to the strategy devised.

A suitable cutting strategy consists in the combination of two cuts, 15 cm deep, from the opposite sides of the 30 cm sample, as confirmed by check tests N 11, 12 and 13, involving half the total number of passes from each side at the same traverse velocity. In these tests the sample was rotated 90° so as to have the two sets of three re-bars near the upper and lower face (with no re-bars in the middle).

Results with garnet appear superior to those obtained with copper slag.

4.2.2 Cut quality

As expected, the cut surface with ASJ (Figure 6) is much rougher than that with diamond wire but this is not a big drawback in a demolition work. However it must be underlined that in the case of abrasive waterjet both cutting rate and cut quality depend on the size and shape of the cross section of the element to be cut through, contrary to DW.

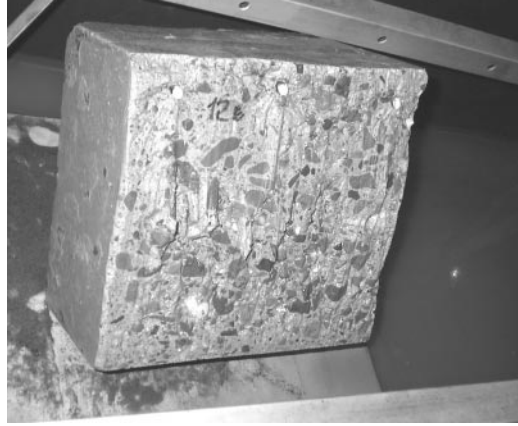


Figure 6. Appearance of the cut surface with the cutting strategy from both sides of the sample.

4.3 Cost evaluation

The unit cost of cutting is given by :

$$C_t = [(C_a + C_d) * Q_a + (C_e * P / R + C_m + C_r + C_s + C_w * 10^{-3} Q_w + D) / V_a]$$

where:

C_t	Unit cost of cutting [US\$/m ²]
C_a	Price of the abrasive: 0.25 [US\$/kg] for garnet and 0.1 [US\$/kg] for copper slag
C_d	Cost of disposal of spent abrasive: 0.1 US\$/kg
Q_a	Abrasive mass flowrate [kg/min]
C_e	Cost of energy: 0.135 [US\$/kWh]
P	Hydraulic power [kW]
R	Transformation efficiency: 0.7
C_m	Cost of manpower: 17.5 [US\$/h]
C_r	Nozzle wear: 0.5 [US\$/h] for garnet and 0.25 [US\$/h] for copper slag
C_s	Cost of spare parts: 6 [US\$/h]
C_w	Cost of water supply: 0.6 [US\$/m ³]
Q_w	Water flowrate [m ³ /h]
D	Depreciation : 21.34 [US\$/h]
V_a	Cutting rate [m ² /h]

For the various tests numbered from 1 to 13 the resulting unit cost of cutting is reported in the bar diagram of Figure 7.

In reality cutting with ASJ suffers from a technical efficiency E not higher than 0.8 because of the need to interrupt the process for filling the bottle with new abrasive, whereas in the case of DW the operation is almost continuous.

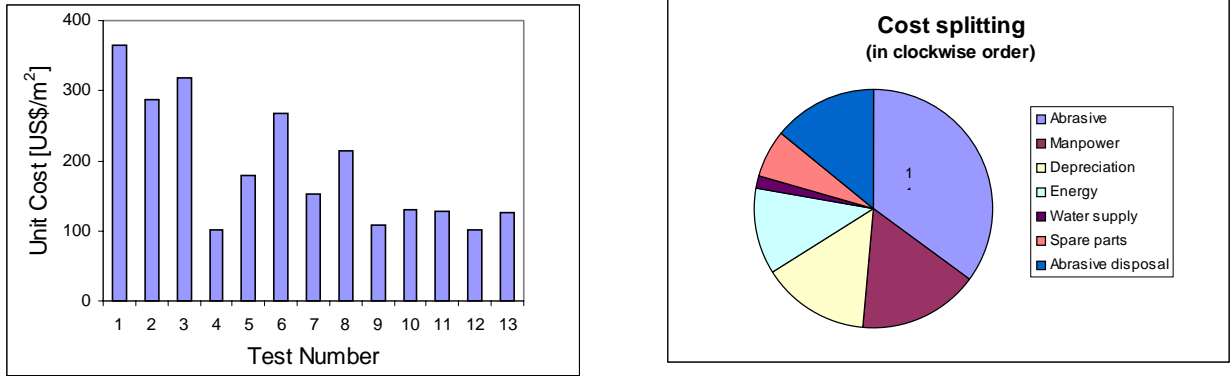


Figure 7. Unit cost of cutting for the various experimental conditions (Table 1) and cost splitting for Test N. 12

The advantage of cutting with multiple passes at relatively high traverse speed of the nozzle is evident: in fact the lowest cutting cost is obtained in tests N. 4 and 12 (with 21 and 14 passes respectively) for which a cutting rate close to 1 m²/h was achieved.

5. TECHNOLOGICAL COMPARISON

Cutting tests in similar conditions show that both technologies are suitable for concrete cutting. However some aspects are worth underlining:

- At optimum operational conditions for each technology, DW appears to be about 30% cheaper than ASJ in terms of unit cost of cutting [US\$/m²];
- regarding the cut area there is no practical limitation for diamond wire with a negligible influence on cutting rate and on the unit cost of cutting, contrary to ASJ (cutting rate gradually decreases and cost increases for larger cut sections);
- cutting deeper than 30 - 40 cm with ASJ would imply a penetration of the nozzle into a wider slot with no great advantage on the technical and economic performance;
- the presence of re-bars is not a major drawback with DW but it poses some problems with ASJ unless they are placed near the surface of the concrete element.

5.1 Fields of application

A comparison of the different methods and technologies applicable in the field of demolition is not easy, due to a great variability of the situations. In fact performance and cost levels vary according to the characteristics of the structure to be demolished (type, position, size, shape, component materials) as well as to a number of side conditions (reliability, safety, environmental impact, disposal or reuse of debris).

Therefore the most appropriate choice must be made for each individual case. However they can be ranked as shown in Table 2, although the indication has only the meaning of a rough orientation.

The respective fields of application of the different methods are summarised in Table 3.

Table 2. Comparison of the various demolition technologies.

INFLUENCING FACTORS	DEMOLITION METHODS AND TECHNOLOGIES				
	EXPLOSIVE BLASTING	MECH. DEMOLITION		CUT-AND-DRAW	
		Excavator	H. Hammer	DW	ASJ
Time: Preparation	xx	X	X	xxx	xx
Operation	-	Xxx	Xxx	xxx	xxx
Debris mucking	xxx	X	X	-	-
Overall Cost	xx	Xx	Xx	xxx	xxx
Flexibility	xx	Xx	Xxx	x	xx
Reliability	x	Xxx	Xxx	xxx	xxx
Loading conditions	x	Xx	Xxx	xxx	xxx
Selectivity	x	Xx	Xxx	xxx	xxx
Material reuse	x	Xx	Xx	xxx	xxx
Safety	x	Xx	Xxx	xx	xx
Environmental impact	xxx	Xx	Xx	x	x
Investment in machinery	x	Xxx	Xxx	xx	xxx

x Low level xx Medium level xxx High level

Table 3. Fields of application of the different demolition methods.

TYPE OF WORK		DEMOLITION METHODS AND TECHNOLOGIES				
		EXPL. BLASTING	MECH. DEMOLITION		CUT-AND-DRAW	
STRUCTURE	MATERIALS		Excavator	H. Hammer	DW	ASJ
Big civil buildings	Concrete	Xxx	x *	xx *		
Small houses	Bricks		Xxx	xxx		
Industrial sheds	Concrete	Xx	xx *	xx	xx	xx
	Steel					xxx
Plants	Concrete	X		x	xx	xx
	Steel					xxx
Monolithic structures	Concrete	Xxx	x *	xx *	xx	
Submerged structures	Steel	X			x	xxx
Nuclear power stations	Mixed					xxx

* In the subsequent phases after the implosion

PARTIAL DEMOLITIONS		X	x	xxx	xxx
---------------------	--	---	---	-----	-----

6. CONCLUSIONS

Demolition of concrete structures with ASJ according to the “cut-and-draw” method is technically and economically feasible. This kind of operation may require a relatively long time

that can however be shortened by using more machines at the same time. On the other hand the method benefits from the lack of debris mucking since the isolated portions of the structure are readily moved away.

Consequently the dismantling cost can be high, also because of the depreciation of expensive machinery, especially in comparison with explosive blasting, although the differences are somewhat reduced if the subsequent phase of debris loading, transportation and disposal is taken into consideration.

Abrasive waterjet, as an alternative to diamond wire, features some advantages concerning flexibility, reliability, operations selectivity, product handling, environmental impact and working safety, provided that adequate care is taken for controlling the risk of accidents.

The possibility of material reuse is good especially if the recovered portions of the structure can find a suitable application as such.

7. ACKNOWLEDGEMENTS

Work carried out within the research projects supported by MURST and CNR.

8. REFERENCES

A – Abrasive Suspension Jet (ASJ)

Agus, M., Bortolussi, A., Ciccu, R., Imolesi, E., Vargiu, A.: Stone Cutting with DIAJet, *Proc. 14th Mining Congress of Turkey*, 1995, pp. 29-35.

Agus, M., Bortolussi, A., Ciccu, R., Vargiu, A.: A comparative study of Suspension and Injection methods in rock cutting with abrasive waterjet, *Proc. 9th American Waterjet Conference*, Dearborn August 1997, pp. 47-60.

Bloomfield, E.J. e Yeomans, M.: DIAJet - a review of progress, *Proc. 1st Asian Conf. on Recent Advances in Jetting Tech.*, Singapore, 1991, p.21-30.

Fairhurst, R.M., e altri: DIAJET - a new abrasive water jet cutting technique, *Proc. 8th Int. Symp. Jet Cutting Tech.*, Durham, England, 1986, p.395-402.

Galecki, G. e Summers, D.A. : Steel shot entrained ultra high pressure waterjet for cutting And drilling in hard rocks, *Proc. 11th Int. Conf. Jet Cutting Tech.*, St. Andrews, England, 1992, p.371-388.

Hashish, M. : Cutting with high-pressure abrasive suspension jets, *Proc. 6th American Water Jet Conf.*, Houston, U.S.A., 1991, p.439-455.

- Kiyoshige, M. : A study of abrasive waterjet cutting using slurried abrasives, *Proc. 9th Int. Symp. Jet Cutting Tech.*, Sendai, Japan, 1988, p.61-73.
- Summers, D.A., e Yazici, S.: The investigation of DIAJet (Direct Injection of Abrasive Jet) cutting of granite, *Proc. 5th American Water Jet Conf.*, Toronto, Canada, 1989, p.343-356.
- Vasek, J., e altri : Influence of properties of garnet on cutting process, *Proc. 7th American Water Jet Conf.*, Seattle, U.S.A., 1993, p.375-387.
- Yao, J., e altri : DIAjet cutting of dolomite & chart - a case study at the St. Louis Arch, *Proc. 6th American Water Jet Conf.*, Houston, U.S.A., 1991, p.529-543.
- Yao, J., e altri : Field trials and developments of the DIAdrill concept, *Proc. 6th American Water Jet Conf.*, Houston, U.S.A., 1991, p.545-559.
- B – Diamond wire (DW)
- Berry P., Bortolussi A., Ciccu R., Manca P.P., Massacci G., Pinzari M.: Optimum use of diamond wire equipment in stone quarrying. *Proceedings APCOM 89*, 21st Int. Symp., Las Vegas, Feb 27 - March 2, 1989 SME AIME, Feb. 1989, pp. 351-365.
- Biasco G.: L'utilizzazione del filo diamantato nel taglio al monte dei materiali non calcarei. *ACIMM for Marble*, 21, 1989, pp. 89-103.
- Bortolussi A., Ciccu R., Manca P.P., Massacci G.: Computer-simulation of diamond wire cutting of hard and abrasive rocks, *Trans. Inst. Min. Metall.* Amin I 103 (May-August 1994), pp. A124-A128.
- Bortolussi A., Ciccu R., Manca P.P., Massacci G.: Simulation and optimisation of rock cutting with diamond wire. In: *Proceedings 22st APCOM*, Berlin, 1990, vol. III, pp. 163-176.
- Ciccu R., Massacci G., Vargiu A.: Prediction of diamond wire performance by computer simulation. *Proc. APCOM 96*, State College, USA, R.V. Ramani Ed., 1996, pp. 165-168.
- Lawn B.R. and Swain M.V.: Microfracture beneath point indentations in brittle solids, *J. Materials Science*, 10, 1975, pp. 113-122.
- J. Wilks and E. Wilks: *Properties and application of diamond*, Butterworth Heinemann, Oxford, 1991 and references quoted therein.
- D.N. Wright: La predizione dell'usura del diamante nella segagione della pietra, *Marmi Graniti e Pietre*, Dicembre 1990.

REDUCING ABRASIVE CONSUMPTION BY USING SUPER-WATER® FOR VENTURI ABRASIVEJET CUTTING

W. G. Howells
Berkeley Chemical Research, Inc.
Berkeley, California

V. L. Imlay
Water Jet, Inc.
Seymour, Indiana

ABSTRACT

Comparisons are made of cutting various materials with abrasive introduced by the Venturi technique when using 0.2% SUPER-WATER® instead of plain water.

Compared to plain water use of SUPER-WATER®, at the same cut speeds, substantially reduces abrasive consumption rates and decreases cut taper.

Edge cut quality is either maintained or improved depending upon the substrate.

The 25 – 30% reduction in abrasive consumption has economic importance especially when considered in conjunction with the 38% cost reduction in operating and maintaining intensifiers and the 31% reduction in horsepower requirement when using SUPER-WATER®.

1. INTRODUCTION

1.1 Background from 10th WJTA Conference

At the 10th American Waterjet Conference in 1999 at Houston three particular papers, presented in different sessions, provide the background for this paper.

They were by Ruppenthal (1), Hashish (2) and Howells (3) and of these the relevant comments of two of them (1,3) were not included in the written proceedings but made only during the oral presentations.

The interrelationship and importance of these comments will become evident in this introduction which deals with reducing abrasive consumption by using a 0.2% solution of a specific polymer named SUPER-WATER[®] as the cutting fluid instead of plain water.

Ruppenthal (1) explained that lower abrasive consumption has an impact on abrasive cost because it contributes to 66% of abrasivejet cutting running costs, as well as on abrasive disposal and waste handling expenses.

1.2 SUPER-WATER[®] Background

Howells has previously described a polymeric additive used commercially since 1974 to significantly increase waterjetting effectiveness by 2 to 50 times (4).

The addition of specific long chain polymers to plain water results in drag reduction prior to the nozzle or orifice and then production of a more coherent jet.

These two advantages, when accompanied by the third step, termed “macromolecular bombardment” (4), lead overall to more jet power per unit area in target penetration.

This increased jet power can be readily observed in waterjet cutting softer materials as a higher quality of the cut surface (5) as well as in the facile removal of hard silica scale, hard coke deposits (5) or, when using special spinning nozzles, in the slotting of granite (6) or precision drilling of concrete (7).

1.3 Definition of Generic Term “Polymer”

When considering the use of polymer additives in the context of this paper there is a very important point that needs to be emphasized.

The term “polymer” (derived from Greek: poly + meros, many parts) is very generic.

In the U.S.A., for example, 35-40% of commercially produced chemicals are polymers.

Not surprisingly, polymers vary in physical form, i.e. they can be solid or liquid. They vary in chemical nature depending upon the monomer (or basic building blocks) used in their synthesis.

They vary in molecular weight, i.e. from several hundred to many millions and, of course, they vary very widely indeed in their applications.

These same generalizations are true for naturally occurring polymers such as silk, cotton, starch, proteins and nucleic acids.

In addition, subtle differences exist but here it is sufficient to note that the term polymer is very generic and thus parallels the word “food” which includes a very wide range of items such as different fruits, breads, wines, meats and cheeses.

The specific polymer used in this study is named SUPER-WATER[®]. It is a 33% active concentration of linear macromolecular partially hydrolyzed polyacrylamide with a molecular weight of 16,000,000 to 18,000,000 and is available as a water-in-oil emulsion.

(*The registered trade marked name is SUPER-WATER[®] concentrated industrial water blasting additive.)

1.4 SUPER-WATER[®]: Increasing the Inherent Long Range Structure of Water

The specific structure, the molecular weight and the concentration of active ingredient of SUPER-WATER[®] are all critical for its ability to increase performance in Venturi abrasivejet cutting. SUPER-WATER[®] functions well in abrasivejet cutting because it has a unique ability not only to retain but even increase the inherent long range structure of liquid water under ultra-high pressure.

Because of the greater structure conferred on the vena contracta by SUPER-WATER[®], its effective cross-sectional area is significantly increased.

This feature was reported by Hollinger (8), who described it as a “piston type action”. This “piston type action” affords a simple understanding of the process being discussed here.

However, just as SUPER-WATER[®] is capable of enhancing the inherent long range structure of liquid water, other ways of perturbing this structure are also evident.

This is readily explained in chemical terms. For example, higher concentrations of SUPER-WATER[®] than 0.2% - in the presence of entrained abrasive – will result in the interference of one hydrated macromolecule with another.

This chain entanglement of hydrated macromolecules, manifested physically as an increase in viscosity, will impair the flow rate from a nozzle and will thereby negatively impact the jet cohesion and the advantageous subsequent steps.

SUPER-WATER[®] has an active ingredient concentration of 33% so in actuality all conclusions with respect to SUPER-WATER[®], at a use concentration of 0.2%, are in fact a result of using only 0.067% of active ingredient.

1.5 Perturbation of Water's Long Range Structure by Other Additives

Hashish (2) showed a 0.25% solution of SUPER-WATER[®] has a calculated coefficient of discharge for a 0.1778 mm diameter nozzle over a pressure range of 49,000 – 99,000 psi of between 0.79 and 0.86 with a maximum of 0.9 at a pressure of 68,000 psi.

By contrast, over this same pressure range (2), plain water has a calculated coefficient of discharge for a 0.1824 mm nozzle of 0.58.

Hashish (2) points out his calculations are very sensitive to orifice size. Although clearly 0.1778 and 0.1824 mm are not identical, a 0.25% SUPER-WATER[®] solution equally clearly has a larger coefficient of discharge than plain water.

The coefficient of discharge is a function of the cross-sectional area of the discharge jet stream divided by the cross-sectional area of the orifice.

Because of the greater structure conferred on the vena contracta by SUPER-WATER[®] its effective cross-sectional area is significantly increased.

Hashish (2) presented data obtained using a 0.25% solution of Polyox[®] for abrasivejet cutting aluminum 5052. He found the Polyox[®] solution was substantially less effective than plain water.

Polyox[®] is a polyoxyethylene glycol available in thirteen distinctly different ranges of molecular weight.

The importance of molecular weight has already been shown above to be critical and the generic nature of polymers previously mentioned is clearly reinforced by this Polyox[®] nomenclature.

The molecular weight of Polyox[®] used by Hashish is only 7,000,000 (9) which means that – per molecule – it is not as capable of bonding as many water molecules as SUPER-WATER[®].

Also, because it is a solid, a 0.25% solution of the Polyox[®] is approximately four times as concentrated as the 0.067% SUPER-WATER[®] active ingredient concentration described above.

When studying the effect of increasing fluid density upon waterjet effectiveness for aluminum 5052, Hashish (2) studied concentrated brine solutions with specific gravities of 1.15 and 1.20.

He found these solutions of specific gravity 1.15 (corresponding to a 20 wt % sodium chloride solution) and 1.20 (corresponding to a 26 wt % solution) were less effective as the sodium chloride concentration increased.

Moreover the depth of cut versus abrasive flow rate at 20,000 psi showed that both solutions of sodium chloride were less effective than plain water.

There is a rational chemical explanation for Hashish's findings. Sodium and chloride ions are well known to strongly bond water molecules. In so doing they destroy or, at least, very strongly minimize the ability for water to retain its inherent long range structure.

This conclusion is even more readily appreciated if Hashish's (2) data are normalized with respect to specific gravity.

Additionally, Hashish (2) presented data which clearly showed that oil with a specific gravity of 0.854 was much less effective than both plain water or 0.25% Polyox[®] solution in abrasivejet cutting of aluminum 5052.

From all of the conclusions discussed so far it is very clear that chemical specificity is of paramount importance.

Specific gravity of "oil" by no means defines the chemistry of the oil.

Oil, even without the intervention of refinery processing, can be paraffinic, alicyclic or aromatic or a mixture of these individuals types of chemical depending upon its geographic origin.

While it is true that each of these molecular structures has a different degree of polarity, hydrocarbons in general only bond together by very weak van der Waals forces, which have considerably less bond strengths than a covalent or even a hydrogen bond.

Hydrocarbons therefore have a very poor ability to form intramolecular structures.

Consequently it is totally clear that "oil" has no long range structure comparable to that of liquid water.

1.6 The Unique Properties of Liquid Water's Structure Under High Pressure: Pauling's Postulation of 1930

"Liquid water has several unique properties, indicating that there is a fundamental difference in structure between water and most other liquids (10).

It was recognized very early that these anomalous properties are due to strong intermolecular interactions leading to association (11)."

It has generally been accepted that these interactions consist mainly of hydrogen bonding between the molecules (12).

The bonds between the oxygen atom and the two hydrogen atoms in liquid water are termed covalent. However liquid water is unique in that it forms very strong hydrogen bonds with other water molecules.

The hydrogen bond which results from a dipole-dipole attraction has a strength of about 5 Kcal/mole, whereas a covalent bond has a strength of about 50 to 100 Kcal/mole.

A fairly recent publication (13) confirmed the original theory, postulated by Pauling in 1930, that under pressure the hydrogen bond of water – which is already strong – partly adopts covalent identity.

This publication in Physical Review Letters (13) has enormous significance for the waterjetting industry, especially in ultra-high pressure work, where the hydrogen bonding and consequent long range structure are crucially important.

The importance of the long range structure of water and the relevance of it to abrasivejetting were pointed out by Howells (3) who cited references 11, 12 and 13 in his oral presentation.

SUPER-WATER[®] with its own capability of bonding 13 to 14 molecules of water to each monomeric unit of the polymer (14), clearly enhances this long range structure, provided it is used at the optimum concentration.

Calculation (15), based on an average molecular weight of 17 million for the SUPER-WATER[®] macromolecule and an average molecular weight of 80 for the monomeric units, shows that each molecule of SUPER-WATER[®] bonds 2.9 million water molecules.

1.7 Examples of SUPER-WATER[®]'s Use in Venturi Abrasivejetting

The first example of SUPER-WATER[®] assisted Venturi abrasivejet cutting was published in 1995.

It was reported that laminated glass, aluminum and stainless steel could be cut with SUPER-WATER[®] plus 100 grit copper slag abrasive 20% faster than with plain water plus copper slag (16).

The technique was later used in France (17), Sweden (17) and Switzerland (18) and these results have been summarized previously (19).

Currently in the U.S.A., Waterjet Inc. of Columbus, Indiana is using SUPER-WATER[®] in a Venturi abrasivejet for cutting a wide range of plastics, aluminum and aluminum alloys, brass, concrete, ceramics, marble, hardwood, various polymeric materials and all types of steel (20) as is A & D Rubber Products, Inc., Stockton, California and companies and/or research facilities in Australia, England, France, Germany, Sweden and Switzerland.

Similarly in Canada, Soheil Mosun Limited, Toronto uses 0.2% SUPER-WATER[®] with abrasive for cutting 304 stainless-, hot and cold rolled-, blue tempered- and Duplex stainless-steel, aluminum, titanium, yellow brass, clear float and laminated glass, marble, ultra-high molecular weight polyethylene and 2-inch thick-acrylic (20).

These ongoing successful industrial applications were recently bolstered by data reported from a preliminary quantitative and carefully conducted study under research engineering conditions (21).

This is the background of the use of SUPER-WATER[®]s in the Venturi technique which prompted the present study by Waterjet Inc. of Columbus, Indiana using industrial equipment available in job shops in North America.

2. DISCUSSION

2.1 Pumps, Conditions and Ancillary Equipment

The objective of these studies, when using readily available industrial job-shop equipment, was to determine the reduction in abrasive consumption that could be achieved with a 0.2% SUPER-WATER[®] solution as a replacement for plain water in Venturi abrasivejet cutting.

A pressure of 50,000 psi – used for all the cutting determinations – was obtained with an Ingersoll-Rand intensifier Model PMH (Streamline I) fitted with a Remcon Inc. abrasive head incorporating a 0.030-inch carbide focus tube and a 0.013-inch jewel.

Universal Mineral (Sharpjet) 80 mesh garnet was used throughout at a standoff distance of 1/8-inch.

The target substrates, 304 stainless steel, A36 hot roll steel, UHMW (ultra-high molecular weight polypropylene), 6061-T6 aluminum and titanium were traversed by a 2-axis gantry robot manipulator.

Solutions of 0.2% SUPER-WATER[®] may be fed from either a DOSATRON INTERNATIONAL Model DI-16 or a Model DI-1500 non-electrical proportional liquid dispenser fitted with a TAH 14-stage static mixer.

The Model DI-16 meters intake fluid in the range of 0.2 – 1.6% and the Model DI-1500 meters in fluid in the range of 0.07-0.2%.

2.2 Abrasive Cutting Results

Roughness was judged on the basis of an Edge Quality scale with Q ratings from 1 through 5 in which higher numerical values indicate better edge finish.

Q = 1. A separation cut: requires force to separate.

Q = 2. A through cut: severe bottom striations.

Q = 3. A clean cut: moderate bottom striations, most commonly used (attained or desired).

Q = 4. A good edge finish: limited striations.

Q = 5. An excellent edge finish: light striations, minimal edge taper.

Table I: **Reduction in Abrasive Consumption** shows the thicknesses of the various materials examined as well as the cut speeds that were used.

In each instance marginally faster cut speeds, e.g. 1.15 versus 1.10, were used with the 0.2% SUPER-WATER[®]/abrasive combination than with plain water/abrasive.

This intentional control was intended to avoid any possibility of the SUPER-WATER[®]/abrasive combination providing a better cut solely on the basis of a slower cut speed.

The Q roughness values were measured on the left side and the right side of the through-cut materials.

In every case the Q values were the same for the SUPER-WATER[®]/abrasive combination as for plain water/abrasive except for A36 hot roll steel where the SUPER-WATER[®]/abrasive showed a Q value of 4 in contrast to a Q value of 3 for plain water/abrasive.

The angle of the cuts, as shown by the number of degrees from the vertical, was better in every instance with SUPER-WATER[®]/abrasive.

This characteristic is most clearly shown in cutting UHMW (ultra-high molecular weight polypropylene) where the angle from the vertical is halved.

It is also noteworthy that the UHMW was cut considerably faster (approximately 4 times) than the other materials of 1-inch thickness.

The objective of these studies to obtain reduced abrasive consumption by using 0.2% SUPER-WATER[®], was achieved.

This is strikingly evident from the abrasive rates, given in pounds/minute.

The reductions shown in the right hand column of Table I range from 25% for aluminum to 30% for A36 hot roll steel.

3. CONCLUSIONS

This paper has described the advantages of using abrasive with a 0.2% solution of SUPER-WATER[®], instead of plain water, for Venturi abrasivejet cutting utilizing readily available industrial equipment.

These advantages include a 25 to 30% reduction in abrasive consumption as well as narrower kerf widths and an equal or better cut quality to those obtained with plain water at the same flow rate.

Because 66% of abrasivejetting costs have been directly attributed to the price of the abrasive this automatically reduces the required overall expenses by 17 to 20%.

Combined with a 38% reduction in intensifier operating and maintenance costs as well as a 31% reduction in required horsepower, both of which result from employing SUPER-WATER[®], these attributes present a distinct economic advantage over the use of plain water.

Water has an inherent and unique long range physical chemistry structure, especially under high pressure, which is markedly enhanced by SUPER-WATER[®].

However this same structural uniqueness of water is nullified by inappropriate additives including the use of polymers, other than SUPER-WATER[®], which are different in structure and molecular weight.

The differences between the advantages of SUPER-WATER[®] and the disadvantages of other additives are readily explained by considering the underlying chemistry.

4. ACKNOWLEDGEMENTS

The authors express their sincere appreciation to Mr. Renato Lombardi of Toronto, Canada, who made suggestions all of which are included in this paper, and to Jan Tubbs and Lois Schwoebel of the WaterJet Technology Association who were kind enough to type this paper in the format required for publication.

5. REFERENCES

1. M. Ruppenthal, "Purchasing and Running a Profitable Abrasive Waterjet", *Proceedings of the 10th American WaterJet Conference*, August 14-17, 1999 (Houston, TX), pp. 707-16.
2. M. Hashish, "Short Course on the Fundamentals and Applications of Waterjet Technology", 10th American WaterJet Conference, August 14-17, 1999 (Houston, TX).
3. W. G. Howells, "SUPER-WATER[®] Jetting Applications from 1974 to 1999", *Proceedings of the 10th American WaterJet Conference*, August 14-17, 1999 (Houston, TX), pp. 363-380.
4. W. G. Howells, "Polymerblasting – a Chemist's Point of View", *Proceedings of the Second US Water Jet Conference*, Rolla, Missouri, USA, May 24-26, 1983, pp. 443-447.
5. W. G. Howells, "Polymerblasting with SUPER-WATER[®] from 1974-1989: a Review", *International Journal of Waterjet Technology*, Volume 1, Number 1, (March 1990), pp. 1-16.
6. D. A. Summers and M. Mazurkiewicz, "Technical and Technological Considerations in the Carving of Granite Prisms by High Pressure Waterjets", *Proceedings of the 3rd U.S. Water Jet Conference* (University of Pittsburgh, 1985), pp. 272-287.

7. W. G. Howells, “*Enhancing waterjetting by use of water soluble additives*”, in *Water Jet Applications in Construction Engineering*, Editor A. W. Momber, publisher A. A. Balkema, Rotterdam, Netherlands, (1998), ISBN 90 5410 698 0.
8. Private communication from R. H. Hollinger to Berkeley Chemical Research, Inc., 1984.
9. Private communication from M. Hashish to Berkeley Chemical Research, Inc., March 2001.
10. G. Nemethy and H. A. Scheraga, “*Structure of Water and Hydrophobic Bonding in Proteins. I. A Model for the Thermodynamics of Liquid Water*”, *J. Chem. Phys.* Vol. 36, pp. 3382-3400, (1962).
11. W. M. Latimer and W. R. Rodebush, *J. Am. Chem. Soc.*, Vol. 42, p. 1419, (1920).
12. H. M. Chadwick, *Chem. Revs.*, Vol. 4, p. 3975 (1927).
13. A. Cunsolo et al., “*Experimental Determination of the Structural Relaxation in Liquid Water*”, *Physical Review Letters*, Vol. 82, Issue 25, 1999, pp. 75-778.
14. S. Majumdar, S. Holay and R. P. Singh, *European Polymer Journal*, Vol. 16, p. 1201.
15. W. G. Howells, “*SUPER-WATER[®] jet cutting, of packaging foams*”, *Packaging Networks*– an internet publication at <http://www.packagingnetwork.com/read/n1200005161/133611> and submitted as a synopsis for publication to *Jet News**.
16. W. G. Howells, “*Additive Improves Abrasive Jet Cutting Jet News**”, December 1995, pp. 5 and 10.
17. D. Weber, letter to the Editor, *Jet News**, February 1997, p. 12.
18. D. Weber, letter to the Editor, *Jet News**, December, 1997, pp. 7 and 8.
19. W. G. Howells, Vincent L. Imlay, Renato Lombardi and Daniel Weber, “*Ultra-high pressure precision jet cutting using SUPER-WATER[®]*”, *Proceedings of the International Composites EXPO*”, Cincinnati, Ohio, May 10, 1999.
20. Private communications from V. L. Imlay, D. Wolford and R. Lombardi to Berkeley Chemical Research, Inc., July 2000 and shown in individual testimonials at www.berkeleychemical.com under CUTTING, Materials Cut with SUPER-WATER[®] and Abrasives.
21. G. Holmqvist and W. G. Howells, “*The Effectiveness of SUPER-WATER[®] in Venturi Abrasivejet Cutting – a Preliminary Examination*”, October, 2000. Not yet released for publication by research sponsors.

*** *Jet News* is a bimonthly publication of the WaterJet Technology Association, St. Louis, Missouri, U.S.A.**

Table I
Reduction in Abrasive Consumption

<u>Substrate</u>	<u>Cut Speed:</u> <u>Inches/min.</u>	<u>Roughness</u> <u>Q*</u>		<u>Degrees</u> <u>From</u> <u>Vertical</u>		<u>Abrasive</u> <u>Rate:</u> <u>1b/min.</u>	<u>Abrasive</u> <u>Rate</u> <u>Reduction</u>
		<u>Left</u> <u>Side</u>	<u>Right</u> <u>Side</u>	<u>Left</u> <u>Side</u>	<u>Right</u> <u>Side</u>		
304 stainless steel: thickness = 1-inch							
Plain water**	1.10	4	4	0.7	0.7	0.97	
0.2% S-W ***	1.15	4	4	0.5	0.5	0.72	26%
A36 hot roll steel: thickness = 1-inch							
Plain water**	1.41	3	3	1.0	1.0	0.99	
0.2% S-W ***	1.46	4	4	0.7	0.7	0.69	30%
Ultra-high molecular weight polypropylene: thickness = 1-inch							
Plain water**	16.1	4	4	1.0	1.0	0.87	
0.2% S-W***	18.0	4	4	0.5	0.5	0.62	29%
Aluminum 6061-T6: thickness = 1-inch							
Plain water**	4.2	4	4	0.7	0.7	0.95	
0.2% S-W***	4.5	4	4	0.5	0.5	0.71	25%
Titanium: thickness = 5/8-inch							
Plain water**	4.4	3	3	0.7	0.7	1.08	
0.2% S-W***	4.6	3	4	0.6	0.6	0.78	28%

***Q values:**

- Q=1. A separation cut: requires force to separate.
- Q=2. A through cut: severe bottom striations.
- Q=3. A clean cut: moderate bottom striations: most commonly used (desired or attained).
- Q=4. A good edge finish: limited striations.
- Q=5. An excellent edge finish: light striations, minimal edge taper.

**** For chemical analysis of plain water please see the attached appendix.**

***** S-W = SUPER-WATER®**

APPENDIX

Waterjet Inc., Seymour, Indiana, uses water from the Indiana-American Water Company (I-AWC), Inc. The water is treated only by passing through a 1-micron filter but is not subjected to ion exchange, reverse osmosis or any other processing.

Chemical analysis of the “plain-water” used in these studies shows:

Total dissolved solid (TDS) concentration is 298 ppm. (It ranges consistently from 295 to 300 ppm.)

The following is taken from: <http://fluid.state.ky.us/ww/ramp/rmhard.htm>

Hardness and water quality

Hardness is due to the presence of multivalent metal ions which come from minerals dissolved in the water. Hardness is based on the ability of these ions to react with soap to form a precipitate or soap scum.

Classification of Water by Hardness Content:

Concentration mg/L CaCO₃

Description -

0 – 75 soft

75 – 150 moderately hard

150 – 300 hard

300 and up very hard

Analytical data by I-AWC for the month of March 2001 showed water hardness ranged from a minimum of 230 (hard) to a maximum of 310 (very hard) with an average of 267 (hard).

Other analytical information from I-AWC showed the pH ranged from 7.7 to 7.9 with an average of 7.8.

Chloride, fluoride and sulfate concentrations were 16.9, 0.79 and 20.8 mg/L respectively.

Calcium, magnesium, sodium and silica (sic) were present at 84, 26, 12 and 12 mg/L respectively.

No iron or potassium was found within the limits of detection.

Of 20 other metallic elements 14 were not detected.

The 6 detected, namely barium, chromium, copper, manganese, molybdenum and strontium were present at 0.047, 0.021, 0.011, 0.010, 0.002 and 0.107 mg/L respectively.

ENVIRONMENTAL EVALUATION AND MANAGEMENT OF AWJ PROCESS

Jiří F. Urbánek,
Brno University of Technology, Faculty of Mechanical Engineering,
Atelier of Process Design, Czech Republic, Europe

ABSTRACT

The principal objectives of following environmental analysis of AWJ processes are a production, dissemination and using of the knowledge and technologies needed to design and development of AWJ processes and create condition for a supply of high quality, environment- and consumer-friendly recycling device which will be competitive on tomorrow's market. An aim is to create reliable technologic system (Device) to treat AWJ process waste. The principal target of consequently proposed Project is to create enforceable and reliable technologic system URrec® - "Under-one-Roof recycling", include the design of need device able to treat all Abrasive Water Jet (AWJ) process waste. AWJ process environmental integration, behavior and influence are tested and evaluated by means of process interactions, inputs, duration, outputs and consequences. The real economics saving of all European countries as a result of massive introduction of recycling devices URrec are counted in expected contribution. It will be source of new economic savings and contribution of cutting technology waste recycling of high pressure AWJ.

1. INTRODUCTION

The principal objectives of following environmental analysis of AWJ processes are a production, dissemination and using of the knowledge and technologies needed to design and develop of AWJ processes and create condition for a supply of high quality, environment- and consumer-friendly recycling device which will be competitive on tomorrow's market. An aim is to create reliable technologic system (Device) to treat AWJ process waste. Environmental sustainable condition is to close waste treatment processes in workshop environment. A core is in recycling of material flows and substances. Workshop environment mustn't suffer any aggravation of the working, safety and hygienic conditions exceed Euro-standards. Partial targets are: to unload an exploitation of abrasive natural sources, water and energy & to reduce an import of the abrasive into countries EC & to improve quality of life and health by preserving the environment & to create economic and ecological contributed device, able to compete overseas solution.

The principal target of consequently proposed Project is to create enforceable and reliable technologic system URrec[®] - "Under-one-Roof recycling", include the design of need device able to treat all Abrasive Water Jet (AWJ) process waste. Parallel targets are:

- to unload an exploitation of abrasive natural sources, (i.e. minimally 60% recycling), water (100 % recycling) and energy (savings of transportation costs 60%);
- to improve quality of life and health by preserving external environment and monitoring of workshop environment;

Preliminary conditions of Project goal:

- The dissemination and using of the knowledge and technologies particularly arisen at European Community INCO-Copernicus project Contract NO. ERB IC15CT98 0821; coursed project title: "Abrasive Water Jet Cutting, a clean technology". The participants of this INCO project are SME "AQUAdem,s.r.o," Brno, CZ; and Brno University of Technology, Brno, CZ
- The project have to fit to Small and Middle Enterprise (SME) participants for the reason of possible grant from EC, 5th Program of Cooperative Research (CRAFT) Thematic Priorities "GROW" – Competitive and Sustainable Growth. Mainly with GROW-1 "Innovative products, processes and organization".
- Project investment back-flow have to come to 24 month of average operation at the latest.
- The URrec have to be competitive on tomorrow's market. It contribute to economic growth increasing, maintain and/or create new jobs in EC countries.
- For Project solution is necessary associated effort of three types of the participants:
 - a) URrec Device designer and coordinator of proposed project engineering works, technologic and environmental process planner. RTD Performer.
 - b) An evaluator of application possibilities and debugger of proposed technology system, future URrec Device user. The SMEs.
 - c) A supplier particular technologic elements , provider of technologic complex made-to measure after consumer requirements, propagator, extender, distributor, transferor and supplier of future URrec Device services. The SMEs.

Expected costs reduction of material inputs to SME users of the URrec brings economical possibility of sustainable and continuing innovation and modernization of manufacturing, processing and services of participating SMEs, so as to improve their competitiveness. It is fully in intention of Community policies that enable competitive and sustainable development. Saving costs from unrealized abrasive import to European Community countries will consist in the savings of external logistic cost and a removal of a dependence at overseas natural sources, include dumping restriction of inorganic substances. An importance of future Project follows from the fact, that more objectives interact here:

The supporting of research activities contributing to competitiveness and sustainability of the development of SME industry. (Industry's role is not only in the collaboration but also in its bringing and integration of Project proceedings). Then arises typically cross-sectored Project along the value chain, so that technology uptake and innovation are more effectively ensured across European industry. Strategic contributions of proposed project significantly include: (a) modernization of industry and adaptation to change; (b) substantially improve overall quality; (c) minimize resource consumption.

International state-of-the-art is given by high quality of the solution above INCO-Copernicus project. The results INCO working group regards of AWJ abrasive waste treatment can be summarized to five type of a solution:

- 1) Used (waste) abrasive is dumped at municipal refuse landfill – common resolution.
- 2) Used abrasive is recycled at extra environment – by other entrepreneurial subject.
- 3) Used abrasive is treated at extra environment – other entrepreneurial subject (e.g. as a ingredient into smelting glass, or solution offered by Brandt and Louis (2000) and others authors.
- 4) Used abrasive is recycled under-one-roof (indoor) AWJ user by means of AWJ machine provider, which supplied device (the common price like a this device is more than 20.000, - EUR).
- 5) Used abrasive is recycled under-one-roof (indoor) AWJ user by means of self-made device (the efficiency like a this device is low, with great environmental risk).

The solution ad 1), 2) and 3) are logistic cost ineffective and may cause environmental risk. A core of our proposed project, will offer a modular under-one-roof device as a recycling system, which will be able to carry-out recycling not only abrasive but even a water and other waste component, include others pollutant and human health harmful substances (noise, dust, bacteria, etc.). In this way the AWJ will be promoted as a clean (without waste) technology.

Real calculation of preliminary price of full supplies (recycled all agents of AWJ process, not only abrasive) will below a boundary 13.500,- EUR, while price competitive overseas device is more than 20.000,- EUR. Other technical limitations is in its great size and ISO 14000 disagreement. The recycling system modularity makes possible to pick out of such solving for users, which will agree with its demands, space and financial conditions. In frames of our solving will offer to the user an environmental audit according ISO EN 14 000, and other European environmental standards. In addition will offer to the user a good possibility to buy yourself chosen modules only. Alternatively possibility will be to assemble whole system step by step.

Concurrent innovation of URrec Device modules will be possible in harmony with stiffen up of environmental standards and law.

to thermal cutting techniques. The amount of recycled abrasives is less than 70% up to date. The increase up to 90% would lead to duplication of the lifetime of the abrasive (70% = 5 cycles to cut; 90% = 20 cycles to cut. It is Louis et al. (1999 - 2002) related project aim.

2. AWJ PROCESS ANALYSIS AND EVALUATION

2.1 Approaches

- **AWJ process environmental integration**, behavior and influence must be tested and evaluated by means of process interactions, inputs, duration, outputs and consequences.
- **A Logistics** is used as process analysis and evaluation instrument. It gives the instruments, methods and technology of a manipulation, processing, monitoring, plan, decision, regulation, control and management of material flow in both the space and the time.
- **The material substance** of AWJ objects is resulted in a possibility to divide their processes. They have their “**micro-logistic**”. and “**macro – logistic**” characteristics. The abrasive is chosen to the demonstration of AWJ environmental engineering.

AWJ process environmental integration, behavior and influence is tested and evaluated by means of process logistic flows, relations, interactions, inputs, duration, outputs, integration and a consequences. It serves to environmental evaluation of the processes and after cut-process components. The core of the paper is abrasive recycling. Method DYVELOP[®] (based at Product Life Cycle) is used for AWJ product and waste recycling analysis, evaluation and management. A synthesis of environmental models of AWJ recycling processes is an instrument for optimized processing way of the abrasive. Complications of environmental relations and their consequence are expressed by material flow productivity in real time and space. Information is shown graphically, very well arranged and computer-able at mathematical point set theory. Electron microscope images serve to abrasive state documentation. Logistic approach is used to final evaluation of environmental influence and productivity of recycling processes.

2.2 AWJ Process “macro – logistic” Characteristics

It is necessary to give attention of whole “Product Life Cycle” (PLC) with regards to abrasive presentation in AWJ processes. For this purpose is good to use method “DYVELOP[®]– i.e. Dynamic Vector Logistic of Processes“. Abrasive recycling is only a part (phase) of abrasive PLC. Figure 1 plots of PLC phases graphic dependence on real time (**t**) and on (non-unit) Value Added (VA). Here abrasive logistic transformation τ is defined as a first derivative of VA' , and/or as a first derivative of real time abrasive price (**P**) to its price spoon ($\Delta P = P_{\max} - P_{\min}$).

$$\tau = \frac{dVA}{dt} = VA' \equiv \left(P \frac{1}{\Delta P} \right)' = \frac{P' \cdot \Delta P - P \cdot \Delta P'}{\Delta P^2} \quad (1)$$

Any PLC is a continuous chain of relations and processes, which must be logistical closed from the point of the view of sustainable development. The PLC can has four phases: production (Pr), distributive (Di), consumer's, user's (Us) and recycling (Re). The graphical interpretation of abrasive transformation τ is shown at Figure 1.

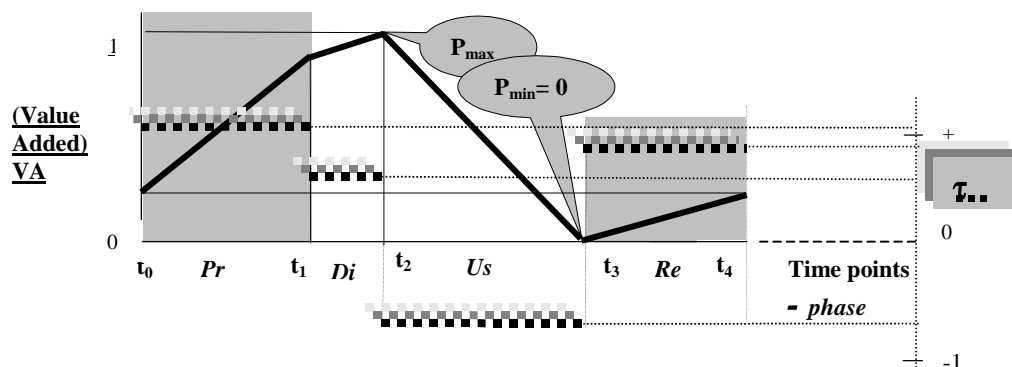


Figure 1. The graphical interpretation of abrasive transformation τ .

The role of real price of the abrasive is important for further logistic evaluation in time nodal point t_3 at the interface of Us/Re phases. If the real price at t_3 of this “after cut-process abrasive” (ACPA) is as on above Figure 1, i.e. $P_{\min} = 0$, then environmental non-harmful ACPA is presupposed. In fact, it is not true. In reality, value $P_{\min} \equiv P_3$ depends upon fabrication technique of abrasive in phase Re. Here if the abrasive is dumped on municipal refuse depot, then with most probability cut-user have to pay it. It manifests negative sign of value P_3 and thereby also τ_3 . More than, latent environmental harmful of ACPA (mixture with mineral oil, non-defined chemical composition of chips) will act of dump refusal. Than it will increase negative value of ACPA, because it will be necessary dumped in special conditions. The difference of P_4 price minus P_3 is necessary costs value of ACPA recycling phase. P_4 price should not be higher than P_1 , to obtain economic efficient of recycling process. If the recycling is made at the site of origin, than P_4 should not be higher than P_1 . As a rule must exist, that recycling abrasive price P_{3II} , (on second (II) cycle- see Figures 3, 4) mustn't to be higher than present-day price P_{3I} , (on primary (I) and/or original (.) previous cycle). Appropriate economic grants, on behalf of requested recycling, they would be manifested as a decreasing of starting price P_3 of recycling phase. It would be an invitation for the recycling during primary phase of abrasive using.

2.2.1 Conditions and rules of abrasive recycling

Natural resources of abrasive are limited. PLC and chains of AWJ abrasive must be logistical closed. i.e. they must course at defined environment. Defined environment means that all and whole AWJ process and its consequence must be environmental defined, monitored and integrated in the sense of environmental standards EN ISO 14000. This standards act about of environmental management of a systems a their processes. If the systems & processes of AWJ are analyzed with an implementation of logistical method DYVELOP[®] then process cell of AWJ can be logistic modeled as is shown at next Figure 2. It uses symbols, operators and procedure of mathematical set theory. A fragment is the recycling in undefined environment.

2.3 AWJ Process-cell “micro – logistic” Behavior

- (1) Nearest Jet environment is influenced by means of: - gravitation field;- laminar enter flow; - kinetic energy;- workpiece position stability; - air characteristics;- the temperature; - abrasive shape and density; - cavitations bubbles; - ecological environment; etc.
- (2) Unusual jet flow physic phenomena are characterized as: - memory functions; - vectors line continuity; - scalar action of flow obstacles (particles shape); - shock waves; - Erosion Front curvature; - non-Newton character of the liquid (compressibility, scalars); - workpiece material changes; - grain impact; - cavitations bubbles; - reaction forces; workpiece abrasive removal;
- (3) Process micro-logistic characteristics are: - composition of jet flow mixture = the water + abrasive + air + removed chips + cavitations vapor bubbles; - workpiece chips removal; - a crushing of the abrasive;- erosion front as a logistic "pipeline" (which has of time-space and information contents); etc.

3. ENVIRONMENTAL MANAGEMENT OF ABRASIVE RECYCLING

The environmental management of abrasive recycling processes needs analysis and describing of its substantial environment. Method “DYVELOP[®]” published by Urbánek (1999) allows practical logistical synthesis of integrated model of all process component, behavior, input/output and ENV. This method is able to express any complication of ENV relations and their consequence, including productivity of processes. It can give any information about material flow even in real time and space, about logistic categories - as a batch, phase, cycle, chain and about modality of material & information processing. All this is expressed graphically, very well-arranged and fast at point set theory, which is suitable to be computerized.

3.1 Macro-logistic Characteristics of AWJ Processes Parameters

technical = transportation + storage + manipulation + means + instruments + accessories

economic = price + value added + costs + expenses + grants + charges + productivity of labor + information + competitions advantage + management

technologic = transformation + material + parameters + productivity + process + know- how + machining ability + accuracy + control + multiplicity + design + process planning + cutting ability + wear + economy + energy

energetic = input + output + physic form + waste energy

distribution = in erosion front + in space + in flow + in gravitation field + in batches + in pipe + traffic conductor + sealing + storage + manipulation + control + multiplicity

informational = plan + program + memory + data + transition + treatment + preservation

management = monitoring + controlling + planning + decision + information

Table 1. Images, symbols and processing modality (the legend) used in next figures

<i>implication; a symbol</i> →		accumulation	Box = environment (ENV) - can be roman numbered;
production phase, [productivity]	[x/y]	sorting	Circle = product life cycle;
distribution and sale	⊘	separation	Double Circle = waste cycle;
consumer's and user	☺	selection	Triangle = customer, user;
recycling phase	↻	dumping	Full Circle = product;
fragment phase	⤿	storage	Annulus = waste;
compost; regeneration;	☀	decomposition	Bold Point = number of point is roman number of the ENV;
Modality of a possibility	◇	arrangement	
		synthesis	

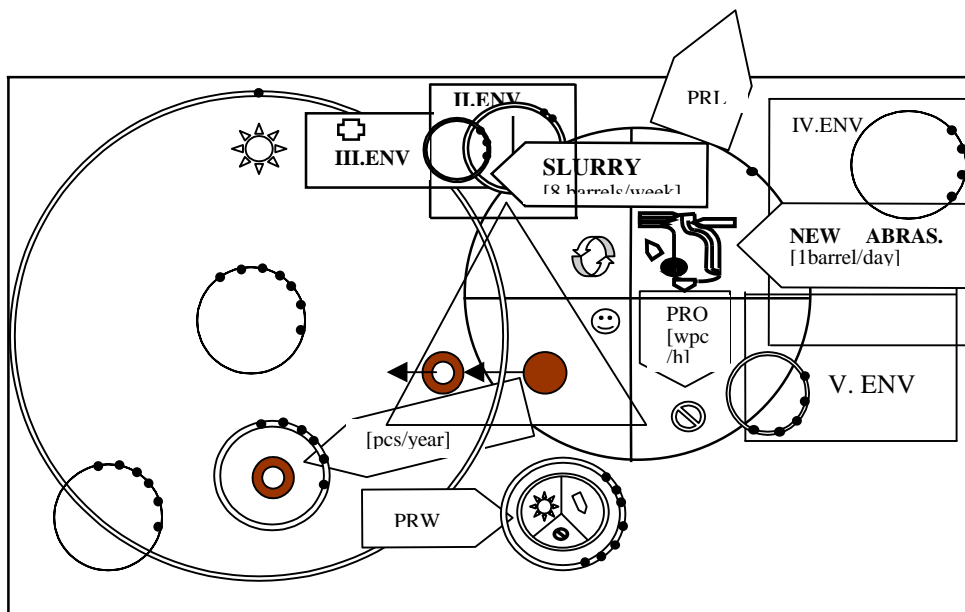


Figure 3. Graphical model of AWJ processes and their environments.

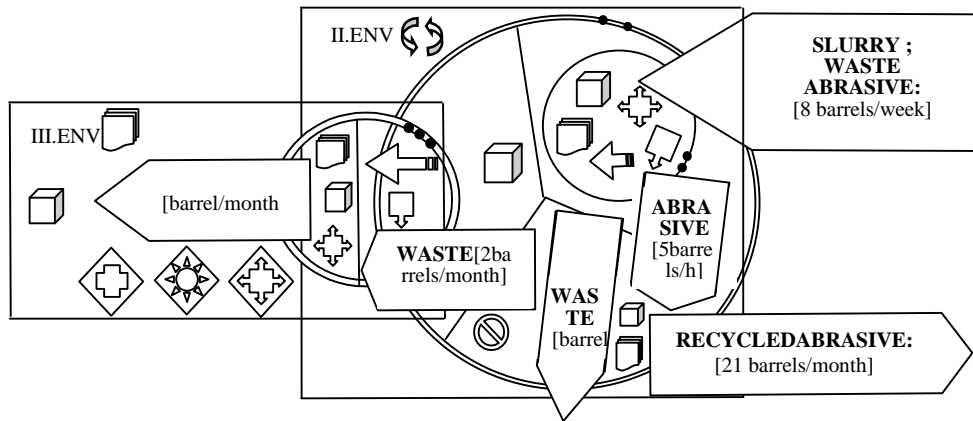


Figure 4. A detail of above (bold linked) graphical model concentrated to abrasive recycling, out of Process Cell, Under-one-Roof (indoor).

Figure 3 shows global level of **I. ENV**. It has known four phases of AWJ processes. The core of it is **I. PLC** of AWJ processes. Semi-products of AWJ processes are flat plate mainly and they are characterized difficult machining-ability. The AWJ processes products are spread at wide **I. ENV**. The **IV. ENV** contains the PLC, which produce new abrasive. It would be ideal to extend **IV. ENV** and it connects with **I. Re** phase of primary AWJ PLC. But with regards to rarely global displacement of raw abrasive locality, it has not economical advantageous. A connection with **II. Re** phase is not necessary, because it have own special logistic pipeline. Figure 4 is a detail of above Figure 3 and it is concentrated to abrasive recycling URrec. Here are expressed relationships, functions and productivity of abrasive recycling (at II. Waste life cycle). **III. ENV** serves to the depot of recycling process not used waste about its must be decided in using at external (outdoor) environments. These models are instruments to optimized environmental and logistic management all AWJ processes.

4. OBJECTIVES AND TECHNIQUES OF THE EVALUATION

The objectives are:

- to analyze and evaluate environmental consequences of AWJ cutting processes with concentration to ACPA;
- to solve abrasive recycling with minimization of ENV loading and economical costs.

DYVELOP[®] method is used as a fundamental evaluation technique for AWJ processes environmental evaluation. This instrument uses the logistic approach. The aids to experimental and practical validation of researched objects are the SEM photographs.

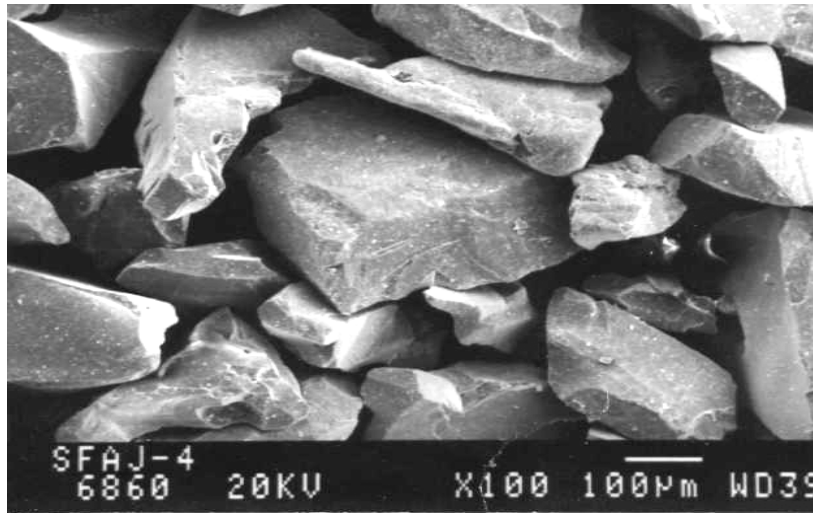


Figure 5. The SEM picture of preliminary crushed abrasive before first using.

Two types of abrasive (Garnet, Mesh 80) were researched: preliminary crushed; preliminary not crushed (it was only extracted from fluvial deposit).

The photographs show visual state of preliminary crushed abrasive. First conclusion is that ACPA obtains better shape (see Figure 6.) because acicular shape of abrasive grain is eliminated. This shape is more regardful to mixing tube. But dust particles occurrence ask its separation and it must be excluded before second using. It allow to express the opinion (which is supported by practical validation by Urbanek 2000) that recycled abrasive (type “preliminary crushed”) is more suitable to cutting process. It brings extension of mixing tube operating time to 20%.

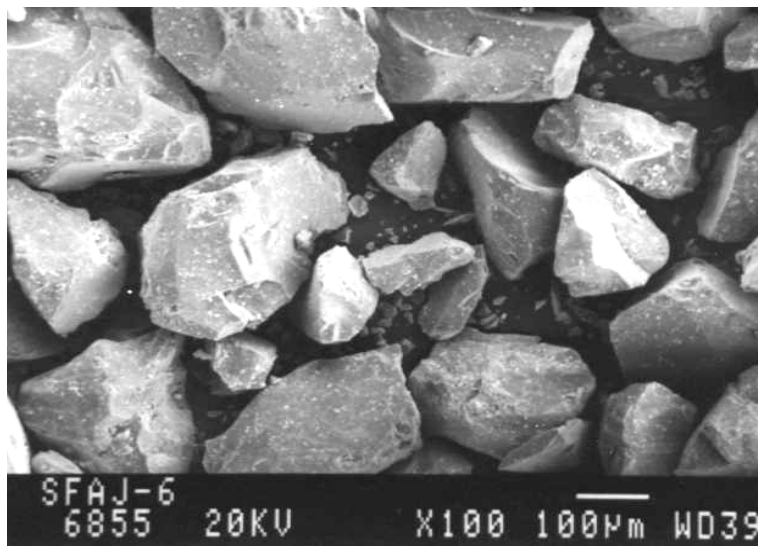


Figure 6. The SEM picture of preliminary crushed abrasive after first using.

Graph 1. shows the distribution of abrasive amount (relative density of an abundance in volume units) in the dependence to grain size of preliminary crushed abrasive. Three column plots represent this distribution:

- NEW ABRASIVE – maximum abundance of mean Mesh 80 of the “Garnet 80TM” is confirmed. The occurrence of other-size components is found regularly but in less amount.
- AFTER CUT-PROCESS ABRASIVE (ACPA) - maximum abundance of mean Mesh 95 is occurred. The shape of distribution plot is more flat and it is inclined to smaller grain-size. Dusty components are plentiful.
- RECYCLING ABRASIVE - recycling process includes drying, sorting, separation and selection. Mean Mesh 90 is obtained. The occurrence of other-size components is eliminated. Dusty components are separated.

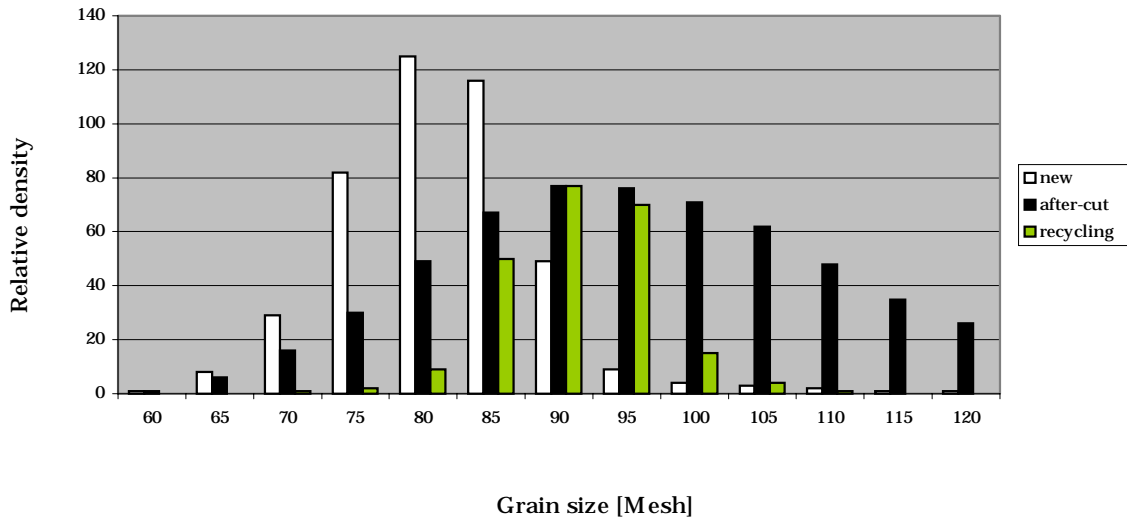
Second conclusion: first phase recycling recovery (yield) is 53 % (in the proportion to output volume of first phase after-cut-process abrasive). 53% volume amount “preliminary crushed” recycling abrasive is able to return to the second phase AWJ cutting process.

Third conclusion: recycling abrasive can be recycled repeat after second presentation in AWJ cutting process. The recovery is after than higher (in the proportion to the output volume of second phase after-cut-process abrasive). It is approximately 65% which is influenced by better shape (acicular shape of abrasive grain is eliminated) of abrasive (owing to lower abrasive breaking (crushing) in cutting kerf).

Four conclusion: “Preliminary not crushed” abrasive (extracted from fluvial deposit) is better to recycling. It gives results near above “abrasive after second presentation in AWJ cutting process” (65%).

Generally is possible to say very restrained estimation that repeated recycling can save 60% raw natural abrasive.

Graph 1. Relation between grain size and relative density of abrasive amount



5. RECAPITULATION AND CONCLUSIONS

The principal objectives of proposed project is a production, dissemination and using of the knowledge and technologies needed to design and develop processes and produce high quality, environment- and consumer-friendly URrec Device which will be competitive on tomorrow's market. Fundamental environmental target is to create enforceable and reliable technologic system able to treat all process waste, which arises during process and after using of Abrasive Water Jet (AWJ) technology. It will be fulfilled by means of environmental sustainable condition - to close waste treatment processes in workshop environment. A core is in the recycling of material flows and substances participated as an AWJ process agent. It must be provided that in a suppression of the disturbing and harmful influences on workshop environs. Inner environment of the workshop must be monitored from the point of view do not suffer any aggravation of the working, safety and hygienic conditions, which exceed European standards specifications and recommendations. Simultaneous targets are:

- by the recycling to unload an exploitation of abrasive natural sources, water and energy
- to reduce an import of natural abrasive into countries EC
- to improve quality of life and health by preserving the environment - refusing of waste abrasive dumping and excluding of waste-water pollution
- to create economic and ecological contributed URrec Device, able to compete overseas solution of this problem.

Fundamental methodological technical instrument of the creation, design, process planning and management, environmental engineering and other tasks of proposed project is Concurrent Engineering. By the methods of Concurrent Engineering and other suitable methods Industrial Engineering will be create a condition for successful project solution.

While fulfilling project aims will be used different progressive methods of industrial engineering, and the focus will be on increasing the productivity and efficiency of processes, and the attention will be paid on a market, a order and a customer. As a result of this, the outcome will be identification of realistic ways, resources, potential, tools and methods in order to increase productivity and above all to increase the competitive advantage of EC SME's industry. Brief planned Project URrec program follows.

5.1 Description of Project Work Program Items

- (1) Qualified description and analysis of real aims, characteristics, structure and environmental behavior of desired processes and systems solved in the project. Background research of successful solutions from overseas and anywhere.
- (2) Terrain research of recycling technology customer demands with marketing goal – to sale continental parties concerned.
- (3) A synthesis of models by applying of process - technologic - logistic – environmental approach. Concurrent engineering.
- (4) A project engineering design of device documentation and Device production process planning - concurrent engineering.
- (5) A debugging of proposed technology system with feedback to Device, process and technology design - concurrent engineering.
- (6) Complete recycling technology providing fellows from the Device production.
- (7) Specific task for all participants is successful dissemination of recycling technology and Device via a publicity.
- (8) Specific task for all participants is to supply of Device material via optimized way of the acquisition. The reserve AWJ system, components, materials and devices for the prototype construction and testing will be acquired.
- (9) A design and construct of prototype via fast prototyping with simultaneous testing and improving of Device produce ability – concurrent engineering.
- (10) A testing and evaluation of prototype with the aim to increasing & improving of using parameter aimed to process and device parameter optimizing. A energy and environmental pollution decreasing.
- (11) Specific task for the RTD Performer is to carry out simultaneously the Environmental Audit and Environmental Management in the sense of standards ISO 14000 and recommendation and laws of all EC countries.

- (12) An expedition of the Device will be fundamental task for SMEs. They will use all efficient means of their connection, the advertisement, publicity and other marketing instruments.
- (13) Specific and permanent task will be staff & experiences exchange via periodical meetings of all proposed project participants.
- (14) Appropriate successful solution of proposed CRAFT-GROW project will be complement final appreciation of all participants.

5.2 Community Added Value and Project Contribution

AWJ technology by its job-shop nature is centered to SMEs mainly. During last 20 years the workshop and terrain application of this technology was implemented nearly from zero number to approximately 1,2 thousand AWJ systems in whole Europe. The origin of industry applicable AWJ technology was in U.S.A and patent protected AWJ device construction is in prevalent rate produced here. But European SMEs takes care of own technology transfer as a technology providers. Here in wide European cooperation they are able to given in high quality and flexibility, after consumers demands, complete technology, including SMEs original components, subsystems and sets – e.g. the control systems, pumps, tables, nozzles, software and other components. Recently is possible to buy AWJ system from exclusive European components. European SMEs are at wide range of AWJ services provider. The interest of SMEs in process waste recycling is very virtuous and creditable, but it is not accidental. It follows from a necessity of the implementation of standard specifications ISO 14000, and all the time more and more severe European and national legislation – environmental sustainability. European competitive SME industry of the AWJ technology should play a key role in a contributing to sustainable development through reduction of material content of the production whilst increasing their service value, and through innovative, safer, cleaner and (in the case of successful recycling) lower natural resource utilization. Also arisen new methods of organizing production, service and logistics should be sought that reduce costs, time-to-market, lead-time, and make improved use of human resources. Since transnational industrial economic strength has increasingly been found in closely webbed interdependencies between firms, organizations and institutions, research objectives have to be considered not just within individual plants, construction sites or industries but throughout the extended value chains from raw materials to end-use products and services.

The abrasive as a raw material is mainly from extra European sources. The price of this abrasive is dictated out of European subjects. Abrasive recycling makes lower dependence at raw abrasive sources. It will save transport expenses and a great deal contributes to European environment preservation, by means of waste refuse excluding. The water recycling is imperative demand of our epoch.

The amount of not AWJ process recycling-able abrasive and waste decrease from former 80 tons/month, 1 AWJ system to future 30 tons, which can be qualified as a defined semi-product for other industrial treatment. So, the Project streams towards to “zero-waste production”. After

recycling out-coming “waste” will be useable as a semi-product of other industrial sectors (glass industry e.g.)

Material cost saving to 1 AWJ system is:

50 x 300,- euro/1 ton = 15000,- Euro.

Device investment back-flow comes after 15 months of average operation:

Planned URrec Device acquisition costs are **13500,-Euro + 35% year's operational (overhead) costs = 18225,- Euro : 15000 = 1,215 x 12 months = 15 months of average operation.**

The real economics saving of all European countries as a result of massive introduction of recycling devices URrec can be count in expected contribution (future state):

1200 continental Devices x 0,5 Project successfulness x average abrasive consumption 80 tons/year/ AWJ machine = abrasive import to Europe 48000 tons/year.

After recycling Device 100% introduction will be spared minimally 60% imported raw abrasive, it is **48000 x 0,6 = 28800 ton/year.** Than if average price is **300 EUR/ton abrasive,** the expected saving from unrealized import is **8.640.000 EUR/year.**

Even if only 33% validity of this opinion will be taken, the future strategic contribution of proposed Project (at planned nearly two years of its duration) will be thrice bigger than ask Project expenditures (approximately 0,5 million Euro) for whole Europe/1 year.

6. REFERENCES AND RELATED PROJECTS

Brandt, S., and Louis, H., “Controlling of High-pressure abrasive water suspension jets,” *15th International Conference on Jetting Technology*, British HR Group, Ronneby, Sweden, 2000, ISBN 1 86058 253 2.

Hashish, M., and Miller, P., “Cutting and Washout of Chemical Weapons with High-pressure ammonia Jets,” *15th International Conference on Jetting Technology*, British HR Group, Ronneby, Sweden, 2000, ISBN 1 86058 253 2.

Pospíchal, Z., and Urbánek, J.F., “Regional Case Study of Waste Recycling,” *1st International Conference on Solid Waste, Technology, Safety, Environment*, Rome, Italy 7-9 April 1999, pages 326 to 332, ICSW –99-1102.

Urbánek, J., Jurová, M., and Dvořáková, I., “Waste Treatment in the Logistical Chains,” *Proceedings of the Fourteenth International Conference on Solid Waste Technology and Management*, Philadelphia, PA U.S.A., The Journal of Solid Waste Technology and Management, 1998, ISSN 1091-8043.

Urbánek, J.F., Skála, Z., and Urbánek, K., “New Instrument of Integrated Waste Management – DYVELOP,” *15th International Conference on Solid Waste Technology and Management, The Journal of Solid Waste Technology and Management*, Philadelphia, PA U.S.A., 1999, ISSN 1091-8043.

Urbánek, J.F., and Kalo• , M., “AWJ Process and Post-processing Consequence to Environmental Protection,” *6th Pacific Rim International Conference on Water Jetting Technology*, Sydney, Australia, 2000, ISBN 1 876315 26 1.

Urbánek, J.F., and Koutný, O., “Environmental System of AWJ After cut-process abrasive recycling,” *15th International Conference on Jetting Technology*, British HR Group, Ronneby, Sweden, 2000, ISBN 1 86058 253 2.

Grant project No. ERB IC15 CT98 0821, Grant European Community INCO – Copernicus, “Abrasive Water Jet Cutting, a clean technology”, Head solver – Universität Hannover, Institut für Werkstoffkunde, Jet-Cutting, Appelstrasse 11, 30 167 Hannover, Germany, duration from 1998 to 2002.

Number of Project 101/00/0890, Grant project of Czech Grant Agency, Národní 3, 110 00 Praha 1, CZ, “An Implementation of Eco-environmental Management System to Machining and Metallurgical Companies”, Brno University of Technology - leder of scientific contents, duration to 2002.

7. NOMENCLATURE

ACPA	=	after-cut-process abrasive
SEM	=	Scan Electron Microscope
AWJ	=	Abrasive Waterjet
CRAFT	=	Cooperative Research
CZ	=	Czech Republic
DYVELOP©	=	Dynamic Vector Logistics of Processes
EC	=	European Community (and/or Countries)
ENV	=	environment
PLC	=	Product Life Cycle
P	=	price
RTD	=	Research, Technology, Development
SME	=	Small and Middle Enterprise
t	=	real time
URrec®	=	Under-one-Roof recycling
VA	=	Value Added
τ	=	transformation

ABRASIVE CUTTING COMPARISONS

R.D. Fossey, D. A. Summers, J. W. Newkirk, G. Galecki
University of Missouri-Rolla
Rolla, Missouri

M. Johnson, D. Burch
Naval Surface Warfare Center
Crane, Indiana

ABSTRACT

Recent years have seen a dramatic increase in the use of high-pressure abrasive waterjets for precision cutting of a wide range of materials, and an even greater increase of their use in hazardous environments as well as the cutting of hazardous materials. Our particular interest lies in the cutting of obsolete munitions and their casings for resource recovery and reuse. When cutting these metal casings, an abrasive is added to the high-pressure water stream. The performance of this cutting system can be controlled by varying the pressure, flow, and traverse velocity of the waterjet and is also influenced by the type of abrasive feed and the operational age of the cutting head.

The paper discusses a test program that evaluated the different types of cutting heads along with their characteristics and performances in head to head comparison cutting. Various specific components of each head will be compared.

1. INTRODUCTION

Several manufacturers offer abrasive cutting heads to industrial users, and each is purported to have advantages. But, as one user put it in the Yahoo waterjet list serve: waterjets@yahoogroups.com,

“...When you work on different nozzles, I do not care because I already have nozzles. Also, the differences will be small and not very significant because manufacturers are not stupid. It is a waste of your time and the sponsors money. Your work on cutting bombs is great but many others in the industry can do that too. Who is going to advance the science? me?”

In a perfect world, all nozzles and cutting heads would, indeed, work virtually the same and there would be no need to analyze performance. Alas, we live in the real world where everything is not always as it seems and the advancement of an industry or science relies on analysis. Previous studies (D. A. Summers, 2001) carried out at the University of Missouri-Rolla have found as much as a 60% operational difference between “identical” nozzles from the same supplier. And this test series showed a considerable difference in cutting ability between the nozzles (Figure 1).

2. BACKGROUND

The demilitarization of munitions using high-pressure waterjets has been an ongoing process, with some giant leaps and some much slower developments over the past decade. The use of abrasive entrained waterjets to cut casings for rapid disassembly of various munitions for resource recovery and recycling appears to be one that has seen only limited development. While the tool has found some use, the economics of the operation can be marginal in an industry where the cost of disposal of the abrasive and contents can be high. Improved economics and performance are essential for the further development of the technology. One target for such development is with its inclusion in a flexible disassembly facility currently under design at the Defense Ammunition Center (DAC) in McAlester, Oklahoma.

Johnson et al (M. Johnson, 1999; Dan Burch, et al., 1999; Dan Burch, et al., 2000) have evaluated the current costs of an existing system and shown its ability to slice a 40mm projectile within 24 seconds using an abrasive waterjet, and 21 seconds for an abrasive suspension jet, although the average time per cut was closer to 35 seconds for the AWJ and 30 seconds for the ASJ. The University of Missouri-Rolla is currently involved in a multi-phase investigation seeking, in part, to optimize both systems and compare total costs per shell to determine the most cost effective method of shell disposal. While many factors are included in the determination of the most efficient system, three “driving” factors include speed of cut, abrasive disposal cost, and nozzle life. As with most industrial operations, cost and speed are the deciding factors.

Preliminary studies carried out at Naval Surface Warfare Center (NSWC), Crane determined that, because of external drivers in the cutting cell cycle, nozzles should be replaced when they had worn to the point that effective cutting speed had to be reduced by 10% over the initial speed achievable. Many manufacturing operations do not have such a stringent requirement for

determining nozzle life, particularly when rough cutting thinner part sections than those of the current study.

This optimization study includes the comparisons of AWJ (Abrasive Water Jets) and ASJ (Abrasive Slurry Jets) performance, but only the first part is included in this paper.

3. APPROACH

The High Pressure Waterjet Laboratory at UMR under funding from NSWC and DAC has begun a study to compare the cutting effectiveness and efficiency of existing commercially available abrasive waterjet nozzles. The performance of six different heads under identical test conditions. Two metrics were used for the assessment of performance, one relating to the energy transfer to the particles, and one being the depth of cut.

The first test matrix evaluated each of the cutting head efficiency in a pristine condition. By analyzing the “throw distance” of the abrasive particles at three pressures and at three abrasive feed rates, a mass transfer efficiency could be determined. By further analyzing the size distribution of the particles as a function of their distance from the nozzle, a determination of the nozzle’s turbulence in the mixing chamber could be relatively evaluated. The abrasive used in these tests was Barton HP 80 garnet that had been sieved to scalp the larger particles (60 mesh and larger) as well as to eliminate any fines (100 mesh and smaller). With this starting point, a determination of the amount of energy absorbed by fracturing the garnet within a cutting head could be determined on a relative basis. For these tests, the cutting heads were positioned horizontally and the stream directed down a 38 foot semi-partitioned tube with holes along the bottom at each 12 inch interval (Figure 2). Following a one-minute run, all abrasives from each foot of the tube were segregated and collected in a tray. Each sample was then sieved and the separated sizes weighed individually.

Concurrently, a precision cut was made under each of the same nine conditions (pressures of 30,000, 40,000, and 50,000 psi with abrasive feed rates of .6, 1.0, and 1.5, pounds per minute) to establish a baseline with which to compare both relative performance and to provide a data base against which to assess the effects of wear on each of the cutting heads. A consistent target material from the same production run (mild steel) was used in all cutting tests. The heads were individually mounted on a precision X-Y table and the traverse velocity precisely controlled over the target sample. Abrasive feed was gravitational and the abrasive for these cutting tests was Barton HP 80 garnet directly from the bag, with no scalping or sieving. Water used for the tests is standard house water that has been filtered to 2 micron absolute and softened. The target samples were triangles of steel which were cut in the plane of the steel. This allowed one side of the cut to be easily removed so that the quality and depth of the cut could be easily determined (Figure 1).

The second mode of testing was to determine the effect of nozzle wear. Various materials were cut with a detailed log of use kept for each cutting head. At five hour intervals approximately, a precise test cut on a triangle of A-108 steel was carried out and the cut evaluated for signs of

wear. In this instance, depth of cut was the only criteria used, on the theory that any energy that was used to widen the kerf would necessarily be reduced from that needed to deepen the cut. All test cuts were performed at 1.5 inches per minute with .6 lbs. per minute of non – sieved Barton HP 80 garnet. The tests were conducted at 40,000 psi. The initial concept was to make a test cut every 5 hours of operation to determine wear. It was up to the operator, however, to increase the frequency of tests if he or she felt that the cut quality deteriorating. When the test cut for a particular cutting head showed a 10% decrease in depth, test cuts were run each hour of operation or more frequently until the head was deemed to be wholly inefficient and the head was removed and disassembled. The various wear components were then analyzed for failure patterns.

Six cutting heads were analyzed, all are readily commercially available. The most current head available from each supplier was purchased, as were spare wear parts. Each supplier was informed that the heads were to be used in competitive testing. All results are reported blindly, and, pending completion of the total research regime, no names will be identified with even partial results. The basic form of all six nozzle designs is roughly the same (Figure 4). The research is ongoing at the time of writing and final conclusions have not been drawn. However, some preliminary results are of interest.

4. RESULTS

All cutting heads tested showed decay of performance that accelerated at some point during testing. The change from baseline to 90% to further degradation was not consistent for each nozzle and occurred at different rates. The portion of the head that was the most obvious cause of performance loss was the focusing tube, which in most cutting heads is designed for easy and rapid replacement. The theorized wear pattern was that of a wave of material erosion beginning at the acceleration section and moving the length of the tube (Figure 5).

In the following discussion it should be noted that the illustrative sections used were obtained by cutting roughly along the axis of the nozzles. While the cut lies close to the axis of the bore, slight deviations can lead to optical distortions not reflecting reality.

Sectioned analysis of a worn tube shows that the erosion is not a simple widening of the tube starting at the throat and moving down the tube. Were this the case, then the tube would get narrower in a step-wise mode moving from the throat to the open end. However it can be seen, (Figure 5), that accelerated zones of wear lie downstream of the throat with some diameter enlargement.

Wear does not progress down the length evenly, but appears to concentrate at certain distances giving the illusion of a swelling and shrinkage over the tube length. This may be evidence of slight misalignment in the self-aligning head causing repeated particle rebound at the same points within the tube. It was also noted that the wear was asymmetrical. SEM inspection of the interior surface of the focusing tube showed different patterns of wear at different locations along the tube.

Within the conic re-alignment section the surface was pitted fairly regularly and consistently by particle impact (Figure 6). As the jet entered the straight tube section the wall was marked by long striations, however as one reached the open end of the tube, the damage was more evenly distributed with pitting and with some deposition of crystals of varying chemistry on the walls of the focusing tube.

For baseline comparison, an unused focusing tube was selected and sectioned. Close observation noted that the EDM penetration in the new tube was not itself symmetrical, which raised the specter that the wear patterns observed might not have been alignment related as previously thought. (Figure 7) More tubes from the different vendors are being evaluated to discern other differences in performance.

Immediately upstream of the focussing tube is the chamber where the water accelerates the abrasive. It has been found that wear in this element, from the incoming abrasive, is also critical to cutting head performance. While all tested cutting heads used basically the same focusing tube configuration, with only minor differences in geometry, the mixing chambers vary greatly from manufacturer to manufacturer in both geometry and material. Abrasives were introduced from an oblique angle as well as perpendicular to the direction of flow. Some heads have a separate replaceable component for mixing while others use a cavity in the head as the space for mixing to occur, and others combine the mixing chamber with the orifice. The first mixing chamber that we analyzed was from the latter and, after this cutting head had failed in service, it was found that the chamber had suffered obvious wear in all the parts that had come in contact with abrasive (Figure 8). A new mixing chamber of the same variety was then sectioned for a comparison and it was determined that there were significant geometrical differences between the two, even discounting wear. Again, comparative analysis was impossible.

Other types of mixing chambers showed less wear, even when the cutting head had fallen to an unacceptable level of performance. Some of the carbide insert chambers showed minimal wear while in others, with separate feed tubes, wear in the interface due to abrasive particle flow, could cause premature failure.

Upstream, in the cutting head, lies the orifice. These are manufactured primarily of sapphire, ruby, or diamond, and usually mounted in a steel fixture. The degree of wear on this part, which doesn't come in contact with abrasive, was surprising. Sectioned views of one sapphire orifice, for instance, show uneven erosion at the entrance section as well as the exit section. This can also be seen in pre-sectioned SEM pictures. It was found that the relatively minor wear on the downstream side of the jewel was exacerbated in the immediately underlying metal tube. The metal was significantly more eroded than the jewel (Figure 9).

When a new jewel insert was sectioned it was noted that there was an imperfect match between the bottom of the jewel and the subsequent tube (Figure 10). It is thought possible this would induce significant turbulence in the vicinity and accelerate local wear. This would have significant degradation in water velocity and concentration, degrading the energy going into the mixing process and reducing the overall particle energy. This would disburse the resulting jet stream leading to faster focusing tube wear and less particle energy as it left the tube (Figure 11).

A comparison of sapphire and ruby jewels showed that a change in jewel type didn't necessarily improve performance (Figure 12). The contrast of entrance sectioned of new and used ruby shows significant beveling as well as the obvious chipping in the used ruby (which was replaced after 18 minutes of use). Again, turbulence could be introduced at this point creating additional wear as well as absorbing energy from the abrasive and reducing cutting ability. Comparison of the cross section of a new orifice and mount might provide some insight for wear patterns and comparison of worn with the new Figure 13.

It was also noted that upon close inspection of the sapphire, ruby, and diamond orifices, particles were found adhered to the interior portions of the jewels. Material inside the throat of an orifice creates additional turbulence and will deflect the jet, and ultimately the abrasives from their intended path.

5. CONCLUSIONS

Basic cutting head design has improved considerably over the years, particularly in the mixing area, but there appears to be some room for further improvement. There are differences in initial performance, and in operational lifetimes between the nozzle designs supplied by different manufacturers. Erosion in the jewel and mixing chamber sections of the nozzle assemblies was as likely to cause premature focusing tube failure and performance degradation as was normal erosion. Minimum standards for water quality must be met since "dirty" water could cause premature failure in the jewel sections of the nozzle. A cost/benefit analysis is a useful tool for evaluating relative benefits of improving component part life. Research on comparative cutting efficiency among the heads available, and between AWJ and ASJ, will continue and the results of these findings will be reported.

6. ACKNOWLEDGEMENTS

The authors gratefully acknowledge the fine work of James Reck and Qingcai Liu in providing exceptional microscopy and Scanning Electron Micrography for this paper. Thanks are also due for the support of James Wheeler and Greg Olson of the Defense Ammunition Center.

7. REFERENCES

- D.A. Summers "Waterjet Use in decontaminating Interior Surfaces" American Nuclear Society Annual Meeting, Spring, 2001 Seattle Washington.
- M Johnson, "Abrasive Cutting of 40mm Projectiles" F/Y 99 annual Report to Defense Ammunition Center, McAlester, OK.

Dan Burch, John Griggs, Mike Johnson, Greg Olson, David Summers, “Abrasive Waterjet Cutting Demilitarization of 40MM Projectiles” 1999 Global Demilitarization Symposium & Exhibition, Tulsa, OK, May 20, 1999

Dan Burch, John Griggs, Mike Johnson, Greg Olson, “Abrasive Waterjet Cutting Demilitarization of 40MM Projectiles”, 2000 Global Demilitarization Symposium & Exhibition Coeur d’Alene, ID, May 18, 2000.

8. FIGURES AND TABLES



Figure 1. Depth of cut comparison for 6 nominally equivalent nozzles from different manufacturers, cutting steel at 40 ksi, 0.6 lb/min at a cutting speed of 1.5 inches/min.



Figure 2. Particle analysis test setup – in a test additional segments were attached to the tube, which extended beyond the door, and a covering tube enclosed the stream.



Figure 3. Computer controlled X-Y table.

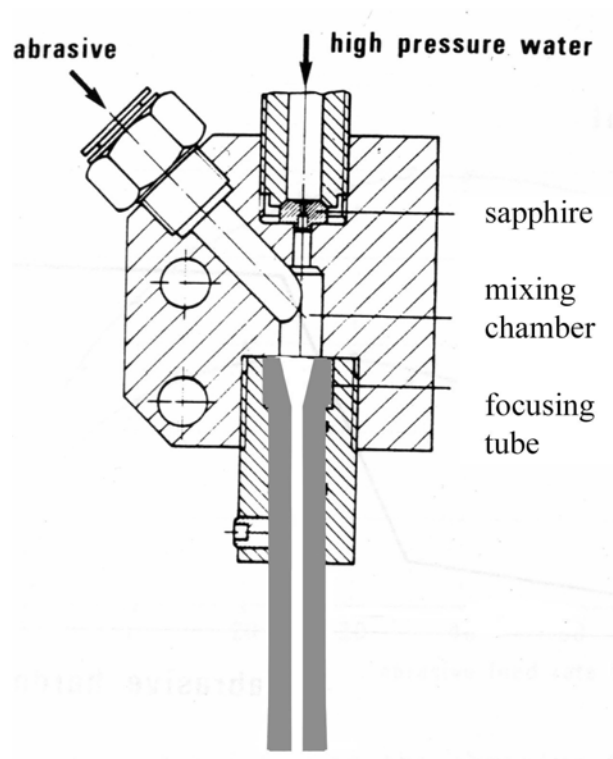


Figure 4. Cutting Head Wear Components.

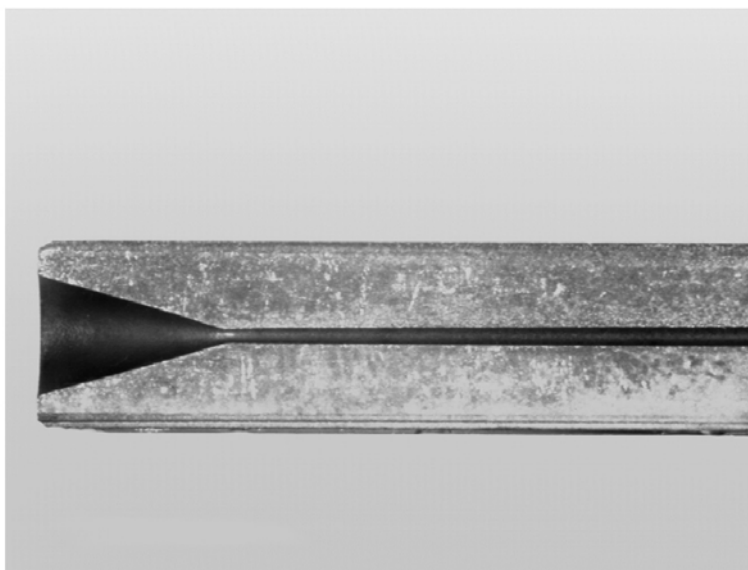


Figure 5. Focusing tube wear.

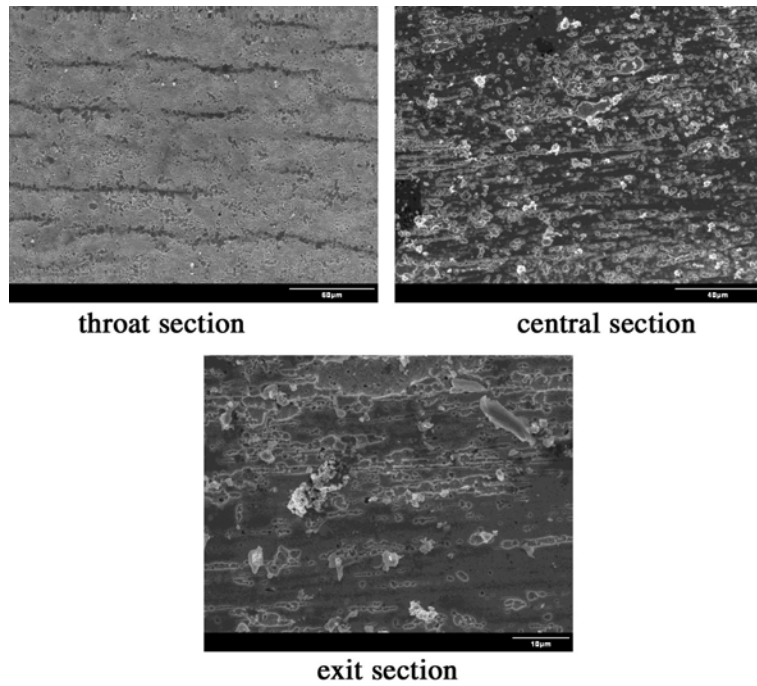


Figure 6. Scanning Electron Microscopy at points along the tube interior wall.

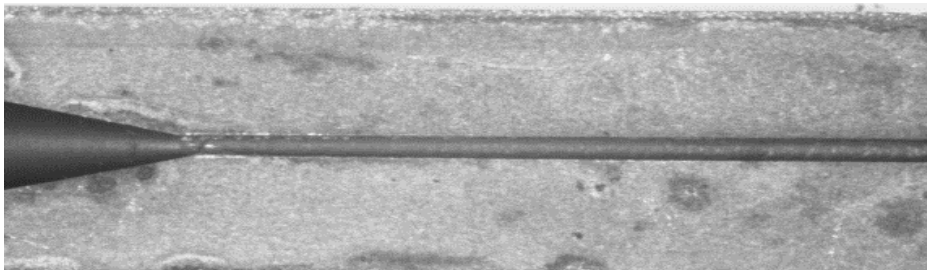


Figure 7. New Focusing Tube, misaligned EDM drilling.

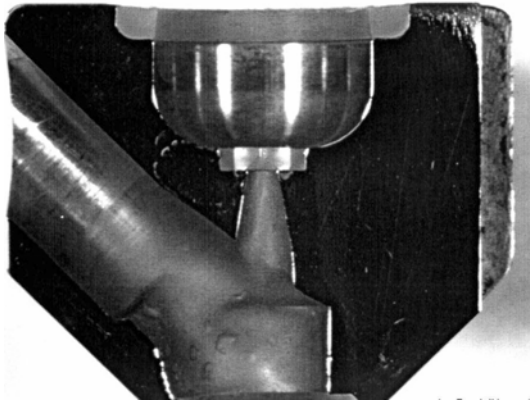
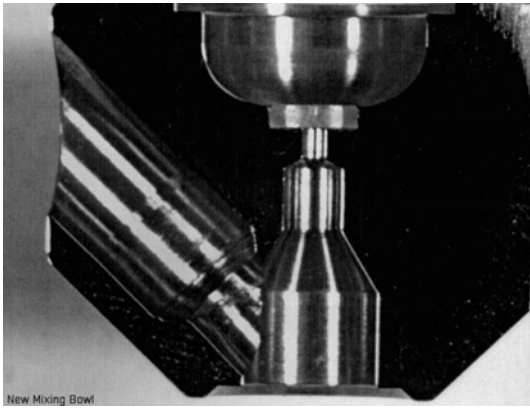


Figure 8. New Mixing Chamber and one used for 50 hours.

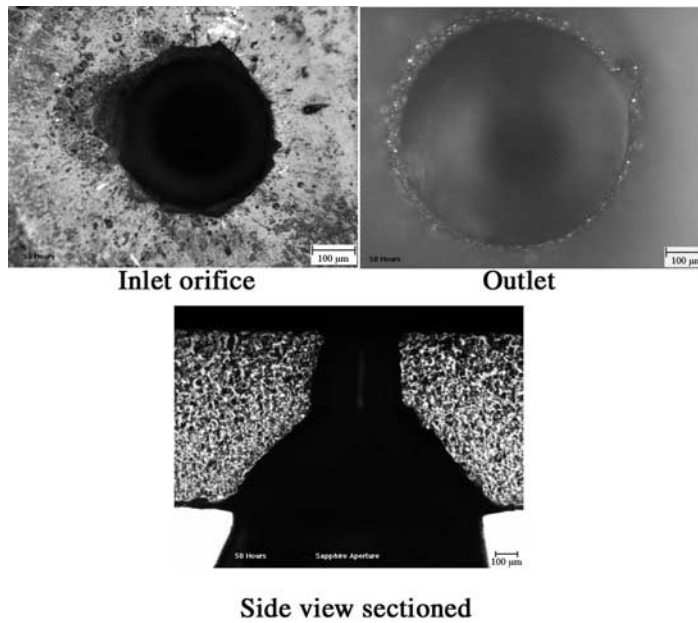


Figure 9. Damaged jewels

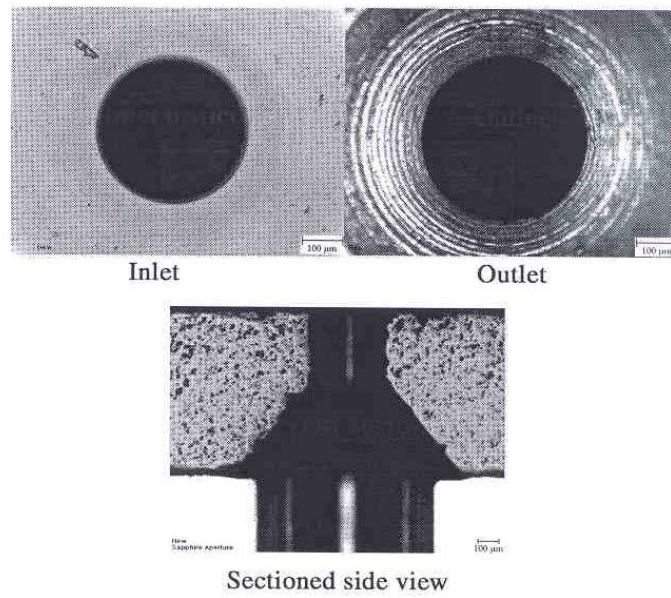


Figure 10. New Sapphire Orifice.

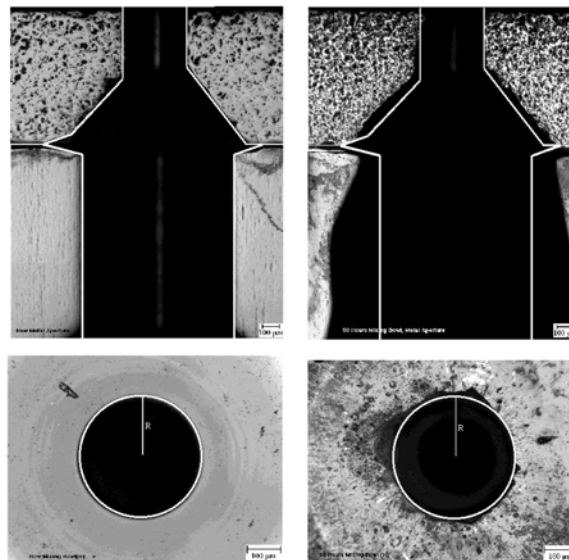


Figure 11. Wear on Sapphire and metal mount.

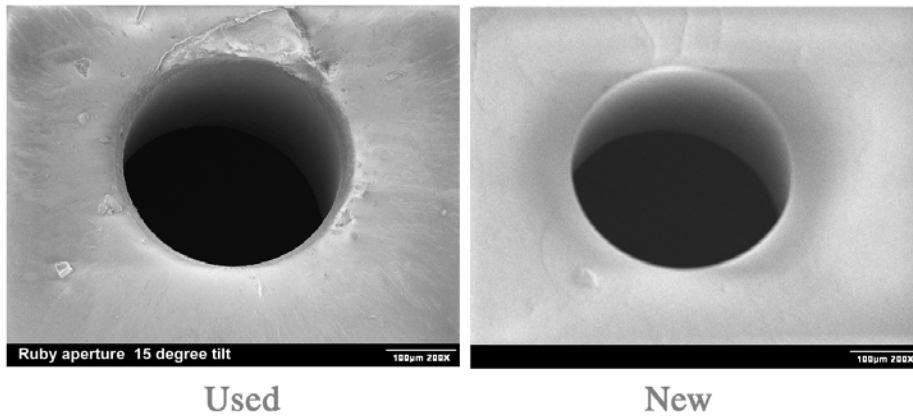


Figure 12. SEM Ruby Orifice Entrance Sections.

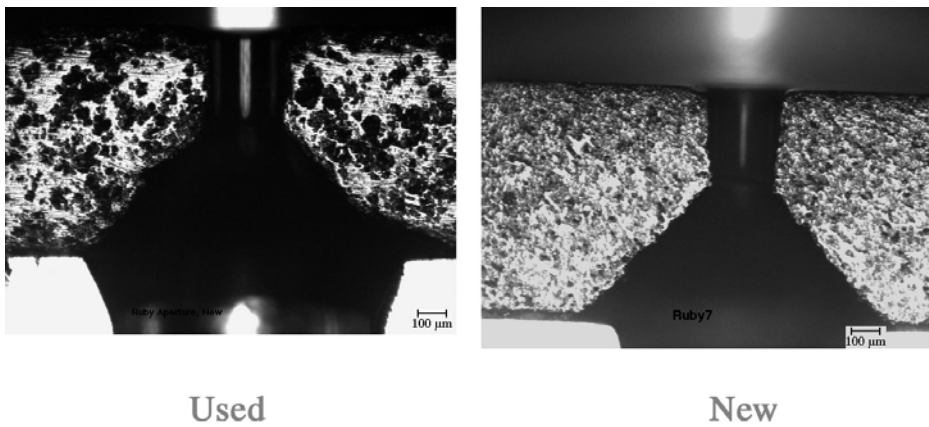


Figure 13. Sectioned Ruby Orifices.

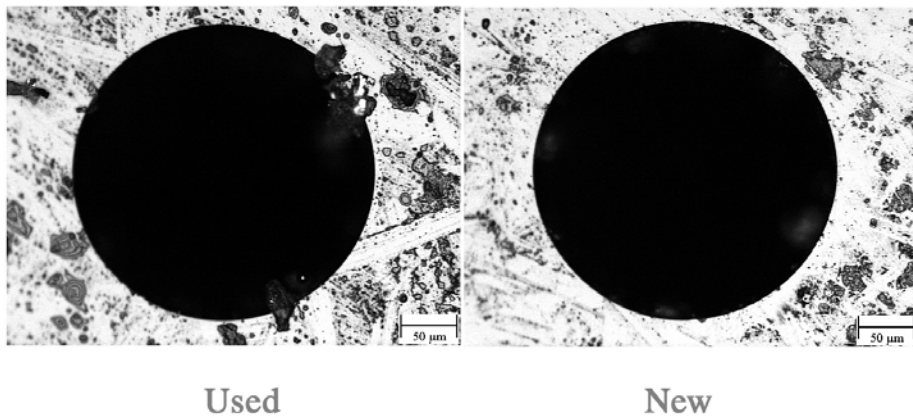


Figure 14. Diamond Orifice Entrance Sections.

ELECTROSTATIC CHARGE GENERATION IN WATERJET SYSTEMS

Paul L. Miller
Gradient Technology
Blaine, MN

ABSTRACT

The use of waterjets can generate electrostatic charges that are potentially hazardous to personnel and harmful to equipment and product. Several serious fires have been attributed to static discharge during waterjet cleaning operations, and static electric arc discharge has been known to damage composite materials. The waterjet industry's trend toward using higher velocity liquid jets and higher purity water increases the risk of electric spark generation as shown by theoretical analysis and empirical testing. This paper identifies the mechanisms related to static electric charge generation during waterjet operations and the corrective measures necessary to control potentially hazardous electrostatic discharge.

1. INTRODUCTION

The presence of static electricity has been known since early Greece, and most likely long before. The modern word “electron” is derived from the Greek word for the material known to us as amber, as it was commonly used for developing a static electric charge. For most technologies throughout time the build-up of static electricity was little more than a nuisance. A century ago the worst effects a person could expect from static electricity was a jolt when touching a doorknob on a winter’s day. It was not until combustible dusts and flammable liquids became more prevalent that the more serious hazards of electrostatic discharge (ESD) became well known. Modern fluid jet equipment has the potential of generating thousands of volts of electricity and has caused several spectacular fires from undesired ESD generation around flammable materials.

1.1 Static Electricity Fundamentals

Static electricity is caused by the buildup of an electrical charge imbalance, with one item’s having an excess of electrons and another item’s having a deficiency of electrons. The transfer of electrons to balance out the systems is called an electrostatic discharge. Since the speed of electricity is functionally the same as the speed of light, or about $3.0 \times 10^8 \text{ m}\cdot\text{s}^{-1}$, when using a good conductor the transfer rate can be extremely fast. Nonconductive materials can substantially slow down the rate of electron transfer and can effectively prevent electrons from flowing.

When two different uncharged materials are in contact, an “electrical double layer” forms where electrons transfer back and forth with a “contact potential” of between 1.0×10^{-3} to 1.0×10^{-1} volts. When two conductive materials are used, the electrons can quickly transfer back and correct any differences in electron balance. However, when a nonconductive (or insulating) material is used, some of the electrons can be “trapped” on its surface and the imbalance in electron quantities can create an electrical potential. The length of time required for the electrical charges to dissipate from a given material is known as the “relaxation time.” The relaxation time for hydrocarbons of different conductivities is shown in Table 1.

1.2 Electrostatic Discharge Damage

Many common modern materials and equipment can be damaged by electrostatic discharge. These items can include computer components, photographic film, electrical equipment, and composite laminates. In some extreme cases, workers can be injured or even metallic structures damaged from ESD.

In most of the cases the ESD damage is from a localized melting of an item due to the extreme levels of heat generated by a miniscule electric arc. Integrated circuit components are especially vulnerable to such discharge and can even be damaged by the amount of electricity accumulated when people walk across a floor. The ESD sensitivity standards for electrical components is shown in Table 2.

Even more important is the potential for ESD to ignite flammable liquids and combustible dusts. As shown in Table 3, the amount of energy required to ignite common flammable materials is rather low. A more unusual concern is in locations where ESD can ignite explosive materials at very low electrical energy levels as shown in Table 4. Explosive materials usually receive extreme attention in such situations, but flammable liquids and gases actually require substantially less energy to ignite, as shown in Tables 3 and 4.

2. ANALYZING AND CONTROLLING ESD HAZARDS

2.1 Creation of a Hazard

Before any accident can occur many intermediate steps must take place to properly set the scene. The first step in creating a hazard is usually that there must be hazardous or sensitive material present in order to cause a problem. The second step is often that certain environmental conditions must be favorable for an event to take place. The third step is that a source of energy is present, while the fourth step is the factor of probability and may take the form of “luck” or of “Murphy’s Law” depending on if it is working for you or against you.

2.2 Eliminating Hazards by Removing Hazardous or Sensitive Materials

The presence of hazardous or sensitive materials is simple to resolve in many cases. We can simply remove the flammable liquids or explosives from the area before we do any work or remove the work to a separate area where there is no exposure to the hazardous materials. For the sake of argument, we will include sensitive electronic equipment in this same group. However, there are certain operations where we might not be able to remove the hazardous or sensitive materials from the area in which we are working, often because we are working directly on these materials or trying to remove other material in close proximity to them.

Flammable liquids and gases are considered hazardous when sufficient quantities are present to exceed their lower flammability limit (LFL) and be below the upper flammability limit (UFL). The LFL and UFL levels for flammable liquids and gases are published in NFPA 325-M (1984) and Zabetakis (1965).

2.3 Environmental Conditions

In order for many materials to become hazardous there must be certain environmental conditions present. The most important one is usually oxygen present in the atmosphere in order to support fire. This environmental condition does not affect explosives, which contain their own oxygen, or electrically sensitive components. In order to eliminate the oxygen in a space an inert gas purge is often used. Inert gas purging requires some special technical considerations depending on the hazardous material and can be extremely dangerous to personnel entering a confined space. Special precautions are required and a safety engineer should be consulted prior to using an inert gas purge in a work area.

Another common environmental factor is temperature. Materials that normally are safe to handle may become flammable if the temperature is substantially raised. The rise in temperature can come from situations such as metal surfaces exposed to sunlight or even from the hot water in a waterjet spray.

To recalculate the LFL of a flammable liquid or gas at an elevated temperature the following equation, shown in Crowl and Louvar (1984), is used:

$$LFL_{\text{elevated}} = LFL_{25} \cdot [1 - 0.75 \cdot (T-25) \cdot \Delta H_c^{-1}] \quad (1)$$

$$UFL_{\text{elevated}} = UFL_{25} \cdot [1 + 0.75 \cdot (T-25) \cdot \Delta H_c^{-1}] \quad (2)$$

where	LFL_{elevated} = lower flammability limit at elevated temperature LFL_{25} = lower flammability limit at 25 degrees C ΔH_c = net heat of combustion ($\text{kcal} \cdot \text{mole}^{-1}$) UFL_{elevated} = upper flammability limit at elevated temperature UFL_{25} = upper flammability limit at 25 degrees C.
-------	---

Another common environmental factor is the presence of water vapor. Sufficient water vapor can act as a conductive material to drain off excess electrical charges and many operations handling explosives or sensitive electronic components are conducted in humidified areas to minimize ESD damage according to NFPA 77 (1993). However, the presence of humidity should not be depended on for reducing the hazard, as in some cases the presence of moisture actually increases the risk as shown in Roux et al., (1993) where HMX explosive is *most* sensitive to ESD at 60% humidity.

2.4 Electrostatic Charging of Liquids

The third factor in the generation of an ESD hazard is the creation of energy. For waterjet operations this is usually caused by the flowing of liquids but can also occur from the impact of crystals against hard targets.

It is a well known phenomenon in safety engineering that flowing liquids can generate large amounts of static electricity. This generation of static electricity from flowing liquids even occurs during the operation of items expected to be “safe.” A classic example is the generation of up to 5,000 volts during the discharge of a carbon dioxide fire extinguisher as described by Petrick (1968).

Usually the liquid must be a poor conductor in order to build a substantial electrical charge. Plain water used for waterjet cleaning is not normally considered a “poor conductor” of electricity, but it can be. As detailed in Reif and Hawk (1974), three very large crude oil carriers (VLCC) were destroyed in December 1969 from electrostatic discharge during washdown by waterjets. Tests performed as a result of these accidents led to the following observations:

- clean seawater sprayed on oil-contaminated walls produced a negative electrical charge
- clean seawater sprayed on clean walls produced a positive electrical charge

- water-containing detergents sprayed on either dirty or clean walls produced a negative electrical charge.

The investigators came to the conclusion that the water spray created a charged cloud of water droplets which was able to store sufficient energy to create an electrical discharge. The charged clouds were able to create between 2.2×10^4 and 1.0×10^6 V during the washing process.

All of these tests were performed with water that would be considered as being highly conduction. In several tests performed in this author's presence, high pressure (350 MPa) waterjet systems also create substantial electrostatic charge buildup as purified water was being used. In these cases the electrostatic charge was sufficient to create a corona discharge, or ionization of the nitrogen in the atmosphere, identifiable by a distinctive pink glowing cloud around the nozzle. As water is purified, either by reverse osmosis (RO) or deionization (DI) technologies, the conductivity of water is substantially reduced. The lack of conductivity is actually used for determining the quality of the purified water.

2.5 Electrostatic Charging Mechanisms

When liquids flow through any system they rapidly build up an electrical charge. If the liquid is conductive, the liquid just as rapidly gives up the electrical charge. For non-conductive liquids, the time to dissipate the electrical charge may be substantial. We refer to the ability of a given liquid to dissipate the electrical charge as the relative dielectric constant (ϵ) and the conductivity of the liquid as its specific conductivity (γ).

Eichel (1967) shows that the relaxation time for a liquid to dissipate the electrical charge built up in it would be:

$$t_r = 8.85 \times 10^{-16} (\epsilon \cdot \gamma^{-1}) \quad (3)$$

where

t_r	=	relaxation time (sec)
ϵ	=	relative dielectric constant (dimensionless)
γ	=	specific conductivity (mho \cdot m ⁻¹)

The double thickness layer is described by Eichel (1967) as the equivalent distance between two plates of a condenser that would have the same capacitance as the interface layer of the fluid flowing through the pipe. The double thickness layer is calculated as:

$$\delta = (D_m \cdot t_r)^{-0.5} \quad (4)$$

where

δ	=	double thickness layer (meter)
D_m	=	molecular diffusion constant (m ² \cdot s ⁻¹)
t_r	=	relaxation time (sec)

The amount of electrons captured or lost by a liquid flowing through a hose or pipe is termed the streaming current. The streaming current for turbulent flow ($R_e > 2400$) adapted from Crowl and Louvar (1984) is:

$$I_s = (1.932 \times 10^{-13} \cdot \text{amp} \cdot (\text{m} \cdot \text{s}^{-1})^{-1} \cdot \text{volt}) \cdot ((d \cdot u \cdot \epsilon \cdot \zeta) \cdot \delta^{-1}) \quad (5)$$

where

$$\begin{aligned} I_s &= \text{streaming current (amp)} \\ d &= \text{pipe diameter (meter)} \\ u &= \text{fluid velocity (m} \cdot \text{s}^{-1}) \\ \epsilon &= \text{relative dielectric constant (dimensionless)} \\ \zeta &= \text{contact potential (volt)} \\ \delta &= \text{double thickness layer (meter)} \end{aligned}$$

The specific parameters for common liquids can be found either in Dean (1985) or in Perry (1950).

The voltage that the liquid accumulates it then calculated by:

$$V_a = I_s \cdot (L \cdot (\gamma \cdot A))^{-1} \quad (6)$$

where

$$\begin{aligned} V_a &= \text{accumulated voltage (volt)} \\ I_s &= \text{streaming current (amp)} \\ L &= \text{length of pipe or hose (meter)} \\ \gamma &= \text{specific conductivity (mho} \cdot \text{m}^{-1}) \\ A &= \text{area of pipe or hose (m}^2) \end{aligned}$$

Likewise, the accumulated charge received by a streaming fluid can be calculated as:

$$Q_a = I_s \cdot t \quad (7)$$

where

$$\begin{aligned} Q_a &= \text{accumulated charge (coulomb)} \\ I_s &= \text{streaming current (amp)} \\ t &= \text{operation time (sec)} \end{aligned}$$

The amount of energy that can be stored in an object with an electrostatic charge is given as either:

$$\text{or} \quad J_a = C_a \cdot V_a^2 \cdot 2^{-1} \quad (8)$$

$$\text{or} \quad J_a = Q_a \cdot V_a \cdot 2^{-1} \quad (9)$$

$$\text{or} \quad J_a = Q_a^2 \cdot (2 \cdot C_t)^{-1} \quad (10)$$

where

$$\begin{aligned} J_a &= \text{accumulated energy (joule)} \\ C_t &= \text{target's capacitance (farad)} \\ V_a &= \text{accumulated potential (volt)} \\ Q_a &= \text{accumulated charge (coulomb)} \end{aligned}$$

Eichel (1967) states that the minimum sparking potential is about 350 volts and that this can easily be achieved by using low conductivity liquids with either high velocity or high volume flow. For high velocity waterjets, the presence of a corona indicates that the potential may be as high as 30,000 volts.

2.6 Control of Static Electricity

There are many ways to control static electricity that are quite effective:

1. Always bond all components together with a grounding cable and have a secure connection to ground.
2. Use conductive piping and hoses. Be careful that gaskets do not insulate the piping from the system.
3. Minimize fluid velocity by using larger diameter piping or hoses. A rule of thumb given by ESCIS (1988) is $1 \text{ m} \cdot \text{s}^{-1}$ maximum fluid velocity.
4. Use humidity to minimize static buildup if it is appropriate for the hazardous material in the area.
5. Eichel (1967) suggests using ionization (either electrically or radioactively) to minimize static buildup.
6. The use of additives to the spray stream to increase the conductivity of the liquid may also be useful, according to Eichel (1967).

2.7 Risk Analysis

The fourth factor mentioned above is the probability of an event's happening. Statistics show that the risk of an undesirable event's happening is based on the amount of energy applied and the number of times the stimulus is applied. Many situations have occurred in which the exact same process was used repeatedly without an accident until the one event occurred during which the accident happened. The most common method for minimizing risk is to minimize exposure to hazardous materials when operating by removing them from the operating area. The next best method, if the materials cannot be removed, is to remove all sources of ignition from the process. It is only through thoughtful planning, rather than "lady luck," that safe operations can be provided.

3. CONCLUSIONS

Those individuals who need to work with waterjets near sensitive or hazardous material should be very familiar with the potential for serious electrostatic charge generation, even in seemingly innocent operations. For this reason any operations in proximity to sensitive or hazardous materials should be evaluated by trained personnel to make sure that the operation cannot

generate sufficient energy to cause an ignition of hazardous materials or damage to sensitive components.

4. REFERENCES

- Brown, F. W., Kusler, D. J., and Gibson, F. C., Sensitivity of Explosives to Initiation by Electrostatic Discharges, U.S. Bureau of Mines Report of Investigations 5002, p. 6, September 1953.
- Crowl, D. A and Louvar, J. F., Chemical Process Safety, Prentice Hall, Englewood Cliffs, NJ, p. 212, 1984.
- Dean, J. A. (ed), Lange's Handbook of Chemistry, 13th edition, McGraw Hill Corp., New York, NY, 1985.
- Eichel, F. G., "Electrostatics", Chemical Engineering, p. 163, March 13, 1967.
- ESCIS (Expert Commission for Safety in the Swiss Chemical Industry), "Static Electricity: Rules for Plant Safety," Plant/Operations Progress, Vol. 7, No. 1, January 1988.
- ESD STM5.1-1998 Revised: Electrostatic Discharge Sensitivity Testing -- Human Body Model. ESD Association, Rome, NY, 1998.
- NFPA 325M, Properties of Flammable Liquids, Gases, and Solids, National Fire Protection Association, Quincy, MA, p. 325M-88, 1984.
- NFPA 77, Static Electricity, National Fire Protection Association, Quincy, MA, 1993. p. 77-6.
- Perry, R. H (ed), Perry's Chemical Engineering Handbook, 3rd edition, McGraw Hill Corp., New York, NY, 1950.
- Petrick, J.T., "Electrostatic Hazards in Processing Explosives," 10th Department of Defense Explosive Safety Seminar, Vol I, 1968. p. 1406. Declassified and downgraded July 7, 2000. Approved for Public Release: Distribution Unlimited
- Reif, R. B. and Hawk, S. A., Review and Evaluation of the Literature on Electrostatic Generation in Tank Cleaning, U.S. Department of Transportation, Coast Guard, DOT-CG-23223-A, 1974. Approved for Public Release: Distribution Unlimited
- Roux, M., Auzanneau, M., and Brassy, C., "Electric Spark and ESD Sensitivity of Reactive Solids (Primary and Secondary Explosive, Propellant, Pyrotechnics) Part One: Experimental Results and Reflection Factors for Sensitivity Test Optimization," Propellants, Explosives, Pyrotechnics, Vol. 18, pp. 317-324, 1993.
- Zabetakis, M.G., Flammability Characteristics of Combustible Gases and Vapors, U.S. Department of Interior, Bureau of Mines Bulletin 627, 1965. p. 60.

Table 1. Relaxation Time for Hydrocarbons of Differing Conductivities (Eichel, 1967)

Conductivity (mho•m⁻¹)	Relaxation Time seconds	Material
10 ⁻²⁰	2.196 x 10 ⁵	hexane
10 ⁻¹⁹	2.196 x 10 ⁴	benzene
10 ⁻¹⁸	2.196 x 10 ³	
10 ⁻¹⁷	2.196 x 10 ²	xylene
10 ⁻¹⁶	2.196 x 10 ¹	toluene
10 ⁻¹⁵	2.196 x 10 ⁰	

Table 2. Electrostatic Sensitivity Levels of Electrical Components – Human Body Model (ESD, 1998)

Class	Voltage Range
Class 0	<250 volts
Class 1A	250 volts to <500 volts
Class 1B	500 volts to < 1,000 volts
Class 1C	1000 volts to < 2,000 volts
Class 2	2000 volts to < 4,000 volts
Class 3A	4000 volts to < 8000 volts
Class 3B	>= 8000 volts

Table 3. Electrostatic Sensitivity Levels of Common Flammable Materials (NFPA 1993 and Crowl and Louvar 1984)

Material	Ignition Energy (J)
Methane	2.9 x 10 ⁻⁴
Propane	2.5 x 10 ⁻⁴
Cyclopropane	1.8 x 10 ⁻⁴
Ethylene	8.0 x 10 ⁻⁵
Acetylene	1.7 x 10 ⁻⁵
Hydrogen	1.2 x 10 ⁻⁵
Gasoline	1.0 x 10 ⁻³

Table 4. Electrostatic Sensitivity Levels of Explosive Materials (Brown, et al 1953)

Material	Ignition Energy (J)
Lead Azide	7.0×10^{-3}
Mercury Fulminate	2.5×10^{-2}
TNT	6.2×10^{-2}
Tetryl	7.0×10^{-3}
PETN	6.2×10^{-2}
Smokeless Powder	1.2×10^{-2}
Black Powder	8.0×10^{-1}

ABRASIVE WATERJET CUTTING A COMPARATIVE STUDY BETWEEN OPEN CATCHER TANK AND WATER CATCHER TANK

J. Munoz, I. Kain
Ingersoll-Rand Waterjet
Bryan, Ohio, U.S.A.

ABSTRACT

This paper compares the Sound Pressure Levels (SPL) generated from the waterjet cutting process between an open catcher tank and an adjustable water level catcher tank (also known as water catcher tank) for two dimensional cutting. It also provides practical measurements of noise levels at different pressures using various cutting nozzle sizes. Further, by continuously monitoring the cutting activities, this paper provides the waterjet user with useful information that can best determine the allowable daily exposure of the operator to the noise level. As a result, the waterjet shops can assess the safety measures and standards that they have to practice, irrespective of the type of job.

1. INTRODUCTION

The waterjet cutting technology has accelerated in recent years to meet the immense expansion of the many new applications. Despite of the rapid growth of this incredible technology, there is always a challenge to develop the safest, simplest, cost effective and powerful turnkey systems. The nature of the phenomena is embedded with a radical challenge that remains the key element in this fastest growing technology. Effective pressurization of water up to and beyond ultra high pressures in order to obtain high cutting efficiency through a supersonic jet, still remains the main core of the business. Thus, noise levels generated by this process will always be an inherent component. The technological advancements have been challenged to determine methods to attenuate and to suppress the noise levels.

The noise levels generated at elevated water pressures during the cutting operation is caused by a few factors some of which are:

- Direct impact of the jet on the workpiece such as piercing routine
- Breakdown of the airways by the jet
- Collision of the jet with the workpiece during the erosion process
- Cavitation and jet speed

2. BACKGROUND

Generally, in abrasive waterjet (AWJ) cutting, catcher tanks serve mainly two purposes. First, they hold and support the workpiece and second, they capture the dispensed abrasive and water from the cutting nozzle including any effluents. During the evolution of the waterjet cutting technology, catcher tanks have witnessed a rapid changing trend in the way they are designed and manufactured.

At the beginning, the vast majority of catcher tanks were configured as solid steel tanks to serve the above purposes. The latter is known as an open catcher tank or standard catcher tank. Currently, with recent innovations of many technological developments, tanks have transitioned into a more fashionable design.

This step is to overcome the intense noise levels generated by the jet. When cutting at various elevated water pressures, catcher tanks absorb and dissipate the remaining energy of the jet that could be exiting at roughly twice the speed of sound. The more the jet is exposed to the ambient environment and to the airways, the more noise is generated. Open catcher tanks generally perform the task to certain point where they act as a compartment or a container to the remaining energy, but do not help reduce the noise carried by this high energy to a level that is tolerable by the operator.

Hazardous noise is any continued and excessive exposure to noise levels at or above 85 decibels. These levels are enough to permanently damage the operator's hearing. Thus, most operators who are subjected to long periods of loudness are required to have earplugs or earmuffs. This tends to be very disturbing and cumbersome to the operator over a long period of time. Giving

operators a choice of work environment, applicable knowledge, and personal comfort are important aspects in reducing the likelihood of noise-induced hearing loss.

To reduce the loudness and to achieve comfortable work conditions, adjustable water level catcher tanks were designed to lower the intensity of the noise. These types of tanks give the user flexibility by adjusting the water level in the tank in order to either partially submerge or fully submerge the workpiece, depending on the material conditions. The noise generated during the cutting course when the workpiece is submerged will be reduced drastically to a permissible level where minimal or no or marginal ear protection is required.

The purpose of this study is to measure the noise generated from the abrasive waterjet nozzle at certain given conditions. These measurements of noise were conducted with different diameters of orifices and focusing tubes, various abrasive flow rates and different water pressures. Other operational parameters, were left unchanged from those normally used in the abrasive waterjet cutting process, i.e., the standoff distance was set to approximately 2.3 mm, the length of the focusing tube was kept at 76.2 mm and the 80 mesh garnet was used during the whole experiment.

3. SETUP & PROCEDURE

Two types of catcher tanks were used to setup and prepare for data collection: an open catcher tank that was basically empty and an adjustable water level catcher tank. The water level in the latter tank was controlled pneumatically and allowed for partial or complete submersion of the workpiece. For test purposes, 25.4 mm HR Steel was used as the workpiece. Three cases were examined:

- The workpiece was placed on the grating on the open catcher tank
- The workpiece was placed on the grating on the adjustable water level catcher tank. The water level was at 19.05 mm below the upper surface of the workpiece
- Same as case 2, but the workpiece was completely submerged with water level up to 12.7 mm above the upper surface

The physical dimensions of both catcher tanks used are about 30.5 cm x 122 cm x 91.5 cm. The Sound Pressure Levels were recorded using a Simpson 884 Type S2A Sound Level Meter at slow response. The instrument was calibrated to take into consideration the influence of the environment and mounted on a tripod approximately 1 m away from the sound source and 1.5 m above the floor where the catcher tank was placed. The ambient noise level was recorded to be 65 dB(A).

The test site was selected to collect noise data that best represents practical measures of typical job shop environment. For comparison purposes only, first, SPLs were recorded without abrasive introduction to the nozzle then, abrasive was entrained into the water stream to begin cutting in order to collect another set of SPLs. This was only to examine the noise generated before and after adding abrasive particles.

4. RESULTS AND DISCUSSIONS

The SPL results of this experiment are presented in this section. The following sets of parameters were selected to collect the data.

First Set

- Nozzle Size: 0.178 mm/0.533 mm (orifice/focusing tube)
- Working Pressures: 103 MPa, 172 MPa, 241 MPa, 310 MPa and 379 MPa
- Abrasive Flow Rate: 0.158 Kg/min

Second Set

- Nozzle Size: 0.254 mm/0.762 mm (orifice/focusing tube)
- Working Pressures: 103 MPa, 172 MPa, 241 MPa, 310 MPa and 379 MPa
- Abrasive Flow Rate: 0.340 Kg/min

Third Set

- Nozzle Size: 0.356 mm/1.092 mm (orifice/focusing tube)
- Working Pressures: 103 MPa, 172 MPa, 241 MPa, 310 MPa and 379 MPa
- Abrasive Flow Rate: 0.567 Kg/min

As aforementioned, a number of measurements were collected to check the noise levels in the two catcher tanks. Table 1 lists the permissible noise level exposures suggested by OSHA. When waterjet users are subjected to sounds exceeding those listed in Table 1, provisions must be implemented to minimize impact on operators. Practically, most of the AWJ cutting processes occur at elevated pressures, i.e., above 310 MPa.

Figures 1, 3 & 5 show the noise levels attained during the AWJ process when using three different nozzle sizes. The SPLs generated when the workpiece was completely submerged proved less impact on the operator. The values ranged from as low as 74 dB(A) to as high as 87 dB(A) depending on the nozzle size and working pressure. When the workpiece was partially submerged, the SPLs ranged from 87 dB(A) to 97 dB(A) also depending on the same previous operational parameters. The noise levels radiated from the nozzles in the open catcher tank showed significantly higher values. They ranged from 90 to the threshold of pain (120 dB(A)). Figures 2, 4 & 6 show the noise levels attained using three different nozzle sizes with no abrasive.

5. CONCLUSIONS

In summary, the noise generated during the course of AWJ cutting must always be taken into consideration for a safe operation. It is always recommend that operators constantly use ear protection devices even if they are exposed to the jet for only short periods of time. The effect of accumulated noise levels over long periods of time can be extremely harmful.

Cutting in submerged conditions on an adjustable water level catcher tank will attenuate noise levels, and in turn, will provide safer working environment for the operator and other personnel

within close proximity. Standard open catcher tanks should become obsolete due to the hard fact that they reverberate noise levels up to and beyond the threshold of pain.

It is obvious that when cutting in an open catcher tank, noise levels exceed the permissible levels listed by OSHA. Even when the workpiece is partially submerged, noise levels remained above 90 dB(A) when using both 0.254 mm/0.762 mm and 0.356mm /1.092 mm nozzle sizes.

6. REFERENCES

- Katakura, H., and Miyamoto, H. "Waterjet-Related Noise and its Countermeasures," *Proceedings of the 9th American Waterjet Conference*, Dearborn, MI, pp. 783-797, 1997.
- Water Jet Technology Association: *Recommended practices for the use of manually Operated high pressure water jetting equipment*, 1994.
- Zaring, K., Erichsen, G., and Burnham, C. "Procedure Optimization and Hardware Improvements in Abrasive Waterjet Cutting Systems," *Proceedings of the 6th American Waterjet Conference*, Houston, TX, pp. 237-248, 1991.
- National Safety Council, "Accident Prevention Manual for Industrial Operations," Seventh Edition, 1974.
- OSHA Noise Exposure Standards, "Occupational Noise Exposure," U.S. Department of Labor, Standard Number 1910.95.

7. NOMENCLATURE

(A):	Weighed dB scale readings of a standard sound level meter that best correspond to the way the human ear perceives sounds
AWJ:	Abrasive Water Jet
dB:	Decibel, unit of measure
OSHA:	Occupational Safety and Health Administration
SPL:	Sound Pressure Level
WJ:	Water Jet

Table 1. Permissible Noise Exposures*

Duration Per day, hours	Sound Level dB(A)
8	90
6	92
4	95
3	97
2	100
1.5	102
1	105
0.5	110
0.25 or Less	115

*When the daily noise exposure is composed of two or more periods of noise exposure of different levels, their combined effect should be considered, rather than the individual effect of each. If the sum of the following fractions: $C(1)/T(1) + C(2)/T(2) + C(n)/T(n)$ exceeds unity, then, the mixed exposure should be considered to exceed the limit value. C_n indicates the total time of exposure at a specified noise level, and T_n indicates the total time of exposure permitted at that level. Exposure to impulsive or impact noise should not exceed 140 dB peak sound pressure level.

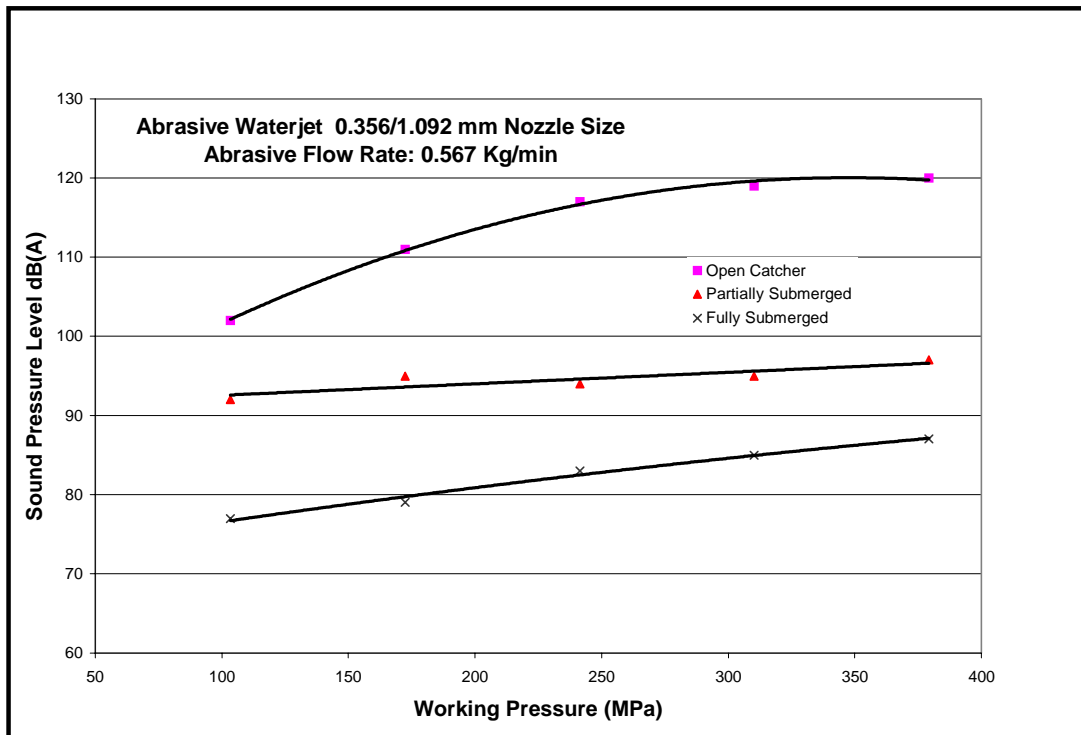


Figure 1: AWJ noise levels when using a 0.356/1.092 mm nozzle at various pressures

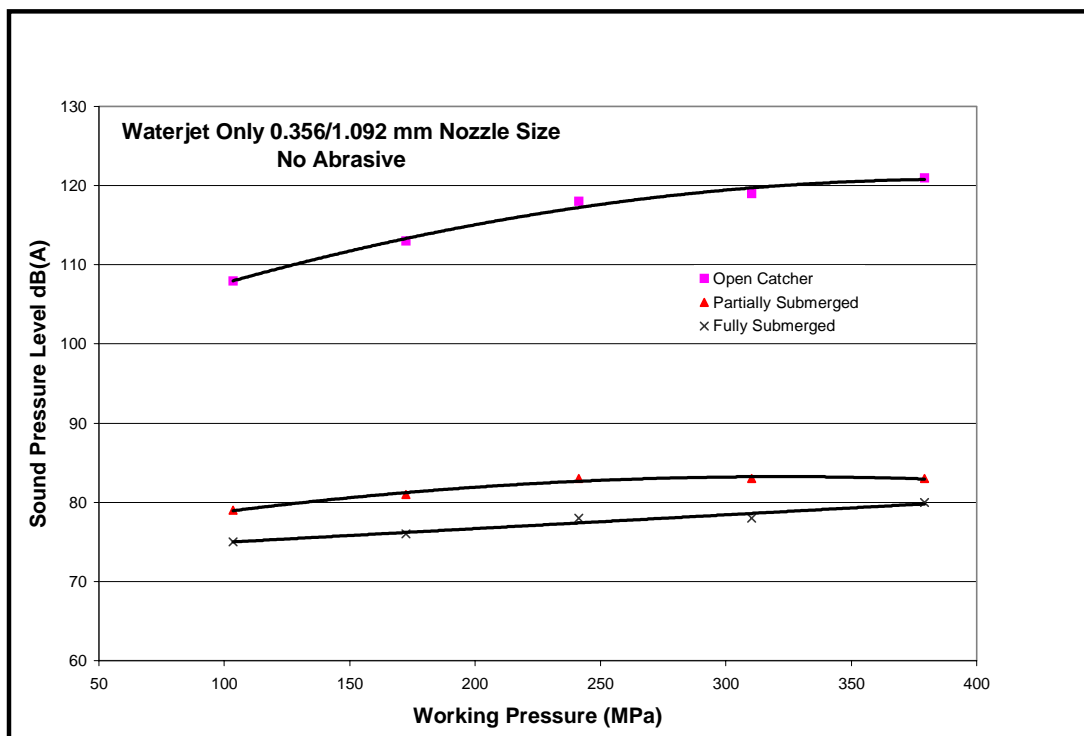


Figure 2: WJ noise levels when using a 0.356/1.092 mm nozzle at various pressures

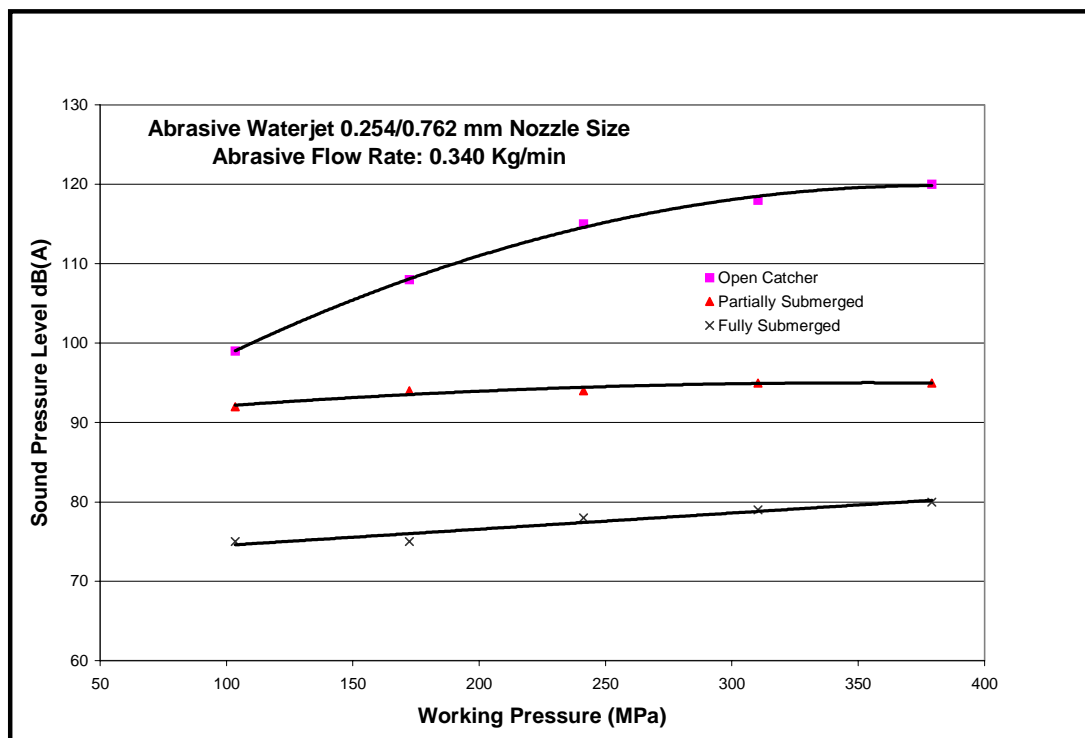


Figure 3: AWJ noise levels when using a 0.254/0.762 mm nozzle at various pressures

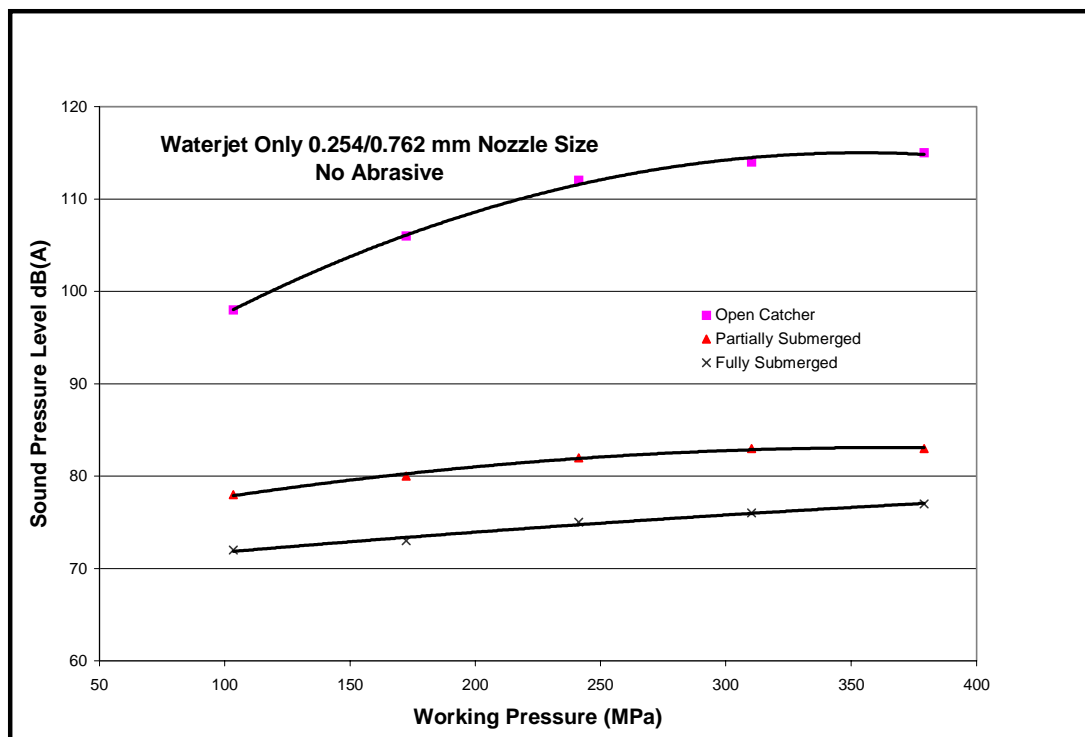


Figure 4: WJ noise levels when using a 0.254/0.762 mm nozzle at various pressures

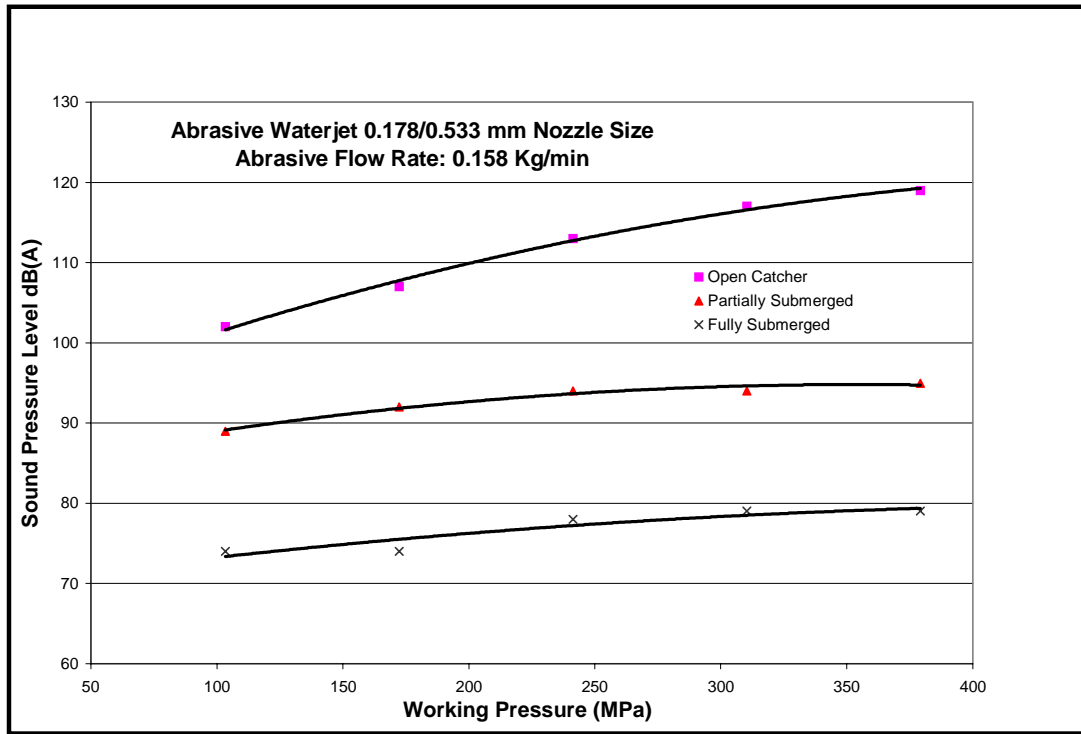


Figure 5: AWJ noise levels when using a 0.178/0.533 mm nozzle at various pressures

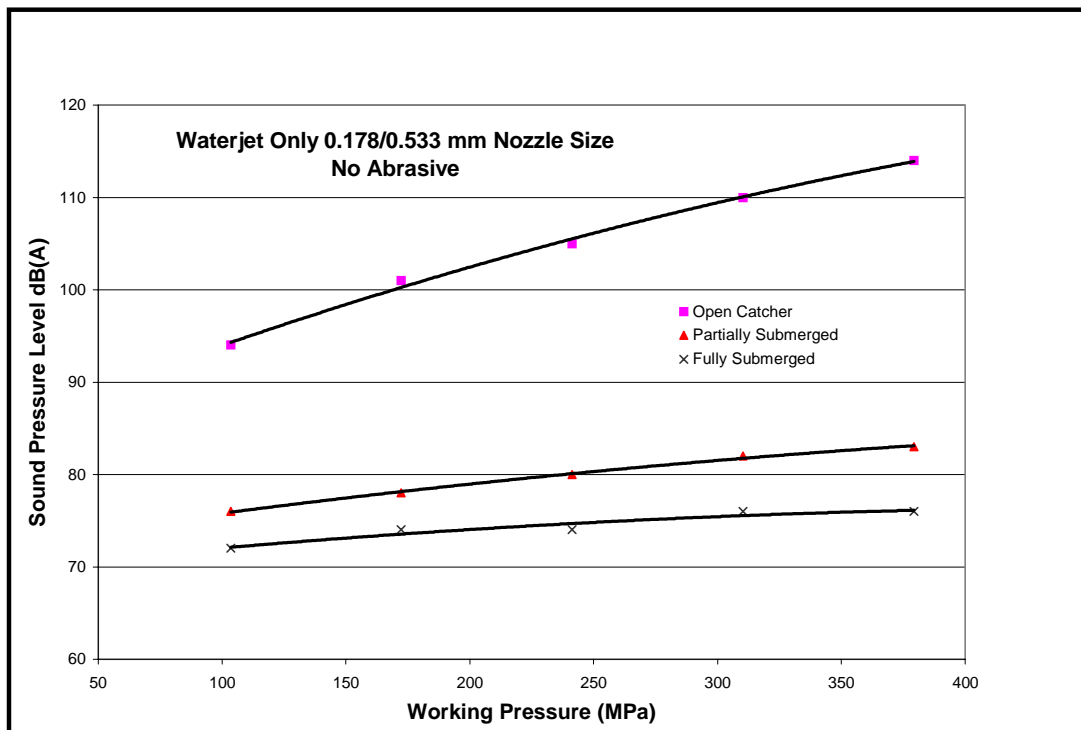


Figure 6: WJ noise levels when using a 0.178/0.533 mm nozzle at various pressures

USING POROUS LUBRICATED NOZZLES TO PREVENT NOZZLE WEAR IN ABRASIVE WATER SUSPENSION JETS (AWSJ)

Umang Anand and Joseph Katz
The Johns Hopkins University
Department of Mechanical Engineering
Baltimore, MD USA

ABSTRACT

This paper reports on an on-going research to develop a method for preventing nozzle wear in abrasive water jets used for jet cutting. This method consists of using a nozzle made of a porous material, which is surrounded with a reservoir containing a high viscosity lubricant. The lubricant is forced continuously through the porous medium as a result of the pressure difference between the reservoir and the high-speed flow in the nozzle. The resulting oil film protects the walls of the nozzle from impact and shear caused by the abrasive particles. Previous tests with a two-dimensional, 0.145 mm wide nozzle with windows enabled observations and measurements of the liquid and abrasive particle velocities using PIV (Particle Image Velocimetry). We have established the proper material characteristics and EDM cutting parameters required to maintain the desired porosity. Over the past year we have been experimenting with an axisymmetric nozzle geometry. The effects of varying the lubricant flow rates and viscosities on the wear have been measured. It was found that the presence of oil substantially reduced the wear of the nozzle walls from 111 % to 10.5 % over the same period. The wear increased as the lubricant injection rate decreased. Lowering the viscosity of the oil for the same nozzle increased the lubricant flow rate, however it had little effect on the wear. The oil film also improved the jet coherence.

1. INTRODUCTION

Abrasive water suspension jets, namely water jets containing abrasive particles, have a considerable niche in the material processing industry. The most troublesome difficulty associated with high-speed slurry jets, which presently limits their usefulness, is wear of the nozzle walls (Conn, 1991, Dubensky et al., 1992). Since the jet speed ranges between 100-500 m/sec, and the particle size can be as high as 40% of the nozzle diameter, it does not take long to destroy a nozzle. Consequently in current systems, nozzles must be replaced frequently, requiring constant maintenance, inspection, loss of accuracy and machine down time. Thus, a solution to the wear problem must still be found, which will expand the use and applications of high-speed abrasive jet cutters. It may be possible to increase the jet speed, and reduce its diameter even further (present sizes range between 100-500 μm), allowing much higher precision, deeper cutting, and wider implementation in problematic materials including ceramics.

2. THE LUBRICATED POROUS NOZZLE

The proposed solution to solve the wear problem is sketched in Figure 1. The nozzle is made of a porous material and is surrounded with a reservoir containing a high viscosity lubricant that is exposed to the same pressure that drives the flow in the nozzle. The lubricant is forced continuously through the porous medium as a result of the pressure difference created due to the high-speed flow in the nozzle.

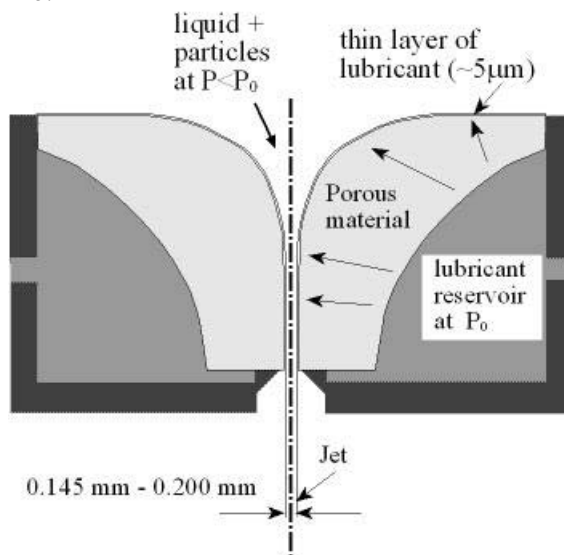


Figure 1. A sketch illustrating the principles of the method for preventing nozzle wear.

The lubricant injection rate, which is controlled by the pressure difference, the nozzle geometry (thickness), permeability and viscosity, is designed to create a thin layer (film), with a typical thickness of 5 μm , on the walls of the nozzle. This film of high viscosity fluid protects the walls of the nozzle from shear and impact of the particles. Since the lubricant is constantly replenished, sites where particles “gouge” the film are repaired, preventing damage to the solid

walls. Provided that the proper lubricant (viscosity), film thickness and nozzle geometry (flow rate through the porous medium) are selected, this approach provides a reliable but yet very simple method to prevent nozzle wear. Due to the differences in viscosity between the water and the lubricant (can be as high as 1500:1), the oil consumption is minimal. Further details can be found in Anand & Katz (2000 a, b) and Katz (1999). The idea of using a porous nozzle but with water injected through the porous nozzle has been introduced before by Tan and Davidson (1990) and Tan (1995, 1998). Their experiments were performed at low pressures of 1.3 MPa, i.e. very low particle velocities.

Initially we studied the flow in a 2-D nozzle with windows on both sides (Anand & Katz, 2000 a, b). This setup allowed us to make direct observations of the flow inside the nozzle. The experiments enabled us to confirm the existence of oil layers on the walls of the nozzle. The oil used in these experiments had a viscosity of $1800 \text{ mm}^2/\text{s}$ (at 25°C). Even though the oil had such a high viscosity, the high shear rates in the nozzle caused considerable entrainment. However, the typical flow rate of lubricant was still very low. Velocity measurements were also performed using Particle Image Velocimetry (PIV). Details on the measurement and analysis method can be found in Dong et. al. (1992) and Roth et. al. (2001). Double-exposure images of tracer nylon particles ($4 \text{ }\mu\text{m}$ diameter, density = 1.14 g/cc) were recorded. The images were then enhanced and auto-correlation analysis was used to measure the liquid velocity. Sample images of the large slurry particles and tracer particles in the nozzle are shown in Figure 2 (a) - (c).

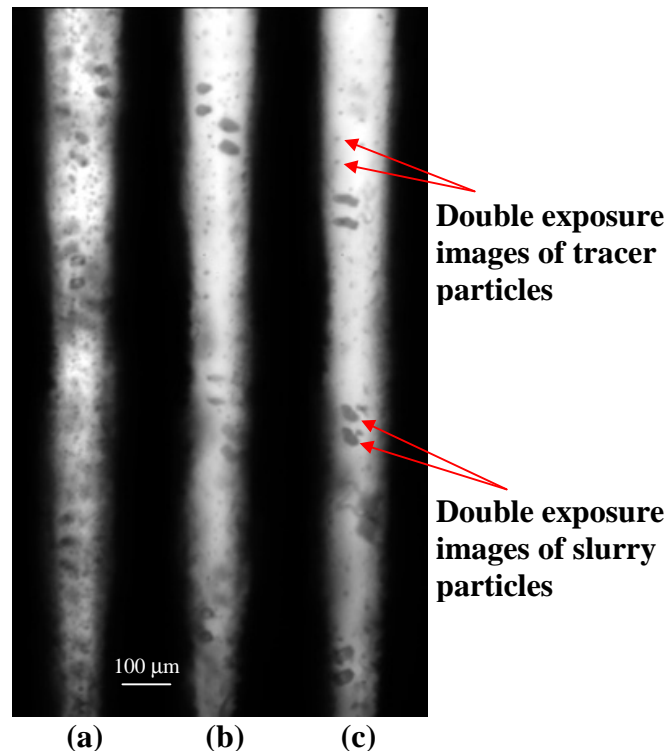


Figure 2. (a), (b), (c) Three samples of double exposure images of the nozzle with water and oil along with slurry (large dark objects) and tracer particles (small dark objects). The flow was from top to bottom.

In order to protect the sapphire windows from being damaged due to the impact from particles during the visualization experiments, we used Celestite (Mohs Hardness 3-3.5, sp.gr. = 3.95) as slurry particles instead of the typical industry standard of Garnet (Mohs Hardness 7-7.5, sp.gr. = 4.0). The velocity of the large slurry particles was measured separately using auto-correlation analysis and subtraction on the enhanced edges of the particles.

We found that there was virtually no change in the centerline velocity when the oil was forced into the nozzle. The slip velocity, which was calculated by subtracting the slurry particle velocity from the average tracer particle velocity in the same region, decreased along the straight section of the nozzle. In fact, near the exit, the slip velocity decreased to negligible levels.

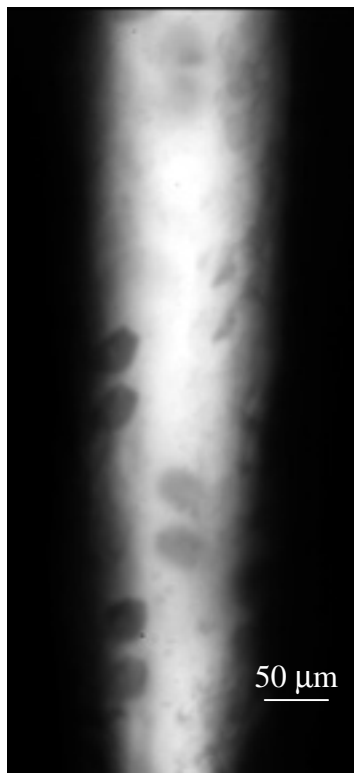


Figure 3. Slurry particles impinging the nozzle walls. The flow was from top to bottom.

Most of the slurry particles appeared to be moving in the center of the nozzle as the sample images in Figure 2 show. However, as shown at the left side of Figure 3, in some cases the slurry particles gouged the oil layer. The images recorded shortly before and after the one in Figure 3 demonstrated that the oil layer immediately replenished itself. Consequently, the integrity of the lubricant layer was not damaged. In order to study the performance of the approach and test the extent of nozzle wear we have also constructed an axisymmetric nozzle facility. The results are discussed in the following section.

3. EXPERIMENTAL OBSERVATIONS AND RESULTS

3.1 Axisymmetric Setup

Figure 4 illustrates the supply system of lubricant and abrasive particles. The water was supplied by a 7.46 kW positive displacement pump whose maximum operating pressure was 68.95 MPa and maximum flow rate was $9.46 \times 10^{-5} \text{ m}^3/\text{s}$. We typically operated at pressures up to 34.5 MPa.

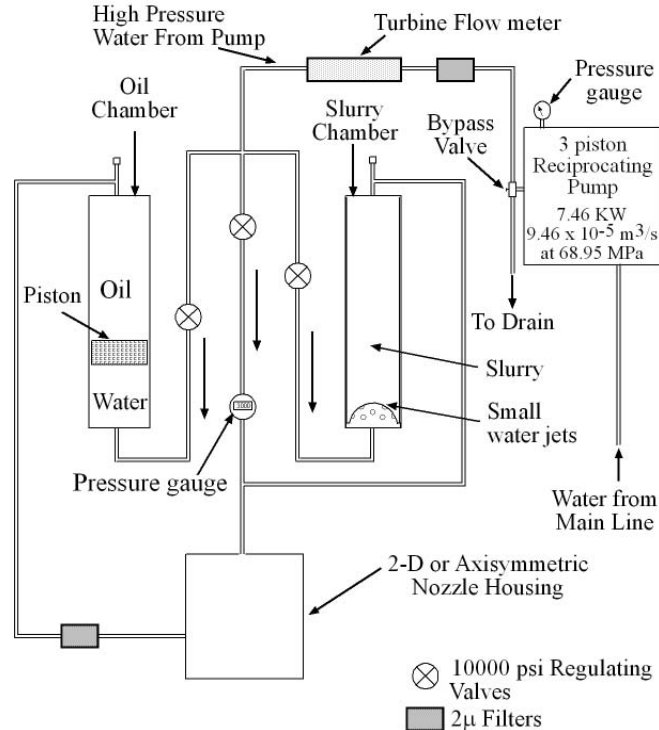


Figure 4. Schematic of the system supplying slurry particles and lubricant to the test chamber.

Using high pressure regulating valves, the pressurized water was used to pressurize both the oil and abrasive slurry chambers. The slurry chamber contained highly concentrated slurry of particles. During an experiment some water was directed towards this chamber from below, entrained some of the particles, and exited from the top of the chamber. Injection into the slurry chamber was from below since the particles were heavier than water and tend to settle. The second reservoir was filled with lubricant and a small loosely fitted piston separated the water from the lubricant. A high pressure gauge and a turbine flow meter were used to record the experimental conditions. Figure 5 (a) shows the components of the axisymmetric nozzle setup and Figure 5 (b) shows a cross-section of the porous nozzle. The nozzle consisted of a short converging section followed by a straight section. The length of the straight section was chosen so that the slurry particles attained nearly the liquid velocity as they exited the nozzle. The abrasive slurry and oil supply tubing are shown in Figure 4. The oil entered through the oil port and collected in the reservoir surrounding the porous nozzle. It then flowed through the porous medium due to the pressure difference to create a thin film on the nozzle walls. The abrasive slurry entered through the upper port.

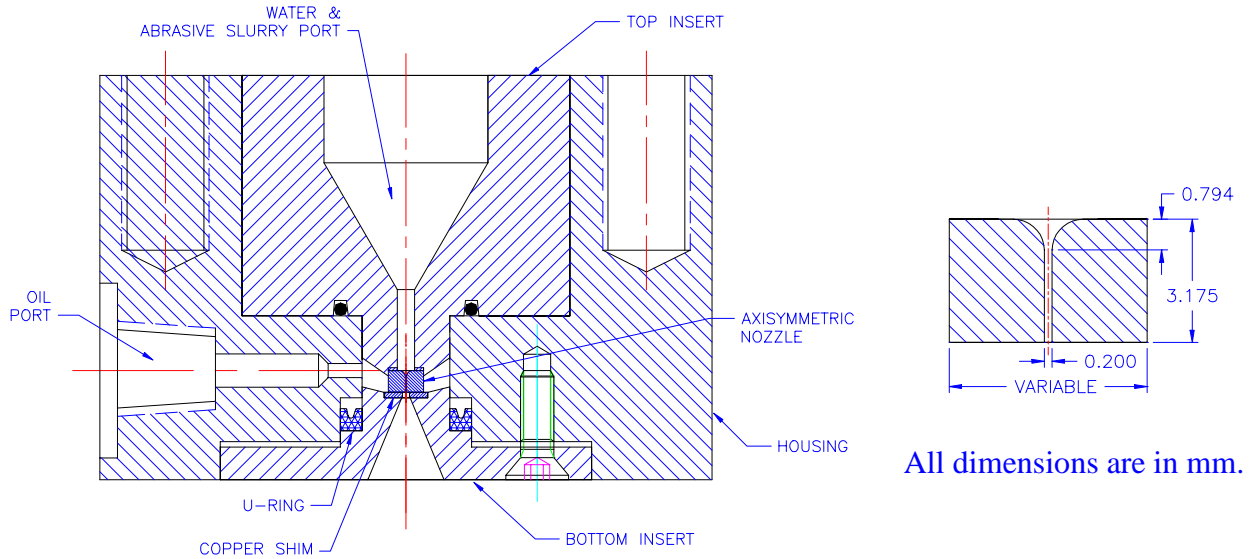


Figure 5. (a) Components of the axisymmetric nozzle housing; (b) Cross-section of the porous nozzle.

The nozzles were made of porous 316-stainless steel and machined using Electric Discharge Machining (EDM). The proper material characteristics and EDM cutting parameters required to maintain the desired porosity have been established and verified by observations using Scanning Electron Microscopy (SEM). Figure 6 (a) and (b) show SEM images of the top and cut section of the porous nozzle.

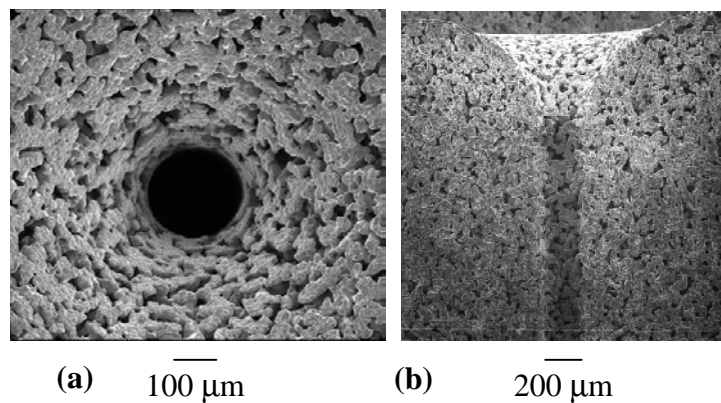


Figure 6. SEM images of the (a) top and (b) cut section of the porous nozzle.

There were several processes for manufacturing the porous material, even for the same porosity (permeability), depending on the particle size, pre-compaction and whether the sintering was based on gravity or on pressure compaction. The quality of the machined surface varied substantially, depending on the method used for manufacturing the porous material. We have experimented with different materials and found an optimum. Using this material, machining by EDM did not “smear” the pores on the surface of the nozzle and uniform pore distribution was maintained. Samples of successful and unsuccessful attempts are shown in Figure 7.

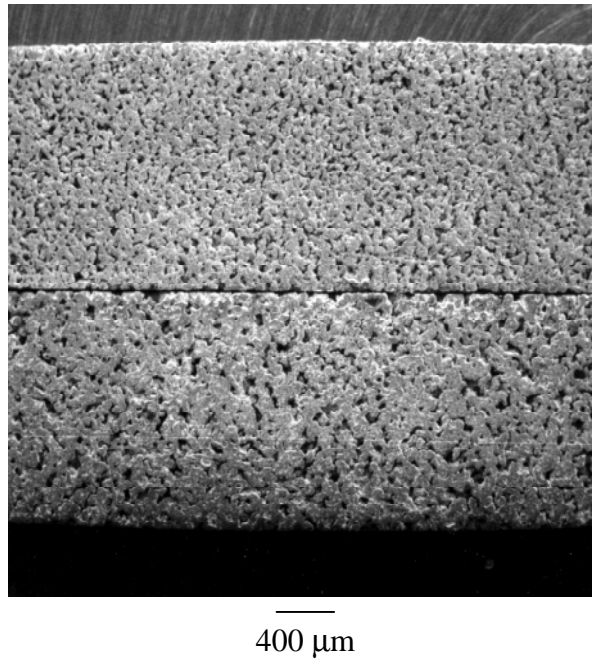


Figure 7. SEM image of EDM'd surfaces of porous materials manufactured using different processes. (Top)– uniform porosity was maintained. (Bottom)–uneven pore distribution.

The EDM cutting parameters, such as energy levels, spark frequencies, cutting speeds, etc., also affected the quality of the surface, as illustrated in Figures 8 (a) and (b). The parameters were optimized to ensure uniform pore distribution on surfaces in the critical regions of the nozzle. The parameters were also adjusted for preventing oil flow in undesired regions of the nozzle.

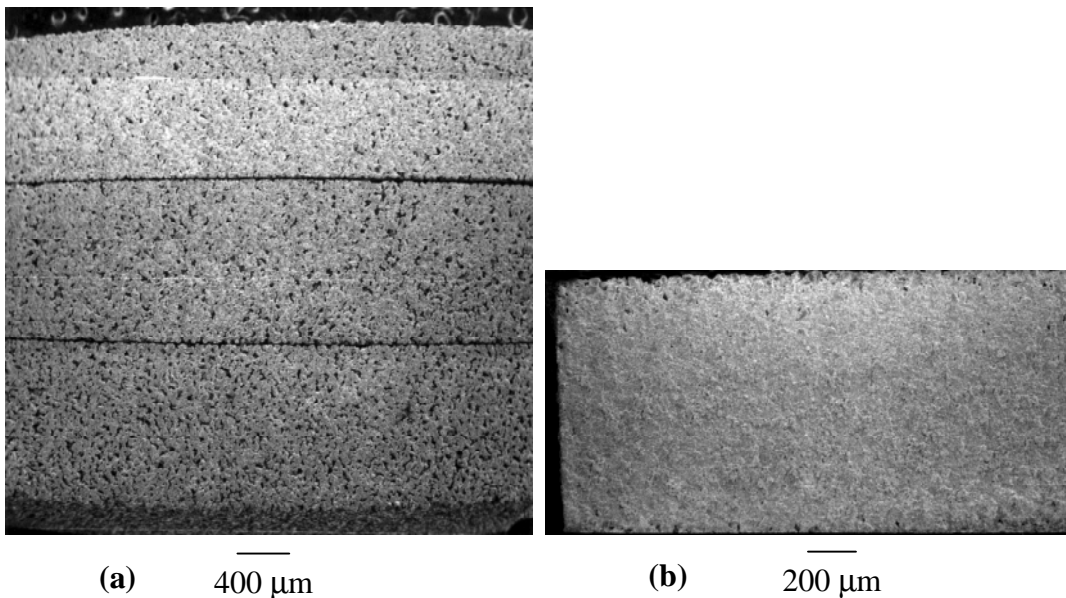


Figure 8. Effects of EDM cutting parameters on the porous surface. SEM images of: (a) Top to bottom – improvements by decreasing the cutting speed and energy level; (b) the result of non-optimized machining – a completely “smeared” surface.

As shown in Figure 4, a 2-micron porous filter was inserted upstream of the nozzle housing. The presence of this element was critical. Experiments performed without this filter resulted in the clogging of the porous medium. Figure 9 (a) and (b) show SEM images of the clogged nozzle surface resulting from experiments with no filter. Figure 9 (a) shows dirt coating the porous surface and Figure 9 (b) shows the same surface with embedded dirt after the surface coating was removed by pressurized air. Figure 10 (a) and (b) show SEM images of the nozzle surface recorded before and after experiments with the in-line filter installed. As is evident, the nozzle surfaces remained unchanged, free from blockage.

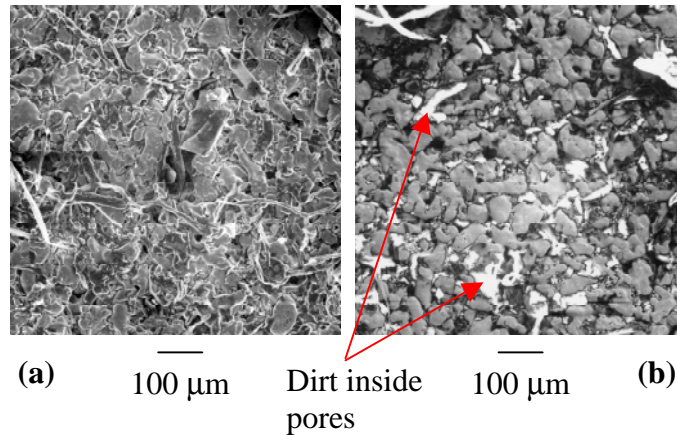


Figure 9. SEM images of the clogged nozzle surface when a filter was not used. (a) Coating of dirt on the surface. (b) Dirt inside the pores.

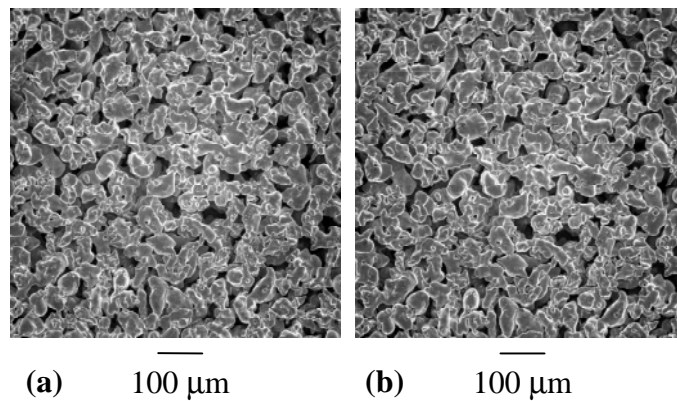


Figure 10. (a), (b). SEM images of the nozzle surface recorded before and after experiments with a filter installed.

3.2 Results

Figure 11 shows the time required to empty the 125 cm^3 oil reservoir as a function of viscosity at an upstream pressure of 14.48 MPa. Also shown is the flow rate of oil relative to that of water. As is evident, the time required to empty the chamber varied linearly with viscosity, in agreement with the Darcy's Law. Accordingly, the relative oil flow rate curve exhibits a hyperbolic behavior.

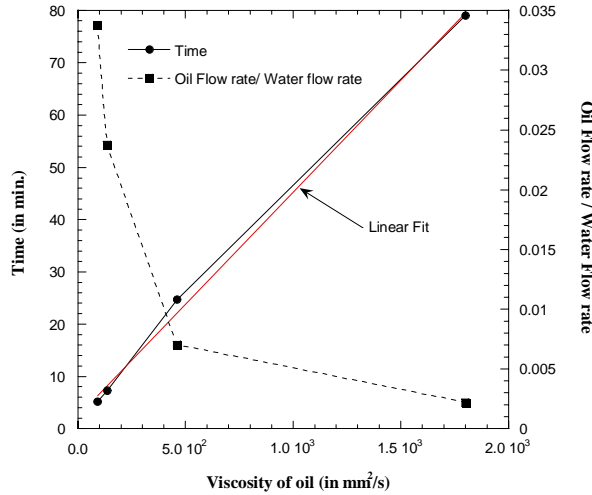


Figure 11. Time taken to use 125 cm³ of four different oils.

We tested the axisymmetric nozzles for wear, using Garnet particles (Nominal size: 25 μm) as abrasive with a slurry concentration inside the slurry chamber of $4.44 \times 10^{-3} \text{ g/cm}^3$. The experiments were performed with different flow rates and viscosities of oil. For all the present results, the upstream pressure was 14.48 MPa and run-time was 1 hour 45 min. We started with a non-lubricated nozzle as a reference case. Figures 12 (a) and (b) show SEM images of the nozzle exit taken before and after the experiments for the non-lubricated nozzle. The exit diameter changed from an initial size of 202 μm to 426 μm based on the diameter of a circle with an equivalent area, i.e. a change of 111 %.

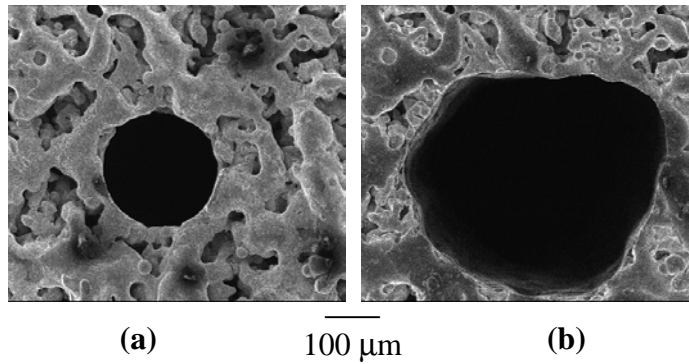


Figure 12. SEM images of the nozzle exit recorded (a) before and (b) after experiments with only abrasive slurry without any oil.

Figures 13 (a) and (b) – 15 (a) and (b) show SEM images of the nozzle exit taken before and after experiments with different conditions. In Figure 13 the viscosity of the oil was 1800 mm²/s (at 25°C) and the ratio of oil flow rate to that of water was 0.0140. The exit diameter changed from an initial size of 210 μm to 232 μm , i.e. an increase of 10.5%. In Figure 14 all the experimental conditions were the same except that the oil flow rate ratio of 0.0099 was lower than before. In this case the diameter changed from 200 μm to 244 μm , i.e. an increase of 22%.

In Figure 15 the viscosity of the oil was $460 \text{ mm}^2/\text{s}$ (at 25°C) and the oil flow rate ratio was 0.0411. The exit diameter changed from $208 \mu\text{m}$ to $248 \mu\text{m}$, i.e. an increase of 19 %.

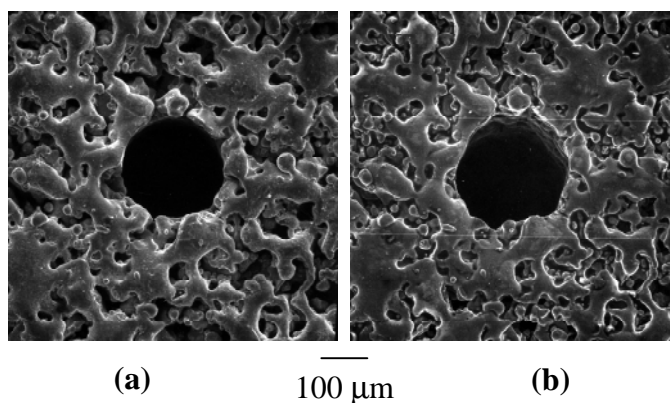


Figure 13: SEM images of the nozzle exit recorded (a) before and (b) after the experiments with oil viscosity of $1800 \text{ mm}^2/\text{s}$. The ratio of oil flow rate to that of water was 0.0140.

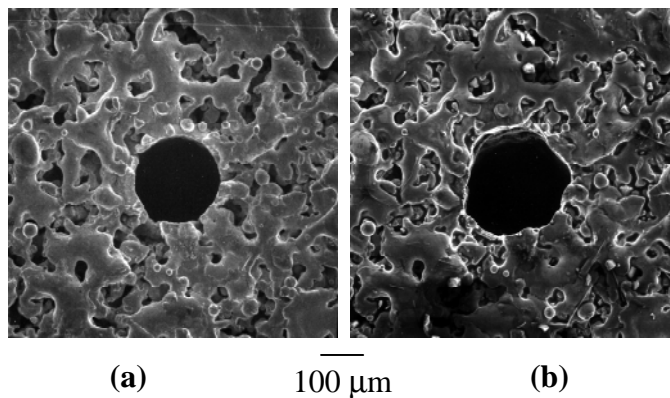


Figure 14. SEM images of the nozzle exit recorded (a) before and (b) after the experiments with oil viscosity of $1800 \text{ mm}^2/\text{s}$. The oil flow rate ratio was 0.0099.

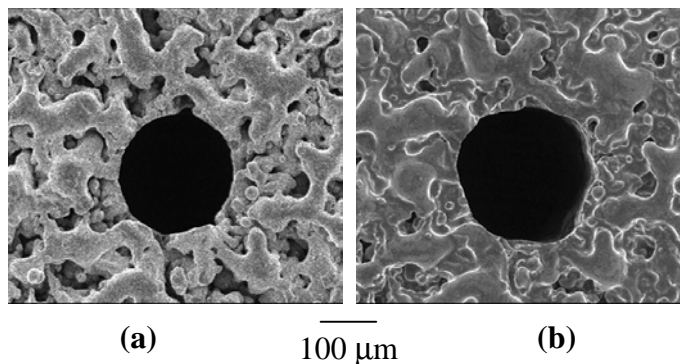


Figure 15. SEM images of the nozzle exit recorded (a) before and (b) after the experiments with oil viscosity of $460 \text{ mm}^2/\text{s}$. The oil flow rate ratio was 0.0411.

From these images it was evident that the presence of an oil film on the nozzle walls had a substantial impact on the extent of the nozzle wear. The lubricant flow rate and the viscosity of the oil (for a given pressure difference) were the primary factors affecting the reduction in nozzle wear. From Figures 13 and 14 it was apparent that for similar experimental conditions the wear increased as the oil injection rate decreased. Comparing Figures 13 and 15 we saw that lowering the viscosity of the oil led to an increase in the oil injection rate but the wear was still higher. However, we have not yet measured the effect of viscosity separately, i.e. determined the wear at the same oil flow rate for different viscosities. These experiments are currently in progress.

We also observed that as long as the oil injection occurred in the nozzle, the jet exit stream was extremely coherent and well defined. Once the oil injection stopped, the jet spread out. This effect could be attributed to the smoothening of the jet walls by the presence of the oil layer.

4. CONCLUSIONS

This paper describes a novel solution for preventing nozzle wear in high-speed slurry jets used for jet cutting. The nozzle was made of porous material and was surrounded by a jacket of lubricating oil. In our setup the oil reservoir was exposed to the same pressure that drove the flow in the nozzle. The oil was forced through the porous nozzle walls and created a lubricating film that protected the walls from impact and shear caused by the abrasive particles. The proper material characteristics and EDM cutting parameters required to maintain the desired porosity have been established. When the particles gouged the oil layer, it immediately replenished itself. It was found that the presence of oil substantially reduced the wear of the nozzle walls from 111 % to 10.5 % over the same period. The wear increased as the lubricant flow rate decreased for similar experimental parameters. When oil of a lower viscosity was used, there was an increase in the lubricant injection rate but it had little effect on the wear. The presence of oil also improved the coherence of the jet. This ability to accelerate the particles to nearly the liquid velocity with minimal damage to the nozzle, even when the nozzle is made of just plain stainless steel, is a major advantage over other presently used technologies.

5. ACKNOWLEDGEMENTS

We would like to thank Jet Edge Corp., USA for providing the support for the project since April 2000. We would also like to thank the National Science Foundation for initial funding and Dr. Andrew F. Conn for his support.

6. REFERENCES

1. Anand, U., Katz, J., "Lubricated Nozzles for High-Speed Slurry Jets", *Proceedings of the ASME Fluids Engineering Division Summer Meeting*, Boston, USA, June 11-15, 2000a.
2. Anand, U., Katz, J., "Prevention of Nozzle Wear in High-Speed Slurry Jets using Porous Lubricated Nozzles", *Proceedings of the 6th Pacific Rim International Conference on Water Jetting Technology*, Sydney, Australia, October 8-11, 2000b.

3. Conn, A., 1991, "A Review of the 10th International Symposium of Jet Cutting Technology", *International Journal of Water Jet technology*, Vol. 1, No. 3, pp. 135-149.
4. Dong, R., Chu, S., Katz, J., 1992, "Quantitative Visualization of the Flow Structure Within the Volute of a Centrifugal Pump, Part A: Technique", *Journal of Fluids Engineering*, Vol. 114, No. 3, pp. 390-395.
5. Dubensky, E., Groves, K., Gulau, A., Howard, K., Mort, G., 1992, "Hard Ceramics for Long Life Abrasive Water Jet nozzles", *Proceedings of the 11th International conference on Jet Cutting technology*, St. Andrews, Scotland, 8-10 Sept.
6. Katz J., 1999, "Lubricated High Speed Fluid Cutting Jet", *United States Patent* No. 5,921,846.
7. Roth, G. I. and Katz, J., "Five Techniques for Increasing the Speed and Accuracy of PIV Interrogation", *Measurement Science and Technology*, 2001, Vol. 12, No. 3, pp 238-245.
8. Tan R.B.H and Davidson J.F., "Cutting by Sand-Water Jets from a Fluidized Bed", *Proceedings of the 10th International Symposium on Jet Cutting technology*, 1990, pp.235-252.
9. Tan R.B.H, "A Model for Liquid-Particle Jet Flow in a Porous Re-entrant Nozzle", *International Journal of Water Jet technology*, 1995, Vol. 2. No. 2, pp. 97-102.
10. Tan R.B.H, "Discharge of Particle-Liquid Jets through Porous Converging Nozzles", *International Journal of Water Jet technology*, 1998, Vol. 3., No. 1, pp. 13-19.

INVESTIGATION OF A NEW CUTTING HEAD CONCEPT BASED ON AN ANNULAR DRIVING JET

U. Suchy
University of Karlsruhe
Karlsruhe, Germany

ABSTRACT

Today, abrasive-waterjet cutting is an established tool for many applications. In order to improve the cutting efficiency, the geometry and use of the cutting head are the subject of many investigations. Yet, conventional mixing heads still suffer from energy losses due to the principle of jet formation process, and from a limited focusing of the jet. Therefore, a new mixing concept was developed. Instead of a spot-like jet, an annular jet encloses the abrasives, thus enabling a “soft” mixing, acceleration and focusing process. The new system works with conventional pressure generation systems, i.e. up to 400 MPa at a maximum water-volume flow rate of 5 l/min. Two different types of geometry are investigated by means of theoretical considerations, CFD-studies, experiments on enlarged models, and original size prototypes. The results indicate the importance of the geometric parameters involved and show that a self-centering effect occurs. During a first parameter study, promising depths of cut were achieved.

1. INTRODUCTION

Since the first applications of abrasive-waterjets to material cutting in the early 80s, mixing heads are the most common systems based on particle injection. This design was developed on the basis of pure waterjet systems which were already known decades before. By pressing water at high pressure through an orifice, a fine “pure” high speed waterjet is generated. In order to add abrasives and accelerate them, the water passes a mixing chamber and enters a well aligned focusing-tube. Along this way, the jet spreads and thus entrains air. This suction effect is used to inject abrasive particles in the mixing chamber as well as in the jet itself. In competition to this system, so called suspension jets were developed on the basis of a common acceleration of the fluid and solid by expelling a slurry through an orifice. Only very few of these systems are used in industrial applications, although they reach similar cutting rates at much lower pump pressures. But especially the wear of the orifice and the high consumption of the abrasives lead to problems where constant cutting properties and low cutting costs are required. Therefore, these systems are mostly found in cases where the lower pressure allows to operate the system with a large distance to the pump, e.g. in under water applications like the decommissioning of oil pipelines or nuclear power plant installations.

Numerous efforts were made to understand and optimize the mixing chamber design as well as investigate the cutting and hydraulic parameters like the traverse rate or the pump pressure. Still, different problems due to the mixing principle limit these improvements: As the particles enter the mixing chamber from the side, they first hit and partly enter the jet at low velocity. After a short acceleration, the particles are pushed out. They hit the inner wall of the focusing tube, rebound, and merge in the jet again. This happens several times until the velocity direction of the particles is nearly parallel to the direction of the jet (see fig. 1, Raissi et al., 1996, Nanduri et al., 1996, Hoogstrate and Lutternvelt, 1997). A comparison of the theoretical and measured velocities of the abrasive waterjet shows that only 35 to 55% of the hydraulic input energy is converted in directed kinetic energy (see Himmelreich, 1993). Until now it has not been investigated how the energy losses are distributed. Most likely, turbulence and wear as well as heat are the main effects: 75 to 80% of the particles brake before they leave the focusing tube. This consumes 3 to 9% of the input energy (Mazurkiewicz and Galecki, 1990). Martinec (1994) showed that apart from a reduction in size, the particle shape is affected by wear during the mixing and acceleration processes. Much more evident is the wear of the focusing tube as well as temperatures up to 58°C at its outer wall (Mohan et al., 1996), factors, which probably play the most important role.

Energy losses due to wall friction lead to another major problem of conventional mixing heads: Focussing the energy of the jet is clearly limited. Considering the cutting rate in dependence of the focus diameter d_F , it shows that the optimum is achieved with an area-ratio of water orifice to focusing tube outlet of 9 to 16 (Blickwedel et al., 1986). Measurements of the particle velocity distribution within the jet (Himmelreich and Rieß, 1991) show that the velocity in the outer part of the jet decreases drastically with a decreasing focus diameter (see Figure 2). This indicates that with smaller focus diameters, the positive effect of a higher energy concentration is compensated by losses caused by friction at the inner wall of the focusing tube.

2. APPROACH

From the very beginning of AWJC, alternative designs for jet formers were investigated. In 1982, Hashish listed different possible approaches and compared three concepts for injection systems. Apart from the common mixing heads used today, he discussed a system with multiple converging waterjets and an annular jet system, both including a central feed of abrasives. He presumed a better mixing efficiency for these systems, but pursued the single-jet, side-feed mixing head for machining reasons.

Yie (1984) applied a system for patent with multiple converging waterjets arranged in a circular pattern with a non-central abrasive entrance. The system was capable of cutting hard materials at water pressures of 100 MPa. Saurwein (1985) applied a similar system with central-fed abrasives for patent.

Apart from multiple jet systems, different designs based on a ring-shaped waterjet were developed. Horii et al. (1990) generated a vortex-flow and proved an excellent focusing and reduction of wear. Nevertheless, the highest reported waterjet velocity is about 35m/s. Hamada et al. (1990) built a mixing head with an annular water outlet which surrounds a steel pipe for abrasive-feeding. The water velocity direction is parallel to the apparatus axis. Due to a relatively wide outlet slit (1.5 mm) and no further focusing of the jet, the authors propose to apply the system for washing, peeling and eroding. The highest reported pressure is 14 MPa.

At the Institute for Machine Tools and Production Science at Karlsruhe University, Germany, a mixing head is developed with an annular driving waterjet, which is focused and encloses the abrasives in its center. Fig 3 shows two possible configurations: Either the waterjet leaves the orifice parallel to the apparatus axis and is then focused by a focusing tube (cylindrical type), or the orifice generates a converging jet (conical type). In this case, only the focusing tube is needed to stabilize the jet.

The system works well with conventional pressure generations systems, i.e. pressures up to 400 MPa and maximum water-volume flow rates at 5 l/min. Due to a better mixing and acceleration process as well as better focusing properties, higher depths and smaller widths of cut are expected.

The aim of the current research is to investigate the influence of the different parameters on the cutting efficiency and to gain a basic understanding of the internal processes. This is mainly done by CFD-studies and investigations on enlarged and original size mixing heads.

3. THEORETICAL CONSIDERATIONS

A major challenge of the new mixing head is to machine the annular slit. By neglecting pressure losses and a change of the water density, the required width can be estimated as

$$s = \frac{\dot{m}_w}{\pi D \sqrt{2 \Delta p \rho_w}} . \quad (1)$$

This leads to a width of 5 to 15 μm , assuming that a similar abrasive entrance area as in conventional mixing heads has to be enclosed by the slit. A comparison with conventional water orifices shows that the mass flow rate will be smaller than the theoretically implemented value due to losses by inner friction. This means that the width of slit can be slightly bigger.

In order to estimate this influence, the total pressure drop within the slit can be estimated as the sum of pressure difference through fluid acceleration (Δp_{dy}), contraction at the slit entrance (Δp_{K}) and inner friction (Δp_{R}):

$$\Delta p = \Delta p_{\text{dy}} + \Delta p_{\text{K}} + \Delta p_{\text{R}} \quad (2)$$

with

$$\Delta p_{\text{dy}} = \frac{\rho_w \cdot \bar{w}^2}{2} \quad (3)$$

$$\Delta p_{\text{K}} = \zeta \cdot \frac{\rho_w \cdot \bar{w}^2}{2} \quad (4)$$

$$\Delta p_{\text{R}} = \lambda \cdot \frac{l_s}{2s} \cdot \frac{\rho_w \cdot \bar{w}^2}{2} \quad (5)$$

Assuming a sharp-edged inlet (flow resistance coefficient $\zeta = 0.5$), this leads to

$$\Delta p = \left(\lambda \cdot \frac{l_s}{2s} + 1.5 \right) \cdot \frac{\rho_w \cdot \bar{w}^2}{2} \quad (6)$$

where λ is the friction factor (see Bohl, 1991). λ depends on the micro and macro geometry of the slit and is experimentally determined for laminar and turbulent flows in annular slits with constant diameters¹:

$$\lambda_{\text{lam}} = \frac{96}{\text{Re}} ; \quad \lambda_{\text{turb}} = \frac{0.427}{\sqrt[4]{\text{Re}}} \quad (7)$$

As λ depends on the Reynolds number, a calculation of the mean velocity in dependence of a given pressure difference must be done in interactions. For turbulent flows, the mean velocity enters with bi-quadratic root into Δp_{R} . Therefore, these pressure losses increase approximately in the same measure as the slit length is increased. Figure 4 shows the results for different lengths and widths of slits for a cylindrical slit of 5.5 mm in diameter at 400 MPa. Due to rising losses, the velocity decreases with an increasing length of slit. This effect is stronger with narrow slits and leads to velocity losses of more than 70% at a slit length of 2 mm. From this viewpoint, the slit should be as short as possible. In this case, the inlet geometry is predominant on pressure

¹ An empirical relation for the friction factor of conical annular slits could not be found.

losses ($\Delta p_K=133$ MPa for $l_s=0$) and the question arises, which length is needed for a “sufficient dimension” of the annular jet. Both questions will be discussed by means of CFD-studies and the enlarged model.

Another important factor that arises from the very narrow slit is the influence of the slit eccentricity on the jet formation. Eccentricity can never completely be avoided and results in a change of flow rates, radial forces, and a different mixing process. In contrast to the other effects mentioned, it is difficult to estimate the influence on the free jet and on the mixing and acceleration processes because of the two-phase respectively three-phase nature of the flows.

It is known that the flow rates rise by 20% (turbulent flow) for cylindrical slits respectively by 150% (laminar flow) when changing from a concentric to an eccentric state (see Figure 5). This effect can be used to compare different designs in terms of achieved concentricity.

Experimental and theoretical studies of hydraulic piston valves show that significant radial forces can occur in the annular slit flow (e.g. Blackburn, 1962). Three cases can be distinguished (see Table 1). In an eccentric annular slit with decreasing width along the flow direction, a centering effect occurs, whereas in the opposite case, the inner part is drawn to the outer part. Only in the case of no conicality, no radial forces occur. Generally, it makes no difference whether the slit width is decreased or increased by the inner or the outer part, respectively a combination of both. This is also valid for laminar and turbulent flows. Yet, only for the laminar case, equations are given for the estimation of the forces (see Blackburn, 1962). Although they are not appropriate for turbulent flows, they give an impression that even for a very small conicality, significant forces must be expected². For the design of the mixing head, this means that

- the use of centering forces must be taken into account,
- the elastic deformation of the inner and outer parts due to the applied pressure can cause radial forces. The design should therefore implement deformations that result in a decreasing width,
- the conical type with parallel surfaces of the inner and outer cone (same angle enclosed) has a centering effect as the tangential taper corresponds to a radial taper,
- a chamfer at the slit inlet causes an additional centering effect.

4. CFD-STUDIES

In order to get a better understanding of the acceleration process within the annular slit, a CFD-study (Computational Fluid Dynamic) was performed by means of the program package STAR-CD. The investigations focus on the length and inlet geometry of the water orifice without taking a possible eccentricity into account. To simplify the model, a 2D modeling method is employed (see fig. 6). Thus, a slice of the slit area is taken, in which “symmetrical planes” are applied on both sides under the assumption that the fluid properties at a cell are independent of the tangential direction. All calculations were done on models with a slit width of 10 μm and a

² e.g. max. force=100 N for: $\Delta p = 350$ MPa; $s_{\min} = 8$ μm ; $e = 8$ μm ; $l_s = 0.3$ mm; $d_0 = 5$ mm; $t = 1$ μm

volume flow of 5 l/min. Considering the velocities and specific geometry, a k- ϵ -Model for high Reynolds-numbers was chosen.

As shown in chapter 3, the slit length has an important influence on the pressure losses caused by inner friction respectively on the loss of mean velocity. Fig. 7 shows the results for the total and static pressure drops. The static pressure drop corresponds to the pressure difference between the pump and the focusing tube i.e. Δp (see chapter 3). Part of this pressure is converted into dynamic pressure (i.e. mass with velocity). This difference is constant as the same mass flow is given as a boundary condition for all models. Therefore, the total pressure difference corresponds to the inner friction losses. As discussed in chapter 3, it increases approximately in parallel with the slit length. Its intersecting point with the pressure coordinate indicates that the pressure losses through the flow contraction at the sharp-edged inlet (angle = 90°) amounts to app. 75 MPa. The static pressure drop for $l_s = 0$ is app. 190 MPa. Using equation (6), this leads to a velocity of 503 m/s respectively to a pressure loss of 63 MPa using equation (4) with $\zeta = 0.5$. In comparison with 75 MPa, this indicates that the “standard” resistance coefficient corresponds well to the numeric results. A second comparison was made at a slit length of 1 mm with a static pressure drop of 400 MPa: The volume flow of 5 l/min (boundary condition) corresponds to a mean velocity of 482 m/s for the considered outlet area. For the same length and width of slit, equation (6) leads to 445 m/s at 400 MPa.

To further investigate the influence of the inlet geometry, six models with a different inlet angle and two other models with round corners of different radius were calculated. The slit length was chosen at 0.5 mm. All other parameters were kept identical to the calculations mentioned before. Figure 7 shows the total pressure drop for angles from 30° to 90°. The results do not indicate a linear relationship. Further investigations on the influence of the discretization scheme used in this case show that this could be explained by numerical imprecision, whereas a further mesh refinement had no significant influence. Still, the results indicate that increasing angles cause rising pressure losses. A round corner significantly reduces these losses, while the resulting pressure difference for a 125 μm and a 250 μm radius is only 1%.

An examination of the velocity distribution shows that after a short way within the slit (app. 50 μm for the sharp-edged inlet), the direction of flow is parallel over the whole width. Still, the velocity profile changes until it is symmetric (after app. 250 μm).

5. ENLARGED MODEL

The calculation of the two-phase and the three-phase flow is difficult, needs a lot of experience and depends on experimental results for validation. In order to understand the mixing and acceleration process in conventional cutting heads, several studies were performed on enlarged models (e.g. Himmelreich, 1993, Schmelzer 1994). A general problem of this method is due to physical reasons, and a complete similarity to the original size is impossible. The specific problem in modeling the WAIS-processes is presence of abrasive particles. With water as model-fluid, it is difficult to keep a similar relation of the forces that interact between the three phases as well as gravity induced forces. Former studies use material of lower density, which allow to suck in the particles but lead to a differing behavior during the acceleration, compared to the

original size mixing heads. Therefore, a model was designed focusing on the flow of water and air without taking the particles into account. This allows the use of a high enlargement factor of 30, which still fits well the important requirements of Reynolds and Weber. Figure 8 shows the modular concept of the model which allows to investigate different types and geometries of mixing heads. The inner part can be moved axially as well as in the eccentric position with the aid of two levers.

Table 2 shows the investigated geometric parameters. The pump pressure was varied from 0..1 MPa. The resulting mass flow was measured by means of an inductive flowmeter.

In a first step, the model was investigated without the focusing tube. The experiments focused on the flow rate and shape of the free jet in dependence of eccentricity, type and geometry of the annular slit. In addition, the occurrence of the self-centering effect was investigated by loosening the holding ring. Thus, the whole inner part can “swim” without losing its water-tightness due to the elasticity of the gasket ring. In a second step, the different focusing tubes (see Table 2) were mounted and the flow inside observed. The results can be summarized as follows:

- The flow rate increases with increasing eccentricity as predicted (see chapter 3). Still, the maximum increase was only 10%. For a slit length-to-width-relationship of less than app. 30, the effect inverts. This effect could be explained with a predominant influence of the inlet flow.
- A slit length (cylindrical type) of even less than 1 mm, corresponding to less than 50 μm in the original size, proves to be sufficient to provide a stable parallel free jet.
- A self-centering effect is shown for the cylindrical and the conical type.
- The conical type shows a suction effect for all configurations whereas with the cylindrical type, water is dammed up in the focusing tubes with a small bore diameter of 15 mm (corresponding to 0.5 mm in original size).
- An examination of the convex part of the focusing tube above the cylindrical bore shows that a part of the water follows the wall geometry whereas another part detaches. For the conical type, a sharp focusing point for the detaching part can be observed (through the abrasive inlet bore). In the case of the centric position and a wide focusing bore, this flow is dominant and results in a clearly defined core jet within the focusing tube. In contrast to that, the flow in the cylindrical type tends to unsymmetrically enter the bore without a clear focusing point which might be a major reason for turbulences and damming.
- The eccentricity results in a zig-zag-flow which continues to the outlet for short focusing tubes but is homogenized for longer focusing tubes.

6. ORIGINAL SIZE PROTOTYPE

The most important part of the mixing head development is the setup of an original size prototype. In a first step, the general problems of the design were investigated which led to the ongoing study of the system in the sense of input and output parameters.

The major requirements for the mixing head design are:

- the stability under water pressure of up to 400 MPa,
- the water-tightness, and
- to provide the annular slit geometry.

The general design problems were already discussed in earlier publications (e.g. Weule and Suchy, 2000) and are therefore not subject of this paper.

Until now, experiments focus mainly on the cylindrical type due to its simpler design. Experiments were performed to compare the different approaches to reach the required accuracy of the annular slit. Based on a measurement of the flow rate, a system was chosen for further investigations which uses a cylindrical gauge for the part assembly (see Weule and Suchy, 2000).

In order to prepare for a parameter analysis, pre-experiments were made to determine the appropriate values for the investigated parameters. These experiments show that the abrasive inlet bore diameter can be reduced to app. 1.0 mm, and that the inner diameter of the focusing tube must at least be 0.9 mm in order to achieve a suction effect for all investigated configurations.

A 2^k-experimental design was chosen in order to identify the significance of geometric parameters, pressure, and the abrasive flow rate. Table 3 shows the upper and lower level for each parameter. All constant parameters are given in Table 4. The depth of cut was measured as target value for all 64 combinations that are possible. Based on these measurements, the “effect” of each parameter was calculated (see Table 3). The values are equivalent to the average increase of depth of cut when the corresponding parameter is increased from mid-level to the upper level. Table 5 shows the calculated “interactions” between all parameters which are equivalent to the additional average increase of depth when both corresponding parameter are increased from mid-level to the upper level.

Apart from the expected strong influence of the pressure, the results show that the annular slit diameter and the enclosed angle of the focusing tube are most important factors for the cutting results. Yet, also the effect of the focus diameter is considerable, as the difference of the chosen levels is rather small. It is surprising that a larger slit diameter causes a deeper cut. An explanation for this could be that the cross-sectional areas of the two cutting heads were different. Indeed, a measurement of the water flow rate showed that it was nearly two times higher for the larger diameter. An examination of the interaction parameters shows that this is probably less caused by lacking machining accuracy or flow losses than by the effect of pressure. Equation (1) explains this: A certain change of the width of slit – e.g. caused by pressure - has a stronger influence on the outlet-area with larger diameters.

The range of depth for all cuts at 200 MPa and the abrasive mass flow 3,7 g/s was app. 1..7,5 mm. This shows the high importance of the combination of geometric parameters and indicates that the optimum is by far not reached yet. This was affirmed by experiments with a variation of the cross-sectional area of the slit: At the same pressure and abrasive mass flow

3,7 g/s, a depth of app. 12,5 mm was measured. The corresponding cut with a conventional mixing head ($d_0=0,4$ mm; $d_F=0,9$ mm) is only 1,5 times deeper.

First experiments with a conical prototype prove the predicted possibility of a suction-effect with a smaller focusing bore diameter of 0.6 mm. Further analysis will be performed later.

7. CONCLUSION

A study of conventional mixing heads shows that these systems suffer from severe momentum transfer losses during the mixing and acceleration process which goes along with a limited ability to focus the jet energy. In a new approach, a mixing head based on an annular driving jet with a central feed of abrasive particles was developed. A major requirement to use similar pumps is a very narrow annular slit. Theoretical considerations, CFD-studies and experiments on enlarged models lead to a very short slit (length-to-width-relation less than 5) with a smooth inlet. They show the existence of a self-centering effect and an increase of the flow rate with growing eccentricity. A comparison of the enlarged models of the conical and cylindrical type with respect to abrasive suction shows that the conical type allows smaller inner diameters of the focusing tube. Experiments on original size prototypes show the high importance of the mixing head geometry. Until now, about 65% of the depth of cut of a conventional head was reached at similar conditions. Future examinations will focus on a detailed investigation of the parameter influence for the cylindrical type, and a further development of the conical type. Additionally, the occurrence of wear in the water orifice and the focusing tube will be investigated.

8. REFERENCES

- Blackburn, J., "Kräfte bei stationärem Betrieb," in: *Fluid Power Control - Regelung durch Strömungsenergie*, Blackburn, J., Reethof, G. and Shearer, J. (ed.), Vol. 2, pp. 154-202, 1962.
- Blickwedel, H., Decker, B. and Haferkamp, H., "Submerged cutting with abrasive water jets," *8th International Symposium on Jet Cutting Technology*, pp. 265-275, Durham, 1986.
- Hamada, S., Kamiyama, S., Tsubota, M. and Yamasaki, T., "The Structure of an annular jet and its characteristics," *10th International Conference on Jet Cutting Technology*, pp. 69-81, Elsevier Science Publishers Ltd, Amsterdam, Niederlande, 1990.
- Hashish, M., "Steel cutting with abrasive waterjets," *6th International Symposium on Jet Cutting Technology*, pp. 465-487, Surrey, England, 1982.
- Himmelreich, U. and Rieß, W., "Laser-velocimetry investigations of the flow in abrasive water jets with varying cutting head geometry," *6th American Water Jet Conference*, pp. 355-369, Houston, USA, 1991.

- Himmelreich, U., "Fluiddynamische Modelluntersuchungen an Wasserabrasivstrahlen," Dissertation, University of Hannover, 1993.
- Hoogstrate, A. M. and Luttervelt, C. A., "Opportunities in Abrasive Water-Jet Machining," *Annals of CIRP*, Vol. 46/2/1997, pp. 697-714, 1997.
- Horii, K. and al., e., "Developments of a new Mixing nozzle Assembly for High Pressure Abrasive Waterjet Applications," *10th International Conference on Jet Cutting Technology*, pp. 193-206, Elsevier Science Publishers Ltd, Amsterdam, Niederlande, 1990.
- Martinec, P., "Changes of garnets during abrasive water jet generation and cutting of materials," *12th International Conference on Jet Cutting Technology*, pp. 543-551, Rouen, Frankreich, 1994.
- Mazurkiewicz, M. and Galecki, G., "Energy consumed for hydro-abrasive jet formation," *International Journal of Water Jet Technology*, Vol. 1, pp. 43-50, 1990.
- Mohan, R., Kovacevic, R. and Beardsley, H., "Monitoring of Thermal Energy Distribution in Abrasive Waterjet Cutting Using Infrared Thermography," *ASME Journal of Manufacturing Science and Engineering*, Vol. 118, pp. 555-563, 1996.
- Nanduri, M., Taggart, D. G. and Kim, T. J., "Wear patterns in abrasive waterjet nozzles," *13th International Conference on Jetting Technology*, pp. 27-44, Mechanical Engineering Publications Ltd, Sardinien, Italien, 1996.
- Raissi, K., Cornier, A. and Kremer, D., "Mixing tube geometry influence on abrasive waterjet flow," *13th International Conference on Jetting Technology*, pp. 247-268, Mechanical Engineering Publications Ltd, Sardinien, Italien, 1996.
- Schmelzer, M., "Mechanismen der Straherzeugung beim Wasser-Abrasivstrahlschneiden," Dissertation, Rheinisch-Westfälische Technische Hochschule Aachen, 1994.
- Weule, H. and Suchy, U., "Mixing head for abrasive-waterjet cutting with an annular driving jet," *15th International Conference on Jetting Technology*, pp. 47-56, Professional Engineering Publishing Ltd, Ronneby, Schweden, 2000.
- Yie, G. G., "Cutting hard materials with abrasive Waterjet," *7th International Symposium on Jet Cutting Technology*, pp. 481-492, Ottawa, Kanada, 1984.

9. NOTATIONS

D_0	water orifice diameter, respectively mean diameter of annular water orifice	Re	Reynolds number
D_F	focus diameter	s	width of annular orifice slit
D_P	geometric mean particle diameter	t	taper of annular orifice slit
E	eccentricity (nominal)	\dot{V}_{centric}	volume flow in centric annular slit
l_F	length of focusing tube	$\dot{V}_{\text{eccentric}}$	volume flow in eccentric annular slit
l_S	length of annular orifice slit	\bar{w}	mean fluid velocity
\dot{m}_A	mass-flow of abrasive particles	α_F	enclosed angle of focusing tube
\dot{m}_W	water mass-flow	δ	eccentricity (relative)
Δp	pressure difference	λ	friction factor
Δp_{dy}	pressure difference through acceleration	λ_{lam}	friction factor for laminar flow
Δp_K	pressure difference through contraction at the slit entrance	λ_{turb}	friction factor for turbulent flow
Δp_R	pressure difference through inner friction	ρ_W	water density

10. TABLES

Table 1. Radial forces caused by eccentric position

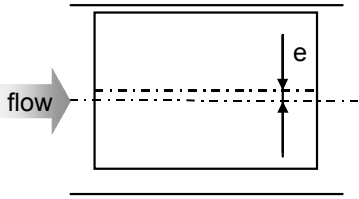
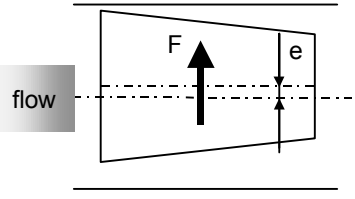
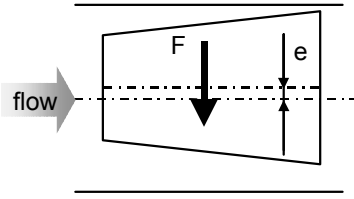
		
No radial forces	Non-centering forces	centering forces

Table 2. Enlarged model: Investigated geometric parameters

		Conical type		Cylindrical type	
		Value	corresponds in original size to	Value	corresponds in original size to
Annular water orifice	cross-sectional area of outlet [mm ²]	0...90	0,075...0,1	67,5/90	0,075/0,1
	included angle [°]	30/60	30/60	-	-
	slit length [mm]	45/87	45/87	3...21	0,1...0,7
	Eccentricity [.]	0...1	0...1	0...1	0...1
Focusing tube	Length [mm]	300/1200	10/40	300/1200	10/40
	included angle [°]	30/60	30/60	30/60	30/60
	diameter of bore [mm]	16/30	0,5/1,0	16/30	0,5/1,0

Table 3. Parameter levels for the 2^K-experiments; effects

Parameter level	d ₀ [mm]	d _F [mm]	α _F [°]	l _F [mm]	p [MPa]	m _A [g/s]
-	3	0.9	15	40	100	2.3
+	4.5	1.1	30	60	200	3.7
Effect [mm]	4.6	-0.8	-3.0	-1.6	14.2	1.3

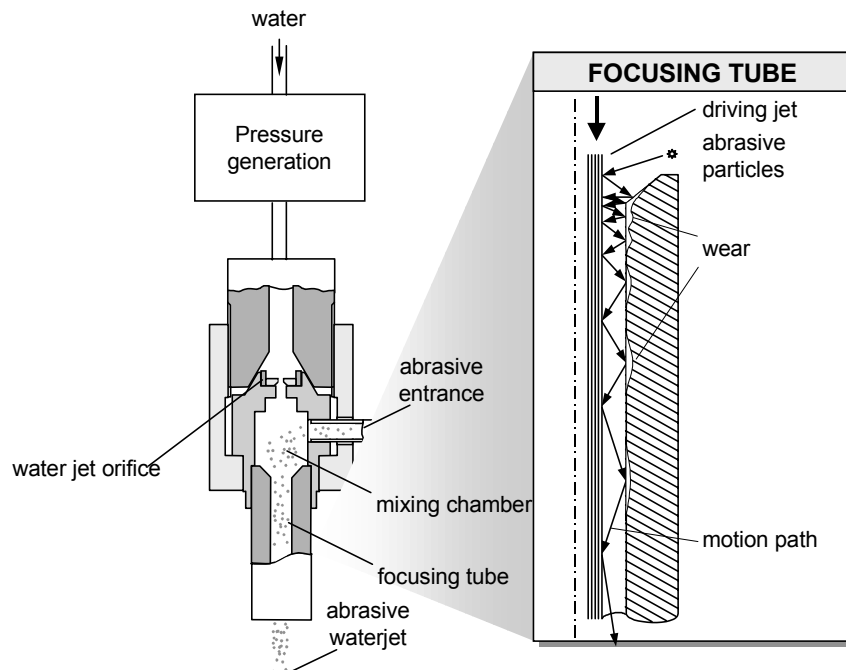
Table 4. Constant parameters

Traverse rate	2 mm/s	Target material	AlCuMg 1
Standoff distance	3 mm	Abrasive material	garnet
Impact angle	90°	Cross-sectional area of annular slit	0,1 mm ²

Table 5. Interaction of parameters (in mm)

	d_0	α_F	d_F	l_F	\dot{m}_A
p	4,72	-2,79	-0,87	-1,58	1,36
\dot{m}_A	1,65	-0,75	-0,11	0,06	
l_F	-1,60	-0,84	0,07		
d_F	-0,64	-0,34			
α_F	-0,21				

11. GRAPHICS

**Figure 1.** General structure and functionality of a conventional mixing head

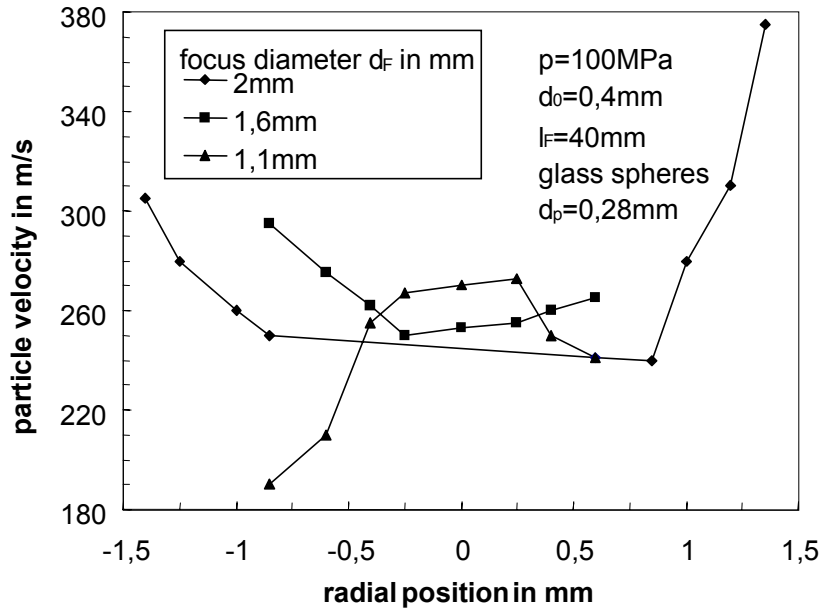


Figure 2. Particle velocity distribution for different focus diameters in conventional mixing heads (Himmelreich and Rieß, 1991)

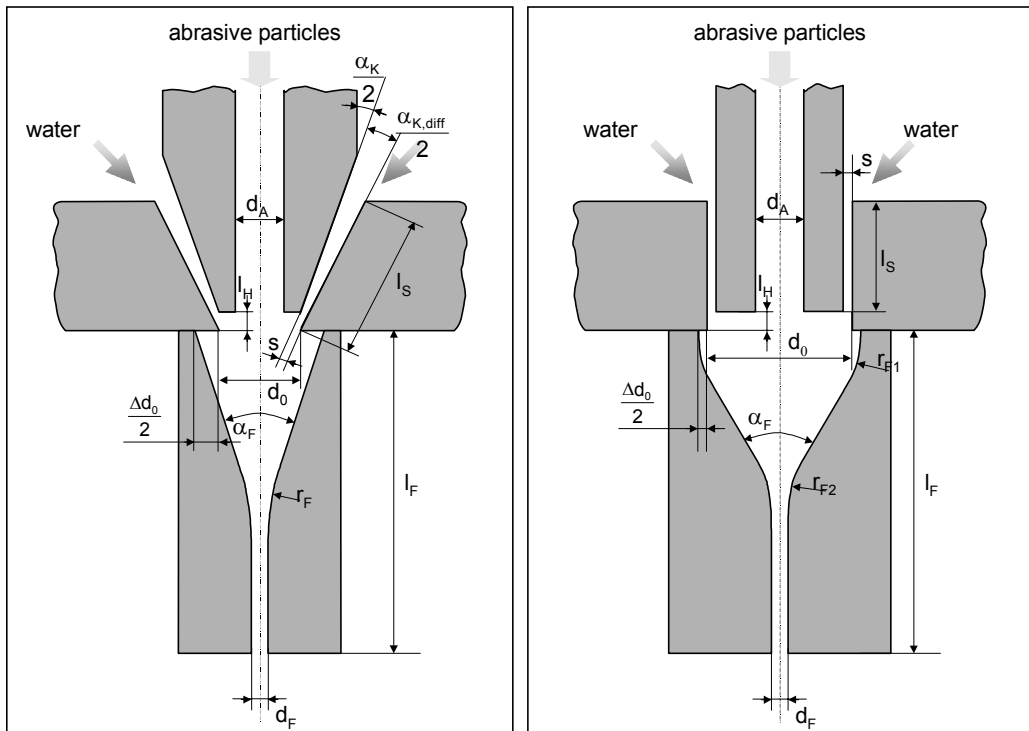


Figure 3. Configurations of a mixing head with annular driving jet

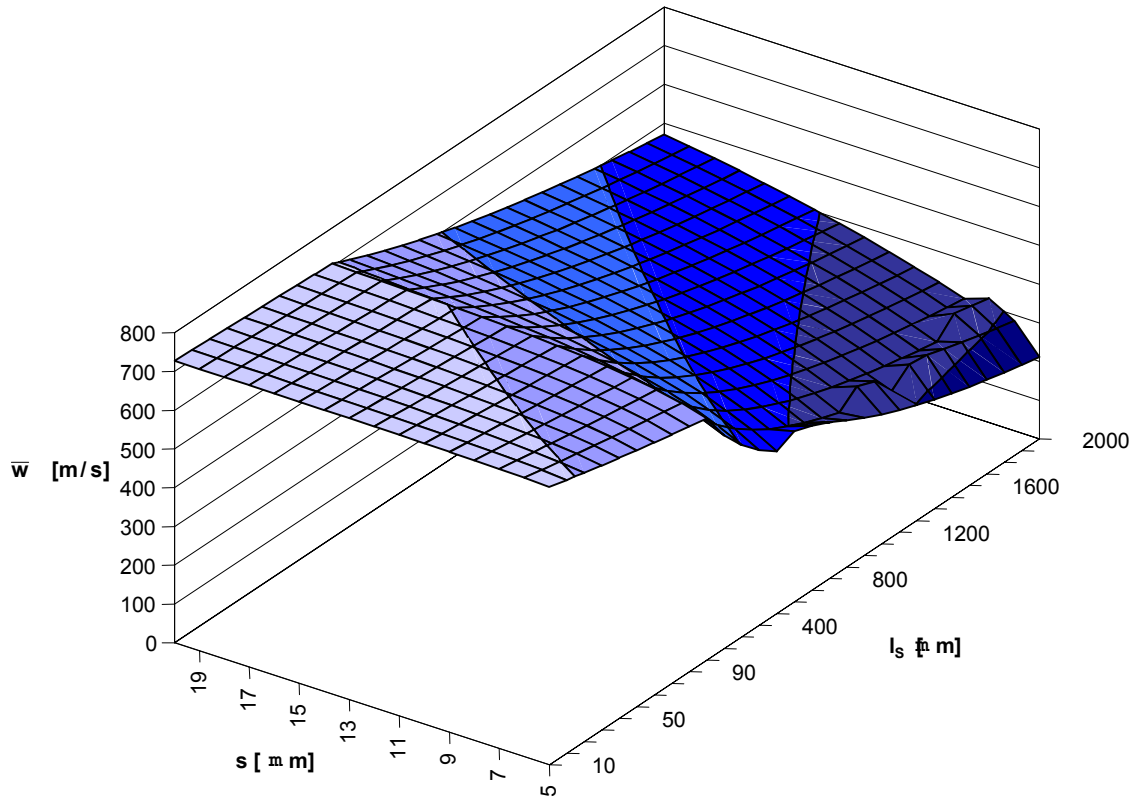


Figure 4. Mean velocity in dependence of the length and width of slit for a cylindrical slit of 5.5 mm in diameter at 400 MPa

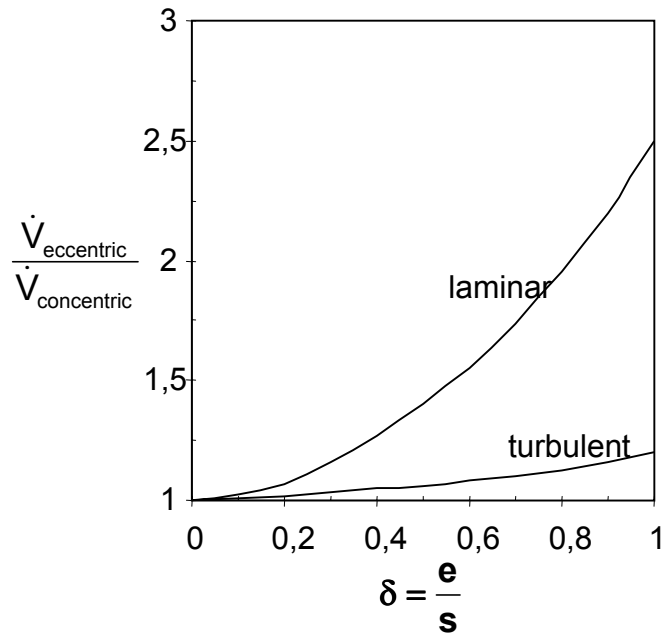


Figure 5. Volume flow in dependence of eccentricity and nature of flow

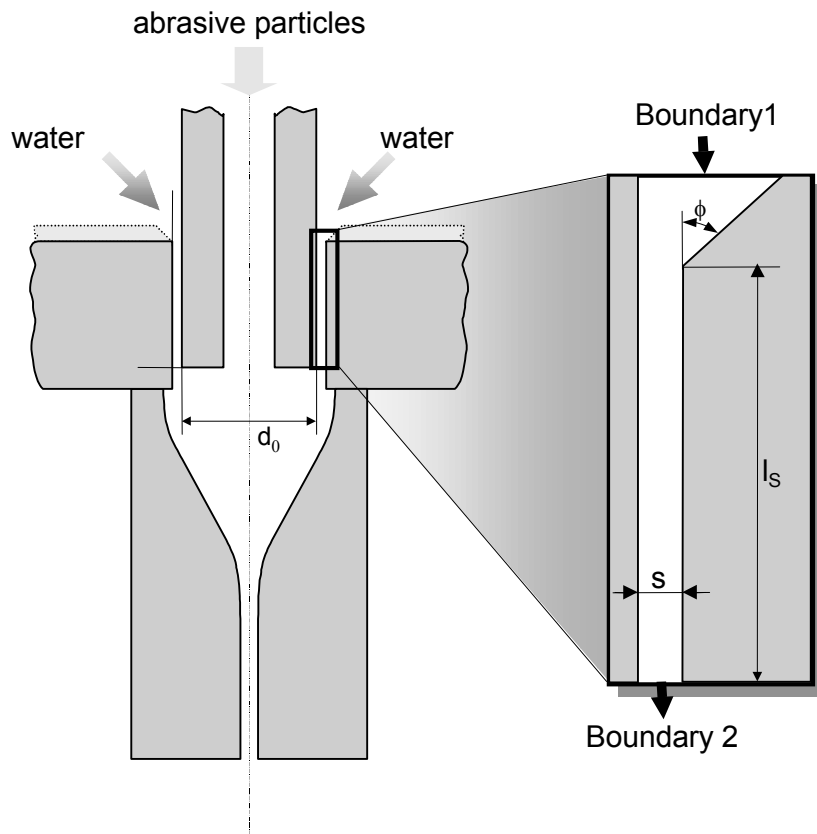


Figure 6. CFD-model

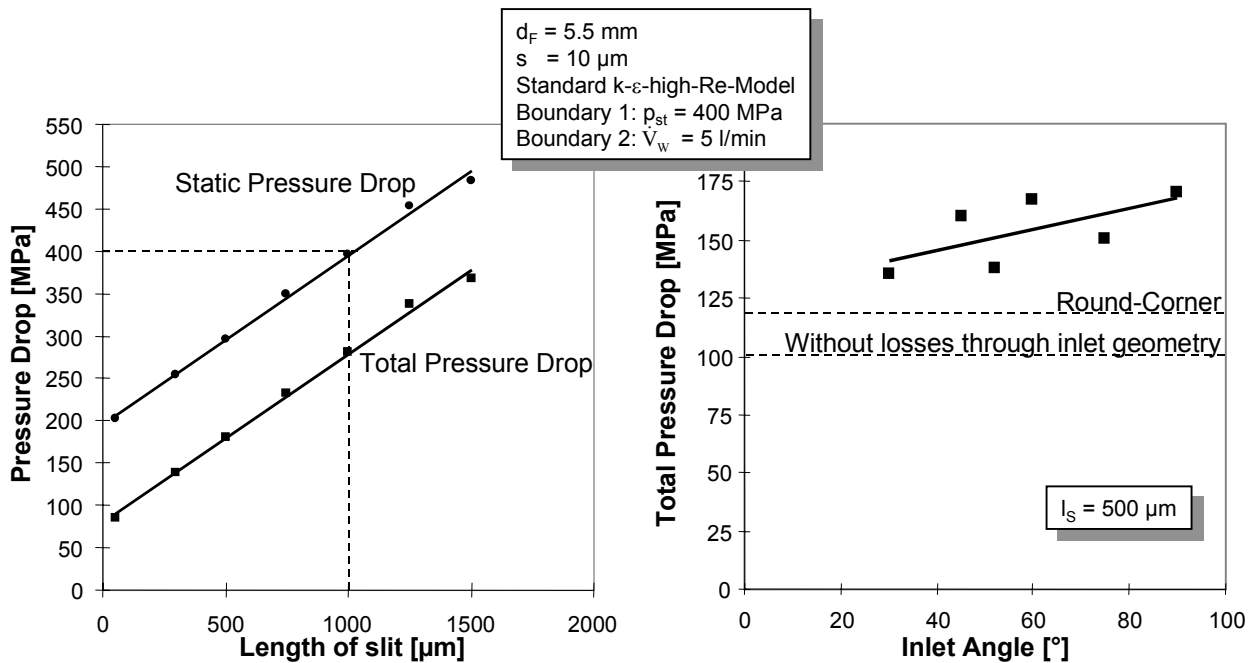


Figure 7. Volume flow in dependence of eccentricity and nature of flow

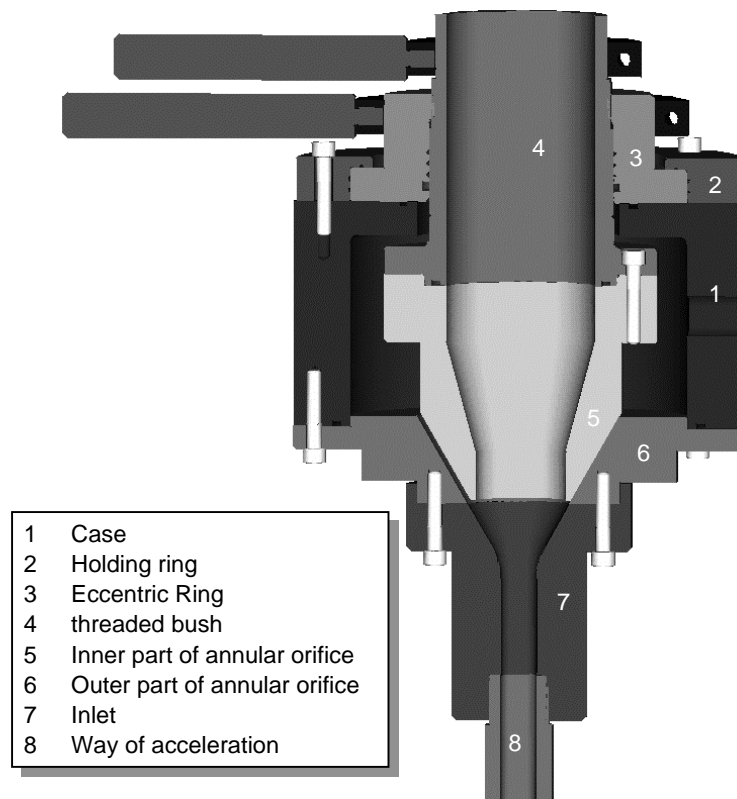


Figure 8. Modular enlarged model (conical type in eccentric position)

RESULTS OF COMPARATIVE NOZZLE TESTING USING ABRASIVE WATERJET CUTTING

D. A. Summers, R. D. Fossey, J. W. Newkirk, G. Galecki
University of Missouri-Rolla
Rolla, Missouri

M. Johnson, D. Burch
Naval Surface Warfare Center
Crane, Indiana

G. Olson
Defense Ammunition Center
McAlester, Oklahoma

ABSTRACT

There is considerable debate about the levels of performance that can be expected from abrasive waterjet (AWJ) systems, and the relative merits of different nozzle designs. In order to provide some standard of comparison, the University of Missouri-Rolla (UMR) has developed a series of tests that compare performance. This paper provides an explanation of test results from an initial suite of six nozzles obtained from the available resources at the time of test. A spread sheet is described that includes abrasive cost, nozzle cost and life in assessing the relative effectiveness of the different nozzles, both with and without abrasive recycling, which is discussed.

1. TEST PROCEDURE

The test procedure for the nozzles has been described in more detail elsewhere (R.D. Fossey, et al. 2001). The tests were broken into three parts, the first evaluated energy transfer to the abrasive, the second the depth of cut achieved under varying test conditions, and the third the decay in performance with time of the nozzles.

2. ENERGY TRANSFER

In essence abrasive waterjets at nine different conditions were first fired down an open tube (Figure 1). The abrasive deposited out of the jet was collected over 1 foot increments from the nozzle and weighed. The average throw distance of the abrasive could then be calculated. This was defined by plotting cumulative weight deposited as a function of distance and determining the 50% point (Figure 2). Tests were carried out at pressures of 30,000 psi; 40,000 psi and 50,000 psi at abrasive feed rates (AFR) of 0.6; 1.0 and 1.5 lb. of 80 mesh garnet per minute. The garnet was prescreened to lie in the size range between 60 and 100 mesh. Average values over the six nozzles are presented in Table 1.

Once these measurements had been made the particles were recombined and the size distribution of the mix was established. The average particle size was then found by plotting average particle size on each screen with cumulative weight retained. The average particle size of the stream, after passing through the nozzle and before hitting the target could then be calculated (Figure 3). Average values for the six nozzles are presented in Table 2. It was noted (by fractional screening) that the smaller particles settled out closer to the nozzle and the larger particles in general were found to be thrown to a greater distance – explicable due to momentum and drag.

3. INITIAL CUTTING TESTS

In order to obtain a standard cut sample triangles of metal (6" x 5" x 1/4") were prepared and aligned so that the jet would cut along a horizontal surface into metal of increasing depth along the cut. The cuts were made in the plane of the sample so that, after cutting, one side could be milled away to expose the cut surface (Figure 3). The depth and quality of the cut could then be measured. It had originally been intended to use the depth at which the jet stopped cutting to the underside of the sample as the measured value. However there were significant segments of the cut that were not cut to this depth in the body of the cut. Instead, therefore, the minimum depth of cut achieved over a four-inch traverse was determined, and recorded. Average and maximum values for the depths of cut achieved, at a traverse rate of 1.5 inches a minute are given (Tables 3 and 4). There was some considerable variation in the results obtained (Figure 4).

4. COMPARATIVE EVALUATION

A plot of average particle throw distance against depth of cut, indicated (Figure 5) that imparting greater energy to the particles resulted in a greater cutting depth. In contrast there did not appear to be as great an effect of particle size (Figure 6). For this reason, and because there is a growing interest in the option of recycling, a series of cutting tests were performed, using the different nozzles, and with recycled abrasive in different size fractions.

5. RECYCLING ABRASIVE

The results showed (Figure 7) that abrasive could be successfully recycled in particle sizes down to 100 μm , or 140 mesh. Below this size fraction there is a significant drop in cutting performance, so that including this material would degrade performance, but within that size fraction a significant savings could be achieved. However the size evaluation achieved with the abrasive shot into the air and described above, did not include the particle crushing that occurs in cutting. When the abrasive was collected from the cutting operation it was found that the amount of abrasive that should be recovered had been further cut in half (Figure 8), although the actual values were, again, a function of the nozzle design which had been used.

6. OPERATIONAL LIFETIME TESTING

Once a comparison of initial cutting conditions had been completed, it was necessary to establish the effective operational lifetime of the nozzle. This was measured by examining the depth and quality of cut at five hour intervals during nozzle use. This proved a little more difficult than the earlier parts of the testing. Bear in mind that we tested, off-the-shelf “brand new” nozzles as supplied to us by the different suppliers. Of the six units we tested two failed with jewel problems within an hour of testing starting, and two failed – possibly prematurely, with excessive wear in the mixing chamber area. Some of those problems are discussed elsewhere (R.D. Fossey, et al. 2001). Because these were given a “second chance” the test program is not yet complete, but two different criteria must be considered in assessing failure. With failure in the jewel or mixing chamber the energy to the particles is dispersed and reduced and cut depth falls away quite markedly (Figure 9). With sustained jewel and mixing chamber life the nozzle fails with focusing tube wear. This is seen in both a reduction in cut depth, and a loss in edge quality but both are quite gradual (Figure 10). Depending on the job being undertaken the loss in edge quality and depth can, to an extent, be overcome by slowing the cutting speed. However, at some point this becomes uneconomical.

7. COMPARISON OF PERFORMANCE

Running at different pressures and AFR changes the cost of the abrasive and the wear on the nozzle. To provide an assessment of the best nozzle a simple process was undertaken. The process relies on costing data originally developed by Johnson (Dan Burch, et al. 1999 and Dan

Burch, et al. 2000) and oriented toward the cutting of 40mm shells. The process is demonstrated with an attached spreadsheet, with the following steps in the process. (Copies of the layout can be obtained). Actions relate to the column letter in the table (Table 5).

Step 1. Costs of the nozzle wear parts, abrasive purchase, abrasive disposal, water, power were input into the table, together with the abrasive flow rate. Required cut depth and cut length were also entered.

Step 2. An equation was inserted describing the cutting depth achieved by the nozzle as a function of time.

Step 3. In column A, time intervals of 30 minutes were laid down in a column.

Step 4. B- Based on the time equation the depth of cut achieved by the jet was calculated.

Step 5. C- The depth was discounted 15% to allow for unacceptable roughness of the bottom of the cut.

Step 6. D- The speed required to achieve the designated cut depth (here the 8.5mm thickness of the 40mm round) was calculated using an exponential variation in cut depth to speed with a 0.86 exponent was used.

Step 7. E – the time to cut the designated length (here the 125 mm cut path length around a 40mm round) was calculated.

Step 8 F – the amount of abrasive used per cut was calculated.

Step 9 G – the cost of the abrasive was calculated.

Step 10 H – the total parts cut is calculated based on the number of parts cut to date plus those cut in the following 30 minutes at the calculated cutting time.

Step 11. – I the amortized cost of the wear parts are calculated to that point by dividing the cost by the number of parts cut.

Step 12. J – the cost of abrasive and nozzle in cutting parts at that time is calculated.

(two additional calculation steps involving water and power costs are not included because of space limitations).

Based on the tabulated results it is possible to see where the cost per part starts to increase and it becomes economical to change the nozzle (in this case after 480 minutes).

It should be mentioned that economic nozzle cutting life of over 40 hours has been established for some of the nozzles we tested.

If the costs of abrasive recycling are included, by adding a modifier to the abrasive flow rate which calculates the percentage of abrasive which is rejected (as a percentage of the abrasive used (Table 6) it is noted that not only is the cost of the cut part reduced, but so also is the cut-off point in the operation.

8. CONCLUSIONS

- Not all nozzle designs cut to the same depth, or with the same lifetime.
- Nozzle life is affected by sapphire and mixing tube life as well as that of the focusing tube.
- Significant cost savings may be achieved by selecting the appropriate nozzle design with optimized cutting parameters.
- Significant cost savings, without affecting overall cutting performance, can be achieved by re-using screened +140 mesh (100 m) abrasive.

9. REFERENCES

- R.D. Fossey, D. A. Summers, J. W. Newkirk, G. Galecki, M. Johnson, D. Burch, "Abrasive Cutting Comparisons" *Proc 11th American Waterjet Conference*, Minneapolis, MN, August, 2001.
- Dan Burch, John Griggs, Mike Johnson, Greg Olson, David Summers "Abrasive Waterjet Cutting Demilitarization of 40MM Projectiles" 1999 Global Demilitarization Symposium & Exhibition, Tulsa, OK, May 20, 1999.
- Dan Burch, John Griggs, Mike Johnson, Greg Olson, "Abrasive Waterjet Cutting Demilitarization of 40MM Projectiles", 2000 Global Demilitarization Symposium & Exhibition Coeur d'Alene, ID, May 18, 2000.

10. FIGURES AND TABLES



Figure 1. Test arrangement to determine the throw and size reduction of abrasive through an AWJ nozzle.

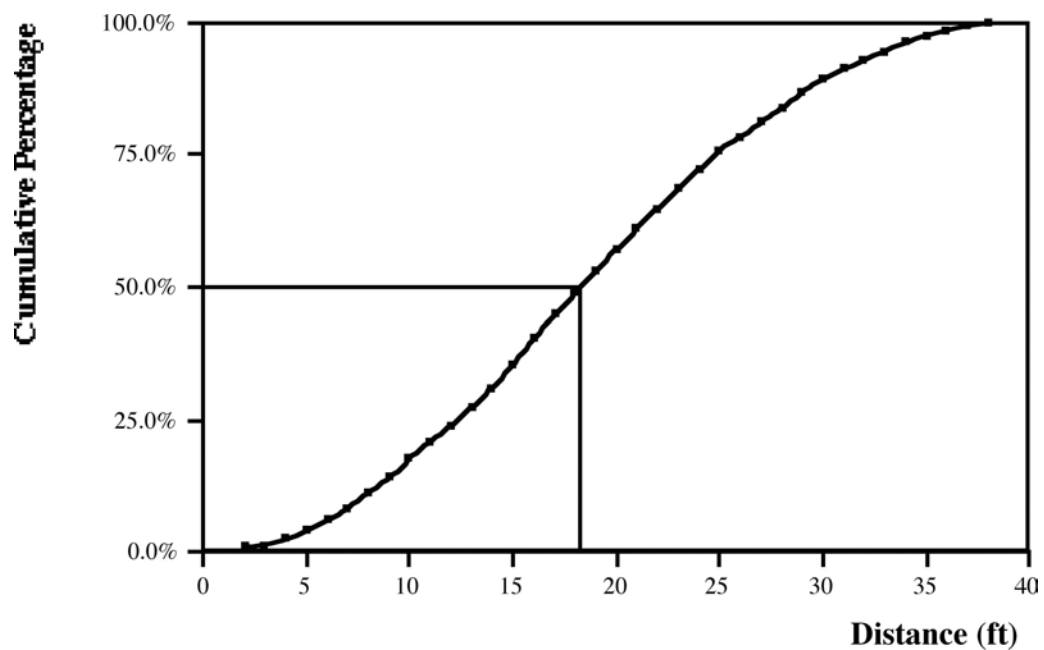


Figure 2. Cumulative weight distribution with distance from a jet at 40,000 psi and 0.6 lb/min.

Throw Distance (ft)	Pressure (ksi)			
AFR (lb/min)	30	40	50	average
0.6	15.0	15.9	17.3	16.1
1	14.3	16.1	16.9	15.8
1.5	13.1	14.5	15.4	14.3
average	14.1	15.5	16.5	15.4

Table 1. Averaged values for throw distance as a function of pressure and AFR.

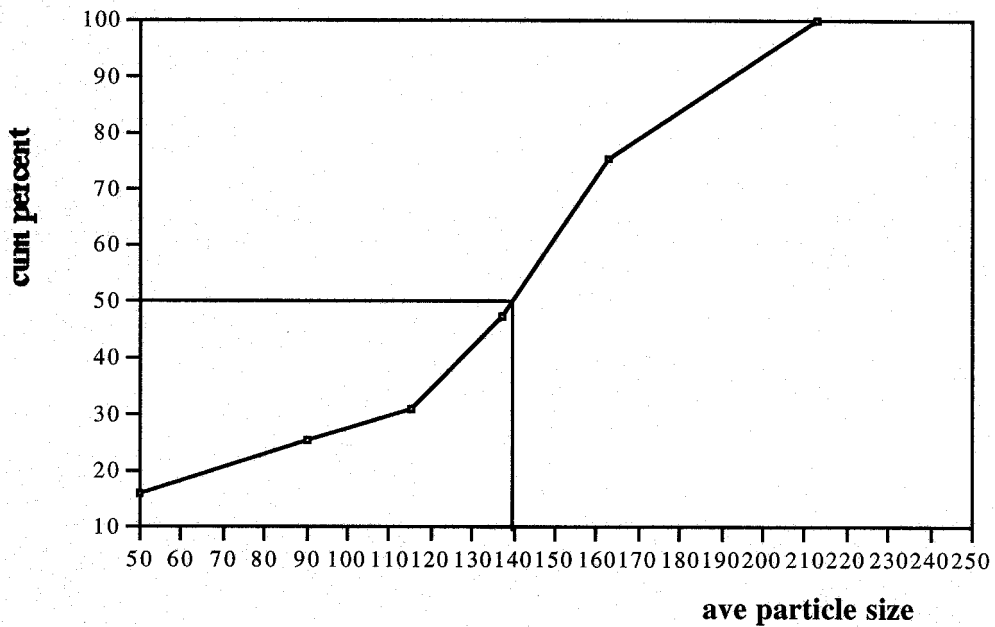


Figure 3. Particle size distribution after passing through the nozzle.

Abrasive Size (μm)		Pressure (ksi)		
AFR (lb/min)	30	40	50	average
0.6	136	129	121	128.5
1	133	126	122	126.8
1.5	132	121	116	122.7
Average	133	125	120	126.0

Table 2. Average particle size produced under the varying conditions of test.

Cut Depth (mm)		Pressure (ksi)		
AFR (lb/min)	30	40	50	average
0.6	30	41	46	39
1	32	46	55	44
1.5	29	44	57	43
average	30	43	53	42

Table 3. Average depths of cut achieved under the conditions of test.

Cut Depth (mm)		Pressure (ksi)		
AFR (lb/min)	30	40	50	average
0.6	36	48	56	46
1	44	57	69	57
1.5	41	61	71	58
average	40	55	65	54

Table 4. Maximum depths of cut achieved under the conditions of test (note these results were not all obtained with the same nozzle).

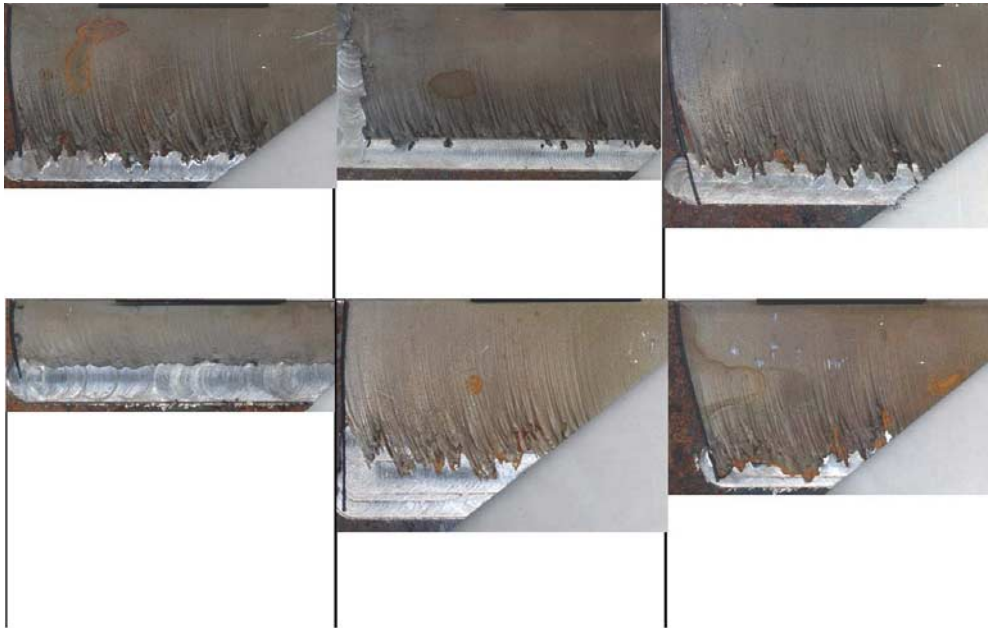


Figure 4. Comparative depths of cut achieved at 40,000 psi and 0.6 lb/min of abrasive feed at a cutting speed of 1.5 inches/min.

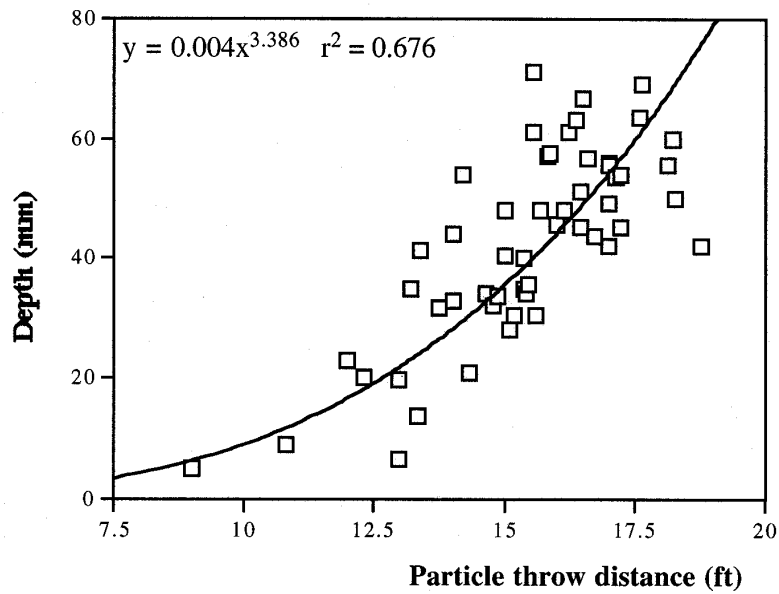


Figure 5. Average particle throw distance against depth of cut for all nozzles and conditions.

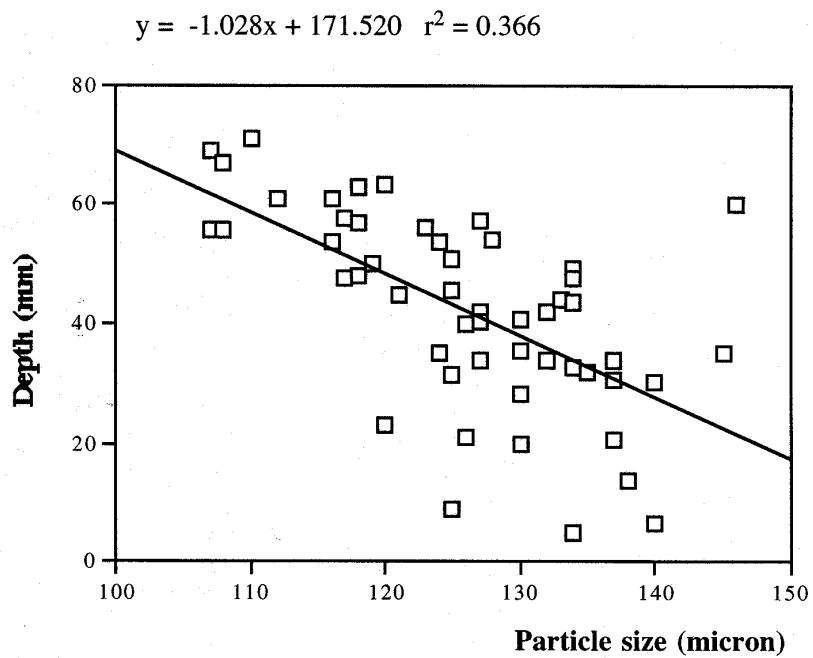


Figure 6. Average particle size against depth of cut for all nozzles and conditions.

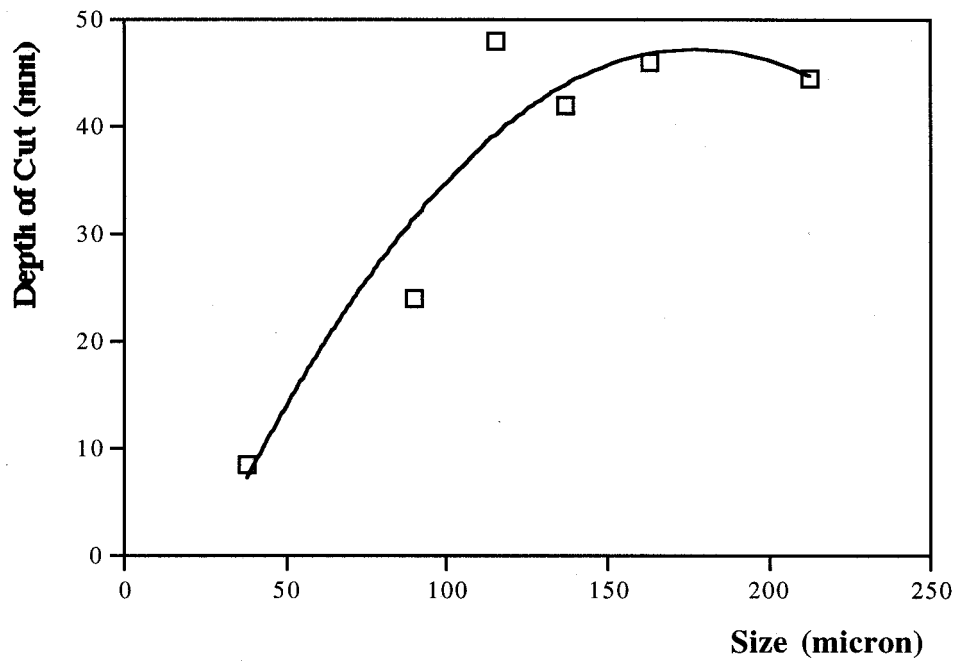


Figure 7. Depth of cut as a function of recycled particle size.

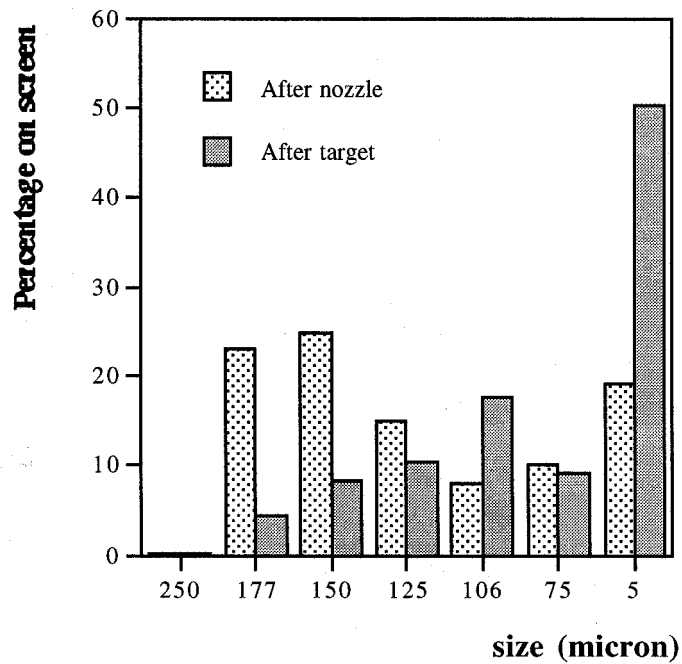


Figure 8. Size distribution after passing through nozzle and one cut on steel target.

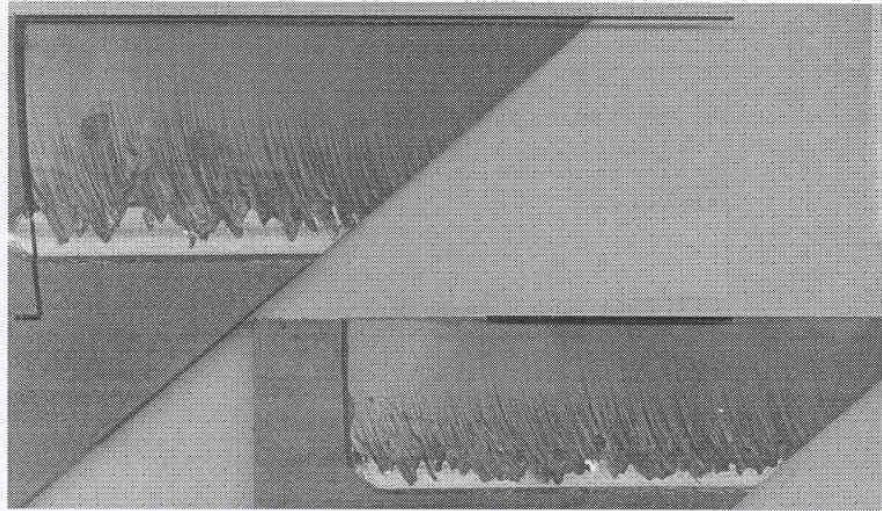


Figure 9. Loss in cut performance with jewel wear – cuts are at 15 and 20 hours.

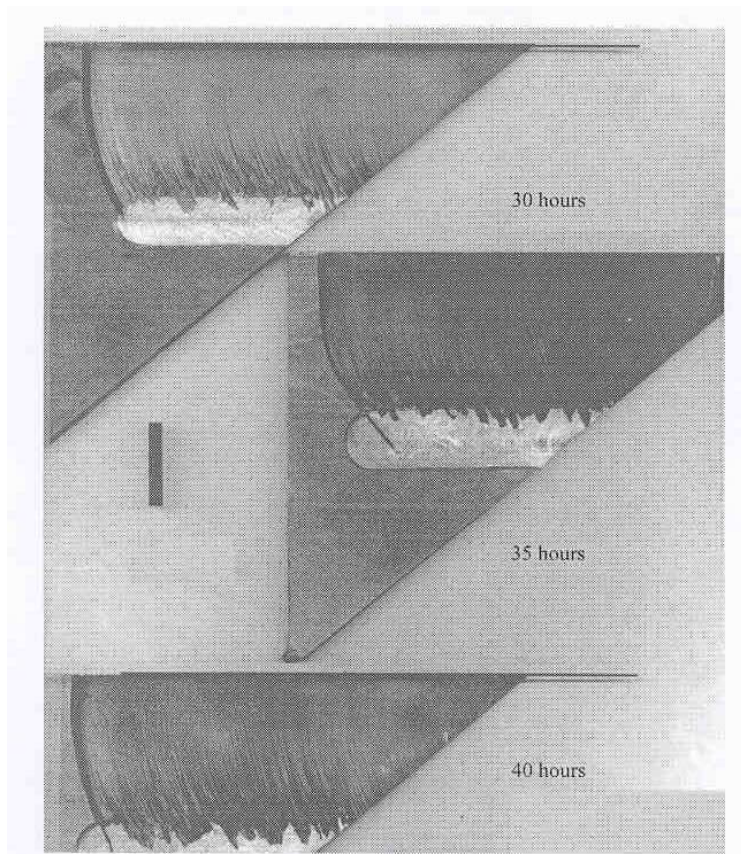


Figure 10. Cut at 40 ksi and 0.6 lb/minute after 30, 35 and 40 hours of use (1.5 in/min feed rate). The black line is 1" long.

Table 5. Cost comparison study without recycling.

PREDICTION OF OPTIMAL PERFORMANCE

nozzle/mix tube	30	focusing tube	118		
total wear part cost	\$148.00		Abrasive flow rate	0.6	lb/min
abrasive cost buy	\$0.48	dispose	\$2.18	total	\$2.66
Wear equation	x^2		x	const	
			-0.727	44.816	
speed	37.5		mm/min		
Depth to cut	8.5		mm		
speed exponent	0.86				
Length of cut	125		mm		
k	814.0632				

A	B	C	D	E	F	G	H	I	J
				cut time	Abrasive Per cut	Abr. Cost Per cut	Total # Parts	nozzle cost per part	total cost per part
Time (min)	Cut depth	85% depth	speed	(sec)	(lb)	\$		0	
0	44.82	38.09	214.54	34.96	0.35	\$0.93	51	\$2.87	\$3.80
30	44.45	37.78	212.52	35.29	0.35	\$0.94	102	\$1.44	\$2.38
60	44.09	37.48	210.50	35.63	0.36	\$0.95	153	\$0.97	\$1.91
90	43.73	37.17	208.48	35.97	0.36	\$0.96	203	\$0.73	\$1.69
120	43.36	36.86	206.47	36.32	0.36	\$0.97	253	\$0.59	\$1.55
150	43.00	36.55	204.46	36.68	0.37	\$0.98	302	\$0.49	\$1.47
180	42.64	36.24	202.45	37.05	0.37	\$0.99	350	\$0.42	\$1.41
210	42.27	35.93	200.44	37.42	0.37	\$1.00	398	\$0.37	\$1.37
240	41.91	35.62	198.44	37.79	0.38	\$1.01	446	\$0.33	\$1.34
270	41.54	35.31	196.44	38.18	0.38	\$1.02	493	\$0.30	\$1.32
300	41.18	35.00	194.44	38.57	0.39	\$1.03	540	\$0.27	\$1.30
330	40.82	34.69	192.45	38.97	0.39	\$1.04	586	\$0.25	\$1.29
360	40.45	34.39	190.46	39.38	0.39	\$1.05	632	\$0.23	\$1.28
390	40.09	34.08	188.47	39.79	0.40	\$1.06	677	\$0.22	\$1.28
420	39.73	33.77	186.48	40.22	0.40	\$1.07	722	\$0.21	\$1.27
450	39.36	33.46	184.50	40.65	0.41	\$1.08	766	\$0.19	\$1.27
480	39.00	33.15	182.52	41.09	0.41	\$1.09	810	\$0.18	\$1.28
510	38.64	32.84	180.55	41.54	0.42	\$1.10	853	\$0.17	\$1.28

Table 6. Cost comparison study with recycling.

PREDICTION OF OPTIMAL PERFORMANCE

nozzle/mix tube	30	focusing tube	118
Abrasive flow rate	0.6lb/min	%age loss	59.27%
total wear part cost	\$148.00	Abrasive flow rate	0.35562lb/min
abrasive cost buy	\$0.48	dispose	\$2.18
Wear equation	x^2	total	\$2.66
		x	const
		-0.727	44.816
speed	37.5	mm/min	
Depth to cut	8.5	mm	
speed exponent	0.86		
Length of cut	125	mm	
k	814.0632		

A	B	C	D	E	F	G	H	I	J
Time (min)	Cut depth	85% depth	speed	cut time (sec)	Abrasive Per cut (lb)	Abr. Cost Per cut \$	total # parts	nozzle cost per part	total cost per part
0	44.82	38.09	214.54	34.96	0.21	\$0.55	51	\$2.87	\$3.43
30	44.45	37.78	212.52	35.29	0.21	\$0.56	102	\$1.44	\$2.00
60	44.09	37.48	210.50	35.63	0.21	\$0.56	153	\$0.97	\$1.53
90	43.73	37.17	208.48	35.97	0.21	\$0.57	203	\$0.73	\$1.30
120	43.36	36.86	206.47	36.32	0.22	\$0.57	253	\$0.59	\$1.16
150	43.00	36.55	204.46	36.68	0.22	\$0.58	302	\$0.49	\$1.07
180	42.64	36.24	202.45	37.05	0.22	\$0.58	350	\$0.42	\$1.01
210	42.27	35.93	200.44	37.42	0.22	\$0.59	398	\$0.37	\$0.96
240	41.91	35.62	198.44	37.79	0.22	\$0.60	446	\$0.33	\$0.93
270	41.54	35.31	196.44	38.18	0.23	\$0.60	493	\$0.30	\$0.90
300	41.18	35.00	194.44	38.57	0.23	\$0.61	540	\$0.27	\$0.88
330	40.82	34.69	192.45	38.97	0.23	\$0.61	586	\$0.25	\$0.87
360	40.45	34.39	190.46	39.38	0.23	\$0.62	632	\$0.23	\$0.86
390	40.09	34.08	188.47	39.79	0.24	\$0.63	677	\$0.22	\$0.85
420	39.73	33.77	186.48	40.22	0.24	\$0.63	722	\$0.21	\$0.84
450	39.36	33.46	184.50	40.65	0.24	\$0.64	766	\$0.19	\$0.83
480	39.00	33.15	182.52	41.09	0.24	\$0.65	810	\$0.18	\$0.83
510	38.64	32.84	180.55	41.54	0.25	\$0.65	853	\$0.17	\$0.83
540	38.27	32.53	178.57	42.00	0.25	\$0.66	896	\$0.17	\$0.83
570	37.91	32.22	176.60	42.47	0.25	\$0.67	938	\$0.16	\$0.83
600	37.55	31.91	174.63	42.95	0.25	\$0.68	980	\$0.15	\$0.83
630	37.18	31.61	172.67	43.44	0.26	\$0.68	1022	\$0.14	\$0.83
660	36.82	31.30	170.71	43.93	0.26	\$0.69	1063	\$0.14	\$0.83
690	36.46	30.99	168.75	44.44	0.26	\$0.70	1103	\$0.13	\$0.83
720	36.09	30.68	166.80	44.97	0.27	\$0.71	1143	\$0.13	\$0.84
750	35.73	30.37	164.84	45.50	0.27	\$0.72	1183	\$0.13	\$0.84

THE HYDRO-CANNON NOZZLE OPTIMIZATION

G. Atanov
Donetsk State University
Donetsk, Ukraine

ABSTRACT

The hydro-cannon is an interesting and promising installation for producing high-speed pulsed liquid (usually water) jets. It uses the inertial principle of the water acceleration. The key feature of the hydro-cannon is that the dynamic pressure of the jet can be many times higher than the static one inside the installation. Hence, the form of the hydro-cannon nozzle is essential for the acceleration process of the water. The paper deals with problems of optimization of the hydro-cannon nozzle. Different approaches to the optimization are considered, and calculation of the nozzle profile to obtain the maximum outlet jet speed is given.

1. INTRODUCTION

Impulsive water jet is a tool for destruction of different hard materials. Therefore the optimum installation for producing the jets is such a one whose demolishing effect is the most.

There are three stages of the existence of an impulsive jet: (a) producing, (b) flight, and (c) impact. Consequently, there are three groups of hydrodynamic aspects related to the impulsive hydrodynamic breaking method: (a) problems of internal ballistics, that is, the processes occurring inside the installations, (b) problems of external ballistics, viz., the motion of the jet and its transformation in the air, and (c) the problems of the interaction of the jet with the target material (Atanov, 1987, 1998).

In order for a breaking process to be optimum, each of its stages must be optimum. Let us consider these stages beginning with the third one.

Different processes proceed in a rock under action of impulsive jets. Each of them can bring to demolition. Interaction of any impulsive jet with a rock begins with the high-speed impact. That leads to the rise of shock waves. The pressure increases strongly, and this is often the main reason of breaking. Besides, while spreading along rock, the shock wave is reflected from different inhomogeneities inside the rock as well as free surfaces as a rarefaction wave, which causes appearance of tensile stresses. As a result, the rock can tear off from a face. The tensile stresses also can arise if the shock waves (or rarefaction waves) are reflected from division boundaries of different rock sheets. If a jet is long enough and its dynamics head is more than the rock liquid limit, the jet takes root into the rock and makes a hollow in it. A zone of the high pressure arises inside the rock, and this internal pressure blows up the rock.

After impact, an impulsive jet starts to spread along the surface of the face. The head of the jet being non-plane, the spreading speed can be more than the speed of the impact because of hydrodynamic cumulative effect. Besides that the surface of the face is rough. Therefore the lowered pressure zones arise behind lugs, and the flow can even tear off. In this case, cavities appear, and closing of them is accompanied with a local hydraulic shock leading to breaking rock. If a rock has cracks (they often arise because of the impact), it breaks under action of a hydraulic wedge. Water penetrates into the cracks under a high pressure and chops off the rock. Intensity of all the above breaking processes depends, in the first place, on the speed of the impact.

There are a lot of other determining factors of both pulse and rock. For example, any pulse is characterized by the form of its pressure impulse, the water mass, the jet momentum, the outlet diameter of the nozzle, the time of action of the jet on the target. A rock is characterized by its percussion viscosity, viscoelastic, fragility, fissuring. The dependence between the stress tensor and speed strain tensor is a very important characteristic by dynamic loading. It is also necessary to take into account manifestation of rock fatigue, decrease of its strength because of unsteady loading. Each of these factors plays its role, and it is to be determined. Only in this case, the breaking criteria can be found which will yield an optimum problem. Future work is required to establish the criteria for fragmentation of the rock and their relationship to the parameters

characterizing the internal ballistics of the impulsive installation producing the jets. Connection between the above parameters only can be found if the motion of the impulsive jet in the air have been studied.

Let us consider the second stage of the jet existence. The target to be demolished is placed at some distance from the nozzle outlet. Moving to the target, any impulsive jet is transformed. There are two reasons for this. Firstly, the jet interacts with the air. It is a very complicated interaction. As the jet speed is supersonic according to the air, shock waves arise in the air, and big forces of resistance develop. Secondly, the process of the pulse is sharply unsteady. It means that the outlet speed is a function of time, and, consequently, the jet speed is changed along the jet axis.

All the above mentioned processes are very complicated. They do not allow using any one-dimensional approximation and must be considered in an axis symmetrical statement. There is also another circumstance that strongly complicates both the mathematical model and calculations, namely unsteady cavitation because of which cavities inside the jet arise. Because of the above mentioned peculiarities of the processes, neither optimization problem can be put according to the second stage of the jet existence, namely its flight.

Let us consider possibilities of the optimization being determined by the interior ballistics of the installation for producing impulsive water jets. Then the optimization problem can be put in a narrow sense. For example, it is possible to demand a maximum of the mass, or momentum, or energy of the jet during the pulse, and these characteristics must be calculated as integrals with respect to time at the nozzle outlet. The time of the integration is a complicated concept that is to be determined. It is not equal to the pulse time. The outlet water speed can be both decreased and increased during the pulse. If it is increased, it means that the water pressure at the nozzle is increased too. More exactly, the module of the gradient of the water speed at the nozzle outlet is increased because the water pressure at the nozzle outlet is equal to the atmospheric pressure (practically to zero). The water outlet speed is decreased when the module is decreased too. In this case, the outlet speed can become less than the speed of the jet, and continuity of the jet can be broken. The jet is torn off. That instant when the discontinuity of the jet arises is the limit of the integration. It has to be determined as a result of calculations. It is the reason owing to which an exponent hydro-cannon nozzle had a very short distance of breaking, namely about 25 cm (Cooley,1972).

There are two parameters of the internal ballistics (water speed and pressure) paying attention to them in the first place. Water speed determines the dynamic head of the jet and, consequently, water pressure on the target. As for a hydro-cannon, its nozzle plays an important role in the pulse process. Its form influences the outlet speed, water pressure inside both the barrel and nozzle. By the first appearance, the optimum nozzle is such a one that guarantees obtaining the maximum outlet speed.

But one and the same water speed can be obtained by different water pressure inside the installation. If a jet is steady, its dynamic pressure is equal to the pressure inside the installation producing this jet. For an unsteady jet, these pressures, in general case, are not equal. The hydro-

cannon dynamic pressure can be superior to the pressure inside the installation several times. This circumstance can be estimated quantitatively with the help of the pressure rise factor k_r . It is determined as a ratio of the maximum jet dynamic pressure

$P_{d \max}$ to the maximum pressure inside the installation $P_{i \max}$ during the pulse:

$$k_r = P_{d \max} / P_{i \max}$$

For the hydro-cannon, $k_r > 1$, and its greatest value obtained in calculations was equal to 3.7 (Atanov and Semko, 1996). But the maximum value of k_r may be only obtained by means of solving an optimization problem.

Neither above-mentioned problem is solved now. The only solution is obtained for a simplified problem. An optimum nozzle profile to obtain the maximum of the mean outlet speed was found under condition that the time of flowing out is set (Atanov 1993, 1997).

2. THE OPTIMIZATION CONDITIONS

A non-percussive hydro-cannon scheme is shown in Figure 1a (Atanov, 1987). The principle of its operation is the following. The air is pumped out from the barrel (4) and nozzle (5). The piston (2) together with water (3) filling some part of the barrel volume is accelerated by compressed gas (1). On reaching the nozzle inlet with a definite speed, the accelerating water flows into it. When the free surface of the water reaches the nozzle outlet, a water outflowing begins. The duration of the pulse is less than 1 ms.

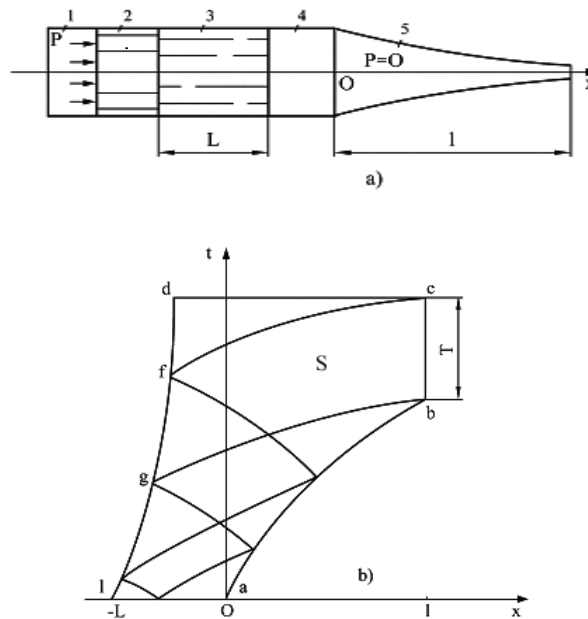


Figure 1. a) Scheme of a non-percussive hydro-cannon;
b) x, t diagram of the process.

Figure 1b shows the x, t diagram of this process (x is a spatial coordinate, and t is time). Here $a-b$ is the trajectory of the water-free surface, $b-c$ is the line of the nozzle outlet, $c-d$ is a first family characteristic limiting the zone of influence designated as S , $d-e$ is the piston trajectory.

Outflow begins at the moment t_b and ends at the moment t_c , and, as we have stipulated, the time of outflowing $t_c - t_b = T = \text{constant}$.

The objective functional is set on the line of the nozzle outlet $b-c$:

$$I = \frac{1}{T} \int_{t_b}^{t_c} u dt \quad (1)$$

The extreme of the functional will be found with the help of the variational methods.

The problem can be solved one-dimensionally. The water flow is described with a system of the unsteady gas dynamic equations:

$$L_1 \equiv \frac{\partial}{\partial t} a^{2/(n-1)} + \frac{\partial}{\partial x} (ua^{2/(n-1)}) + ua^{2/(n-1)} \frac{d \ln F}{dx} = 0 \quad (2)$$

$$L_2 \equiv \frac{\partial u}{\partial t} + \frac{\partial}{\partial x} \left(\frac{u^2}{2} + \frac{a^2}{n-1} \right) = 0$$

where u is the water speed, a is the sonic speed in the water, F is the nozzle cross-sectional area, and $n = 7.15$ is the water adiabatic index (the Tait equation is taken as the water state equation). The equations remain invariant in a dimensionless form if the following scales are used: the initial sonic speed $a_0 = 1460$ m/s for u and a , the length of the nozzle l for x , and the value l/a_0 for t . The dimensionless form will be used henceforth but $F(x)$ is nondimensionalized.

The system (2) is of the hyperbolic type.

The initial conditions are put on the segment $a-e$:

$$u = u_0, \quad a = 1 \quad (3)$$

where u_0 is the initial water speed obtained during the acceleration process in the barrel. The boundary conditions are applied to the lines of the free surface and piston. On $a-b$, the water pressure is equal to zero, and the sonic speed, consequently, is equal to its initial value

$$L_3 \equiv \frac{dx}{dt} - u = 0 \quad (4)$$

$$a = 1 \quad (5)$$

On $d-e$, the equation for the piston motion under the action of the water pressure is written as follows:

$$L_4 \equiv \frac{dx}{dt} - u = 0 \quad (6)$$

$$L_5 \equiv \frac{du}{dt} + A(a^{2n/(n-1)} - 1) = 0, \quad A = \frac{1}{n} \frac{l}{L} \frac{m}{M} \quad (7)$$

where L is the initial length of the water charge in the barrel, m is the mass of the charge, and M is the mass of the piston.

On the nozzle outlet line $b-c$, the boundary condition is set if the outflow is subsonic. It consists in the constancy of the water pressure and, consequently, the sonic speed, and has the form (6).

Let us take the derivative dF/dx as the controlling function designating it as follows:

$$L_6 \equiv \frac{dF}{dx} - \omega = 0 \quad (8)$$

Then the variational problem can be formulated as follows: within the interval $0 \leq x \leq 1$, the function $F(x)$ should be found that has the given values $F(0)$ and $F(1)$ and provides the maximum to functional (1) if there are algebraically conditions (3) and (5) and differential conditions (2), (4), (7) to (8).

The present problem involves a conditional extreme in the zone S (see Figure 1b). To find the solution, the general method of indefinite Lagrangian multipliers will be used, which was worked out for solving steady gas dynamics problems and was first applied to unsteady gas dynamics problems in works. The method consists in (a) building an auxiliary functional (Lagrangian functional) in which all of the above conditions are introduced with the help of the indefinite multipliers (Lagrangian multipliers), (b) determining its first variation, and (c) choosing multipliers such that the coefficients at the independent variations, except those of the controlling function, would be equal to zero.

The Lagrangian functional is

$$I_L = \frac{1}{T} \int_{t_b}^{t_c} u dt + \int_0^1 C_0 L_6 dx + \int_0^{t_b} C_1 L_3 dt + \int_0^{t_d} (C_2 L_4 + C_3 L_5) dt + \iint_S (h_1 L_1 + h_2 C_2) dx dt \quad (9)$$

where $h_1(x, t)$, $h_2(x, t)$, $C_1(t)$, $C_2(t)$, $C_3(t)$, $C_0 = \text{constant}$ are the indefinite Lagrangian multipliers. The function $F(x)$ yielding the extreme to functional (10) also provides it to functional (1) with the above conditions.

The first variation of the functional (9) is a sum of (a) the terms outside the integral at the points b , c , d ; (b) the contour integrals along the lines of the free surface $a-b$, nozzle outlet $b-c$, the piston $d-e$ and the line $c-d$ ($t = \text{constant}$); (c) the surface integral all over the zone S .

In the zone S the following conditions are found:

$$\begin{aligned} \frac{\partial h_1}{\partial h_2} + u \frac{\partial h_1}{\partial h_2} + a^{2/(n-1)} \frac{\partial h_2}{\partial x} &= a^{2/(n-1)} \frac{\omega}{F} h_2 \\ \frac{\partial h_2}{\partial t} + u \frac{\partial h_2}{\partial x} + a^{(2n-4)/(n-1)} \frac{\partial h_1}{\partial x} &= \frac{u\omega}{F} h_2 \end{aligned} \quad (10)$$

This system defines multipliers h_1 and h_2 .

On the free surface line $a-b$,

$$h_2 - C_1 = 0, \quad \frac{dC_1}{dt} - C_1 u \frac{\omega}{F} - h_1 \frac{du}{dt} = 0 \quad (11)$$

Along the piston line $d-e$,

$$\begin{aligned} \frac{dC_3}{dt} + C_3 + a^{2/(n-1)} h_2 &= 0 \\ \frac{dC_1}{dt} + \frac{2}{n-1} a^{3-n/(n-1)} \frac{da}{dt} h_2 + \frac{du}{dt} h_1 &= 0 \end{aligned} \quad (12)$$

$$nAa^{2/(n-1)} C_3 - h_1 = 0$$

On the nozzle outlet line $b-c$,

$$uh_1 + h_2 + \frac{1}{T} = 0 \quad (13)$$

On the line $c-d$,

$$h_1 = 0, \quad h_2 = 0 \quad (14)$$

At the points b (on its lower side) and d , accordingly,

$$C_1 = 0, h_2 = \frac{u_c - u_b}{u_b T} \quad (15)$$

$$C_2 = C_3 = 0 \quad (16)$$

Equating the expression near the variation of F to zero, we obtain an equation for C_0 :

$$\frac{dC_0}{dx} + \frac{\omega}{F} E_0 = 0, \quad C_0(x) = \int E_0 \frac{\omega}{F} dy + C_0(1), \quad E_0 = \frac{1}{F} \int_{a-b}^{t_c} h_2 u a^{2/(n-1)} dt \quad (17)$$

The $C_0(1)$ value is found from the condition that values of $F(0)$ and $F(1)$ are given.

The above choice of the Lagrangian multipliers allows exclusion of all the variations, except that of the controlling function, from the variation of the functional (9). Thus the Lagrangian functional variation will have only one term:

$$\delta I_L = \int_0^1 E(x) \delta \omega dx \quad (18)$$

where the function $E(x)$ is the gradient of both functional (9) and functional (1) with respect to the controlling function. It is given by

$$E = E_0 - C_0 \quad (19)$$

The above relations pose a conjugate or a reverse problem, and its solution is obtained as follows. A nozzle profile is assumed (the first approximation), and the system (2) with conditions (3) to (7) is solved (the direct problem). Then, the system (10) with conditions (11) to (16) is solved backwards in time, and all the Lagrangian multipliers, except C_0 , are found. Then, C_0 and E are defined with the help of equations (17) and (19) by the well-known $C_0(1)$. After that, $\omega(x)$ is corrected by means of the gradient method:

$$\omega^{(i+1)} = \omega^{(i)} + \alpha E^{(i)} \quad (20)$$

where i is the number of iterations and $\alpha = \text{constant}$ is the gradient method step. Numerous calculations showed that α can change within a wide interval and its real value for each problem must be determined experimentally.

The cross-sectional area of the nozzle is defined by the formula

$$E(x) = F(0) - \int_0^x \omega dy \quad (21)$$

The described process is repeated until E becomes less than a given value for $0 \leq x \leq 1$. This iterative process allows $C_0(1)$ to be found easily, and thus $C_0(x)$ can be defined with the help of formula (19). From relations (19) to (21),

$$\int_0^1 E dx = 0, \quad C_0(1) = \int_0^1 \left(E_0 - \int_0^x \frac{\omega}{F} E_0 dy \right) dx \quad (22)$$

The resultant correlations make up a closed system of the optimization equations.

3. THE NUMERICAL SOLUTION

Traditionally, gas dynamics variational problems are solved via the numerical method of characteristic. But this problem has a peculiarity. According to the conditions (13) to (15), each of the Lagrangian multipliers h_1 and h_2 has two values at points b and c . It means that h_1 and h_2 are broken at these points, and discontinuities of them arisen. These discontinuities spread along characteristics $b-f$ and $c-g$ and their reflection. The multiplicity of the discontinuities obviates the advantages of the method of characteristics. Another solution technique is needed.

The direct and conjugate problems were solved by the same method (Atanov, 1988). It is a shock-capturing method that was successfully applied for open channels, in which the flow is described by analogous hyperbolic equations and variational problems are characterized by a large number of the Lagrangian multiplier discontinuities (Atanov, Evseeva and Work 1998). The solution was constructed on an immovable grid. The number of grid cells increased in the nozzle and decreased in the barrel according to the motion of the boundaries.

By $T \rightarrow 0$, the problem corresponds to an optimization one to get the maximum inflow speed. As it was shown theoretically in works (Atanov, 1993), the optimal nozzle has fractures in this case.

Figure 2 shows the results obtained for the hydro-cannon with $L/l = 1$ and the initial water speed $u_0 = 150$ m/s.

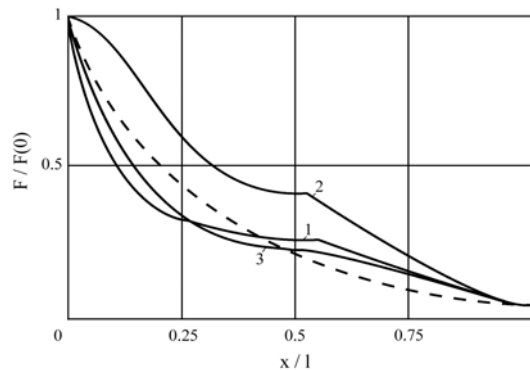


Figure 2. The cross-sectional area of the optimum nozzles.

The dashed line gives the initial profile assumption, and curves 1 and 2 are for $A = 0.01$ and $A = 0.5$ by $T \rightarrow 0$ (4 time steps). Curve 3 corresponds to $A = 0.01$ and $T = 100$ time steps. It has no fracture at $x > 0$. For curve 1, the outlet speed increased from 1170 m/s for the initial nozzle to 1440 m/s (23 per cent) for the optimum one.

4. CONCLUSION

In the paper, concept of the optimization of the impulsive hydrodynamic method of breaking is considered. It is shown that the full optimization includes that of three stages of jet existence: producing, flight, impact. The factors influencing on breaking and the jet are discussed: properties of rocks, transformation of the jet in the air, parameters of internal ballistics of the installations.

A problem of finding the optimum profile of the hydro-cannon nozzle to get the maximum outlet speed is put and its numerical solution is given. Such a nozzle can allow gain in the outlet speed more than 20 per cent.

5. REFERENCES

- Atanov, G.A. The hydroimpulsive installations for breaking rock formation in the mines. Kyiv, Vyshcha Shkola, 1987 (In Russian).
- Atanov, G.A. A method for integration of the gas dynamics equations. *Izvestija Akademii Nauk USSR, Mechanica Zhidkosti i Gasa*, N4, 1988. Pp 184-189 (In Russian).
- Atanov, G.A. Optimization of the hydro-cannon nozzle in the outlet speed. *Teoreticheskaya i Prikladnaya Mechanika*. Kiev, Vyshcha Shkola, N24, 1993. Pp 53-57 (In Russian)
- Atanov, G.A. The optimal control problem of profiling the hydro-cannon nozzle to obtain the maximum outlet speed. *Proceedings of the Institution of Mechanical Engineers*, V 211, Part C, 1997. Pp 541-547.
- Atanov, G.A. Impulsive hydrodynamic method of breaking rocks and concrete. *Water jet applications in construction engineering*. A.A. Balkema, Rotterdam, Brookfield, 1998. Pp 73-89.
- Atanov, G.A., Evseeva, E.G., and Work, P.A. The variational problem of water level stabilization in open channels. *Journal of Hydraulic Engineering*, V 124, N1, 1998. Pp 50-55.
- Atanov, G.A., Semko, A.N. The pressure rise factor for power hydro-cannon. *Proceedings of the 13th International Conference on Jetting Technology*. (Sardinia, Italy, 1996). Pp 91-103.

Cooley, W. Rock breakage by pulsed high-pressure water jets. Proceeding of the 1st International Symposium on Jet Cutting Technology (Coventry, England, 1972), paper B7, pp 101-112.

Krayko, A.N. Variational problems of gas dynamics. Moscow, Nauka, 1979 (In Russian).

Miele, A. (Ed.) Theory of optimum aerodynamic shapes. New York, Academic Press, 1965.

6. NOMENCLATURE

a - sonic speed in water,
 $C_0, C_1, C_2, C_3, h_1, h_2$ - indefinite Lagrangian multipliers,
 E - gradient of functional,
 F - nozzle cross-sectional area,
 k_r - pressure rise factor,
 l - nozzle length,
 L - initial length of the water charge,
 m - water charge mass,
 M - piston mass.
 n - water adiabatic index
 P_d - jet dynamic pressure,
 P_i - water pressure inside the installation,
 t - time,
 T - time of outflowing,
 u - water speed,
 x - space coordinate,
 α - gradient method step,
 ω - controlling function.

NUMERICAL SIMULATION OF ABRASIVE WATER JET

D. H. Ahmed, E. Siores, F. L. Chen
Industrial Research Institute Swinburne
Swinburne University of Technology
Hawthorn, Victoria, Australia

J. Naser
School of Engineering and Science
Swinburne University of Technology
Hawthorn, Victoria, Australia

ABSTRACT

A Computational Fluid Dynamics (CFD) method has been developed to find out the particle and air velocity distributions at the exit of the focus tube that are encountered during Abrasive-Air-Water jet processing. The study has been carried out using a multi-phase approach. The abrasive particles were treated as a solid granular continuous phase. The air used for pumping the abrasive particles into the jet device was treated as a continuous phase and the water was treated as the principle continuous phase. The governing equations were discretized using the finite volume approach. The solution was obtained using the Inter-Phase Slip Algorithm (IPSA). The governing equations were closed using the K- ϵ turbulence model. The abrasive particles enter the nozzle and the focus tube where the particles distributed themselves along the solid wall surface and flew along the solid wall, while the air phase concentrated in the central region of the mixing tube. The distribution pattern of the air and water phase suggests a possible oscillation in the focus tube. The simulation was performed using different abrasive inlet angles and abrasive inlet positions. The results clearly show the effect of abrasive inlet angle and its positions on velocity distribution at the exit of the focus tube. It was found from the simulation that the optimum abrasive inlet angle depends on its position in the mixing chamber. Lower angles are beneficial when the abrasive inlet position is near the taper part ie. lower portion of the mixing chamber, and higher angle are preferred when the abrasive inlet position nears the orifice ie. upper portion of the mixing chambers. The velocities and volume fractions of air, water and abrasive particles at the exit were compared with the available experimental data. The simulated results showed good agreement with the experimental data.

1. INTRODUCTION

Velocity distribution in abrasive water jet for precision cutting is very important parameter. Experimental results for finding the velocity of water and abrasive have been obtained using different methods. But in actual case the abrasive water jet encompasses the flow of three phases (water, air and solid). Most researchers have carried out experiments for the abrasive particles and water, since it is difficult to measure the velocity of air at the exit of the focus tube.

Scharner et al. (1998) calculated the air flow rate according to the abrasive flow rate. It is clear from their paper that the geometry of the mixing chamber has a great influence on the airflow rate. Abduka and Crofton (1989) showed that the vacuum pressure inside the mixing chamber is increased with the increase of the water pressure and that also depends on the orifice diameter. Neusen et al. (1994) showed that the composition of abrasive water jet on a volume basis is approximately 4% to 6% water, 0.2% to 0.5% abrasive and 93% to 95% air. Tazibt et al. (1996) showed that the air is sucked with the abrasive particles occupies more than 90 percent of the volume of an abrasive water jet and hence there is a great influence of air in abrasive water jet. Some authors have tried to simulate the abrasive water jet but they have only considered two phases (water and solid). Jain Ye (1996) attempted to simulate the abrasive water jet considered the particle motion and trajectories with Lagrangian equations of particle motion. He showed that the tapered inlet angle has profound influence on the particle concentration and kinetic energy distribution at the nozzle exit. J Ye and R Kovacevic (1999) have also simulated the abrasive water jet for two phases and in both simulations they used a direct injected abrasive water jet (DIA jet). In this paper we have tried to simulate abrasive water jet considering three phases for conventional entrainment jets.

Computational Fluid Dynamics (CFD) analysis for abrasive water jet is very useful tool for finding out the velocity distributions of the different phase existing during AWJ processing. The software CFX-4 was used for these simulations. Water and solid was considered to be incompressible flow and air as compressible flow.

This paper addresses the simulation of abrasive water jet for three phases existing in a conventional entrainment system and for different abrasive inlet angles and abrasive inlet positions in the mixing chamber.

2. MATHEMATICAL MODELING

Abrasive water jet is obviously a turbulent flow according to the Reynold's number. Water is generally passing through the orifice with high velocity whereas air and abrasives flow with comparatively small velocity. There is a transfer of energy from the high-speed water to the abrasive particles, which impact the work piece. Therefore, the cutting performance of an abrasive water jet is a function of the total mass of impinging particles and their velocity at impact. The average velocity of the total mass of abrasive particles is a quantity, which must be determined to improve the cutting head design. To find out the velocity distribution at the nozzle exit using simulation, the water, air and solid system needs to be treated as multi-phase flow. The simulation also carried out for steady state, turbulent flow and considering heat transfer. Water

was considered as the primary phase. Simulations were developed with K-ε turbulence model (turbulent kinetic energy and energy dissipation) using the CFX-4 software.

2.1 Equations of the Simulation

The three phases were labeled by Greek indices α , β and γ representing water, air and solid respectively and N_p denotes the number of phases. The volume fraction of each phase is denoted r_α . As the simulation was carried out using a cylindrical coordinate system, the variable had three components like; $U = U(r, \theta \text{ and } z)$. All the three phases were modeled with Eulerian approach.

From the continuity equation

$$\frac{\partial}{\partial t}(r_\alpha \rho_\alpha) + \nabla \cdot (r_\alpha \rho_\alpha U_\alpha) = 0 \quad \dots\dots\dots(1)$$

From the momentum equation

$$\begin{aligned} \frac{\partial}{\partial t}(r_\alpha \rho_\alpha U_\alpha) + \nabla \cdot (r_\alpha (\rho_\alpha U_\alpha \otimes U_\alpha - \mu_{\alpha eff} (\nabla U_\alpha + (\nabla U_\alpha)^T))) \\ = r_\alpha (B - \nabla p_\alpha) + \sum_{\beta=1}^{N_p} c_{\alpha\beta}^{(d)} (U_\beta - U_\alpha) + F_\alpha \quad \dots\dots\dots(2) \end{aligned}$$

$$\text{where} \quad \mu_{\alpha eff} = \mu_\alpha + \mu_{T\alpha} \quad \dots\dots\dots(3)$$

$$\text{and} \quad \mu_{T\alpha} = C_\mu \rho_\alpha \frac{k_\alpha^2}{\varepsilon_\alpha} \quad \dots\dots\dots(4)$$

and the energy equation (for incompressible flow)

$$\frac{\partial}{\partial t}(r_\alpha \rho_\alpha H_\alpha) + \nabla \cdot (r_\alpha (\rho_\alpha U_\alpha H_\alpha - \lambda_\alpha \nabla T_\alpha)) = \sum_{\beta=1}^{N_p} c_{\alpha\beta}^{(h)} (T_\beta - T_\alpha) \quad \dots\dots\dots(5)$$

where H_α is the static enthalpy, $H_\alpha = h_\alpha(T_\alpha)$

So, the algebraic equation of state and the constitutive equation for each phase are as follows:

$$\rho_\alpha = \rho_\alpha(T_\alpha, p_\alpha) \quad \dots\dots\dots(6)$$

$$h_\alpha = h_\alpha(T_\alpha, p_\alpha) \quad \dots\dots\dots(7)$$

Considering that the volume fractions sum is unity:

$$\sum_{\alpha=1}^{N_p} r_{\alpha} = 1$$

The general advection-diffusion equation is:

$$\frac{\partial}{\partial t}(r_{\alpha} \rho_{\alpha} \Phi_{\alpha}) + \nabla \cdot (r_{\alpha} (\rho_{\alpha} U_{\alpha} \Phi_{\alpha} - \Gamma_{\alpha} \nabla \Phi_{\alpha})) = r_{\alpha} S_{\alpha} + \sum_{\beta=1}^{N_p} c_{\alpha\beta} (\Phi_{\beta} - \Phi_{\alpha}) \quad \dots\dots\dots(8)$$

The term $c_{\alpha\beta} (\Phi_{\beta} - \Phi_{\alpha})$ describes inter - phase transfer of Φ between α and β .

$c_{\alpha\alpha} = 0$, $c_{\alpha\beta} = c_{\beta\alpha}$. Hence, the sum over all phases of all inter - phase transfer terms is zero.

Equation of volume fraction

$$\frac{\partial}{\partial t}(r_{\alpha} \rho_{\alpha}) + \nabla \cdot (r_{\alpha} \rho_{\alpha} U_{\alpha} - \Gamma_{\alpha} \nabla r_{\alpha}) = 0 \quad \dots\dots\dots(9)$$

where $\Gamma_{\alpha} = \frac{\mu_{T\alpha}}{\sigma_{\alpha}}$

The turbulent dispersion of volume fraction was modeled using the Eddy diffusivity hypothesis.

Assuming that the transport equation for k and ε in a turbulent phase takes the same form as the generic scalar advection-diffusion equation

$$\begin{aligned} \frac{\partial}{\partial t}(r_{\alpha} \rho_{\alpha} k_{\alpha}) + \nabla \cdot \left(r_{\alpha} \left(\rho_{\alpha} U_{\alpha} k_{\alpha} - \left(\mu + \frac{\mu_{T\alpha}}{\sigma_k} \right) \nabla k_{\alpha} \right) \right) \\ = r_{\alpha} S_{k\alpha} + \sum_{\beta=1}^{N_p} c_{\alpha\beta}^{(k)} (k_{\beta} - k_{\alpha}) \quad \dots\dots\dots(10) \end{aligned}$$

$$\begin{aligned} \frac{\partial}{\partial t}(r_{\alpha} \rho_{\alpha} \varepsilon_{\alpha}) + \nabla \cdot \left(r_{\alpha} \left(\rho_{\alpha} U_{\alpha} \varepsilon_{\alpha} - \left(\mu + \frac{\mu_{T\alpha}}{\sigma_{\varepsilon}} \right) \nabla \varepsilon_{\alpha} \right) \right) \\ = r_{\alpha} S_{\varepsilon\alpha} + \sum_{\beta=1}^{N_p} c_{\alpha\beta}^{(\varepsilon)} (\varepsilon_{\beta} - \varepsilon_{\alpha}) \quad \dots\dots\dots(11) \end{aligned}$$

The source terms were considered to be the same as their single - phase analogous and thus :

$$S_{k\alpha} = P_{\alpha} + G_{\alpha} - \rho_{\alpha} \varepsilon_{\alpha} \dots\dots\dots(12)$$

$$S_{\varepsilon\alpha} = \frac{\varepsilon_{\alpha}}{k_{\alpha}} (C_{1\varepsilon} (P_{\alpha} + C_{3\varepsilon} \max(G_{\alpha}, 0)) - C_{2\varepsilon} \rho_{\alpha} \varepsilon_{\alpha}) \dots\dots\dots(13)$$

where P is the shear production
and G is production due to the body forces.

The constants were set as $C_{\mu} = 0.09$, $C_1 = 1.44$, $C_2 = 1.92$, $C_3 = 0$, $\sigma_k = 1.00$ and $\sigma_{\varepsilon} = 1.217$

Since air was considered as compressible flow, its density will then change with changes in pressure. The ideal gas law:

$$\rho = \frac{pW}{RT} \dots\dots\dots(14)$$

where $p = P + P_{ref}$

The pressure P which was stored and solved for by the code actually the difference between the thermodynamic pressure p and fixed reference pressure P_{ref}

2.2 Geometry and Parameters

The cylindrical coordinate system was used to create the geometry for the conventional entrainment jet. The schematic diagram is shown in Figure 1. For three-phase flow (water, air and solid) the surrounding was considered to be in atmospheric condition. For that reason extra blocks were created and treated as the pressure boundary with atmospheric pressure and 100% air. Whilst the water pressure was considered as 276 MPa. The dimensions of the geometry and parameters are shown in Table 1. The abrasive inlet angle and its position are shown in Figure 2.

3. VALIDATION OF THE SIMULATION

Although the simulation was developed for three phases, it was very difficult to measure the velocity of the three phases in order to fully validate the theoretical results. However, the velocity distribution at the exit of the focus tube was verified with experimental data for a two-phase flow published by Zoltani and Bicen (1990). Fully turbulent, two phase round jet of 25.4 mm in diameter, exit velocity of 20 m/s and containing 80 μm beads with a density of loading of 1.5% was examined in their tests. They used laser-Doppler velocimetry to measure the velocity of air and solid for several positions at the exit. The results presented in Figure 3 to Figure 5

show that the numerical simulations developed are in good quantitative agreement with the experimental study.

Some other experimental findings that provided measurements of the volume fractions of the three phases at the exit and analysis for water, air and solid were also utilized to validate the simulated results. For example, Neusen et al. (1991) measured the volume fraction of air, water and solid at the outlet using scanning X-ray densitometry. The X-ray scanner produced a very thin (0.125mm) beam of X-ray, which passed through the jet and was attenuated by interaction with mass contained in the jet. The intensity of the X-ray beam was measured using a scintillation detector. The absorption coefficients were then used to estimate local average substance volumetric fraction for air, water and abrasive. They used pressure ranging from 207 to 345 MPa, and abrasive flow rate from 0.34 to 0.57 kg/min to measure the volume fractions for 4mm stand off distance. The volume fractions from the simulation were compared with these experimental results. The volume fractions from the simulation are taken at the exit of the focus tube i.e. 0mm standoff distance. The simulated volume fraction of water at the exit of the focus tube was higher near the wall. This may lead to possible oscillation of the jet assembly. The compared volume fraction results are shown in Figures 6, 7 and 8.

4. EFFECT OF ABRASIVE INLET ANGLE AND ITS POSITION

The simulation was developed for different abrasive inlet angles and its position in the mixing chamber. The velocity distributions at the exit of the focus tube are presented in this section. The jet velocity at the exit was found to be dependent on the mixing processes at the mixing chamber and the time taking for the acceleration process of the abrasive particles, as well as the momentum transfer from water to abrasive particles. The simulated conditions for the conventional entrainment system are given in table 1.

For precision cutting, the jet velocity near the central axis is important and it should be the maximum velocity near the center position of the jet. Three different abrasive inlet positions were used for obtaining the optimum inlet position (Figure 2). The center distance of the abrasive inlet was 2.25mm from the taper part of the assembly. Another two positions of the abrasive inlet 5.25mm and 6.75mm from the lower part of the mixing chamber were also considered. For different abrasive inlet angles, the air and the solid will bounce from different positions in the mixing chamber, taper part and the focus tube. Table 2 shows these phenomenon.

It is clear from Table 2 that at 2.25mm position, of abrasive inlet from the taper part, the abrasive will hit the inclined surface, if the inlet angles in between 20.56 to 55.56 degrees. If the inlet angle is less than 20.56 degree, it will hit the mixing chamber. Figure 9 shows the water speed at the outlet of the focus tube for different abrasive inlet angles. For 30-degree inlet angle the water speed was found to be higher than the others along the radius. Similarly Figures 10 and 11 show the air and solid speed for different abrasive inlet angle. From Figures 9 to 11 it is clear that for 30-degree abrasive inlet angle, the jet speed becomes maximum for this configuration of the nozzle geometry. But if the geometry is changed like mixing chamber length and diameter, taper inlet angle etc., the optimum abrasive inlet angle may change at maximum jet speed. It should also be mentioned here that for 30-degree abrasive inlet angle, the velocity of the different

phases along the radius is not in well pattern. This indicates that the mixing process in the mixing chamber are not quiet enough for getting the maximum velocity at the center position of the jet.

Figure 12 shows the average speed of the jet for different abrasive inlet angles. It is clear that for 30 degree abrasive inlet angle (29 degree of abrasive inlet angles are also used for obtaining an accurate pattern), the average speed of the jet is maximum. Figure 13 shows the speed of water, air and solid near the central axis and it can be seen that for 30-degree abrasive inlet angle, the respective velocities of the different phases are maximum and follow a almost similar pattern. In the case of 75 degree, the speeds of the three phases are similar but not maximum.

The next step was to find out the effect of inlet position for different abrasive inlet angles. Considering the results illustrated in Figure12 simulations were developed for different abrasive inlet angles (30, 45 and 60 degrees) and for different inlet positions.

The new abrasive inlet position was 6.75mm from the taper part and simulations were carried out for abrasive inlet angle 30, 45 and 60 degrees. An additional simulation was carried out using the abrasive inlet angle of 45 degrees with the inlet position being 5.25mm. For the precision cutting jet velocity should be maximum near the central region of the jet. Figures 14 to 16 show the velocity distribution at the exit plane along the radius for the abrasive inlet angle 30 degrees and for two different inlet positions. A better result was obtained though for the former inlet position. But in the case of 45 degrees inlet angle, better results were obtained for the inlet position of 5.25mm. These are shown in Figures 17, 18 and 19. But in the case of abrasive inlet angle of 60 degree (Figures 20, 21 and 22) better results were found when 6.75mm abrasive inlet position was used. So it is clear that for the inlet position near the orifice or the upper side of the mixing chamber, a higher angle is the optimum abrasive inlet angle. For upper position of the abrasive inlet angle, the velocity profiles show that the maximum velocity is near the central line of the jet.

5. CONCLUSION

If the abrasive inlet position is closed to the taper part i.e. bottom of the mixing chamber, a lower angle will be the optimum abrasive inlet angle when considering the maximum velocity of the jet.

If the inlet position is changed towards the orifice (i.e. upper position of the mixing chamber) a higher abrasive inlet angle will be the optimum.

A higher position of the abrasive inlet angle i.e. near the orifice velocity profile, indicated that the maximum velocity of the jet is near the central axis. This also indicates that the mixing process in the mixing chamber is optimum and therefore the oscillation of the jet is minimized and hence precision jet cutting can be carried out.

6. ACKNOWLEDGMENTS

The authors would like to thank the Australian Research Council (ARC) for the support of this work.

7. REFERENCES

- Abduka, M., and Crofton, P. S. J., "Theoretical Analysis and Preliminary Experimental Result for an Abrasive Water Jet Cutting Head." *Proceedings of the 5th American Waterjet Conference*, pp. 79-87, Water Jet Technology Association, Toronto, Canada, 1989.
- Neusen, K. F., Alberts, D. G., Gores, T. J., and Labus, T. J., "Distribution of Mass in a Three-Phase Abrasive Waterjet Using Scanning X-Ray Densitometry, " *Proceedings 10th International Symposium on Jet Cutting Technology*, BHRG Fluid Engineering, Amsterdam, Netherlands, pp. 83-98, 1991.
- Neusen, K. F., Gores, T. J., and Amano, R. S., "Axial Variation of Particle and Drop Velocities Downstream From an Abrasive Water Jet Mixing Tube," *12th International Symposium on Jet Cutting Technology*, pp. 93-103, 1994.
- Scharner, M., Weseslindtner, H., Trieb, F., Herbig, N., and Haase, C., "Study on the Influence of Mixing Chamber Dimensions in Abrasive Waterjet Cutting Heads on Cutting Efficiency," *14th International Conference on Jetting Technology*, BHR Group Conference Series, Publication No. 32, pp. 169-183, 1998.
- Tazibt, A. Q., Parsy, F., and Abriak, N., "Theoretical Analysis of the Particle Acceleration Process in Abrasive Water Jet Cutting," *Computational Material Science*, Vol. 5, pp. 243-254, 1996.
- Ye, J., "Numerical Simulation of Particle Concentration at the Exit of a Direct Injected Abrasive Water Jet Nozzle," *Particulate Science and Technology*, Vol. 14, pp.75-88, 1996.
- Ye, J., and Kovacevic, R., "Turbulent Solid-Liquid Flow Through the Nozzle of Premixed Abrasive Water Jet Cutting System," *Proc. Instn Mech Engineers*, Vol.213, Part B, pp. 59-67, 1999.
- Zoltani, C. K., and Bicen, A. F., "Velocity Measurement in a Turbulent, Dilute, Two-phase Jet," *Experiments in Fluids*, Vol. 9, pp. 295-300, 1990.

8. NOMENCLATURE

B	Body force
c	Inter-phase term
C	Constant
D	Focus tube diameter
F	Inter phase non-drag forces
G	Production due to body force
h	Thermodynamic enthalpy
H	Total enthalpy or static enthalpy
k	Kinetic energy
N_p	Total number of phases
p	Thermodynamic pressure
P	Pressure/ Shear Production
P_{ref}	Reference pressure
r	Radius
R	Universal Gas Constant
S	Source term
t	Time
T	Temperature
U	Velocity
U_{om}	Jet velocity
W	Molecular Weight
x	Distance from the exit
θ	Cylindrical coordinate
θ_1, θ_2	Calculated angles in the taper inlet part
φ	Abrasive inlet angle
Φ	Physical property
ρ	Density
σ	Turbulent Prandtl Number
ε	Dissipation of turbulent of kinetic energy
λ	Thermal conductivity
μ	Molecular viscosity
μ_T	Turbulent viscosity
Γ	Eddy diffusivity
Subscripts	
a	Air
p	Abrasive particles
w	water
T	Turbulent
α, β, γ	Phases
Superscripts	
d	Drag
h	Heat transfer
T	Tensor

9. TABLES

Table 1. Simulation Conditions

Nozzle dimension		
Orifice diameter		0.33 mm
Mixing chamber diameter		6 mm
Mixing chamber length, L_c		12 mm
Taper inlet angle		51.75^0
Focus tube diameter, d_f		1.27 mm
Focus tube length, L_f		75 mm
Abrasive inlet diameter		3 mm
Water density		1000 kg/m^3
Air density		1.29 kg/m^3
Abrasive density		4100 kg/m^3
Abrasive diameter		180 μm
Inlet conditions		
Water pressure		276 MPa
Air pressure		0.76 MPa
Abrasive mass flow rate		0.45 kg /min
Air flow rate		2.67 lit/min
Abrasive Inlet Angle, ϕ		$0^0, 15^0, 30^0, 45^0, 60^0, 75^0, 90^0$

Table 2

Distance from the taper part (mm)	Angle range, θ_1 (air and abrasive will hit the inclined surface)	Angle range θ_2 (air and abrasive will pass through the focus tube)
2.25	$20.56^0 - 55.30^0$	$55.30^0 - 65.75^0$
5.25	$41.20^0 - 66.22^0$	$66.22^0 - 74.00^0$
6.75	$48.40^0 - 69.55^0$	$69.55^0 - 76.37^0$

10. FIGURES

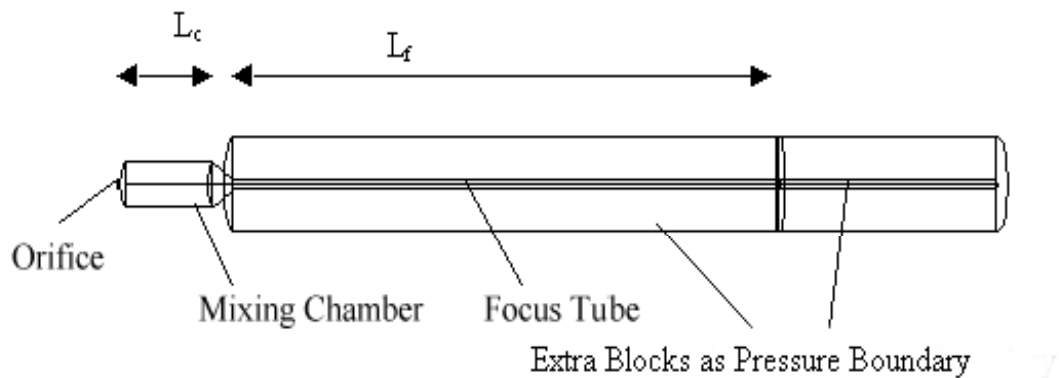


Figure 1 Schematic of AWJ Nozzle

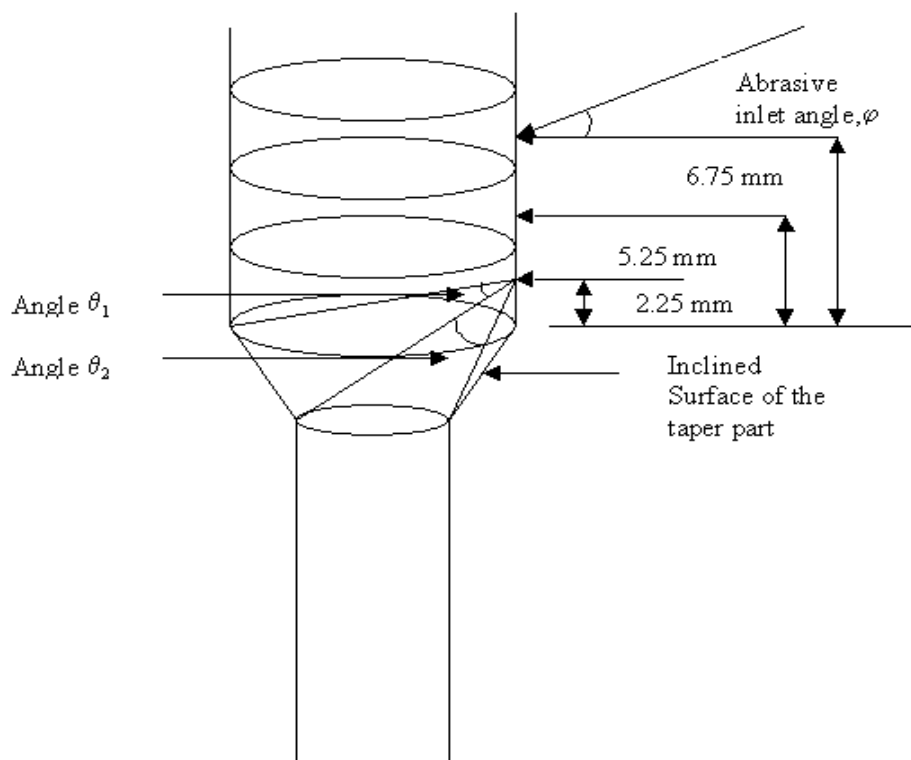


Fig. 2 Grid in the mixing Chamber and Grid space

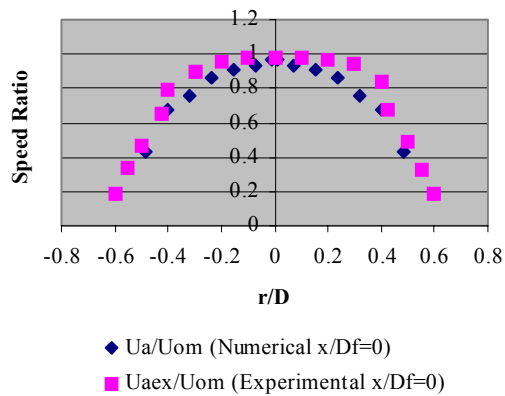


Figure 3 Speed ratio of air

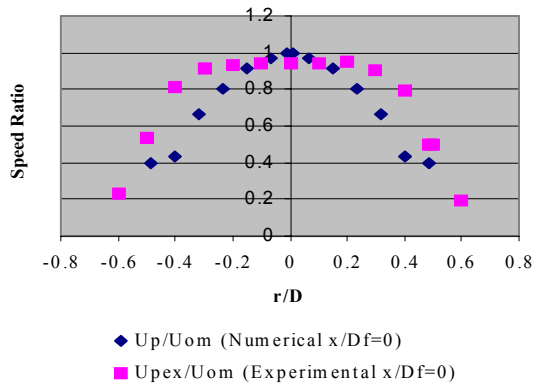


Figure 4 Speed ratio of solid particle

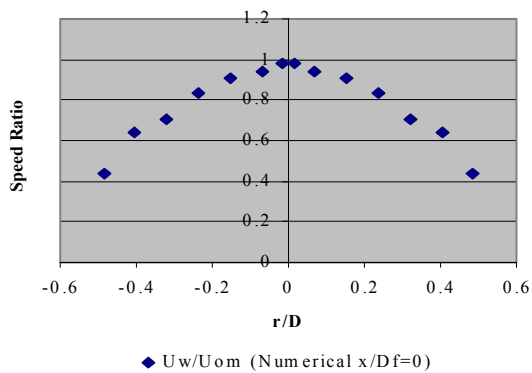


Figure 5 Speed ratio of water

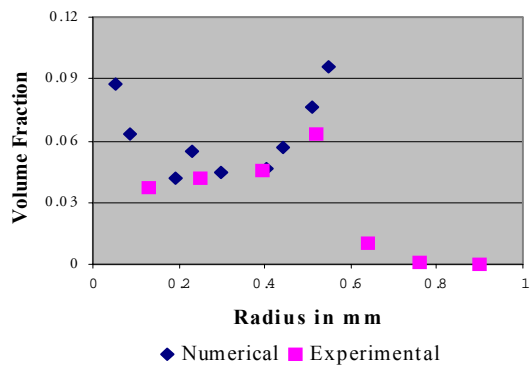


Figure 6 Volume fraction of water

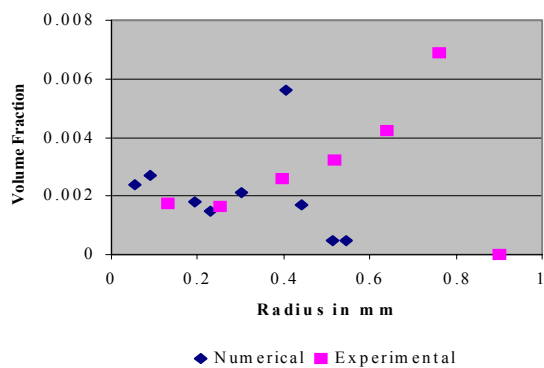


Figure 7 Volume fraction of abrasives

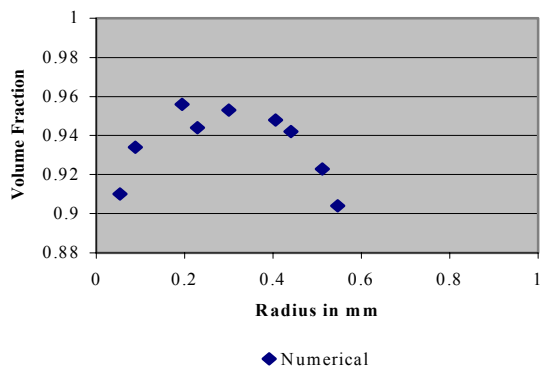


Figure 8 Volume Fraction of air

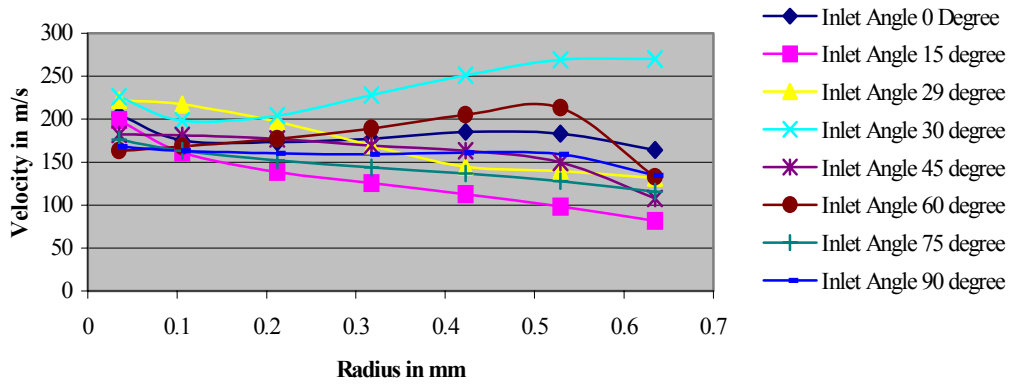


Figure 9 Water velocity along the radius at the exit of the focus tube

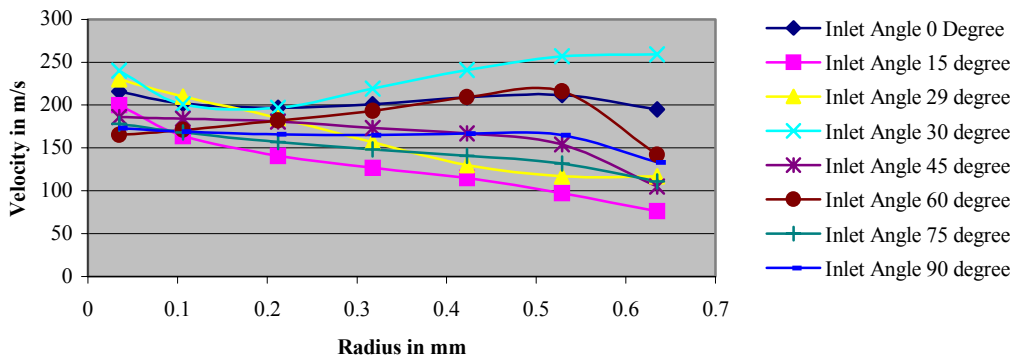


Figure 10 Air velocity along the radius at the exit of the focus tube

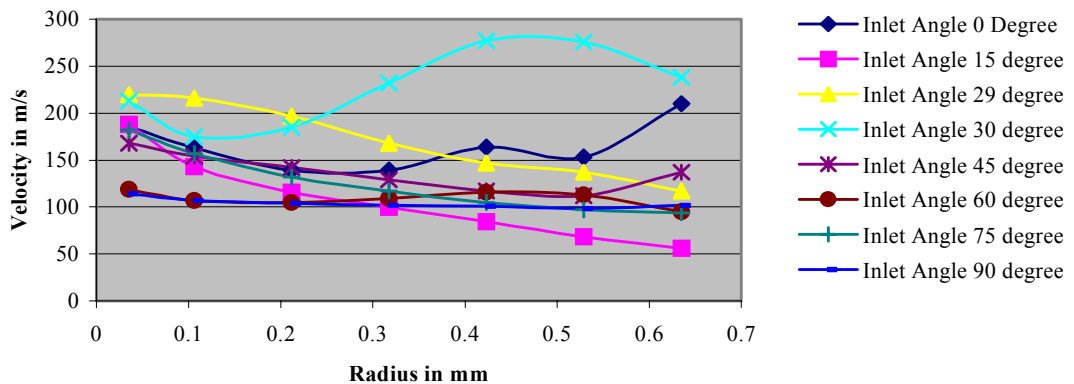


Figure 11 Solid velocity along the radius at the exit of the focus tube

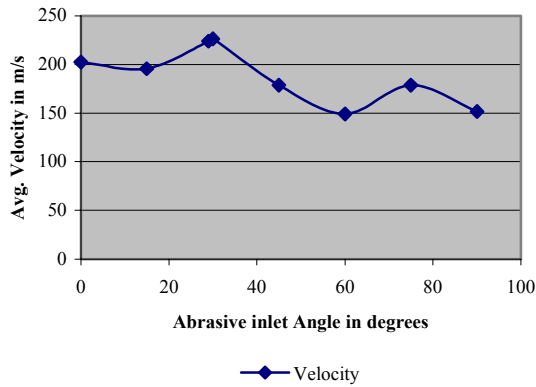


Figure 12 Average speed of the jet for different abrasive inlet angle

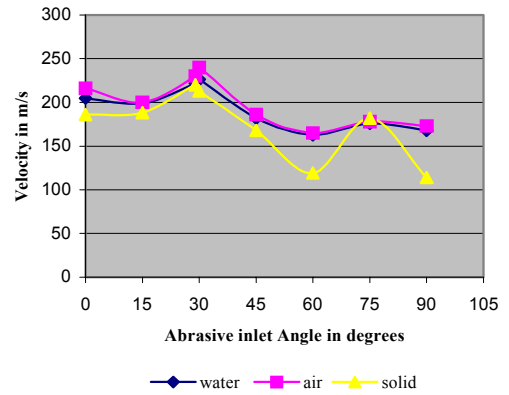


Figure 13 Velocity of the phases near the central line of the jet for different abrasive inlet angle

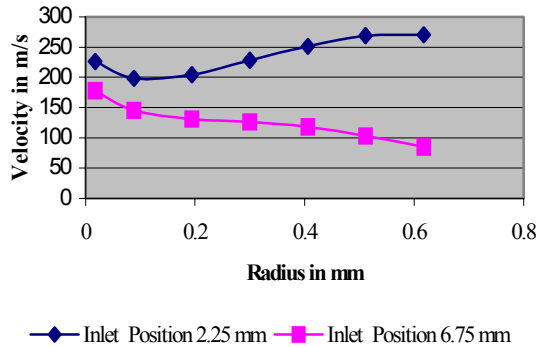


Figure 14 Water velocity for 30 degree abrasive inlet angle for two different positions

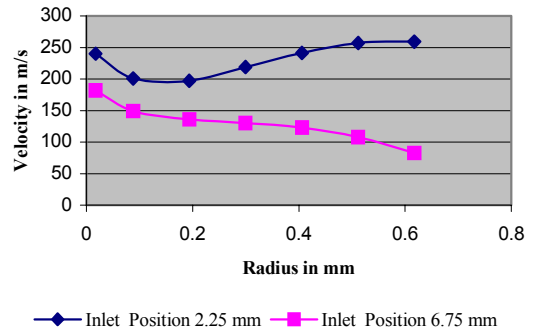


Figure 15 Air velocity for 30 degree abrasive inlet angle for two different positions

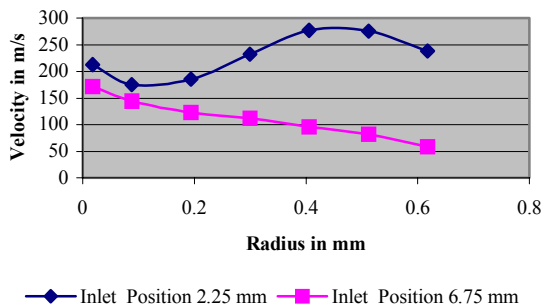


Figure 16 Solid velocity for 30-degree abrasive inlet angle for two different positions

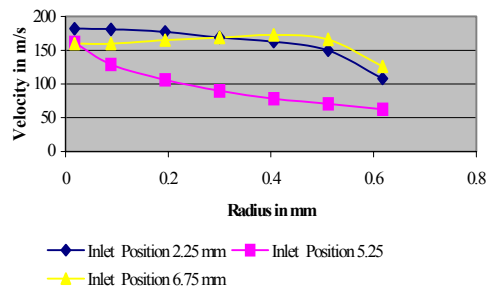


Figure 17 Water velocity for 45-degree abrasive inlet angle for three different positions

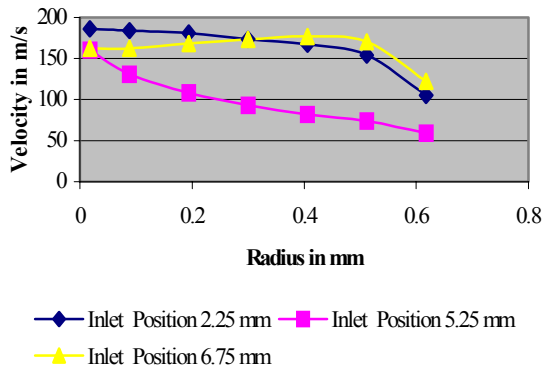


Figure 18 Air velocity for 45-degree abrasive inlet angle for three different positions

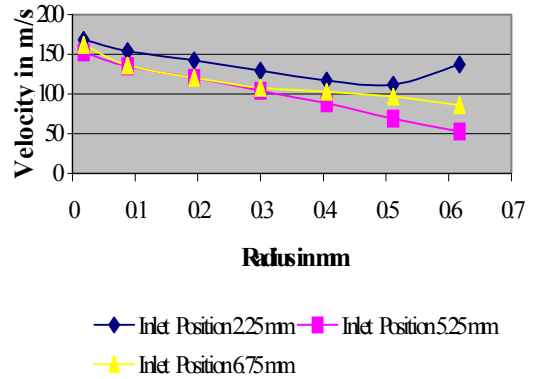


Figure 19 Solid velocity for 45 degree abrasive inlet angle for three different positions

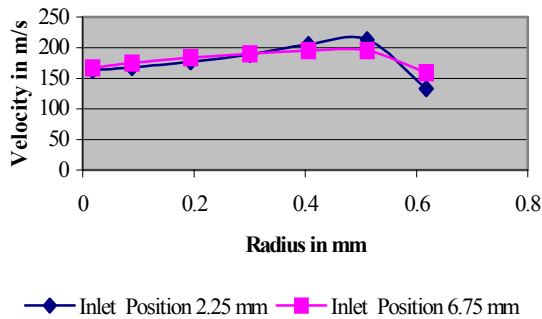


Figure 20 Water velocity for 60-degree abrasive Inlet angle for two different positions

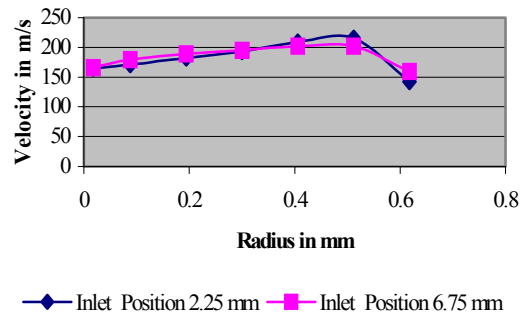


Figure 21 Air velocity for 60 degree abrasive inlet angle for two different positions

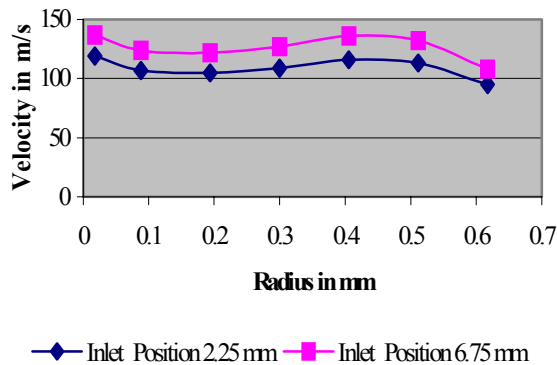


Figure 22 Solid velocity for 60-degree abrasive inlet angle for two different positions

STUDY ON THE FLOW CHARACTERISTICS OF FREE WATER JET BASED ON HYPERBOLA FLOW LINE STRUCTURE

Jiang Shan
Beijing Special Engineering Design and Technology Institute
Beijing, PRC

Fang Mei
University of Science and Technology Beijing
Beijing, PRC

ABSTRACT

In the present report, the author investigated theoretically and experimentally the flow characteristics of free water jets based on hyperbola flow line structure, the conservation of momentum flux and the conservation of mass flux of free water jet. It has been developed the equation of hyperbola flow line, dynamic pressure distribution, velocity distribution and density distribution of free water jet. The theoretical equation are simple and practical, which could express the characteristics of the free water jet in any surrounding liquid medium, water and air, i.e., in all regions, initial region, main region and final region. The good agreement between the experimental and theoretical values of dynamic pressure and velocity in a free water jet is obtained.

1. INTRODUCTION

Till now, the behavior of a submerged or unsubmerged free water jet was investigated analytically and experimentally by many researchers, but the theoretical result was not whole and practical. Unfortunately, the theoretical result [1,2] just express the characteristics of submerged jet in the final region. There are very few published papers to attempt to establish the characteristics of the unsubmerged free water jet in air basis on the theoretical analysis. Yanaida [3, 4, 5] based on that the width of the jet spread is proportional to square root of distance, had carried out a lot of theoretical research, obtained the half experimental and half theoretical equation about the characteristics of unsubmerged jet in the main region and final region, but which was not simple and united.

In the present report, the analytical relations of momentum theory are proposed on that the flow line pattern in free water jet is proved to be hyperbola. It has been developed the equation of hyperbola flow line, dynamic pressure distribution and velocity distribution of free water jet. The theoretical equation are simple and practical, which could express the characteristics of the free water jet in any surrounding liquid medium, water and air, i.e., in all regions, initial region, main region and final region. The good agreement between the experimental and theoretical values of axial dynamic pressure and axial velocity in a free water jet is obtained.

2. BASIC CHARACTERITIC OF FREE WATER JET

2.1 Hyperbola Flow Line Structure of Free Water Jet

In essence, the free water jet is a flow beam surrounded by nozzle, its structure is shown in Figure1. The free water jet consists of: initial region, main region and final region. In the initial region, which is near the nozzle, there is a jet core in submerged or unsubmerged water jet [1]. In jet core, the jet particle keep the velocity at the nozzle exit, and each flow line almost parallel the jet centerline. In the main region, the flow line deviates gradually from the jet centerline because the jet particle turbulence spreading and exchanging momentum with surrounding liquid. In the final region, the jet particle spread along straight line which all join at the jet source [1]. Consequently it is reasonable that the pattern of each flow line in free water jet is hyperbola. If the jet source is treated as origin O, the jet centerline is treated as x-axis, the perpendicular line of jet centerline is treated as radial axis r-axis, the general equation of hyperbola flow line is

$$\left(\frac{\bar{r}}{a}\right)^2 = 1 + \left(\frac{\bar{x}}{b}\right)^2 \quad (1)$$

The first derivative of the Eq. (1) with respect to a is

$$\frac{\bar{r}d\bar{r}}{ada} = 1 + \left(\frac{1}{b^2} - \frac{ab'}{b^3}\right)\bar{x}^2 \quad (2)$$

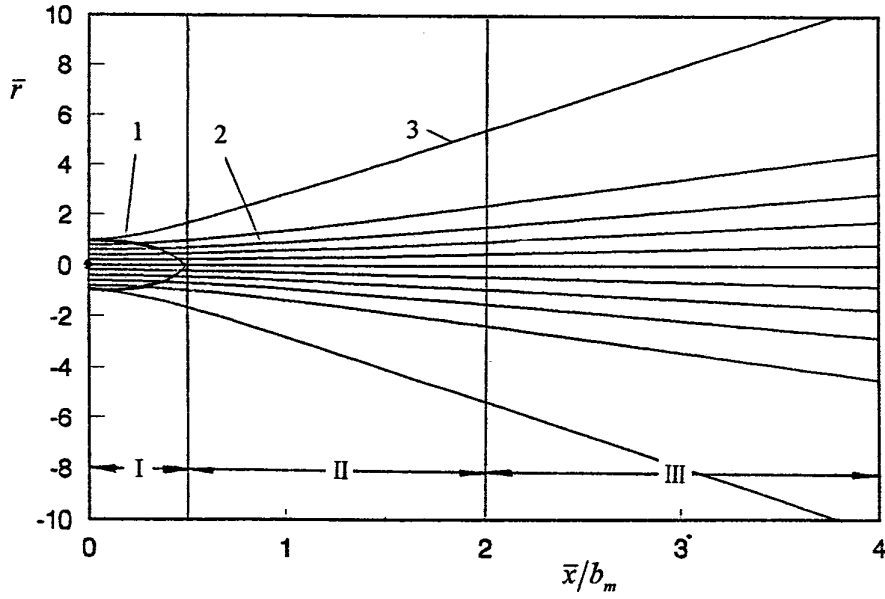


Figure 1. Structure of hyperbola flow line in free water
 I-initial region; II-main region; III-final region.;
 0-jet source; 1-jet core boundary; 2-hyperbola flow line; 3-jet boundary

2.2 Conservation of the Momentum Flux of Free Water Jet

Because there is not pressure gradient in free water jet field, and there is not almost axial effection among jet flow beams, we can assume that the axial momentum flux of any flow beam in free water jet remains essentially constant at any distance downstream of the nozzle exit. Then, the momentum flux of the flow beam between a and $a + da$ at any distance downstream of the nozzle exit is equal to the momentum flux at nozzle exit, which can be rewritten as follow

$$\rho u^2 2\pi \bar{r} d\bar{r} = \rho_0 u_0^2 2\pi a da \quad (3)$$

From last equation, we have

$$\frac{p}{p_0} = \frac{a da}{\bar{r} d\bar{r}} \quad (4)$$

From the conservation of momentum flux of jet, the momentum flux of jet at any distance downstream of the nozzle exit is equal to the momentum flux at nozzle exit. Integrating the Eq.(3), we have

$$\int_0^\infty p 2\bar{r} d\bar{r} = p_0 \quad (5)$$

2.3 Conservation of the Mass Flux of Free Water Jet

Jet particle moves along flow line, it has small radial motion, but it makes interval among flow line and cause surrounding flow attracted in interval. The collision between jet particle and surrounding flow particle is complete plastic collision, so the surrounding flow velocity is equal to the jet velocity in flow beam of free water jet.

From the conservation of mass flux, the mass flux of the flow beam between a and $a + da$ at any distance downstream of the nozzle exit is equal to the mass flux of jet at nozzle exit and the mass flux of surrounding flow fulling interval, which can be rewritten as follow

$$\bar{r}d\bar{r}\rho u = ada\rho_0u_0 + \left(\bar{r}d\bar{r} - \frac{ada\rho_0u_0}{\rho_0u} \right) \rho_s u \quad (6)$$

2.4 Velocity Distribution in Final Region of Free Water Jet

The velocity distribution equation in final region of submerged free water jet has been induced by many researchers [1, 2] with Prandtl free turbulent flow theory, which is

$$\frac{u}{u_m} = \frac{1}{\left[1 + A \left(\frac{\bar{r}}{\bar{x}} \right)^2 \right]^2} \quad (7)$$

In the final region of unsubmerged free water jet, the droplets of water jet are very small and uniformly distributed [4], the density of jet is very small and gradually tend to surrounding flow density, and

$$\rho = \rho_m$$

the flow characteristic in the final region of unsubmerged free water jet is similar to the flow characteristic in the final region of submerged free water jet, so the velocity distribution can be also expressed by Eq. (7).

Therefore, the distribution of dynamic pressure in final region of free water jet is:

$$\frac{p}{p_m} = \frac{\frac{1}{2}\rho u^2}{\frac{1}{2}\rho_m u_m^2} = \frac{1}{\left[1 + A \left(\frac{\bar{r}}{\bar{x}} \right)^2 \right]^4} \quad (8)$$

3. ANALYSIS ON EQUATION OF HYPERBLA FLOW LINE IN FREE WATER JET

Substituting Eq. (2) into Eq. (4), we have

$$\frac{p}{p_0} = \frac{1}{1 + \left(\frac{1}{b^2} - \frac{ab'}{b^3} \right) \bar{x}^2} \quad (9)$$

At the final region of free water jet, which is $\bar{x} > 2b_m$, Eq. (9) can be simplified as follow

$$\frac{p}{p_0} \approx \frac{1}{\left(\frac{1}{b^2} - \frac{ab'}{b^3} \right) \bar{x}^2} \quad (10)$$

At the centerline of free water jet, $a=0$, $b=b_m$ Substituting this two equation into Eq. (10), we obtain the centerline dynamic pressure in final region as follow

$$\frac{p_m}{p_0} = \frac{1}{\left(\frac{\bar{x}}{b_m} \right)^2} \quad (11)$$

From Eq. (8) and Eq. (11), we obtain as follow:

$$\frac{p}{p_0} = \frac{1}{\left[1 + A \left(\frac{\bar{r}}{\bar{x}} \right)^2 \right]^4 \left(\frac{\bar{x}}{b_m} \right)^2} \quad (12)$$

Substituting Eq. (12) into Eq. (5), we obtain as follow:

$$\int_0^\infty \frac{d\bar{r}^2}{\left[1 + A \left(\frac{\bar{r}}{\bar{x}} \right)^2 \right]^4 \left(\frac{\bar{x}}{b_m} \right)^2} = 1$$

Solving this equation, we obtain

$$A = \frac{1}{3} b_m^2 \quad (13)$$

Besides, from Eq. (1), we know that the hyperbola flow line has the characteristics as follow when $\bar{x} > 2b_m$.

$$\left(\frac{\bar{r}}{\bar{x}}\right)^2 = \left(\frac{a}{b}\right)^2$$

Substituting last equation and Eq. (13) into Eq. (12), we obtain the dynamic pressure distribution in final region of free water jet

$$\frac{p}{p_0} = \frac{1}{\left[1 + \frac{1}{3}\left(\frac{b_m a}{b}\right)^2\right]^4 \left(\frac{\bar{x}}{b_m}\right)^2} \quad (14)$$

Substituting Eq. (14) into Eq. (10), we obtain as follow:

$$\frac{1}{b^2} - \frac{ab'}{b^3} = \left[1 + \frac{1}{3}\left(\frac{b_m a}{b}\right)^2\right]^4 \frac{1}{b_m^2}$$

Solving last equation, we obtain function b of a :

$$\left(\frac{b}{b_m}\right)^2 = \frac{1}{3} \left[(1-a^2)^{\frac{1}{3}} + (1-a^2)^{\frac{2}{3}} + (1-a^2) \right] \quad (15)$$

Then, substituting Eq. (15) into Eq. (1), we obtain the equation of hyperbola flow line of free water jet:

$$\left(\frac{\bar{r}}{a}\right)^2 = 1 + \frac{3}{(1-a^2)^{\frac{1}{3}} + (1-a^2)^{\frac{2}{3}} + (1-a^2)} \left(\frac{\bar{x}}{b_m}\right)^2 \quad (16)$$

From last equation, we can see that the flow line pattern is decided by b_m imaginary half axis of hyperbola flow-line in centerline. The pattern of hyperbola flow line in free water is showed in

Figure 1. From Figure 1, we see that each flow line in the initial region almost is straight line paralleling the jet centerline, which form the jet core. From Eq.1, we know that $\bar{r} \approx a$ when $\bar{x} = \frac{1}{2}b$, and we consider the length of jet core $\bar{x}_c = \frac{1}{2}b_m$. So from Eq.15, we obtain the boundary equation of jet core as follow:

$$\left(\frac{\bar{x}}{\bar{x}_c}\right)^2 = \frac{1}{3} \left[(1-a^2)^{1/3} + (1-a^2)^{2/3} + (1-a^2) \right]$$

4. ANALYSIS ON THE DYNAMIC PRESSURE DISTRIBUTION

Substituting Eq. (15) into Eq. (9), we obtain the equation of dynamic pressure distribution of free water jet:

$$\frac{p}{p_0} = \frac{1}{1 + \left(\frac{1}{1-a^2}\right)^{4/3} \left(\frac{\bar{x}}{b_m}\right)^2} \quad (17)$$

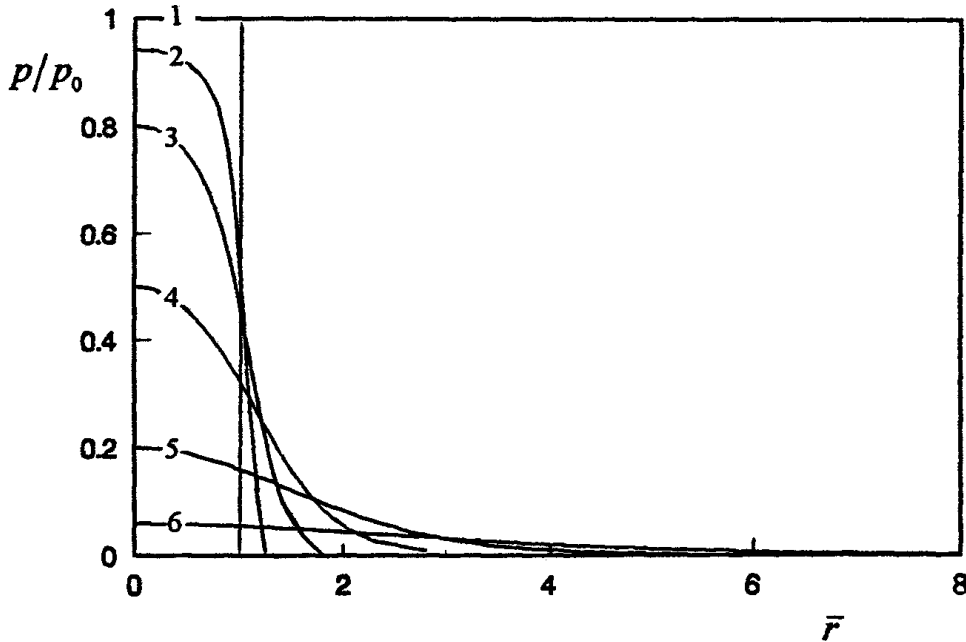


Figure 2. Dynamic pressure distribution of free water jet
1- $\bar{x}/b_m = 0$; 2- $\bar{x}/b_m = 0.25$; 3- $\bar{x}/b_m = 0.5$; 4- $\bar{x}/b_m = 1$; 5- $\bar{x}/b_m = 2$; 6- $\bar{x}/b_m = 4$

We can see that the dynamic pressure at point (\bar{x}, \bar{r}) in free water jet depends on \bar{x} and a . Therefore, we can obtain dynamic pressure at any point from Eq. (16) and Eq. (17). Figure 2 is dynamic pressure distribution diagram drawn according to Eq. (16) and Eq. (17).

4.1 Dynamic pressure distribution in centerline of free water jet

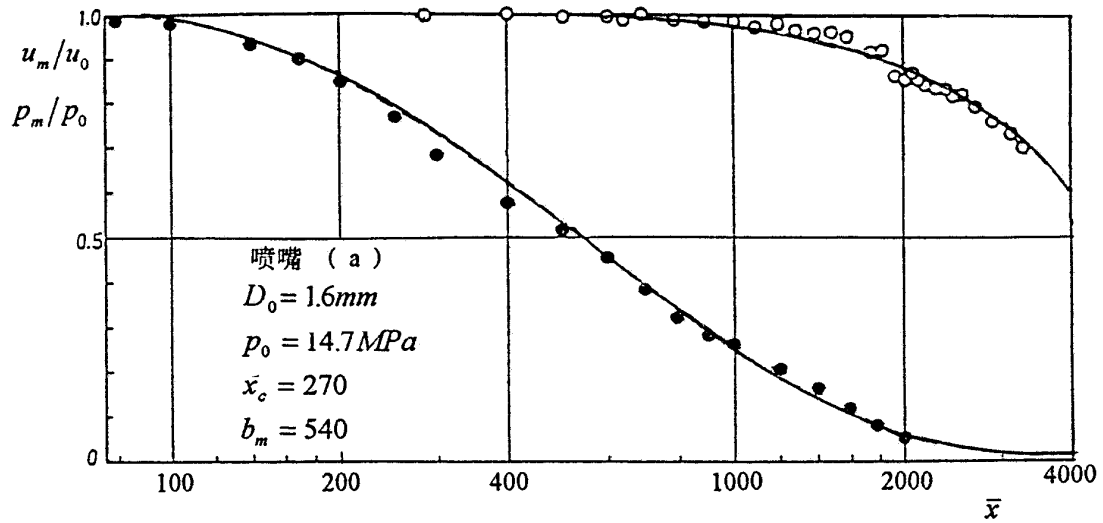


Figure 3. Comparison of theoretical and experimental values on the dynamic pressure and velocity in centerline of free water jet

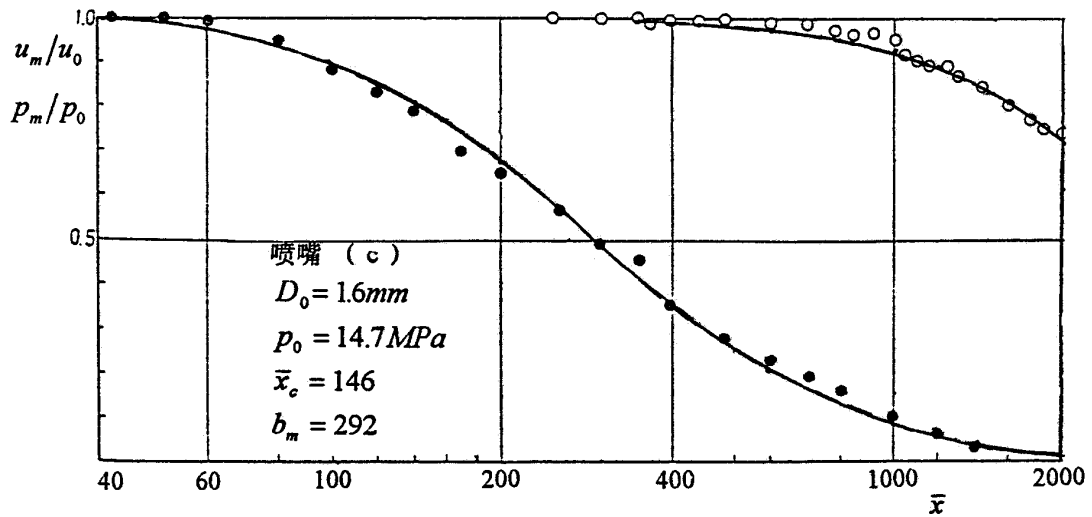


Figure 4. Comparison of theoretical and experimental values on the dynamic pressure and velocity in centerline of free water jet

Substituting $a = 0$ into Eq. 17, we have the dynamic pressure distribution in centerline of free water jet:

$$\frac{p_m}{p_0} = \frac{1}{1 + \left(\frac{\bar{x}}{b_m}\right)^2} \quad (18)$$

From Eq. 18, we know that the dynamic pressure distribution depends on b_m .

Figures 3 and 4 depict the theoretical curve (under curve from Eq. 18) of the variation of the centerline dynamic pressure along the jet, and they show experimental points from papers by Yanaida [5]. It is apparent from these figures that the experimental results are in good agreement with the theoretical values for the all regions of free water jet.

4.2 Dynamic pressure distribution in section of free water jet

From Eq. (17) and Eq. (18), we have dynamic pressure distribution in section of free water jet, which is rewritten as follow:

$$\frac{p}{p_m} = \frac{p}{p_0} * \frac{p_0}{p_m} = \frac{1 + \frac{\bar{x}^2}{b_m^2}}{1 + \left(\frac{1}{1-a^2}\right)^{4/3} \left(\frac{\bar{x}}{b_m}\right)^2} \quad (19)$$

In section $\bar{x} = 0$ of the initial region, $p = p_m$, it is even distribution:

In section $\bar{x} = b_m$ of the main region, the dynamic pressure distribution is

$$\frac{p}{p_m} = \frac{2}{1 + \left(\frac{1}{1-a^2}\right)^{4/3}}$$

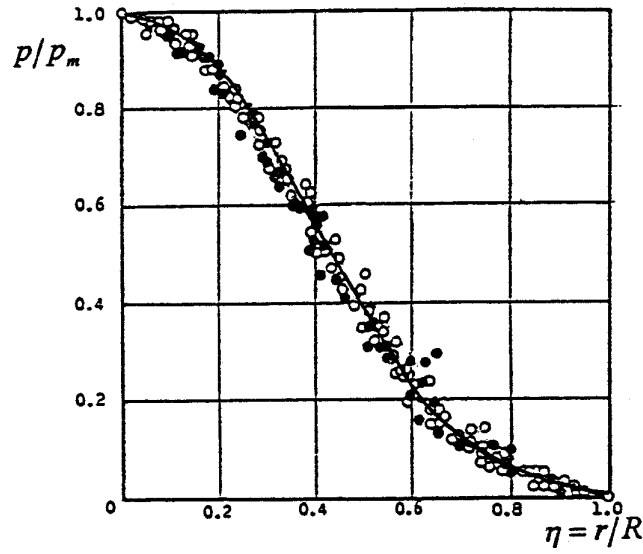


Figure 5. Comparison of theoretical and experimental values on the dynamic pressure in Section $\bar{x} = b_m$ of free water jet.

Figure 5 depicts the theoretical curve (from Eq.19) of the dynamic pressure in section $\bar{x} = b_m$ of free water jet. And it shows experimental points from papers by Yanaida [3]. Good agreement between experimental and theoretical values of the dynamic pressure in section of free water jet is achieved too. In the section $\bar{x} > 2b_m$ of final region, the dynamic pressure distribution is

$$\frac{p}{p_m} = (1 - a^2)^{4/3}$$

Last equation indicates that the dynamic pressure distribution in section of final region only depends on real half axis a of hyperbola flow line, and is similar to each other.

5. ANALYSIS ON VELOCITY DISTRIBUTION AND DENSITY DISTRIBUTION OF FREE WATER JET

Solving equations set of the conservation Eq. 3 of the momentum flux and the conservation Eq. 6 of the mass flux (equation of continuity), we obtain the velocity distribution and density distribution as follow:

$$\bar{u} = \frac{-(1 - \bar{\rho}_s) + \sqrt{(1 - \bar{\rho}_s)^2 + 4 \frac{\bar{r} d\bar{r}}{a da} \bar{\rho}_s}}{2 \frac{\bar{r} d\bar{r}}{a da} \bar{\rho}_s} \quad (20)$$

$$\bar{\rho} = \frac{2(1 - \bar{\rho}_s)\bar{\rho}_s}{-(1 - \bar{\rho}_s) + \sqrt{(1 - \bar{\rho}_s)^2 + 4\frac{\bar{r}d\bar{r}}{ada}\bar{\rho}_s}} + \bar{\rho}_s \quad (21)$$

From Eq. (16) , Eq. (20) and Eq. (21), we can extract the velocity and density in any point of free water jet.

In the centerline of jet, from Eq. (16) or Eq. (2), we have

$$\frac{\bar{r}d\bar{r}}{ada} = 1 + \left(\frac{\bar{x}}{b_m}\right)^2$$

Substituting last equation into Eq. (20), we obtain the velocity in centerline of jet as follow:

$$\bar{u}_m = \frac{-(1 - \bar{\rho}_s) + \sqrt{(1 - \bar{\rho}_s)^2 + 4\left(1 + \left(\frac{\bar{x}}{b_m}\right)^2\right)\bar{\rho}_s}}{2\left(1 + \left(\frac{\bar{x}}{b_m}\right)^2\right)\bar{\rho}_s} \quad (22)$$

5.1 Velocity Distribution in Centerline of Submerged Free Water Jet

In water, $\bar{\rho}_s = 1$ substituting this equation into Eq. (22), we obtain the velocity in centerline of submerged free water jet as follow:

$$\bar{u}_m = \frac{1}{\sqrt{1 + \left(\frac{\bar{x}}{b_m}\right)^2}} \quad (23)$$

Last equation can indicate the centerline velocity in all regions of submerged free water jet. From last equations, we can obtain that the centerline velocity in final region of submerged jet is inversely proportional to range, which is identical with the experimental and theoretical results by many other researchers.

5.2 Velocity Distribution in Centerline of Unsubmerged Free Water Jet

The density of dry air is $\rho_s = 1.2kg / m^3$. there is not only air but also steam attracted into the water jet, the density of the all gas attracted into jet is several times bigger than density of dry air, but it is still very much smaller than density of water, $\bar{\rho}_s \ll 1$. Expanding the radical of Eq.

(22) into Taylor series, and simplifying it, we obtain the velocity distribution in centerline of unsubmerged free water jet

$$\bar{u}_m = 1 - \bar{\rho}_s \left(1 + \left(\frac{\bar{x}}{b_m} \right)^2 \right) \quad (24)$$

Figure 3 and Figure 4 depict the theoretical curve (upper curve from Eq. 24) of the variation of the centerline velocity along the unsubmerged water jet, and they show experimental points from papers by Yanaida [5]. In Figure 3, $\bar{\rho}_s = 7 \times 10^{-3}$. In Figure 4, $\bar{\rho}_s = 6 \times 10^{-3}$. It is apparent from these figures that the experimental results are good agreement with the theoretical values for the all regions of free water jet. Figure 3 and Figure 4 show that initial region and main region with the constant jet centerline velocity.

6. CONCLUSIONS

The following conclusion can be drawn from this paper.

1) According to the flow line pattern and the dynamic pressure, the free water jet is divided into 3 regions: initial region ($0 \leq \bar{x} \leq \frac{1}{2}b_m$) with the constant centerline dynamic pressure, main region ($\frac{1}{2}b_m < \bar{x} \leq 2b_m$) with the constant centerline velocity, and final region ($\bar{x} > 2b_m$).

2) Any flow line in free water jet is hyperbola, the equation of flow line in free water jet is

$$\left(\frac{\bar{r}}{a} \right)^2 = 1 + \frac{3}{(1-a^2)^{1/3} + (1-a^2)^{2/3} + (1-a^2)} \left(\frac{\bar{x}}{b_m} \right)^2$$

3) The shape of jet core is similar a half ellipsoid, its length is $\bar{x}_c = \frac{1}{2}b_m$.

4) Equation of dynamic pressure distribution in free water jet is

$$\frac{p}{p_0} = \frac{1}{1 + \left(\frac{1}{1-a^2} \right)^{4/3} \left(\frac{\bar{x}}{b_m} \right)^2}$$

5) Equation of centerline dynamic pressure in free water jet is

$$\frac{p_m}{p_0} = \frac{1}{1 + \left(\frac{\bar{x}}{b_m}\right)^2}$$

This equation has good agreement with the experimental values in initial region, main region and final region, it is simple and practical.

6) Dynamic pressure distribution in section of free water jet changes from even distribution to similar uneven distribution.

7) Equation of velocity distribution in free water jet is

$$\bar{u} = \frac{-(1 - \bar{\rho}_s) + \sqrt{(1 - \bar{\rho}_s)^2 + 4 \frac{\bar{r} d\bar{r}}{ada} \bar{\rho}_s}}{2 \frac{\bar{r} d\bar{r}}{ada} \bar{\rho}_s}$$

8) Equation of centerline velocity in submerged free water jet is

$$\bar{u}_m = \frac{1}{\sqrt{1 + \left(\frac{\bar{x}}{b_m}\right)^2}}$$

9) Equation of centerline velocity in unsubmerged free water jet is

$$\bar{u}_m = 1 - \bar{\rho}_s \left(1 + \left(\frac{\bar{x}}{b_m}\right)^2\right)$$

7. REFERENCES

1. Sun, J.J., "Cut Technology of Water Jet, " *Press in China University of Science and Technology*, pp. 8-24, 1992.
2. Huang, D.S., "The Speed Distribution of Submerged Free Water Jet," *Journal of High Pressure Water Jet*, Vol.1, 1987.
3. Yanaida, K., "Flow Characteristics of Water Jets," *2nd Intern. Symp. Jet Cutting Tech*, pp. A2-19-32, 1974.

4. Yanaida, K., Flow Characteristics of Water Jets in Air, *4th Intern. Symp. Jet Cutting Tech*, pp. A3-39-54, 1978.
5. Yanaida, K., Flow Characteristics of Water Jets in Air, *5th Intern. Symp. Jet Cutting Tech*, pp. A3-33-44, 1980.
6. Jiang S., 1996, The Study of Machinism and Technology of Comminution Particles by High Pressure Water Jet, *Report of Post Doctor Research in University of Science and Technology of Beijing*, pp. 14-29, 1996.

8. NOMENCLATURE

A — a coefficient related to the quality of free water jet

a — real half axis of hyperbola flow line in free water jet

b — imaginary half axis of hyperbola flow line in free water jet, b is function of a

b_m — imaginary half axis of hyperbola flow line in centerline

$p = \frac{1}{2} \rho u^2$ — the dynamic pressure of free water jet at point (x, r)

\bar{x}_c — dimensionless length of jet core, $\bar{x}_c = \frac{1}{2} b_m$

$u, \bar{u} = \frac{u}{u_0}$ — velocity and dimensionless velocity of free water jet at point (x, r)

u_0 — velocity of free water jet at nozzle exit

u_m — centerline velocity at point $(x, 0)$

$\rho, \bar{\rho} = \frac{\rho}{\rho_0}$ — density and dimensionless density of free water jet at point (x, r)

ρ_0 — density of free water jet at nozzle exit

ρ_m — density of free water jet at centerline of jet

$\rho_s, \bar{\rho}_s = \frac{\rho_s}{\rho_0}$ — density and dimensionless density of surrounding flow

NUMERICAL STUDY OF THE TURBULENT FLOW INSIDE A PURE WATERJET

K. Babets, E. Geskin
New Jersey Institute of Technology
Newark, NJ

ABSTRACT

The numerical simulation of the water flow in a nozzle was studied using numerical techniques. The standard system of governing equations describing the turbulent flow were modified to be applied to the description of the formation of the waterjet in a nozzle. The standard $k-\varepsilon$ turbulence model was used. The numerical solutions were obtained in terms of velocity fields, pressure, the turbulent kinematic energy k and dissipation ε . The validity of the computational scheme and the obtained results could be checked, by comparing the outlet velocity profile and its magnitude with the available experimental results of other researches. The abrasive slurry was approximated as a three-phase flow, where the primary phase is the jet, the second phase is the entrained air, and the third phase is the abrasive particles mixed in the flow. The computational domain in this study was limited to the cutting head of a conventional waterjet nozzle. It was shown that the volumetric fraction of air in the nozzle can be estimated to be greater than or equal to 85%. This result was in a total agreement with previously reported experimental results.

1. INTRODUCTION

The efficient application of waterjets to industrial surface decontamination requires a thorough understanding of the influence of different parameters involved in the process. The independent parameters involved in abrasive waterjet surface decontamination can be divided in two several groups (Hashish, 1991). The first group of parameters is process related and it includes nozzle traverse rate, standoff distance, number of passes, degree of overlap and the desired degree of surface cleanliness. The second group of parameters is jet-related and can be subdivided into hydraulic, abrasive and mixing (internal) parameters. The hydraulic parameters include water pressure, water flow rate, abrasive parameters include abrasive type, abrasive particle size and flow rate. A special attention needs to be paid to the internal parameters of the waterjet nozzle. These parameters consist of the internal diameters of a waterjet nozzle such as mixing tube diameter, mixing tube length and air flow rate through the abrasive inlet port. The reason a special attention should be paid to this group of parameters is because it is the least studied group and is the most difficult to control and optimize.

The importance of studying the flow characteristics inside a waterjet flow have resulted in quite a few experimental and numerical studies of this phenomena. A fair number of experimental studies was concerned with velocity measurements of the waterjet. The techniques most often used for non invasive measurements were limited to high-speed digital photography (Sawamura et al, 1999), Laser Transit Anemometry (LTA) (Chen and Geskin, 1990), Laser Doppler Velocimetry (LDV) (Neusen et al, 1992), etc. Neusen et al (1992) have shown that with the cutting head in place but with abrasive flow rate 0.0 kg/min, the exit mean velocity reduces substantially as compared to pure waterjet velocities after primary nozzle, Figure 1. It was suggested that the reason for the velocity drop is the momentum exchange between the liquid and gas phases in the mixing process. Next they show that after abrasive particles were mixed in the stream the mean exit velocity remained relatively constant, at approximately 260 m/sec, even though the abrasive mass flow rate was varied by 150% , and pressure was varied by 67%, Figure 2.

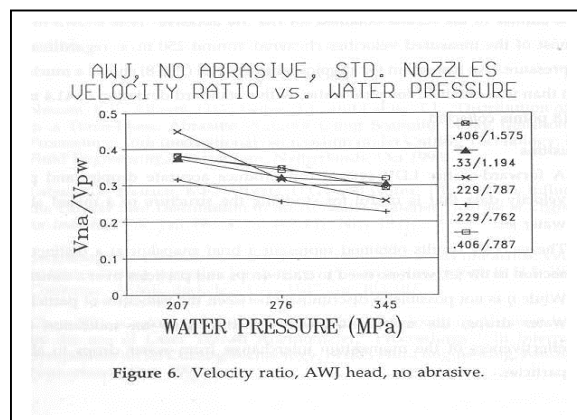


Figure 1. Velocity Ratio for AWJ with no Abrasive (Neusen et al, 1992)

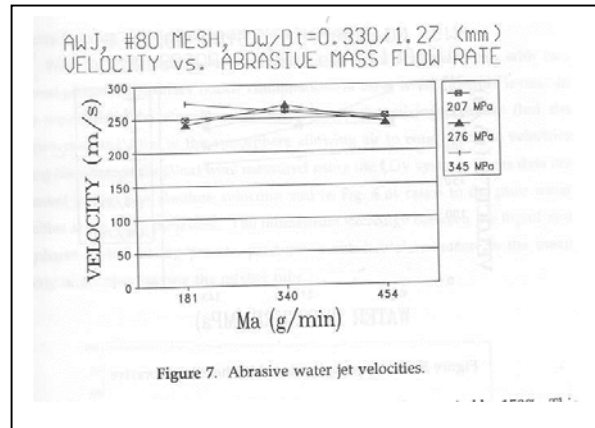


Figure 2. Abrasive Waterjet Velocities (Neusen et al, 1992)

Sawamura *et al* (1999) has shown that, on the contrary, approximately 9% velocity loss is found when the media flow rate is 0.0 kg/min. The velocity loss increases with the increase in the abrasive flow rate and it could reach up to 60% of theoretical value when the flow rate reaches 0.2 kg/min (Figure 3).

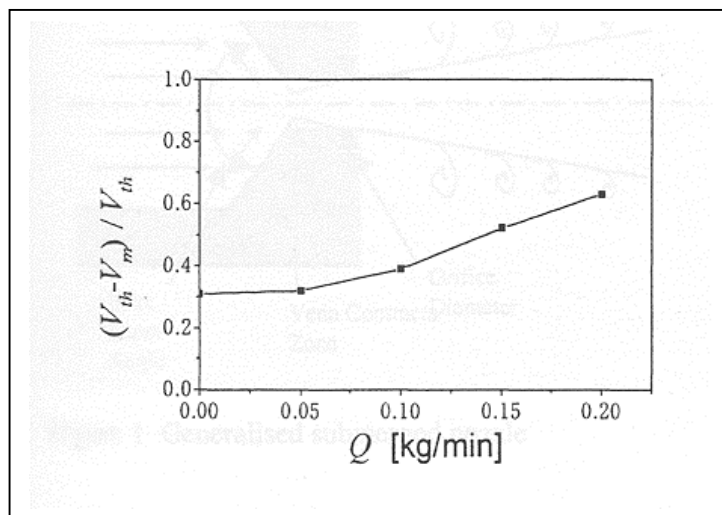


Figure 3. The Relation Between the Velocity Loss and the Abrasive Flow Rate (Sawamura et al, 1999)

Our own experimental studies of the velocities of the abrasive waterjets have shown, that the pure waterjet velocity closely follows the velocity predicted by the Bernoulli equation, as was corroborated by Neusen et al, (1992), (Figure 4).

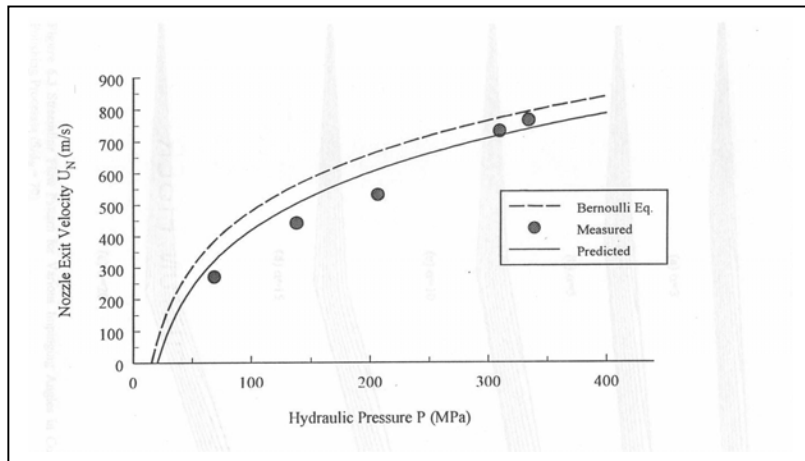


Figure 4. Calculated and Measures Nozzle Velocities as Function of Hydraulic Pressure

The numerical simulation of the flow inside a nozzle is an economical and efficient way to predict such flow characteristics as velocity and pressure fields, turbulent characteristics and to suggest an optimized nozzle design.

There have been limited studies in jet analysis, and very few works on the jet behaviour inside a waterjet nozzle. Flow characteristics of waterjet in air was investigated by Yanaida and Ohasi (1978). The authors have characterized the waterjet into three regions: continuous flow region, droplet region and diffused region based on axial velocity and break up length. Eddingfield et al (1981) proposed a two-dimensional axisymmetric multicomponent mathematical model which coupled the three flow fields such as continuous water, entrained air, and droplets. Amano et al (1982) carried out theoretical and experimental investigation of the turbulent axisymmetric jets impinging on a flat plate. He has employed the two equation (k-E) turbulence model in his computations. He has solved the standard Navier-Stokes equations together with two-equation turbulence by the hybrid scheme of central and backward finite difference scheme. Vijay et al. (1993) investigated the application and dynamics of cavitating jets. The authors have investigated different nozzle configurations in their numerical investigations and found that the performance of artificially submerged cavitating jets operating at identical conditions surpassed that of fully submerged or noncavitating jets.

Several numerical studies were undertaken to investigate flow characteristics inside a waterjet nozzle. A numerical approach was suggested by Lai et al. (1991) to predict the flow characteristics inside three nozzles. The authors have shown numerically that a center body insert into a conical nozzle results in superior performance due to the increased cavitation. Khan (1994) have investigated the flow characteristics inside waterjet nozzle. He has used the finite element method to solve the turbulent flow fields. His numerical results were validated through the experimental study of the waterjet characteristics by using velocity measurements with Laser Transit Anemometer, and force measurements with piezoelectric force transducer. He has used the high speed filming to reveal the dynamics and behaviour of the jets. Thus it was shown that at the micro level the high speed jet is a sequence of disintegrated slugs, but at the macro level the jet is the normal turbulent flow.

Most of the numerical studies of the turbulent flow patterns inside a waterjet nozzle carried out up-to-date neglect the presence of the air phase inside the nozzle, although the later takes up to 90-95% of the three-phase mixture volume (air + water + abrasive) according to (Neusen et al, 1990, Osman et al, 1996). Moreover the effect of air flow rate is shown to both affect the jet coherence ultimately causing the jet break up, and reduce the exit velocity of particles by up to 40% (Tazib et al, 1994). The velocity loss is also connected with the flow rate of abrasive media.

Raissi et al (1996) has investigated in detail the influence of internal nozzle parameters on three-phase waterjet flow in a nozzle. In his work he takes into account the presence of air in the cutting head (90% of volume occupation), flow turbulence (eddy viscosity model) and abrasive particle interactions. As the outcome of the study, authors suggest that the numerical tools are very helpful in nozzle design optimization.

2. NUMERICAL STUDY OF THE TURBULENT FLOW INSIDE A PURE WATERJET NOZZLE

2.1 Modeling of the Turbulent Flow

The numerical simulation of a turbulent flow involves modification of governing equations for case of laminar flow. For modeling of turbulent flow a standard two-equation (k-ε) model was applied. For the flow involved in this study being turbulent, steady, incompressible, isothermal, chemically homogeneous and without body forces the following equations, modified for the case of turbulent flow, apply:

$$\frac{d\bar{U}_i}{dx_i} = 0 \quad (1)$$

$$\rho U_j \frac{\partial K}{\partial x_j} = \frac{\partial}{\partial x_j} \left(\frac{\mu_t}{\sigma_k} \frac{\partial K}{\partial x_j} \right) + \mu_t \frac{\partial \bar{U}_i}{\partial x_j} \left(\frac{\partial \bar{U}_i}{\partial x_j} + \frac{\partial \bar{U}_j}{\partial x_i} \right) - \rho \varepsilon \quad (2)$$

$$\rho U_j \frac{\partial \varepsilon}{\partial x_j} = \frac{\partial}{\partial x_j} \left(\frac{\mu_t}{\sigma_k} \frac{\partial \varepsilon}{\partial x_j} \right) + C_1 \mu_t \frac{\varepsilon}{K} \frac{\partial \bar{U}_i}{\partial x_j} \left(\frac{\partial \bar{U}_i}{\partial x_j} + \frac{\partial \bar{U}_j}{\partial x_i} \right) - C_2 \rho \frac{\varepsilon^2}{k} \quad (3)$$

where $i, j = 1, 2$, $\mu = \mu_0 + \mu_t$, and $\mu_t = \rho C_\mu k^2 / \varepsilon$, as proposed by Kolmogorov- Prandtl.

The above equations contain empirical constants C_1 , C_2 , σ_k , σ_ε and C_μ . Over the years the k-ε model has been tested and optimized against the wide range of flow problems. For the turbulent flow inside the nozzle the following values of these empirical constants was selected: $C_1=1.44$, $C_2=1.92$, $\sigma_k=1.00$, $\sigma_\varepsilon=1.30$ and $C_\mu=0.09$.

2.2 Near-Wall Modeling

The standard $k-\varepsilon$ turbulence model is valid mostly for the flows with high Reynolds number. In a problem involving a solid boundary, there is always a special viscosity-affected near wall region, which contains the viscous sub-layers. Therefore a problem arises when we try to apply the standard $k-\varepsilon$ turbulence model to a near-wall regions. Thus a special modeling approach is needed to simulate a turbulent flow in a near-wall region. Another reason a special considerations should be given to the near-wall region is that in order to resolve the sharp variations of flow variables in near-wall regions, a prohibitively large number of grid points must be used, which leads to expensive computation. There are two approaches to modeling of the near wall region. In the so-called wall function approach the special semi-empirical formulas are used to bridge the viscosity-affected region between the wall and the fully turbulent region. In this study the Wall Function approach was used to overcome the viscosity affected regions of the flow.

2.3 Problem Description

The computational domain for this problem was limited to the pure waterjet nozzle geometry. There are many variations of the sapphire nozzle geometry, but for this study we have limited ourselves to the standard convergent nozzle. The nozzle geometry is presented in Figure 5. Two variations of the conventional nozzle geometry was used for numerical simulations. The geometrical parameters of nozzles used in this study is presented in Table 1.

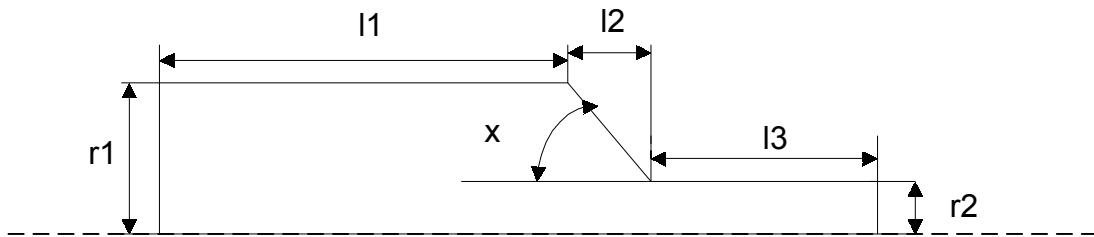


Figure 5. Computational Geometry

Table 1. Geometrical Parameters of Pure Waterjet Nozzles

Nozzle #	Angle x	R1(cm)	R2 (cm)	L1 (cm)	L2 (cm)	L3 (cm)
1	60°	0.1598	0.0178	1.598	1.68	1.935
2	90°	0.1598	0.0178	1.68	0	1.935

2.4 Mesh Development and Boundary Conditions

The computational domain was discretized into 12300 elements using the GAMBIT software. The four node, quadratic elements have been employed. The numerical grid is shown on Figure 6.

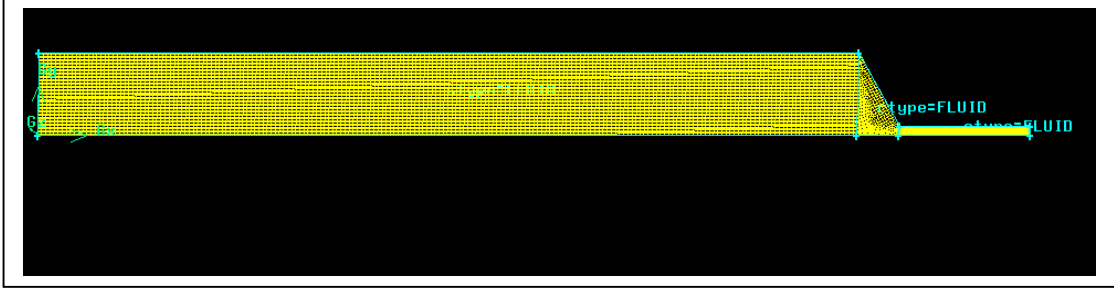


Figure 6 Computational Domain

The domain (Figure 6) over which the problem is to be solved is comprised of the inlet section, outlet, the axis of symmetry and the wall.

It is required to provide appropriate boundary conditions for k , and ε on the boundaries of the computational domain. The inlet plane is positioned upstream of the regions of interest. At the inlet section the water is prescribed a uniform velocity which was calculated from the constant volume flow rate. The turbulence quantities at the inlet section are determined using the following empirical relations,

$$k = 0.1U^2 \quad (4)$$

$$\varepsilon = \frac{k^{3/2}}{0.05r} \quad (5)$$

where r is the radius of the sapphire nozzle.

At the outlet boundary, the Neumann i.e., the zero gradient boundary condition in the axial direction is applied for U , k , ε . At the wall, the near-wall modeling approach is applied for those regions of the computational domain, which coincide with the solid boundary. On the solid wall u , k , ε are set to zero.

The finite element package FLUENT was used for the numerical solution of discretized equations.

2.5 Results and Discussion

The numerical solutions of the turbulent flow representing the jet flow in the pure waterjet nozzle were obtained in terms of velocity fields, pressure, the turbulent kinematic energy k and dissipation ε . The velocity field on the outlet section of the nozzle is of the most interest here, because it directly translates into the exiting energy of the jet, it's primary characteristics. Also the validity of the computational scheme and the obtained results could be checked, by comparing the outlet velocity profile and its magnitude with the available experimental results of other researches. Table 2 summarizes the results of velocity computations for nozzle #1 and different pressures.

Table 2 Predicted Velocity and Bernoulli Velocity

Mass Flow Rate (g/s)	Water Pressure (MPa)	Outlet Velocity (m/s)	Velocity from Bernoulli (m/s)	LTA Measured Velocity (m/s)
36.45	138	441	504	460
44.6	207	500	617	550
51.6	276	585	712	N/A
57.6	345	674	796	730

The velocity in column four was calculated using the Bernoulli equation:

$$V_{\text{bern}} = k*(2p/\rho)^{1/2} \quad (6)$$

where k was taken to be equal 0.96.

The experimental values of velocity at different intensifier pressures were measured by Li (1996) with the help of Laser Transit Anemometer. Here we can see that the predicted values of velocities indeed follow the ones predicted by Bernoulli equation pretty closely. The maximum relative error for the tested ranges does not exceed 20%. The relative error of prediction is even less in case we compare our prediction results with LTA measurements done by Li, (1996). Thus we could agree, based on this numerical results that the jet in the primary nozzle could be closely approximated by the conventional two-equation turbulence model and the exit velocity can be approximated with pretty good accuracy by the Bernoulli equation. Figures A1 through A4 in the Appendix show the results of the numerical simulations for the waterjet nozzle 0.354 mm and intensifier pressure 276 MPa. Contours of velocity magnitude (Figure A1) and stream function (Figure A2) give us an accurate idea regarding the velocity flow field in the nozzle. Thus it could be inferred that the highest velocity occurs exactly after the primary nozzle entrance. And exactly this velocity is best approximated by Bernoulli equation. Immediately after the entrance a not significant velocity loss occurs. The highest pressure is achieved at the orifice entry. The spatial velocity distribution (Figures A3, A4) is similar for both nozzles used in the study and it is uniform and there is no flow separation in the nozzle. Again it suggests that the flow can be

represented as the conventional turbulent jet. Thus the results show that the convergent nozzle produces concentrated high-energy jet.

3. MODELING OF TWO PHASE FLOW IN THE WATERJET CUTTING HEAD

As it was pointed out earlier, the flow in a waterjet-cutting head is not a simple one-phase turbulent flow. Instead this flow can at best be approximated as a three-phase flow, where the primary phase is the jet, the second phase is the entrained air, and the third phase is the abrasive particles mixed in the flow. In order to approach this problem, the volume of the fluid (VOF) model was used. The VOF model is a technique designed for two or more immiscible fluids, where the position of the interface between the fluids is of interest. In the VOF model, a single set of momentum equations is shared by the fluids, and the volume fraction of each of the fluids is tracked throughout the domain. The tracking of the interface(s) between the phases is accomplished by the solution of a continuity equation for the volume fraction of the phases. For the q^{th} phase, this equation takes the following form:

$$\frac{\partial \alpha_q}{\partial t} + u_i \frac{\partial \alpha_q}{\partial x_i} = 0 \quad (7)$$

The volume fraction equation will not be solved for the primary phase, instead the primary phase volume fraction will be computed based on the following constraint:

$$\sum_{q=1}^n \alpha_q = 1 \quad (8)$$

The properties appearing in the transport equations are determined by the presence of the component phases in each control volume. In general, for an N-phase system, the volume fraction averaged property would take a form:

$$p = \sum \alpha_q p_q \quad (9)$$

where p is some volume fraction averaged property (e.g. density, viscosity, etc).

A single momentum equation is solved throughout the domain, and the resulting velocity field is shared among the phases. The momentum equation depends on the volume fractions of all the phases through the properties ρ and μ . In the case of turbulence quantities, a single set of transport equations is solved, and the variables κ and ε are shared by the phases throughout the field.

3.1 Dispersed Phase Modeling

In this study the Lagrangian approach for two-phase flow modeling is used to model the ice particles mixing process. The underlying concept here is what is usually called dispersed two-phase flow. The idea is to consider one of the phases to be dispersed (abrasive particles) in the

other phase (waterjet). At the same time strong coupling occurs between phases. The Lagrangian model represents the dispersed phase as a continuous stream of particles moving through the carrier phase. The governing equations for the carrier phase are given in the standard in fluid dynamics Eulerian frame of reference, while the motion of the particles is described in a Lagrangian coordinate system. The information transfer between phases is accounted for by the momentum along particle paths.

The motion of each particle of the dispersed phase is governed by an equation that balances the mass- acceleration of the particles with the forces acting on it. For a particle of density ρ_p and diameter D_p the governing equation is:

$$\rho_p \frac{dU_i^p}{dt} = \frac{1}{\tau} (U_i - U_i^p) + (\rho_p - \rho)g_i + \rho_p f_i^p \quad (10)$$

where U_p is the particle velocity, U is the velocity of the carrier phase, f_p is the combination of forces acting on the particle, and τ is the particle's relaxation time, defined by Equation 11.

$$\tau = \frac{4\rho_p D_p^2}{3\mu C_D \text{Re}^p} \quad (11)$$

where μ is the viscosity of the fluid, Re^p is the particle Reynolds number defined by:

$$\text{Re}^p = \frac{D_p |U_i - U_i^p| \rho}{\mu} \quad (12)$$

and C_d is the drag coefficient. There exist many models, mostly empirically based for the drag coefficient. Among the most commonly used ones is the polynomial model given by:

$$C_d \text{Re}^p = 24(a + b\text{Re}^p + c(\text{Re}^p)^2 + d / \text{Re}^p) \quad (13)$$

where a , b , c , and d are constants.

The first term on the right hand side of (10) is the generalization of the classical Stokes Drag on a particle. The second term is the buoyancy force, important in simulating the sedimentation of solid particles in liquid, and the third term represents different forces that appear in particulate motion in fluid.

A particle trajectory is obtained by the solution of the particle momentum equation (10) coupled with kinematic equation:

$$U_i^p = \frac{dx_i}{dt} \quad (14)$$

where x_{pi} is the position coordinate of the particle at time t .

3.2 Problem Description

The computational domain in this study is limited to the cutting head of a conventional waterjet nozzle. In the cutting head three phases are mixing up to constitute the abrasive-air-water jet flow. The air enters the cutting head through the abrasive port. The cutting head itself consists of mixing chamber and focusing tube. In mixing chamber the mixing of the water stream, air and solid additives occurs, and the three-phase stream is then accelerated in the focusing tube. The computational domain along with process boundary conditions is given in the following chart. To reduce the computer time, the length of the focusing tube was taken smaller then it is in reality, with the assumption that after this length the flow is fully developed and no significant change of properties occurs.

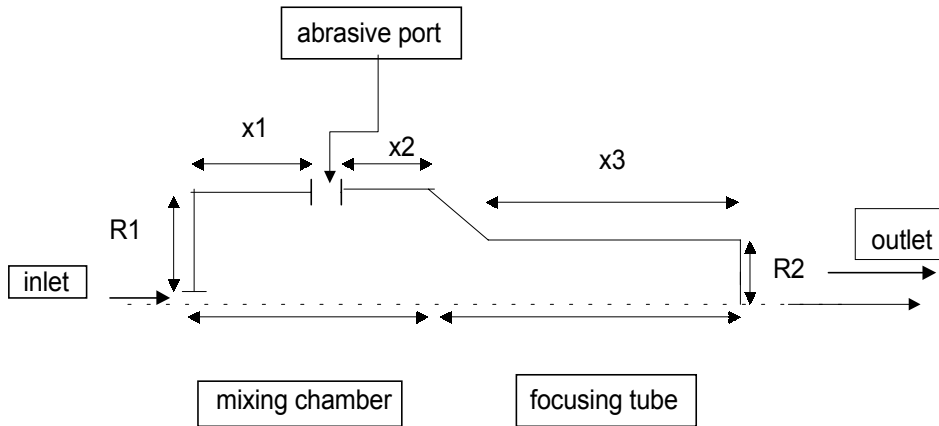


Figure 7. Nozzle Geometry

Table 3 Nozzle Dimensions

Waterjet Cutting Head Dimensions					
X1	X2	X3	R1	R2	Inlet
0.244	0.3556	1.5	0.203	0.116	0.017
(sm)	(sm)	(sm)	(sm)	(sm)	(mm)

3.3 Boundary Conditions

It is required to provide appropriate boundary conditions for k , u , ε on the boundaries of the computational domain. The inlet plane is positioned upstream of the regions of interest. The boundary condition for U is prescribed uniform at the inlet and set to be equal to 600 m/sec. The

volume fraction of air is taken to be equal to zero at inlet, and unity at abrasive port inlet. The turbulence quantities at the inlet section are determined using the empirical relations (4 – 5).

At the outlet boundary, the Neumann i.e., the zero gradient boundary condition in the axial direction is applied for U , k , ε . At the wall, the near-wall modeling approach is applied for those regions of the computational domain, which coincide with the solid boundary. On the solid wall u , k , ε are set to zero.

3.4 Discussion and Presentation of Results

The result of the analysis is presented in Figures A.5 through A.12. The contours of velocity magnitude show that after the primary nozzle, centerline velocity dominates the flow. There is a velocity loss along the centerline, not exceeding 10% of the velocity magnitude after the primary nozzle. The average centerline velocity at secondary nozzle exit, for the given operating conditions is 250 m/s. These results are in a good agreement with results available in the literature (Raissi et al 1996, Neusen et al, 1996). The turbulent quantities increase closer to mixing tube and grow even stronger on the jet periphery, further from the jet centerline. This could be explained by the increasing intensity of the jet break up in the secondary nozzle. The volumetric fraction of air in the nozzle can be estimated to be greater than or equal to 85%. This again is in a total agreement with previously reported experimental and numerical results. (Raissi et al, 1996, Osman et al, 1996).

4. REFERENCES

- Hashish, M. 1991. "Optimization Factors in Abrasive- Waterjet Machining", *Journal of Engineering for Industry*, Vol. 113, pp. 29-37.
- Hashish, M. 1993. "Prediction Models for AWJ Machining Operations." *Proceedings of the 7th American Water Jet Conference*, Seattle, Washington, pp. 205-216.
- Sawamura T., Fukunishi Y., Kobayashi R. 1999. "The Effects of the Abrasive Flow Rate on Abrasive and Water Velocities." *Proceedings of the International Symposium on New Applications of Water Jet Technology*, Ishinomaki, Japan.
- Osman A.N., Buisine D., Thery B., Houssaye G. 1996. "Measure of Air Flow Rate According to the Mixing Chamber Designs." *Proceedings of 13th International Conference on Jet Cutting Technology*, Sardinia, Italy.
- Neusen K.F., Gores T.J., Labus T.J. 1992. "Measurement of Particle and Drop Velocities in a Mixed Abrasive Waterjet Using a Forward-Scatter LDV System." *Jet Cutting Technology*, Kluwer Academic Publishers.
- Yanaida, K., and Ohashi, A. 1978. "Flow Characteristics of Water Jets in Air." *Proceedings of Forth International Symposium on Jet Cutting Technology*. A3-39 – A3-54.

- Eddingfield, D. L., Evers, J. L., and Setrok, A. 1981. "Mathematical Modeling of High Velocity Water Jets." *1st U.S. Waterjet Conference*. 1: I-3.1 – I-3.14.
- Chen W-L., Geskin E.S. 1990. "Measurements of the Velocity of Abrasive Waterjet by the Use of Laser Transit Anemometer", *Proceedings of 10th International Symposium on Jet Cutting Technology*, BHRG Fluid Engineering.
- Chen W-L. 1990. "Correlation Between Particle Velocities And Conditions Of Abrasive Waterjet Formation", *Ph.D. Dissertation*, New Jersey Institute of Technology.
- Tazib A., Schmitt A., Parsy F., Abriak N., Thery B. 1994. "Effect of Air on Acceleration Process in AWJ Entrainment System." *Proceedings of 12th International Symposium on Jet Cutting Technology*, Rouen, France.
- Raissi K, Cornier A., Kremer D., Simonin O. 1996. "Mixing Tube Geometry Influence On Abrasive Waterjet Flow." *Proceedings of 13th International Conference on Jet Cutting Technology*, Sardinia, Italy.
- Amano, R.S. and Neusen, K. F. 1982. "A Numerical and Experimental Investigation of High-Velocity Jets Impinging on Flat Plate." *6th International Symposium on Jet Cutting Technology*. 6: c3.107-c3.122.
- Vijay, M. M., Hu, S. G., and Lai, M. K. Y. 1993. "Enhancing the Performance of Cavitating Water Jets." *Proceedings of 7th American Water Jet Conference*.
- Lai, M.K.Y., Vijay, M.M., Zou, C. 1991. "Computational Fluid Dynamics Analysis of Submerged Cavitating Water Jets." *Proceedings of the 6th American Waterjet Conference*, Waterjet Technology Association, St. Louis, Missouri.
- Khan, E. 1989. "Investigation of the Dynamics of Abrasive Waterjet Formation." *MS Thesis*, New Jersey Institute of Technology.

5. APPENDIX

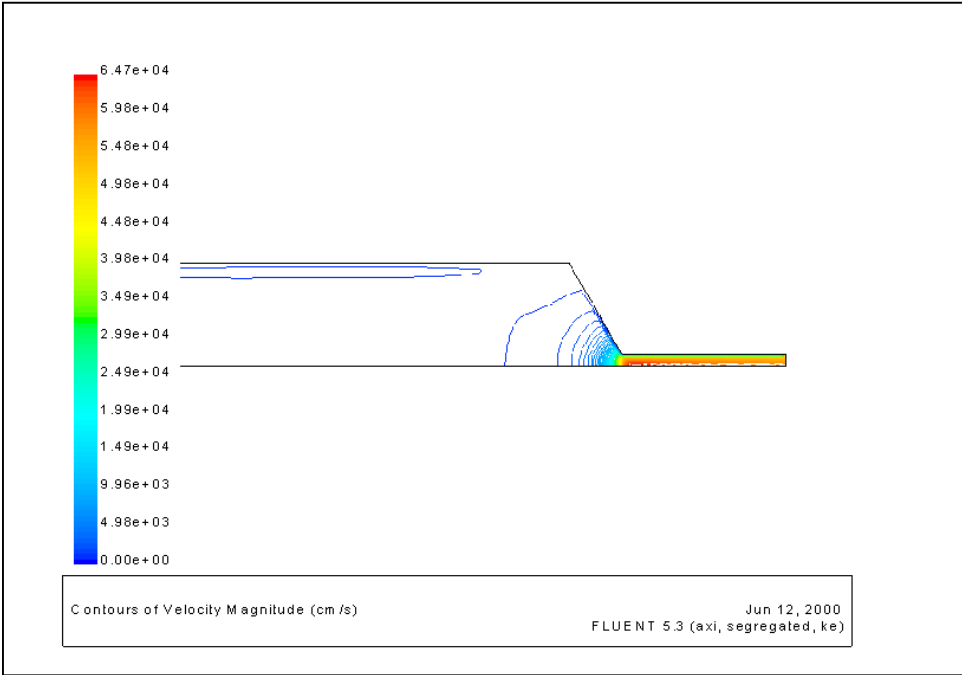


Figure A.1 Contours of Velocity Magnitude (cm/s) for Nozzle #1 and Mass Flow Rate 52 g/s

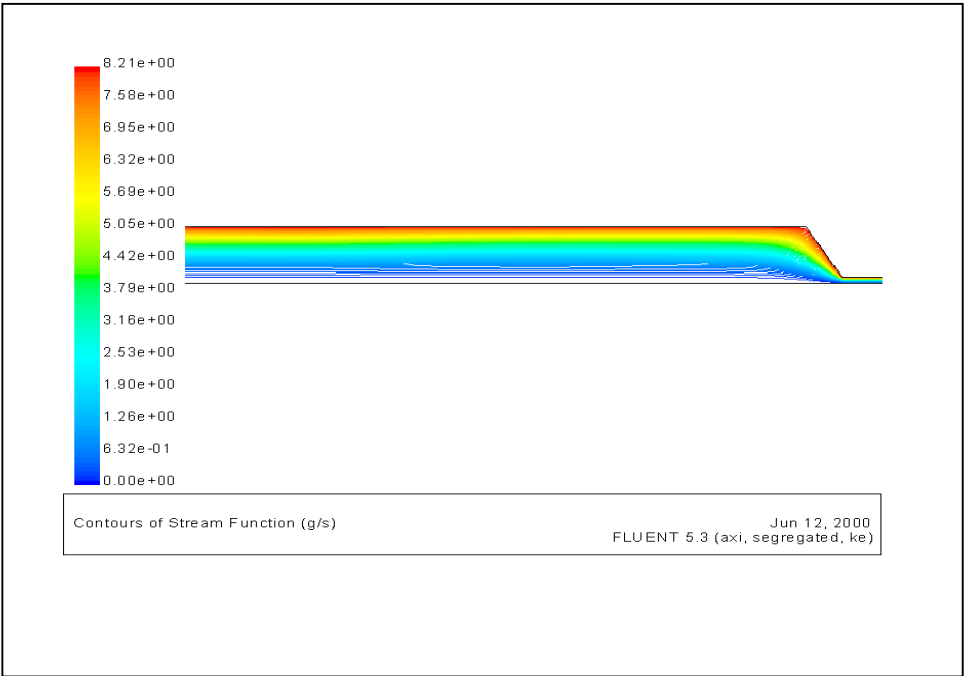


Figure A.2 Stream Line Contours For Nozzle #1 and Mass Flow Rate 52 g/s

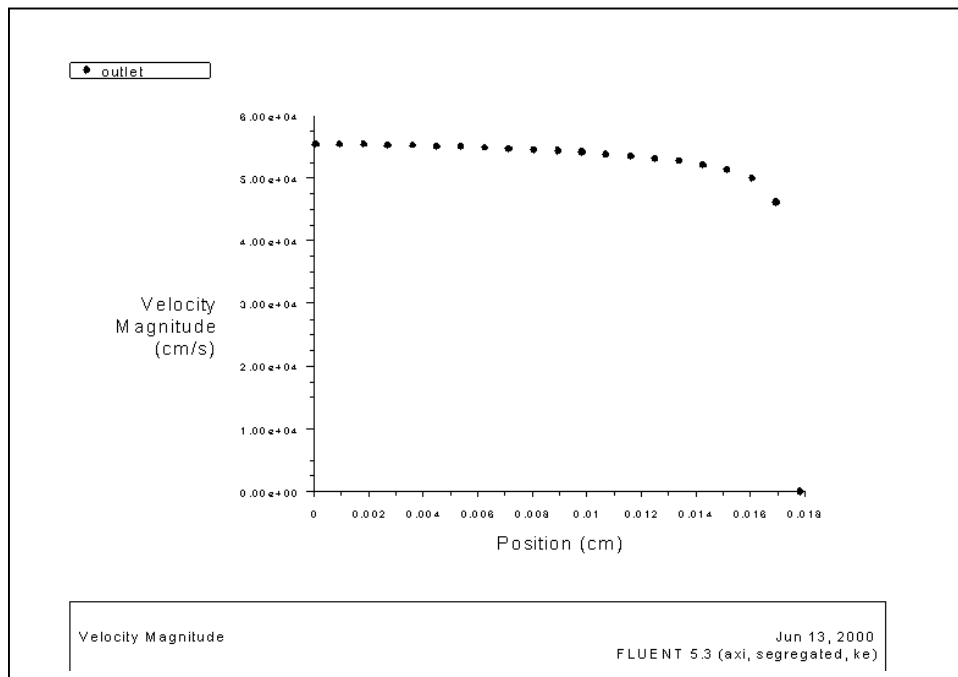


Figure A.3 Outlet Velocity Magnitude, Nozzle #2, Mass Flow 52 g/m

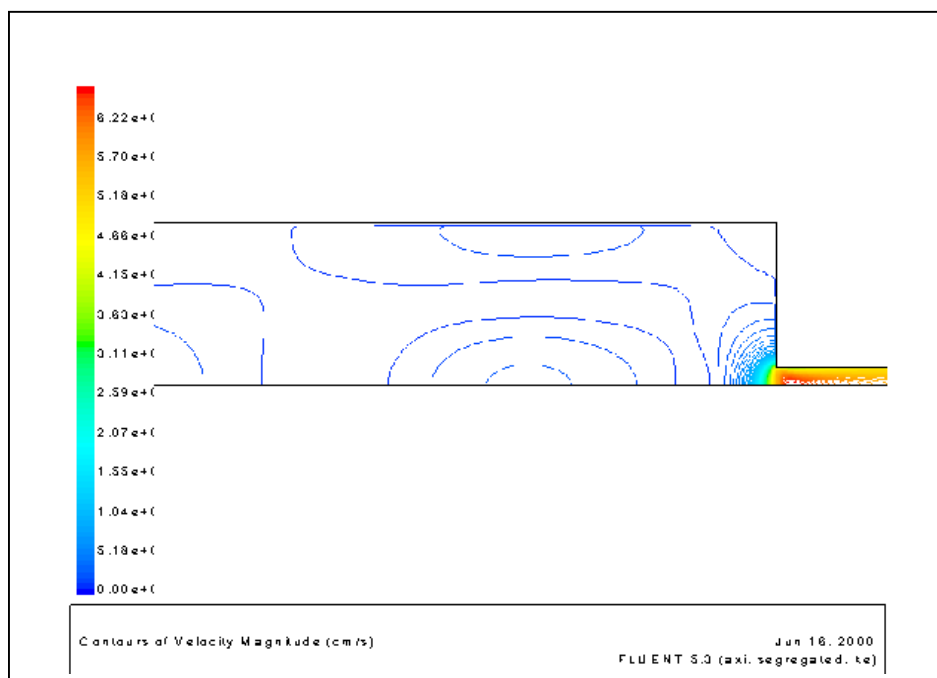


Figure A.4 Contours of Velocity Magnitude (cm/s)

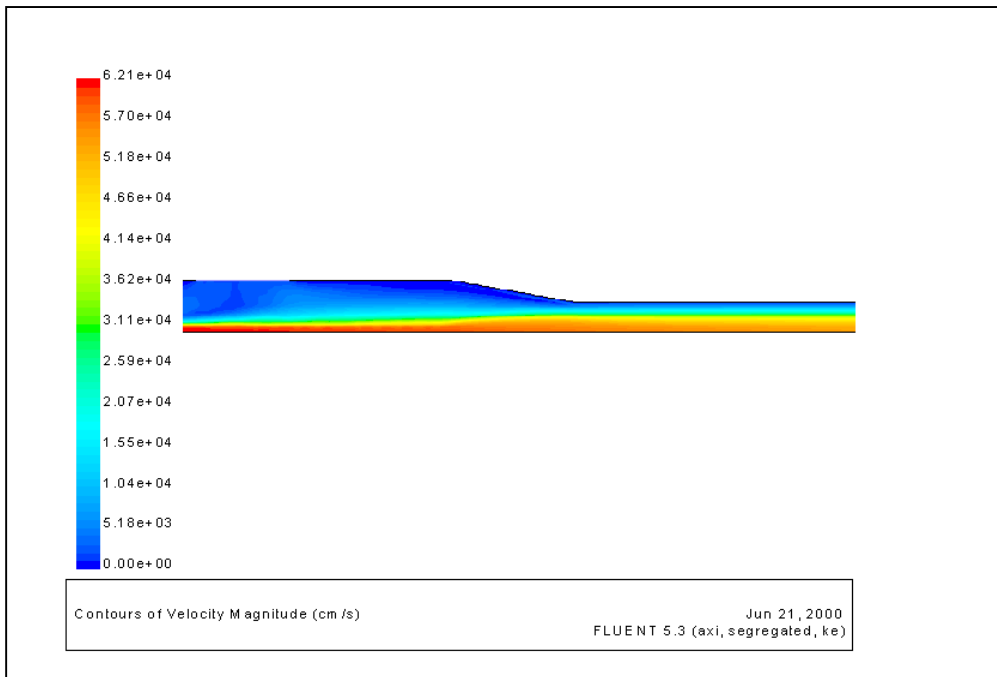


Figure A.5 Contours of Velocity Magnitude

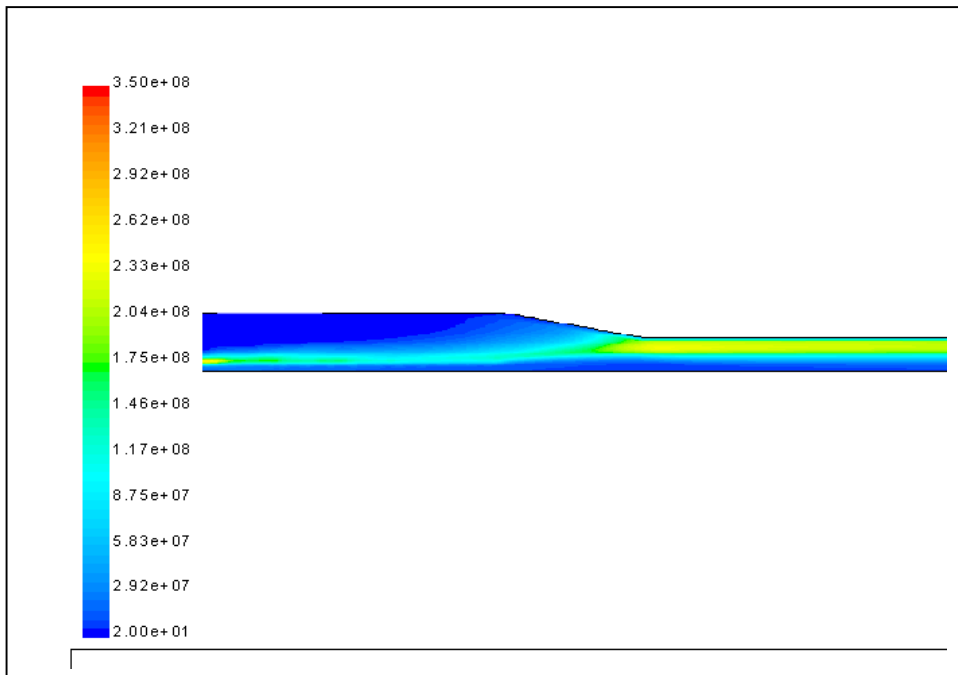


Figure A.6 Contours of Turbulent Kinetic Energy (k)

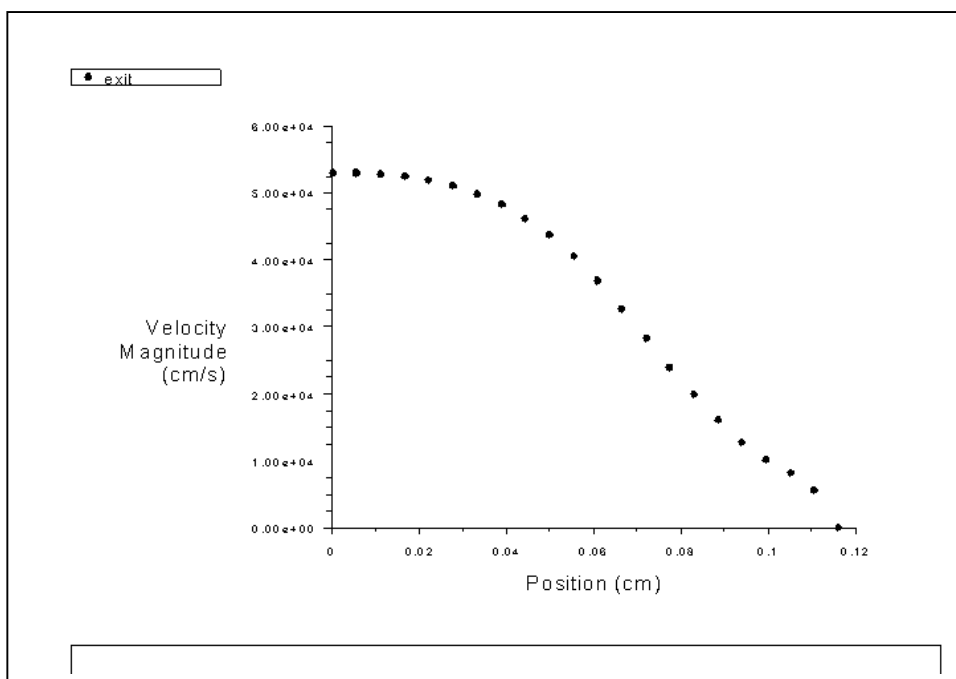


Figure A.7 Velocity Magnitude at Nozzle Exit

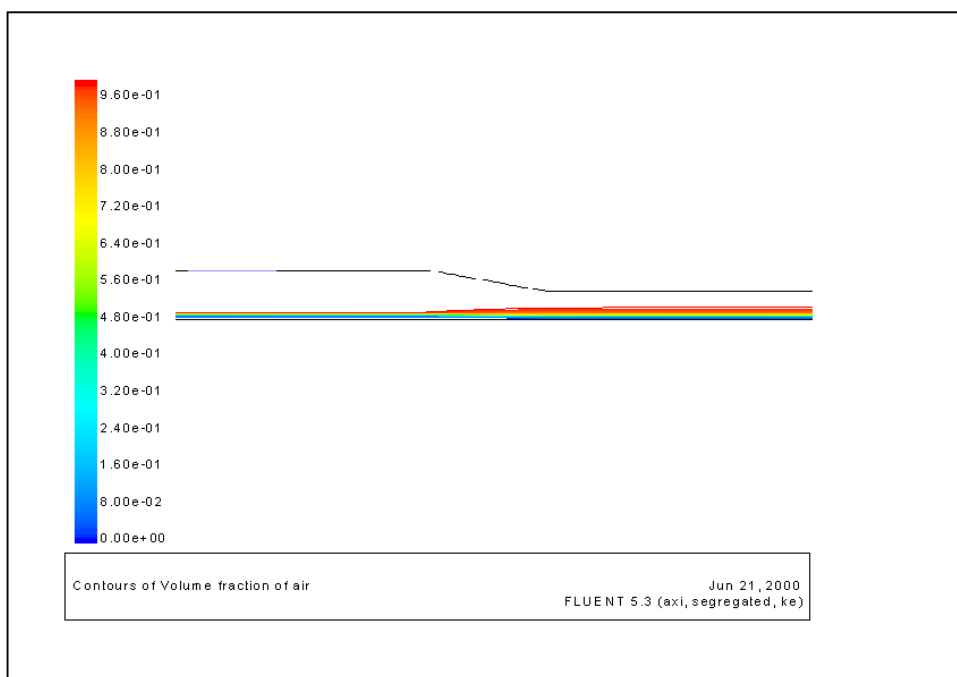


Figure A.8 Contours of Volume Fraction of Air

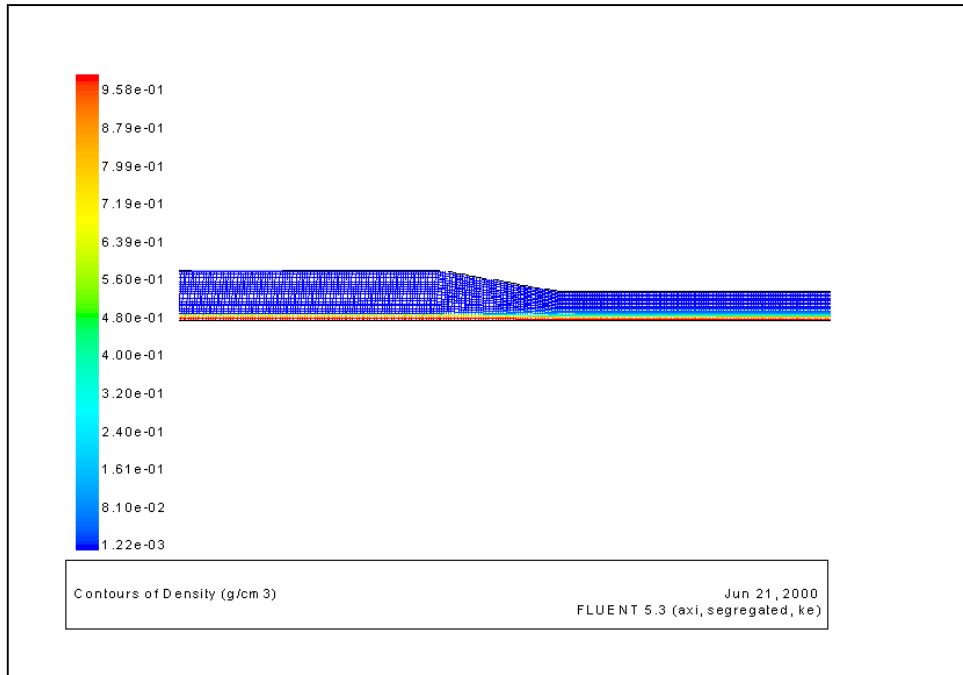


Figure A.9. Density Contours (g/sm³)

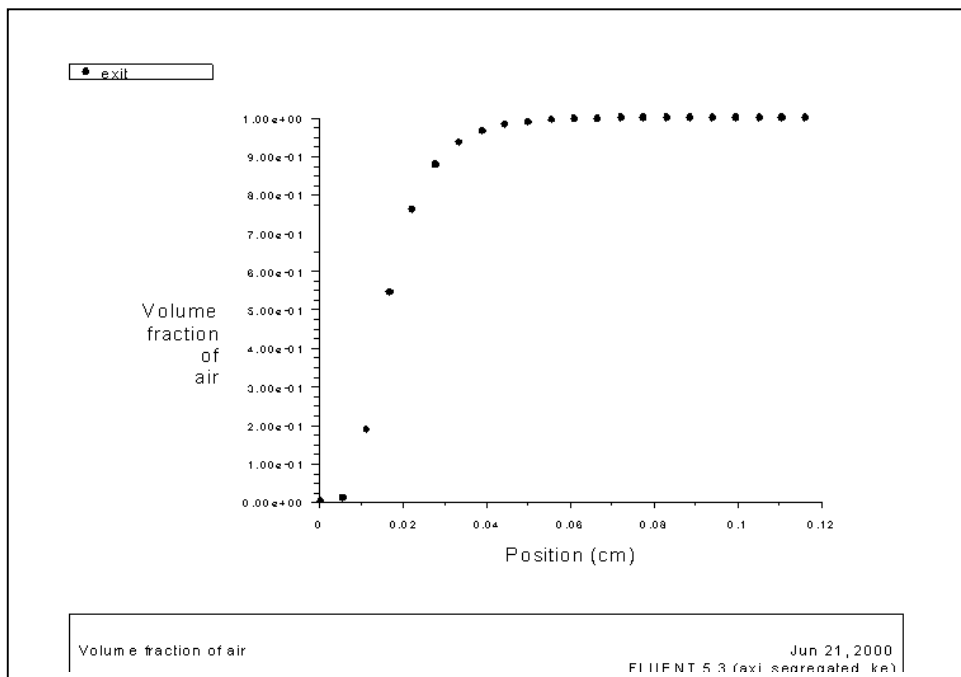


Figure A. 10 Volumetric Fraction of Air at the Nozzle Exit

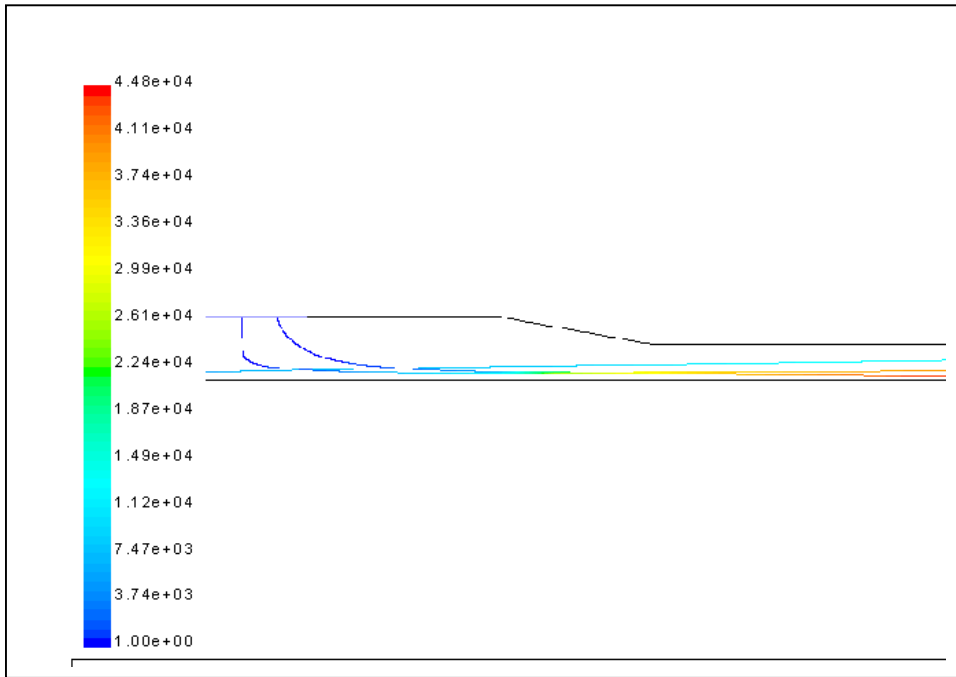


Figure A.11 Particle Traces Colored by Particle Velocity Magnitude (sm/s)

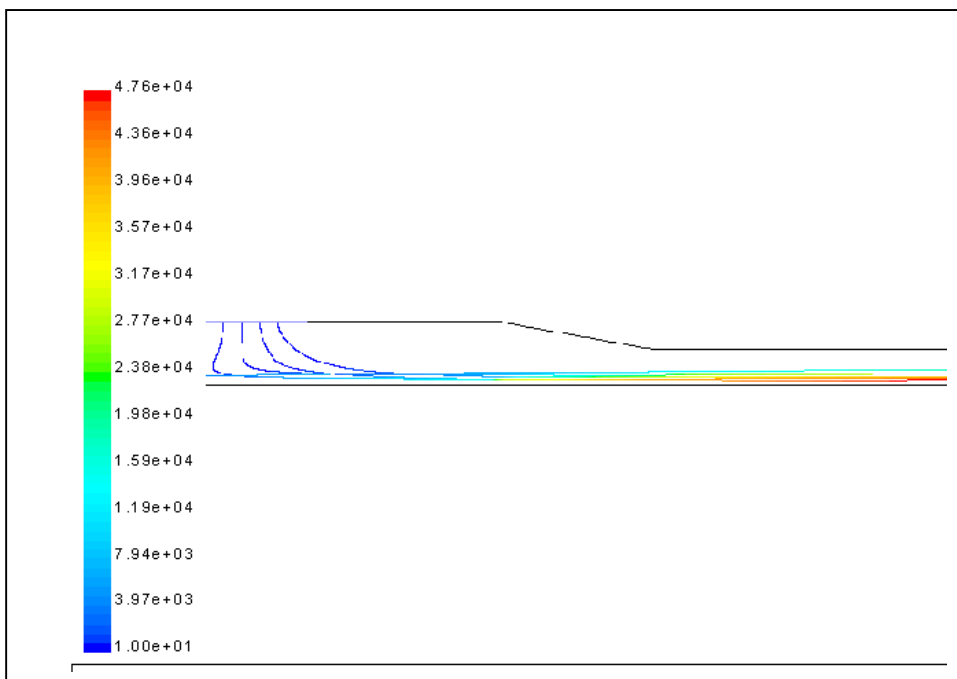


Figure A.12 Particle Traces Colored by Particle Velocity Magnitude (sm/s)

NUMERICAL INVESTIGATION OF CHAOTIC MOTION FOR CAVITATION BUBBLE IN OSCILLATING PRESSURE FIELD

Zhang Fenghua, Tang Chuanlin, Yang Lin
Zhuzhou Institute of Technology
Zhuzhou, Hunan, P. R. China

Liao Zhenfang
The Institute of Mechanical Engineering
Chongqing University
Chongqing, P. R. China

ABSTRACT

Radial motion of single cavitation bubble in oscillating pressure field has been investigated numerically after accounting for the liquid compressibility. It is shown that the bubble motion presents intense nonlinear feature and there will be bifurcation and chaos under some condition. Double-periodic bifurcation is one of the ways that the radial motion of single cavitation bubble reaches chaos. The indetermination of the cavitation bubble motion in oscillating pressure field has been revealed.

1. INTRODUCTION

The gaseous nuclei in water are essential to cavitate. The cavitation phenomenon is composed of the nucleation, growth and collapse of bubbles. The cavitation inception and bubble growth in cavitating water jet are in oscillating pressure field. A lot of experiments show that there are indeterminations in cavitation phenomenon and dispersion for experimental data (Ooi, 1985, Ran et al., 1994). The famous ITTC experiments (Johnsson, 1969) indicate that the data are also dispersed widely for the same model in different experimental devices. The data are often deviated even for the same model and experimental devices tested at the different time. Indeed, it is an important reason to cause data dispersion that the factors affecting cavitation are such much that it does not simulate all of the factors in the test. But nonlinear theory tells us that even if the external affecting factors can maintain constant in the test, the chaos, which originates from the internal indeterminations of the matter itself, can cause the data dispersion. So, the investigation of the chaos phenomenon of cavitation bubble motion is very important.

The study of nonlinear theory is still developing, there is not a general calculating method for common nonlinear equation. Thus, the numerical solution becomes important one of the methods to investigate nonlinear dynamics.

2. DYNAMIC EQUATION

The motion of single spherical cavitation bubble in infinitive boundary and incompressibility field is described with the Rayleigh-Plesset equation:

$$R\ddot{R} + \frac{3}{2}\dot{R}^2 = \frac{1}{\rho} \left(p_v + p_g - p(t) - \frac{2S}{R} - 4\mu \frac{\dot{R}}{R} \right) \quad (1)$$

“.” above the letters is substituted for $\frac{d}{dt}$ (the same as follows).

After accounting for the liquid compressibility, the bubble motion is described with Keller's form (Keller et al., 1956):

$$\left(1 - \frac{\dot{R}}{c} \right) R\ddot{R} + \frac{3}{2} \left(1 - \frac{1}{3} \frac{\dot{R}}{c} \right) \dot{R}^2 = \frac{1}{\rho} \left(1 + \frac{\dot{R}}{c} + \frac{R}{c} \frac{d}{dt} \right) \left(p_v + p_g - p(t) - \frac{2S}{R} - 4\mu \frac{\dot{R}}{R} \right) \quad (2)$$

Assume that the gas in bubble is adiabatic, it can be obtained

$$p_g = p_{g0} \left(\frac{V_0}{V} \right)^\gamma = p_{g0} \left(\frac{R_0}{R} \right)^{3\gamma} \quad (3)$$

The oscillating pressure is

$$p(t) = p_0 + p' \sin(2\pi ft) \quad (4)$$

Make

$$\left. \begin{aligned} x &= \frac{R}{R_0} \\ y &= \frac{K_0}{R_0} \dot{R} \\ z &= \frac{t}{K_0} \end{aligned} \right\} \quad (5)$$

where

$$K_0 = R_0 \sqrt{\frac{\rho R_0}{2S}} \quad (6)$$

If $\tau = \frac{t}{K_0}$, the equations (2), (3) and (4) change into

$$\left. \begin{aligned} \frac{dx}{d\tau} &= y \\ \frac{dy}{d\tau} &= g(x, y, z) \\ \frac{dz}{d\tau} &= 1 \end{aligned} \right\} \quad (7)$$

where

$$\left. \begin{aligned} g(x, y, z) &= \frac{1}{(1 - a_1 y)x + a_1 a_2 a_5} (A + B + C) \\ A &= -\frac{3}{2} \left(1 - \frac{1}{3} a_1 y\right) y^2 \\ B &= a_2 (1 + a_1 y) [x^{-3\gamma} + a_3 - a_4 x^{-1} - a_5 y x^{-1} - a_6 (1 + a_7 \sin a_8 z)] \\ C &= a_1 a_2 x [a_4 y x^{-2} + a_5 y^2 x^{-2} - 3\gamma x^{-3\gamma-1} - a_6 a_7 a_8 \cos(a_8 z)] \end{aligned} \right\} \quad (8)$$

Each coefficient is

$$\left. \begin{aligned} a_1 &= \frac{R_0}{cK_0}, \quad a_2 = \frac{K_0^2 p_{g0}}{\rho R_0^2}, \quad a_3 = \frac{p_v}{p_{g0}}, \quad a_4 = \frac{2S}{p_{g0} R_0} \\ a_5 &= \frac{4\mu}{p_{g0} K_0}, \quad a_6 = \frac{p_0}{p_{g0}}, \quad a_7 = \frac{p'}{p_0}, \quad a_8 = 2\pi f K_0 \end{aligned} \right\} \quad (9)$$

Differential equation (7) is not solved analytically and the numerical method can be used commonly.

3. THE DOUBLE-PERIODIC BIFURCATION AND CHAOS OF NUMERICAL SOLUTION

We solve the equation (7) with standard four-order Runge-Kutta method. Choose $R_0 = 10\mu m$, $p_0 = 0.1MPa$, $p' = 0.09MPa$. The oscillating frequency f is a parameter.

3.1 Quasi-linear Response

When oscillating frequency $f = 265kHz$, we obtained Figure 1. Figure 1(a) represents the ratio of bubble radius R/R_0 versus time t (part of the curve). Figure 1(b) is the power spectrum corresponding with Figure 1(a). Thus it can be seen that it has higher order frequency components besides the fundamental frequency different from the linear oscillation. We call it quasi-linear response.

Figure 1(c) is a phase plane map that represents $\dot{R} \sim R/R_0$. Figure 1(d) is a Poicare map. It is thus clear that the phase map has the feature of limiting circle and there is one point on the Poicare map under the condition of quasi-linear oscillation. It is called the periodic-1 solution.

3.2 Double-periodic Bifurcation

With the decrease of frequency f , the solving form of equation (7) changed. Figures 2~3 indicate the course of double-periodic bifurcation.

Figure 2 shows that periodic-2 solution for equation (7) appears as $f = 250kHz$. It makes clear from Figure 2(a) that the oscillating period of bubble is twice as large as one of pressure field. There are two points on Poicare map. The secondary resonant frequency, which is lower than frequency f and equal to $f/2$ at periodic-2 solution, appears in figure 2(b). It shows that the omen of chaos emerges.

When $f = 240kHz$, the solutions are shown in Figure 3. More secondary resonant frequencies appear. There are 4 points on the Poicare map. That is, the period doubles again.

3.3 Chaos

After periodic-4 solution, the periodic-8 solution appears with decreasing the oscillating frequency f . Next, the periodic rule can not be found for the data of numerical calculation. It is stated that the chaos arrives.

The chaotic motion of cavitation bubble is shown in figure 4 as $f = 233kHz$. The oscillation is not periodic and the power spectrum presents the feature of wide-band noise spectrum. The

phase map has not the feature of limiting circle and becomes unclosed trace. Some data are given only on the phase map, or the map will become black and the trace is not distinguished. The Poincare map will consist of infinite points. There are 200 points in Figure 4(d) and the shape of Strange Attractor is emerged.

3.4 Bifurcating Map and Feigenbaum Number

Figure 5 is a bifurcating map in which abscissa is a parameter f and ordinate is a dimensionless radius of bubble in Poincare section. It shows that there is an evident phenomenon from double-periodic bifurcation to chaos as the frequency f decreases from $270kHz$ gradually.

Chaotic theory has proved that it should follow the Feigenbaum rule from double-periodic bifurcation to chaos (Moon, 1987). That is, as $n \rightarrow \infty$, the parameter λ should be satisfied with

$$\delta = \frac{\lambda_n - \lambda_{n-1}}{\lambda_{n+1} - \lambda_n} \Big|_{n \rightarrow \infty} = 4.6692016 \quad (10)$$

$\delta = 4.6692016$ is called Feigenbaum number.

From the course of double-periodic bifurcation in figure 5, we obtained that the bifurcating point $f_1 = 258.934kHz$ from period 1 to period 2, $f_2 = 241.3kHz$ from period 2 to period 4 and $f_3 = 237.35kHz$ from period 4 to period 8. Thus

$$\frac{f_2 - f_1}{f_3 - f_2} = 4.4643 \approx \delta \quad (11)$$

The ratio of parameter f is equal to Feigenbaum number roughly. The error comes mainly from numerical calculation. Every point corresponding to abscissa in bifurcation map is calculated independently and f_n value produces error unavoidably.

4. CONCLUSION

After accounting for the liquid compressibility, the radial motion of single cavitation bubble in oscillating pressure field has been investigated numerically. Thus, we can conclude as follows:

- (1) The bubble motion presents intense nonlinear feature and there will be bifurcation and chaotic behavior under some condition.
- (2) Double-periodic bifurcation is one of the way that the radial motion of single cavitation bubble in oscillating pressure field reaches chaos.
- (3) The indetermination of the cavitation bubble motion is revealed.

5. ACKNOWLEDGMENTS

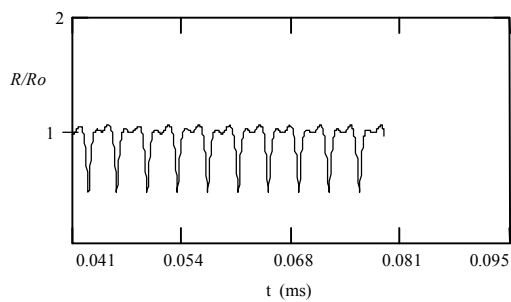
This research project is funded from the National Natural Science Foundation of China (No. 59874033).

6. REFERENCES

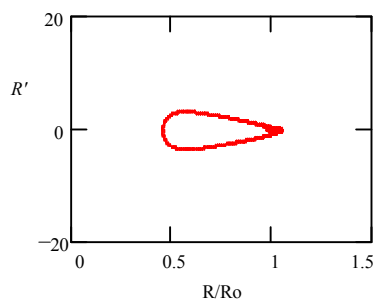
- Johnsson, C.A., "Cavitation Inception on Head Forms, Further Tests," *Proceedings of the 12th ITTC*, pp.125-131, Rome, 1969.
- Keller, J.B. and Kolodner, I., "Damping of Under Water Bubble Oscillations," *J. Appl. Phys.* Vol. 27, pp.87-93, 1956.
- Moon, F.C., "Chaotic Vibration," *John Wiley & Sons Ltd*, 1987.
- Ooi, K. K., "Scale Effects on Cavitation Inception in Submerged Water Jets: a New Look," *Journal of Fluid Mechanics*, Vol. 151, pp.367-390, 1985.
- Ran, B. and Katz, J., "Pressure Fluctuation and Their Effect on Cavitation Inception within Water Jets," *Journal of Fluid Mechanics*, Vol. 262, pp.223-263, 1994.

7. NOMENCLATURE

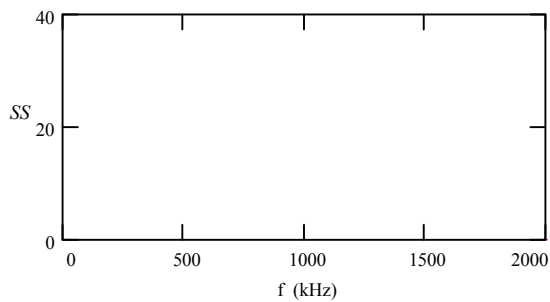
- c : sound velocity in water, m/s
- f : oscillating frequency, Hz
- p_0 : average pressure of field, Pa
- p_g : partial pressure of gas, Pa
- p_v : partial pressure of vapor, Pa
- p_{g0} : initial partial pressure of gas, Pa
- $p(t)$: field pressure, Pa
- p' : amplitude of oscillating pressure, Pa
- R : radius of cavitation bubble, m
- R_0 : initial radius of cavitation bubble, m
- S : surface tension of the liquid, N/m
- V : volume of cavitation bubble, m^3
- V_0 : initial volume of cavitation bubble, m^3
- ρ : liquid density, kg/m^3
- μ : liquid viscosity, Ns/m^2
- γ : polytropic index



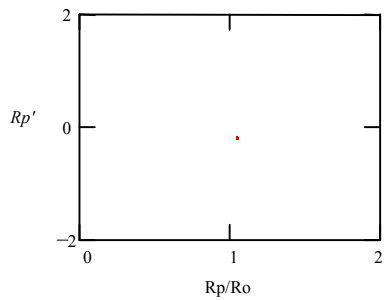
(a)



(c)

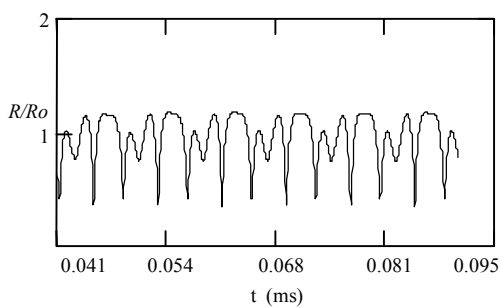


(b)

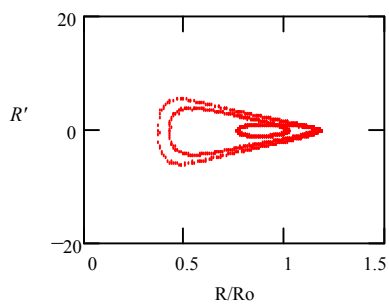


(d)

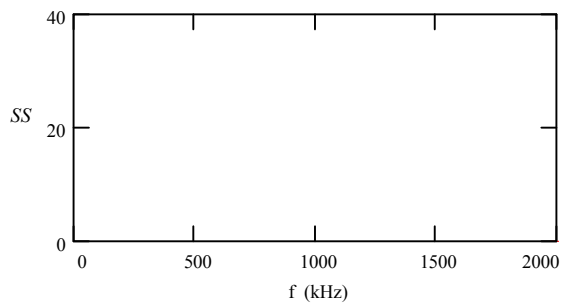
Figure 1. Quasi-linear Response----Periodic-1 Solution ($f=265$ kHz)



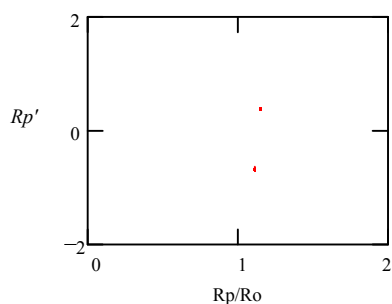
(a)



(c)



(b)



(d)

Figure 2. Periodic-2 Solution ($f=250$ kHz)

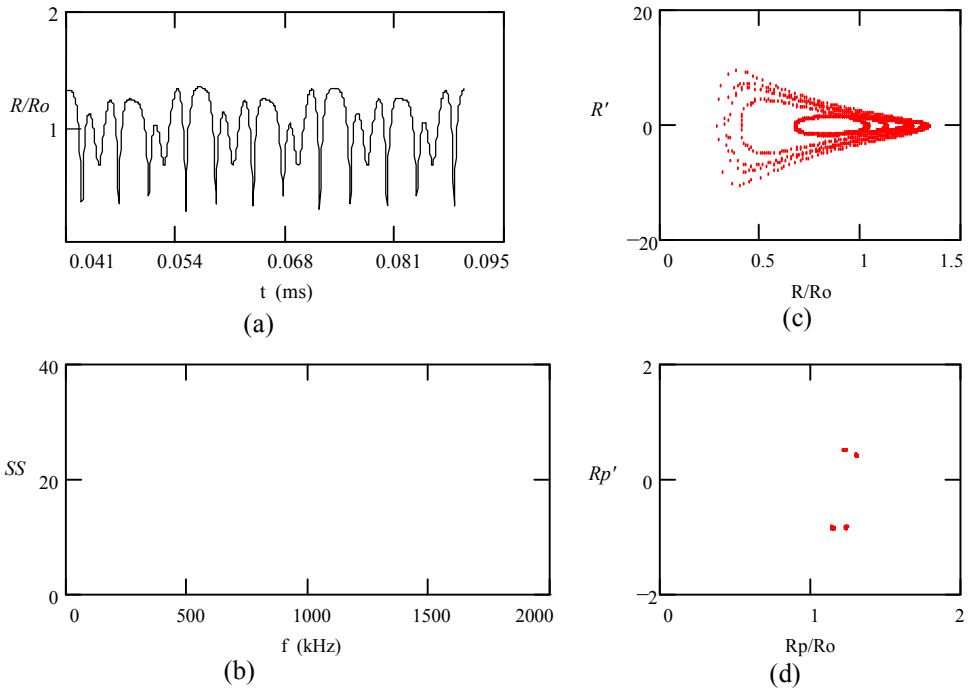


Figure 3. Periodic-4 Solution ($f=240$ kHz)

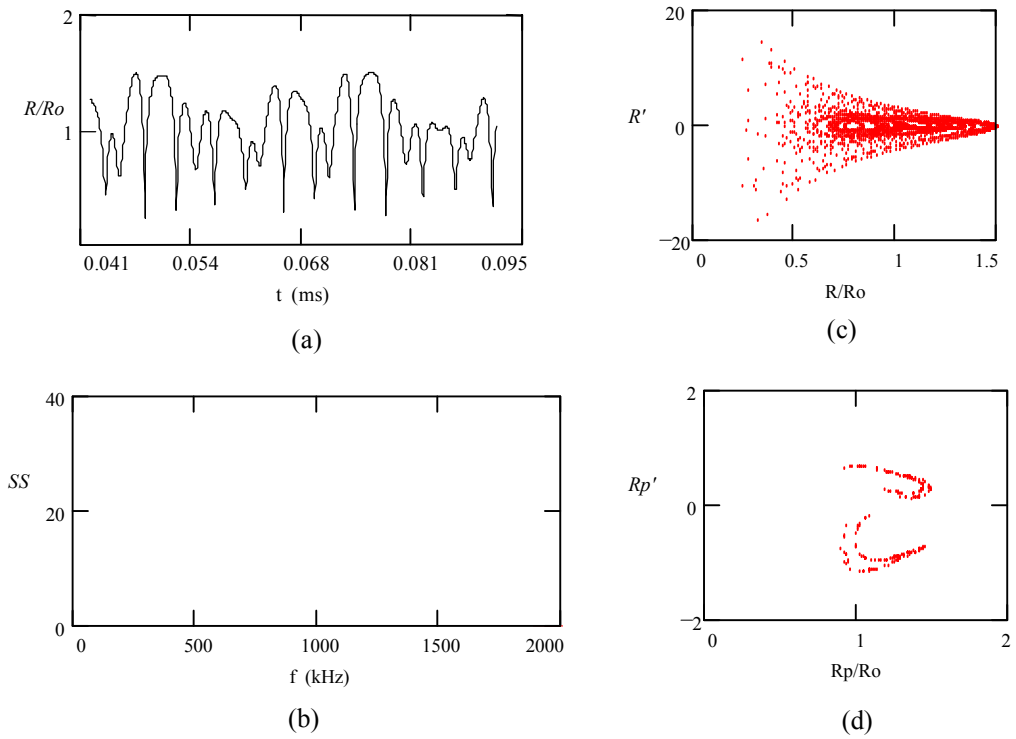


Figure 4. Chaotic Motion of Cavitation Bubble ($f=233$ kHz)

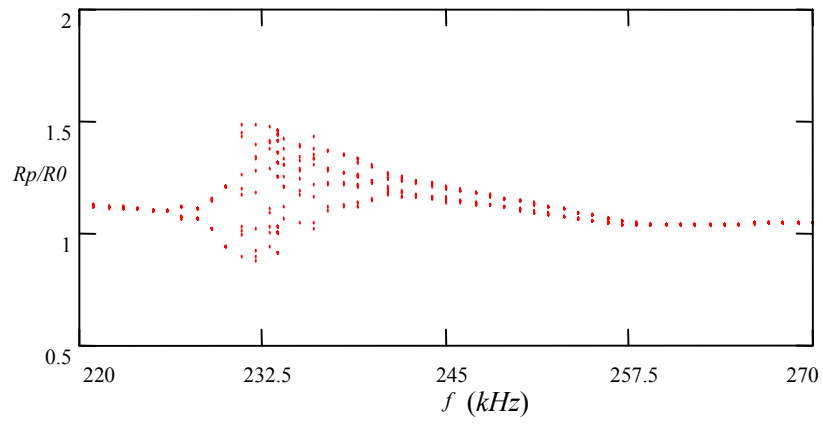


Figure 5. Bifurcating Map

EXPERIMENTAL STUDIES OF JET CAVITATION NOISE SPECTRUMS IN OIL WELL CASING

Li Gensheng Huang Zhongwei Zhang Debin Niu Jilei
University of Petroleum, East China
Dongying, Shandong, P.R. China

ABSTRACT

For the submerged jet with high velocity, cavitation is easily produced at the low pressure core area of the turbulent vortex, which will change the liquid stable condition and bring about liquid pulsation; also, the bubble's collapse can erode the nearby solid surface because of such partial area's high pressure and the production of high noise. This paper presents the jet cavitation noise spectrums at different exiting speeds in oil well casing. Spectrums at different stand-off distances from the nozzle also have been measured.

In the experiment, signals such as auto-spectrum, time-amplitude etc., are measured spontaneously at different frequency bands. The experiment results show that in the hydrophone's frequency responding range (0-100kHz), those signals change with the nozzle exiting speed across the whole frequency band. However, the strongest noise is concentrated below 20 KHz. With the increase of the standoff distance, the signal power will decrease, especially at higher frequency bands.

1. INTRODUCTION

Cavitation is the process that occurs when local pressure in liquid decreases, and the air bubble, inside the liquid or at the interface between the liquid and solid wall, forms, develops and collapses. In any case, cavitation can not appear in air or solid media. This process is categorized by its generating conditions and main physical features. There are cruising, fixed, vortex and oscillating cavitation (Konype,1981). When cavitation happens, a single micro-bubble will experience such complex processes as developing, collapsing, rebounding and recollapsing, and creating sharp sound pulse and flash (Qi, 1999). In fact, such phenomenon is a very complicated non-stable random process. Although its characteristics in every stage have not been studied thoroughly, it is known through calculation that when a micro bubble collapses, the pressure can be as high as 6GPa and the temperature can be more than over 4000K (Phlipp et al, 1998; Yuri, 1999). The material erosion experiment also proved that cavitation has a destructive function (Konype, 1981).

As the jet emerges at a higher Reynold number, the liquid will form central cone area without vortex close to the nozzle outlet, in which the velocity reaches a maximum and remains constant for some distance. When the shear layer spreads to the jet center, the velocity will decrease because of the energy exchange between differential liquid speeds. So, it is most probable that cavitation will happen around the shear layer with low pressure. It's already known that the strongest cavitation noise appears at the distance of 5 times the nozzle diameter down stream (Konype, 1981).

The factors affecting cavitation initiation are:

1. impurity characteristic;
2. liquid physical features
 - a. viscosity
 - b. surface tense
 - c. temperature
3. liquid dynamics features
 - a. pressure
 - b. velocity
 - c. geometry dimension of flow path
4. surface conditions
 - a. smoothness
 - b. micro-crack containing gas

This paper presents the experimental results of tests of varying nozzle exiting velocities in an oil well casing at different stand-off distances.

2. ANALYSIS OF THE NOISE SOURCES

In addition to the background noise, the noise spectrum results from two kinds of noise sources: cavitation and the friction noise generated when a high speed fluid flows through the nozzle

outlet. According to the noise source's emittance and direction features (Ma, 1987), the friction noise belongs to quadruple source. That is, the only reason for noise lies in the fluid viscous stress. For the subsonic flow, the total noise power of the quadruple source is in direct proportion with flow velocity of V^8 , which shows that noise power will increase significantly when flow velocity increases slightly.

The spectrum of cavitation noise has a wide frequency band. Such noise has been measured at the range of 5 Hz--180 KHz (Jiang et al, 1998). Because of the fast attenuation of higher frequency signals, the main signal power is concentrates below 20 KHz. In this experiment, no signal over 20 KHz can be detected at a shorter stand-off distance. Therefore, the spectrum at higher frequency bands (>20 KHz) has not been analyzed in this paper.

3. EXPERIMENTAL METHODS

3.1 Experiment Conditions

For the measurement convenience, the casing was laid horizontally. There may be some differences from the actual conditions at the well bottom. Also, the factors such as temperature and ambient pressure were neglected. In the experiment, the medium is clean tap water, and the nozzle diameter is 4 mm.

3.2 Experimental Setup

As shown in Figure 1, a 5 1/2" oil-well casing, with the length of 8 meters, was fixed horizontally upon 4 concrete bases. Along its axial direction, 15 square windows, 100 mm×100 mm, were cut and covered with plexiglass. For the convenience of expression, these windows were specified numbers as #1, #2 etc according to the distance from the nozzle. An open steel tank, with the size of 200 mm×200 mm×1800 mm, can be fixed against any one of these glass windows with good seal. The hydrophones will be placed in it. At one end of the casing, the nozzle was set up at the center axial; at the other end, a vortex-street flow meter was installed to calculate exactly the nozzle's exiting speed, which was adjusted through a additional valve fixed on the inlet pipe line.

The signal was detected and analyzed with a Type 2825 double channel real time analysis system manufactured by B&K Co of Denmark. The system used in this experiment includes two hydrophones, 8103/8105, a NEUX 2692 charge amplifier, two Type 3016 data acquisition/conversion modules and Pulse-Labshop software, with frequency responding range of 102.4 KHz. Through fast Fourier transformation (FFT), such function types as time-amplitude, auto spectrum, cross spectrum, coherence, signal-to-noise ratio, auto-correlation, cross-correlation, frequency response, etc can be measured and displayed in the screen. Using a Main cursor or a Delta cursor, a peak value or the average value in some frequency ranges can be read exactly. There are three kinds of signal average modes able to be selected: liner, exponential and peak average, through any one of which a maximum 10^5 average times can be set to eliminate random difference as much as possible.

3.3 Experiment Methods

In this experiment, 6 kinds of flow rates read by the vortex-street flowmeter were set by adjusting the valve, corresponding to the jet's exiting velocity as 52, 65, 77, 88, 100 and 112 m/s respectively. Along the casing's axial direction, the measurements were taken at 6 windows, one by one, with stand-off being 0, 200, 400, 600, 800 and 900 mm.

Using the interface of the software, the line number on the horizontal axis was set at 3200, so that when the low-pass was selected as 102.4 KHz, the band-width became 32 Hz automatically. At every window under every flow velocity, such real time functions as time-amplitude, auto spectrum, cross spectrum and coherence were measured at the same time. Also, as far as the measurement efficiency is concerned, the average time was set at 500. Before the experiment, the static signal was measured as a reference. That is, when the signal over 20 KHz nearly overlapped with the static signal, it could be determined that the noise resulting from cavitation has attenuated completely. Measurement was stopped here. Based on this point, the signals at only 6 windows (maximum stand-off 900 mm) were measured.

4. EXPERIMENTAL RESULTS AND ANALYSIS

As shown in the expression of the cavitation number K (Konype, 1985),

$$K = \frac{P_0 - P_b}{\frac{1}{2} \rho V_0^2}$$

where:

- P_0 -- absolute pressure;
- P_b -- saturated vapor pressure;
- V_0 -- flow velocity;
- ρ -- fluid density.

The value of K will decrease when the flow velocity V_0 rises if other conditions remain constant. Then, the cavitation in the shear layer will be enhanced dramatically. Because of the signal attenuation, the curves of spectrum-velocity are various at different windows. In this paper, only the signals at the #2 window (200 mm stand-off) were analyzed because under the same velocity, its noise power was strongest among this windows.

4.1 The Relationship Between Signal Power and Velocity at Different Frequency Band

Figure 2 shows the tendency of the power spectrum at different bands changing with velocity measured at #2 window. The reference of the vertical coordinate value dB was set at 10^{-12}Pa^2 . It was found that the value of the signal power increases clearly with the increment of velocity at every frequency band. In addition, the signal power at lower frequencies is more sensitive to flow velocity than that at higher ones. For instance, when the flow velocity rises from 52 m/s to

112 m/s, the signal power at 4-7 KHz soars from 130.8 dB to 171.3 dB correspondingly, an increment of 40.5 dB. However, for the power at the band of 18-20 KHz, this value is only 23.7 dB.

When the flow velocity changes from 65 m/s to 80 m/s, a sudden increase in high frequency band curves appears. Correspondingly, when the flow velocity rises from 65 m/s to 88 m/s, the signal power value increases by 22.8 dB at the band of 4-6 KHz. But there is little change when the velocity ascends from 88 m/s to 112 m/s. For the band of 18-20 KHz, the two changes are 16.2 dB and 5.4 dB, corresponding to velocity changes above. In other curves of different frequency bands, there is a similar result. In the author's opinion, there is a critical velocity about water jet cavitation in oil well casings. When the flow velocity becomes higher than this point, that is, about 80 m/s, cavitation will happen dramatically, emitting strong noise while the micro-bubble collapses dramatically. When the velocity exceeds 88 m/s, only the cavitation range becomes large, while the signal power is unchanged.

4.2 Relationship between Noise Signal Power and Stand-off

As shown in Figure 3, the general tendency of the signal power at the band of 0-20 KHz decreases with the increment of stand-off. While under the lower velocities (<88 m/s), it changes to a great degree as the measurement point moves farther away the nozzle. At the same time, the signal power value rises to a larger extent when flow velocity increases. For example, at the velocity of 65 m/s, the power value decreases 17 dB within 900 mm axially, and such value at the stand-off 600 mm is 166.8 dB; when the velocity becomes 77 m/s, these two values are 10 dB and 175.4 dB. That is, at this axial point, it increases 8.6 dB under a velocity increase of 12 m/s. When flow velocity exceeds 88 m/s, the curves becomes different. It can be seen that when this value changes from 88 m/s to 100 m/s, and the velocity gradient is 12m/s, there is almost no change in signal power at the same stand-off. Such phenomena accords well with the results in 4.1. After fully cavitation, the amplitude of noise in the fluid will hardly increase with the jet velocity.

4.3 Relationship between Attenuation Coefficient and Noise Frequency

With respect to the wave attenuation in viscous media, according to the single dimension N-S Equation (B.Z. Hu, 1996), the wave amplitude attenuation can be expressed as:

$$A = A_0 e^{-\alpha x} \cdot e^{j\omega \left(t - \frac{x}{c} \right)},$$

where:

A_0 – wave amplitude when no attenuation;

α – attenuation coefficient

ω – angular frequency, $\omega=2\pi f$

x – propagation distance

c – propagation velocity in a specified media

Therefore, for two points, x_1 and x_2 , along wave propagating direction, α can be developed through above equation as:

$$\alpha = \frac{1}{x_2 - x_1} \ln \frac{A_2}{A_1}$$

Figure 4 indicates the relationship between α and frequency, which is the average of three α values calculated with the signal power data at #1, #2 and #5 windows. Compared with general law, in which attenuation coefficient rises with frequency, there appears an unexpected tendency below 5 KHz under this experimental condition. That is, a local peak value (at about 3 KHz) exists in the frequency band of 0-5 KHz, after which the coefficient soars with frequency as usual. Also, as for different flow velocities, the coefficient runs differently. When the flow velocity is lower than 66 m/s, it almost stays smooth with the increment of frequency. After that, except at 100 m/s (to be proven later), the higher the flow velocity is, the higher the soaring rate is, which means even for signals at the same frequency point, those generated from higher flow velocities will attenuate faster than that from lower velocities. The authors still can not clearly explain this phenomena. It may have some relation to the casing wall resonance.

4.4 Time-Amplitude Curves at Different Velocities

As shown in Figure 5, the signal amplitude can be seen directly from these figures. Once again, the critical point of velocity at 88 m/s is proven here. That is, when it rises above this point, there is less increment of vibration amplitude with the enhancement of flow velocity. In Figure 5-a, the maximum amplitude under 52 m/s is about 600 Pa, while 65 m/s, 4 KPa. After 88 m/s, this value stays approximately at 20 KPa, even at 112 m/s in Figure 5-f. On the other hand, through calculation, there exists at about 70 Hz a low frequency wave in Figure 5-a. However, such waves becomes more and more ambiguous with the rise in flow velocity.

5. CONCLUSIONS

1. Generally, with the increase of nozzle exiting velocity, the cavitation noise in oil well casings will become strong. However, there exists a critical velocity point (at about 80 m/s). Around this point, the noise power will ascend to a high degree; once exceeding it, the power value becomes smooth with the increment of flow velocity.

2. The noise power attenuates along the casing's axial direction. Within the measured range, the descending gradient is higher at lower velocities than at higher ones. In addition, the three curves (drawn from the velocities above 88 m/s) almost overlap this figure.
3. Under these experimental conditions, there appears to be an abnormal phenomenon in the attenuation coefficient figure. That is, only for the noise signals above 5 KHz, will their power attenuation go up with the increment of frequency.
4. In the time-amplitude figures, there is about 70 Hz waves at lower flow velocities. Also, the fluid vibration amplitude soars with the velocities. However, when the velocity exceeds 88 m/s, that low frequency wave becomes ambiguous. At this time, the vibration amplitude will not rise with the velocities.

6. ACKNOWLEDGEMENTS

The research was supported by China National Natural Science Fund. Also, the authors would express their thanks to Professor Li Zhongyi and Professor Qiao Wenxiao for their help on the experiment setup and signal analysis.

7. REFERENCES

- Hu, Bozhong., "*Oil Production with Wave Field*", pp 8-11, 1996.
- Jiang, Guojian. , "*A Mathematic Model of Ship Propeller Cavitation Noise*", Acoustics Journal, Vol. 23, No.5, 1998.
- Konype, R.T., "*Cavitation and Corosion*", pp 96-97, pp 160, translated in1981.
- Ma, Dayou., "*Noise Control*", pp 180-183, 1987.
- Phlipp A., and Lauterborn, W., "*Cavitation Erosion by Single Laser-produced Bubble*", Fluid Mechanics, Vol. 361, pp 75-116, 1998.
- Qi, Dingman. , "*A Study of the Feature of Cavitation Noise Spectrum*", Vibration and Impact, Vol.18, No.3, 1999.
- Yuri, T.D., "*Hot Spot during Cavitation in Water*", American Chemical Society, Vol.121, pp 5817-5818, 1999.

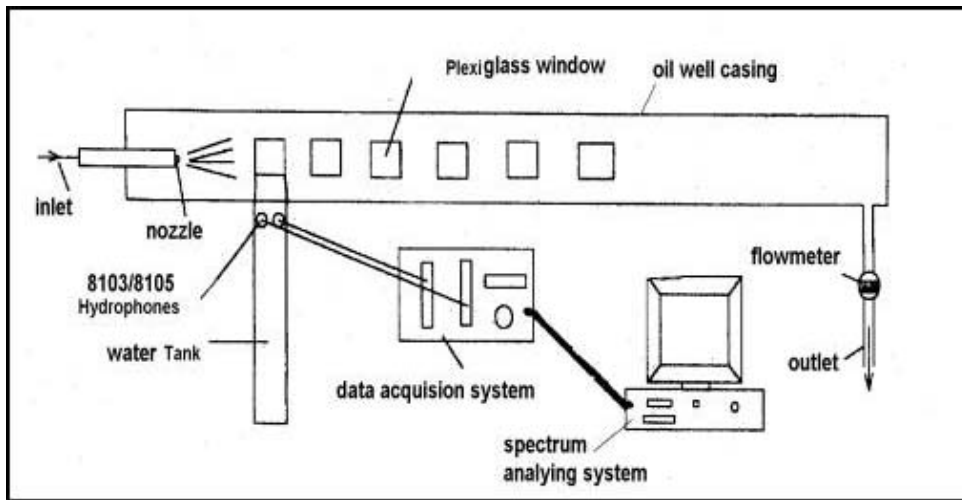


Figure 1. Schematics of Experimental Setup

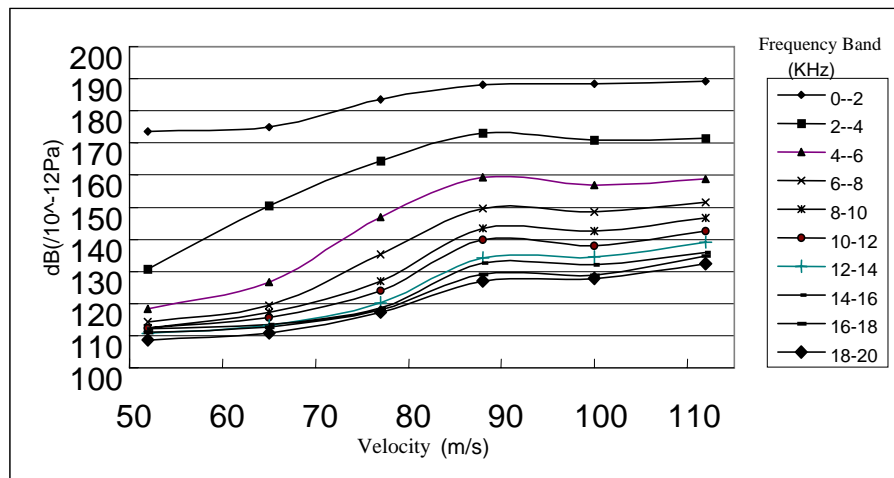


Figure 2. Relationship between Signal Power and Velocity at Different Frequency Band

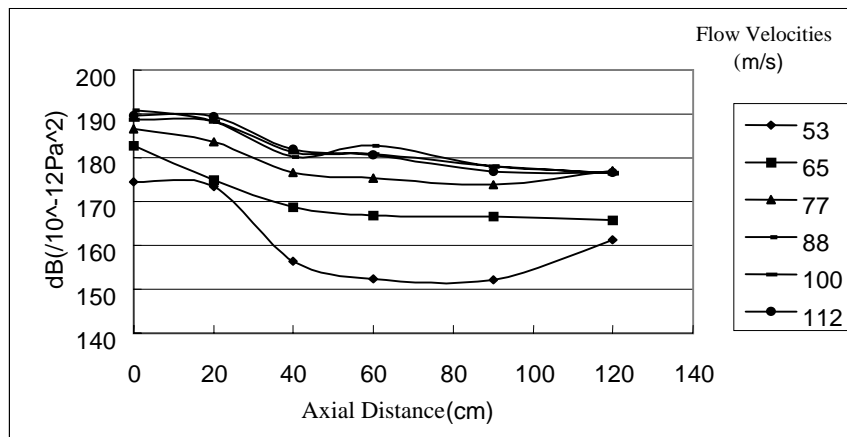


Figure 3. Relationship between Noise Signal Power and Stand-off

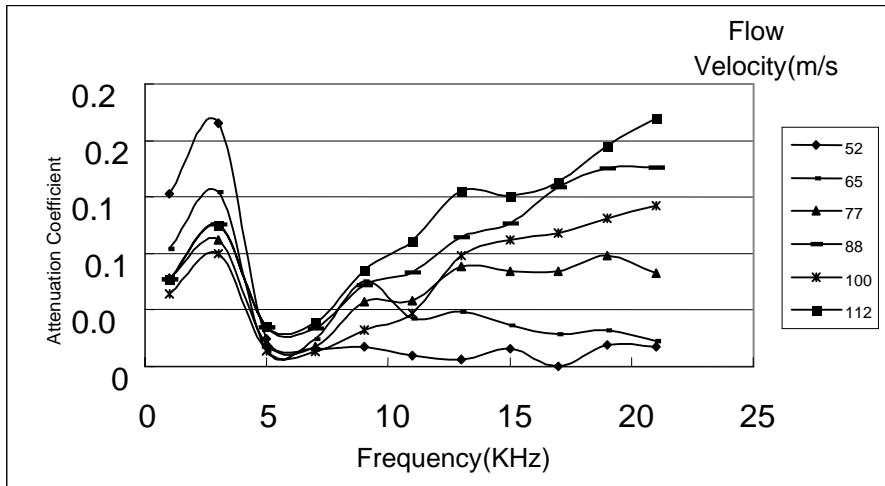


Figure 4. Relationship between Attenuation Coefficient and Frequency

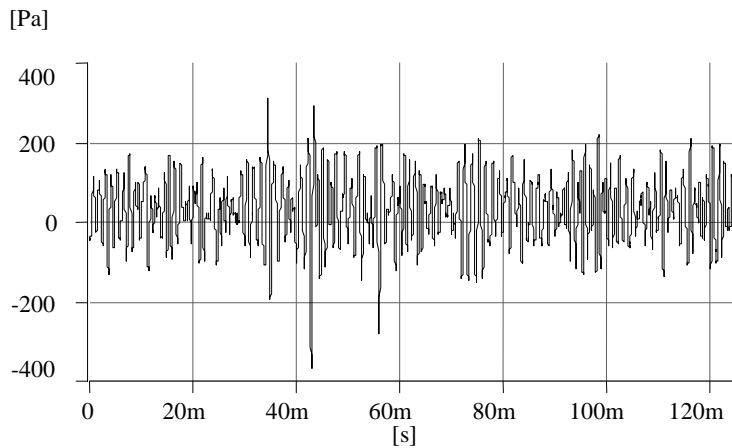


Figure 5-a. Time-Amplitude Curves at the Velocities of 52m/s

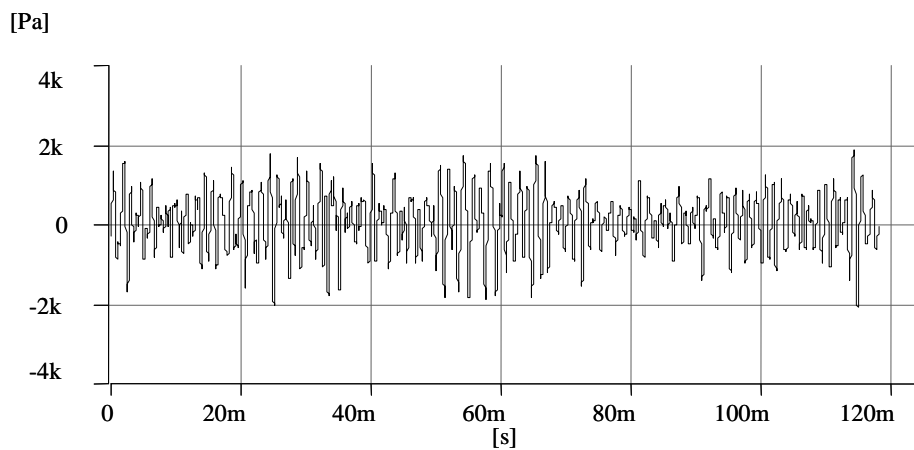


Figure 5-b. Time-Amplitude Curves at the Velocities of 65m/s

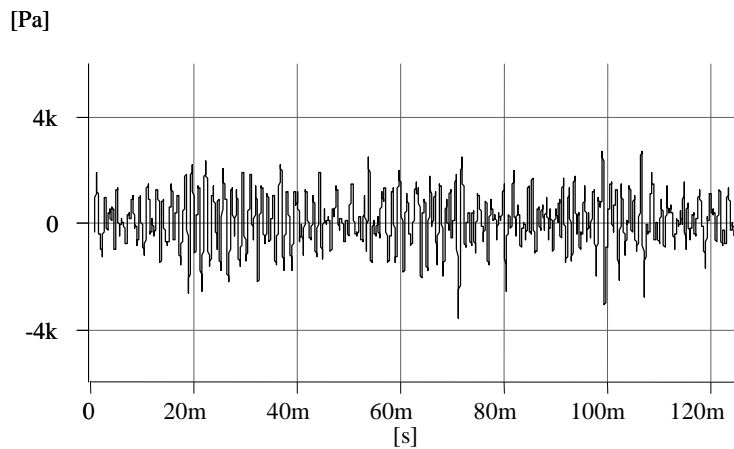


Figure 5-c. Time-Amplitude Curves at the Velocities of 77m/s

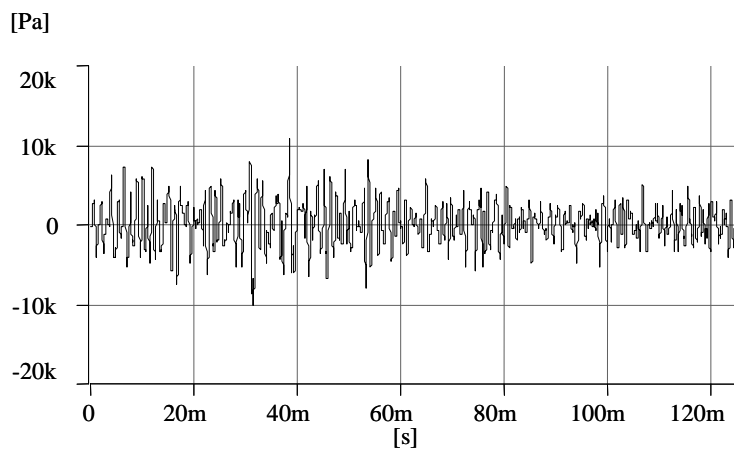


Figure 5-d. Time-Amplitude Curves at the Velocities of 88m/s

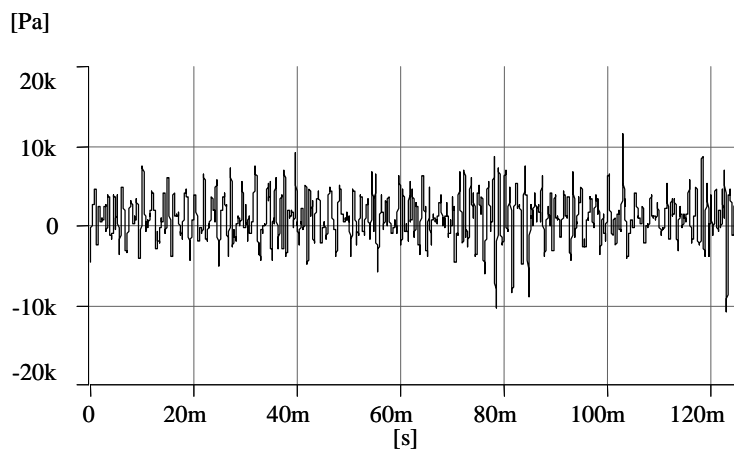


Figure 5-e. Time-Amplitude Curves at the Velocities of 100m/s

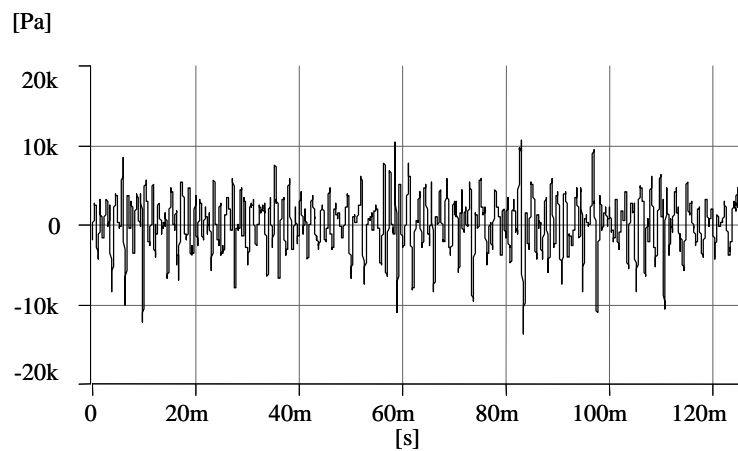


Figure 5-f. Time-Amplitude Curves at the Velocities of 112m/s

TESTING OF MINERAL TYPES OF ABRASIVES FOR ABRASIVE WATER JET CUTTING

J. Foldyna, P. Martinec, L. Sitek
Institute of Geonics of the Czech Academy of Sciences
Ostrava, Czech Republic

ABSTRACT

Comparative tests of olivine and three types of garnet almandine abrasives used in high-speed water jet cutting were performed in the Institute of Geonics in Ostrava. Tests of both cutting efficiency of abrasives and wearing effect on focusing tube were performed. The cutting efficiency of abrasive materials was tested according to the methodology developed in the Institute of Geonics in Ostrava. The testing procedure is based on carrying out of cuts in wedge shaped samples (made from granodiorite and mild steel) under the standard conditions. Test results are expressed as a comparison of cutting ability of tested abrasive materials with cutting ability of reference abrasive (Barton HP80). The results obtained in these tests indicate significant differences in cutting efficiency of individual tested abrasives. The wearing effect of abrasive materials on focusing tube was tested according to methodology developed in the Institute of Geonics in Ostrava. The methodology is based on measurement of focusing tube mass loss as a function of time (rate of mass loss) and thus allows prediction of focusing tube life. Test results are expressed as a comparison of wearing effect of tested abrasive material with wearing effect of reference abrasive (Barton HP80). The results obtained in these tests indicate quite distinct wearing effects of tested garnet almandine abrasives and, on the other hand, significant difference in wearing effects of olivine abrasive compared to that of garnet almandine abrasives.

1. INTRODUCTION

Research of abrasives in the Institute of Geonics of the Czech Academy of Sciences in Ostrava is, among others, oriented at determination of suitability of commercially available mineral types of abrasives for the use in abrasive water jet cutting. In the paper, study of three types of almandine garnet abrasives and one type of olivine abrasive is presented as an example of such a research of mineral types of abrasives. These abrasives were selected for the tests with respect to their relatively low price and commercial availability on the Czech market.

Abrasive material evaluation was performed using following standard procedures: grain size distribution of input abrasive concentrate was determined according to Czech standard EN 933-2 (72 1184), density of abrasive concentrate was determined according to Czech standard 72 1154, cutting tests and tests of wearing effect of abrasive material on focusing tube were performed according to methodologies developed in the Institute of Geonics of the Czech Academy of Sciences in Ostrava (IG methodologies) and published by Martinec & Foldyna (1997), Martinec et al. (1998) and Foldyna et al. (2000).

2. TESTED SAMPLES OF ABRASIVES

Both standard cutting tests on steel and granodiorite samples were performed using all tested abrasives in as delivered condition.

Macroscopic description, mineralogical analysis and basic properties of tested samples of abrasives are summarized in following sections and Table 1. Grain size distributions of input samples and crushed abrasives after slot cutting under experimental conditions defined in the IG methodology (Martinec & Foldyna (1997), Martinec et al. (1998)) are presented in Tables 2 to 6.

2.1 Garnet I

The abrasive consists of polygonal mineral grains of garnet – almandine (almandine with low content of pyrope and spessartine components (about 92%), and almandine with low content of pyrope component (about 2%)), and admixture of other minerals (magnetite and titanomagnetite (about 6%), zircon and rutile (less than 1%), quartz, micas, feldspars (less than 1%)). Grains of almandine garnet comprise diverse shapes represented by combination of abraded rounded grains and polygonal angular ones (see Figure 1-a). Primary surface of garnet grains is partially rounded. Crushing of bigger primary grains formed angular grains – new surfaces were created by separation of stable parts along natural fracture cracks (Figure 1-b). Leaching out of mineral inclusions forms cavities on the primary surface of grains. The surface of new grains after crushing is rough and jagged, with deposition of secondary minerals (Figure 1-c).

2.2 Garnet II

The abrasive consists of polygonal mineral grains of garnet – almandine (almandine with low content of pyrope and spessartine components (about 80%), and almandine with low content of pyrope component (about 8%)), and admixture of other minerals (magnetite and titanomagnetite (about 10%), zircon and rutile (about 2%), quartz, micas, feldspars (less than 1%)). Grains of

almandine garnet are rounded, without sharp edges (Figure 2-a). Primary surface of grains is typical for natural garnet sand (garnet after aqueous abrasion) – Figure 2-b. Grains are fractured by natural cracks that creates preferred planes for breaking-up in the process of interaction of garnet grains with high-speed water jet – Figure 2-c.

2.3 Garnet III

The abrasive consists of crushed mineral grains of garnet – almandine separated from massive rocks (almandine with low content of pyrope component (about 90%), almandine with low content of pyrope and spessartine components (about 2%)), and admixture of other minerals (pyrite, chalkopyrite and magnetite (about 3%), leukoxen and rutile (about 1%), quartz, micas, feldspars (about 4%)). The concentrate exhibits various shapes of individual grains (Figure 3-a). Garnet grains are sharp edged, polygonal. All grains demonstrate massive damage by net of cracks. These cracks are both natural and induced by technological processes of grinding and separation (Figure 3-b). Crack-walls are planar with conchoidal fracture (Figure 3-c). The fine net of cracks enable easy and deep destruction of primary grains during interaction between abrasive grain and high-speed water jet.

2.4 Olivine

The abrasive consists of grains of natural olivine separated from the massive rocks (olivine with dominance of Mg_2SiO_4 component (about 92%), and low content of Fe_2SiO_4 component (about 8%)), and admixture of opaque ore minerals (less than 0.5%). Grains are consistent both in size and shape (Figure 4-a). Grains are polygonal, non-regular, damaged by fine net of cracks (Figure 4-b). Two types of cracks can be determined in grains: (1) non-regular cracks induced by technological processes of grinding and separation and (2) planar cracks oriented parallel to (001) plane in olivine crystal (natural cracks) – Figure 4-c. Combination of this two systems of cracks can initiate new fracture planes and consequently create very easy and deep destruction of abrasive grains in interaction processes with high-speed water jet.

3. TESTING OF CUTTING PERFORMANCE OF ABRASIVES

Cutting tests with almandine garnet and olivine abrasives were performed according to IG methodology (Martinec & Foldyna (1997), Martinec et al. (1998)). The testing procedure is based on carrying out of cuts in wedge shaped samples (made from granodiorite and mild steel) under the standard conditions. Tests were performed using commercially available cutting head for generating of abrasive water jet “Jet Edge Permalign Abrasive Cutting Head” (mixing chamber part No. 36329) at two operating pressures (250 and 350 MPa), other cutting parameters were maintained constant: nozzle diameter 0.25 mm, focusing tube diameter 1.0 mm, focusing tube length 76 mm, stand-off distance 2 mm, abrasive feed rate 250 g/min at pressure of 250 MPa and 300 g/min at pressure of 350 MPa.

Firstly, five cuts at constant traversing velocity (100 mm/min for steel sample and 250 mm/min for granodiorite sample) were performed at pressure of 250 MPa and abrasive feed rate of 250 g/min. Next, another five cuts were performed at pressure of 350 MPa and abrasive feed rate of 300 g/min at the same traversing velocities.

The maximum thickness of the sample cut through by the abrasive jet was measured for all cuts performed in both types of testing samples. Average values of depth of cut (corresponding to maximum depths of cut achievable in given material under given cutting conditions) and their standard deviations were calculated for individual materials and operating pressures.

Testing results were expressed as a comparison of cutting ability of tested abrasive materials with cutting ability of reference abrasive - almandine garnet Barton HP80. All tested abrasives are compared according to relative cutting depth. See Figure 5 for results in steel and Figure 6 for results in granodiorite.

Results indicate that the best cutting performance in mild steel sample (comparable to that obtained with reference abrasive) was obtained using Garnet III abrasive at both operating pressures. The cutting performance of Garnet I and Garnet II was slightly lower at pressure of 350 MPa and significantly lower at pressure of 250 MPa compared to performance of reference abrasive. The cutting performance of olivine abrasive was slightly lower compared to performance of reference abrasive at both pressures.

On the other hand, the best cutting performance in granodiorite sample (higher in comparison with performance of reference abrasive) was obtained using Garnet I abrasive at both operating pressures. Slightly lower performance at both pressures was obtained using Garnet II abrasive. The cutting performance of Garnet III abrasive was almost identical to the performance of reference abrasive. The cutting performance of olivine abrasive was 26 to 27% lower compared to performance of reference abrasive at both pressures.

The cutting performance of Garnet I and Garnet II abrasives is likely influenced by the fact that these abrasives contain significant amount of bigger grains. The higher content of bigger grains influences the cutting performance in a positive way when cutting granodiorite, and in a negative way when cutting steel sample. On the other hand, the presence of bigger grains in garnet III abrasive has almost no influence on cutting performance – these grains break-up during the interaction with high-speed water jet due to their massive damage by net of cracks.

The results obtained with garnet abrasives indicate that the cutting efficiency is also influenced by the genesis of the abrasive material – garnet abrasives separated from “heavy sands” does not contain grains with internal stress and also extremely damaged parts of grains are removed from the material by the natural processes.

4. TESTING OF WEARING EFFECTS OF ABRASIVE MATERIAL ON FOCUSING TUBE

In spite of excellent cutting performance, certain types of abrasives may not be suitable for application in abrasive water jet cutting due to their excessive wearing effects on focusing tube. Therefore, the methodology of determination of wearing effect of abrasive material on focusing tube was developed in the Institute of Geonics CAS in Ostrava (Foldyna et al. (2000)). The methodology is based on measurement of focusing tube wearing by determination of focusing tube mass loss as a function of time (rate of mass loss) and thus allows prediction of focusing tube life.

The measurement of wearing effect of tested abrasive materials on focusing tube was performed under standard conditions: operating pressure 350 MPa, nozzle diameter 0.30 mm, and abrasive feed rate 350 g/min. Commercially available focusing tube Flow (part No. 010460-30-30) with diameter of 0.8 mm, and length of 76 mm was used in the test.

Before measurement, the weight of new tube, w_0 , was determined using scales with precision of 0.1 mg. Then, cutting was performed under above-mentioned conditions. After one hour of cutting, the focusing tube was removed from cutting head, dried, cleaned and the weight of tube, w_1 , was determined. The same procedure was repeated after two hours of cutting. Again, weight of tube, w_2 , was determined.

To evaluate results obtained from the above test, rates of mass loss of the focusing tube for each hour of cutting Δw were calculated using following formulas:

$$\Delta w_1 = w_0 - w_1 \quad (1)$$

$$\Delta w_2 = w_1 - w_2 \quad (2)$$

Average rate of mass loss of the focusing tube $\bar{\Delta w}$ can be calculated as follows:

$$\bar{\Delta w} = \frac{w_0 - w_i}{i} \quad (3)$$

Assuming that focusing tube life is determined by increase of the inner diameter of the tube from 0.8 mm to 1.50 mm (in average), the nozzle life t can be roughly estimated using following formula:

$$t = \frac{0.1\rho}{\bar{\Delta w}} \quad (4)$$

Testing results are expressed as a comparison of estimated relative nozzle life using tested abrasive material with estimated relative nozzle life using reference abrasive (almandine garnet Barton HP80). Results of the test are presented in Figure 7.

Results indicate that relative nozzle life differs significantly for tested garnet – almandine abrasives. If one uses Garnet II abrasive, the relative nozzle life can be 25% higher compared to use of reference abrasive or Garnet I abrasive. This is probably due to the fact that Garnet II is natural garnet sand with rounded grains and without sharp edges. It is of interest to note that use of olivine abrasive can increase relative nozzle life more than nine times compared to reference abrasive.

5. CONCLUSIONS

Depths of cut obtained using garnet – almandine and olivine abrasives in steel and granodiorite samples indicate quite significant differences in cutting efficiency of individual tested abrasives. Authors believe that the cutting efficiency of all tested abrasives could be improved by the better sorting and selection of proper grain size for given material – i.e. coarser grains for cutting granodiorite and finer grains for mild steel.

Cutting efficiency of olivine abrasive in granodiorite cutting is relatively low compared to reference abrasive almandine garnet Barton HP80. Therefore, authors cannot recommend this abrasive for cutting of very hard rock and similar materials.

Wearing effects of tested almandine garnet abrasives are up to 25% lower compared to reference abrasive almandine garnet Barton HP80. Therefore, these abrasives can be recommended for utilization in abrasive water jet cutting.

Wearing effects of olivine abrasive are more than nine times lower compared to reference abrasive. If one takes into consideration also its satisfactory cutting efficiency in mild steel sample, olivine abrasive can represent suitable, operating cost saving alternative of almandine garnet abrasives when cutting metal materials.

6. ACKNOWLEDGEMENT

Presented work was performed within the framework of research project of the Czech Academy of Sciences No. K3012103 and INCO-Copernicus project No. IC15-CT98-0821. Authors are thankful for the support.

7. REFERENCES

- Martinec, P., and Foldyna, J., “Methodology of determination of cutting efficiency of abrasive materials in abrasive water jet cutting,” *Geomechanics 96 (Proceedings of the International Conference Geomechanics 96, Rožnov p. R. / Czech Republic / 3-6 September 1996)*, pp. 397–401, A. A. Balkema Publishers, Rotterdam, Netherlands, 1997.
- Martinec, P., Mašláň, M., Hlaváč, L., Foldyna, J., Sitek, L., and Malík, J., “Mathematical modeling of mineral grain failure caused by high pressure water and abrasive jet action, mineralogy of abrasives and the way of failure of garnets for two isomorphous series”, Final report of grant project of Grant agency of the Czech Republic No. 205/96/0931, Ostrava, Czech Republic, 1998.
- Foldyna, J., Martinec, P., and Sitek, L., “Testing of industrial types of abrasives for abrasive water jet cutting”, *Proceedings of the 6th Pacific Rim International Conference on Water Jet Technology, Sydney, Australia*, pp. 143-147, CMTE, Australia, 2000.

8. NOMENCLATURE

i	duration of the test [hours]
S_0	sorting coefficient [-]
S_k	symmetry coefficient [-]
t	estimated nozzle life [hours]
w_0	weight of a new focusing tube [mg]
w_1	weight of a focusing tube after one hour of cutting [mg]
w_2	weight of a focusing tube after two hours of cutting [mg]
w_i	weight of a focusing tube after i hours of cutting [mg]
Δw	rate of mass loss of the focusing tube [mg/hour]
$\overline{\Delta w}$	average rate of mass loss of the focusing tube [mg/hour]
ρ	density of focusing tube [kg m^{-3}]

Table 1. Properties of tested abrasives

Abrasive	Garnet I	Garnet II	Garnet III	Olivine
Mineral	Garnet-almandine	Garnet-almandine	Garnet-almandine	Olivine
Locality	India	Australia	Ukraine	Norway
Grain size [Mesh]	80	80	80	80
Mineralogical purity [%]				
Color	Transparent light violet-red to brown red	Transparent light violet-red to dark brown red	Transparent dark brown red to transparent light violet-red	Transparent very light gray-green
Color after oxidation at 900°C	Dark red-brown	Very dark red-brown (cocoa)	Very dark red-brown (cocoa)	Very light red-brown (brick)
Massive damage (% of number of grains)	10 – 20	30 – 40	70 – 80	85 – 95
Roundness of grains (Pettijohn) [-]	0.2 – 0.6	0.4 – 0.8	0.2 – 0.6	0.0 – 0.8
Sphericity of grains (Wahlstrom) [-]	0.0 – 0.4 (0.6)	0.25 – 0.8 (1.0)	0.0 – 0.25 (0.4)	0.0 – 0.15
Density of powdered material [kg.m^3]	4052	4084	4091	3332
Bulk density of grains [kg.m^3]	4051	4060	4077	3071
Hardness – Mohs [-]	7	7	7	7

Table 2. Grain size distribution of tested abrasives at the input to the mixing chamber – focusing tube system, sorting

	Garnet I	Garnet II	Garnet III	Olivine
Grain size	% of weight			
Below 0.09 mm	0.1	0.3	2.5	2.7
0.09-0.12mm	0.4	0.9	5.4	5.5
0.12-0.25 mm	33.3	37.2	43.1	80.5
0.25-0.315 mm	45.0	59.3	32.1	10.9
Over 0.315 mm	21.2	2.3	16.9	0.4
Average grain size [mm]	0.273	0.263	0.247	0.187
Sorting coefficient S_0	1.20	1.20	1,32	1.25
Symmetry coefficient S_k	0.89	0.85	0.84	0.96

Table 3. Grain size distribution of tested abrasives after the slot cutting in mild steel at 250 MPa

	Garnet I	Garnet II	Garnet III	Olivine
Grain size	% of volume			
Below 1 micron	0.7	0.9	1.2	1.0
1-12 microns	4.9	7.1	11.3	10.4
12-48 microns	27.1	29.8	33.4	36.1
48-96 microns	45.6	43.8	42.2	43.0
96-192 microns	21.7	18.4	11.9	9.5
Average grain size [microns]	71	66	55	51

Table 4. Grain size distribution of tested abrasives after the slot cutting in mild steel at 350 MPa

	Garnet I	Garnet II	Garnet III	Olivine
Grain size	% of volume			
Below 1 micron	1.0	1.4	2.2	1.4
1-12 microns	8.0	11.7	18.9	15.5
12-48 microns	31.5	36.9	40.4	40.5
48-96 microns	43.8	41.1	33.3	36.8
96-192 microns	15.7	8.9	5.2	5.8
Average grain size [microns]	64	48	37	41

Table 5. Grain size distribution of tested abrasives after the slot cutting in granodiorite, 250 MPa

	Garnet I	Garnet II	Garnet III	Olivine
Grain size	% of volume			
Below 1 micron	2.2	2.8	3.4	3.3
1-12 microns	14.2	17.9	19.9	22.2
12-48 microns	23.5	24.3	28.5	32.4
48-96 microns	39.0	36.7	36.6	35.9
96-192 microns	21.1	18.3	11.6	6.2
Average grain size [microns]	69	64	44	39

Table 6. Grain size distribution of tested abrasives after the slot cutting in granodiorite, 350 MPa

	Garnet I	Garnet II	Garnet III	Olivine
Grain size	% of volume			
Below 1 micron	3.9	4.0	4.3	3.5
1-12 microns	23.0	22.2	23.7	21.9
12-48 microns	30.0	26.5	30.2	30.5
48-96 microns	34.4	34.3	35.1	36.3
96-192 microns	8.7	13.0	6.7	7.8
Average grain size [microns]	40	44	38	40

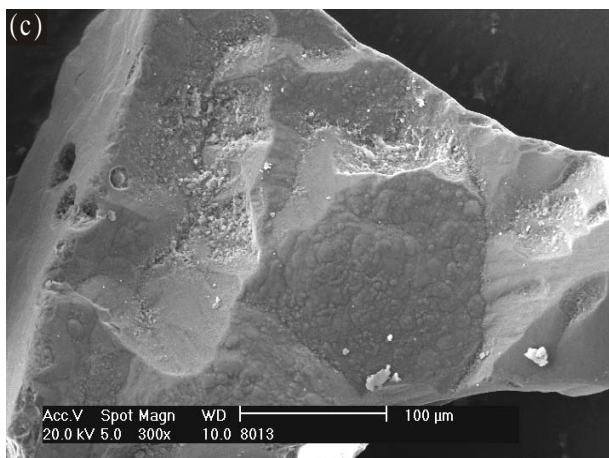
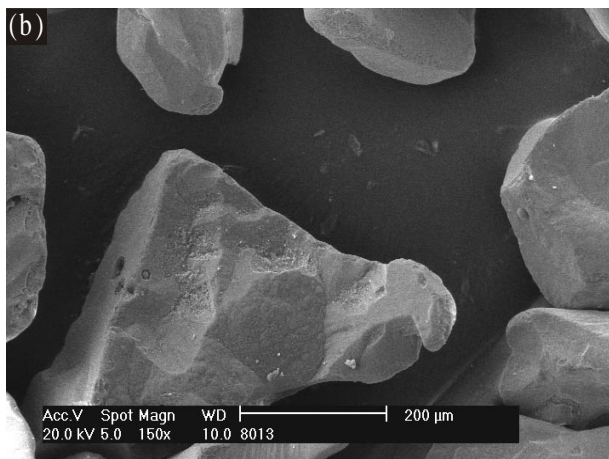
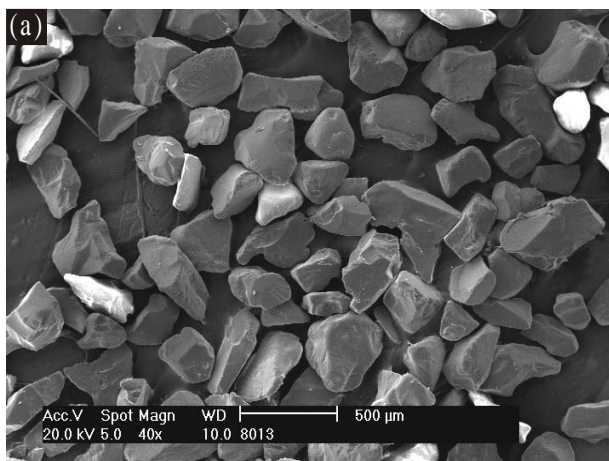


Figure 1. Morphology of grains of garnet I.
(SEM microphotography, magnification is
indicated on pictures by abscissa)

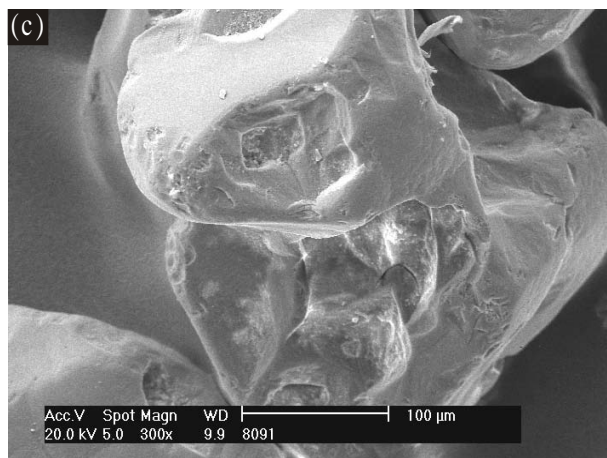
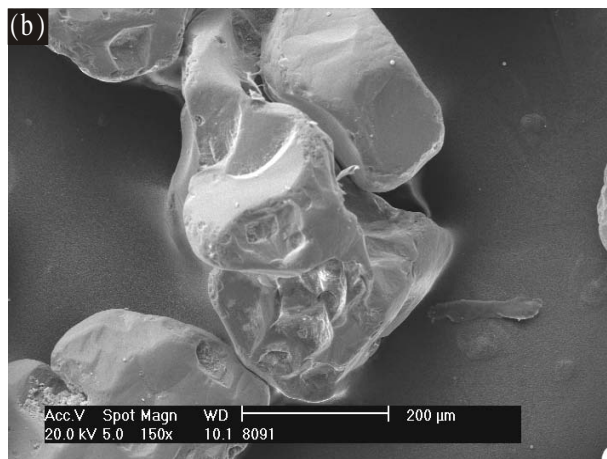
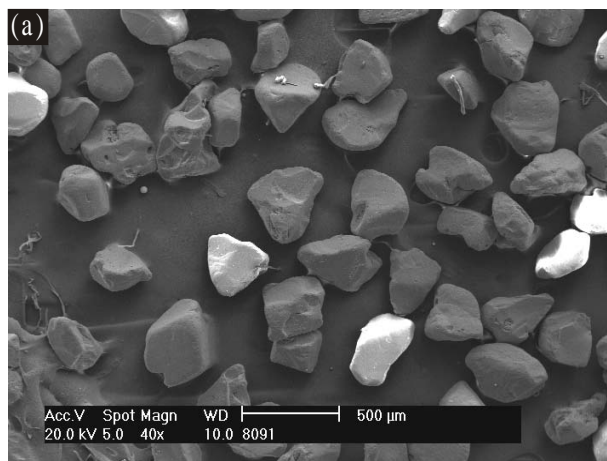


Figure 2. Morphology of grains of garnet II.
(SEM microphotography, magnification is
indicated on pictures by abscissa)

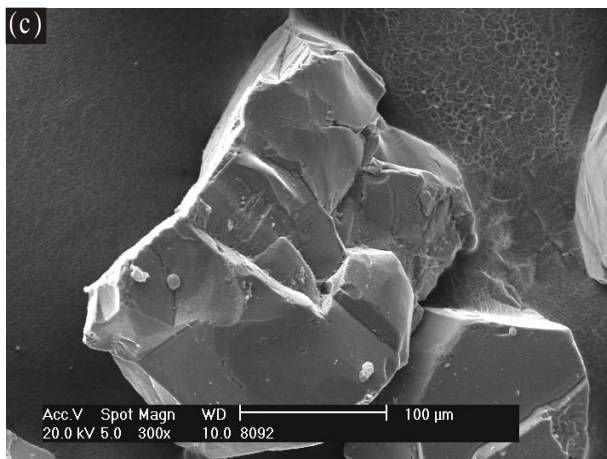
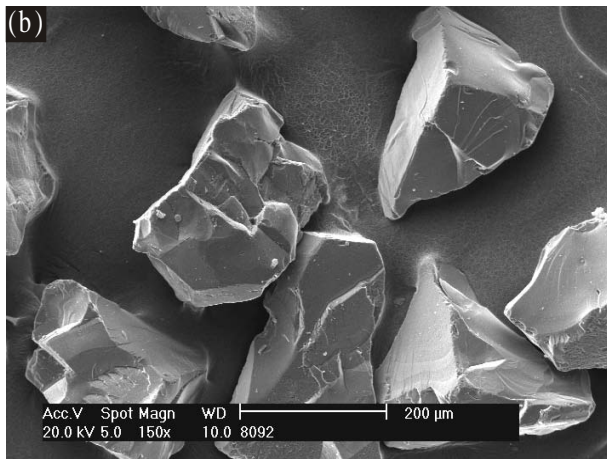
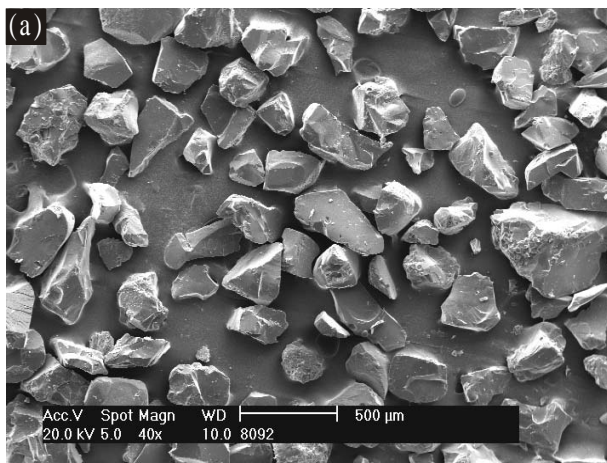


Figure 3. Morphology of grains of garnet III.
(SEM microphotography, magnification is indicated on pictures by abscissa)

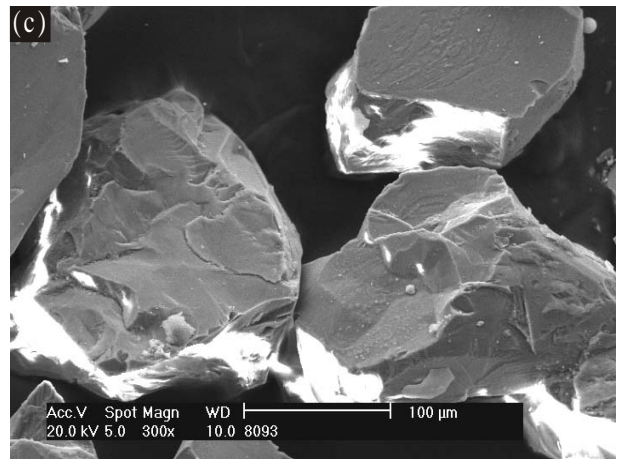
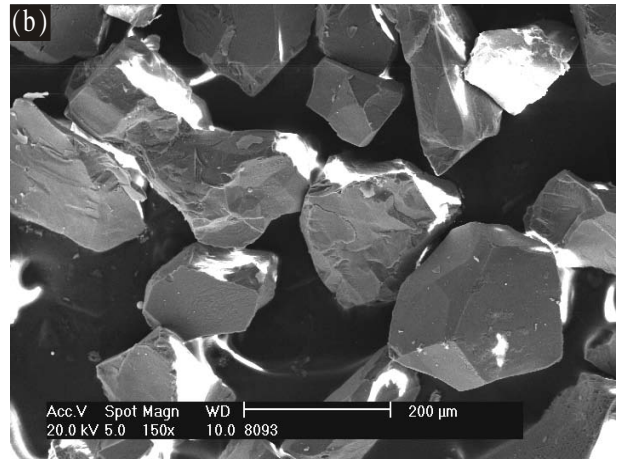
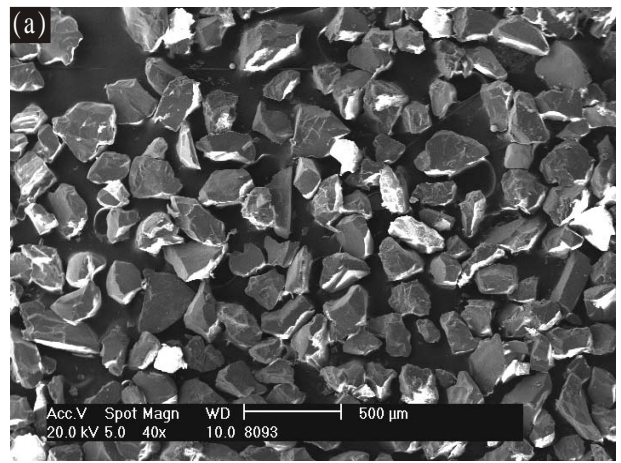


Figure 4. Morphology of grains of olivine.
(SEM microphotography, magnification is indicated on pictures by abscissa)

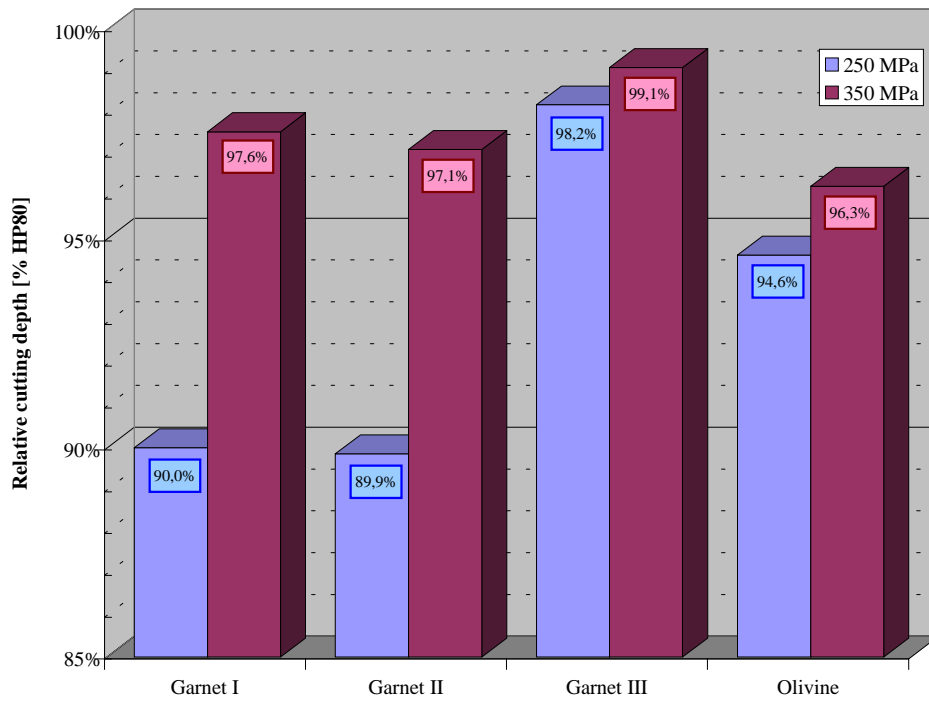


Figure 5. Relative cutting depths for tested abrasives obtained in mild steel.

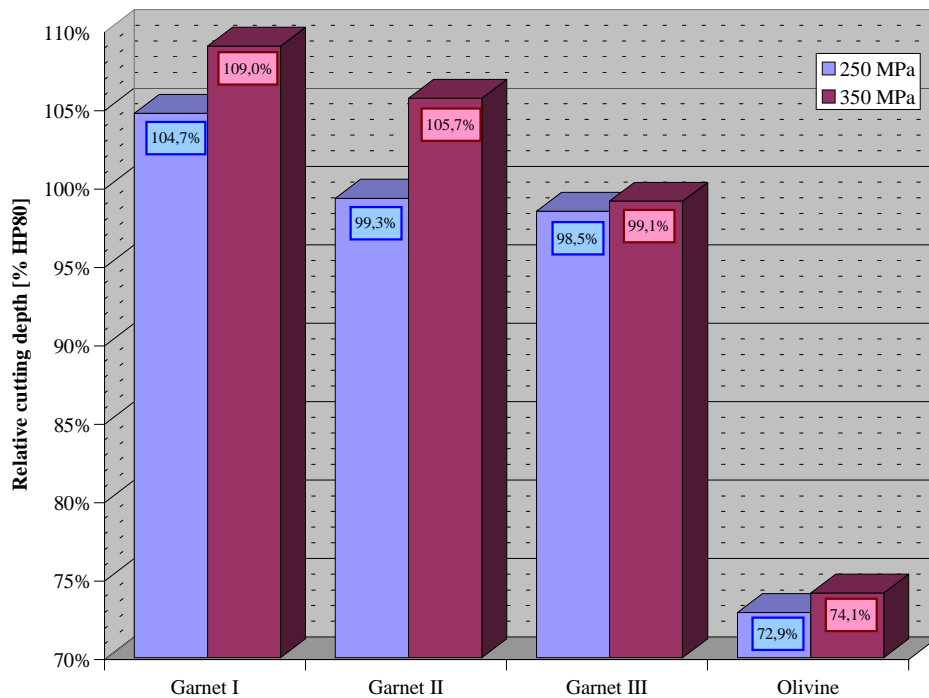


Figure 6. Relative cutting depths for tested abrasives obtained in granodiorite.

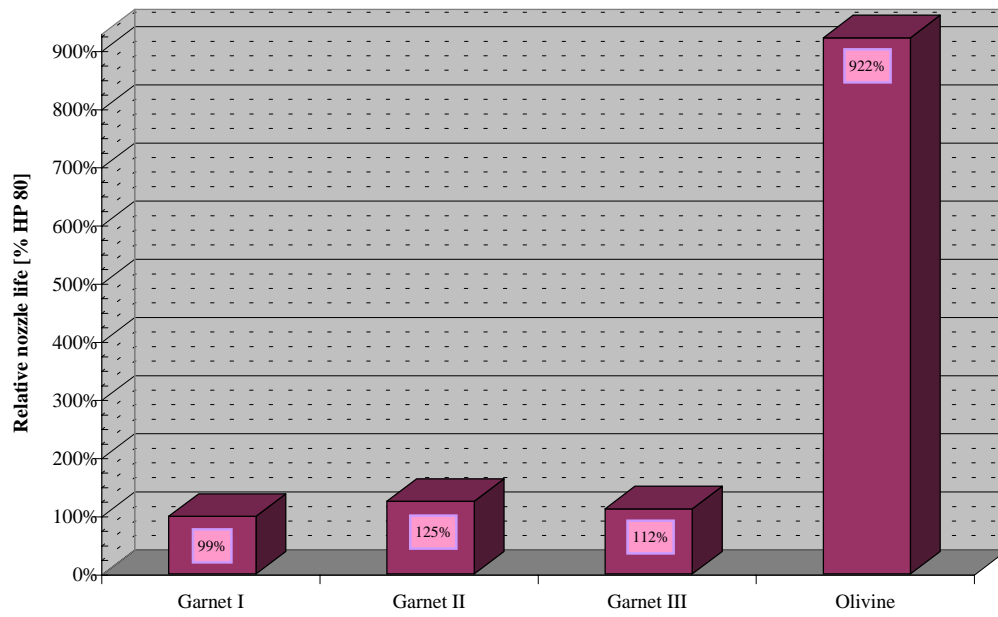


Figure 7. Estimated relative nozzle life for tested abrasive materials.

AWJ TO MACHINE FREE FORM PROFILES IN NATURAL STONE

L. Carrino, W. Polini, S. Turchetta
Dipartimento di Ingegneria Industriale
Università degli Studi di Cassino
Cassino (FR), Italy

M. Monno
Dipartimento di Meccanica
Politecnico di Milano
Milano, Italy

ABSTRACT

Artistic works represent a wide field of application in natural stone. Free-form profiles are involved in internal and external paving of civil house and monument. Once realised manually, the mosaic paving are now mass-produced by means of traditional or innovative machining technologies.

The traditional process uses a diamond mill, which rotates on its own axis, cutting a marble marquetry characterised by a free form profile. This is an old technology that involves both process and tool parameters whose values are defined on the base of the experience of builders and end-users.

The Abrasive Water Jet cutting of marble is a relatively recent process and, therefore, it needs to be completely understood and optimised.

This work shows the results of an experimental study on the influence of AWJ parameters on stone cutting of free-form profiles. It aims to identify the applications where the AWJ results profitable with respect to traditional technology. A shape has been identified, choosing from the typical decorative applications, in order to define the experimental geometry. A set of experimental cuts have been statistically planned and realised by means of AWJ and diamond mill technologies. The quality and the efficiency of the two alternative processes have been investigated and compared. Technical and economical aspects have been discussed.

1. INTRODUCTION

The world stone production has increased, in the last years, up to 110 millions of tons in 1999. It involves marbles, granites and stones, both raw and machined products. The stone products are more and more used for outside and inside flooring, outside and inside covering, home and urban furnishing, civil building (public, commercial or housing) and sacred art.

Nevertheless, the actual marble, granite and stone diffusion may be further increased partially due to the intrinsic difficulty of machining this material. In fact the inclusion of seaweed and fossils in a matrix of calcite crystals has pointed out the limits of the traditional diamond removal manufacturing processes. It is impossible to act on stone composition in order to modify its machinability. Moreover, the pressing request of stone products has made evident the need of optimised cutting methods able to increase the machining efficiency by minimising the production time and, if possible, the costs. Further requirements are the reduction of the discards, with a consequent decreased impact on environment, and of the noise, the improvement of the worker conditions and the safety. Hence, the growing interest of marble has stimulated the study of innovative manufacturing processes in which tools are replaced by an energetic beam.

In this field, the thermal machining processes (laser, plasma, etc.) have limited applications due to the high temperatures imparted to the marble that can cause structural or mechanical changes without cutting the material. These changes are mainly unknown at now.

Among the innovative manufacturing processes that have shown their suitability in marble machining, Abrasive Water Jet (AWJ) may satisfy the demand of non thermal, high productivity, tolerance observant process. A limit of AWJ technology is the quality of the cutting surfaces: the morphological characteristics of AWJ generated surfaces present a great scattering as the process variables are changed or as the distance from the impinging surface is increased (Miranda et al., 1993). A critical aspect in the stone field is the aesthetic appearance. This means that the quality of the manufactured products is a fundamental variable, but it seems not to be influenced by the morphological parameters, such as roughness or waveness, of the cutting groove surface. The functionality of the stone products is preserved whatever the value of the morphological parameters.

Different approaches exist in literature studying the relationship among process parameters and cutting efficiency. Cheung et al. (1976) compares a submerged water jet with a free jet operating in air for concrete and red granite cutting in terms of cut depth. Matsuki et al. (1988) deepen the comparison considering the influence of the impinging angle and stand off distance on the depth of cut in rock machining. Koyohashi et al. (1990) introduce further parameters, such as rock temperature, physical properties of the rock, water jet pressure, nozzle diameter, traverse speed rate and stand off distance whose influence on cut depth is analysed. Bortolussi and Ciccu (1993 and 1996) studied the relationship between the cutting specific energy or the specific erosion and the jet parameters on one side, and the rock-related properties on the other. Miranda et al. (1996) analysed the fractured surfaces machined with different values of the water pressure, the abrasive flow rate and the feed rate on Rosa de Borba marble and Moca Creme calcareous stone. All these works consider only the penetration capability of jet inside the stone material involving the

minimum cutting energy without taking into consideration the further important factor that is the machined quality.

The present work reports an experimental study on the influence of the AWJ cutting variables on the quality of marble free-form cuts, that is on the deviations of the machined profile from the designed one. The cutting of free-form profile, generally called contouring, represents the main application of AWJ together with the quarry excavation. It is commonly used to produce decorations or ornamental products, such as flooring, covering and so on.

The followed approach is mainly an experimental one, aiming to the definition of an empirical relationship between process variables and quality parameters. It deepens the consideration of Carrino et al. (2000).

In the first part of this work the influence of some process variables on the quality of AWJ cutting profiles has been analysed and “transferred” to statistical models. A set of experimental free-form cuts has been performed on Perlato Royal Coreno marble and the generated profiles have been measured in order to identify which process variables significantly influence the geometric deviation of the actual profile from the designed one. Then a family of statistical relationship has been identified and validated by means of the regression analysis.

In the second part of the work the problem of the costs optimisation has been investigated.

All the obtained results, both technological and economical, have been compared with the technological and economical characteristics of the technology traditionally used in this field: the diamond milling.

2. INTERNAL FLOORING

The use of natural stones is very important for the carrying out of flooring, as regards the functional and perceptive aspects, they guarantee an excellent reaction when put into practice. It is in the perceptive field that their performance and expressive capacities are compared to those of many other materials susceptible to analogous destination and gain a characteristic quality thanks to the possibility of original decorative creations, particularly sought after for delegation places and for personalized environmental solutions.

The superficial aspect of the flooring determines important consequences on the spatial perception of the internal environment and takes on formal implications which the designers very often consider in an inadequate way.

It is enough to think of the effects that design and colour of the flooring produce on the perception of a three-dimensional space: floors and ceilings are at par, even if they only define horizontal surfaces that outline the environment, they are able to influence the entire internal space.

It is not enough to plan the building as a functionally integrated whole of inhabited spaces, carried out by closing and carrying structural elements, and an operative device of technological systems etc. However, a specific plan of each single internal flooring is necessary. In fact the flooring can constitute the characterizing element of certain premises or the starting point to plan the alterations of an internal environment.

The generating elements of the design of flooring, which in architectural terms can create the aesthetic and perceptive values, are the type of material, the colour, the surface finishing and the geometry-laying. The material used for the flooring can be of both type: natural and artificial. Naturalness and artificiality have different properties, but most of all they have different ways of perception, which although subjective, meet with the cultural reference and the collective memory of the consumers.

The appearance of natural stones has marked their history which man has written only starting from the last pages, those related to the extraction of the rock and the surface finishing.

The interest for natural stone material started when man observed the colour that the stones gained when more smooth or wet, even before being able to use tools and work the stone. Therefore, man started to seek and work stone focusing more on its use for building.

The relationship between man and colour has a great influence on our way perceiving the space in an architectonic environment. It has the possibility of creating sensations of deepness or approach of the surfaces of the walls, the ceiling and the flooring, but also of changing the perception of their geometrical proportions.

Even if it is not easy to individualize precise rules, the colours spreading out on vast surfaces determine optical illusions and create perspective effects which are sometimes useful to improve the quality of internal spaces.

The sensation of the colour not only depends on the type of material, but also on the conditions of the surface which can be more or less smooth or rough, shiny or opaque, bright or dull, which the material shows at the moment of the extraction or is given by subsequent surface processing.

The geometry-laying of a flooring is influenced by the used type of elements. It is possible to take these elements back to two fundamental typologies: it turns out that one is based on the use of trimmed slabs, while the other on the use of tiles.

Trimmed slabs carry out flooring where the choice and the processing of the material take place only on the basis of a precise work order. On the other hand the dimension and the conformation of each slab are fixed on the basis of a plan especially elaborated in relation to the architectonic characteristics of the environment and of the designer's constituent aim.

Therefore, it is a very personal solution able to guarantee the utilisation of the decorative valence of natural stone material, moreover it allows to insert specific ornamental motifs able to satisfy all the needs of prestigious environments. The other typology of implementation, based on the use of mass-produced tiles with standard dimensions according to the producers' choice, are

widely differentiated from the solution of trimmed slabs. This is due to the fact that as the design of the flooring is bound to the prefixed shapes and dimensions for tiles, but also to the possibility of matching them.

Polished tiles allow to simplify and quicken the lay down, as they can be put in practice through gluing and do not need further finishing.

Geometry-laying is linked to the decision of producing stone elements in conformity with standard size, from which the name laying derives. It is carried out by mass-produced elements or it can be prepared in accordance with planned measures, from which the name lay down derives, carried out by elements which are not part of a mass-production.

The flooring made from elements which are not taken mass-produced is obtained by using slabs with given dimensions, shapes and veins which are selected in the planning stage. These slabs are selected based on the plan of the environment. In this range of solutions there are various types of lay down geometry (UNI 9379). They include: lay down geometry with polygonal elements and lay down geometry for elements with curved sides. The first can be made up of designs which are complex, unique or repetitive. They require a specific planning of details for the reproduction of geometrical and chromatic schemes and have a remarkable decorative effect. The second one is analogous to the first, however, it is more difficult to implement due to the adoption of elements from various curve shapes. Marquetry coverings also belong to this category of flooring – flooring which displays particular designs such as rosettes, décor and centres of premises. They are achieved with marquetry techniques or gluing with shapes and combinations of suitable material in order to obtain their aesthetic characteristics. The marquetry technique is achieved by inserting thin elements into the predisposed area in the bigger and thicker slabs. The gluing technique makes provisions for element assembling, having complementary shapes. This is done on a base which is made up of a slab with a thickness which is lower than the final one. At the same time it bears a shape which is the same as the final one. Using these solutions helps obtain designs which are located in defined areas or developed all over the flooring. They may have remarkable chromatic and decorative properties which are due to the ability of geometric compositions bearing more complex shapes and curved lines.

3. FLOORING QUALITY

The production process of flooring that is constituted by curved elements consists of the following stages:

1. the cutting of the components which make up the flooring
2. the assembling of the components
3. gluing and puttying
4. surface finishing
5. packaging (if necessary)

The critical stage of the process is the cutting of the components. The final quality of the product strongly depends on the quality of the cut of every single component. At the moment regulations

regarding the rules and measurement procedures for the quality standards of products being tested do not exist. The required standards can be divided into two categories: medium and high standard of quality. Medium standard of quality makes provisions for the manufacturing of components which, upon assembling, allow for the presence of a space between a piece and another with a 1 mm length. It is only under one condition that the problems tied to the quality details of the cut surface do not exist. This is when the cut simply runs through the material such as the coinciding of the cut grooves, the wave on the wall of the groove and the roughness, which are evaluated on a width of 10 mm, do not obstruct the assembling of the components. For the processing which requires a high standard of quality, in other words, or for products assembled with minimum leak lines of 0.5 mm, more accurate cut operations are required compared to the first type. This is so in order to obtain coinciding parameters and form error which are contained. A relevant aspect for the quality of the product is related to the dimensional control of the cut profile. This kind of error determines both the size and the constancy of the leak along the profile once various elements have been assembled. This is important especially when cutting natural stone using water-jet because even by using the correct radius of water jet, the obtained real profile may at times manifest evident distortions in comparison with the plan.

Distortions of this type are due to the nature of the material and to the acceleration and deceleration transistor of the machine's axle. Natural stone materials can display strong structural characteristics that are characterised by a strong anisotropy, with different areas in the part that offer resistance to variable removal. Depending on the trajectory taken from the top of the cut compared to the weaving of the material, cuts with variable lengths can be obtained and are hard to control. Another characteristic is the porosity of the material which, in a way, can help the cutting process however it may also cause problems as far as the prediction of cut length is concerned. The complexity of the trajectory that has to be taken in some parts of the profile causes an acceleration (the speed of advancement) which is different from the one established. This is due to the fact that the lengths of the spaces for acceleration and deceleration which are necessary to reach the established cut speed, can be greater than the pieces of profile which are present between two discontinuities. Consequently, there will be areas with nominal cut speeds alternating in areas in which speed cut is inferior, with a greater erosion on the jet's behalf. Therefore giving a groove length of greater cut. These elements do not usually obstruct the composition of the final product, however, they might provoke a defect such as the presence of stucco in various lengths among the single components. This has a negative effect on the appearance of the assembled product. Furthermore, the quality of the product depends on the used process parameters. Currently, companies that work natural stone do so based on the empirical indications received from the tool supplier. This usually becomes a solution, however, none of the work is done to optimise the tools, the labour, the reduction of waste to lessen its impact on the environment, or to improve the working conditions for the labourers involved.

4. EXPERIMENTAL PROCEDURE

4.1 Test material

A stone material exhibits a hardness, which renders it difficult to machine, and a very low thermal expansion coefficient, which makes it suitable for external applications.

The experimental material was Coreno Perlato Royal marble. It is mainly constituted by CaCO_3 with inclusions of seaweed and fossils that produce light and dark spots appreciated from an aesthetic point of view. Its mechanical properties are higher than those of White Carrara marble, as shown in Table 1, indicating that this material could play an important role in many civil applications.

4.2 Experimental phase

There are a lot of possible 2D shapes of a marquetry constituting a flooring that may not be classified on the base of standard feature, such as circle, square and so on. In general they are very complex, because of their irregular profiles, making the machining very hard. This means that the cutting shape deeply influences the resulting quality when it is related with the process parameters. Therefore, it is needed to accurately analyse the cutting shape before starting the machining in order to optimise the choice of the process parameters. It is not possible to define general considerations, which result independent by the shape to cut, in order to ease the machining. The attention has been focus on a 2D shape that is industrially used for decorative applications (see Figure 1). It has a complex geometry that may be schematically represented by a sequence of arcs of circles that are characterised by many different radii, as shown in Figure 2. This shape has been used as experimental geometry in the following and it has been cut by slabs of 10 mm thickness. In fact 10 mm is the value of the flooring thickness commonly used for decorative applications.

The traditional technology uses two diamond mills to cut the experimental shape. A mill of 15 mm diameter that produces a rough geometry and divides it from the slab, as shown in Figure 3. Finally a finishing cut produces the marquetry shape by a mill of 3 mm diameter (see Figure 3). The tool characteristics are the result of a specification particularly suitable for machining Coreno Perlato Royal material, as recommended by diamond tool producers. The value of the tool rotation speed industrially used is about 5000 rpm, while the feed rate is a function of the tool diameter. Its value is higher for 15 mm mill than for 3 mm mill. This is due to the reduced tool resistant section. An equivalent feed rate may be calculated by considering the ratio between the cutting length and the whole cutting time: it is equal to about 112 mm/min. A sample of six shapes has been produced by means of traditional technology with the previously defined parameters.

The machining of stone or marble represents the main field of AWJ application together with gasket cutting. However, the choice of process parameters needs to be optimised. Therefore, the first step is represented by the analysis of the influence of the process parameters on cutting efficiency and quality. A set of experimental cuts has been designed and machined. The three process parameters deeply influencing the material removal mechanism, as discussed in the previous work (Carrino et al. 2000), have been considered as factors of the experimental plan. The levels of the process variables have been selected in order to maximise cutting efficiency.

The remaining process parameters have been considered fixed during the experimental phase. The values of all the process parameters are shown in Table 2. In particular the abrasive is barton garnet, which is widely used for AWJ machining; also the two mesh values of the abrasive are extremely diffused. As can be derived from Table 2, each cut has been replicated three times,

yielding a total of 54 cuts. The experimental cuts have been performed in a random sequence, in order to reduce the effect of any possible systematic error.

4.3 Measurement procedure

The quality of a decoration is generally measured in terms of reduced deviation from the designed shape. The designed shape is the 2D profile developed by means of a CAD software. This profile was used to define the part program of the CNC machining centre or of the AWJ equipment: it means to translate it into a set of co-ordinate of points that define the tool path related to the machine reference frame. During this step the mill diameters have been measured and their values have been used to define the trajectory of the tool axis. The focuser diameter has been used for the trajectory of the abrasive water jet.

Once machined, the 2D profile has been measured by a co-ordinate measuring machine. The actual contour of each cut shape has been obtained by probing the profile at 338 discrete measuring points. The distance between two following points is equal to 2 mm. In particular the actual profile has been measured at a distance of 2 mm and 7 mm from the upper cut edge. In this way it has been possible to evaluate the decrease of the jet efficiency with depth along the cutting groove. In fact the lower profile is covered during application and is, therefore, not critical from an esthetical point of view. The used probe has a 3 mm diameter in order to minimise the effect of the mechanical filtering.

The deviations of the measured points from the 2D CAD model have been calculated for each cut shape. These deviations represent the errors of the actual profile from the nominal one due to the machining process: they include form, orientation and location errors (see Figure 4). They are a function of the geometry of the profile: in this case they depend by the radii of the arcs of circles constituting the shape of the flooring marquetry. They are caused by the chippings between tool, jet or mill, and the material being cut.

The result of the measuring procedure has been the distributions of the geometric deviations: 108 distributions for AWJ technology and 12 distributions for the traditional milling technology. Each distribution has been characterised by the first four statistical moments: mean, variance, skewness and kurtosis. The mean is a commonly used measure of the centre of a batch of data. The variance is a measure of how far the data are spread about the mean. The skewness is a measure of asymmetry, while the kurtosis is a measure of how different the deviations distribution is from the gaussian distribution. Moreover, the median value has been calculated too because of the non-normality of the distribution data. It is used to indicate where the centre of the data is. The median is in the middle of the data: half the observations are less than or equal to it, and half are greater than or equal to it.

Finally, the suitability of the produced profiles implies that the taper of the cutting grooves is not so elevated to compromise the profiles joint. In a previous work it has been verified that the taper obtained on a thickness of 19 mm is very small (Carrino et al., 2000). Therefore, it is possible to assume that the taper on a thickness of 10 mm is further reduced and it does not compromise the flooring setting.

5. RESULTS DISCUSSION

5.1 Study of the influence of AWJ process parameters on geometric deviations

In this work the analysis of variance model was employed to determine the influence of the AWJ cutting parameters on the distributions of the geometric deviations (Neter et al, 1974). This means to define the influence of the process parameters on the statistical variables mean, median, variance, skewness and kurtosis related to the different deviation distributions.

The fundamental hypotheses of the ANOVA applicability to the experimental data (that are the normality and the homogeneity of the variance of the residuals) have been verified. When these hypotheses have not been satisfied, the Kruskal-Wallis and the Mood's median non parametric tests were applied (Deshpande et al. 1995).

Moreover, the response trend (increase or decrease) as a function of the process parameters has been evaluated by means of the Main Effects Plots.

The results of these analyses show that, apart from abrasive mesh, all the process parameters that are involved in the material erosion process influence the variables of deviations, as summarised in Table 3.

The abrasive mass flow rate and the feed rate are the main cause of variation of variables mean, median and variance: an increase in the abrasive mass flow rate or a decrease in the feed rate produce a lower geometric deviation from the nominal profile. This means that the distribution of the geometric deviations is centred very near to zero and its shape is narrow and narrow, due to the decrease of variance values as shown in Figures 5, 6. These results are independent by the measurement position along the cutting grooves: they are the same for 2 mm and 7 mm positions, even if the mean values increase along the cutting depth. This is probably due to the shape of the jet that has a very reduced diameter and remains better focused for high values of abrasive mass flow rate and low values of feed rate. Moreover, a decrease of the feed rate gives to the high number of abrasive particles included in the water-jet the time needed to accurately erode the cut volume.

The shape of the deviations distribution was described by skewness and kurtosis. These two variables are mainly influence by abrasive mass flow rate: an increase of this process parameter causes an increase in the asymmetry and in the sharpness of the distribution. This is due to the increase of skewness and kurtosis when the abrasive mass flow rate increases. The mean values increase along the cutting depth, even if the general behaviour remains the same. A high abrasive mass flow rate implies a high number of abrasive particles included in the water-jet; each particle contributes eroding an elementary volume and all the eroded volumes gives the last shape of the contour profile. Therefore, increasing the abrasive mass flow rate means to increase the probability to change the shape of profile and therefore to have a distribution of deviation harder and harder foreseeable that means asymmetric and sharp.

At last, the abrasive mesh does not significantly affect the geometric deviations of the obtained profile, while its effect on morphological characteristics of the cutting surface seems to be very

strong. This is confirmed by many analysis on metal material where the roughness of the cutting surface is a very important morphological parameter by a functional point of view (Capello et al., 1996).

It can be stated that the profile of the flooring marquetry depends on the interaction between the material and the jet shape, that is, by the abrasive mass flow rate and the feed rate. Therefore, in operative conditions the values of these two process variables must be fixed and controlled in order to decrease the geometric deviation from the CAD designed profile.

5.2 Predictive model of the AWJ geometric deviations

After the analysis of the effects of process variables on the geometric deviations between machined and nominal profiles, the regression analysis has been used to exploit the quantitative character of this relationship (Neter et al., 1974). In particular, the application of some simple models has been investigated, which can be easily adapted to practical cases.

The regression analysis was focused only on the mean and the median of the deviations distribution because these two statistical parameters allow to foresee the mean behaviour of data near or far from normal distribution. Some statistical procedures were used to verify the normality of the residuals and the homogeneity of the variance, which are the hypotheses that must be verified when performing a regression analysis.

The regression analysis has identified a unique statistical model for the upper (2 mm) and for the lower (7 mm) parts of the kerf. It was observed that mean and median related to geometric deviations of the profile depends in a similar way on the cutting parameters.

The functional form of the regression model is linear:

$$\ln(M) = a + b \cdot m_a^2 + c \cdot m_a + d \cdot u$$

The left side of this relation is a logarithmic transformation of mean and median of the deviations distribution, while the values of the constants a , b , c and d are shown in Table 4.

Because of the empirical approach followed, the statistical relationship is valid inside the experimental range.

The statistical model identified can be used to foresee the obtainable free-form profile error once the values of the process variables have been fixed, and vice versa. Moreover, these equations can be used to control AWJ marble machining: the comparison between the theoretical and the measured values allows to verify if the process is in a control state. Therefore, these equations are the first step to optimise the AWJ machining of marble in order to reach the most efficient application of this non traditional manufacturing process to marble cutting.

5.3 Comparison between AWJ and diamond milling

A visual inspection of the cuts underlines that those machined by diamond mill present a wider chipping spreading on the upper cut edges than those obtained by AWJ technology. The situation is inverted for the lower cut edges.

A deep analysis was carried out on the distributions of the geometric deviations of the actual profile from the nominal one. The distribution obtained merging the six samples machined by diamond mill was compared with the distributions of minimum and maximum errors due to AWJ technology. The first is formed by the samples that were cut with the highest value of abrasive mass flow rate (500 g/min) and with the lowest value of feed rate (350 mm/min) as previously described. The second distribution is constituted by the samples cut with the lowest value of abrasive mass flow rate (300 g/min) and with the highest value of feed rate (750 mm/min).

The mill and the AWJ distributions were compared in terms of location (median) and dispersion (variance) by the Kruskal-Wallis and Mood test. The results are shown in Table 5. It can be seen that the distribution of the AWJ minimum deviations is characterised by a median lower than this of mill distribution and by a standard deviation upper, even if very near, than this of mill distribution.

The distribution of AWJ maximum deviations is characterised by a median and a variability that range from six to ten times the corresponding values of milling distribution.

Therefore, an important technological result is that AWJ technology allows to reproduce the designed profile of the flooring marquetry more accurately than milling technology permits if its process parameters are opportunely choosen. This result together with the possibility to cut profiles whose bending radius is one tenth of that for milling makes AWJ technology the most promising process to cut the free-form profiles of decorative applications, such as flooring, civil covering and so on, by a technological point of view.

6. COST OPTIMISATION

The total cost of AWJ machining can be divided into the cost figures reported in Table 6, which have shown to be the most relevant ones (Monno, 1997).

The most relevant costs are the abrasive one, the cost of the water and the cost of the energy. These three costs, together with the cost of the focuser and nozzle wear and the cost of labour, are affected by the selection of the process variables. Hence, an effective optimisation of the machining can be performed if one of these costs is reduced.

Therefore, the optimisation of the process parameters can lead to a significant reduction of the total AWJ machining cost.

The total cost of milling machining can be divided into the cost figures reported in Table 6, which are the costs of energy, water, tool wear and labour. These costs were calculated for the values of the process variables commonly used in practice and previously described.

The abrasive water jet allows to decrease the machining cost more than 50% independently by the values of the process parameters inside the experimental range, as shown in Figure 7. This is mainly due to the feed rate values that are very higher than those of milling for a 10 mm slab thickness: this is due to breakage of the mechanical tool. Therefore, the choice of the AWJ process parameters is related to the solution of the trade off between the increase or the decrease of the abrasive mass flow rate aiming to minimise the geometric deviations of the AWJ machining with respect to the CAD model or the machining costs respectively. The same considerations may be applied to feed rate. Both the solutions allow to considerably decrease the machining costs with respect to the traditional technology.

Therefore, the technological and economical advantages of AWJ, when compared with traditional milling, are very considerable in the field of decorative applications.

7. CONCLUSIONS

The AWJ technology results to be very competitive in the field of decorative applications. It allows to reproduce the designed profile more accurately than traditional technology does, once chosen the process parameters. The geometric deviations from the designed 2D shape may be strongly decreased by increasing the abrasive mass flow rate or decreasing the feed rate. This result together with the possibility to cut profiles whose bending radius is one tenth of that for milling makes AWJ technology the most promising process to cut the free-form profiles of decorative applications, such as flooring, civil covering and so on, by a technological point of view.

Moreover, the AWJ machining costs allows to decrease the milling one more then 50%, independently by the values of the process parameters on a slab thickness of 10 mm.

8. ACKNOWLEDGMENTS

The research reported in this paper was partially supported by MURST and CNR – National Research Council. The authors are grateful to Pellegrino Marmi, Formia, Italy for supporting the experimental activities and to sig. Zola, President of Union for the exploitation of Coreno Perlato Royal for supplying the experimental material.

9. REFERENCES

Agus, M., Bortolussi, A., Ciccu, R., Kim, W.M., Manca, P.P., “The influence of rock properties on waterjet performance”, *Proceedings of the 7th American Water Jet Conference*, pp. 427-442, Water Jet Technology Association, St. Louis, Missouri, 1993.

- Agus, M., Bortolussi, A., Ciccu, R., Vargiu, A., "Abrasive-rock interaction in AWJ cutting", *Proceedings of the 13th International Symposium on Jet Cutting Technology*, pp. 509-519, BHRA Fluid Engineering, Cranfield, Bedford, England, 1996.
- Capello, E., Monno, M., Polini, W., Semeraro, Q., "AWJ Machining: Surface quality as a constraint", *Proceedings of the 13th International Symposium on Jet Cutting Technology*, BHRA Fluid Engineering, Cranfield, Bedford, England, 1996.
- Carrino L., Monno M., Polini W., Turchetta S., "Study of cutting quality and efficiency in stone production", *Proceedings 15th International Symposium on Jetting Technology*, pp. 133-146, BHRA Fluid Engineering, Cranfield, Bedford, England, 2000.
- Cheung, J.B., Hurlburt, G.H., "Submerged water-jet cutting of concrete and granite", *Proceedings of the 3rd International Symposium on Jet Cutting Technology*, pp. 49-62, BHRA Fluid Engineering, Cranfield, Bedford, England, 1976.
- Deshpande, J.V., Gore, A.P., Shanubhogue, A., "Statistical analysis of nonnormal data", *John Wiley & Sons*, 1995.
- Koyohashi, H., Kyo, M., Rekiguchi, R., Matushita, Y., Tokioka, M., "Experiments and multivariate analysis of hot dry rock cutting with high pressure water jet", *Proceedings of the 10th International Symposium on Jet Cutting Technology*, pp. 27-43, BHRA Fluid Engineering, Cranfield, Bedford, England, 1990.
- Matsuki, A., Okumura, K., Nakadate, H., "Some aspects of slot cutting of rocks with high speed water jets both in air and in water", *Proceedings of the 9th International Symposium on Jet Cutting Technology*, pp. 495-511, BHRA Fluid Engineering, Cranfield, Bedford, England, 1988.
- Miranda, R.M., Lousa, P., Mouraz Miranda, A.J., Kim, T., "Abrasive water jet cutting of portuguese marbles", *Proceedings of the 7th American Water Jet Conference*, pp. 443-457, Water Jet Technology Association, St. Louis, Missouri, 1993.
- Miranda, R.M., Kim, T.J., "Abrasive waterjet cutting of marble and calcareous stones: a phenomenological study", *Proceedings of the 13th International Symposium on Jet Cutting Technology*, pp. 415-424, BHRA Fluid Engineering, Cranfield, Bedford, England, 1996.
- Monno M., "Selection of Process Parameters for AWJ cutting", *International Conference on Cutting Technologies (ICCT '97)*, Hannover, March 5-6, 1997.
- Neter J., Wasserman W., "Applied Linear Statistical Models", *R.D. Irwin, Inc.*, Homewood, Illinois, 1974.

10. NOMENCLATURE

a, b, c, d	= proportionality factors (see eq. (1))
C_m	= machining cost [\$/m]
C_{en}	= energy cost [\$/m]
C_{abr}	= abrasive cost [\$/mg]
C_w	= water cost [\$/m]
C_{f_n}	= focuser and nozzle cost [\$/m]
C_t	= diamond tool cost [\$/m]
C_l	= labour cost [\$/m]
c_{KW}	= specific energy cost [\$/KWh]
c_w	= specific water cost [\$/m ³]
c_{abr}	= specific abrasive cost [\$/Kg]
c_t	= specific diamond tool cost [\$/h]
c_{f_n}	= specific focuser and nozzle cost [\$/h]
c_l	= specific labour cost [\$/h]
h	= material thickness
h_{mach}	= machined depth of cut [mm]
m_a	= abrasive mass flow rate [Kg/min]
P	= water pressure [MPa]
P_w	= milling power [kW]
$Q(P)$	= water volume flow rate [m ³ /s]
Q_w	= water volume flow rate for milling [m ³ /s]
u	= feed rate [m/min]

Table 1. Mechanical properties of Coreno Perlato Royal and White Carrara

Material properties	Coreno Perlato Royal	White Carrara
Density [kg/m ³]	2740	2705
Water absorption [%]	4.0	0.06
Compressive strength [MPa]	163	131
Compressive strength to ageing by frost [MPa]	162	126
Young modulus [MPa]	72000	75000
Flexural strength [MPa]	12,8	16.9
Abrasion resistance	0.95	0.52
Impact resistance [cm]	32	61
Knoop hardness [MPa]	2001	1463

Table 2. AWJ experimental plan

Fixed factors	Levels	Variable factors	# Levels	Levels
Water pressure [MPa]	350	Abrasive mass flow rate [g/min]	3	300-400-500
Orifice diameter [mm]	0.30	feed rate [mm/min]	3	300-500-750
Nozzle diameter [mm]	1	Abrasive mesh	2	80 - 120
Abrasive kind	garnet			
Standoff distance [mm]	2			
# passes	1			

Replications	3
Total cuts	54

Table 3. Influence of AWJ process parameters on geometric deviations

		ANOVA results								
		mesh			m _a			u		
	Deviations Variables	F	p	SSF/ SST	F	p	SSF/ SST	F	p	SSF/ SST
2 mm	Mean	0.01	0.91	0.6	95.18	0	56.7	45.34	0	22.7
	Median	7.84	0	1.7	134.9	0	62.4	53.29	0	23.6
	Variance	0.71	0.41	2.3	16.34	0	42.4	4.52	0.02	10.9
	Skewness	0.49	0.49	0.3	14.03	0	41.4	1.91	0.17	5.4
7 mm	Mean	1.31	0.26	1	29.77	0	47.4	13.93	0	20.7
	Median	0.62	0.44	0.5	28.74	0	45.6	15.86	0	22.7
	Variance	3.10	0.09	5.2	9.40	0	29.9	1.23	0.30	4.16
	Skewness	0.62	0.44	0.8	17.73	0	44.8	0.84	0.44	2.3
		Kruskal-Wallis Test								
		H	p		H	p		H	p	
2 mm	Kurtosis	0.80	0.37		12.7	0		2.87	0.24	
7 mm	Kurtosis	0	0.99		16.3	0		1.91	0.38	

Table 4. Regression coefficients.

		a	b	c	d	R ²
2 mm	ln(mean)	5.24	+0.000033	-0.0322	+0.00185	89.8%
	ln(median)	3.93	+0.000025	-0.0266	+0.0024	90%
7 mm	ln(mean)	3.99	+0.000025	-0.0249	+0.00165	67.8%
	ln(median)	2.50	+0.000015	-0.0181	+0.00216	76.3%

Table 5. Comparison between AWJ minimum error and milling

			Kruskal-Wallis Test			Mood Test		
	Level		Median	H	p	Q3-Q1	χ^2	p
2 mm	1	Milling	0.18	321.23	0	0.225	334.37	0
	2	AWJ	0.09			0.133		
7 mm	1	Milling	0.17	28.58	0	0.107	47.84	0
	2	AWJ	0.14			0.163		

Table 6. Machining Costs of AWJ and milling

AWJ		Diamond milling	
Energy cost	$C_{en} = c_{KWh} \cdot \frac{P \cdot Q(P)}{u}$	Energy cost	$C_{en} = \frac{c_e \cdot (P_w \cdot 0.6)}{u}$
Water cost	$C_w = c_w \cdot \frac{Q(P)}{u}$	Water cost	$C_w = c_w \cdot \frac{Q_w}{u}$
Abrasive cost	$C_{abr} = c_{abr} \cdot \frac{m_a}{u}$	Tool cost	$C_w = \frac{c_t}{u}$
Focuser and nozzle wear cost	$C_{f_n} = \frac{(c_f + c_n)}{u}$	Labour cost	$C_l = \frac{c_l}{u}$
Labour cost	$C_l = \frac{c_l}{u}$		

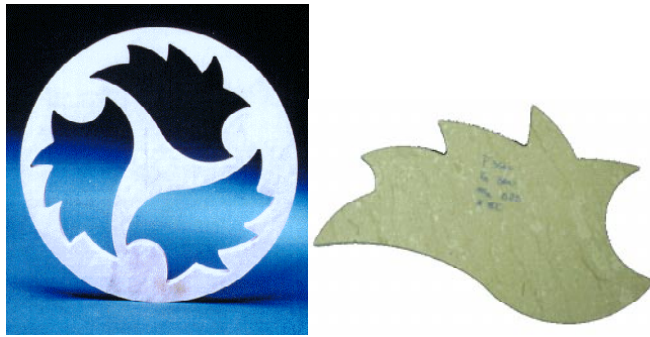


Figure 1. Decorative application (Courtesy Brembana Machine)

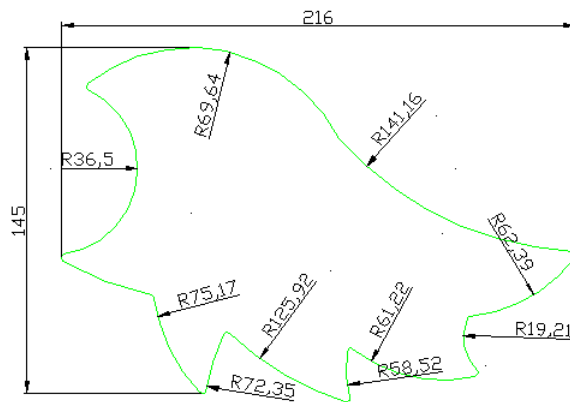


Figure 2. Experimental 2D shape

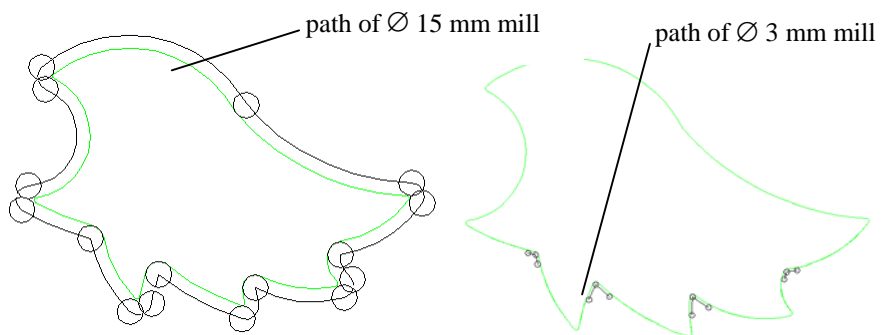


Figure 3. Milling trajectory

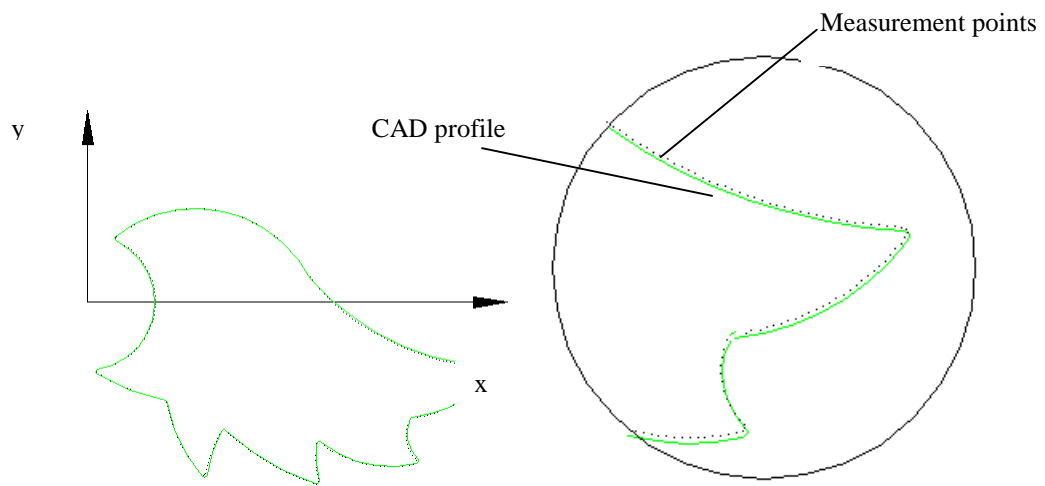


Figure 4. Measurement procedure

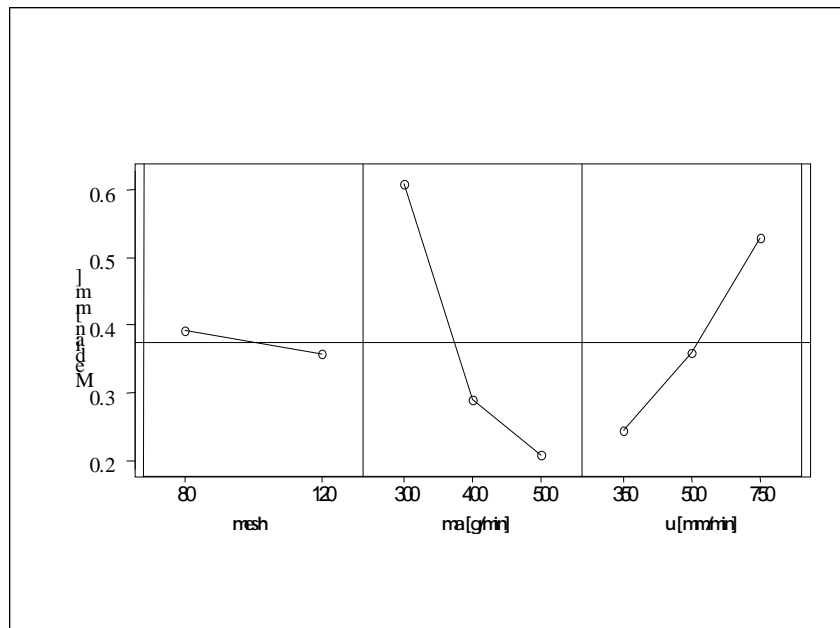


Figure 5. Main Effect Plots of the median of the deviation distribution at 2 mm

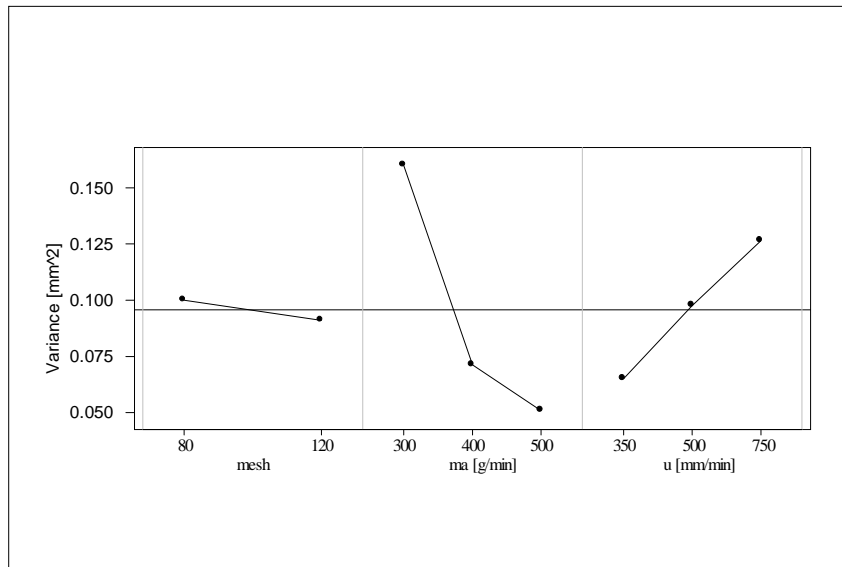


Figure 6. Main Effects Plot of the variance of the deviations distribution at 2 mm

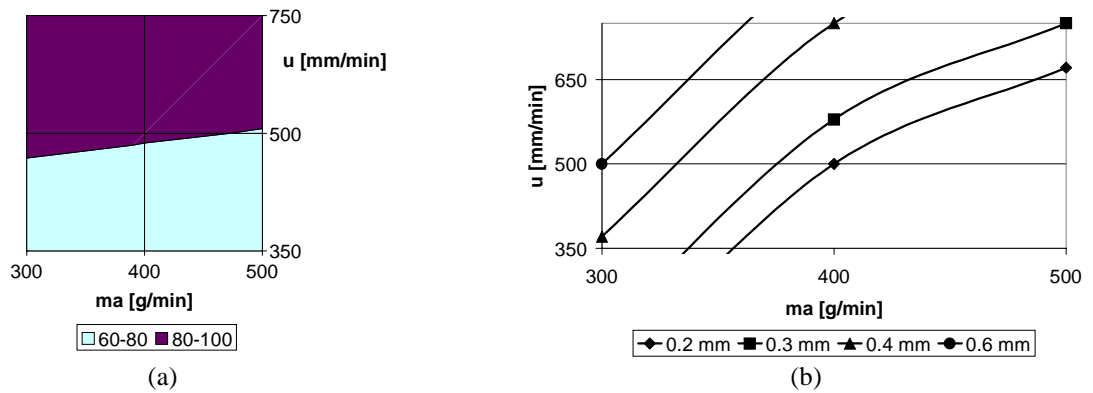


Figure 7. Technological and economical considerations:
 (a) costs difference between milling and AWJ
 (b) iso-curve of geometric deviations for AWJ machining

ABRASIVE WATER JET MACHINING OF ALUMINUM WITH LOCAL ABRASIVES

O. V. Krishnaiah Chetty, M. Kantha Babu
Manufacturing Engineering Section
Indian Institute of Technology Madras
Chennai, India

ABSTRACT

This paper details the studies on Abrasive Water Jet Machining of Aluminum with garnet abrasives available in southern India. Design of Experiments using L27 Orthogonal Array and ANOVA analysis helped in the determination of significant cutting parameters. The influence of abrasive particle size distribution along with process parameters like pressure, traverse rate, and abrasive flow rate on the target parameters has been studied. American Foundrymen's Society Fineness number, depth of cut, kerf width (top & bottom), kerf taper, surface roughness at three sections (upper, middle and lower) are targeted. Response equations are developed for the target parameters.

1. INTRODUCTION

Abrasive Water Jet Machining (AWJM) an emerging technology has found a variety of applications world over as it offers wide ranging benefits and is very effective even in machining difficult-to-machine materials. The intensity of the cutting process depends on several AWJM process parameters (Hashish, 1991b and Momber et al., 1988). Among these parameters, certain abrasive parameters such as size, shape, and particle size distribution (PSD) influence the fragmentation of abrasives, depth of the cut, kerf width, kerf taper and surface roughness.

Cost of abrasives contributes substantially to the production cost. Industries prefer garnet abrasives (one of the popular abrasives) drawn from established sources. Indian industries are focusing attention to the possible benefits of using AWJM in their production systems. Abrasives, locally available may prove economical than imported ones. Industries can be encouraged to use this efficient technology if cost reductions are demonstrated. This will provide them a competitive edge in manufacturing. This ongoing research therefore aims at analyzing the locally available garnet abrasives (obtained from southern part of India) to determine their suitability. Preliminary work done in this connection reported by Krishnaiah Chetty et al. (1999) concentrated on depth of cut. In our research, cost reductions are planned through choice of abrasives, and optimization of parameters specific to applications.

This paper analyzes the performance of local garnet abrasive and reports the findings achieved through L27 Orthogonal Array (OA) Experimental Design on the effect of American Foundrymen's Society Fineness number (AFS number) at nozzle exit and after cutting, depth of cut, kerf width (top and bottom), kerf taper, surface roughness in machining Aluminum. The allocation in L27 OA has been decided based on the ANOVA results of L9 OA in surface roughness measurement at the middle section of the work piece by Krishnaiah Chetty et al. (2001). The identified least significant factor AFR is studied without interaction effects, while other key parameters are considered for interaction effect. The responses equations (Montgomery, 1991) are also established.

2. EXPERIMENTAL SETUP AND PROCEDURE

Injection type IP236-22 AWJ machine supplied by M/s WOMA has been used in this work. The equipment details are given in Table 1. The present work attempts to investigate the influence of abrasive PSD along with process parameters pressure (P), traverse rate (TR), and abrasive flow rate (AFR) on cutting Aluminum as shown in Table 2 with three levels. The abrasive samples (AS) are chosen to have three different distributions of abrasive particles. The ranges of P, TR, and AFR parameters are selected based on productivity and industrial practice, while the AS is formulated to include abrasive particles collected from single, three and five individual sieves as shown in Table 3. The AS are formulated to have nearly the same (AFS Number) as well as average particle size proposed by Guo et al. (1992) based on momentum method. The stand off distance is maintained at 3mm, the jet impact angle being 90°, with a single pass cutting. To study the influence of variable process parameters on the disintegration behavior of abrasives, abrasive particles are collected at the exit of the focusing nozzle and after cutting aluminum. Collection is done through a special catcher, consisting of a cylindrical drum with a screening

cloth. These abrasives are cleaned (Aluminum debris is dissolved by adding 20% NaOH Solution), dried and sieved. The AFS number is calculated from the sieve analysis.

In order to minimize the number of experiments, statistical experimentation using L27 OA has been used. Randomized experimentation without replication has been done. The AFS number at nozzle exit and after cutting, depth of cut, kerf width (top and bottom), kerf taper (ratio of top kerf width to bottom kerf width) and surface roughness (SR) are measured and responses equations established. A trapezoidal work piece is cut and the depth of machining has been computed. Perthometer is used to measure SR.

3. RESULTS AND DISCUSSION

Analysis considering AFS number at nozzle exit and after cutting, the depth of cut, kerf width (top and bottom), kerf taper, and surface roughness are presented hereunder.

3.1 AFS Number at nozzle exit

ANOVA analysis in Table 4 indicates that P is significant at 99% confidence level. The AS, and interaction effects PxAFR, and ASxAFR are significant at 90% confidence levels. Their linear, quadratic and components of interaction effects are shown in the Table 4. Abrasives at nozzle exit are collected when it is stationary. The mean responses in Fig. 1 indicate that P3 results in increased fragmentation. High P normally results in higher particle fragmentation because of increase in kinetic energy (Hashish, 1989). Among the abrasive sample, AS3 results in increased fragmentation, due to the presence of more number of larger size particles than AS1 and AS2. In the interaction effect, P3xAFR2 and AS3xAFR1 result in more particle fragmentation. The response equation for the above, Y_{AN} is:

$$Y_{AN} = 87.606 + 0.533(P-225) + 3.061 \times 10^{-4}(P-225)^2 + 32.844(AS-0.281) + 108840(AS-0.281)^2 - 2.888(AFR-1) - 0.035(P-225)(AFR-1)^2 + 1.30 \times 10^{-3}(P-225)^2(AFR-1) - 2.24 \times 10^{-4}(P-225)^2(AFR-1)^2 + 666.7(AS-0.281)(AFR-1)^2 + 692640(AS-0.281)^2(AFR-1)^2 \quad (8)$$

3.2 AFS Number after cutting Aluminum

ANOVA analysis in Table 5 indicates that P and AS are significant at 99% and 90% confidence levels. The linear and quadratic effects of P and AS are shown in Table 5. It is observed that particle disintegration after cutting Aluminum material depends on P and AS. The mean responses in Fig. 2 indicate that high P (P3) results in more particle fragmentation. Abrasive sample AS1 is subjected to tremendous fragmentation during cutting. On the other hand AS3 consisting of larger as well as smaller size particles seem to fragment less than AS1 or AS2 after cutting. The response equation for the above, Y_{AC} is:

$$Y_{AC} = 105.518 + 0.109(P-225) - 4.34 \times 10^{-4}(P-225)^2 + 0.024(AS-125) - 566.6(AS-0.281) + 42120(AS-0.281)^2 - 1.00(AFR-1) \quad (9)$$

3.3 Depth of cut

ANOVA analysis in Table 6 indicates that P, TR, AFR, and the interaction effect PxAS are found to be significant parameters. The linear effect of individual parameters P, TR, and AFR are significant at 95% confidence levels, while their quadratic effects are not significant. Considering the components of interaction effects, P_{QxAS_L} and P_{QxAS_Q} are significant at 90% and 95% confidence levels respectively.

The mean responses in Figure 3 indicate that high P, low TR and high AFR result in increased depth of cut. With increase in pressure, the higher energy of the jet results in enhanced depth of cut (Hashish, 1989; Kovacevic, 1992). Lower TR implies prolonged exposure time and hence increased depth of machining. Increase in AFR increases the depth of cut in the selected range, since more number of abrasive particles will be involved in the mixing and cutting processes.

Considering the interaction effect, although AS is not significant individually, its interaction effect with pressure, P_{2xAS3} is found to be significant and results in increased depth of cut. This may be due to the fact that the abrasive sample AS3 consists of combination of five different sizes of abrasives particles of which some are larger and heavier than AS1 and AS2, and hence possess increased energy for cutting. When P is increased from P1 to P2, though fragmentation of abrasives is found to increase (Figure 9), the increase in kinetic energy seems to aid the cutting, resulting in increased depth of cut. With further increase of pressure from P2 to P3 the combined effect of higher abrasive fragmentation and the increased kinetic energy seems to increase the depth of cutting as compared to P1, but not as compared to P2. Hence the maximum depth of cut is observed at P_{2xAS3} . The response equation for the depth of cut, Y_{DOC} is:

$$Y_{DOC} = 13.69 + 0.064(P-225) - 7.579 \times 10^{-4}(P-225)^2 - 0.0696(TR-125) + 5.445 \times 10^{-4}(TR-125)^2 + 228.963(AS-0.281) + 10.85(AFR-1) + 9.588(AFR-1)^2 - 0.195(P-225)^2(AS-0.281) - 102.957(P-225)^2(AS-0.281)^2 \quad (1)$$

3.4 Kerf width

Kerf width (average of three measurements using optical microscope) is measured at the top and bottom surfaces of the cut. The kerf taper is computed in each case. It is observed that the bottom kerf width is smaller than the top kerf width, resulting in a convergent cut.

3.4.1 Top kerf width

ANOVA analysis in Table 7 indicates that interaction effect PxAS is only significant at 90% confidence level and its component P_{QxAS_Q} is significant at 95% confidence level. The mean responses in Figure 4 indicate that minimum kerf width (efficient machining, since minimum material is lost) is at P_{1xAS3} . The response equation for the top kerf width, Y_{KWT} is:

$$Y_{KWT} = 1.230 - 4.93 \times 10^{-4}(TR-125) - 8.1(AS-0.281) + 0.077(AFR-1) - 1.664(P-225)^2(AS-0.281)^2 \quad (2)$$

3.4.2 Bottom kerf width

ANOVA analysis in Table 8 indicates that only TR is significant at 95% confidence level. Its linear and quadratic effects are significant at 95% and 90% confidence levels respectively. The mean responses in Figure 5 indicate that bottom kerf width reduces with an increase in the TR. At increased TR there is not enough time for spread hence the decrease in kerf width at bottom side. This result is similar to that reported by Momber et al. (1998) for ductile materials. The response equation for the bottom kerf width, Y_{KWB} is:

$$Y_{BKW} = 0.809 + 2.066 \times 10^{-4}(P-225) - 8.4 \times 10^{-4}(TR-125) + 9.6 \times 10^{-6}(TR-125)^2 + 2.9(AS-0.281) + 0.071 (AFR-1) \quad (3)$$

3.5 Kerf taper

ANOVA analysis in Table 9 indicates that TR is significant at 99% confidence level. The AS, and the interaction effect of PxTR are significant at 95% confidence level and TRxAS is significant at 90% confidence level. The significance of linear, quadratic and the components of interaction effects are also shown in Table 9. It is also observed that error (E) also plays a significant role at 95% confidence level, indicating highly complex conditions. The mean responses in Figure 6 indicate that minimum taper is obtained with low TR and with AS3 abrasive sample. The low TR implies increased exposure time, and AS3 consists of larger size particles compared to other samples resulting in improved cutting, leading to reduction in kerf taper. In the interaction effect, P1xTR1 and TR1xAS1 result in minimum taper. It is also observed from the mean responses that the interaction effect of TR and AS3 generally results in reduced taper. The response equation for the kerf taper, Y_{KT} is:

$$Y_{KT} = 1.445 - 3.86 \times 10^{-4}(P-225) + 7.06 \times 10^{-4}(TR-125) - 2.29 \times 10^{-5}(TR-125)^2 - 15(AS-0.281) - 720(AS-0.281)^2 - 0.33(AFR-1) - 1.47 \times 10^{-5}(P-225)(TR-125) + 5.68 \times 10^{-8}(P-225)(TR-125)^2 - 0.1146(TR-125)(AS-0.281) + 3.94 \times 10^{-3}(TR-125)^2(AS-0.281) \quad (4)$$

3.6 Surface roughness

As the abrasive waterjet cuts through the material, the upper cut section will be smoother, while striations are observed at lower section. Surface roughness (Ra), measurements are made using Perthometer at three locations of the cut surface. a) Upper section (2 mm below the top surface), b) middle section, and c) Lower section (two third heights from the top surface).

3.6.1 Upper section

ANOVA analysis in Table 10 indicates that no parameter is significant at the upper section. The mean responses are given in Figure 7 and the response equation for the upper section, Y_{SRU} is:

$$Y_{SRU} = 9.47 + 8.89 \times 10^{-3}(P-225) + 8.88 \times 10^{-3}(TR-125) - 75.6(AS-0.281) - 0.924 (AFR-1) \quad (5)$$

3.6.2 Middle section

ANOVA analysis in Table 11 indicates that TR, AS, and interaction effect PxTR are significant at 95% confidence levels. The significance of linear, quadratic and the components of interaction effects are also shown in Table 11. From the mean responses in Figure 8 it is found that TR1 and AS3 result in minimum SR. Generally higher TR increases the jet deflection, which in turn results in higher surface roughness. The increase in the number of impacting particles at lower TR contributes to the reduction in surface roughness. Since the additional particles serve to smoothen the surface that the forgoing particles have generated. This is in line with the general findings (Singh et al., 1991, and Hashish, 1991b). Abrasive sample AS3 has more number of larger size particles as well as finer particles than AS1 and AS2. It is also found that the AFS number of AS3 at nozzle exit is higher (Figure 1) due to fragmentation of abrasive particles. These two factors result in improved surface roughness.

Considering the interaction effect of PxTR, in the present case it is found that P2xTR1 result in minimum SR. The response equation for the middle section, Y_{SRM} is:

$$Y_{SRM} = 10.125 - 0.299(P - 225) + 1.393(TR - 125) - 2.016 \times 10^{-4}(TR - 125)^2 - 91.1(AS - 0.281) - 65400(AS - 0.281)^2 + 0.567(AFR - 1) + 2.66 \times 10^{-5}(P - 225)(TR - 125) + 1.088 \times 10^{-6}(TR - 125)^2(P - 225) - 4.92 \times 10^{-6}(P - 225)^2(TR - 125) - 7.33 \times 10^{-8}(P - 225)^2(TR - 125)^2 \quad (6)$$

3.6.3 Lower section

ANOVA analysis in Table 12 indicates that P and its linear effect are significant at 90% confidence level. Momber et al. (1988) reported that the influence of pressure is more at the lower section. The influence of waterjet pressure on surface roughness increases as the depth of cut increases (Kovacevic, 1991). During cutting, the upper and middle sections of the work piece are directly attacked by abrasive particles. Then the kinetic energy is continuously decreased as the jet travels, in addition to the jet deflection, the abrasive particle size distribution becomes non uniform as a result the cutting action becomes cyclic leading to striations on the cut surface at lower section (Matusi et al., 1991 and Hashish, 1991a). From the mean responses in Figure 9 it is found that P1 results in minimum SR. The response equation for the lower section, Y_{SRL} is:

$$Y_{SRL} = 10.96 + 0.020(P - 225) - 5.65 \times 10^{-5}(P - 225)^2 + 0.012(TR - 125) - 114.4(AS - 0.281) - 0.633(AFR - 1) \quad (7)$$

4. CONCLUSIONS

Abrasives in Abrasive Water Jet Machining contribute significantly to the cost of production and play an important role. Therefore the use of local garnet abrasives will be advantageous. Investigations on the influence of the abrasive particle size distributions on the cutting performance are limited in literature. This paper studies the use of local garnet abrasives obtained from southern India for cutting Aluminum. Its behaviour is analysed through L27 Orthogonal Array Design of Experimentation. Experiments have been conducted to study the

influence of abrasive particle size distributions along with pressure, traverse rate, and abrasive flow rate on the target parameters like AFS number at nozzle exit and after cutting, depth of cut, kerf width, kerf taper, surface roughness at three levels. ANOVA analysis indicated the statistically significant parameters and their linear and quadratic effects at various confidence levels. The investigations proved that the local abrasives behave similar to imported abrasives. The response equations have been developed. The response equations will be useful to the production managers to select suitable combination of parameters for a specific application of Aluminum cutting with local abrasives.

5. ACKNOWLEDGEMENTS

The authors express sincere thanks to Science and Engineering Research Council of Department of Science & Technology, Government of India, for the financial support for the equipment. They also acknowledge the financial assistance for research interactions with German counterparts under the DST-DAAD project based personnel exchange program 1999.

6. REFERENCES

- Guo. N.S., Louis, H., Meier, G., and Ohlsen, J., "Recycling Capacity of Abrasives in Abrasive Water Jet Cutting," *Proceedings of 11th International Conference on Jet Cutting Technology*, pp.503-523, Scotland, 1992.
- Hashish, M., "Pressure Effects in Abrasive WaterJet Machining," *Transactions of ASME Journal of Engineering Materials and Technology*, Vol. 111, pp.221-228, 1989.
- Hashish, M., "Characteristics of Surfaces Machined with Abrasive WaterJet," *Transactions of the ASME Journal of Engineering Materials and Technology*, Vol.113, pp. 354-362, 1991a.
- Hashish, M., "Optimization Factors in Abrasive WaterJet Machining," *Transactions of ASME Journal of Engineering for Industry*, Vol. 113, pp.29-37, 1991b.
- Krishnaiah Chetty, O.V., and Ramesh Babu, N., "Some Investigations on Abrasives in Abrasives WaterJet Machining," *Proceeding of 10th American WaterJet Conference*, pp. 419-430, WaterJet Technology Association, USA, 1999.
- Krishnaiah Chetty, O.V., and Kantha Babu, M., "Studies on the Use of Local Abrasives in Abrasive Water Jet Machining of Aluminum," Accepted for presentation and publication in the *Proceedings of 17th International Conference on CAD/CAD, Robotics and Factories of the Future*, Trinidad, West Indies, 2001.
- Kovacevic, R., "Surface Texture in Abrasive WaterJet Machining," *International Journal of Manufacturing System*, Vol. 10, pp. 32-40, 1991.

- Kovacevic, R., "Monitoring the Depth of Abrasive WaterJet Penetration," *International Journal of Machine Tools and Manufacture*, Vol.32 (5), pp725-736, 1992.
- Matsui, S., Matsumura, H., Ikemoto, K., Tsujita, K., and Shimizu, H., "High Precision Cutting Method for Metallic Materials by Abrasive WaterJet," *Proceeding of 10th International Conference on Jet Cutting Technology*, pp.263-278, 1991.
- Momber, A.W., and Radavan Kovacevic., "Principles of Abrasive WaterJet Machining," Springer, Great Britain, 1998.
- Montgomery, D.C., "Design and Analysis of Experiments," John Wiley & Sons Inc, Singapore, 1991.
- Singh, P.J., Wei-Long Chen, and Jose Munoz., "Comprehensive Evaluation of Abrasive WaterJet Cut Surface Quality," *Proceeding of 6th American WaterJet Conference*, pp. 139-161, WaterJet Technology Association, Houston, 1991.

Table 1. The Details of Equipment

Abrasive Water jet Machining System	Injection type IP236-22, M/s WOMA, Austria
Power	22 kW, 50Hz
Max. Discharge pressure	360 MPa
Abrasive feeding system	Vibratory conveyor with heating facility
CNC work table	Two-axis control (X=1000,Y=1000)
Primary nozzle diameter, mm	0.25, (Sapphire)
Secondary nozzle diameter, mm	0.8, (Carbide)
Secondary nozzle length, mm	70

Table 2. Variable Process Parameters

S. No	Variable Parameters	Low 1	Medium 2	High 3
1	Pressure [MPa]	150	225	300
2	Traverse rate [mm/min]	50	125	200
3	Abrasive flow rate [g/s]	0.5	1.0	1.5
4	Abrasive sample code	AS1	AS2	AS3

Table 3. Details of Abrasive Sample Codes

Abrasive Sample code	Percentage of abrasives Sieve designation, Mesh size (Average particle size, mm)					AFS number	Average Particle size, mm
	#44 (0.355-0.400)	#52 (0.315-0.355)	#60 (0.250-0.315)	#72 (0.200-0.250)	#80 (0.180-0.200)		
AS1	-	-	100%	-	-	52.0	0.283
AS2	-	33.33%	33.33%	33.33%	-	52.0	0.278
AS3	20%	20%	20%	20%	20%	52.8	0.282

Table 4. ANOVA Analysis - AFS Number at Nozzle Exit

Source	P	DF	S	V	F	• , %	Remarks
P		2	1,218.25	609.14	444.51	77.30	***
P _L		1	1200.45	1200.45	876.24	76.25	***
P _Q		1	17.80	17.80	12.99	1.05	*
AS		2	44.96	22.48	16.40	2.69	*
AS _L		1	0.50	0.50	0.364	0.05	Ns
AS _Q		1	44.46	44.46	32.45	2.74	**
AFR	Y	2	2.741	1.370	1.000	0.00	Ns
E		8	156.30	19.54	14.25	9.24	*
P x AS		4	15.26	3.82	2.78	0.62	Ns
P x AFR		4	83.48	20.87	15.23	4.96	*
P _L x AFR _L		1	0.30	0.30	0.21	0.00	Ns
P _L x AFR _Q		1	16.00	16.00	11.67	0.93	*
P _Q x AFR _L		1	53.77	53.77	39.24	2.49	**
P _Q x AFR _Q		1	13.37	13.37	9.75	0.62	*
AS x AFR		4	51.48	12.87	9.39	2.93	*
AS _L x AFR _L		1	1.33	1.33	0.97	.002	Ns
AS _L x AFR _Q		1	25.01	25.01	18.25	1.50	**
AS _Q x AFR _L		1	0.11	0.11	0.08	0.00	Ns
AS _Q x AFR _Q		1	25.03	25.03	18.27	1.07	*
(e)		2	2.74	1.37	-	2.27	-
Total		26	1,572.52	60.48	-	-	-

Table 5. ANOVA Analysis - AFS Number After Cutting

Source	P	DF	S	V	F	• , %	Remarks
P		2	1,252.66	626.37	112.00	60.37	***
P _L		1	1216.82	1216.82	108.78	58.90	***
P _Q		1	35.84	35.84	6.40	1.47	Ns
TR		2	62.74	31.37	5.61	2.51	Ns
AS		2	151.19	75.59	13.52	6.81	*
AS _L		1	144.52	144.52	25.83	6.75	**
AS _Q		1	6.68	6.68	1.20	0.06	Ns
AFR	Y	2	11.19	5.59	1.00	0.00	Ns
E		6	257.11	42.85	7.66	10.87	Ns
P x TR		4	175.70	43.93	7.85	7.46	Ns
P x AS		4	101.93	25.48	4.56	3.87	Ns
TR x AS		4	43.93	10.98	1.96	1.05	Ns
(e)		2	11.19	5.60	-	7.07	-
Total		26	2,056.52	79.097	-	-	-

Table 6. ANOVA Analysis - Depth of Cut

Source	P	DF	S	V	F	• , %	Remarks
P		2	523.91	261.96	10.42	15.74	**
P _L		1	414.98	414.98	16.51	12.95	**
P _Q		1	109.01	109.01	4.34	2.79	Ns
TR		2	547.70	273.85	10.89	16.53	**
TR _L		1	491.41	491.41	19.55	16.33	**
TR _Q		1	56.29	56.29	2.24	1.87	Ns
AS		2	112.92	56.46	2.25	2.08	Ns
AFR		2	564.20	282.10	11.22	17.08	**
AFR _L		1	529.75	529.75	21.07	17.60	**
AFR _Q		1	34.44	34.44	1.37	1.14	Ns
E		6	334.51	55.75	2.22	6.10	Ns
P x TR	Y	4	100.55	25.14	1.00	0.00	Ns
P x AS		4	438.27	109.57	4.36	11.22	*
P _L x AS _L		1	28.83	28.83	1.15	0.12	Ns
P _L x AS _Q		1	9.16	9.16	0.32	0.00	Ns
P _Q x AS _L		1	120.78	120.78	4.80	3.18	*
P _Q x AS _Q		1	279.50	279.50	11.12	8.45	**
TR x AS		4	387.30	96.82	3.85	9.53	Ns
(e)		4	100.55	25.14	-	21.72	-
Total		26	3,009.34	115.74	-	-	-

* Significant at 90 % Confidence level,

** Significant at 95 % Confidence level,

*** Significant at 99 % Confidence level,

Ns -Not Significant, Y- Pooled.

Table 7. ANOVA Analysis - Top Kerf Width

Source	P	DF	S	V	F	• , %	Remarks
P		2	0.025	0.013	3.250	5.94	Ns
TR		2	0.028	0.014	3.500	6.99	Ns
AS		2	0.030	0.015	3.750	7.69	Ns
AFR		2	0.027	0.014	3.500	6.64	Ns
E		6	0.050	0.008	2.000	9.09	Ns
P x TR	Y	4	0.016	0.004	1.000	0.00	Ns
P x AS		4	0.088	0.022	5.500	25.17	*
P _L x AS _L		1	0.001	0.001	0.250	0.00	Ns
P _L x AS _Q		1	0.009	0.009	2.250	1.75	Ns
P _Q x AS _L		1	0.004	0.004	1.000	0.00	Ns
P _Q x AS _Q		1	0.073	0.074	18.50	24.13	**
TR x AS		4	0.025	0.006	1.500	3.15	Ns
(e)		4	0.016	0.004	-	36.36	-
Total		26	0.286	0.011	-	-	-

Table 8. ANOVA Analysis - Bottom Kerf Width

Source	P	DF	S	V	F	• , %	Remarks
P		2	0.005	0.002	1.00	0.33	Ns
TR		2	0.090	0.045	22.50	28.48	**
TR _L		1	0.071	0.071	35.50	22.85	**
TR _Q		1	0.018	0.018	9.00	5.30	*
AS	Y	2	0.005	0.003	1.50	0.33	Ns
AFR		2	0.028	0.014	7.00	7.95	Ns
E		6	0.102	0.017	8.50	29.80	Ns
P x TR		4	0.024	0.006	3.00	5.30	Ns
P x AS		4	0.031	0.007	3.50	7.62	Ns
TR x AS		4	0.018	0.005	2.50	3.31	Ns
(e)		2	0.005	0.002	-	17.22	-
Total		26	0.302	0.012	-	-	-

Table 9. ANOVA Analysis - Kerf Taper

Source	P	DF	S	V	F	• , %	Remarks
P		2	0.032	0.016	3.98	3.33	Ns
TR		2	0.150	0.075	18.80	19.69	***
TR _L		1	0.051	0.051	12.64	6.52	**
TR _Q		1	0.100	0.100	24.96	13.31	***
AS		2	0.105	0.052	13.11	13.45	**
AS _L		1	0.103	0.103	25.65	13.73	***
AS _Q		1	0.002	0.002	0.57	0.00	Ns
AFR		2	0.022	0.011	2.76	1.94	Ns
E		6	0.193	0.032	7.177	23.44	**
P x TR		4	0.114	0.028	6.352	13.59	**
P _L x TR _L		1	0.082	0.082	20.419	10.82	**
P _L x TR _Q		1	0.021	0.021	5.329	2.36	*
P _Q x TR _L		1	0.007	0.007	1.849	0.42	Ns
P _Q x TR _Q		1	0.004	0.004	0.884	0.00	Ns
P x AS	Y	4	0.018	0.004	0.000	0.28	Ns
TR x AS		4	0.077	0.019	4.305	8.46	*
TR _L x AS _L		1	0.022	0.022	5.547	2.50	*
TR _L x AS _Q		1	0.005	0.005	1.296	0.14	Ns
TR _Q x AS _L		1	0.049	0.049	12.321	6.24	**
TR _Q x AS _Q		1	0.000	0.000	0.027	0.00	Ns
(e)		4	0.018	0.004	-	14.63	-
Total		26	0.711	0.027	-	-	-

Table 10. ANOVA Analysis - Surface Roughness at Upper Section

Source	P	DF	S	V	F	• , %	Remarks
P		2	8.667	4.333	2.151	3.77	Ns
TR		2	8.000	4.000	1.986	3.23	Ns
AS		2	7.796	3.898	1.935	3.06	Ns
AFR	Y	2	4.029	2.014	1.000	0.00	Ns
E		6	22.793	3.799	1.886	8.70	Ns
P x TR		4	20.867	5.217	2.590	10.41	Ns
P x AS		4	14.218	3.554	1.764	5.01	Ns
TR x AS		4	36.631	9.158	4.546	23.23	Ns
(e)		2	4.029	2.014	-	42.58	Ns
Total		26	123.000	4.731	-	-	Ns

Table 11. ANOVA Analysis - Surface Roughness at Middle Section

Source	P	DF	S	V	F	• , %	Remarks
P		2	4.364	2.182	2.856	2.37	Ns
TR		2	15.705	7.852	10.277	11.85	**
TR _L		1	7.996	7.996	10.465	6.04	**
TR _Q		1	7.709	7.709	10.089	5.80	**
AS		2	19.745	9.872	12.921	15.22	**
AS _L		1	3.735	3.735	4.888	2.48	*
AS _Q		1	16.010	16.010	20.954	12.74	**
AFR	Y	2	1.528	0.764	1.000	0.00	Ns
E		6	35.124	5.854	7.662	25.52	**
P x TR		4	25.341	6.335	8.292	18.62	**
P _L x TR _L		1	0.067	0.067	0.088	0.00	**
P _L x TR _Q		1	0.841	0.841	1.101	0.06	*
P _Q x TR _L		1	17.223	17.223	22.541	13.75	***
P _Q x TR _Q		1	7.211	7.211	9.437	5.39	**
P x AS	Y	4	5.082	1.271	1.663	1.70	Ns
TR x AS		4	12.804	3.201	4.189	8.15	*
(e)		6	6.609	1.101	-	16.59	-
Total		26	119.687	4.603	-	-	-

Table 12. ANOVA Analysis - Surface Roughness at Lower Section

Source	P	DF	S	V	F	• , %	Remarks
P		2	44.464	22.232	9.105	10.56	*
P _L		1	43.861	43.861	17.964	11.05	*
P _Q		1	0.603	0.603	0.247	0.00	Ns
TR		2	15.766	7.883	3.229	2.90	Ns
AS		2	15.264	7.632	3.126	2.77	Ns
AFR	Y	2	4.883	2.442	1.000	0.00	Ns
E		6	64.473	10.746	4.401	13.30	Ns
P x TR		4	81.322	20.331	8.326	19.10	Ns
P x AS		4	60.369	15.092	6.181	13.50	Ns
TR x AS		4	88.143	22.036	9.025	20.92	Ns
(e)		2	4.883	2.442	-	16.94	-
Total		26	374.707	14.412	-	-	-

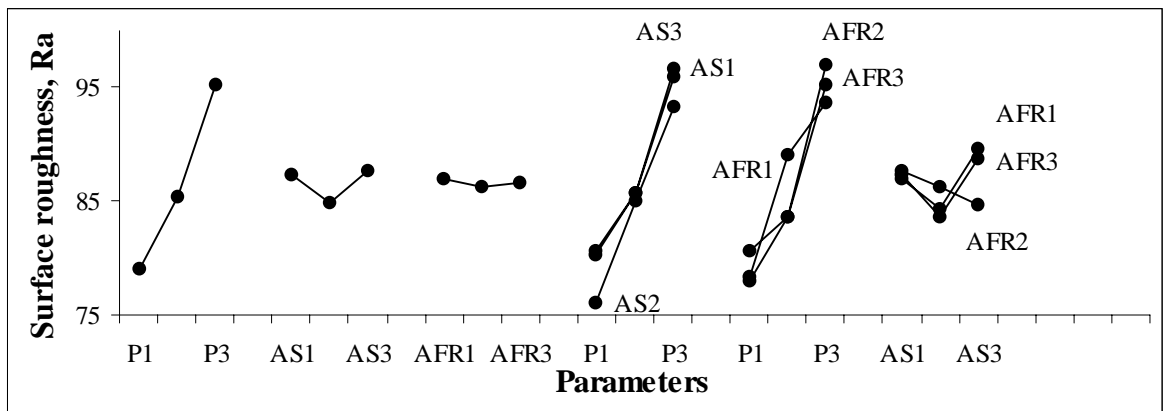


Figure 1. Mean Responses – Parameters Vs AFS Number at Nozzle Exit

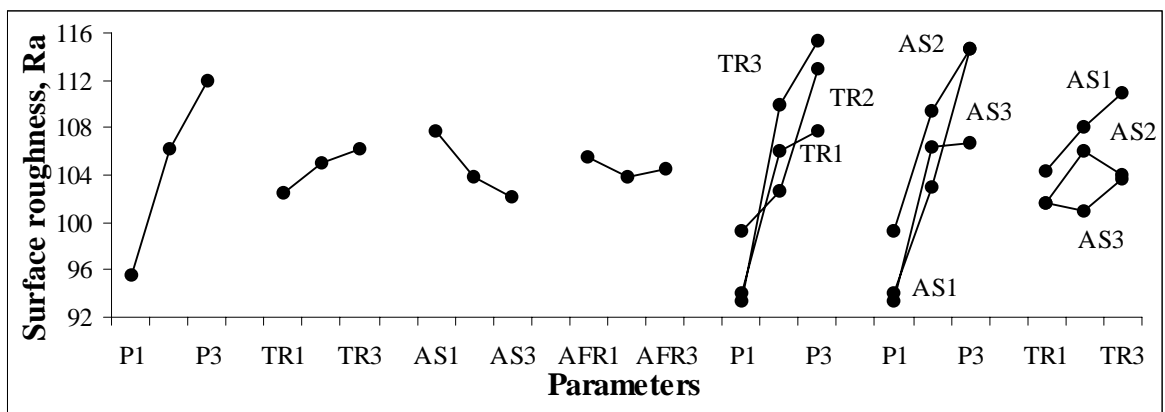


Figure 2. Mean Responses – Parameters Vs AFS Number After Cutting

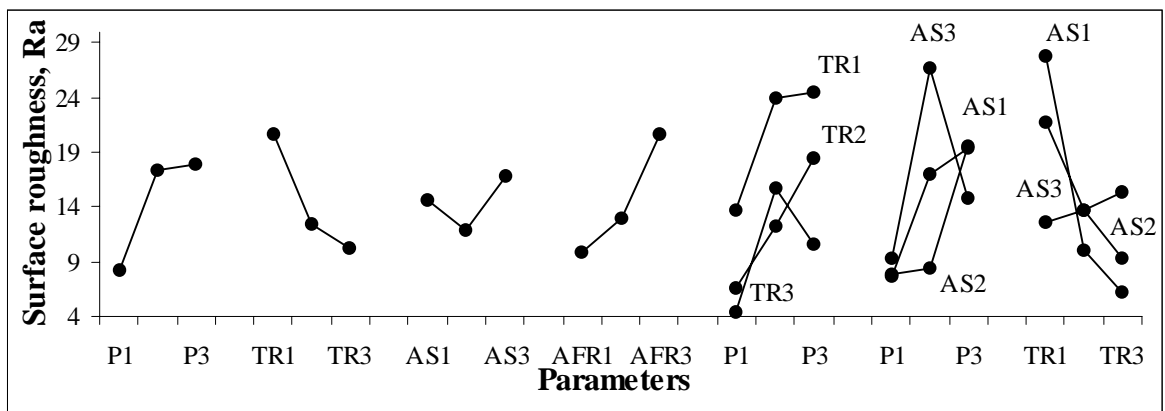


Figure 3. Mean Responses – Parameters VS Depth of Cut

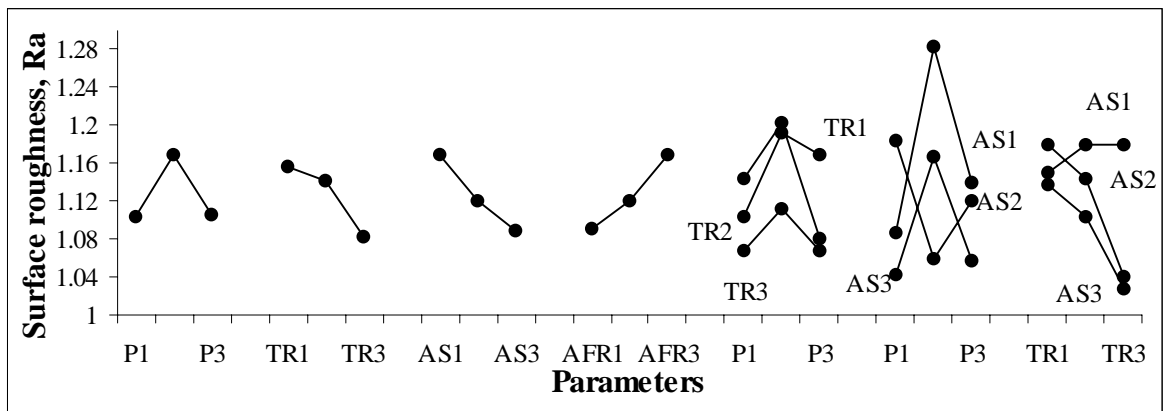


Figure 4. Mean Responses – Parameters Vs Top Kerf Width

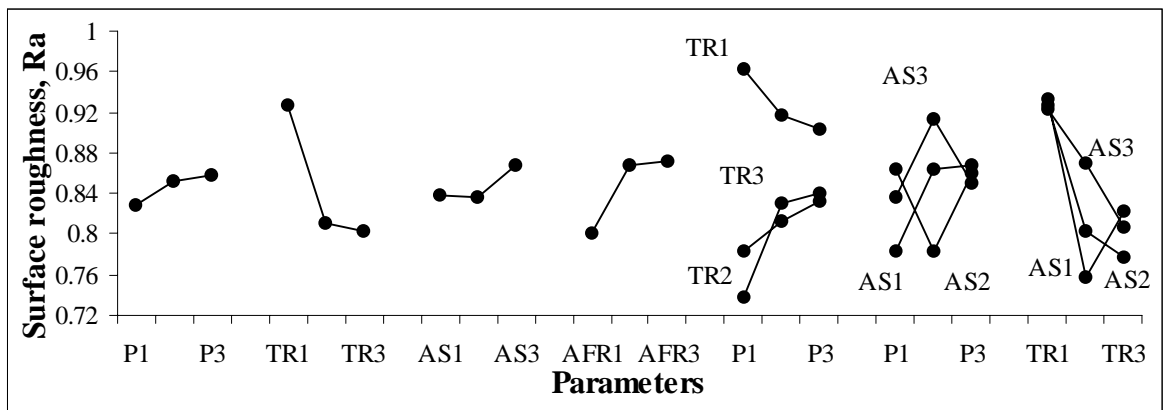


Figure 5. Mean Responses – Parameters Vs Bottom Kerf Width

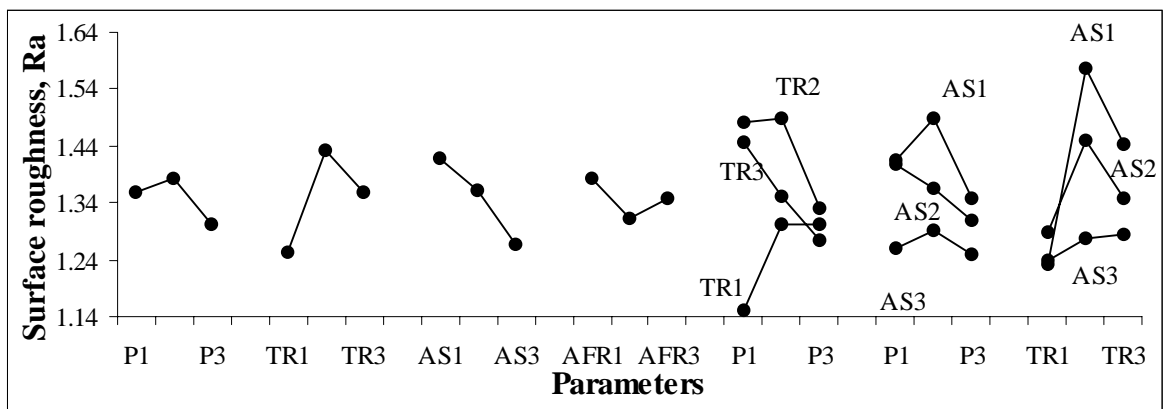


Figure 6. Mean Responses – Parameters Vs Kerf Taper

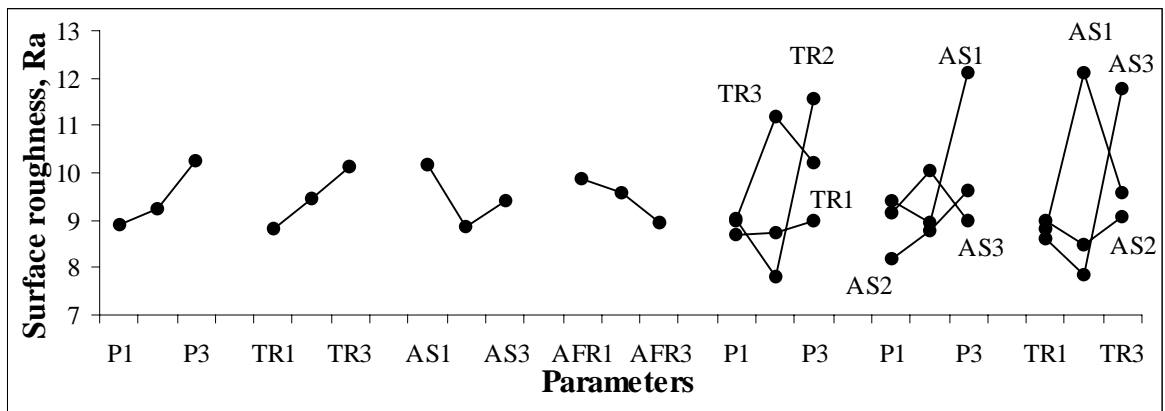


Figure 7. Mean Responses – Parameters Vs Surface Roughness at Upper Section

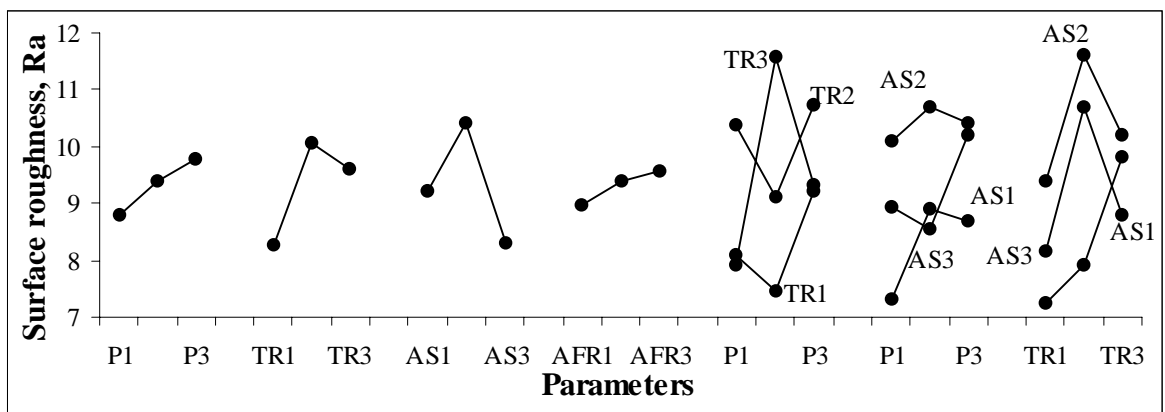


Figure 8. Mean Responses – Parameters Vs Surface Roughness at Middle Section

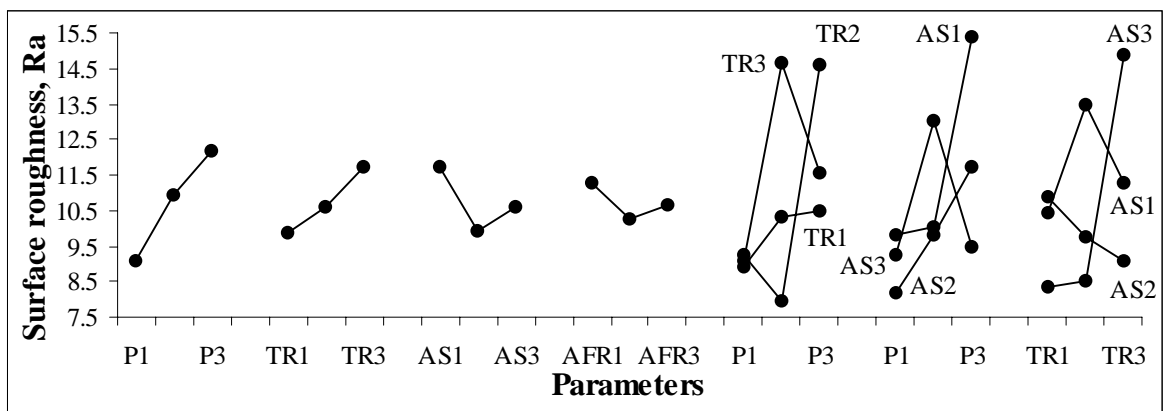


Figure 9. Mean Responses –Parameters Vs Surface Roughness at Lower Section

ULTRA HIGH PRESSURE WATERJET PEENING

PART I: SURFACE TEXTURE

S. Kunaporn and M. Ramulu
University of Washington
Seattle, Washington, USA

M. Hashish and J. Hopkins
Flow International
Kent, Washington, USA

ABSTRACT

An experimental study was conducted to investigate the influence of high-pressure waterjet peening conditions on surface characteristics of a 7075-T6 aluminum alloy. Surface profilometry and scanning electron microscopy (SEM) were used in characterizing the surface texture and topography. Surface characteristics in terms of surface texture on peened specimens in relation to peening conditions were analyzed and discussed. It was found that the magnitude of erosion on material surface by the impingement of high-pressure waterjets was strongly dependent on the applied peening conditions.

1. INTRODUCTION

Waterjet peening is a recent surface treatment technique that has been developed to improve the fatigue performance of materials as an alternate to the conventional shot peening process [1-5]. Most of the surface processing methods not only affects the surface layers but also alters the surface microstructural irregularities. The local irregularities or the surface roughness is the stress concentrations, which reduce the fatigue limit of the material. In addition, surface roughness and tolerance are also closely related, and it is generally necessary to specify a smooth finish to maintain a fine tolerance in the finishing process. For many practical design applications, it is the tolerance and strength requirements that impose a limit on the maximum allowable roughness. The reliability of manufactured components is often critically dependent upon the quality of surface produced by machining, and the surface layer may drastically affect the strength and chemical resistance of the material

Prior studies [6-16] have reported that the high-pressure flow of water at supply pressure below 150 MPa have the same deformation effects as conventional shot peening, but with negligible changes in surface roughness and topology. However, the common problem of using peening is the introduction of surface and subsurface damage and erosion on the target. Erosion and micro-fracture induced by the jets are expected if the applied process conditions are beyond a certain threshold values of target material. Process conditions that include pressure, traverse rate, stand off distance, jet exposure time, and the types of jets (round or fan). There is no systematic investigation is conducted to study the surface textures generated by waterjet peening process that includes the round and fan jets.

The objective of this study is to evaluate the performance of high-pressure waterjets ($P \geq 150$ MPa) on a 7075-T6 aluminum alloy through an examination of surface characteristics. Surface characteristics induced by different jet conditions were evaluated and discussed to define suitable peening conditions. Surface characteristics of the component in general, are discussed, in terms of surface texture and surface integrity [18]. Surface texture is a term used to describe the exterior features of the surface such as surface roughness, lay, and pits etc., while surface integrity is defined as the inherent condition of a surface layer, which pertains to properties such as micro-structural transformations, hardness alternation, residual stress distribution etc. The investigation of both surface texture and surface integrity of materials after peening will provide useful information on the states of materials, which will be later employed for the fatigue performance study.

2. MATERIAL AND METHODS

The aluminum alloy 7075-T6 was employed in this study. The Al7075-T6 has an elastic young modulus of 72 GPa, a yield strength and ultimate tensile strength of 516 and 587 MPa, respectively. The waterjet peening studies were performed on two types of test specimens: the 64 mm thick plate and 6.3mm diameter circular cross section test specimens.

The waterjet peening process involves accelerating water to very high velocities with the high intensifies pump before accelerating the water out of the nozzle to impact against the surface. Figure 1 schematically shows the parameters relevant to waterjet peening in this study. Jet velocity at the nozzle exit can be calculated using Bernoulli's law:

$$V_j = \sqrt{\frac{2P}{\rho}} \quad (1)$$

where ρ is the density of the water. The high-pressure waterjets coming out of the nozzle are considered to contain the kinetic energy, which can be calculated by [19]

$$E = \frac{1}{2} m_w V_j^2 \quad (2)$$

where m_w is the resulting mass of the water, which is equal to $\rho A_n V_j T_e$, and A_n is the cross section area of the nozzle, and T_e is the exposure time of the jets on material surface.

The waterjet peening system employed a high-pressure pump with control unit, capable of generating waterjet pressures up to 400 MPa. The pressurized water was directed through a 0.3-mm diameter sapphire orifice before entering a nozzle specially designed for the purpose of waterjet peening. The nozzle was oriented perpendicular to the surface of the test specimen. With the test specimen fixed in a holder, the nozzle was moved and adjusted to obtain an appropriate nozzle-to-surface standoff distance, X (Figure 2). Table 1 listed the peening conditions. Number of passes and nozzle feed speed were varied to observe the effect of jet energy on material surface.

As received and waterjet peened surfaces were examined using SEM and optical microscopy to investigate surface characteristics. The surface texture resulting from the machined and peened samples was measured using contact profilometry with a commercial profilometer and 5 μ m stylus. All measurements were obtained according to *ANSI B46.1-1986* [17] using a 0.8 mm cutoff length and 3.5 mm traverse length. Conventional roughness parameters, including the arithmetic average roughness (R_a), peak to valley height (R_y), root mean square roughness (R_q) and ten-point height (R_z) were calculated from each profile. Various statistical and random process methods were used in addition to standard roughness parameters to analyze the peened surface characteristics.

3. RESULTS AND DISCUSSIONS

The implementation of two (round and fan-jet) nozzles for waterjet peening played an important role on the peened surface condition. Surface finish, texture, the degree of induced subsurface hardness and compressive residual stresses.

3.1 Surface Examination

The surface roughness and statistical parameters data for the flat test specimens (conditions A-C) using round and fan-jet nozzles are shown in Figure 3. It is evident that the water peening using the round-jet nozzle caused rougher surface than those using the fan-jet nozzle for stand off distance greater than 36 mm. In the case of fan-jet nozzle, although the kinetic jet energy was increased, there were little changes in roughness parameters again at standoff distance greater than 36 mm. However, at low stand off distance (less than 30mm) had significant effect on surface roughness parameters with fan-jet nozzle.

Peening conditions that have been implemented on the flat surface were applied to the circular cross section specimens. Note that all specimens were waterpeened using the fan-jet nozzle under the same supply peening pressure, 310 MPa (condition D). The distribution of surface roughness parameters with respect to different standoff distances of the circular cross section test specimens are shown in Figure 4-a, while Figure 4-b shows the distribution for those with respect to different jet exposure times (the nozzle feed rates and a number of passes). All surface roughness gave similar values of the arithmetic surface roughness (R_a) and the root-mean-square (RMS) roughness (R_q), while maximum peak-to-valley height (R_y) and the ten-point roughness (R_z) were within the scatter of less than 5%. It was observed that the average surface roughness parameters obtained between peened and unpeened surface have little difference in magnitude, however, maximum peak-to-valley height (R_y) and the ten-point roughness (R_z) varied and had a minimum value at 46mm stand off distance. Surface roughness parameters were clearly dependent on the jet exposure time as shown in Figure 4b. Best surface treating condition was associated with the jet exposure time of 0.2s and is at a stand off distance 46mm. Therefore, R_a and R_q values might not be the parameters that can indicate the surface characteristics or distinguish the effect of the jets on material surface.

Optical examination of peened surface was conducted and surface profile corresponding to the examined surface was analysed for each specimen to discern the waterpeened surface topography under different peening process conditions. Figure 5 showed the optical micrographs and the corresponding surface roughness profile of each specimen. It was noticed that there was surface deformation in the test specimens waterpeened at the standoff distance lower than 43 mm in the form of pronounced machined feed marks. Little changes of surface finish are noticed in the specimens waterpeened at the standoff distance greater than 44 mm. Increasing the peening time by varying the nozzle transverse speed and a number of jet passes showed increase in all surface parameters can be seen increasing surface damage in Figure 5b. It is found that waterjet peening under the same peening time yielded similar surface roughness parameters and surface finish, although the nozzle feed rate and a number of jet passes were different. It can be explained by that under the same peening time, the resulting kinetic energy of the jet on those specimen surfaces was equal. Results of weight loss of each specimen as compared to that of the unpeened conditions are plotted in Figure 6. The weight loss of specimens increased when the standoff distances decreased and peening time increased.

3.2 Surface Texture

Statistical parameters i.e. surface height distribution, bearing ratio, power density spectra, auto-correlation function were applied to evaluate the randomness of the surface texture. Statistical parameters, skewness and kurtosis, for specimens waterpeened by the fan-jet nozzle and the round-jet nozzle were examined. Surface skewness is the term that defines the nature of an asymmetrical surface distribution with respect to a purely symmetric or "Gaussian" spread, while kurtosis is used to identify the relative peakedness or flatness of the distribution compared with the normal distribution. A negative skewness is ideal for bearing surfaces that require large effective contact areas and lubrication reservoirs within the valleys of the lay. Positive skewness is more effective in minimizing fatigue failures through free abrasive erosion. Metals with greater resistance to abrasive penetration would be prone to exhibit a negatively skewed surface. Materials responsive to abrasive wear are more likely to exhibit a positively skewed surface due to the reduction in wear resistant surface stress concentrations [20]. Surface height skewness and kurtosis were calculated from the surface profile data using two different types of the nozzles and are shown in Figure 7. Fan-jet nozzle peened surfaces was Gaussian and had a kurtosis and skewness nearly equal to 3 and zero. The surfaces waterpeened by the round jet nozzle skewed negatively with higher value of kurtosis as compared to those specimen waterpeened by the fan-jet nozzle. This may be due to that the round jet nozzle eroded material surface causing pits or flaws by the penetration of the jet. These pits and flaws are undesirable because they may act as a crack initiation site and may reduce fatigue life of material. Therefore, the fan jet nozzle is more suitable for waterjet peening.

Figure 8 shows the height distribution and its height cumulative distribution, corresponding to the surface profiles of the round specimens shown in Figure 5. The normal distribution is a probability function that gives the probability of the surface profile that has a certain height at any positions of the surface, while the Abbot-Firestone curve or bearing ratio is the terminology used to describe the percentage of material to air of the surface profiles at any contact surface level [20-21]. It is observed from Figure 8a that the normal distribution of the all specimens waterpeened under standoff distance from 38 mm to 48 mm (condition D) showed almost similar bearing ratio, and Gaussian properties with lower peak in the specimen waterpeened at shorter standoff distances. The specimens waterpeened at longer peening time showed a more broad range in profile height distribution, with negative skew of the peak with different bearing ratio characteristics. Moreover, the bearing area fraction decreased as the peening time increased.

The stochastic properties of the surface were further examined by using power spectral density and auto correlation relations. Figure 9 shows the typical power spectrum density (PSDF) function and the auto-correlation function corresponding to the unpeened surface and the peened surface profiles shown in Figure 5b. The PSDF curve shows that with increasing peening time and decreasing standoff distances, the spectrum weight corresponding to a peak of the curve increased with the higher frequency ($\omega/2\pi$) of the wave. Note that the inverse of the frequency in the PSDF is the period of the repeated pattern on the surface in millimeters, which can be obtained in the autocorrelation functions. The autocorrelation decreased from decreased rapidly from 1 to zero stabilized. The typical correlation wavelength of waterpeened specimens at X of 38 mm and 41 mm were identical to that of unpeened specimen which was about 50 μm . However, correlation wave length of the specimen waterpeened at longer peening time was at

about 40 μm . Comparison of the normal distribution and the bearing ratio curves in Figure 8, it becomes evident that the waterjets cause the surface rougher when peening at lower standoff distance and longer peening time. Peening using standoff distance greater than 46 mm under condition D revealed negligible changes in surface texture as compared to that of the unpeened surface.

3.3 Surface and Sub-Surface Microstructure

Micro hardness measurements made on peened flat surfaces are shown in Figure 10. Results obtained from micro hardness measurement showed that a maximum increase in micro hardness of specimen waterpeened using the fan-jet nozzle was about 30 % greater than that of the base material. In contrast, there was less improvement of the micro hardness in waterpeened by the round-jet nozzle.

Compressive residual stress measurement was made on specimen surface by x-ray diffraction method. The residual stress results obtained from the specimens waterpeened by both the fan-jet nozzle and the round-jet nozzle are depicted in Figure 11. Results did show that waterjet peening induced the compressive residual stress in material surface. It was found that the degree of induced surface residual stress by the round-jet nozzle was greater than that of the fan-jet nozzle (Figure 11a). An increase in jet exit pressure and a decrease in a nozzle-to-surface distance increased the compressive residual stresses. Although the degree of surface compressive residual stresses induced by the fan-jet nozzle was generally lower than those by the round jet nozzle, it appears that waterjet peening by the round jet nozzle trended to cause rougher surface or greater surface erosion with little improvement of the subsurface micro hardness. As a result, the fan jet nozzle was chosen for conducting for further study on waterjet peening. In comparison to those in the unpeened specimen, all those specimens exhibited an increase in compressive residual stresses. The magnitude of residual stress was found to increase when the standoff distance increased with the magnitude lies between 200 MPa to 600 MPa. The results of induced compressive residual stress by waterjet peening in this study were in agreement with those obtained in shot peening by Was et al [3]. Moreover, increasing peening time, the compressive residual stress decreases as shown in Figure 11b. This might be due to the presence of the significant mass removal that was detected in the specimens as discussed in previous section.

4. CONCLUSION

Results from the investigation of surface characteristics showed that changes of surface produced by high-pressure waterjets were strongly dependent of peening parameters. It was found that waterjets did induced plastic deformation on material surface. A decrease in compressive residual stress was expected at longer peening time and shorter standoff distance when material removal occurred. Statistical functions have been used to distinguish and define appropriate standoff distance for waterjet peening. Results also showed that the changes in surface roughness and topology are directly influenced by the kinetic energy that has been transferred to target material. Therefore the same surface characteristics on the target material are obtained by

using an equal amount of energy supplied by the jet. These results might be the useful information in waterjet peening application and further study.

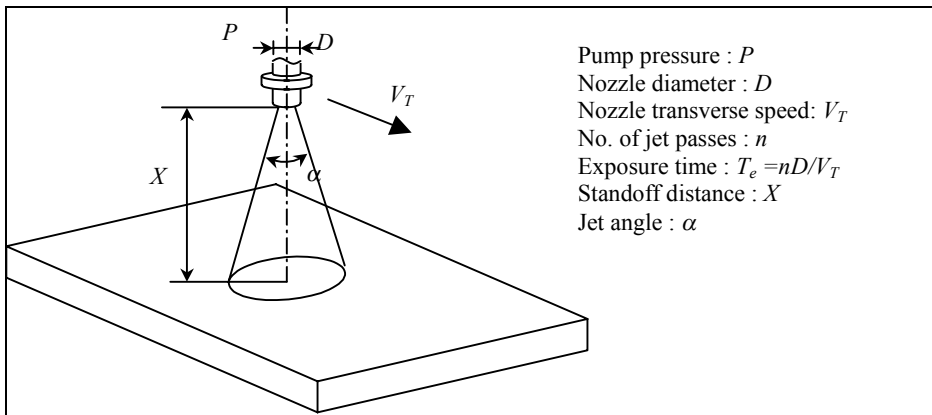
5. REFERENCES

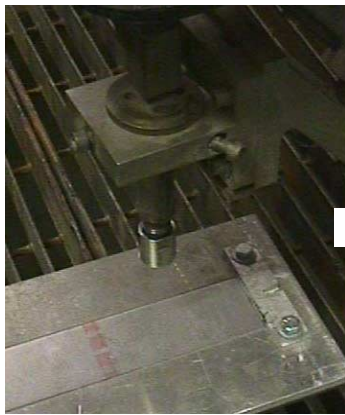
1. A Niku-Lari, "Shot Peening," 1st International Conference on Shot Peening, Paris, 14-17 September 1981, pp.1-21.
2. Hammond, D.W., "Crack Propagation in the Presence of Shot-peening Residual Stress," *Engineering Fracture Mechanics*, Vol.37, No.2, 1990, pp. 373-387.
3. Was, G.S., Pelloux, R. M. and Frabolot, M.C., "Effect of Shot Peening Methods on The Fatigue Behavior of Alloy 7075-T6," 1st International Conference on Shot Peening, Paris, 14-17 September 1981, pp.445-451.
4. Marsh, K.J., *Shot Peening: Techniques and Applications*, Engineering Materials EMAS Ltd., Warley, UK, 1993.
5. Verport, C.M., and Gerdes, C., "Influence of Shot Peening on Material Properties and the Controlled Shot Peening Blades", 1st published in Metal Behavior and Surface Engineering, ITTT-International, 1989.
6. Blickwedel, H., Haferkamp, H., Louis, H. and Tai, P.T., "Modification of Material Structure by Cavitation and Liquid Impact and Their Influence on Mechanical Properties," *Erosion by Liquid and Solid Impact*, Proc. 7th International Conference on Erosion by Liquid and Solid Impact, 7-10 September 1987, pp.31.1-31.6.
7. Tonshoff, H.K, Kroos F, and Hartmann, M., "Water Peening – An Advanced Application of Water Jet Technology," 8th American Water Jet Conference, August 26-29, 1995, paper 33, pp. 473-486.
8. Daniewicz, S.R., and Cummings, S.D., "Characterization of Water Peening Process", Transaction of the ASME, Vol. 121, July 1999, pp. 336-340.
9. Yamaushi, Y., Soyama, H., Adashi, Y., Sato, K., Shindo, T., Oba, R, Oshima, R., and Yamabe, M., "Suitable Region of High-Speed Submerged Water Jets for Cutting and Peening," *JSME International Journal*, Series B, Vol.8, No.1, 1995, pp.31-38.
10. Mathias, M., Gocke, A. and Pohl, M., "The Residual Stress, Texture and Surface Changes in Steel Induced by Cavitation", *Wear*, Vol.150, 1991, pp. 11-20.

11. Colosimo, B. M.; Monno, M., Semeraro, Q., "Process Parameters Control in Water Jet Peening" *International Journal of Materials and Product Technology*, Vol. 15 (1-2), 2000, pp. 10-19.
12. M. Ramulu, S. Kunaporn, M.Jenkins, M. Hashish and J.Hopkins, "Peening with High Pressure Waterjets" *SAE technical Paper Series No. 1999-01-2285. Aerospace Manufacturing Technology Conference and Exposition*, Bellevue, Washington, June 8-10,1999.
13. M. Ramulu, S. Kunaporn, D.Arola, M. Hashish and H.Jordon., " Waterjet Machining and Peening of Metals" *ASME Journal of Pressure Vessel Technology*, Vol 122, (1), 2000, pp.90-95.
14. Arola, D. and McCain, M. L., "Abrasive Waterjet Peening: A New Method of Surface Preparation for Metal Orthopedic Implants," *Journal of Biomedical Materials Research: Applied Biomaterials*, (in press) 2000.
15. Arola, D. and M. Ramulu, "Material Removal in Abrasive Waterjet Machining of Metals. Part I: Surface Integrity and Texture," *Wear*, Vol. 210 (6), 1997, pp. 50-58.
16. Arola, D. and M. Ramulu, "Material Removal in Abrasive Waterjet Machining of Metals: A Residual Stress Analysis," *Wear*, Vol. 211 (2), 1997, 302-310.
17. ANSI Standard B46.1, " Surface Texture (Roughness, Waviness & Lay)", American National Standard Institute, Washington, D.C., 1986.
18. Kalpakjian, S., *Manufacturing Processes for Engineering Materials*, 3rd ed., Addison Wesley Longman, CA, 1997.
19. Tikhomirov, R.A., Babanin,V.F., Petukhov, E.N, Starikov, I.D, and Kovalev, V.A., *High-Pressure Jetcutting*, ASME Press, New York, 1992.
20. Whitehouse, D.J., *Handbook of Surface Metrology*, Bristol; Philadelphia : Institute of Physics Pub., c1994.
21. Thomas, E.R., *Rough Surfaces*, Longman Group Limited, London and New York, 1982 G.S. Was, R. M. Pelloux and M.C. Frabolot, " Effect of Shot Peening Methods on The Fatigue Behavior of Alloy 7075-T6," 1st International Conference on Shot Peening, Paris, 14-17 September 1981, pp.445-451.

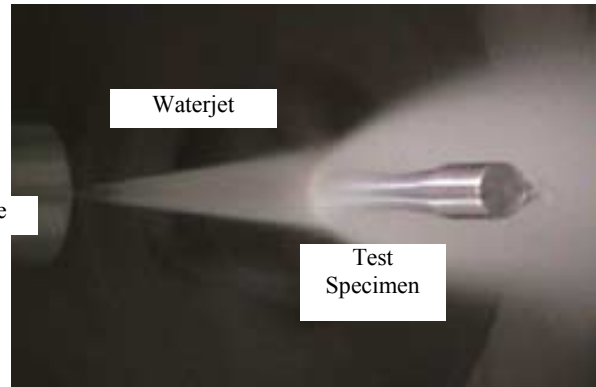
Table 1: Waterjet Peening Conditions

Condition	P (MPa)	V_j m/s	X (mm)	V_t mm/s	No. of Jet Pass	T_e (s)	E_k (kJ)	Nozzle Type	Specimen Type
A	310	787	45-109	6.98	4	0.2	3.9	fan	flat
B	310	787	36-102	6.98	4	0.2	3.9	round	flat
C	310	787	25-36	12.7	4	0.1	2.2	fan	flat
D	310	787	38-48	12.7	4	0.1	2.2	fan	round
			46-48	1.27	4	1.0	21.7		
			46-48	12.7	40	1.0	21.7		

**Figure 1. A Schematic Representation of Waterjet Peening Parameters [7].**



(a)



(b)

Figure 2. Waterjet peening operation on (a) a flat specimen and (b) a circular cross section of round specimen.

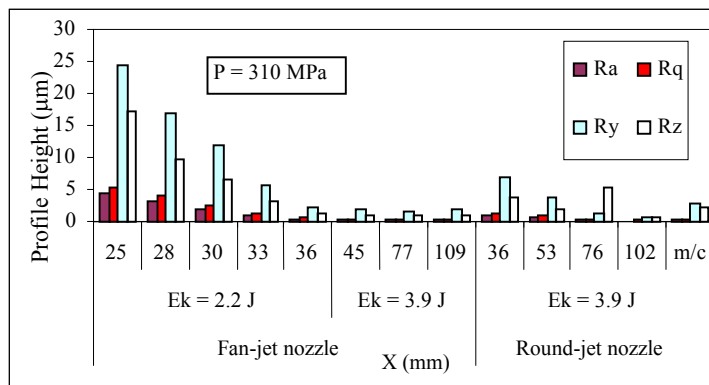


Figure 3. Surface Roughness Distribution (Condition A–C).

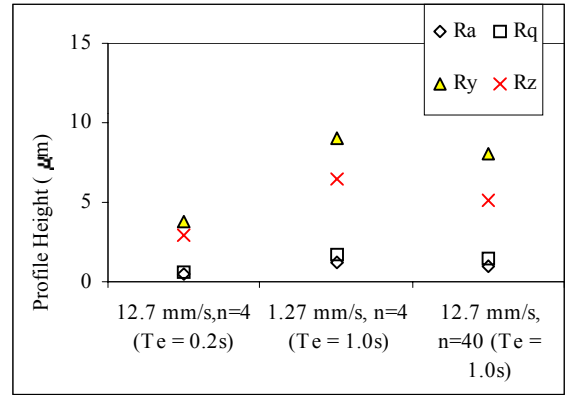
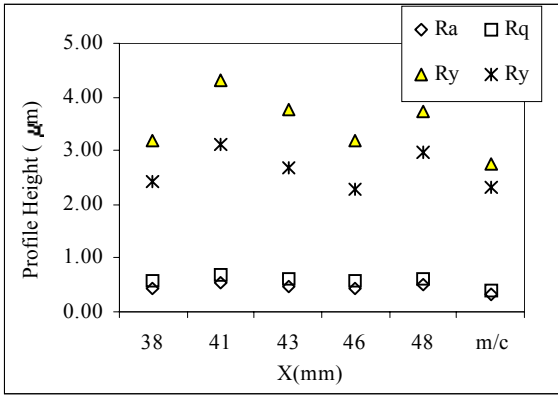


Figure 4. (a) Surface Roughness vs. X of Condition D (circular cross section fatigue test specimens), $V_T = 12.7$ mm/s, (b) Surface Roughness vs. T_e (X = 48 mm).

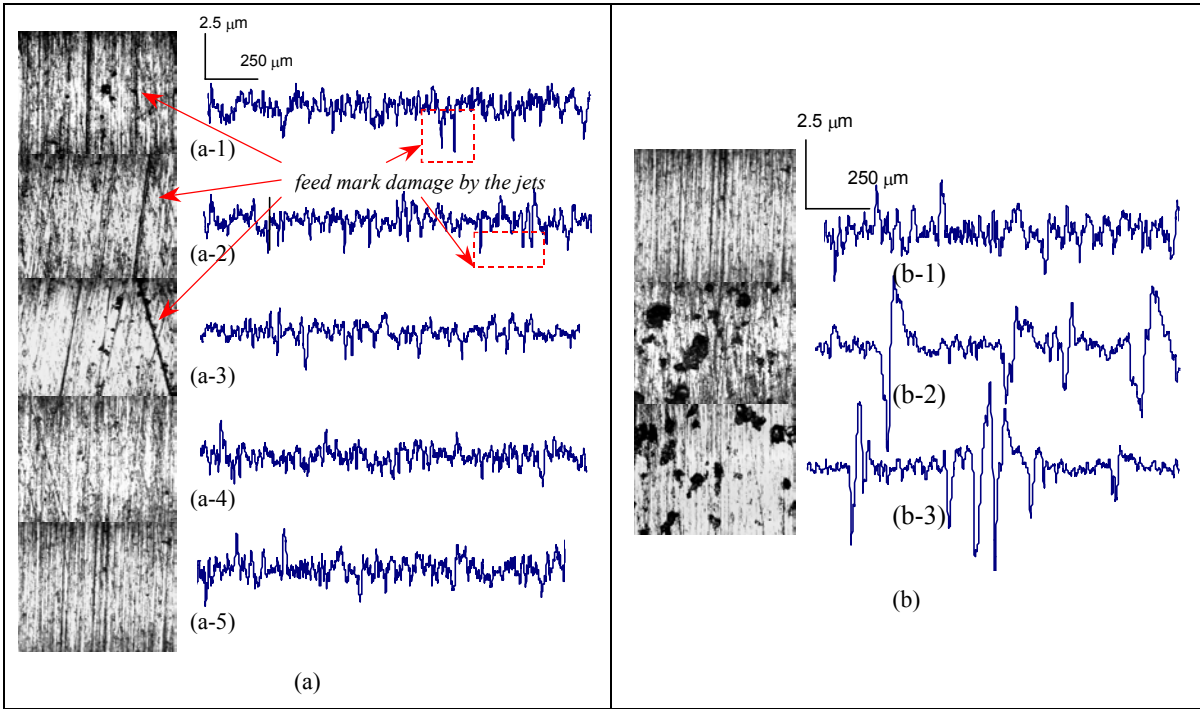
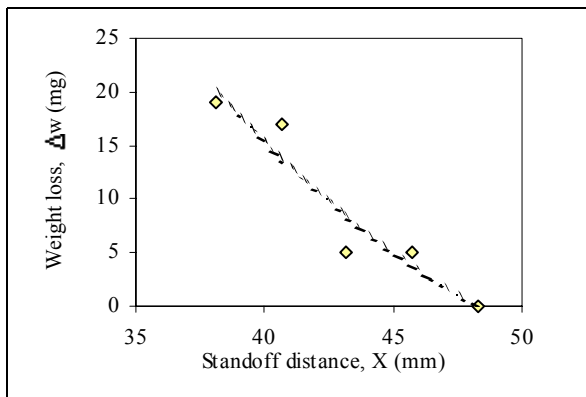
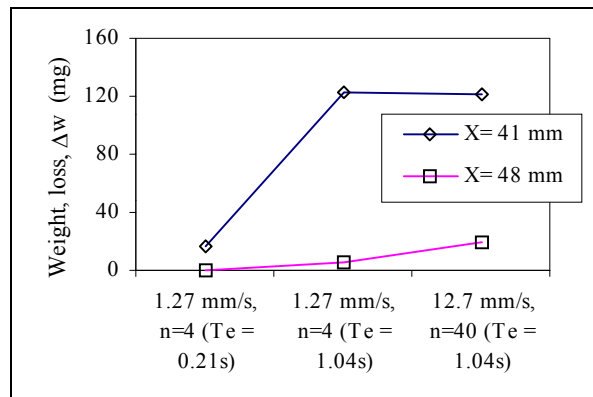


Figure 5. (a) Micrographs and corresponding surface profiles, peening condition D: (a-1) X = 31 mm, (a-2) X = 41 mm, (a-3) X = 43 mm, (a-4) X = 46 mm, and (a-5) X = 48 mm.; (b) Micrographs and corresponding surface profiles, peening condition D, X = 48 mm: (b-1) $V_T = 12.7$ mm/s, n=4 ($T_e = 0.21$ s), (b-2) $V_T = 1.27$ mm/s, n=4 ($T_e = 1.04$ s), (b-3) $V_T = 1.27$ mm/s, n=40 ($T_e = 1.04$ s).



(a)



(b)

Figure 6. (a) Weight loss (Δw) vs. X , condition D ($V_T = 12.7$ mm/s), (b) Weight loss (Δw) vs. Te .

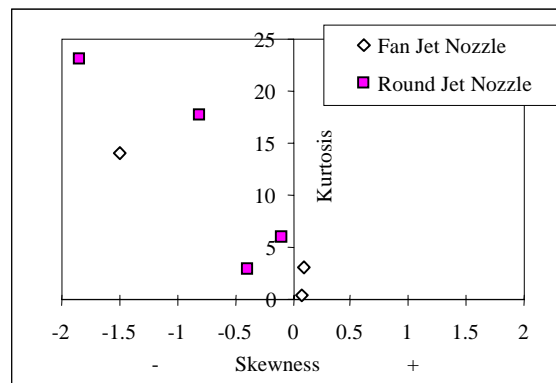


Figure 7. Skewness vs. Kurtosis (Conditions A and B).

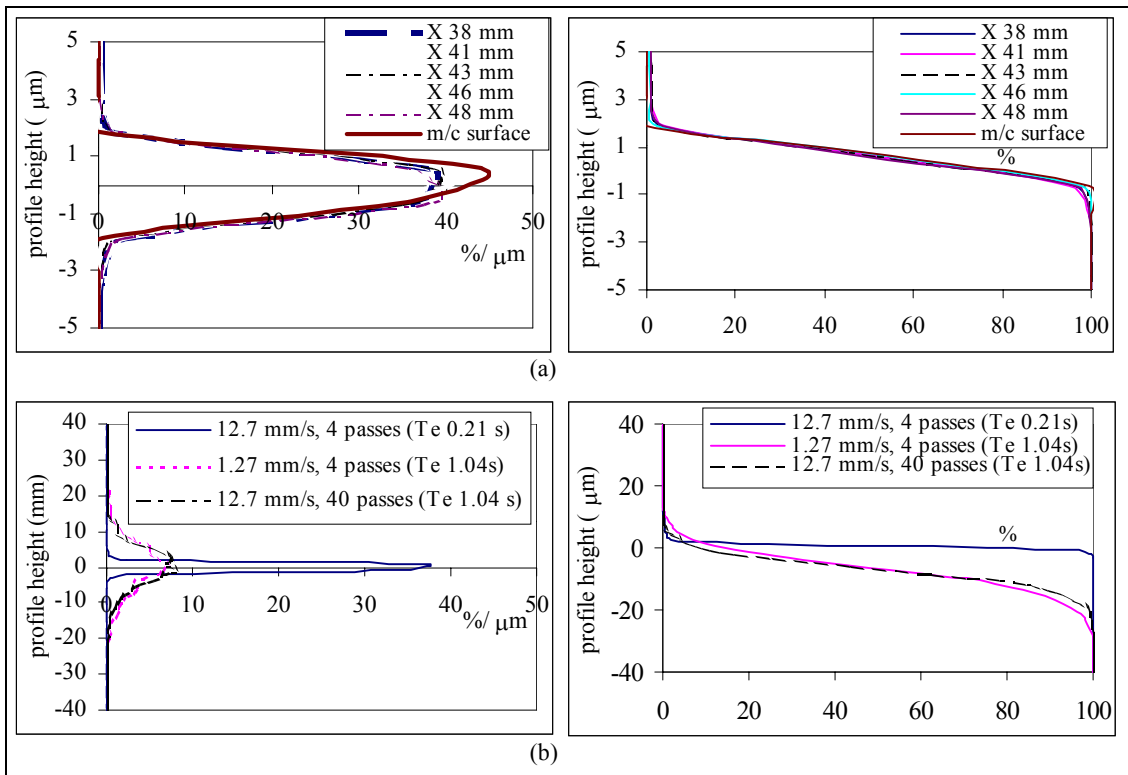


Figure 8. Typical height distribution and corresponding bearing ratio curve: (a) P= 310 MPa, $T_e=0.21$ s/mm (b) P= 310 MPa, SOD = 41 mm.

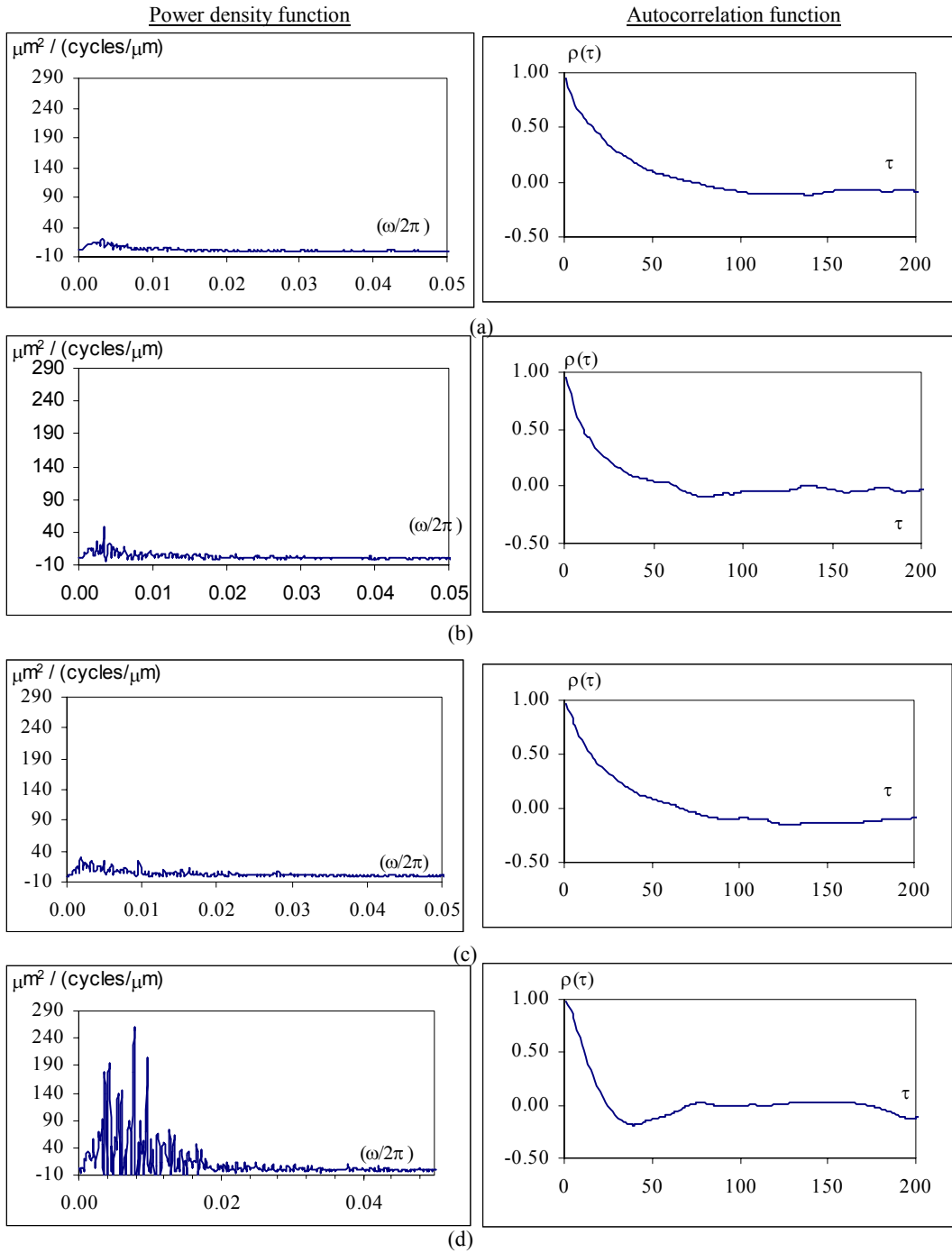


Figure 9. Power spectrum density function and autocorrelation function, condition D (a) unpeened surface, (b) $X = 38 \text{ mm}$, $T_e = 0.21 \text{ s}$, (c) $X = 41 \text{ mm}$, $T_e = 1.04 \text{ s}$ (d) $X = 41 \text{ mm}$, $T_e = 1.04 \text{ s}$.

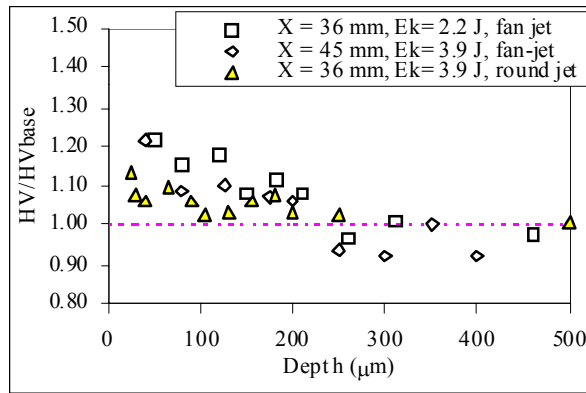


Figure 10. Typical micro hardness distribution.

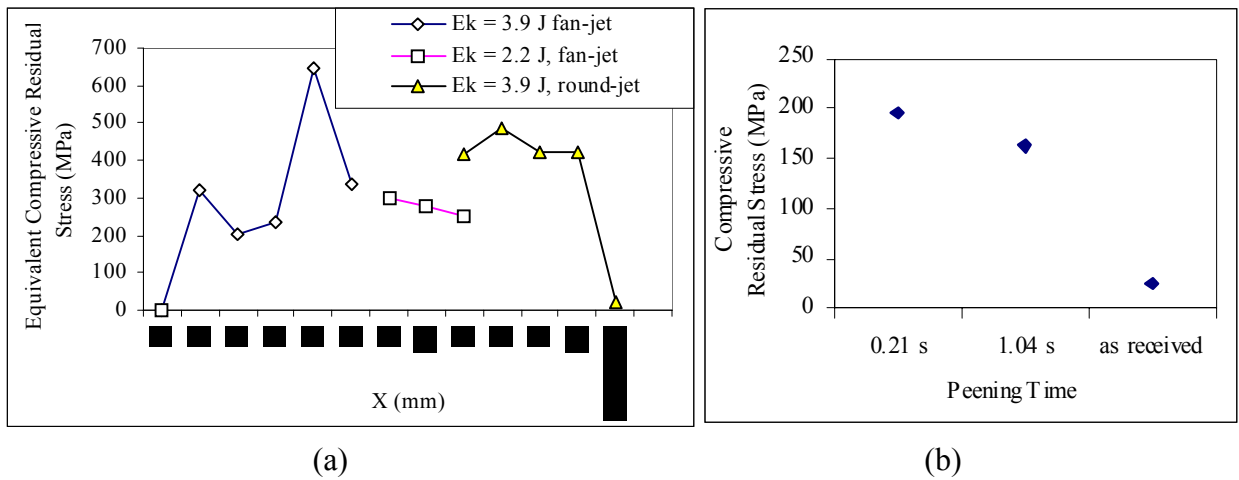


Figure 11. (a) Residual Stress vs. X, condition A-C (b) Residual Stress vs. T_e (Condition D), $X = 28 \text{ mm}$.

ULTRA HIGH PRESSURE WATERJET PEENING PART II: HIGH CYCLE FATIGUE PERFORMANCE

S. Kunaporn and M. Ramulu
University of Washington
Seattle, Washington, USA

M. Hashish and J. Hopkins
Flow International
Kent, Washington, USA

ABSTRACT

Waterjet peening has recently emerged as one of the alternative surface treatment processes to improve the fatigue life of the components. Part I of this experimental study has been concentrated on surface characteristics of waterjet peened material. In this part of the study, un-notched hourglass shaped circular cross section test specimens were fabricated and surface treated for selected waterjet peening conditions. Completely reversed rotating bending fatigue tests were conducted on peened aluminum specimens to evaluate fatigue performance (S-N curves). Fracture surfaces were evaluated by scanning electron microscopy (SEM) to identify the fatigue mechanisms. Results show that waterjet peening can enhance the fatigue strength by 20-30% to that of unpeened Al7075-T6 material.

1. INTRODUCTION

Alternative surface treatment processes to shot peening called waterjet peening have been recently introduced using high-pressure waterjets to impinge the material surface. The development of this process was realized from the concept of jet breakup that was observed in the jet structure. Generally, high-pressure jets have the continuous solid flow characteristics in the initial region or at short distance from the nozzle exit. At longer distance, the jets, which stay coherent in the initial region, will start to breakup into a number of droplets. The impingement of each droplet is found to generate force acting normal to the surface [1]. This high force induced plastic deformation in the surface and near surface layers of the workpiece material thereby producing compressive residual stresses and increasing subsurface work hardening [1-9].

Shot peening studies [10-14] have shown that induced compressive residual stresses are beneficial to fatigue life of the components. In general, improvements of the fatigue strength by the peening process could be achieved if compressive residual stresses and work hardening were sufficiently induced in the layer of the workpiece material. The degree of fatigue improvement by the peening process, however, is strongly dependent on many factors i.e. the magnitude of induced residual stresses and the resulting surface finish. It is known that the main limitation of shot peening is a high degree of resulting surface roughness on target material. Surface alternations such as microcracks can be anticipated in the peening operation. Metallurgical studies and fatigue testing revealed that the microcracks can act as crack nucleating sites in fatigue resulting in the degradation of fatigue strength. It has been reported that the shot peening process improved fatigue strength by 25~55% in reversed bending fatigue cycling when a compressive residual stress approached 60% of material's ultimate tensile strength in high strength aluminum alloys [16]. Al-Obaid [17] also revealed that the maximum residual stress was developed at the surface for soft material while the maximum compressive stress was observed at about 125~250 μm below the surface for hard materials in general or for soft materials peened at high peening intensity or impact energy. Several recent investigations [1,3-7] have revealed that waterjet peening produced similar processing and performance results as conventional shot peening. Most of these studies were conducted either using low to moderate pressures or using round nozzles. However, published literature available on waterjet peening using fan-jet nozzles was limited.

Therefore, an experimental investigation of waterjet peening with fan-jet nozzles was conducted to further explore the potential application of this process. In the first part of this waterjet peening study, we have shown the effects of waterjet peening process conditions on material surface topography. Peened surface characteristics were evaluated and suitable peening conditions have been identified. The intent of this paper is to report the effects of waterjet peening on fatigue strength in 7075-T6 aluminum alloy.

2. EXPERIMENTS AND PROCEDURES

The test material was 7075-T6 aluminum alloy whose yield strength and ultimate strength are 516 and 587 MPa respectively [18]. Test specimens were fabricated into hourglass, circular cross section as per specification recommended in the instruction manual for RR Moore machine [19] and is shown in Figure 1. After fabrication, the gage section of each test specimen was surface treated by waterjet peening according to the process conditions listed in Tables 1. The process conditions chosen in this experimental investigation based on the results from previous study. Note that the peening time, T_e of each condition was the jet exposure time calculated per the nozzle diameter and jet traverse speed using $T_e = n \frac{D_n}{V_T}$, where n is the number of jet passes, D_n is the nozzle diameter, and V_T is the nozzle traverse speed.

The waterjet peening system employed a high-pressure pump with control unit, capable of generating pump pressures, P , up to 400 MPa. The pressurized water was controlled and directed through a 0.3-mm sapphire orifice before entering a nozzle specially designed for the purpose of waterjet peening. The nozzle was oriented perpendicular to the surface of the test specimen while the test specimen was rotated with the speed of 500 RPM. An appropriate nozzle-to-surface standoff distance, X , was obtained by moving and adjusting the nozzle.

Both peened and unpeened test specimens were fatigue life tested in completely reversed rotating bending ($R = S_{min}/S_{max} = -1$) until fracture. A commercial R.R. Moore rotating bending fatigue test machine (4-point flexure) was used at rotational speeds up to 10,000 RPM at alternating stress, S , that ranged from 200 to 430 MPa. The number of cycles to fracture along with corresponding applied stress amplitude were recorded for each test for later analysis. As received and waterjet peened surfaces were examined prior to fatigue testing using SEM to discern distinguishing surface features. Fracture surfaces of failed test specimens were examined both by optical and scanning microscopy to assess the mode and origin of fatigue failure.

3. RESULTS

3.1 Surface and Sub-surface Characteristics

Figure 2 shows the surface roughness parameters obtained from the surface profiles recorded in this series of experiments. Note that the changes in the arithmetic average surface roughness (R_a) and the root-mean-square (RMS) roughness (R_q) are negligibly small between peened and unpeened specimens. However, the maximum peak-to-valley height (R_y) and the ten-point average roughness (R_z) magnitudes were greater in peened specimens as compared to as-machined or unpeened specimens. It is interesting to see that the small change in values of surface roughness parameters in the peened specimens as compared to the unpeened specimens might be the result of deformation induced during waterjet peening process.

SEM micrographs of the specimen surfaces, which were water peened using nozzle-1, under the lowest standoff distance with varying supply pressures are shown in Figure 3. Peened surfaces clearly revealed no sign of surface erosion even at high-pressure used in this series of experiments. In contrast, the results obtained with nozzle-2 showed that there was erosion damage induced by the jets on the specimen surface of Set 5-6 as can be seen in Figure 4. However, the typical hardness profiles of the surface damage specimens (Set 5-7) showed an increase in surface micro hardness as shown in Figure 5.

3.2 High cyclic fatigue life

Fatigue life (S-N) curves of the hourglass, circular cross section fatigue life specimens under three different jet pressures using nozzle-1 are shown in Figure 7. It can be seen that waterjet peening improved the fatigue limit of 7075-T6 aluminum alloy. Fatigue limit or the endurance strength was evaluated for 10^8 fatigue life cycles. The maximum improvement of the fatigue limit in 7075-T6 aluminum alloy was about 25% higher than that of as-machined specimens. This improvement was found with the specimens waterpeened at $P=310$ MPa and $X=44$ mm (Figure 6). Waterjet peening at some conditions such as low pressure or those waterpeened at greater standoff distances showed little fatigue improvement even though there were no changes in surface roughness of these specimens. Moreover, by increasing the pressure and peening time (decreasing nozzle transverse speed, V_T) may yield an increase in surface hardness (Figure 5), but fatigue limit will rapidly degrade when surface erosion or damage presented. Indeed, the surface erosion induced in specimens peened by nozzle-2 clearly reduced the fatigue lives as shown in Figure 7. Therefore, nozzle and jet characteristics will have a significant effect on peening in addition to pressure and peening time.

3.3 Fatigue crack origin

Fractographic examination of fracture surfaces of both peened and unpeened test specimens were conducted. The typical SEM micrographs are shown in Figure 8. It can be seen from the micrographs that crack was initiated from the outer surface of the as-machined test specimen whereas the fatigue crack initiation site was located about 100-200 μm beneath the surface in the water peened specimens. The extent of the waterjet peening deformation layer was clearly a function of supply pressures as shown in Figure 8b-d. The greater the applied pump pressure, the deeper the surface hardening layer and the fatigue crack initiation sites.

4. DISCUSSIONS

Apparently, the degree of fatigue improvements was strongly dependent on peening conditions as observed in the S-N curves. The maximum improvement of the fatigue limit in 7075-T6 aluminum alloy was about 15-25%. Comparing this water peened alloy fatigue limit to that of published data [20] on fatigue limit of 160 MPa found for rotating and bending shows about 43% of improvement. The degree of fatigue life improvement achieved by waterjet peening in 7075-T6 aluminum alloy is less than that in case-hardened steel [1]. However, it is expected that the

materials with greater tensile strength tend to have greater fatigue benefit from the peening process [16].

Fatigue test results shown in Figure 7 revealed that localized surface irregularities such as eroded pits induced by the jets could serve as very effective stress concentrations at the specimen surface. Although waterjet peening did induce deformation at the surface, but the induced deformation degraded rapidly without significant effect on the sub-surface as observed in specimens Set 5-7. Therefore, the critical concern and a word of caution is noted in waterjet peening is to minimize the stress concentrations posed by surface erosion and localized deformation.

Results from SEM micrographs showed that there was no erosion on the surface due to the jets in specimens Set 1-3. However, surface roughness data showed that the R_y and R_q roughness values of the waterpeened specimens were about 4 times higher than those of as-machined specimens. The high values of surface roughness might be the results from machining operations or localized plastic deformation. In general, an increase in surface roughness might affect the components by reducing their fatigue limit. The higher the surface finish, the lower the fatigue limit of the components. Nevertheless, with the increase in surface roughness in the waterpeened specimens, the fatigue limit did increase appreciably due to surface hardening. Therefore, we are currently examining the direct effect of waterjet peening on fatigue life improvement by considering a correction factor for interactions of surface finish, and depth of subsurface layer and will be reported in future.

5. CONCLUSION

Fatigue performance study of waterjet peened specimens under ultra-high pressure conditions by using a fan-jet nozzle was conducted on 7075-T6 aluminum alloy. Within the experimental conditions used in this study, the following conclusions were made:

1. Waterjet peening is capable of inducing surface plastic deformations similar to shot peening. Plastic deformation in waterjet peened test specimens caused fatigue crack to initiate in the interior of test specimens.
2. The degree of fatigue life improvement by waterjet peening was found to be dependent on peening conditions i.e. jet pressure, standoff distance, nozzle type, jet velocity and peening time. This study showed that the fatigue improvement by waterjet peening could be achieved.
3. Surface erosion and pits induced due to the impact of the jets has a marked influence on fatigue strength of material. To improve fatigue strength by waterjet peening, it is important that peening conditions must be appropriately chosen to ensure that waterjets will not induce surface erosion.

4. The maximum fatigue improvement found in the waterpeened specimens of high strength alloy (Al-7075-T6) was about 25 %, which is comparable to that of shot peened specimens of the same material.

6. REFERENCES

1. Tonshoff, H.K., Kross, F. and Marzenell, C., "High-pressure water Peening – a New Mechanical Surface-Strengthening Process", *Annals of the CIRP*, Vol. 46, No.1, 1997, pp 113-116.
2. Zafred, P. R., "High Pressure Water Shot Peening", *European Patent Specification*, Publication #EP 0218354B1, November 7, 1990.
3. Blickwedel, H., Haferkamp, H., Louis, H. and Tai, P.T., "Modification of Material Structure by Cavitation and Liquid Impact and Their Influence on Mechanical Properties," *Erosion by Liquid and Solid Impact*, Proc. 7th International Conference on Erosion by Liquid and Solid Impact, September 7-10, 1987, pp.31.1-31.6.
4. Yamauchi, Y., Soyama, H., Adashi, Y., Sato, K., Shindo, T., Oba, R., Oshima R., and Yamabe, M., "Suitable Region of High-Speed Submerged Water Jets for Cutting and Peening," *JSME International Journal*, Series B, Vol.8, No.1, 1995, pp.31-38.
5. Daniewicz, S.R., and Cummings, S.D., "Characterization of Water Peening Process", *Transaction of the ASME*, Vol. 121, 1999, pp. 336-340.
6. Mathias, M., Gocke, A. and Pohl, M., "The Residual Stress, Texture and Surface Changes in Steel Induced by Cavitation", *Wear*, Vol.150, 1991, pp. 11-20.
7. Colosimos, B.M., Monno, M., and Semeraro, Q. "Process Parameters Control in Water Jet Peening", *International Journal of Materials and Product Technology*, Vol. 15, 2000, pp. 10-19.
8. M. Ramulu, S. Kunaporn, D. Arola, M. Hashish and J.Hopkins, "Waterjet Machining and Peening of Metals", *Journal of Pressure Vessel Technology*, *Transactions of the ASME*, Vol.122, No.1, 2000, pp. 90-95.
9. M. Ramulu, S. Kunaporn, M.Jenkins, M. Hashish and J.Hopkins, "Peening with High Pressure Waterjets" *SAE technical Paper Series No. 1999-01-2285*. Aerospace Manufacturing Technology Conference and Exposition, Bellevue, Washington, June 8-10,1999.
10. Niku-Lari, A., "Shot Peening," First International Conference on Shot Peening, Paris, September 14-17, 1981, Pergamon Press Ltd., pp.1-21.

11. Marsh, K.J., Shot Peening: Techniques and Applications, Engineering Material Advisory Services Ltd., London, 1993.
12. De los Rios, E.R., Walley, A., Milan, M.T. and Hammersley, G., "Fatigue Crack Initiation and Propagation on Shot-peened Surfaces in A316 Stainless Steel" *International Journal of Fatigue*, Vol. 17, No 7, 1995, pp. 493-499.
13. Hammond, D.W. and Meguid, S.A. "Crack Propagation in the Presence of Shot-peening Residual Stresses", *Engineering Fracture Mechanics*, Vol. 37, No.2, 1990, p.373-387.
14. Was, G.S., Pelloux, R.M. and Frabolot, M.C., "Effect of Shot Peening Methods on The Fatigue Behavior of Alloy 7075-T6," First International Conference on Shot Peening, Paris, September 14-17, Pergamon Press Ltd., 1981, pp. 445-451.
15. Luo, W., Noble, B. and Waterhouse, R.B., "The Interaction between Shot-Peening and Heat Treatment on the Fatigue and Fretting-Fatigue Properties of the High Strength Aluminum Alloy 7075," Impact Surface Treatment, Elsevier Applied Science Publishers, 1986, pp.57-67.
16. Oshida, Y. and Daly, J., "Fatigue Damage Evaluation of Shot Peened High Strength Aluminum Alloy", 2nd International Conference in Impact Surface Treatment, England, September 22-26, Elsevier Applied Science Publishers, London, 1986, pp. 404-416.
17. Al-Obaid, Y.F., "A Rudimentary Analysis of Improving Fatigue Life of Metals by Shot Peening", *Journal of Applied Mechanics*, Vol.57, 1990, pp. 307-312.
18. Properties and Selection; Nonferrous Alloys and Special-Purpose Materials, Metals Handbook, American Society of Metals, V.2, 1991, pp. 17.20.
19. Instruction Manual for R.R. Moore High Speed Fatigue Testing Machine, SATEC Materials Testing Equipment. 1997.
20. Fatigue and Fracture, ASM Handbook, ASM International, OH, 1996, Vol.19, pp.785-800.

Table 1. Waterjet Peening Conditions of Circular Fatigue Test Specimens.

Set	P (MPa)	V (m/s)	X (mm)	V_T (mm/s)	Number of jet passes, n	Peening Time, T_e (s)	Nozzle Type
1	103	454	24	12.7	4	0.10	Fan (Nozzle-1)
2	103	454	36	12.7	4		
3	207	643	36	12.7	4		
4	310	787	44	12.7	4		
5	310	787	60	4.2	4	0.31	Fan (Nozzle-2)
6			64	4.2		0.31	
7			64	12.7		0.10	

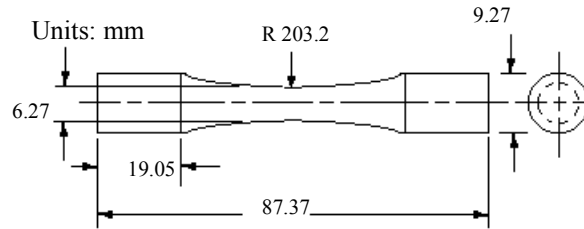


Figure 1. Geometry and Dimensions of Hourglass, Circular Cross-section Fatigue Life Test Specimens.

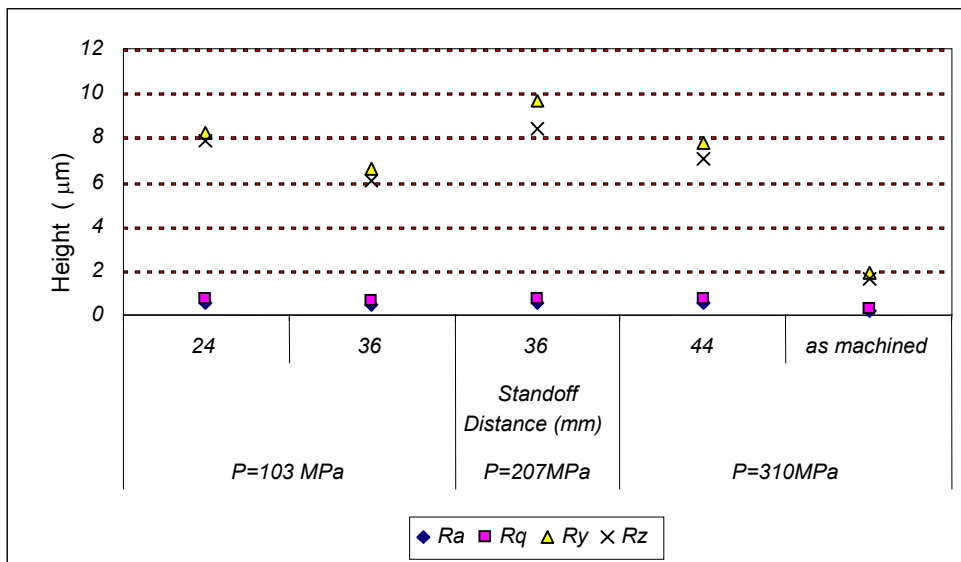
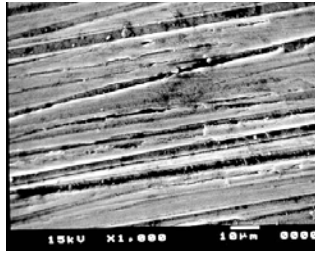
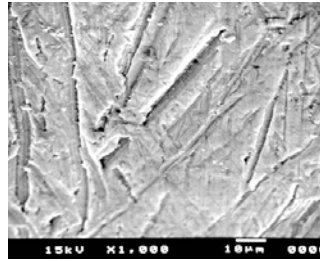


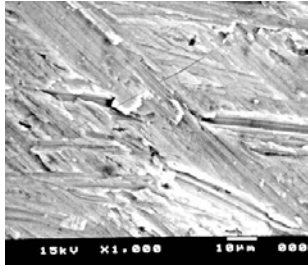
Figure 2. Average surface roughness parameters obtained on waterjet peened specimen surfaces.



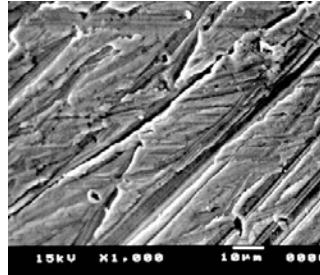
(a) unpeened surface



(b) $P = 103 \text{ MPa}$, $X=24\text{mm}$.

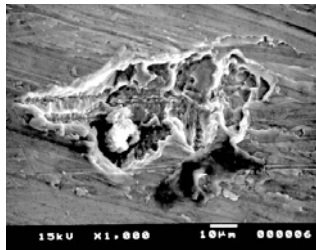


(c) $P = 207 \text{ MPa}$, $X=24\text{mm}$.

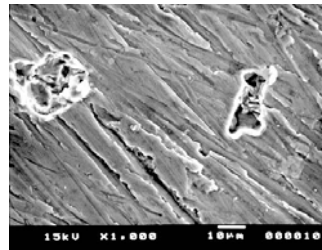


(d) $P = 310 \text{ MPa}$, $X=44\text{mm}$.

Figure 3. SEM Micrographs of Fatigue Specimen Unpeened and Peened Surfaces at Different Applied Pressures using Nozzle-1.



(a) $P = 310 \text{ MPa}$, $X=60\text{mm}$
 $T_e = 0.31 \text{ s}$



(b) $P = 310 \text{ MPa}$, $X=64\text{mm}$
 $T_e = 0.31 \text{ s}$

Figure 4. SEM Micrographs of Fatigue Peened Surfaces using Nozzle-2.

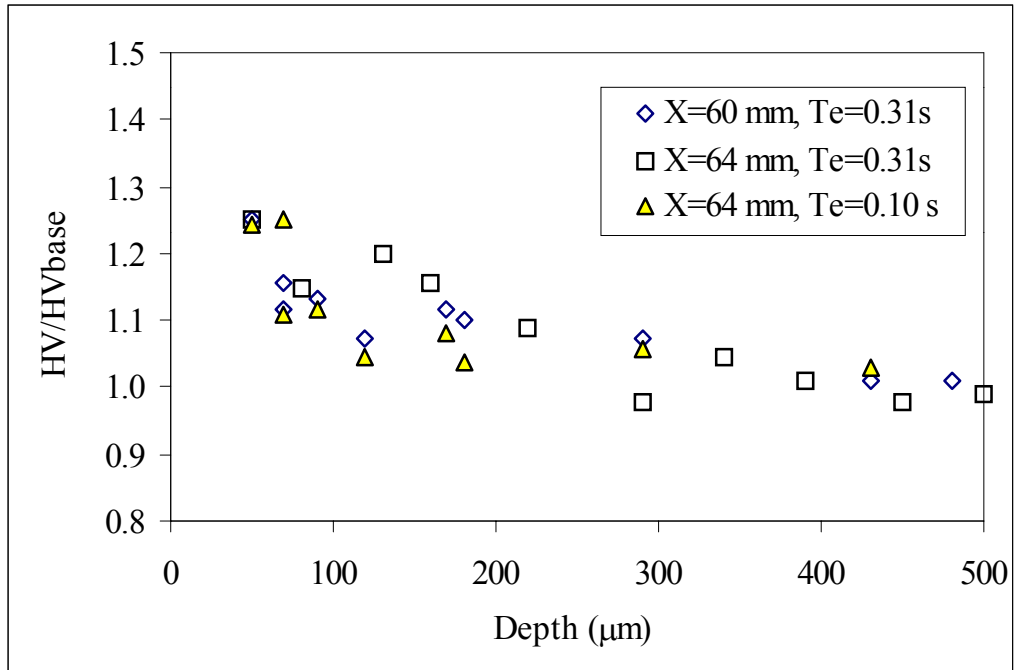


Figure 5. Hardness Distribution of Waterpeened Specimens (Set 5-7, P=310 MPa).

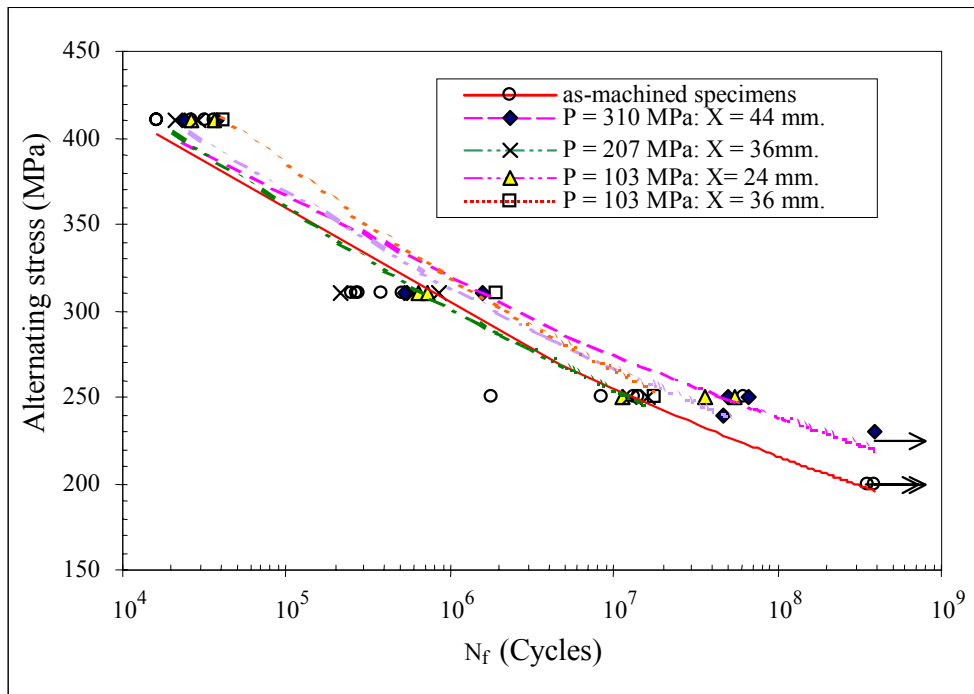


Figure 6. S-N Curves of the Waterpeened Specimens, Set 1-4 using Nozzle-1.

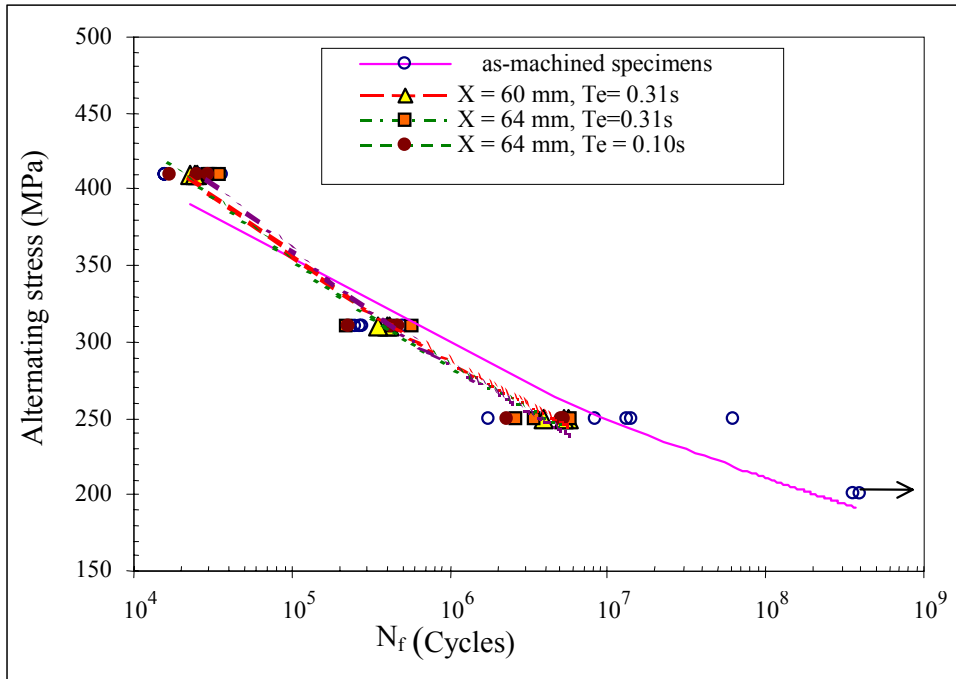
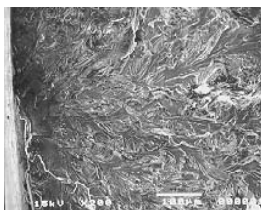
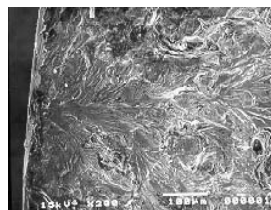


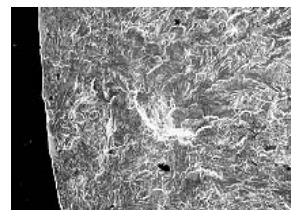
Figure 7. S-N Curves of the Waterpeened Specimens, Set 5-6 using Nozzle-2.



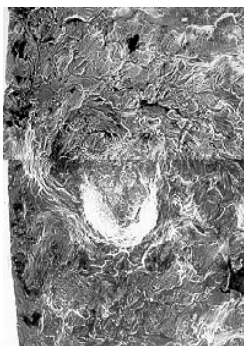
(a) unpeened



(b) waterpeened (P = 103 MPa)



(c) waterpeened (P=207MPa)



(d) waterpeened (P = 310 MPa)

Figure 8. SEM Fractography of Fracture Surfaces Tested at Mean Stress = 250 MPa.

DEVELOPMENT OF A TECHNOLOGY FOR FABRICATION OF ICE ABRASIVES

D.V. Shishkin, E.S. Geskin, B. Goldenberg
New Jersey Institute of Technology
Newark, NJ

ABSTRACT

The mission of this project was to develop a practical technology for formation of ice abrasive. Our previous works demonstrated the effectiveness of the use of ice-air mixture as a cleaning media. However a practical technology for fabrication of ice particles of a desired size and at a desired temperature is still under development. The physical properties of ice (tendency to agglomerate, boundary variation due to absorption of water and melting, etc.) make formation and transportation of ice abrasives extremely difficult. We developed a process for controllable generation of ice particles using a rotational crusher embedded into a heat exchanger. Water was supplied at the bottom of the heat exchanger and as it moved along the rotating auger ice was formed and crushed. Refrigerant and liquid nitrogen was used as a cooling media. At the exit of the heat exchanger the air stream entrained the generated particles. In the course of operation the cooling conditions and the auger rotation were maintained constant while the water flow rate was changed. The rate of production and the geometry of the generated particles were monitored. We also investigated the temperature distribution along the heat exchanger and the corresponding distribution of the particle size. As the result of the study process phenomenology was developed and a design of the system for formation of ice abrasive was suggested.

1. INTRODUCTION – ICE AS AN ABRASIVE MEDIA

A number of the surface processing technologies based on the use of the air-ice stream has been previously suggested. A car washing machine constituted the first attempt of practical utilization of the ice particles (US Patent, 1955). Another technology used a stream of charged ice particles directed at treated surfaces (Kanno et al, 1991). Szijcs (1991) proposed cleaning of the sensitive surfaces by the impact of fine grade ice entrained into the air stream. The atomization of the liquid in the air stream and subsequent freezing of the generated fine droplets formed the blast material. The freezing was achieved by the addition of the refrigerant (N_2 , CO_2 , Freon) into the stream in the mixing chamber or by the addition of refrigerant into the jet after the mixing chamber. Another technology involved the use of ultra-clean ice particles, having the uniform grain size, for cleaning surface and grooves of ferrite block (Tomoji, 1992). Ice blasting device utilizing stored particles was suggested by Harima (1992). S. Vissisouk (1994) proposed to use ice particles near melting temperature for surface decoating. Meshner (1997) developed a nozzle for enhancement of the surface cleaning by ice blasting. Shinichi (1997) suggested inexpensive cleaning various surfaces by mixing ice particles, cold water and air. Niechial (1998, 1998a) proposed an ice blasting cleaning system containing an ice crusher, a separator and a blasting gun. Settles (1998) suggested producing ice particles of a size range below 100 micrometers within the apparatus just prior to the nozzle.

Although the potential use of ice blasting was suggested by a number of inventors, the practical use is much more limited. Herb and Vissisouk (1996) reported precision cleaning of zirconium alloys in the course of production of bimetallic tubing by ice pellets. It was shown that ice blasting improved the quality of bimetal. The use of air-ice blasting for steel derusting was reported by Liu et al (1998). The following operational conditions were maintained: air pressure: 0.2-0.76 MPa, grain diameter: below 2.5 mm, ice temperature $-50^{\circ}C$, traverse rate 90 mm/min, and standoff distance 50 mm. At these conditions the rate of derusting ranged from 290 mm²/min at the air pressure of 0.2 MPa to 1110 mm²/min at the air pressure of 0.76 MPa. The quality of the treated surfaces complied with ISO 8501-1 Sa 2.

In the final analysis, the adoption of the ice-jet technology is determined by the effectiveness of the generation and handling of ice abrasives. Regular abrasives are stable at practically feasible operational conditions, while ice particles can exist only at subzero temperature. Maintaining such a temperature prior, within and outside of the nozzle is an extremely difficult task. The adherence between the particles increases dramatically as the temperature approaches $0^{\circ}C$. At this condition ice tend to pack and clog the supply lines. Thus these lines must be maintained at a low temperature. This and other problems similar problems prevent adoption of the ice jets by industry. In order to assure the acceptance of the ice abrasives, it is necessary to develop a practical technology for their formation, transportation and acceleration.

2. PROPERTIES OF WATER ICE

The practical application of the water ice as a machining media is determined by the physical properties of the solid water. Practical importance has the properties of Ice I existing at the modest pressure (below 200 MPa). An important feature of ice I is the reduction of a melting

temperature at an increase of the pressure. The minimum temperature of the liquid water is attained at the pressure about 200 MPa and is equal to -20 C. Another important feature determining particle behavior in the course of impact is ice elasticity. At the temperature range of - 3 C to - 40 C ice is an almost perfect elastic body. Hook's Law is obeyed if the stresses in the ice are below than certain level and are applied during a short period of time. The dynamic elastic properties of ice at -5 C are characterized by the following data: Young modulus (E) = 8.9-9.9 GPa, Rigidity modulus (G) = 3.4-3.8 GPa, Bulk modulus (K) =8.3-11.3 GPa, Poison's ratio (χ) = 0.31-0.36. For comparison, for Aluminum Alloy 1100-H14 E = 70 GPa and G= 26 GPa. For silica glass E = 70 GPa. If the columnar ice is stressed perpendicular to the long direction of the column the static Young modulus in bars is determined by the equation:

$$E=(5.69-0.64T)*10^4 \quad (1)$$

where, temperature T is given in C. The dynamic Young modulus of ice increases almost linearly from 7.2 GPa at -10 C to 8.5 GPa at - 180 C, and is independent from direction of loading. The data above shows that the ice powder can be consider as a soft blasting material and used accordingly.

One of the main issues in the use of the ice powder is sintering of particles and their adhesion to the surface of the enclosure. The strength of the adhesion depends on ice temperature. This dependence is shown in Figure 1 (a). As it follows from this figure it is necessary to maintain ice temperature below -30 C to prevent sintering of the particles. Sintering also depends on the duration of particle contact. The radius of the neck, which forms between two ice spheres, brought into contact during time t at temperature T (Figure 1 b) is determined by the equation

$$\left(\frac{x}{r} \right)^n = \frac{A(T)}{r^m} t \quad (2)$$

where x is the radius of the neck, r is the radius of sphere, A(T) is a function of the temperature, n and m are the constants. The function A(t), as well as the constants m and n are determined by the mechanism of sintering. As it follows from equation (2) it is necessary to prevent the contact between particles in order to avoid particles sintering as well as their adherence to a solid surface. Ice tends to adhere to a solid surface where the ice nuclei are generated.

Moisture contained in the atmosphere in the course of ice transportation enhances the adherence of the ice to walls as well as sintering of ice particles. Both, ice melting and moisture absorption result in the plug formation and clogging of the conduits.

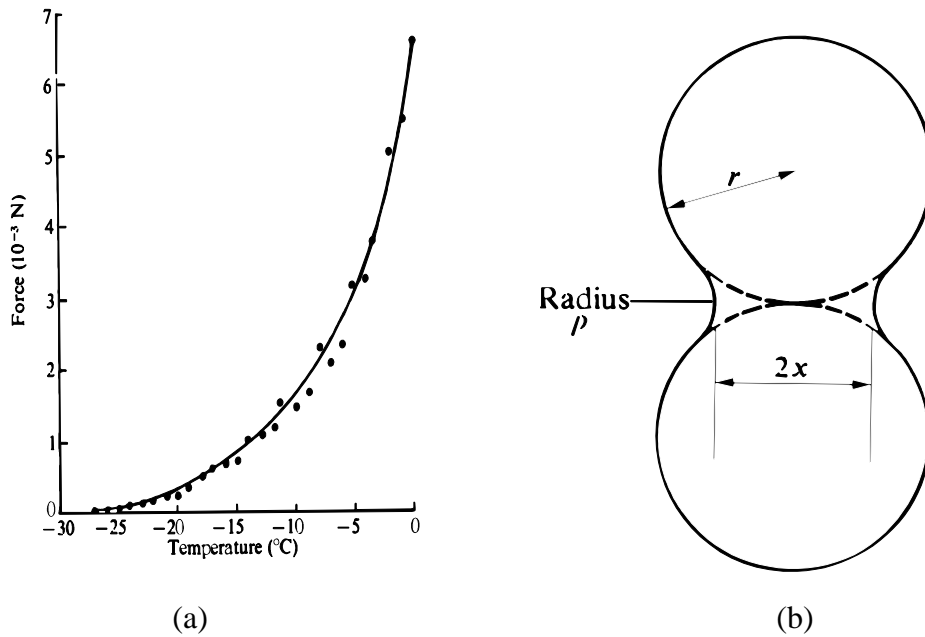


Figure 1 (a) strength of the adhesion of ice particles, (after Hobbs, 1974) and (b) schematic of the sintering of ice particles (after Hobbs, 1974).

3. EXPERIMENTAL SET UP FOR FABRICATION OF ICE ABRASIVE

In our previous experiments several systems for ice powder formation were tested. One of such systems depicted in Figure 2 was selected for further experiments. The system consisted of the following functionally separated blocks:

- ice making block which includes the evaporator, auger, auger driver, sealing and liquid nitrogen cooling apparatus;
- ice unloading mechanism
- nozzle block which includes parallel nozzles and focusing device.

In our experiment water entered the heat exchanger via a special port. As it moved along the rotating auger water solidified and an ice plug was formed. Solidified ice plug moved forward along the auger helical ways. Decomposition of this plug brought about formation of the ice powder. It was determined however, that it is absolutely necessary to eliminate any obstructions to ice flow in order to prevent jamming of the heat exchanger. The heat exchanger and the auger of the icemaker constituted a modified commercial icemaker of Hoshizaki America, Inc. The design of these parts will be changed in the next generation of the device. The cooling was carried out by the refrigerant Galden HT-55 supplied by the TurboJet refrigeration apparatus or by liquid nitrogen stored in a tank. In both cases supply of a cooling media was determined by the characteristics of a source, the refrigeration system or the nitrogen tank. We replaced Hoshizaki auger driver by a more powerful device in order to prevent jamming of the ice. The rotation momentum of the auger 4 was provided via a gearbox with gear-ratio 1:100. However

the selected driver operated at a constant speed of 100 rpm. At these conditions, the size and the temperature of particles were determined by the rate of the water supply to the port 8, which changed gradually from 0 to 200 ml/min. Water flow rate was precisely controlled by a special valve (Figure 2 (a)). In the final analysis, we were able to generate a desired kind of the particles at given cooling conditions by the selection of the water flow rate. The attempts to improve ice production by the increase of the water pressure or were unsuccessful. It is quite obvious that the conditions of the ice production (specific cost and energy consumption, process stability, uniformity of the generated particle, output per 1 kg of the facility or 1 cm² of the outlet crosssection area etc.) will be dramatically improved by the process optimization.

At the outlet of the heat exchanger the powder was entrained by the unloading mechanism which directed it to the nozzle block (5). Nozzle block consisted of two air guns (6) and a special focusing device. Three different sizes of the nozzles were used however in all cases the nozzle-to-focusing tube ratio was 1:2. An unloading mechanism delivered ice particles via flexible plastic tubes to the abrasive port of the air gun. In the gun the air supplied into the insulated nozzle block at a room temperature accelerated the particles. The ice-airjet was formed and directed to the substrate surface.

The ice crystallization was monitored through a set of thermocouples and resistance gauges 10 imbedded into the evaporator (Figure 2(b)). Data acquisition card processed the signals generated by the gauges. As the result the diagrams of the temperature along the wall of the heat exchanger and resistance distribution within the ice block were obtained.

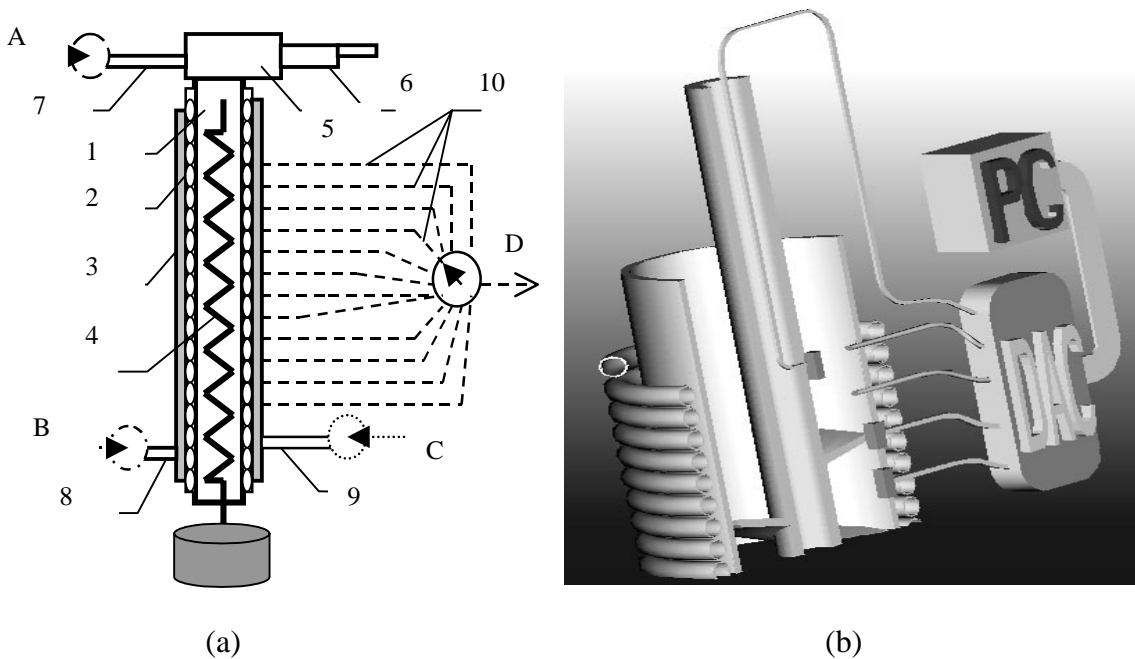


Figure 2 (a) schematic of auger type II system where: 1 – evaporator, 2 – refrigerant coils, 3 – insulation, 4 – auger, 5 – ice reloading device, 6 – air gun, 7 – air supply port, 8 – water supply port, 9 – cooling media port, 10 – gauges, A – air flow rate valve, B – water flow rate valve, C –

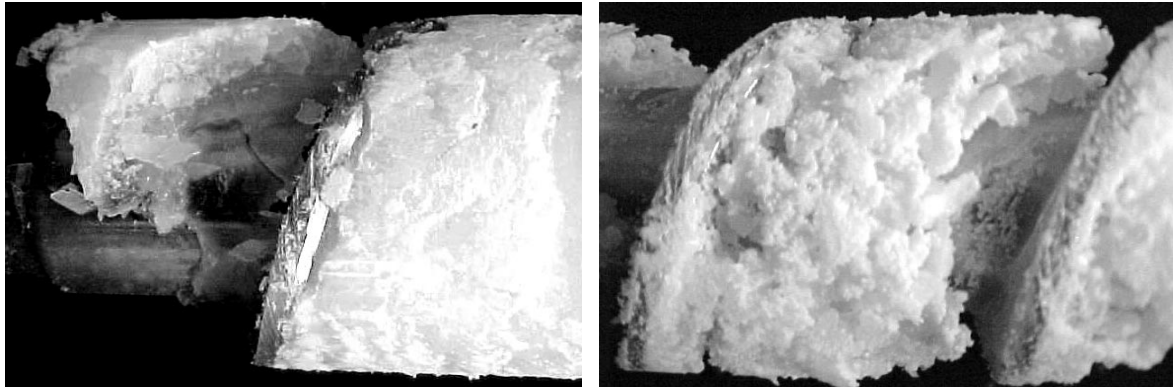
cooling media valve, D – data acquisition card, and (b) schematic of gauges placement inside of the evaporator with their distance calibrated from water inlet port (water zero level).

A shear number of the control variables (rate of the supply of the water and coolant, rate of the auger rotation, the diameter and the length of the heat exchanger, distribution of the temperature and heat flow along the refrigerator, the geometry of the auger) practicality excluded empirical process optimization. At the same time complexity of the phenomena that occur in the course of the powder formation (water freezing and simultaneous decomposition in the spiral moving layer) rendered impossible to construct a physical model of the process. Thus the only practical approach to the process design entailed experimental study of the distribution of water properties within the icemaker, construction of the process phenomenology using the acquired information and then the use of commercial packages (Pro/ENGINEER, FIDAP, etc) to evaluate the design parameters of the icemaker as well as the correlation between input variables and the ice properties.

Special experiments were carried out in order to examine the state of the solid ice in the course of solidification and particles formation. In order to attain this goal the auger was stopped during normal operations and then extracted from the heat exchanger. The solid phase, which remained at the ways of the auger, was visually examined. The state of the ice is depicted on Figures 3. The anatomy of the ice in the course of freezing and particle formation was investigated using the developed set of pictures. This information was supplemented by the ice temperature and electrical resistance monitored prior to the auger extraction. Extensive database acquired in course of these experiments was used to develop a hypothetical mechanism of ice particle formation. The suggested hypothetical process phenomenology is described below.

4. PHENOMENOLOGY OF ICE BLOCK DECOMPOSITION

Powder formation is a complex process involving solidification, stress development in the solid phase, super cooling of the solid with cracks propagation inside the block, concentration of the structural and thermal stresses within the solid and finally decomposition of ice blocks. According to our hypothesis ice block solidification occurs at the first flight of the auger helical way. The formation of a solid block and its initial decomposition are depicted on Figure 3. At this stage the formation of the ice structure is completed and further cooling brings about only reduction of ice temperature. Thus particles size can be controlled only at the initial stages of the process.



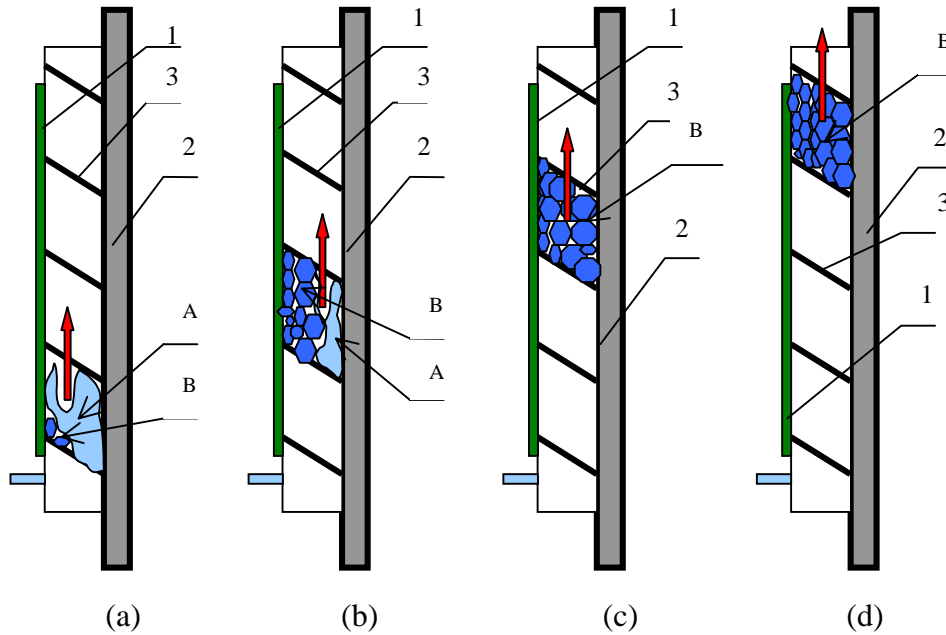
(a)

(b)

Figure 3. The solid ice block decomposition at the two distinct stages of ice powder formation: a) initial stage of block formation, and b) the intermediate stage of block decomposition.

The following phenomenology of particle formation at the nitrogen cooling has been suggested. Ice nucleation originates as water flow reaches evaporator wall having the temperature of -196°C . The crystals grows is randomly oriented from the walls of the evaporator and the auger stem. Ice nucleation and crystal growth depended on the conditions of cooling and the auger spiral movement. The ice plug formed and propagated along the auger stem. The generated ice acquires a multilayer pattern. A super cooled ice layer directly adjacent to the evaporator and a moderately cooled layer in the vicinity of auger can be identified. An explosive character of water freezing near the evaporator wall leads to thermal ice expansion inside the volume constrained by the evaporator and the auger and subsequent formation of the ice plug. This resulted in the compression of the solid and cracks nucleation. The nucleation of cracks under compressive stress is generally due to the dislocation pile-up at the grain boundaries and relief of stress concentration by parting along the grain boundaries. The phenomenon of crack nucleation has been well investigated for low to moderate loading conditions by A. Sanderson. The generated cracks as well as the cracks initially developed in the solid ice propagate within the ice body and eventually fracture the solid block. Block decomposition occurred almost instantaneously and could be consider as an explosive destruction. The ice temperature at this region ranges from -15°C to -150°C ($D = 10 - 24$ mm from water level zero).

The following hypothetical mechanism of ice formation and decomposition (Figure 4) was suggested. Liquid water freezes and forms ice plug at the first ways of the auger. Thermal expansion essentially stops ice advance, and develops the intensive stresses within the plug. This brings about formation and development of cracks and eventually fracturing the solid and formation of ice fragments. The density of cracks developed in the course of freezing determines the size of particles. The cracks density in turn depends on the rate of water-cooling. This explains the effect of the rate of water supply on the size of particles. At a low rate of water supply that is at a high rate of freezing the fine particles are generated. The objective of the process control is to generate such temperature and stress fields within the ice plug, which brings about formation of the ice of the desired size at the desired rate.



↑ - direction of auger spiral movement.

Figure 4. Hypothetical schema of ice plug formation and decomposition in auger spiral movement.

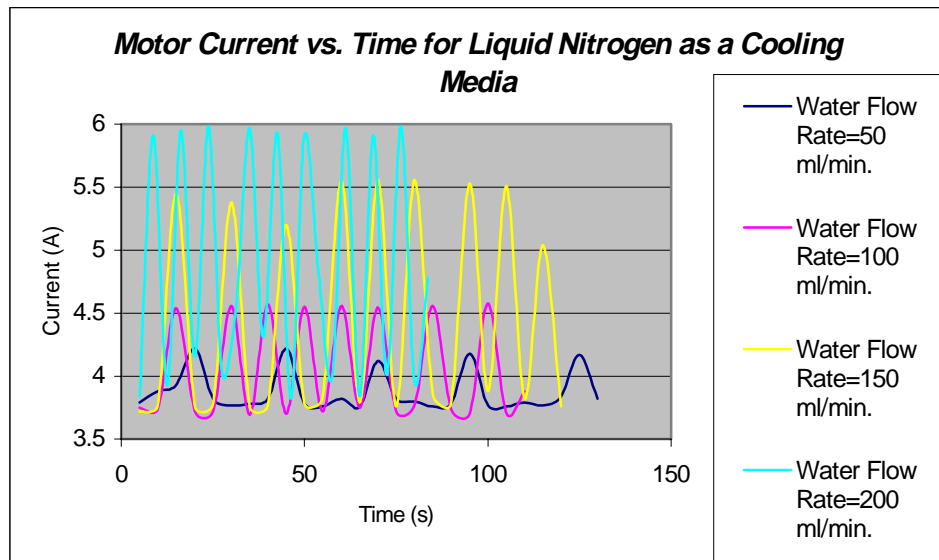


Figure 5. The correlation between driver current and water flow rate in time. Notice distinct frequencies of current extremum value appearance for different water flow rates.

The periodic mode of the formation and decomposition of ice blocks determine the periodical character of ice motion and driver operation. Indeed, the ice powder exits the icemaker periodical and periods of the ice exit exactly coincide with those of driver operation shown on Figure 5.

Before plug formation water and ice flow freely along the auger and thus loading of the driver is minimal. As long as the plug stops the ice motion, the torque of the driver increases dramatically, but drops almost instantaneously when the plug is decomposed. (Figure 5). After the plug decomposition, the geometry of particles does not change and heat exchange results in ice cooling only.

5. CHARACTERIZATION OF THE GENERATED ICE ABRASIVE

Our previous work showed the possibility of the use of ice abrasive for a wide variety of surfaces processing operations. However it was found that each specific technology is attainable only at a narrow range of particle size and temperature. Derusting of steel for example requires particles ranging from 3 to-7mm, while the biomedical applications require highly homogeneous ice powder in the range 0.25 mm-0.3 mm.

The proposed mechanism of particle formation enables us to design a technology providing a desired kind of particles. At our experiments the control strategy was developed by the selection of the cooling media and the water flow rate. The effect of the cooling media (the refrigerant HT vs. liquid nitrogen) on the particles size is shown on Figure 6 (a), while Figure 6(b) demonstrates effect of water flow rate on this parameter. It must be pointed out that the exit particle temperature is also important operational parameter, because it determines particles stability and hardness.

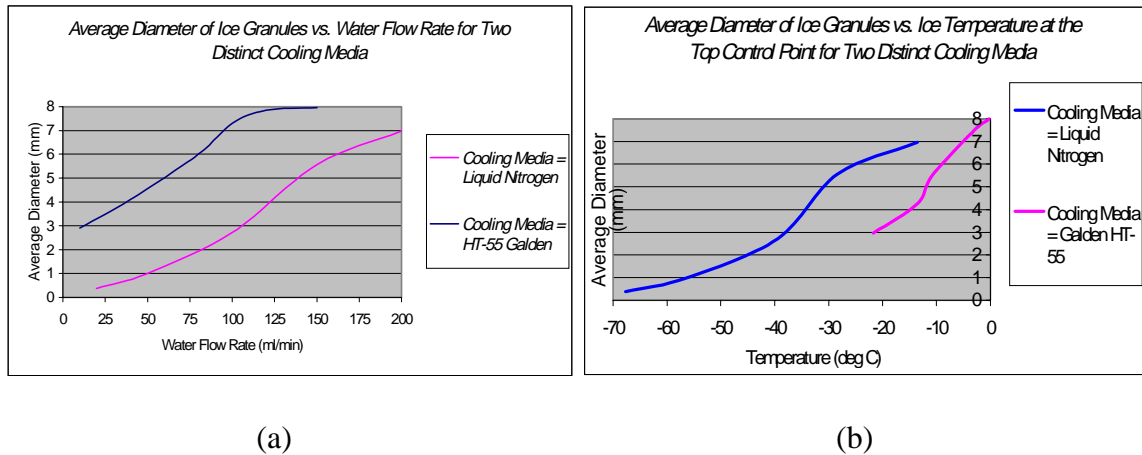


Figure 6. Size distribution of ice particles for refrigerant and liquid nitrogen cooling media as a function of the water flow rate and ice particles temperature.

The actual entrainment of stable low temperature particles is shown on Figure 7. The streams containing low and high concentration of ice particles are depicted on this figure.



Figure 7. Pictures show the high and low density ice-airjet streams (air pressure = 0.544 MPa, ice particles flow rate is in a range 20g-60g).

6. SELECTED APPLICATIONS OF ICE ABRASIVE

A series of the experiments were carried out in order to demonstrate the potential of application of the ice-air jet for various surface-processing operations.

6.1 Biomedical Applications of IJ Technology

The experiments were conducted on two distinct types of skin, the chicken skin and the pigskin. The paint was deposited on the skin in question by a waterproof marker. Then the ice-airjet was used to remove this paint. The feasibility of the paint removal without damaging of the underlying layers as well as selective removal of the epidermis layer of the skin without damaging of further layers was demonstrated - Figures 8(a) and 8(b). The depainting was performed without disturbing the skin structure as well as without creating a temperature gradient in the impingement zone.

6.2 Decontamination of the Heavily Polluted Machine Parts

The deposit consisted of the mixture of dry grease and dust and was moderately adhered to the substrata. The selected area of part surface was decontaminated - Figure 9(a) The visual inspection confirmed the cleanness of the generated surface.

6.3 Decontamination of the Highly Adhesive Layer

Two plastic discs were glued together with highly adhesive glue. Then the glue remaining on the plastic disc surface was removed by the ice-airjet - Figure 9(b). No surface damage was found. Notice that it was not possible to remove this deposit using mechanical means. Another example involved removal of a thin layer of fresh rust formed from the steel surface - Figures 10 (a) and (b).

7. CONCLUSION

The suggested mechanism of the formation of ice powder enables us to design an effective industrial scale device for ice jet formation. The extensive use of this device is envisioned.

8. ACKNOWLEDGEMENTS

The study was supported by NSF grant DDM9312980 "Development of Ice Jet Machining Technology".

9. REFERENCES

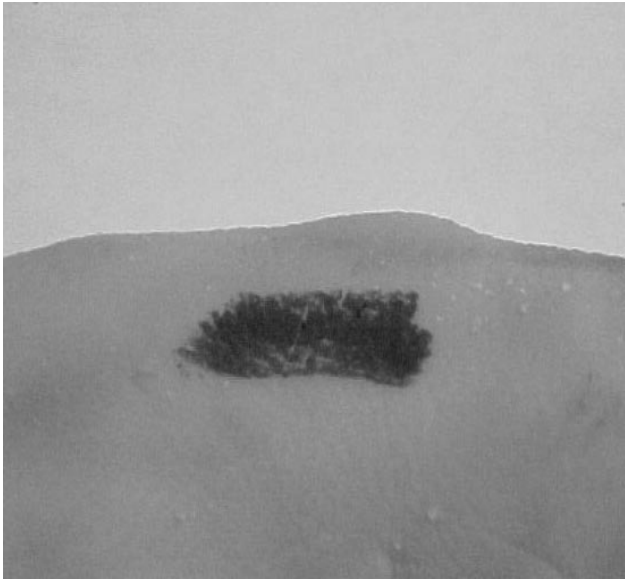
- Kanno et al (1991) Cleaning Device Using Fine Frozen Particles, US Patent 5,074,083.
- J. Szijcs, 1991, A Method for Cleaning Surfaces, European Patent 0 509 132 B1.
- M.Tomoji (1990), A Precision Cleaning Method, Japanese Patent 04078477.
- I. Harima (1992) Ice Blasting Device and Manufacture of Ice Blasting Ice Grain, Japanese Patent 04360766 A.
- S. Vissisouk and S Vixaysouk, 1994, Particles Blasting Using Crystalline Ice, US Patent 5,367,838.
- T. Mesher (1997), Fluidized Stream Acceleration and Pressurizer Apparatus, US Patent 5,607,478.
- H. Shinichi, 1997, Surface Cleaning Method and Device, Japanese Patent 09225830 A.
- R. Niechcial, 1998, Ice Blasting Cleaning System, US Patent 5,820,447.
- G. Settles, Supersonic Abrasive Ice blasting Apparatus, US Patent 5,785,581.
- B. Herb and S. Visaisouk, 1996, Ice Blast Technology for Precision Cleaning, in Precision Cleaning, Witter Publishing Company, Anaheim CA, pp. 172-179.

B. Liu et al, 1998, Research on the Preparation of the Ice Jet and its Cleaning Parameters, Jetting Technology, Ed. H. Louis, Professional Engineering Publishing, Ltd, London, UK, pp. 203-211.

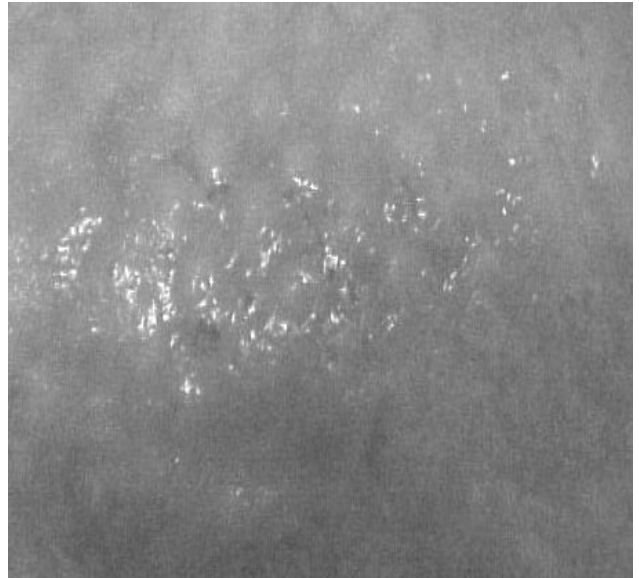
Ice Physics by Hobbs, Peter, Clarendon Press, Oxford 1974.

Hoshizaki America, Inc.-Peachtree City, GA. 1998.

Sanderson, T.J., Ice Mechanics: risks to offshore structures, Graham & Trotman, London, UK 1988.

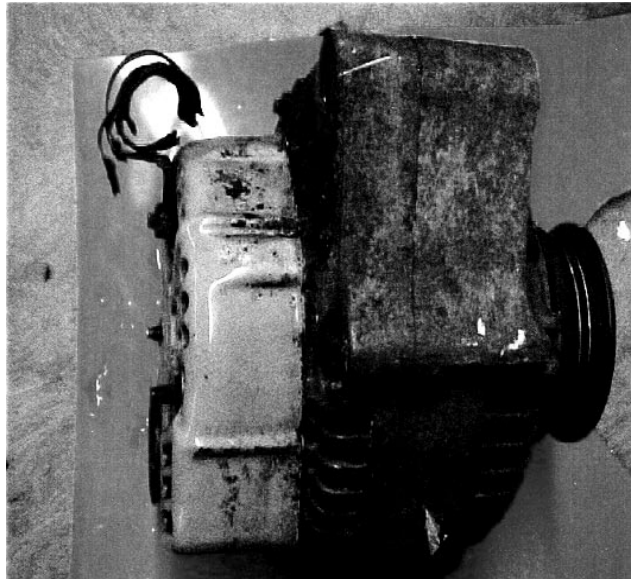
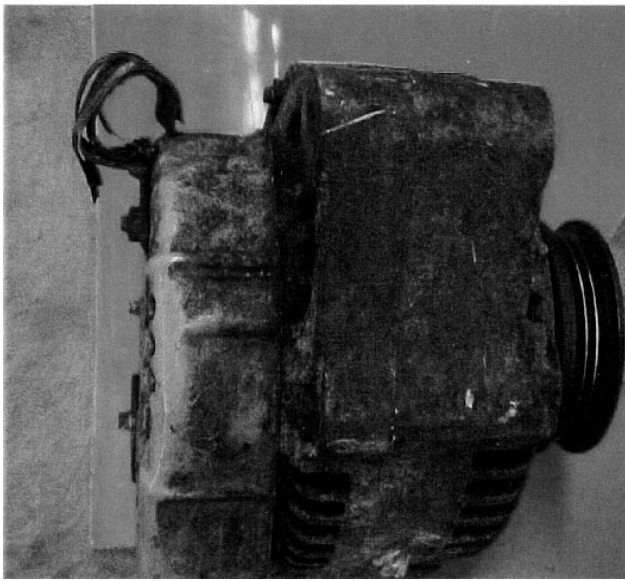


(a)

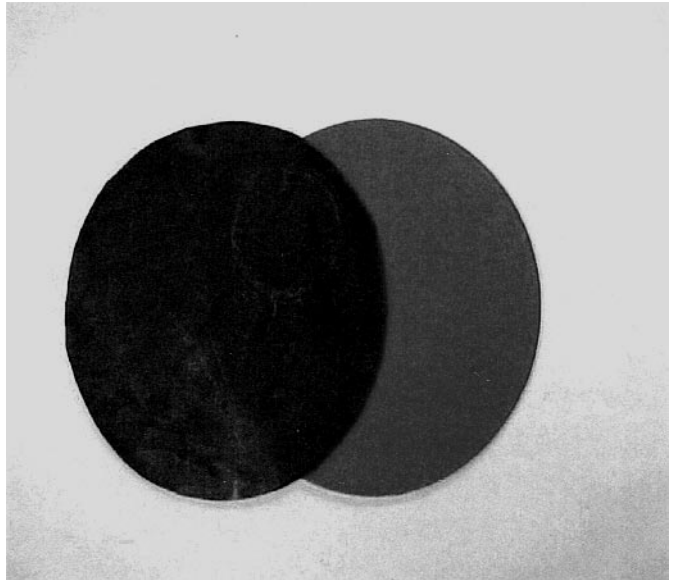
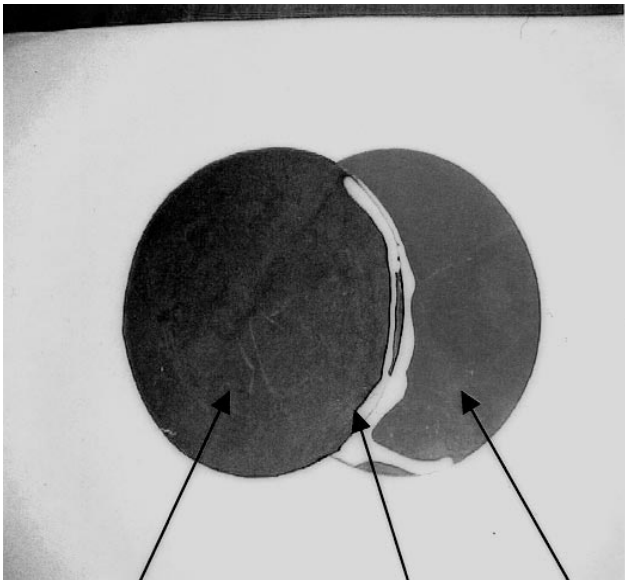


(b)

Figure 8 (a) waterproof marker was partially removed from the epidermis layer of the pork skin. Then the epidermis layer was removed too. No damage to the underneath layers was determined, and (b) waterproof marker was removed from the highly sensitive surface of the chicken skin. No damage to the epidermis was observed in course of the cleaning procedure.

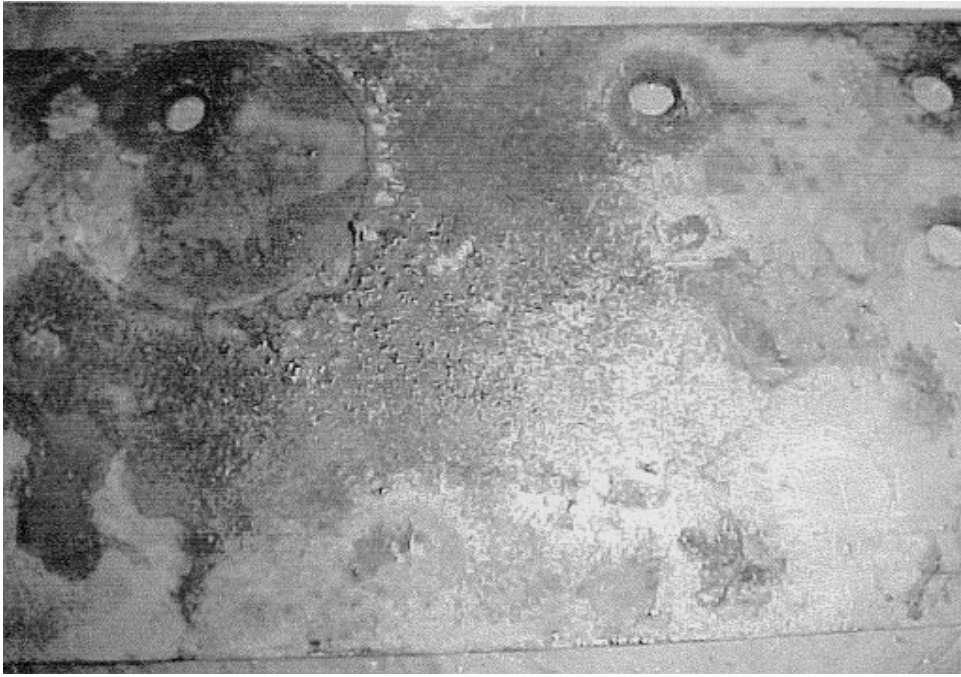


(a)



(b)

Figure 9 (a) decontamination of the heavily polluted machine part, and (b) removal of highly adhesive glue layer from the plastic surface.



(a)



(b)

Figure 10 (a) rusted carbon steel surface. Notice that newly formed rust layer is highly adhesive, and (b) carbon steel plate was partially derusted (middle part of the plate).

LABORATORY RESEARCH FOR WATER JET MATERIAL SURFACES CLEANING

S. Radu, N. Iliș, A. Magyari, A. A. Magyari
University of Petroșani
Petroșani, Romania

ABSTRACT

High pressure water jets are often used to clean degraded surfaces or whose protecting coat is deteriorated, such as the surfaces of technological equipment, the ship bottoms which are covered by limestone deposits, painted surfaces which need undergo a degrading process.

The paper presents the experiments conducted for the cleaning of the belts and ash deposited on the doors of the ovens used at the Coal Processing Plant.

1. INTRODUCTION

The paper is among the first of this kind and presents the use of medium and high pressure water jets for the cleaning of material surfaces.

The aim of this research is to establish the efficiency of water jets in cleaning the ash deposited during the process of coal chocking on the doors and the frames of the ovens at the Coal Processing Plant in Calan and in cleaning the coal or other materials attached on the belts used in open pit coal mining.

2. THE DESIGNING OF A WATER JET CLEANING MECHANISM

At present, the doors and the frames of ovens are cleaned manually, which involves the use of a large number of unskilled workers, a poor cleaning quality, heat losses caused by the opening of the doors over large periods of time, as well as the emission of noxious gases into the atmosphere. Another cleaning methods the use of the charging machine, a complex mechanism which also performs other operations. The shortcomings of this method are the non-uniform cleaning and the rapid wear of the brushes.

Starting from the existing mechanical cleaning installation and slightly changing it, we designed a new mechanism whose cutting tools are the water jets provided by the hydromonitors. Thus, we took over the existing automatic mechanism in which we replaced the brushes with a nozzle support system mounted on six lateral trolleys (figure 1).

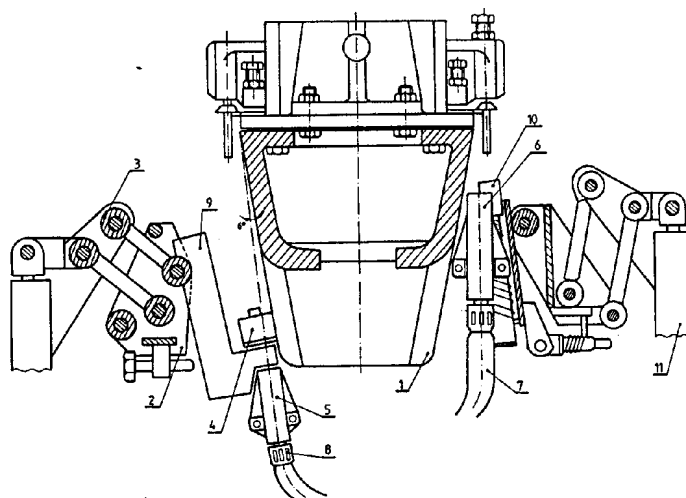


Figure 1. Water jet cleaning mechanism

1. mounted door; 2. support; 3. handle; 4. guide roll; 5. nozzle support frame with tangent jet;
6. nozzle support frame with direct jet; 7. hose; 8. quick joint with staples;
9. fixing board; 10. bolt; 11. body

The cleaning of the door is achieved in two complete trolley movements on the door perimeter, one of them clockwise and the other counter clockwise. The nozzle support frames with direct jets (6) alternate with those with tangent jets (5).

In order to avoid the sprinkling of the brick wall, the whole assembly is provided with a metallic tightening frame fixed on the lateral surface of the door before the beginning of the cleaning operations. The frame also collects and guides the hydraulic agent towards the basin situated under the door cleaning mechanism.

3. DESIGN OF THE BELT CLEANER WITH HIGH PRESSURE HYDRAULIC JETS

Starting from the need of working out a belt cleaner with high-pressure hydraulic jets, we have designed two variants of such equipment, in accordance with the Figures 2 and 3.

The equipment shown in the Figure 2a is made up by a metallic part (nozzle support) placed under the empty arm of the conveyer belt, having a width of 1 mm. On the frame there are placed two supports (3) for passing in by thread of the nozzles (4) of particular design. The metallic part is propped and fixed on the metallic frame (2) by means of a bolt (7) and a nut.

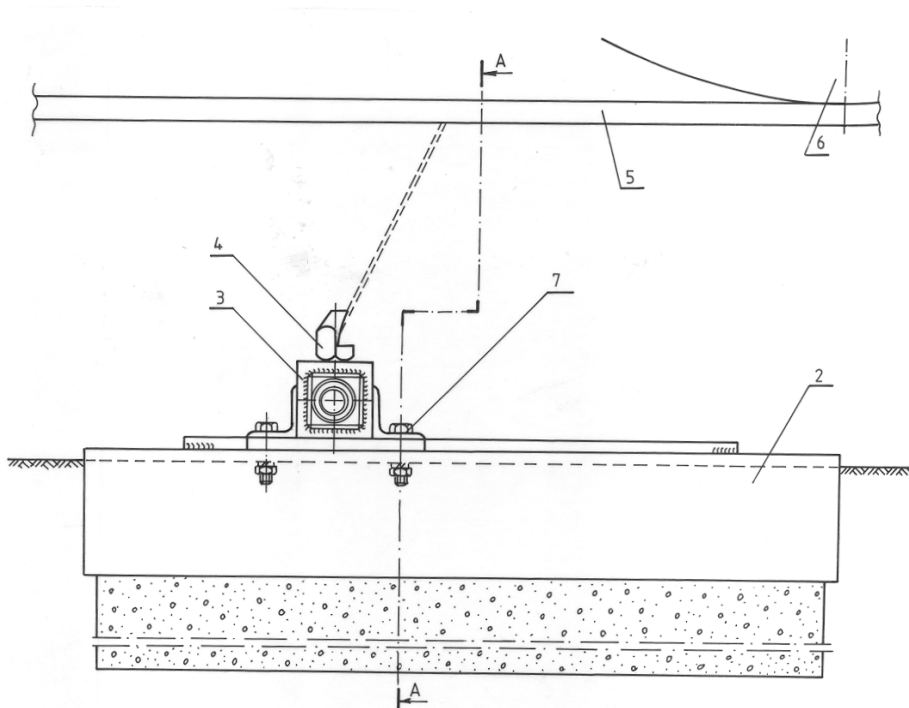


Figure 2a. The belt cleaner system - Lateral view.

In the designed device we have foreseen a collecting tank for water flowing and recycling. This tank is made of concrete and at the superior part it is foreseen with holes for screws mounting at the superior part.

The metallic part on which are placed the nozzles can be supplied with water under pressure at both of the ends. The transport of the fluid under pressure from the supplying hydraulic pump is conveyed by flexible pipes which are joint at the end of the nozzle-holder by a fast joining system with hooks.

Between the metallic frame (2) and the nozzle-holder part there are mounted some spacers (8) made of steel, as the frame, too.

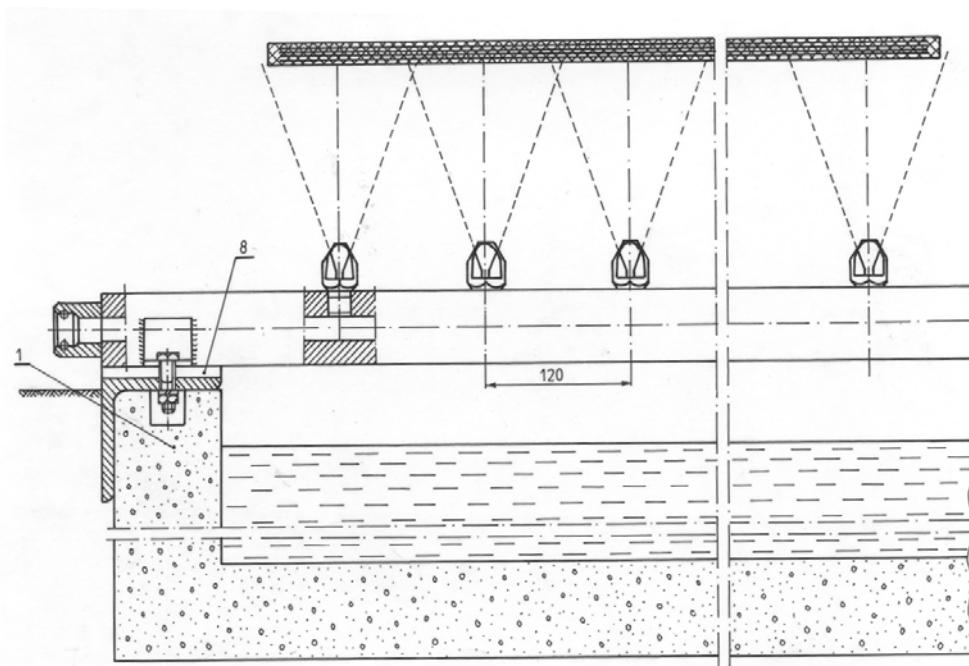


Figure 2b. The belt cleaner system – Section view.

The nozzles has a special design, so that the water jet should have a shape of a fan in order to cover a working range of about 130 mm, at a distance of 150 mm from the belt. Therefore the nozzles are placed at 120-mm distance between them. They are made of steel, thermally treated in order to resist to pressures up to 25 MPa. The 2,252-model pump, made in Germany has a maximum outflow of 325 l/min at a maximum pressure of 25 MPa.

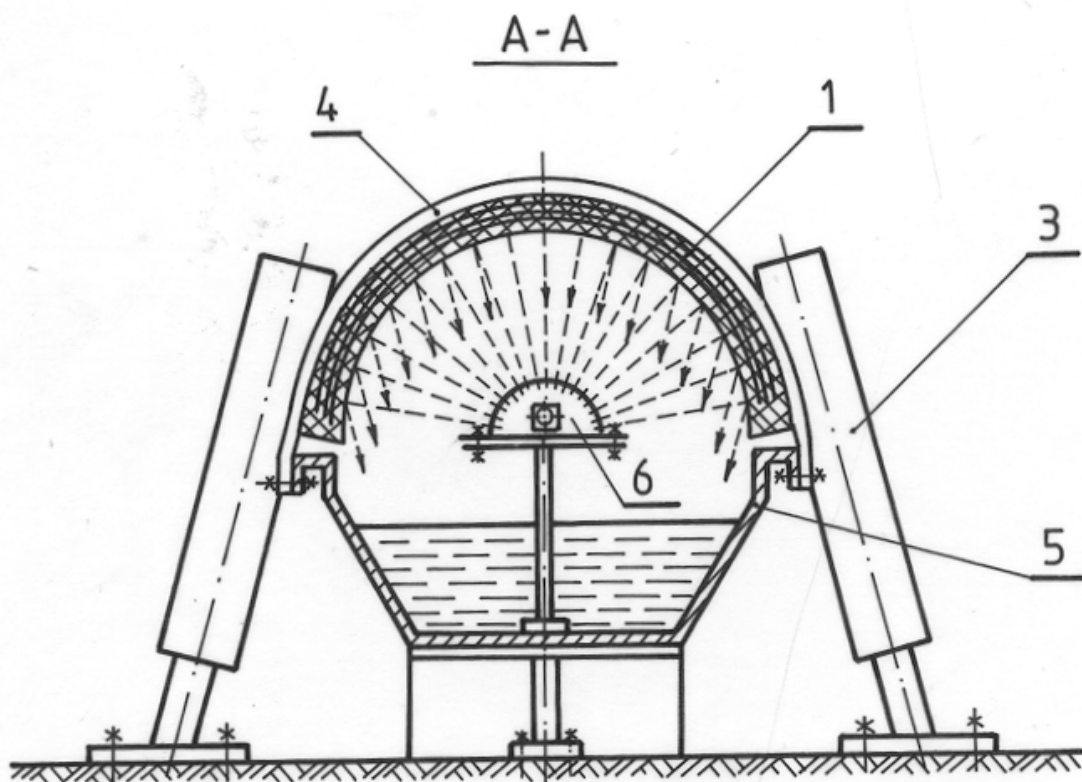
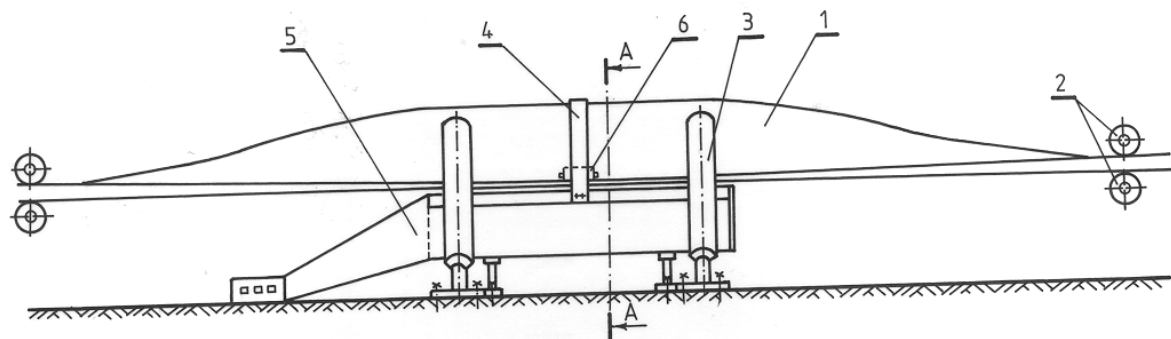


Figure 3. The second cleaning device.

The strength required for the pump driving motor is 160KW. The selecting of this type of pump proceeds from a calculus related to the maximum number of nozzles or holes required for cleaning of a conveyor belt having a width of 1,400 mm. Taking into consideration that between the nozzles there is a distance of 120 mm, 12 nozzles are required for this belt, with the outlet diameter of $d_0 = 5$ mm.

The second cleaning device, Figure 3, presents a different conception of the cleaning device (6) that has a semicylinder shape, with an interior cylindrical conduit. It is fixed on a support by some holding screws. On the exterior of the semicylinder some nozzles are placed after a certain scheme, not being all of them in the same plane perpendicular on the axle of the cleaning device.

For a better cleaning of the belt, on the lateral parts of the belt two orientation rolls are placed that confers the belt the shape from the figure. In order to maintain the belt in this position, a leading part of the belt is placed, over the belt. This part has in its composition a metallic band at the part of contact with the conveyor belt coated with a rubber lay, smoother than the belt rubber.

The tank (5) in which the water and the cleaned matter are deposited is designed so that at its inferior part there are holes for matter discharge toward the pump and the right wall can be disassembled, so that the tank may be cleaned periodically by the matters deposited on its bottom.

The shape of the cleaning device allows the conveying of the jets all over the surface of the cleaning belt and the general design of the equipment ensures a concentration of water and the matter released from the belt into tank (5).

Because in the case of this device the reduced number of the nozzles diameter balances the higher number of them, the flow of the pump is enough for supplying of the cleaning device.

4. THE MOD OF ACTION WITH THE PROPOSED BELT CLEANER EQUIPMENTS

In order to carry out the cleaning of the conveyor belt, water having a pressure up to 105 MPa is forwarded by pump through pipe toward the nozzle support that forwards the thin water jets under a certain angle toward the conveyor belt. Water, together with the matter are deposited in tank (Figure 3) that is divided so that the matter deposited at the bottom should not break into the area in that the filter, from the vacuum pipe is placed. From the tank, the pump absorbs the filtered water.

The supplying of the nozzle support can be carried out at both of the ends, the scheme allowing the less pressure loss.

Taking into consideration the amount of mater released by the used water flow and the way of carrying out of the tank, in one of the two variants or in the case of the leading system of the hydraulic mass the period and way of cleaning of the tank are chosen.

5. CONCLUSIONS

The equipment can be placed both underground and especially ground surface, having an increased reliability and ensuring a better cleaning of the belts.

After the carrying out and testing, conclusions about the optimal cleaning pressure, working period of the nozzles and the required flow for each variants of designed equipment may be drawn.

6. REFERENCES

- Ilias N., Magyari A., Radu S., Achim M., Magyari A.A., “Water Jet and Abrasive Water Jet Performances in Material Cutting”, *Proceedings of the 5th Pacific Rim International Conference on Water Jet Technology*, New Delhi, India, 1998.
- Radu S., Ilias N., Magyari A., Magyari A.A., “Laboratory Experiments for Cleaning and Polishing the Surface with Hydraulic Jets”, *Proceedings of the 10th American Waterjet Conference*, volume II, pp.595-598, Houston, Texas, U.S.A., 1999.

INVESTIGATION OF METAL PIERCING USING HIGH –SPEED WATER SLUGS

E. S. Geskin, B. Goldenberg, O. Petrenko
New Jersey Institute of Technology
Newark, NJ, U.S.A.

G.A. Atanov
Donetsk Institute of Social Education
Donetsk, Ukraine

ABSTRACT

The objective of this study is to develop a knowledge base necessary for the design and implementation of a manufacturing tool based on the use of the string of the high speed water slugs. We designed and constructed a prototype of the device for formation of this jet termed water extruder. At this stage the extruder was suitable for generation of single slugs. The series of experiments involving piercing of steel and aluminum samples were performed. As the result the feasibility of the use of the selected device for slug formation was demonstrated and an avenue of process improvement was identified. The available computational techniques suitable for process optimization were explored and a procedure for process optimization was selected.

1. INTRODUCTION

The goal of the study is to develop a knowledge base of the use of a string of super-high speed water slugs for material processing. This string termed impulsive waterjets (IWJ), constitutes one of the most efficient material removal tools. The slug impacting the material surface at the speed above 1.0 km/sec effects the substrate similarly to the charge of an explosive deposited on the substrate surface. In fact, IWJ replaces explosives in the course of mining and rocks breakage.

One of avenues of IWJ formation involves the use of the water extruders. In the course of the extruder operation the fast moving piston impacts the water contained in a barrel and expels a portion of water via a converging nozzle. The expelled water forms a high-speed slug, moving in the direction of the nozzle axis. The string of the slug forms IWJ. Water acceleration in a converging nozzle due to the impact was investigated in details [1-7]. However, the previous use of water slugs was limited to mining and construction industries. It is the objective of this study to investigate the feasibility of the jet application in manufacturing. One of the conditions of the manufacturing application of high-speed slugs is reduction of the slug diameter. In order to assure the accuracy needed for material removal the slug diameter should not exceed fraction of millimeter. The exit diameter of existing extruders is more than 1 cm.

In order to investigate the extruder properties we constructed a prototype of the device and examined its operation. We selected a powder as a power source because a gun constitutes the simplest device, which can be used for the acceleration of the water slugs. We used the Remington power actuated tool and conventional power load to investigate the formation and behavior of the slugs. The constructed device is suitable for firing a single shot and then to be recharged. The frequency of the recharging needed for formation of the IWJ will be attained at the following stages of the work. The current study also involved theoretical process examination. The numerical technique needed for prediction the pressure in the barrel and the slug velocity was developed as the result of this study.

2. EXPERIMENTAL SET UP FOR FORMATION OF THE WATER SLUGS

A schematic of the set up constructed for process investigation is shown in Figures 1 and 2. All principal parameters of this device (barrel length and diameter of the barrel and the nozzle, dimensions of the slug, the dimensions and the travel distance of the piston) are changeable. At this stage our objective was to construct the simplest device suitable for piercing of hard substrates by water droplets. The desired gun (Figure 3) was constructed by the modification of the barrel of the Remington power actuated tool. The modification involved the change of the barrel geometry, attachment of a nozzle and addition of provisions for formation of a water slug within the barrel. The main issue at this stage was momentum transfer from the explosion products to the water. The principal advantage of the constructed device was its simplicity. While no special machining or other treatments were needed, the constructed device was suitable for the experimental study of metal piercing.

The following design issues were addressed. It was necessary to place a water slug of the desired size in the barrel. The piston designed for the acceleration of the steel nails did not suit the conditions needed for the impact of the water slug. The barrel diameter far exceeded the desired diameter of water slug. It was necessary to attach a converging nozzle to the barrel. It was also necessary to position a gun with respect of a target. Three versions of this device shown in Figure 4 differ by the mode of energy transfer from the source (explosion products) to the water slug. We explored the direct gas-slug energy exchange (Figure 4a), acceleration of a piston impacting the slug (Figure 4b) and finally acceleration of the piston impacting the another piston adjacent to the water slug (Figure 4c).

The experiments involved the impact of steel and aluminum substrates attached to the nozzle. The base having an opening coaxial with the nozzle supported the targets. The power of the charge, the travel distance of the piston, the mass of the slug, the thickness of the target and the diameter of the opening in the base were changed in the course of testing.

3. EXPERIMENTAL RESULTS AND DISCUSSION

Selected samples generated in the course of our experiment are shown in Figures 5-11 and the results of the piercing are summarized in the Table 1. The principal finding of these experiments was demonstration of the feasibility of metal piercing and deformation using our set up. It was noticed that at similar conditions the explosion products brought about a slight deformation of the substrate. Thus, the use of a slug as a momentum transfer media is necessary.

As it was expected the increase of the amount of the powder and the reduction of the target thickness increase the probability of the piercing. However the relationships between operational and design parameters are clearly rather complicated. It was evident that non-linear relationships exist between the power of explosion and the nozzle diameter, travel distance of the piston and the slug mass, between the mass of the slug and the nozzle diameter, etc. It was noticed that the use of the intermediate piston (Figure 4c) improves the process of piercing. This improvement, however, can be due to enhancement of the energy transfer from the gases to the water or to better conditions of the water containment in the barrel.

3.1. Discussion

We observed 3 modes of the material deformation determined by the ratio between the diameters of opening in the base the nozzle. If this ratio approximately less than 3 the slug penetrates through a metal target. The hole almost replicates the form of the opening. If the opening is round, the diameter of the generated hole is equal to the diameter of the opening. The mechanism of the piercing is most probably is due to the metal shear.

If the diameter of the opening exceeds the nozzle diameter in approximately more than 5 times, the slug forms a dimple due to the plastic deformation of the impact zone. The dimple has a spherical form and its diameter is equal to that of the opening. If the diameters ratio is

less than 5 and more than 3 the slug forms a spherical dimple, however at the bottom of the dimples the slug forms a hole. The hole diameter is equal to that of the nozzle. The hole formation in this case is most probably due to the metal shear.

It was found that depending of the geometry of the impact zone, the slug-workpiece interaction bring about results similar to different static loading (Figure 12). Thus these loading resulted in the formation of the stress fields similar to that generated by the dynamic impact. These phenomena can be used for monitoring and investigations of the impact conditions.

The performed experiments clearly indicate feasibility of metal piercing at a wide variety of conditions of the slug formation. At the same time it was shown that process optimization will enable us to improve the results of the treatment.

4. EVALUATION OF THE BARREL GEOMETRY

One of the principal design characteristics of the water extruder is the distance of the piston travel. The speed of the slug is determined by the speed of the piston prior to the impact. This speed can be evaluated by the solution of the Lagrange problem of the propelling of a solid body by a gas expanding in the barrel (Atanov, 1987).

The gas pressure in the barrel is defined by the equation of the Poisson adiabat

$$p_2 = p_0(V_{g0} / V_{g2})^k \quad (1)$$

where V_g is the gas volume, P is the gas pressure, the subscript “0” represents the initial while the subscript “2” represents the current state. If the energy dissipation is negligible, the kinetic energy of the piston equals to the energy lost by the gas. Then the piston velocity can be obtained from the equation:

$$v_2 = \sqrt{\frac{2p_0 V_0 [1 - (V_0 / V_2)^{k-1}]}{(k-1)m_1}} \left(1 + \frac{m_1}{m_2}\right) \quad (2)$$

Where m_1 and m_2 are masses of the piston and the barrel respectively.

The distance of the piston acceleration is defined by the equation:

$$l_p = \frac{V_0}{F_2} \left\{ \left[1 - \frac{(k-1)E_g}{p_0 V_0} \right]^{-\frac{1}{k-1}} - 1 \right\} \quad (3)$$

where E_g , is the energy gained by the piston,
 F_2 is the piston cross section area.

The optimal size of the receiver V_0 corresponds to the minimum of V_2 , because then the total size of the device is minimal. This value is determined by the equation

$$V_{2\min} = k^{\frac{k}{k-1}} \frac{E_g}{p_0} \quad (4)$$

Then, the minimal (optimal) distance of acceleration which assure the piston energy of E_g is

$$l_{popt} = (k^{\frac{k}{k-1}} - k) \frac{E_g}{p_0 F_2} \quad (5)$$

and the optimal ratios between the initial and the final parameters of the gas cavity are

$$\frac{V_2}{V_0} = k^{\frac{1}{k-1}} = 2.32 \quad (6)$$

$$\frac{l_{popt}}{l_{pmin}} \cong k^{\frac{k}{k-1}} - k = 1.84 \quad (7)$$

The numbers were calculated for a diatomic gas. Equations of (6) and (7) will be used in the course of the extruder design.

5. NUMERICAL MODELING

The process of water extruder firing is an unsteady process, which involves wave motion and energy dissipation and could be solved in 2D axially symmetric arrangement. However the duration of the discharge is many times longer than the time needed for acoustic wave to travel along the water charge. Also, Reynolds number at water slug speed of $U=500m/s$ and nozzle diameter $h=2.5mm$ is

$$Re = \frac{Uh\rho}{\mu} = \frac{500m/s \cdot 2.5 \cdot 10^{-3}m \cdot 10^3 kg/m^3}{1.003 \cdot 10^{-3} kg/m \cdot s} \approx 1.25 \cdot 10^6$$

This allows us to use 1D non-dissipating quasi-stationary model for estimation of water pressure and velocity. The model used is represented by the following equations:

$$\left\{ \begin{array}{l} \frac{dp}{dt} = n(p+1) \left(\frac{1}{m} \frac{dm}{dt} + \frac{1}{1-x} \frac{dx}{dt} \right) \\ \frac{dm}{dt} = -\alpha \sqrt{(p+1)^{\frac{n-1}{n}} - 1} \\ \frac{dx}{dt} = v \\ \frac{dv}{dt} = \beta(C - p) \end{array} \right. \quad (8)$$

Where

- p – water pressure in the nozzle;
- m – water mass;
- x, v – piston displacement and speed;
- t – time;
- n – adiabatic exponent, $n=7.15$.

Here the first equation is the equation of entropy balance, second – is the dependence of outflow speed on pressure in the nozzle. And the last two equations are the law of piston movement.

All values are dimensionless quantities. For nondimensionalization we used $B=304.5kPa$, m_0 which is the water mass in the nozzle, v_0 – initial piston speed, reduced nozzle length which is the ratio of the nozzle volume and the nozzle cross-section area, and l_c/v_0 for time nondimensionalization.

α, β, C are the similarity criteria of the set-up:

$$\begin{aligned} \alpha &= \sqrt{\frac{2}{n-1}} \frac{c_n}{v_0} \frac{F_a}{F_1} \\ \beta &= \frac{1}{n} \left(\frac{c_n}{v_0} \right)^2 \frac{m_0}{m_p} \\ C &= \frac{p_g F_2}{B F_1} \end{aligned} \quad (9)$$

Where

- F_a, F_1, F_2 are respectively the area of the nozzle cross-section on exit, at the entrance, and the area of the barrel;
- m_p – is the piston mass;
- m_0 – is the water load at $t=0$;

v_o – is the piston speed at $t=0$;
 p_g – gas pressure during firing, which can be assumed to be constant;
 c_n – is the sound speed at normal conditions;

Initial conditions are:

$$p = n c_n v_o / B; m = 1; v = 1; x = 0; \quad (10)$$

The results of numerical integration of the system (9)-(10) are presented in Figures 13 through 15.

6. CONCLUDING REMARKS

The performed work evidently demonstrated both feasibility of metal punching by water slugs at the wide variety of the slug properties (the conditions of our experiments were determined by the design of the Remington tool) as well as feasibility of process improvement (the variation of operational conditions significantly effect process results). The number of the process and design variables effecting the operation of the device Figure 4 exceeds 8. Thus special techniques is needed for optimization of this technology.

We will combine experimental study using the device Figure 2 and analytical study using numerical technique for modeling of shock waves in the 2-dimentional fluid flow (Godunov, 1976).

7. REFERENCES

- Atanov, G.A. (1987) "Hydro-Impulsive Installations for Rocks Breaking", *Vishaia Shcola*, Russian), Kiev.
- Atanov, G.A., (1991), "Foundations of One-dimensional Unsteady Gas Dynamics", *Vishaia Shcola*, (in Russian) Kiev.
- Voitsehovsky, B.V., Izosimov, V.A., Olenkov, N.F. (1962) "About Availability of Impulsive Water Extruder Decomposition Application For Rocks Decomposition", *Izvestia Sibirskogo otd. AN SSSR. Ser. tehn.* – No. 9, pp.72-75.
- Godunov, S.K. "Numerical Solution of Multidimensional Problems of Gas Dynamics", *Nauka, Moscow*, 1976, pp.168-193.
- Lavrentyev, M.A., Antonov, E. A., Voitsehovsky, B.V., "The Questions of theory and practice of impulsive water jets", *Novosibirsk: Institute of Hydrodynamics of Siberian Branch of SA USSR*, 1961.
- Atanov, G.A., "Powder impulsive water jetter", *Proceedings of the 11th International Conference on Water Jet Cutting Technology*, September, St. Andrews, Scotland, pp. 295-303, 1992.

8. ACKNOWLEDGEMENT

The study was supported by the NSF grant DMI 9900247.

Table 1. Summary of Metal Deformation by Impacting Slugs

[illegible]

N - number of the picture representing a sample; Dsn- mode of the acceleration of the water according to the Fig. 3; P-level of power load, according to the existing commercial standards; V- volume of the water slug, cm^3 ; D_1 -barrel diameter, mm; m-mass of the piston, g; D_2 - nozzle diameter, mm; d_1 - diameter of the opening in the base, mm; L_1 - travel distance distance of the piston, mm; l_2 -stand off distance, mm; TM- target materials (SS-stainless steel, Al- aluminum, LCZ- low carbon steel coated with zinc); r- thickness of the target , mm; d_2 - diameter of the hole in the target, mm.

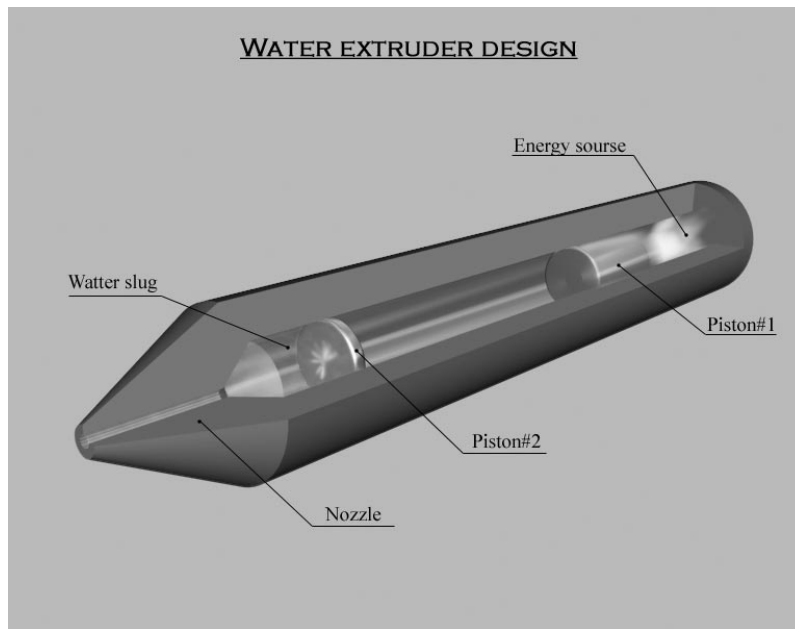


Figure 1. Schematic of the water extruder

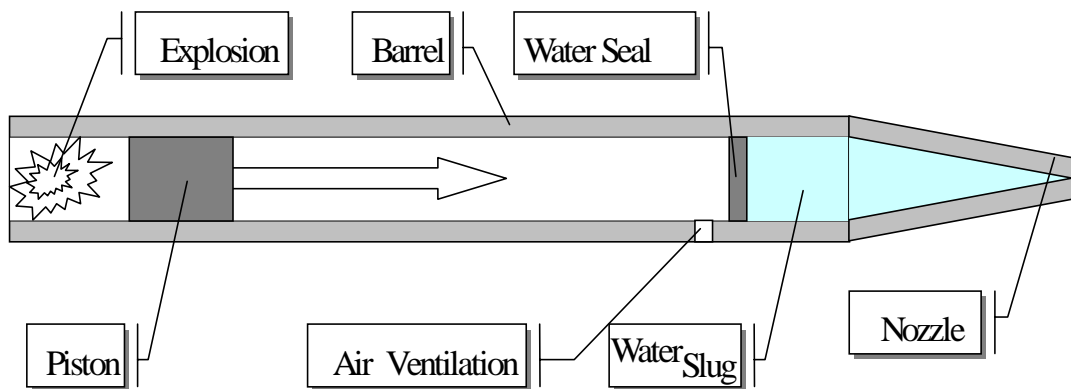


Figure 2. Schematic of the experimental setup for investigation of slug formation. Parameters of the setup will be varied in a wide range. The following parameters will be varied: Inner barrel/Piston diameter; Piston path length; Piston mass; Explosion energy; Water slug mass; Nozzle geometry.

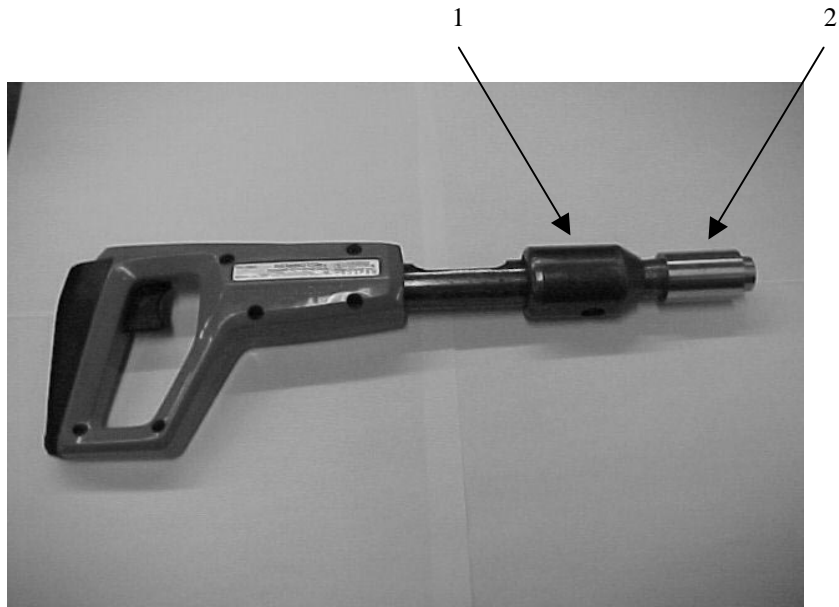


Figure 3. Experimental set up formation of high speed water slugs.
1 – power actuated tool; 2- attachment for loading of the water slug.
Notice simplicity of the modification of a commercial gun.

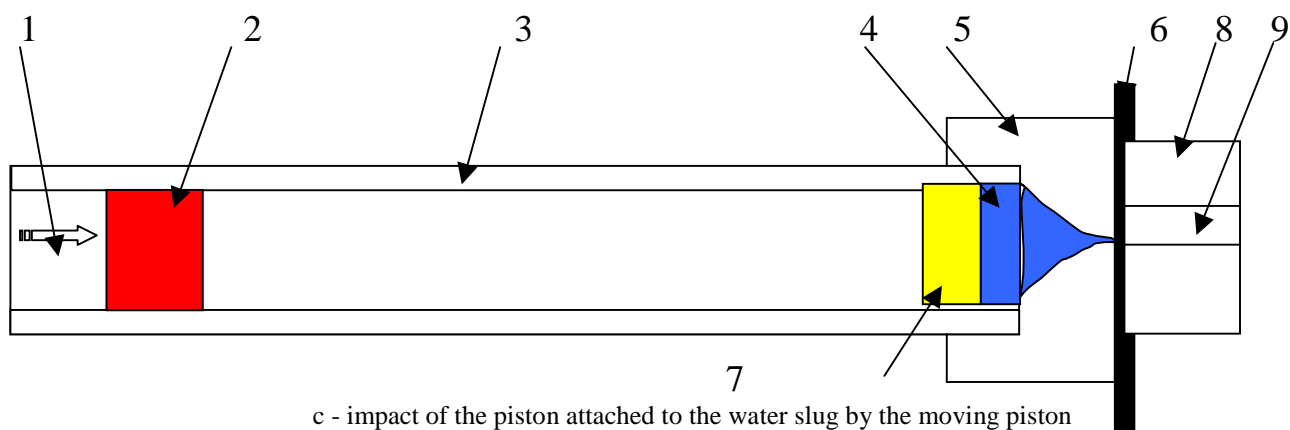
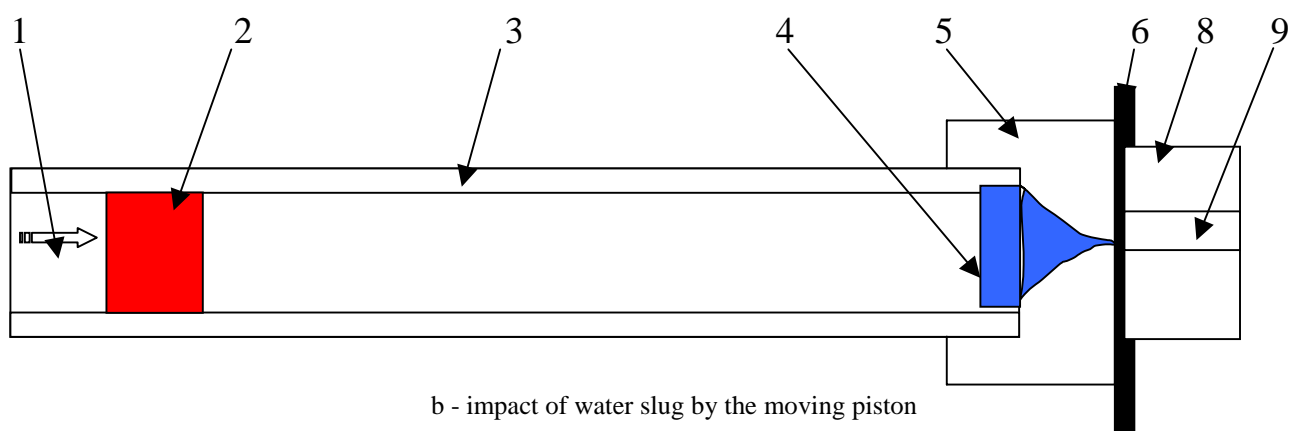
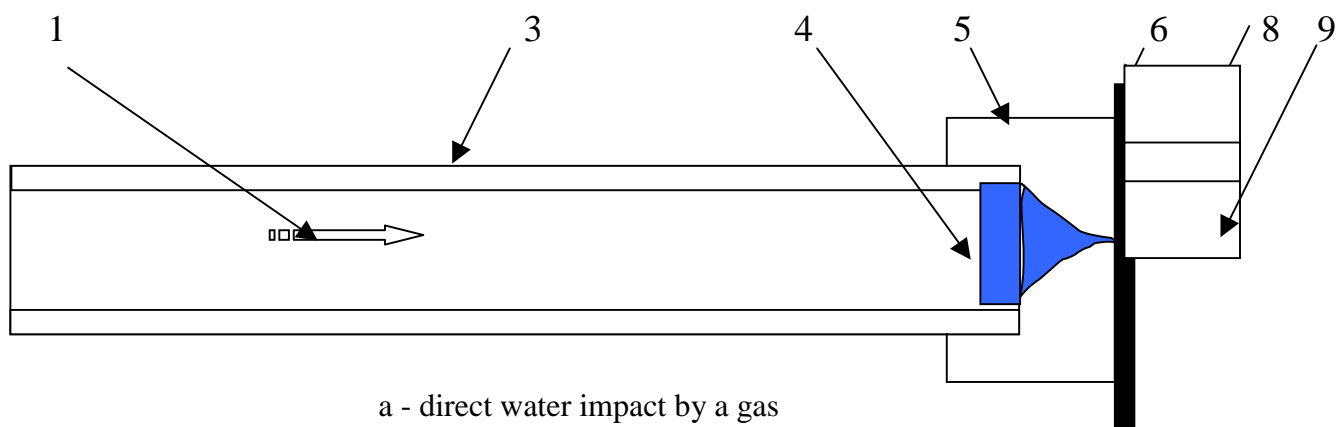


Figure 4. Schematic of the water slug acceleration
 1-product of explosion; 2- piston attached to an explosive; 3- barrel; 4 – water slug; 5- nozzle;
 6- target; 7- piston attached to the water slug; 8 - base of a target; 9- opening in the base.

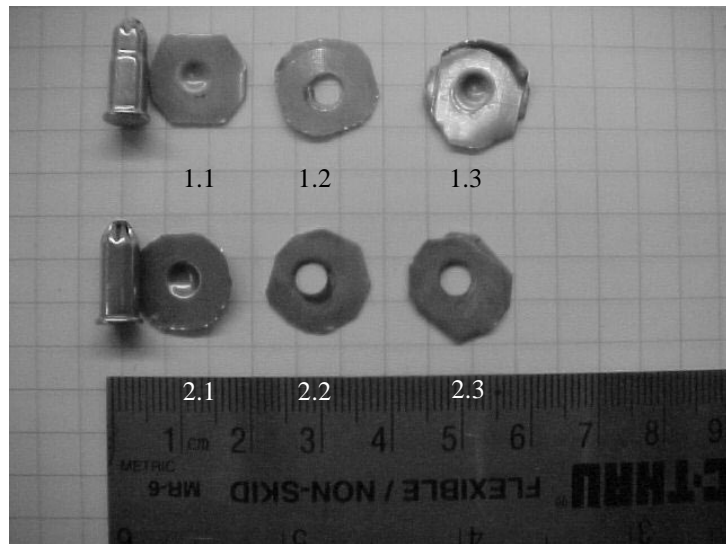


Figure 5. Piercing of the stainless samples (Figure 3a , Table 1).
 Samples 1.1&2.1 were impacted by gas stream only.
 Samples 1.2, 1.3, 2.2, 2.3 were impacted by the water slugs.
 The thickness of the samples 1.3&2.3 two times more than other samples.
 The samples 1.1, 1.2, 1.3 were pierced by the low power explosive.
 The samples 2.1, 2.2, 2.3 were pierced by the high power explosive. Notice deformation only of samples 1.1, 2.1 and 1.3 and piercing of samples 1.2, 2.2, 2.3.

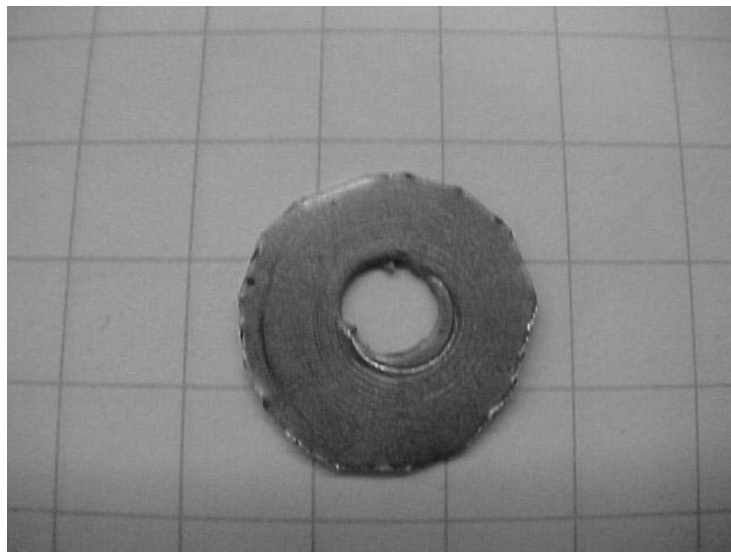


Figure 6. Sample 2.2 at magnification x 3. Notice shear of the steel by impacting slug.

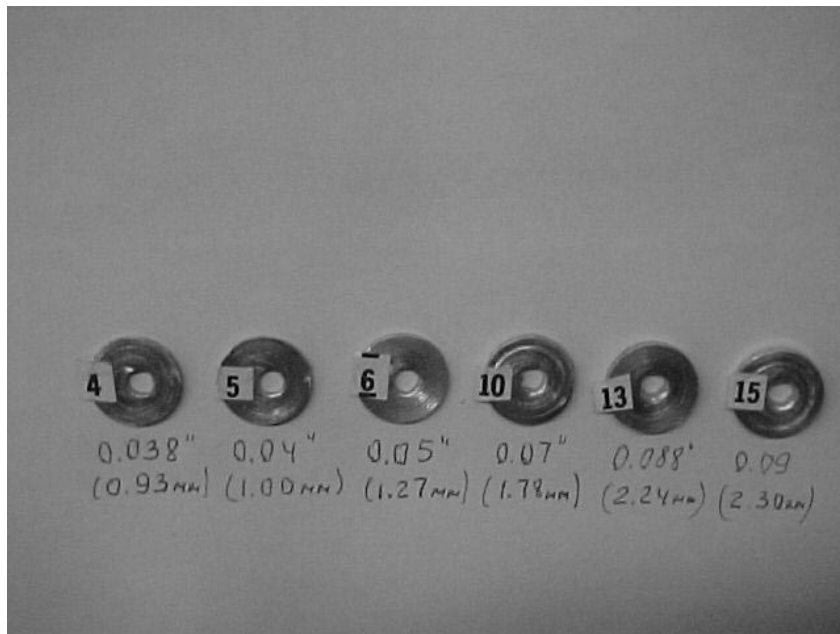


Figure 7. Piercing of aluminum samples. Notice formation of the round holes in all samples.



Figure 8. Piercing of stainless steel sample (21) at non round opening in the base (B). Notice geometrical similarity between the hole in the sample in the opening in the base.

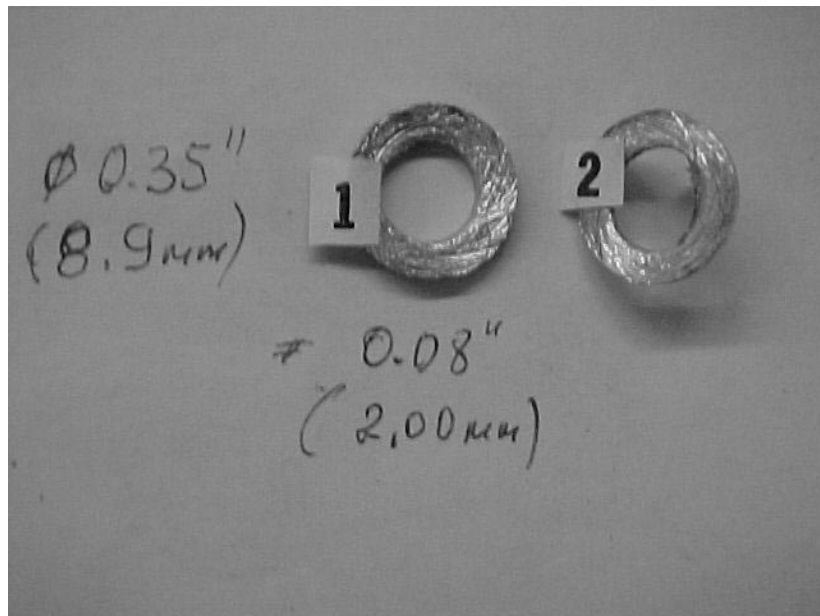


Figure 9. Piercing of large holes in aluminum samples. Notice generation of large round holes (diameter =8.9mm) using smaller nozzle (diameter =4.3 mm).

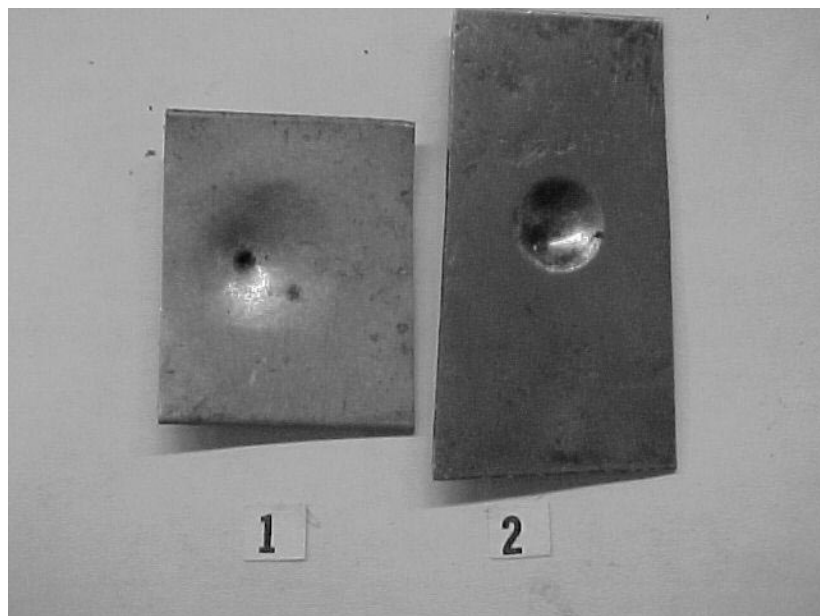


Figure 10. Piercing of holes in steel samples at very large opening in the base. Notice formation of spherical dimples having diameter equal to that at the base opening. Also notice formation of holes in the bottom of the dimples having diameter equal to the diameter of the nozzle.

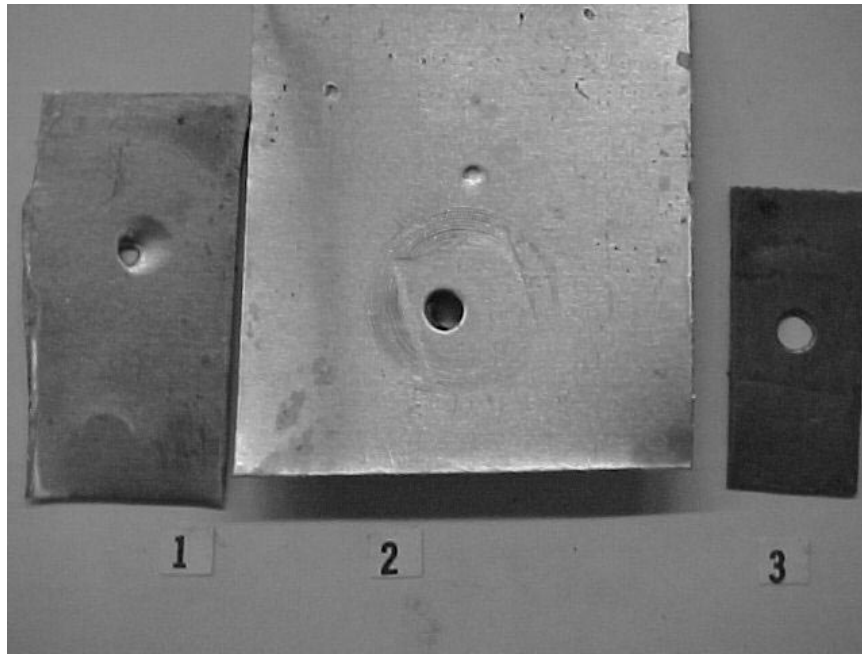


Figure 11. Piercing of steels and aluminum samples at different kinds of the fixture. The steel sample 1 was attached to the base having opening diameter much larger than the diameter of the nozzle.

The aluminum sample 2 and the steel sample 3 were attached to the bases having opening comparable with the nozzle diameter. Notice formation of the holes at the non deform surface and formation of the smaller hole at the sample dimples at the sample 1.

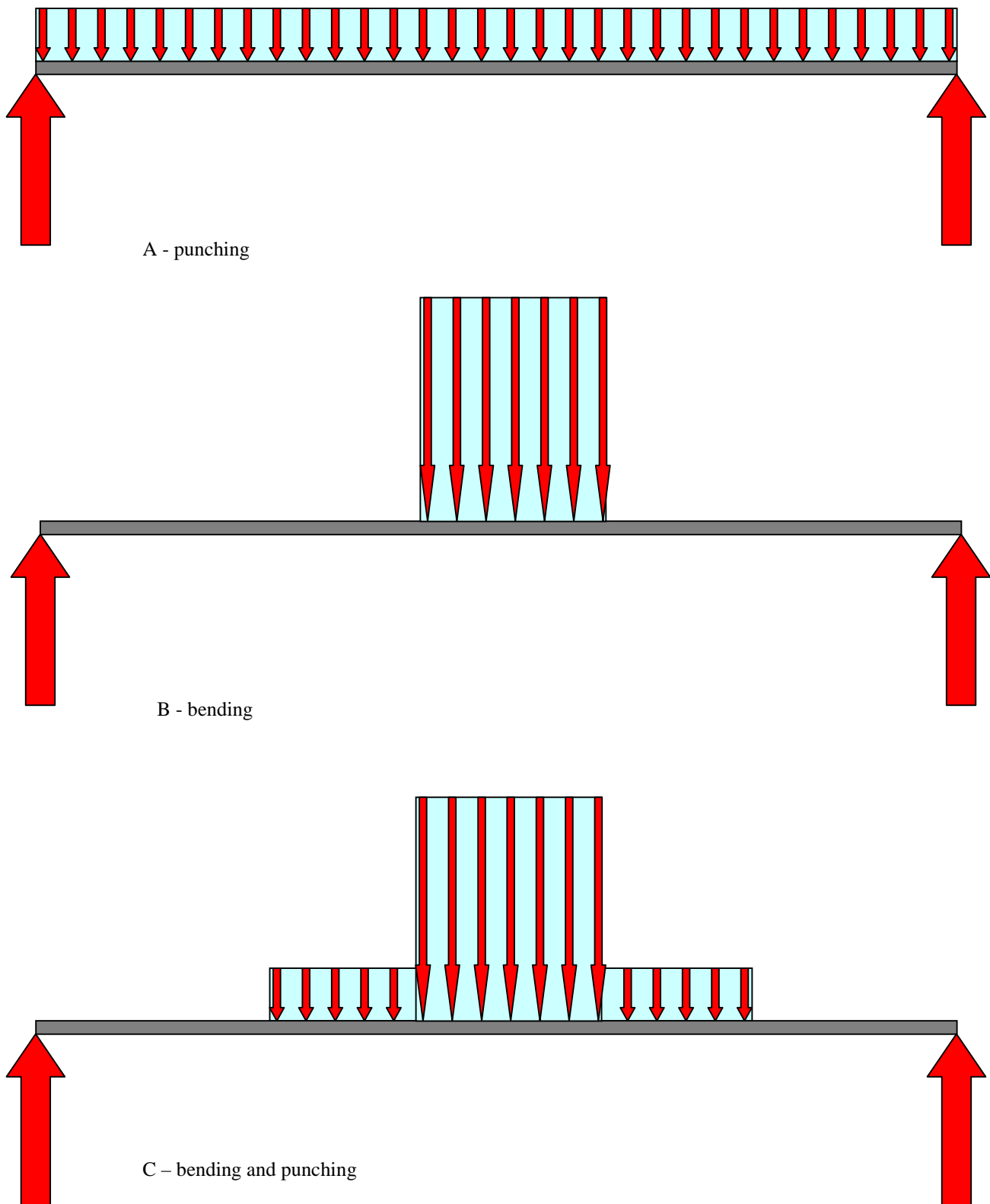


Figure 12. Schematics of the substrate loading resulting the deformation identical that of the water slugs. Case A corresponds the ratio between the base opening and the nozzle diameter less than 3, Case B corresponds to this ration higher than 5 and Case C represents intermediate conditions.

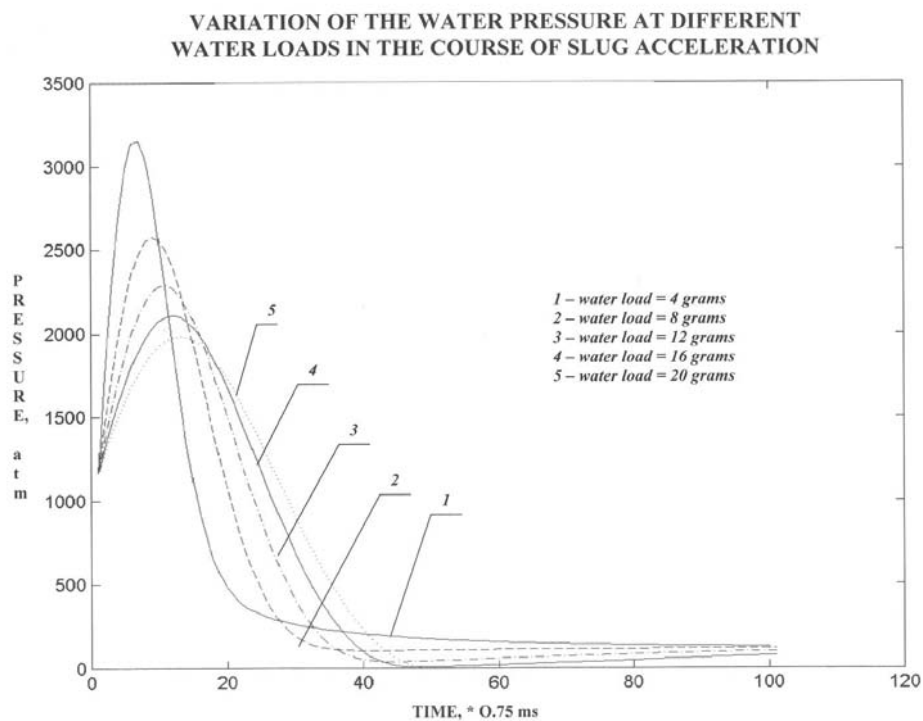


Figure 13. Pressure in the barrel during firing at different water loads

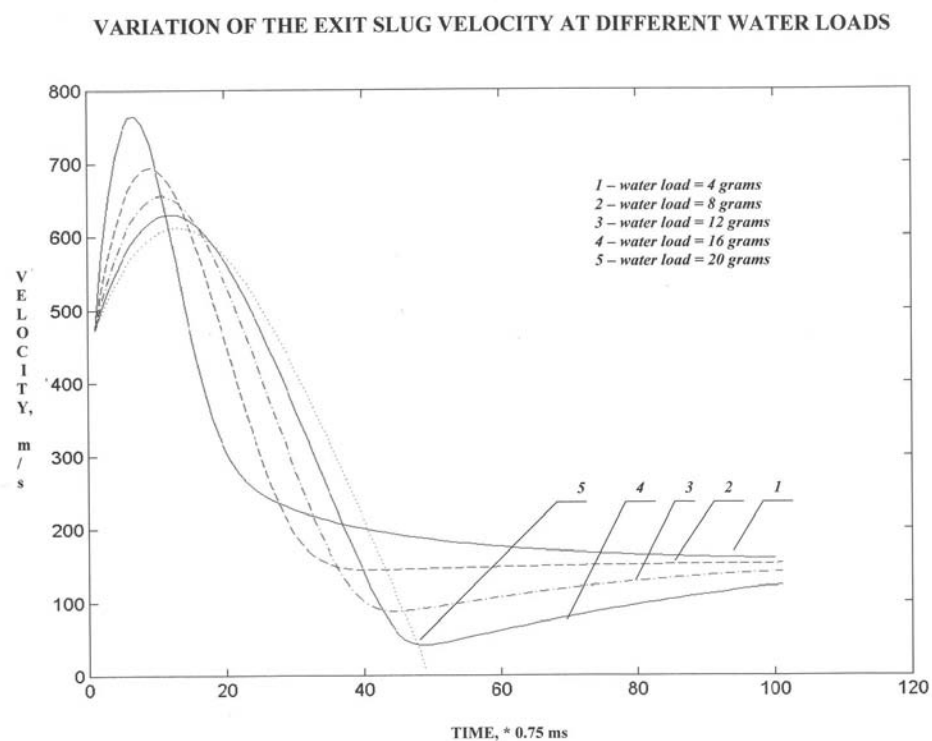


Figure 14. Change of exit slug velocity during firing at different water loads

EFFECT OF THE WATER LOAD ON THE WATER
PRESSURE IN THE COURSE OF SLUG ACCELERATION

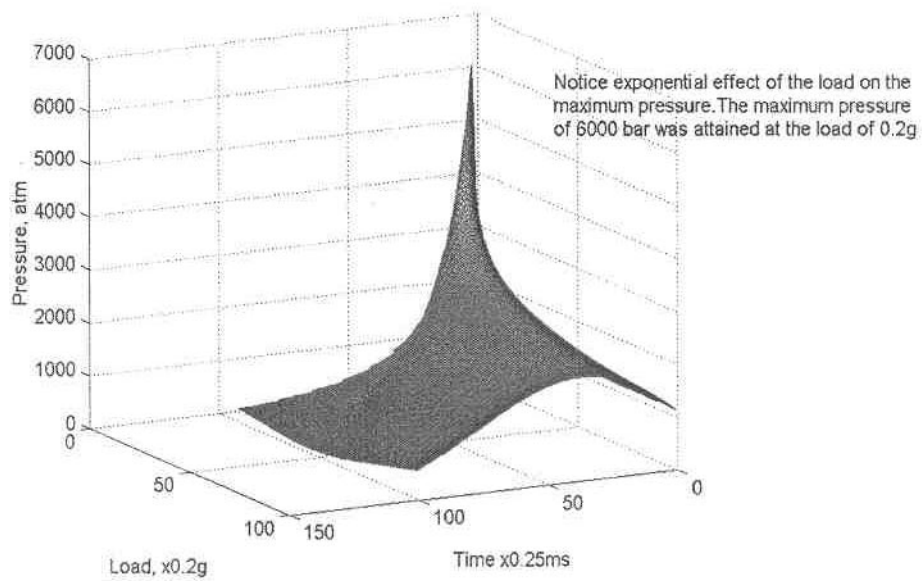


Figure 15. Water pressure in the course of slug acceleration

ABRASIVE WATERJET & METAL MATERIAL INTERACTION DYNAMICS

Jiří F. Urbánek
Brno University of Technology
Faculty of Mechanical Engineering, Atelier of Process Design
Czech Republic, Europe

ABSTRACT

Special model is based at a shock waves theory. The model requires cutting process presence of arbitrary material and it is situated in cutting kerf. Dynamical removal phenomena initiates shock wave and an echo is consequence at jet interface, at erosion front mainly. The arrangement of the experiments was aimed to catch a phenomena dynamics by means of high-speed camera. Specific setting of Abrasive Waterjet (AWJ) process parameters of the cutting flow at the interface - final workpiece margin/free space - faces to a nose creation. The nose is bounded as a triangle and it is a consequence of overshooting phenomenon. A special test specimen is designed for cutting/machining ability of AWJ processes. It provides job-shop tests according the requirements to quick and cheap, but enough exact and repeatable, operative proofs. The test is founded at nose measurement and obtained dependencies serves to fast and exact evaluation of cutting process efficiency. It will be source of new economic savings and contribution of cutting technology of high pressure AWJ.

1. INTRODUCTION

A statement was vindicated in past paper by Urbánek (2000): “The Abrasive Waterjet (AWJ) has a behavior as it would have a shape memory in cutting kerf”. Today is possible to go even further and can be affirmed: “The AWJ in cutting kerf has virtual memory of one binary unit (bit) as a solid on workpiece final margin”. Its behavior is as a “clip-clap” element here. Its dynamics can be simply expressed as aN “unruptured jet” model (the abbreviation URjet would be used).

URjet model is based at a shock theory (in literal, also transferred meaning of word sense).

This model requires cutting process presence of arbitrary material. The boundary conditions are: The existence of the cutting process between the entry and an exit surface is a function of the relative velocities \mathbf{w}_{cran} ; and \mathbf{w}_{dors} of the jet and the workpiece in cutting kerf. The vectors \mathbf{w}_{cran} ; \mathbf{w}_{dors} are space perpendicular.

Necessary experimental conditions are: generated (working) pressure of AWJ generator is 350 MPa and vector $\mathbf{w}_{\text{ventr}}$ must be controlled. The impact velocity of flow \mathbf{w}_{cran} is faster than air sound velocity magnitude. The URjet model start from image that a flow compressibility has real quantity (water specific mass is increased in cranial direction at least in cutting kerf doubtless). The evidence is a workpiece burr at jet surface of exit. But lateral sides of cutting kerf act the jet centric (cross-sections) compressibility beside. The evidence would be given by “overshooting” process analysis in next chapters. Both above those compressibility have a character of shock waves rather than evident (visible) turbulence. The source of turbulence damping are abrasive and other solid particles and cavitations bubbles, which eliminate of turbulence chaos in workpiece interactive flow. Further reason for “turbulence model” abandon and URjet model enthronement is a duration from micro- to nano-second’s of the jet-workpiece interactions. The flow compression is compensated by re-active shock and consequent force makes material extraction from the cutting kerf surface. This phenomenon together with dominant initial erosive function of abrasive particles and together with cavitations, delaminating and other sources of removal effects make for a cutting ability of AWJ in ductile (metal) workpieces. This paper is not aspiring about exact mathematics of watching phenomena. But rather it refers to their real existence, and offers of partial explanation, verified and supported by the experiments.

2. PROCESS ANALYSIS AND MODEL SYNTHESIS

The stress state of abrasive flow in interaction with workpiece isn't possible to view only linear, nor only flat, but even spatially and in addition in two mutually dynamically affected, and significantly one another transformed environments. Catch-able effects on interface of these environment is hardly possible to identify at static model.

The hydrodynamic URjet shape is a self-formed “pipeline,” depicted as a tube in Figures 2 and 7. The various regions, definitions, and fundamental interaction relations of the flow was shown by Urbánek (2000). An occurrence of relative organized dissipate flow is condition of successful cutting through of the workpiece. It is originated after exit surface abandonment. It has a character of submerged flow here. The normal fluid dynamic fluctuation, scalar and vector

physical quantities can be defined here; but the abrasive, chips, and bubbles in the flow are special components of the AWJ flow.

The arrangement of the experiments was aimed to catch a phenomena dynamics by means of high-speed camera. Specific setting of AWJ process parameters of the cutting flow at the interface: - final workpiece margin/free space - faces to a nose creation. The nose (bounded as a triangle of the points A, B, C – Figure 3) is a consequence of a phenomenon, which was named an “overshooting” by Urbánek (1997). While position B \equiv B' points are stable during overshooting the position A and C is changed in Figure 3. The nose shape is nearly similar to rectangular triangle, if the leg A'B' against of a right angle is taken as a line. Than triangles ABC and A'B'C' are self similar rectangular triangles with conjunct ϕ'_{nose} . Than is valid, if the ϕ is entered jet diameter.

$$tg \phi'_{nose} = \frac{B'C' - \frac{1}{2}\phi}{h_{nose}} = \frac{B'C'}{A'C'} \quad (1)$$

The further experiment necessary common conditions are here:

- The plane of final margin must be parallel to within $\pm 5^\circ$ of the vector w_{cran} (see Figure 1). Than the AWJ cutting flow is stable process to the time point of the “overshooting”. When AWJ jet axis exits the final marginal surface - dissipate flow overshoots from dorsal to ventral side of final margin. A duration of this process is to the 0.1 sec. Virtual “memory” consist in a fact there, that the overshooting is untouched sooner as long as AWJ $\frac{1}{2} \phi$ do not exceed of final margin. And/or as long as the axis of impacted AWJ (point O - see Figure 2) do not cross final margin respectively.
- The URjet flow separating/dividing (“like as an edge”) was not observed simultaneously to ventral and dorsal side of the “nose” for time duration of the overshooting. Fluent bypassing (flow round) simultaneously of both sides of the nose (“like as at a blade edge”) was not observed. Stable bypassing (fluent, not divided, flow) is possible at one side of edge only – i.e. “jet coherence memory”. Stable bypassing is possible at one side of nose only (clip-clap effect) – AWJ is coherent. The condition is an existence of AWJ flow feed - w_{ventr} , or an existence of workpiece feed - w_{dors} . The fluid flow did not separate from either a convex or a concave area at the working surface. Bypassing of convex area was not observed by Hashish and Stewart (2000). Bypassing of concave area is connected with erosion front creation always.
- The parameter h_{nose} (Figure 1) is value which is useful in workpiece machinability and/or abrasive flow cutting-ability determining. Likewise it is suitable for cutting ability evaluation of the abrasive in UR test here.

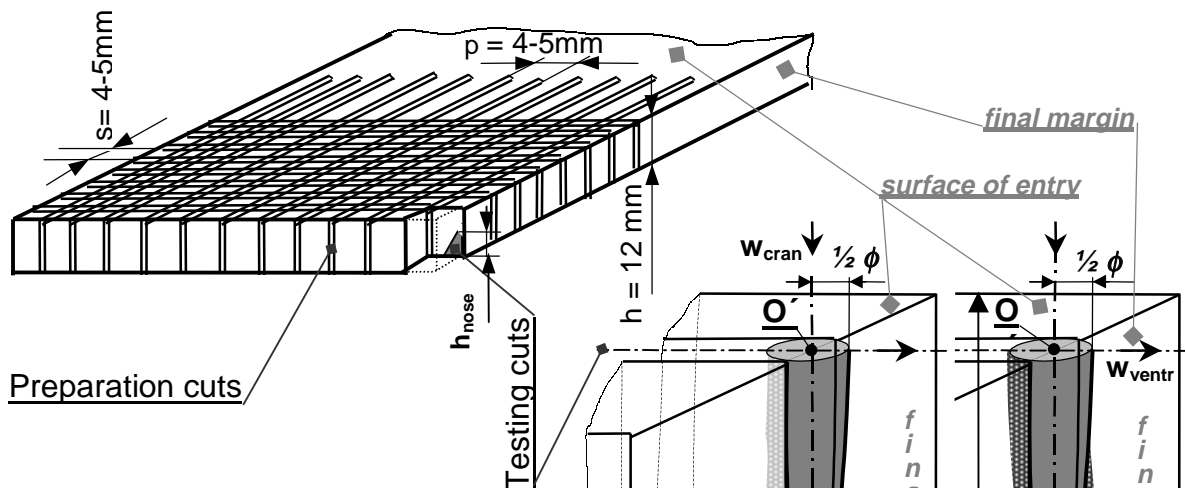


Figure 1. An URtest metal specimen with typical spike-tooth p and span s of h_{nose} testing – AWJ cutting.

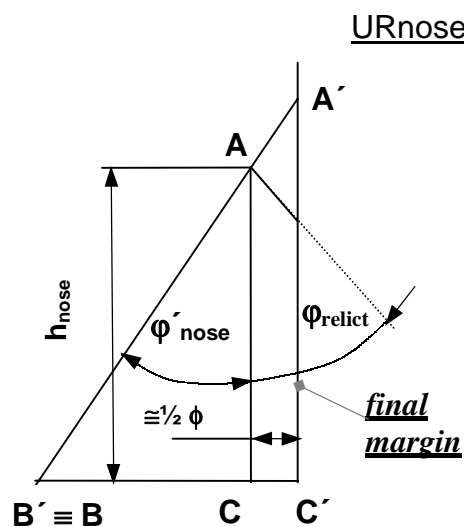


Figure 3. A scheme of URnose creation. Time sequence is from (comma letters) $t' = t - \delta t$ to t .

Figure 2. A detail of URjet. At this clip the AWJ dissipate flow "overshoots" from dorsal to ventral side of final margin. Comma letters show state of overshooting start in real time $t' = t - \delta t$, where t is real time of overshooting end.

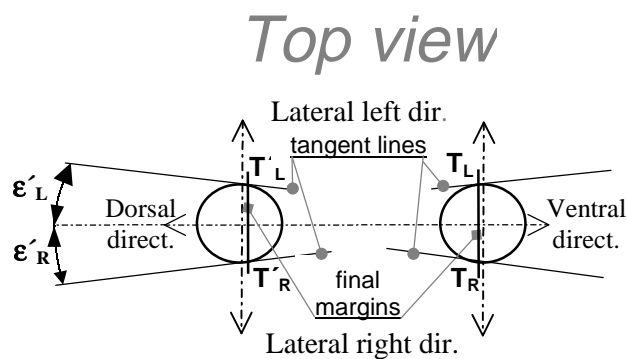


Figure 4. Cranial top view of the URjet clip. Final margin position predetermines the lateral sides points $T_{L,R}$, them pass through tangent lines, which angles ϵ determine dissipate flow direction during the overshooting.

The experiments at URtest specimens were carried-out for the verification and check of real recycled abrasive cutting ability. It was made as a part a solving of project “Under-one-Roof Recycling” - (the abbreviation URrec[®] is used for this project - product of Grant Agency of Czech Republic 101/000890).

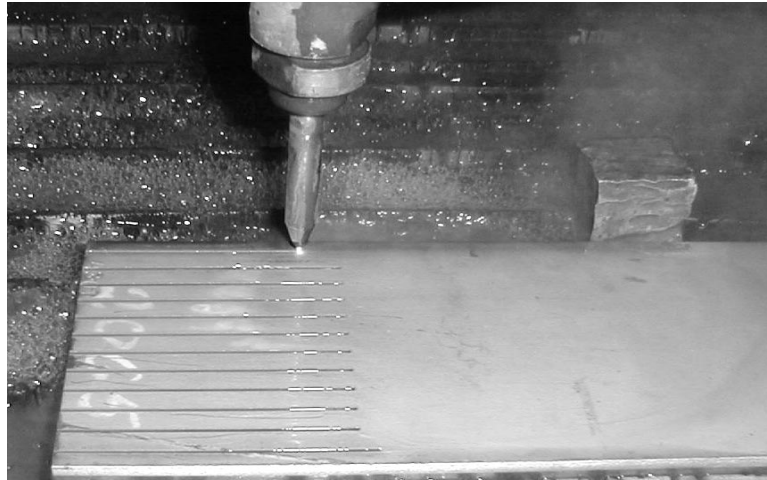


Figure 5. The picture of production process of URtest specimen at real workpiece configuration. Preparation cuts.

The explanation of dynamic behavior of AWJ working in cutting kerf (erosion front) of workpiece arose as a “by-product” of above experiments.

An URtest specimen design was started from requirements to quick and cheap, but enough exact and repeatable, operative proofs. The specimen production need not any other machine. Its adjustment does not need any other arrangement for its preparation. It is completely producible by means disposable AWJ arrangement, where it serves for its testing then. Otherwise, a compliance above-mentioned conditions of specimen contours is fully in competency dispensable AWJ system. At Figure 5 is the picture of production process (preparation cuts) of URtest specimen at real workpiece configuration. The URtest specimen properties, contours and arrangement is fully subordinated of the economic, time and informative effectiveness of the test. Up to now the execution of workability or cutting ability tests by the help of edge samples needs cumulative time (preparation + implementation) in order the hours. While our URtest offer more and precise information already under several minutes. Therefore it is multiple cheaper and it is suitable for job-shop exams of machine/cutting ability of AWJ technology. Shape of our specimen is like a “Un-cut Rack” (from this originates the abbreviation URtest).

URtest[©] metal specimen is drawn with typical spike-tooth p and span s in Figure 1. The possibility of h_{nose} testing and measuring follows from next figures. Figure 2 is a detail of URjet. At this clip the AWJ dissipate flow “overshoots” from dorsal to ventral side of final margin. Comma letters show state of overshooting start in real time $t' = t - \delta t$, where t is real time of overshooting end. At Figure 3 is a scheme of URnose creation. The Figure 4 shows clip at cranial top view of the URJet. Final margin position predetermines the lateral sides points $T_{L,R}$,

passing through tangent lines, which angles ϵ determine dissipate flow direction during the overshooting. If real value of sum

$$\epsilon_L + \epsilon_R \geq 0 \quad \text{than dissipate flow keep dorsal direction.} \quad (2)$$

But if

$$\epsilon_L + \epsilon_R < 0 \quad \text{than dissipate flow is overshoot to ventral direction.} \quad (3)$$

The Figure 6 is plotted graph for two different properties of workpiece material: - ductile (stainless-steel 14 301) with cranial thickness $h_{DU} = 12$ mm;

and brittle (granite stone) with $h_{BR} = 60$ mm. They both were tested at nose creation in given boundary conditions. The graphs of dependence $h - h_{nos} = f(w_{ventr})$ was obtained at special URtest samples.

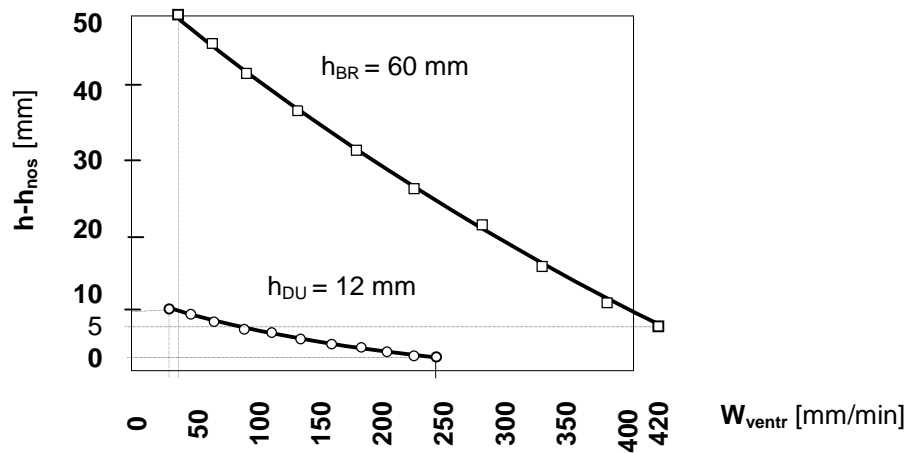


Figure 6. The workpiece material dependence $h - h_{nos} = f(w_{ventr})$.

Above graph confirms the ability of value h_{nose} as a cutting/ machining ability measure, there with regard to feed rate has almost linear dependence. The value h_{nose} dependence to the workpiece material scratch resistance by Vickers was very close correlation as was achieved by Urbánek (1996). The dependencies to other AWJ parameters have to be tested in our next experiments. Value h_{nose} serves for fast and exact evaluation of cutting process efficiency. It will be source of new economic savings and contribution of cutting technology of high pressure AWJ.

3. CONCLUSIONS AND DISCUSSIONS

The Abrasive Waterjet in erosion front has a phenomenology different from that of water jets with slow flows of Newton liquid. The experiments show that an effort for the turbulence visualization or turbulence verification is inefficient and at the adventure level only. Flow cavitations effects originating in the turbulence have not enough time and space in AWJ metal workpiece erosion front. But enormous stress gradient originates in the transition from the high-

pressure region at the workface to the high velocity flow in the fluid, distant from the workface. The model of shock waves (or echo waves) was developed using Cylindrical Micro Segments analysis. Occurrences of echo waves which keep the “shape memory” of URjet was evidenced by Urbánek (2000) at acoustic emission graphs. They were made by means of Acoustic Emission Analyzer AED FTA 16. The record and plot of workpiece acoustic emissions were expressed over the frequency range 30 kHz to 2 MHz. A typical acoustic emission record is a plot of the number of acoustic events as a function of time in seconds. This record is a very good indicator of the cutting process. The peaks in the record correspond to periods of rapid removal of material at the workpiece face. The background at 4000-6000 counts represents the signal from rebounding (echo) amplification. This background occurs whether or not there are abrasive particles in the wAWJf flow. It can be argument for neutrality of solid particles presence at echo abundance.

The absence of the background was observed by Urbánek 1999 in the quiet periods (without jet/workpiece interaction). The pressure fluctuations (which can relate with cavitations bubbles collapse too) are main removal phenomena if the abrasive is absent in the URjet. It makes possible cutting process without the abrasive. Head source of cavitations bubbles are echo dependent pressure fluctuations in the jet flow. Synchronized camera record, dynamometer plot and acoustic emission graphs give full survey (visual, force and acoustic) about dynamical phenomena which was observed at transitive states between free space/workpiece.

The hydrodynamic AWJ flow's shape, working in erosion front, keeps a self-formed “pipeline,” depicted as an dorsal concave curved tube (cross-sections 0 – 10) expanding in cross-sections 5 – 10 in Figure 7. A dissipate flow, with the characteristics of a “submerged flow,” occurs at the exit of the flow from the bottom surface of the workpiece (5 – 10 cross-sections). At each transversal plane (cross-sections 0 – 5) in workpiece cutting kerf the flow is bounded by the semicircular erosion front at the workface (ventral direction) and the semicircular fluid/air interface (dorsal direction). For whole this dynamic process of removal interactions the resulting circle cross-sections 0 – 5 are kept. They are kept even if a cranial depth of cutting kerf is longer (multi-pass cutting) than a length, where the submerged flow occurs, if the jet fly through the free space.

It seems that an existence of the coherent AWJ flow between workpiece entry (0) and an exit (5) needs a resistance against material removal and/or lateral walls of cutting kerf at least. The good possibility of “multi-pass cutting” was described by Ciccu et al.(1996). Here the lateral wall is the “memory factor”. The high-speed fluid dynamic fluctuation, scalar and vector physical quantities can be defined here; but the abrasive, chips, and bubbles in the flow are special (scalar) components of the AWJ flow here.

The largest displacement of stress distribution is manifested by $\delta\sigma_{RR}$ relative increasing in the radial plane of the CMS (see Figure 8). The erosion front existence and shape is determined by: - the sum of the material removal processes (abrasion, cavitations, delaminating, etc., described by Urbánek and Bumbálek (1998)) and the large kinetic energy of the fluid flow; - in workpiece medial plane, concave curvature of the erosion front with curvature Q_{iM} (see Figure 7). The centripetal acceleration of the fluid is caused by the reaction forces R_i at the Q_{iM} . The sum of cutting centrifugal and above centripetal forces and other in medial plane results to general force F_{ventr} , which is surprise very small and oscillates around zero $\pm 2N$ as was documented by Urbánek (2000).

“Control” stress of the shock wave is given as a difference $\delta\sigma_{CR}$ along URjet radial direction. It is initiated by erosive, cavitation and delaminating interactions in erosive front. Its speed of sound radiates like shock wave in environment of the jet, whereas multiplex echo occurs on jet/ other environment interface. However dominant “control” direction is given by solid semi-cylindrical erosive front as is shown at Figure 9. The result is high concentration of the stress in the jet center, which discharges (relax) in one free only direction, so in axial direction (jet longitudinal line). This reactionary stress vector is concentrated with analogy waters ejaculation after drop in a stone on water-plane. In the center radii it then happen to tension concentration of the shock waves. Reaction consequence is a change of dominant vector of diffused shock waves. However, this mechanism can operate only in cutting kerf, where semi-circular erosive front initiates and forms echo interface. The jet flying in freeway space hasn't enough solid echo interface. It forms still more diffusive taper in addition. Than here indeed the echo results to submerged flow. Staggered parallel offers for the echo function with laser lights origin in its active generator. Longitudinal diffusive echo-waves are operated like feedback controlled continuance of jet with dorsal curvature in erosive front so long, as long as angles sum $\epsilon_L + \epsilon_R$ obtain negative value (under zero). At that moment lateral sides cutting kerf controlling function is lost. The jet begins its behavior so, as it fly through free space, the “overshooting” process proceeds.

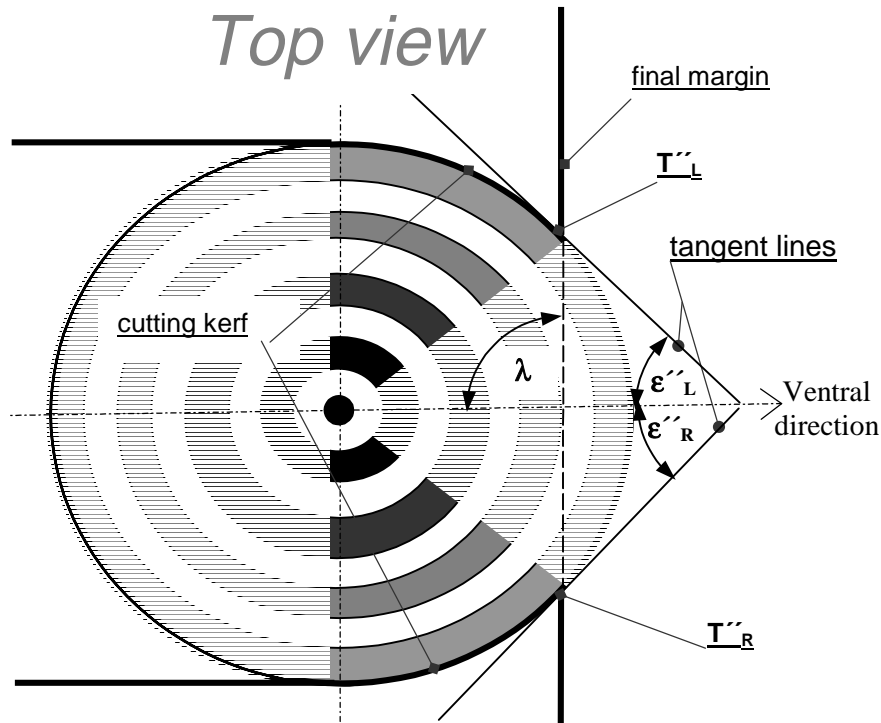


Figure 9. Echo shock waves visualization.

Cross shock waves result to shock echo in longitudinal direction, where effective to material removal is cranial direction at kerf surface (erosion front). Slant angle λ final margin in relation to ventral direction (not perpendicular) have to be a target of our next experiments. Here a URjet model of an interaction would be supported or refuted. A thesis is that slant final margin makes for the striations. Lateral-lateral-ventral surfaces of cutting kerf have an effect as an initiator of concentric shock waves as is shown in Figure 9. They paradoxical keep transversal cross-section jet as a circle shaped. They don't permit a disruption of the jet flow in any direction. The consequence is the dissipate flow keeping in dorsal direction. This state of stress keep dissipate flow in dorsal direction to the time of the overshooting. A start of overshooting comes after an intersection of the jet center of workpiece final margin. The overshooting duration is under 0,1 sec. A result is a change of dissipate flow from dorsal to ventral direction. Like a this behavior explains an AWJ multi-pass-cutting, as well as other unusual phenomena, include “memory” (clip-clap) of URjet function. A statement can be expressed: “The AWJ in cutting kerf has virtual memory of one binary unit (bit) as a solid on workpiece final margin”.

4. REFERENCES

- Agus,M., Bortolussi,A., Ciccu,R., and Vargiu,A., “Abrasive-rock Interaction in AWJ Cutting,” *Proceedings of 13th International Conference on Jet cutting Technology*, Cagliari, 1996.
- Hashish,M., and Stewart,J.,, “Observations on Precision Turning with AWJ,” *15th International Conference on JETTING TECHNOLOGY*, Ronneby Sweden, 2000.
- Urbánek,J., “Characteristics of the Interaction Between Abrasive Water Jet and a Workpiece,” *13th International Conference on JETTING TECHNOLOGY*, Sardinia, I, 1996, ISBN 186058 011 4.
- Urbánek,J., and Bumbálek,L., “ Abrasive Waterjet Removal Phenomena in the Workpiece Erosion Front, ” *Review AIRAPT-16&HPCJ-38*, Japan, Kyoto, 1998, ISSN 0917-639X.
- Urbánek, J.F., “The Flow Interactive Characteristics of Abrasive Water Jet (AWJ),” *Review AIRAPT-17*, U.S.A., Honolulu, 1999.
- Urbánek, J.F., “Interaction Phenomena and a Cavitation of Abrasive Water Jet,” *6th Pacific Rim International Conference on Water Jetting Technology*, Sydney, Australia, 2000, ISBN 1 876315 26 1.

5. NOMENCLATURE

a-p line – antero-posterial line

AWJ - The Abrasive Waterjet

CMS – Cylindrical Micro Segment

F_{ventr} – general force

h – specimen thickness

h_{nose} – measure of the nose

l-t line – longitudinal line

p – test specimen spike-tooth of

Q_{IM} – erosion front curvature

R_i – reaction forces

s – test specimen span

t – time

t-v line – transversal line

Urjet – Un-Ruptured jet

URrec[®] – Under-one-Roof recycling

URtest[®] – Un-cut Rack test

w_{cran} – cranial velocity

w_{dors} – dorsal velocity (feed rate)

ε – angle of tangent line

ϕ – jet diameter

φ – angle of nose

λ – slant angle of final margin

σ – normal tension

τ – tangential tension

IMPACT INITIATION MECHANISMS OF HIGH EXPLOSIVE MATERIALS DURING WATERJET DEMILITARIZATION

Paul L. Miller
Gradient Technology
Blaine, MN

ABSTRACT

Safety is paramount in the demilitarization of high explosive ordnance. The use of waterjets for the demilitarization of high explosive ordnance has increased in pressure from the early 24 MPa (3500 psi) units first used in the early 1950s to the current generation of fluid jets cutting high explosives at pressures exceeding 350 MPa (50,000 psi). Analytical safety tests were performed independently by both Los Alamos National Laboratories and the author on high explosive initiation using fluid jets and theoretical models were generated from the empirical data. This paper identifies the shock initiation mechanisms and examines safety testing related to impact shock initiation of high explosive materials during waterjet operations and the control measures necessary to prevent initiating the explosives during demilitarization.

1. INTRODUCTION

Waterjets have been used by the US military and their civilian contractors for demilitarization of weapons since the early 1950s as reported by Yeakley and McQueen (1964). Prior to this time the use of low pressure steam had been used by the military for the demilitarization of conventional explosives, not for the kinetic effects of the steam jet but rather to melt the explosives. The initial reluctance to adopt waterjets as a method for demilitarization is understandable given the sensitivity of high explosive materials to impact under normal circumstances, let alone the potential for increased sensitivity in aged or contaminated explosives found in old weapons. Typical high explosives detonate when subjected to low level impact shock, such as from a falling weight, and the energy requirements for most explosives are characteristically very low. In addition to the shock sensitivity, most explosives are also very sensitive to friction, spark, and temperature. These extreme sensitivities restricted the use of waterjets for the demilitarization of high explosive filled devices for many decades until adequate safety testing was performed.

2. DISCUSSION

2.1 Background

The earliest examples of waterjets used for demilitarization, according to Padgett (1962) were by Thiokol in the 1950s and 1960s to wash out rocket motors. The first washout systems used pressures of 24 MPa (3000 psi) with flow rates of $0.82 \text{ liter} \cdot \text{sec}^{-1}$ (13 gpm) through a 1.59 m^{-3} (0.063-inch) orifice. By the 1960s these systems had evolved from curiosities into a well-defined and developed technology using 35 MPa (5000 psi) at $19 \text{ liter} \cdot \text{sec}^{-3}$ (300 gpm) through a 6.35 m^{-3} (0.25-inch) orifice as reported by Yeakey and McQueen (1964). These waterjet systems eventually were standardized by the U.S. Army as an *Ammunition Peculiar Equipment* (APE) 1300M1 by the late 1960s. However, by the end of that decade the U.S. Navy had effectively put on hold any future use of waterjet washout of bombs or projectiles, according to Palmer (1969), based on safety concerns raised by both the British and Canadians.

In the 1980s an effort was made by several different U.S. Government agencies, acting independently, to evaluate the effects of jet impact on high explosives. The U.S. Navy through the Naval Surface Warfare Center – Crane Division (NSWC-Crane) attempted to establish the limits of safety using waterjets on explosives, while Los Alamos was independently investigating the use of high velocity jets (Mader and Pimbley, 1981) to intentionally initiate explosives. Completely unaware of the government's efforts, researchers working under a commercial independent research and development (IR&D) program (Miller, 1992) had established the safety of the fluid jet cutting process through theoretical research and empirical testing by the mid-1990s. These systems have since been used extensively for demilitarization and disposal of conventional ordnance.

The commercial IR&D program to qualify entrainment fluid jets for use on high explosive weapons was originally conceived, according to Miller (1996), from research performed for the National Aeronautical and Space Administration (NASA) by various researchers such as

Thiruvengadam and Rudy, (1969), Engel (1970), and Thiruvengadam and Gunasekaran (1970) on modeling the impact of raindrops on aircraft and turbine engines. From this research on high velocity raindrop impact data a predictive model was generated and the safety of the fluid jet cutting process was predicted as discussed later in this paper.

2.1.1 High Explosives

The three general types of military energetic materials are propellants, explosives, and pyrotechnics (PEP). Explosives are chemical compounds that contain either a bound oxidizer or sufficient molecular stress to release the stored chemical energy in a short duration. Explosives are further classified as to being either a *primary* or a *secondary* explosive. Primary explosives are very sensitive materials used in low quantities to initiate an explosion while secondary explosives are much more powerful and stable. Classic explosive materials of the primary type include lead azide (LA), mercury fulminate (MF), and pentaerythritol tetranitrate (PETN). Secondary explosives used today are typically nitroaromatics such as 1, 3, 5-trinitro, 2-methylbenzene (TNT), or nitramines like hexahydro-1,3,5 trinitro-1,3,5 triazine (RDX), or octahydro-1, 3, 5, 7 tetrahydro-1, 3, 5, 7 tetrazocine (HMX). These three explosives alone amount to over 95% of all explosives used by the military.

High explosive (HE) projectiles typically contain only about 20% of their mass as actual explosive fill. The remaining mass of the projectile is the metallic casing weight. The heavy projectile casing is required for the projectile to remain intact during the tremendous forces present during gun launch. These forces may exceed 10,000 Gs in high performance weapons. The heavy projectile walls complicate the demilitarization and disposal of unwanted or surplus projectiles. Standard metal cutting processes generate substantial amounts of localized heat which typically initiate some percentage of the projectiles with predictably disastrous effects.

2.1.2 Impact Shock Sensitivity

The drop test apparatus was adopted in the early twentieth century, according to Deck (1926), as one method of attempting to apply a quantitative ranking to the impact shock sensitivity of explosives. In these tests a 2.0 kg weight is dropped onto the sample from varying heights to determine if the test sample will explode at that impact level. Gibbs and Popolato (1980) report that tests conducted with a 2 kg drop weight on PETN required only a 0.0125 meter drop; HMX, a 0.026 meter drop; PBX 9404, a 0.042 meter drop; and TNT, about a 0.157 meter drop. A list of explosive sensitivities is given in Table 1. Considering the extremely low heights that are required for an explosion to occur it is no wonder that shock and impact sensitivity are serious concerns with the demilitarization of explosively loaded munitions.

2.1.3 Problems with Drop Testing for Impact Initiation

Although explosive scientists throughout the world use the drop test machine for determining the sensitivity of explosive materials, there are serious problems with scaling impact tests and correlating these tests with physical or chemical mechanisms (Fedoroff and Sheffield, 1975). Coffey, et al. (1982) researched the initiation of explosives on thermal indicating paper from impact testing. The indication on the paper identified that the initiation site was not at the center

of the impact but rather toward the periphery of the explosive material. The most probable explanation is that the initiation of the explosives is due to the high velocity shear rather than from compressive effects of the dropped weight.

2.1.4 Projectile Impact Initiation

A better method of evaluating the shock sensitivity of explosives is through the use of either an explosive “card-gap” test or a “projectile impact” test as shown in Weiss and Litchfield (1967) and Watson (1973). It has long been recognized that fragments, bullets, or projectiles impacting high explosives can initiate a detonation in the target explosive material. Early work on projectile initiation of explosives dates back to before the Second World War. These original tests were to evaluate the impact of bullets fired during armed conflict’s striking explosively loaded weapons and causing them to prematurely detonate. Watson’s (1973) paper indicated that the projectile velocity required to initiate 50% of the explosive targets (V_{50}) for PETN was only $310 \text{ m}\cdot\text{s}^{-1}$ and for TNT was only $780 \text{ m}\cdot\text{s}^{-1}$.

2.1.5 Water Jet Impact Velocity

For a nominal 345MPa (50,000psi) waterjet, the estimated jet velocity is $830 \text{ m}\cdot\text{s}^{-1}$ based on Hashish (1989). The velocity of a waterjet is approximated by the equation:

$$V = (2P \cdot p^{-1})^{0.5} \quad (1)$$

where V = jet velocity
 P = pressure upstream of the orifice
 p = density of the liquid.

Since the projectile V_{50} stated above for PETN and TNT is less than the velocity of the nominal waterjet velocity, it would be reasonable if you only looked at those numbers to conclude that waterjets should initiate these explosives on a routine basis. Fortunately is not the case, however, in actual practice.

Chan (1985) of NASA's Jet Propulsion Laboratory researched the effects of impacts on explosives and concluded that not only was velocity critical, but projectile diameter was also critical. He stated that the drop test data should be recalculated to threshold velocity data using the equation:

$$V_t = (2gH_{50})^{0.5} \quad (2)$$

where g = acceleration due to gravity
 H_{50} = 50% drop height.

2.1.6. Shock Hugoniot

One of the additional “missing pieces” in the explosive sensitivity research was the effect of the shock Hugoniot on both the impacting projectile and the target material. When one item is struck by another, shock waves propagate through both the projectile and the target. These shock waves, according to Noonan (1961), are based the product of the sonic velocity and the

density of the material which, in turn, varies with the pressure the substance. This is known as the acoustic impedance.

The ability of shock to transfer energy from one item to another is highly dependent on the similarity of the two shock Hugoniot of the items. A mismatched set of Hugoniot (also known as impedance mismatch) between the projectile and the target reduces the likelihood of effective energy transfer. The ability of a waterjet to transmit the shock energy into an explosive material is governed by both the Hugoniot of the explosive and the water.

As shown in Figure 1, the shock pressure from an impacting slug of water traveling at a given velocity is substantially less than that of metals traveling at the same speed. Consequently, water must travel significantly faster than metals in order to achieve a similar pressure in the target material.

The pressure generated by a liquid impact against a rigid target can now be approximated, according to Brunton (1965), by:

$$\begin{array}{ll} P_i &= pCV \\ \text{where } P_i &= \text{impact pressure} \\ p &= \text{density of the liquid} \\ C &= \text{shock Hugoniot of the liquid} \\ V &= \text{jet velocity} \end{array} \quad (3)$$

2.1.7 Jet Initiation

Finally, research performed by Mader (1981) of Los Alamos Scientific Laboratories (LASL) showed that the relationship of a liquid jet initiation of a given high explosive is actually related to the product of the density (p) of the liquid in grams per cubic centimeter, the square of the liquid's velocity (V) in mm/microsecond, and the diameter (d) of liquid impact in millimeters, or pV^2d . LASL's data were generated by using high velocity shaped charges with various liner materials, including water. The test data were then modeled on impact simulation computer programs and the results correlated. According to Mader (1981) the pV^2d for any given target explosive is a constant and is predictable from any type of shaped-charge jet material. Test data from actual tests performed by Mader (1981) and Giltner (1993) show close correlation to the formula's prediction.

Likewise, high speed liquid jets, such as waterjets, *can also initiate* high explosives from impact as verified by Giltner, et al. (1993). The critical question is not “**if**” a fluid jet can initiate a detonation in an explosive, but “**how likely**” can an inadvertent initiation occur under normal operating conditions.

2.1.8 Abrasive Fluid Jet Behavior

Knowing that the density, velocity, and impact diameter are the three critical parameters for the impacting jet projectile, we can now establish these parameters for an abrasive entrainment fluid jet system.

The jet velocity of an abrasive fluid jet is slower than the plain fluid jet velocity due to the mixing of a massive amount (up to 15% by mass) of slow moving, dense abrasive and large volumes of air into the high velocity jet stream. Tests have shown that the velocity of the mixed three-phase jet stream (air, water, and abrasive) drops to less of the original velocity. In order to maximize our safety margin, we will retain the original fluid jet velocity and accept that the mixed abrasive fluid jet velocity will always be less than this speed.

A standard entrainment fluid jet orifice is 3.56×10^{-4} m (0.014-inch) diameter and the abrasive mixing tube is 1.10×10^{-3} m (0.043-inch) inside diameter. A standard amount of liquid will flow through the fluid jet orifice over a given time frame. For 345 MPa fluid jets, the orifice and focusing tube typically use water at a rate of 3.8 kg per minute and abrasive at 0.57 kg per minute. The garnet abrasive has a density of about $4000 \text{ kg}\cdot\text{m}^{-3}$. Assuming that the garnet has only the density of water, the density of the three-phase mixture drops to only 11% of the density of water due to the influx of air into the system. This drop can be shown by the fact that the area of the water exiting the first orifice is $9.931 \times 10^{-8} \text{ m}^2$, and the three phase mixture exiting the second orifice occupies an area of $9.369 \times 10^{-7} \text{ m}^2$, or nine times the area for the same mass of material. Research data suggest that the actual density of an abrasive fluid jet mixture may be significantly lower.

Abrasive particles used in the abrasive fluid jet process start out as nominally 180 micron (80-mesh) particles. These particles are tightly distributed in size to assure that an exceptionally large particle will not plug an orifice. The abrasive particles are shattered when they enter the high velocity fluid stream and impact inside the jet nozzle prior to exiting from the abrasive fluid jet. Scanning electron microscopy has shown that recovered garnet particles are typically less than 100 microns in size. Although these particles fracture and decrease in size prior to impacting the target surface, we will assume that these particles remain at 180 microns for this analysis to eliminate the potential for a rogue particle's passing through untouched.

With the information and assumptions stated above, the pV^2d of the abrasive fluid jet can be calculated as always being less than:

$$\begin{aligned} p &= 1000 \text{ kg}\cdot\text{m}^{-3} (1 \text{ gm}\cdot\text{cc}^{-1}) \\ V &= 830 \text{ m}\cdot\text{s}^{-1} (0.830 \text{ mm}\cdot\text{sec}^{-1}) \\ d &= 1.09 \times 10^{-3} \text{ m} (1.09 \text{ mm}) \end{aligned}$$

Therefore, the pV^2d for an abrasive fluid jet would be calculated at $7.524 \times 10^5 \text{ kg}\cdot\text{s}^{-2}$ ($0.751 \text{ mm}^3\cdot\mu\text{s}^{-2}$). The behavior of the explosive and how it might respond to such an impact shock must now be defined. The pV^2d given by Mader (1989) for PBX 9404 is given as $1.50 \times 10^8 \text{ kg}\cdot\text{s}^{-2}$ ($150 \text{ mm}^3\cdot\mu\text{s}^{-2}$). Since the sensitivity of PBX 9404 is approximately that of tetryl, a very sensitive high explosive, the choice of this material may be too sensitive for real-world analysis, but should provide an ample margin of safety.

2.2 Fluid Jet/Explosive Interaction

The waterjet computed figure of $7.524 \times 10^5 \text{ kg}\cdot\text{s}^{-2}$ ($0.751\text{mm}^3\cdot\mu\text{s}^{-2}$) compares very favorably with the published 50% pV^2d impact product for PBX-9404 of $1.50 \times 10^8 \text{ kg}\cdot\text{s}^{-2}$ ($150 \text{ mm}^3\cdot\mu\text{s}^{-2}$). The standard deviation (sigma) of Mader's test data for the waterjet initiation of PBX-9404 was calculated to be $1.346 \times 10^7 \text{ kg}\cdot\text{s}^{-2}$ ($13.46 \text{ mm}^3\cdot\mu\text{s}^{-2}$). The U.S. Army typically uses a figure of merit for safety of "one chance in a million" for most explosive operations. Therefore, an abrasive waterjet cutting operation should not be expected to be a hazardous operation (based on a $p=1\times 10^{-6}$ accident criteria) as long as the calculated pV^2d product for waterjet remains below a statistical 4.76 sigma margin, which would yield a probability of 0.97×10^{-6} .

For PBX 9404 the statistical safety margin would require subtracting the product of 4.76 times the test sigma of $1.346 \times 10^7 \text{ kg}\cdot\text{s}^{-2}$ ($13.46 \text{ mm}^3\cdot\mu\text{s}^{-2}$) to achieve $6.4 \times 10^7 \text{ kg}\cdot\text{s}^{-2}$ ($64 \text{ mm}^3\cdot\mu\text{s}^{-2}$) which must be subtracted from the average value of $1.50 \times 10^8 \text{ kg}\cdot\text{s}^{-2}$ ($150 \text{ mm}^3\cdot\mu\text{s}^{-2}$). The results give the $p=1\times 10^{-6}$ accident criteria at a pV^2d impact product of $8.6 \times 10^7 \text{ kg}\cdot\text{s}^{-2}$ ($86 \text{ mm}^3\cdot\mu\text{s}^{-2}$). Given that the calculated product for a typical waterjet is only $7.524 \times 10^5 \text{ kg}\cdot\text{s}^{-2}$ ($0.751\text{mm}^3\cdot\mu\text{s}^{-2}$), the waterjet system should be safe to operate routinely on high explosives. This conclusion has also been seen in empirical testing.

2.3 Empirical Testing

Miller (1992a) performed a series of actual tests against explosives using both fluid jets and abrasive fluid jets starting with water as the cutting fluid at 345MPa and an estimated jet velocity of $830 \text{ m}\cdot\text{s}^{-1}$. Various types of secondary high explosives were tested in metal confinement to explore the sensitivity of explosives to fluid jet impact and shock. None of the secondary high explosives reacted.

2.3.1 Ultra-High Pressure Fluid Jet

In order to validate the safe operation of fluid jets at nominal velocities of $830 \text{ m}\cdot\text{s}^{-1}$, a series of tests were performed using glycol and glycerin at pressures at the theoretical upper limit of waterjet cutting. The pressure of approximately 1,000 MPa (1GPa) was chosen as the upper limit due to thermodynamic limitations of water. The secondary high explosive targets selected for the 1 GPa ultrahigh pressure waterjet were TNT and PETN. PETN and TNT were chosen as the test candidates as these two explosives represent the two extremes of the secondary explosive inventory. Since PETN is so sensitive, see Table 1, any operation safe to use with PETN would be safe to use with all other secondary high explosives. The use of glycol and glycerin was required because water freezes at room temperature when subjected to pressures approaching 1 GPa. The 1 GPa ultrahigh pressure system provided a jet velocity of approximately $1255 \text{ m}\cdot\text{s}^{-1}$ based on equation (1).

The TNT pellets were cast cylinders $1.585 \times 10^{-2}\text{m}$ (0.624-inch) in diameter by $1.626 \times 10^{-2}\text{m}$ (0.640-inch) in height. The PETN was packaged in small metal cans $4.572 \times 10^{-3}\text{m}$ (0.18-inch) in diameter by $9.144 \times 10^{-3}\text{m}$ (0.36-inch) in height. The dimensions of these explosive targets

were chosen to exceed their respective critical diameters in order to insure detonation. Approximately fifty (50) samples were prepared and at least 45 shots were achieved in order to establish a 95% safety margin with a 90% confidence interval.

As shown in Figure 2, the pellets were directly impacted and none of them either burned or detonated. Some of the pellets showed a slight discoloration as shown in Figure 3, but the same discoloration was also observed in the control pellets that were not impacted by the fluid jet. As a further examination of the material stability, the residual materials were tested using HPLC for energetic breakdown products. Although there were various colors present in the sample bottles, as shown in Figure 4, no decomposition products was discovered during laboratory analysis.

2.3.2 Follow-On Research

Following the tests on high explosive materials, high explosive projectiles were tested using an abrasive entrainment fluid jet. Approximately 500,000 high explosive projectiles were eventually cut without event using several different systems. Among the liquids tested against live weapons were water, glycols, oils, and anhydrous ammonia, as described by Miller (1998) and Miller and Hashish (1999).

Using the data that were gathered from both the research and empirical testing, the V_{50} curves were calculated showing the velocity required for a 50% probability of initiation for various explosives. These curves are shown in Figure 5.

The fluid jet research was independently reviewed by the U.S. National Research Council (1999), a subset of the United States National Academy of Sciences, on behalf of the U.S. Army for the purpose of evaluating the safety of the process for the disposal of chemical weapons. Their findings concluded what our research had shown for years:

“The use of high pressure water or ammonia to cut explosive-loaded ordnance and/or to wash out energetic materials from ordnance casings is a proven technology.”

3. CONCLUSIONS

The use of high pressure waterjets or other fluid jets can be used successfully on energetic materials with an acceptably low risk associated with initiation due to jet shock or impact initiation. Nevertheless, the reader is cautioned always to ensure that proper safety is observed in all areas of operation. Fires and explosions have been documented from munition handling operations that have used waterjets, but these event occurred due to secondary operation failures.

4. REFERENCES

- Brunton, J. H., "The Physics of Impact and Deformation: Single Impact. 1. High Speed Liquid Impact," *Phil. Trans. A.*, Vol. 260, 1965. p. 81.
- Chan, C.K., "Predicting Effects of Impacts on Confined Explosives," NPO-16258/5720, NASA Jet Propulsion Laboratory, March 1985.
- Coffey, C. S., DeVost, V., Jacobs, S. J. and Kayser, E. G., "A Review of Recent Impact Sensitivity and Hot Spot Investigation," 20th Department of Defense Explosive Safety Seminar, p. 1437, 1982. Approved for Public Release: Distribution Unlimited.
- Deck, H. S., "Safety in Explosive Plants," *Army Ordnance*, July-August, 1926. pp. 33 –39.
- Engel, O. C., Basic Research on Liquid-Drop-Impact Erosion, National Aeronautics and Space Administration, CR-1559, June 1970.
- Fedoroff, B. T. and Sheffield, O. E. (ed.), "Impact Tests," *Encyclopedia of Explosives and Related Items*, Vol 7, US Army Research and Development Command, PATR 2700, 1975. p. I-35. Approved for Public Release: Distribution Unlimited.
- Gibbs, T. R. and Popolato, A. (ed.), *LASL Explosive Property Data*, University of California Press, 1980. pp. 449-453.
- Giltner, S. G., Sitton, O. C., and Worsey, P. N., "The Reaction of Class 1.1 Propellants and Explosives to Water Jet Impact," 24th International ICT Conference, Karlsruhe, FRG, June 29 - July 2, 1993.
- Hashish, M., "Pressure Effects in Abrasive-Waterjet (AWJ) Machining," *Trans. of the ASME Journal of Engineering Materials and Technology*, Vol. 111, p. 222, July 1989.
- Mader, C.L., "Numerical Modeling of Impact Involving Energetic Materials," in J.A. Zukas (Ed.), *High Velocity Impact Dynamics*, John Wiley & Sons, NY, pp. 879-888, 1990.
- Mader, C.L., "Numerical Modeling of Detonations," *Los Alamos Series in Basic and Applied Science*, Univ. Calif. Press, p. 80, 1979.
- Miller, P. L. "NASA's Connections," Invited Presentation, American Chemical Society National Convention, 1996.
- Miller, P. L. and Hashish, M., "Demilitarization of Chemical Weapons Using High Pressure Ammonia Fluid Jets," 10th American Waterjet Conference, WJTA, Aug. 1999.
- Miller, P.L., "Accessing Chemical Munitions Using Ammonia Fluid Jets," 28th Department of Defense Explosive Safety Seminar, 1998. Approved for Public Release: Distribution Unlimited.

- Miller, P.L., "The Effects of Ultrahigh-Pressure Waterjet Impact on High Explosives, 25th Department of Defense Explosive Safety Seminar, 1992. Approved for Public Release: Distribution Unlimited.
- Miller, P.L., "The Mechanisms and Parameters of Abrasive Waterjet (AWJ) Cutting of High-Explosive Projectiles," 25th Department of Defense Explosive Safety Seminar, 1992. Approved for Public Release: Distribution Unlimited.
- Nonnan, E. C., "Gap Test," Minutes of the Third Explosive Safety Seminar on High Energy Solid Propellants, Department of Defense Explosive Safety Board, p. 60, August 1961. Declassified and downgraded July 7, 2000. Approved for Public Release: Distribution Unlimited.
- Padgett, H. L., "Recovery of Motor Cases from Reject or Over-Age Solid Propellant Rocket Motors," Minutes of the Fourth Explosive Safety Seminar on High Energy Solid Propellants, Department of Defense Explosive Safety Board, p. 231, December 1962. Declassified and downgraded July 7, 2000. Approved for Public Release: Distribution Unlimited.
- Padgett, H. L., "Recovery of Motor Cases from Reject or Over-Age Solid Propellant Rocket Motors," Minutes of the Fourth Explosive Safety Seminar on High Energy Solid Propellants, Department of Defense Explosive Safety Board, p. 231, December 1962. Declassified and downgraded July 7, 2000. Approved for Public Release: Distribution Unlimited.
- Palmer, J. L., "Explosives Demilitarization," Minutes of the Explosive Safety Seminar (11th), Department of Defense Explosive Safety Board, pp. 659-660, September 1969. Declassified and downgraded July 7, 2000. Approved for Public Release: Distribution Unlimited.
- Petersen, R., "Susceptibility of Explosives To Accidental Initiation," 20th Department of Defense Explosive Safety Seminar, Vol II, p. 1406, 1982. Approved for Public Release: Distribution Unlimited.
- Review and Evaluation of Alternative Technologies for Demilitarization of Assembled Chemical Weapons, Appendix G., National Research Council, U.S. Army Contract DAAG55-97-C0044 National Academy of Sciences, National Academy Press, Washington, DC, pp. 413-420, August 1999.
- Swanson, R.K., Kilman, M., Cerwin, S., and Tarver, W., "Study of Particle Velocities in Water Driven Abrasive Jet Cutting," ASME Proceedings 4th U.S. Waterjet Conference, p. 107, 1987.
- Thiruvengadam, A. and Rudy, S., Experimental and Analytical Investigations on Multiple Liquid Impact Erosion, NASA CR-1288, 1969.

Thiruvengadam, A. Rudy, S., and Gunasekaran M., Experimental and Analytical Investigations on Multiple Liquid Impact Erosion, NASA CR-1638, 1970.

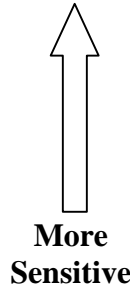
Watson, R. W., Card-Gap and Projectile Impact Sensitivity Measurements, A Compilation, U.S. Bureau of Mines Information Circular 8605, 1973.

Weiss, M. L. and Litchfield, E. L., Projectile Impact Initiation of Condensed Explosives, U.S. Bureau of Mines Report of Investigations 6986, 1967.

Yeakey, R. A. and McQueen, H. F., "Rocket Motor Case Reclamation," Minutes of the Sixth Explosive Safety Seminar on High Energy Solid Propellants, Department of Defense Explosive Safety Board, pp. 215-237, August 1964. Declassified and downgraded July 7, 2000. Approved for Public Release: Distribution Unlimited.

5. TABLES

Table 1. Explosive Sensitivities (Petersen, 1982)



Explosive	Relative Sensitivity
PETN	37
RDX	54
Tetryl	67
PBX 9404	68
OCTOL	94
PBXN-105	97
CYCLOTOL	101
COMP B	105
TNT	174

6. FIGURES

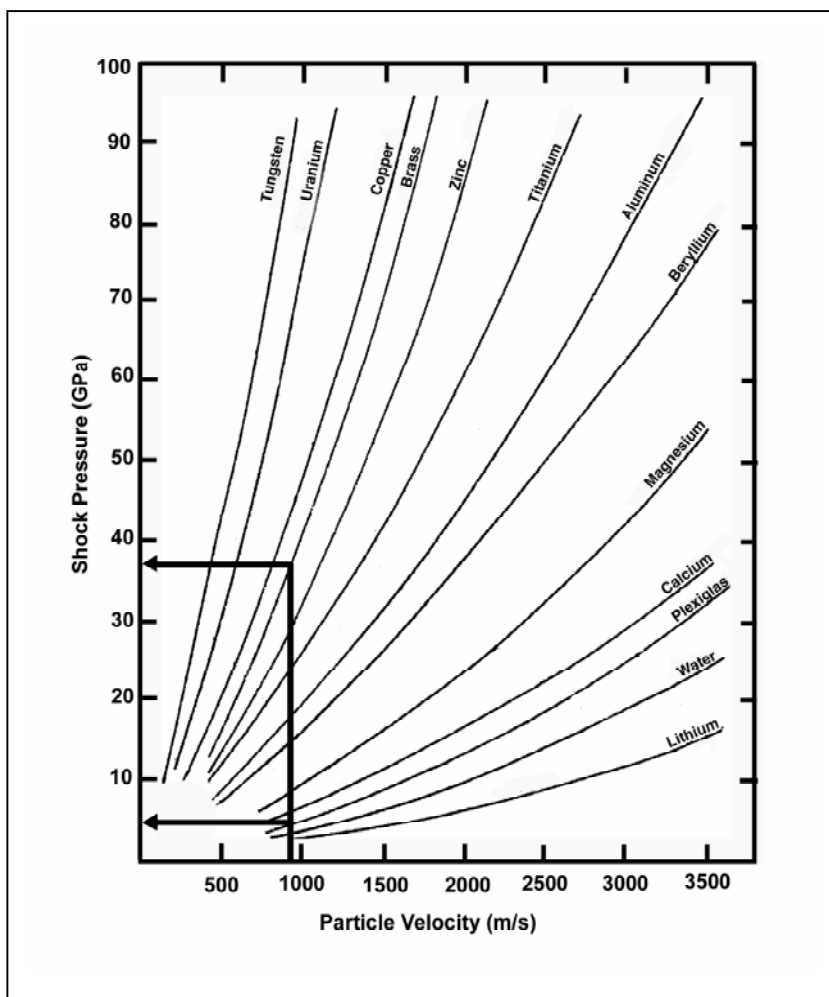


Figure 1. Shock Hugoniots for Several Materials Comparing Shock Pressures Generated by Water vs. Brass at the Same Particle Velocity

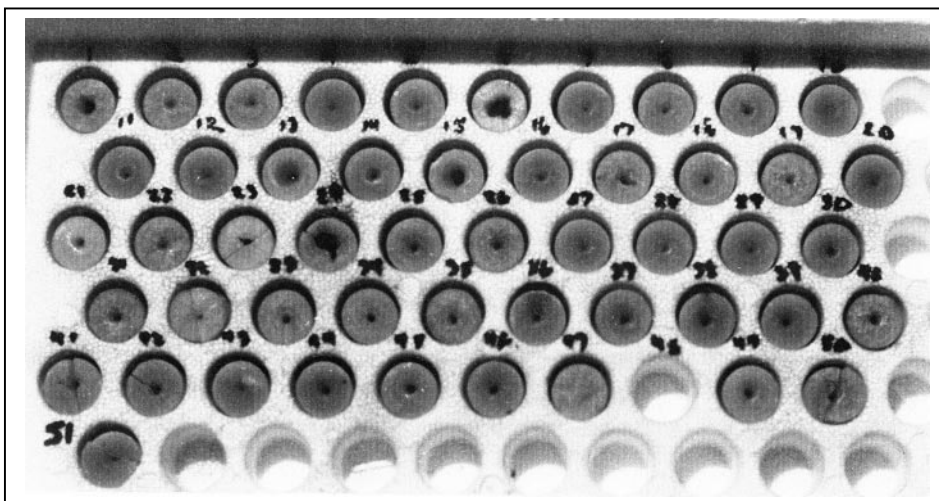


Figure 2. TNT Samples Shot at 1,000 MPa

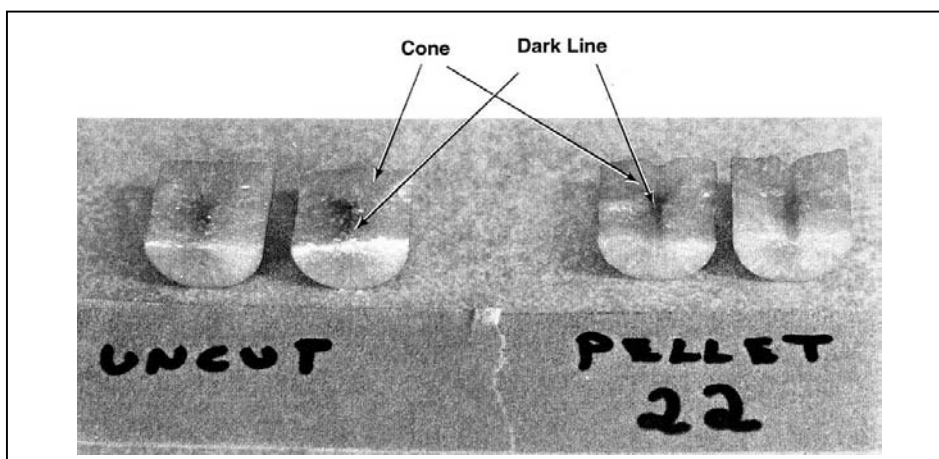


Figure 3. TNT Samples With Dark Lines

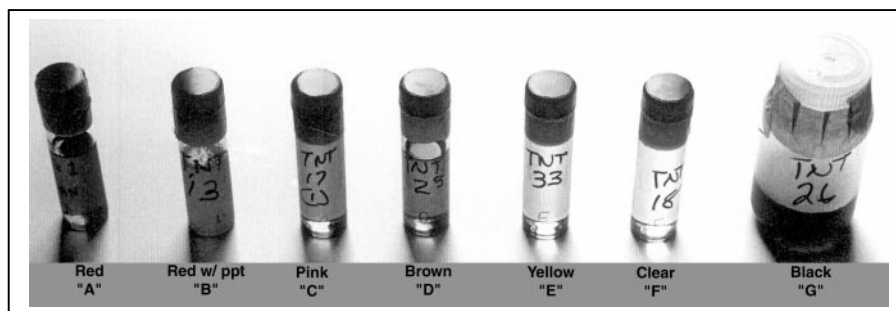


Figure 4. Post Test TNT Liquids Showing Color Variations

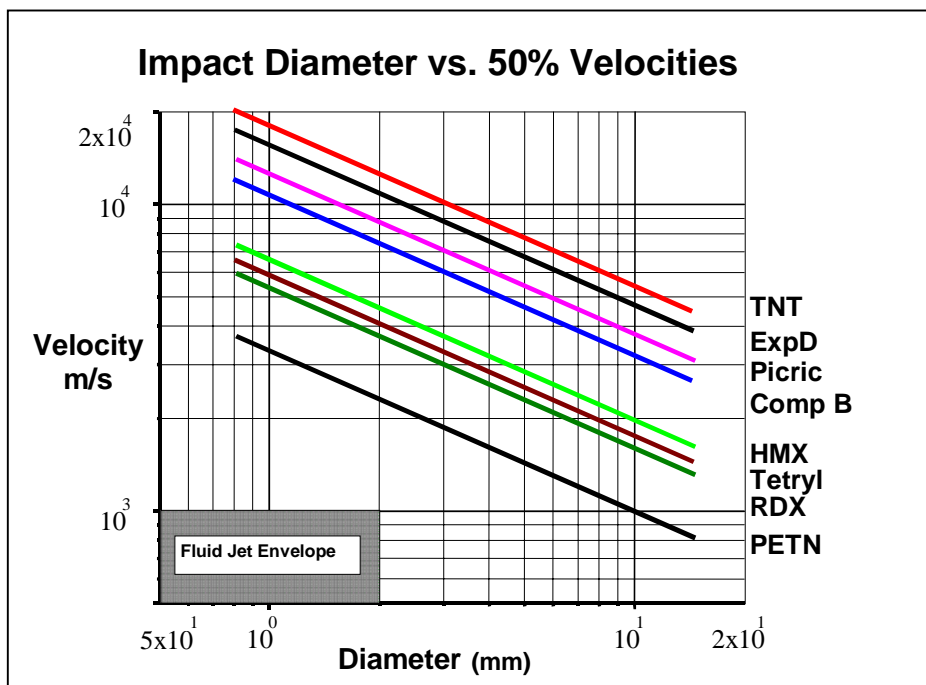


Figure 5. Probability Curves for the 50% Probability Initiation Velocities of Various Explosives

WATERJET USE IN SCULPTING LARGE AND SMALL OBJECTS

D.A. Summers, J.G. Blaine, L.J. Tyler
University of Missouri-Rolla
Rolla, Missouri

ABSTRACT

The High Pressure Waterjet Laboratory recently completed the large sculpture entitled "Millennium Arch," which was then presented, as a gift from a private donor to the University of Missouri-Rolla. During the course of preparing the parts of the sculpture a number of different waterjetting techniques were used (E. Sandys, et al., 1999). This was necessary to achieve the artistic design called for by the artist, Edwina Sandys. Following completion of that piece a number of smaller versions of the work, and other sculptures have been completed, using both abrasive and plain high-pressure waterjet streams. Waterjet assisted polycrystalline diamond cutters have been found useful in planing the surface of the stone prior to polishing.

1. INTRODUCTION

Edwina Sandys had created two sculptures using abrasive waterjets, prior to the subject of this paper. The first of these was “The Branches of Promise” installed at Monsanto World headquarters in 1989 (Figure 1). This is a 15-ft. high sculpture of glass and steel, and was, at the time of construction the world’s largest glass sculpture. It was followed by the construction of a sculpture, prepared from parts of the Berlin Wall, and located on the Westminster College Campus in Fulton, MO. This piece, entitled “Breakthrough” was made from eight four-foot sections of the wall. The profile of two figures was carved through the reinforced concrete wall, and was dedicated by President Reagan in November 1990 (Figure 2). What was intriguing was that the artist was left with two solid cut-outs 12-ft. high, these were accordingly named “Break Free” and installed as a separate sculpture at the Franklin D. Roosevelt Library in New York.

A meeting after the dedication of “Breakthrough” led to an UMR alumnus, Scott Porter, commissioning the work “Millennium Arch” to be located on the UMR campus as a memorial to his parents, The Rev. G. Scott Porter and Helen Porter, and Scott’s late wife Barbara Porter. This work was to be carved from Missouri granite and be located next to Castleman Hall, the Center for the Performing Arts on campus (Figure 3).

2. CUTTING THE PIECES

Blocks of rock were brought from a quarry in Graniteville, MO, to the High Pressure Waterjet Laboratory (HPWL) on campus and a specially prepared cutting table was built by UMR students to carve the rough blocks into the shapes required for the two legs of the main sculpture. The blocks, as shipped from the quarry, measured roughly 16-ft. by 4-ft. by 7-ft. They were trimmed to two blocks measuring 15.5-ft. by 2.5-ft. by 5-ft. The trimming was carried out using a lance containing two diverging nozzles. The nozzles were threaded into a holder at an included angle of 55° , and had a diameter of 0.03 inches. The lance was attached to a rotary coupling and turned by a hydraulic drive at a speed of around 400 rpm. The lance and rotation assembly were mounted on a platform, which could be raised and lowered over approximately 30 inches. Thus, during the cutting, the lance had to be extended three times. This was, in part, because of a lack of clearance between the top of the stone, as received, and the roof of the building in which the cutting took place. (As an aside rebounding granite particles from the cutting were still able to reach up and punch a hole through the roof). Cuts were made all around the blocks (Figure 4) to define the shapes required. The blocks were then turned onto their sides (Figure 5) and returned to the table. The table was lowered 4-ft. for the figure cutting.

No abrasive was used in the cutting process. It had been initially planned to cut the blocks and figures using an ASJ system. However, early experiments with cutting the granite showed that the slot which would result would be very narrow. This would make separation of the blocks very difficult where the slot was 0.2 inches wide and 30 inches deep around a 7-ton sculpture, with the surrounding 14-ton column to be undamaged during the movement. After debate it was agreed that the cuts would be made some 1-inch wide using the rotating waterjets.

The outer cuts were made at 15,000 psi to give a rough finish and with nozzle inserts in a holder. This produced a cut that was too wide for the separation cut between the figures and the columns. A much smaller holder was therefore prepared, fitting onto a smaller diameter feed-pipe, to cut the separation cuts around the figures. It was noted that the nozzle holders wore out in cutting some 10 inches into the granite around the 22-ft. long cutting path. Thus, nozzles had to be replaced. This change produced a slight difference in the cut width, which created some problems later in the preparation of the piece since the surfaces outlining the figures and the holes had to be ground flat and polished. Where the cuts were made around the figures the jet pressure was increased to 20,000 psi. The female figure was cut in a period of 22 hours. Slots were cut up to 0.5 inches on each pass, before advancing into the slot that amount. A program had been written by UMR students under the direction of John Tyler so that this process would run automatically. Unfortunately, due to variations in the granite structure, the slot depth was not consistently achieved, and thus, the cuts had to be continually monitored. Manual control to overcome localized "hard spots" led to localized widening of the slot and rough spots on the final figure surface.

3. FIGURE FINISHING

Once the figures had been cut and removed from the columns (Figure 6) it was necessary to grind the surfaces flat and then polish the interior cuts in the columns and the surfaces of the figures. Grinding the surfaces flat by hand takes over 24 hours per surface, using a special set of pads on a body grinder. A fixture was built, (Figure 7), using a set of four polycrystalline diamond composite cutters with high pressure (10,000 psi) waterjets directed at their contact point with the surface. This was mounted on the frame of the cutting table, spun at 200 rpm and moved over the flat surface of the female figure. It ground a much more accurately flat surface and cut the surface in about half of the time that would have been required for the manual grinding, removing up to half-an-inch of material from the surface over the 11-ft. by 5-ft. flat surface in around 8 hours. The diamonds, being cooled, stood up well to the cutting. However, due to scheduling problems and the abundance of students, only one surface was completed this way. The rest were all done by hand. (It should be noted that the head would have worked considerably better, in hind-sight, if it had been rotated about four-times faster.) Once the figure and inner surfaces had been ground, they were hand polished to a high reflectivity. The artist was concerned, however, that the initially carved surface of the two columns would appear too regular and artificial. In order to overcome this we agreed to distress the block. This required that we hand-hold a lance operated with a 0.03 inch diameter nozzle and operated at 15,000 psi (Figure 8). For an optimal effect, the jet had to be moved in a spiral or oscillating mode with less than half an inch between adjacent passes. Repeated passes in one area and more widely spaced traverses in others provided relief for the columns.

In the same way, when the capstone was received it was delineated with drill holes and clear edges (Figure 9). In order to make it more like a boulder, the rough collars were hand-milled down using the hand-held lance as with the columnar distressing. Because of the location and length and depth of the drilled holes in the block (Figure 8) much more rock was removed by

hand and significant sculpting of the block was achieved. Where the holes were too deep or badly oriented, they were filled with granite chips mounted in resin.

4. MOUNTING THE PARTS

In carving the blocks it was noted that the jet would preferentially attack any weakness planes in the block. In this way, it became clear that there were several crack lines in the block which would, over the centuries, lead to block failure. Because these were delineated it was possible to provide prophylactic action. This was achieved by drilling small holes down through the potential failure areas and inserting reinforcing rods. A similar procedure was also used to insert rods into the feet of the figures so they would be held securely in place on the mounting plinth.

The narrow width at the bottom of the feet meant that the holes must be of small diameter. At the same time, the hole size must be only slightly larger than the rod size if the resin bolts were to be most effective. The holes were therefore drilled at 10,000 psi with a slow (4 inches/min.) feed rate. The holes created were slightly larger than the drilling lance and provided a good anchor for the rods. The back half of the hole was grouted first, and the glue allowed to set around the pins. A tension was then applied to the pins and more grout used to fill the hole to the collar. This applied a slight compressive force across the failure surface. After the outer glue had set the pins were sawn off along the edge of the block.

5. MOUNTING THE CAPSTONE

The vertical columns were mounted on an 18-inch thick reinforced concrete pad, and concrete poured around the legs to ensure stability. Once the legs were secure, a wooden template was prepared showing the shape and location of the top of the columns. This was then used to locate two shallow wells which were carved into the capstone. These were located over the legs so that they would penetrate some 6 inches into the block. The recesses were carved using a traversing mechanism to cut a series of slots into the block, and then mechanically removing the intervening ribs. Significant protrusions were then removed using the hand-held lance described earlier. The capstone was then mounted on the legs. A small amount of grout was inserted between the block and the legs to distribute the weight and fill any voids caused by the waterjet cut roughness of the mating surfaces.

The figures were mounted on their plinth (Figure 10), some 50-ft. from the rest of the arch and the entire composite sculpture, "Millennium Arch" was dedicated on May 13, 2000.

6. SUBSEQUENT WORK

The large table has been used to prepare smaller figure sculptures and sheets of granite for smaller works of art. Blocks of granite some four-inches thick have been used to create 1/12th scale models of the sculpture. These have been cut using an X-Y table and abrasive waterjets.

The total geometry is loaded into the table computer and the blocks and figures are cut under computer control.

The cuts which are achieved are very regular and clean, which helps since it virtually removes the need to grind the figures, which need polishing before they can be used. The front and back face of the figures must still, however, be ground flat, and this is done conventionally and manually.

The Arch pieces (cut as a single block rather than in three pieces) is too regular for final use. Thus, the surfaces are again distressed with a 15,000 psi hand-held lance. This lance can remove significant amounts of material and care must be taken to leave enough material around the excised figure locations. When completed the assembly has been mounted on black-painted aluminum and has found some critical acclaim.

7. ACKNOWLEDGEMENTS

This work could not have been carried out, without the generous donation by Scott Porter; nor the artistic talents of Edwina Sandys. The work was accomplished with the assistance of many students who wrote programs, designed and built cutting systems and monitored cutting progress until the job was done. They then spent many hours grinding and polishing the final pieces. Supervision was provided by Bob Fossey, Jim Blaine and John Tyler, who were also called in to help with the cutting and moving. Norbert Maerz provided great help in the grinding and polishing of the granite.

8. REFERENCES

E. Sandys, ARBS; S. Porter, OPHIR RF; D. Summers, G. Galecki, R. Fossey, J. Blaine, J. Tyler, University of Missouri-Rolla, "The Carving of the Millennium Arch," 10th American Waterjet Conference, Houston, TX, August 14-17, 1999.



Figure 1. The Branches of Promise (photo by Richard Kaplan).



Figure 2. Break Through.



Figure 3. Sketch of the possible location of the Arch (Edwina Sandys & Dr. Summers).



Figure 4. Cutting the original block shapes.



Figure 5. Turning the blocks.

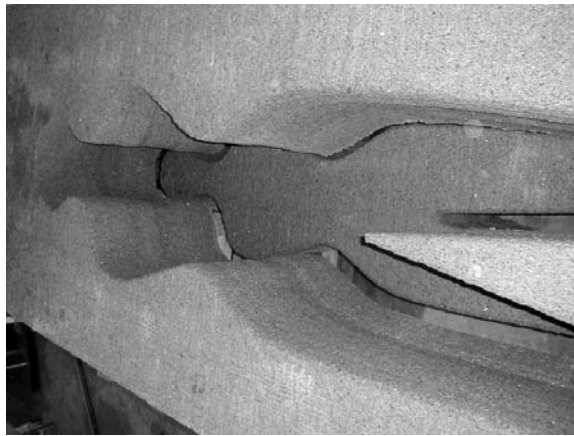


Figure 6. Separating the pieces.

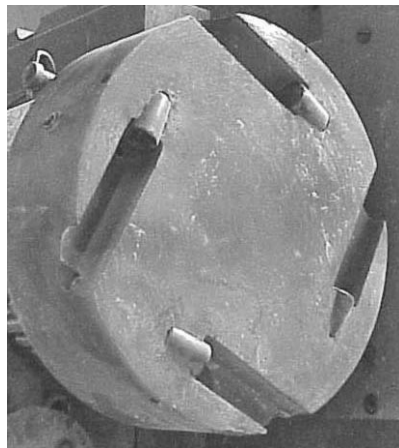


Figure 7. PDC cutters in holder for grinding the figure faces.



Figure 8. Distressing the blocks with a hand-held lance.



Figure 9. Capstone as received.



Figure 10. Dedication.



Figure 11. First Winter (Jim Bogan).



Figure 12. One-twelfth scale model of Millennium Arch.

PERFORMANCE OF WATER JET CUTTING SYSTEM IN DIMENSION STONE

C. T. Lauand, G. R. Martín C., W. T. Hennies
University of São Paulo
São Paulo, SP, Brazil

M. Agus
University of Cagliari
Sardinia, Italy

ABSTRACT

High-pressure water jet technology for cutting is currently employed for a very wide range of materials including rocks, more specifically dimension stone. This advanced technology is applied not only to drilling and excavation of hard rock for winning blocks with opening of holes or slots, but also for end products in the field of dimension stone final beneficiary. In recent years, the increasing world-wide use of advanced machinery, as new and advanced technology replaces conventional procedures, and has led to fully automated technique that use CAD/CAM processes to manufacture high quality end products. A Brazilian Research Program in this field began in 1999 with the acquisition and installation of a sophisticated equipment of high pressure abrasive water jet system that was imported from USA, with financial support of FAPESP. This paper presents some results of researches about the main technological characteristics of Brazilian dimensional stone, determined in laboratory with granite and marble samples using this advanced technology. Laboratory determination of linear and curvilinear kerf cuts on test samples of appropriate geometry were performed and the results indicate that this procedure will provide important data for optimisation of the cutting process. The surface finishing quality of the cut was also examined, and some recommendation of there is given. Used abrasives are also an important element in the process and will be discussed as cost and optimisation factor. The test were performed on samples of commercial granite and marble that are very appreciated in the domestic market and also on rocks exported to the international markets.

1. INTRODUCTION

In Brazil, the advanced high pressure or high speed water jet technology for cutting engineering materials, currently employed for a very wide range of materials including rocks, was practically unknown at the beginning of the 90. One of the Authors has had the opportunity to visit at this time some beginning research made by Prof. Raimondo Ciccu at the University of Cagliari, in Italy. Some years later a second visit in Ostrava at the Geonic Institute at Czech Republic, was a opportunity to see a more advanced system and the parts of rock gears made in them.

These makes that a non-conventional excavation methodology, as a research line on the mining engineering department of the São Paulo University were created, to bring to light this advanced technology. Thus in 1998, a program was presented, to cut rocks with high pressure water jet in the study of Master of Engineering and another Ph. D. associated with the acquisition and importation of a modern system for rock cutting. The São Paulo State Research Foundation (FAPESP), approved this Program in the beginning of 1999. Then the acquisition starts and importation of the water jet system, an OMAX 2652A model, which was finally put in operation in January 2000.

The detail of this Brazilian Water Jet Program was presented last year at Calgary, Canada, in an International Meeting (Lauand et al., 2000a). Also some, preliminary data collected as first laboratory results were presented last year at Athens, in Greece during the Mine Planning and Equipment Selection meeting in which three paper were presented. The first one, deal with the determination of the rock technological parameters useful for the water jet cutting systems (Lauand et al., 2000b) that consists the work of a graduate program in Master of Engineering of the second of above authors. The second paper deals with the technological characterisation of abrasives for high pressure water jet systems (Martín C. et al., 2000) and is the work of a graduate program in Ph. D. of the third author. Additionally on this same meeting, a third paper was presented but related with safe cutting of steel ducts used at the transportation of gas and oil, not with abrasive water jet, but with suspension water jet (Mendes et al., 2000).

Only to complement this introduction, in the field of non-conventional excavation techniques of the Mining Engineering Department of USP two activities may be registered. The first one, in were Prof. Stellin Junior are leading a graduate program of Ph.D. in the electro-hydraulic or plasma application to rock blasting (Silva et al., 2001), and the other are some former researches in the application of flame jet to win granite blocks (Hennies et al., 1998).

The present paper deals mainly with the experience acquired during the first year of theoretical studies, and experimental laboratory work using the bought OMAX system in the testing of samples of some commercial dimension stones in the State of São Paulo. The system performance was tested to cut linear and curvilinear kerfs, and the examination of the surface finishing of this cuts were realised with SEM photography. Suggestions are made to use the Italian Norm for definition of surface finishing roughness in the smooth cut region of the kerf.

2. GENERAL ASPECTS

Water jet is a very old tool to excavate or desegregate and transport mineral resources as a pulp to the dressing plant in mining. Its beginning date from the early years of the 18th century in Russia. This processes to win by open cast extraction sand, gravel and clay, are used also today in Brazil as described in a paper presented in Poland the last years (Soares et al., 1998).

As technology developed, a water pump was able to furnish jet with higher pressure and with lower quantity of water that has show more efficacy to cut stronger rocks. Today, in the field of excavation strong granites can be depth slotted to win blocks of dimension stone (Savanick, 1999).

The first studies intended to check the new equipment behaviour and its performance for cutting different kinds of rocks. Three granite and one marble specimens of commercial quality ornamental rocks from the State of São Paulo were selected, and preliminary samples cut for testing the system, as well as to determine major technological parameters and behaviour of this rocks under the new cutting system.

Another purpose was to determine test parameters of different abrasive options for the water jet system, not only because of the issues with imported garnet, as mentioned above, but also because of the fact that synthetic, or manufactured, abrasives normally have more constant chemical and physical properties than those of natural minerals.

Field trips to collect rock samples were the first part of the work. Then these samples were shaped according to standard procedures, with conventional diamond blades, prior to the test with the water jet cutting nozzle of the OMAX System. The next phase was the actual test of system, when several rock samples were cut at different transverse speed and with different kinds of abrasives.

Finally, the test results and some general conclusions about the main technological parameters for the optimisation of the abrasive water system were established and will be described in the following paragraphs.

Unfortunately, the initial evaluation tests with the synthetic aluminium oxide and silicon carbide produced in Brazil by Alcoa, were not satisfactory and the use of these products is not recommended. Thus, the only suitable product for our test program was the imported 80-mesh grain size garnet, from Flow that was bought in São Paulo.

3. THE ROCK SAMPLES

The three commercial granite quarries selected are the valued Capão Bonito red Granite, the Interlagos silver Granite and the Piracaia black Granite. The mining sequence of the red granite with jet piercing channelling was presented at MPES'99 realised in Dnipropetrovsk, Ukraine (Hennies, et al., 1999).

The other two are the silver Interlagos Granite that is explored from Parelheiros, a district in São Paulo city, and the black Piracaia Granite, localised north of São Paulo near to Piracaia city, at a distance of about one hundred km from São Paulo city.

The Figure 1 shows the slot open by jet flaming technology at the Capão Bonito Quarry.

The Piracaia black Granite is generally used for funeral arts as cemetery tombstones, but also to façade of buildings. All these granite are of Precambrian age and belongs to the crystalline Brazilian shield. Figure 2 shows, the extraction by diamond wire of the Piracaia Black Granite Quarry.

One first curiosity is that the Parelheiros silver granite is exploited after the cover is explored for fine sand aggregate that is extracted using the old hydraulic mining system. Normal monitors shown in Figure 3 make the sand extraction. The system works with a pressure of 0,245 MPa with a flow rate of 450 cubic meters of water per hour with recycling and use four monitors of 2.54 cm (1 inch).

Another curiosity of the application of the black Piracaia granite for the façade of buildings belongs to the history of the dimension stone exploitation in Brazil. Thus, in Figure 4, is presented an old photograph from 1938 of a block that is about 10 m (30 feet) long, 1.60 m (5 feet) wide, and 0.60 m (2 feet) thick, that was transported by special prepared structure of cow car to the nearest railway station of the Piracaia village and then to the São Paulo city.

In Figure 5 the façade of Sport and Tourism Secretary of São Paulo is shown in were this block was installed as the roof of the entrance in the centre of the city.

Finally, the marble is a dolomite marble that is partially exploited as dolomite limestone for special white cement production, other part for ground soil corrective purposes, and also marble blocks as dimension stone or also as unpolished, ornamental stone. This marble comes from a bed found in the Precambrian migmatites that occurs near the city of Campos do Jordão in the Mantiqueira Mountains, State of São Paulo.

Figure 6 shows the location of the four quarries in the State of São Paulo.

4. TECHNOLOGICAL ROCK CHARACTERISTICS

Some of the major technological characteristics of the collected rocks are presented in Table 1. This data were in part collected from sources of the following papers: Capão Bonito red Granite (Hennies et al., 1999); Interlagos silver Granite (Born et al. 1996); Piracaia black Granite and Campos do Jordão dolomite Marble in the work of Ornamental Stones of State of São Paulo published by IPT the São Paulo Research Institute (Caruso et al, 1990).

Other data as mineralogical description and photographs of the polished rocks of three of the samples appears in the last work of Caruso et al, 1990.

5. SAMPLE PREPARATION AND LABORATORY ASSAYING

After a field trip to collect the rocks, test samples were prepared according to a specific shape for the new cutting system.

A regular 7 cm x 15 cm x 50 cm parallelepiped prism was first cut with a diamond saw blade with and then split in two at a 30° angle at the middle of the shortest distance to provide two samples for assay.

Figure 5 shows a design of these rock samples for the abrasive water jet system-cutting test used in the rectilinear erosion. These samples of the four selected rocks were then cut to determine some of the kerfs topographical features.

The adopted hydraulic parameters were for all cuts were the following: pump pressure of 290 MPa (42,000 psi) and jewel opening $d_0 = 0.3556$ mm (0.014 "). The ceramic mixing or focus tube was 110 mm long with 0.762 mm (0.03 ") diameter. The mean distance of the nozzle to the rock surface was about 5 mm. The abrasive used in the tests was the imported garnet from Flow, 80 Tyler mesh and 0.180 μ m as mean grain size.

Two different laboratory assays of the four rocks were performed, a rectilinear cut with greater traverse velocity and a circular cut with lower traverse velocity to test the performance of the resulting kerf.

To characterise the various topographic entities of the kerf the following parameters were measured:

- 1 Top width of the cut (b_T)
- 2 Bottom width of the cut (b_B)
- 3 Taper of the cut (T_R)

Additionally, there were two distinct cut regions, an upper, smooth finished kerf zone, and a lower, wavy kerf zone on the samples. These data are:

- 4 High of the smooth kerf
- 5 High of the wavy kerf
- 6 Total kerf high.

All the above mentioned topographic measures are illustrated in Figure 6, from the papers of N. S. Guo, 1994 and D. Arola & M. Rumulu, 1993 in (in: Momber & Kovacevic, 1998).

6. ASSAYING RESULTS

The first series of assays were straight cuts in the rock samples using default values for granite and marble machining, and considering a 5 cm theoretical thickness of the target material. The

system's machining control software provides 5 quality settings with corresponding mean traverse speed in mm per second, according to Table 2.

The laboratory test results for these characteristics with default transverse cutting speed for granite and marble, and 80# garnet is presented in Table 3. In this table, the results values for straight linear cut ranging from quality levels 1 to 5 are presented.

Figure 7 exhibits the bottom view of the rectilinear cut of the three granites and the dolomite marble, whose slab thickness is approximately 70 mm. The samples' bottom view indicates full cut length for quality 5 setting. This figure also indicates that at the bottom view, for any quality setting from 1 to 5, there is a maximum of smooth kerf height. In the higher quality settings 4 and 5, the sample was completely cut, not as a straight kerf, but in the wavy kerf zone. If we look at next quality setting (3) the sample was not completely cut, and the same happens with quality settings 2 and 1.

Figure 8 illustrates the same straight cuts from the samples top view for the four assayed rocks. In this figure it is possible to notice the effect of the garnet's impact on the kerfs' edges, as the kerfs are wider and with round instead of straight edges.

The second series of tests consisted of cutting two concentric circles with 25 mm diameter and 50 mm diameter, respectively, on 50 mm thick samples at quality settings ranging from 3 (average) to 5 (high). Table 4 displays the system's average cut speed.

Figure 9 illustrates the top view of the cylindrical cut with 25 mm and 50 mm diameter respectively of the four assayed rocks. Slab thickness was 50 mm, and just two test settings were performed, quality 3 and quality 5. Figure 9 (a) illustrates the red Capão Bonito granite, 9 (b) the silver Interlagos granite, 9 (c) the black Piracaia granite, and, 9 (d) depicts the white Campos do Jordão dolomite marble. As mentioned above, these cut tests were performed at quality 3 on right side and quality 5 on the left.

Finally, Figure 10 illustrates the bottom view of the same circular cut tests from the previous figure. It is noticeable that while quality 3 setting for the granites only accidentally cut through the full sample thickness. The marble sample was completely cut, but in the wavy zone of the kerf. Otherwise, quality 5 settings at lower speed provided good results for marble and granite.

7. SURFACE FINISHING

To have some data about surface finishing, different cut specimen of the rocks were examined. So, nine finished surfaces were prepared that are: a cut by a diamond saw, the water jet in the smooth region, and in the wavy region, and pieces of a fracture plane or prepared by sand paper with different mesh sizes as 60#, 120#, 220#, and, 400#, and finally a polished end surface of the seller from the red granite and the marble. After a conductive layer coverage these surfaces were examined under a SCAN camera and photography of them were obtained at various amplifications. Figures 13 and 14 show SEM images of marble and granite cut by abrasive waterjet (smooth and rough zones).

Roughness determination of eight of the prepared slices are shown in Figure 15.

Table 5 shows the name of the surface finishing of the Italian Norm, and the comparison of the obtained waterjet cut surface in the smooth region is about the middle of the two first name terminology then the used garnet has 80# size. In the wavy region there is very high differences between the waves so it is not possible to compare the results.

The result of the more important quantitative data as the average Roughness R_A and waviness W_T can be observed on Table 6.

8. CONCLUSIONS

Some important conclusions can be achieved with a carefully observation of the rock kerf, the rectilinear assay and also on the curvilinear assay. As rocks are constituted by polycrystalline materials in where different minerals are subjected to variable erosion, and thus makes that with a same transverse speed of the water jet nozzle can given more or less depth cuts.

The irregular kerf in the bottom view of the curvilinear cut of the granite in Figure 11, or the test in the straight cut in the bottom view of the Figure 10 shown this effect.

9. REFERENCES

- Born, H; Soares, L. & Braga, J. M. S., Caracterização “Tecnológica dos Materiais de construção de Jazida localizada em área urbana, São Paulo – SP,” *EGATEA: Revista da Escola de Engenharia*. Universidade Federal do Rio Grande do Sul, n. esp. pp. 323-31, nov. 1996./Apresentado ao 4. Congresso Ítalo Brasileiro de Engenharia de Minas, Canela, 1996.
- Caruso, L.G. et al. “Catalog of Dimension Stones of the State of São Paulo,” Secretaria da Ciência, Tecnologia e Desenvolvimento Econômico - *SCTDE - PRÓ-MINÉRIO IPT* Instituto de Pesquisas Tecnológicas do Estado de São Paulo, Publicação IPT 1820 122 pp., 1990.
- Hennies, W. T., Stellin Junior, A., Cretelli, C., “Jet piercing application for red granite block mining in São Paulo, Brazil,” *Proceedings of the 8th International Symposium on Mine Planning and Equipment Selection*, pp. 21-26, Dnipropetrovsk National Mining University of Ukraine, 1999.
- Lauand, C.T., Martín C., G.R., Hennies, W. T., Ciccu, R., “The Brazilian Program of High Pressure Water Jet to Cut Ornamental Rocks, *Proceedings of the 6th International Conference on Environmental Issues and Waste Management in Energy and Mineral Production*, pp. 711-716, Calgary, Canada A. A. Balkema, Rotterdam 2000a.
- Lauand, C.T.; Martín C., G.R.; Hennies, W. T., Ciccu, R. “Rock Technological Parameters Useful to Water Jet Cutting Systems,” *Proceedings of the 9th International Symposium on*

Mine Planning and Equipment Selection, pp. 625-630, Athens, Greece Eds. G. N. Panagiotou e T.N. Michalakopoulos A. A. Balkema, Rotterdam, 2000b.

Martín C., G.R., Lauand, C.T., Hennies, W. T., Ciccu, R. “Abrasives in Water Jet Cutting Systems,” *Proceedings of the 9th International Symposium on Mine Planning and Equipment Selection*, pp. 641-645, Athens, Greece Eds. G. N. Panagiotou e T.N. Michalakopoulos A. A. Balkema, Rotterdam, 2000.

Mendes, M.L.A., Soares, L.; Hennies, W.T., Ciccu, R., Botulussi A., “Application of Pre Mixed Abrasive Water Jet for Maintenance of Oil and Gas Ducts,” *Proceedings of the 9th International Symposium on Mine Planning and Equipment Selection*, pp. 653-656, Athens, Greece Eds. G. N. Panagiotou e T.N. Michalakopoulos A. A. Balkema, Rotterdam, 2000.

Momber, A. W.; Kovacevic, R. *Principles of Abrasive Water Jet Machining* Springer Verlag London Limited 394 pp. 1998

Savanick, R. C. Hydraulic Mining. *Fluid Jet technology: fundamentals and applications*, pp. 6.1-6.12 4th Ed. Labus, T. J. Water Jet Technology Association, Saint Louis, 1999.

Silva, C.M.M., Stellin Jr., A., Costa, E.G., Hennies, W.T., “Electrohydraulic rock blasting for mining in urban areas,” *Environmental Management and Health*, Vol. 12, Number 1 pp. 27-34, 2001.

Soares, L.; Fujimura, F.; Hennies, W. T., Braga, J. M., “Continuous mining of sand at São Paulo, Brazil,” *Proceedings of the 5th International Symposium on continuous surface mining*, pp. 303-311. WROCLAW, Oficyna Wydawnicza Politechniki Wroclawskiej, 1998.

10. FIGURES



Figure 1. An overview of the Red Capão Bonito Granite Quarry

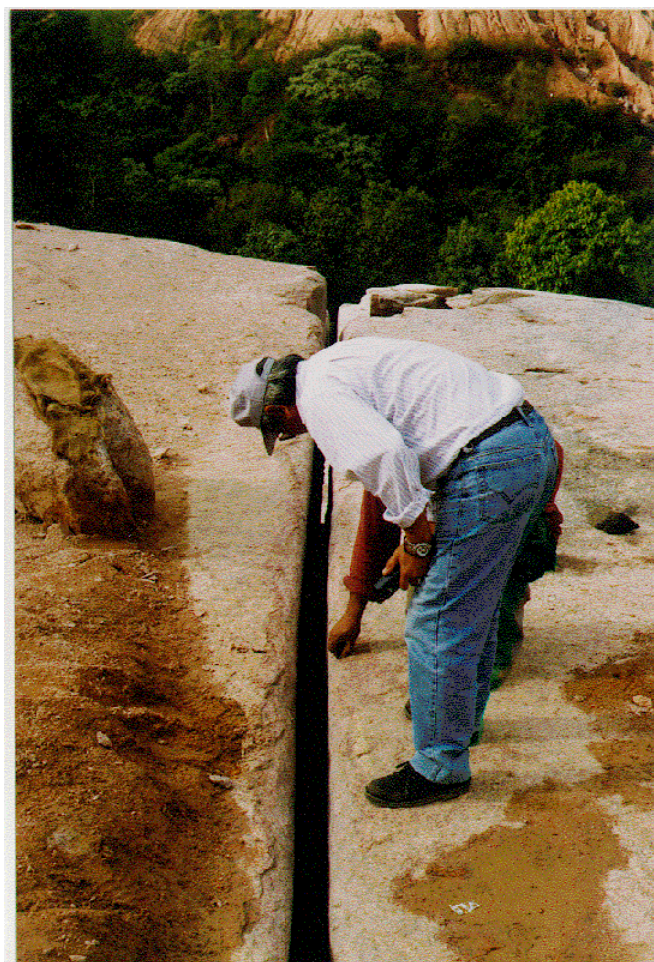


Figure 2. Jet piercing slot open in the Capão Bonito Granite Quarry.

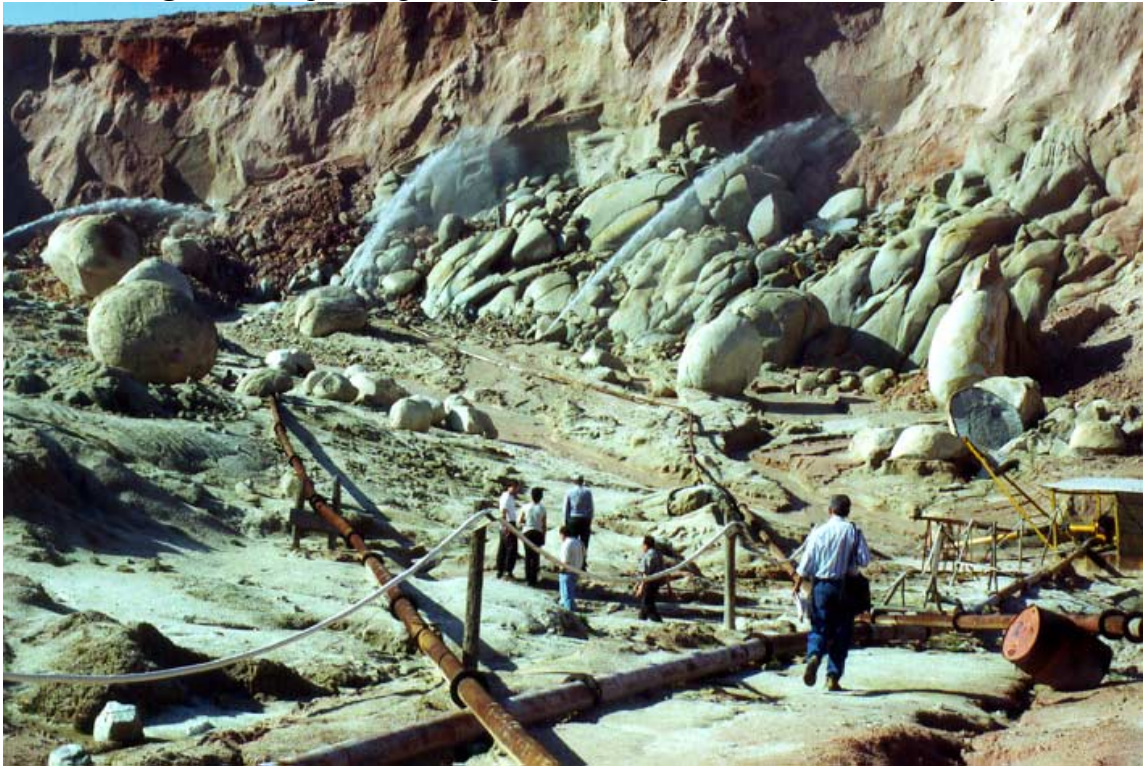


Figure 3. Hydraulic mining at Parelheiros, São Paulo, Brazil



Figure 4. Diamond wire block winning at Piracaia Black Granite Quarry



Figure 5. Piracaia black granite block with 10 m long by 1.60 m wide and 0.60 m high exploited in 1938 and his transport structure of cow car.



Figure 6. Façade of the Sport and Tourism Secretary of São Paulo in the centre of the city with the roof of the Piracaia granite.

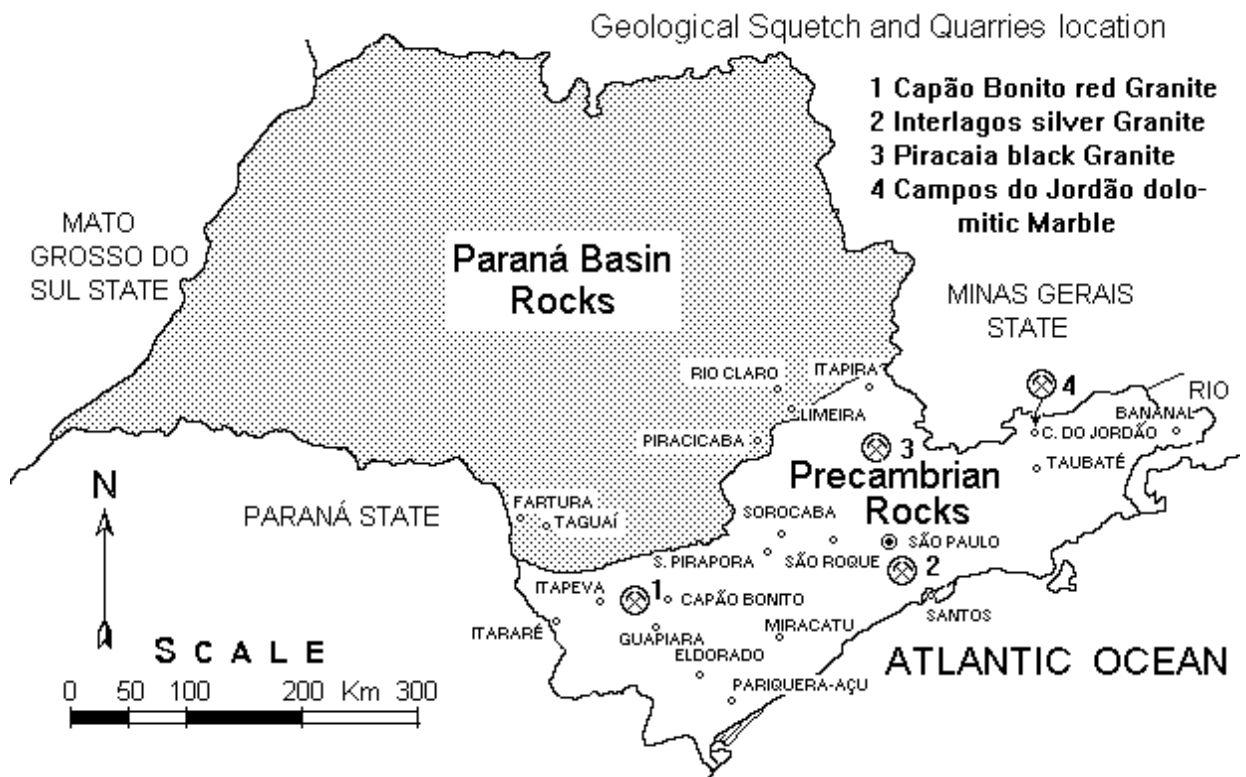


Figure 7. Location of the Granite and Marble Quarries in the São Paulo State.

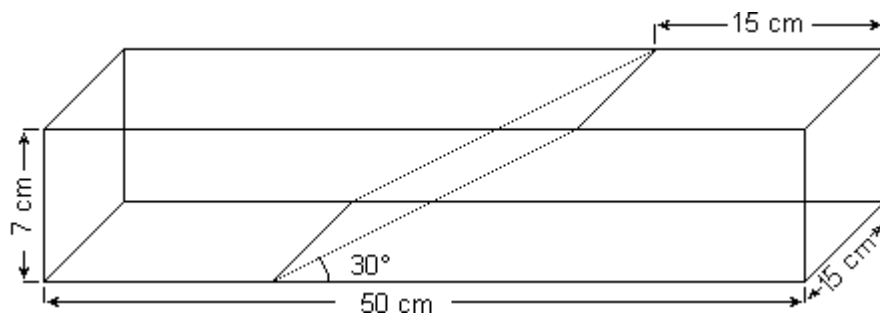


Figure 8. Geometry of samples for the rectilinear cut with AWJ.

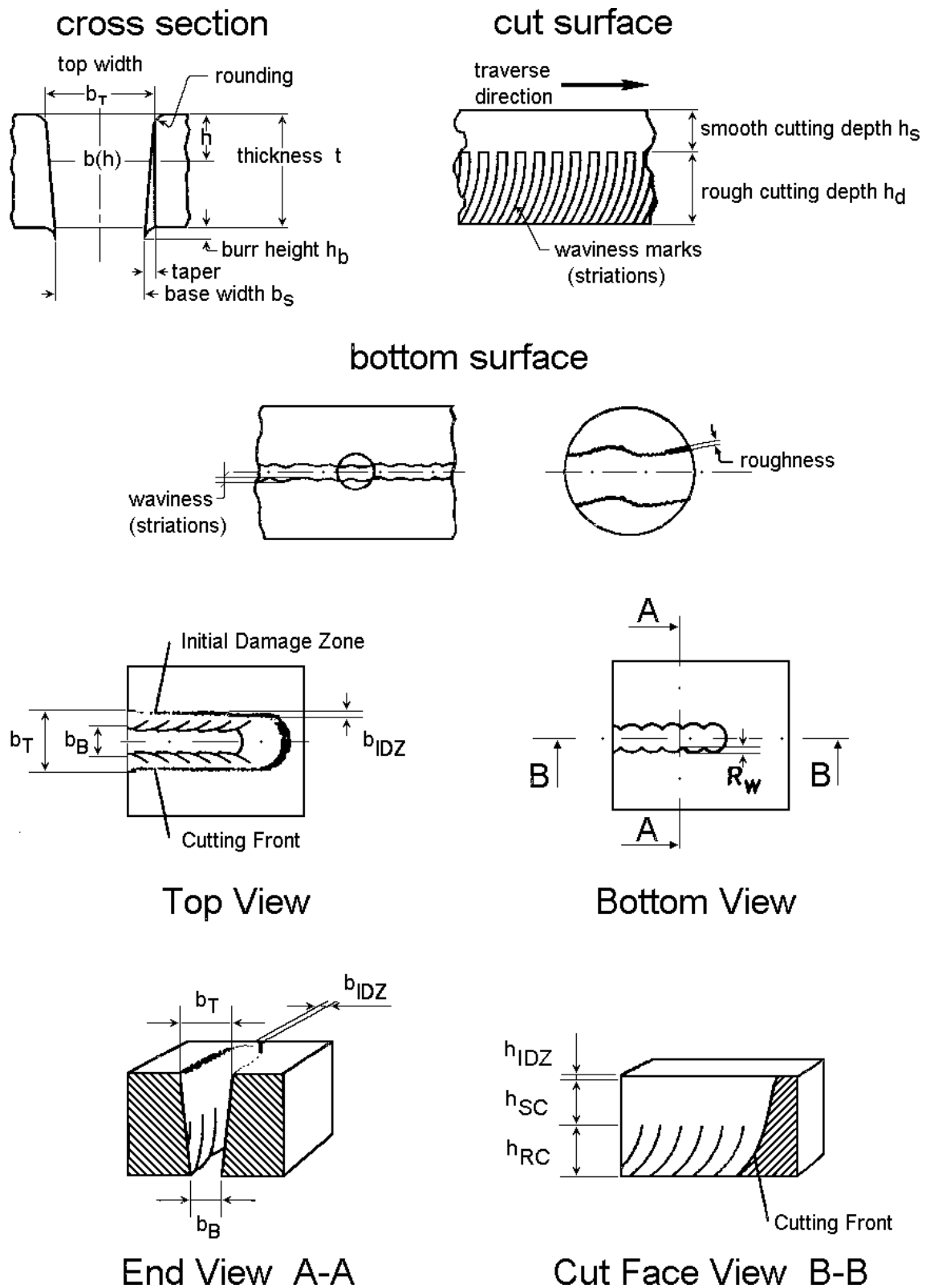


Figure 9. Topographic measures of the kerf (apud Guo in Momber & Kovacevic, 1988)

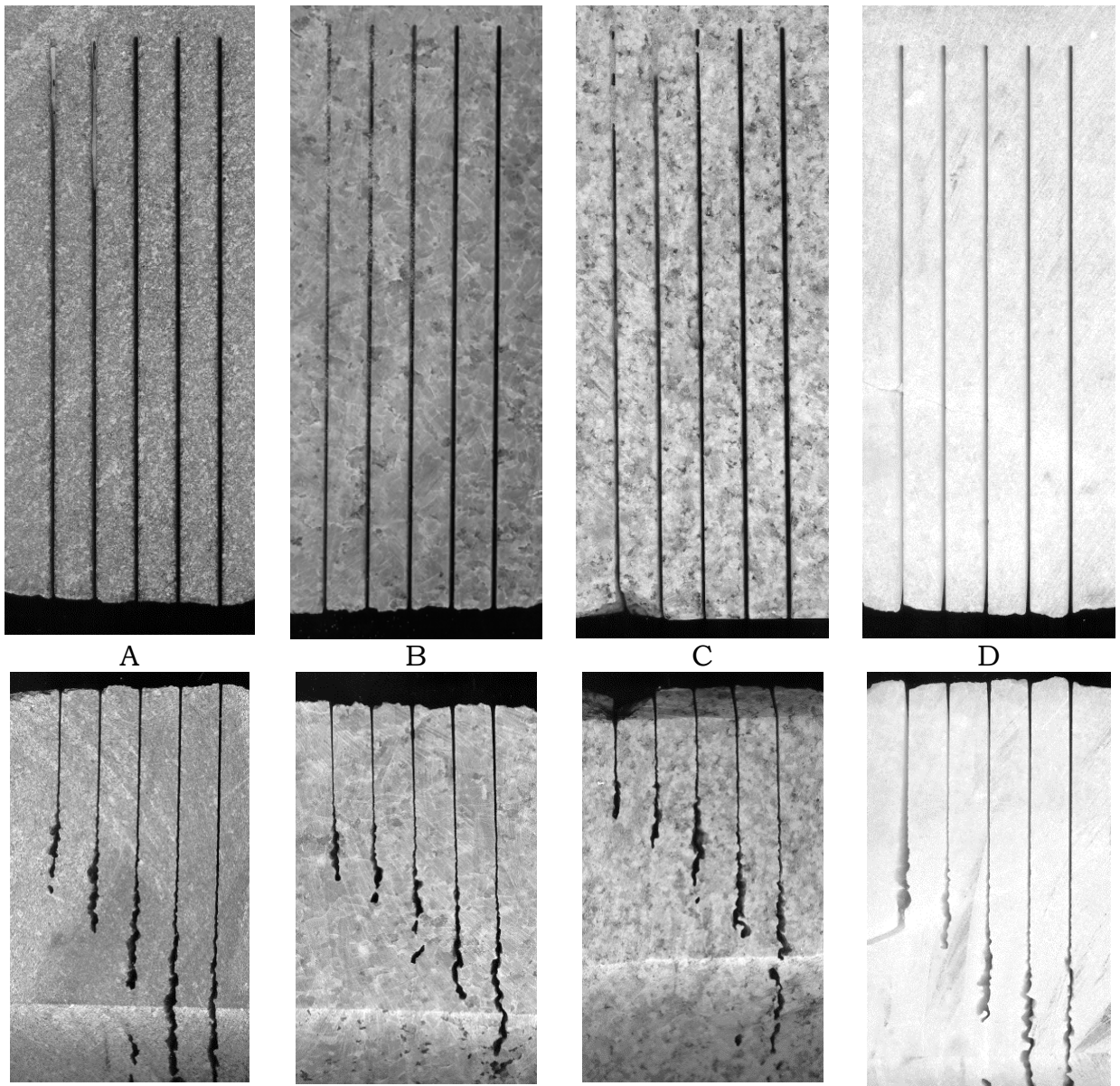


Figure 10. Retilinear waterjet cutting. Above, top view, below bottom view. A) Piracaia Black Granite. B) Capão Bonito Red Granite. C) Interlagos Silver Granite. D) Campos do Jordão White Marble.

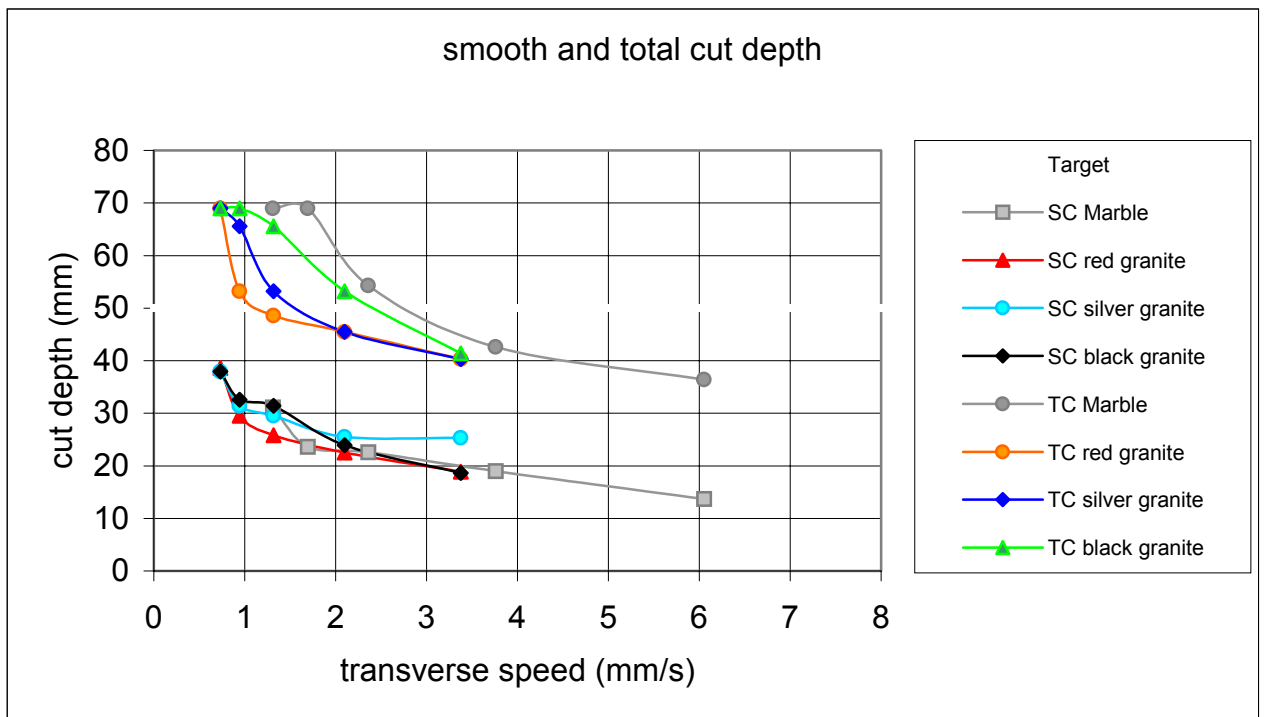


Figure 11. Smooth kerf and total kerf depth

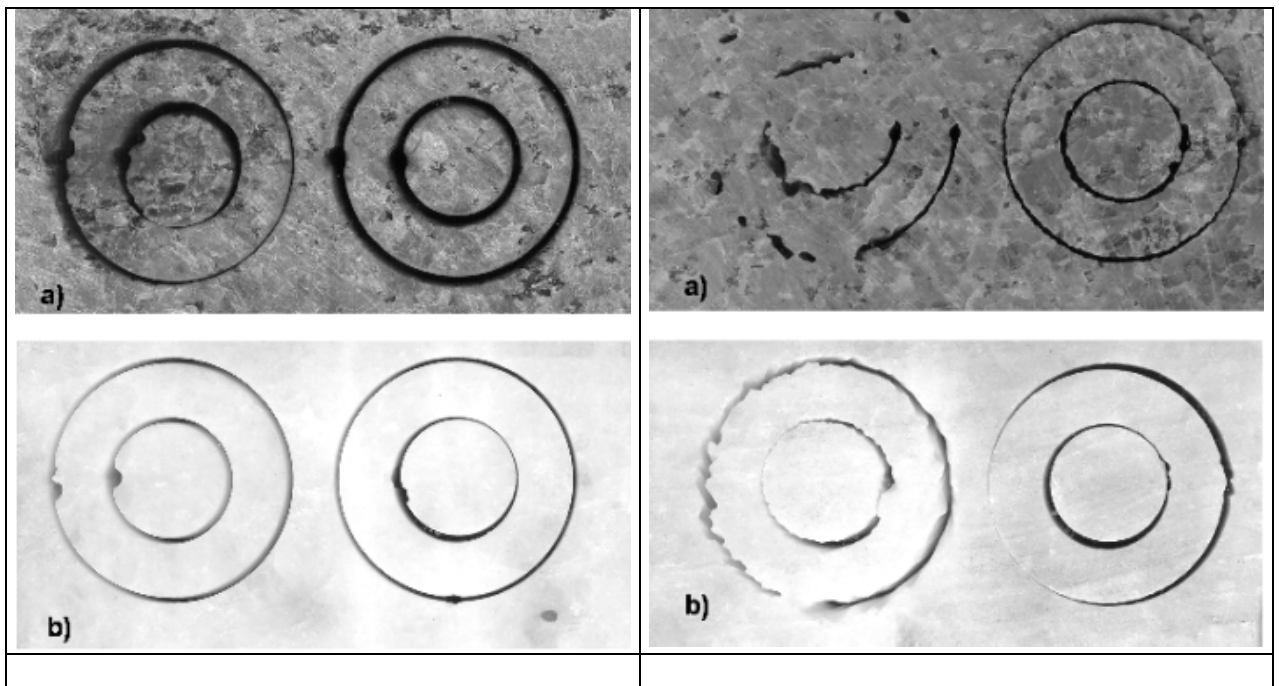


Figure 12. Curvilinear waterjet cut. Right side top view. Left side bottom view. a) Capão Bonito Red Granite, b) Campos do Jordão White Marble.

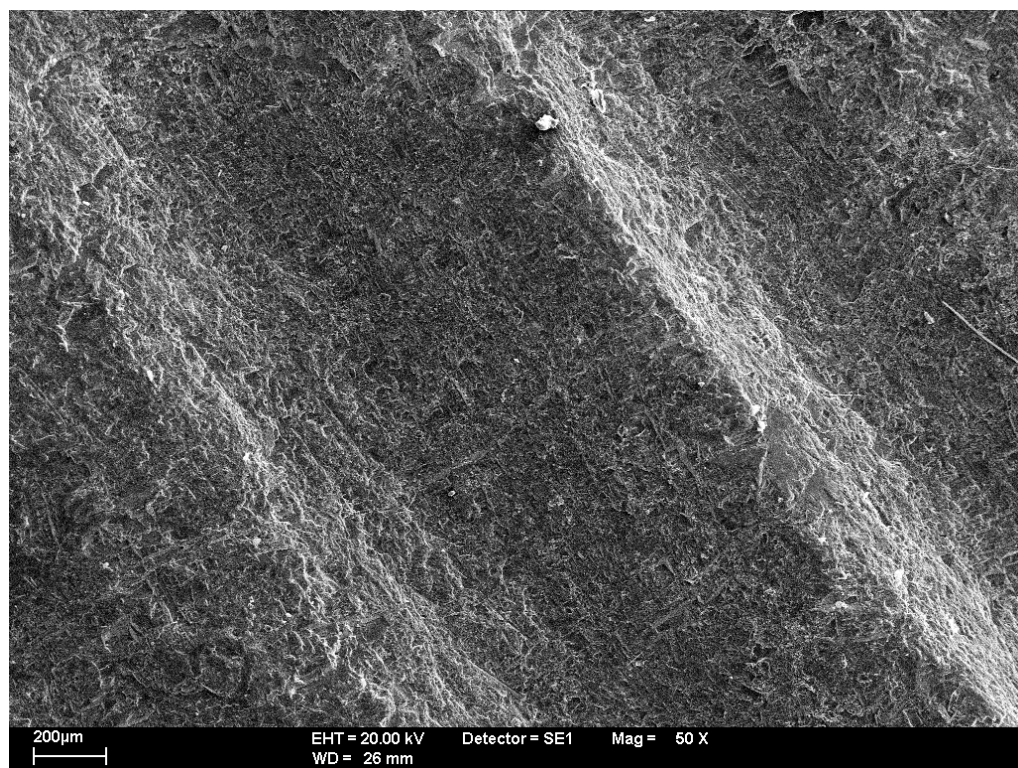
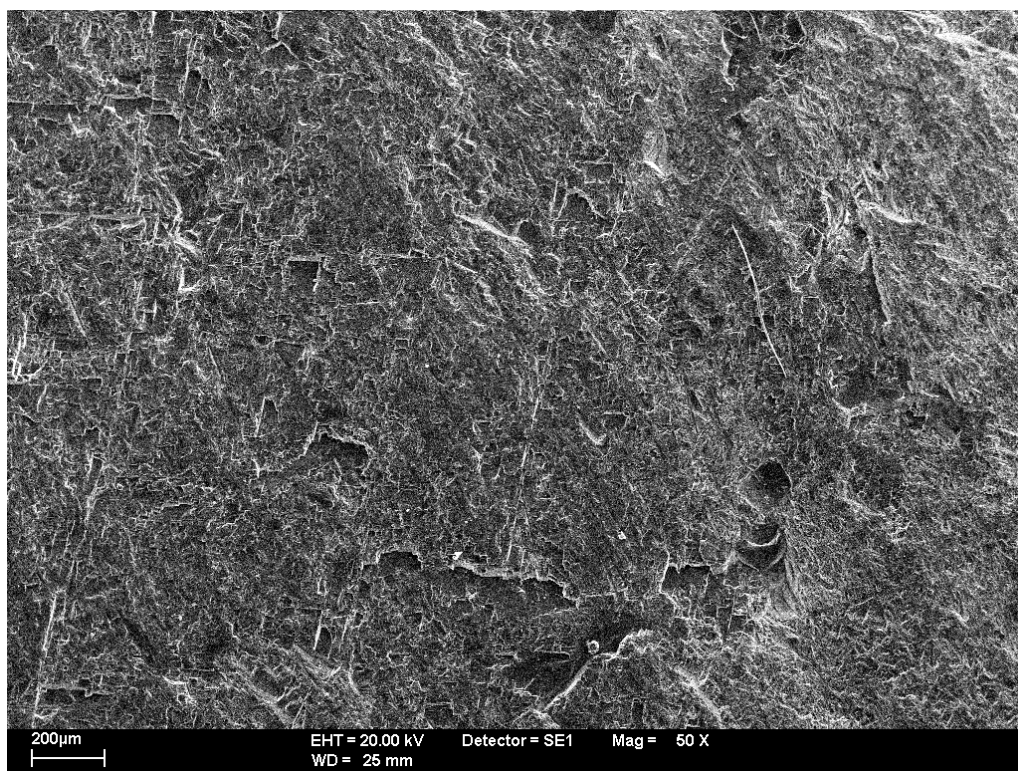


Figure 13. SEM images of Campos do Jordão White Marble cut by abrasive waterjet. On top, smooth zone. On bottom, rough zone.

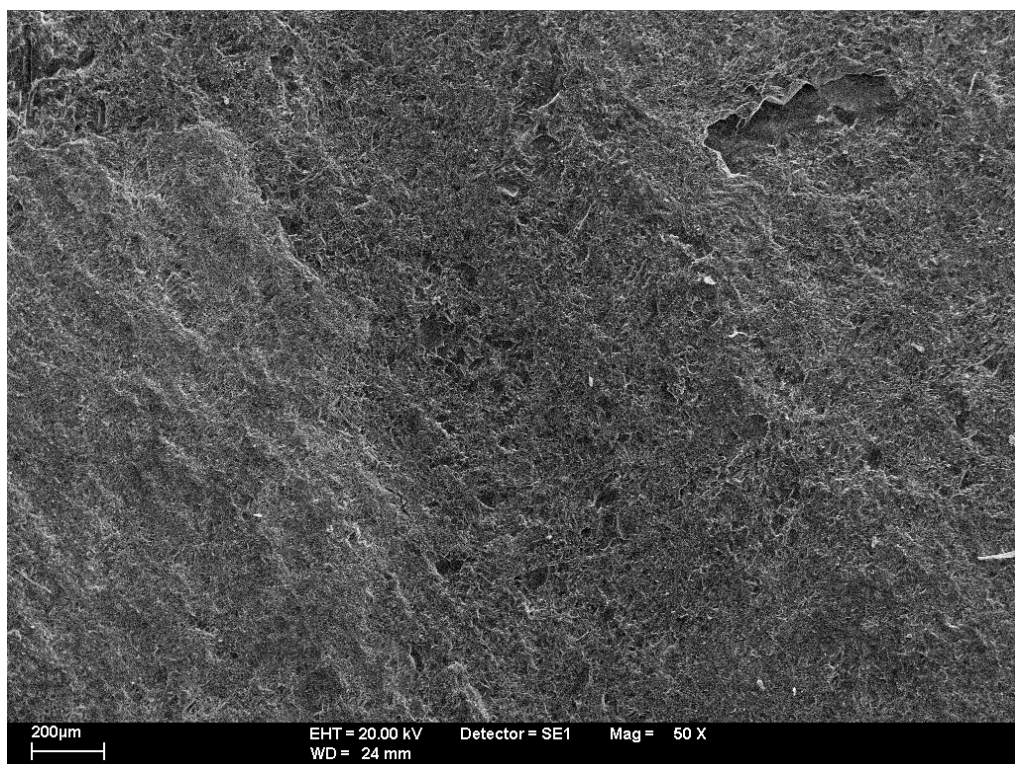


Figure 14. SEM images of Capão Bonito Red Granite cut by abrasive waterjet. On top, smooth zone. On bottom, rough zone.

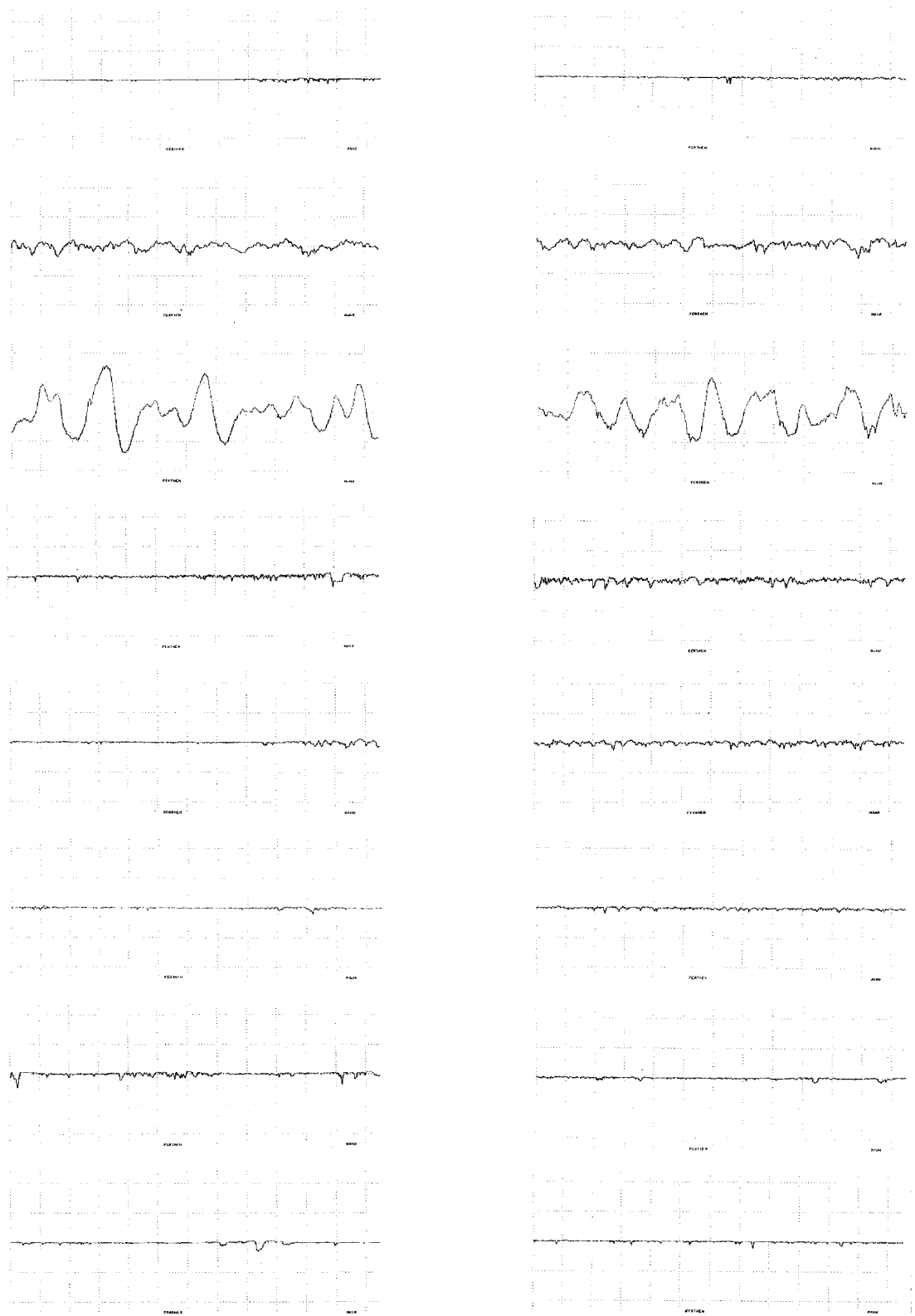


Figure 15. Roughness of surfaces. Left side granite, right side marble. From top to bottom, polished surface, waterjet cut at smooth region, waterjet cut at wavy region, diamond saw, and grinding by 60#, 120#, 220# and 400# sandpaper.

11. TABLES

Table 1. Physical, Mechanical and some other technological parameters of the analysed granites and marble samples.

Property	Capão Bonito red Granite	Interlagos silver Granite	Piracaia black Granite	Campos do Jordão white Marble
Dry Density	2,625 kg/m ³	2,625 kg/m ³	2,803 kg/m ³	2,816 kg/m ³
Apparent Porosity	0.68 %	0.78 %	0.52 %	0.87 %
Water Absorption	0.26 %	0.28 %	0.19 %	0.31 %
Amsler Wear Test	0.60 mm	0.64 mm	0.68 mm	3.84 mm
Impact Strength Test	0.51 m		0.38 m	0.22 m
Linear Thermal Expansion	8.9 mm/m °C x 10 ⁻³		9.3 mm/m °C x 10 ⁻³	11 mm/m °C x 10 ⁻³
Compression Breaking Load at Natural State	133 MPa	179 MPa	170.0 MPa	77 MPa
Compression Breaking Load after Freezing/Thawing	134 MPa			
Modulus of Rupture	9.2 MPa			
Bending Test	13.2 MPa	14.1 MPa	17.8 MPa	6.0 MPa
Static Deformability Modulus	56.1 GPa		32.963 GPa	55.277 GPa
Knoop Micro hardness	6789 MPa			
Ultrasonic Pulse Velocity	5380 m/s			
Ammonium Hydroxide (NH ₄ OH)	Unaltered aspect			
Sodium Hypochloride (NaClO ₂ H ₂ O)	Unaltered aspect			

Table 2. Linear traverse speed of nozzle in straight cut

Rock	Granite	Marble
	mm/s	mm/s
Quality 1	3.376	6.054
Quality 1	2.097	3.761
Quality 1	1.316	2.359
Quality 1	0.945	1.695
Quality 1	0.731	1.311

Table 3. Results of the laboratory assaying.

Rock	Granite			Marble
	Red	Silver	Black	White
Quality 1				
b _T	1.3	1.3	1.4	1.3
b _B	0.5	0.6	0.9	1.0
T _R	2.6	2.3	1.6	1.3
smooth kerf	18.9	25.3	18.6	13.7
wavy kerf	21.4	13.9	22.8	22.7
total kerf high	40.3	40.3	41.4	36.4
Quality 2				
b _T	1.3	1.4	1.4	1.3
b _B	0.3	0.5	0.6	0.7
T _R	4.3	2.8	2.3	1.9
smooth kerf	22.5	25.5	23.9	19.0
wavy kerf	19.5	20.0	29.3	23.6
total kerf high	42.0	45.5	53.2	42.6
Quality 3				
b _T	1.3	1.4	1.4	1.3
b _B	0.4	0.5	0.5	0.5
T _R	3.3	2.8	2.8	2.6
smooth kerf	25.8	29.5	31.4	22.6
wavy kerf	22.8	23.7	34.2	31.7
total kerf high	48.6	53.2	65.6	54.3
Quality 4				
b _T	1.3	1.4	1.4	1.3
b _B	0.3	0.4	0.5	0.5
T _R	4.3	3.5	2.8	2.6
smooth kerf	34.6	38.4	32.6	23.6
wavy kerf	32.4	25.9	> 36.4	> 45.4
total kerf high	67.0	63.4	> 69	> 69
Quality 5				
b _T	1.3	1.4	1.4	1.3
b _B	0.3	0.4	0.5	0.5
T _R	4.3	3.5	2.8	2.6
smooth kerf	36.7	38.6	37.9	31.1
wavy kerf	> 32.3	> 30.4	> 31.1	> 37.9
total kerf high	> 69.0	> 69.0	> 69.0	> 69.0

Table 4. Traverse speed of nozzle in curved cut

Rock	Granite	Marble
	(mm/s)	(mm/s)
Quality 3		
(25 mm) circle	0.773	1.356
(50 mm) circle	1.156	2.036
Quality 5		
(25 mm) circle	0.189	0.274
(50 mm) circle	0.282	0.503

Table 5. The Italian Norm to surface finishing evaluation

Name	Equivalent Granulation
“Levigated”	60#
Middle or Normal “Levigated”	120#
Fine “Levigated”	220#
Half Lustrous surface	400#

Table 6. The roughness determination of surface

Kind of Surface	Average Roughness R_A (μm)		Wawiness W_T (μm)	
	Granite	Marble	Granite	Marble
Polished Surface	0.9	1.8	7.5	2.6
Water Jet Smooth Cut	9.9	8.7	54.2	48.8
Water Jet Rough Cut	47.8	40.0	232.5	226.3
Diamond Saw	3.1	5.5	14.2	50.2
60# Grinding	2.0	4.4	18.3	9.6
120# Grinding	1.4	2.1	13.3	5.5
220# Grinding	3.2	1.8	10.7	7.6
400# Grinding	2.0	1.1	8.7	8.4

DISINTEGRATION OF ROCKS EXPOSED TO LASER BEAM BY WATERJET

L.M. Hlaváč

**VŠB - Technical University Ostrava
Ostrava, Czech Republic**

P. Martinec

**Institute of Geonics, Czech Academy of Sciences
Ostrava, Czech Republic**

A. Jančárek

**Faculty of Nuclear and Physical Engineering of the Czech Technical University
Prague, Czech Republic**

ABSTRACT

The wide experience with disintegration of heated rocks by water jet led to the idea to utilize the advantages provided by water jet on such rocks for deep kerfing. The idea is based on combination of two modern disintegration technologies - laser beam and water jet. The interest in disintegration of heated materials also grows up both in the research area and in practice. The advantages of preheating of the rock like materials by laser beam are particularly two: modification of material properties by inner transformations of a phase (reduction of strength) and the generation of a cobweb of micro-cracks especially in the direction of a laser beam. The paper contains both the theoretical physical investigation of the problem and the package of the experimental data. The large scale of problems rising in both spheres of research (theoretical and experimental) has been widely analysed and discussed as well.

1. INTRODUCTION

The research of laser beam interaction with rock materials started in the Czech Republic in 1989. Within the framework of the government research task II-6-1.04.03 under the direction of Vašek the first kerfs were made by CO₂ laser with continuous operation (Vašek et al., 1989). Those experiments were performed namely for the purpose of energy balance calculations, nevertheless, the material structure attracted the physics in the research group and they started to analyze the modifications of material and phase transformations of material components.

The second stage of research was included into the project of Grant Agency of the Czech Republic No. 106/93/2338 directed by Hlaváč. Several rock materials and rock like materials were submitted to the pulse laser beam operation. The obtained kerfs were again studied mostly regarding the amount of removed material.

The third stage of research was started within the framework of the project of the Grant Agency of the Czech Republic No. 106/98/1354 directed by Mádr (2000). The project was aimed at rock like materials in non-traditional physical conditions. Therefore, the heated rocks were tested and certain attributes of the physical state of matter seemed to be similar to the ones known from the laser made kerfs. The optical microscopic research of the rock materials transformed by laser beam started again and was deepened and largely elaborated by Martinec (2001). The most important results of the up-to-date group are included into this paper together with theory of laser beam energy utilization and hypotheses of rock material behaviour under the laser beam impact.

2. LASER BEAM IMPACT

Two types of CO₂ lasers were used for experiments – the continuous one with output 1500 W and the pulsing one with frequency 5000 Hz and output 25 W. Laser beam is coherent (the divergence is generally about 5 mrad for used CO₂ lasers) and output optics focuses it on a very small area (with a diameter of the order of the tenth of millimetres). When focused, the density of laser beam power increases up to values of the order $10^8 - 10^{10} \text{ W.m}^{-2}$. The behaviour of material influenced by laser beam results from that fact – it melts and evaporates creating even plasma. The effective temperature increases up to values about 10^7 K in the focus plane. The temperature gradient and temperature time evolution depend on a traverse rate of the laser beam spot on the material surface. For our parameters the temperature gradient is located in the interval from 10^5 to 10^9 K.m^{-1} and the temperature time evolution can reach values from 10^3 to 10^5 K.s^{-1} . The parameters were determined by basic theories of high-power laser jets (Letochov, 1982). However, the exact values need further measurements transcending the frame of our up-to-date research.

The traverse rates had values: 1, 1.5, 2.5, 5, 10, 25 mm.s⁻¹ for the continuous 1500 W CO₂ laser
1, 2.5, 5, 10, 20, 40 mm.s⁻¹ for the pulse 25 W 5000 Hz CO₂ laser

The rock samples used with a continuous laser were prepared from sandstone (Figure 1). The samples loaded by laser beam with pulse jet were prepared from several rock materials – sandstone (Figure 2), siltstone, granite, syenite, granodiorite, marble, dolomite and composite made from

marble pieces fasten together by concrete. In general, the energy delivered to the target removes the volume of material determined by width, depth and length of the kerf made by laser beam. The depth can be calculated by equation (1), provided all necessary parameters are known or determinable.

$$h = \frac{\alpha P_v t_K}{\varepsilon_v n_o D_K l_K} \quad (1)$$

The laser beam diameter in the focus plane can be determined from initial parameters through the equation (2) and the kerf diameter D_K is considered to be nearly of the same value.

$$D_f = \frac{\lambda_o f_o}{\pi D_o} \quad (2)$$

The length of kerf is determined by traverse rate and the time of kerfing, i.e. equation (3).

$$l_K = v_P t_K \quad (3)$$

The length of the intensive zone of a focused laser beam behind the focus distance can be determined, according to laser beam theories published by Engemann (1993), from the equation (4)

$$L_C = \frac{2 \pi D_f^2}{\lambda_o} \quad (4)$$

This length should correlate with the depth of penetration of the laser beam into the rock material provided the correction resulting from a velocity factor is considered. The speed of penetration has only limited value. Therefore, the depth of penetration is obtained as the result of composition of both velocity vectors, the traverse rate and speed of penetration, acting along the time calculated from the laser beam diameter and traverse rate. The speed penetration is determined by rate of the atom evaporation for target material. Nevertheless, contrary to the water jet there is a certain zone of thermally influenced material round the kerf made by laser beam. Material in this zone is transmuted and disturbed. The couplings among atoms are weakened and a lot of small fissions, crannies and breaks grow up. This disturbed rock material can be disintegrated more efficiently.

3. DESCRIPTION OF THE EXPERIMENTAL MATERIAL

Two blocks of light green medium grained glauconite sandstones from the Godula Unit in Beskydy Mountains (the West Carpathian in the Czech Republic) were selected for description in this paper. This type of sandstone was used for many experiments with water jets and abrasive water jets in the past. The analytical numbers of samples inscribed at the Institute of Geonics are 1780B (Figure 1) and 5355 (Figure 2). Both sandstone samples are composed of detrital quartz, quartzite grains, quartz-feldspars aggregate in grains, feldspars (orthoclase, oligoclase-andesine) grains and irregular detrital flakes of various types of mica (medium grain size 0.3 mm). Detrital grains of quartz and

feldspars are sub angular in shape, ranging from 0.2 to 0.5 mm in grain size. Diagenetic corrosion and outgrowths of quartz are quite frequent. The matrix is compound of clay matter (illit, mica) with authigenic cement as carbonates (individual crystals of Fe-dolomite-ankerite series) and with fine silicification. Minerals as glauconite, which formed small yellow-green pellets (approximate maximum size 0.5 mm), have an authigenic origin. Sorting of detrital grains is bad. Texture is psammitic, from a sub angular up to an angular shaped, medium grained.

4. METHODS OF KERF STUDIES

A perpendicular profile of kerfs made by laser beam was studied in thin section by means of optical microscopy with system of image analysis LUCIA 2 (Ščučka, 2001). Sample No. 1780B was loaded by a high power continuous laser beam and sample No. 5355 was loaded by a medium power pulse laser beam. Identification of minerals, identification of mineral transformations and formation of glass were studied by means of optical microscopy, X-ray powder diffraction and infrared spectroscopy.

The following parameters were determined:

- Estimation of percentage of individual mineral grains in the kerf section by evaluation of the portion of individual minerals on the kerf wall.
- Description of physical phenomena guiding laser beam interaction with individual minerals on the kerf walls.
- Description of glass origin in the kerf, glass identification and determination of the melting temperature and flow points for the whole sandstone.
- Specification of geometrical parameters of the kerf section shape by image analysis (Ščučka, 2001): the depth of kerf, the width of kerf on the surface of the block, the width of kerf at the half depth of the kerf and the total area of the kerf.

5. RESULTS

This section is devoted to the description of changes made in rock material by laser beam impact.

5.1 Laser beam interaction with rock material and minerals

Interaction of a laser beam with rock materials produced three effects:

- melting of minerals in the kerf;
- the origin of new minerals or glass phases in the kerf and in the vicinity of the kerf wall made by laser beam in the rock material;
- the origin of a thermally induced crackling in the mineral grains or in the rock material texture.

Laser beam interaction with a rock material texture proceeds on the level of individual mineral grains or the matrix (very fine particles of mica, clay minerals and mineral cement). Intensity of mineral

melting and transformation depends on the temperature distribution in the vicinity of the kerf walls that correlates with the temperature in the beam focus (being inside the kerf). The melting point of the quartz is 1713°C and quartz grains are locally melted by this temperature. The primary quartz glass is produced. The same situation sets in for K-feldspars (melting point 1150°C) or oligoclase (melting point 1450°C). Melting of feldspars produces alkaline glass. Mix of both new-formed glass (quartz one and alkaline one) in the kerf constitutes a new, secondary glass phase. Glass fills the kerf and it is stiffened there in the form of several chemical types of glass.

Nevertheless, we have many more indicators of temperature in the rock material structure. In the case of laser beam interaction with glauconite sandstone the glass is foaming and erupting out of the kerf on the block surface. Grains, better said crystals of carbonates (Fe-dolomite – ankerite) in the matrix, are dissociated within the temperature range 720 - 870°C and CaO, MgO, FeO and CO₂ are produced. The Fe²⁺ based in the carbonate structures is oxidized to the Fe³⁺ form on temperatures above 500°C. Transformation of glauconite into new mullite-spinel phases is another well detectable feature. It proceeds between temperatures 850°C and 950°C. The total dehydroxilation of glauconite structure is observed within the temperature interval 550 - 600°C. Oxidation process of Fe²⁺ is started in the glauconite structure approximately in the temperature range 400 - 500°C and produces changes in colour of minerals – from the yellow-green one to the dark red and even brown one. Dispersed coal matter, however, is carbonised or oxidized near the temperature point 400°C. These relationships between material changes and temperature state of the matter make to map the temperature field round the kerf produced by laser beam possible. The progress of the temperature field can be also studied and described. This is the base for modelling of simultaneous application of laser beam and water jet for rock material disintegration.

5.2 Rock material crackling

Formation of fissions, crannies and breaks is connected with two principal mechanisms. The first one is a well-known phase transformation of α to β quartz (572.7 °C) which induces a net of crannies in quartz grains. The second one is a formation of parallel open fissions caused by heating and cooling of the rock texture: different coefficients of thermal dilatibility for individual components of rock materials (mineral grains and matrix) in the vicinity of a laser beam interaction zone are responsible for them. Frequent destruction of the kerf mouth and its vicinity is the result of different distribution of temperature in this part of material and in the rest one. The thermal reactions and crackling of minerals or the base rock texture are also very good natural indicators of temperature distribution in rock material mass along the kerf walls.

5.3 Composition of the rock samples and local composition of sandstone in kerfs

Each section of the kerf made in sandstone has its own individual mineral composition. Estimation of volume percentage of individual mineral grains in kerfs marked A through F was made as a portion of individual minerals on the kerf wall. This portion of minerals and matrix was determined by optical microscopy in thin section. The results proved that both materials used for samples have the same composition. Molar ratios of selected compounds, melting points and other parameters were also determined for whole rock samples. The values are presented in Table 1.

5.4 Shape of kerf, deposition of glass and geometry of kerfs

Standard profiles of kerfs together with types of glass location in the kerf cross section profile are illustrated in Fig. 3. Photos of thin sections of kerfs from sample No. 1780B and sample No. 5355 are presented in Fig. 4 and Fig. 5 respectively. The main geometry parameters of the kerf (the depth, the width in half of depth, the width of the kerf mouth on the material surface and the area of the kerf section) are quantified in Table 2.

6. DISCUSSION

Sandstone, as a poly-component and a poly-dispersed mineral system, is a special event of laser beam interaction with rock material. Interaction of laser beam passes out firstly with the individual minerals in the rock material. Grain sizes of many minerals fall within the interval $<0.1;0.5>$ mm and the maximum kerf width lie in the range from 0.22 to 0.6 mm. Secondary interaction of a laser beam with the primary glass melted from individual minerals provokes formation, better said homogenisation, of a new composition of alkaline glass. This glass is injected into cracks in the rock material and minerals. The cracks are formed in the vicinity of the kerf walls. Difference between individual depths of kerfs is a function of local mineral composition and grain size of minerals (quartz and feldspars).

Typical changes in the mineral structure are good indicators of distribution of temperature in rock material starting from the kerf wall inward the rock mass (oxidation, dehydration, dehydroxilation, formation of new mineral phases, oxidation of dispersed coal matter, etc.). Further research is to be aimed at the theoretical description of these problems. Nevertheless, our previous experiences with application of water jet on heated rock materials (Hlaváč, 1999, Mádr et al., 2000) allow us to predict that penetration of water jet in rocks influenced by laser beam will increase even at rocks cooled off to the normal temperature. It is caused by the facts that rock material is disturbed both directly and indirectly. Material parameters are modified as it is described in section 5.1 and a cobweb of fissions and crannies is generated as it is described in section 5.2. The amount of disintegration should be more increased when water jet is applied on rock material in the instance after a laser beam pass. This application makes possible to utilize the effect of rapid cooling off by water jet inducing additional disturbances and simultaneously the fact that couplings in the hot material are weakened. The increase of efficiency is demonstrated in Fig. 6. The curve in Fig. 6 is evaluated for the same type of sandstone according to theories presented by Hlaváč (1995, 1999). The points in Fig. 6 are experimental results obtained during research of interaction of water jet with heated rock materials.

7. CONCLUSIONS

Experimental data proved that in the vicinity of laser beam impact on rock type materials a great number of physical changes proceed. According to our up-to-date research the following parameters were determined to play the key role:

- transformation of rock forming materials;

- dehydroxilation of some building unites of rock matter;
- oxidation processes in rock matter;
- dissociation of certain rock forming minerals;
- melting of minerals and clay matter;
- evaporation of liquids formed by molecules of melted rock matter;
- origin of fissions, crannies and breaks round the interaction zone;

Laser beam interaction with rock type materials can serve for increase of water jet efficiency in appropriate applications. Nevertheless, further research is still needed, especially the one aimed at concurrent laser beam and water jet impact. Unfortunately, limited financial budget caused that we were not able to realize such experiments yet.

8. ACKNOWLEDGMENTS

The authors are grateful for support of the work presented in this paper to the Grant Agency of the Czech Republic (projects No. 106/93/2338, 205/96/0931 and 106/98/1354), to the Grant Agency of the Czech Academy of Sciences (project No. K1-012-601(3141)) and to the Ministry of Industry and Trade (project No.FB-C3/05).

9. REFERENCES

- Engemann, B.K., Herbrich, H., Kessler, B., and Langemann, M., “Schneiden mit Laserstrahlung und Wasserstrahl,” *Expert verlag*, 179 p., Germany, 1993. (in German)
- Hlaváč, L.M., “Physical Analysis of the Energy Balance of the High Energy Liquid Jet Collision with Brittle Non-Homogeneous Material,” *Proceedings of the 8th American Waterjet Conference*, M. Hashish (ed.), pp. 681-697, Water Jet Technology Association, St. Louis, Missouri, 1995.
- Hlaváč, L.M., “Theoretical and experimental investigation of a high energy waterjet efficiency on thermally treated rocks,” *Proceedings of the 10th American Waterjet Conference*, M. Hashish (ed.), pp. 497-506, Water Jet Technology Association, St. Louis, Missouri, 1999.
- Letochov, V.S., and Ustinov, N.D., “High-power lasers and their utilization,” *ALFA*, 110 p., Bratislava, 1982. (in Slovak)
- Mádr, V., Hlaváč, L., Hlaváčová, I., Poláček, J., Sosnovec, L., Kušnerová, M., and Valíček, J., “Disintegration of rocks in non-traditional conditions by liquid jets,” *Report of the project GACR No. 106/98/1354 Disintegration of materials in non-traditional conditions by liquid jets*, 19 p., VŠB-Technical University Ostrava, Ostrava, 2000. (in Czech)

Martinec, P., and Hlaváč, L., “Interaction of coherent electromagnetic radiation with rock materials,” *Final report of works made in the framework of several projects*, 82 p., Institute of Geonics and VŠB-Technical University Ostrava, Ostrava, 2001. (in Czech)

Ščučka, J., “Study of kerfs induced by laser beam in rocks by image analysis,” *Proceedings of Geonics 2001*, Kožušníková, Konečný (eds.), PERES Publishers, Prague, 2001. (in print)

Vašek, J., Hlaváč, L., Foldyna, J., and Horák, J., “Energy balance of the process of rock material disintegration by high-pressure water jet,” *Controllable stage E 03 of the framework II-6-1.03.04*, 89 p., Mining Institute of the Czechoslovak Academy of Sciences, Ostrava, 1989. (in Czech)

10. NOMENCLATURE

α	absorption of the target material ...[-]
D_o	output diameter of laser beam ...[m]
D_f	diameter of laser beam at the focus plane ...[m]
D_K	kerf width ...[m]
ϵ_v	evaporation energy per atom ...[J]
f_o	focus length of the output optics ...[m]
h	depth of material disintegration ...[m]
λ_o	wavelength of the laser radiation ...[m]
l_K	kerf length ...[m]
L_C	length of the focused beam (diameter of focused beam divided by divergence) ...[m]
n_o	number of atoms in volume unit ...[-]
P_v	output power of laser beam ...[W]
t_K	time of kerfing ...[s]
v_p	traverse rate ...[m]

11. TABLES

Table 1. Molar ratios of selected compounds and melting points for whole rock samples.

Sample No:	1780B	5355
SiO ₂ /Al ₂ O ₃ [-]	17,15	17,26
(SiO ₂ +Al ₂ O ₃)/ (MgO+CaO+Fe ₂ O ₃ +K ₂ O+Na ₂ O) [-]	10,24	12,54
Loss of ignition [%]	3,84	2,88
Deformation temperature ID [°C]	1460	1410
Softening temperature ST [°C]	1500	1435
Melting point [°C]	1570	1540
Flow point [°C]	1640	>1650

Table 2. Kerf shapes, glass location in the kerf and kerf parameters.

Kerf	Shape	Glass	Traverse rate	Depth	Width (half depth)	Width (surface)	Area of the kerf section
			[mm.s ⁻¹]	[mm]	[mm]	[mm]	[mm ²]
Sandstone, sample No.1780B							
A	A	C	1	9.19	2.14	3.08	20.08
B	A	C	2.5	5.14	1.26	2.06	6.52
C	A	D	25	0.80	0.99	2.18	0.80
D	A	C	10	1.98	1.08	1.38	1.09
E	B	D	5	3.19	0.98	2.07	3.42
F	A	D	1.5	7.56	(1.78)	(2.48)	(10.62)
Sandstone, sample No. 5355							
A	A	C	1	1.35	0.37	0.57	0.559
B	A	C	2.5	0.70	0.36	0.37	0.251
C	A	D	5	0.47	0.37	0.38	0.147
D	A	C	10	0.37	0.20	0.32	0.068
E	B	D	40	0.13	0.15	0.22	0.017
F	A	D	20	0.17	0.23	0.62	0.049

12. GRAPHICS

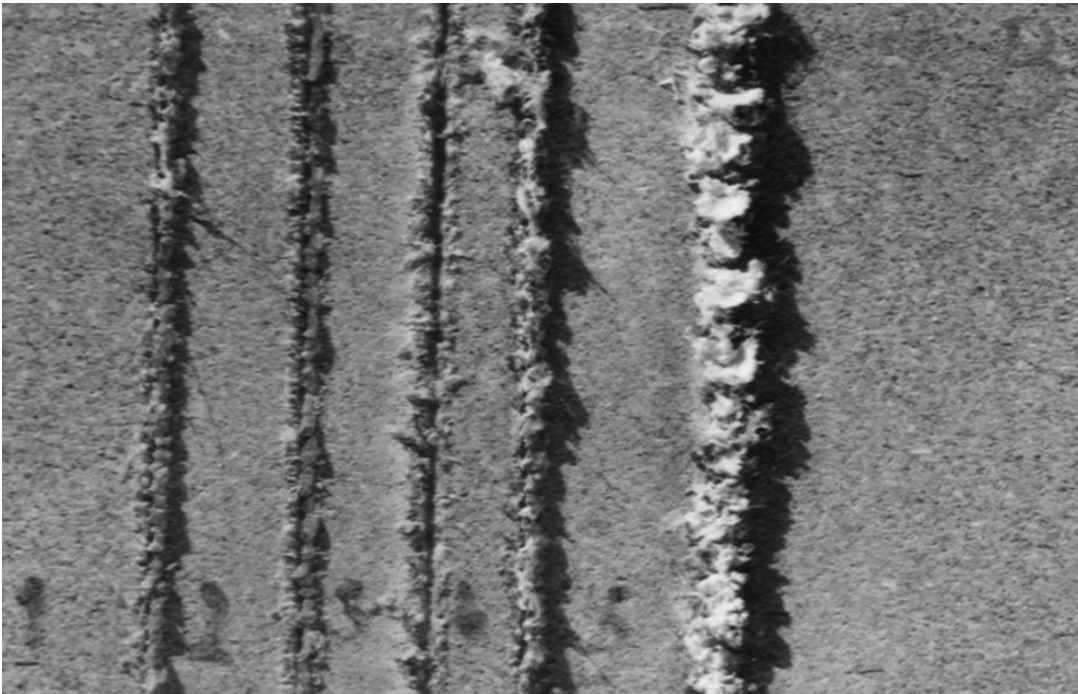


Figure 1. Kerfs made by a high power continuous laser beam in the sample 1780B.

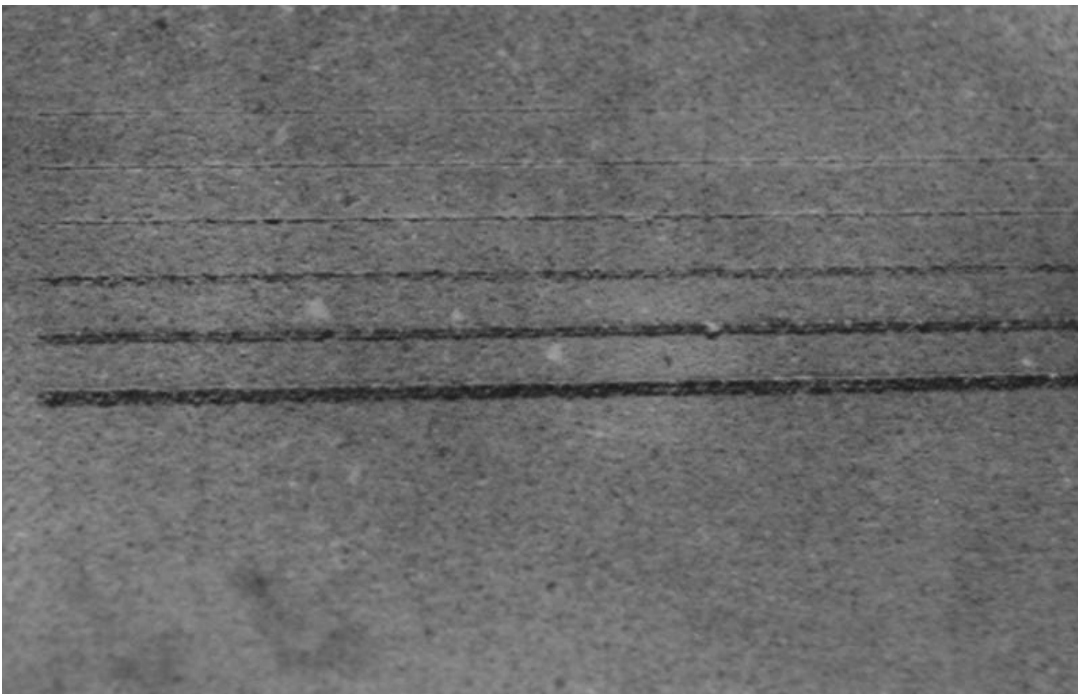


Figure 2. Kerfs made by a medium power pulse laser beam in the sample 5355.

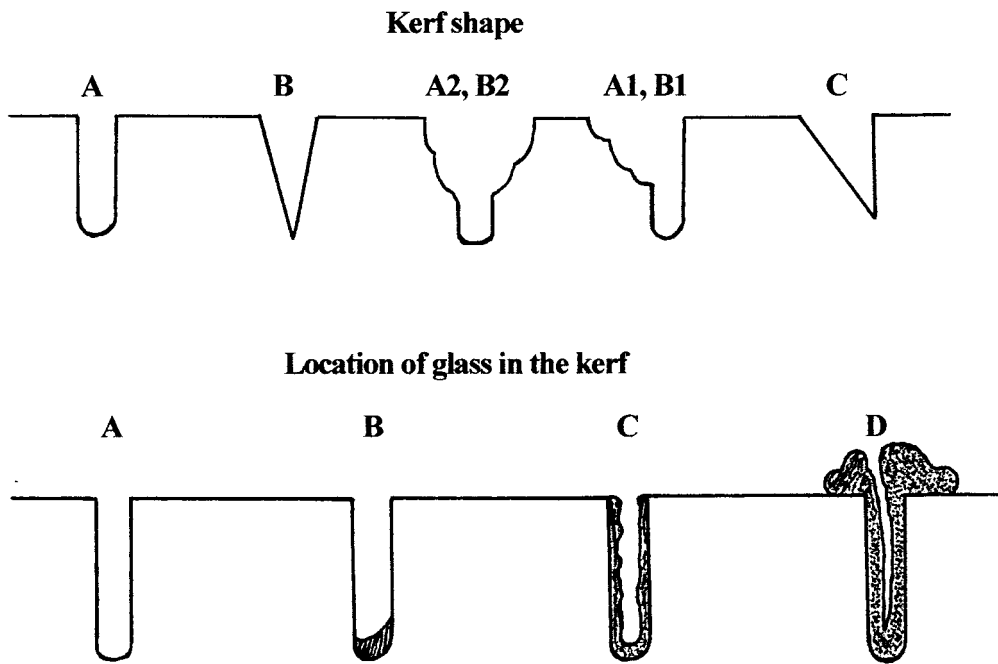


Figure 3. Schemes of the kerf cross sections. *Simple kerf shapes*: A – rectangular, B – triangular, C – asymmetrical. *Compound kerf shapes* – simple shape plus breaks in the upper part of the kerf: 1 – one sided, 2 – both sided. *Location of glass*: A – no glass in the kerf, only products of decomposition possible, B – glass in the bottom of the kerf, C – glass located in the kerf, either on the walls with central cavity or filling the whole kerf, D – glass fills the kerf and it is even melted out from the kerf forming various patterns on the material surface.

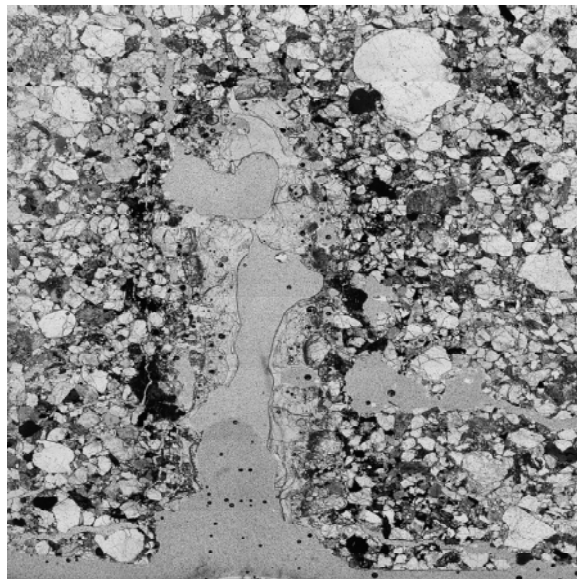


Figure 4. Cross section of the kerf made by laser beam in sandstone sample 1780B.

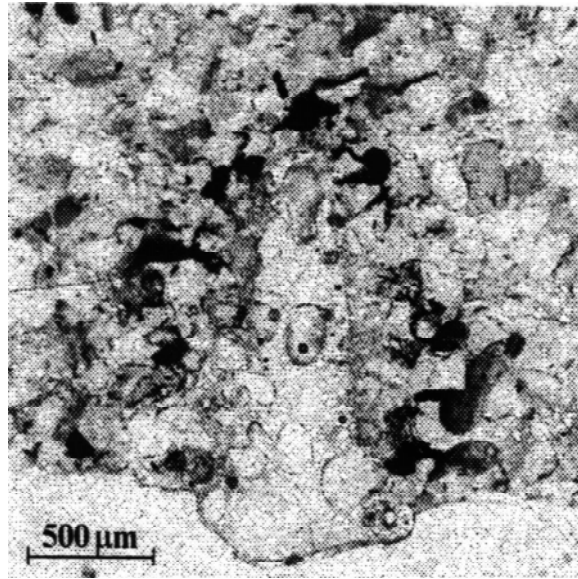


Figure 5. Cross section of the kerf made by laser beam in sandstone sample 5355.

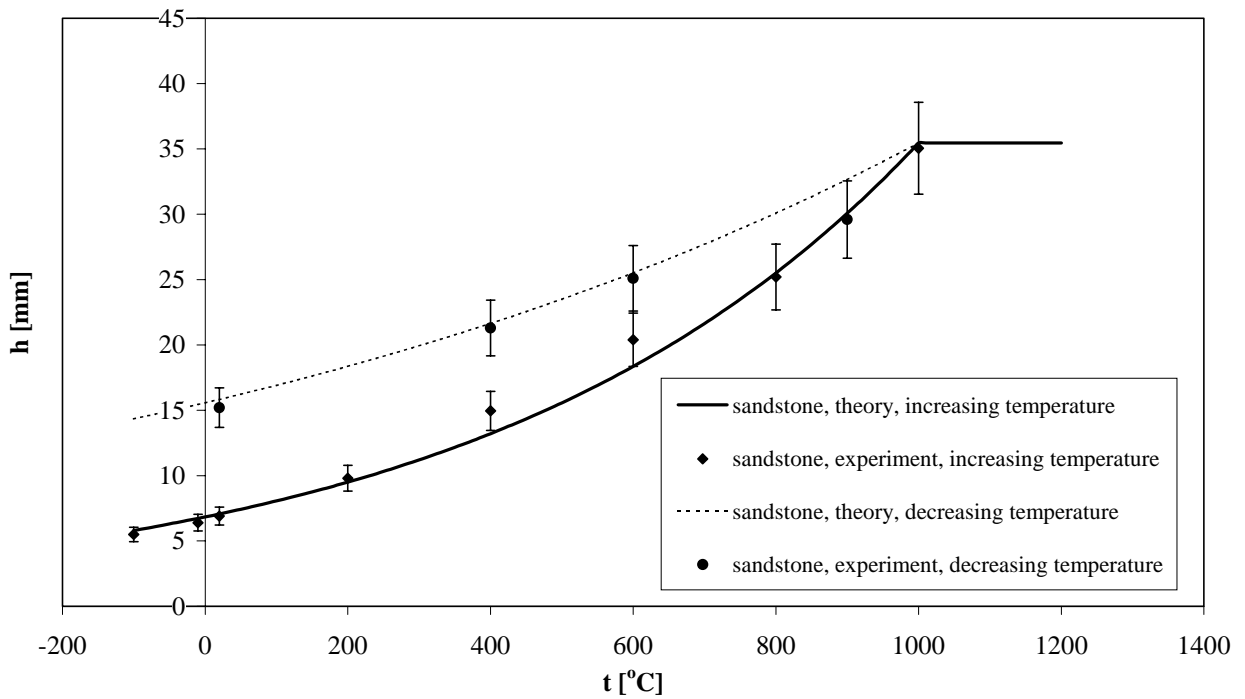


Figure 6. Comparison of the theoretical and experimental depth of disintegration made in thermally treated sandstone sample by water jet.

LIMITATIONS TO THE USE OF WATERJETS IN CONCRETE SUBSTRATE PREPARATION

G. Galecki, N. Maerz, A. Nanni, J. Myers
University of Missouri-Rolla
Rolla, Missouri, U.S.A.

ABSTRACT

Repair and strengthening of concrete structures with fiber reinforced materials (FRP) involves the use of externally bonded sheets, prefabricated laminates, and bars mounted near the surface. Studies have shown that the load-carrying ability of FRP materials is integrally related to the bonding characteristic of the epoxy to the substrate. This is very significant to the construction industry for identifying optimal bond characteristics since current specification requirements for the use of FRP repair and strengthening techniques have no methodology to identify these optimal conditions.

Over the years custom applications have become a standard option and some standards have to be established for specific applications. This paper discusses a roughness index of concrete surfaces produced with waterjets under different conditions.

1. INTRODUCTION

Waterjets offer advantages in the specific application of concrete removal. In-depth review of all aspects of waterjet applications in construction engineering is given by Momber (1993, 1998) and Summers (1995). Utilizing the operating flexibility of waterjets, depending on the type of work, different requirements to concrete removal rates can be achieved.

With settings for the minimum material removal, the surface can be textured or well washed at the extreme. Since Fiber Reinforced Polymer (FRP) materials have tremendous potential for repairing and strengthening structures that have deteriorated (Nanni, et al., 1993), (Myers, et al., 1999) such as columns, beams, and slabs, the interest lies in proper application of said materials. Load carrying ability of FRP materials is related to the bonding characteristic of the epoxy to the substrate. The bonding characteristic is a function of the surface roughness of the concrete, thus, identifying optimal bond characteristics is of great significance to the construction industry.

2. CONCRETE SURFACE PREPARATION

To prepare the bond surface for FRP laminating, the surface needs to be cleaned and roughened. Cleaning is required to remove foreign substances from the concrete substrate, and to remove weakened or damaged parts of the substrate. After cleaning, one of the principal factors affecting the bond behavior between the prepared concrete and epoxy is the roughness of the concrete surface. To enhance the bond characteristics of the substrate, different methods can be used to produce a rough surface. While an optimal level of roughness has not been characterized to date, preliminary bond characterization work has indicated that the level of roughness impacts the loading level at which de-lamination between the two materials occurs. Based on the initial study, improper surface preparation results in less than optimal bonding characteristic. The International Concrete Repair Institute (ICRI) has identified and prepared plastic models of nine different Concrete Surface Profiles (CSP), (International Concrete Repair Institute 1997), Fig.1. This provides a simple tool for specifying roughness. It is however a very subjective measure and lacks the objectivity that is needed.

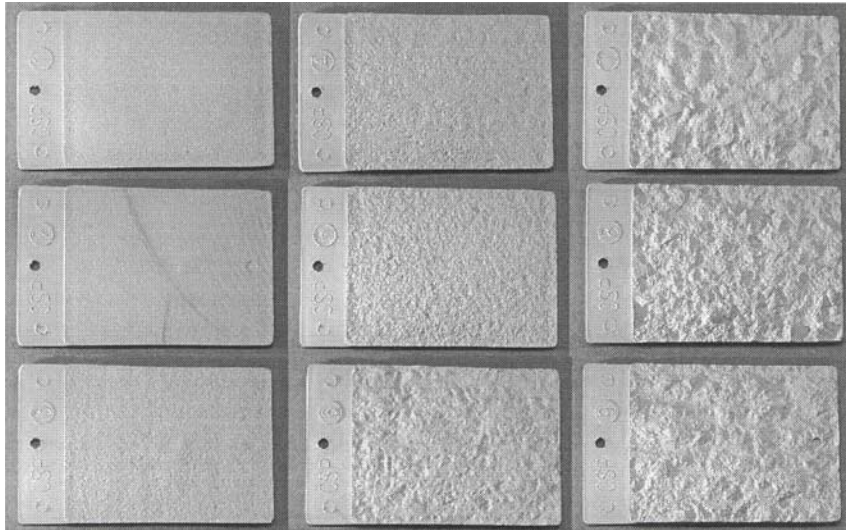


Figure 1. Plastic model concrete surface profiles. The profiles are ordered 1 to 9 in order of increasing roughness, and correspond to acid etching, grinding, light shotblast, light scarification, medium shotblast, medium scarification, heavy abrasive blast, scabbing, and heavy scarification.

Surface preparation of industrial structures is a problem. Surface preparation is the process by which sound, clean, and suitably roughened surfaces are produced on concrete substrates for the application of the specified protective system. Methods used will determine the substrate topography required for the different type of coatings. According to ICRI (International Concrete Repair Institute, 1997), method selection must be guided by the following principles of sound practice:

- The structure to be coated should not be damaged.
- The reinforcing steel should not be damaged nor its bond with the concrete loosened.
- Vibration, impact, or thermal loads applied should not weaken the concrete.

To produce a suitably roughened surface, different methods for preparing concrete surfaces can be employed. The methods of surface preparation include: detergent scrubbing, low-pressure water cleaning, acid etching, grinding, sand blasting, shot blasting, scarifying, needle scaling, scabbing, high-pressure water jetting, flame blasting, and milling. Each of these methods has its advantages and disadvantages, which need to be considered in light of existing conditions and requirements.

Though the rough surface can be produced by different methods, there is a difference in the surface quality. For instance, the surface prepared using hand held tools results in a higher probability of interface failure at pull-off test (Silfwerbrand, 1990). When compared between sand blasting, jack hammering, and water jetting methods of surface roughening, the percentage of interface failure for each of the listed methods is 38%, 31%, and 7% respectively. This is related to the profile length, which in the case of a waterjet is the longest, providing the best anchoring effect. According to Frenzel, (2001), there are three reasons why water jetting should

be selected as a method of surface preparation. These reasons are environmental requirements, process economics, and health and safety issues.

Based on assumptions that concrete is a brittle material and the aggregates are stronger than the matrix, chipping and/or liberation of the aggregates can dominate the erosion mechanism of concrete. Since concrete has a porous structure, it is expected that under the load induced by waterjets, all weak bridges connecting individual voids will be damaged and washed away. This is especially important to the outer skin of concrete casting structures where high concentration of air bubbles and much less of large aggregates can be found in the surface vicinity. When a jet moves transversely over the empty space of a pore, it will fill it up creating the cushion for a new oncoming segment of the jet. The presence of water in a pore will reduce the material removal efficiency by the damping action of water cushion. This has to be considered as a positive aspect in surface roughening, contrary to hydrodemolition.

The porosity of concrete, together with other of its properties, will control to a degree, obtainable roughness. The cushioning effect of the water trapped in the pores may be different in preparation of flat surfaces in horizontal applications than in overhead or vertical applications due to the presence or lack of water in the pores. However, there is no data available on this. Also, the ratio of the jet diameter to the pore dimension and the aggregate size and type will determine the concrete resistance against water jetting.

3. EXPERIMENTAL SET UP

To produce roughness, concrete samples were moved under a single nozzle, rotating the cutting head with variable rotational speed, Fig 2. The waterjet struck the surface at 80 degrees.

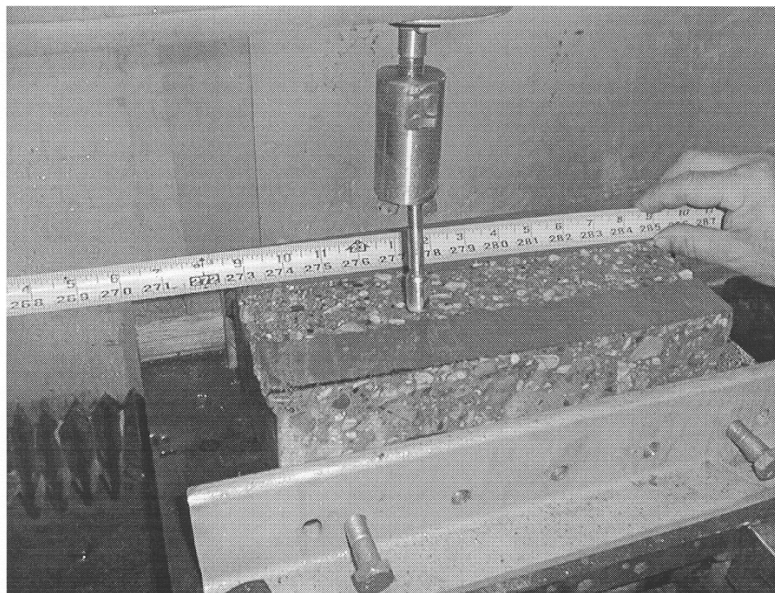


Figure 2. Test rig--general view.

3.1 Test Conditions

A stand-off distance of 6 mm, an angle of attack of 80 degrees, and a traverse speed of 0.5 m/min were kept constant during these tests.

Taking into consideration the fact that any application of waterjets is generating waste water that needs to be disposed of, it was decided to use very small diameter nozzles, Gatti type 2720 of 0.1 mm and 0.2 mm in order to produce the minimum of waste amount. Waterjets were generated under pressure levels of 70 MPa, 140 MPa, and 210 MPa. The selection of initial parameters, in part, was guided by the experience gained in the use of waterjets for drilling in sandstone (Galecki, 1983).

The relationship between the traverse speed and the rotational speed of the cutting head affects the texture produced (Galecki, 1999). To analyze this effect, the rotational speed was changed in a relatively wide range, varying from 210 rpm to 2,160 rpm. Disruption of the jets caused by the centrifugal force and its effect on the jet quality was not analyzed.

In any type of field applications, it is obvious that the set parameters might be disturbed by the outer conditions. One of these parameters, which may be affected, is stand-off distance. To simulate changes in stand-off distance, a stepped sample and an inclined sample with two inch in vertical drop were used.

3.2 Baseline Roughness

Currently, there is no means to effectively measure roughness of concrete. It can only be done by subjective comparison of the concrete surface to surface profiles in the form of plastic models provided by ICRI (International Concrete Repair Institute, 1997). In order to prepare the base-line roughness, surfaces of six concrete slabs were prepared using disk grinding and sandblasting. Then an imaging device was employed to measure the roughness of the concrete surface (Maerz, et al., 2001). Therefore, test results will no longer vary based on the disposition of an operator.

The image and roughness numbers of prepared surfaces are shown in Figure 3. Note the difficulties in distinguishing the difference in surface roughness obtained by using different methods.

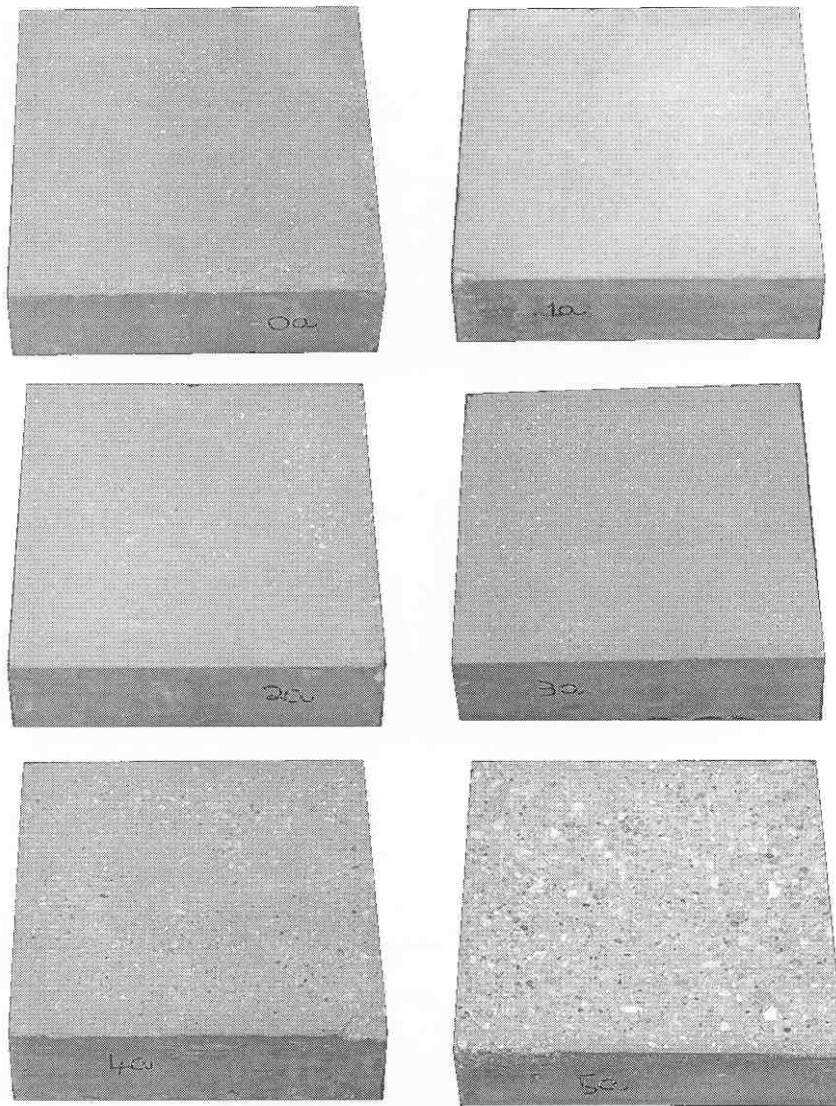


Figure 3. Concrete surfaces used for testing: block 0--surface roughened with a grinding wheel, blocks 1-5 sandblasted with an increasing duration of sandblasting media.

3.3. Water Jetting Parameters

In these preliminary tests, a combination of waterjet diameter, rotational speed of the cutting head, pressure, and stand-off distance was used. Test conditions are given in Table 1. It was decided that for studying the bonding effect between concrete and FRP, surfaces with roughness indexes corresponding to specimens 3, 7, 9, 13, and 15 were selected, Figure 4. The pull-off test results are not published in this paper, since they are part of a thesis, which has not been defended at this time.

Table 1. Test conditions and surface roughness index Ia..

Ia=average surface angle degrees

SAMPLE #	PRESSURE (MPa)	NOZZLE (mm)	ROTATIONAL SPEED (RPM)	ROUGHNESS INDEX (Ia)
1	210	0.2	1080	16.8
2	Clogged nozzle			no results
3	140	0.1	210	11.5
4	210	0.1	210	18.4
5	210	0.1	1080	15.1
6	210	0.1	1080	11
7	210	0.1	2160	11.1
8	210	0.1	360	15
9	210	0.1	360	14.8
10	140	0.1	2160	8.7
11	140	0.1	1080	10.4
12	140	0.1	360	12.6
13	140	0.1	210	13.1
14	70	0.1	210	9.7
15	70	0.1	360	9.7
16	70	0.2	360	12.2
17	105	0.2	360	14.4
18	140	0.2	360	14.8
19	140	0.2	720	13.9
20	140	0.2	360	17.3
21	140	0.2	360	N/A
22	70	0.2	360	15.7
23	140	0.2	720	16.5
24	140	0.2	1080	17.7
25	140	0.2	2160	16.6
26	140	0.2	2160*	13.1
27	140	0.2	1080*	13.9
28	140	0.2	1080*	14.9
29	140	0.2	720*	16.7
30	140	0.2	720**	13.8/13.8
31	70	0.46	720**	13.1/14.7
32	140	0.46	720**	N/A

*50 mm vertical drop

** inclined sample

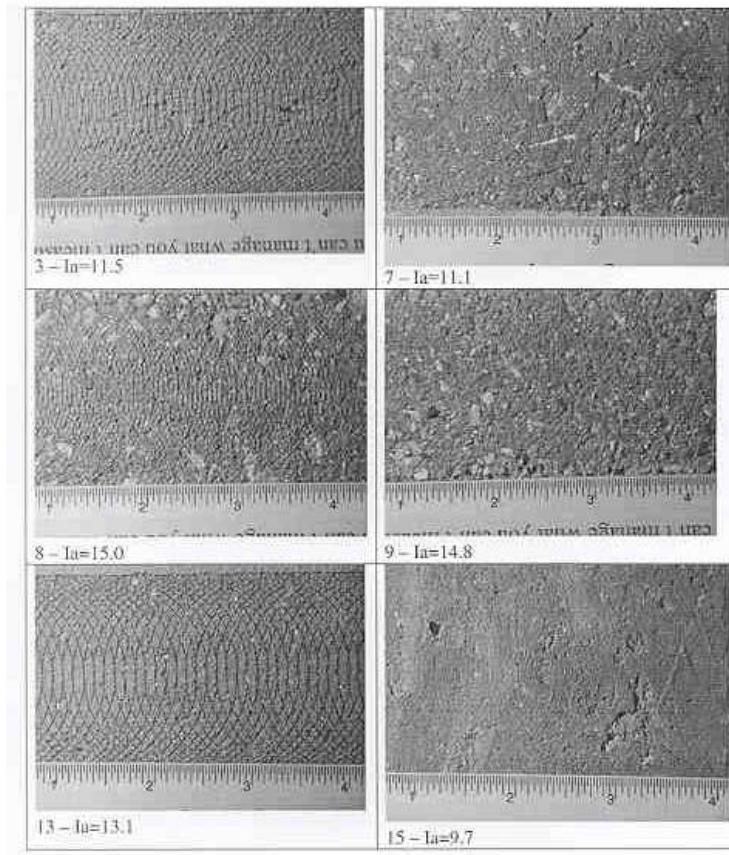


Figure 4. Images and the roughness indexes of concrete surfaces prepared under different conditions; image number corresponds to the test number in Table 1.

4. DISCUSSION OF RESULTS

Due to the complex nature of interaction between the waterjet and concrete surface, the surface roughness of the given concrete is related to all operational parameters. Though these parameters do not act independently, but as a group affecting the surface topography, attempts to discuss the influence of some main parameters on the surface roughening process with waterjets are made in the following sections.

4.1 Pressure

Material removal rate is strongly dependent on waterjet energy imparted to the cutting zone. When examining the influence of pressure only, it can be seen, that the change from 20,000 psi to 30,000 psi resulted in roughness index change from 3-Ia=11.5 to 4-Ia=18.4. A much gentler change in pressure from 105 MPa to 140 MPa, resulted in a roughness index change from 17-Ia=14.4 to 18-Ia=14.8. These two sets of different conditions very well illustrate how much the surface roughness can be controlled by change in pressure.

Though the roughness index is used to determine the change in surface topography, these numbers are meaningless unless the relationship between the roughness index and the bond strength will be established. Again, the roughness index is established to objectively compare the surface condition.

4.2 Rotational Speed

Since chipping and/or liberation of the aggregates can dominate the erosion mechanism of concrete, the concrete properties (mainly the size of aggregates) will determine the pitch of the waterjet passes. The pitch will control the wash-away process of the soft matrix in order to release the harder and bigger components. The pitch of waterjets is the result of the traverse speed and the rotational speed of the cutting head.

It is important to note that the pitch of waterjet passes can be maintained in a wide range of operating parameters. The contact time between waterjets and the concrete surface will vary depending on the speeds at which the surface is roughened. The higher the surface preparation rates, the shorter the exposure time of the surface to waterjets that is needed. To illustrate the effect of the exposure time to waterjets on the surface roughness, the rotational speed was changed from 360 rpm to 2,160 rpm. The traverse speed was maintained at the same level of 0.5 m/min. As a result of these changes, the roughness index dropped from 8-Ia=15.0 to 7-Ia=11.1 (see Figure 4). As depicted in Fig.4, the influence of the rotational speed on surface roughness is significant, therefore, this parameter can be used in the process control.

Both, density, as well as the distribution of waterjet passes, contribute to the surface roughness index. The surface coverage by waterjets was studied by Galecki (1999). Since concrete is a non-homogeneous material, it can be expected that under the same conditions roughness may vary from area to area.

4.3 Nozzle Diameter

Nozzle diameter, together with jet velocity as a function of pressure, will determine the energy imparted to the collision zone on a concrete surface. Adjusting one or the other parameter, the performance the waterjet can be controlled. The questions of what and why should always arise at the beginning of any application. The environmental issues and economics of the process of applying FRP materials were the reasons why small diameter nozzles were used. Small diameter nozzles give low discharge and it is always easier and less expensive to dispose of waste in smaller quantities. For the purpose of applying FRP materials, the minimum of surface material has to be removed which can be achieved with low energy waterjets.

Although the condition for optimal bonding between epoxy and substrate is not yet known, it is obvious that excessive roughness of the surface will require larger quantities of primer, putty, and epoxy, which in turn increases the cost of the job performed.

Investigation into the relationship between the nozzle diameter and the surface roughness index was carried out with nozzle sizes of 0.1 mm to 0.2 mm at 70 MPa, in experiments 15 and 22 of Table 1. When nozzle diameter was changed from smaller to larger, the roughness index increased from 15-Ia=9.7 to 22-Ia=15.7. No data is available at the moment on how the difference in surface roughness may influence the bond strength.

4.4 Stand-Off Distance

Waterjets lose their cutting effectiveness as a function of stand-off distance. Since roughening with high pressure waterjets is a stand-off distance sensitive operation, it was decided to investigate this parameter by using stepped samples with a 50 mm vertical drop, Fig. 6. The roughness produced on the lower and upper surfaces on sample 29: 29-Ia=15.8 and 29-Ia=15.5, respectively. Closeness of these measurements overcame expectation, since subjective investigations showed a difference in surface conditions. In this particular case it was possible to show the usefulness of the imaging device.

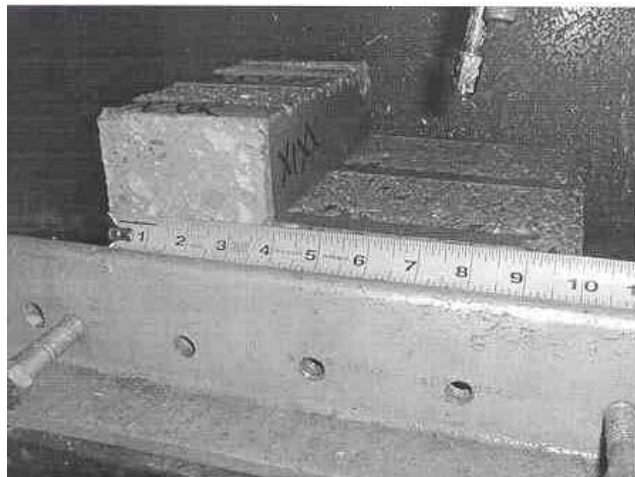


Figure 5. Stepped sample to investigate the influence of stand-off distance.

5. CONCLUSIONS

Repair and strengthening of concrete structures with fiber reinforced materials is mainly performed on existing structures with unknown properties. As expected, the properties of concrete will vary from structure to structure. As shown in previous sections, water jetting with high pressure is a very flexible process in sensitive surface preparation. It seems to be a logical approach to run a test on a concrete surface under selected parameters to identify the property of the concrete by the roughness index. Then, necessary adjustment of the operational parameters has to be made to produce the optimal surface condition. A waterjet end effector can be integrated with an imaging module for automated surface roughening.

6. ACKNOWLEDGEMENTS

The financial support by the Federal Highways Administration and American Concrete Institute is greatly appreciated. The authors are thankful to Dr. David Summers, University of Missouri - Rolla, for his valuable comments.

7. REFERENCES

Frenzel, L.M., Advisory Council, Private Communication, April 2001.

Galecki, G., 1983, "Drilling in Sandstone at Pressure Above 100 Mpa," Reports of the Institute of Machine Building Technology," Wroclaw Technical University, No. 23/83 - for Central Institute of Mining, Katowice.

Galecki, G., 1999, "Cutting/Cleaning Head Path Simulator," - unpublished material.

International Concrete Repair Institute, 1997, "Selecting and Specifying Concrete Surface Preparation for Sealers, Coating, and Polymer Overlays," Technical Guideline No. 03732".

Maerz, N.H., Chepur, P, Myers, J., and Linz, J., 2001, "Concrete Roughness Measurement Using Laser Profilometry for Fiber Reinforced Polymer Sheet Application," Presented at the Transportation Research Board 80th Annual Meeting, Jan. 7-11 2001, 12 pp.

Momber, A.W., 1993, "Handbuch Druckwasserstrahl-Technik," Beton-Verlag, GmbH, 1st Edition, Dusseldorf.

Momber, A.W., Ed. 1998, "Waterjet Applications in Construction Engineering," Balkema, Rotterdam, pp 163-175.

Myers J., Raghu, A., Mettemeyer, M., Nanni, A., "An Assessment of In-Situ FRP Shear and Flexural Strengthening of Reinforced Concrete Joists," Publication--ASCE Structures Congress, Philadelphia, PA, May 2000.

Nanni, A., Ed., 1993, "Fiber-Reinforced-Plastic (FRP) Reinforcement for Concrete Structures: Properties, Developments in Civil Engineering," Vol. 42, Elsevier, Amsterdam, The Netherlands, pp.450.

Silfwerbrand, J., 1990, "Improving Concrete Bond in Repaired Bridge Decks," Concrete Intern. 12 (9).

Summers, D.A., 1995, Waterjetting Technology, E & FN Spon, London, pp. 322-339.

DEVELOPMENT AND DESIGN OF SELF-ROTATING FORCED PULSED WATERJET: BASIC STUDY AND APPLICATIONS

W. Yan, C. Bai, A. Tieu and M.M. Vijay
^VL_N Advanced Technologies Inc.
Ottawa, Ontario, Canada

ABSTRACT

A nozzle body for producing rotating forced pulsed waterjets was designed, fabricated and tested. Several factors needed to be considered in the design: (i) self-rotation, (ii) acoustical tuning of the swivel, in addition to other requirements, and (iii) critical areas of the flow upstream of the orifices. The body consisted of four orifices - the inner two to generate the main forced pulsed waterjets and the outer two providing the torque necessary to rotate the nozzle. Tests were carried out to investigate: (i) the effect of several variables such as, the angles of the jets, and (ii) the potential of rotating forced pulsed waterjets for several industrial applications, particularly the removal of hard coatings. The pressure and flow were ≤ 69 MPa (10,000 psi) and 49 l/min (13 usgpm) respectively. The paper includes the details of fundamentals, and sample applications of the removal of hard coatings. Depending upon the type of coatings, removal rates varying from 0.66 m²/hr (7.1 ft.²/hr) to well over 23.2 m²/hr (250 ft.²/hr) were achieved. This compares favorably with the rates achieved with the ultra-high pressure ($\approx 30,000$ psi) continuous waterjet systems.

1. INTRODUCTION

Vijay and his co-workers have reported in several publications the mechanics of generating forced pulsed waterjets and their potential for a variety of industrial applications [Vijay (1992), Vijay & Foldyna (1994), Vijay, et al. (1995), Vijay, et al. (1997), Vijay (1998a), Vijay, (1998b), Vijay, et al. (1998c), and Vijay, et al. (1999)]. In all of these earlier studies a single-orifice non-rotating jet was investigated. Nonetheless, the results obtained on the removal of hard marine coatings were quite impressive [Vijay (1998a) and Vijay (1999)]. Removal rates of the order of $6.5 \text{ m}^2/\text{hr}$ ($70 \text{ ft}^2/\text{hr}$) were achieved with the single jet at a pressure of only 40 MPa (6,000 psi) and a flow of 22.7 l/min (6 usgpm). However, compared to the rates reported in the literature, achieved with the ultrahigh-pressure ($\geq 207 \text{ MPa}$; 30,000 psi) continuous waterjet systems [Kamareddine, et al. (1998)], it was realized that the rate of $6.5 \text{ m}^2/\text{hr}$ ($70 \text{ ft}^2/\text{hr}$) is not competitive, and hence the performance of pulsed waterjet system must be improved further.

One method of accomplishing high removal rates would be to move the single jet in successive adjacent paths ($\approx 5 \text{ mm}$ in width). Since the impact pressure of a pulsed waterjet is quite high compared to the corresponding continuous jet, it can be moved over the target at fairly high traverse rates (otherwise, substrate will be eroded). However, even with automation, it would be difficult to produce a smooth surface because of the striation effect (small rough widths between two adjacent swaths). Oscillating jets would probably leave the same effect. Thus, developing a rotating pulsed waterjet system seemed to be the best option as it would cover a swath $\geq 25 \text{ mm}$ (1 in) per pass, although it is not the most efficient way to distribute the jet energy over a surface. As there was no information on the rotating forced pulsed waterjet systems in the literature, careful attention had to be paid to several factors which were expected to influence the design. For instance, what effect would the geometry of the passage upstream of the orifices have on the characteristics of the pulses? Taking into careful consideration all of these factors, a rotating forced pulsed waterjet system was manufactured and successfully tested both in the laboratory and in the field. The details are given in the following Sections:

2. DESIGN CRITERIA

The criteria, both from the standpoint of performance and to satisfy the specifications dictated by industrial standards (e.g., NACE) for surface preparation, etc., were:

- To keep the pump pressure at or below 69 MPa (10,000 psi). This offers many advantages such as, ease of maintenance, low operating costs, etc.
- To limit water consumption to 49 l/min (13 usgpm), depending on the application.
- For hand-held operations, incorporate special features so that the weight of the gun is compensated by the reaction forces when pressurized. Currently, as the ultrasonic transducer is mounted on the gun [Vijay (1999)], it is slightly heavier than a conventional waterblast gun.
- To keep the system operator friendly. The operator should be able to operate the gun, pump and associated equipment with relative ease.
- Competitive performance compared to the existing ultrahigh-pressure continuous waterblasting systems.

3. DESIGN AND FABRICATION

The main design work was focused on the rotating part consisting of the swivel and the nozzle body. A major problem was the uncertainty whether well-defined pulsed waterjets will be produced by the nozzles inclined to the axis of rotation for self-rotation (see below). For this reason a four-orifice nozzle configuration was selected (see Figures 1 and 2), assuming that the two outer orifices would provide the torque required for self-rotation, while the two inner (main) orifices would generate pulsed waterjets to perform the actual work. The angles of the outer nozzles (see Figure 2) could be varied as required.

3.1 Effect of Inner Configuration of Multiple-Orifice Nozzle on Performance

In a rotating system (be it self-rotating or otherwise), generally two or more orifices are used. The concept of rotating nozzle systems is not new. In fact, a perusal of the literature shows that extensive work has been done, and continues to be done on the nozzles, swivels and other accessories including the mechanism of interaction between the jets and the target [Barker & Selberg (1978), Chen, et al. (1998), Feistkorn & Knickmeyer (1984), Harris & Brierley (1976), Hilaris & Bortz (1980), Hlaváč, et al. (1994), Hoshino, et al. (1976), Klich, et al. (1995), Lefin & Hurel (1984), Li, et al. (1997), Nagano, et al. (1974), Reichman & Cheung (1978), Wright, et al. (1999) and Zhang, et al. (1992), to name only a few]. This clearly indicates that the search for acceptable performance and reliable rotating waterjet systems has not abated [Wright, et al. (1999)]. In the case of a forced pulsed waterjet, the requirements are even more severe, particularly selecting proper dimensions of the inner passages and the swivel, as discussed below.

In the single-orifice forced pulsed jet shown in Figure 3, there is no interruption to the passage of water between the microtip and the nozzle exit. Although all the variables indicated in this figure influence the performance of the pulsed waterjet [Vijay & Foldyna (1994)], the velocity fluctuations induced in the flow by the tip pass freely through the orifice producing well-defined pulses [Vijay, et al. (1995)]. However, as shown in Figure 2, this would not be the case when the flow stream is divided into two or more branches to achieve self-rotation. The flow in the zone between the tip and the uncut part of the metal between the orifices becomes quite complex. Furthermore, what happens to the acoustic field in this zone is quite difficult to grasp theoretically or otherwise. Thus, some loss (probably considerable) in performance is inevitable. Indeed the data shown in Figure 4 bear this out. In this figure, the jets were not rotated and the symbols, such as 'a' have the meaning indicated in Figure 3 (A_m is the amplitude setting on the ultrasonic generator which corresponds to 0.45 kW of ultrasonic power = 2.6% of total hydraulic power). Mass loss of aluminum sample was used as a measure of performance. The performance of the dual-orifice nozzle is of the order of 40% of that achieved with a single-orifice of equivalent diameter. The advantage of the rotating system stems from the fact that the target experiences multiple passes (plus multiple impacts in the case of pulsed waterjet) of the jets over the same path [Hlaváč, et al. (1994)].

It must be noted that this loss also occurs in the case of continuous waterjet systems, may be to a lesser degree. It is possible, however, to minimize these losses by careful design of the nozzle profile upstream of the orifices [Barker & Selberg (1978), Reichman & Cheung (1978), Hilaris & Bortz (1980), Li, et al. (1997) and Wright, et al. (1999)].

3.2 Angle of the Jet

Just as in the case of a continuous waterjet, the angle of impingement of the rotating pulsed waterjet has significant influence on the performance. Since the orifices in the rotating head were not placed apart from each other, that is, their axes intersected the axis of rotation, the swath on the target would depend on the included angle between the jets and the standoff distance. This angle must be as large as possible without adverse effect on performance. In order to arrive at appropriate angles some tests were conducted. The results depicted in Figure 5 clearly indicate that the performance remains virtually intact up to an angle of inclination of about 10° . Although the performance deteriorates somewhat when the angle is increased to 20° , it could be used for some applications. However, when the angle increases beyond 20° , the performance decreases drastically. In the initial design, the value of the included angle was 12° .

3.3 Components for Self-Rotation

3.3.1 Outer Orifices for Self-Rotation

The sole purpose of the two outer orifices was to provide the torque necessary to rotate the two main inner jets. This choice was made as there was no certainty whether well-defined pulses would be formed if only the two inner orifices were selected (Figure 1). The diameters of the outer orifices and their separation (arm length) were just enough to provide the thrust force, and hence the torque required for self-rotation. For instance, at a pressure of 69 MPa (10,000 psi), two 0.51 mm (0.02 in) orifices at an arm length of 51 mm (2.0 in), provided a threshold torque of 0.113 N-m (25 in-lbf) which was considered to be adequate for self-rotation.

3.3.2 Swivel

As mentioned in **Section 3.1**, due to special requirements, it was not possible to simply purchase a readily available commercial swivel. It had to be custom designed to satisfy the requirements, particularly the internal diameter, length and the threshold torque. These requirements made the swivel larger than those commercially available, rated for the same pressure and flow. Although this increased the magnitude of the threshold torque, the outer jets took care of that requirement.

4. ENERGY DISTRIBUTION OVER THE TARGET

In the case of a rotating jet, any point on a sample is under repeated loading condition. At a particular point on a sample, the loading condition is equivalent to a rapidly changing impact by the jet. The total number of impacts a point receives depends upon the rotating speed, traverse speed of the jet, the diameter of jet at the target (a function of standoff distance), and the location of point relative to the centre of rotation of the jet. The number of impacts can be calculated by:

$$n_i = 2 \frac{w_p}{V_{tr}} N$$

where,

n_i - Number of impacts on the sample by a dual-orifice rotating nozzle,

w_p - diameter of jet at the target surface, *mm*

V_{tr} - jet traverse speed, *m/min*,

N - rotating speed of nozzle head, *RPM*

For instance, for a jet diameter of 5 mm (0.2 in) at the target surface, rotational speed of 3000 RPM, and a traverse speed of 1.27 m/min (50 in/min), a point 'A' (Figure 6A) near the moving center of the rotating head will receive 24 impacts by the jet from a dual orifice nozzle.

For the same conditions described above, a point 'B' (Figure 6A) near the inner edge of the rotating jet and perpendicular to the moving direction receives about 150 impacts. This is estimated by:

$$n_i = 4 \frac{\sqrt{w_p D}}{V_{tr}} N$$

where, D - the distance between the two orifices, *mm*.

The dwell time of each impact at any given point is a function of w_p , V_{tr} and N . However the duration of impact is sensitive to the sequential number of the impacts. While the duration is minimum for the first and the last impacts, it is longest (maximum) for the middle impact. The longest duration for a single impact, for the parameters used above, is 1.25 ms. In this period, this particular point receives a total of 25 additional impacts by the forced pulsed jet! This is why the pulsed jet has considerable advantage over continuous waterjet, and can do the same job at lower pump pressure and hydraulic power.

5. EXPERIMENTAL WORK

Both laboratory and field tests were conducted to evaluate the performance of the newly developed rotating forced pulsed waterjet gun shown in Figure 7. To date, the results have not only been quite promising, but also quite useful for incorporating further improvements.

5.1 Laboratory Tests

5.1.1 Visualization of the Jet

In order to ensure that forced pulses are indeed formed by the rotating dual-orifice nozzle, a few visualization tests were conducted using a combination of STROBOTAC (General Radio Model 1538-A, Maximum RPM = 150,000), a regular 8-mm video camera and a Mini-DV digital camera. Since the characteristics of the pulsed jet is not affected significantly by rotation, the tests were

conducted with no rotation, and at a pressure of 13.8 MPa (2,000 psi). In a dark room, with the ultrasonic generator on, the strobe was tuned gradually until a quasi-stationary stream of pulses could be seen. A series of digital video pictures was then taken. A typical photograph is illustrated in Figure 8. The pulses can be seen quite clearly, and the appearance is identical to the photograph shown in Figure 9, taken with a pulsed laser by Vijay, et al. (1995). As discussed by these authors, the superior performance of the pulsed waterjet compared to the corresponding continuous waterjet stems from the large mushroom shaped pulses.

5.1.2 Removal of Coatings

In this series of tests, several types of coatings were removed with the rotating pulsed waterjets, all at pressures ≤ 69 MPa (10,000 psi). The rotational speed was measured to be approximately 2,800 RPM. Both hand-held and automatic (that is, mounting the samples on the X-Y gantry) operations were conducted. The performance indicators were (a) surface finish (profile) and (b) area removal rates. It should be pointed out that no quantitative measurements were taken to assess the surface profile. However, based on the inspection made by the clients, it is believed that the profiles met the specifications of NACE, or other organizations.

Heavily Rusted Samples: Figure 10 shows the rusted samples mounted on the gantry. It is clear that the rust is completely removed to bare metal finish. The area removal rate was about $9.6 \text{ m}^2/\text{hr}$ ($103 \text{ ft}^2/\text{hr}$), deemed to be competitive with the rates achieved with sandblasting.

Automobile Bumper Caster: This particular caster (Figure 11) had about 14 layers of hardened paint [Vijay, et al. (1997)]. All the layers are removed to bare metal finish. The area removal rate was about $23.2 \text{ m}^2/\text{hr}$ ($250 \text{ ft}^2/\text{hr}$). The width of the swath per pass is almost 50 mm (2.0 in).

Automobile Support Racks (Figure 12): These supports are used for mounting various automobile components for painting. Over a period of time they become completely covered with several layers of paint which need to be removed on a regular basis. Once again all layers of paint were removed to the satisfaction of a potential client. It should be noted that with automatic operation, about 60 racks per hour could be processed with the pulsed jet technique, almost four times the desired rate.

Marine Samples: Several types of coatings are used in the marine industry [Vijay, et al. (1998a) & (1999)]. Generally, they are epoxy based coatings. The hardness (that is, the bond to the metallic substrate) can be gaged by the variations in the removal rates achieved with the jets at the same operating parameters. The sample shown in Figure 13A, consisting of three layers (1-GP-171 @ 2 mils, 1-GP-207 @ 6 mils and 1-GP-207 @ 6 mils), is used in special (critical) areas of the ships. The fact that the area removal rate at 69 MPa (10,000 psi) was only $0.66 \text{ m}^2/\text{hr}$ ($7.1 \text{ ft}^2/\text{hr}$) confirms that the coating is indeed very hard. The sample depicted in Figure 13B also had three layers (Amercoat 160 @ 2 mils, Amercoat 185 HS @ 1.5 mils and 1-GP-61 @ 1.5 mils) and yet the removal rate was almost $25.5 \text{ m}^2/\text{hr}$ ($275 \text{ ft}^2/\text{hr}$) at the same operating pressure. These data clearly indicate that the removal rates are highly dependent on the strength of the bond (hardness) to the substrate.

Irregular Shaped Components: These are jigs used to support automotive parts for glueing. Figure 14A shows the components before exposure and Figure 14B after the exposure to pulsed waterjet.

The magnitude of pressure was only about 45 MPa (6,500 psi). The total time taken to remove the baked-on adhesive from all the components was of the order of 60s.

5.2 Field tests

Field Demonstration in the USA: This demonstration took place at an automotive plant in the USA. The purpose of the demonstration was to prove that forced pulsed waterjet technology is a cost-effective technique, and could be used to replace chemical stripping or burning (in the incinerators). Figures 15A and B show the various types of racks used by the company for mounting and painting automobile parts (for example, side moldings). The demonstration was conducted with the hand-held gun which the operator had no problem in handling as the weight was balanced by the reaction forces. Figure 15C shows a close-up view of the painted rack and Figure 15D clearly shows the layers (up to 20 layers) removed to bare metal finish.

Paper Mill Contract Job: This work is described in great detail in a parallel paper at this Conference [Tieu, et al. (2001)]. Figure 16 shows the head of roller after cleaning with the rotating forced pulsed waterjet machine. As concluded by Tieu, et al., the job was quite successful.

6. CONCLUSIONS

A rotating forced pulsed jet system was developed and tested. Both laboratory and field trials at fairly low operating pump pressures (≤ 69 MPa; 10,000 psi) have clearly established its potential for many industrial applications, particularly industrial cleaning and coatings removal.

7. ACKNOWLEDGMENTS

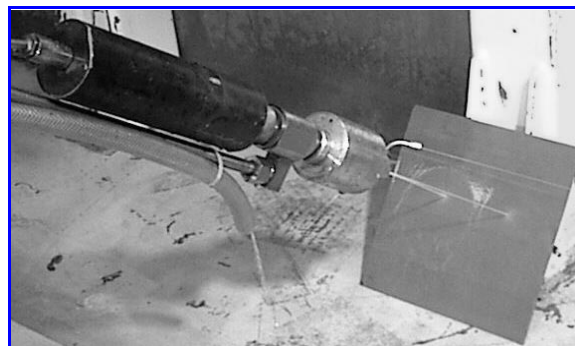
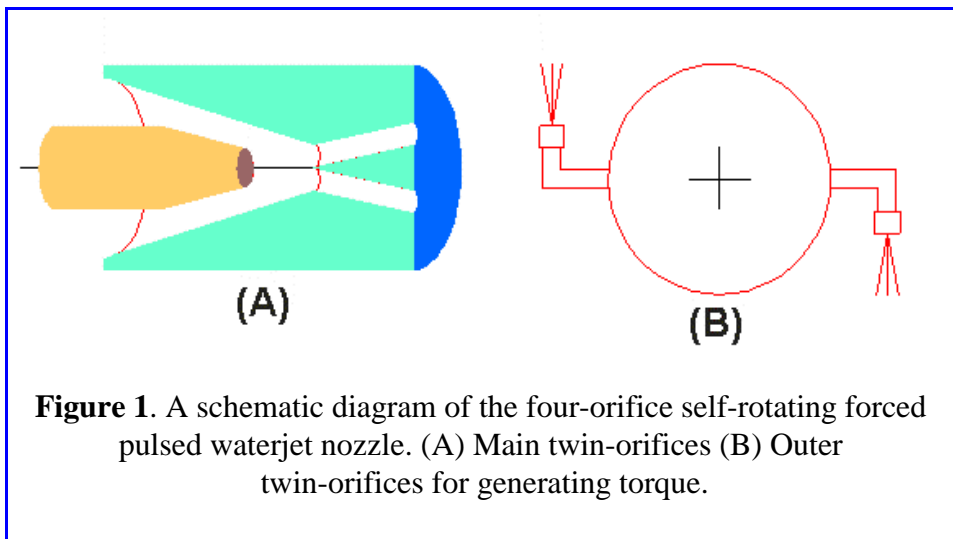
The work described in this paper was partially funded by the Government of Canada (IRAP - Industrial Research Assistance Program administered by the National Research Council of Canada, and SR&ED Credit administered by the Canada Customs & Revenue Agency). This is gratefully acknowledged.

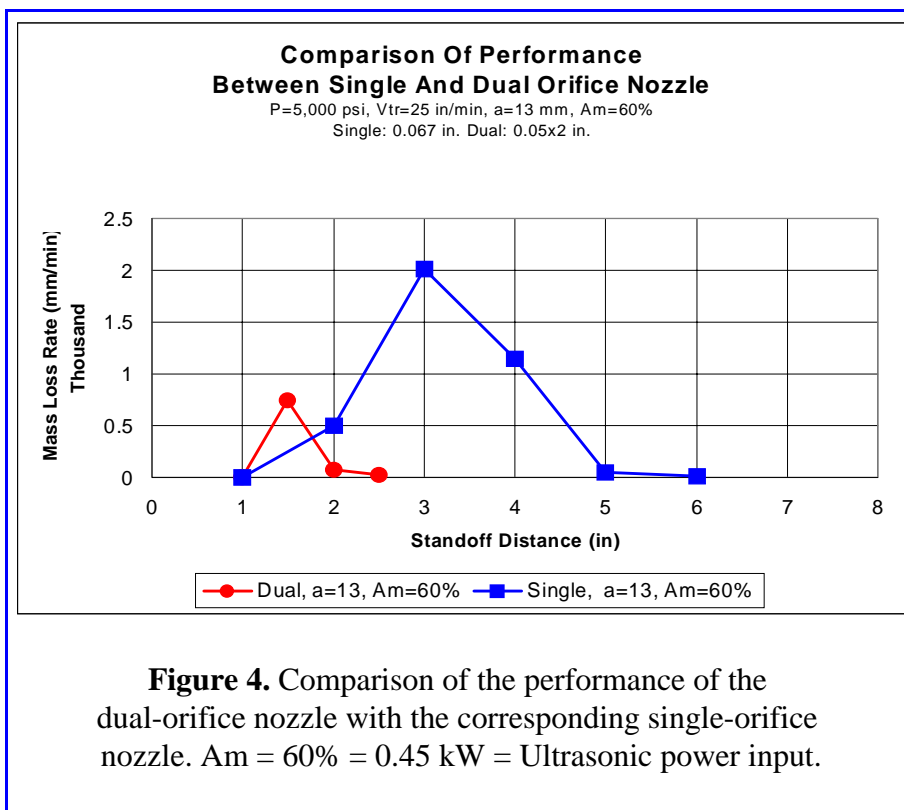
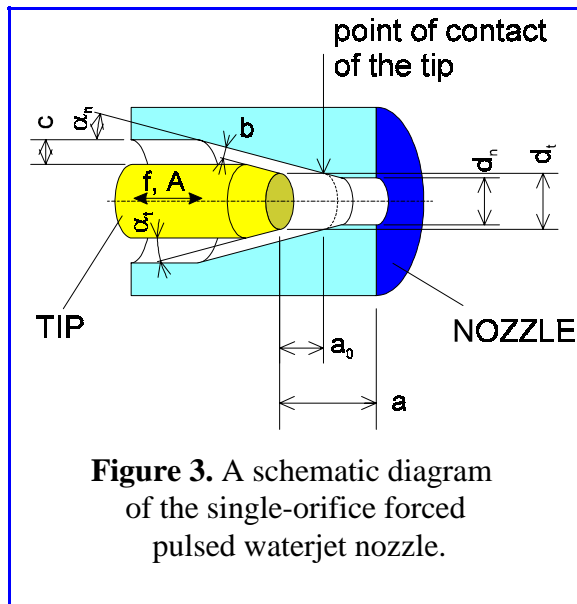
8. REFERENCES

- Barker, C.R., and B.P. Selberg, "Water Jet Nozzle Performance Tests," *Proceedings of the 4th International Symposium on Jet Cutting Technology*, Paper A1, BHRA Fluid Engineering, Cranfield, Bedford, England, 1978.
- Chen, Z.W., S.X. Xue, W.P. Huang, Y.B., Fan and H.J. Peng, "Technology of Rotary Heads for Oil Pipes' Inner and Outer Surfaces Cleaning," *Proceedings of the 5th Pacific Rim International Conference on Water Jet Technology*, pp. 182-187, WJTSJ, Tokyo, Japan & ISWJT, Ottawa, Canada, 1998.

- Feistkorn, E., and W. Knickmeyer, "Tests on Water Jet Assisted Drilling of Shot Firing Boreholes in Abrasive Rocks," *Proceedings of the 7th International Symposium on Jet Cutting Technology*, Paper H5, pp. 469-480, BHRA Fluid Engineering, Cranfield, Bedford, England, 1984.
- Harris, H.D., and Brierley, W.H., "Removing Rock with a Rotating High Speed Water Jet," *Proceedings of the 3rd International Symposium on Jet Cutting Technology*, Paper G3, BHRA Fluid Engineering, Cranfield, Bedford, England, 1976.
- Hilaris, J.A., and S.A. Bortz, "Field Study for Highway Maintenance Application of Jet Cutting Technology," *Proceedings of the 5th International Symposium on Jet Cutting Technology*, Paper C2, pp. 97-104, BHRA Fluid Engineering, Cranfield, Bedford, England, 1980.
- Hlaváč, L.M., L. Sitek and J. Vašek, "Using of the Physical Model to the Evaluation of an Efficiency of the Tools Creating Multiple-Motions of the Nozzles," *Proceedings of the 12th International Conference on Jet Cutting Technology*, pp.255-264, BHR Group Conference Series, Publication No. 13, Cranfield, Bedford, England, 1994.
- Hoshino, K., T. Nagano, K. Takagi, Y. Narita and M. Sato, "The Development and the Experiment of the Water Jet Drill for Tunnel Construction," *Proceedings of the 3rd International Symposium on Jet Cutting Technology*, Paper E4, BHRA Fluid Engineering, Cranfield, Bedford, England, 1976.
- Kamareddine, I., D. Girard and R. Schmid, "Fully Automated Systems for Surface Preparation with the Ultrahigh-pressure Waterjet," *Proceedings of the 14th International Conference on Jetting Technology*, pp.499-510, BHR Group Conference Series, Cranfield, Bedford, England, 1998.
- Klich, A., A. Kalukiewicz and L. Jarno, "Construction and Investigation of the Polish Roadheading Machine with High-Pressure Water Jet Assistance," *Proceedings of the 4th Pacific Rim International Conference on Water Jet Technology*, pp. 311-322, WJTSJ, Tokyo, Japan, 1995.
- Lefin, Y., and A. Hurel, "Rotary Drilling Assisted by Water Jets and Other Recent Developments of High Pressure Water Jets for the Cutting of Rocks in France," *Proceedings of the 7th International Symposium on Jet Cutting Technology*, Paper H3, pp. 439-454, BHRA Fluid Engineering, Cranfield, Bedford, England, 1984.
- Li, G., J. Ma, X. Shen and H. Chen, "A Study of Descaling of Water Injection Tubing by Water Jet," *Proceedings of the 9th American Water Jet Conference*, pp.603-611, Water Jet Technology Association, St. Louis, Missouri, USA, 1997.
- Nagano, T., K. Hoshino and Y. Narita, "The Development of a Water Jet Drilling Machine," *Proceedings of the 2nd International Symposium on Jet Cutting Technology*, Paper E1, BHRA Fluid Engineering, Cranfield, Bedford, England, 1974.
- Reichman, J.M., and J.B. Cheung, "Waterjet Cutting of Deep-Kerfs," *Proceedings of the 4th International Symposium on Jet Cutting Technology*, Paper E2, BHRA Fluid Engineering, Cranfield, Bedford, England, 1978.

- Tieu, A.H, W. Yan, C. Bai, M.M. Vijay and J. Szemeczko, "The Removal of Hardened Grease Deposits from Steam Dryers in a Paper Mill: First Successful Contract Application of Forced Pulsed Waterjet," *Proceedings of the 11th American Water Jet Conference*, Water Jet Technology Association, St. Louis, Missouri, USA, 2001.
- Vijay, M. M., "Ultrasonically Generated Cavitating or Interrupted Jet," U. S. Patent No. 5,154,347, 1992.
- Vijay, M.M., and J. Foldyna, "Ultrasonically Modulated Pulsed Jets: Basic Study," *Proceedings of the 12th International Conference on Jet Cutting Technology*, pp.15-36, BHR Group Conference Series, Publication No. 13, Cranfield, Bedford, England, 1994.
- Vijay, M.M., M. Jiang & M. Lai, "Computational Fluid Dynamic Analysis and Visualization of High Frequency Pulsed Water Jets," *Proceedings of the 8th American Water Jet Conference*, pp.557-572, Water Jet Technology Association, St. Louis, Missouri, USA, 1995.
- Vijay, M.M., E. Debs, N. Paquette, R. Puchala & M. Bielawski, "Removal of Coatings with Low Pressure Pulsed Water Jets," *Proceedings of the 9th American Water Jet Conference*, pp.563-580, Water Jet Technology Association, St. Louis, Missouri, USA, 1997.
- Vijay, M.M., "Design and Development of a Prototype Pulsed Waterjet Machine for the Removal of hard coatings," *Proceedings of the 14th International Conference on Jetting Technology*, pp.39-57. BHR Group Conference Series, Cranfield, Bedford, England, 1998a.
- Vijay, M.M., "Pulsed jets: Fundamentals and Applications," *Proceedings of the 5th Pacific Rim International Conference on Water Jet Technology*, pp. 9-23. WJTSJ, Tokyo, Japan & ISWJT, Ottawa, Canada, 1998b.
- Vijay, M.M., J. Remisz, J. Foldyna & P.E. Grattan-Bellew, "Preweakening of Hard Rocks with Ultrasonically Generated Pulsed Waterjets," *Proceedings of the 5th Pacific Rim International Conference on Water Jet Technology*, pp. 479-496. WJTSJ, Tokyo, Japan & ISWJT, Ottawa, Canada, 1998c.
- Vijay, M.M., W. Yan, A. Tieu & C. Bai, "Removal of Hard Coatings from the Interior of Ships Using Pulsed Waterjets: Results of Field Trials," *Proceedings of the 10th American Water Jet Conference*, pp.677-694, Water Jet Technology Association, St. Louis, Missouri, USA, 1999.
- Wright, D., J. Wolgamott and G. Zink, "Nozzle Performance in Rotary Applications," *Proceedings of the 10th American Water Jet Conference*, pp.905-919, Water Jet Technology Association, St. Louis, Missouri, USA, 1999.
- Zhang, L., Q. Zhang and Yang, J., "Movement Track and Parameter Optimization of a Space Type Rotary Cleaning Head," *Proceedings of the 3rd Pacific Rim International Conference on Water Jet Technology*, pp. 295-304, WJTSJ, Tokyo, Japan, 1992.





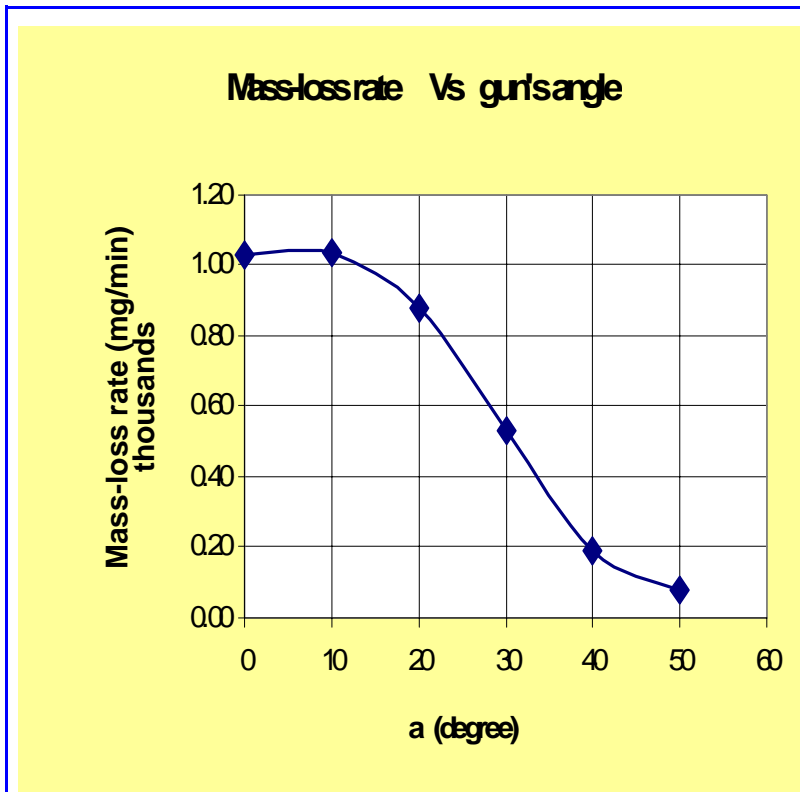


Figure 5. Plot showing the effect of angle of impingement (angle of the jet with respect to the axis of rotation) on performance, using mass-loss of aluminum samples as measure of performance.

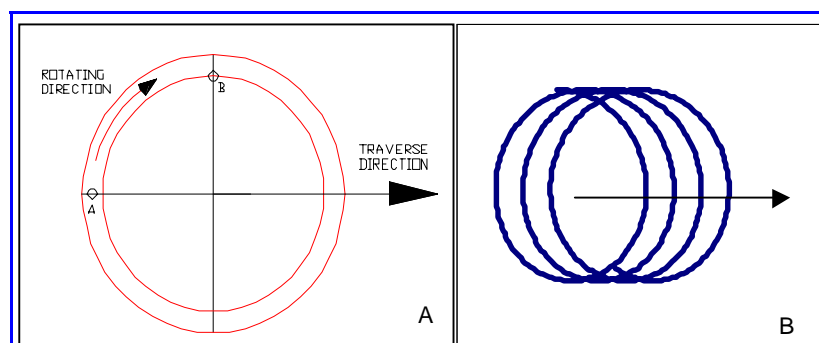


Figure 6. Schematic diagram for analysis of the effect of location relative to moving direction on impact time. (A) Location of points relative to rotation center and moving direction; (B) Pattern made by rotating jets.

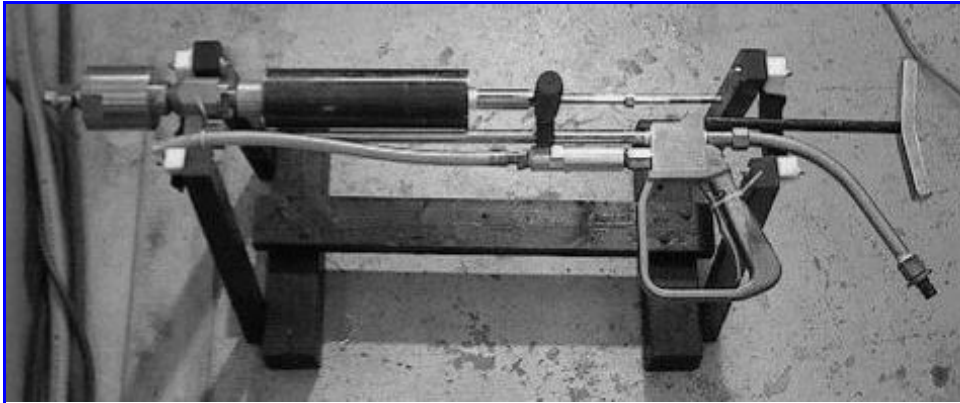


Figure 7. A general view of the new hand-held gun for operating with the self-rotating forced pulsed waterjets.



Figure 8. Typical appearance of the forced pulsed waterjet from a dual-orifice nozzle.

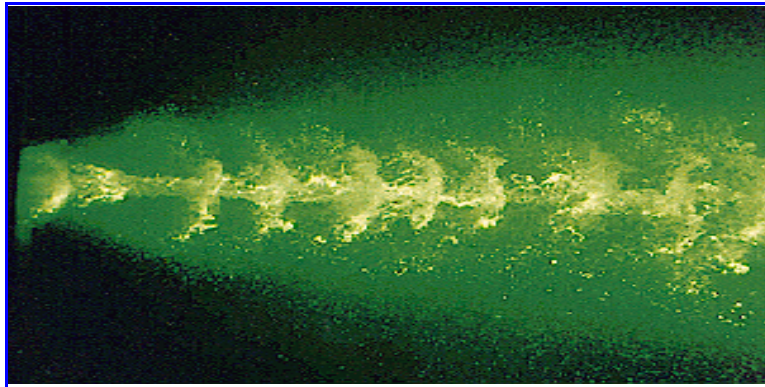


Figure 9. Appearance of a pulsed waterjet taken with a 4-6 ns duration Nd-Yag laser [Vijay, et al. (1995)].

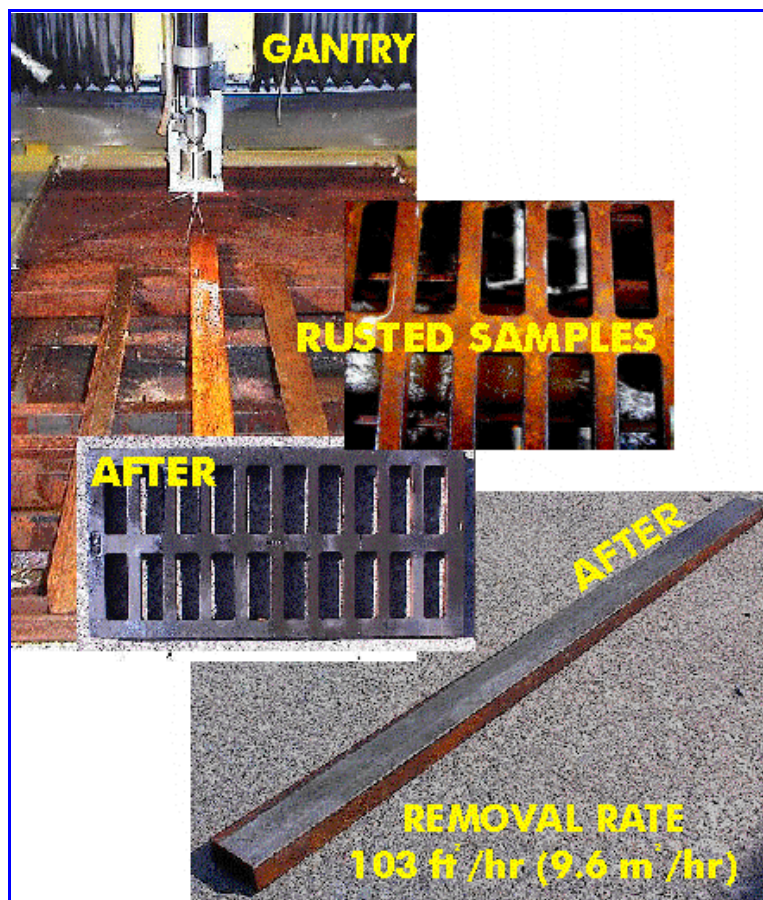


Figure 10. Gun with the rotating head on the gantry showing the heavily rusted samples before and after exposing to rotating forced pulsed waterjet.



Figure 11. Multiple layers (~ 14 layers) of paint removed with the rotating forced pulsed waterjet from the auto bumper casters. (B) Closed-up of the surface finish.

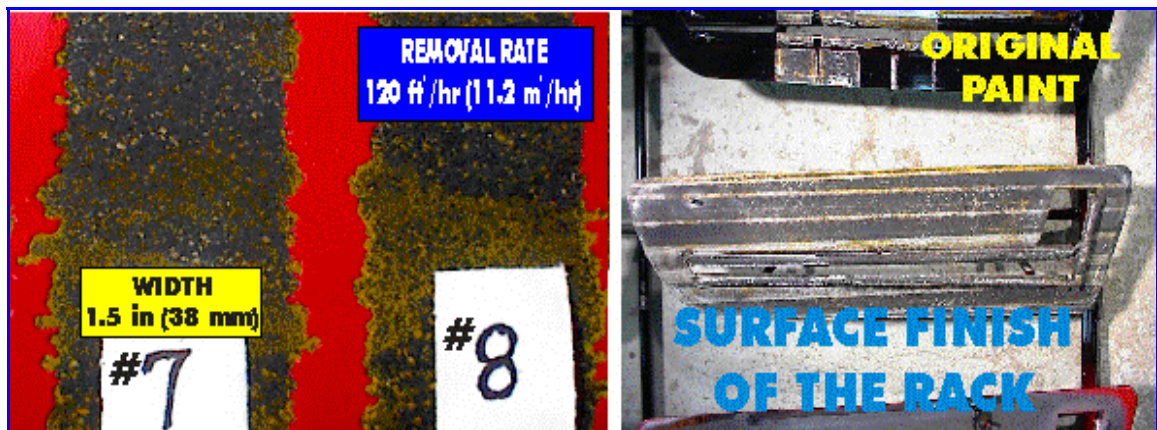


Figure 12. Multiple layers of paint removed from the support racks used for mounting various auto components for painting. Photos show typical widths removed per pass and removal rate.

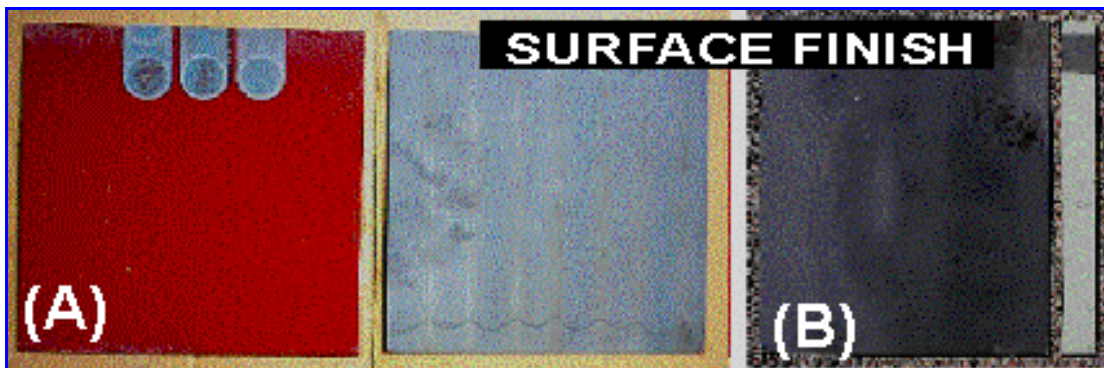


Figure 13. A general view of the marine coatings removed with the rotating pulsed waterjet. (A) Removal rate = $0.66 \text{ m}^2/\text{hr}$ ($7.1 \text{ ft}^2/\text{hr}$), (B) Removal rate = $25.5 \text{ m}^2/\text{hr}$ ($275 \text{ ft}^2/\text{hr}$).

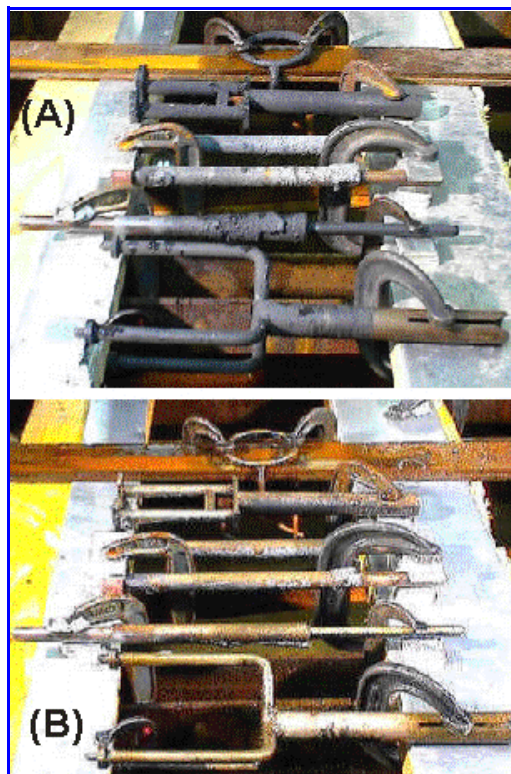


Figure 14. The removal of very hard coatings (combustion deposits) from several irregular shaped components.

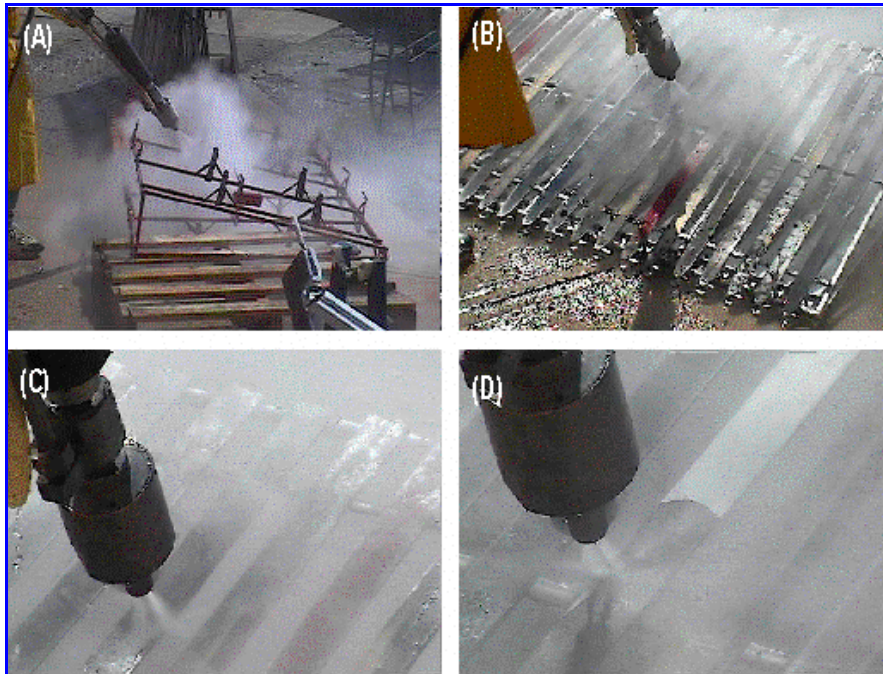


Figure 15. Field demonstration of the rotating system for the removal of hard paint (up to 20 layers) from automobile racks for a client in the USA. (A) & (B) general views of the racks; (C) close-up view of the rotating jets; (D) close-up view of the coatings removed to bare metal finish.



Figure 16. A general view of the head of the roll after cleaning with the forced pulsed waterjet (rust is believed to be acceptable).

THE USE OF THE THEORY OF SONICS FOR PRODUCING HIGH PRESSURE PULSATORY WATER JETS

A. Magyari, N. Ilias, Gh. Roman, S. Radu
University of Petrosani
Petrosani, Romania

ABSTRACT

In order to generate high pressure pulsatory water jets, in this paper, a sonic pressure amplifier is used, which is based on the sonorous resounding phenomenon. The increase of the liquid pressure is caused by the water by an alternative moving mobile piston. At a certain oscillation frequency of the piston linked with the active length of the amplifier, stationary waves of the pressure occur, with knots and antinode loops, the pressure being periodically capable of reaching very high values. By releasing from the amplifier in these moments a part of the liquid, the pulsatory water jet is generated. The compensation of the evacuated liquid is made using a low pressure pump.

1. INTRODUCTION

It is well known that pulsatory water jets are more efficient in the crushing and dislocation of materials than continuous jets, because of their dynamic action.

The molding of the pulsatory front (plane, cylindrical or spherical) has a tremendous effect on the value of the pressure developed in the impact point. Pulsatory jets have an important penetrating and crushing potential of the materials, but instead they are not suitable for accurate cutting of the materials.

So far, there have been built many types of devices for producing pulsatory jets, which differ from one another as to the way in which the pulsations are being produced: producing one or more low frequency impulses; modulation of a continuous jet in order to produce the pressure pulsations.

In this paper, in order to amplify the pressure the phenomenon of sonorous resonance is being used. Due to the multiple reflection of the waves produced in water by a piston, an important increase of the pressure amplitude takes place, the water under pressure being released periodically from the amplifier, forming the pulsatory jet.

2. PRINCIPLE OF THE METHOD

The principle used in this paper to create high pressures is based on the fact that every elastic medium of a certain geometrical shape can constitute a resounding cavity for mechanic waves of a specific frequency. For this frequency there is the possibility to determine the geometrical parameters of this cavity, in such a way that after this is filled with water, due to a pulsatory mechanic energy against the liquid column, stationary waves energy in this cavity, that use a given number of knots and antinode loops, having a constant position in time. If from outside, supplying with pulsatory energy continues (without introducing water in addition), with the frequency of which the resounding cavity has been built, the water pressure increases in such a way that it can lead to the mechanic destruction of the cavity.

The fundamental principles that lay to the basis of the calculus of the resounding cavity for mechanic energy are the following:

- the propagation of the mechanic energy is made on an elastic medium;
- the mechanic energy propagates in the elastic medium by means of longitudinal mechanic waves;
- the propagation of the energy in the elastic medium obeys the principle of Huygens;
- the reflection of a mechanic wave against a stiff wall is produced with a periodicity, equal to half of the wave length or by changing of the phase.

The principle described is illustrated in Figure 1.

The piston, which is driven by a rod-crank mechanism or by an eccentric mechanism, pulses alternatively with constant speed at the end of a fully filled liquid pipe.

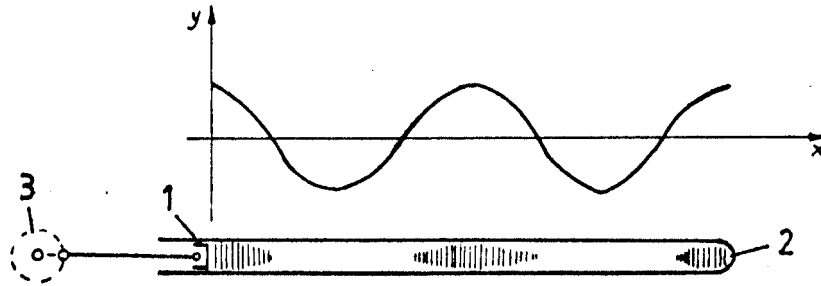


Figure 1. The principle of the generating of stationary waves

The longitudinal wave generated by the first pulse of the piston propagates to the opposite end of the pipe which is shut by a stiff wall, reflects by changing the phase and then reaches the piston against where it suffers a second phase changing reflection. If the length of the pipe is a whole number of wave semilengths ($L = n \lambda / 2$), then the reflected wave on the stiff wall, when reaching the piston, supraposes in phase with the new created wave and thus, when the next pulse of the piston takes place, a higher amplitude wave will propagate through the pipe. The condition of resonance being imposed, stationary waves of pressure, with minimums and maximums will be generated in the pipe.

If the piston continues its alternative movement with the same frequency, the value of the pressure in the maximum points increases very much, leading to a possible mechanical destruction of the pipe.

In principle, if in a point of minimum pressure of the pipe, additional liquid is injected, and if in a point of maximum pressure a liquid evacuation nozzle is mounted, it is possible to obtain a high pressure pulsatory liquid jets generator.

3. THE MATHEMATICAL ASSESSMENT OF THE PHENOMENON

The phenomenon of generating and amplifying the pressure of the liquid can be assessed using the dependence relations in the theory of sonics, theory in which the phenomenon of conveying the mechanical energy through elastic mediums is dealt with using the analogy with the phenomenon of alternative electric current propagation in electric circuits.

3.1 Sonic Currents

The continuous flowrate in short pipes is:

$$\dot{v} = v w \quad (1)$$

where v is the cross-sectional area of the pipe and w is the current moving speed.

The flow rate produced by a simple alternative moving piston inside a cylinders:

$$i = I \sin (at + \varphi) \quad (2)$$

The amplitude of the sonic current:

$$I = r a \Omega \quad (3)$$

The angular speed:

$$a = 2 \pi n \quad (4)$$

The number of the driving mechanism rotations:

$$n = \frac{1}{T} \quad (5)$$

where T is the period of the complete run of the piston.

The efective value of the flow rate:

$$I_{2ef}^2 = \frac{1}{T} \int_0^t i^2 dt = \frac{I^2}{2} \quad (6)$$

The efective speed of the fluid:

$$v_{ef} = \frac{I_{ef}}{\varpi} \quad (7)$$

The volume displaced by the piston after a complete run:

$$\delta = 2 r \Omega = 2 \frac{I}{a} \quad (8)$$

3.2 Sonic Pressures

The changing pressure produced by the piston inside the pipe is:

$$p = H \sin (at + \varphi) + p_m \quad (9)$$

where H is the maximum alternative pressure and p_m is the average existing pressure in the pipe.

The minimum and maximum pressure:

$$p_{\min} = p_m - H \quad (10)$$

$$p_{\max} = p_m + H \quad (11)$$

The instant sonic pressure between two points is:

$$h = p_1 - p_2 = H \sin (at + \varphi) \quad (12)$$

The effective sonic pressure:

$$H_{\text{ef}} = \frac{H}{\sqrt{2}} \quad (13)$$

The pressure function of the flow rate:

$$h = R i \quad (14)$$

where R is the resistance due to the friction

$$R = k \rho \frac{1}{\omega} \quad (15)$$

where k is a coefficient and ρ is the density of the liquid.

3.3 The Sonic Power

$$W = \frac{1}{T} \int_0^T Ri^2 dt = \frac{RI^2}{2} \quad (16)$$

$$W = \frac{RI^2}{2} = \frac{HI}{2} = H_{\text{ef}} \cdot I_{\text{ef}} \quad (17)$$

3.4 Sonic Displacement

$$\delta = \int_{t_1}^{t_2} i dt \quad (18)$$

where δ is the volume of the displaced fluid in the $t_2 - t_1$ time interval.

If the flow rate is a simple harmonic function, than

$$i = I \cos at \quad (19)$$

$$\delta = I \int_{t_1}^{t_2} \cos at = \frac{I}{a} (\sin at_2 - \sin at_1) \quad (20)$$

The amplitude of the sonic displacement:

$$\Delta = \frac{I}{a} \quad (21)$$

$$I = a \Delta = r a \Omega \quad (22)$$

$$\Delta = r \Omega \quad (23)$$

3.5 Hydraulic Capacities and Condensers

As a hydraulic capacity it has considered an accumulating tank or a free piston inside a cylinder, which is in connection with a spring device which communicates with a pipe filled with liquid.

The sonic capacity is:

$$C = \frac{\delta}{h} \quad (24)$$

$$\delta = \omega f = C h \quad (25)$$

where f is the displacement of the piston and h is the pressure of the liquid.

If the piston is retained by a spring,

$$f = A F \quad (26)$$

where A is a constant of the spring and F is a force that drives the piston.

$$F = \omega h \quad (27)$$

$$f = A \omega h \quad (28)$$

$$\text{or} \quad C = A \omega^2 \quad (29)$$

$$\text{and} \quad F = \frac{f}{A} = \frac{f \omega^2}{C} \quad (30)$$

The capacity of the liquid columns in the pipes:

$$C = \frac{V}{E} \quad (31)$$

where V is the volume of the liquid and E is the elasticity coefficient of the liquid.

In the case of water:

$$C = \frac{V}{20000} \quad (32)$$

The sonic capacity of a pipe:

$$C = \frac{l\omega}{E_1} \quad (33)$$

where E_1 is the coefficient of elasticity of the metal of the pipe.

3.6 Sonic Inertia

The inertia is influenced by the moving mass and by the area which the force that caused the moment is applied:

$$L = \frac{M}{\omega^2} = \frac{G}{g\omega^2} \quad (34)$$

The inertia of a column of liquid inside a pipe is:

$$L = \rho \frac{1}{\omega} \quad (35)$$

The relations referred to above, completed with others, used in the strength of materials have been the basis for the designing calculus of the pressure amplifier presented in this paper.

4. THE CONCEIVING OF THE SONIC PRESSURE AMPLIFIER

Using the principle described above, a sonic pressure amplifier has been conceived for the generating of a pulsatory water jet.

The imposed final pressure was 100 MPa for a flow rate of 80 l/min. The functioning regime of the amplifier is the resounding one ($L C a^2 = 1$), for which, a wave length of 6.283 cm has resulted. The dimensions and the sonic parameters are determined in such a way that the imposed

performance parameter are ensured, resulting an active length of the amplifier of 94.25 cm. The external diameter is about 15 cm, and the length is 100 cm.

The constructional scheme of the amplifier can be seen in Figure 2.

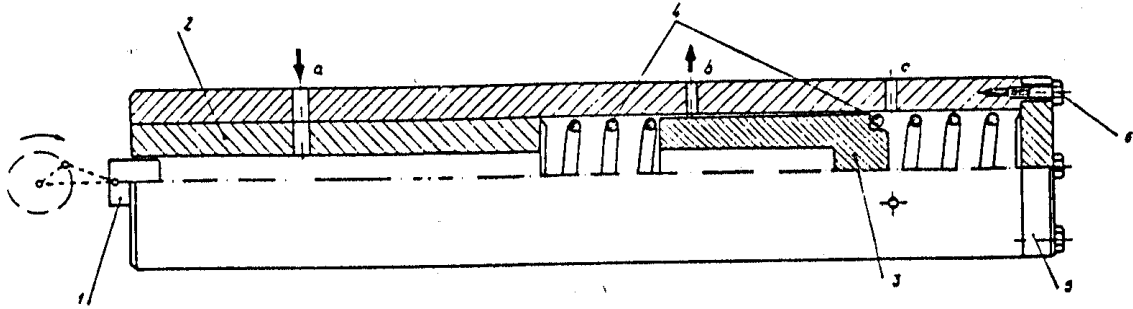


Figure 2. Constructional scheme of the sonic amplifier

The piston 1 generates longitudinal waves in the column of liquid with a wave length determined by calculations. The inertia and the capacity of the liquid in the cylinder 2, of the internal piston 3 and the elicoidal springs 4 are in such a way determined that there is a wave centre in point “b” and a knot in point “a”. While the piston 1 is functioning, water is being introduced through the orifice “a” from low pressure pump. Due to the multiple reflection of the waves, an important increase of the amplitude of the pressure takes place, the orifice “b” opens and some of the water leaves the cylinder.

Because the orifice “b” is placed in a point of maximum of wave, a high pressure water jet will go out through it. After the liquid jet is delivered, the oscillation amplitude of the piston 3 decreases and the process begins again. This way the installation is able to generate high speed pulsatory liquid jets.

Water drips caused by the untightness of the piston 3 are eliminated through the orifice “c”.

The general scheme of the installation is shown in Figure 3.

The supplying with water of the cylinder “A” is made using the low pressure pump “C”, protected by the valve “E”, through a hydrostatic accumulator “D” and the direction valve “B”.

The installation is capable of generating a pressure of 100 MPa, with a frequency of the pulsatory jet of 25 pulsation per second, at a flow rate of 80 l/min. The driving power required is 20 kW.

Having tested experimental model, the performance parameters are not reported to have been altered compared to the designed ones.

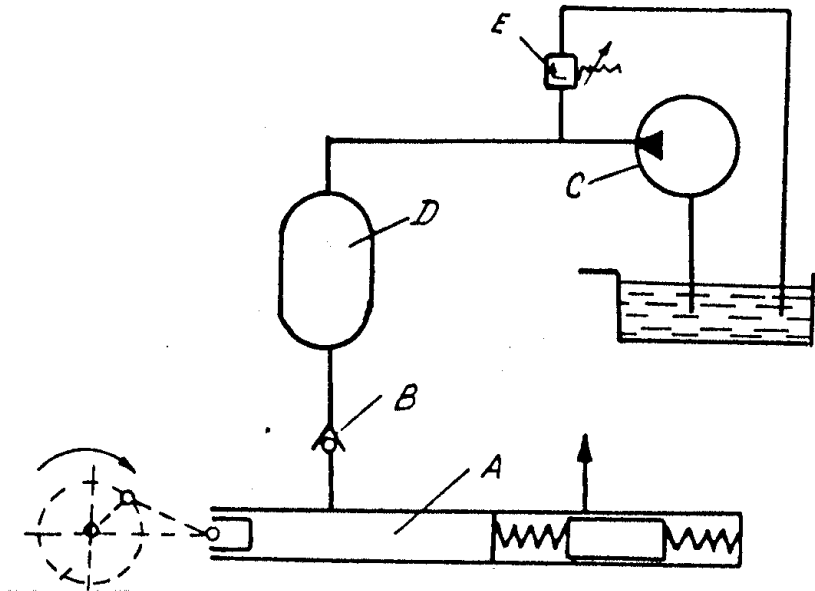


Figure 3. The general scheme of the installation

5. CONCLUSIONS

The use of sonics for the amplifying of the pressure stands out in a very high efficiency compared to the differential pressure amplifiers, requiring a lower energy consumption.

The installation is also remarkable for its simple design, small sizes and high reliability.

6. REFERENCES

Ilias, N., Magyari, A., and Radu, S. "Devices and apparatus for creating and measuring the parameters of water jets", Proceedings of the 3rd International Symposium on Mine Mechanisation and Automation, Lulea, 1995.

Ilias, N., Magyari, A., Radu, S. et al. "A new type of dynamic plough", Scientific Papers of the I.M. Petro• ani, Vol. XVIII, 1986.

7. NOMENCLATURE

ω -	cross-section of the pipe (cylinder)
v -	current moving speed of the liquid
r -	length of the crank or the eccentricity
a -	angular speed of the crank
Ω -	cross section of the piston
φ -	angle of the phase
r -	number of the driving mechanism rotation
T -	period of a complete run of the piston
H -	maximum alternative pressure
p_m -	average existing pressure in the pipe
R -	hydraulic resistance due to the friction
ρ -	density of the liquid
l -	length of the pipe
δ -	volume of the displaced fluid
Δ -	amplitude of the sonic displacement
C -	hydraulic capacity
h -	pressure of the liquid
E -	elasticity coefficient of the liquid
E_1 -	elasticity coefficient of the metal of the pipe
L -	sonic inertia
V -	volume of the liquid

MODULATED VS. CONTINUOUS JETS: PERFORMANCE COMPARISON

J. Foldyna, L. Sitek
Institute of Geonics of the Czech Academy of Sciences
Ostrava, Czech Republic

ABSTRACT

Forced modulation of a continuous stream of water represents the most promising method of pulsed jet generation because of its simplicity and practicality. Experimental results obtained with the ultrasonic vibration of a tip situated inside the nozzle indicate that using this technique one can achieve performance of the jet even order of magnitude higher in comparison to continuous jet at the same hydraulic parameters (Vijay & Foldyna, 1994). Regardless the fact that experimental results presented so far were obtained using mostly empirical approach, they proved that the forced modulation of high velocity water jets could serve as viable method for further increasing of the efficiency of the technology. Performance of ultrasonically modulated jets in cutting of various materials was tested in laboratory conditions in the Institute of Geonics in Ostrava. In this paper, results obtained in cutting of brass, mild steel, rock and concrete samples using modulated water jets are presented. The performance of the jet was evaluated in terms of rate of mass loss and/or depth of cut. The results are compared with those obtained with continuous jets at the same operating parameters. Potential of forced modulation of the jet is discussed.

1. INTRODUCTION

Despite the impressive advances made in the field of water jet technology during the last decades, the use of water jets for hard rock mining and other underground engineering applications remains unattractive. The main reason for this apparent lack of interest is that the performance of water jet techniques is not competitive with the existing conventional mechanical systems. Therefore, extending the use of water jets to these areas requires significant improvement in their performance.

From an analysis of the impact of a water jet on a target, it can be shown that the impact pressure generated by a slug of liquid is considerably higher than the corresponding stagnation pressure generated by a continuous jet. Therefore, if a continuous jet could be divided into a train of slugs, the resulting pulsed jet could significantly improve the performance in the cutting of hard rocks. Furthermore, one can assume that additional effects (for example, enhanced penetration and the subsequent crack propagation in the material) due to impact of pulsed jets may provide new methods for the cutting and fracturing of hard and brittle materials.

Since the early seventies, incessant attempts have been made for generating various types of pulsed water jets (Vijay, 1994). In this paper, attention is focused on a particular method of generating pulsed jets that involves modulating a continuous stream of water with an ultrasonic vibrator situated upstream of the nozzle exit.

Unlike single pulse and interrupted jets, a modulated jet escapes from the nozzle as a continuous stream of liquid having unsteady velocity (cyclically modulated over time). Slow and fast portions of each cycle tend to flow together, forming a train of “bunches” in the free stream, which eventually separate.

At present, an extensive research program is performed in the Institute of Geonics in Ostrava oriented at the evaluation of potential of modulated jets in cutting of various materials as well as at the understanding of fundamental processes occurring both within and outside the nozzle during ultrasonic modulation of the jet. In this paper a brief discussion on force effects of modulated jets compared to that of continuous jet is given, followed by examples of cutting performance of the modulated jet in metallic, rock and concrete samples. The results are compared to that obtained with continuous jets at the same operating parameters.

2. BACKGROUND

The method of ultrasonic modulation of the jet was described in detail by Vijay et al. (1994), and Vijay & Foldyna (1994). A detailed description of the concept and configuration of the ultrasonic nozzle can be found in Puchala & Vijay (1984) and Vijay (1992). The modulation of a jet is produced by the vibrating tip of an ultrasonic velocity transformer located inside a nozzle. The vibration is generated by an ultrasonic transducer connected to the velocity transformer.

The geometric configuration of the nozzle with the vibrating tip inserted upstream the nozzle exit is shown in Figure 1. The tip vibrates axially with amplitude A so that both the distance a and the gap b periodically changes from maximum to minimum values. The ultrasonic nozzle can be

“tuned” by setting the distance a to obtain maximum modulation of the high-speed water jet. However, the distance a has to be large enough to avoid contact between the nozzle surface and the tip.

3. TESTING EQUIPMENT

The tests presented in the paper were performed using plunger pump capable to deliver up to 43 l/min of water at pressure up to 120 MPa. Ultrasonic nozzle was equipped with piezoelectric transducer vibrating at 20 kHz (at maximum power of 600 W). Force effects of the jet were measured by the apparatus for the measurement of stagnation force of the jet, consisting of piezoelectric force sensor and charge amplifier. The apparatus was developed at the Institute of Geonics in Ostrava (for more details on apparatus and measurement method, see Vala, 1994, and Foldyna & Sitek, 2000). Data acquisition and processing was performed using PC-based measuring system. The measured time domain signal was transformed using FFT to obtain frequency domain of the signal.

4. RESULTS AND DISCUSSION

4.1 Force Effects of Modulated Jet

Series of measurement of force effects of the modulated jet was performed under following testing conditions: operating pressure of 20 MPa, nozzle diameter of 1,98 mm, and ultrasonic power of 600 W. Standoff distance was changed during the tests. To compare force effects of modulated jet with force effects of continuous jet, another series of measurement was performed with continuous jet under the same operating parameters (except the ultrasonic power was set to 0 W).

The results of the measurement of force effects indicate significant difference between modulated and continuous jets. The time domain of stagnation force shows that the stagnation force of the modulated jet varies periodically from minimum to maximum values. At certain standoff distance, valleys of the signal equal to zero stagnation force – this corresponds to the complete separation of the jet into individual slugs of water. An example of time and frequency domains of stagnation force of modulated jet can be seen in Figure 2. The time domain indicates that the amplitude of stagnation force of the modulated jet varies in time within the range from 0 up to 400 N. The frequency domain exhibits relatively flat spectrum with strong peak of 128 N at frequency of about 20.2 kHz that corresponds to the modulation frequency of the jet (i.e. exciting frequency of piezoelectric transducer).

On the other hand, the time and frequency domains of stagnation force of continuous jet show that the stagnation force oscillates around certain level of the force – this corresponds to static load with relatively small dynamic component. An example of time and frequency domains of stagnation force of continuous jet is presented in Figure 3. Flat frequency spectrum with gradual increasing of the amplitude towards higher frequencies corresponds to impact of continuous stream of water accompanied by impact of small droplets of water due to natural break-up of the jet.

4.2 Cutting of Metallic Samples

Two types of materials were selected for the tests of cutting of metallic samples: mild steel CSN 11 375 of the low carbon range (C max. 0.20%, P max. 0.05%, S max. 0.05%, minimum tensile strength 363 MPa, minimum yield strength 235 MPa, density 7850 kg/m³) and brass CSN 423223 (58% Cu, 40% Zn, 2% Pb, minimum tensile strength 412 MPa, density 8300 kg/m³). Thin discs 40 mm in diameter and 5 mm thick were manufactured and used as test specimens.

Tests were conducted at pressure of 40 MPa, nozzle diameter was 1.98 mm, standoff distance 140 mm, traversing velocity 30 mm/min, and ultrasonic power was set to 600 W. The standoff distance of 140 mm was found to be optimum for the operating parameters specified above in previous tests. In order to compare the performance of modulated jet with the continuous jet, tests with the latter were performed using standard nozzle for continuous jet and at the same values of operating parameters. Rate of mass loss calculated using following equation was used as a measure of performance:

$$\Delta m_s = \frac{\Delta m \cdot v_{tr}}{s} \quad (1)$$

Experimental results are presented in Figure 4 for mild steel samples and Figure 5 for brass samples. In both cases, while the modulated jet formed an irregular slot both in shape and depth, the kerf produced by the continuous jet is hardly visible. The rates of mass loss obtained for steel and brass samples were 705.7 mg/min, and 1077.6 mg/min respectively for cuts made using modulated jet. On the contrary, rates of mass loss were 19.3 mg/min for steel sample and 1.6 mg/min for brass sample only.

4.3 Cutting of Rock Samples

Medium grained sandstone (locality Řeka) and medium grained granodiorite (locality Žulová) were selected as testing materials for tests of cutting of rock samples. Physical properties of sandstone and granodiorite were as follows: sandstone – compressive strength 115 MPa, tensile strength 5.8 MPa, Young's modulus 19.7 GPa, density 2652 kg/m³, unit weight 2495 kg/m³, porosity 5.8%; granodiorite – compressive strength 144.5 MPa, tensile strength 11.3 MPa, Young's modulus 45 GPa, density 2648 kg/m³, unit weight 2610 kg/m³, porosity 1.41%.

Tests were performed at pressure of 40 MPa, nozzle diameter was 1.98 mm, standoff distance 140 mm, and ultrasonic power was set to 600 W. Again, the standoff distance of 140 mm was found to be optimum for the operating parameters specified above in previous tests. Cuts in rock samples were conducted at two traversing velocities – 0.10 and 0.25 m/min in sandstone, and 0.5 and 1.0 m/min in granodiorite. Again, in order to compare the performance of modulated jet with the continuous jet, tests with the latter were performed using standard nozzle for continuous jet and at the same values of operating parameters. Average depth of cut calculated from five arbitrary measurements taken along the path of the jet was used as a measure of performance of the jet.

Results are presented in Figure 6 for sandstone and in Figure 7 for granodiorite samples. In sandstone samples, both jets formed quite regular slots at both traversing velocities. However,

average depths of cut obtained with modulated jet are 2 to 3 times higher compared to that obtained with continuous jet. In granodiorite samples, while modulated jet formed fairly regular slots again, slots produced by continuous jet are irregular both in shape and depth, being formed mostly by breaking out of rock chips. Again, average depths of cut produced by modulated jet are 2.8 to 3 times higher compared to that produced by continuous jet.

4.4 Cutting of Concrete Samples

Concrete samples were prepared according to prescriptions given in Table 1. Two classes of concrete were obtained by the change of grit component in concrete No. 2. Compressive strengths and densities of concrete samples are also given in Table 1.

Tests were conducted at pressure of 40 MPa, nozzle diameter was 1.98 mm, standoff distance 140 mm, and ultrasonic power was set to 600 W. Yet again, the standoff distance of 140 mm was found to be optimum for the operating parameters specified above in previous tests. Cuts in concrete No. 1 samples were conducted at two traversing velocities – 2 and 5 m/min, cuts in concrete No. 2 at the only traversing velocity of 2 m/min. In order to compare the performance of modulated jet with the continuous jet, tests with the latter were performed using standard nozzle for continuous jet and at the same values of operating parameters. Average depth of cut calculated from five arbitrary measurements taken along the path of the jet was used as a measure of performance of the jet.

Results are presented in Figure 8 for concrete No. 1 and in Figure 9 for concrete No. 2 samples. In both classes of concrete, both types of the jet formed quite irregular slots both in shape and depth at both traversing velocities, being formed mostly by breaking out of cement chips along larger grit grains. However, slots formed by modulated jet are more regular, especially at higher traversing velocity (see Figure 8c and 8d). In all cases, average depths of cut obtained with modulated jet are approximately 1.5 times higher compared to that obtained with continuous jet.

5. CONCLUSIONS

Measurement of stagnation force of the modulated high-speed water jet shows that there is significant difference between force effects of modulated and continuous jets. While the modulated jet produces only dynamic load on the target with high level of peaks at certain standoff distances, the load on the target produced by the continuous jet is static with relatively small dynamic component.

Results obtained in cutting of metallic samples show clearly the potential of modulated jets. The performance of modulated jet was approximately 36 times higher in mild steel and even more than 670 times higher in brass compared to performance of continuous jet at the same operating parameters if one takes the rate of mass loss of the sample as a measure of the jet performance.

In rock and concrete cutting, the performance of modulated jet was 2 to 3 times higher in rock and about 50% higher in concrete compared to performance of continuous jet at the same operating parameters if the average depth of cut is taken as a measure of the jet performance. Authors believe, however, that the performance of modulated jet can be further improved,

especially in rock and concrete cutting, by proper matching of operating parameters, such as operating pressure and traversing velocity. Investigations in these areas are in progress in the laboratory.

6. ACKNOWLEDGEMENT

Presented work was performed within the framework of research project of the Grant Agency of the Czech Republic, project No. 105/00/0235. Authors are thankful for the support.

7. REFERENCES

- Foldyna, J., and Sitek, L., "Methodology of evaluation of nozzles for high-speed water jet generation", *Proceedings of the 6th Pacific Rim International Conference on Water Jet Technology, October 9 – 11, 2000, Sydney, Australia*, pp. 127-131, CMTE Australia, 2000.
- Puchala, R.J., and Vijay, M. M., "Study of an ultrasonically generated cavitating or interrupted jet: Aspects of design", *Proceedings of 7th International Symposium on Jet Cutting Technology*, Paper B2: pp 69-82, Ottawa, Canada, 1984.
- Vijay, M. M., Foldyna, J., and Remisz, J., "Ultrasonic Modulation of High-Speed Water Jets", *In: Geomechanics 93 (Proceedings of the International Conference Geomechanics 93, Hradec/Ostrava/Czech Republic/28-30 September 1993)*, pp. 327 – 332, Z. Rakowski, Editor, A. A. Balkema Publishers, Rotterdam, Netherlands, 1994.
- Vijay, M. M., "Ultrasonically generated cavitating or interrupted jet", *U. S. Patent No. 5,154,347*, 1992
- Vijay, M. M., "Power of pulsed liquid jets", *In: Geomechanics 93 (Proceedings of the International Conference Geomechanics 93, Hradec/Ostrava/Czech Republic/28-30 September 1993)*, pp 265-274, Z. Rakowski, Editor, A. A. Balkema Publishers, Rotterdam, Netherlands, 1994.
- Vala, M., "The measurement of the non-setting parameters of the high pressure water jets", *In: Geomechanics 93 (Proceedings of the International Conference Geomechanics 93, Hradec/Ostrava/Czech Republic/28-30 September 1993)*, pp 333-336, Z. Rakowski, Editor, A. A. Balkema Publishers, Rotterdam, Netherlands, 1994.
- Vijay, M. M., and Foldyna, J., "Ultrasonically Modulated Pulsed Jets: Basic Study", *In: 12th International Conference on Jet Cutting Technology*, pp 15-35, N. G. Allen, Editor, BHR Group Conference Series, Publication No. 13, Mechanical Engineering Publications Limited, London, 1994.

8. NOMENCLATURE

A	amplitude of vibration of the tip of the velocity transformer [mm]
a	distance from the tip of velocity transformer to the exit plane of the nozzle [mm]
b	clearance between conical sections of the transformer and the nozzle [mm]
d	nozzle diameter [mm]
h	average depth of cut [mm]
Δm	mass loss [mg]
Δm_s	rate of mass loss [mg/min]
p	operating pressure [MPa]
P_U	ultrasonic power [W]
s	cut length [mm]
S	standoff distance [mm]
v_{tr}	traverse velocity [mm/min]

Table 1. Prescriptions and basic physical properties of concrete samples.

	Concrete No. 1	Concrete No. 2
Prescriptions		
Cement	CEM I 42.5 R Mokrá (412 kg)	CEM I 42.5 R Mokrá (412 kg)
Sand 0 – 4 mm	Locality Žabčice (780 kg)	Locality Žabčice (780 kg)
Grit 8 – 16 mm	Amphibolite - locality Želešice (1020 kg)	Digged sand - locality Žabčice (1020 kg)
Water	210 kg	210 kg
Basic physical properties		
Density	2526 kg/m ³	2367 kg/m ³
Compressive strength	37.3 MPa	28.0 MPa

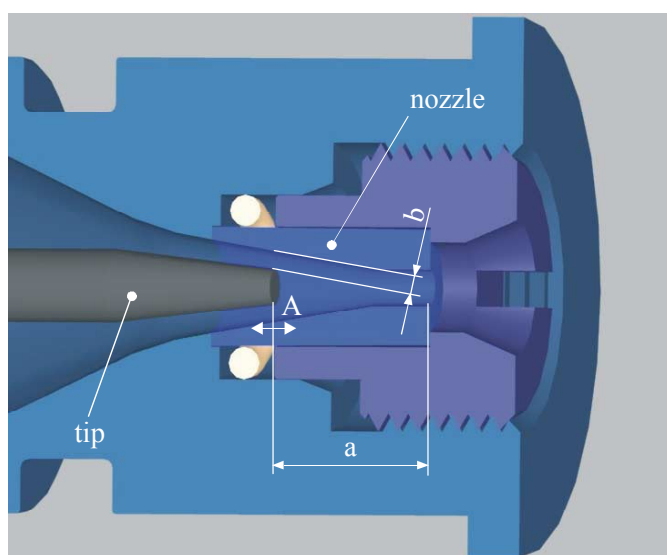


Figure 1. Geometric configuration of the ultrasonic nozzle.

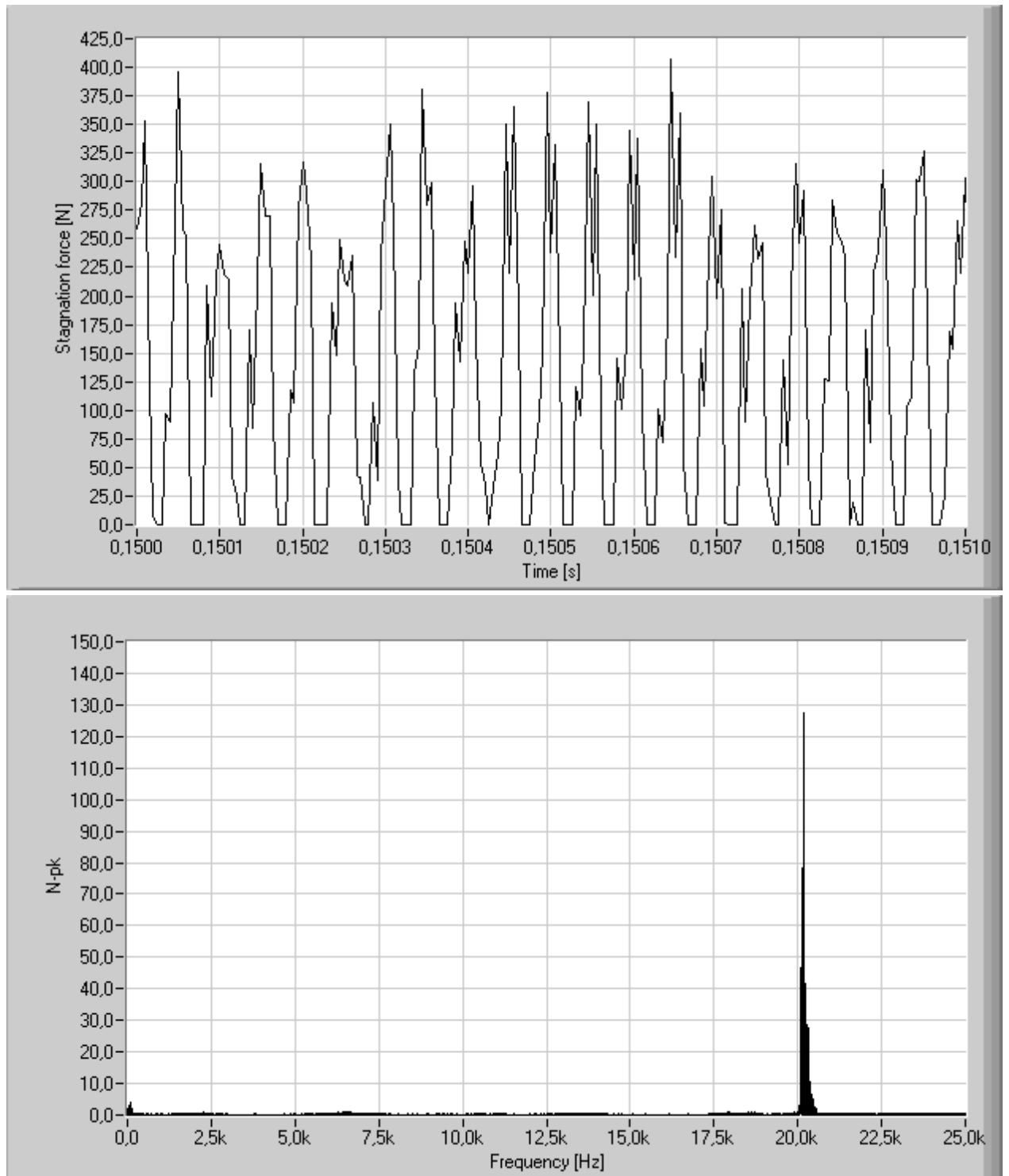


Figure 2. Time and frequency domains of stagnation force of modulated jet. Testing conditions: $p = 20$ MPa, $d = 1.98$ mm, $P_U = 600$ W, $S = 40$ mm.

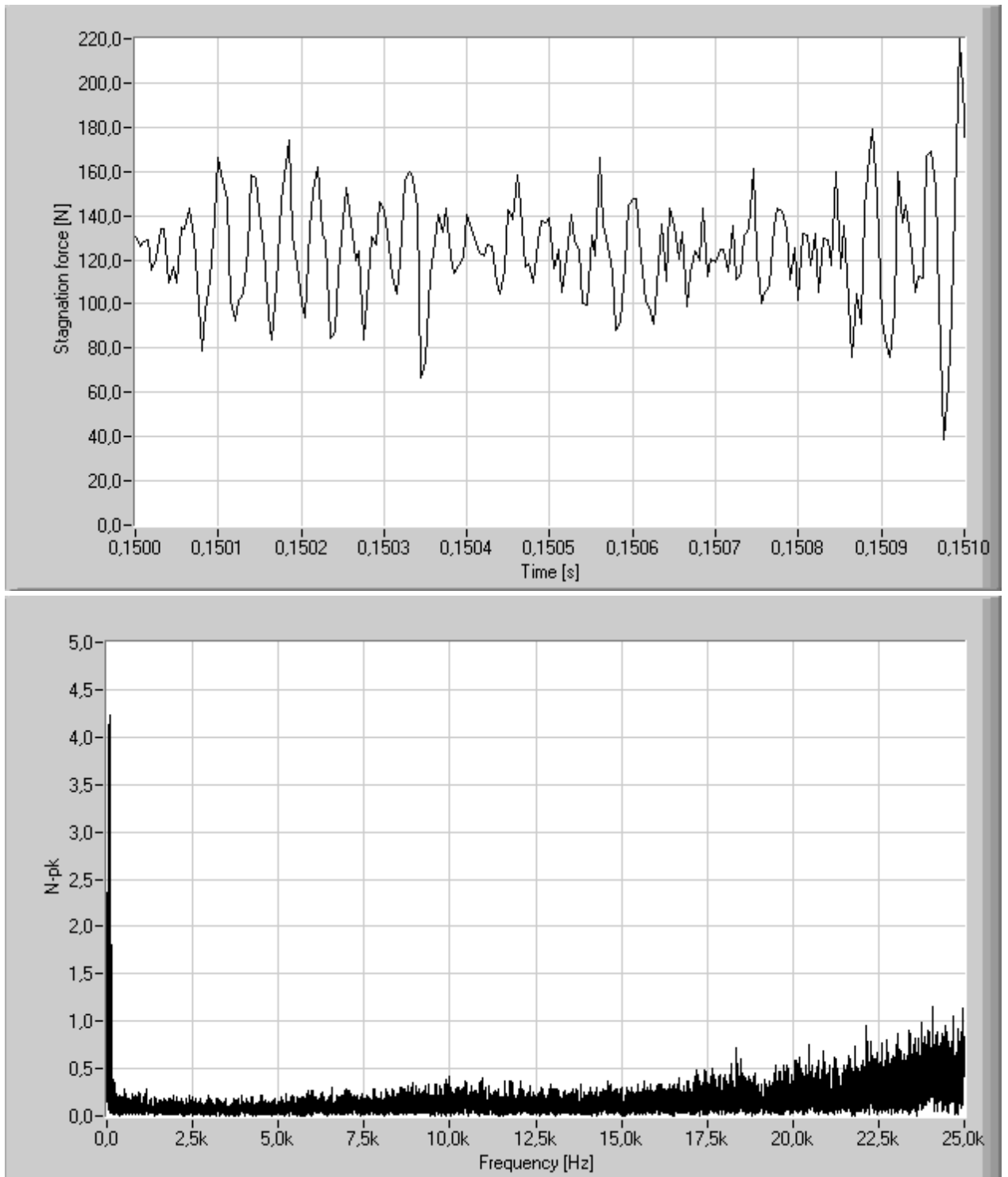


Figure 3. Time and frequency domains of stagnation force of continuous jet. Testing conditions: $p = 20$ MPa, $d = 1.98$ mm, $S = 40$ mm.

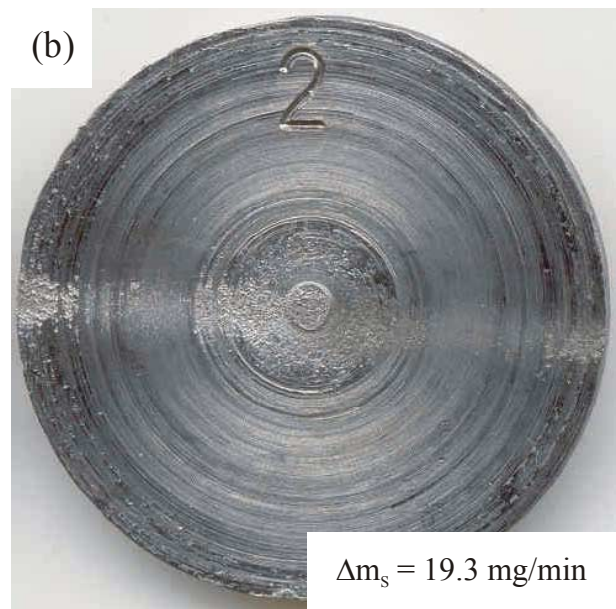
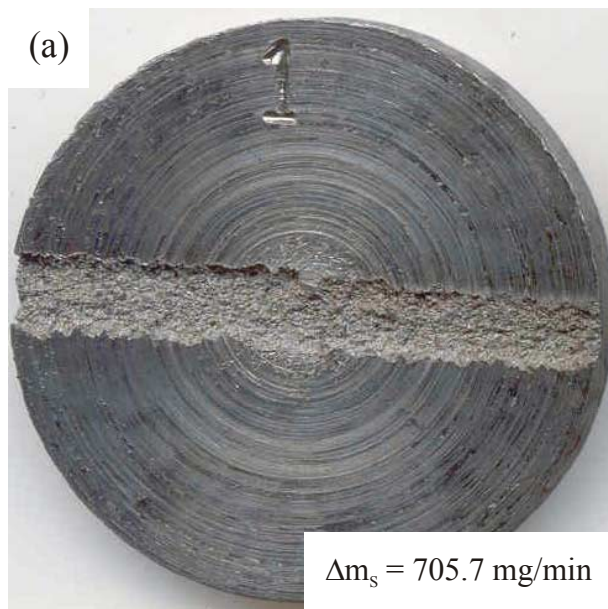


Figure 4. Mild steel CSN 11 375 exposed to (a) modulated jet and (b) continuous jet. ($p = 40 \text{ MPa}$, $d = 1.98 \text{ mm}$, $v_{tr} = 30 \text{ mm/min}$, $S = 140 \text{ mm}$)

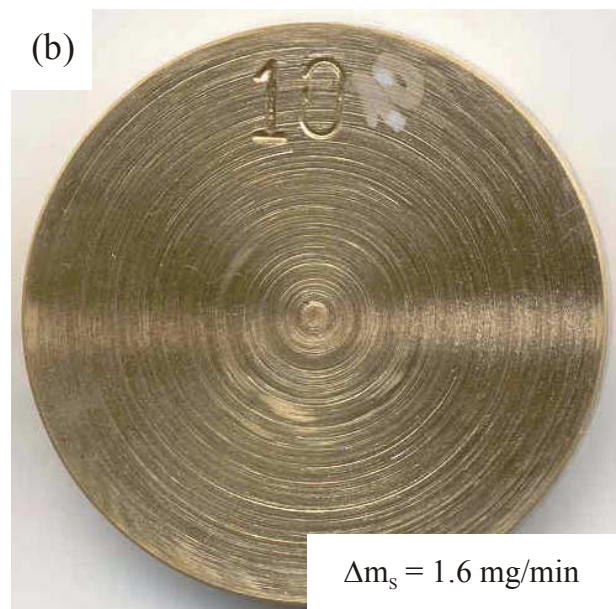
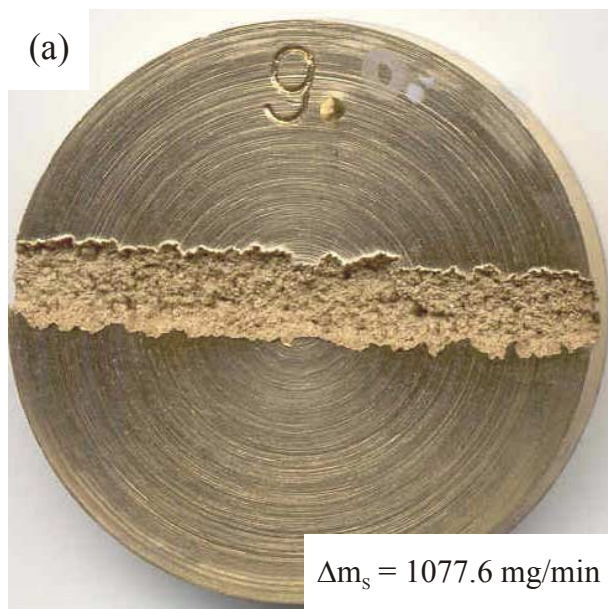


Figure 5. Brass CSN 423223 exposed to (a) modulated jet and (b) continuous jet. ($p = 40 \text{ MPa}$, $d = 1.98 \text{ mm}$, $v_{tr} = 30 \text{ mm/min}$, $S = 140 \text{ mm}$)

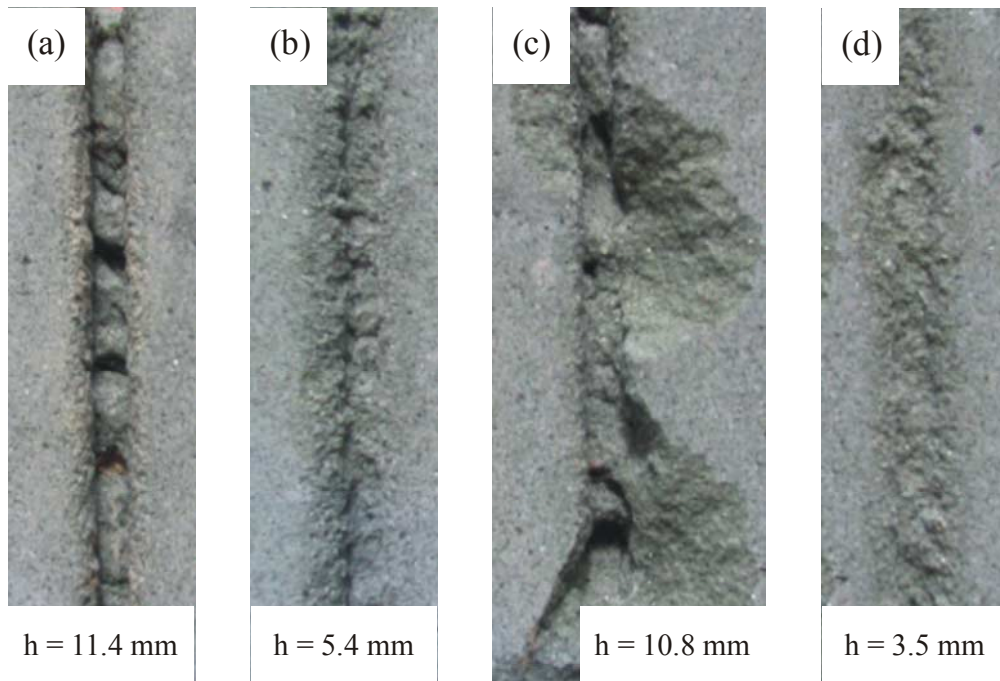


Figure 6. Sandstone exposed to modulated jet (a, c) and continuous jet (b, d). ($p = 40$ MPa, $d = 1.98$ mm, $v_{tr} = 100$ mm/min (a, b), and $v_{tr} = 250$ mm/min (c, d), $S = 140$ mm)

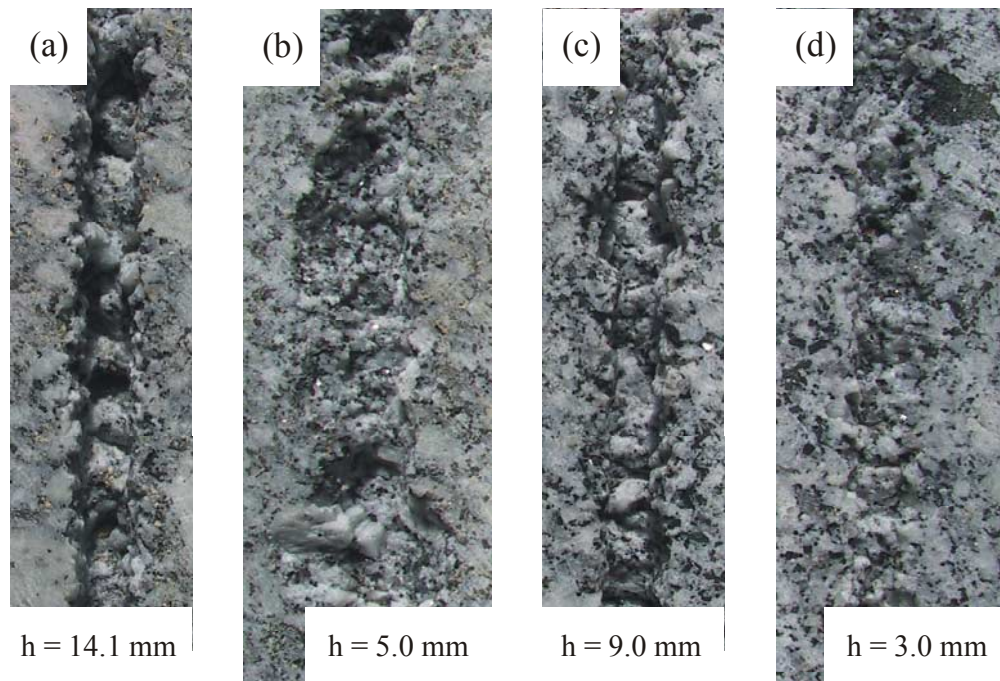


Figure 7. Granodiorite exposed to modulated jet (a, c) and continuous jet (b, d). ($p = 40$ MPa, $d = 1.98$ mm, $v_{tr} = 500$ mm/min (a, b), and $v_{tr} = 1000$ mm/min (c, d), $S = 140$ mm)

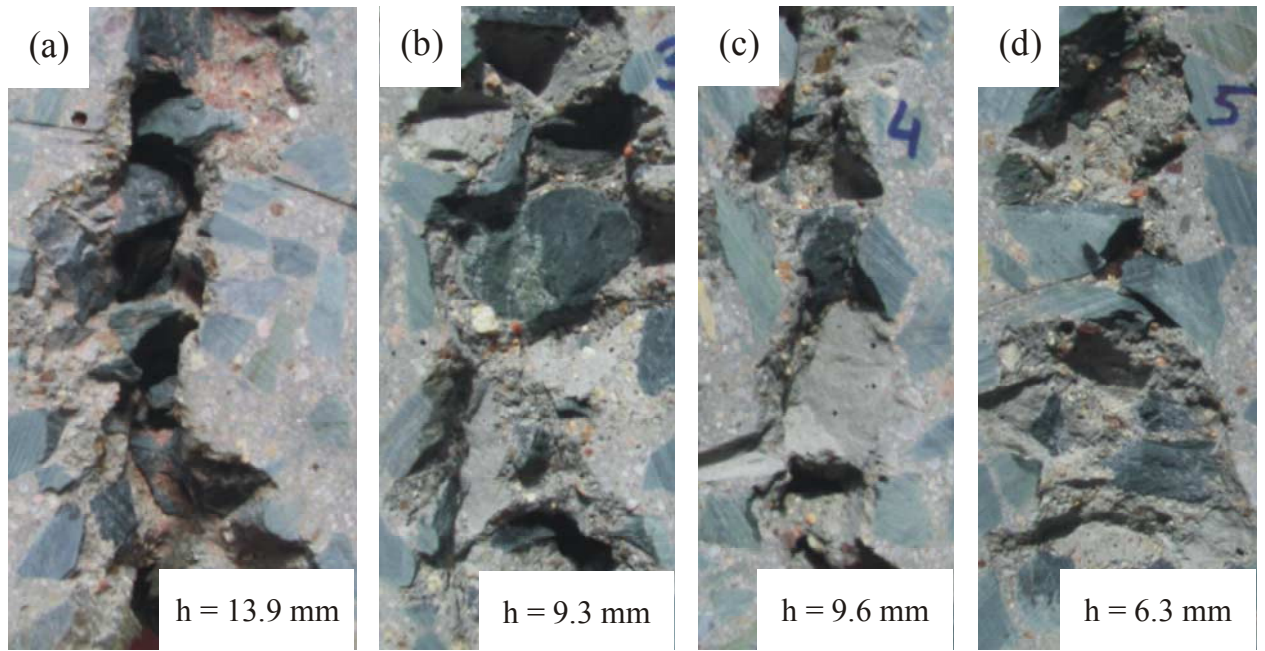


Figure 8. Concrete No. 1 exposed to modulated jet (a, c) and continuous jet (b, d). ($p = 40$ MPa, $d = 1.98$ mm, $v_{tr} = 2000$ mm/min (a, b), and $v_{tr} = 5000$ mm/min (c, d), $S = 140$ mm)

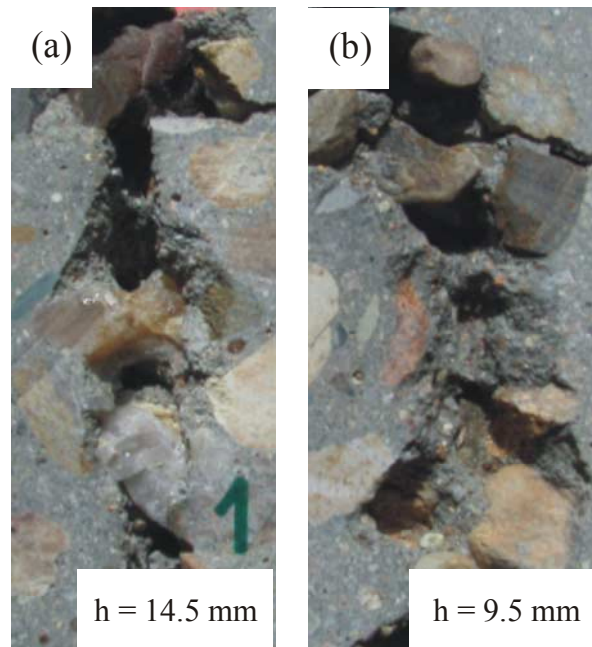


Figure 9. Concrete No. 2 exposed to modulated jet (a) and continuous jet (b). ($p = 40$ MPa, $d = 1.98$ mm, $v_{tr} = 2000$ mm/min, $S = 140$ mm)

HYDRODYNAMIC GENERATOR FOR ULTRASONIC MODULATION OF THE JET: BASIC STUDY

J. Foldyna, L. Sitek
Institute of Geonics of the Czech Academy of Sciences
Ostrava, Czech Republic

Z. Říha, L. Lhotáková
Faculty of Mechanical Engineering, Brno University of Technology
Brno, Czech Republic

ABSTRACT

It is well known that the impact pressure on a target generated by a slug of water is considerably higher than the stagnation pressure of a corresponding continuous jet. Thus, it is possible to significantly improve the performance of a continuous jet by modulating it to generate a train of slugs. The process of ultrasonic modulation by hydrodynamic generator placed upstream the nozzle outlet was studied using CFD methods. This paper presents numerical simulation of turbulent, one phase, incompressible fluid flow inside 3D geometry of the nozzle for high-velocity jet modulation using CFD code. The CFD model of one-phase (water) incompressible flow in hydrodynamic generator was developed and results obtained are presented in the paper. The dynamics of the modulated flow was studied also experimentally using method of direct measurement of frequency and amplitude of modulation. The results obtained from CFD model are compared with results from experimental measurement and certain design recommendations following from the study are discussed.

1. INTRODUCTION

It is well known that the impact pressure on a target generated by a slug of water is considerably higher than the stagnation pressure of a corresponding continuous jet. Thus, it is possible to significantly improve the performance of a continuous jet by modulating it to generate a train of slugs. An attempt was made to develop ultrasonic nozzle equipped with hydrodynamic generator placed upstream the nozzle exit.

2. BACKGROUND

Under hydrodynamic generators can be grouped sonic and ultrasonic generators employing high velocity liquid or gas stream. Most of the early studies in the propagation of ultrasonic waves in water and gases utilized whistles and sirens (Crawford 1955).

The tested generator is based on vortex movement of liquid (see Figure 1). It possesses one characteristic not experienced with other forms of jet generators, namely its frequency dependence on the input pressure. The generator consists basically of tube of circular cross section into which water is introduced tangentially, creating a vortex by a rapid rotation. During passage from the larger diameter to the smaller the speed of rotation of the water stream will be increased according to the law of conservation of angular momentum. As the fluid approaches the tube exit plane, it becomes unstable and periodic fluctuations in the motion are produced (Chanaud 1963). A whipping of the vortex is occurring as it leaves the confines of the tube. It thus appears that at the outlet the vortex is no longer stable but whips round at an angular velocity approximating to its rotational frequency. An attempt was made to exploit this instability for modulation of the high-speed jet.

The process of ultrasonic modulation by the hydrodynamic generator was studied using CFD methods. The paper presents numerical simulation of turbulent, one phase, incompressible fluid flow inside 3D geometry of the nozzle for high-velocity jet modulation using CFD code. The objective of turbulent flow numerical simulation was to find flow behavior in the nozzle with determined boundary conditions. The results obtained from CFD model are compared with results from experimental measurement.

3. CFD MODEL OF THE NOZZLE

3.1 Geometry of Computational Model

Geometry of solved area can be seen in Figure 2. Shape of geometry could not be simplified for numerical solution (axis, symmetry, periodicity, etc.). The geometry was created exactly according to design drawings. The biggest area of solved geometry contains quadrilateral cells; rest of geometry (tangency transitions at the inlet and outlet) was created from tetrahedral and pyramid cells.

3.2 Physical Description of the Fluid Flow Through Solved Geometry

The fluid flow through ultrasonic jet model was solved as 3-dimensional incompressible, turbulent, non-stationary one phase water flow with density $\rho = 998.2 \text{ kg/m}^3$ and viscosity $\mu = 0.001003 \text{ Pa}\cdot\text{s}$.

Turbulent water flow was solved with Reynolds stress model. Flow near the wall was described by non-equilibrium function.

3.3 Initial and Boundary Conditions

Total pressure at the inlet is 32 MPa. Turbulent intensity at the inlet is 0.5%. Zero static pressure was set at the outlet of solved area.

Real geometry at the outlet was extended by cylinder with the same diameter as outlet hole of the nozzle (1.37 mm). The wall of this extended cylinder was determined without friction. Set of boundary conditions is illustrated in Figure 2.

Initial boundary condition was set as nonzero field of velocity, pressure and others scalar values computed by k- ϵ turbulent model with the same boundary conditions as mentioned above.

3.4 Numerical Simulation

The time step value was defined with respect to instability appearance of velocity profile. These instabilities were observed at the nozzle outlet. The time step was $2 \cdot 10^{-6} \text{ s}$. Control-volume-based technique was used for solution of Reynolds equations describing turbulent flow. SEGREGATED – implicit solver was chosen for algebraic equations solution. Discretization of time step was made by second-order implicit. Relaxation parameters and discretization in the numerical solution are given in Tables 1 and 2.

Relative static pressure in place of pressure sensor (p_5) and flow rate in cross section at the end of cylinder (place of flux Q record) were recorded during computation, see Figure 2.

3.5 Results

The Figure 3 shows dependency of static pressure p_5 and flow rate Q on time. There are only small changes of recorded values during computation.

The geometry of the model was cut by several cross sections to visualize the fluid flow inside of the nozzle. Sections were made in all directions of coordinate system. Positions of sections are given in Figures 4 and 5. First section x_1 , perpendicular to axis x , shows geometry in tangential connection of inlet and large cylinder, see Figure 2. Second section x_2 , perpendicular to axis x , shows geometry in conical part of the generator. Last two sections x_3 and x_4 , perpendicular to axis x , shows geometry in small cylinder and in place of tangential connection of small cylinder and outlet cylinder upstream the nozzle.

Section y_1 is perpendicular to axis y . Axis of large and small cylinders lies in section y_1 . Sections z_1 and z_2 are perpendicular to axis z . Axes x and y determined plane of section z_1 . Section z_2 is parallel with section z_1 .

First picture in Figure 5 shows contours of velocity and static pressure in sections x_1 , x_2 , x_4 , z_2 . There are features of complicated fluid flow. Geometry contains fields with very low and high Reynolds numbers. Lowest flow velocities are near of axes of large and small cylinders. Highest velocity and lowest static pressure is at the nozzle outlet. Because of position of inlet cylinder to large cylinder, the fluid starts to rotate about axis of cylinders and simultaneously moves in direction of x axis. This situation is illustrated in Figures 7, 8, and 9. Shape of geometry affects fluid flow at the end of small cylinder. Flow direction is changed from axis x to y and initialize velocity vortices in small cylinder in Figure 6. Shape and size of velocity vortex varies during time. It creates soft fluctuations of recorded values of pressure and flow rate in time.

Velocity and pressure fields at the nozzle outlet are presented in Figure 10. There is visible tangential velocity component in outlet flow profile and asymmetrical velocity profile with respect to axis of symmetry of the outlet diameter, which is defined by cylindrical part of the nozzle outlet.

3.6 Conclusions from CFD Model

Numerical simulation of the fluid flow in the ultrasonic nozzle for modulation of the jet based on hydrodynamic generator did not confirm presence of considerable pressure and flow rate pulsations that could initialize forced break-up of the jet emerging from the nozzle. Recorded values of static pressure and flow rate are nearly constant in time. This conclusion is valid under presumption that fluid flow inside the nozzle does not depend on compressibility of the fluid flow and forced break-up of the jet appears only in case of considerable changes of velocity at the nozzle exit in time. The incompressibility presumption does not have to be valid especially in the area of outlet cylinder where velocities exceed 200 m/s.

Conclusion of numerical simulation is necessary to be confirmed by experimental measurement.

4. EXPERIMENTAL MEASUREMENT

To verify conclusions from the CFD model, an experimental measurement was performed in the lab. The ultrasonic nozzle (with the same geometry as was used in the model) was manufactured. The nozzle was equipped with pressure transducer connected to the PC based data acquisition system. The measured time domain signal was processed by FFT to obtain frequency domain of the signal to identify presence of pressure fluctuations in the nozzle. The example of the measurement can be seen in Figure 11. It can be said that the measurement confirmed the conclusion from the numerical simulation. Frequency domain of the pressure signal indicates, that in addition to low frequency peaks caused by the pump pressure fluctuations, there are low-level peaks only at frequencies of about 2.8 kHz and their harmonics in the signal.

5. CONCLUSIONS

Both numerical simulation of the fluid flow in the ultrasonic nozzle for modulation of the jet and direct measurement of pressure effects did not confirm presence of considerable pressure pulsation in the nozzle. This indicates that the changes in nozzle design are necessary to improve the modulation of the jet.

However, the consistency of results from the numerical simulation and direct measurement will allow to utilize the CFD model of the nozzle in design of the new ultrasonic nozzle with hydrodynamic generator without necessity to actually manufacture number of variants of the nozzle.

6. ACKNOWLEDGEMENTS

Presented work was performed within the framework of research project of the Grant Agency of the Czech Academy of Sciences, project No. A2086001. Authors are thankful for the support.

7. REFERENCES

- Crawford, A.E., “Ultrasonic Engineering with Particular Reference to High Power Application”, *Butterworths Scientific Publication*, pp. 113 – 136, 1955.
- Chanaud R.C., “Experiments Concerning the Vortex Whistle”, *The Journal of The Acoustical Society of America*, pp. 953 – 960, July 1963.

8. TABLES

Table 1. Under – relaxation factors

Pressure	0.3
Momentum	0.7
Turbulence kinetic energy	0.8
Turbulence dissipation	0.8
Reynolds stresses	0.5

Table 2. Schemes for discretization

Pressure	Second-Order
Momentum	Second-Ordered Upwind
Pressure-velocity	SIMPLE
Turbulence kinetic energy	Second-Ordered Upwind
Turbulence dissipation	Second-Ordered Upwind
Reynolds stresses	Second-Ordered Upwind

9. FIGURES

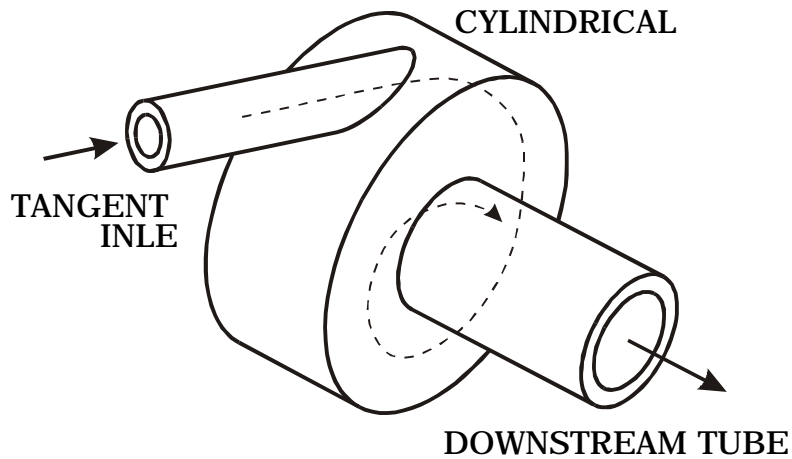


Figure 1. Scheme of hydrodynamic generator based on vortex movement of liquid.

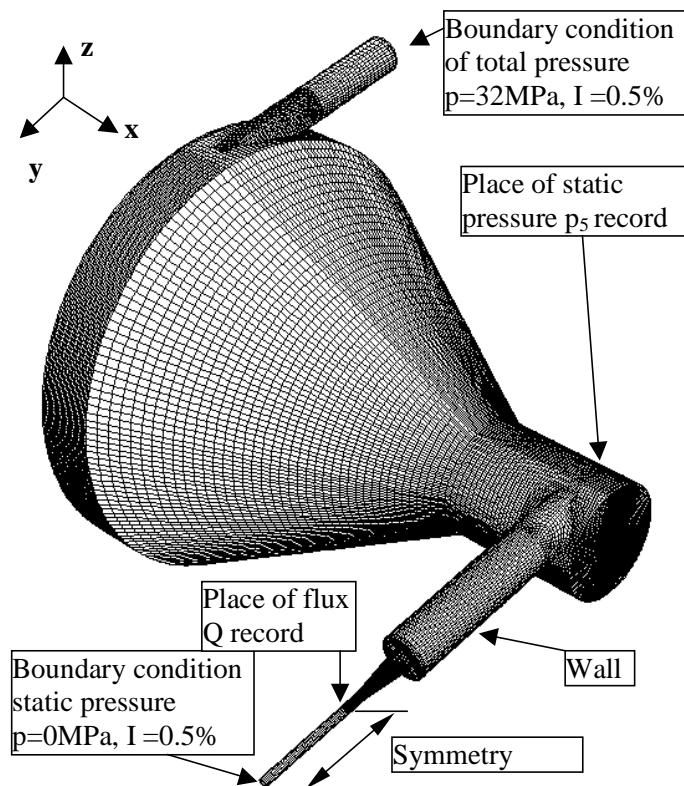


Figure 2. Computational geometry with mesh on the walls, about 200 000 cells

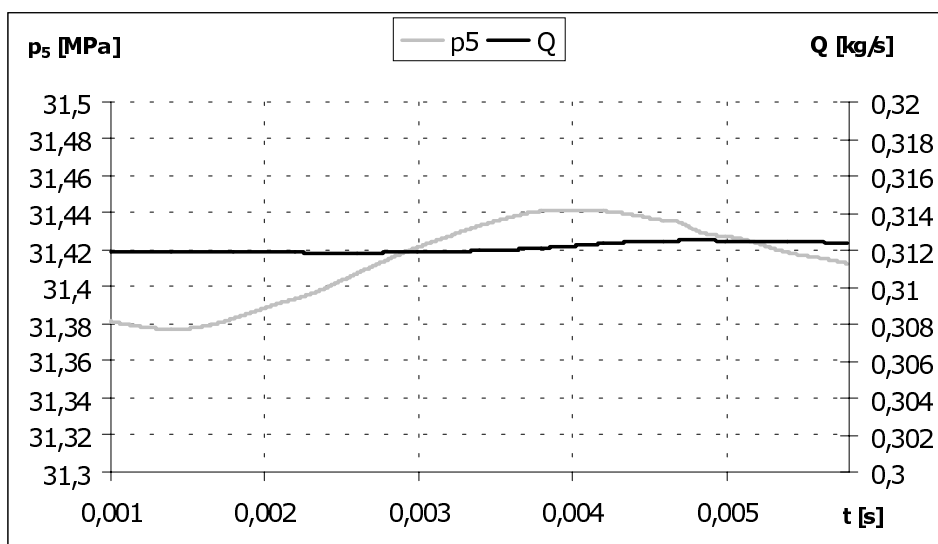


Figure 3. Pressure and flow rate variation in time

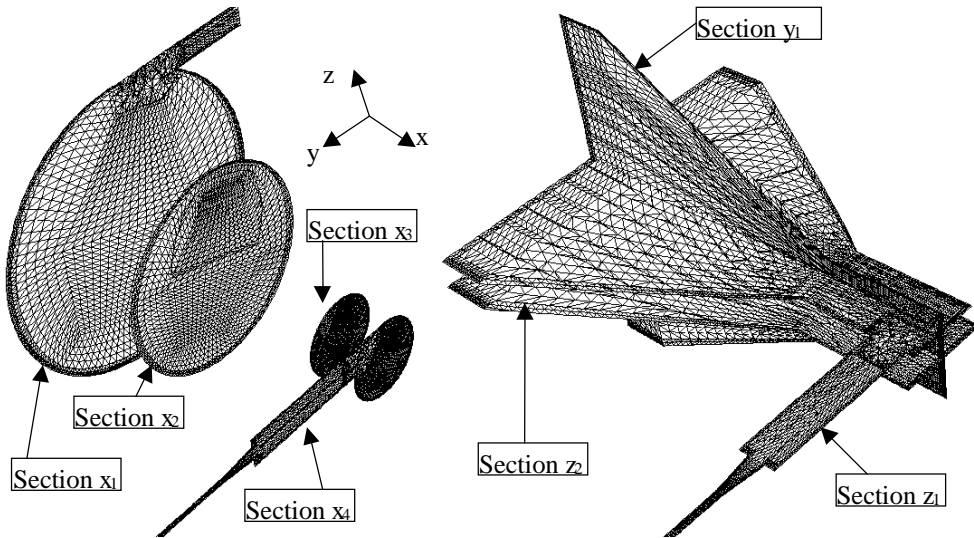
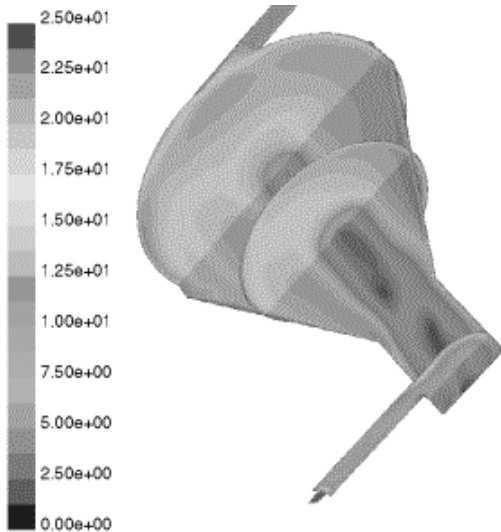
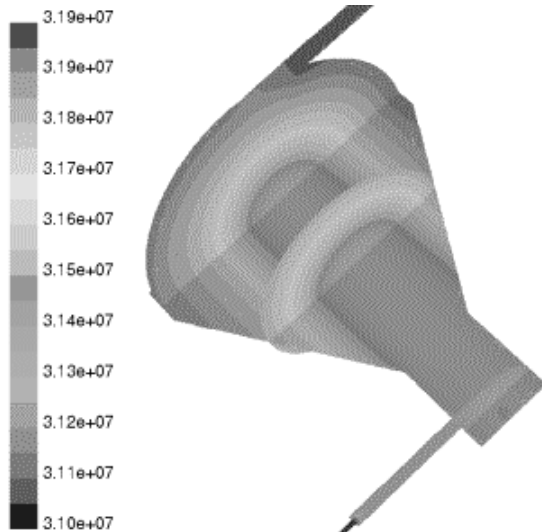


Figure 4. Geometry sections of the model

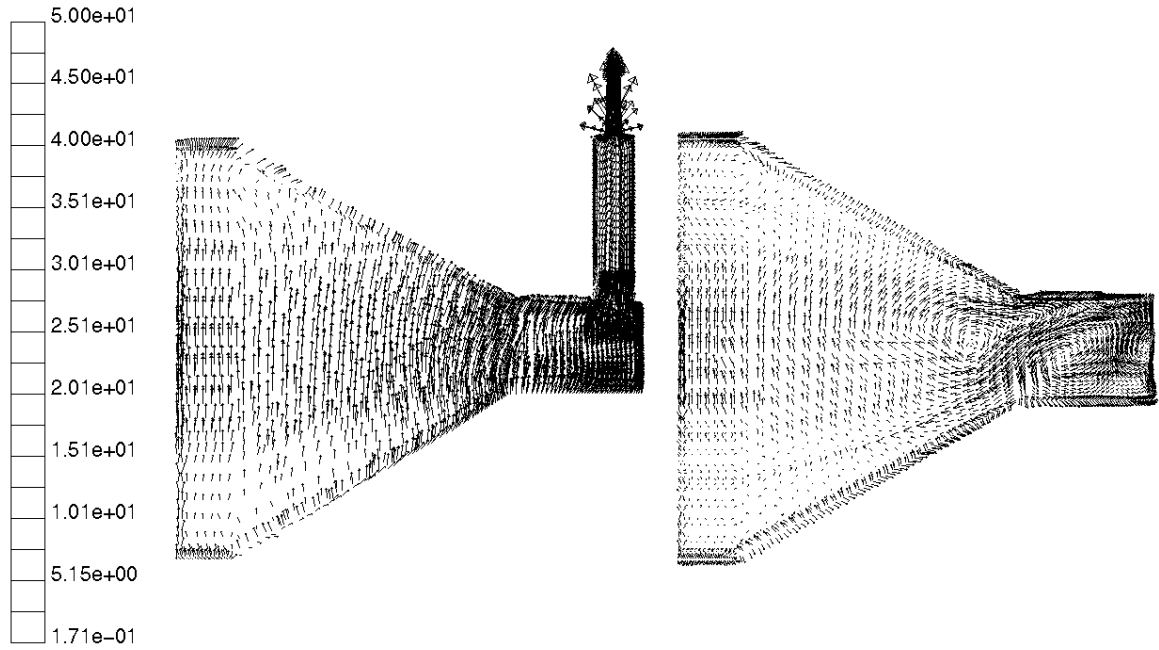


a) contours of velocity in sections x_1, x_3, z_2 [m/s]



b) contours of static pressure in sections x_1, x_3, z_2 [m/s]

Figure 5. Contours of velocity and static pressure in sections x_1 , x_3 , z_2



a) velocity vectors in section z_1 [m/s]

b) velocity vectors in section z_2 [m/s]

Figure 6. Velocity vectors in sections z_1 , z_2

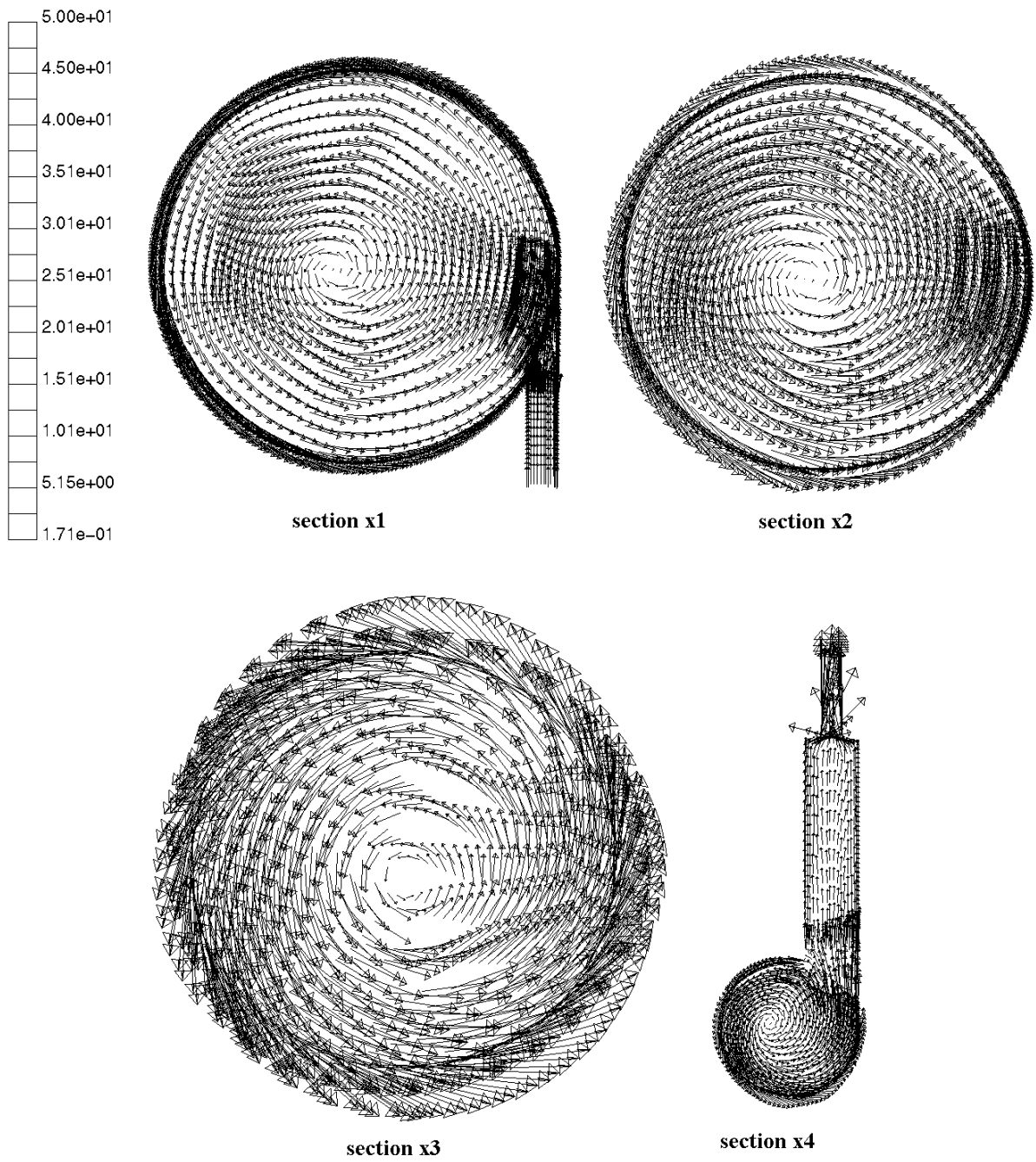


Figure 7. Velocity vectors in sections x_1 , x_2 , x_3 , x_4 [m/s]

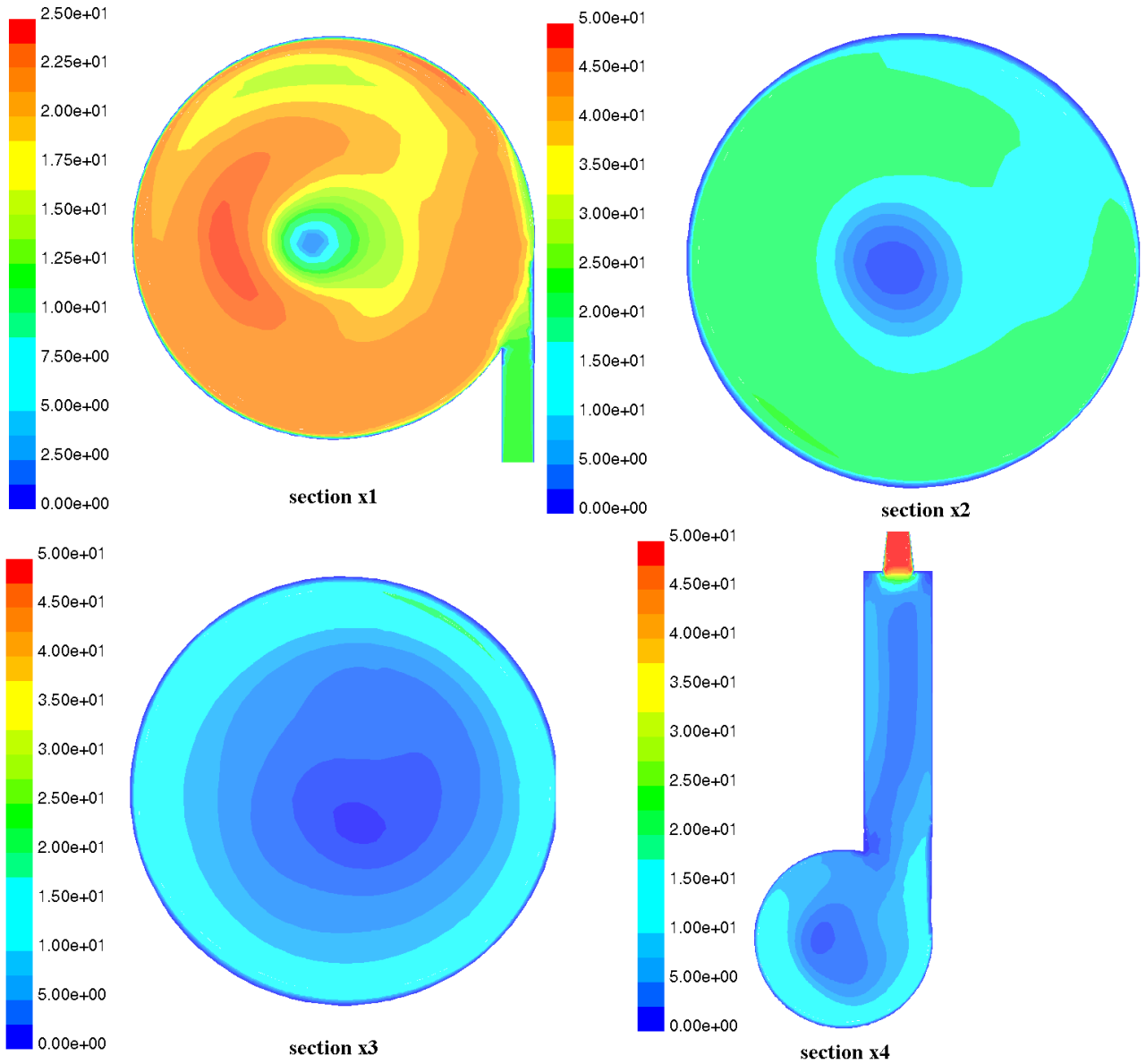


Figure 8. Velocity contours in sections x_1 , x_2 , x_3 , x_4 , [m/s]

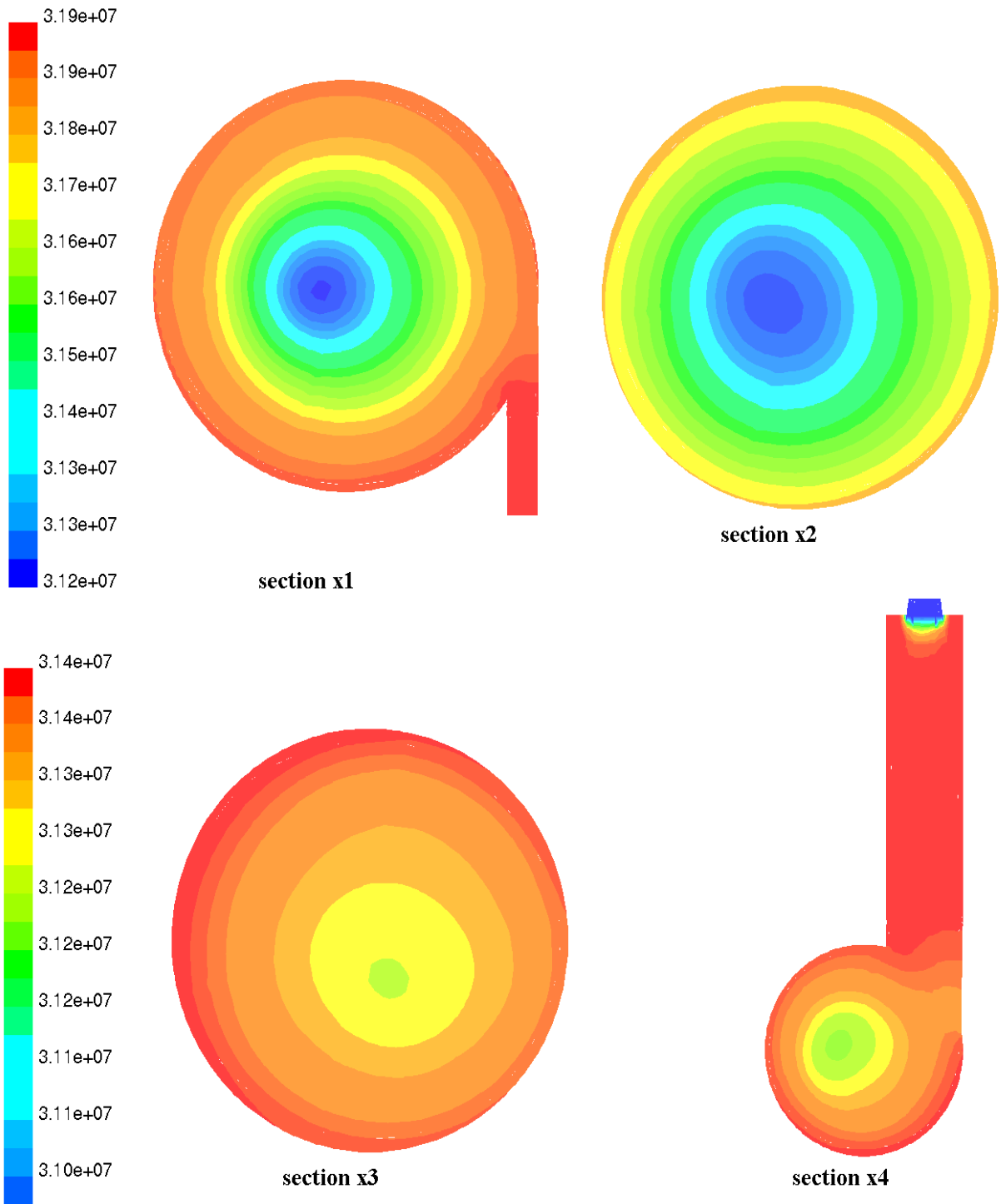
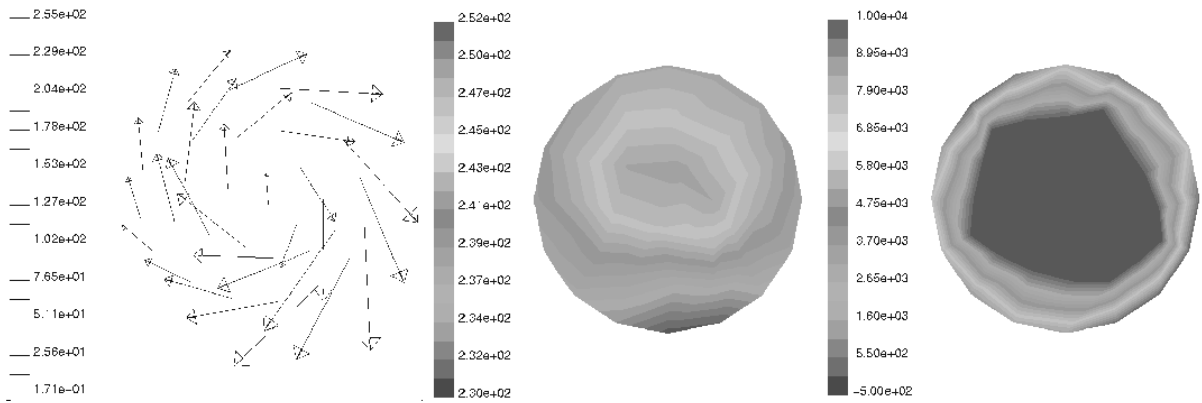


Figure 9. Contours of static pressure in sections x_1 , x_2 , x_3 , x_4 , [Pa]



a) velocity vectors at the outlet from the nozzle [m/s]

b) contours of velocity at the outlet [m/s]

c) contours of static pressure at the outlet [Pa]

Figure 10. Velocity and static pressure at the outlet from the nozzle

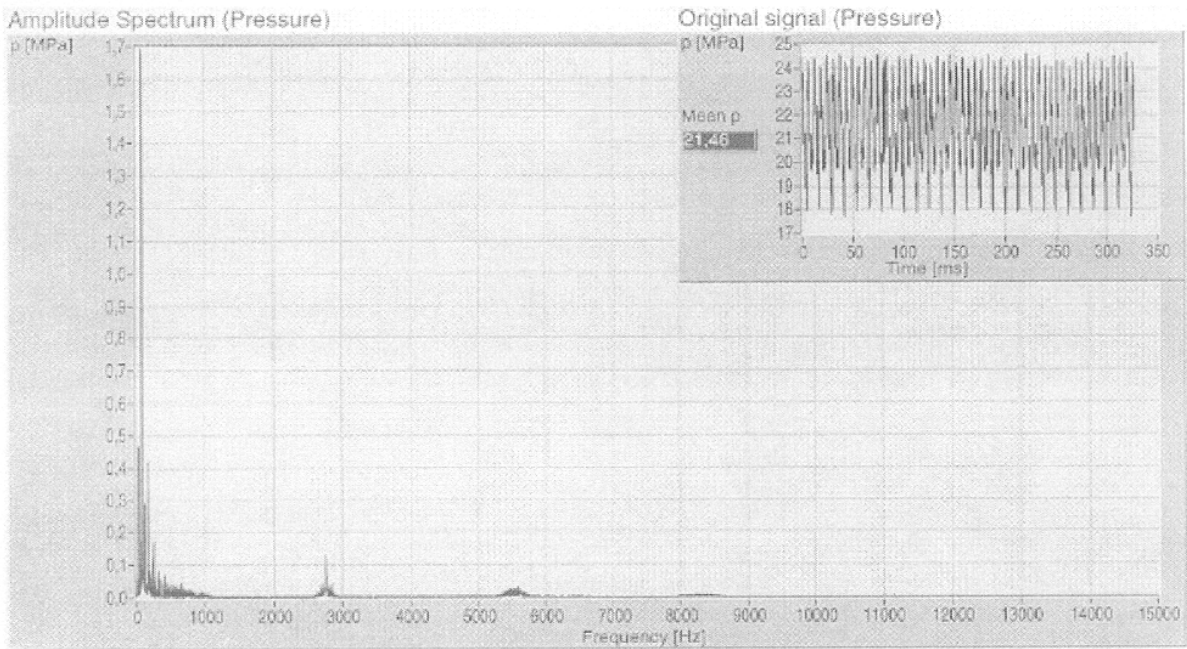


Figure 11. Time and frequency domain of the pressure signal in the ultrasonic nozzle (input pressure 30 MPa, nozzle diameter 1.37 mm).

WATERJET CLEANING OF TRUCK-MOUNTED CONCRETE MIXING TANKS

Arthur L. Miller and Grant W. King
Spokane Research Laboratory
National Institute for Occupational Safety and Health
Spokane, Washington

George A. Savanick,
U.S. Bureau of Mines (retired)

ABSTRACT

Manually removing hardened concrete from inside concrete mixing tanks using tools such as pneumatic chipping hammers has been identified by the National Institute for Occupational Safety and Health (NIOSH) as being a hazardous occupation. Engineers at NIOSH's Spokane Research Laboratory (SRL) teamed up with students from Gonzaga University to design an automated cleaning method for such tanks. The team built a prototype consisting of a remotely controlled lance with two opposing waterjet nozzles mounted on one end. The lance and its drive assembly are mounted on a control pedestal, which allows the lance to be adjusted for optimizing tank entry. The pedestal is supported and elevated by a scaffold-type frame. The system was tested using a 1,000-psi pump supplying up to 215 gal/min of water to the nozzles. It was shown that semi-cured concrete could be removed effectively from the tank walls. In cooperation with an industry partner, Central Pre-Mix Concrete Co. of Spokane, WA, the system will be demonstrated at a concrete mixing plant as a daily or weekly cleaner, and the results will be compared to current rinsing and cleaning methods. The goal is to reduce the build-up of concrete over time, thereby reducing or eliminating the need to chip concrete manually from inside the tanks.

1. INTRODUCTION

The Spokane Research Laboratory (SRL) of the National Institute for Occupational Safety and Health (NIOSH) focuses on providing engineering solutions to occupational health and safety hazards in the mining and construction industries. This paper summarizes a project that addresses the hazards associated with cleaning hardened concrete from inside truck-mounted mixing tanks.

The project was born out of a hazard recognized by both NIOSH and the Occupational Safety and Health Administration (OSHA). It addresses the exposure of construction workers to a multiple-hazard situation while cleaning concrete mixing trucks. The workers are exposed to extremely high noise levels, high concentrations of respirable dust that may contain silica, hand and arm vibrations from the use of pneumatic tools, the possibility of traumatic injuries from falling debris, and musculoskeletal disorders from lifting chunks of concrete and heavy tools inside confined work spaces. The goal of this project is to design an automated cleaning process that will remove a worker from this hostile environment.

In 1997, the Wisconsin OSHA consultation program, in conjunction with the Sentinel Event Notification System for Occupational Risks (SENSOR) program, did a preliminary investigation of this problem and cited silica exposure as a “serious hazard” (i.e., can cause a health hazard exposure resulting in death or serious physical harm). Searches of Bureau of Labor Statistics data by NIOSH researchers indicated that 570,417 workers at 60,222 establishments could be involved. It appeared that the hazards of cleaning out concrete tanks were a serious health hazard that had been overlooked for a variety of reasons. Therefore, assessing the problem and providing methods for reducing worker exposure to these hazards lay directly within NIOSH’s mission.

2. BACKGROUND

The ready-mixed-concrete industry is a vital part of modern life and many other industries depend on it. Every day, millions of tons of ready-mixed concrete are transported from concrete plants to job sites via mixing tanks mounted on trucks. The tanks have a helical screw system of baffles to mix the concrete or to force it out the back of the drum when pouring, depending on the rotational direction of the drum (Figure 1). After months of use, concrete builds up on the baffles, causing a loss in efficiency of the baffles and a decrease in the volume the trucks are able to transport. As much as 1-1/2 yd³ of concrete per load, depending on drum size, can be lost because of build-up.

Two cleaning processes are commonly used to clean concrete haulage tanks. The first involves flushing out the tank daily with a large volume of water. The specifics of this process vary somewhat, but typically the tank is flushed for 5 to 10 min following every load of concrete and for approximately 15 min at the end of each work shift. In some cases, operators will add coarse aggregate to the tank to improve scouring of semi-hardened concrete. Despite this treatment, concrete hardens and builds up on tank surfaces over time.

The second process is to chip the built-up, hardened concrete manually from the inside of the tank. This is done on an as-needed basis, typically about one to three times per year, and entails sending

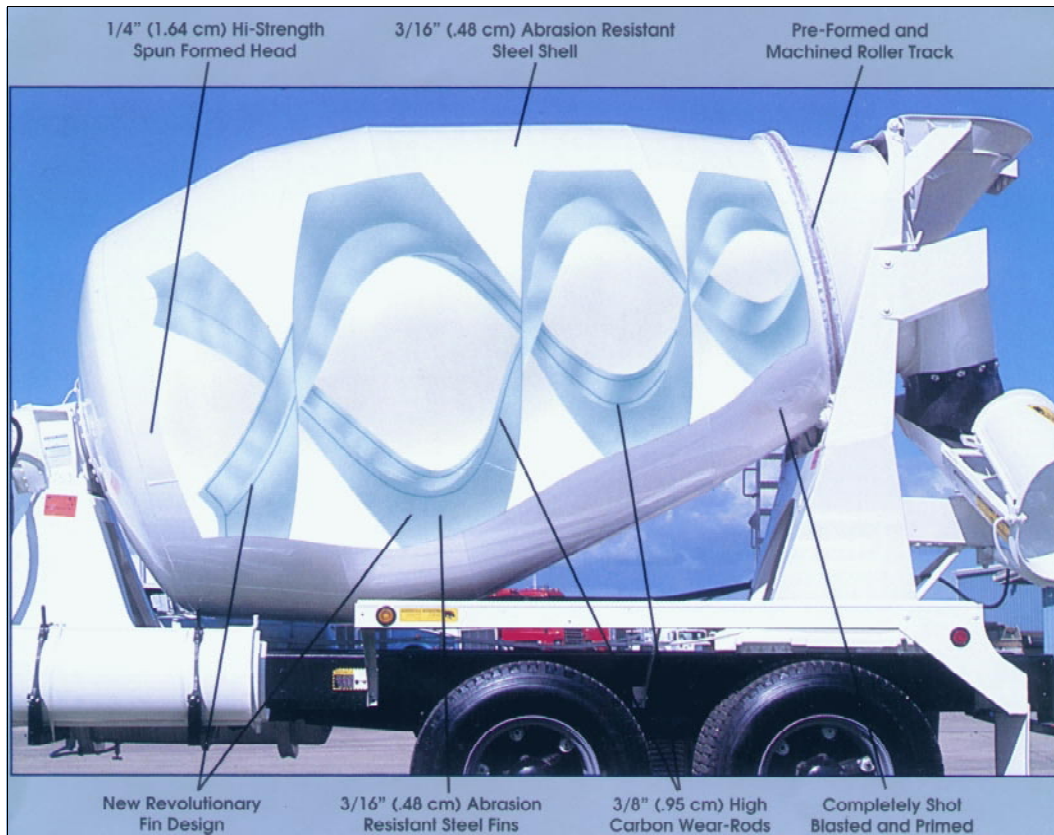


Figure 1. Tank geometry. This cutaway illustrates the complexity of the twin helical mixing baffles.

an employee into the tank with pneumatic tools such as hand-held chippers and jackhammers. The procedure takes between 1 and 8 hr and places the employee in an enclosed, hazardous environment that may even require a confined-space permit. According to a recent study, this task could cause negative health effects, such as hearing loss and silicosis (Williams and Sam 2000a, 2000b; Sam and Williams 2000). The number of times this chipping must be done varies, depending on the type of concrete mixed and how effective the flushing process has been. The criteria used to decide when it is time to chip out a tank are—

1. When the discharge from the tank becomes inefficient because the mixing baffles are heavily coated with concrete,
2. When the weight of the empty truck is excessive because of the accumulation of hardened concrete (up to 10,000 lb of concrete can build up inside the tank), and
3. When the capacity (i.e., delivery volume) of the tank is reduced significantly because of the accumulation of hardened concrete.

Both cleaning processes are somewhat complicated by the interior geometry of the tanks (Figures 1 and 2). In the case of the tank rinsing technique, the agitated water easily scours the rear sides of

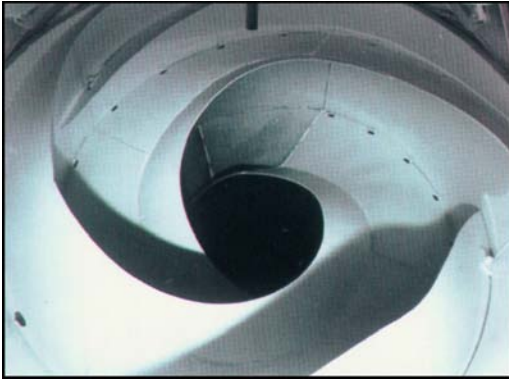


Figure 2. Mixing baffles. This view from inside an unused tank shows the surfaces that will become coated with concrete.

the baffles as it is propelled out of the tank by the rotating baffles. However, because the front sides are protected, concrete tends to build up preferentially on the front side of the baffles. During the chipping process, the baffles make maneuvering inside the tank difficult. The odd geometries of the baffles create hard-to-reach spots and also present more surface area for concrete to adhere to. The complex geometry and concrete build-up on the front sides of the baffles were a major consideration in developing design concepts for automated cleaning systems.

In addition to hazards associated with cleaning, there are economic disadvantages to continuing these work practices. A preliminary economic feasibility study¹ was conducted that indicated haulage productivity could be reduced by as much as 15% because of reduced delivery volumes resulting from concrete build-up inside the tanks and reduced fuel economy. Such reductions would translate into a significant loss of income for concrete mixing companies and might easily justify the cost of an automated cleaning system.

The goal of this research project is thus to build and field test an automated tank cleaner so that the industry will have hard data on which to make decisions about whether to incorporate such technology into their work practices.

3. RESEARCH APPROACH

NIOSH researchers called on the talent of engineering students at Gonzaga University, Spokane, WA, to help tackle this problem. Through the Gonzaga Center for Engineering Design, a group of fourth-year mechanical engineering students was assigned the problem as a senior design project. The design team consisted of students, an adjunct professor who served as project advisor, and two liaison engineers from SRL. The team's mission was to design, build, and test a prototype automated tank cleaning system.

The team assessed the problem in brainstorming sessions, via phone conversations with industry representatives, and by field trips to a local concrete mixing plant. This preliminary assessment led to the selection of hydroblasting as the technology of choice for solving the problem, and further design work therefore focused on hydroblasting techniques. The team generated a list of design requirements and then developed five unique preliminary design concepts using these requirements as a guide (Lazenga et al. 2000). The concepts were evaluated using a weighted decision matrix.

¹Lazenga, Nathan J. Economic Analysis of the Installation and Application of an Automated Concrete Removal System for the Ready-Mixed Industry. Proposal prepared for Engineering Economics course, School of Engineering, Gonzaga University, Spokane, WA, Nov. 2000, 14 pp. Available from authors of this paper.

The “winner” became the concept that was developed further for testing. Below is a list of the requirements and a brief overview of the various preliminary concepts.

3.1 Design Requirements

3.1.1 Functional Requirements

- Cleaning should prevent the accumulation of hardened concrete in the tank.
- Cleaning must remove uncured and semi-cured concrete from 90% of the tank interior.
- Cleaning system must not damage the tank or truck.
- System must accommodate standard truck geometries. Design should focus on the McNeilus Bridgmaster truck, which is a truck commonly used in the industry.
- Cleaning time must not exceed the current cleaning cycle time of 15 min.
- Prototype must be rugged and dependable to withstand impacts of falling debris within the tank.
- All components must be capable of operating in a wet environment.
- Jet(s) must be capable of being guided through the rear entry and baffles.
- Use of an external water supply must be easy.

3.1.2 Operational Safety Requirements

- System must be semiautomatic, i.e., operable by one semiskilled technician.
- Failsafe system must ensure that the jets operate only inside the tank.
- Jets must shut off if any part of the apparatus gets tangled or obstructed.

3.2 Additional Parameters

In addition to the design requirements listed, several other issues were taken into account.

- In discussions with workers who regularly clean tanks, it was noted that most of the build-up is deposited on the front sides of the baffles, i.e., the side that faces the front of the truck. During the rinsing process, the back side of the baffles (where the water discharges from the tank) acts as a trough in which water collects. Agitation of this water prevents the semi-hardened concrete from being deposited on tank surfaces. Conversely, water on the front sides of the baffles is not agitated, and therefore concrete builds up rapidly. This location is where cleaning efforts must be focused.
- Environmental regulations restrict the methods used for draining and disposing of wastewater and materials. Wastewater will likely need to be captured in a settling pond and cleaned before disposal or re-use.
- Every mixing tank has a side access panel through which a person enters the tank to chip the concrete free. Although it is feasible that this panel could be used as an access for an automated system, this is not desirable because it can take over an hour to remove and replace the panel.
- Concrete can build up in the tank to a thickness of nearly 18 in.



Figure 3. View showing limited access to tank interior.

- Access to the tank interior is quite restricted due to the limited clearance at the rear of the tank (Figure 3).
- Differences in initial truck heights and the amount of height reduction caused by the increasing weight of accumulated water in the tank during the cleaning process (“truck squat”) may require that an automated system be vertically adjustable.

4. PRELIMINARY DESIGN CONCEPTS

Using the list of design requirements and additional parameters as a guide, the following preliminary design concepts were generated (Lazenga et al. 2000).

4.1 Locking Chain Waterjet Deployment

This design incorporates a specially designed chain link that can be curled up in one direction, but when unrolled in the other direction, locks to form a rigid wand. This mechanism would allow the waterjet to be deployed from above the truck through the limited-access hopper and into the drum. While the tank spins, the jet sprays and cleans the interior of the tank.

4.2 Locking Chain System, Deployment from Side of Tank

In this design, the existing side access panel is used to gain entry to the tank interior. A hose deployment apparatus, perhaps the locking chain, would enter the hole and spray the baffles.

4.3 Baffle-Guided Crawler

This design entails a simple frame with wheels or rollers on the bottom and side. The apparatus rests in the trough of the baffle and rolls down the inside of the tank as it slowly rotates. An arm with a waterjet(s) on it is attached to the top of the frame and drapes over the top of the baffle. As the crawler moves, the waterjet sprays the backside of the baffle the crawler is resting on. The crawler is tethered to the pump by means of a high-pressure water hose.

4.4 Chaos Waterjet Ball

This concept incorporates a ball tethered to the pump by means of a shielded high-pressure hose. As the tank spins, the ball moves down the tank baffles in the same manner as the crawler. The water is shot out of an asymmetrically positioned nozzle in the ball. Due to the force of the water, the ball twists and spins so the stream is randomly directed throughout the inside of the tank.

4.5 Helix-Mounted Waterjets

This design would require a permanently mounted track of waterjets welded on top of the baffles. The waterjets point at the back of the previous baffle. A pipe along the top of the baffle connects all the waterjets and provides pressurized water that cleans the baffles. A pump is connected to the pipe from outside the drum, providing pressure to the waterjet's baffles.

4.6 Lance-Mounted Waterjet

A waterjet is mounted on a lance that moves in and out of the spinning tank. The waterjet sprays the tank interior, removing built-up concrete. The set-up and alignment of the apparatus is the most difficult part of the cleaning cycle. Access to the tank is limited (figure 3), and misalignment could be disastrous to the entire system. However, with the right control system, this design could be made practical.

4.7 Concept Evaluation

The design concepts were assessed using an evaluation based on a weighted decision matrix. This technique, known as Pugh's method, allowed all proposed concepts to be compared directly. The first step in Pugh's method is to choose the criteria to be compared. These criteria were derived from the design requirements and from discussions among team members. A weighting factor was assigned to each relative to its overall importance. One concept was then selected as a datum. The design team chose to use the locking chain waterjet deployment as the datum. The datum was assigned values of zero on the decision matrix, while the other concepts were given a score ranging from -3 to +3.

A score of +3 indicated that the given concept met the evaluation criteria much better than the datum, while -3 indicated that the datum was far superior to the concept. Each of these values was then multiplied by the weighting factor. The weighted values were then summed for each concept to give a weighted total. The concept that best met the list of evaluation criteria was that concept that had the highest weighted total on the decision matrix. The decision matrix is shown in Table 1.

Table 1. Weighted decision matrix

Criterion number	Criterion	Weighting factor	Side, tank	Baffle-guided crawler	Chaos waterjet ball	Helix-mounted jet	Lance-mounted waterjet
1	Easily inserted	8	-2	-1	-1	3	1
2	Accurately inserted	10	0	1	1	3	1
3	Setup time	8	-3	-1	-1	3	-1
4	Position nozzle effectively to clean 90% of tank	10	-2	0	-3	-1	0
5	Mechanical reliability	8	0	1	2	-2	2
6	Resistance to entanglement	10	1	-2	-3	3	1
7	Cannot damage tank interior	10	-1	-1	-3	0	1
8	Resistance to debris impact	8	-1	-1	2	-3	1
9	Quick cycling time for cleaning	7	-2	-2	-3	-3	0
10	Easy to remove from tank in case of failure	4	-2	-1	1	-3	1
11	Sensitivity to varying internal geometry	8	0	-2	2	3	0
12	Sensitivity of varying truck heights	8	1	2	2	3	-1
13	Dependence on support structure	5	0	1	1	3	0
14	Cost to build	4	-1	2	3	-3	2
15	Cost to operate	8	-2	-1	-1	1	0
16	Ease of maintenance	7	-1	1	2	-3	1
17	Cost to maintain	7	0	1	1	-3	1
18	Resistance to water and rust	8	0	0	1	-2	1
19	Ease of operation	9	0	-2	-1	2	0
20	Ease of fabrication	5	0	1	2	-3	1
21	Mechanical simplicity (number of moving parts)	7	0	1	3	2	2
22	Breakdown time	8	-3	-2	-1	2	-1
23	Ease of storage	2	0	2	3	3	-1
24	Compactness	3	0	1	2	2	-2
25	Safe	10	-1	-2	-2	3	0
26	Weather-resistant	8	0	2	2	2	0
27	Easily transported and redeployed	3	0	2	3	-3	-1
28	Simplicity of control system for insertion	8	0	1	2	3	1
29	Simplicity of control system for cleaning cycle	8	-1	-1	1	-3	0
30	Ease of nozzle replacement	4	0	2	2	-3	0
31	Avoidance of obstacles	9	0	-2	-2	-3	0
32	Navigation of obstacles	9	0	1	2	-3	-1
33	Aesthetically pleasing	4	0	2	-1	-2	-1
34	Aesthetically robust	4	0	0	2	-3	1
35	Does not require tank modification	10	0	0	0	-3	0
36	Does not require access panel removal	8	-3	0	0	0	0
Weighted totals			-175	-41	56	40	88

NOTE: Weighted totals at the bottom of each column are calculated by multiplying rating number (either -3 or +3) for each criterion by the corresponding weighting factor, then summing all products. The locking chain option was used as the datum (0) and therefore had a weighted total of 0.

Based on this evaluation, the design team chose to continue development of the lance-mounted waterjet. This concept ranked highest because it was safe, simple, and inexpensive to build. Other advantages were that it allowed reliable surface coverage in a single pass and required the least amount of operator intervention. It would also clean the tank quickly by allowing the tank to rotate.

5. FINAL DESIGN: LANCE-MOUNTED WATERJET SYSTEM

5.1 Support and Controls

The prototype cleaning system includes a 24-ft-long jetting lance with two opposing nozzles mounted at the tip of the lance. The lance and drive system are mounted on a control pedestal (Figure 4). The pedestal allows both vertical and horizontal adjustment. The drive system propels the lance 15 ft along its axis by means of specially contoured urethane wheels driven by a 1/2-hp dc permanent magnet motor. Since the tilt angle of the tank is fairly constant on different trucks, the lance tilt was made adjustable using a simple manual system, i.e., a pinned support rod. The lance must enter the tank along the centerline, as shown in Figure 5, and therefore care must be taken to align the system properly during field use. Left-right lateral movement is controlled remotely from an operator's station that communicates with an electric motor, and a manual hydraulic foot pump controls vertical adjustment of the pedestal. The system is supported and elevated by a 6-ft-high scaffold (Figure 6).

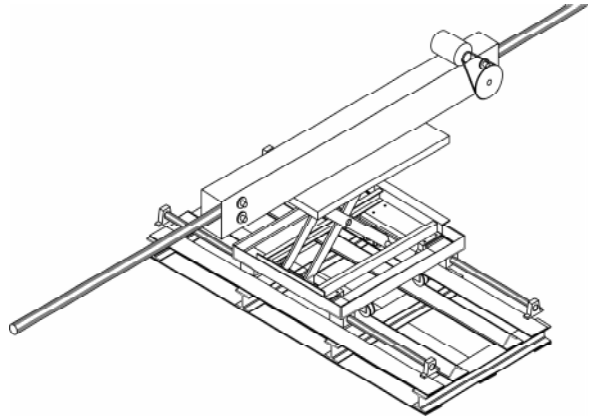


Figure 4. Control pedestal.

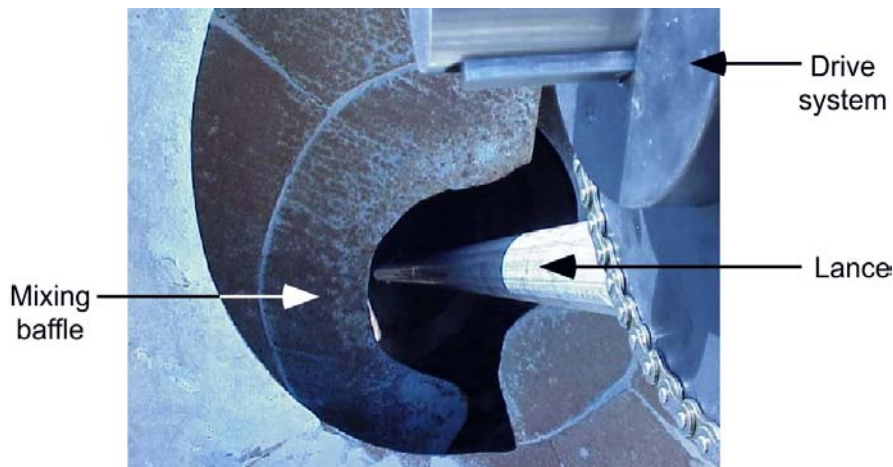


Figure 5. View of rear of tank as lance is inserted.

5.2 Hydroblasting Subsystem

A key decision for this subsystem was whether to address removing hardened concrete or to focus on preventing build-up on tank surfaces via regular daily or weekly cleanings. Preliminary tests conducted with a 5,000-psi, 15-gal/min hydroblasting pump indicated that standoff distances were

excessive and curtailed removal of hardened concrete. A second test conducted with an extension wand alleviated the standoff problem, but introduced another problem—the interaction between the extension wand and the mixing baffles. After these preliminary tests, the team concluded that the



Figure 6. Scaffold-mounted system.

more practical approach would be to use a streamlined lance for ease of insertion and couple it with a higher-volume, lower-pressure hydroblasting source. With less horsepower, this combination would deliver a more stable (albeit lower pressure) jet stream to the tank surface. It was hypothesized that such a system could be used as a daily or weekly cleaning device to prevent concrete build-up. Also, it would be simpler and cheaper to build and operate. In the worst case, such a system would slow the build-up of concrete, which would still offer a great advantage in terms of increased delivery volumes for the trucks and therefore in economics. In the best case, it would obviate the need for the manual chipping process.

5.3 Sizing the Waterjet

The system required a waterjet that would deliver enough pressure to remove semi-hardened concrete at a standoff distance of about 3-1/2 ft. The hardness of the concrete as it sets up on the mixing baffles is unknown. According to ASTM standards, portland cement must have an initial set in 1 hr, final set in 10 hr, and achieve a strength of 1,200 psi in 3 days. The initial set of cement is checked by resting upon it a 1/12-in-diameter, blunt cylinder supporting a 1/4-lb weight. When the flat end of the cylinder no longer dents the cement, initial set has occurred. The final set is checked in a similar manner using a 1/24-in-diameter needle and a 1-lb weight.

Based on this information and extrapolations of the data (dotted line) presented in Figure 7, strength of 1-day-old concrete was estimated to be around 400 psi. Assuming that effectively removing the concrete would require at least half again this amount of impact pressure, it was decided the target stagnation pressure at the tank surface would be 600 psi. Using a graph of the Tollmein equation for jet degradation (Figure 8) adapted from Miller et al. (1997), we estimated the jetting parameters necessary to achieve this pressure.

With a known standoff distance of 42 in, a likely nozzle size (for example, 1/4 in) was assumed, which gave the result that $x/d = 168$. The graph gives a value of $P_s/P_n = 0.8$ at that point (see dotted lines on Figure 8), which is the ratio between stagnation pressure (P_s) at a given distance and original nozzle pressure (P_n). Using a desired stagnation pressure of 600 psi, the resulting nozzle pressure is $P_n = 600/0.8 = 750$ psi. Using the Bernoulli equation, the exit velocity was calculated at 328 ft/sec, which results in a flow rate of 100 gal/min for two nozzles.

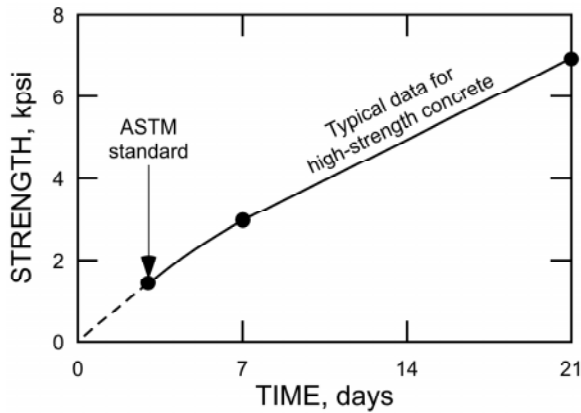


Figure 7. Data for determining compressive strength of concrete.

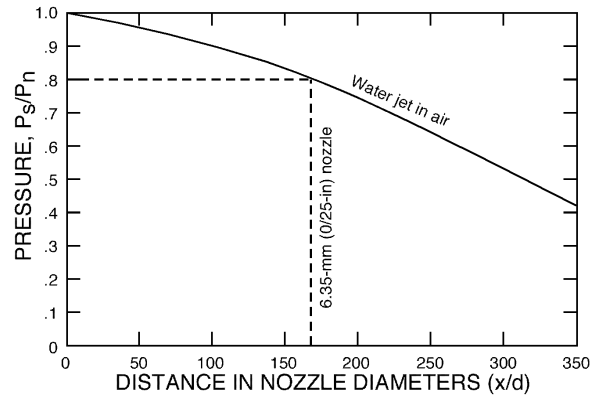


Figure 8. Variation in stagnation pressure with standoff distance for a waterjet in air.

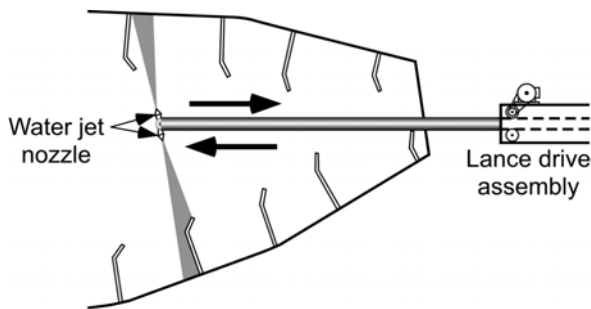


Figure 9. Sketch of lance inside mixing tank showing jetting angles.

Similar calculations using nozzle sizes between 1/8 and 3/8 in led to the conclusion that the system would function well with a pump that could generate somewhere between 680 psi at 215 gal/min and 1,200 psi at 35 gal/min. The pump chosen for the first tests was a seven-stage, axial flow, centrifugal pump capable of generating 1,000 psi at up to 235 gal/min.

To balance the forces at the tip of the lance, the opposing nozzles were similar in diameter, with the downward nozzle slightly enlarged to offset the force of gravity on the extended lance. To optimize the cleaning action of the jets, the nozzle angle and/or the lance insertion angle can be varied to achieve the result shown in Figure 9. This allows best coverage of the mixing baffle surfaces, i.e., the slightly larger jet would blast the front of the mixing baffles where concrete build-up is more pronounced.

5.3 Water Management

For field tests, a system for water management similar to that used at a local cement mixing company was selected. This entailed drawing gray water from the still end of a settling pond and returning it to the opposite end (Figure 10). A hydroblasting pump was placed near the still end to draw water directly from the pond, taking care to suspend the suction hose off the bottom and to use a screen to filter out debris. The water was pumped through a hose to fill and pressurize the 2-in (inside diameter) lance, supplying flow to the nozzles. After the water left the concrete mixing tank (along with a considerable amount of concrete debris), it was captured in a catch tank. From the catch tank, it was pumped back to the head of the settling pond using an 8-hp trash pump.

5.4 System Operation

The final field-ready system will be designed for use by specially trained truck drivers. When a fully functional system is installed at a mixing plant site (Figure 10), the following steps show how the system will be operated, presumably by a trained driver, at the end of each shift.

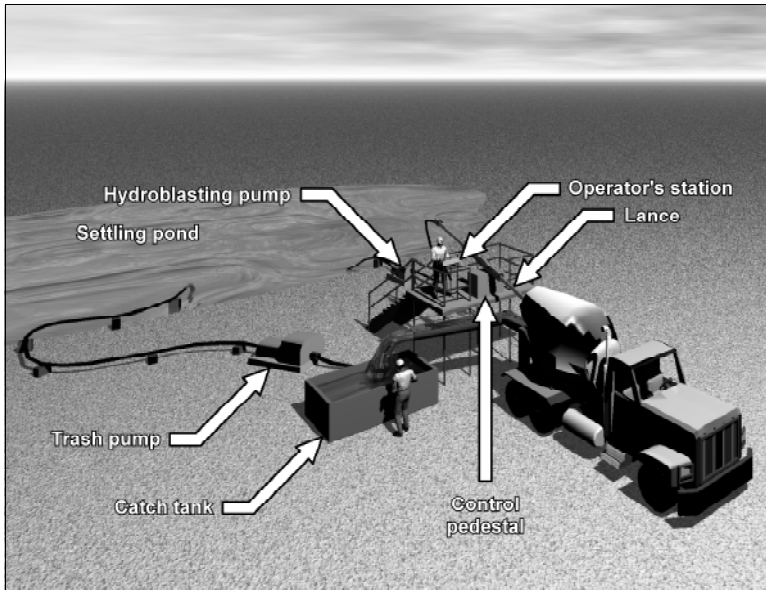


Figure 10. Artist's sketch of cleaning system at field site.

- System is in the neutral position.
- Truck is backed into place using guides or stops and lowers outrigger wheels. The driver then—
- Sets brakes.
- Starts tank rotation.
- Climbs onto scaffold and goes to control station.
- Turns system “ON.”
- Manipulates positioning controls to align lance with tank entry.
- Operates lance drive until lance enters tank.
- Powers up pump.
- Advances/retracts lance for one or more cycles.
- Shuts down pump.
- Retracts lance to neutral position.
- Turns system “OFF.”
- Continues spinning tank to discharge waste.
- Stops tank rotation.
- Drives away.

6. TESTING

Initial tests of the cleaning system were completed at SRL on April 20 (Figure 11). The truck was provided by Central Pre-Mix Concrete Co. Because a proper wastewater disposal system was not available, the initial tests were performed on a relatively clean truck. The objectives were to ensure that the lance could be properly positioned using the lateral and vertical motion systems and to determine the optimum height and angle of insertion for the lance. Testing was also necessary to ensure that the fully inserted lance would not come into contact with the tank interior during rotation.

Several cleaning cycles were completed. The angle of insertion of the lance was adjusted to optimize ease of insertion while ensuring that the lance would not contact the tank interior during rotation. The platform was also raised about 12 in, which improved ease of insertion. As expected, the limited clearance to the tank interior required careful positioning of the waterjet delivery system, but the lateral and vertical motion devices accomplished insertion and retraction of the lance smoothly and at a controllable rate. Thus, the results of the initial tests were considered positive.

Field tests of the cleaning system were done at Central Pre-Mix on April 27 (Figure 12). For these tests, trucks were cleaned when they returned from job sites in Spokane and the interiors of the tanks were coated with a layer of uncured and semi-cured concrete.



Figure 11.—Preliminary tests at SRL.

The team found that not all trucks could be cleaned. Because truck design tends to vary somewhat from year to year and the trucks are not designed to allow straight-line access to the tank interior via the rear orifice, some trucks possess features that block access to the tank interior. The cleaning system could not be used on these trucks. However, many newer truck models have

features that are compatible with the cleaning system, such as an upper loading hopper that can be raised out of the way and a lower hopper with a geometry that does not block the tank orifice. Another difficulty was that some trucks are not capable of driving in reverse with the rear set of wheels in the “down” position, which is necessary to permit the cleaning system to be operated. The driver must lower the wheels—because the axle blocks the tank entrance when in the up position—and then back the truck to the cleaning station.

Successful tests were performed on several newer trucks with an upper hopper capable of being raised and capable of being driven in reverse with the rear wheels in the down position.

Parameters monitored during the tests included total cleaning-cycle time, total volume of water used, and effectiveness of cleaning. Positive results were obtained in all three areas. The test team and Central Pre-Mix employees present determined that only one cleaning pass—from one end of the tank to the other and back—was required. The time required for this pass was 1 to 2 min, which was a fraction of the team’s initial goal of 10 min. Roughly 200 gal of water were used for each cleaning cycle versus the 500 to 1,000 gal required for the current flushing method, and the wastewater leaving the tank was visibly dirty at the beginning of the cleaning cycle and clear at the end of the cycle.

Central Pre-Mix employees had positive responses to the cleaning system. They stated that the system was more effective in removing uncured and semi-cured concrete from the tank than the flushing method currently used. The employees were also enthusiastic regarding the small volume of water required for the cleaning cycle; smaller volumes of water processed through the settling pond place less stress on the settling pond system



Figure 12. Field testing the cleaning system at Central Pre-Mix Concrete Co.

than larger volumes. The short cycling time was also a great improvement on the current time of 10 to 15 min.

7. CONCLUSIONS

Cleaning hardened concrete from mixing tanks has been identified as a hazardous occupation. NIOSH researchers and Gonzaga University students teamed up to develop an alternate solution. They hypothesized that a daily or weekly tank cleaning using a remotely controlled hydroblasting system could prevent build-up of concrete on tank surfaces. They built a prototype automated tank cleaning system and demonstrated its effectiveness in cleaning semi-hardened concrete from concrete mixing tanks. A prototype was demonstrated that could offer companies an economical alternative to current cleaning methods while providing workers with a higher level of safety while on the job. Results from this project could conceivably prevent numerous job-related injuries every year and save the concrete mixing industry considerably in terms of medical expenses, injury leave time, and legal settlements. It is recommended that this work be taken to the next level, which would include improving the of the system and conducting long-term field tests.

8. RECOMMENDATIONS

- Because the lance tends to rotate while being inserted and retracted from the tank, the next lance should employ an anti-rotation device, such as a keyed system.
- The linear bearings used in the lateral motion system are sensitive to misalignment, so other methods of preventing tipping of the system should be explored.
- Interchangeable nozzles should be employed to allow for differences in cleaning tasks.
- The scaffolding or platform should be mobile, which would allow the operator to move the entire system to the truck to be cleaned. One possibility would be to mount the scaffolding on rails.
- Use of alternative hydroblasting pumps should be explored. The pump used for the experimental cleaning system is rather unique and not commercially available at a price that would make it conducive to wide-scale use. It is also possible that if the tanks are cleaned regularly, a lower-pressure pump might suffice.
- A control system should be developed that includes safety mechanisms such as limit switches and emergency stops. Controls for vertical motion, lateral motion, and the waterjet delivery system should be located on a single control panel.

9. ACKNOWLEDGMENTS

The bulk of the work on this project was done by engineering students from Gonzaga University, and their hard work is greatly appreciated. Two different student teams participated in the work.

Members included Nathan Lazenga, Jeremiah Pappé, Vincent Petersen, Ryan Wade, Adam Baron, Vanedee Moua, and Dave Quadracci. We would also like to thank Gonzaga University's faculty project advisor, Thomas Zysk, for his excellent technical and motivational leadership of these student teams.

10. REFERENCES

Lazenga, Nathan J., Jeremiah Pappé, Vincent Petersen, and Ryan Wade. "NIOSH Concrete Mixing Drum Cleaning Apparatus, Interim Report." Project 2000 ME-1. Sponsored by NIOSH, Spokane Research Laboratory, Spokane, WA, and Gonzaga University, School of Engineering, Spokane, WA, Dec. 2000, 33 pp. Available from authors of the current paper.

Miller, Art, Dan Daly, and Steve Connors. "Reach Enhancement of a Submerged Waterjet Using Air Shrouding." Paper 24. *9th American Waterjet Conference* (Aug. 23-26, 1997, Dearborn, MI). Waterjet Technology Association, 1997, pp. 347-363.

Sam, Kwasi, and Donald R. Williams. "Control Measures for Reducing Employee Exposure to Concentrations of Total and Respirable Silica in the Ready-Mixed Concrete Industry during Truck Drum Cleaning." Abstract and table. Illinois On-Site Consultation Program, Illinois Dept. of Commerce and Community Affairs, Chicago. [2000] 2 pp. Available from authors of the current paper.

Williams, Donald R., and Kwasi Sam. "Illinois Ready-Mixed Concrete Association Industrial Hygiene Study." Illinois On-Site Consultation Program, Illinois Dept. of Commerce and Community Affairs, Chicago. [2000a] 16 pp. Available from authors of the current paper.

Williams, Donald R., and Kwasi Sam. "Nine Ways To Give Drum Chippers 'Nine Lives.' " *Concrete Producer*, Dec. 2000b, 3 pp.

**THE REMOVAL OF HARDENED GREASE DEPOSITS
FROM STEAM DRYERS IN A PAPER MILL FIRST SUCCESSFUL
CONTRACT APPLICATION OF FORCED PULSED WATERJET**

A. H. Tieu, W. Yan, C. Bai, M.M. Vijay
V_LN Advanced Technologies, Inc.
Gloucester, ON., Canada

J. Szemeczko
Advanced Waterjet Applications Inc.
Oakville, ON., Canada

ABSTRACT

Paper mills systematically inspect all the steam rollers about every 5-7 yrs for possible shell and head cracks due to the extreme service conditions, basically high temperature and pressure. Dryer head surface testing requires that it be free of scale, dirt grease, paint etc., in order to get accurate indication of possible cracks. Some dryer heads can build grease deposits that exceed 13 mm (½-in.) in thickness. In the case of excessive amount of baked-on grease, high-pressure waterblasting up to 138 MPa (20,000 psi) has been known to be the most efficient technique to remove the build-up thoroughly. In this paper, on the other hand, it is shown that the job can be accomplished at much lower pressures (\approx 50 MPa; 7,000 psi) using the patented forced pulsed waterjet technology. Complexities encountered during the dryer head cleaning job are also highlighted.

1. INTRODUCTION

Steam dryers in paper mills are subjected to harsh operating conditions, namely, continuous application of high internal pressure, and corrosion in a high humidity environment. Crack inspection on a roll head by magnetic particle testing requires that it must be free from rust scales, baked on dirt and grease, oil film, and paint so as to leave an exposed metal surface.

A common method for cleaning is to use low pressure blasting (20 MPa, 3,000 psi) with wire brushing after the surface has been treated with a cleaning solvent. However, this is only effective for rolls with thin deposits. Furthermore, some solvents can cause environmental problems to effluent system and are harmful to workers. Other methods used in the past, such as caustic solutions and abrasive waterjet (AWJ) blasting, are not recommended as they are considered to be dangerous, ineffective and the problem of ingress into bearings and drive mechanisms.

The cleaning job discussed in this paper was performed by Advanced Water Waterjet Applications using the forced pulse waterjet machine manufactured by V_{L_N} Advanced Technologies [Vijay (1998a) and Vijay, et al. (1999)]. The forced pulse waterjet was able to effectively clean all areas of the paper machine at 45 MPa (6,500 psi) that would have otherwise required high-pressure blasting at pressures in the neighbourhood of 140-170 MPa (20,000-25,000 psi).

1.1 Background

To maintain a safe operating order of steam dryers, they must be thoroughly inspected every 5-7 yrs. Roll inspection can only be performed once the rolls are properly cleaned to a specified level set out by the industry standard for roll inspection.

According to the standards set out by regulatory societies, such as ISO (International Standard Organization), NACE [National Association of Corrosion Engineers; e.g., NACE No.5; Frenzel (1999)] and SSPC (Society for Protective Coating), the dryer head needs to be 'Clean Almost to Bare Substrate'. Invisible contaminants such as salts, chemicals, or water soluble substances are not of concern since the surfaces are not painted.

When a crack develops through the thickness of the cap, loss of heat from the rollers occurs resulting in inadequate drying of the paper. Additional wear factors such as the fast rolling speed can introduce cyclic loading at the journal and end plate junction, and can cause cracks to be developed at weld joints, or even bolts from stress corrosion cracking. Consequently, many of these dryers are not in the same operating condition as when they were made, and may need to have their operating pressure reduced, or the dryer replaced.

Roll inspection requires that all roll heads be carefully examined using either 'Wet Fluorescent Magnetic Particle', or 'Dry Powder Magnetic Particle Testing'. Although these dryers are rated for high burst pressure, most of them when hydrostatically tested, rupture in the head well below the design burst pressure. Therefore, careful inspection of the heads is crucial. This is normally done by a certified metallurgist immediately after cleaning the dryers.

1.2 Forced Pulsed Waterjet

A detailed description of the forced pulsed waterjet technique is beyond the scope of this paper. Vijay and his co-workers [Foldyna & Vijay (1994), Vijay (1992), Vijay & Foldyna (1994), Vijay et al. (1995, 1997, 1998c & 1999) and Vijay (1998a & 1998b)] have described in great detail the technique for generating forced pulsed waterjet. However, for the sake of clarity, a brief description is reported here (see also, the paper by Yan et al. in these Proceedings). Basically, the forced pulsed waterjet is produced by modulating a continuous stream of water flowing through a conventional nozzle. The modulation is achieved by oscillating the tip of a probe (generally designated as 'microtip') at ultrasonic frequencies (≥ 15 kHz) placed inside the nozzle upstream of the exit. Generally, electrical signals from an ultrasonic generator are used to excite a piezoelectric crystal which energizes the probe. Pressure fluctuations at the tip of the probe modulates the flow. Consequently, the waterjet that emerges from the nozzle resembles a string of pearls when viewed with a stroboscope. This is called 'forced pulsed waterjet' which is far more powerful than the natural pulsed waterjets produced by several different methods [for example, self-resonating nozzles, Chahine, et al. (1983)]. Improvement in performance occurs because the impact pressure on the surface to be treated is the waterhammer pressure which is significantly higher than the usual stagnation pressure of a continuous waterjet

2. CONTRACT REQUIREMENTS

The contract called for a complete cleaning of the steam roller heads to bare metal finish on the tending and driving sides. As shown in Figures 1 & 2, the rolls are arranged in three separate sections, and some extend to a height of 9 m (30 ft). The location of the roll heads, 0.9 m (36 in.) and 1.0 m (42 in.) in diameter, varied throughout the paper machine. Spent water was required to be collected and filtered for large particles before being released into the sewer system of the plant.

The mill was shut down for 7 days in September 2,000, and the cleaning task was required to be completed within the first couple of days. The contract also specified the waterblasting to be self-contained, and the work should not affect other operations in progress in the adjacent wet-end or pit areas.

2.1 System Setup

Two electrically driven pumps delivering a total flow rate of 38 l/min (10 usgpm) at 45 MPa (6,500 psi) were used to pump city water. A single 1.22 m (48 in.) hand-held gun was used with a self rotating nozzle assembly. The pump was equipped with a 3 kW ultrasonic generator to drive the piezoelectric transducer in the gun to modulate the waterjet. A Mobile Processing and Containment Unit (MPCU) rated for 10 usgpm was used to collect, filter and separate the oil from the spent water from the pit. All necessary peripherals were provided by the contractors, including safety apparels, cleaning agents, scaffolding, and plastic sheet covers.

2.2 Cleaning Logistics

The dryer section was over 36 m (120 ft.) in length (see Figure 1). As 15 m (50 ft.) long hoses were employed, it was convenient to move the forced pulsed waterjet machine and the additional pump to the different dryer sections. Since the units were quite compact [Vijay, et .al. (1999)], it was easy for one person to move and place them close to the working area (see Figure 3). The hose length was long enough to conveniently reach the highest roll at 9 m (30 ft.) above ground level.

Two crews of three men each worked 12-hour shifts alternately. Based on the number of rolls, it was possible to manage a 16-hour of continuous cleaning time allowing for breaks and contingencies. As the rolls were all linked together by massive gearing on the drive side (Figure 4), they were indexed to expose hidden spots behind support structures.

Since a catwalk was not available on the drive side, a temporary scaffold had to be set up for the cleaning and be shifted along side as the cleaning progressed. The pit was unusually shallow and was conveniently used as a collecting basin for the spent water with plastic sheets laid over them. Plastic sheets were also used to cover the main walkway on the tending side of the machine from back splash and stray waterjets from the drive side.

2.3 Cleaning Operation

The dirtiest rolls were cleaned first as they were very difficult to reach and the heads were most heavily baked with grease. Some rolls were situated mid-way between catwalks and had to be blasted from the top and bottom catwalks.

Bearing blocks laden with grease (see Figure 5) required careful attention to avoid knocking the grease back onto the cleaned surfaces. In some tight spaces, a single non-rotating waterjet had to be used for it delivered a long and more powerful waterjet into hard to reach areas.

Rolls were cleaned section by section so that head inspection can be carried out concurrently. The rolls were rotated at least 3 times in order to completely clean all the surfaces that were hidden from structural supports. This proved to be the most time consuming activity as the entire gear train and the rolls had to be rotated manually by turning a pinion that often required up to four people. Throughout the cleaning period, the roll inspector would make random checks and comment on the quality of the surface finish. The rolls were treated with a gentle degreaser solution on a final rinse to remove the stubborn oil film and leave it dry to the touch. The surfaces cleaned were examined by the inspector and were certified for testing.

The drive side (Figure 4) proved to be the trickiest side to clean as the rolls were guarded by a dense web of gears and spokes. These massive gears were laden with synthetic lubrication which made it very difficult to get around. In addition, the catwalk was not available on the drive side, so a scaffolding system had to be brought in and set up to move along that side as the cleaning progressed.

Three operators were contracted for the job. While the first operator was blasting, the second was preparing the rolls to be blasted, and the third person was responsible for manoeuvring the waterjet machine. They rotated their tasks about every twenty minutes with adequate breaks during a 12-hour shift.

2.4 Assessment of Performance

The assessment was based on: (i) surface finish as examined by the inspector and (ii) estimation of the actual rate of area removal (cleaning). Typical appearance of a head of the roll after cleaning is shown in Figure 6. As these are made of cast iron, the formation of flash rust was inevitable. However, this was believed to be acceptable as they are covered once again with grease. As noted by the inspector, the surface finish was acceptable.

With regard to the rate of removal, it was rather difficult to assess precisely due to the many interruptions encountered during the cleaning process. However, a comparison of the total recorded time for the entire job with the time estimated originally furnished a reasonable estimate of the actual waterjetting and non-waterjetting times.

The actual duration of waterjetting was approximately 15 hours, about 20 percent of the total working time. Total roll surface to be cleaned was 128.2 m² (1380 ft.²) which took 78 hours to complete.

The rate of cleaning was estimated as follows:

Gross removal rate: $128.2 \text{ m}^2 (1380 \text{ ft.}^2) / 78 \text{ hrs} = 1.644 \text{ m}^2/\text{hr} (17.7 \text{ ft.}^2/\text{hr})$

Actual removal rate: $128.2 \text{ m}^2 (1380 \text{ ft.}^2) / 15 \text{ hrs} = \underline{8.55 \text{ m}^2/\text{hr} (92 \text{ ft.}^2/\text{hr})}$

Considering that the operating pressure was only 45 MPa (6,500 psi), the actual removal rate is considered to be quite remarkable.

3. DISCUSSION

Paper mills differ in their cleaning requirements depending on the type of paper being processed, the age of the mill and the type of dryers used. Cleaning for roll inspection requires careful consideration to the type and condition of the deposits to be removed, space and accessibility, and machine structural layout that may hinder cleaning efforts.

The waterjet machine used in this contractual job functions in dual mode of operation, namely, as a regular (continuous), and forced pulsed waterblasting. Loose dirt and oil stains were easily removed by regular blasting at 41- 48 MPa (6,000-7,000 psi). However, when hard tar-like coatings were encountered, forced pulsed blasting at a pressure of only 45 MPa (6,500 psi) was found to be quite effective. This dual mode of operation, a very attractive feature, gave the operator a choice: either to use regular low pressure waterjetting, or pulse mode, just with the flick of a switch. The

pulse mode was essentially equivalent to very high-pressure regular waterjetting (≥ 138 MPa; 20,000 psi), without using such high-pressure pumps [Vijay & Foldyna (1994)].

The completion time of 78 hours was higher than the originally estimated time of about 50 hours. The main factors for this overrun are intrinsic to the paper mill. For example, to rotate the dryers for thorough cleaning, three (occasionally, four) people were required taking at least $\frac{1}{2}$ hour to make a 90 degree turn. Waterblasting was frequently interrupted due to poor lighting conditions as the gun operator had to examine the quality of the surface closely. Needless to say that flash rusting (see Figure 6) added to this problem until it was realized that this was not of major concern. As stated before, considerable time was spent in constructing a mobile scaffold on the drive side (due to absence of catwalk).

Initially, a large rotary coupling was used for the self-rotating nozzle. The rotary system coupled with the 1.22 m (4 ft.) long gun proved to be too heavy for the operators to manipulate, especially in the hard to reach areas. In such cases, *ad-hoc* solutions were improvised, for instance, shortening the gun to 0.91 m (3 ft.) and/or replacing the rotary system with a single-orifice, non-rotating nozzle (see Figure 7).

Although only 20 percent of the total number of rolls were extremely dirty, they required almost 50 percent of the overall cleaning time. As this involved the removal of baked on oil and grease, careful attention was taken not to re-contaminate the surfaces already cleaned. In addition, blasting with cold water made the tough grease even tougher to remove in that it had a tendency to smear rather than flake off. The heavy tar build-up around bolt heads and seams were easily removed by the forced pulse waterjet in a single pass. Sometimes a light brushing with a degreaser and a final blasting proved to be very effective. Throughout the entire operation, the waterjet machines performed very well with no failures of any kind (seals, ultrasonic generator, etc.).

This work was conducted without a prior visit to the paper mill. Such a visit could have made it possible to plan and isolate some of the problems (such as tight space). This could have reduced the overall time taken for the job.

4. CONCLUSIONS

The conclusions from this first successful contractual application of forced pulsed waterjet are:

- The entire cleaning operation was conducted at a pressure of 45 MPa (6,500 psi). The performance is believed to be equivalent or superior to that of continuous waterblasting at pressures greater than 100 MPa (15,000 psi).
- Since the forced pulsed waterjet machine worked without any problems in a harsh environment, its reliability for very demanding contractual jobs was established. Furthermore, problems of broken seals, plungers, stuffing box, engines, tumbling block and worn swivels, hoses, nozzles, etc., often encountered with very high-pressure systems [Gracey (1999)], were virtually eliminated. Less maintenance means less downtime and more time for cleaning.
- The actual waterjetting time for cleaning was only 20% of the total time taken to complete the

job. This excess time was intrinsic to the paper mill and was beyond the control of the waterjetting contractor.

- Apart from the problems intrinsic to the paper mill, no mechanical problems occurred during the entire cleaning operation.
- Although waterjetting is becoming increasingly popular in the surface preparation industry, it is essential for contractors to remember the importance of having a reliable waterjetting system.

5. ACKNOWLEDGMENTS

The authors are thankful to the management of Sonoco Products Company, Montreal, Québec, Canada, for providing this excellent opportunity to prove the potential of the novel forced pulsed waterjet technology for industrial cleaning applications, and its mill rights for their support during the entire cleaning operation.

6. REFERENCES

- Chahine, G.L., A.F. Conn, V.E. Jr. Johnson and G.S. Frederick, "Cleaning and Cutting with Self-Resonating Pulsed Water Jets," *Proceedings the 2nd U.S Water Jet Conference*, pp. 167-175, Water Jet Technology Association, St. Louis, Missouri, USA, 1983.
- Foldyna, J., and M.M. Vijay, "Potential of Ultrasonically Modulated Pulsed Water Jets for Cutting Metals," *Manufacturing Science & Engineering, ASME 1994. Vol.1., PED-Vol. 68-1*, pp. 397-404, ASME, New York, USA, 1994.
- Frenzel, L.M., "A Comparison of Surface Preparation for Coatings by Waterjetting and Abrasive Blasting," *Proceedings of the 10th American Water Jet Conference*, pp.645-660, Water Jet Technology Association, St. Louis, Missouri, USA, 1999.
- Gracey, M.T., "Using 40,000 psi Water Waterjetting for Field Work," *Proceedings the 10th American Water Jet Conference*, pp. 717-724, Water Jet Technology Association, St. Louis, Missouri, USA, 1999.
- Vijay, M. M., "Ultrasonically Generated Cavitating or Interrupted Jet," U. S. Patent No. 5,154,347, 1992.
- Vijay, M.M., and J. Foldyna, "Ultrasonically Modulated Pulsed Jets: Basic Study," *Proceedings of the 12th International Conference on Jet Cutting Technology*, pp.15-36, BHR Group Conference Series, Publication No. 13, Cranfield, Bedford, England, 1994.
- Vijay, M.M., M. Jiang & M. Lai, "Computational Fluid Dynamic Analysis and Visualization of High Frequency Pulsed Water Jets," *Proceedings of the 8th American Water Jet Conference*, pp.557-572, Water Jet Technology Association, St. Louis, Missouri, USA, 1995.

Vijay, M.M., E. Debs, N. Paquette, R. Puchala & M. Bielawski, "Removal of Coatings with Low Pressure Pulsed Water Jets," *Proceedings of the 9th American Water Jet Conference*, pp.563-580, Water Jet Technology Association, St. Louis, Missouri, USA, 1997.

Vijay, M.M., "Design and Development of a Prototype Pulsed Waterjet Machine for the Removal of hard coatings," *Proceedings of the 14th International Conference on Jetting Technology*, pp.39-57. BHR Group Conference Series, Cranfield, Bedford, England, 1998a.

Vijay, M.M., "Pulsed jets: Fundamentals and Applications," *Proceedings of the 5th Pacific Rim International Conference on Water Jet Technology*, pp. 9-23. WJTSJ, Tokyo, Japan & ISWJT, Ottawa, Canada, 1998b.

Vijay, M.M., J. Remisz, J. Foldyna & P.E. Grattan-Bellew, "Prewakening of Hard Rocks with Ultrasonically Generated Pulsed Waterjets," *Proceedings of the 5th Pacific Rim International Conference on Water Jet Technology*, pp. 479-496. WJTSJ, Tokyo, Japan & ISWJT, Ottawa, Canada, 1998c.

Vijay, M.M., W. Yan, A. Tieu & C. Bai, "Removal of Hard Coatings from the Interior of Ships Using Pulsed Waterjets: Results of Field Trials," *Proceedings of the 10th American Water Jet Conference*, pp.677-694, Water Jet Technology Association, St. Louis, Missouri, USA, 1999.

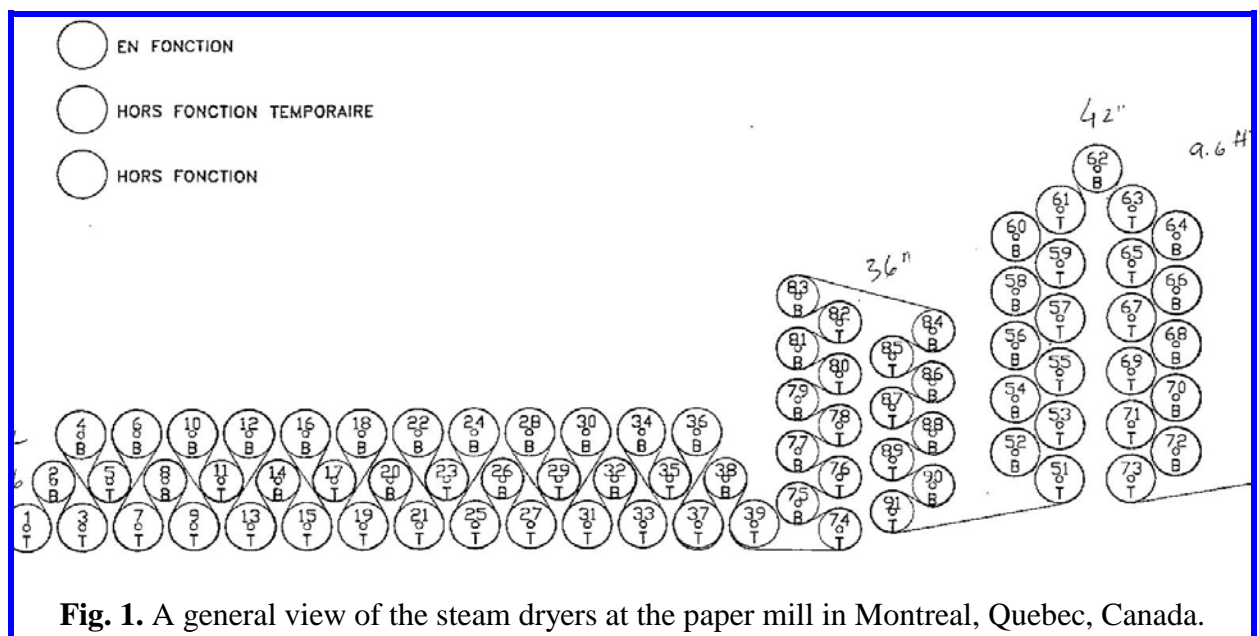


Fig. 1. A general view of the steam dryers at the paper mill in Montreal, Quebec, Canada.



Fig. 2. A general view of the plant showing the various hardware covered with both soft and hardened grease.



Fig. 3. Photograph showing the forced pulsed waterjet machine in the vicinity of the working area and the operators.



Fig. 4. A general view showing massive gearing to drive the rolls.



Fig. 5. A general view of the roll showing the bearing at the centre covered with grease.



Fig. 6. A general view of the head of the roll after cleaning with the forced pulsed waterjet (rust is believed to be acceptable).



Fig. 7. A general view of the shortened gun fitted with a non-rotating single orifice nozzle.

REMOVAL OF NON-SKID COATINGS FROM AIRCRAFT CARRIER DECKS

J. Van Dam, T. Kupscznk
NLB Corp.
Wixom, MI

ABSTRACT

This paper documents the removal of non-skid coating from aircraft carrier decks utilizing a high production UHP waterjet tool. Shot blasting, which has been the preferred method of removal, is able to meet required production rates, but has two major problems. Firstly, shot blasting fails to remove all of the chlorides from the ship decks. Secondly, the shot blasting machines can not contain all of the media used in the blasting process.

Previous attempts at using waterjetting as a removal tool addressed the two main limitations of grit blasting, (containment of media and chloride removal), but failed to meet the required removal rates. The NLB Non-Skid Removal System is the first to combine the advantages of UHP waterjetting into a system that can meet required removal rates with a single machine.

1. INTRODUCTION

1.1 Anti-Skid Coatings - A Brief History

Non-skid coating is a two-part epoxy coating which contains 80% aluminum oxide, a sharp, sand like material. The Oxide creates a sandpaper type surface that provides traction for the aircraft, tow tractors, and personnel aboard naval ships. There are 13 U.S. Aircraft Carriers with an average of 300,000 sq./ft of non-skid on each flight deck. However, there can be as much as an additional 100,000 sq./ft of non-skid coating on the ships. The majority of this is on the floor of the hanger bays where aircraft are stored and on the well deck levels where ammunition and supplies are stored. In addition to the carriers, there are 41 amphibious warfare ships that each has approximately 200,000 sq./ft of non-skid coating. So, while aircraft carriers make up the single largest application for non-skid removal, the coating can, in fact, be found on nearly every naval vessel in service today.

2. THE CIRCUMSTANCES SURROUNDING AND RAMIFICATIONS OF COATINGS FAILURES

2.1 Reasons for Coatings Failure

There are many reasons that non-skid coatings fail, but the most prevalent reason is corrosion cells that are encapsulated by the coating at the time of application. These cells are most commonly caused by either trapped chlorides in the steel deck (Figure 1) or steel shot left over from the removal process (Figure 2).

2.2 Ramification of Coatings Failure

Non-skid is generally considered to be the most critical coating on naval ships. If non-skid coatings fail, the ship cannot launch, or, if it is already at sea it must cease recovering aircraft. Failing non-skid can become ingested by the intakes of jet engines causing millions of dollars of damage as well as the possible loss of life. During the Persian Gulf War there was a non-skid failure on an U.S. carrier and the ship stopped all flights until the coating could be repaired.

3. THE SHOT BLASTING METHOD FOR REMOVAL OF NON-SKID COATINGS

3.1 The Steel Shot Method

Prior to 1998, non-skid was primarily removed through the use of Wheelabrator™ shot blasting equipment. There are a number of variations on this type of machine, but they generally are self-propelled, electric powered machines that use paddle type devices to accelerate the steel shot and direct it towards the surface to be cleaned. Once the steel shot impacts the surface, a vacuum system is employed to recover the shot in order for it to be recycled.

A typical non-skid removal project that utilizes shot would see anywhere from 6 to 10 units lined up across the deck of a ship. These units would consume about 2,000 pounds of steel shot for each 10,000 sq/ft² of non-skid removed. The average flight deck of a U.S. carrier ranges from between 180,000 sq./ft. to 240,000 sq./ft. This means approximately 40,000 pounds of steel shot is consumed per project.

3.2 Problems Associated with the Steel Shot Method

The steel shot method of removal has a number of drawbacks. The machines are very high maintenance tools and require large investments in personnel and spare parts to keep running. The nature of the machines makes them quite self-destructive and the process of replacing vacuum seals and the paddles that accelerate the shot is an ongoing one.

While there are very real problems associated with maintaining the equipment that applies the shot, the larger problem exists in the shot itself. Carrier decks are riddled with padeyes or tie-downs (Figure 3) that are utilized to secure equipment during transit. These small depressions on the flight deck cause the shot blast machines to lose vacuum and allow the steel shot to escape out onto the deck of the carrier. This shot escapes at a high velocity and is capable of injuring nearby personnel. The loose shot can roll across the deck and end up in adjacent areas where re-coating is occurring. The shot becomes encapsulated in the coating and creates a corrosion cell.

Another type of corrosion problem is the shot becoming entrained in the ship's deck drain system. This steel shot gets wet when water enters the drain system and the oxidation of the shot causes a reddish stain to appear on the sides of the ships immediately below the drains.

Even the best efforts to contain the shot during the removal process are met with limited success. Once the deck has been re-coated, hundreds of sailors are employed to scour the deck with shop vacs and magnets in efforts to reclaim all the loose shot. Even these efforts are not enough. Once a ship sets sail the motion causes any stray shot to become dislodged, often finding its way onto the flight deck. There are reports of shot being present on deck as long as 45 days after a ship first set sail. This loose shot not only causes a safety concern for personnel, but also has been attributed to jet engine failures.

4. USING UHP WATER FOR NON-SKID REMOVAL

4.1 Advantages of Water

UHP water provides a superior method for removing non-skid coatings. Not only does it eliminate many of the maintenance concerns surrounding the shot blast machines; it more importantly eliminates the shot itself. The spent media (water) is much easier to control than steel shot, and reclamation efforts are much more successful. In addition, UHP water removes the soluble salts (chlorides) from the deck of the ship, eliminating one of the main causes of the corrosion cells that form under the non-skid coating (Figure 4). Waterjetting with UHP water does not disrupt other work that needs to be done on the deck of the ship.

4.2 First Generation Systems

The original process for removing non-skid coatings from ship decks with UHP water utilized devices that were originally developed for vertical surface preparation work (Figure 5). The first job completed by this device was on the U.S.S. George Washington Aircraft Carrier at the Norfolk Naval Shipyard. The project required the removal of 200,000 sq./ft. of non-skid material.

While this original system was successful enough to earn the approval of the Navy, it had a number of drawbacks. In order to meet production requirements contractors were required to run as many as four devices at once. Each of these systems required its own operator, pumping unit and vacuum source. The seal design was not capable of maintaining suction over the padeyes on the deck. Typical production rates ranged from 100 to 150 sq./ft. per hour per device.

4.3 Next Generation Systems

The next generation of non-skid removal systems has now arrived and provides major advancements over previous systems (Figure 6). These devices utilize UHP water and provide production rates from 250 to 1000 sq./ft per hour. These improvements in production have been made possible through a number of advancements.

4.3.1 Control of Nozzle Rotation Speed

The control of nozzle rotation has proven to be a major contributor to improved production rates. Operators are now able to speed up or slow down nozzle head RPM, which provides superior control over nozzle dwell time. This makes it possible to make adjustments on the fly and match dwell time to coatings thickness.

4.3.2 Traversing Nozzle Head

The first generation of systems to utilize UHP water were simple crawler type devices that provided only a single axis of movement. The new generation systems can not only traverse backwards, but can index the nozzle array from side to side allowing for up to an 85" cleaning path (Figure 7).

4.3.3 Vacuum Seal Technology

Maintaining a positive vacuum seal is important as escaping water can create a spot of flash rust on the deck. Any form of oxidation on the steel deck is unacceptable and will cause the project to come to a halt. Advancements in vacuum seal technology have provided a system that not only gives superior seal life, but creates a vacuum seal which is unaffected by the variations in the flight deck. Small depressions in the deck, as well as the aforementioned padeyes do not cause the vacuum seal to fail.

5. OTHER APPLICATIONS

While non-skid removal has proven to be the largest application for systems of this type to date, there are a number of other applications that look promising. The same systems can be used for concrete surface prep as well to perform light to heavy scarification of concrete surfaces (Figure 8). Epoxies as well as rubber type waterproofing compounds can easily be removed at higher production rates than multiple shot blasting machines, eliminating multiple operators and the need for clean-up.

6. CONCLUSION

Non-skid is one of the most important coating systems utilized by the U.S. Armed Forces. The premature failure of these coatings can cease the operation of the most powerful method of air power deployment available.

Systems that utilize UHP water for non-skid removal have provided a solution to one of the Navy's largest coating removal problems. Advancements in traversing techniques and vacuum seal design have addressed many of the limitations of the first generation systems.

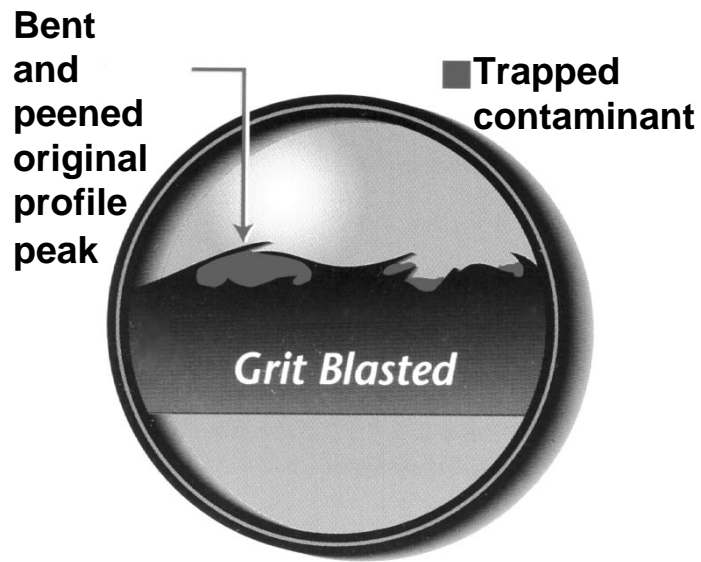


Figure 1. Blasting with steel shot causes chlorides to become trapped under the original profile, causing corrosion cells.

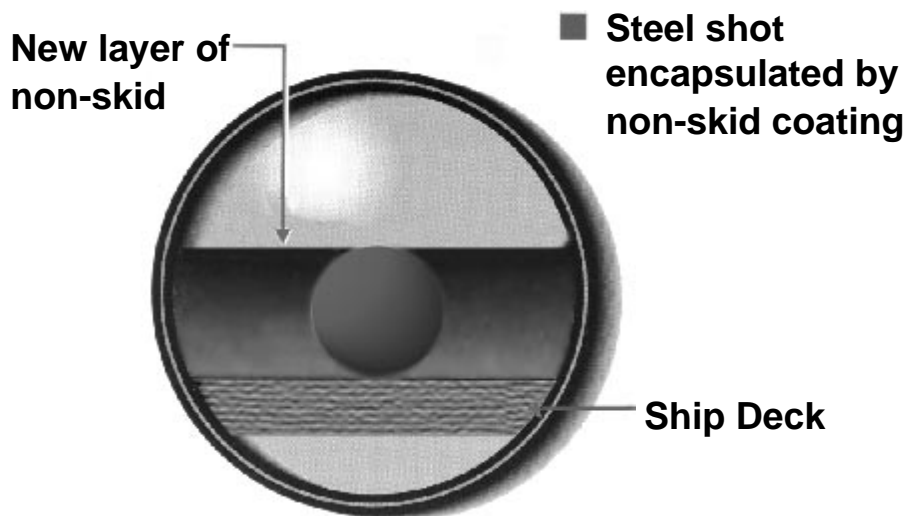


Figure 2. The steel shot that remains on the deck compromises the new layer of non-skid coating.



Figure 3. Tie downs or "padeyes" provide areas where steel shot can escape onto the deck of the carrier.

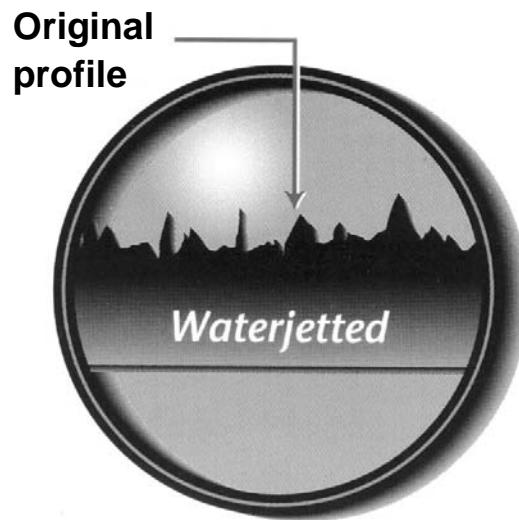


Figure 4. Waterjetting removes the chlorides from the steel deck, eliminating a major cause of corrosion cells.



Figure 5. The original process for removing non-skid coatings from ship decks with UHP water utilized devices that were originally developed for vertical surface preparation work.



Figure 6. Second generation non-skid removal systems combine the advantages of the original systems with new features that improve productivity.



Figure 7. Second generation systems not only traverse backwards, but can index the nozzle array from side to side allowing for up to an 85" cleaning path.

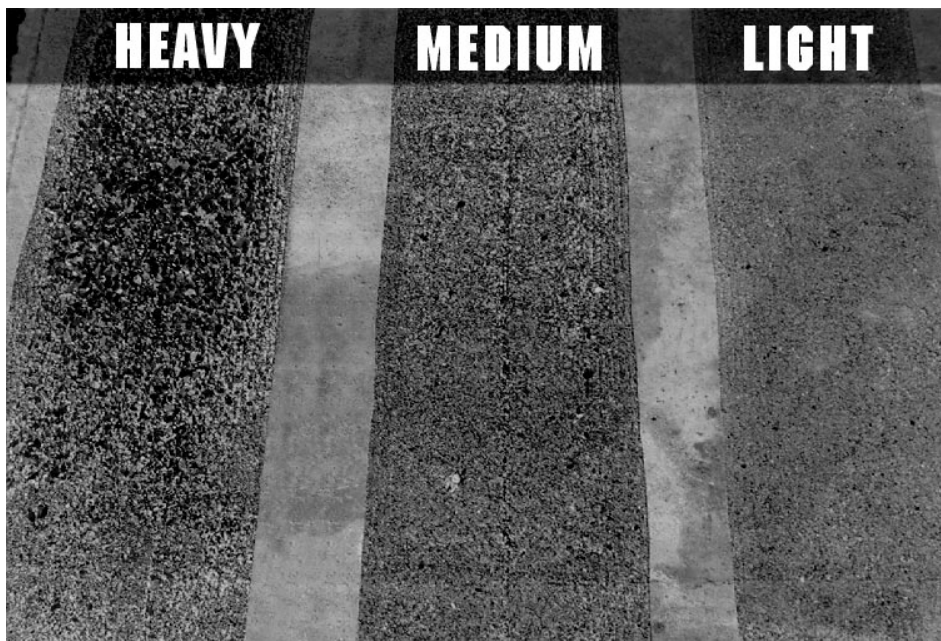


Figure 8. Additional applications include various levels of concrete scarification.

**DIFFERENCE AND SIMILARITY OF GLUE REMOVAL
FOR AIRPORT CONCRETE RUNWAY AND BITUMEN RUNWAY**

Xue Shengxiong, Fan Yibin, Peng Haojun, Huang Wangping, Chen Zhenwen
General Machinery Research Institute
Hefei, Anhui Province, P. R. China

Jiang Tao
Guangzhou Baiyun Airport
Guangzhou, Guangdong Province, P. R. China

Wang Leqin
Zhejiang University
Hangzhou, Zhejiang Province, P. R. China

ABSTRACT

It is a spreading new technology to use high pressure waterjet technology for removing airports runway glue and improving its friction factor, safety and service life. The basic requirements for glue removal equipment are complete removal of glue to raise friction factor to no less than 0.5 and having no injury to runway. Aiming at the situation that concrete and bitumen runways exist at the same time in civilian airports in China, we developed the vehicle for airport runway glue removal. The difference between structures of two types runway leads to the different mechanism of glue removal and different requirements for equipment. In this paper, we discussed the difference and sameness of glue removal for these two kinds of airport runway using the 70MPa, 150HP glue removal equipment developed by us and summarized the successful experiences including complete function of equipment, application of various waterjet forms, working process and procedure and relative quality control.

1. INTRODUCTION

Recent years, it becomes a more and more urgent problem for the 140 civilian airports including nearly 40 international airports in China to remove glue adhering on runway with the increasing flights especially international flights. Larger airports such as Beijing Capital International Airport and Shanghai Hongqiao International Airport have imported glue removal vehicles, other airports have to rely on professional high pressure waterjet cleaning companies and clean their runways once every year or even longer. Now, there are both concrete and bitumen runways existing at the same time in China. The reason for this situation is that the bitumen runways are mainly constructed on the concrete runways that are broken and can not be repaired to extend their service lives. Because of this, the bitumen runways have to be existed, though they are only makeshifts and fewer in use.

To solve this problem, we developed the tractive airport runway glue removal vehicle in thought of the situation that two kinds of runway coexist in Chinese airports. After one year testing, we have gained successful experiences. It will be recommended to users after further improvement.

2. AIRPORT RUNWAY GLUE REMOVAL VEHICLE

The rotating surface cleaners of imported glue removal vehicles in China like products of Harbon Company, the Great Britain (working under pressure of 70MPa and flow rate of 70L/min) and WOMA Company, Germany (working under pressure of 75MPa and flow rate of 180L/min) are all fixed on the front of cleaning automobiles and move along with them. These types of cleaning units have to occupy large vehicle, have large volume and are costly. So they are hard to spread in Chinese market. The design of glue remover for airport runway put forward by the authors adopts high pressure reciprocating pump set driven by diesel engine. The main part of equipment is placed on a trailer and drawn to move by other vehicle during cleaning process. Rotating surface cleaner is separated from the main unit and pushed forward manually. It also has the design of moving automatically driven by mechanism. This design has been approved by more than 10 airports in China for its lower manufacturing cost and maintenance fee.

Specified working pressure of the three-piston high pressure reciprocating pump used in our design is 70MPa. Its maximum flow rate is 70L/min. Seal adopted is a combination of clearance sleeve and kevlar packing. It can guarantee the main pump working reliably no less than 500 hours. The power of diesel engine used is 150HP. Rotation speed of the engine can be adjusted automatically by a negative feedback system controlled by pressure signal from main pump to stabilize system's working pressure at a set pressure, which can be preset by operator through pressure regulation valve. Total equipment weighs about 3 tons and has a compact arrangement shown in Figure 1. Normally, the capacity of water transportation automobiles used in airports is 7 to 8m³. So it needs to supplement water to these water transportation trucks every 1.5 to 2 hours when the glue removal vehicle working continuously.

There are two types rotating surface cleaner. One is the self-rotating cleaner pushed forward manually. Its rotating driven force comes from the hydraulic torque generated by two or four eccentrically installed nozzles. Because there is only one high-pressure water hose connected at

rear of the cleaner, it is light and handy. Its disadvantages are the uneven glue removal occasionally occurred and possibility of injury to runway surface brought by artificial stop. These are all resulted from the uneven moving speed generated by the form of manually driven. The other cleaner is the mechanically driven one propelled and controlled mainly by hydraulic technology. Its characteristic is that the rotation speed of nozzle head and moving speed of whole cleaner are even and can be adjusted separately according to operator's command. Its weaknesses are the weight and the inconvenience while working because of the three hoses connected at the rear part of cleaner (one high-pressure water hose, two hydraulic oil hoses). Compared the advantages and disadvantages of two types cleaners, we chose the mechanically driven cleaner in our design. Tests show that it has more advantages, especially in fulfilling the demands of both clean glue removal and having no injury to runway surface. Figure 2 shows the schematic diagram of hydraulic driven surface cleaner.

3. TESTS

Tests have been carried out four times on concrete runway at Luogang Airport in Hefei and bitumen runway at Baiyun Airport in Guangzhou. Equipment used in tests includes the runway glue removal trailer and surface cleaner, lighting truck, water transportation trucks and friction factor measuring car, etc. These unit sets worked together, moved once every 50m long runway cleaned. Friction factor was measured after cleaning runway several hundred meters long. Figure 3 shows the equipment for glue removal on airport runway.

Figure 4 shows the testing ground on concrete runway. Surface cleaner was driven by hydraulic motors. Its maximum moving speed was not less than 10m/min, cleaning width was 600mm. Cleaning effect can fully fulfill the desired quality index.

Moving speed of surface cleaner was varied from 6 to 15m/min according to thickness of glue adhering to bitumen runway. By adjusting working conditions, cleaning on bitumen runway can reach the evenly white base observed effect. At the mean time, there is no evident injury to runway observed, that is to say, no evidently visible sand and stone drop from the base of runway. But this will be varied when trying to raise working pressure and lower moving speed to improve cleaning quality. The hydraulic system worked under pressure of 10MPa. Two hydraulic motors are driven by pressurized hydraulic oil from one gear pump.

4. DIFFERENCE AND SAMENESS OF GLUE REMOVAL ON TWO KINDS OF RUNWAY

Tests show that the first sameness is that the chosen working parameters of cleaning unit can fulfill the glue removal demand well on both kinds of runway. Table 1 shows the results of tests on two runways using four $\varnothing 1.2\text{mm}$ cylindric hole nozzles installed opposite each other, Table 2 shows tests results of rotating nozzle head consisting of 26 pieces $\varnothing 0.2\text{mm}$ micro-hole atomizing diamond nozzles. From this data, we can see that when using four opposite installed cylindric nozzles, cleaning pressure only needs to be 45MPa on concrete runway and 65MPa on bitumen runway. If working pressure is raised higher than these critical pressures, the runway will be

injured though the cleaning effect will be better. So it is not acceptable. When working with atomizing nozzle head and cleaning pressure set to 65MPa, the cleaning effect is well satisfying and no injury occurs or injury is within the acceptable range. Generally speaking, working pressure during cleaning on either runway is within the unit's specified working pressure range chosen by the authors, flow-rate of the main pump can also satisfy working needs. These all show that working parameters of total unit we chose are appropriate.

Another sameness of cleaning on two runways is that their working procedures are basically same. Before cleaning on runway, the equipment must be regulated and debugged in advance to ensure it is in good condition and can work properly. In this step, works are focused on checking whether the inlet and outlet valves of high pressure reciprocating pump can open and close normally or not, whether there is unusual sound from main pump and diesel engine or not, whether the connecting screws become loose or not, whether the hydraulic pump, motors and control valves work properly or not, whether the rotating nozzle head rotates fluently or not and whether the nozzles are blocked or not, etc. After these thorough checks, we can connect the water supplying pipe, high pressure water hose and hydraulic oil hoses in sequence, start the diesel engine, begin a test cleaning after main pump works normally. If result of test cleaning is good, we can go in the regular cleaning process. When cleaning finished, glue particles removed from runway surface must be swept away by vacuum cleaning vehicle or flushed outside the runway using waterjet guns.

Besides above sameness, there are still differences existing in glue removal on concrete runway and bitumen runway, they are determined by the different structural characteristics of the two runways. From the eye of structure analysis, concrete runway is compact and has a relatively smooth surface while the bitumen runway is loose and has a relatively rough surface. This difference leads to different glue adhering mechanisms as shown in Figure 5. Glue adherence caused by high speed friction between runway and airplane's tires during landing and taking off on concrete runway appears to be a flat style, all glue adheres to surface of runway and can not penetrate into the base, so there is a distinct dividing line between the places with and without glue adherence. But for bitumen runway, glue not only adheres on its surface, but also penetrates and fills in the holes and gaps under surface because of its loose structure. So it is hard to distinguish the adhering glue from bitumen and remove the glue completely while having no injury to runway.

The basic requirements for runway glue removal are both removing glue completely and having no damage to runway surface, that is to say, excessive removal of runway base material is not allowable. For concrete runway, its smooth surface, flat glue adhering style and compact structure make it easy to remove glue from runway because of the difference in strength between glue and concrete. The cleaning effect on this runway is good and evident. Working under critical pressure, no matter what kind of nozzle head is used, glue can be cleaned thoroughly and no injury to runway surface occurs. Of course, the higher the working pressure and longer the cleaning time, the better the cleaning effect. When cleaning on concrete runway, the main problem is that the moving speed of surface cleaner must fit in with the structure and type of chosen nozzle head to avoid spiral pattern appearing on runway. If the spiral pattern appears, it indicates that the moving speed is fast and cleaning is not thorough. It must put more emphasis on this problem especially when using two or four opposite installed cylindric nozzles head and

having a long period of interval between two cleaning process. If using the micro-hole atomizing diamond nozzle head to clean runway, this problem is not severe because this type of rotating nozzle head has a wider cleaning width compared with cylindric nozzle head. So, it is recommended to use the micro-hole atomizing diamond nozzle head instead of cylindric nozzle head. The later is used only when glue layer is so thick that cleaning speed is too low using the atomizing nozzle head.

For bitumen runway, many holes and gaps in its loose base are easy to be filled with glue particles, meanwhile, components of bitumen are similar to glue material in strength, hardness and chemical composition compared with concrete. The special glue adhering mechanism on bitumen runway and similarities between glue layer and runway surface material make it easy to damage runway surface while cleaning with waterjet. This brings about much more difficulties in meeting the demands of both complete removal of glue layer and having no injury to runway base material. So it must be paid more attention when cleaning bitumen runway. Before cleaning large area, test must be done in a small place to determine appropriate cleaning parameters. Regular cleaning process can be carried out only the conditions of both even glue removal and damage to runway surface within acceptable range being confirmed. During cleaning process, working parameters such as pressure and moving speed of surface cleaner must be adjusted according to changing thickness of glue layer in different area to ensure complete glue removal in presupposition of having no harm to runway surface.

Besides, tests show that rotating cylindric jet head is not fit for cleaning bitumen runway because of its larger impact force and easiness to damage runway surface. So only the rotating micro-hole atomizing jet head consisting of 26 pieces $\varnothing 0.2\text{mm}$ diamond nozzles can be applied in cleaning bitumen runway. This type of cleaning head makes waterjet atomize evenly, enlarges its striking area and meanwhile, reduces its striking force slightly. After cleaning, runway surface can be evenly whitened (as shown in Figure 6). Nozzles on rotating head must be installed closely as far as possible from rotation axis, especially when working with self-driven rotating head. For self-driven rotating head, installation angle of spraying rods must be considered. For compelled-driven rotating head, nozzles can be vertical to runway surface. Because stripping is more effective than braking in higher cleaning efficiency and less injury to runway surface during cleaning bitumen runway, installation of spraying rods must ensure that there is an angle existing between direction of waterjet flow line and vertical line. This angle lies in the range from 45° to 60° according to test results. When cleaning concrete runway, it seems not to be a serious problem. If rotating jet head is propelled by external force, this angle can be omitted.

5. PROBLEMS

Tests were all carried out during period of no flight in airport. Some problems were revealed after summarizing the tests and must be put more emphasis on. First is that no leakage oil is permitted because it will reduce friction factor sharply. This requires the components of unit such as diesel engine, hydraulic pump, motors and valves are carefully selected and bought from qualified manufacturers and carefully checking the connection joints of hoses. Leakage is the first enemy to our cleaning equipment and must be avoided by improving reliability of the total

unit. In addition, weight of surface cleaner must be reduced as low as possible to make it light and mobile.

To guarantee the cleaning process being conducted smoothly, the cleaning unit must be maintained and repaired when not working. Test running must be done before formal cleaning if necessary to confirm the whole equipment being in good condition. Before cleaning, emphasis must be put on checking operators' dressing and connection of high pressure hoses according to requests listed in "Safety Guidance for Running High Pressure Waterjet Equipment". A special person must be assigned to be safety supervisor at working area and work must be definitely divided to every operator before cleaning to avoid confusion during working.

6. CONCLUSIONS

Tests verify the authors' design of 70MPa, 150HP waterjet cleaning equipment is totally appropriate for purpose of airport runway glue removal, larger parameters are not necessary. Two types of rotating head are developed, each has its own usage and the rotating atomizing jet head has a wider scope of usage. Their speeds and qualities of glue removal can fully meet the maintenance demands for modernized airports.

7. ACKNOWLEDGEMENTS

Our work and tests have gained support from Hefei Airport and Guangzhou Airport. Great thanks should be given to them.

8. REFERENCES

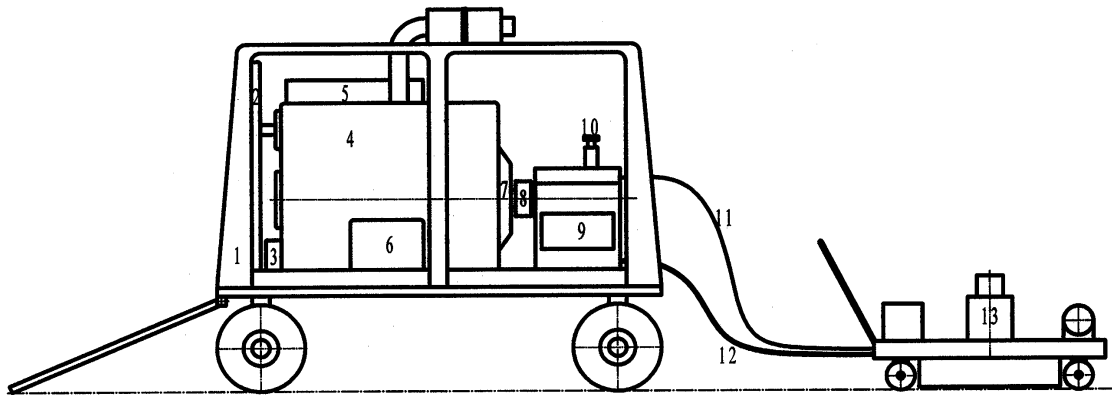
- JB/T 8093-1999, "High Pressure Water Jet Equipment", *Industrial Standard of People's Republic of China*, issued by Bureau of Mechanical Industry, P. R. China.
- JB 8526-1997, "Safety Guidance for Running High Pressure Waterjet Equipment", *Industrial Standard of People's Republic of China*, issued by Bureau of Mechanical Industry, P. R. China.
- Xue Shengxiong, Huang W. P., Chen Zh. W., Fan Y. B., Peng H. J., "High Pressure Waterjet Technology and Its Applications", Mechanical Industry Press, Beijing, 1998.
- Xue Shengxiong, Huang W. P., Chen Zh. W., Shi D. J., "Test Research of Super High Pressure Reciprocating Seal", *Proceedings of the 8th American Waterjet Conference*, pp 547~556, Water Jet Technology Association, Houston, Texas, 1997.
- Zhou Dan, "Runway Cleaning at Shanghai's New Airport", *Jet News*, Nov. 2000.

Table 1 Tests of Runway Glue Removal Using Four Opposite
Installed Cylindric Nozzles Jet Head

Type of Runway	Working Pressure MPa	Rotation Speed of Nozzle Head Rpm	Moving Speed of Surface Cleaner m/min	Cleaning Effect
Concrete Runway	20	800	3	Not clean
	30	800	3	Basically clean, thick glue layer can not be cleaned
	40	800	3.5	All cleaned
	40	800	5	Basically clean, thick glue layer can only be partially cleaned
	45	800	5	All cleaned
	>45			Damage appears
Bitumen Runway	45	800	5	Partly cleaned, no damage to runway surface
	50	800	3	Better than above, no damage to runway surface
	65	800	3	Most glue layer removed, little damage to runway surface, sand and stone can be seen with naked eye
	65	800	1	Nearly all glue removed, obvious sand and stone can be seen, middle degree damage to runway surface

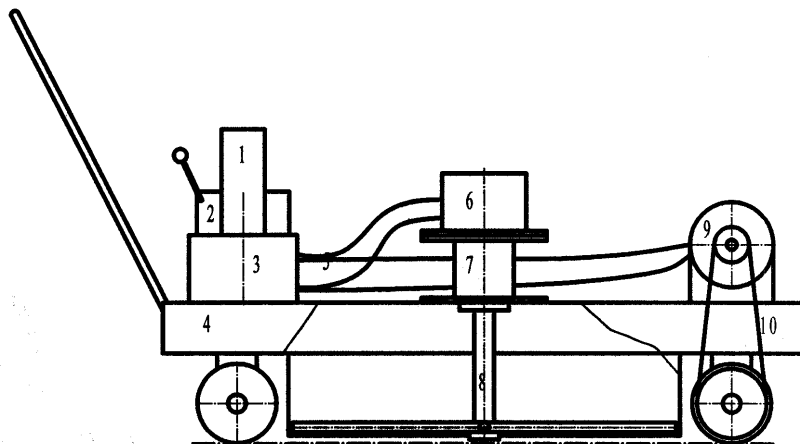
Table 2 Tests of Runway Glue Removal Using Micro-hole
Atomizing Nozzles Jet Head

Type of Runway	Working Pressure MPa	Rotation Speed of Nozzle Head Rpm	Moving Speed of Surface Cleaner m/min	Cleaning Effect
Concrete Runway	65	700	10.5	All glue layer removed, base of runway appears, no injury to runway
Bitumen Runway	65	600	8.2	Nearly all of thicker glue layer can be cleaned, no sand and stone can be seen with naked eye All of thinner glue layer is cleaned, base is exposed, micro sand and stone can be seen, but not many



1. Car 2. Water Cooler 3. Hydraulic Pump 4. 150HP Diesel Engine
 5. Hydraulic Oil Tank 6. Negative Feedback Control System 7. Clutch
 8. 9. High Pressure Pump 10. Pressure Regulation Valve 11. High Pressure Water Hose
 12. Hydraulic Oil Hoses 13. Surface Cleaner

Figure 1. Overall Arrangement of Runway Glue Removal Vehicle



1. Speed Regulation Valve 2. Directional Valve 3. Valve Seat Block
 4. Dolly 5. Hydraulic Oil Hoses 6. Rotation Driven Motor
 7. High Pressure Rotating Seal 8. Spraying Rods and Connections
 9. Movement Driven Motor 10. Chain Transmission System

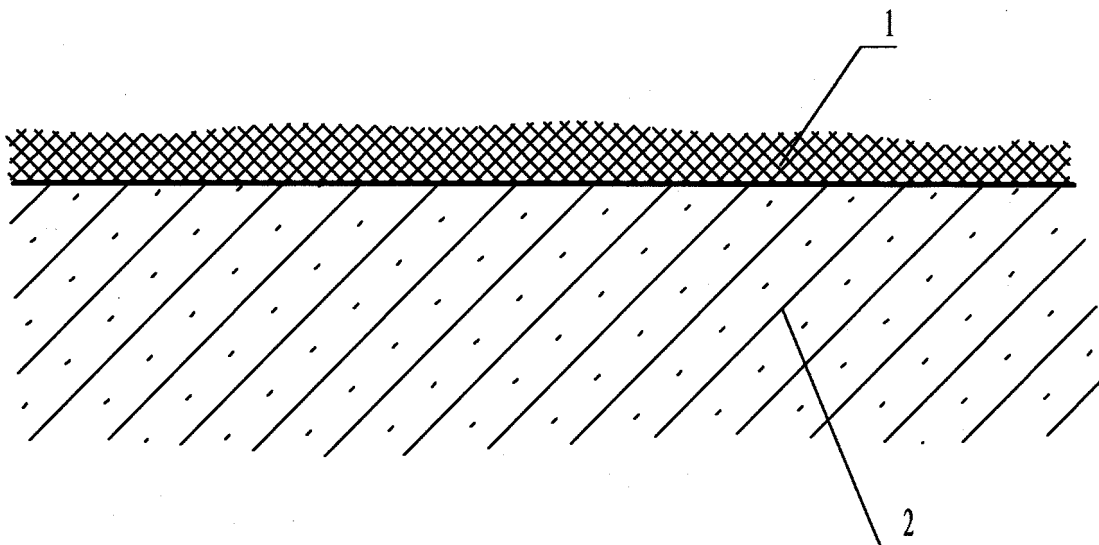
Figure 2. Schematic Diagram of Hydraulic Driven Surface Cleaner.



Figure 3. Equipment for Glue Removal on Airport Runway

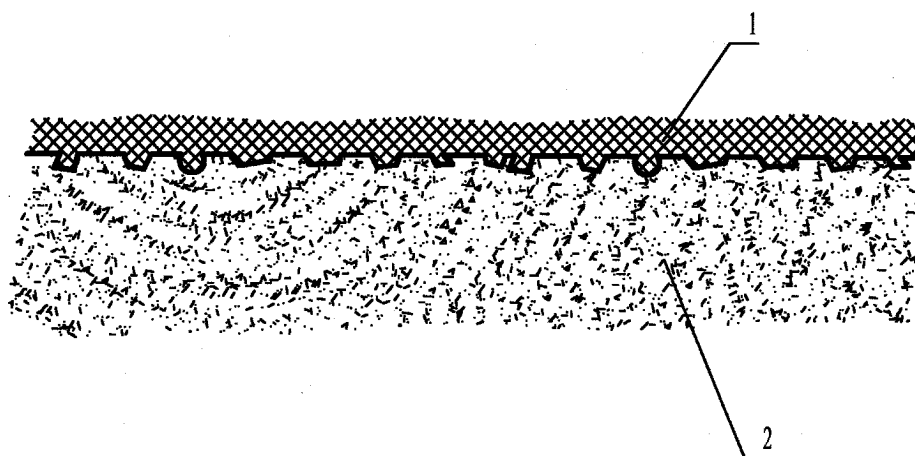


Figure 4. Testing ground of Glue Removal



1. Glue Layer 2. Base of Concrete Runway

Figure 5a. Glue Adhering Mechanism for Concrete Runway



1. Glue Layer 2. Base of Bitumen Runway

Figure 5b. Glue Adhering Mechanism for Bitumen Runway

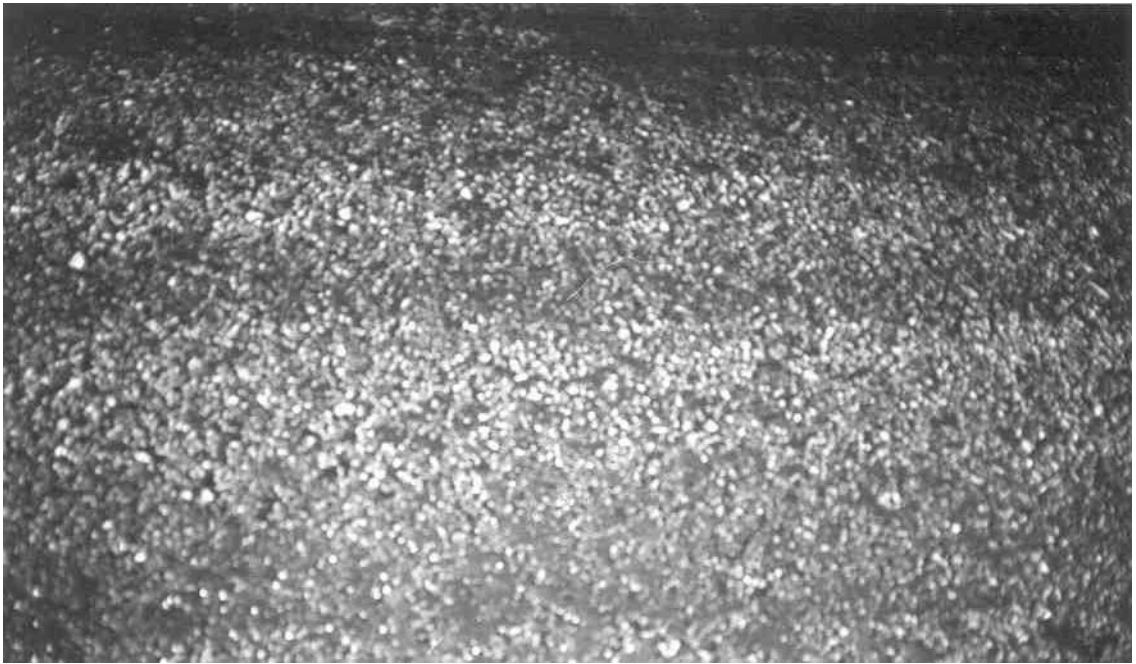


Figure 6. Bitumen Runway after Glue Removal

HIGH PRESSURE WATER JET FOR MINING RED SEA EGYPTIAN PHOSPHATE

Ahmed A. El-Saie, Ph.D.
Tabbin Institute for Metallurgical Studies
Cairo, Egypt

ABSTRACT

High-pressure water jet technology is used for extract, transport, and concentrate the phosphate ore from underground Egyptian mine economically at the Red Sea area. This is the first time this technology is used for underground phosphate mining in the world and it is the first time this technology used in mining in Egypt.

This method is performed practically by using the high-pressure water jet. Special nozzle and lacing are designed to break down only the phosphate ore from the mine pillars into small grain size –5 mm. This article describes the equipment used for applying this technology in the Red Sea Phosphate mining. The water and phosphate ore, slurry, are transported to a collection tank. Slurry pumps are used to transport that slurry from underground to the surface. The slurry is feeding a classifier to separate the phosphate ore from the water and clay. The product has a very high grade, 31-33 % P_2O_5 , and very small percentage of water, 11-14 %. After sun drying the water content is ranging from 6 to 8 %

This article describes the high-pressure water nozzle, lacing and monitor, which are used to hydraulically mine the phosphate ore from underground mine. Also, it describes the labor management.

1. INTRODUCTION

Many applications can be realized by using high-pressure water jet for mining coal, ores, and rocks. Water jet mining and slurry transport are attractive alternatives for the mining industry. Coal is fragmented by water jet impact and transported as slurry in former USSR (Okhrimenk et al 1974), Japan (Otsuka 1981), and Canada (Parks and Grimley 1975). In United States the phosphate mining industry uses hydro-monitors and slurry pumps for slurring and transporting phosphate ore on the surface (Cooley, 1976), (Jet News, June/July 2000).

This new technology is used for extract, transport, and concentrate the phosphate ore from underground Egyptian mine economically. This is the first time this technology is used for underground phosphate mining in the world and it is first time this technology used in mining in Egypt.

This paper describes the equipment used and labor management to produce the phosphate ore from underground phosphate pillars, which are left after the conventional room and pillars mining method.

2. HYDRAULIC MINING METHOD

This mine is located in Hamrwain area at the Red Sea Governorate, Egypt, see Figure 1. Underground fresh water is found in most mines in this area under 38 meter above the sea level. The dimensions of these pillars vary from 2 by 2 meters to 5 by 5 meters.

2.1 Equipment Used

- High pressure water pumps
- High pressure water monitor and its carrier
- Slurry pumps.
- Collection tank with agitator.
- Submersible slurry face pumps.
- Spiral classifier
- Multi-stage water pumps.
- Steel slurry pips.
- Water pipes.
- High and low pressure hoses.

2.2 Water Source

The fresh water is drawn from the underground water in the mine using multi-stage water pump, see Figure 2. The fresh water is used for:

1. To fill the high-pressure pumps feeding tank.
2. To adjust the water-phosphate concentration in the collection tank.

3. To facilitate the collection-tank screen operation, to pass the phosphate and remove the refuse oversize rock.
4. To help the slurry flowing easily in the channels.

2.3 High Pressure System Nozzle and Monitor

Special nozzle and lacing are designed to break down only the phosphate ore from the mine pillars into small grain size –5 mm. and leave the waste material having large size, see Figure 3.

2.3.1 High pressure water pumps

Three high-pressure pumps are used each has capacity of 75 l/m at a pressure 200 bars. It operates with electric motor, which has a power 37.5 kW. A relief pressure valve adjusts the pressure, which is capable of adjusting pressure from 0 to 400 bar.

2.3.2 High pressure water nozzle

A special nozzle, see Figures 4, and 5, is designed to satisfy the requirement of jet coherency and to reach a stand off distance of more than 4 meters. It is made from stainless steel. The nozzle internal surface was polished to provide a smooth surface to reduce the turbulence of the flow near the nozzle exit, and to supply a jet with coherent core and further cutting action, i.e., long stand off distance.

2.3.3 High pressure water lacing

A special lacing, see Figure 6, is designed to allow the nozzle to advance nearer to the face or far from it. Also, the design allows the operator to work at a distance from the face, about 4m, i.e. in safe distance to be further from any water splashes or flying rock. The operation showed that the operator is in very safe distance from the face. The operator can read the pressure in the lacing, which is very close to the pressure at the nozzle, see Figure 6.

2.3.4 High pressure water monitor

Special monitor, see Figure 6, is designed to allow the nozzle to move up and down, right and left. Also, the monitor is allowing the nozzle to advance nearer to the face or far from it in small increments from 0 to 600 mm, as well as, it is allowing the nozzle to move in large increment 600 mm to 3000 mm. The operator can see the face and the nozzle action as well as the direction of cutting, see Figure 6.

2.3.5 High and low pressure hoses

A 25-mm low-pressure hose is used to increase the water flow in the slurry channels to help the phosphate slurry flowing.

A 25-mm high-pressure hose is used to connect the high pressure water steel pipe to the monitor.

2.4 Roof Supporting

The roof of the mine was holding very well. In spite of this, the author tried three different methods of roof support. The first one is building pillars from the waste rock found in the mine after the removal of the phosphate ore, see Figure 7. The second support system was using wood props to protect the operator and monitor, see Figure 8. The third method was leaving portion of the ore pillars to protect the labors and equipment, see Figure 9. It is found the last two options were very satisfactory.

2.5 Hydraulic Transportation

Water and phosphate ore, slurry, are flowing in channels dug in the mine floor, see Figure 10, to a collection tank, and see Figure 11. These channels must have enough inclination, more than 10 degrees, to allow the slurry to flow free without deposition in the bottom of these channels. If the grade of the channels do not allow for this free slurry flowing, a small tank with screen should be erected and submersible pumps should be used for the horizontal or near the horizontal passages. The submersible pump will feed the collection tank or the nearest flowing channel. There is a screen installed over the submersible pump tank with 10 mm opening to prevent the large size rocks from entering the submersible pump case and line. Also, there is a screen installed over the collection tank with an opening of 5 mm to allow the -5 mm phosphate and clay to pass through to the collection tank. The + 5 mm is removed from the screen manually. Slurry pumps, see Figures 12 and 13, are used to transport that slurry from underground collection tank through underground entries pipeline, see Figure 14. Then this slurry transported to the surface through pipeline, see Figure 15.

2.6 Concentration Facility

On the surface, the slurry is feeding a spiral classifier, see Figure 16, to separate the phosphate ore from the water and clay. Water and clay are directed to near-by valley, see Figure 16. Water goes back through the cracks and fissures to the underground water table. Some of this water is used to irrigate nearby small farm.

2.7 Phosphate Concentrates

The product has a very high grade, 31-33 % P_2O_5 , and very small percentage of water, about 11 to 14 %, see Figure 17. The phosphate concentrate produced from the spiral classifier is spread in a sun dryer to reduce the amount of water content in the phosphate concentrate. After sun drying the water content ranges from 6 to 8 %. The sun dryer is just a leveled floor with thin layer of concrete (150 mm), the concentrate can be turned over periodically to allow the sun to dry it.

2.8 Labor Management

Eleven workers and supervisor per shift per face were performing the following functions:

- Two workers on the monitor.

- Two workers on the slurry channels and submersible pump if present.
- Two workers on the collection tank and screen.
- Two workers for supports and services.
- One mechanic.
- One electrician.
- One on the surface nearby the classifier
- One by the multi-stage water pumps.

3. MAIN ADVANTAGES OF THIS MINING METHOD

1. It is a selective mining method.
2. No need for using drilling and blasting. Explosives costs about 25 % of the selling price.
3. No need to transport the country rocks and wastes from underground to the surface then to the dressing plant.
4. No need to a complicated dressing plant's flow sheet, the dressing is performed very simply right on the mine mouth.
5. No need for crushing and grinding.
6. Convergence is very small compared with the drill and blast mining methods.
7. All operations are clean, no pollution, and environment friendly. There is no dust, which the workers inhale during the mining, transportation, screening, crushing, grinding, and at the dressing plant.
8. This method conforms with sustainable development concept.
9. It preserves the Egyptian mineral wealth. Most of underground mining methods leave about 30 to 50 % from the ore in pillars without extraction. This hydraulic mining method can extract about 100 % of the ore from underground deposits.
10. Conserve the energy by reducing the number of conventional operations such as crushing, grinding, screening, and concentration processes.
11. The ability of this method to re-open the closed mines because the high cost of explosives, drilling, and haulage, or for de-pillaring the mines.
12. Increase the reserves in the mine, due to the usability of the ore in the supporting pillars (mine losses). Also, mine's ore under water level can be extracted due to draining the water and lower its level, then that ore can be extracted.
13. The simplicity of the operations and high efficiency of equipment, such as pumps.
14. The economics of this method is high because it integrates many conventional operations, such as drilling, blasting, transportation, and concentration in one operation.

4. CONCLUSION

This method of mining phosphate deposit is applicable for underground or surface mines as long as the source for water is available near the deposit. This method of mining is a selective one. This method can extract the phosphate deposit economically and profitably. It can be used for exploitation of the deposit, as well as, for development as long as the height of the seam is enough for workers to perform their duties and functions.

5. ACKNOWLEDGEMENT

The author thanks all the employees and engineers of JETECH Company, for their effort to make this pioneer work become reality. The author fully recognizes the encouragement of Chairman of Red Sea Phosphate Co. Also, thanks him for giving this idea a chance to transform from a dream to reality and for his confidence in the author's ability to perform this work successfully. The author, also, appreciates the cooperation and long discussions of Prof. Dr. Samir I. Youssef, which generated the solutions for many problems.

6. REFERENCES

1. Cooley, (1976), "Survey of Water Jet Coal Mining Technology," Proc. 3rd Int. Symp. On Jet Cutting Technology, Chicago, USA.
2. El-Saie, A. A., (1977) "Investigation of Rock Slotting by High Pressure Water Jet For Use in Tunneling," Ph.D. Thesis, University of Missouri-Rolla.
3. El-Saie, A. A., (1993) "Rock and Metal Cutting by High Pressure Water Jet," TIMS Bulletin, Vol. 61.
4. Jeremic, M.L., (1983) "Elements of Hydraulic Coal Mine Design," TRANS TECH PUBLICATIONS, Germany, and GULF PUBLISHING COMPANY, Houston.
5. Jet News, "Hydraulic Mining," Water Jet Technology Association, June/July 2000.
6. Momber, W., Andreas, (1998) "Water Jet Applications in Construction Engineering," A. A. Balkema, Rotterdam, Netherland.
7. Okhrimenki, V. A., Nuprim, and A. I., Ishchuk, I. G., (1974) "Underground Hydraulic Mining of Coal," Nedra Publishers, Moscow.
8. Otsuka, T., (1981) "The Hydro-Mine Sunagawa," Glukauf, v. 117, No. 24.
9. Parks, D. M., and Grimley, A. W., (1975) "Underground Hydraulic Mining of Coal," Coal Convention of Am. Min. Congress, Pittsburgh, Pa USA.

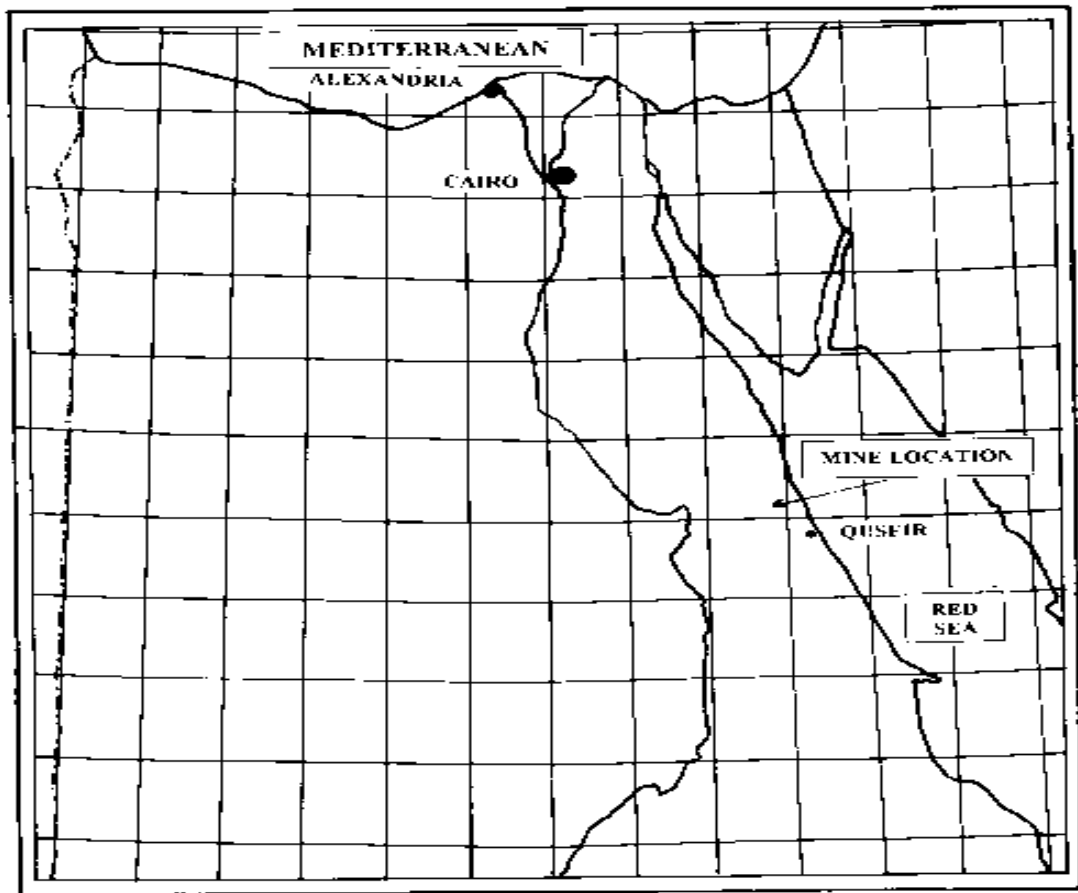


Figure 1. Map of Egypt showing the mine location.



Figure 2. The fresh water is drawn from the underground water in the mine using multistage water pump.



Figure 3. The high-pressure monitor, cutting the phosphate seam.

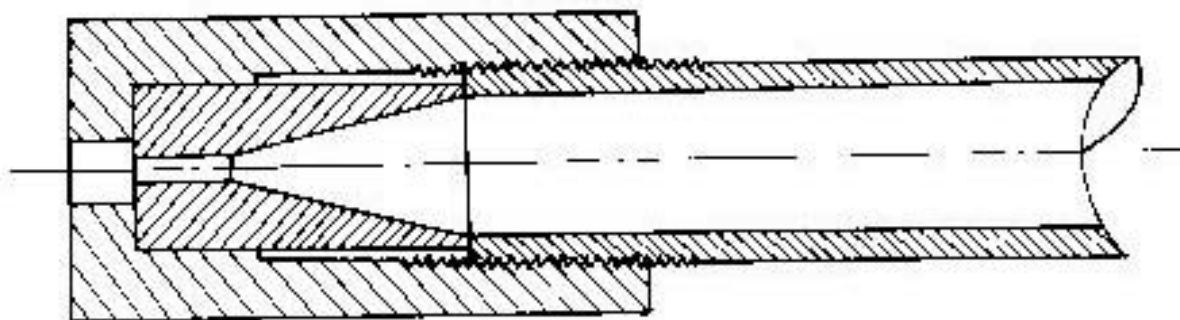


Figure 4. Special nozzle design cross-section.

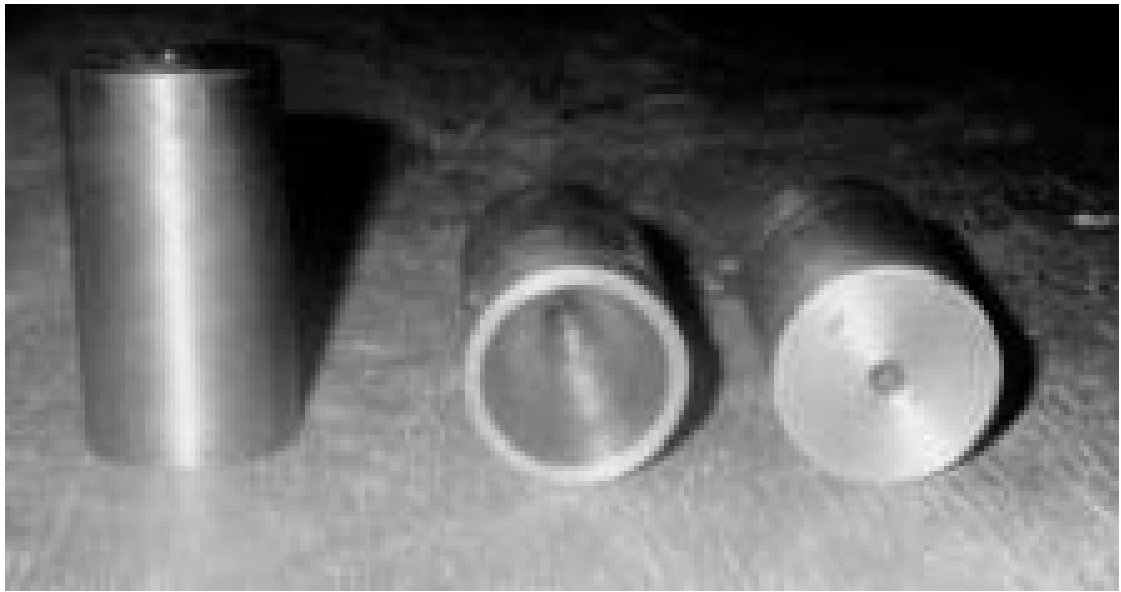


Figure 5. The configuration of the nozzle's inside.

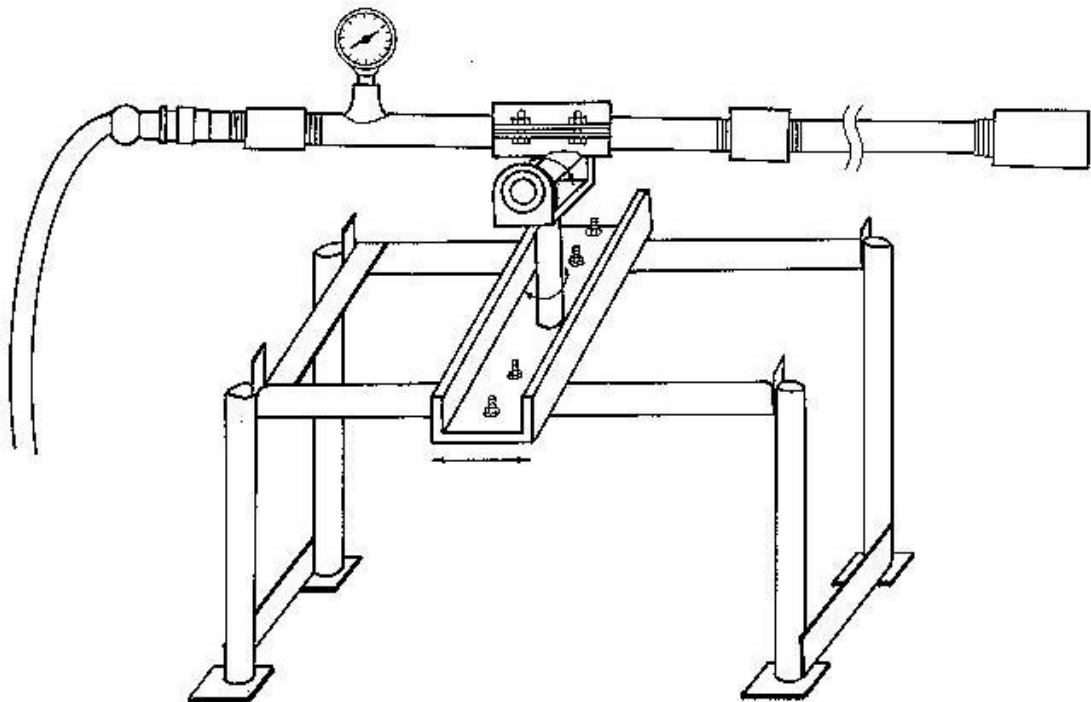


Figure 6. A special monitor design.



Figure 7. Roof support by building rock pillars.



Figure 8. Roof support by installing wood props.



Figure 9. Roof support by leaving portion of the ore pillar.



Figure 10. The High Pressure Monitor, cutting the phosphate seam, water-phosphate slurry flow through dug channels in the mine floor.



Figure 11. Slurry collection tank and agitator installed on it.

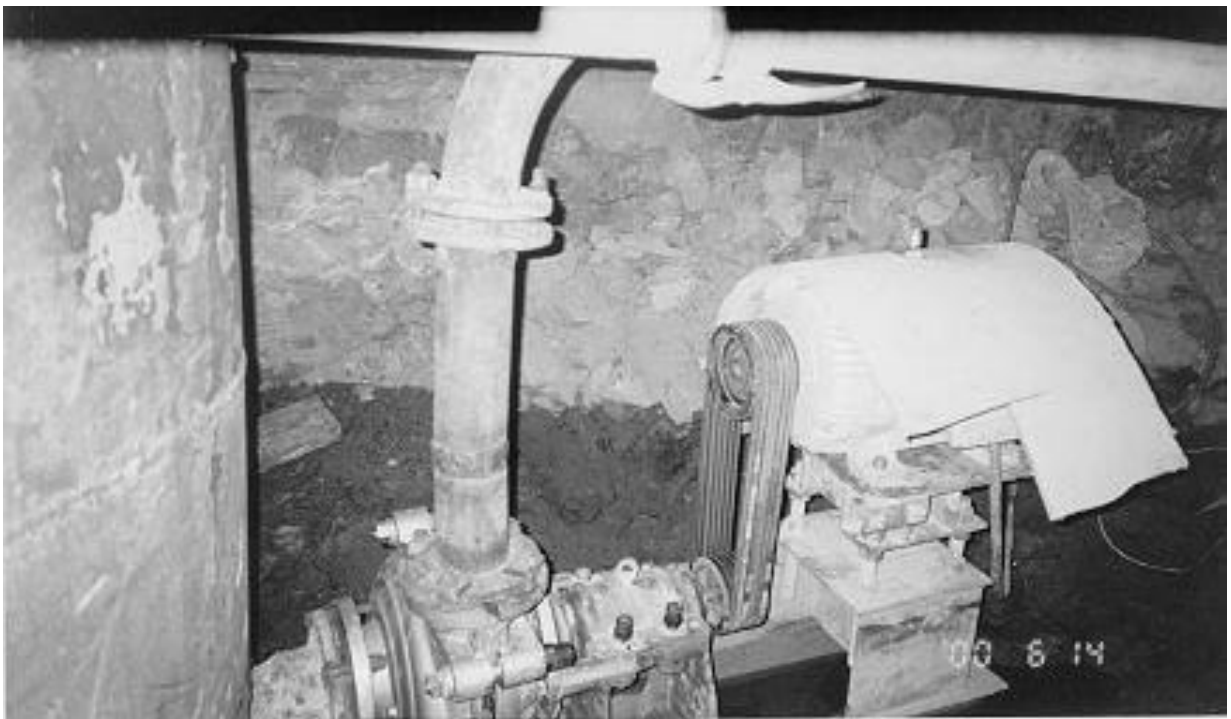


Figure 12. First slurry pump connected to the slurry collection tank.



Figure 13. The third slurry pump installed in one of the mine entries.

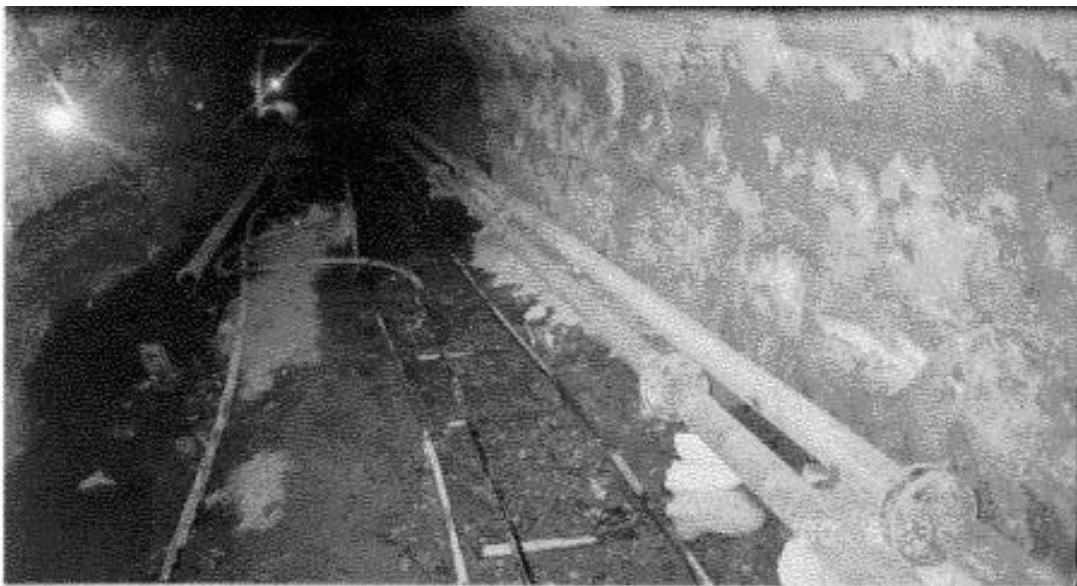


Figure 14. Water-phosphate slurry flow through pipeline in underground entries.



Figure 15. Water-phosphate slurry flow through pipeline on the surface to the classifier.



Figure 16. Water-phosphate slurry flow through pipeline to the classifier, water and clay are directed to nearby valley. Some of this water is used to irrigate nearby small farm.



Figure 17. The phosphate concentrate produced from the spiral classifier.

RESEARCH OF WATERJET INTERACTION WITH SUBMERGED ROCK MATERIALS

**L.M. Hlaváč, I.M. Hlaváčová, M. Kušnerová, V. Mádr
VŠB - Technical University Ostrava
Ostrava, Czech Republic**

ABSTRACT

The material properties of submerged rocks and rock like materials are different from the dry ones measured in air. Simultaneously, there are some problems in practice solvable by using the waterjet technology for disintegration of such materials directly “in situ“. Therefore, one part of the theoretical and experimental research in the Institute of Physics at the Technical University Ostrava has been aimed at these problems. The pressure vessel was prepared for testing of both the material properties up to certain depth of submersion and the influence of the water jet on them. The experimental results obtained in the vessel are presented in the paper, discussed and analyzed both from the point of view concentrated on material properties and from the point of view focused on decay of waterjet efficiency in liquid medium. Some theoretical models are also presented. The experimental data are correlated with results of the theoretical analyses and largely discussed.

1. INTRODUCTION

This research is a part of the project devoted to the interaction of water jet with rock type material situated in non-traditional conditions. One of such states of material is submersion. The efficiency of tools with rotating, swinging or vibrating nozzled heads is decreased in water (oil or another liquid). Nevertheless, there are certain events in practice for which it is good to have some alternative chance prepared. We tried to study the efficiency of the water jet in water medium without pressure, it means near the level. It was done in order to have any idea how the change of density of the surrounding medium influences the jet flow. The water jet efficiency in certain depth under the level was then also investigated. A special pressure vessel was prepared for this purpose (Figure 1).

2. THEORETICAL BACKGROUND

The basic theoretical presumption presented by Hlaváč et al. (1999) concerning the attenuation of water jet in the medium between the nozzle outflow and target material surface was based on theories of cumulative charge (Lavrentjev, 1957). The equation for attenuation coefficient ξ was derived from the relationships describing the cumulative charge. The coefficient is related to the parameters of the liquid continuum surrounding the nozzle. This derivation was carried out because both phenomena resemble each other from the physical point of view. According to this theoretical assumption the coefficient ξ can be calculated from the equation 1 for any continuum which the liquid jet is moving through.

$$\xi = \frac{C_x}{\mu} \frac{\rho_{env}}{\rho_o d_o} \quad (1)$$

In accordance with theories of Lavrentjev and other specialists on physics of cumulative charge we supposed that the attenuation coefficient (better said the jet penetration length) in any continuum is determined directly by the density of the continuum. This basic relationships had to be proved by tests made in the pressure vessel alike other hypotheses.

Opposite to the decrease of water jet efficiency due to the density of medium between nozzle and target the increase of disintegration effect was expected due to a rock material drop in strength caused by soddenness. The increase of pressure in water surrounding the target material should cause a further drop in water jet efficiency because the density of liquid increases with increasing of its pressure. Nevertheless, we had no possibility to measure coefficient ξ directly. We have only some possibility to determine it more exactly by introduction of some additional factors (except those resulting directly from the modification of physical conditions, e.g. pressurized water density or non-omissible change in difference of the pressure inside and outside the pump). Therefore, we modified equation 1 and the equation 2 was obtained:

$$\xi = \frac{C_x(p)}{\mu} \frac{\rho_{env}}{\rho_o d_o} \frac{\eta_a}{\eta} \quad (2)$$

All other theoretical relationships were used from our previous theoretical investigations, especially the ones presented by Hlaváč (1992, 1995, 1999). The equations resulting from the theory and applied for calculations in this paper are presented here in the form valid for one pass as equations 3 and 4 (for depth of disintegration and coefficient of jet velocity loss).

$$h = \frac{\pi d_o \sqrt{2 \rho_o \mu^3 p^3 \gamma_R^3 e^{-5(\xi L)} (1 - \alpha^2) \cos \theta}}{4 \chi \rho_M v^{\frac{\rho_o}{\rho_M}} \left[\alpha^2 e^{-2(\xi L)} \mu p \gamma_R + \frac{\rho_o}{\rho_M} \sigma \right]} \quad (3)$$

$$\alpha = 1 - \frac{C_d^2 \sqrt{2 \mu^3 p^3 \gamma_R^3 \rho_M^* k^*}}{8 \sqrt{\rho_o} \eta \sigma_s a e^{3(\xi L)}} \quad (4)$$

3. DESCRIPTION OF EXPERIMENTAL MATERIAL

The blocks of light green medium grained glauconite sandstones from the Godula Unit in Beskydy Mountains (the West Carpathian in the Czech Republic) were selected for experiments. This type of sandstone was used for many experiments with water jets and abrasive water jets in the past and it is used also for experiments with a laser beam. This very hard and abrasive sandstone is composed of detrital quartz, quartzite grains, quartz-feldspars aggregate in grains, feldspars (orthoclase, oligoclase-andesine) grains and irregular detrital flakes of various types of mica (medium grain size 0.3 mm). Detrital grains of quartz and feldspars are sub angular in shape, ranging from 0.2 to 0.5 mm in grain size. Diagenetic corrosion and outgrowths of quartz are quite frequent. The matrix is compound of clay matter (illit, mica) with authigenic cement as carbonates (individual crystals of Fe-dolomite-ankerite series) and with fine silicification. Minerals as glauconite, which formed small yellow-green pellets (approximate maximum size 0.5 mm), have an authigenic origin. Sorting of detrital grains is bad. Texture is psammitic, from a sub angular up to an angular shaped, medium grained. The mean value of the specific volume weight of sandstone (including pores) is 2500 kg.m⁻³, the specific weight of sandstone matter (without pores) reaches 2640 kg.m⁻³ and the values of uniaxial compression strength and tensile strength are determined to be 128 MPa and 9 MPa respectively.

4. EXPERIMENTAL PROCEDURE

The water jet penetration length is a hard indictable parameter and the methodology for its measurement is still in the preliminary stage. The efficiency of water jet was determined from the depth of disintegration on rock materials. Up-to-date the above described model rock was used for experiments because it is very homogeneous with a small amount of disorders and failures. The blocks of this sandstone were prepared at a diamond saw without any additional treatment. The dimensions of the blocks were approximately 10 x 10 x 2 cm. Each block was fixed in the support

of the motional device inside the pressure vessel in the beginning of the experiment. The vessel was closed and filled with water except the case when the tests for comparison were performed in air. Water inside the vessel was either without pressure or pressurized. Pressurizing of water was ensured by inflow from the cutting nozzle and regulating overflow valve. Pressure inside a vessel was indicated by mechanical pressure meter installed at the vessel body. The kerfs were made by water jet in the sandstone samples at various traverse rates. The depths of kerfs were measured and applied as the criterion for efficiency comparison.

5. RESULTS AND DISCUSSION

Some of our up-to-date results are presented in Table 1. It can be mentioned that the difference between results obtained in air and non-pressurized water is very small, within the uncertainty of the measurement, determination of both rock and water jet parameters. Nevertheless, the results are in good correlation with theoretical presumptions - see the graph in Figure 2. The curves were calculated using above presented theoretical equations and the points were determined as the average values of measured data. The further experiments are prepared but could not be realized yet. They are aimed at monitoring the relationship for stand-off distance. This relationship could help us to solve the problem with determination of the appropriate method for coefficient ξ measurement.

6. CONCLUSIONS

The theoretical relationships derived previously could not be used for correlation with experimental data directly. It was caused by the fact that the primary theoretical expectations differed from the experimental results greatly. The difference was not in the character of the relationship but only in the quantitative values. These disproportions were eliminated by modification of the theoretical equation for calculation of the attenuation coefficient. The theoretical expectations derived from the adjusted model are in a good correlation with our present data; not only a qualitative one but also a quantitative one. The up-to-date results show that the theoretical equations for efficiency can be used without any substantial change provided that coefficient of water jet attenuation is determined correctly. The modified equation for calculation of the coefficient of water jet attenuation in the medium filling the space between the nozzle outlet and target surface could not be proved yet, however.

7. ACKNOWLEDGEMENTS

The authors are grateful for support of the work presented in this paper to the Grant Agency of the Czech Republic by project No. 106/98/1354.

8. REFERENCES

- Hlaváč, L., “Physical description of high energy liquid jet interaction with material,” *Geomechanics 91*, pp. 341-346, Rotterdam, Balkema, 1992.
- Hlaváč, L.M., “Physical Analysis of the Energy Balance of the High Energy Liquid Jet Collision with Brittle Non-Homogeneous Material,” *Proceedings of the 8th American Waterjet Conference*, M. Hashish (ed.), pp. 681-697, Water Jet Technology Association, St. Louis, Missouri, 1995.
- Hlaváč, L.M., “Theoretical and experimental investigation of a high energy waterjet efficiency on thermally treated rocks,” *Proceedings of the 10th American Waterjet Conference*, M. Hashish (ed.), pp. 497-506, Water Jet Technology Association, St. Louis, Missouri, 1999.
- Hlaváč, L.M., Hlaváčová, I.M., Mádr, V., “Quick method for determination of the velocity profile of the axial symmetrical supersonic liquid jet,” *Proceedings of the 10th American Waterjet Conference*, M. Hashish (ed.), pp. 189-199, Water Jet Technology Association, St. Louis, Missouri, 1999.
- Lavrentjev, M.A., “Cumulative Charge and Principles of Its Work,” *Achievements in Mathematics*, Volume 12, Number 4, pp.41-56, 1957. (in Russian)

9. NOMENCLATURE

α	coefficient of losses in liquid jet velocity during interaction with material ...[-]
a	material grain size ...[-]
γ_R	compressibility factor ...[-]
$C_{x^*}, C_x(p)$	coefficient of liquid (water) jet forehead resistance and pressure dependant coefficient of liquid (water) jet forehead resistance in the medium ranging between nozzle outlet and target surface respectively ...[-]
C_d	coefficient of resistance of the material structure to the liquid (water) jet ...[-]
d_o	liquid (water) nozzle diameter ...[m]
η	liquid (water) dynamic viscosity ...[N.s.m ⁻²]
η_a	air dynamic viscosity ...[N.s.m ⁻²]
h	depth of disintegration in material ...[m]
θ	angle of an incidence of the liquid (water) jet measured between a normal line at the point of jet's axis projection through material surface and jet axis ...[rad]
k^*	material dynamic permeability ...[m ²]
L	stand-off distance ...[m]
μ	nozzle discharge coefficient ...[-]
ξ	coefficient of attenuation of jet caused by resistance of the medium between nozzle outlet and target surface ...[m ⁻¹]
p	liquid (water) pressure before the nozzle inlet ...[Pa]
p_v	water pressure inside a pressure vessel ...[Pa]

ρ_o	liquid (water) density in the non-compressed state ...[kg.m ⁻³]
ρ_{env}	density in the non-compressed state of the medium ranging between nozzle outlet and target surface ...[kg.m ⁻³]
ρ_M	specific volume weight of material (including pores) ...[kg.m ⁻³]
ρ_M^*	specific weight of material (without pores) ...[kg.m ⁻³]
σ	material compressive strength or combined strength ...[Pa]
σ_s	material shear strength ...[Pa]
v	modified traverse rate ...[m.s ⁻¹]
χ	coefficient of reflected jet expansion due to mixing with disintegrated material ...[-]

10. TABLES

Table 1. The experimental results (depths of kerfs) performed with the following parameters: water pressure in the pump $p = 350$ MPa and $p = 200$ MPa, the water nozzle diameter $d_o = 0.2$ mm, the stand-off distance $L = 13$ mm, the angle of impact $\theta = 0$ rad, the pressure of pressurized water in the vessel $p_v = 1.2$ MPa.

traverse rate	350 MPa			200 MPa		
	depth in air	depth in water	depth in pressurized water	depth in air	depth in water	depth in pressurized water
[mm.s ⁻¹]	[mm]	[mm]	[mm]	[mm]	[mm]	[mm]
10	11.7	10.7	7.1	5.3	5.2	3.2
20	9.3	9.3	6.7	4.8	4.5	2.8
30	8.2	7.9	5.2	4.4	3.9	-
40	7.1	-	-	-	-	-
50	6.6	6.5	4.2	3.4	2.6	1.4
75	6.2	5.7	3.8	3.1	2.3	1.2
100	5.0	4.9	3.1	2.7	2.0	0.9

11. FIGURES



Figure 1. The mobile pressure vessel for testing of water jet in pressurized surrounding water up to 5 MPa.

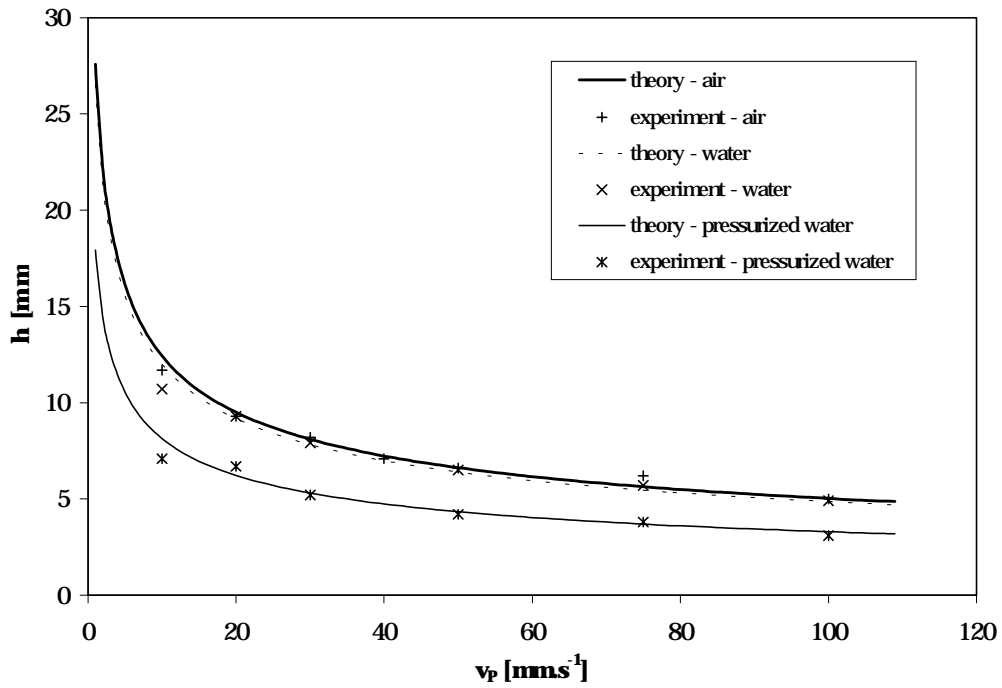


Figure 2. Comparison of theoretical and experimental results of the depth of kerf obtained for water pressure 350 MPa.

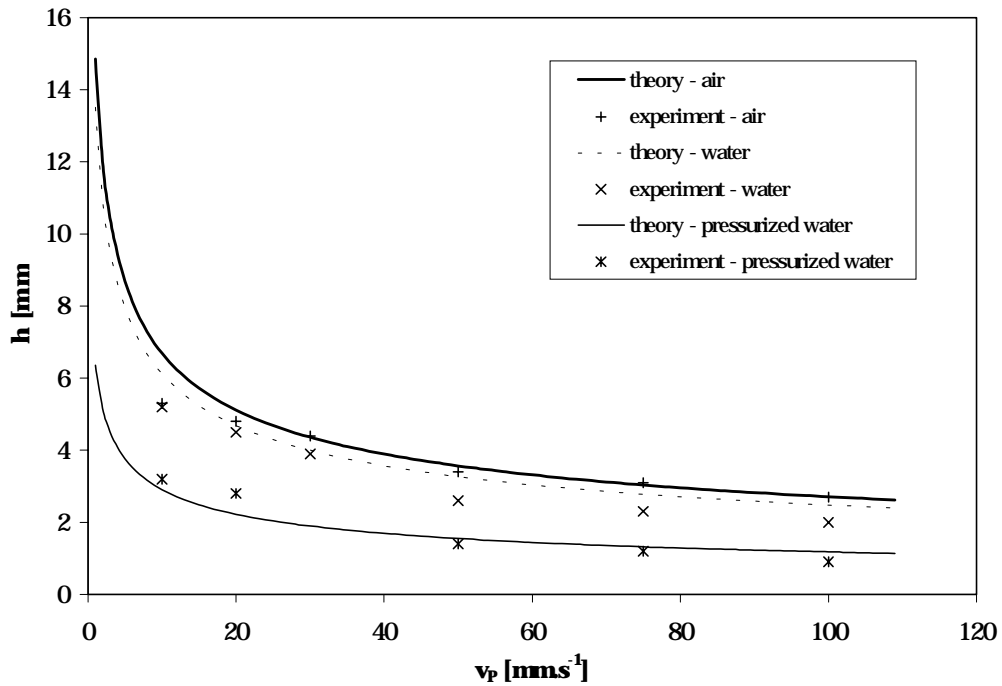


Figure 3. Comparison of theoretical and experimental results of the depth of kerf obtained for water pressure 200 MPa.

**THE STUDY ON THE BREAKER OF SELF-EXCITED
OSCILLATION PULSED JET TO SCOUR THE HARD
CLAY AND ROCKY BEDS UNDER WATER**

Tang Chuanlin, Zhang Fenghua, Yang Lin
The Zhuzhou Institute of Technology
Zhuzhou, Hunan, P. R. China

Liao Zhenfang
The Institute of Mechanical Engineering
Chongqing University
Chongqing, P. R. China

ABSTRACT

It is essential that the hard clay should be broken and the ore deposit should be loose for exploiting beach placer under water with sand pump or airlift. The feasibility of the nozzle of self-excited oscillation pulsed jet (SEOPJet) as the breaker and loosening device for the airlift or centrifugal pump is researched. The dynamic characteristics of the SEOPJet to crush the hard clay and loose the layer of ore deposit are explored experimentally under the submerged condition. It is shown that the SEOPJet not only effectively breaks the hard clay or loose the particles of sand on the placer bed, but also produces fluctuating uplift forces acting on particles of sand. The oscillating radial flow caused by the SEOPJet makes particles of sand move to the end of the suction pipe quickly. Velocities of the airlift to penetrate the hard clay and concentration of the solids for the solid-liquid mixture sucked by the airlift or sand pump are increased obviously.

1. INTRODUCTION

The devices which have been used to mining under water, dredging the river or lake and excavating the channel are mainly the mechanical dredger, submersible pump, airlift and jet pump. Operating under water to use mechanical dredger, its efficiency is low, cost is high, the depth to excavate under water isn't enough. There are these shortages for sealing device of submersible motor is unreliable, vane type pump wears seriously and the operating is discontinuous, when the submersible pump has been applied to dredge ore deposit under water. So, the airlift and jet pump are the ideal devices to break, lift and transport the clay and ore deposit under water for these possess simplified structure, good wear-resistance, reliable running and high dredging depth. The key parts of these devices are the breaker and lift equipment. As to the breaker, the mechanical cutter device and the ordinary continuous jet have been used usually in the operating field. Some problems have been resulted from these breakers. They are that:

- (1) They can't break the hard clay and sand gravel (over grade IV)
- (2) The crushed particles of the hard clay and sand gravel are frequently held to the bottom of water by large differential pressure (static pressure and dynamic pressure of jet). The radial velocity adjacent to the suck head of the airlift (jet pump) is not enough to push them to move quickly. It is to change the concentration of solids of solid-liquid-air mixture sucked by the airlift and makes the quantity of solid to decrease.

It is well known that the impacting characteristic of pulsed jet is superior to that of ordinary jet. Therefore, authors try to use the self-excited oscillation pulsed jet as the breaker of the airlift (jet pump) to resolve these problems. Some laboratory and field tests have been carried out.

2. EXPERIMENTAL SYSTEM AND MEASUREMENTS

2.1 Experimental System

The sketch of the experimental system is shown in figure 1. It is made up of the airlift, breaker, transporting riser and measuring system. The air-lift device consists of airlift 6, pipe supplying compressed air 7 and riser 8. The breaker includes centrifugal pump 1, valve 2, pipe 3, hinge joint 4 and the nozzle of self-excited oscillation pulsed jet 5. The pressure transducers 9, signal processor 10, mini-computer 11 and oscillograph 12 constitute measuring system.

2.2 Measurements

2.2.1 Pressure Measurement

Under the submerged condition, the dynamic stagnation pressure and radial impingement pressure distributions are measured. It is shown in figure 2,3,4, 5. From these figures, the nozzle of the SEOPJ can produce strongly oscillating pulsed jet whose fundamental frequency is about 5~50Hz. The average peak dynamic stagnation pressure is (1.75~2.5) times that of

ordinary jet, the standoff distance in which the mean dynamic pressure at the axial of the jet can erode the target increases greatly. It is shown experimentally that the sharper the oscillating pressures fluctuate, the larger the standoff distance in which jet can crush rock. The radial peak dynamic velocity of the SEOPJ is larger than that of ordinary jet. In other word, it makes the particles of clay be pushed quickly when the radial velocity on the chips increases. The distribution of the difference pressure (which is equal to subtracting radial mean pressure from radial peak fluctuating pressure) is given in figure 5. It shows that the region of flow along the bottom of the test cell where the peak fluctuating pressure is greater than the mean pressure. The particles of clay located directly beneath the nozzle exit would not experience a lifting force. But within this region a lifting force is available to aid in the particles of clay removal. It is shown in figure 6 that the forces acting on the particles of clay are gravity G , float force G_f , pushing force F_r resulted by the radial flow, friction force F_f and lifting force ΔF resulted by the SEOPJ. They are given by:

$$G = \frac{4}{3}\pi(d_m/2)^3 \rho_s g \quad (1)$$

$$G_f = \frac{4}{3}\pi(d_m/2)^3 \rho_L g \quad (2)$$

$$F_r = k\pi(d_m/2)^2 \rho_L V_r^2 / 2 \quad (3)$$

$$F_f = \mu [G - G_f + (P_a + \rho_L gh) \pi (\frac{d_m}{2})^2 - \Delta F] \quad (4)$$

$$\Delta F = \frac{1}{4}\pi d_m^2 \Delta P \quad (5)$$

It is necessary that the driving force F_r be larger than the friction force F_f for the particles of clay to be moved to the end of the suck pipe. Let it be supposed that:

$d_m=0.68\text{mm}$, $\rho_s=2450\text{kg/m}^3$, $\rho_L=1000\text{kg/m}^3$, $k= 0.17$, $f_1=0.55\sim 0.65$. V_r and ΔP can be taken from Figure 4 and Figure 5. It has been shown by calculating that F_r is greater than F_f in the region of $0.17 < r/H < 0.35$. This behavior is consistent with the analyzing results of M. R. Well and is demonstrated by the simulating test.

2.2.2 Simulating Scouring Test

The artificial hard clay, whose mechanical property similar to that of field, has been positioned on the bottom of the test cell. This target has been impacted by the SEOPJ. The standoff distance is equal to 10 times the diameter of the nozzle, the water-head of the centrifugal pump is

about 20m, 30m, 40m, 50m, 60m, 110m. The test results are shown in figure 7. It is shown that the scour depth is a function of the peak oscillating velocity, oscillating frequency when the other parameters aren't changed such as standoff distance, radial distance, the diameter of nozzle, the depth of water et al. The relationship between the scour depth and the peak oscillating velocity as well as oscillating frequency may be described by:

$$s_d = \frac{U_p}{fd} \quad (6)$$

$$\frac{e}{d} = k_1 s_d^n \quad (7)$$

It can be concluded that the greater the oscillating peak velocity is, the larger the scour depth. Moreover, the ordinary jet cannot scour the hard clay and gravel (grade IV~VI), but the SEOPJ can do it, on the same conditions, because the peak amplitude of the oscillating velocity is (1.32~1.55) times that of ordinary jet.

3. FIELD TEST

According to experimental results above, authors have designed a set of airlift on which the breaker of the SEOPJ is installed. Field tests have been conducted in Wenchong, Hainan for two years. In the test water area, its depth of water is 3~15m, the geological condition is soft soil and sand (under the water 3~8 meter), hard clay and gravel (under the water 8~13 meter) and sand (below 13 meter). During the course of test, it is found that the airlift penetrates the hard clay and rocky bed by using the breaker of the SEOPJ. But the airlift with the breaker of ordinary jet can operate continuously under the water from 6 to 12 meters, with the aid of mechanical cutter. The quantity of solid-liquid mixture and concentration of solids are measured by weighing the weight of the specimen. Measuring results are given in Table 1. From Table 1, the concentration of solids for the solid-liquid mixture sucked by the airlift is increased obviously when the breaker of the SEOPJ is used. This can indicate that the breaker of the SEOPJ has large scouring ability and lifting force that makes the particles of the hard clay and gravel move easy.

4. CONCLUSIONS

- (1) There is a region ($0.17 < r/H < 0.35$) in which the radial peak oscillating pressure (upward) is larger than the mean dynamic pressure (downward). During this region, the particles of hard clay and gravel can move easy.
- (2) The breaker of the SEOPJ can scour the hard clay and gravel which isn't scoured by ordinary jet, on the same condition.
- (3) The concentration of solids of the solid-liquid mixture sucked by airlift with the breaker of SEOPJ increases by about one-half.

- (4) The SEOPJ has intensive oscillating characteristic, the oscillating rate that is equal to difference pressure (between the maximum oscillating pressure and the minimum oscillating pressure) divided by the mean pressure is about 40% above.

5. ACKNOWLEDGMENTS

This project is supported by the National Natural Science Foundation of China (59874033). The authors wish to extend thanks to Mr. Zen Shaoping, Xiang Qian , economic develop company, Hanan, for their help with experimental works.

6. REFERENCES

Cheatham J.B.Jr., Yarbrough J.G., “Chip Removal by A Hydraulic Jet,” *SPEJ*, pp21-24, 964.

Liao, Z., Tang, C., “A New Type of Nozzle for Oil Well Drill Bits,” *Proceedings of the 10th International Symposium on Jet Cutting Technology*, pp135~144, Elsevier Science Publishers Ltd. London UK, 1991.

M.R. Wells, “Dynamic Rock Chip Removal by Turbulent Jetting,” SPE 14218.

Tang, C., Liao, Z., Yang, L., “The Application of the Airlift and the Self-excited Oscillation Pulsed Jet on Exploiting Beach Placer,” *Proceedings of the 14th International Symposium on Jetting Technology*, pp375~386, BHR Group, Brugge, Belgium, 1998.

7. NOMENCLATURE

d: The diameter of nozzle, m

H: The standoff distance, m

r: Radial distance from jet axis, m

P: The instantaneous pressure of jet, Mpa

P_p : The average peak dynamic pressure at stagnation point, Mpa

P_r : The average peak dynamic pressure, Mpa

P_{r1} : The mean dynamic pressure, Mpa

ΔP : Net lifting pressure, Mpa

P_0 : Pressure drop across nozzle, Mpa

g: Acceleration due to gravity, m/s^2

d_m : The average diameter of particles, m

ρ_1 : Density of water, kg/m^3

ρ_s : The mean density of solid, kg/m^3

G : Gravity of the particles on the bed, N

G_F : Float force of the particles, N

F_r : Pushing force, N

V_r : The velocity of radial flow, m/s

k : Experimental constant

μ : Frictional coefficient of the particles

ΔF : The lifting force, N

P_a : Atmosphere pressure, Mpa

H : The depth of water, m

V_p : The amplitude of the peak dynamic velocity, m/s

f : The frequency of the dynamic pressure, Hz

n, k_1 : Experimental constant

e : The scouring depth, m

Table 1 The Measuring Data in Field

Parameter Type of jet	The depth of water (m)	The lifting height above water level (m)	The flow rate of solid-liquid mixture (m^3/s)	The concentration of solid (%)
SEOPJ	9~15	2~2.5	305~335	15~25
Ordinary jet	9~15	2~2.5	317~350	8~15

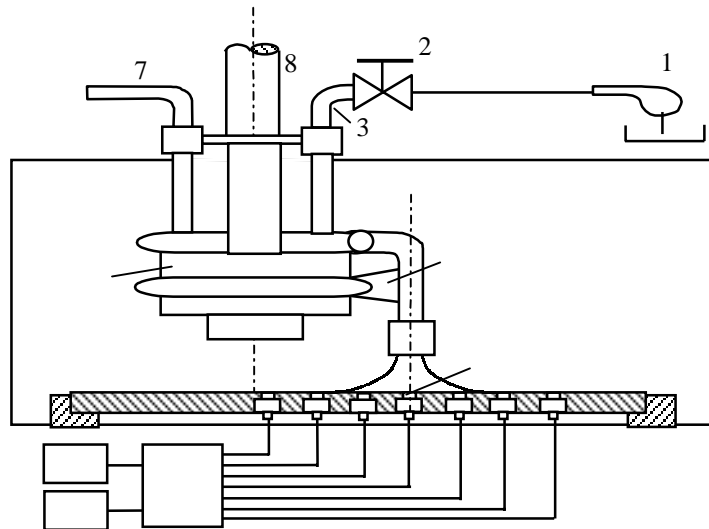


Figure 1. Sketch of the Experimental System

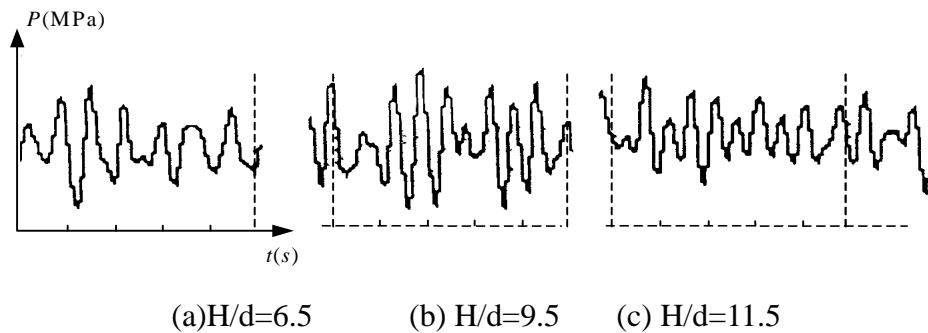


Figure 2. The Instantaneous Dynamic Pressure at Stagnation Point under the Submerged

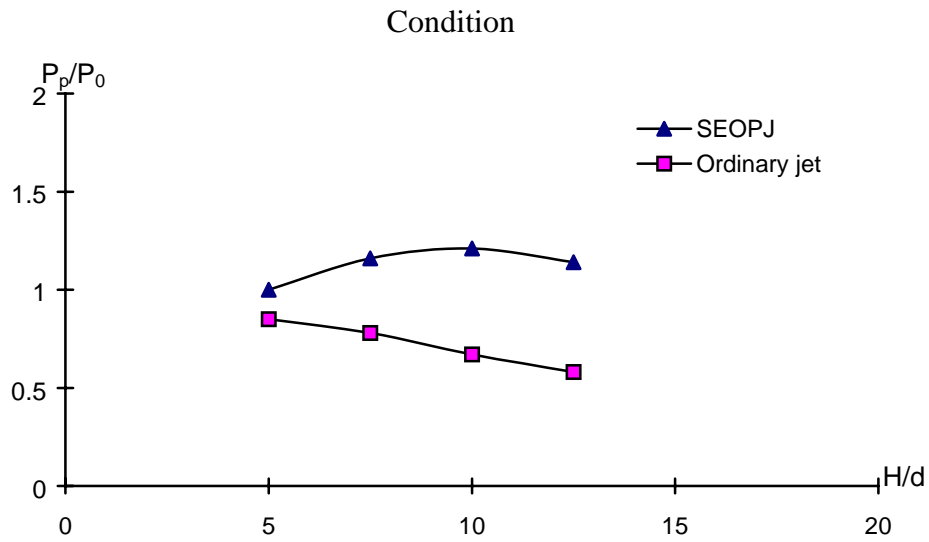


Figure 3. The Peak Dynamic Pressure at Stagnation Point under the Submerged Condition

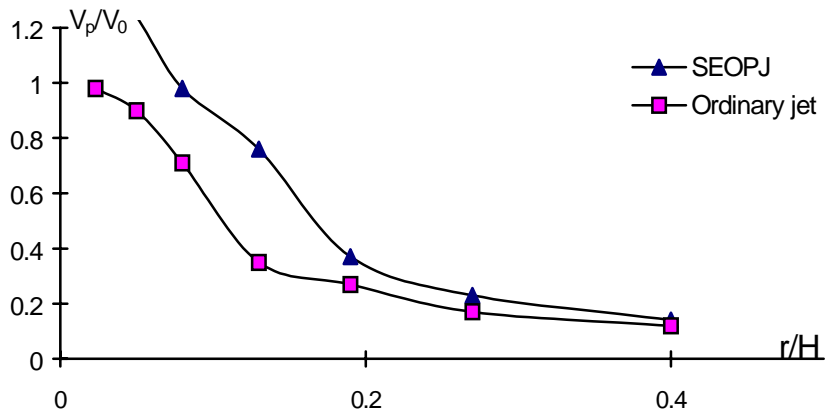


Figure 4. The Radial Velocity Distribution Under the Submerged Condition

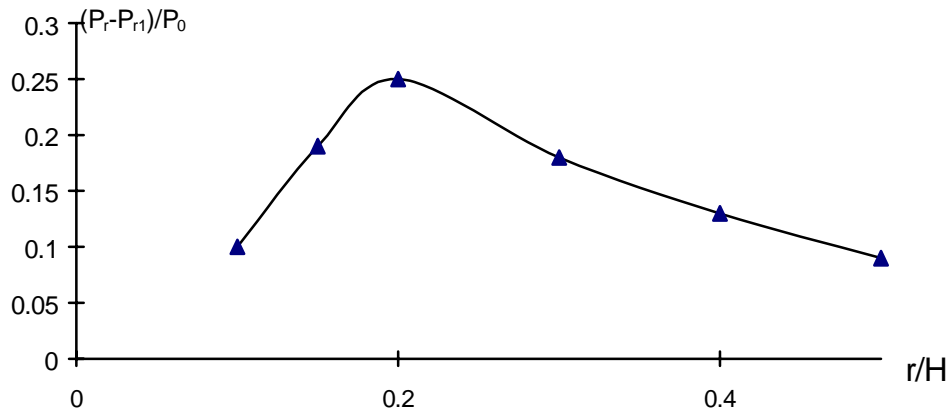


Figure 5. The Lifting Pressure Distribution

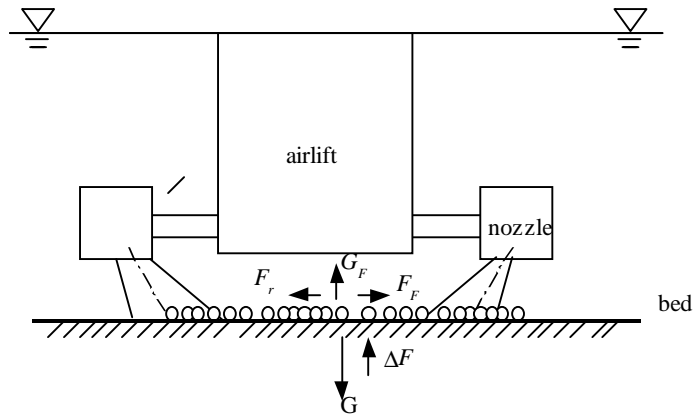


Figure 6. The Forces Acting on the Particles of the Clay

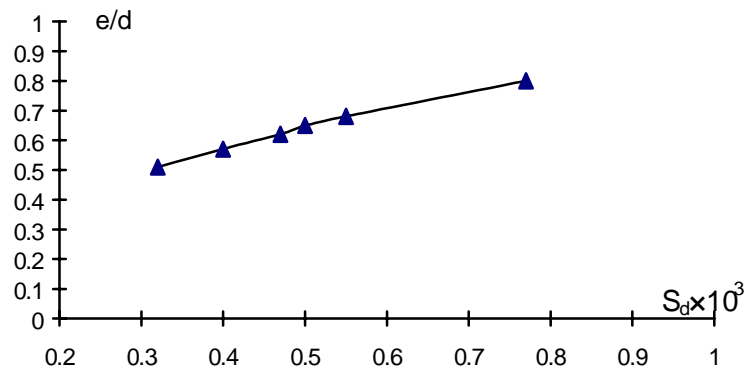


Figure 7. The Relationship between the Scouring Depth and Oscillating Velocity and Frequency

EMPIRIO-ANALYTICAL METHOD A GOOD MEANS OF WATER JETTING TECHNOLOGY INVESTIGATIONS

B.V.Radjko
Lugansk College of Eastukrainien State University
Lugansk, Ukraine

ABSTRACT

This paper presents some results of empirio-analytical investigations of statistical data of hydraulic breaking coefficient obtained with using monitor plain water jets while subsidiary development in coal seams. Statistical data reflect geological conditions of coal seams from low dip till high dip. It is investigated influence of some active factors on forming of the hydraulic breaking coefficient value while coal water jet extraction from the face in pillar boards. These are the factors: dip angle of coal seams, coal ash, volatile matter of coal, gas content in coal, depth of mining and duration of hydraulic breaking of splits. It is shown how change dispersion of the statistical data in dependence on increasing the number of active factors if their influence character have been taken into account correctly. To make clear advantages of empirio-analytical method to investigate water-jetting technology the graphs of meeting together statistical data and calculation ones are given as an example. For comparison the influences of quantity of the active factors taken into account correctly on the meeting statistical and calculation data the graphs are made for two, three, four, five and six factors separately. These graphs reflect how dispersion of the statistical data diminish and empirical values approach to calculation ones with increasing number of the active factors taken into consideration. The empirio-analytical method gives possibility to investigate water-jetting technologies using not only experimental statistical data but industrial ones too. Besides, It permits to reveal influence power each of the actives factors separately as well as their common effect on forming statistical phenomenon.

1. INTRODUCTION

Empirio-analytical method of the statistical data investigations has been elaborated to analyze the results of industrial employment of the hydraulic breaking of the coal seams with plain water jets. It consists of some steps:

- acquiring statistical data population (industrial ore experimental);
- revealing active factors forming statistical data;
- study of the statistical dots diapasons to each of the active factors;
- determination of the “key points” quantity to have statistical sample;
- definition the number of statistical dots in “key point”;
- preparing statistical data sample volume limited;
- revealing analytical character of twofold dependencies along each of the active factors;
- construction of twofold empirio-analytical dependencies to each of the active factors;
- unification some twofold empirio-analytical dependencies into mathematical model of multi factors;
- making graph of meeting together statistical values and calculation ones to have clear result attained;
- calculation of variation coefficient.

Revealing of the active factors that form statistical data are made by study early experience, papers, investigations, construction check empirical graphs etc. To minimize errors in the parameters of constructed empirio-analytical dependencies are studying statistical dot diapasons to each of the active factors. As quantity of the “key points” makes influence on statistical sample volume to get last limited and fitted adequacy with statistical population the “key points” is selected according to the principle “other things being different” (Radjko, 1995). The number of the statistical dots in “key point” is defined using principle of damage minimizes. To avoid mistakes of principle in constructed mathematical model the characters of the twofold dependencies are revealed by analytical investigations (Radjko, 1999). Construction of twofold empirio-analytical dependencies to each of the active factors is made using statistical sample of limited volume prepared. It is executed by employing a number of reduction steps to exclude distorting effect of the factors taken into account earlier. Then all twofold empirio-analytical dependencies are combined to have mathematical model of multi factors. To check obtained result graph of meeting together statistical and calculation values is constructed and estimated quantitatively using coefficient of variation also. Graph of meeting is needed to control correctness of quantity and influence character of active factors taken into consideration. Symmetrical location of the statistical dots near theoretical curve and small dispersion are significant of correctness.

Quality of empirio-analytical method of the statistical data investigations is displayed on example of data of the hydraulic breaking coefficient of the coal seams obtained in different conditions. Value of the last have been calculated out of the statistical data sample using the General equation of the hydraulic breaking process of solids with plain water jets (Radjko, 1998).

2. STATISTICAL DATA SAMPLE

Statistical data sample is presented with 29 splits extracted by monitor jet in pillar boards in the coal seams with different geological conditions. This statistical data sample was not prepared as a representative one but use only as an example to display possibilities of the empirio-analytical investigation method. Values of the hydraulic breaking coefficient and active factors on each of the splits are given in the Table 1.

3. HYDRAULIC BREAKING COEFFICIENT DEPENDENCIES ON ACTIVE FACTORS

To display quality of the empirio-analytical method of the statistical data investigations dependencies of the hydraulic breaking coefficient make on one, two, three, four, five and six active factors. Then dependencies above are used to make graphics of meeting together statistical and calculation values. Result depends on correctness of active factor registration: influence character, quantity and consecution of introduction.

Figures 1-6 show meeting together statistical and calculation values of the hydraulic breaking coefficient for dependencies with different active factors taken into account.

3.1. Dependencies on one factor

Figure 1 shows meeting together statistical and calculation values for twofold dependencies of the hydraulic breaking coefficient on each of the six active factors. Out of the graphics one can see that there is faint tendency to meeting together statistical and calculation dots in the dependencies $R(Ac)=f(R_o)$, $R(H)=f(R_o)$, $R(Vc)=f(R_o)$, $R(t)=f(R_o)$ and nothing of the kind in $R(\cos\alpha)=f(R_o)$ and $R(I)=f(R_o)$.

All six factors are active but their influence on meeting together statistical and calculation data of the hydraulic breaking coefficient realize in various.

3.2. Dependencies on combinations of two factors

Figure 2 presents meeting together statistical and calculation values for the dependencies of the hydraulic breaking coefficient on combinations of two active factors. It is seen out of the graphics that character of meeting together in $R(Vc,t)=f(R_o)$ and $R(I,t)=f(R_o)$ remain the same as in $R(t)=f(R_o)$; in $R(I,Ac)=f(R_o)$ and $R(H,Ac)=f(R_o)$ - as in $R(Ac)=f(R_o)$; in $R(H,\cos\alpha)=f(R_o)$ and $R(Vc,\cos\alpha)=f(R_o)$ - as in $R(\cos\alpha)=f(R_o)$. So the characters of meeting together statistical and calculation values under the two factors taken into account determined by the last factor introduced.

Registration of two active factors does not give guarantee to have tendency of meeting together statistical and calculation data of the hydraulic breaking coefficient.

3.3. Dependencies on combinations of three factors

Figure 3 shows meeting together statistical and calculation values for the dependencies of the hydraulic breaking coefficient on combinations of three active factors taken into account. Out of the graphics follows that tendency of meeting together has appeared practically in all combinations of the three factors. It is curious that even destroying effect of the factor “ $\text{Cos}\alpha$ ” (look Figure 2) changes his nature: look $R(V_c, t, \text{Cos}\alpha) = f(R_o)$.

If is necessary to get tendency of meeting together statistical and calculation data one have to take into registration three active factors as minimum.

3.4. Dependencies on combinations of four factors

Figure 4 offers meeting together statistical and calculation values for dependencies of the hydraulic breaking coefficient on combination of four active factors taken into account. It is clear out of the graphics that tendency of meeting together remains in all combinations of the four factors. But character of meeting together statistical and calculation values has became no best then was before practically in all combinations with the exception of $R(Ac, H, t, V_c) = f(R_o)$. In $R(Ac, t, \text{Cos}\alpha, H) = f(R_o)$ character of meeting together gets much worse then in $R(V_c, t, \text{Cos}\alpha) = f(R_o)$.

Registration of four active factors do not give essential improving of meeting together statistical and calculation values of the hydraulic breaking coefficient.

3.5. Dependencies on combinations of five factors

Figure 5 shows meeting together statistical and calculation values for dependencies of the hydraulic breaking coefficient on combinations of five factors taken into account. Out of the graphics one can discover that tendency of meeting together is remained in all combinations. But character of meeting together statistical and calculation values have improved only in three of those: $R(Ac, t, \text{Cos}\alpha, H, I) = f(R_o)$, $R(I, Ac, H, \text{Cos}\alpha, t) = f(R_o)$, $R(H, \text{Cos}\alpha, Ac, I, t)$ and practically have not changed in three another combinations – $R(I, t, Ac, V_c, H) = f(R_o)$, $R(V_c, \text{Cos}\alpha, I, t, H) = f(R_o)$, $R(Ac, H, t, V_c, \text{Cos}\alpha) = f(R_o)$. In the first case all combinations consist of the same factors, in the second – those changed.

What is the reason of that division? May be there are factors compatible and no compatible?

3.6. Dependencies on combinations of six factors

Figure 6 displays meeting together statistical and calculation values for dependencies of hydraulic breaking coefficient on combinations of the six active factors taken into account. It is understandable out of the graphics that addition sixth active factor into combinations of them gives different results: improve character of meeting together statistical and calculation data in one case – $R(Ac, t, \text{Cos}\alpha, H, I, V_c) = f(R_o)$; do not change its in three cases –

$R(I,t,Ac,Vc,H,Cos\alpha)=f(R_o)$, $R(Vc,Cos\alpha,I,t,H,Ac)=f(R_o)$, $R(Ac,H,Vc,Cos\alpha,I)=f(R_o)$; make its worse in two cases – $R(I,Ac,H,Cos\alpha,t,Vc)=f(R_o)$ and $R(H,Cos\alpha,Ac,I,t,Vc)$.

It follows out of the comparison of influence of six factor combinations on meeting together statistical and calculation values of the hydraulic breaking coefficient there is suitable one to be utilized in practical intention. That is $R(Ac,t,Cos\alpha,H,I,Vc)=f(R_o)$. Empirio-analytical Method of water jetting technology investigations gives possibility to reveal such combination of active factors and construct mathematical model of multi factors good for applied calculations.

4. INTERACTION INFLUENCE OF ACTIVE FACTORS

Interaction influence of the active factors on meeting together statistical and calculation values of the hydraulic breaking coefficient displays at the Figure 7. It is the same as the Figure 6 left above. To reveal interaction influence of the active factors statistical dots paint in different colour. Those corresponding minimum values of the factors range get blue colour, middle values – crimson colour, maximum values – yellow colour. That is blue dots have range at coal ash – $7.2\div 9.3\%$, duration of hydraulic breaking of splits – $9\div 100$ min., dip angle of coal seams – $10.5\div 20^\circ$, depth of mining – $90\div 100$ m, gas content in coal – $2.5\div 3.5$ m³/t. Crimson dots have - at coal ash – $12.3\div 18\%$, duration of hydraulic breaking - $110\div 200$ min., dip angle - $33\div 38^\circ$, depth of mining - $115\div 160$ m, gas content – $4.9\div 7.8$ m³/t, volatile matter – $21.5\div 36.7\%$. Yellow dots have - at coal ash – $21.8\div 29\%$, duration of hydraulic breaking - $225\div 330$ min., dip angle - 86° , depth of mining - $270\div 300$ m, gas content – $17,7$ m³/t, volatile matter – $37.4\div 42,5\%$.

At the Figure 7a distribution of the statistical dots is made at coal ash, Figure 7b – at duration of hydraulic breaking of splits, Figure 7c – at dip angle of coal seams. Distribution of the statistical dots at depth of mining, gas content and volatile matter in coal is given at the Figures 7d, 7e and 7f accordingly.

Out of analytical investigations (Radjko, 1999) is known influence character of active factors on the hydraulic breaking coefficient of coal seams. It grows with increasing dip angle of the coal seams and gas content in coal and with decreasing coal ash, duration of hydraulic breaking of split and depth of mining. Volatile matter in coal makes complicated influence on the hydraulic breaking coefficient: with increasing volatile matter that grows at first and diminishes then. Maximum of that corresponds to middle of range. That is maximum values of the hydraulic breaking coefficient one can wait in the beginning of range such factors as coal ash, duration of hydraulic breaking and depth of mining; in the end of range – as dip angle, gas content and in middle of range – as volatile mater. But as follows out of the graphs that is not quite so.

Logic above is observed at Figures 7b, 7e and 7f where maximum values of the hydraulic breaking coefficient coincide with beginning, end and middle of active factor range accordingly. The rest graphs logic “is infringed”. At the Figure 7e dots with maximum values of the hydraulic breaking coefficient have minimum ones of dip angle. At the Figures 7a and 7d dots with maximum values of the hydraulic breaking coefficient have the same values of coal ash and mining depth accordingly. The reason is as follows. Statistical dots of that sample are formed

under influence of different active factors. Some of them make effect stronger then other ones. That we see. It concerns this statistical sample only. In different statistical sample illustration can be another.

It is seen out of the graphs too there is not clear delimitation between statistical dots of different range parts. The reason is influence another factors.

5. CONCLUSION

Empirio-Analytical Method of statistical data investigations is good means to study water-jetting technology using both industrial and experimental facts. It gives possibility to reveal influence of different active factors individual and having interaction and analyze mechanism of factors interaction also. That Method allows to find the best combination of the active factors to utilize its in applied aims, construct mathematical model of multi factors for calculating results of water jet action acceptable to practical use, project water jet working in different conditions etc.

6. ACKNOWLEDGMENTS

Author is thankful to Mr. President G.A.Savanick, Ph.D., for invitation to take part in the 2001 American Waterjet Conference.

7. REFERENCES

1. Radjko, B.V., "Empirico-Analytical Investigations of Coal Seams Breaking Process with Plain Water Jets", *Proceedings of the 8th American Water Jet Conference*, Vol. II, pp. 867-878, Water Jet Technology Association, Houston, Texas, 1995.
2. Radjko, B.V., "General Equation of Hydraulic Breaking Process of Solids with Plain Water Jets", *Proceedings of the 5th Pacific International Conference on Water Jet Technology*, New Delhi, India, 1998.
3. Radjko, B.V., "Analytical Investigations of Hydraulic Breaking Coefficient of Coal Seams", *Proceedings of the 10th American Water Jet Conference*, Water Jet Technology Association, Houston, Texas, 1999.

Table 1. Data of the Splits in the Pillar Boards

Hydrocomplex	Hydraulic breaking coefficient, R_0 , m/kN	Dip angle, α , leg.	Coal ash, A_c , %	Volatile matter V_c , %	Gas content, I , m ³ /t	Mining depth, H , m	Breaking duration, t , min
Krasnoarmey-skaya, m ⁵	9319,1	10,5	29	41,3	3	140	11
	3987,9	10,5	29	41,3	3	140	305
	3310,7	10,5	29	41,3	3	140	272
	3896,9	10,5	29	41,3	3	140	225
	2883,5	10,5	29	41,3	3	140	330
	6934,8	10,5	29	41,3	3	140	98
Novodonets-kaya, l ₃	5903,4	10,5	23,3	38,5	3,5	115	200
	7720,4	10,5	23,3	38,5	3,5	115	90
	7285	10,5	23,3	38,5	3,5	115	60
	9576,7	10,5	23,3	38,5	3,5	115	30
Pioner, l ₇ m ⁰ ₄ m ² ₄	18476,2	13	9,3	37,4	4,9	160	9
	15382,6	13	9,3	37,4	4,9	160	42
	13580,3	13	12,3	36,7	7,8	300	30
	12890	13	12,3	36,7	7,8	300	65
	11265,6	13	7,9	36,1	7,7	280	21
	6983,4	13	7,9	36,1	7,7	280	195
	14599,6	13	7,9	36,1	7,7	280	12
Belianka, h ₇	15776,9	20	7,2	21,5	17,7	270	85
	22825,8	20	7,2	21,5	17,7	270	55
Zimogorie, m ₃	7931,7	33	21,8	42,5	2,5	95	100
	6879,4	33	21,8	42,5	2,5	95	130
	8751,7	33	21,8	42,5	2,5	95	66
	5365	33	21,8	42,5	2,5	95	78
Privoljnians-kaya, m ₃	8878,2	38	18	41,3	2,5	90	100
	9478	38	18	41,3	2,5	90	58
Lutuginskaya, l ₂	7380,5	86	15,6	40,8	2,5	100	165
	10319,3	86	15,6	40,8	2,5	100	110
	8800	86	15,6	40,8	2,5	100	125
	12608	86	15,6	40,8	2,5	100	30

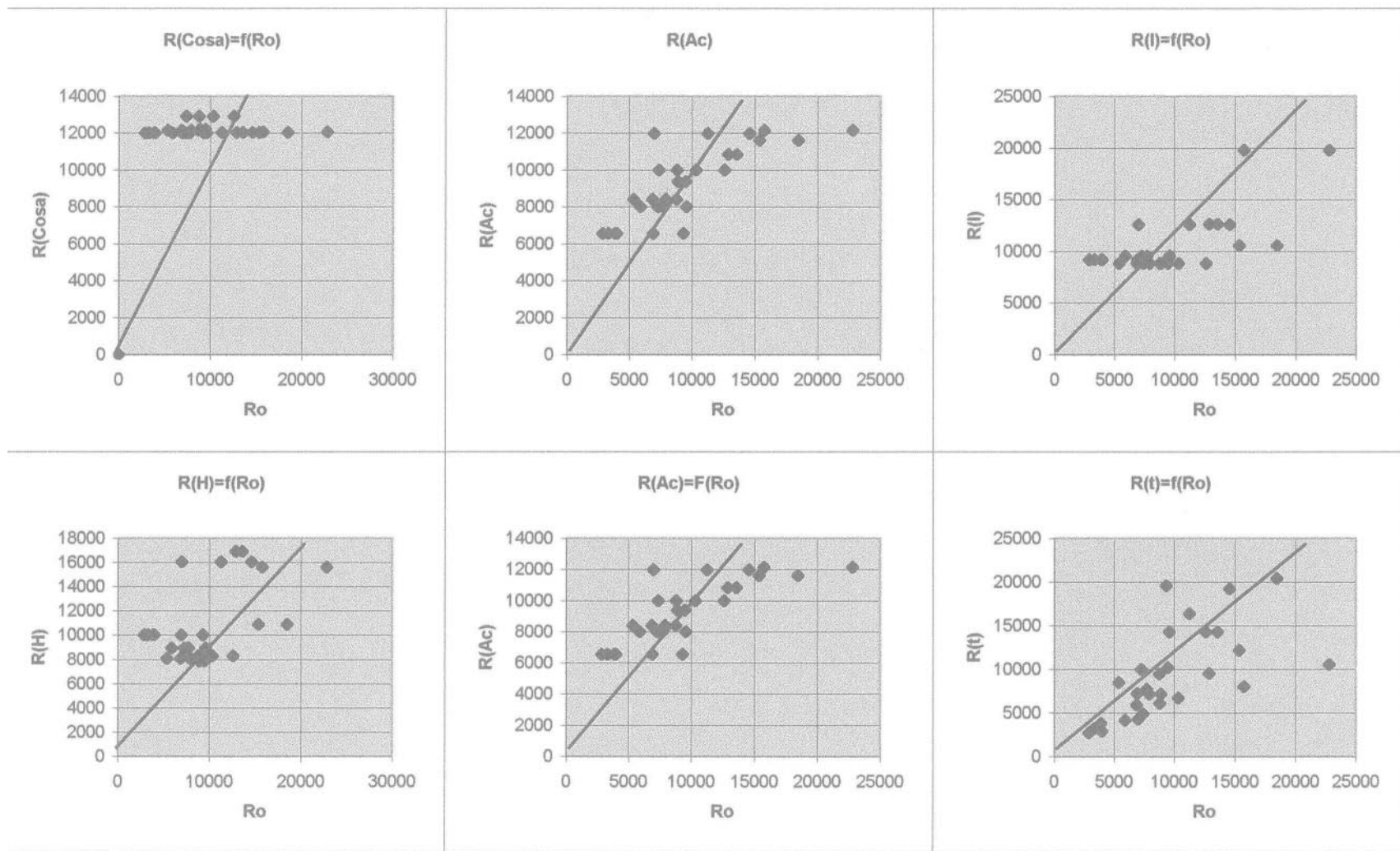


Figure 1. Graphs of meeting together statistical and calculation values of coefficient R_o for dependencies with one factor taken into account

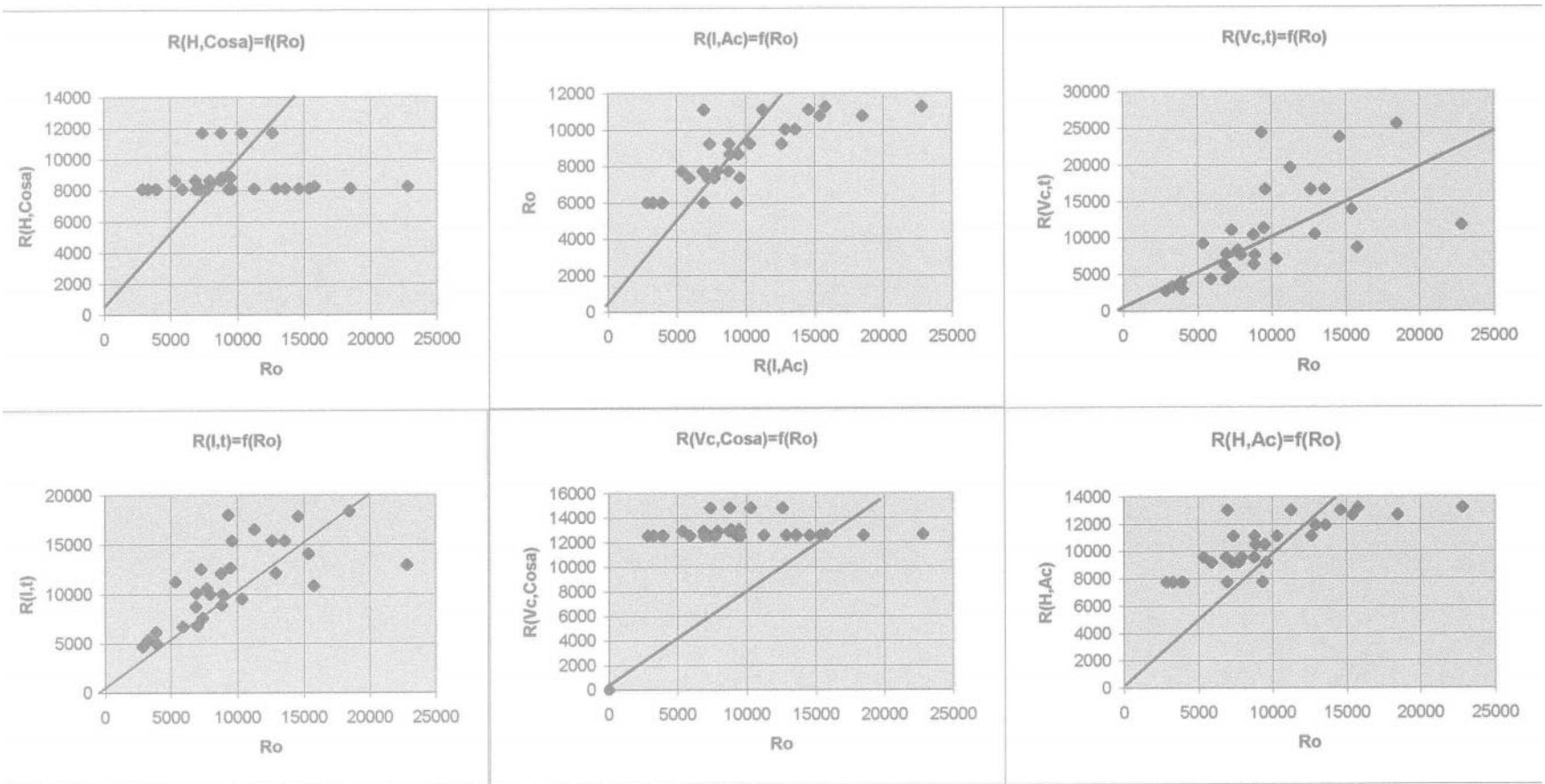


Figure2. Graphs of meeting together statistical and calculation values of coefficient R_o for dependences with two factors taken into account

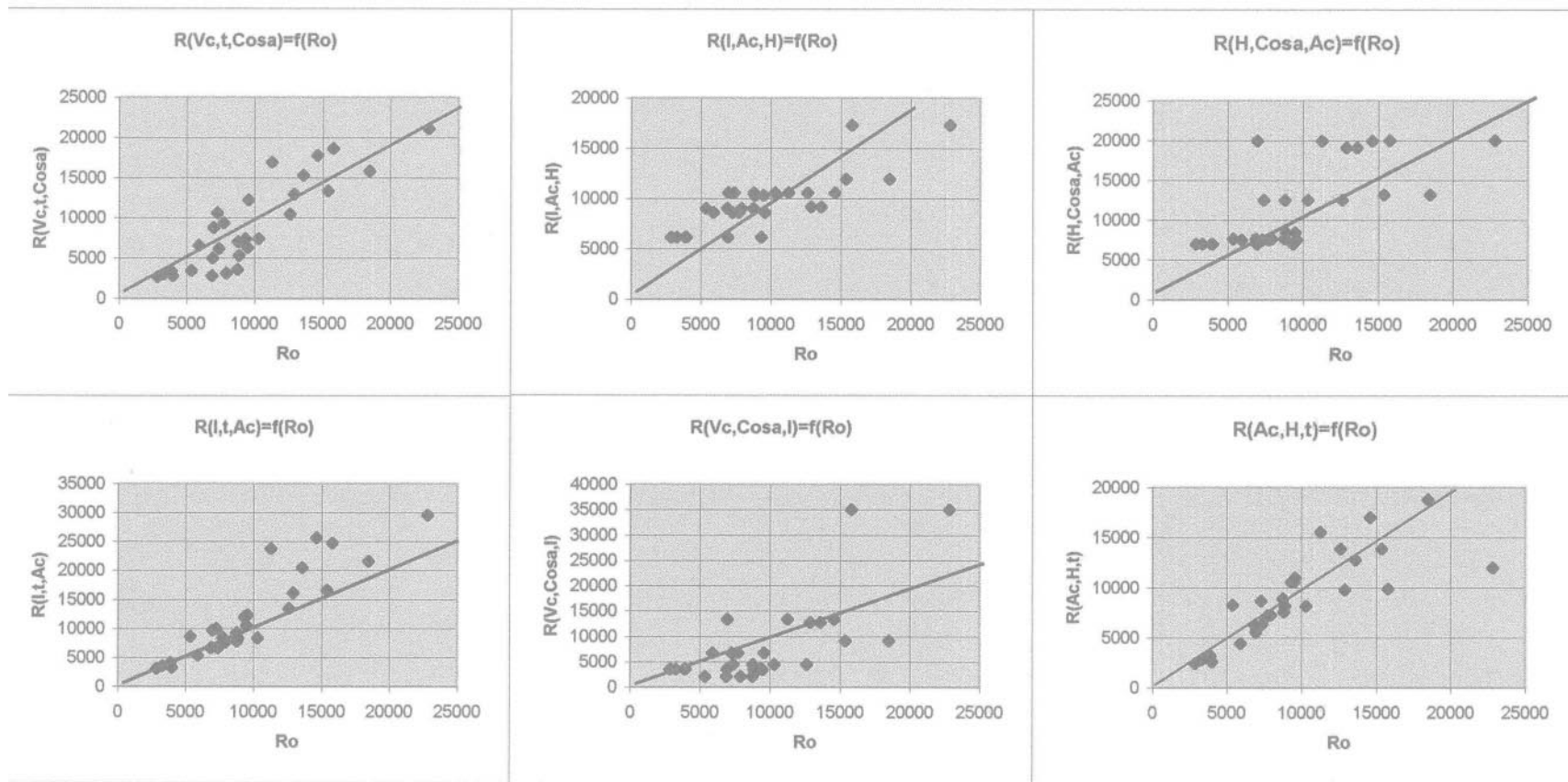


Figure3. Graphs of meeting together calculation and statistical values of coefficient R_o for dependences with three factors taken into account

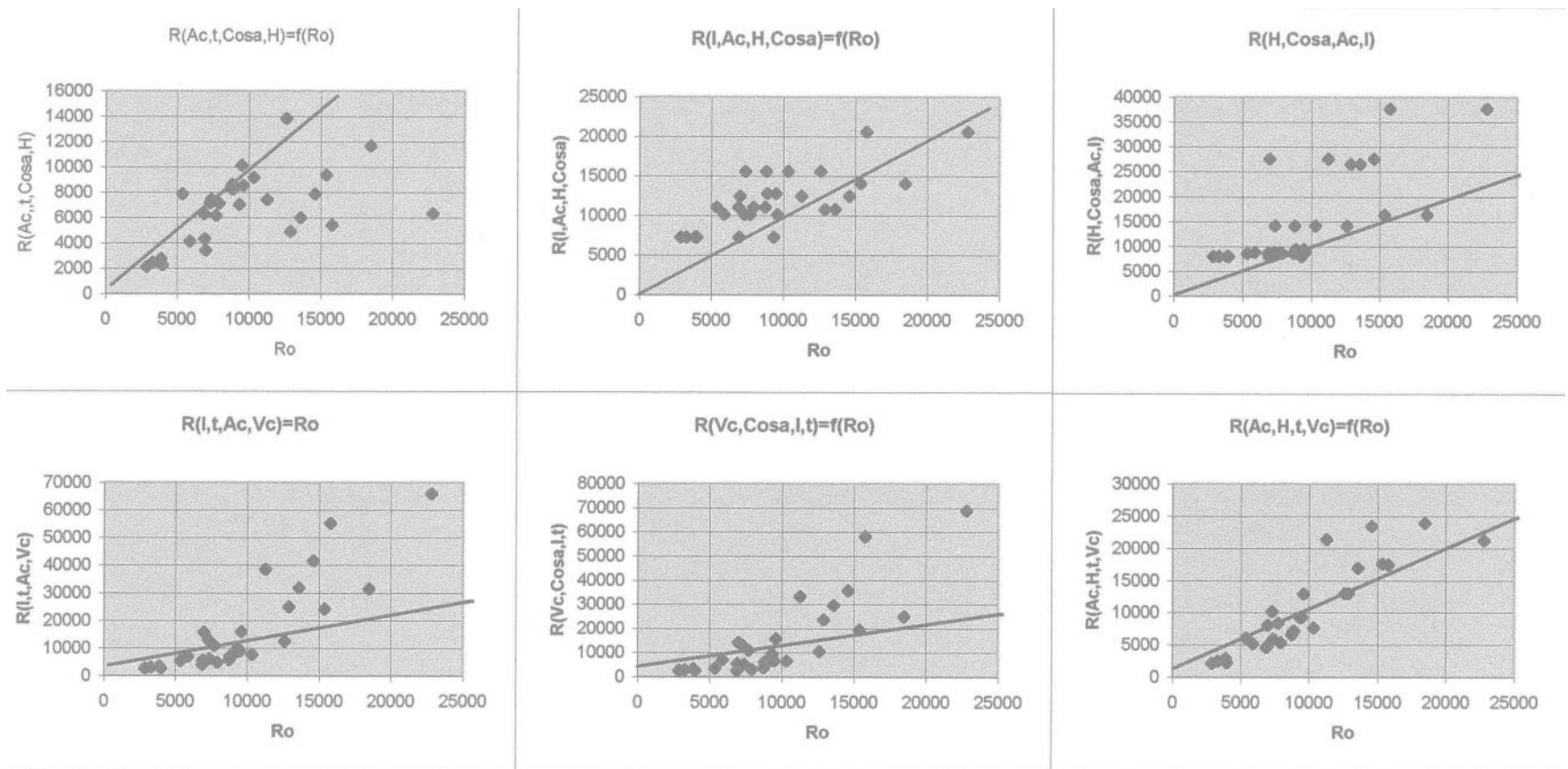


Figure 4. Graphs of meeting together statistical and calculation values of coefficient R_o for dependencies with four factors taken into account

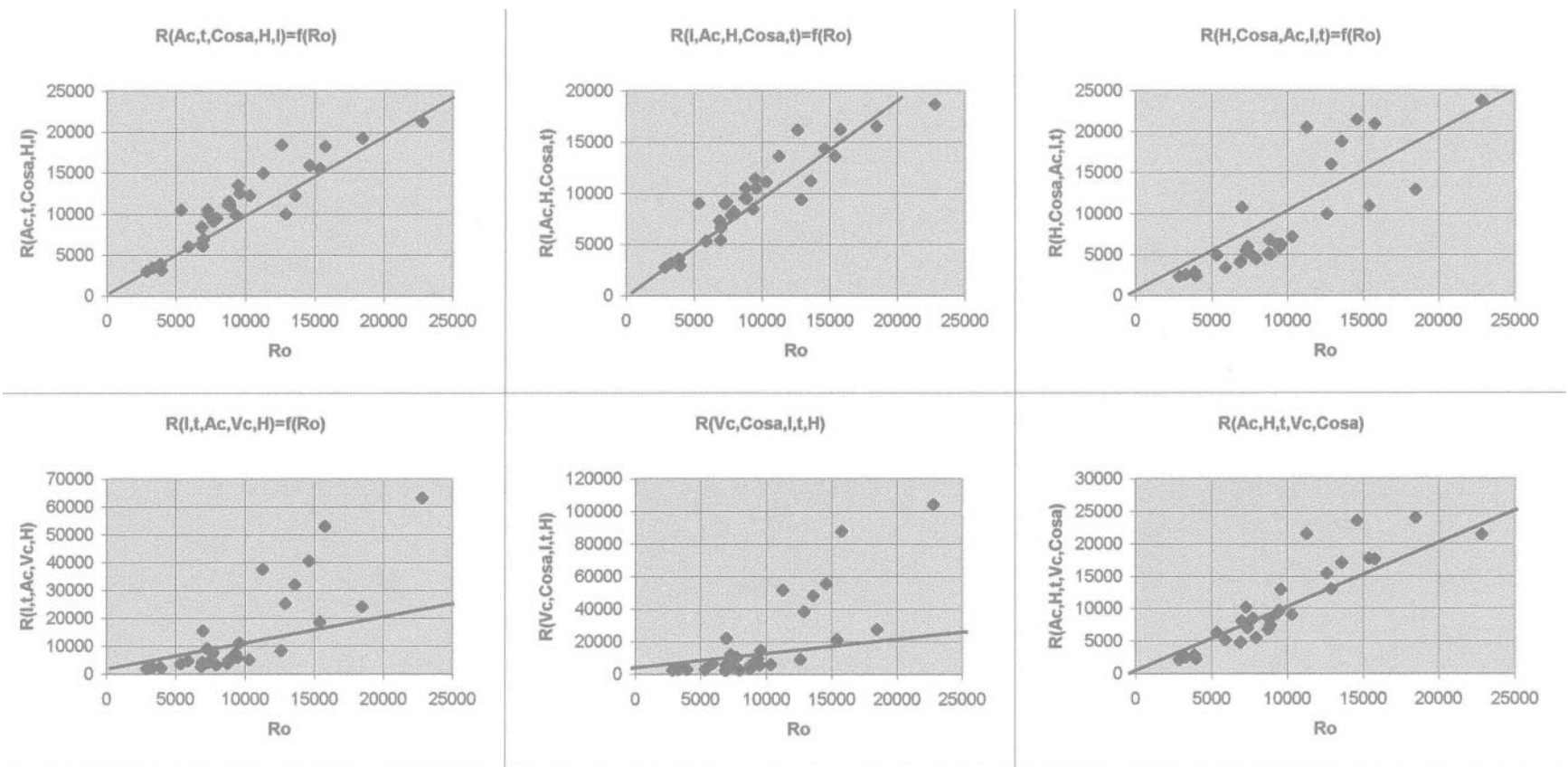


Figure 5. Graphs of meeting together statistical and calculation values of coefficient R_o for dependencies with five factors taken into account

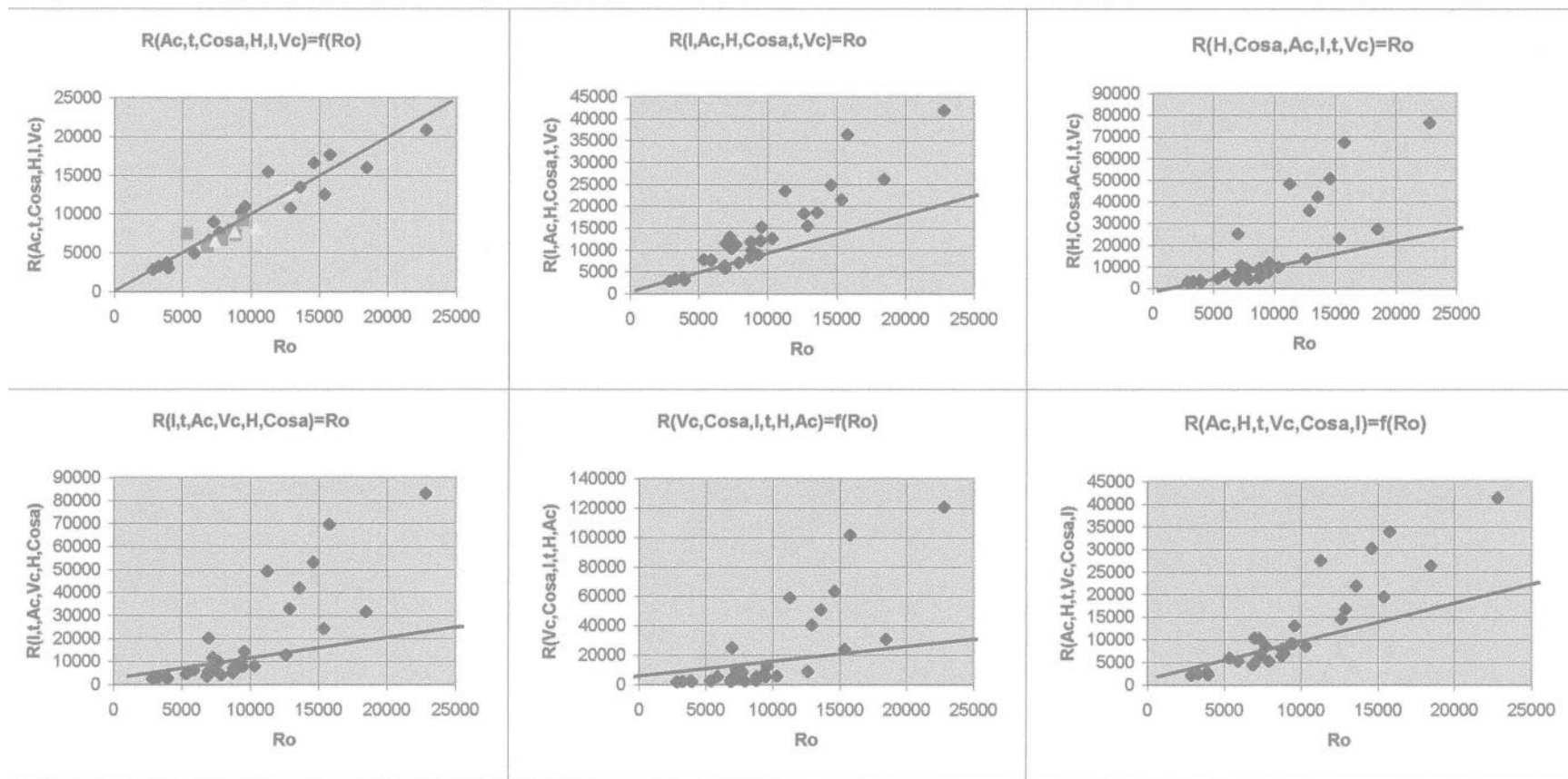


Figure 6. Graphs of meeting together statistical and calculation values of coefficient Ro for dependencies with six factors taken into account

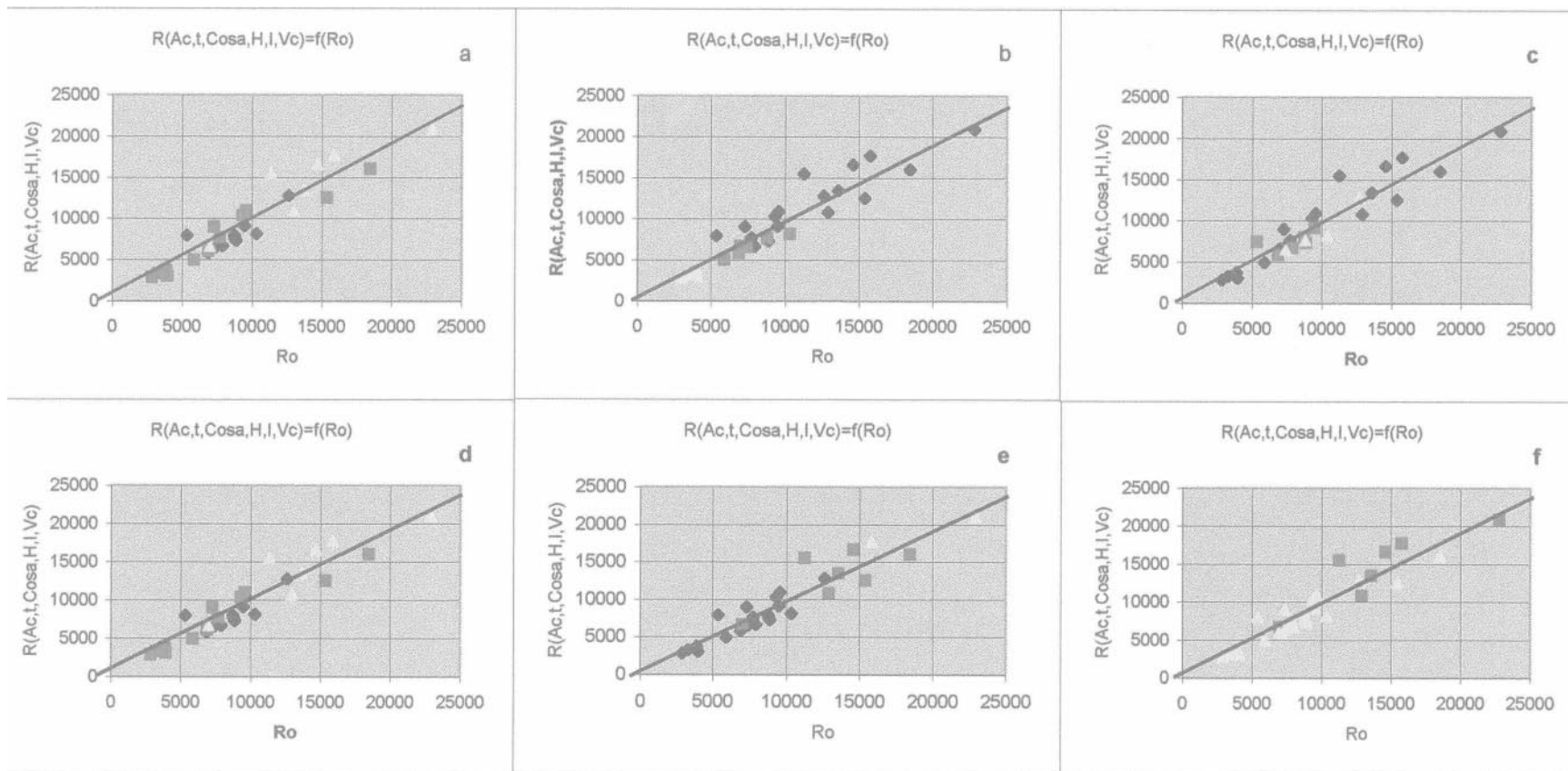


Figure 7. Influence of interaction factors on hydraulic breaking coefficient values

EXPERIMENTAL STUDIES ON SWIRLING JET FOR HOLE DRILLING

Yang Yongyin, Wang Ruihe, Zhou Weidong, Shen Zhonghou
University of Petroleum (East China)
Dongying, Shandong, P.R.China

ABSTRACT

Jet expanding is vital for swirling jet to drill a big diameter hole in Ultra-Short Radius Radial Horizontal Well drilling, so it is important to understand the property or velocity distribution of submerged swirling jet through experimental studies. This paper concerns the studies with PIV flow measurement technology on submerged swirling jet in a confining cell, and presents velocity components distribution profiles in jet axisymmetrical plane and on different jet cross sections. Experiment result shows that swirling jet mean flow velocity develops into self-similarity zone beyond a certain standoff distance in confining submergence condition, and the tangential and radial components are more significant than that of conventional non-swirling jet.

When abrasive particles were added in the same swirling jet fluid to increase drilling efficiency, the fluid-borne abrasive velocity in the jet were also studied through the same method indicating that while abrasive velocity distribution profiles approximately take on the same pattern as that of the surrounding or carrying fluid, slip velocity exists in the jet flow field between abrasive particle and its surrounding fluid.

1. INTRODUCTION

Swirling jet shows its great efficiency in drilling of large holes in diameter in USRRHW (Ultra-Short Radius Radial Horizontal Well) drilling technology. Because of the existence of swirling flow, swirling water jet expands very much in diameter along its way downstream than conventional jet does (Wang et al, 1998). In applications of USRRHW drilling, such polymers as polyacrylamide (or PAM hereafter) are generally added to drilling fluid to increase its capacity for debris transport, and to prevent bore holes from collapsing. While increasing the viscosity of fluid, polymers have influence on the performance of the jet. However, the knowledge about effects of polymers on the jet velocity profile lacks in general at present. And comprehensive studies on the properties of swirling polymer-thicken water jet generated by a built-in impeller in nozzle are generally lacking, too. Thus, it is of great importance and necessity to make clear the velocity profile of swirling jet when polymer is added to water.

In this paper, with two-dimensional PIV velocity measurement technology, the velocity profile of the swirling jet of Purely Hydrated Polyacrylamide (or PHP) fluid with PAM concentration of 0.1% by weight was systematically studied. At constant flow rate, axial and radial velocity components on the axisymmetrical plane, and tangential velocity on the cross sections at various SODs were measured. The measurement covered from 0.5do to 11do, which is greater than the standoff distance generally used in practical drilling of USRRHW.

The purpose of this study is to investigate the probability of studying three-dimension time-averaged flow velocity of swirling jet with two-dimensional PIV technology, and to further study the velocity profile of swirling PHP fluid abrasive suspension jet. This study can help not only further understand properties of swirling jet flow, but also improve the nozzle design, and lay a reliable foundation for computational stimulation of swirling jet flow.

2. EXPERIMENT SETUP AND PRINCIPLES

Particle Image Velocimetry has been developed into a powerful velocity field measurement technology, and found its increasing applications in experimental fluid dynamics. The PIV system used in this study was made by TSI Incorporated, America in 1999. And it shows good properties in image capture and processing methods. To meet the requirements of both the PIV measurement system and the abrasive jet flow production under submergence condition, the experiment setup includes the following units (See Figure 1):

- (1) **PIV system:** consisting of a synchronizer of Ver. 6.1c, two laser producers of Laserpulse Mini Yag 12 , a camera of PIVCAM 10-30 CCD, and a measurement control and image processing computer.
- (2) **Platform:** with 3D coordinator, for support and regulation of the CCD camera and laser head.
- (3) **Nozzle:** with 7 mm in diameter, 60° in contraction angle, and 6mm in cylindrical exit length.

- (4) **Round glass tube and glass water vessel unit:** for confining and simulating jet under submergence condition, and with an elliptic light reflection mirror inserted in 45°angle within the round tube for obtaining images on jet cross section.
Glass tube: $\Phi_190\text{mm}\times800\text{mm}$: Glass water vessel: $400\text{mm}\times400\text{mm}\times600\text{mm}$.
- (5) **Pump:** $50\text{MPa}\times1\text{ l/s}$.
- (6) **Abrasive delivering unit:** for adding, at required delivering rate, abrasive particles into circulation pipe between pump and jet nozzle.
- (7) **EH Prowirl 70F flowmeter:** with full range 2 l/s and precision $\pm0.5\%$, and for the control of fluid flow at constant rate in experiments.

The polymer thicken fluid, i.e. PHP, was made by adding PAM water to the concentration of 0.1% by weight as an instance in this study of swirling jet. When PAM is mixed into water, the big molecule hydrates and attracts a lot of free water molecules around itself, which help to thicken the water and increase its capability to suspend solid abrasive particles.

The measurement under each condition was conducted at a constant fluid rate to study time-averaged velocity field of jet flow. The PIV system in this study can capture 15 pairs per second of particle images of desired flow field. To capture more than 300 pairs of images for obtaining more accurate mean velocity field takes only a few minutes for each experiment condition.

The velocity of jet at nozzle exit was controlled at around 30 m/s on average. And separating time is 0.01 or 0.02 ms between taking A and B of each pair of images. The inquiring spot size were around $1\text{mm}\times1\text{mm}$ in the fluid velocity measurement, and $3\text{mm}\times6\text{mm}$ in abrasive velocity measurement. And the processing results show that velocity vectors above 90% are good vectors in instant velocity fields.

3. EXPERIMENT RESULT AND ANALYSIS

Velocity measurement of the swirling jet with tow-dimensional PIV system in this study includes two parts. First one, the flow field was selected on jet axisymmetrical plane to probe the axial and radial velocity components of the jet; Second one, with the help of a light reflection mirror, the measurements of the tangential component on its different cross sections were studied.

3.1 Axial Velocity Distribution

Axial velocity components of swirling jet for PHP fluid are plotted in Figure 2, which presents the transversal distributions of the velocity components at different radius and SOD. The normalized velocity was obtained by dividing the maximal velocity at nozzle exit center point. From Figure 2, it is shown that, under submergence condition, great changes take place about the axial velocity distribution compared to swirling water jet. In PHP fluid swirling jet, the axial velocity components distribution curve along radius at identical SOD does not resemble “M” form that is the case in swirling water jet in short SOD (Wang et al, 1999), but show a curve pattern of normal distribution density function with the maximum on the axial line.

When the axial velocity components were normalized with the corresponding maximal value at the jet center of identical SOD, another distribution pattern was obtained shown in Figure 3, which presents the characteristics of self-similarity of the axial velocity distribution in the zone from 4d0 to 11d0. This result confirms the result of theoretical analysis on swirling jet flow (Yang Y et al, 1999). Through data regression, the self-similar velocity can be expressed as a formulation like normal distribution density function as following:

$$\frac{U_{r,SOD}}{U_{0,SOD}} = \frac{A}{\sqrt{2\pi} \cdot \sigma} e^{-\frac{(r/SOD)^2}{2\sigma^2}} \text{-----(1)}$$

$$U_{0,SOD} = 2 \times 10^{-6} \cdot SOD^5 - 2 \times 10^{-4} \cdot SOD^4 + 3.8 \times 10^{-3} \cdot SOD^3 - 0.0383 SOD^2 + 0.0952 SOD + 0.9395 \text{-----(2)}$$

in which: constants $A=1.25$, $\pi=3.14159$, $\sigma=0.15165$. r and SOD stand for radial and standoff distance coordinates of the flow field in the range $r>0$ and $SOD>4$ do, and $U_{r,SOD}$ and $U_{0,SOD}$ stand for axial velocities of the points (r, SOD) and $(0,SOD)$.

3.2 Radial Velocity Distribution

From Figure 4, it can be seen that radial velocity components are quite lower, the flow direction are however complicated. Generally, in the outer of the jet at short SOD, fluid flows toward the jet centerline resulted from entrainment of ambient fluid into the jet. But inside the jet, there is a core with positive radial velocity, the radius of the core fluctuates and ultimately increases with the increase of SOD. The corresponding values of the positive velocity component decrease in a wavy mode with the increasing of SOD. The wavy changing of the radial velocity component along its way downstream flow is probably related to the development and merge of eddies in jet boundary.

3.3 Tangential Velocity Distribution

Tangential velocity is an inherent characteristic of swirling jet. In the experiment, tangential velocity distributions were measured on various cross sections of the swirling jet from 1do~10do. And it is shown that the patterns of tangential velocity distribution along the radial at different SODs bear some resemblance. And tangential distribution patterns indicate there exists a vortex core inside the jet along the jet axis.

Figure 5 presents, as an instance, the distribution pattern of time-averaged tangential velocity on the cross section at 2d0 in SOD. It is shown that in the core of the jet, tangential velocity increases linearly with the increase of jet radius, which shows the property of potential vortex flow in the inner area of the jet. And outside the core tangential velocity decreases gradually, which means the decrease of the influence of center vortex core on the flow in outer jet area.

Along jet axis, the radius of the vortex core varies little within $3d_0$ in SOD and increases linearly with SOD beyond $4d_0$ like a taper (see Figure 6). Through regression of the data, an equation can be obtained. And the expanding angle of the taper core is about 35° beyond $4d_0$ in SOD.

Figure 7 presents the variation or attenuation of the maximal tangential velocity of swirling jet vs. SOD. Experiment results show that there are two linear decreasing stages. The first stage is within $4d_0$ in SOD where tangential velocity decreases faster, and the second stage is beyond $4d_0$ where the tangential velocity component decreases in a slow rate.

The linear decrease in tangential velocity value and the linear increase in vortex geometry diameter with SOD increase further mean or imply swirling jet also approaches a more regular or self-similar flow in jet developed flow region.

3.4 Axial Velocity of Abrasive Particles in Swirling Jet

When some abrasive particles of 0.2mm in diameter were added into the above fluid, the jet became an abrasive suspension jet. In the process of the experiment, the abrasive particles dispersed uniformly throughout the flow field. Then the axial velocities of abrasive particles were measured with PIV system. The time-averaged velocity field was obtained by averaging the instant velocity fields. And the result was normalized with the maximal fluid velocity at nozzle exit, and is plotted on Figure 8. By comparing Figure 8 with Figure 2 it is shown that the axial velocity transverse distribution pattern and the downstream velocity attenuation trend of the abrasive particles within the jet bear some resemblance with those of the fluid, although the values of the abrasive particle velocities are relatively lower. The lower velocity of the abrasive particle than the fluid means the fact that there is a velocity slip between the particle and the fluid in jet flow.

Because the abrasive concentration in the abrasive suspension jet was only about 0.2% by volume, the influences between abrasive particles are much lower. Then the fluid velocity can be regarded as little change when the abrasive particles were added into the jet. When the particle axial velocity value is subtracted from the fluid axial velocity, we could get the particle axial slip velocity in the abrasive suspension jet flow (see Figure 9), which indicates the slip velocity is greater near the nozzle exit. With the increase of SOD, the slip velocity decreases, and will be smaller than 10% of the fluid maximal velocity at nozzle exit when SOD is beyond $7d_0$.

4. CONCLUSION

It has been proved that PIV technology can be well used to measure the three dimensional velocity components of jet, which provide a good method for future study of different type of jet. And through this study, we can reach the following conclusions.

- (1) It is feasible using modern 2D PIV velocity measurement system to study three dimensional mean velocity components of submerged jet flow at constant flow conditions.

- (2) Polymers have great influence on the axial velocity transverse distribution pattern. For jet fluid of PAM concentration at 0.1% by weight, the maximum of the axial velocity of swirling jet is still on jet centerline.
- (3) Axial velocity of swirling jet approaches, like non-swirling jet, a self-similarity distribution through development in transition flow. In self-similar flow region, the standardized axial velocity can be expressed as standard normal distribution density function of (r/SOD). For jet fluid of PAM concentration of 0.1% by weight, the self-similarity region of the swirling jet is $SOD > 4d_0$.
- (4) The radial velocity is marginal while its transverse distribution complicated. In the outer area of the jet there exists a flow toward its axisymmetric centerline, while in the core of the jet fluid flows off the centerline.
- (5) Tangential velocity is an inherent characteristic of swirling jet. The tangential distribution shows that there exists a vortex core inside the jet along the jet axis. Along jet centerline, the vortex spin speed attenuates with standoff distance increasing, and the geometric form of vortex core expands like a taper.
- (6) The linear decrease in tangential velocity value and the linear increase in vortex geometry diameter further mean the jet approaches a more regular flow.
- (7) Axial velocity transverse distribution pattern and velocity attenuation trend of the abrasive particles within the jet downstream bear some resemblance with that of the fluid.
- (8) There is a velocity slip between abrasive particles and the surrounding fluid in swirling abrasive jet. Axial slip velocity is greater near the nozzle exit, and decreases with SOD increase.

5. ACKNOWLEDGEMENTS

This work was supported by China National Petroleum Corporation under development agreement No.970507. Any opinions, findings, conclusions, or recommendations expressed within the article are those of the authors and do not necessarily reflect the views of the CNPC.

6. REFERENCES

Wang, R., Xu, L., Shen, Z., “*Theoretical and Experimental Study on the Conical Swirling Water Jet Flow*”, Journal of Hydrodynamics, Ser. B,3 Vol.10 No.3 (1998).

Wang, R., Zhou, W., Shen, Z., Yang, Y., “*Study on Mechanism of Rock-Breaking by Swirling Water Jet*”, China Safety Science Jour. Vol.9, WJTSI, 1999 (10.).

Yang, Y., Wang, R., Shen, Z., Bu, Y., “*Theoretical Analysis and Mechanics Model of Submerged Swirling Jet Flow*”, China Safety Science Jour. Vol. 9, WJTSI, 1999 (10).

7. NOMENCLATURE

USRRHW:	Ultra-Short Radius Radial Horizontal Well;
PAM:	Polyacrylamide, with molecular weight• 20~24• $\times 10^6$ particularly in this study;
PHP:	Purely Hydrated Polyacrylamide;
PIV:	Particle Image Velocimetry;
CCD:	Charge Coupled Device;
do:	Nozzle diameter;
z:	Axial dimension of jet with z=0 at nozzle exit;
r:	Radial dimension of jet at different SOD;
SOD:	Standoff Distance;
St. SOD:	Standardized SOD, SOD/do;
St. Radius:	Standardized Radius, r/do;
U:	Axial velocity component of swirling jet;
V:	Radial velocity component of jet;
W:	Tangential velocity component of jet;

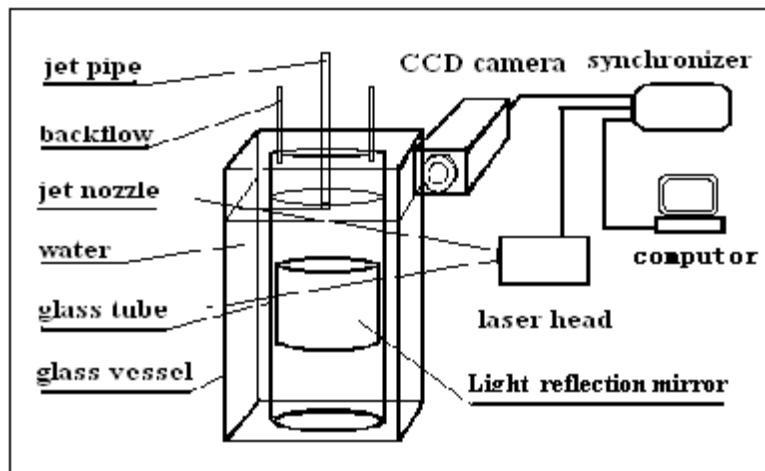


Figure 1. Schematics of Velocity Measurement System

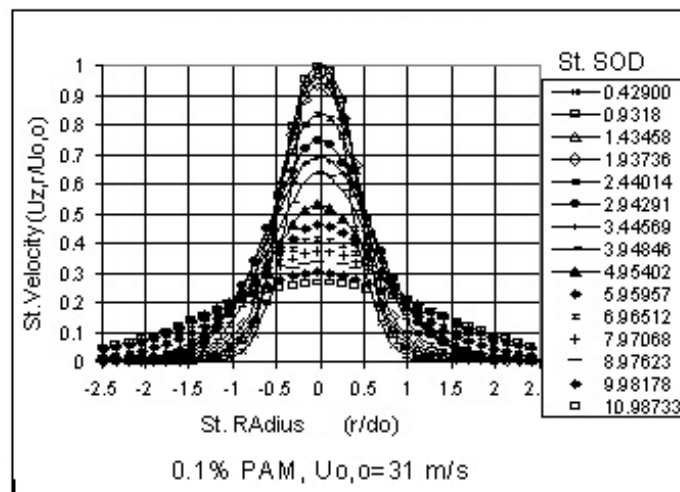


Figure 2. Axial Velocity Distribution of Swirling Jet

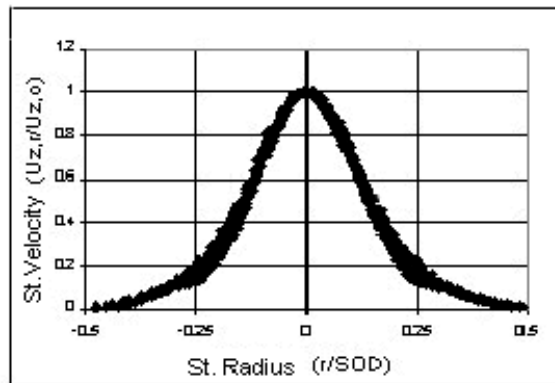


Figure 3. Self-resemblance Property of Axial Velocity of Swirling Jet

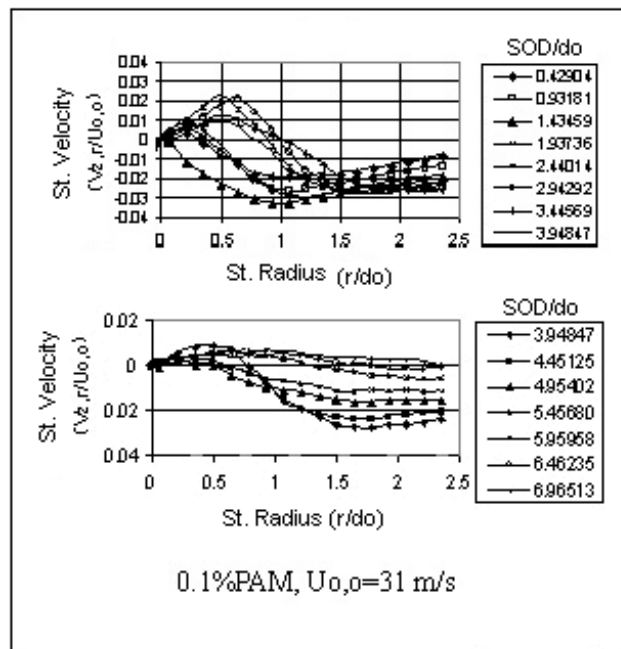


Figure 4. Radial Velocity Distribution of Swirling Jet

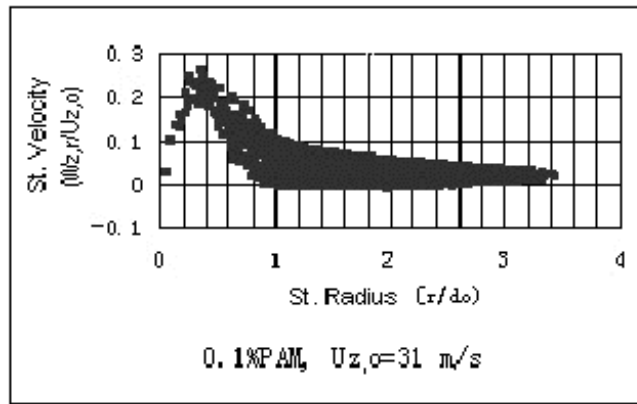


Figure 5. Tangential Velocity Distribution on Jet Cross Section at SOD of $2d_n$

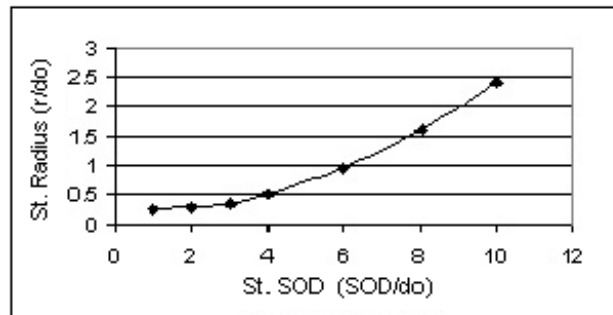


Figure 6. Radius of Vortex Core in Swirling Jet vs. SOD

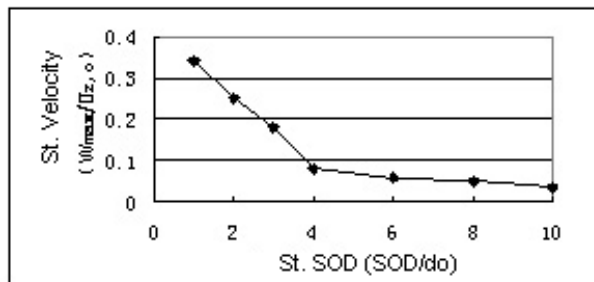


Figure 7. Linear Attenuation of Maximal Tangential Velocity vs. SOD

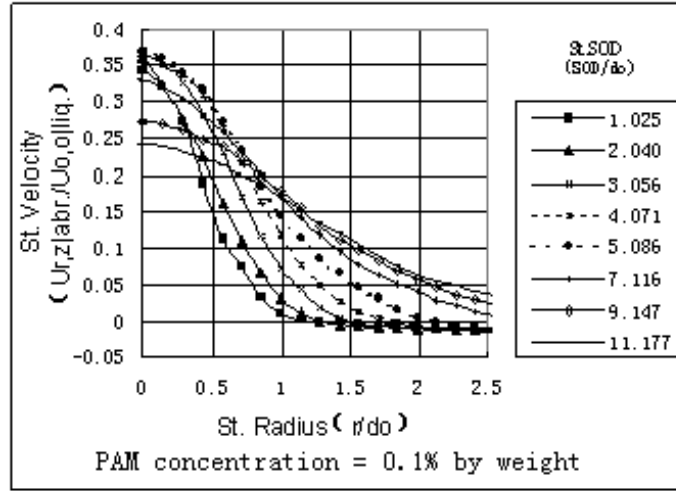


Figure 8. Axial Velocity Profile of 0.2mm Abrasive Particles in Swirling Jet of PHP Fluid

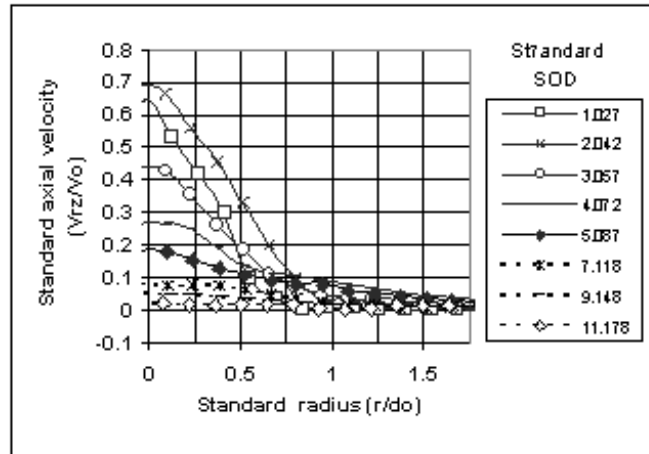


Figure 9. Slip Velocity Profile of 0.2mm abrasive particles in 0.1% PHP Fluid Swirling Jet

OPTIMIZING WATER BLAST POWER

D.Wright, J. Wolgamott, G. Zink
StoneAge, Inc.
Durango, Colorado

ABSTRACT

Effective waterblasting requires a minimum combination of pressure and flow to clean a surface. To achieve cleaning at further distances, or to complete the job faster, additional power in the form of greater flow or pressure is needed. The purpose of this research was to determine if there is an optimum combination of pressure and flow for a given power at various standoff distances.

Jet power deteriorates as the jet moves through the air. The rate of deterioration of the jet is a function of the nozzle diameter. Total power is the combination of pressure and flow. Therefore, at the same power, there exists the choice of a large jet at low pressure or a small jet at high pressure. At a given standoff distance, the large jet will not have deteriorated as much as the small jet, but the small jet started with a higher pressure at the nozzle.

Jet penetration was measured at various standoff distances in two materials with different properties. Pressures from 21 to 231 MPa (3,000 to 33,000 psi) and flows from 19 to 170 lpm (5 to 45 gpm) were used. In all cases a clearly defined optimum pressure and flow was found. Additionally, it was found that the optimum nozzle size at a given standoff held constant over a range of powers.

1. INTRODUCTION

The power of a waterblast system is the combination of the water pressure and the flow rate. Once a jet exits the nozzle orifice, the water pressure is converted to velocity. The velocity of the jet is then converted into a stagnation pressure at a surface; this stagnation pressure along with the mass flow rate of the jet will determine the effective cleaning power or impact of the jet on a surface.

Since the pressure of a system is much easier to measure than the velocity or the stagnation pressure of the jet, the power of the jet is commonly referred to in terms of the system pressure. For example, we refer to the “threshold pressure” of a material. The pressure value in this case is the pressure the operator reads off the gauge on the pump. In most materials, a minimum threshold pressure must be reached before any material is removed. In many materials there appears to be an optimum pressure, above which increased power is best applied with increased flow.

Ideally, the distance from the jet to the surface being cleaned, referred to as standoff distance, should be kept as small as possible, since a jet loses power as it travels through the air. However, in many waterblast operations, large standoff distances are common, and cannot be efficiently avoided. The rate at which a jet loses power as it travels through the air is dependent on the size of the nozzle. Therefore, at a given standoff distance, a larger jet will have deteriorated less than a smaller jet.

If two jets of equal powers are considered, one a large jet at a lower pressure, and the other a small jet at a higher pressure, the higher pressure jet will have a greater effect at the surface at a short distance. As the standoff distance is increased, the continual deterioration of this jet will result in an impact equal to, and finally less than the larger jet at the lower initial pressure. Meanwhile, the larger jet has been deteriorating as well, but not as rapidly. However, since this jet started out at a proportionally lower pressure to the minimum required threshold pressure to attack the material, it cannot be allowed to deteriorate as much.

This paper explores the effect of the proportions of the pressure and flow to determine if there is an optimum combination at various standoff distances.

2. TEST PROCEDURE

The tests consisted of series of constant power values divided proportionally into pressures ranging from 35 to 231 MPa (5,000 to 33,000 psi), and flows from 19 to 170 lpm (5 to 45 gpm). Carbide nozzles with flow straighteners, all of the same design, were used. Orifice sizes ranged from .71 to 3.96 mm (.028 to .156 in.) A 25 cm (10 in.) straight pipe was used upstream of the nozzle.

Test samples consisting of machineable wax, with a threshold pressure between 35 and 42 MPa (5,000 and 6,000 psi), and a cement and sand mixture with a threshold pressure of 10.5 MPa (1,500 psi) were used. Single jets were traversed at standoff distances from 5 to 127 cm (2 to 50 in.) Passes were made at the constant rate of 30 cm/sec (1 ft/sec). The jet kerfs were measured for depth and volume.

3. RESULTS

3.1 Constant Power, Increasing Standoff Distance

The first series of tests were conducted at 71 Kw (95 hp), with combinations of pressure and flow from 36 MPa, 121 lpm to 231 MPa, 19 lpm (5,100 psi, 32 gpm to 33,000 psi, 5 gpm). The results are shown in Figure 1. At a 5 cm (2 in.) standoff, the depth of cut increased with an increase of pressure, although the trend leveled off between 147 and 231 MPa (21,000 and 33,000 psi), about 5 times the threshold pressure of the material. As the standoff distance increased, the maximum pressure for optimal effect decreased to between 70 and 84 MPa (10,000 and 12,000 psi), and occurs on a narrow peak, where the jet power reaching the surface exceeds the minimum required threshold pressure.

Figure 2 shows the results of an identical 71 Kw (95 hp) test conducted at the 127 cm (50 in.) standoff distance with a cement and sand mixture. Even though this material was much more easily attacked by a jet, and had a much lower threshold pressure, the optimum condition at this standoff distance occurred at nearly the same pressure, between 70 and 77 MPa (10,000 and 11,000 psi). This indicates that the optimum conditions at larger standoffs are not strongly dependent on the threshold pressure of the material.

3.2 Depth compared to Volume

The results of the 71 Kw (95 hp) tests in terms of volume removed are shown in Figure 3. This shows similar results, with the exception of the optimum at close standoffs occurring near 105 MPa (15,000 psi), while higher pressures show decreasing efficiency. The higher pressure conditions resulted in greater depth of cut, but the smaller nozzle diameters did not create as wide of a kerf as the lower pressures with larger orifice diameters. The curves at larger standoffs resemble those produced by depth of cut, with the optimums occurring between 70 and 84 MPa (10,000 and 12,000 psi).

3.3 Increasing Power, Fixed Standoff Distance

Tests were also conducted at 106 Kw (142 hp), at standoffs of 20, 51, and 127 cm (8, 20, and 50 in.). These results are shown in Figure 4. The optimum pressures shifted upward, with the optimum at 127 cm (50 in.) occurring between 105 and 140 MPa (15,000 and 20,000 psi). This upward trend is illustrated in Figure 5, which shows powers of 71, 86, 98, 106 and 135 Kw (95, 116, 131, 142 and 181 hp) at a standoff of 127 cm (50 in.). This trend is due to the increase in orifice size at each pressure with the increasing power. The standoff distance in nozzle diameters is decreasing, resulting in less deterioration of impact at the surface.

If the optimum pressures at each power are used, and a nozzle diameter calculated to match the pressure and power, the resulting orifice diameters at each standoff are approximately the same. These orifice diameters are plotted versus the standoff distance in Figure 6. The standoff distance divided by nozzle diameter is plotted against the standoff distance in Figure 7. The relationship of optimum orifice size at a given standoff distance is expressed in Figure 8, where depth of cut versus

the orifice diameter at a standoff distance of 127 cm (50 in.) is plotted for powers ranging from 71 to 135 Kw (95 to 181 hp). These charts show the optimum performance is dependent on orifice size for a given standoff distance. An optimum orifice size should be selected based on standoff distance, and increased power should be applied through increased pressure and flow while keeping this orifice diameter constant.

4. CONCLUSIONS

The results of these tests showed an optimum pressure and flow combination for a given power at a given standoff distance. The optimum does not appear to be dependent on the threshold pressure of the material. As standoff distances increase, the optimum conditions become more sharply defined.

In addition, these tests showed that the optimum conditions occur at a fixed value in terms of nozzle diameters at each standoff, and an increase in power should be applied by increasing pressure and flow through the optimum orifice size, defined by the standoff distance.

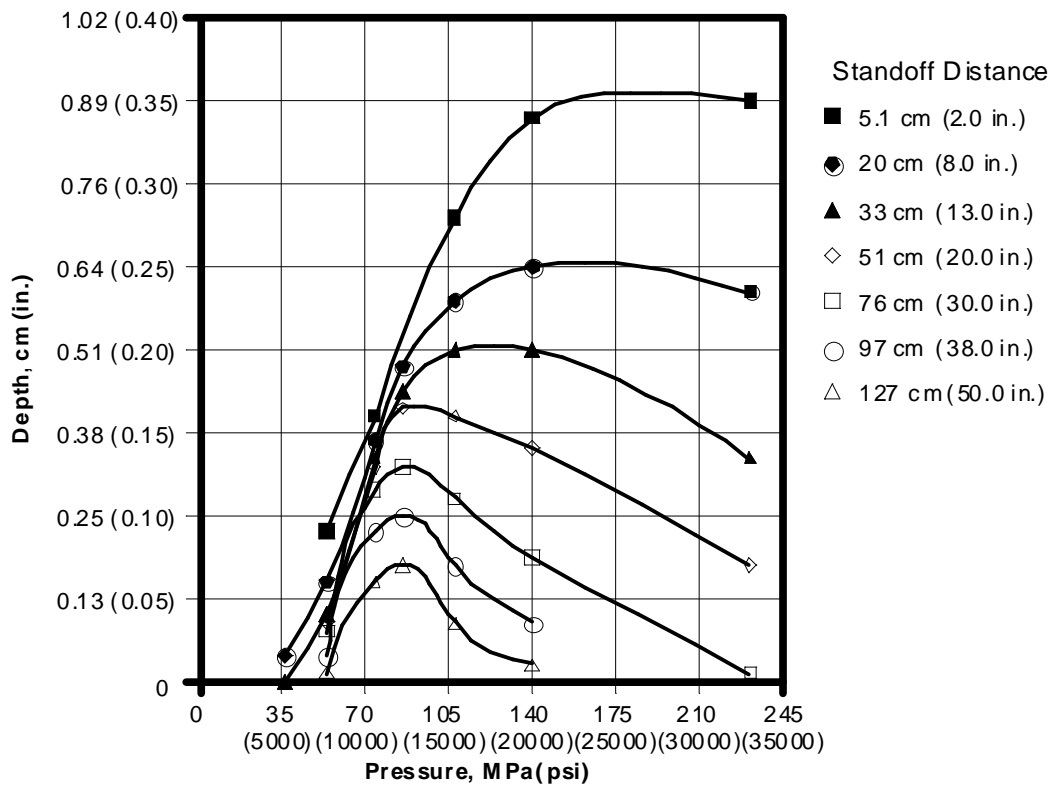


Figure 1. Depth of Cut in Wax at 71 kw (95 hp), vs. Pressure

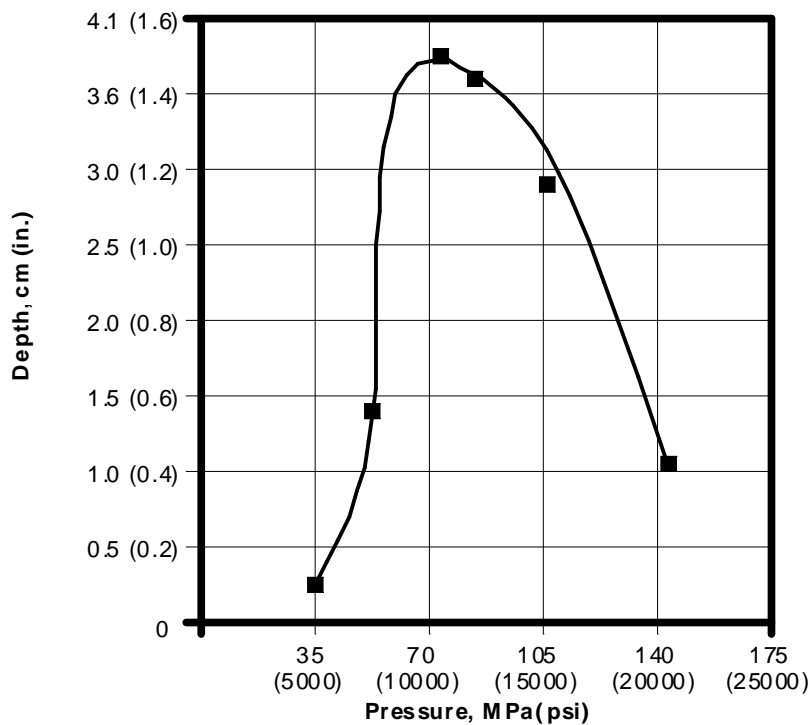


Figure 2. Depth of Cut in Cement/ Sand Mixture at 127 cm (50 in.) Standoff

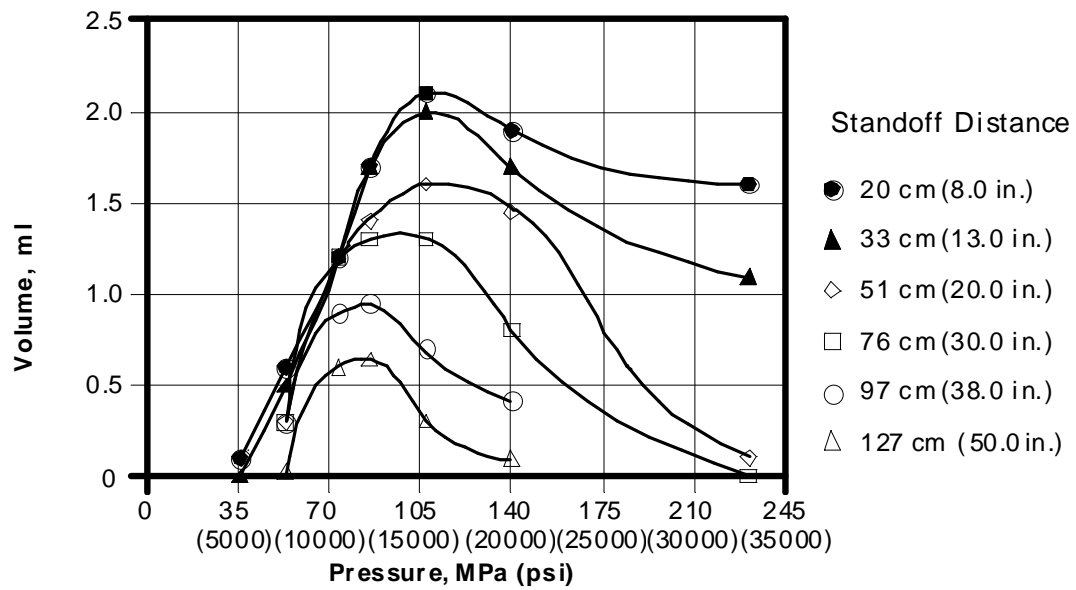


Figure 3. Volume Removed in Wax at 71 Kw (95 hp), vs. Pressure

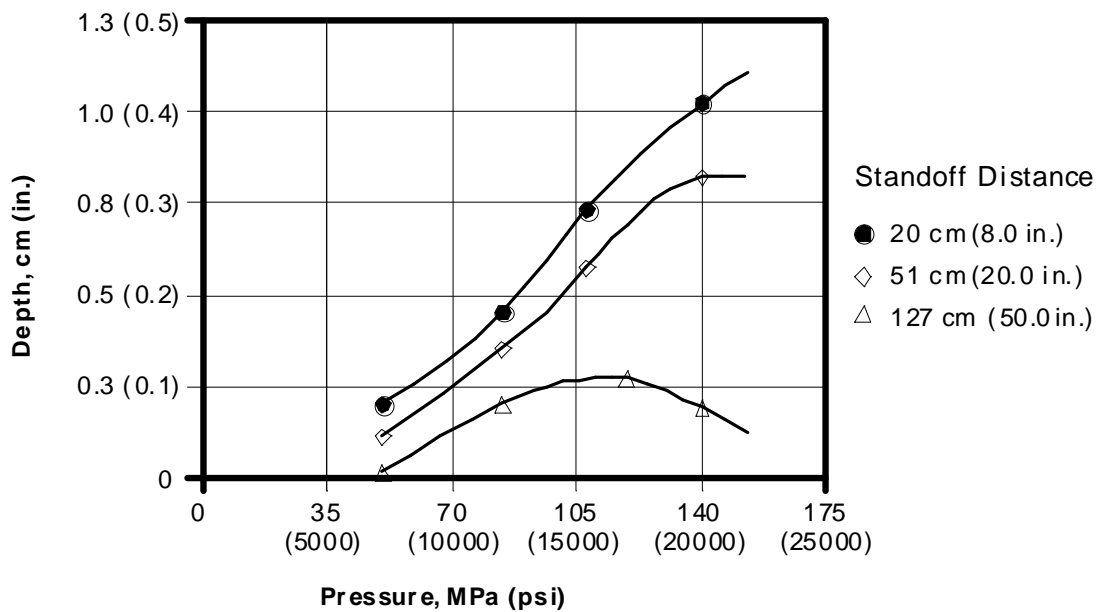


Figure 4. Depth of Cut in Wax at 106 Kw (142 hp), vs. Pressure

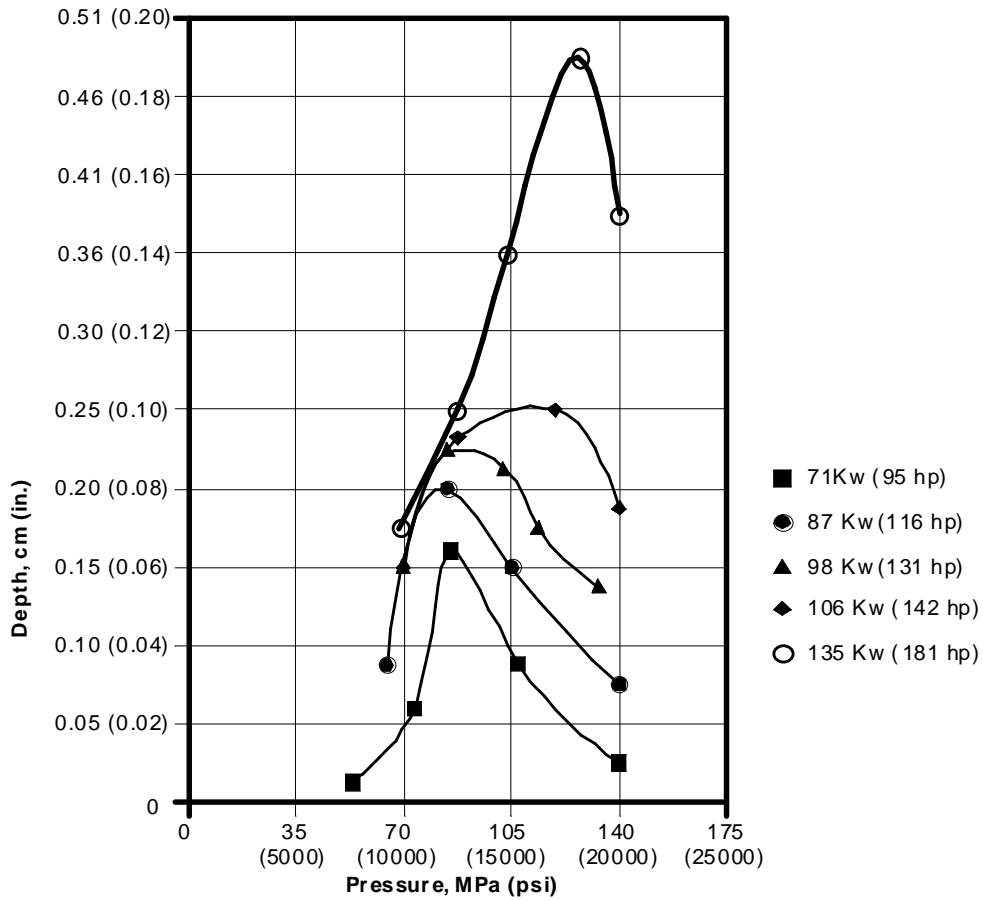


Figure 5. Depth of Cut in Wax at 127 cm Standoff (50"), vs. Pressure

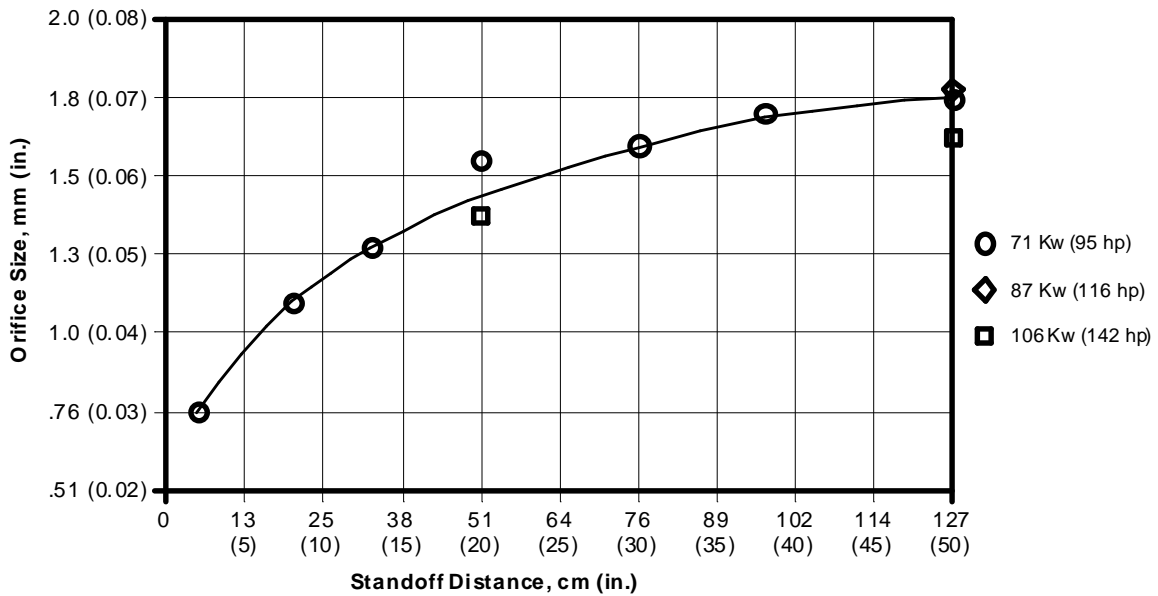


Figure 6. Optimum Orifice Diameters at Standoff Distances

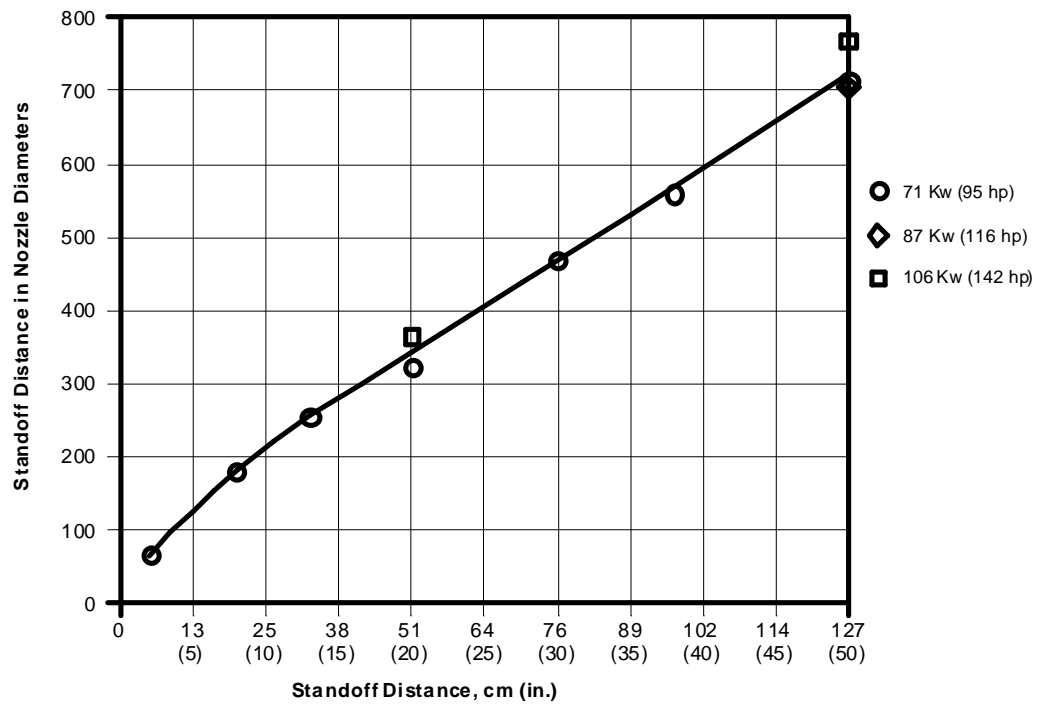


Figure 7. Optimum Nozzle Diameter Standoffs

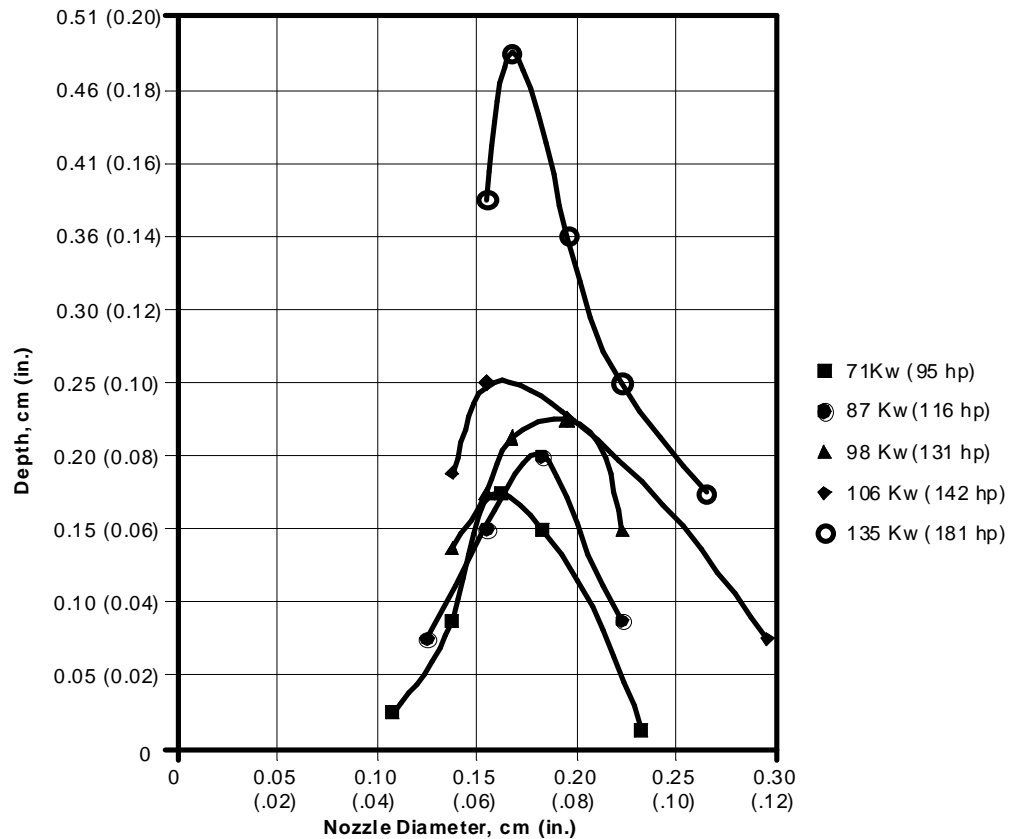


Figure 8. Depth of Cut in Wax at 127 cm Standoff (50"), vs. Nozzle Diameter

WATERJET TECHNOLOGY CHALLENGE TO MEET NEW EXPECTATION

Jack Russell
Dow
Freeport, Texas

ABSTRACT

This paper is being presented from the perspective of an end user of waterjet technology and a representative of the petrochemical industry.

In today's competitive global environment the waterjet industry, industrial process cleaning companies, and the petrochemical industry are faced with new challenges. To overcome the problems and perceptions that exist with industrial process cleaning companies will require a culture shift to meet the demands of their customers. To understand what must be done we need to analyze past practices, address key points, and define new concepts. This analysis will improve field applications and resolve trust issues between waterjet customers and industrial process cleaning companies, to take waterjet technology to the next level.

1. INTRODUCTION

Waterjet technology has proven to be successful in petrochemical plants for process cleaning applications. Along with their success, there have been failures and there are still obstacles to overcome. In today's global competitive environment, the petrochemical industry is being challenged to produce higher quality at lower cost. Waterjet service providers are faced with improving the effectiveness of their technology to meet the same demand. In order to meet the demands, a change in culture on behalf of the waterjet industry is required. A new perspective for identifying the energy and force requirements for removing foulants must be addressed. To justify my position on this topic, we will look at the following issues from the end users perspective.

- The Requirements of the Petrochemical Industry
- A New Cultural Shift in Industry
- WaterJetting Companies Capabilities
- Perceptions or Misperceptions
- Process for Designing a Cleaning System
- Ensuring a Bright Future for WaterJetting
- Conclusion

2. THE REQUIREMENTS OF THE PETROCHEMICAL INDUSTRY

Our world has realized that we operate in a global market place. This means that there are more than one kid on the block providing products and services. The petrochemical industry is no exception to this fact. They must provide their customers products at the lowest cost with the highest quality to maintain a competitive advantage. In an effort to survive in this global environment, the petrochemical industry must become more efficient and reduce cost. They must:

- Identify and resolve high cost problems
- Increase run time and reduce down time
- Produce more, with higher quality, with less variability
- Identify suppliers and service providers that are willing to meet the same challenges

These challenges need to be addressed without compromising safety or environmental impact. The points made are not rocket science; in fact they are concepts we have all pursued for years. What makes it different is the urgency and how we approach solving these problems today for future business growth. Solving the problems will take teamwork between the petrochemical industry and waterjet industry.

3. CULTURE SHIFT IN THE PETROCHEMICAL INDUSTRY

There is a required urgency to solve petrochemical industry's problems for business growth. A culture shift is necessary to reach the objectives. The most important areas that require attention are:

- Utilization of the appropriate resources
- Knowledge and experience for pre-job analysis
- How works have been accomplished and evaluate their cost efficiency (manpower, work process, procedures, best technology, and tools).
- Develop new ways to solve problems, collaboration, and partnering.
- Make decision based on data.
- Challenge standard practices (no more comfort zone or accepting it as the only way).
- Root cause evaluations to eliminate or reduce high cost problems.
- Improving and implementing new technology.

3.1 Examples of Cultural Change

Since the mid-nineties, the petrochemical industry has undergone cultural changes. These changes have made a significant impact on the way business is conducted. Listed below are a few examples:

- Educating the workforce to make better decisions that effect their work. This is accomplished by identifying the boundaries they can work within.
- Less management for supervising and approving decisions.
- Taking risk through the use of data and testing to incorporate beneficial technology without compromising safety or environmental factors.
- Created cooperative relationships with suppliers (labor, services, and products).
- Focus attention on the needs of their external customers.

4. WATERJETTING SERVICE PROVIDER'S CAPABILITIES

Why is a waterjet service provider important? The question is the same as, " who is the most important .. an Engineer, a Farmer or a Laborer?". The answer to the questions is the farmer, because without food the engineer and the laborer could not exist. The same scenario is true of a plant environment. It takes engineers, operators, and craftsmen to operate a plant; however, without the ability to clean the internal components, it will not run efficiently. Without the knowledge and experience of the waterjet industry, the petrochemical industry would find it difficult to operate and be competitive.

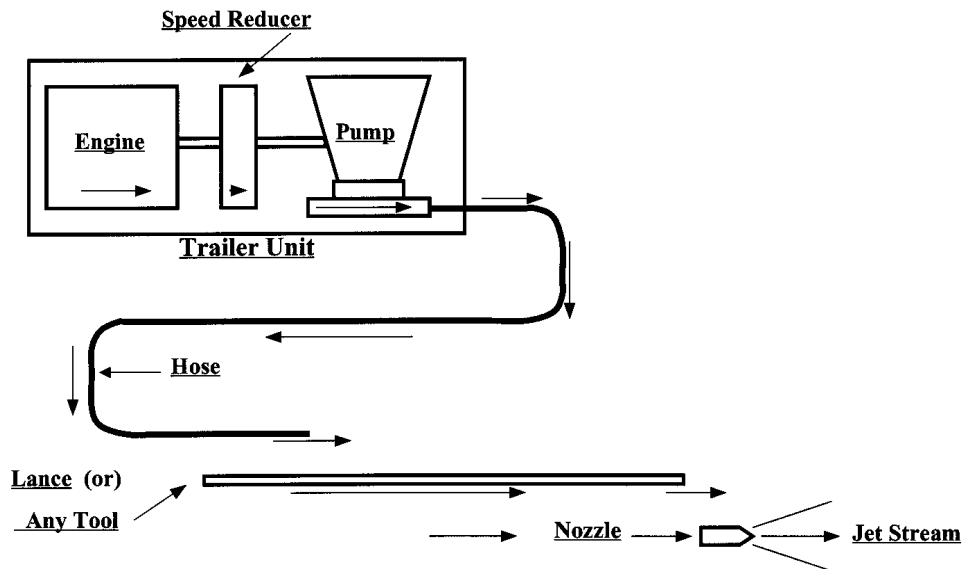


Figure 1. Basic Hydroblasting System

4.1 Basic Hydroblasting System

Figure 1 illustrates the basic hydroblasting system. How does plant maintenance and operation personnel perceive this system? They see a motor, pump, hose, and a cleaning tool to squirt water. In reality it is a highly sophisticated, mathematically supported system. To illustrate the mathematical processes involved (calculating energy losses), let's look at each components of a hydroblasting system.

Motor/Engine – An electrical motor or diesel engine is the power source that initiates the energy (measured in horsepower-Hp). As the energy is being produced it is transferred to the shaft (measured in break horsepower-BHp). The power source is generating mechanical energy that has losses due to friction of the moving parts.

Speed Reducer – As the speed reducer receives the remaining mechanical energy from the power source, it transfers the mechanical energy to the pump shaft. Speed reducer is designed to lower the speed of the pump shaft (measured in RPM).

Pump – The remaining mechanical energy after the speed reducer is induced into the pump. The pump is designed to convert the mechanical energy into hydraulic fluid energy (measured in hydraulic horsepower-HHp) as it is discharged from the pump. The amount of fluid being pumped is a function of the number of pistons, piston diameters, pistons stroke length, and revolution per minute. The pressure is dependent on the restriction down stream. Pressure and flow must be synchronized in order for the pump to be efficient.

Hoses – The remaining hydraulic fluid energy from the pump is delivered to the hoses. Hoses are designed to carry the hydraulic fluid energy to the cleaning tool. In most cases the hoses, fittings, and other connections are usually where the greatest losses occur due to friction and turbulence.

Cleaning Tool – The remaining hydraulic energy that is left from the losses of the power source shaft, speed reducer, pump and hoses is delivered to the cleaning tool chosen to perform the work (shotgun, slab cleaner, lances, 3D-rotary head, etc.).

Nozzle – The remaining hydraulic fluid energy at the end of the hose is delivered into the nozzle. The “**nozzle**” is the very heart of the whole system. Without the calculation of the system losses there is no way the nozzle can be designed to work efficiently. The nozzle orifice(s) also dictate the amount of mechanical and hydraulic fluid energy produced (measured in hydraulic horsepower-HHp).

Jetstream – The remaining hydraulic fluid energy that is exiting the nozzle’s orifice is converted to mechanical energy that performs work (measured as impact force).

Capturing the above system in another term is that the power source is producing mechanical energy and has about 30 to 35 more horsepower than the pump. The pump receives the mechanical energy and converts the energy to the pump horsepower hydraulic fluid energy. There are basically two types of pumps used:

- **Variable displacement hydraulic pump (VDHP)** referred to as intensifier 40,000 psi. Ultra-high pressure.
- **Reciprocating positive displacement hydraulic pump** ranging from 5,000 psi to 36,000 psi.

These pump flow capabilities range from 6 gpm to 250 gpm and the amount of flow is dependent upon the amount of pressure required. The three pump pressure ranges are classified as conventional pressure (10,000 psi), high-pressure (20,000 psi), and ultra-high (40,000 psi). The hoses, with an inner core, spiral wound wire reinforcements, and protected cover transports the fluid to the cleaning tool. The pressure and flow is dependent on inner core diameter of the hose. The selection of the cleaning tool is based on the energy required, location, access points, and design of the equipment internals. The nozzle’s orifice(s) is designed to match a working pressure, obtain the impact force of the fluid and shape the jetstream. As the jetstream exits the nozzle, the hydraulic fluid energy is converted to mechanical energy. The principle job of the jetstream is to cut, fracture, or peel the foulants. The angle and stand-off-distance is also critical for the jetstream to be efficient. To evaluate the alternatives a process should be followed in selecting the pump, hoses, cleaning tool, and nozzle.

5. PERCEPTIONS OR MISPERCEPTIONS

Communications between the customer and service provider is one of the major problems in getting work accomplished efficiently. Does perceptions or misperceptions cause some of the problems dealing with communication? Trying to understand the perceptions of people is difficult. In some cases to understand how people really feel about a situation, they have to be encouraged to express their feelings. In other instances, the real feelings are not expressed until a situation has come to a boiling point. When perceptions are realized, the task is to determine if they are justifiable. If they are not, then they are misperceptions. The only way to combat

misperceptions is to understand how they are created. Some of the perceptions that I have identified with waterjet service providers are listed below.

Perception of Customer	Why
Focus on billable hours	<ul style="list-style-type: none">• Long cleaning times• Sometimes repeat job• Unrealistic time quotes
The technology is not seen as technical	WaterJet service providers should provide the customer with better understanding of the pre-job planning process
Limited technical people	<ul style="list-style-type: none">• Switching out equipment often• Limited training of hands-on people• High personnel turnover rates
Limited trust	<ul style="list-style-type: none">• Results are not up to expectations
Very limited knowledge	<ul style="list-style-type: none">• Appears that testing is required for every job

From the customer's viewpoint, here are some comments of what they want the waterjet service providers to eliminate:

- Reinvent the wheel on repeated jobs
- Continue to “fight the fire” with the same old shovel
- The assumption that there is only one approach or solution
- Over looking that technical expertise has been developed for use in process cleaning applications
- Not using the most economical technology
- Trial and error methodology in cleaning

I have worked for the past twelve years with waterjet technology by bringing waterjet service providers into our plants. In the last four years I have realized that the customer's perceptions of the waterjet service providers should be taken seriously.

Let me explain my meaning. In 1998, I became aware of some perception issued and started working to resolve some of these issues. These are issues from a customer’s viewpoint. They want waterjet companies to focus on:

- Using the best available technology (most economical/safest)
- Learning and documenting what works well in repetitive applications
- Identifying high cost problem areas, and work to reduce or eliminate
- Recognizing that a culture shift has taken place in the petrochemical industry
- Creating cooperative relationships with customers (team relationship)
- Improving the utilization of manpower and equipment
- Increasing technical knowledge
- Knowing the real capabilities of the equipment
- Developing a professional image at all levels of the company (managers to lance operators)

From a waterjet service provider's point of view, they want the petrochemical industry to:

- that they can reduce cleaning problems
- Recognize that they can decrease equipment downtime
- Recognize their ability Recognize that waterjetting is a highly technical field
- Recognize that waterjet service providers employ experts
- Have confidence in their ability
- Recognize to reduce cost
- Trust that they will get it done

5.1 Point of Views

Waterjet service providers and the petrochemical industry seem to want to accomplish the same goal .. to perform a job safely and make a profit. The problem is both have looked at the perceptions from different viewpoints. **Both have failed to focus in on what is truly causing the perceptions.** The fact is “waterjetting is being accomplished by the only means available”. From the very beginning, the waterjetting industry has focused their attention on using more energy and ways to apply it, rather than looking at the characteristics of the foulants.

To illustrate this concept, visualize a picture of the hydroblasting equipment used in the plants performing their normal job without the foulant being in the picture. This would show the area where their knowledge and experience lies. To complete the whole picture, they would need to add knowledge of the foulant characteristics to the existing picture. This same picture could be used for plant personnel. They look only at the foulant without looking at the hydroblasting equipment.

5.2 Proving a Concept

Looking back at Figure 1, I stated that hydroblasting is a sophisticated technology. Hydroblasting systems are composed of a blasting unit, hoses, fittings, cleaning tools, and finally the very heart of the system, the nozzle. If the nozzle is designed correctly, the blasting system will produce the energy required to do the work. Also, the nozzle's jetstream must approach the foulants at the appropriate angle, stand off distance, and dwell time to work efficiently. The processes for determining these parameters have utilized previous experience and trial and error due to the lack of understanding of the characteristic foulants.

6. PROCESS FOR DESIGNING A CLEANING SYSTEM

Choosing the right equipment for every cleaning application requires an information exchange between the equipment owner and the service provider. A site visit is necessary to obtain

adequate information. Let's take a look at some of the key questions that should be addressed by the waterjet service provider:

Key questions in a job setup:

- Is the equipment on the ground or in the structure?
- Are there utilities available? If so, how far from the equipment?
- How much available room exists around the equipment?
- What are the foulants being removed?
- What is the consistency of the foulants?
- What are environmental, safety, and disposals concerns?
- Has it been done before, and if so, how?
- Where are the entry points, and what are their dimensions?
- Are there any internal obstacles?
- What is the material of construction?
- What other jobs, equipment, or personnel will be in the area?
- When do they want this done?
- What is your definition of clean?
- Any specific question related to the application and technology.

Every question is important in evaluating a cleaning application. In order for the cleaning system to be sized properly (by calculating all the losses), the waterjet service provider should evaluate the foulants to determine the energy required at the nozzle. The person with the most knowledge and experience selects the nozzle and energy for the application. This is the point where the waterjetting industry needs to make the culture shift.

The waterjetting industry needs to place more emphasis on the energy exerted past the nozzle (impact force) as it relates to the foulants. This statement is supported by the following facts:

- The jobs last longer than planned
- There are multiple pump changes
- There are multiple nozzles selected during a job
- Application and method changes
- Failures to reach the desired level of clean
- The workers are blamed for the equipment's inefficiencies

These facts exist because the waterjet service provider believes that jobs can be accomplished in the same manner as on previous visits. In order for the job to be treated as it was on the previous visit, it would have to meet all the conditions listed below:

- The process used the same feed rates
- No process upsets
- No adjustments in ratio of components
- Used the same operator all times
- Variable did not change

- Maintained the same temperatures
- Equipment shutdown in consistent manner
- Equipment had the same runtime
- No changes in design

One of the most important factors in the culture shift for the waterjet industry is understanding the characteristics of the foulants being removed. Plant upsets pose different cleaning problems to be solved by waterjet service providers. In some instances it is a guessing game to determine what will work. To address the solution let's look at the foulants characteristic and how the waterjet stream effect them.

Foulants Characteristics Properties

Foulants	Type of Build-Up	Impact Force	Jetstream Strategy
Hard	Thickness	Pressure	Cut
Soft	Multi-Layers	Volume	Fracture
Oily	Different Layers	Mixture	Tear
Gummy	Different Thickness	Additives	Peel
Stain			Wash

Once the foulants characteristics are known, how is the hydraulic fluid energy determined? To make this determination, the questions below should be addressed:

- How much energy does the foulants take away from the working energy?
- What is the breakaway energy required removing the foulants?
- What is the energy needed to attack the foulants (cut, fracture, peel, tear, etc.)?
- What is the dwell time?
- What is the standoff distance?
- What is the best angle of approach?
- What is the time requirement to complete the job?
- What is the best system design (pump, hoses, tool, and nozzle)?

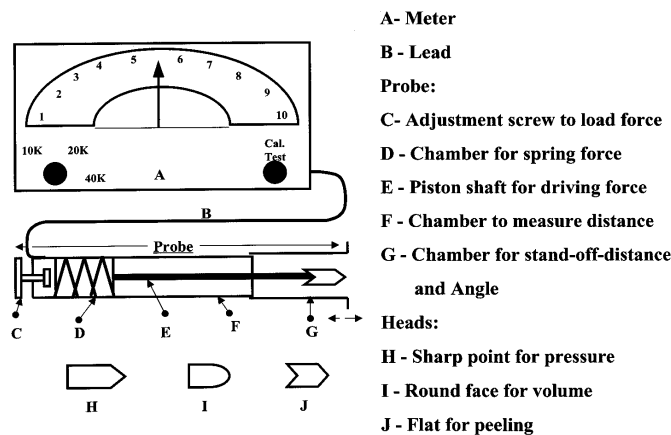


Figure 2. Russell Foulant Characteristic Tester (RFCT)

Instead of trial and error methods of finding the breakaway energy, waterjet service providers need a tool to assist in defining the foulant characteristics. Above we talked about the key points to remove foulants effectively. In Figure 2 is a conceptual design of the Russell Foulant Characteristic Tester (RFCT). This is a tool concept to gain knowledge of the foulants' unknown characteristics. It is designed to measure the energy required to remove a foulant. How does the Russell Foulant Characteristic Tester (RFCT) work? (Please refer to Figure 2 for a better understanding of this explanation.)

The probe is design to be placed against the foulant.

“C” is a setscrew used to apply a measurable load on the spring - "D".

“D” is a spring with a known force. When the force of the spring is released it will push the piston - "E" - forward, with a foulant-measuring tip ("H", "I" and "J") into the foulant.

“E” is a piston that has a flat surface on the back of the shaft for the spring force to push on to drive it forward into the foulant. The front end of the shaft is threaded so different types of heads can be screwed on. The piston shaft is transferring the loaded force of the spring to the head to penetrate, fracture, or peel the foulant.

“F” is the chamber that is measuring the distance that the piston is moving forward.

“G” is representing the chamber that will move back and forth like a micrometer to measure effective standoff distances. The flat surface of the footing can be adjusted to certain angles for finding the best angle of approach.

“H” is representing a pointed head for measuring the quality of pressure reaction on the foulant.

“I” is representing a rounded, blunt head for measuring the quality of force, or energy dissipation, of the foulant.

“J” is representing a thin, flat head for measuring the bond of the foulant.

“B” is representing the lead that is transferring the signals of the force, penetration depth, or movement distance at certain standoff distances back to the meter.

“A” is representing the meter that is converting all the information from the probe into hydraulic energy that is needed to properly calculate a system design to get the work accomplished.

Another factor in the culture shift is teamwork. In an effort to develop the RCFT, teamwork may be necessary. Non-Destructive testing instrument manufacturer may hold the solution to instrumentation. The opportunity for teamwork exists.

8. ENSURING A BRIGHT FUTURE FOR WATERJETTING

The petrochemical industry cannot continue to clean their equipment using technology in the old culture. The cost of cleaning and loss of production time is critical in lowering cost to compete on the global market. New tools for assisting job analysis and performance are growing vastly in other fields. I cannot expect any less from the waterjet industry with their knowledge and experience. Waterjet service providers need new tools technology to gain knowledge of the foulants characteristic. Without the new technology, the following cannot be accomplished:

- Recognize that waterjetting is a highly technical field
- Recognize that waterjet service providers employ experts
- Have confidence in their ability
- Recognize that they can reduce cleaning problems
- Recognize that they can decrease equipment downtime
- Recognize their ability to reduce cost
- Trust that they will get it done.

The prototype of the RCFT has not been developed. I challenge the waterjet industry to develop this tool to evaluate cleaning jobs and improve customer satisfaction. I would like to mention that our best resource are those of you who are hands-on skilled workers. Think about how you would like to improve equipment and discuss it with your technology support groups. Your ideas may make all the difference. You are our experts.

9. CONCLUSION

I hope I have effectively presented the major concerns and expectations of the petrochemical industry and the waterjet service providers. Communication and teamwork is the key to reaching our desired outcomes. We can provide our customers products and services at the lowest cost with the highest quality and maintain a competitive advantage.

THE ELECTRO-AEROSOL JET CLEANING THE GREASE AND IMPURITY ON THE METAL SURFACE

Liao Zhenfang, Zhang Shijin, Deng Xiaogang
Institute of Mechanical Engineering
Chongqing University
Chongqing, P. R. China

Zhang Fenghua, Tang Chuanlin
Zhuzhou Institute of Technology
Zhuzhou, Hunan, P. R. China

ABSTRACT

Generating principle of the electro-aerosol jet and its application extent are mainly introduced. The cleaning mechanics of the electro-aerosol jet are analyzed. The electro-aerosol jet can clean the metal surface with very low pressure.

1. INTRODUCTION

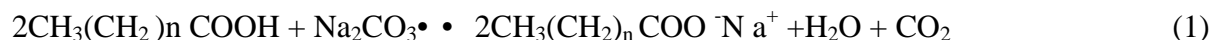
To clean the grease and impurity on the metal surface, two methods are used at present: (1) Use organic solvent or water-base scouring agent (2) Use abrasive water jet. Organic solvent is easy to catch fire, the consumption of water-base scouring agents is large and needs the cooperation of some mechanical action (such as steel brush) to come to consummate consequence. Abrasive jet has consummate impact in removing rust and impurity, but it is less effective in removing oil grease. Moreover, it will take a lot of investment at the beginning and abrasive must be recovered. Therefore, to complete some special cleaning job, we must seek a new type jet to clean grease and impurity without abrasive. The electro-aerosol jet is provided by authors for cleaning the grease and impurity on the metal surface which has many merits as follows: (1) It needs low pressure (we can use a centrifugal pump which has a large flow and a lower pressure). (2) It is safe and reliable. (3) The structure is very simple and the apparatus is very cheap. The electro-aerosol jet is especially fitful to clean the great oil tank, ship's hold, oil container and chemical container etc.

2. OPERATING PRINCIPLE OF THE ELECTRO-AEROSOL JET

Operating principle of the electro-aerosol jet is showed by Figure 1. The water jet is broken into dropping water by compressed air, and forms the aerosol jet. The direct-current electrical field with high voltage (about 6 KV) is imposed between supersonic-speed nozzle and low-pressure nozzle. As aerosol jet through supersonic-speed nozzle, the high voltage electrical field makes water to be electrified and the electro-aerosol jet is formed.

3. PRINCIPLE OF REMOVING GREASE OF THE ELECTRO-AEROSOL JET

The main ingredients of superficial active agent used in the research are composed of fatty acid and soda.



The molecule of carboxylic acid is comprised of polarity-base (-COOH) and negate-polarity-base (alkyl). Polarity-base can resolve in water easily. On the contrary negate-polarity-base have not be dissolved in water but in organic dissolvent easily (such as oil).



The polarity-radical and negate-polarity-radical in the molecule of fatty acid sodium salt can react with water and grease respectively. In the water solution, much of alkyl in the molecule of carboxylic acid is attracted by Van Derward's force. They draw close each other, after that form a spherical micelle, and polarity carboxylic acid base negative ion is on the surface of spherical micelle. In general, grease does not be resolved in water but can resolve in the internal of micelle that is comprised of molecule of carboxylic acid salt. In other words, oil is absorbed by affinity oil radical and extern of micelle is surrounded by affinity water base, so extern of micelle can

easily resolve in water. Therefore, grease and micelle of carboxylic acid salt are mixed together and dispersed in the water. Under the operation of the jet, and the grease is removed.

The polarity of anode and cathode of high voltage direct current power assemble can be exchanged in accordance with a certain frequency, and polarity of aerosol water particles will be relevantly changed. When aerosol water particles deposit on the metal surface, under the influence of aerosol-jet volume-electric charge electrical field, surface tension between the interfaces of impurity and cleaning mixture will be changed. At the same time, electrical field will change the attachment-character of electrified particles and the formation time of adhesive layer. It is these factors determine that the change of surface tension has characteristic time and that the electric charge particle has influence on the cleaning strength. It is well known that the impact of removing impurity and the speed of cleaning are decided by surface tension of cleaning mixture.

At the beginning instant, water flow particles (dropping water) deposit on faint conducting layer formed by impurity on which some remaining electric charge accumulates, and the direction of electromotance points to the articles waiting for cleaning, so it increases attachment performance of oil. When electric-charge-liquid-flow-particles of opposite polarity deposit on the impurity, they will make grease or impurity lost electric charge and appear neutrality, and make accumulated volume electric charge had the same sign as liquid-flow-particles-electric-charge. The direction of electric force will change, and this change will make grease and impurity separate from the metal surface, then they can be removed. By the way, in order to make liquid flow electrified, a little sodium salt is needed to add in the water.

In some special situation, high voltage electric power permit of no use, the device can be also adopted without high voltage electric field. Of course, without high voltage electric field, the cleaning efficiency will be decreased.

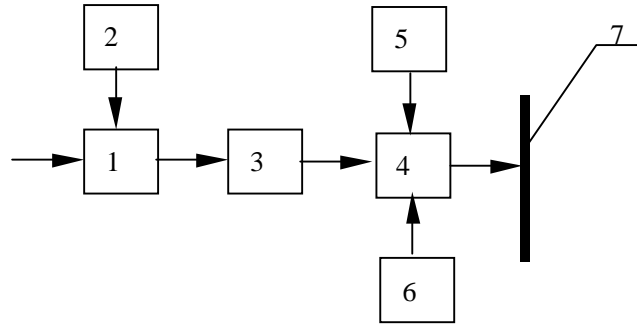
4.THE RUSHING EFFECT OF THE ELECTRO-AEROSOL JET

When jet flushes the surface of piece of work, affinity oil base inserts into oil drop, and breaks oil into small particles, which are surrounded by a layer of affinity water base. Affinity water base resolves in water, it makes the oil which do not resolve in water disperse in water. At the same time, liquid flow particles carried electric charge under the co-operation function of superficial active agent, electric agent and jet scouring and impacting effect, grease and impurity will be remove.

A piece of steel plate coated with different kinds of engine oil and butter with different thickness has been tested. The results showed that compared with some conventional water jet with superficial active agent, the electro-aerosol jet has higher efficiency in cleaning grease and impurity. The main reason for it is that the inside diameter of electro-aerosol nozzle is too bigger, the cleaning area has increased drastically. It is calculated that the efficiency of electro-aerosol jet is as 10 times as that of available water jet when the consumption of water is same, the cleaning quality can satisfy the user completely.

5. ACKNOWLEDGMENTS

This research project is funded from the National Natural Science Foundation of China (No. 59874033).



- | | |
|------------------------------|-------------------------------|
| 1 - Pressure water flow | 5 - High voltage power source |
| 2 - Superficial active agent | 6 - Compressed air |
| 3 - Low-pressure nozzle | 7 - Cleaned piece of work |
| 4 - Supersonic nozzle | |

Figure 1. Schematic diagram of the electro-aerosol jet

ADVANCED HIGH-PRESSURE WATERJET CLEANING SYSTEMS FOR INVESTMENT CASTING FOUNDRIES

J.J. Tebbe
Triplex Systems, Inc.
Minneapolis, Minnesota, U.S.A.

ABSTRACT

The paper explores the use of high-pressure waterjetting techniques and systems for primary and secondary operation ceramic shell removal from investment castings. The author will compare the waterjetting process to different traditional methods for removing ceramic shell and various casting cleaning processes practiced today. The author will discuss environmental, ergonomic and productivity benefits related to the use of waterjets as the primary means for effectively cleaning investment castings.

1. INTRODUCTION TO THE INVESTMENT CASTING PROCESS

The investment casting process or lost wax process has been around for thousands of years. Today the investment casting process is one of the premier high technology processes for producing complex near net shape cast parts from common metallurgies to super alloys. Investment castings have both aerospace and commercial applications ranging from precision cast airfoils, compressor stators, nozzles, turbocharger wheels to gun parts, pump housings, impellers to golf club heads. Investment castings have become so elaborate that often a single complex casting geometry eliminates previous fabrication methods involving machining, sheet metal work, welding and fastening technologies.

Investment denotes the mechanical method of obtaining a mold rather than the material used. It is the process of investing a three-dimensional pattern in all of its dimension details to produce a single piece destructible mold into which molten metal will be poured.

The principal feature of investment molding is that a fluid mixture flows around the pattern providing excellent detail. This mixture sets with the aid of a hydraulic bond. The pattern is expendable and removed by burning or melting.

The mold is then fired to the temperature of the metal alloy to be cast. Metal is then introduced into mold vessel or tree via gravity or vacuum. The cast mold tree is allowed to cool and now encases the precision cast parts. The destructible mold material must be removed to reveal the precision cast parts. The destruction of the mold material without damaging precision castings is the basis for this paper.

2. TRADITIONAL METHODS FOR DESTRUCTION OF MOLDS

The last operations of the investment casting process occur in the post cast area or casting finishing. The removal of the mold material, cleaning, cut-off and grinding operations occur in post cast (after metal is poured).

The mold materials used in investment casting consist of refractory fillers and refractory binders for purpose of discussion we shall refer to these refractory materials as the ceramic shell. Removal of the ceramic shell mold material is very labor intensive and has required in the past several mechanical operations to remove the shell material and clean the castings. For purposes of discussion the removal of shell material shall be divided into two categories, *primary and secondary operation cleaning*.

Primary operation cleaning is defined as gross removal of ceramic mold material from the investment cast tree. *Secondary operation cleaning* is defined as fine removal of ceramic materials from blind holes, internal passageways, recesses or areas that are not accessible with primary operation cleaning. The following briefly reviews the *traditional processes* and the *advantages and disadvantages* of each process for removal of ceramic molds:

- **Knock-Out Process:** The process ranges from manual hammering to reciprocating air hammer for removal of mold materials. This process is labor intensive and relies on percussive hammering and vibration to remove the mold materials. The *advantage* of this process is rapid *primary operation cleaning* when the process is mechanized. The *disadvantages* are; labor intensive process, potential for vibration induced stress cracking, loud process requiring sound deadening or hearing protection, dry process, produces airborne silica dust requiring adequate ventilation and respiratory protection.
- **Shot-Blast Process:** The process is mechanically hurling steel shot at the remaining mold material. The process is typically a *secondary operation cleaning* technique, however mold material may still remain in cavities and recesses requiring further cleaning. The *advantage* of this process is, high production rates and speed from batch processing. The *disadvantages* are; potential for casting surface and edge damage, high maintenance machinery, dry process releases airborne silica dust requiring adequate ventilation and respiratory protection and the blast media is an expendable.
- **Abrasive Blast Process:** The process is typically manual or mechanized batch processing. This process is labor intensive and relies on compressed air entrained abrasive particles for removal of mold material. The process is typically a *secondary operation cleaning* technique. The *advantage* of this process is moderate production rates are achievable. The *disadvantages* are potential for casting surface damage, labor intensive manual operation, compressed air costs, dry process releases airborne silica dust requiring adequate ventilation and respiratory protection and the blast media is an expendable.
- **Chemical Leaching Process:** The process is typically a batch cleaning process and is used for both *primary operation cleaning* of delicate parts and *secondary operation cleaning* for complete removal of investment from the castings. The *advantages* of this process are: high production rates and removes all mold material external and internal passageways. The *disadvantages* are; requires another operation cleaning chemical surface residue, produces large amounts of hazardous waste, posing expensive disposal issues, uses large amounts of potentially dangerous chemicals, hot process requiring a lot of energy to heat the chemical bath continuously, requires special ventilation for chemical vapors.

To summarize the *traditional processes*, these processes have historically been used in all foundry applications as the only means of removing mold material effectively. Most foundries utilize all four of the above listed processes to achieve one goal, removal of mold material. Each of the traditional process has its *advantages* all of the processes have greater *disadvantages* associated with each process. The author will show implementation of a *non-traditional cleaning process*, offers greater advantages for productivity with fewer disadvantages related to ergonomics and environmental issues.

3. ADVANCED HIGH PRESSURE WATERJET CLEANING SYSTEMS

The non-traditional cleaning process that competes directly with the four traditional cleaning processes is the use of advanced high-pressure waterjet cleaning techniques. The use of high-pressure waterjets for cleaning castings continues to gain greater acceptance as an important finishing process for investment castings.

The use of waterjets for cleaning aluminum casting has become common practice over the years and is the preferred cleaning method for this softer metal alloy. In the case of aluminum castings, the casting and its surface can easily be damaged by more aggressive cleaning processes such as the Knock-Out, Shot-Blast, Abrasive Blast and Chemical Leaching Processes for shell mold removal.

In waterjet cleaning of aluminum castings, the pressure range is a limited band, generally between 3000 psi (204 bar) and 6000 psi (408 bar). By staying within this pressure band, optimum cleaning results occur. Below the band, productivity drops off; above the band productivity increases, but the risk of casting damage also increases. So in the case of aluminum, parts damage is the limiting factor and determines the maximum system pressure.

In the case of steel and high temperature alloys, waterjetting is in direct competition with the four traditional cleaning processes. Each cleaning process has its advantages and disadvantages. For high temperature alloy castings in general the waterjet cleaning process must be comparable to traditional methods, better than the alternatives or offer benefits that eliminate finishing process steps.

For high temperature alloy castings, the waterjet cleaning pressure range is much broader, generally between 10,000 psi (680 bar) and 20,000 psi (1360 bar). In the past, waterjetting systems were limited to 10,000 psi (680 bar) and this in turn also limited the application of waterjets for investment casting foundries. Through research and development, 15,000 psi (1020 bar) has been determined to produce optimum cleaning results with no damage to the casting for most applications. Pressures of 20,000 psi (1360 bar) and greater have limited applications and these are generally determined by test cleaning.

To best understand the water-jet casting cleaning process, like traditional cleaning operations, waterjetting can be divided into primary and secondary operation cleaning steps. Advanced waterjet cleaning offers both primary and secondary operation cleaning, to work in place of or in conjunction with existing traditional cleaning methods.

4. PRIMARY OPERATION WATERJET CLEANING PROCESS

Primary operation waterjet casting cleaning is defined as gross removal of ceramic mold material from investment cast trees. The objective is to remove as much mold material as possible and to clear gating areas in preparation for cut-off. With waterjetting 90%-100% of the mold material can be removed depending on the complexity of the castings. Current waterjet cleaning systems include manual and automatically operated machines. Benefits of primary operation cleaning

with waterjets are: (1) eliminating damaged parts, (2) high production rates are attainable with automation, (3) better cleaning of recesses and passageways (4) Ergonomic operation with minimal body stress issues (5) elimination of airborne silica dust hazard, (6) Eliminates two to three traditional cleaning process steps. The primary disadvantage is the initial capital investment for the waterjetting equipment. However equipment justification can easily show a one – two year payback on the investment. With properly designed automation and material handling high production rates are achieved directly impacting reduction of cleaning steps and improved cleaning efficiency and productivity.

5. SECONDARY OPERATION WATERJET CLEANING PROCESS

Secondary operation waterjet casting cleaning is defined as fine removal of ceramic mold materials or core materials from blind holes, internal passageways, recesses or area that are not accessible with primary operation cleaning. Secondary operation waterjet cleaning has applications no matter what the primary method of cleaning is.

The objective of secondary operation waterjet cleaning is to remove 100% of the remaining investment. Secondary operation waterjet cleaning would compete with shot-blasting, abrasive blasting and chemical leaching.

In waterjetting, the secondary operation cleaning occurs after primary operation cleaned trees are processed through the cut-off operation (removal of cast parts from the gating). A typical secondary operation waterjet cleaning involves either repositioning individual casting in workholding tools for a second pass through the existing waterjet cleaning center or loading castings into an additional carousel style automatic waterjet cleaning center. A properly designed system can offer automatic primary cleaning and manual or automatic secondary operation cleaning in the same machine. Very high production rates can be achieved with the addition of secondary operation waterjet carousel style cleaning centers.

6. ADVANCES IN CASTING HANDLING AND MANIPULATION

There have been major advances in handling and manipulating entire investment cast trees using a new, powerful and compact rotary clamping device. The *patented rotary clamping tool* is designed to capture the conical shaped pouring cup remnant that is present on the investment cast trees. The pouring cup area of the investment casting is the area of the mold where the molten metal is funneled into the mold vessel and solidifies. The solidified metal consists of the metal formation of the pouring cup area, down sprue, gating feeders to the cast parts all encased in the fired ceramic mold. The patented rotary clamping device captures the metal pouring cup remnant of the investment casting as follows: When the clamp is actuated the three jaws advance along the closing rings angular cam surface, thus surrounding the pouring cup remnant at the minor diameter of the cone. Once the three jaws contact the minor diameter of the cone a fourth point of contact on the jaw actuator plate, contacts the base of the major diameter of the pouring cup and rams the pouring cup and jaws into the closing ring, achieving a captured pouring cup

and holding the investment cast tree rigid with the powerful clamps holding force. The *patented rotary clamping tool* family consists of three basic clamp sizes as illustrated in **Figure 1**.

Since the majority of investment castings fall within the jaw capacity range of the *Size #2 clamp*, further discussion will focus on this size clamp. The rotary clamping tool is designed to operate from a compressed air source up to 100 psi (7 bar) or a hydraulic pressure source up to 250 psi (17 bar) with no clamp modification. To compare clamping forces review the chart in **Figure 2**.

The *Size #2 clamp's* compact size, 9.0" diameter x 12.0" height (229 mm x 305 mm), and powerful clamping force capabilities, allows this clamping mechanism to hold heavy castings rigid in any plane, including horizontal, with overhung loads to 36" (914 mm). The *Size #2 clamp* can hold castings up to 100 lbs. (45 kg).

By using these clamping tools as an integral component of an entire cleaning system, optimum cleaning results and productivity can be achieved. The proper presentation and manipulation of castings is necessary for productive cleaning and ergonomic loading and unloading of the castings.

Specialized workholding tools have been developed to present individual or multiple castings in the proper direction for secondary operation cleaning. When a workholding tool is evaluated a three dimensional model is reviewed and the proper location of the casting on the tool is established. The workholding tools are designed to be loaded into the *patented rotary clamping tool* for presentation to the waterjets during the secondary operation cleaning cycle.

The *patented rotary clamping tool* has proven to be a valuable tool for investment casting foundries. The devices compact rotary design eliminates the need for large turntables. The rotary clamps ability to hold cast tree rigid in the horizontal plane, has lead to new system designs. With the rotary clamping tool in the horizontal plane a waterjetting nozzle can now track the entire length of the casting similar precision machining techniques. The invention of the *patented rotary clamping tool* has lead to new inventions to improve the investment casting process. Among these inventions are the *patented long reach clamping tool* and the *patented abrasive wheel cut-off machine*.

7. RAM (RANDOM AUTOMATIC NOZZLE MOVEMENT)

In high-pressure water jetting systems, water is usually directed to one or two high-pressure nozzles. A properly designed nozzle delivers the high pressure water in a focused stream to the surface to be cleaned. Like any method a foundry may use for cleaning – whether accelerating high velocity water streams, hurling steel shot or abrasive media—the kinetic energy dissipates almost as rapidly as it is imparted into the media. So it is very important to take advantage of the cleaning energy at it's most effective range. In waterjet cleaning of castings, nozzle distances of 6" to 12" (152mm to 305mm) are typical. High-pressure waterjetting with higher water volume to the nozzle can effectively double the cleaning distance for larger castings.

High-pressure waterjet casting cleaning systems typically require between 75 hp to 150 hp (56 kw to 112 kw) per nozzle as a baseline for estimating power requirements. With these power requirements per nozzle it is important to design cleaning systems with the minimum number of nozzles to remain cost effective as a casting cleaning process. The optimum cleaning system utilizes one (1) zero degree nozzle to keep the cleaning power requirements to a minimum. Through research and development *Random Automatic Nozzle Movement, RAM* (patent pending) was developed. For an automatic casting cleaning systems to be both productive and cost effective, the challenge of utilizing one (1) nozzle, nozzle movement and casting manipulation become very important factors. The *RAM* automation process incorporates linear nozzle movement, rotary movement and rapid X-Y movements of the waterjet nozzle. The simultaneous movements have proven to be very effective for fast and effective removal of ceramic mould materials from investment castings. The *RAM* movements are PLC controlled utilizing a single program that produces repeatable results in diverse complex casting configurations. The only parameters need to be entered is the casting height in inches (mm) and cycle time in minutes. The cleaning efficiency using *RAM* automation techniques has reached 99% to 100% cleanliness with cycle times of 1 to 2 minutes on high temperature alloy castings.

8. CONCLUSIONS

Comparisons of Random Automatic Nozzle Movement incorporated in advanced high-pressure waterjetting systems and traditional cleaning process has revealed, labor reduction, elimination of two to three traditional cleaning processes, elimination of airborne silica dust and increases in productivity and ergonomics.

Through extensive engineering, all mechanical mechanisms for imparting movement, oscillation and rotation have been designed to be outside the severe cleaning environment. The refinement of RAM automation techniques has eliminated the need for high- pressure waterjet rotary unions and multiple waterjetting nozzles. The RAM technique has produced very predictable cleaning results. The waterjetting process for casting cleaning has shown: (1) fast destruction of mold materials (2) no destruction of castings and casting surfaces (3) deeper penetration of recesses and passageways.

The future of the waterjet cleaning process for investment castings holds excellent potential for productivity, ergonomics, safety and improvement of environmental issues. With the potential elimination of several *traditional process* cleaning steps, post cast cleaning operations could be combined with post cast finishing (cut-off and grinding). Waterjet cleaning and post cast finishing could eventually be configured into a manufacturing work cell environment. A typical manufacturing work cell would include the waterjet cleaning process, cut-off and grinding operations.

The manufacturing work cell concept has productivity, ergonomic and environmental potential. Productivity and ergonomics are improved with fewer cleaning steps and less movement of castings through departments. The wet process eliminates airborne silica dust; water can be recycled, and the demolished inert ceramic mold material can be further recycled for use as filler material for construction applications.

9. ACKNOWLEDGEMENTS

Beeley, P.R., Smart, R.F., Bidwell, H.T., "Investment Casting" pp. 183-212, Finishing Investment Castings, Institute of Materials Publication, 1995.

Bidwell, H.T., editor, "Investment Casting Handbook," Investment Casting Institute Publication, 1997.

Klotzin, E., "Metalcasting & Molding Processes," pp. 39-70, American Foundry Society Publication, 1981.

Tebbe, J.J., Inventor, U.S. Patent 5,044,421 "Rotary Pneumo-Hydraulic Clamp".

Tebbe, J.J., Inventor, U.S. Patent 6,119,677 "Apparatus For Clamping And Precisely Cutting Castings".

Tebbe, J.J., Inventor, U.S. Patent Serial No: 09/198,240 "Clamping Jaw Device".

Tebbe, J.J., Inventor, U.S. Patent Pending "Random High Pressure Water Jetting Nozzle For Cleaning Castings".

10. GRAPHICS

Tool family consists of three clamp size ranges:

- 1.0 (Size #1) Jaw clamping range, .50"- 2.5"
- 2.0 (Size #2) Jaw clamping range, 2.5"- 4.75"
- 3.0 (Size #3) Jaw clamping range, 3.5"- 7.25"

Compressed Air Source

100 psi (7 bar), equivalent to 2827 lbs. (1285 kg.) of force, (1.4 ton).

Hydraulic Pressure Source

250 psi (17 bar), equivalent to 7069 lbs. (3213 kg.) of force, (3.5 ton).

Figure 1
Clamp Tool Capabilities

Figure 2
Clamp Pressure-to-Force
Conversion Chart

FIELD EXPERIMENTS OF A CITY STREET FENCE WATER JET CLEANER

Wang Jiansheng
Wuyi University
Jiangmen, Guangdong, P. R. China

Yang Lin
Chongqing University,
Chongqing, P. R. China

Jing Shuangxi & Liu Wei
Jiaozuo Institute of Technology,
Jiaozuo, Henan, P. R. China

ABSTRACT

The city street fences, made of iron bars and pieces with different shapes, are very difficult to clean by man traditionally. This method usually has a hard physical intensity, a lower efficiency and a higher cost. A new type of a cleaning machine, a City Street Fence Water Jet Cleaner (CSFWJC) has been designed and manufactured, which consists of two main parts of water jetting and rotary brush rubbing and can be equipped on spraying cars easily. First, the lower pressure water jets to the city street fences and cleans down the dust on them. Then the rotary brushes rub off the dunghill adheres to the city street fences. And last, the lower pressure water sprays to and scours the city street fences again. Field experiments show that a CSFWJC has a feasible structure, reliable performance, simple structure and ideal effect. The cost of cleaning street fences using the city street fence water jet cleaner can decrease to about 18.5 percent of that by the artificial method.

1. INTRODUCTION

There are thousands of kilometers of the city street fences in big cities or middle cities, which made of many kind of shapes of steel pipes, steel bars and steel pieces. The height of the fences is in the range of 0.8 m to 1.5 m. The city street fences or barriers are used to separate high-speed and low-speed ways or up and down roadways. The following are three main ways to clean the city street fences.

- Manual-cleaning method. The main streets in the middle and big cities, such as Beijing, Shanghai, Guangzhou, and so on, are the windows for external opening and a civilized symbol of a city, so a lot of men are needed to clean the street fences for a certain period of time. This cleaning way not only has a hard physical intensity, lower efficiency, higher cost and more danger, but also has a bad effect on the city's feature.
- Water washing by a fire hydrant or a spraying car, needs a great amount of water and has a bad cleaning effect.
- Lacquering the fences is a usually way in each city in P. R. China at the time of evaluating civilized cities.

The street fences are the faces of a city, which reflect the sanitation degree of the city, which are almost not cleaned in all over cities in P. R. China. It is a serious problem for city street fences cleaning, especially in the cities of north China, which has a little rainfall and big fly sand and ash. So it is necessary to develop a high efficiency mechanized machine for cleaning street fences.

2. DESIGN SCHEME AND GENERAL LAYOUT OF A CSFWJC

Rinsing and brushing are two basic cleaning functions. Water with a certain speed can remove away the dust on the surface of the street fences, and the higher water speed, the better cleaning effect. But the water speed is not allowed over high because the high-speed water can peel off the paint coating (Sui Jiajun, 1992 & Cui Muoshen et al, 1991). Brushes can easily rub off the dunghill tightly adhered to the city street fences, for example phlegm. Combining water rinsing and brush rubbing together is the main design idea of the new city street fence water cleaner. First, the lower pressure water jets to the surface of the fences and cleans down the dust on them, and can pre-wet the dunghill tightly adhered to them. Then the large rotary brush rubs off the dunghill pre-wetted easily. And last, the lower pressure water sprays to and scours the city street fences again.

It is the most reasonable cleaning method that we clean the both sides of the street fences once. But it is very difficult to do it because there has not a standard of the city street fences and have so many of billboards, signposts, electric light poles and so on. So we adopt the method of cleaning single side once, the two sides of the fences can be cleaned over when a spraying car go and back once. The single side cleaning method has several advantages, such as a higher cleaning speed and efficiency, single structure, lower cost and so on.

As shown in Figures 1 to 4, a city street fence water jet cleaner consists of two main parts of rotary brush rubbing and water jet rinsing. The two parts are equipped on a support frame fixed on the safety bar in the front of the spraying car.

The part of the rotary brush rubbing consists of a driven wheel, a tense spring, a flexible shaft, a support frame, two bearings, a round brush and so on. The driven wheel, being pressed on cartwheel forcefully by a tense spring and driven by the cartwheel, can run the rotary brush via a flexible shaft.

The part of water jet rinsing consists of a pump in the car, a flexible tube and a water jet tube. Water from the water jet tube fixed over the support frame jets from top to bottom, which has three functions. First, it removes off and pre-wetted the dust on the surface of the street fences. Second, it assists the rotary brush to rub. Last, it rinses away the dust rubbed off by the rotary brush.

3. DESIGN OF A TEST-MACHINE

Design parameters are that water pressure of the pump in the spraying car = 0.8-1.1 MPa, rate of flow = 5-8m³/h, speed of the spraying cars = 5-10 km/h and the height of the street fences = about 1 meter.

3.1 Rotary Brush

The 0.6-meter-diameter rotary brush of 1.2-meter long consists of an axis with one bearing in each side, a round brush base and 1-mm-diameter hard nylon hair. The two bearings are fixed in two bearing seats fixed on support frame. The up end of the rotary axis is connected with a flexible axis and is driven by it.

It is a reasonable rubbing way when the brush hair move along the bars or pieces of the street fences that are usually up and down, so that we fixed the axis of the rotary brush on the support frame with an angle of 45 degree of back high.

3.2 Water Jet Tube

Experiments show that the faster of water speed, the larger water impact force, and the better of the cleaning effect. When the water pressure is less than 1 MPa, the water can only rinse away the dust not tightly adhered to the city street fences. With water pressure increasing, the rinsing effect become better and better. When the water pressure is higher than 3 MPa, the water can rub away all dust and adhesive substance, such as phlegm, but this water pressure jet is danger to passengers and drivers passed by. So we chose operating water pressure in the range of 0.8 to 1.2 MPa.

The water jet tube with some nozzles is fixed on the top of the support base and about 0.3 meter over the rotary brush. Water spouts down to the street fences from the water jet tube. The nozzles on the water jet tube are divided into three groups. The first group nozzles at the front end of the

tube can rinse down the dust on the surface of the street fences and pre-wets the fences, the flow rate of which is about 60 percent of total rate of flow. The second group nozzles in the middle of the tube can assist the rotary brush to rub. The third group nozzles at the back end of the tube can rinse away the dust rubbed off by the rotary brush.

4. FIELD EXPERIMENT AND ANALYSIS

- As shown in Figures 2 to 5, the field experiments show as following.
- It is a feasible design way of CSFWJCs;
- The cleaning efficiency of the thicker diameter nozzles at lower pressure is better than that of thinner diameter nozzles at higher pressure. The optimal pressure is in the range of 0.8 MPa to 1.2 MPa.
- Consume power of the new cleaner is about 0.6 to 1.3 KW, which does hardly influence the operating functions of the spraying car.
- The 0.6-m-diameter of the rotary brush is too thicker, and the nylon hair is too denser
- The most of the adhesive substance can be rubbed off, but not all.
- The weight of the new cleaner is about 50 kilogram.

5. ECONOMIC BENEFIT

The spraying car runs at about 5 to 10 kilometers per hour. The cleaning speed of the two sides of the fences is about 2.5 kilometer per hour. Following are the cleaning costs of the new cleaner:

- Hour wage of a driver and an assisted man = 10 RMB Yuan
- The running cost of the spraying car = 20 RMB Yuan
- Water cost = 5 RMB Yuan
- The running cost of a CSFWJC = 2 RMB Yuan
- Other costs = 0-13 RMB Yuan
- Total cost is about 37 to 50 RMB Yuan

The cleaning costs of the manual-cleaning method are as following.

- Hour wage of a man = 4 RMB Yuan
- Hour wage of 50 men = 200 RMB Yuan

A city street fence water jet cleaner can relieve men of their heavy work, and reduce cleaning cost down to 18.5 to 25 percent.

6. CONCLUSIONS

- The water pressure and flow rate of the spraying car can meet the request of A CSFWJC.
- The power of a CSFWJC is about 0.6 to 1.3 KW, which does hardly influence the operating functions of the spraying car.
- The optimal diameter of the rotary brush is about 0.4 meter
- A CSFWJC equipped on a spraying car without alteration has several advantages, such as a single structure, a lower cost and convenient uses.
- Most of the adhesive substance can be rubbed off.

It is necessary that some problems of CSFWJCs must be solved before they come into use.

- It must establish a rule of city street fences and reduces the billboards, signposts, electric light poles and so on as possible as we can.
- The design schemes must be optimized, for example, adopting the rotary brush driven by a hydraulic system and keeping a constant pressure of the rotary brush on the fences automatically.

7. ACKNOWLEDGMENTS

The authors would like to thank the Henan National Natural Foundation of China for her financial support.

8. REFERENCES

- Sui Jiajun, "Water Jet Cutting Technology", *Publishing House Of China University Of Science And Technology*, pp187-230, Xiuzuo, P. R. China, 1992
- Cui Muoshen, Sui Jiajun. High-Pressure Water Jet Technology. *Coal Industrial Publishing House*, pp142-158, Beijing, P. R. China, Oct. 1993

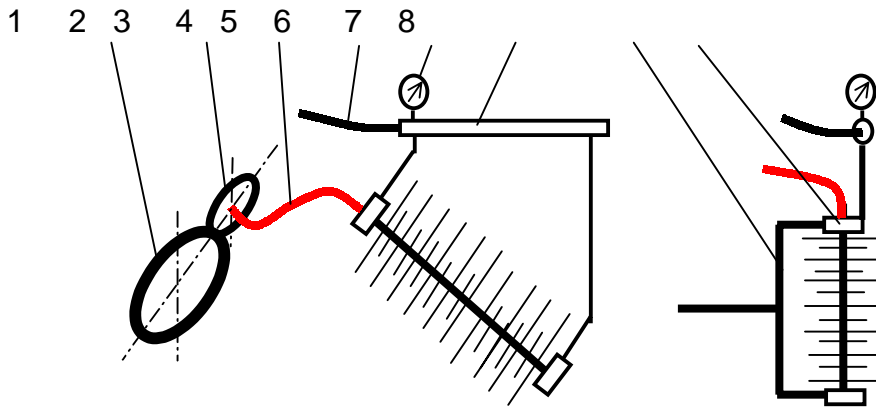


Figure 1. The Sketch of a CSFWJC
 1-cartwheel, 2-driven wheel, 3-flexible axis, 4-flexible tube, 5-pressure gauge
 6-water jet tube, 7-support frame, 8-bearing and bearing site



Figure 2. No. 1 Experimental Photo of the CSFWJC Test Machine



Figure 3. No. 2 Experimental Photo of the CSFWJC Test Machine



Figure 4. No.3 Experimental Photo of the CSFWJC Test Machine



(a) Before Cleaning



(b) After Cleaning

Figure 5. The Photos of the Street Fences Before/After Cleaning by the CSFWJC

DEVELOPMENT OF THE PREMAJET DERUSTING MACHINE

Dongsu Zhang, Benli Liu, Beihua Jia, Lihong Liu
Huainan Institute of Technology
Huainan, Anhui, P.R. China

ABSTRACT

The structure, working principles, and main technological parameters of the premajet derusting machine are introduced in this paper. Experiments have been made to test the relationship between such jet parameters as working pressure, rate of water flow, abrasive weight consistency and derusting efficiency. Suitable parameters have been decided. Results prove that the derusting machine is characterized by its high derusting efficiency (as high as $20\text{m}^2/\text{h}$), good derusting quality (as good as ISO8501-1 Sa 2.5), and low specific power consumption (about $0.3\text{kW}\cdot\text{h}/\text{m}^2$). Therefore it is a new type of high efficiency derusting machine.

1. INTRODUCTION

Premajet is a new technique developed since the last decade. The main principle of this technique is to add abrasive into the high-pressure water pipe system by means of special technical methods. A complete mixture of the abrasive and high pressure water jets out through the nozzle and forms an extremely high speed of abrasive jet. The system is called PREMAJET (premixed abrasive jet) because the mixing process of abrasive and high-pressure water is completed before the jetting. Compared with the pure pressure water jet, premajet changes the continuing static pressure action of pure water jet on the target object into the action of high frequency strike and erosion by abrasive jet. The effect is greatly improved. Compared with injection abrasive jet, premajet can fully mix the abrasive and water, and lengthen the time of acceleration, so it acquires higher energy and becomes more effective on the target object. Therefore the working pressure can be greatly reduced.

Premajet is our patent technique (Patent No. 88109149.9). After continuous hard work, we have solved such technical problems as abrasive screen classification, abrasive tank filling, and abrasive consistency regulation, which are essential in the application of this technique. This has made possible the practical application of the technique. The present paper is a general introduction of our premajet derusting machine.

2. THE STRUCTURE OF THE MACHINE AND ITS WORKING PRINCIPLES

The premajet-derusting machine is composed of four main parts: a premajet producer, an abrasive screening device, an abrasive tank filling system, and electric equipment control cupboard. The schematic figures of the structure of the machine and its water supply system are shown in Figure 1 and Figure 2.

2.1 The abrasive jet producer

This part consists of a high-pressure pump station, an abrasive supply device, and a jet gun. The high pressure pump station is made up of a triplex plunger pump, an over flow valve, a pressure regulating valve, and a water tank, which are used to supply high pressure water to the whole system. The abrasive supply device is composed of an abrasive tank, an abrasive stop valve, a local slurring device, and a one-way shunt pipeline. It is used to supply well-mixed abrasive slurry. The amount of the supply of abrasive can be regulated through regulating the water flow in the shunt pipeline. A one-way valve is fixed on the shunt pipeline in order to prevent the return of the abrasive in the abrasive tank. Closing the stop valve on the bottom of the abrasive tank can produce pure pressure water jet. The abrasive slurry jets out through the nozzle of the jet gun to form a high-speed abrasive jet.

2.2 The abrasive screening device

This part consists mainly of a submerged screen, an abrasive store funnel, a coarse sand funnel, and a discharge residue valve. The function of this part is to screen the raw abrasive or to retrieve the used wet abrasive. After screening the abrasive in accord with the demands falls directly into

the abrasive store funnel, while pellets of sand of bigger diameters and other substances fall into the coarse sand funnel at one end of the screen, which are removed at intervals. A small-size belt-delivering device is used to feed the screen in order to reduce the intensity of labor (This is not shown in Figure 1).

2.3 The abrasive tank filling system

This part consists mainly of a slurry pump, a water-sand delivering convertible valve, a high-pressure stop valve, a slurry-mixing device, and some pipelines. The function of this part is to fill the screened abrasive into the abrasive tank. Before filling, the unload valve and the pressure relief valve should be opened to set the tank in a low-pressure condition. Then open the high pressure stop valve, start the slurry pump, and turn the water-sand delivering convertible valve to its sand delivering position. The abrasive in the store funnel can be filled into the abrasive tank. In the meantime, the surplus water in the abrasive tank returns to the bottom of the store funnel through another high pressure stop valve and is used for further mixing process. When the filling process is completed, reverse the whole procedure and it can work for another cycle.

2.4 The electric equipment control cupboard

This part is used to control the high-pressure water pump, the screen device, the slurry pump, and the belt-delivering device.

3. THE ABRASIVE JET PARAMETERS

To test the relationship between parameters and the derusting efficiency of the machine, we made some experiments to form the parameters of the working pressure, the rate of water flow, and abrasive consistency, and decided the derusting specific power consumption. The derusting specific power consumption in this paper is defined as the ratio of the consumption of power to the efficiency of derusting. The jet power consumption may be calculated with the following formula:

$$N = P \times Q / 60$$

N - jet power consumption (kW)
P - jet pressure (MPa)
Q - rate of water flow (L/min)

The experiments were done on steel plates of about the same rusting degree. The jetting was done by hand, 10 minutes each time. The derusted area was measured and the corresponding derusting efficiency was obtained. The quality of derusting was decided as ISO8501-1 Sa 2.5 with eye-measurement after one jetting. The standoff of jet was 0.5 m, and the jet angle was 75°. The sand used in the experiment was ordinary river sand with diameters less than 0.5mm.

3.1 The pressure parameter

Conditions of experiment: The rate of water flow off the nozzle was 30L/min, the abrasive weight consistency was 30%. According to the hydraulic formula of the rate of water flow,

pressure, and diameter of nozzle:

$$Q=2 \times D^2 \times \sqrt{P}$$

Q - rate of water flow (L/min)
P - pressure (MPa)
D - diameter of the nozzle (mm)

with consistent rate of water flow, by using nozzles of different diameters, we got sure that the only variable was pressure in the experiment. The grades of pressure in the experiment were 2.5, 5, 7.5, 10, and 12.5MPa. The results of the experiment were shown in Table 1. The effect tendency of derusting efficiency and derusting specific power consumption under different pressure is shown in Figure 3.

As is shown in the Figure 3, with the pressure of jet increasing, derusting efficiency increases significantly, and derusting specific power consumption decreases significantly. But once the pressure surpasses 10MPa, the increasing tendency of derusting efficiency subsides, while the tendency of specific power consumption goes up. According to the results of experiment stated above, and considering that over high pressure may bring some unfavorable effect on the target metal object, the suitable working pressure should be better settled at 10MPa.

3.2 The flow parameter

Conditions of experiment: the working pressure was 10MPa, the abrasive weight consistency was 30%, and the rates of water flow were 11, 18, 24, and 30 L/min. The results of experiment are shown in Table 2. The effect tendency of derusting efficiency and derusting specific power consumption with different rate of water flow is shown in Figure 4.

As is shown in the Figure 4, derusting efficiency increases considerably with the increase of the rate of water flow, while the change of specific power consumption is not very great. It falls slightly down. According to the results of the experiment, and considering that bigger rate of water flow may cause stronger reaction, which might be unsafe in operation, the suitable rate of water flow should be 30~35 L/min. If further derusting efficiency is required, the rate of water flow and number of nozzles can be multiplied.

3.3 The abrasive weight consistency parameter

Conditions of experiment: the working pressure was 10MPa, the rate of water flow was 30L/min. The abrasive weight consistency was 10.1%, 21.5%, 30% and 38.3%. The results of experiment are shown in Table 3. The effect tendency of derusting efficiency and derusting specific power consumption under different abrasive consistency is shown in Figure 5.

As is shown in Figure 5, with the increase of abrasive weight consistency, both derusting efficiency and derusting specific power consumption decrease considerably. But when the abrasive weight consistency surpasses 30%, the change of both slow down. According to the result of the experiment, the suitable abrasive weight consistency should be about 30%.

4. MAIN TECHNOLOGICAL PARAMETERS OF THE DERUSTING MACHINE

Jet parameters :

working pressure	8 ~ 11 MPa
water flow	30 ~35 l/min

PREMAJET producer :

volume of abrasive tank	0.4 m ³
abrasive weight consistency	30 %

Screening device :

motor power	1.1 kW
screen opening size	1 mm

Abrasive tank filling system:

motor power	1.5 kW
consistency of carry sand	55~ 60 %
filling efficiency	• 80 kg/min

Performance parameters:

derusting efficiency	20 m ² /h
derusting specific power consumption	260 W·h/m ²
derusting quality	ISO 8501- 1 Sa 2.5

5. CONCLUSION

- Premajet improves the mixing mechanism of abrasive and water. The abrasive receives bigger kinetic energy in the process of acceleration through the nozzle. Therefore, the quality of this type of jet is better than any other types.
- The jet parameters of premajet derusting machine have significant influence on derusting efficiency and derusting specific power consumption. The reasonable parameters should be as follows. Working pressure: 10MPa, rate of water flow: 30L/min, and abrasive weight consistency: 30%.
- The premajet derusting machine is an assembly of abrasive screening, and machine filling abrasive. Under the derusting quality standard of ISO 8501-1 Sa 2.5, its efficiency can reach 20 m²/h, and derusting specific power consumption is about 0.3 kW•h/m². So it is a new type of high efficiency derusting equipment.

6. REFERENCES:

1. Benli Liu, Moshen Cui, "Experiment of the premixed abrasive jet to cut metal plate", *Proceedings of 9th International Symposium on Jet Cutting Technology*, pp.85-98, BHRA, The Fluid Engineering Center, September , 1988.
2. Benli Liu, Dongsu Zhang, Beihua Jia, "The Premixed Abrasive Jet Derusting System", *Proceedings of 1st Asian Conference on Recent Advances in Jet Technology*, pp.80-85, CI-PREMAER PET.LTD, SINGAPORE, May 1991.
3. Dongsu Zhang, "Development of premixed abrasive jet derusting equipment", *Mining & processing equipment*, Volume 27, pp.53-54, 1999.

Table 1. Impacts of working pressure on derusting efficiency

Working pressure (MPa)	2.5	5.0	7.5	10.0	12.5
Jet power (kW)	1.25	2.50	3.75	5.00	6.25
Derusting efficiency (m ² /h)	1.8	6.0	12.7	19.3	21.7
Derusting specific power consumption (W·h/m ²)	694	417	295	259	288

Table 2. Impacts of water flow rate on derusting efficiency

Water flow rate (l/min)	11	18	24	30
Jet power (kW)	1.83	3.00	4.00	5.00
Derusting efficiency (m ² /h)	4.8	8.2	13.6	19.3
Derusting specific power consumption (W·h/m ²)	381	366	294	259

Table 3. Impacts of abrasive weigh consistency on derusting efficiency

Abrasive weigh consistency (%)	10.1	21.5	30.0	38.3
Jet power (kW)	5.0	5.0	5.0	5.0
Derusting efficiency (m ² /h)	4.7	11.7	19.5	17.9
Derusting specific power consumption (W·h/m ²)	1062	427	256	279

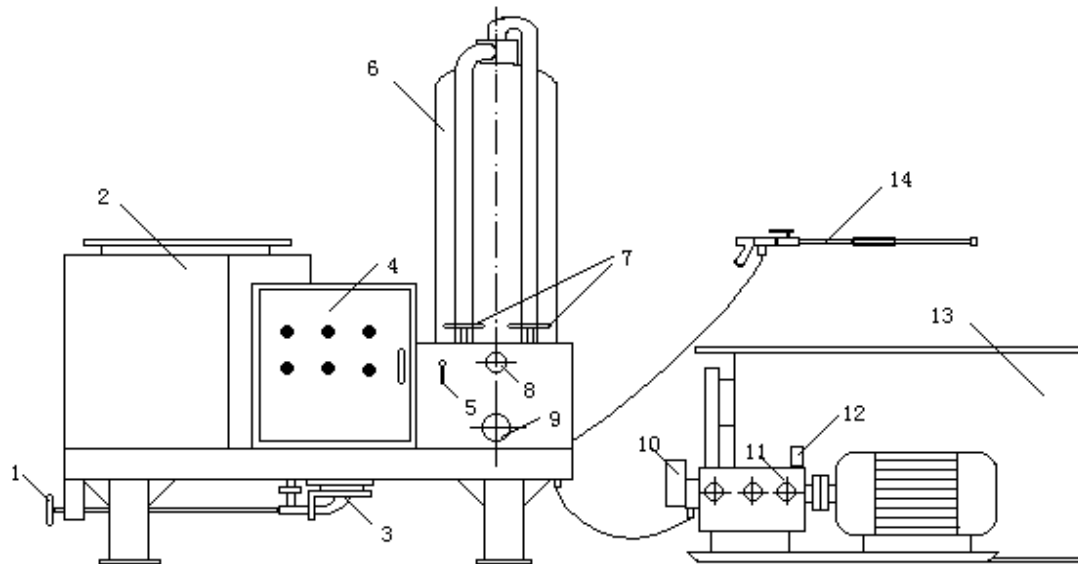


Figure 1. The schematic figures of the structure of the machine

1.The water-sand delivering convertible valve 2. Abrasive screening device 3. Abrasive tank filling system 4. Electric equipment control cupboard 5.Unload valve 6. Abrasive tank 7. High pressure stop valve 8. Pressure relief valve 9. Stop valve of the abrasive tank 10. Pressure regulating valve 11. High pressure pump 12. Safety valve 13. Water tank 14. Jet gun

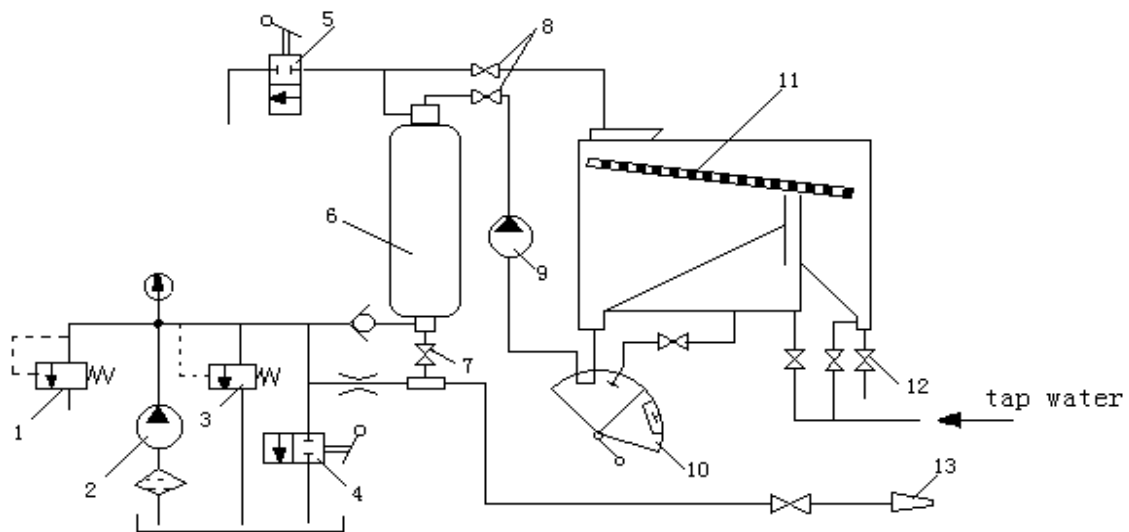


Figure 2. The figures of the water supply system

1. Safety valve 2. High pressure pump 3. Pressure regulating valve 4. Unload valve 5. Pressure relief valve 6. Abrasive tank 7. Stop valve of the abrasive tank 8. High pressure stop valve 9. Slurry pump 10. The water-sand delivering convertible valve 11. Abrasive screening device 12. Discharge residue valve 13. Jet gun

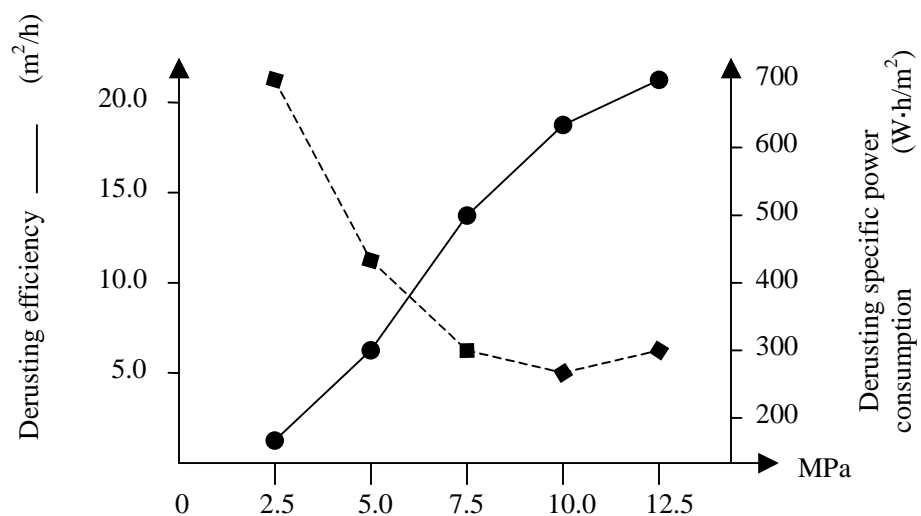


Figure 3. The effect tendency of derusting efficiency and derusting specific power consumption under different working pressure

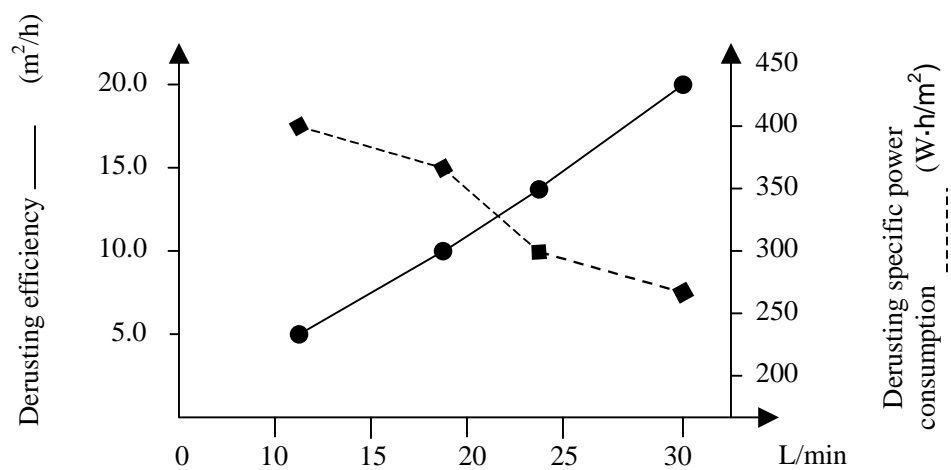


Figure 4. The effect tendency of derusting efficiency and derusting specific power consumption under different rate of water flow

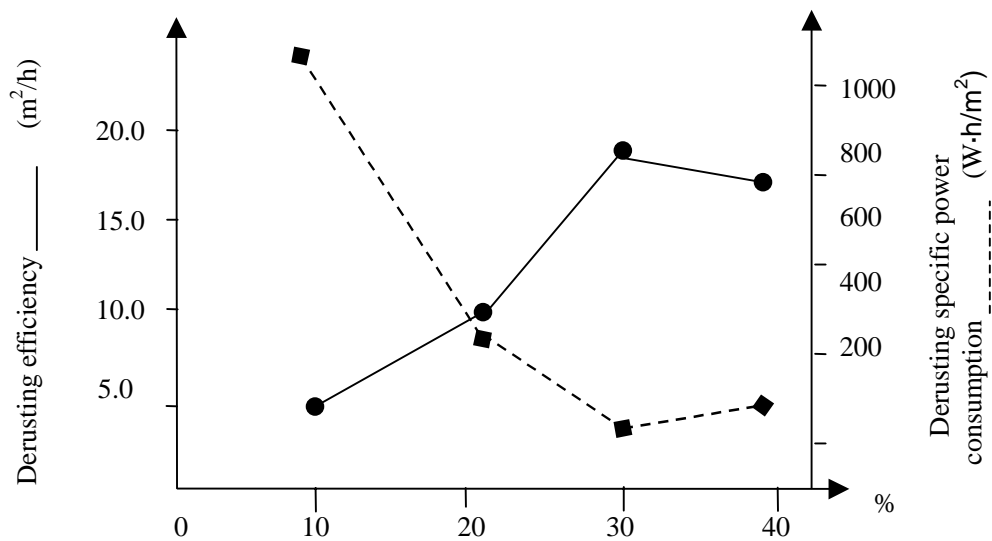


Figure 5. The effect tendency of derusting efficiency and derusting specific power consumption under different abrasive weight consistency

ADVANCED WATERBLAST TOOLS

PAY FOR THEMSELVES

John Wolgamott, Mark House, Doug Wright
StoneAge, Inc.
Durango, Colorado USA

ABSTRACT

How does a contractor justify the purchase of the more advanced and expensive waterblast tools? If he is just trying to offer bids with the lowest price per hour then he probably can't see the benefits. However, if he is interested in improving his safety, quality, productivity, profits, and competitive abilities, then these tools are a necessity.

This paper discusses the many benefits of using advanced waterblast tools in the form of rotating nozzles and mechanized systems to effectively apply the jet power. They can improve safety by moving the operator away from the jet and splash back. Rotary nozzles are very effective and can shorten cleaning times and improve quality. Mechanized systems can apply more power than can be handled manually. They also avoid confined entry problems and the need for scaffolding, cool down, cleanup and isolation. These tools benefit both the contractor and the customer hiring the work to be done. A key task for the contractor is to educate and sell the plant operator on the value these tools offer. Several applications are presented to exemplify the advantages of using modern waterblast tools.

1. INTRODUCTION

“Why spend money to work faster if I get paid by the hour?” A bit short sighted, but still a common question when considering buying new equipment to improve productivity. The correct answer is “to deliver more value to your customer”. By investing in new and improved tools the contractor can offer better service that will benefit both him and his customer. Advanced equipment and accessories can provide; improved safety, higher productivity, lower costs, reduced labor needs, better quality work, and increased capabilities. All of these are benefits that can be of great value to both the contractor and the customer.

Often, the real challenge is getting the customer to recognize the value of using a well equipped contractor. The purpose of this paper is to assist in identifying the benefits of advanced waterblast tools and the value they add to the operation. By presenting a clear list of benefits the customer will be better able to see the value and be willing to pay for it. Certainly not every customer will recognize the benefits immediately. However, most will over time, with proper education in the complete costs of the “cheaper alternative”. The contractor must gain the confidence of the customer that he can provide the best solution to his waterblast needs. “Best” in terms of safety, quality, and performance, as well as overall costs. This approach may lose an occasional job to the customer who is just looking for the lowest bid price. But, isn’t it better to be aligned with customers who do value your abilities to provide a better solution?

2. BENEFITS

The value of state-of-the-art waterblast tools can be measured in several ways:

- Improved Safety
- Higher Productivity
- Reduced Labor
- Lower Costs
- Better Quality
- Increased Capabilities

2.1 Improved Safety

Everybody loses when an accident or injury occurs on the job; the operator, the contractor/employer, and the customer. Several issues become involved; individual pain and suffering, lost time, financial responsibility, reporting requirements, bad publicity, and collateral liability. Investigating an accident takes time of management that would be better spent running an efficient operation. A maintenance manager’s career is largely based on their ability to run an on-time, incident free turnaround. Reliable and safe contractors are worth more money.

Waterblasting is a powerful technology and therefore potentially dangerous. A waterjet that can be used to cut concrete or remove epoxy coatings can certainly injure a human body. It is critical therefore, that every effort be made to protect the operator and minimize the potential for injury.

Advanced tools and mechanized equipment offer the best solution for both protecting the operator and getting the job done effectively.

Safety can be greatly improved simply by keeping the operator away from the jet nozzle. Mechanized waterblast equipment is designed to securely hold the jet and control its direction. This eliminates accidents where the hose nozzle gets away and comes back on the operator, or when the gun operator slips and inadvertently turns the jet on himself or a co-worker.

Being away from the jet also has the advantage of being away from the splash back. This allows the operator to see better what is going on around him and avoid danger to himself and others. And, often the splash back can carry abrasive particles or even dangerous chemicals from the object being cleaned. This is especially true in tube bundle cleaning.

A further safety advantage of having the jet held by a machine instead of a man is simply the elimination of physical exertion. An operator who is continually muscling against the reaction force of a powerful jet is less alert, and less capable of thinking about safety. He is concentrating on keeping his balance, avoiding the worst of the splash back, and pointing the jet in the right direction.

A tube lancing machine is a good example of where mechanization can improve safety by moving the operator away from the jet (Figure 1). This equipment is used on the common waterblast job of unplugging and cleaning heat exchanger tubes. Instead of manually inserting and twisting the jet nozzle, the lancing machine operator stands at a control panel. Instead of the jet being on the end of a loose flexible hose, it is on a rigid steel lance and securely guided. The lancing machine is not only much safer, but also more productive and more capable of cleaning the hardest of tubes.

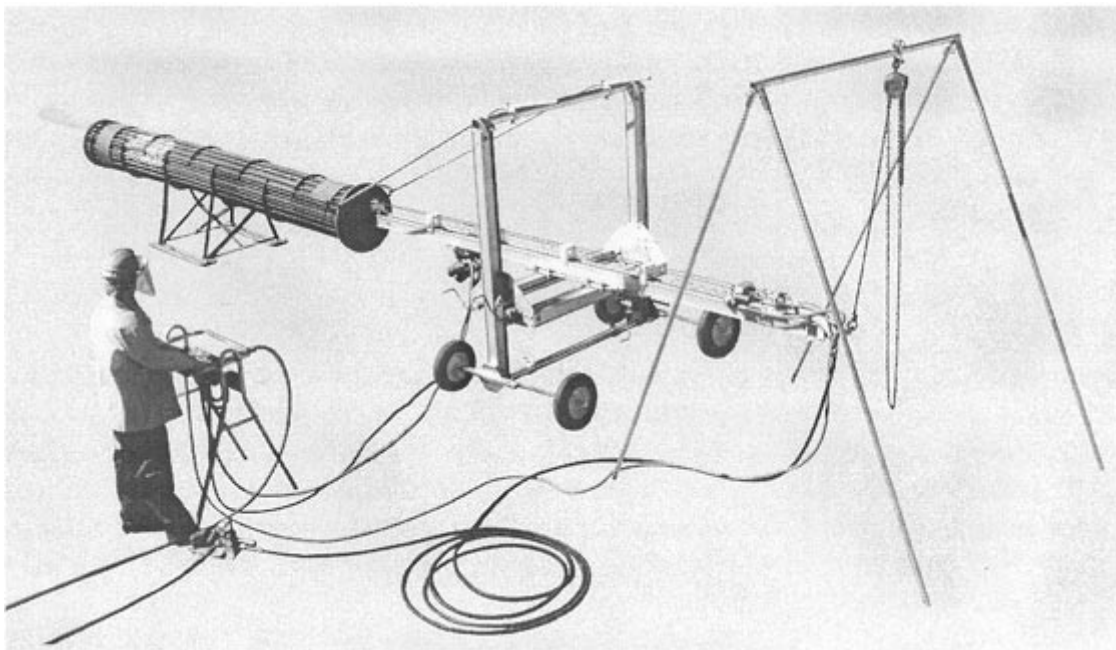


Figure 1. Tube Lancing Machine

With mechanized equipment, scaffolding can often be eliminated entirely. Many modern waterblast tools can be suspended on a cable or positioned by a mechanical boom. This reduces all the risks associated with assembling/disassembling the scaffolding, and of the operators falling off. It is very awkward handling a jetting gun, resisting the reaction force, dragging a stiff high pressure hose, while wearing a heavy rubber suit, and a wet scaffold does not help. Boiler fireboxes over 100 ft high have been cleaned by hoisting rotary nozzles with high flow rates.

Eliminate risk and confined entry requirements by putting a tool in, not a person. There are many excellent models of rotary nozzles specifically designed for cleaning tanks and vessels. They generally have two axes of rotation to allow them to jet in all directions, hence they are called three dimensional or 3D nozzles (Figure 2). These nozzles can simply be lowered into the vessel or positioned on the end of a boom. The operator stays completely out of the tank, safe and dry.

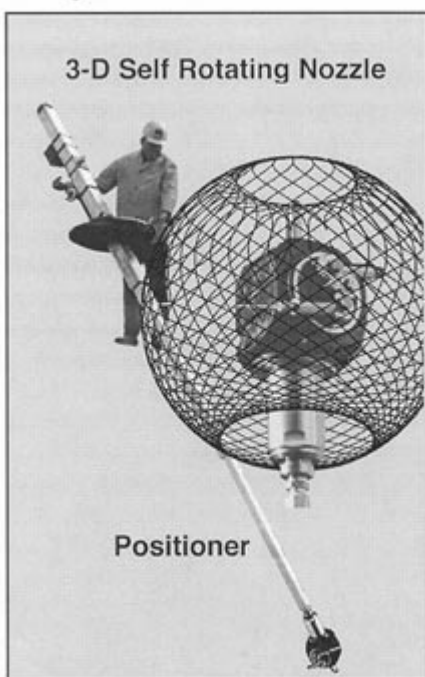


Figure 2. Positioner Boom and 3D Nozzle

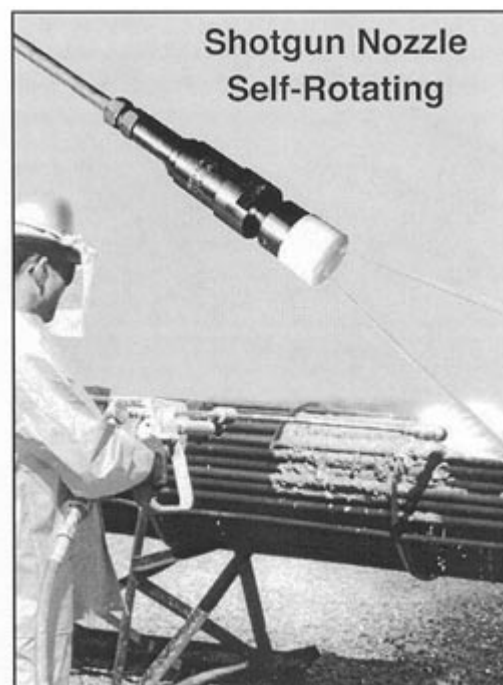


Figure 3. Rotary Shotgun Nozzle

Where conditions warrant, advanced waterblast equipment can even be designed to operate in complete isolation. The blasting area can be totally contained and the cleaning operation automated and controlled remotely. This helps protect the environment as well as the operator.

2.2 Higher Productivity

Modern waterblast tools offer many opportunities for improved productivity. Mechanized equipment can handle more power and operate continuously without needing a break. The delays in waiting for cool down, degassing or scaffolding, can be eliminated. It is important for

the contractor to learn the value of a quicker turnaround to the customer. Get the customer involved in the search for better equipment and techniques.

A rotary nozzle on a shotgun (Figure 3) is a simple example of technology paying for itself with higher productivity. Waterjets are effective because they concentrate energy and impact on a small area. However, they must be constantly moved to get any work done. By spinning the powerful jets, more surface area is covered, with less work by the operator.

Time-savings are important, especially when either the window of opportunity is limited, or when downtime is expensive. Many jobs allow only a set amount of time and the goal is to get as much done as possible before the next operation starts.

For many maintenance operations, the lost revenue during down time is much greater than the actual cost of waterblast cleaning. So even a major increase in tooling costs that save cleaning time, may be well worth it to the customer.

One example is cleaning black liquor evaporators in the pulp and paper industry. These units can have thousands of tubes and only a few days allocated to the cleaning operation. Severely plugged tubes can take 20 minutes or longer to clean with conventional nozzles. Using controlled rotation nozzles (Figure 4), the tubes can be cleaned in about 1½ to 3 minutes, a dramatic increase in productivity. The rotary nozzles cost more and require some maintenance, but the results are more than worth it.

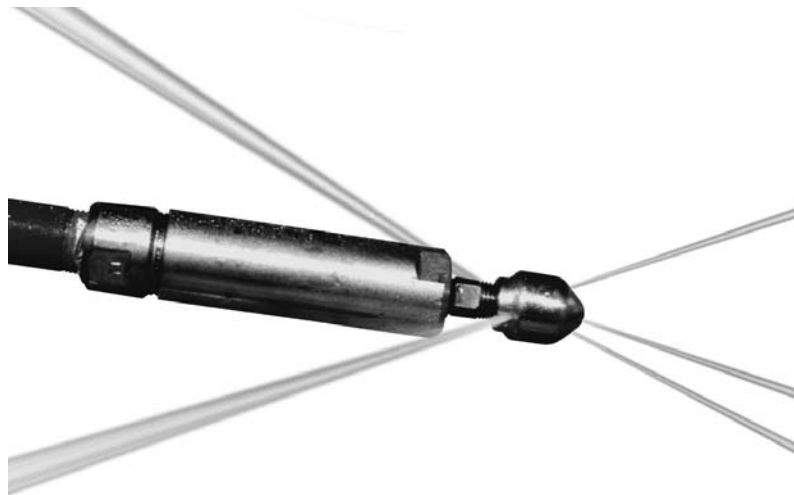


Figure 4. Rotary Tube Nozzle

Advanced waterblast equipment can apply much more power than a man can handle. The typical gun operator can handle a maximum of about 70-150 hp depending on the pressure. This limit comes from the back thrust a man can safely handle, usually recommended to be no more than 1/3 the operators weight. Many times it is impractical to put multiple people on a job simply due to space limitations. A single mechanized tool can apply over a 1000 hp and this allows more cleaning to be done in less time.

Mechanized tools keep working without the need for rest breaks or operator change-out. This keeps the expensive pressure pumps doing productive work more minutes per hour.

The use of mechanized tools can eliminate delays and save time. No need to wait for vessel cool down or degassing if only equipment is going inside and not a person. Scaffolding time can often be eliminated if the right tool is used. There are waterblast tools that can be hoisted, slid on a cable, or positioned on a boom.

Operators can enjoy using a good tool and will take greater interest in being professional and more productive. A good operator can be motivated to produce more by giving them better tools.

2.3 Reduced Labor

The use of mechanized equipment can reduce the manpower needed on a job. A single operator can control tremendous cleaning power. His work will be much less physically demanding and he will not require as much rest time to stay productive.

The use of mechanized equipment will require fewer employees, but they will need to be more skilled and mindful. The operation and maintenance of advanced equipment is best handled by experienced and trained individuals. It is a more pleasant job function however than doing manual blasting. It is easier, cleaner and less dangerous. This attracts a higher quality employee and also helps reduce turnover. Having fewer and higher skilled employees also translates into fewer accidents and the many costs associated.

A good example would be in concrete renovation by hydro demolition. A robotic machine (Figure 5) can take the place of several men with handguns. It can handle more power and provide more consistent results.



Figure 5. Concrete Demolition Equipment

Cleaning with a 3D rotary nozzle in a tank instead of an operator eliminates the need to have standby personnel watching out for them. The result is one less person and an easier job for the operator remaining.

Another example of labor savings is in tunnel cleaning. Large railway or subway tunnels can be cleaned by building a special car equipped with an array of rotary waterjet nozzles (Figure 6). They can cover the entire surface in one pass and require only 1 or 2 operators. In smaller fluid transport lines, a custom trolley can be designed to hold rotating nozzle arms in the center, windmill style. The mechanized designs both require very little labor and each offer a superior result in time-savings and quality of the finished job.



Figure 6. Tunnel Cleaning

2.4 Lower Costs

The use of advanced waterblast tools can reduce overall job costs. By being more efficient there will be cost savings in terms of; less labor, less wear on the pump, less fuel use, and even less water needed. There will also be intangible savings in reducing the potential for accidents and reducing labor turnover.

The initial cost of a new advanced tool can seem rather high, but not when compared to the savings over time. The investment in a high pressure pump and operator is substantial and a tool that can improve their efficiency 50% is potentially worth half of that investment. Buying tools will also be cheaper than paying for more people. A wide variety of tools and accessories will allow the contractor to best utilize his investment in pumps and operators. He will be able to solve customer's different tasks in the most efficient manner.

Again, an example is in cleaning black liquor evaporators in the pulp and paper industry. These vertical bundles can have thousands of tubes from 30 to 60 ft long. They require the operator to handle heavy waterblast hose by feeding it down the tube then pulling it back up. This is hard work in a hot and cramped space. An efficient rotary nozzle described earlier, can speed up the actual cleaning but will do nothing to reduce the amount of heavy lifting. An air operated hose reel however can eliminate the manual lifting entirely (Figure 7). It will also improve safety and job quality. On a recent job with 65 ft tubes an operator with the hose reel and rotary nozzle was routinely cleaning 40 tubes per hour. That was three times faster than without advanced equipment and definitely lowered the cleaning costs.

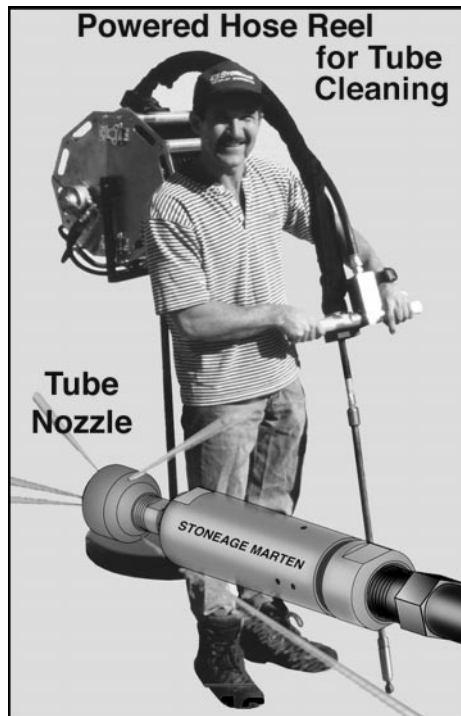


Figure 7. Powered Hose Reel

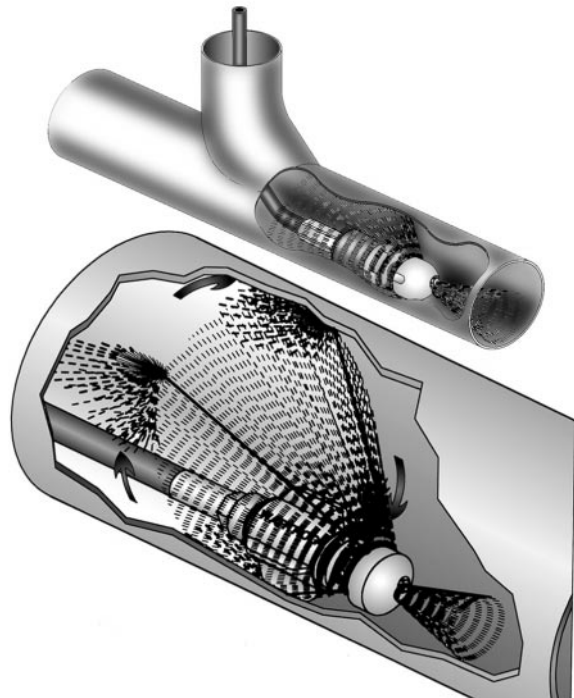


Figure 8. Sewer Cleaning with Dynamic Nozzles

Another example is in sewer cleaning (Figure 8). Using modern dynamic nozzles the cleaning can be done with less water and less time. This allows more footage to be cleaned for each truck of water, saving time in driving and refilling.

In the chemical process industry there are significant related costs to vessel cleaning. There is expensive lost production time for cooling and ventilating, cleanup, isolation, erection of scaffolding, and procedural administration of confined space requirements. It's far too expensive a preparation for a contractor who works for the lowest available hourly rate! Putting rotary waterblast equipment inside is much faster overall and less expensive than manual cleaning.

2.5 Better Quality

Mechanical equipment will produce more uniform results than manual methods. The right equipment will be less susceptible to human error and allow better control over the process.

Waterjets are very powerful but strike in only a pinpoint. It is necessary to move the jet quickly and smoothly to avoid streaking and patchiness. With automated jets the entire surface can be assured of receiving the same distribution of jet power.

For example, paper suction rolls are thick steel cylinders with thousands of tiny holes that get plugged with fiber. Unplugging them is a tedious and time-consuming operation. Manual methods are lucky to obtain even 80% effectiveness while mechanized waterblast tools can achieve close to 100%.

Rotary nozzles in pipelines are more effective and give better cleaning than non-rotary nozzles. By putting the power into only a few jets, each will be bigger and will therefore carry farther and hit harder. And, by spinning the jets at a fast but controlled speed, the entire surface will be struck by the jets, thus resulting in better and more uniform cleaning. They can be used in cleaning piping and ducts from one inch to several feet in diameter. For larger lines, a skid or centralizer may be used to hold the spinning nozzles in the center (Figure 9). The nozzles can even pull themselves several hundreds of feet depending on the pump power available. Controlled rotary nozzles are becoming quite popular because of their effectiveness and quality of cleaning.

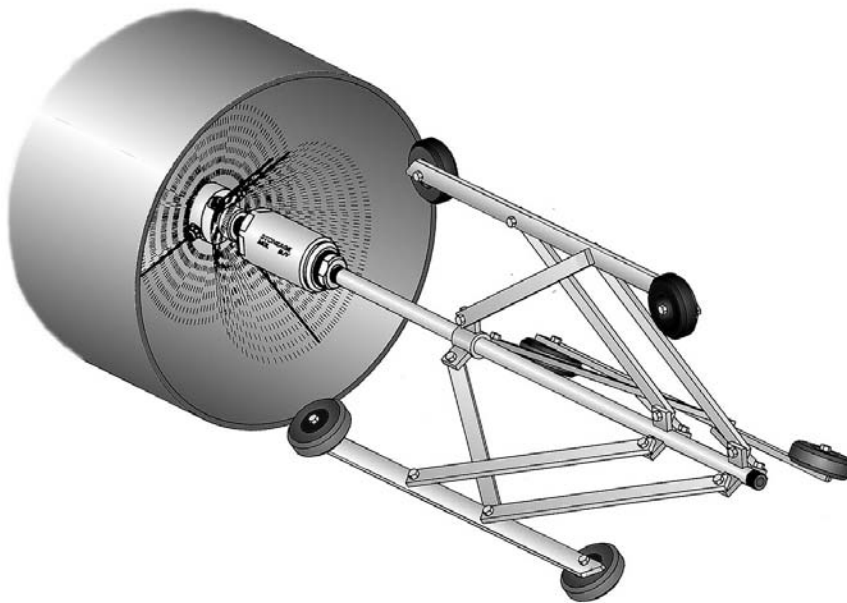


Figure 9. Rotary Pipe Cleaning Assembly

Modern equipment can combine suction with blasting for a better operation environmentally. The blast water and product can be collected immediately preventing any contamination of the surrounding area. Separation and recycling of the water is possible and important in some applications.

Another example where advanced waterjet equipment can provide better quality is in petrochemical manufacture. Typically several batches of material are processed before stopping to do the required cleaning. The frequency of cleaning is determined by many things including;

line plugging, volume reduction in the vessel, and product contamination by leftover material. Automated waterblasting equipment can be installed as part of the manufacturing process (Figure 10). By cleaning after every batch the task is easier to do and results in a product that is more uniform and of higher quality. In one case a plastics manufacturer is able to provide a product of such superior quality that it commands a premium price. Process operations may require custom equipment simply due to their unique installations.

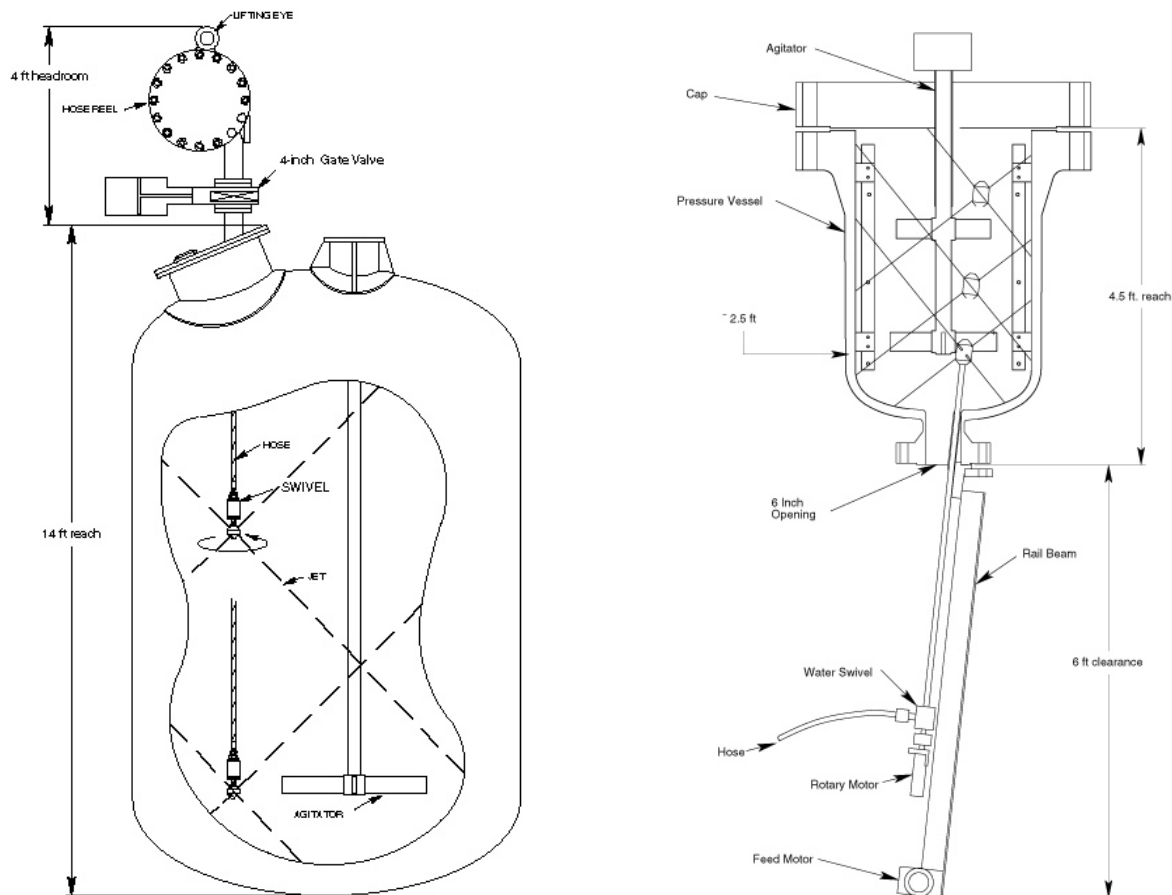


Figure 10. Automated Vessel Cleaning

2.6 Increased Capabilities

Some jobs just can't be done practically without using modern equipment. The new advanced tools can be used effectively: at very long distances (very deep in oil wells), in tight areas (small ID heat exchange tubes) or in large spaces (100 ft diameter storage tanks), submerged (sewer cleaning), and in hot (online boiler blasting) or hazardous environments not suitable for confined space entry (reactor cleaning).

A recent example of newer tools being more capable was in cleaning air preheater tubes. A power plant that had routinely allowed 13 days during shutdown to clean the thousands of tubes. In the several years of the plants operation no one had been able to clean even half of them in the allotted time. A contractor offered to do the job with controlled rotary nozzles and the plant

agreed to pay an hourly cost for the advanced tools. The contractor was able to finish 100% of the tubes in only 10 days. This was of tremendous value to the plant and the contractor is expecting to be awarded work at two more plants by the same owner.

Modern waterblast equipment is capable of operating reliably at very high pressures and large flow rates. They can remove very hard coatings and provide a superior bonding surface for new coatings (Figure 11), while eliminating the mess, debris and hazard of sandblasting.



Figure 11. WJ Paint Removal with Suction

Custom equipment can be designed to fit into crowded plant layouts and adapt to existing constraints. Large amounts of power can be delivered through hoses and piping to remote or awkward locations. In some situations it makes sense to permanently install the special nozzle equipment and then bring the pump for periodic cleaning. This has been done for conveyor belt and vessel cleaning.

Stack cleaning and large vessels can be cleaned effectively and safely with mechanical equipment (Figure 12). Controlled rotary nozzles can be suspended in the stack and lifted or lowered while cleaning, with the operator staying safely outside. Vessels in excess of 80 ft in diameter and stacks over 900 ft tall have been cleaned successfully with mechanized equipment.

Advanced waterblast tools can do jobs better than older alternative methods such as flushing, sandblasting, grinding, shotblasting, jackhammering, hand chipping, etc. The increased capabilities of modern waterblast tools present a variety of possible applications:

- Open and clean plugged drill pipe
- Gently clean glass mirrors for solar energy collection (Fig 13)
- Plate cleaning of glue residue in pressboard plants
- Abrasive jet cold cutting to reduce risk of explosion and fire hazard

- Removal of NORM (naturally occurring radioactive material) from oil field tubulars
- Propellant and explosives recovery from old munitions and rockets
- Waterjet assisted drilling in soil and rock
- Removing asbestos from old buildings and piping
- Online conveyor chain or dryer belt cleaning
- Provide ultraclean surfaces for critical components

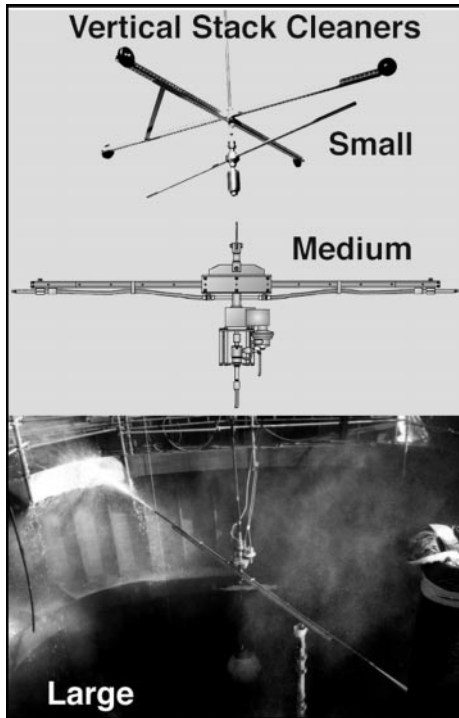


Figure 12. Stack Cleaning

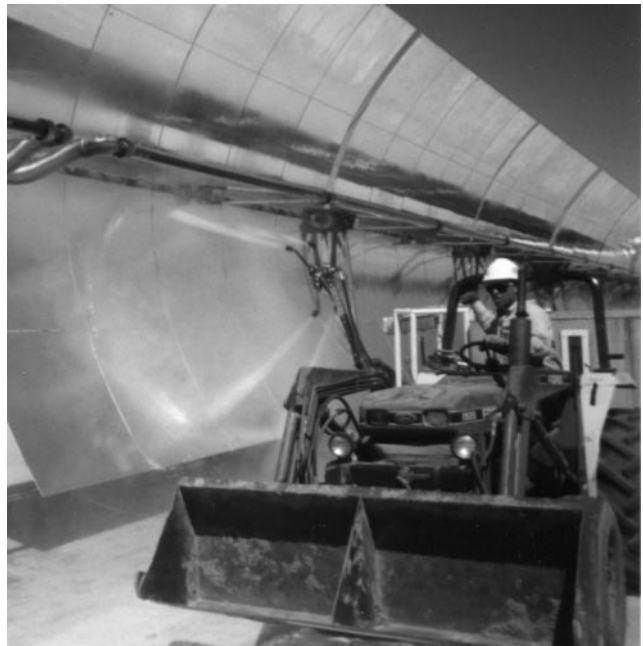


Figure 13. Solar Mirror Cleaning

The same basic pump unit can be used with different tools to accomplish many different tasks. Waterblasting is an expanding market. Every day there are new customers, new industries, and new applications being found. By solving the customer's tough problems, you improve the chances of getting the easy jobs as well.

3. CONCLUSION

There are many good reasons to utilize advanced waterblast tools. Their use can benefit both the contractor and the customer. The cost of waterblasting is small compared to the overall economics of a customer's typical operation. A better waterblast tool therefore can have a very high value-in-use. Less downtime for cleaning maintenance can mean big dollar savings to the customer.

The contractor benefits by:

- Being better able to solve customer problems.

- Building a company based on offering best value to customer.
- Staying ahead of competition that just tries to do it cheaper.
- Being able to do jobs quicker.
- Have capabilities to do jobs that others can't, which insure better margins.
- Reducing costs associated with accidents, employee turnover, and supervision hassles.
- Providing higher quality work and getting paid for it.

The customer benefits by:

- Getting better quality work performed.
- Lowering overall costs. Perhaps higher cost/hour but with fewer hours and/or associated costs.
- Having difficult jobs accomplished.
- Saving downtime and possible disruption to other operations.
- Having safer operations on site, perhaps better environmental record.
- Being able to use state of the art solutions to solve maintenance problems.
- Needing less supervision of contractor who is professional and partnering.
- Knowing that they are working with a contractor who is knowledgeable, professional and doing business in a way that will insure that he is available in future.

An investment in advanced waterblast tools (and appropriate training) can have a big payoff for the contractor as well as the customer.

TURNING A LIABILITY INTO AN ASSET!

THE STORY OF AN OLD POWER PLANT

Richard Dupuy and Robert Ashworth
UHP Project, Inc.
Newport News Virginia

Lydia Frenzel, Ph.D.
Advisory Council
San Marcos, Texas

ABSTRACT

The Lower Colorado River Authority, Austin, Texas, refurbished the Comal County Utility Plant located in New Braunfels so that it can be used for public, commercial businesses. The story is the transformation of a power plant, built in 1926, which contained asbestos and lead based paint (lbp) and had been closed for decades, into an asset for the community.

1. INTRODUCTION

Every project starts out with a where, when, what, how statement. This coatings project involved removal by manually held ultra-high-pressure waterjetting (UHP WJ) of approximately 410,000 square feet of lead based paint from the historically significant Comal County Power Plant located in New Braunfels, Texas. The project combines renovation, but not restoration, and historic preservation. The owner is Lower Colorado River Authority, the coating manufacturer is Wasser High-Tech Coatings, the contractor is UHP Projects Inc. The coating removal portion started around September, 1999, and continued through June, 2000. This project was the first time the contractor had worked with the owner.

Every project has more to the story than “just the facts.” Every project involves interaction and representation of the three points of view that must come together in the bid specification for the surface preparation and coating application to be successful and flow smoothly. (See Frenzel for further discussion) These points of view are:

- owner,
- coatings manufacturer, and
- contractor.

Certainly any project that deviates from a traditional blasting and painting must have the upper management of the owner firmly in support of the process. The owner or operator of the facility initiates and controls the project often with the assistance of an engineering or planning firm who may act for the owner. In this project, the owner selected early in the process a coating system based on past history. The question then became how to write the specifications for public bidding and how to select a qualified contractor.

The Bid Specification language allows people to work together on projects. When all three viewpoints- owner, contractor, and coatings manufacturer come together- a “new or emerging” process becomes an accepted process. Responsibility is shared between the three parties. The owner, coatings manufacturer, and contractor can get together and discuss solutions that are mutually beneficial. Often the result is that the coatings manufacturer and the contractor work together to supply cooperative warranties or guarantees to the owner.

2. THE OWNER

2.1 Who is the Owner and What Role does the Comal Plant play in the community?

The Owner is a conservation and reclamation district that generates hydroelectric power, manages the waters of the Colorado River, operates parks and assist communities in economic development. (See LCRA News).

Water is a major recreational and economic source for New Braunfels founded in 1845. For many New Braunfels residents, the Comal Plant has been a city landmark, guarding the entrance to Landa Park, the "Largest in Texas" for more than seven decades. Community interaction and

response was a top priority for the owner. (New Braunfels Chamber of Commerce, Landa Park literature).

The power plant is 20 feet from the pristine Comal River with three endangered species and sixty-three species of flora and fauna in the immediate vicinity. Comal Springs feeds a 1.5 million gallon pool in the park. The nearby Schlitterbahn Waterpark Resort is one of the nation's largest waterparks, featuring 65 acres of water recreational areas. The Comal plant is very visible as it is located two blocks from the historic town square and across the street from Wurstfest Hall, a major Texas celebration and tourist attraction.

Williams described the interaction of the LCRA with the community. The Comal power plant was built in 1926, before the owner was created. The owner subleased Comal from the Guadalupe-Blanco River Authority in 1942 and gained full title in late 1972. After prices on natural gas continued to spiral, the owner pulled the plug in 1974, but not their involvement and commitment to the community.

The owner has a strong eco-friendly policy. They do the right thing for air quality, water quality, the community, occupational safety and health, and general environmental enhancement. "We're recycling a power plant," said John Gosdin, LCRA manager of parks and conservation services, who has overseen the work. (See Williams). In the late 1970's, LCRA leased the 37 acre site to the City of New Braunfels and New Braunfels utilities. The plant lay dormant. It was discovered in 1986, that salvagers of the equipment and steel had damaged some interior insulation, included friable asbestos in the 1979-82 time period. Starting in 1989, the owner removed 6,300 cubic yards of contaminated asbestos-containing insulation and contaminated materials. Soil contaminated with fuel oil and PCB's, and on-site landfills were remediated.

The removal of the paint and repainting is just one step in a multi-year, multi-stage project. For this refurbishment project, the owner has spent more than a decade on the environmental cleanup and other site work, including the asbestos, PCBs, landfills, and repairs on the Comal Dam, which helps control the level of nearby Landa Lake. The investment could total as much as \$11 million. (See Launius and Williams).

2.2 How did the Owner Decide to Abate the Site?

There were three choices.

- Mothball the building. This leads to a board-up building with future legal and financial risks to the owner and the city.
- "Shell" the building. Removing remaining equipment, stripping the building to its exterior walls, concrete floors and structural steel- would cost an estimated \$7 million.
- Tear down the building. This would cost almost as much as "shelling" the building.

The owner opted to shell the building and develop the site, based on guidelines drawn up by the owner and local community leaders. New Braunfels Utilities and the city agreed to give up its lease on the building and most of the site. In this manner future revenues can be generated. The owner would provide the land and building under a long-term lease and receive a percentage of

any project revenues to help recover some of their remediation costs. Now the Comal Power Plant site could generate tax revenues for the city the first time since the early 1940's. The new jobs and support service could create an economic impact for the city of at least \$12 million a year. (See Williams).

The removal of the lead based paint (lbp) and repainting is nearly the last step to be taken. Bids went out in Spring 1999, before they knew the final use of the building. The coatings work began in fall 1999. In January 2000, it was announced that the owner and a developer had an agreement to redevelop the plant for use as a hotel, restaurant, and conference center. (See New Braunfels Herald-Zeitung). The removal and repainting of the structure was completed in July 2000.

2.3 What was the condition of the Site?

The metal exposed during the asbestos remediation had accumulation of piles of rust on the floors. Pigeons roosted in the beams; small animals made their homes in the building. Most of the windows were cracked, but in place. Analysis of the paint systems (See Table 1) showed that the levels of lead content in the paint ranged from 0.3 to 13.5% by weight.

Because this was to be used for the general public and might be turned into apartments, U.S. Department of Housing and Urban Development's (HUD) Lead Based Paint- Interim Guidelines for Hazard Identification and Abatement in Public and Indian Housing were followed. This is an unusual requirement for an industrial lbp project. Pre-job lead wipes provided results from 220 to 11,790 µg/sq. ft.

Asbestos and lead in the air did not exceed permissible exposure limits if there is no activity in the building to stir up the dust. The asbestos was removed prior to the painting contractor arrival on the premises.

The amount of structural steel contained in the structure is deceptive.

Interior Structural Steel	363,700 ft ²
Exterior Structural Steel	21,250 ft ²
Interior Masonry	28,600 ft ²
Exterior Masonry	5,400 ft ²

To put this into perspective, the walls and flat surfaces covered 55,000 sq. feet (5,500 square meters) or slightly over one American football field. The steel beams, complex shapes with difficult access of 363,700 sq. feet (36.4 square meters) correspond 7.6 American football fields. Imagine, cleaning 7.6 football fields of area all in the shape of the goalposts. (Figures 1, 2).

Going into the project, the known hazards were:

- Physical safety concerns including hazards from falling objects, i.e. fire bricks, holes in the floors, and water or bird/animal feces.

- Health hazards from lead paint, asbestos, and the presence of large amount of bird feces. There is the potential for one to contract hypersensitivity pneumonitis, or bird fancier's lung, through exposure to organic debris.

2.4 How The Owner Decides to Include WJ as a process?

It has been noted that the owner seeks environmentally friendly solutions, but they always examine the dollar cost of every project.

The owner has prior experience in removal of hazardous paint in environmentally sensitive areas (See Johnson Hydroreview, MP, and JPCL) with the Wirtz Dam. Prior to the Wirtz Dam project in 1995, the owner had been using dry abrasive blasting specifications. As the owner of the facility, the owner had been paying for the disposal of the waste as a separate part of the project. As the EPA and OSHA regulations continue to become more comprehensive concerning air, water, and soil quality and worker safety, the costs to remove paint became greater. Between 1990 and 1995, the owner noticed a great increase in the dollar amount to remove paint and disposal of the waste streams.

In 1995, the owner changed their specifications to ask the contractor to estimate the amount of waste to be disposed at the end of the project. The owner began to include that cost in the project bid and would allow the contractor to be within 15% of the tonnage. If the actual tonnage was more than 15% of the estimated, the contractor would pay for the overage.

It turned out that the cost drivers of the projects were:

- location and mobilization costs,
- containment, and
- waste disposal.

The owner worked with coatings manufacturers to supply coatings that could go over tightly adherent existing coating or tight primer. They found that field abatement, not total removal, would be cost and performance effective. Field encapsulation of existing tightly adherent coatings to date has given quite satisfactory performance. The hazardous waste generation decreased significantly when all of the lbp did not have to be removed. The owner has also found that high and ultra-high pressure WJ was saving them considerable amounts of money in waste disposal and containment costs.

The bid document remains open to all types of technologies including dry blasting, wet abrasive blasting, waterjetting, and power tool cleaning as appropriate. The bid document includes consideration of the amount of material released to the air and the total amount of hazardous waste to be disposed. Over the past few years, the owner has shifted to more WJ as a surface preparation process in maintenance projects based on economics. The use of WJ without abrasive is possible because these older surfaces already have a primary surface preparation.

The owner also shifted towards greater consideration for the experience and qualifications of the contractor. The successful contractor is a SSPC QP-1 and QP-2 qualified contractor. On this

project, the contractor used waterjetting, low pressure water washing, chemical stripping, and hand/power tools.

2.5 Reviewing the Specifications and Selecting the Paint System

The owner already had a history of 5-6 years performance with moisture-cured (MC), single component, micaceous iron oxide (MIO) urethane coatings in prior industrial and dam projects over a waterjetted cleaned surface. The coatings were very successful and are performing well. Touch-up and recoating is not needed after six years exposure.

The owner feels that the high solids, low volatile organic compounds (VOC) approach that meets California air emissions is part of their commitment to pollution prevention and waste minimization.

3. THE COATINGS MANUFACTURER

In this project, the owner selected a coating system based on past history. (See Johnson). Two different technical representatives worked on the project. A technical representative in New Orleans from the earlier projects worked with the owner initially. The New Orleans technical representative assisted the owner in reviewing the general request for bid and selecting a coating system suitable for industrial and commercial usage as there would be an indeterminate time before the building was occupied.

As the project started, a technical representative moved to New Braunfels, Texas where the Comal Power Plant is located. Even though this was the New Braunfels technical representative's first WJ project, he had 20 years of military maintenance experience and 15+ years of coating experience working with the clients, contractors and various on-site people and welcomed this new learning opportunity.

3.1 The Coating System

The owner's typical specification for an industrial project has MIO in all three coatings.

- Primer: one coat of moisture cured urethane- MC- Miozinc which is zinc-rich/micaous iron oxide, single component, applied for 3 mils DFT. The VOC is not to exceed 2.8 lbs per gallon.
- Intermediate Coat: MC- Miomastic or MC- Ferrox -B
- Top Coat: MC- Ferrox-A- MIO-filled, single component, moisture-cured urethane. VOC- not to exceed 2.8 lbs per gallon.

3.2 Surface Preparation

For abrasive blasting, the coatings manufacturer felt that a change from SSPC SP-10 to SP-6 or for SSPC WJ-2 to WJ-3 would be sufficient for quality performance. (See Frenzel). Tightly adherent, sound coatings could remain. Since it was unknown what the final developer would

want as a color scheme, the coatings manufacturers felt comfortable that the primer could be put on with an open end recoat time. The stricture was that the primer would have to be cleaned before recoating. This could be a cost savings to the owner because they had originally specified a three coat industrial coating and now the owner was down to a single coat.

However when a potential developer became identified during the course of the project, the owner went with a primer and semi-gloss topcoat to take advantage cost savings of the scaffolding already in place so that the building would not have to rescaffold again for coatings application. The coatings manufacturer felt that the two coats would be quite sufficient because this is a low stress exposure with no UV exposure. For all interior structural steel, interior plates, ladders, doors, windows and exterior signs, windows and frames, awnings, ladders and door, the coating system was primer and an attractive semi-gloss, luster top coat with the desired finish color to match existing colors on doors, windows, signs, and ceiling. The exterior concrete coating system was a buff primer and a luster top coat to hide the multiple tones of the underlying concrete.

The coating, a single-component moisture-cured urethane (MCU) is very reliable, easy to use, and very user friendly. The contractor can pop the lid on the can; stir it up; and put it into suspension. The paint can be applied with brush, roller, or spray without addition of thinner with a very long pot life. The coating can be applied under adverse conditions, of rain or cool, damp weather. There is very little to no down time from a contractor's point of view. Cost savings is found in less thinner, less downtime, and the MCU system is typically one-half the thickness of an epoxy system.

4. THE CONTRACTOR

The public bid process included responses of dry abrasive blasting, but the selected process was UHP WJ. The contractor was SSPC QP-1 and QP-2 qualified with a history of similar projects throughout the world. (See Dupuy).

One of the principals has over 25 years experience as a general contractor with dry abrasive blasting. Over the past seven years, he has found UHP WJ to work well in all sorts of maintenance projects. The contractor started in 1993 and has grown to 150 employees, multiple vacuum systems, and 12-13 UHP WJ pumps. The two principals met in 1989-90 on the USS Enterprise in which 265,000 square feet of bilges and machinery rooms was cleaned with WJ and painted. The coatings have lasted without failure to date. The contractor handles on-shore and offshore projects, large and small, from the one-two day to multi-year contracts.

The first impression during the pre-bid conference when the estimators walked into the Comal Plant was the Gomer Pyle Syndrome "GOLLY!" UHP Manager Bob Ashworth said "We Looked up- It was a large job. Piping was being removed along with the last of the asbestos. There is a lot of steel in this plant- maybe more so than on a ship or bridge. The steel just goes on forever and ever. It was a challenge to see all the building." (Figures 1 and 2).

Ashworth feels “There is no other company in the world that has the caliber of the people that we do. It was a very exciting job. It was a job that we are very well suited for. Our people are trained in these types of jobs. It was a difficult job and a kind of job that we like to take on.” Their projects managers bring dedication, loyalty, and outstanding experience to each site. This attitude comes out in their work and public response.

The contractor breaks down all large projects as multiple small jobs in each small section and put it all together for estimation. The contractor made several trips to the site. As Ashworth said, “LBP does not strike the fear in us as they may in an abrasive blaster. When you use water to remove lbp, it’s not the hazard it is with dry blasting. Your people are not exposed to the hazard of air borne contaminants. It’s a much safer application. We do not have to do full containment. We contain water. We do blood lead levels. We do full training.”

One of the challenges of the bid was to meet the acceptance criteria for lead wipe levels as negotiated with the owner.

5. THE PROJECT

5.1 Startup

The most difficult part of every project is just getting the equipment set up and mobilized. The contractor tackled environmental details first. Lined, sand-filled, bermed containments for all of the equipment and pumps were set up to contain any diesel spills with easy clean up. The contractor set up plumbing to make ensure water volume to the farthest areas. They built the gutter work for the windows.

A comprehensive health and safety plan is implemented early, especially for the people they hired from the community. Word-of-mouth brought people to the site. The contractor management was very impressed with the quality of people. The contractor hired several people from the community and trained them to be waterjetters, and hired local painters and general labor. Everyone learned and came to work with a very good attendance record.

The contractor brought about 7 people down. There were 60-65 people total working at one time between the WJ, painting, scaffolding, electricians, and environmental personnel. The financial investment in a very good training program and training trailer paid dividends throughout the project. The contractor had complete control of the building and work force. Some of the new personnel found permanent positions. The community benefited with a payroll about \$10-12,000 per day.

5.2 Safety Meetings

A full time safety person was on the job each and every day and held a 15-minute safety meeting each and every morning. They went over every safety problem as they were identified. The owner was at every meeting. The coatings technical representative was there several times. The employees notified the contractor of each and every problem as they saw it, not later. Every job

will have some safety violations, but when you have a program running like on this job, it gives the contractor the sense of security that you will not be caught for a flagrant violation.

5.3 Obstacles and Challenges Found During the Project

On any project, there is always the potential that obstacles and differences can escalate into major objections that cannot be resolved. All the parties met, resolved differences, and made compromises that did not affect the quality of the work.

5.3.1 Windows

Windows, Windows everywhere. Windows are an integral part of the project with over 300 panes and frames. Most were broken and could not be shut tightly. If dry blasting had been selected, it would have been almost impossible to contain the dust and debris inside the building. The WJ made the dust easy. (Figures 1 and 3).

The windows proved to be fairly easy to clean. The lbp removal went just as planned with a change in pressure and nozzles to fit the conditions. The contractor rigged troughs under each window to catch both interior and exterior water from the cleaning operations and direct the water into the building for the collection sump. Ground tarps and geotextile material were placed to collect any chips. The work on the exterior of the building of the building was performed with man-lifts and swing-stages. (Figure 3).

The painting of the muttuns and cross-pieces was exceedingly time consuming. All of this work had to be done with small, fine hand brushes. It was very tedious and the opening mechanism is chain driven that couldn't be seen when it is shut. You had to get up close and personal before you could see the full extent of the problem. The contractor finally worked out a system to speed up the job. (Figure 4).

5.3.2 Brick Surfaces

The surfaces varied from old steel with multi-layered paint, to hard brick, to horse hair filled mortar and very soft, old brick. The paint over the soft interior stucco and concrete was softened with biodegradable chemical strippers and washed down gently. Concrete and brick were not repainted. Some of the substrate was soft brick made in 1922. Some of the mortar was sandstone and horsehair.

5.3.3 Appearance of WJ-3 compared to SSPC SP-6 (See Frenzel).

For the most part, the existing paint system was easily removed to the NACE No. 5- SSPC SP-12 surface preparation of WJ-3 with retention of tightly adherent primer. However, early in the project, the contractor had been routinely delivering a WJ-2 because they were training the new employees. After the initial training program, the contractor switched to the specified WJ-3. The third party inspector from a nation-wide engineering firm that deals with power plants representing the owner had not seen WJ before. Because he had been getting a WJ-2 visual cleanliness, the third party inspector, simply through lack of experience, did not want to accept a

WJ-3 surface. The WJ-3 appearance was not a problem for the coatings representative. This issue was resolved with a joint meeting of the owner, the contractor, the coatings technical representative, and looking at representative photos of WJ-2 and WJ-3 from Dr. Frenzel as well as photos from prior owner projects of WJ-3 in which the same coating system had been used and was performing well. (See Johnson and Lever papers on Wirtz Dam). (Figure 5).

The contractor hit one section that had a tightly adherent black layer that was very difficult to remove. It was initially identified as paint, but proved to be mill scale. The jetters would "grind" on the mill scale until it was removed. This term does not mean that they were using mechanical grinders. The WJ industry has adopted the term "grinding" to reflect that the nozzle is rotating and a circular pattern is produced.

5.3.4 Apparent Specification Contradiction

During the first month, it was discovered that the specification had a contradiction that had not been discussed in pre-bid or pre-start meetings. The bid called for WJ-3 or SP-6 in the surface preparation section and complete removal of all lead-based paint (lbp) in the remediation and abatement section. The contractor had bid with WJ-3 as the surface preparation with the appropriate HUD closure requirements for lead wipe samples. The third party inspector was calling for complete removal, or WJ-1.

The surface preparation section contained language that took into consideration both abrasive blasting and water jet cleaning. "Surface finish shall be visually free of all oils, greases, dirt, and foreign contaminants. Rust, rust scale, and loose mill scale shall be removed except that a thin layer of tightly adherent corrosion may remain in the bottom of the pits or inert brown ferric oxide or black magnetic iron oxide stains may remain as a tightly adherent thin film on the corroded steel surface. All existing paint shall be substantially removed to the metal substrate (SSPC SP-6/ SSPC SP-12/WJ-3). A thin film of prime coat on the metal substrate or shadows of prime coat in the metal substrate profile may remain provided the remaining paint has been fully subjected to the water blast intensity. A profile of 1.8 to 2.1 ml should be sufficient to provide good adhesion and bonding of prime coat and overcoat."

The abatement section stated: "Visible lead-based paint shall be removed from accessible surfaces interior to the building. "Following coatings abatement, perform visual inspection. If deteriorated painted surfaces and/or visible amounts of dust are still present, these conditions must be eliminated. Conduct wipe tests on abated masonry substrates to ensure complete removal of lead-based coatings. Conduct wipe tests on abated steel substrates following application of primer to ensure complete removal of lead-based coatings.

The contractor interpreted this to mean that the check for visible lbp would be made at closure after the primer and topcoat had been applied. The third party inspector interpreted the abatement statement to mean a SSPC- SP-10 or WJ-1 should be achieved prior to painting. The owner and contractor came to the resolution that the visible lbp statement was invoked after the primer and topcoat was applied.

5.3.5 Staging

It was initially thought that the interior of the building could be cleaned from manlifts with a minimum of rigging . This was the case for the turbine room. The estimated 240,000 sq. ft. in the turbine room was removed and then painted within the same time period. There were 12 jetters, 4 supervisors, and 8 painters working simultaneously. However for most of the building, scaffolding and dance floors had to be constructed. A national firm was hired for the staging. It was found that the WJ and painting could proceed faster than the staging could be erected and moved.

5.4 Project Air Monitoring

The PM-10 test for particulate matter with a mean diameter of 10 micrometers or less was not applicable because of lack of visible dust in the working area.

Ambient Air monitoring was measured for the first ten days. Fifteen samples were taken with only one above the “no detection” level. The detected sample was $40 \mu\text{g}/\text{m}^3$ with an average of $2.7 \mu\text{g}/\text{m}^3$. Air monitoring of the jetters personal breathing zone is given in Table 2.

After the air monitoring results were reviewed on this project, project management made the decision to remove the respirator requirements initially enforced during the testing procedures and to implement a random sampling as necessary to insure personnel safety. These types of readings are typical on UHP lead abatement projects.

The personal safety precautions focused on personal hygiene, i.e., washing hands and face, and changing clothes in the change room. The emphasis is “Do not take lead home.” Personal hygiene is the major precaution on a WJ job as compared to the requirement of full face, air supplied hoods, and engineering controls of negative full containment on dry blasting projects.

5.5 Project Waste Management

To meet the HUD guidelines for closure on the building, the entire structure was pressure washed before wipe tests were taken. All areas were prepared to provide closure wipe tests agreed upon by the owner and the contractor.

The river is right next to the plant. On the river side, they built a double 4 foot high silt fence and bermed with soil. From the building to silt fence, they put down a double layer enviro screen. They collected any water that came from the building through gutters and put it back into the building where it was stored. There was no contamination in the soil.

The contractor was able to direct almost all the water back to inside when working on the windows by building special gutters. On some of the windows and outside areas, the paint was coming off in chunks. They used 100 mesh enviro screens to clean the water and collect the paint chips as we went along. The screens were placed out 30 feet from the building.

At least one month was spent on clean-up, closure and final painting details. In addition to the main building, two separate pump houses, a bridge and a gate valve on a concrete bulwark in the river were refurbished.

Most of the wastewater used on the project was collected on the concrete floors in the interior of the building and pumped to a holding tank and a large sump area. The solids were allowed to settle during the project. Retained water evaporated during this time. The water was separated from the solids through decanting and filtrations. After the water was tested for heavy metals by an independent lab using the TCLP method (Table 3), the non-hazardous 400,000 gallons of effluent water was disposed through the municipal water treatment facility at a cost of \$2.79/1,000 gallons (0.003 dollars per gallon) or a total cost of \$1,126.

The painting process generated approximately 44,000 pounds of hazardous waste (paint cans and other solids) that were disposed of by the owner. This waste stream included an estimated 4,000 pounds of waste paint thinner. This waste stream would be present whether waterjetting or dry blasting was used to clean the building. The contractor kept all of the ground tarpaulins for future use.

Another 10,000 gallons (estimated 50 tons) of hazardous waste sludge comprised of the solids that settled from the water was disposed by the owner. The total estimated costs for this hazardous waste disposal was estimated at approximately \$20,000.

Let's compare the above with the waste disposal profile of the scenario of using dry abrasive blasting. If dry abrasive blasting had been used for the surface preparation, an estimated 6-10 pounds abrasive/square foot for the coating removal would have been required. With the assumption of 8 pounds per square foot, the spent abrasive, which would have been mingled with lead paint, would amount to 3,280,000 pounds (1640 ton). The containment and cleanup of this abrasive and generated dust would have presented a major effort and would have been very labor and time consuming.

For comparison, non-hazardous abrasive disposal varies somewhat and costs approximately \$65 to \$75 per ton in the Norfolk, Virginia area. This calculates to \$106,600 for non-hazardous abrasive disposal. It costs about \$0.25/pound if the abrasive stream is hazardous, or an estimated cost of \$820,000.

Look at this project from a waste minimization viewpoint. The assumption is made that the amount of waste paint and thinner materials would be the same whether using WJ or abrasive blasting. Compare the volumes 10,000 gallons of hazardous sludge generated on the project with the calculated 3,280,000 pounds of abrasive. Assuming 100 pounds abrasive per cubic foot, this calculates to 32,800 cubic feet or 246,000 gallons. The project, in terms of 50 gallons drums, would have generated 200 drums WJ sludge compared to an estimated 4920 drums of spent abrasive. The volume of hazardous spent material is reduced 25 times.

6. OVERALL PROJECT FEELING

All three participants, the owner, the coatings supplier and the contractor approached this project with a "win-win" attitude. Resolve differences early in the start-up. Work towards a solution to educate the inexperienced personnel. Maximize safety and pollution prevention. Get the maximum performance. The project turned out good with an extremely well appointed building.

6.1 Lasting impression from the coatings technical representative

This section is a summary of interview remarks made by the New Braunfels coatings technical representative near the end of the project.

This project is neat. We are taking an old building that had all the hustle and bustle of a power plant. For years, it has been essentially abandoned and had deteriorated into a derelict condition. Now the building is being recycled as a viable entity. The owner is bringing it back into the life of the community providing future service to New Braunfels.

To go in this building and dry blast it, in my mind, would have probably polluted the building and the surroundings with abrasive media to the point that it would have been falling out of the cracks for years to come. The UHP WJ, is very effectively removing the old lbp. WJ allows the contractor to get the paint down on the floor. They are putting the paint and water into a large cistern. They are not getting the media permeated into the nooks and crannies of the building.

Another advantage is the coating and UHP WJ is almost a marriage made in heaven. The coating can go on in damp environments. You can literally apply it in parts of the building while they are WJ in other parts of the building. You couldn't do that with dry abrasive blasting. Dry blasting would have extended the time out considerably longer if they tried to blast and then coat. It would take forever to get the dust to settle.

HP or UHP WJ is very clean when you compare to the dry blast. The coatings technical representative has been associated with slurry blast and you still have a lot of stuff to clean up. With the HP WJ, not only does it clean the pores of the steel, you do not have the problems of residual dust which gets into everything.

The side issue of a little rust bloom is minimal. Because you are doing manual WJ, you tend to get a light rust bloom afterwards. Wasser's moisture cured urethane coatings are made for that environment of a light rust bloom. It works long term on steel which is not perfectly prepared so you do not need a SP-5 or SP-10, or WJ-1 or WJ-2. The single component, zinc based, micaceous iron oxide moisture cured urethane provides a tenacious coating. The barrier properties are combined with active corrosion protection in case of a breach.

From a coatings and cleaning aspect, the contractor had very little down time from equipment. When you go in and look at their work, it is very clean. There is virtually no collateral damage to the building. The coatings are removed to the edge without damage to the brick. The edges of the beam are where the paint ends. The paint application work is pristine; it doesn't go onto the brick. The quality is very professional.

When I talked to the owner, they all agreed that UHP WJ is doing an exceptionally fine job. The owner is quite pleased with the removal, coatings, application, and the treatment the contractor is giving to the building. It has been a joy to the coatings technical representative to work on the building and with the people. It is a joy to see someone like the owner who takes the time to re-designate what the building is to be used for, and to recycle it to be an asset to the community. Everyone is working towards that common goal.

6.2 Lasting Impression- Contractor

This section is a summary of interview remarks made by the contractor project manager near the end of the project.

The use of WJ is safer for the community. If you had abrasive blasted, there is no way you could have kept all the dust and debris inside the building. The containment costs would have been enormous. The owner involved the community in the planning; they are in tune with what is going on around them. We are only two blocks from the main square. When the general public sees a cloud of dust coming out of an old building, the first thing they would think is lead poisoning. This didn't happen. We had people stopping by and telling us "How great the building looks."

Most all of the people we brought down here from Virginia fell in love with New Braunfels. Some of them have tried to desert us and stay here. The vendors and suppliers have been great. If they didn't have it, they would call around and help us find it. It's has been a real pleasure. That's what we will remember about this project.

7. BENEFITS AND SAVINGS ON THIS PROJECT

There are savings in the project costs attributed to reduced health risks associated with generation of lead dust and reduction in the amount of containment.

The lead remediation was completed with no detrimental effect to the surrounding tourist and recreational areas and the pristine river with its 3 endangered and 63 species of flora and fauna. There was not contamination to the surrounding environment or disruption to local activities.

It is estimated that the project saving were over \$500,000 by using UHP WJ technology over abrasive blasting. These savings resulted from minimal containment requirements, reduced waste disposal, and high production rates.

The exposure to health risks for all employees was greatly minimized and confined to the actual work areas. The containment due to airborne dust was negligible and presented few problems.

8. SUMMARY

For lead abatement projects, the advantages are:

- greatly reduced waste streams and costs
- minimal environmental impact, and
- greatly reduced liabilities.

Worker and surrounding area exposure to contaminants are minimized. The advantage of knowing approximate disposal costs prior to the start of each project makes budgeting easier.

Coatings manufacturers have accepted this surface preparation technology and are approving their products in conjunction with properly prepared surfaces using UHP WJ. Many have issued standards for their own products or have endorsed published standards. The industry has successfully cleaned and recoated millions of square feet of area in a variety of application. (See Dupuy).

UHP WJ surface preparation technology has earned its place as an accepted surface preparation technique. The large numbers of projects that are being completed each year add to the database of information that has proven this technology to be a cost effective, environmentally friendly technology for many maintenance coating applications.

9. ACKNOWLEDGEMENTS

Thanks is given to the Lower Colorado River Authority, UHP Projects Inc., Wasser High-Tech Coatings, Texas Natural Resource Conservation Commission, and, most especially, the sponsors of the Advisory Council.

10. REFERENCES

Dupuy, Richard, "Ultra High Pressure Waterjetting for Maintenance Coating Applications," Proceedings of the Seminars, SSPC 2000, p. 255-265, Nashville, Tennessee, 2000.

Frenzel, Lydia, "A Comparison of Surface Preparation for Coatings by Water Jetting and Abrasive Blasting," Proceedings of the 9th American Waterjet Conference, Houston, Texas, 1999.

Williams, John "Comal Plant gets new lease on Life," LCRA News, p. 4-7, September, 1999.

Johnson, Mark, "Get the Lead Out! Removing Lead-Based Paint on Hydro Plant Structures," Hydro Review, May, 1996; Lever, Guy, "Hydroblasting permits safe, cost-effective Dam Rehabilitation," Materials Performance (MP), April 1996, pp 38-41; Lever, Guy, "WaterJetting Cuts Hazardous Waste at Dam," Journal of Protective Coatings and Linings (JPCL), p. 37, April, 1996.

Launius, Kenneth W. and Vanderglas, Brian, "Comal Power Plant Remediation Project," paper # 636," Air & Waste Management Conference, Orlando, Florida, June, 2001.

New Braunfels Herald-Zeitung, January 26, 2000.

Landa Park Brochures, The Greater New Braunfels Chamber of Commerce Brochures

11. TABLES

Table 1. Initial tests for the Paint Systems over Various Interior Areas

Parameter,	Action Limit TRNCC 335.568	Comal Building Paint Solids Analysis
total cadmium	0.5 mg/L	<0.50 to 143 mg/Kg
total Chromium	1 mg/L	54- 8,592 mg/Kg
total Lead	1.5 mg/L	3100- 135,600 mg/Kg

To put this in simpler terms, the lead paint content of 135,600 mg/Kg corresponds to 13.5 %.

Table 2 Air Monitoring, Jetters Personal Breathing Zone

Blasters personal breathing space	$\mu\text{g}/\text{m}^3$ Lead, 8-hour TWA,
10/01/1999	BDL
10/01/1999	BDL
10/05/1999	BDL
10/05/1999	BDL
10/14/1999	BDL
10/14/1999, enclosed room	120
10/15/1999	BDL
10/15/1999	40
10/15/1999	BDL
10/15/1999	20
10/15/1999	BDL
10/15/1999	BDL
10/18/1999	BDL
10/19/1999	BDL
10/19/1999	30
10/19/1999	BDL
10/19/1999	BDL
10/20/1999	20
10/20/1999	70
10/21/1999	BDL
10/21/1999	BDL

The detection limit was $20 \mu\text{g}/\text{m}^3$. The Action Limit is $30 \mu\text{g}/\text{m}^3$. TWA=Time weighted average. BDL- below detection limit

Table 3 Analysis of Decanted Water

TCLP Metals	Analysis of Decant Water	Reporting Limit	Regulatory Limit
Component	Result mg/L	mg/L	mg/L
Arsenic	< 0.10	< 0.10	<5.0
Barium	<1.0	<1.0	<100
Cadmium	<0.10	<0.10	<1.0
Chromium	<0.20	<0.20	<5.0
Lead	<0.20	<0.20	<5.0
Selenium	<0.10	<0.10	<1.0
Silver	<0.10	<0.10	<5.0
Mercury	<0.01	<0.01	<0.2

12. FIGURES



Figure 1

Extensive structural steel on the interior of the building to be cleaned and recoated with a moisture cured urethane.



Figure 2

Another picture of the steel to be cleaned and recoated.



Figure 3

Trough under window to direct water into sump areas.



Figure 4

Close up of painted window mechanism.

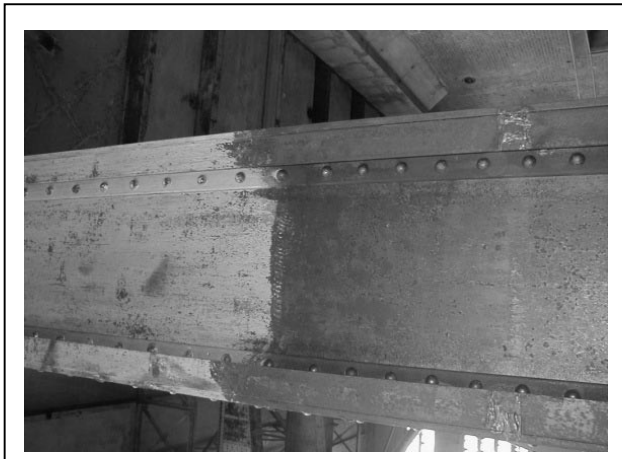


Figure 5

Beam in initial condition on left side and cleaned to WJ-2 on right side.

COMPARISON OF SURFACE PREPARATION USING DIFFERENT METHODS

Eng. Luis E. Ortega Trotter
Acquablast Tratamento de Superfícies Ltda.
Pinhais, PR, Brazil

ABSTRACT

In a Pulp Mill we make a comparison of four different surface preparation methods:

- a) Abrasive paper pneumatic grinder;
- b) Pneumatic needle;
- c) Dry Blasting Copper slag;
- d) Hydroblasting.

Since the Mill is close to the shore, $\frac{3}{4}$ mile only, it's atmosphere is highly corrosive due to two sea breeze (chlorine), geographical environmental aspects were taken in consideration. Also bleaching chemicals contamination like sodium hydrochloride, sodium hydroxide, hydrochloric acid, chlorine dioxide, sulfuric acid and overflow from tanks, leakages, equipment maintenance and others. We studied all these surface cleaning methods to obtain a maximum of four micrograms/cm² of salt contaminants recommended by two great paint manufacturer, before the painting process. Cost for the paint project – Housekeeping/2000 were also take under analysis. Other measurement were done at different times after the surface cleaning process, so as to observe the salt contamination and determine the best period to paint. Also visual study by a Scanning Electron Microscope for visible contamination were made. This Pulp Mill became ISO 14001 certificated and the preparation process was also studied and evaluated under this point of view.

1. INTRODUCTION

Doing hydroblasting in the largest Pulp Mill in the world, after near by two years of job we achieved a huge technical experience. Aracruz Housekeeping/2000 project took about 6 months of work. General information about geographical localization, local weather, temperature and other factors have to be taken in consideration for that magnitude of job.

So it is very important for the Mill owner which method of depainting and rust removing system to be applied. Also a whole computer program was made with all interface and interference that could happens with the different contractors.

The owners great concern was the possibility of his product be contaminated (cellulose – 98% for export). After beginning of the job we made a study we called “*Comparison of Surface Preparation with different Methods*”:

- a) Abrasive Paper with Pneumatic grinder;
- b) Pneumatic needle;
- c) Copper slag blasting;
- d) Ultra High Pressure Hydroblasting.

After this study, owner and contractors were convinced about the quality of Ultra High Pressure Hydroblasting method. But during the job, other kind of problems merged, like: After Hydroblasting how long could we keep surface quality for the painting? The Mill is situated just $\frac{3}{4}$ mile from shore. Chlorine and Sulfate containing environment (typical in Pulp Mills) could contaminate the prepared for painting surfaces. This required a second study to determine maximum elapsed time between hydroblasting and painting.

2. JOB LOCALIZATION AND CORROSION ASPECTS

Since the Housekeeping budget was limited to just US\$ 550,00.00 they prioritized which equipment to be treated first. Also the geographical localization was taken into consideration concerning corrosion aspects. Humectation time for that place, based on ISO 9223 chart for humidity >90% is according to the Figure 1.

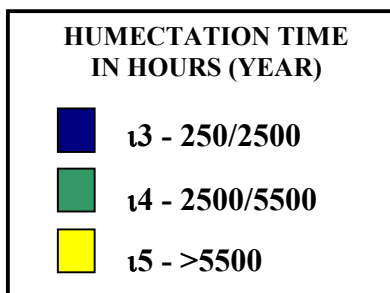


Figure 1. Industry localization



The map indicate 2.500 to 5.500 hours with annual humidity over 90% that means classification category 4 by ISO 9223.

Classification of atmospheric corrosivity

Category of corrosion	Agresivity
C1	Very low
C2	Low
C3	Medium
C4	High
C5	Very high

Table 1.

Classification of humectation time and contamination by SO₂ and Cl ISO 9223.

Category	Time of humectation Hour/year	Contents of SO ₂ /m ² day	Contents of Cl mgCl/m ² day
1	> 10	≥ 10	≥ 3
2	10 – 250	10 – 35	3 – 60
3	250 – 2.500	35 – 80	60 – 300
4	2.500 – 5.500	80 – 200	300 – 1.500
5	> 5.500		

Table 2.

3. BROOKS DETERIORATION INDEX

We also studied our geographical localization from Brooks deterioration index.

The classification for SO₂ contents as category 3 – 4 and for Cl category 3 – 4 after our local study




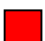
BROOKS CORROSIVITY INDEX	
	>5 → HIGH
	2-5 → MEDIUM
	1-2 → LOW
	<1 → VERY LOW



Figure 2.The map indicated a moderate index between 2 and 5.

Formulae for this index is:

$$I = \frac{(HR - 65) P}{100}$$

HR = relative annual humidity.

P = Steam saturation pressure corresponding to the annual media temperature.

4. ELETROCHEMICAL CORROSION

The most common corrosion process in this area is electrochemical corrosion. This is a process which happens in presence of water, usually at ambient temperature, it forms a corrosion cell (Battery). If we have water or salt like NaCl, SO₂, Cl⁻, etc, temperature up to 40°C (or over) on a steel plate (C or D), the electrons go from anode to cathode; this happens due to many reasons:

- a) inclusion, segregation, crack, blister
- b) different metal tension
- c) different polishing
- d) different heat treatment
- e) different size and angle of the grain
- f) material produced at different time
- g) different temperature and humectation

We can represent a corrosion cell (battery) or galvanic cell (battery) as Figure 3.

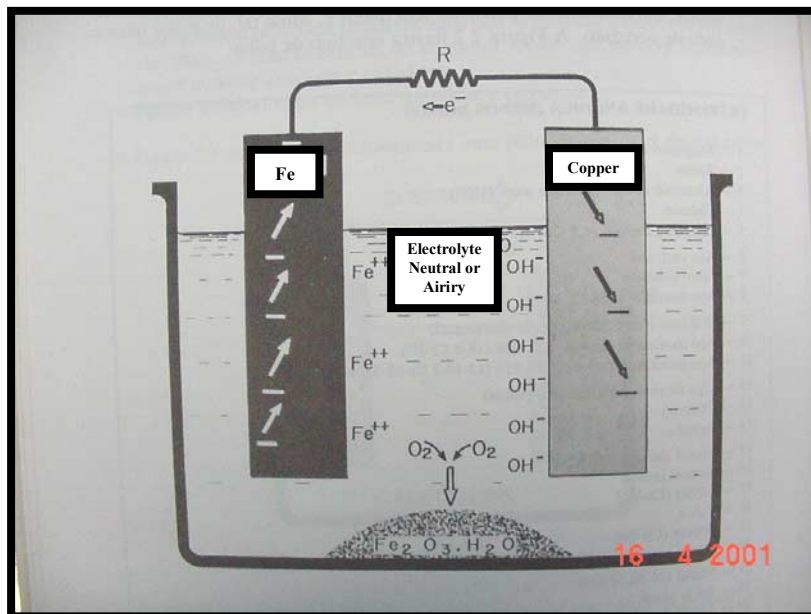


Figure 3.

Based in all these information, we can get a final representation of annual corrosion of steel in microns referred to SO₂ and Cl⁻ in mg/m² day.

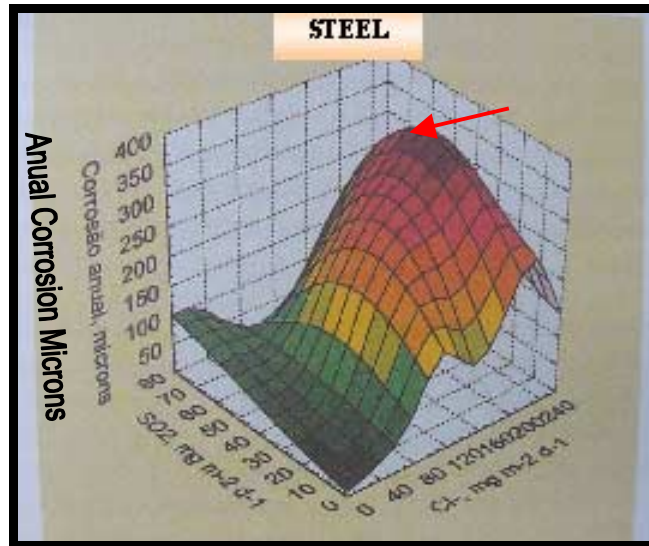


Figure 4.

After chemicals analysis with chlorine (25ppm/day) and sulfates (9,62 ppm/day) over a surface of 10cm² we obtain at Figure 4 the maximal annual corrosion rate: over 400µm a year. That means a very high aggressive environment for all industrial paints. The best possible surface preparation have to be taken in consideration. Elapsed time between surface preparation and painting have to be considered to 1 or 2 hours. After this period we recommend high pressure blasting of the surface with 200 bar (3.000psi) – 20 lts/min. with rotating nozzle. From data based calculation and climate observation, we see the Mill is in brown zone indicated by the arrow (Figure 4). For a better localization we also take my Ultra light airplane and took an airview from 360mt high (1.200 feet).

Also we can see wind blowing smoke, so the wind direction at that moment (04.16.2001) 07:10 AM was North-West (Figure 6).



Figure 5.



Figure 6.

5. COMPARISON OF SURFACE PREPARATION WITH DIFFERENT METHODS

5.1 Housekeeping/2000 paint project

The pulp mill is now ISO 14001 certificated and Engineering and Maintenance Departments were looking for a cleaner process for surface preparation.

Sand or copper slag blasting was held as high polluted system. Large amounts of pulp production have been contaminated many times by sand or copper slag. Also abrasive paper with pneumatic grinder demonstrated same problems. Pneumatic needle demonstrated to be a too slow and high cost process.

Surface quality was not taken in consideration, because no information was available at that time.

The budget for Housekeeping/2000 job was US\$ 522.000,00 (related only for paint purpose Table 3) equivalent to 28.363 m² (305.185 ft².)

Company	US\$	%
Paint Supply cost	122.000	22,1
Painting cost	108.00	20,71
Scaffolding cost	81.180	15,11
Hydroblasting cost	226.00	42,08
Total	537.800	100

Table 3.

Now we can see that surface preparation was the heaviest part of the budget (42,08%).

Under such magnitude of investment any company (contractors) must have criterious management, quality and correct proceedings to obtain best painting life span. If one of the contractors would delay his program, others would suffer for that or have to pay the amount of labor cost for the rest. From this point of view harmony and good sense to do the job in time was necessary. Weather problems like rain and humidity over 80% have to be recovered at weekends. Normally hydroblasting work time was from 07:00 AM to 03:00 PM, paint process from 03:00 PM to 06:00 PM or later if humidity conditions permitted.

5.2 Background

To demonstrate for Maintenance and Engineering Department that hydroblasting process is used in some countries like Germany, England, France, Spain, USA, Canada, Japan, and others, we decided to make comparison between three different methods normally used and hydroblasting. It is not easy to use hydroblasting in this country, because of paradigms. We have to break a whole of old concept in surface preparation.

Based in Nace n° 5 (National Associate of Corrosion Engineers – and SSPC – SP12 (Society for Protective Coatings) has determined the different aspects for non visible contaminants for

surface preparation. This was also a new concept in surface preparation for the Industry and the Paint contractor.

SC-1. An SC-1 surface shall be free of all detectable levels of contaminants as determined using available field test equipment with sensitivity approximating laboratory test equipment. For purposes of this standard, contaminants are water-soluble chlorides, iron-soluble salts, and sulfates.

SC-2. An SC-2 surface shall less than 7 $\mu\text{g}/\text{cm}^2$ chloride contaminants, less than 10 $\mu\text{g}/\text{cm}^2$ of soluble ferrous ion levels, and less than 16 $\mu\text{g}/\text{cm}^2$ of sulfates contaminants verified by field or laboratory analysis using reliable, reproducible test equipment.

SC-3. An SC-3 surface shall have less than 50 $\mu\text{g}/\text{cm}^2$ chloride and sulfate contaminants as verified by field or laboratory analysis using reliable, reproducible test equipment.

Invisible contaminants like Cl, SO_2 , grease, oil and large variety of chemical components like sodium hydrochloride, sodium hydroxide, hydrochloride acid, chlorine oxide, chloride dioxide, sulfuric acid produce failure of coatings. The removal of all these invisible contaminants leads for longer performance by the coating system. We asked two different paint manufacturers and explain that limit up to 4 mg/cm^2 of salt contamination would adhere better and longer coatings with Ultra High Pressure Hydroblasting. Over 4 mg/cm^2 of salt contamination would produce failure of coatings in an exponential basis.

5.3 Technology

Waterjetting can be described as a series of small droplets in the 5-10 micron range hitting the surface at supersonic speeds (Ultra High Pressure Hydroblasting over 1.700 bar – water velocity 566 m/sec – 2.037 km/hr). The droplets implode (cavitate) and destroy coatings, rust, remove salts; then spread laterally and shear at the interface, like ultra sonic cleaning, lifting all kind of materials. A series of microscopic “pock marks” from on the macro surface. The craters and pits get “deep cleaning”.

Using hydroblasting we don't change the existing profile. Abrasive erodes the surface from the top, and non visible contaminants, are driving into the surface or form pocket of metal in which these contaminants are buried. It happens the same process in a more aggressive way using pneumatic needle.



Figure 7.



Figure 8.

5.4 Chlor-Test

We made the test with chloride test kit for measurements of Chlor salt contamination of the sample. It was also possible to make the same test by computerized spectrometry. Using this second system we found different amounts of Chlor components like sodium hypochloride, hydrochloric acid, chlorine oxide, chlorine dioxide, sulfuric acid and others. The first method demonstrates to be quicker and practical for the contractor because three Ultra High Pressure Waterjet equipment were working at the same time.

5.4.1 Test with abrasive paper using pneumatic grinder



- ❖ Measurement: $7 \mu\text{g}/\text{cm}^2$.
- ❖ Classification SC-2.

Figure 9.

In the photo (n° 9) we can see the kind of steel plate that was eroded about 2 millimeters.

5.4.2 Pneumatic needle

This test was conducted on the steel plate with pneumatic needle. This very high salt contamination was because all needle drive not only steel oxide but also all kind of salt into the surface or better; form a pocket of metal in which all these contaminants are buried.



- ❖ Measurement: $65 \mu\text{g}/\text{cm}^2$.
- ❖ Classification SC-3.

Figure 10.

Immediately they will form a galvanic current due of the different electrical potential of the involved elements. This is the next step to destroy the paint. Normally this happens after 9 months of paint application in this mill.

5.4.3 Copper slag blasting

Here we used a tube as sample (Figure 11), that was corroded to classification C, no paint coverage.



- ❖ Measurement: $7 \mu\text{g}/\text{cm}^2$.
- ❖ Classification SC-2.

Figure 11.

5.4.4 Ultra High Pressure Waterblasting

Here was used an own build Ultra High Pressure Equipment with 6 plungers, 230 HP (2.000 bar) diesel engine, also a Pneumatic Rotating Gun (2.000 RPM) with 4 concentrate nozzle jets operating at 1.800 bar and 16 lt/min, using cold clean potable water and filtered to 1 micron.

This was conducted in the most contaminated Industrial area, also over steel.



- ❖ Measurement: $0 \mu\text{g}/\text{cm}^2$.
- ❖ Classification SC-1.

Figure 12.

5.5 Conclusion for this test

There was no doubt that Ultra High Pressure Waterblasting was the best process for surface preparation (Figure 13).

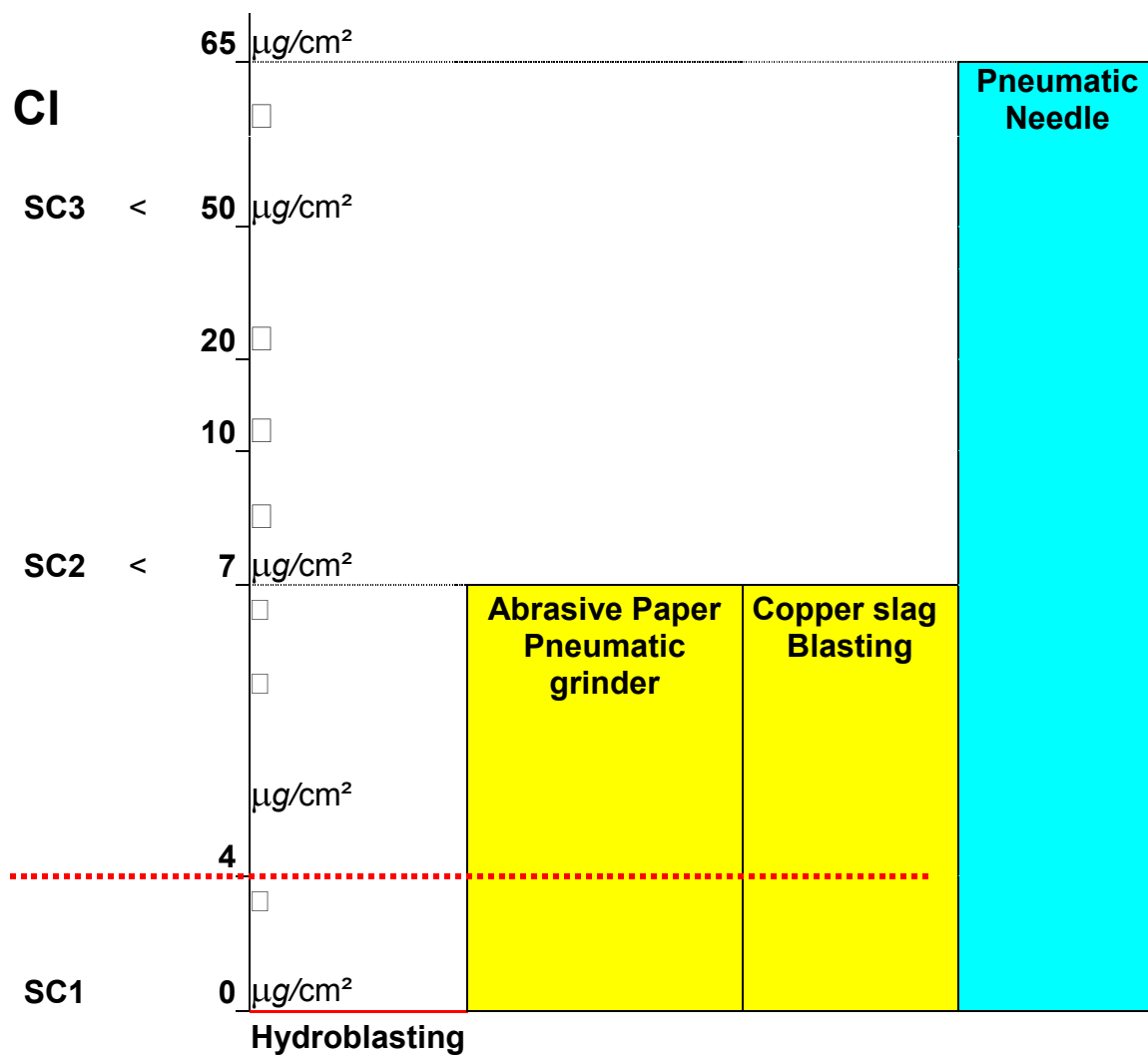


Figure 13.

6. CONTAMINATION IN PROGRESS

Since industrial and marine contamination never stops, there was great doubt about how long could be wait between hydroblasting and the paint process. Normally was hydroblasted from 07:00 AM to 03:00 PM. The paint process began at 03:00 PM and ended at 06:30 PM or sooner if problems with humidity over 80% appears.

We put 2 samples (Figure 14), one in front of the Recovery Island, closer to the sea (Test II) and another close to the Lime Kiln (Test I).

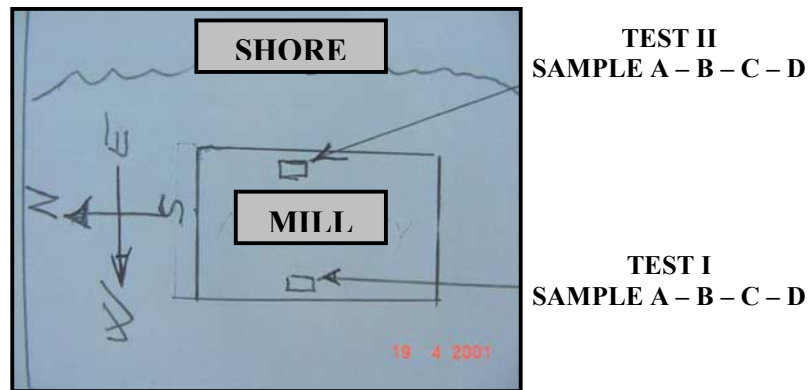


Figure 14.

Both samples were hydroblasted to 1.700 bar, and we had 8 samples analyzed with an Dianex instrument. Each test was made after 3, 6, 9 and 24 hours of local exposition. With this result it demonstrates that we can paint after hydroblasting not later than two hours.

SAMPLES	"A" After 3hr	"B" After 6hr	"C" After 9hr	"D" After 24hr
TEST I	Chloride 1,48 Sulfate 4,93	Chloride 8,59 Sulfate 9,125	Chloride 20,89 Sulfate 7,20	Chloride 25,99 Sulfate 9,203
SUBTOTAL I	6,41ppm	17,71ppm	28,09ppm	35,19ppm
TEST II	Chloride 7,74 Sulfate 6,68	Chloride 7,53 Sulfate 5,78	Chloride 12,872 Sulfate 6,22	Chloride 10,41 Sulfate 9,45
SUBTOTAL II	14,42ppm	13,31ppm	19,09ppm	19,86ppm
Σ ÷2	10,41ppm	15,51ppm	23,59ppm	27,52ppm

Table 4.

We used a computerized spectrometer to see the result of Cl, NaCl and SO₂ contents (Figure 15).

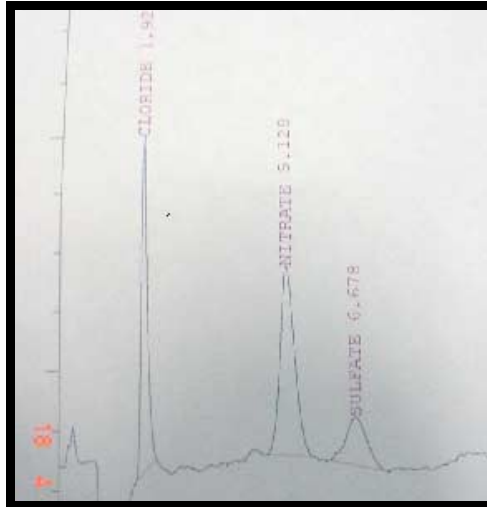


Figure 15.

7. VISIBLE TEST

7.1 Uncleaned steel plate

We used a heavily rusted steel plate (C classification). This pitted new steel 1020 (Figure 15a) without magnification. Scanning Electron Microscope (JEOL – T330A – Semafore) 150 magnification (Figure 17). We observe the heavy rust, debris and salt crystallization of NaCl, Chloride and sulfates. We observe salt crystallization with 500 magnification (Figure 18). The uncleaned steel had a measured anchor pattern of 0,20 millimeter. The cross section of the surface (Figure 16) shows a pocket fold in the metal. When used sandblast or pneumatic needle over a surface with two spikes they come together forming a pocket trapping all kind of debris, salt, iron oxide etc. If we use abrasive paper only the top of the spikes will be removed. For heavily corroded steel (D classification), anchor pattern over 2 millimeter or more a plate or a structure could easily reach the strength limit.

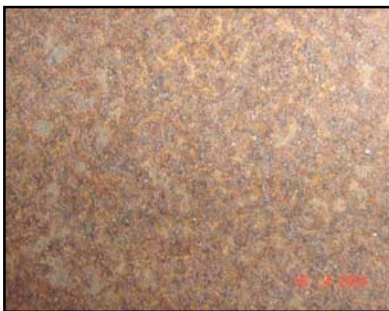


Figure 15a.

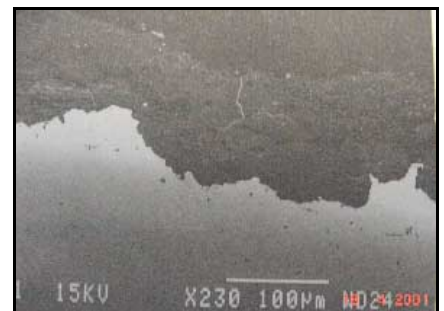


Figure 16.

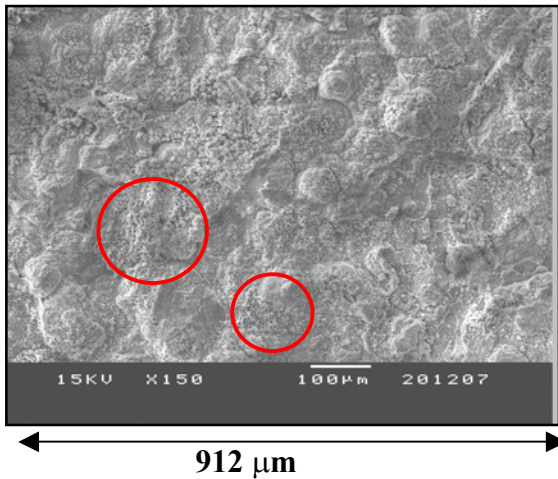


Figure 17.

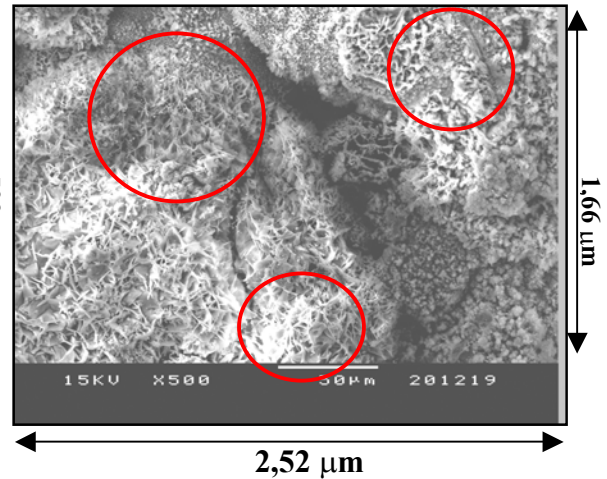


Figure 18.

○ Salt contamination all rest is rust.

7.2 Abrasive paper with pneumatic grinder

In the Figure 19 without magnification we see hundreds of corrosion pits, places where abrasive paper untouched the corrosion. All kind of debris, steel rust and all kind of salt may stay after treatment, forming after painting a electrochemical corrosion cell.

Figure 20 with 150 magnification we see clearly where the abrasive paper works. The remaining areas are contaminated with Chlor – other salts like NaCl, sulfates and corrosion.

Figure 21, a closer view, (X 500) we observe better a great area when abrasive paper have cleaned the surface Painting over such kind of surface treatment obviously electrochemical corrosion will be present after 6 months or one year.



Figure 19.

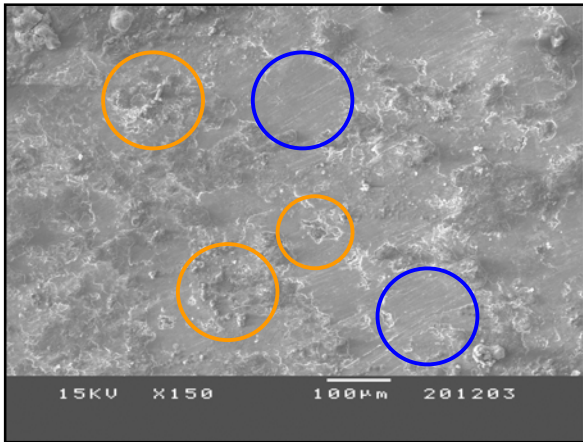


Figure 20.

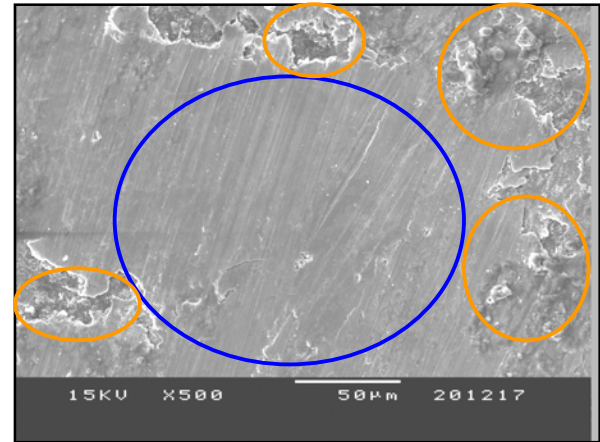


Figure 21.

○ Clean areas.

○ Steel corrosion and salt contamination

7.3 Pneumatic needle

In Figure 22 we observe clearly how the surface was treated with the heavy impact of the new needle. All kind of steel corrosion and salt contamination were literally compacted at the surface of the steel plate. The depressions of the impact reached close to 40 μm . That's the reason when making Chlor-Test it reached 65 $\mu\text{g}/\text{cm}^2$ of salt contamination. Such kind of surface preparation will be corroded in a very short period because of hundreds of electrochemical corrosion cells to be found in only 1 cm^2 . In Figure 23 we don't observe metal pockets, but they surely exist caused by the great impact and steel deformation. We observe also a deep depression of about 40 μm . Chlor-Test and other salt is to be found over all surface. In Figure 24 (magnification X 500) we observe dramatic Chlor salt contamination, other salt and steel corrosion.

Normally pneumatic needle user estimate that it has done a good job (unknowing non visible contamination) because the treated surface looks "bright". When using new needle, they impact the steel surface producing micro clean surfaces according to new sharp needle pattern. It reflects like mirror.



Figure 22.

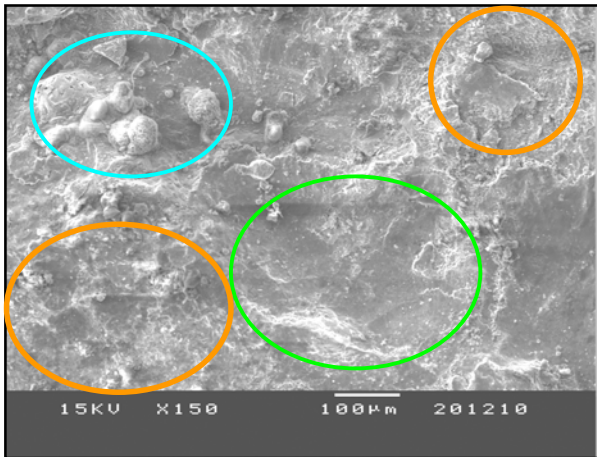


Figure 23.

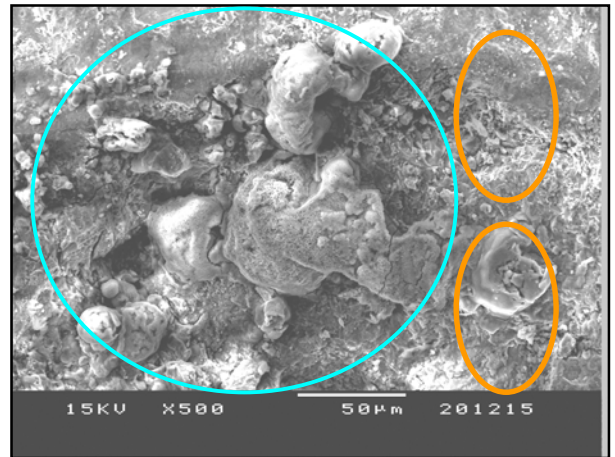


Figure 24.

- Steel corrosion and salt contamination
- Chlorine
- Deep depression 40µm

7.4 Dry Blasting Copper slag

We used good quality copper slag. The surface became white metal finished. At Figure 25 we see that some little darker points rest of abrasive trapped at the steel surface. The surface was literally corroded and little pocket have also to be observed, where all kind of salt, surface oxide can be found. Figure 26 also crack of the surface can be seen. At Figure 26 rest of trapped abrasive everywhere and deformation of the surface producing waves of steel deformation, under this waves can be found any kind of contamination. With this kind of surface preparation, electrochemical corrosion will appear after 2 years in this industry due to: changes of temperature, industrial contamination, sun rays, electrochemical cell, NaCl etc.



Figure 25.

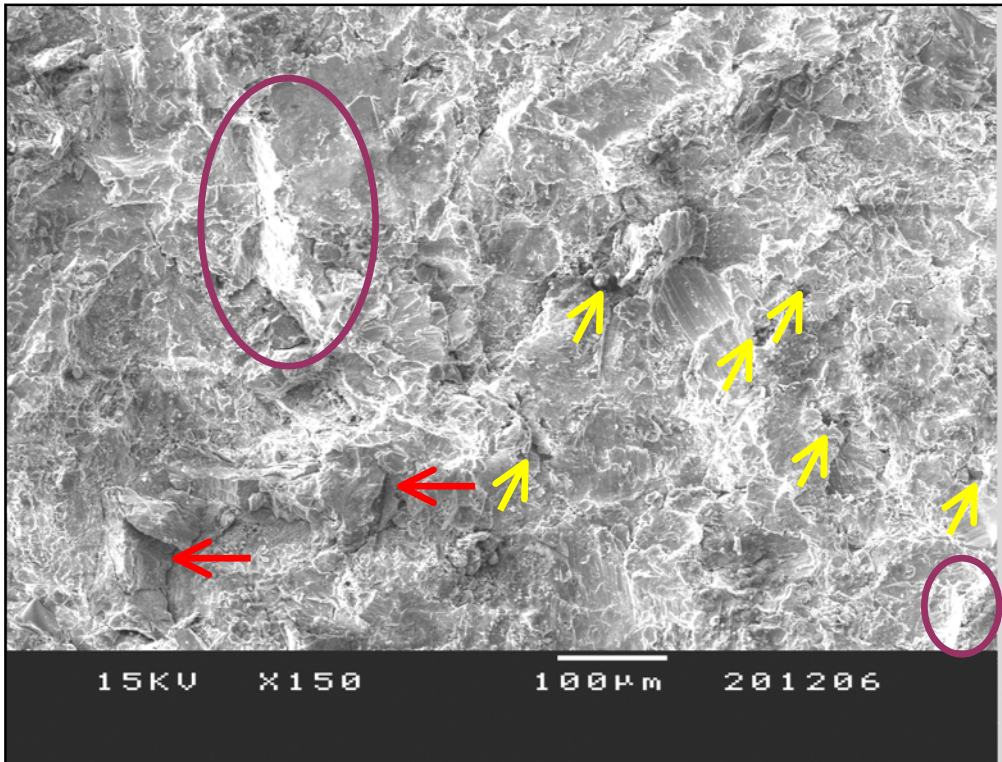


Figure 26.

↑ Pockets. ↑ Crack. ○ Waves, steel deformation.

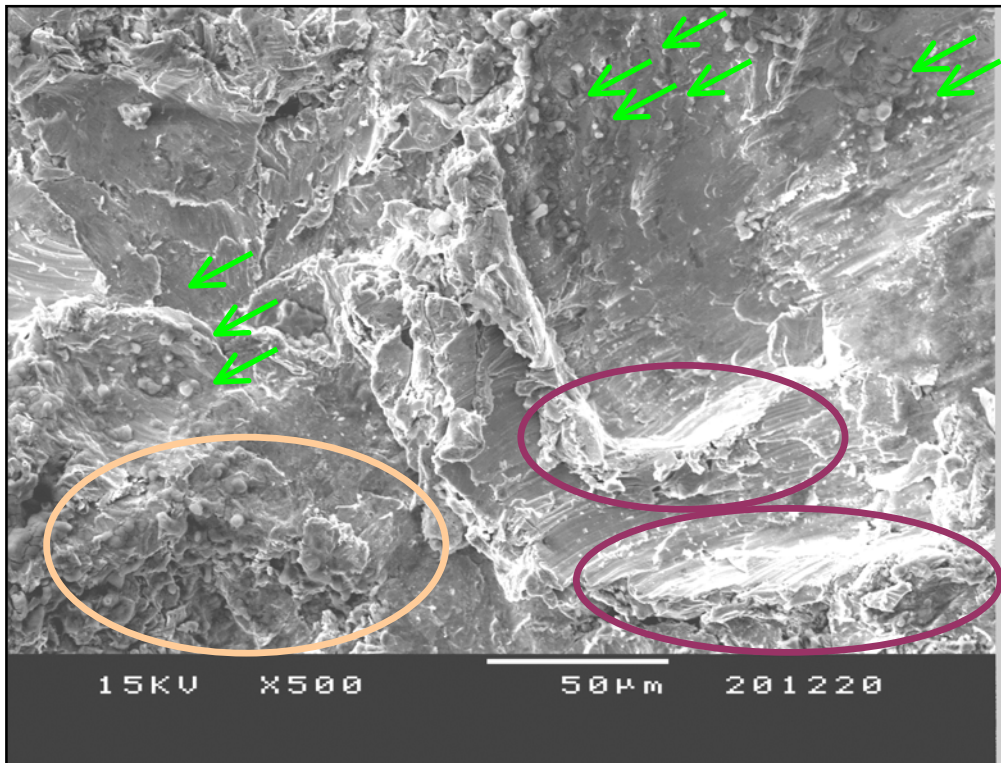


Figure 27.

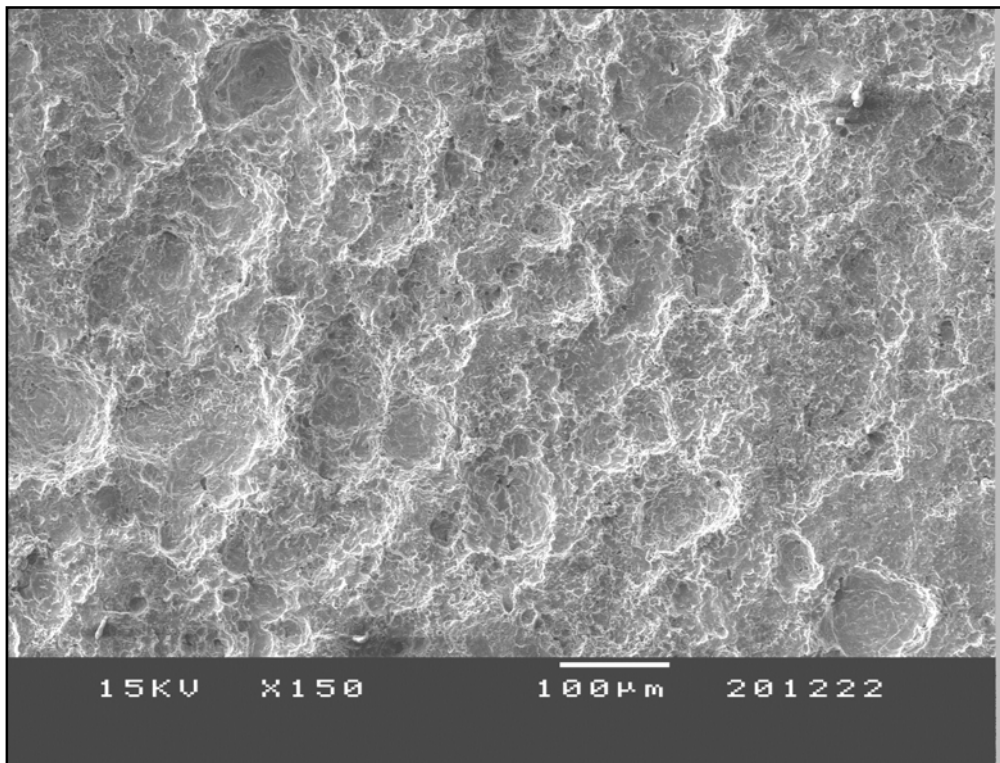
↑ Rest of trapped abrasive. ○ Salt contamination. ○ Waves, steel deformation.

7.5 Ultra High Pressure Hydroblasting

We took a first photo after 10 minutes (Figures 28, 29 and 30) of surface preparation. We used 1.700 bar, pneumatic rotating gun (2.000 RPM) with nozzle 15° to the surface at 50 millimeters distance. Figures 31 and 32 were taken about 4 hours after surface treatment, we observed a light flush rust. We could paint (according paint specs) up to moderate flush rust (International Paint – Hydroblasting Standards). In Figures 28 and 29 we observe a real clean area without chemical contamination, rust, debris etc. At Figure 30 (X 500 magnification) we observe little caves that has been cleaned deeply. In Figure 32 to be sure that this “contamination” was flush rust, an analysis was made, and the electronic microscopy indicates only Fe and O₂.



Figure 28.



**Figure 29. No rust. No salt contamination. No surface deformation. No cracks.
After 10 minutes Hydroblasting.**

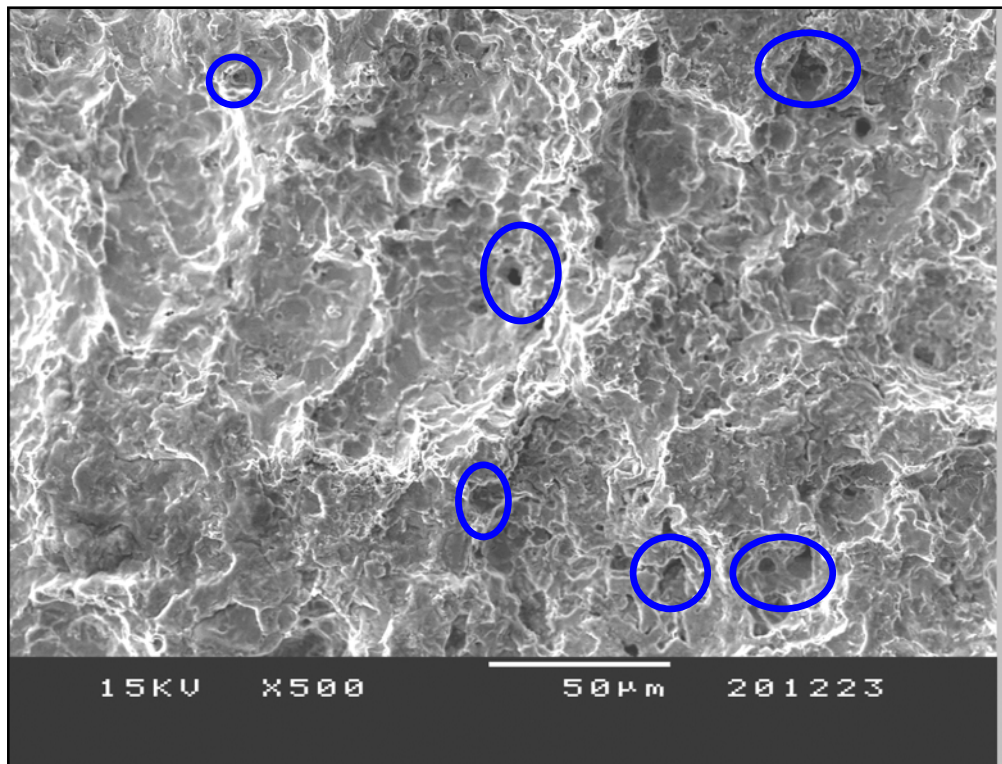


Figure 30. After 10 minutes Hydroblasting.

○ Clean pocket.

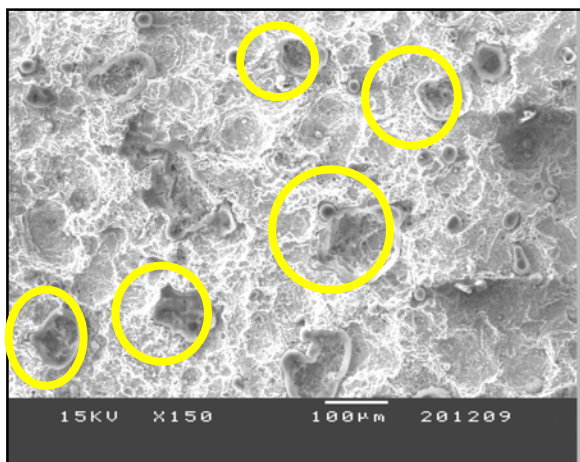


Figure 31. After 4 hours (X150).

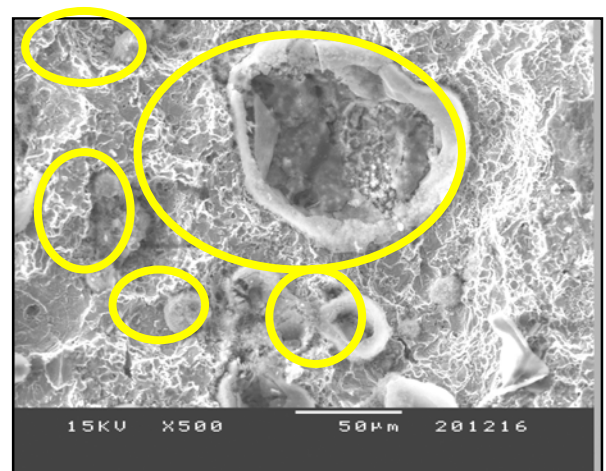


Figure 32. After 4 hours (X500).

○ Light flash rust.

8. CONCLUSION

The current effort seeks to demonstrate the importance of whole view for a big maintenance painting procedure where hydroblasting was introduced as a new surface cleaning process. Also was demonstrated the high quality of the surface preparation, that means much longer lifetime for paintings.

There was also demonstrated the possibility to follow the sequence established in whole MS Project and to maintain also the programmed budget.

We also demonstrated that only 22,1% of the budget was designed for paint supply; this means that the rest, 77,3% of the total budget cost for a good surface preparation, will means a huge responsibility for the contractor. Geographical localization, marine and industrial contamination have to be considered for a better understanding in the procedure of surface preparation and the painting process. As discussed by Lydia Frenzel et al (1999) “to make water work in a project, you have to understand that Three Viewpoints must converge in bid specifications and they must all be represented in the negotiations and planning of the project. These points of view are – OWNER – CONTRACTORS – COATING MANUFACTURER. People are driven to include water by environmental, safety and economic consideration. They are not embracing water for the benefit of enhanced performance.” This is absolutely true! We tested these proposition!

9. ACKNOWLEDGMENT

Thanks to Aracruz Cellulose S.A. / ES – Brazil in special to Eng. Karen Medeiros Günther, Eng. Fernando Ramiro Martins Junior, Eng. Áureo Machado Neto responsible for Housekeeping/2000 Project, Mr. João Manoel Ventura Rodrigues responsible for all the hydroblasting security norms, Mr. Gil Ribeiro Peres, Mr. Sebastião Miguel da Silva and Eng. Gilmar Luiz Mattedi responsible for R&D Department and Eng. Edgar Becker – Revestodur Company. To Acquablast and to Mr. Leonardo Reis Milagres (typing and copilot) and also for all my family.

10. REFERENCES

- Frenzel, Lydia, “A Comparison of surface Preparation for coatings by waterjetting and abrasive blasting” - Proceedings of the 11th American Waterjet Conference, P.P. 645, Water Jet Technology Association, St. Louis, Missouri, 1999.
- Marcillo, M., Almeida, E., “Corrosion and Protection of Metals in the atmosphere in Ibero-merica”, Project MICAT, X.V 1/CYTED, 1998.
- Nunes, L. P. and Lobo, A. C., “Pintura Industrial”: *Na proteção anticorrosiva*. Rio de Janeiro - Brasil: Livros Técnicos e Científicos, 1994.
- Trotter, Luis Ortega, “15º Congresso Brasileiro de Manutenção”, *Hidrodecapagem: Um Novo Processo de Manutenção e Aspectos Ambientais*, TT118, September 18-22, 2000, Vitória – ES, Brasil.

DEVELOPMENT OF A GENERIC PROCEDURE FOR MODELING OF THE WATERJET CLEANING

K. Babets, E.S. Geskin
New Jersey Institute of Technology
Newark, NJ

ABSTRACT

A practical procedure for utilization of available information, both numerical and linguistic, for identification of the operational conditions of the waterjet cleaning is presented. Neural Networks based prediction models were constructed using previously available information. The model constituted a knowledge base of the procedure. Then a single parameter, the erosion strength was determined experimentally or by the use of an expert knowledge. The fuzzy logic technique enabled us to determine weight of each preliminary constructed model for the process in question. Thus the first approximations of the operational conditions are determined. In the course of further operation the developed model is improved. The developed procedure will assist a practitioner in the selection of a decontamination technology for an unknown surface.

1. INTRODUCTION

The effective material decontamination is one of the major industrial concerns nowadays. It is difficult to imagine a single manufacturing process where material decontamination is not involved at some level. The technology includes such important and vital issues as disinfecting and wound cleaning in hospitals and extends to road deicing, maintenance of building and bridges, paint stripping from aircrafts, and etc., etc., etc.

Currently, the most usable approach for material decontamination involves chemical cleansers. The technology of chemical cleaning is very well studied and understood. Chemical cleansers are comparatively inexpensive, in many cases readily available and extremely effective. The problem with chemical cleansers is that they are potentially hazardous to worker's health and environmentally unfriendly. These and other problems with chemical cleansers (such as disposal of used agents, separation of debris from cleaning agents, etc.) demand an application of alternative methods for effective material decontamination based on physical coating removal technologies.

Physical coating removal technologies take advantage of differences in physical properties between the coating and the substrate to destroy the bonding and/or abrade the coating from the underlying substrate. Physical coating removal technologies use one or more of four general types of physical mechanisms (USPA, 1994):

- Abrasive technologies wear the coating off with scouring action.
- Impact technologies rely on particle impact to crack the coating to remove it.
- Cryogenic technologies use extreme cold to make the coating more friable and induce differential contraction to debond the coating.
- Thermal technologies use heat input to oxidize, pyrolyze, and/or vaporize the coating.

These technologies include but not limited to: plastic media blasting, wheat starch blasting, sodium bicarbonate wet blasting, high pressure water blasting and cryogenic blasting. It is clear that the water blasting constitutes the most effective technology. Water is readily available, comparatively inexpensive, and induces no damage to environment. The complete separation of water and debris facilitates material recovery. Therefore complete pollution prevention is feasible.

Although numerous extensive studies of waterjet-based material cleaning have been implemented, and this topic is a current topic of many researchers, there is no a universal technique that will allow practitioners to bridge the gap between the available information about the process (numerous case studies, etc.) and a current need of a practitioner to remove a specific contaminant from a specific deposit. This difficulty renders the process unusable for most practical applications. Therefore a goal of this research to implement such a modeling tool that will assist in practical implementation of such a technology.

2. DEVELOPMENT OF A GENERIC MODELING TOOL

The experimental studies of material decontamination enabled us to identify the range of the application of waterjet technology for surface cleaning as well as to acquire a database for development of modeling and optimization techniques. The theoretical study resulted in the development of corresponding algorithms and computer codes. However, the ultimate goal of the process investigation is to provide practitioners with an effective and practical approach for processing all information available to practitioner, regardless of the form and accuracy. First, a generic and easily obtainable coefficient characterizing any substrata - to be cleaned - deposit -to be removed must be identified and explained. Second, a generic modeling procedure, utilizing this surface coefficient must be identified and constructed. And, finally the suggested procedure must be tested on several experimental samples with different types of deposits.

2.1 Determination of the Erosion Strength

In our work the following approach was used to obtain a generic coefficient that would characterize any combination of substrata and deposit. Following the results available in the literature (Conn A.F., 1990) we define the area cleaning efficiency E_a as the ratio of area cleaned per unit time and power delivered by the nozzle (4).

$$E_a = \frac{\text{Area cleaned per unit time}}{\text{Power delivered by nozzle}} = \frac{\dot{A}}{P} \quad (4)$$

where area cleaning rate A is in m²/hour, and

$$P = \Delta p \cdot Q \quad (5)$$

where : Δp – pressure drop across nozzle,
 Q – is the flow rate;

Thus E_a has the units of [m²/Kw-hr], that is a unit area cleaned per unit of energy expended by the nozzle.

The idea of characterizing a material's ability to resist erosion is far from new. Thiruvengadam (1967) in his studies of cavitation erosion has suggested a concept of erosion strength that was based on a strain-energy absorption concept. Heymann (1970) has suggested a concept of relative erosion strength. Thus utilizing ideas of both Thiruvengadam and Heymann, Conn A.F., (1990) relates the area cleaning rate, \dot{A} , an erosion strength for cleaning S_c and an erosive intensity I , for a given waterjet nozzle and fixed set of waterjet parameters (water pressure, traverse rate, angle of impingement, standoff distance, etc.,) as:

$$\dot{A} = \frac{I}{S_c} \quad (6)$$

or

$$E_a = \frac{I}{P \cdot S_c} \quad (7)$$

Combining expressions 4 and 7 results in

$$E_a \propto S_c^{-1} \quad (8)$$

The relation 8 is the basic relation, used to derive the curves, representing the dependence of the area cleaning efficiency E_a and erosion strength for cleaning S_c (Figure 1).

2.3 Determination of the Erosion Strength based on the Available Cleaning Examples.

The available experimental database reflecting material decontamination with pure waterjet was compiled, and the area cleaning efficiencies were calculated for deposit types given in Table 1. The data in Table 1 was used to derive the relationships between area cleaning efficiency E_a and erosion strength for cleaning S_c (Figure 1). The point of departure for the line 276 - 310 MPa in Figure 1 was the data for Item 1 from Table 1. The calculated cleaning efficiency for removal of deposit Epoxy #1 was assigned an Erosion Strength $S_c=10^3$, relative units. This line, per relation (8) was plotted at a slope 1:1 on log-log chart. The rest of the data points on line 276-310 MPa were located based on calculated area cleaning efficiencies and working water pressure.

Table 1. Cleaning Examples

Item	Deposit	WP	ND	Flow Rate	Area Cleaning Rate	Power Delivered by Nozzle	Area Clean Effect
	Type *	(MPa)	(mm)	m3/sec	(m2/hour)	Kw	m2/Kw-hr
1	Hard Epoxy	276	0.305	4.610E-05	0.52	12.71	0.0408
2	Hard Epoxy	138	0.305	3.260E-05	0.04	4.50	0.0085
3	Hard Epoxy	103	0.3556	3.837E-05	0.02	3.97	0.0048
4	Rust	310	0.254	3.391E-05	0.99	10.52	0.0938
5	Weak* Rust	310	0.1778	1.662E-05	0.52	5.16	0.1040
6	Oil Based	138	0.254	2.262E-05	0.69	3.12	0.2201
7	Oil Based	69	0.254	1.599E-05	0.17	1.10	0.1541
8	Weak Epoxy*	276	0.3554	6.259E-05	1.04	17.26	0.0603
9	Auto Paint*	138	0.254	2.262E-05	0.14	3.12	0.0434

- Deposits were used for model testing only.

To derive line for 138 MPa (Figure 11) items 1 and 2 were compared. Since the Erosion Resistance for the deposit type Epoxy #1 is known ($Sc=1000$ relative units) and is constant, the first point for line 138 MPa thus could be located. Similarly to derive the line for 70-100 MPa item #6 was located at the 138 MPa line and compared with item #7.

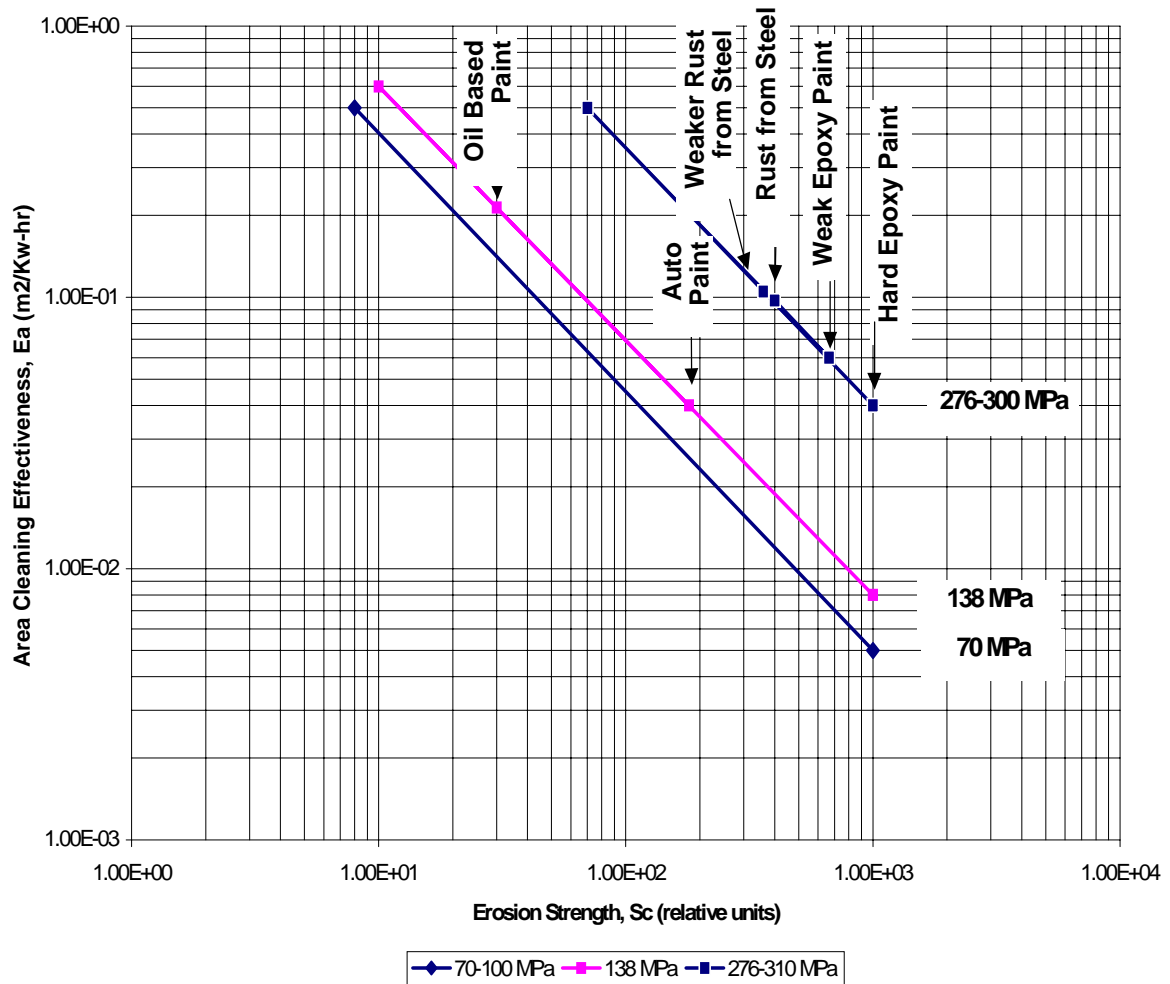


Figure. 1 Graphical Relationship Between E_a and Sc

The main result that could be inferred from the Graphical Relationship between the Area Cleaning Efficiency E_a and Erosion Strength Sc shows that there is a definite relationship between E_a and Sc and that Erosion Strength for cleaning of similar materials is closely spaced together, and consequently the Sc coefficient can be used to characterize an unknown deposit-substrata combination. On the other hand, it should be emphasized, that relations in Figure 1 as was presented by Conn (1990) and verified by our experimental studies do not constitute an exact relation, at best they represent an order of magnitude comparison only.

3. DEVELOPMENT OF GENERIC PREDICTION TECHNIQUE

The problem, that most of the waterjet practitioners face when dealing with an unknown surface is the lack of information about the process or in other words the unavailability of a generic technique that could be used as a first approximation of a process. This section is concerned with the development of such an approach. The idea behind such an approach is to combine the previous knowledge about the process in question and based on that, make an inform decision as to which waterjet parameters to apply, as a first approximation. We are using the notion of Erosion Strength (Sc) developed in the previous section to classify an unknown surface together with Neural Networks Fuzzy Reasoning technique, suggested by Takagi et al. (1991), for information processing.

The prediction technique construction begins with the development of fuzzy universe for Erosion Strength, Sc . The experimental database allows us to construct three fuzzy sets, based on the number of experimental situations available. The items 1,2,3,4,6,7, representing the removal of three basic deposit types (Hard Epoxy, Rust and Oil Based Paint) from Table 1 with corresponding Erosion Strengths 1000, 400 and 30 (from Figure 1) were assigned the degrees of membership of unity in either of three sets. Then the working space of the universe for Sc on a semi log scale was equally divided between the tree classes, as shown in Figure 2.

Thus each of the classes in Figure 2 is represented (with degree of membership 1) by a specific deposit type available in our experimental database. In other words these three fuzzy sets cover the ranges of all possible values for the materials with erosion strength for cleaning from 1 to 10000 relative units. Similarly, if we identify a deposit substrata combination with some value of erosion strength, Sc , and this value happens to be inside the range [1,10000], then we can identify the degree of membership of such a deposit substrata combination in the three fuzzy sets (Figure 2). This procedure alone can be very useful when trying to classify some unknown deposit-substrata combination.

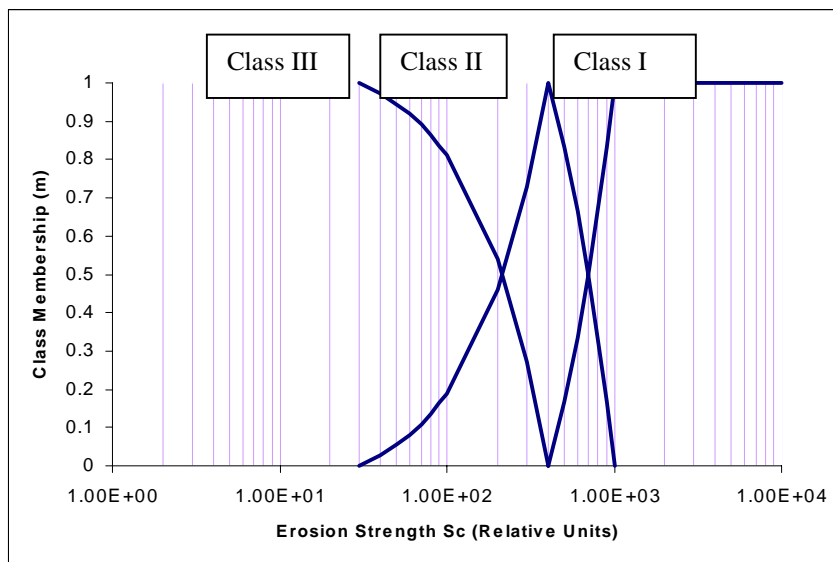


Figure 2. The Fuzzy Universe for Erosion Strength, Sc .

It should be emphasized that for each of the three basic deposits an extensive experimental study was undertaken. Since we possess a required empirical knowledge for these processes, the appropriate numerical representation of each process can now be made with the help of artificial neural networks. The procedure of the application of a neural network for process modeling and optimization was described earlier (Babets, Geskin, 1999). Thus, after each network has been created, properly trained and tested we have obtained reliable numerical models for the three base deposits, or equivalently three fuzzy base classes of the universe Erosion Strength (Sc). Therefore, it can now be stated, that a process of material cleaning of material with erosion resistance coefficient in the range $[1, 10000]$ can now be approximated as some combination of the base models. The computational procedure follows the following steps. For an unknown deposit, a practitioner makes a simple experiment that allows him to calculate Area Cleaning Efficiency for a working water pressure. Then using the computed E_a we can determine the corresponding Erosion Resistance coefficient (Sc) for this surface from the Figure 1, for the given water pressure. Once a corresponding Sc coefficient was found, the fuzzy membership in the three classes on Figure 2 can be determined. The above procedure can be described on example of the item number 8, Table 1. Separate experiments were made for the auto paint deposit removal with plain waterjet. The computed area cleaning efficiency was calculated as $E_{a \text{ auto paint}} = 0.04 \text{ m}^2/\text{Kw-Hr}$. From Figure 1 the corresponding coefficient Sc was found to be $Sc=180$ relative units. And from Figure 2, the degree of membership (μ) in the three basic classes can be calculated as $\mu_{(\text{class I})} = 0$, $\mu_{(\text{class II})} = 0.4$, $\mu_{(\text{class III})} = 0.59$. These degrees of membership can be interpreted as follows. The Erosion Resistance of the Auto Paint deposit is approximately midway between that of the Hard Epoxy Paint and rust deposit. Now that the surface was identified we could use the base models given by the neural networks to get a first approximation to the process. We supply a set of input parameters (Water Pressure, Nozzle Traverse Rate, Nozzle Diameter, and Standoff Distance) as an input into the base models represented by the neural nets. The corresponding output in terms of the single strip width is obtained by each of the network. The final result is obtained by defuzzifying the output according to Eq. 9.

$$y_i^* = \frac{\sum_{s=1}^r \mu_{A^s}(x_i) \cdot u_s(x_i)}{\sum_{s=1}^r \mu_{A^s}(x_i)}, i = 1, 2 \dots n \quad (9)$$

In equation 9, μ - is the membership value of a deposit with Erosion Strength Sc in the three base classes, U_s - is the output of the s^{th} neural network, and y^* is the final defuzzified output.

The output of the model is the single clean width of the strip produced on the surface by the supplied combination of the input parameters, which then can easily be converted to process productivity. This procedure is sketched on Figure 3.

4. EXPERIMENTAL VERIFICATION OF PERFORMANCE

In order to experimentally verify the suggested modeling approach an additional experimental database was acquired. The experimental samples consisted of the three types of deposits - auto paint, weaker rust, and weak epoxy paint, (items 5,8,9 Table 1). Waterjet parameters varied in these additional experiments were limited to the water pressure, nozzle traverse rate, standoff distance, and nozzle diameter. Experimental setup and procedures were similar to those described in the previous chapters. Area cleaning efficiencies for removal of these deposits was used to identify the corresponding erosion resistance coefficient from Figure 1, and the degrees of belonging of these deposits to the three base classes were identified with the help of Figure 2. Table 2 shows the results for the test deposits along with the deposits representing the base classes.

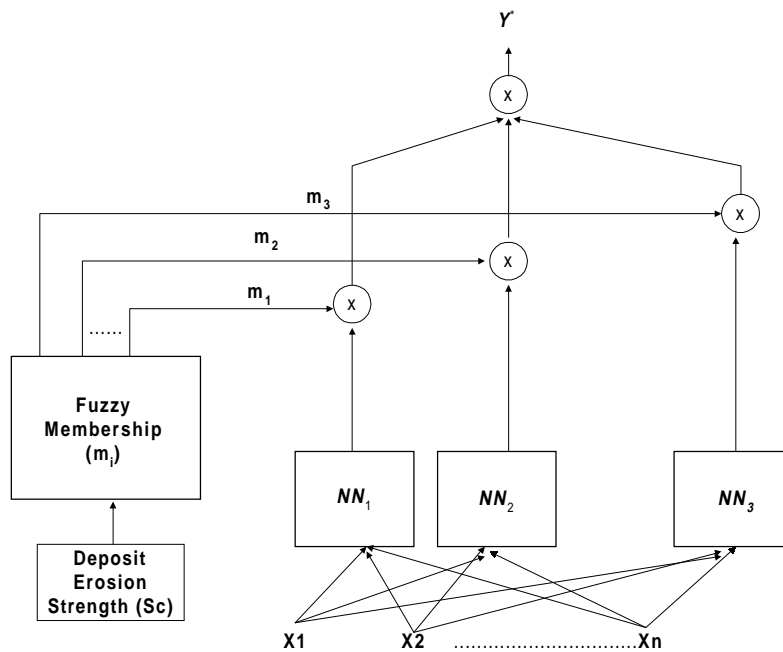


Figure 3. Generic Modeling Approach.

NN1, NN2, NN3 - Artificial Neural Network models for the three base classes.

X1, X2, ..., Xn - Process input variables.

The model performance was tested on each of the test deposits by providing the model with a set of waterjet input parameters within the working space (delimited by equipment capabilities), obtaining the corresponding output in terms of the single width of strip and comparing the results with experiments.

Table 2. Cleaning Samples

N	Deposit	Area Cleaning Efficiency (m ² /Kw-hr)	Erosion Strength (Relative Units)	Degree of Membership		
				Class I	Class II	Class III
1	Hard Epoxy Paint	0.04	1000	1	0	0
2	Weak Epoxy Paint	0.06	665	0.41	0.58	0
3	Rust from Steel	0.0975	400	0	1	0
4	Weaker Rust from Steel	0.105	360	0	0.89	0.1
5	Auto Paint	0.04	180	0	0.4	0.59
6	Oil Based Paint	0.21	30	0	0	1

5. DISCUSSION OF RESULTS

The model for prediction of the results of waterjet cleaning described in the previous sections was tested on several additional test deposits. Figures 4 - 9 present the results of prediction. Analyzing the results, it is clear that the model prediction results are acceptable at both relative error of prediction (~20 %), and at following the trend of the process, which is also important for any cleaning study. Although a relative error of prediction may at the first glance be considered high, it should be kept in mind that standard deviation of experimental measurements was in the vicinity of 25 ~ 30 %, and it really is difficult to expect the model performance to be more accurate than that. Nevertheless, as a first estimation of a cleaning productivity for a given type of deposit, these results constitute a reasonable approximation. Furthermore, since it is shown that the model is also capable of predicting the trend of the process, meaning that the change in one independent input results in, say, increase of the output, allows using this model for the process optimization. We suggest using the Genetic Algorithms for this purpose.

However it should be noted, that at the current stage the prediction technique was tested only in the middle of the problem space. At the outskirts of the problem space the veritable results could not be obtained. The reason for this lies in the limitations in the development of the three base models. Since the ranges of experimental parameters used for the construction of models were different in each case, and there was no coordinated experimental setup, but rather the data was compiled at later stages, there are inconsistencies in choosing the levels of process parameters in case of a test cleaning space. These inconsistencies are due to the poor ability of neural networks to extrapolate. For example, if for a base model development the rate of nozzle traverse was in the range from 1000 mm/min to 2500mm/min, and a test cleaning case was run at 1500~4000 mm/min, the reliable model performance will be in the intersection of these ranges. The way to cure the above problem is to cover all the parameter space (limited by equipment capabilities) for each process variables in all the base models. Of course it results in quite extensive experimentation, but on the good side it needs to be done only once, when developing the base

models. Also the current model does not cover the full range of all possible erosion strength of different materials, but by extending the procedure with additional base models for lower or higher degrees of erosion strength for cleaning (Sc), this limitation can be reduced or eliminated.

6. REFERENCES

- Babets, K., Geskin, E. S., Chaudhuri B. 1999. "Neural Network Model of Waterjet Depainting Process", *10th American Waterjet Conference*, Houston, TX.
- Babets, K., Geskin, E. S. 1999. "Optimization of Jet Based Material Decontamination", *International Symposium on New Applications of Water Jet Technology*, Ishinomaki, Japan.
- Conn, A., 1990. "A Relative Cleanability Factor", *Proceedings of 10th International Symposium on Jet Cutting Technology*, BHRG Fluid Engineering.
- Conn, A., Chahine, G., 1995. "Ship Hull Cleaning with Self-Resonating Pulsed Waterjets", *Third American Waterjet Conference*, Pittsburgh, USA
- Takagi H, Hayashi I. 1991. "NN-Driven Fuzzy Reasoning." *International Journal of Approximate Reasoning*, Vol. 5, No. 3, pp. 191 – 212.
- Thiruvengadam, A. 1966. "The Concept of Erosion Strength." *Erosion by Cavitation or Impingement*, American Society for Testing and Materials, ASTM.
- United States Environmental Protection Agency, Office of Research and Development. 1994. "Guide to Cleaner Technologies." *EPA/625/R-93/015*, Washington DC 20460.

7. FIGURES

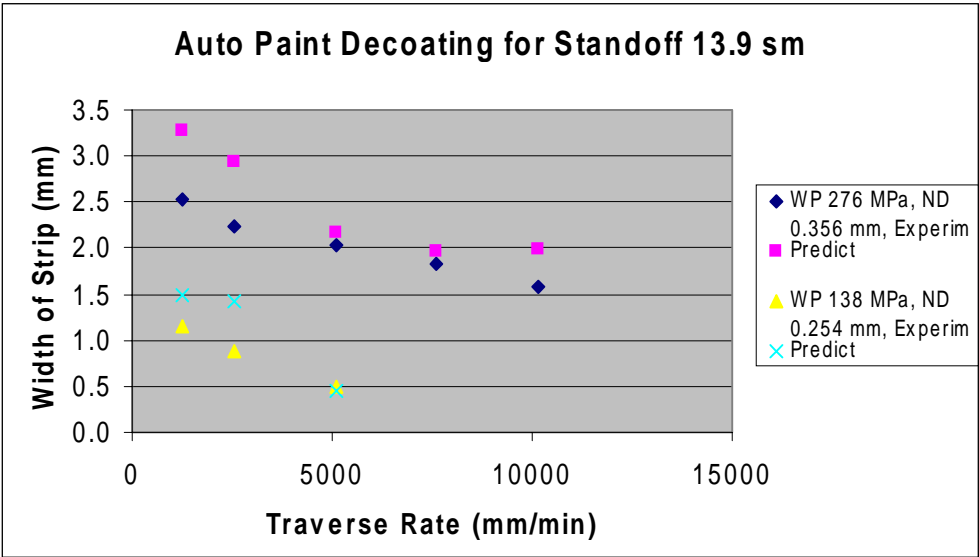


Figure 4. Auto Paint Removal

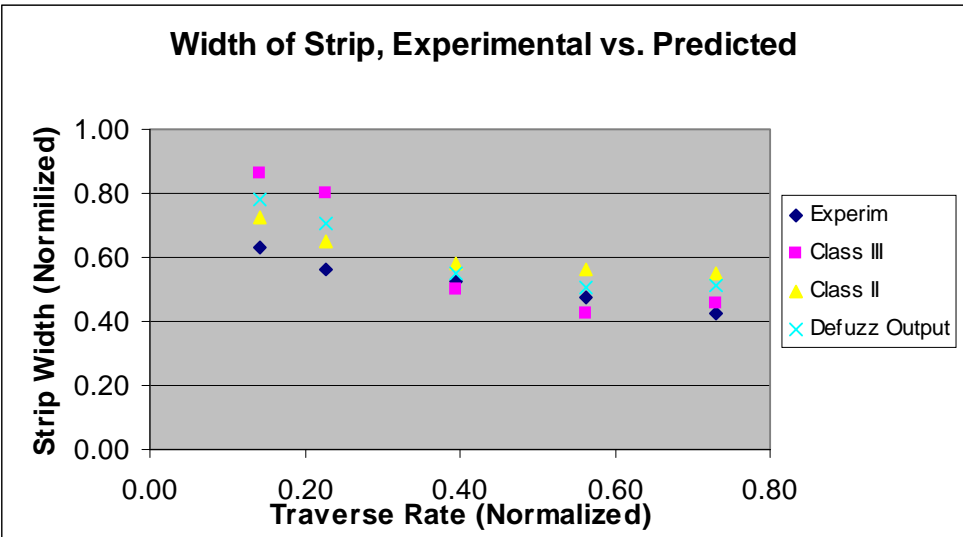


Figure 5. Auto Paint Removal

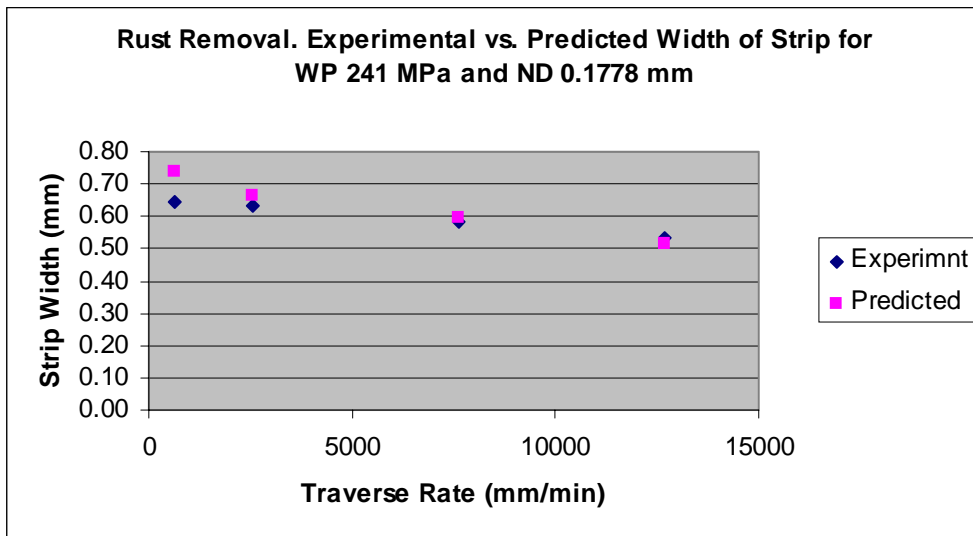


Figure 6. Removal of Weak Rust

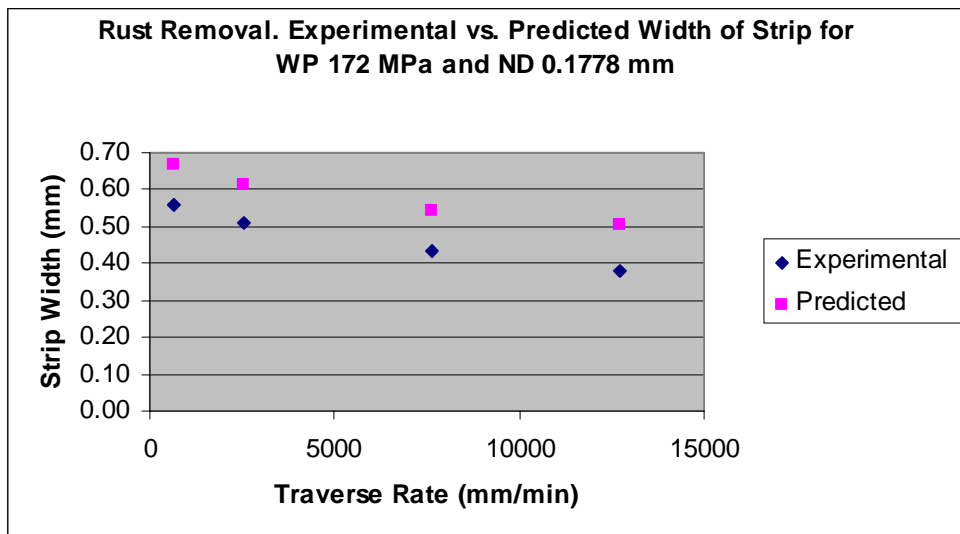


Figure 7. Removal of Weak Rust

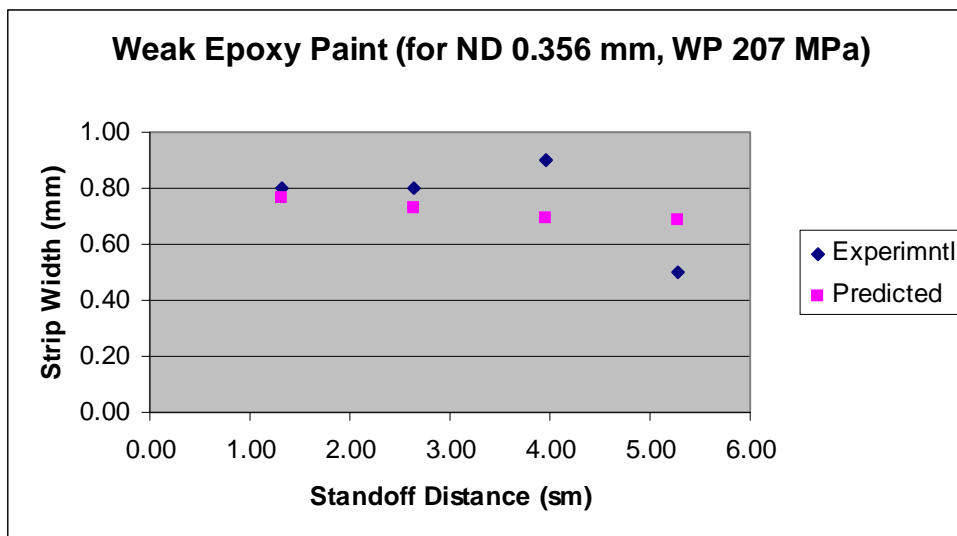


Figure 8. Removal of Weak Epoxy

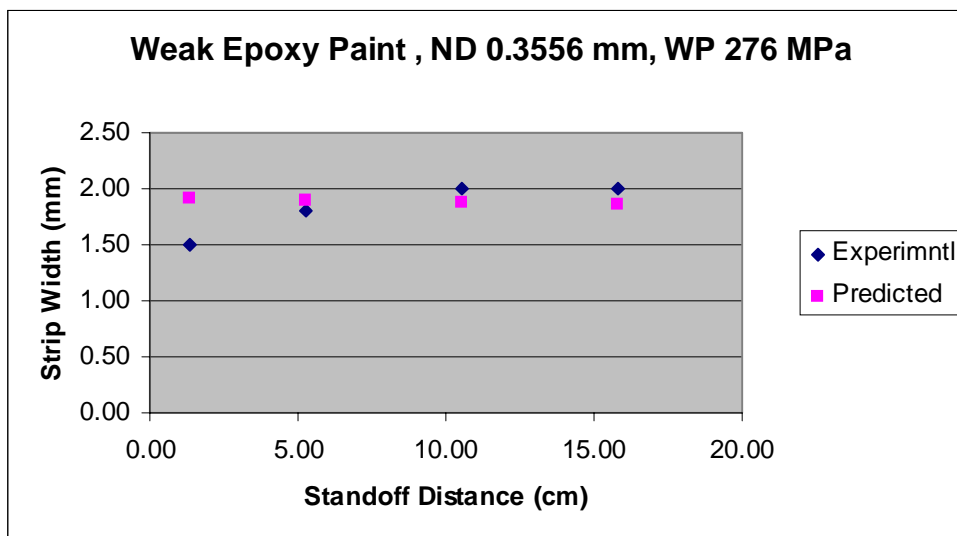


Figure 9. Removal of Weak Epoxy

THE DEVELOPMENT OF IMPROVED HIGH PRESSURE VALVES

G. G. Yie
Jetec Company
Grants Pass, Oregon

ABSTRACT

In order to circumvent the well-known shortcomings in performance, ease of operation, and reliability of existing valves available for high-pressure water jetting applications, a new valving method has been developed. This method involves the use of a pilot fluid circuit to operate a floating valve poppet situated in a cavity for controlling the fluid flow through an inlet and an outlet. The movement and the position of this valve poppet in respect to the outlet port determines the flow continuity. The energy contained in the fluid is utilized to move the valve poppet and to open and close the outlet port. This method is utilized to construct a variety of valves that have features well suited for high-pressure water jetting applications. This paper describes the unique features of these valves.

1. INTRODUCTION

An on-off valve is an important component in all fluid systems; it allows the fluid flow to stop and start in a way similar to a switch in an electrical system. At low fluid pressures, there are many suitable valves for both liquid and gas operations. These valves are commonly identified by their mode of operation or by the shape of the key valving element involved, such as cock valves, ball valves, butterfly valves, poppet valves, needle valves, and stem valves. By moving the key valving element with an external force, the valve port will be opened or closed. The required external force can be supplied by human hand or foot, compressed air, hydraulic oil, or electrical means.

When the fluid pressure is increased, the stresses created by the fluid inside the valve cavity increase accordingly. As a result, many on-off valve designs are no longer suitable for various reasons. At fluid pressure above 690 bar (10,000 psi), for example, the usable valves are limited to some ball valves, stem valves, and needle valves. At such pressures, a fluid such as water can cause erosion on metal during the on-off operation if the valve port is opened or closed slowly. Needle valves, for example, are used widely in high-pressure fluid operations in which the valve needle is raised or lowered slowly into the valve port such that serious erosion of the needle and valve port can occur at very high fluid pressure. It is much preferred that such valve port be opened and closed quickly. Unfortunately, a manual rotating valve can be turned by human hand only a quarter turn at a time and high-pressure valves require the use of fine threads to operate the valve needle.

To instantly open or close a valve has its problems at high fluid pressures. One is the high external force required to operate the valving element. At very high fluid pressures, the external force must be raised to a high level in order to overcome the fluid induced forces inside the valve cavity such that manual operations become difficult or impossible. The other is the metal fatigue from the constant pounding between the valving elements. And yet, many waterjetting processes today are operating at pressures well above 690 bar (10,000 psi) and many applications require that an on-off valve be operated by human hand reliably and safely at high on-off frequencies. As a result, there are problems.

2. STATE OF THE ART

At present, manually-rotated stem valves and needle valves are commonly used in high-pressure fluid systems. In such valves, a valve stem or needle is raised or lowered against a mated valve port with a rotating handle. The process is slow and the valving elements can be subjected to severe erosion at very high pressures. Once erosion occurred, the valve may be subjected to extreme torque in closure, thus resulting in metal deformation and further damage to the valving elements. Therefore, existing high-pressure manual valves are not suitable for use that requires frequent on-off operations.

When instant manual on-off operations are required, such as in waterjetting processes, the selection of suitable valves is limited to stem valves and ball valves at pressures up to 1380 bar (20,000 psi), and only the stem valves at pressures above 1380 bar. There are hand-operated so-called “dump” valves in use today at pressures up to 1380 bar but they are leak-prone, difficult to use, and have poor

reliability. There are no reliable and easy-to-use hand-operated shutoff valves in the market today for use at water pressures above 1380 bar. For example, there are no toggle valves for high-pressure waterjetting operations.

A common approach for providing instant on-off operation in a valve is to use an air-operated actuator to supply the force required for moving a valve stem. There are several such valves available for waterjetting at pressures up to 3800 bar (55,000 psi); all of them are based on the stem-valve design in which a slim valve stem is moved against a valve port by the force from the air actuator. One end of this valve stem is situated inside a valve cavity and is mated with the valve's outlet port while the other end abutts the piston rod of the air actuator. When the fluid pressure is low, the fluid-induced force on the valve stem is also low and the valve stem can be moved easily. When the fluid pressure is very high, the fluid exerts tremendous force on the valve stem in the outward direction. To push the valve stem toward the valve's outlet port requires an external force greater than the fluid induced force. For example, if a valve stem of 2 mm (0.078 inches) in diameter is exposed to 3800-bar (55,000 psi) water in a valve cavity, the valve stem is subjected to a pushing force of about 120 kg (263 lb). To close this valve, the air actuator must supply a pushing force significantly greater than 120 kg on the valve stem until it engages the valve port and seals the outlet.

The example valve reveals several conditions that are vital to the valve's performance. The 120-kg (263-lb) force is much more than what human hand can supply, thus eliminating the possibility of operating this valve by hand. With an air actuator at say 4 bar (60 psi), the piston must be of sufficient size (2.5 inches in diameter) in order to supply the required force. The magnitude of this force is high for the slim valve stem involved if the stresses are of concern. Finally, the valve's outlet port must be considerably smaller than the diameter of the valve stem, thus limiting the flow capability of the valve. Today, a typical 3800-bar (55,000 psi) air-operated on-off valve has a 2-mm (0.078-inch)-diameter valve stem and a 1.1-mm (0.045-inch)-diameter valve outlet port. To increase the valve's outlet port would require the use of a larger valve stem, which can be operated only by using a larger or more powerful air actuator. Today, air-operated on-off valves used in field waterjetting process typically have 178-mm (7-inch)-diameter air actuators.

In addition to the bulkiness and low flow capability, currently available air-operated instant on-off valves are leakage prone due to several reasons. One reason is that closure of the valve outlet port depends purely on the external force applied to the valve stem. This force must be sufficiently greater than the fluid force and the valve stem must mate well with the valve port if positive closure is desired. If the valve is operated at a high frequency, the valve stem will pound on the valve port frequently, thus creating fatigue problems. Another reason is that the external force is applied directly and abruptly to the valve stem such that force alignment and water-hammer effect can be problems.

In short, all currently available manually operated or powered high-pressure on-off valves, and particularly instant on-off valves, have performance and reliability problems when they are used under today's waterjetting pressures; improved valves have been in need for quite some time. Jetec Company has been aware of this situation and has devoted considerable effort in developing better

valves as evidenced by the six U.S. patents on valves granted to date. This paper describes Jetec's most recent and most successful effort in the valve development project.

3. JETEC'S SOLUTION

Jetec's new valve involves the use of a floating poppet to open and close an outlet port, a fluid circuit to aid the operation of the valve poppet, and the utilization of fluid force to move and to seat the valve poppet. The valve poppet is situated entirely inside the valve cavity and straddles across two separate fluid chambers, as shown in Figure 1. The lower chamber is the main fluid chamber that has a fluid inlet and a fluid outlet. The lower end of the valve poppet mates well with the valve seat of the outlet port. The upper chamber is called the actuating chamber as it is responsible for moving the valve poppet. The two chambers are separated by a poppet seal. The valve poppet has a central fluid passage equipped with a check valve and a parallel side passage that connects the two chambers at all times. There is a fine actuating pin having one end in contact with the central passage of the valve poppet and the other end in contact with a source of external force. There may be an internal bias spring that urges the valve poppet to be detached from the valve's outlet port.

This valve can be a normally-closed one if a constant external force is applied to the actuating pin that pushes the valve poppet down to close the outlet port. When a pressurized fluid enters into the valve, it flows into both lower and upper chambers and exerts force on the upper end of the valve poppet to close the outlet port tightly. This force can be very substantial if the fluid pressure is high, the valve poppet is quite large, and the valve port is only slightly smaller than the valve poppet. Since the seating of the valve poppet is basically accomplished by the fluid force, the closure of the outlet port will never be in doubt. If the outlet port is in a conical shape, the valve poppet must seal the port at its upper circumference and its diameter should be somewhat smaller than the diameter of the valve poppet. Consequently, there will be a prescribed surface area of the valve poppet's lower end that will be exposed to the pressurized fluid when the outlet port is closed by the valve poppet. This surface area supplies the fluid force necessary for opening this valve.

As an example, if the valve poppet has a diameter of 8 mm (0.312 inches) and the sealing circle around the outlet port is 6.4 mm (0.250 inches) in diameter, the valve poppet will be pushed down against the valve seat by a fluid force in the actuating chamber of about 695 kg (1,530 lb) if the water pressure is 1380 bar (20,000 psi). In the lower chamber, a fluid force of about 249 kg (548 lb) is pushing the valve poppet upward. Therefore, the net valve closure force is about 446 kg (982 lb). This force is sufficiently large to assure positive valve closure.

As the valve is closed, the actuating pin seals the central passage of the valve poppet. The external force is responsible for this sealing duty. Since the passage is small and the actuating pin has a conical shaped tip, the required sealing force is quite small. A slight leakage here will not affect the closure of the valve. For example, if the actuating pin has a diameter of 2 mm (0.078 inches) and the fluid pressure is 1380 bar (20,000 psi), a force of 45.5 kg (100 lb) applied to the external end of the actuating pin would move the pin and seal the fluid passage.

To open the valve requires the removal of the external force or the application of a counter force to overcome the existing force on the actuating pin. As a result, the pin is moved away from the valve poppet, thus exposing the central passage of the valve poppet. The fluid in the actuating chamber quickly loses its pressure and the fluid force in the lower chamber quickly moves the valve poppet upward, thus opening the valve port. The presence of the check valve inside the valve poppet makes sure that the fluid will not flow upward through the central passage once the outlet port is open. The bleed passage inside the valve poppet is deliberately made small such that the fluid pressure inside the two chambers will not be equalized quickly. Once the valve poppet's lower end is detached from the valve seat, it is exposed to the fluid completely. Thus the valve poppet is pushed upward by the full fluid force until it reaches its upmost position. There will be no hesitation as the valve-opening fluid force is very substantial. Using the earlier example, the initial valve-opening force is about 249 kg (548 lb) and is increased to about 695 kg (1,530 lb) quickly. Since there is fluid in the upper chamber, the valve poppet is well cushioned and there will be no bang whatsoever.

Once the valve is open, the fluid pressure inside the two chambers is equalized. The valve poppet will stay at its high position as the actuating pin is fully retracted. The pressurized fluid will flow through the main valve cavity from the inlet to the outlet. Since the outlet port can be quite large, the pressure drop through the valve is negligible. The outlet port can be as large as 5 mm (0.200 inches) in diameter if the valve poppet has a diameter of 8 mm (0.312 inches). It is worthy to note that the diameter of the valve poppet in Jetec's new valves is not related to the diameter of the actuating pin. This means that the external force required for moving the actuating pin can stay small even though the valve's outlet port is very large. This is not at all possible with any existing valves.

To close the valve again. The external actuating force is resumed and the actuating pin makes contact again to the valve poppet and "gently" pushes it down until stopped by the valve seat. The fluid force then takes over and closes the outlet port tightly.

4. BENEFITS

The valve design described above is suitable for constructing on-off valves of many types for use with all types of fluids at a very wide range of pressures. It is particularly well suited for use at high fluid pressure because of high energy available for operating the valve. The benefits achieved by this valve design can be summarized as follows:

- High and wide pressure and flow capabilities.
- Positive opening and closure of the valve port by the strong fluid force.
- Absence of pounding between the valve poppet and the valve seat.
- Absence of destructive water hammer effect due to the piloted operation.
- Versatile design allowing various modes of operation.
- Compact size due to much reduced size of the valve actuator.
- Much improved reliability and reduced operating cost.

5. AVAILABLE TYPES

Jetec's new valve design has been applied for constructing several different types of valves for testing. An air operated on-off valve suitable for 2800-bar (40,000 psi) operations is shown in Figure 2. This valve has a 5-mm (2-inch)-diameter air piston operating at about 5.5-bar (80 psi) air and is mated with an actuating pin of about 2 mm (0.078 inches) in diameter. Increasing the air piston to 6.4 mm (2.5 inches) in diameter allows the valve to be operated at water pressures up to 3800 bar (55,000 psi).

By changing the actuating pin and by adding a pressure gauge as well as an air valve to the air-operated 2800-bar (40,000 psi) valve turns the on-off valve into an air-operated automatic pressure relief valve, as shown in Figure 3. The air actuator is filled with air up to a prescribed pressure that corresponds to the water pressure inside the valve that is designated as the operating pressure. When the water pressure exceeds this set pressure for whatever reasons, the valve will open automatically and let out water from the valve cavity. The valve will close again when the water pressure inside the valve falls below the set point. This valve can withstand frequent operations because of its unique features discussed previously.

A hand-operated normally-closed valve is shown in Figure 4. This valve has a die spring of prescribed rating pre-compressed to provide the force necessary to close the valve at the desired operating water pressure. A hand-operated lever is provided for supplying a counter force against the die spring so as to free the actuating pin of the valve. Once the force is removed, the water force inside the main cavity will then quickly open the valve. By virtue of Jetec's unique valve design, the force required for operating the lever is well within the capability of human hand. Holding the lever at the open position is made easy as the water inside the valve aids this effort. This valve is ideally suited for constructing handheld waterjet lances operating at pressures up to 2800 bar (40,000 psi). This normally-closed valve can be easily made into a foot-operated one by configuring the lever differently, as shown in Figure 5.

A hand-operated normally-open valve is shown in Figure 6. This is a so-called "toggle" valve commonly available for fluid systems at low pressures but not available for high-pressure applications until now. It is constructed by placing a die spring between the actuating pin and a cam actuator. The cam supplies a predetermined compression to the die spring, which then provides a prescribed force against the actuating pin to closed the valve. To open the valve, the cam actuator is rotated a quarter turn to release the spring compression. It is clear that the cam actuator does not touch the actuating pin directly, thus the pin is not subjected to unwanted stresses. Jetec's valve design allows such toggle valve be made and used for high-pressure fluid for the first time. Such toggle valves can find many applications in today's waterjet systems.

By removing the cam actuator from the valve and replacing it with a threaded cap to the spring cylinder, a spring-operated automatic pressure relief valve is created, as shown if Figure 7. The die spring is compressed to a predetermined level so as to provide the desired valve-closing force. When the water pressure inside the valve exceeds the set point, the valve will automatically open and let out the water. An ordinary 19-mm (3/4-inch)-diameter die spring can be used for constructing pressure relief valves suitable for use at water pressures up to 2800 bar (40,000 psi) because of the

unique features of Jetec's valve design. Until now, spring-operated pressure relief valves are not suited for waterjetting processes at high pressures; they are used primarily on car-washing systems.

Jetec's air-operated on-off valves are ideally suited for operating an abrasive waterjet nozzle, such as that marketed by Jetec, as shown in Fig. 8. By virtue of its reliability, it is perfect for high-cycle operations. Its piloted operation and absence of water hammer effect protect the hose and the orifice.

6. SUMMARY

A new valve design has been developed. Available data have shown that it is very well suited for use at high fluid pressures, such as waterjetting pressures. This design can be readily applied for providing valves of many types to serve different purposes. These valves will be made available for commercial applications shortly.

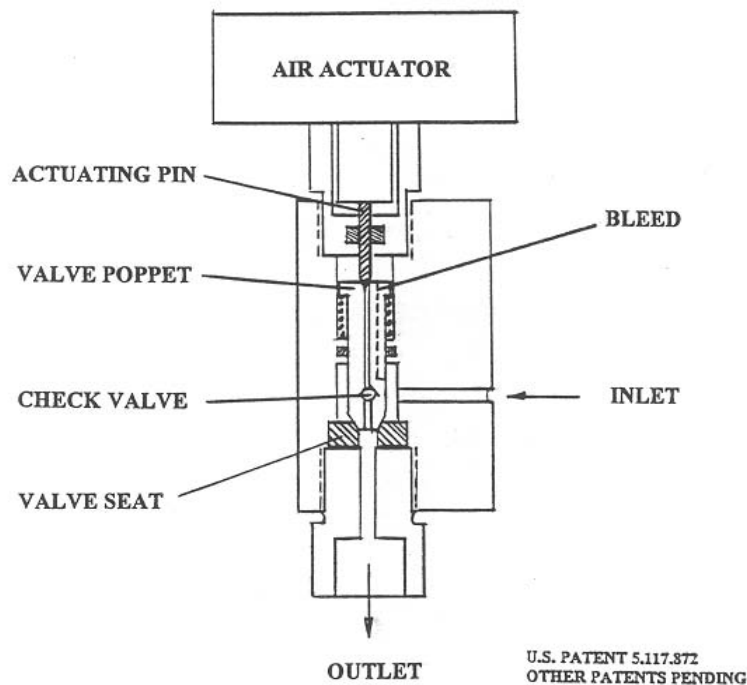


Figure 1. Schematic Drawing of Jetec's High-Flow On-Off Valve



Figure 2. An Air Operated 2800-Bar On-Off Valve

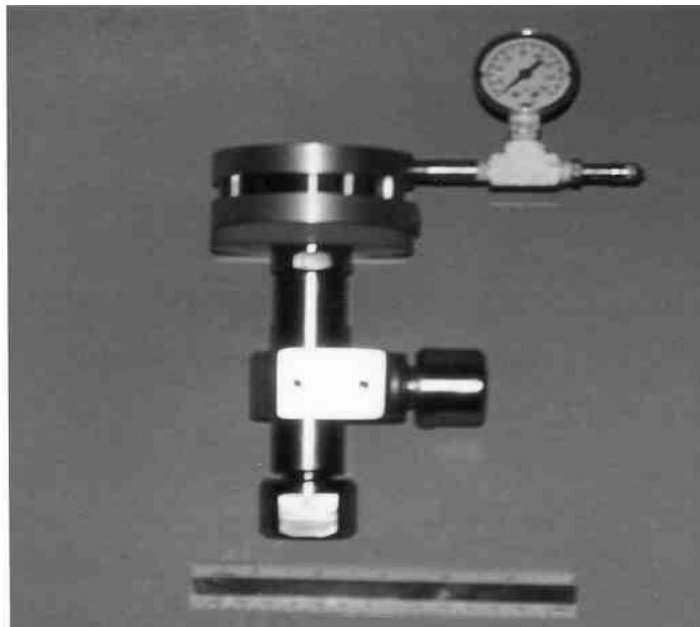


Figure 3. An Air Operated 2800-Bar Automatic Bypass Valve

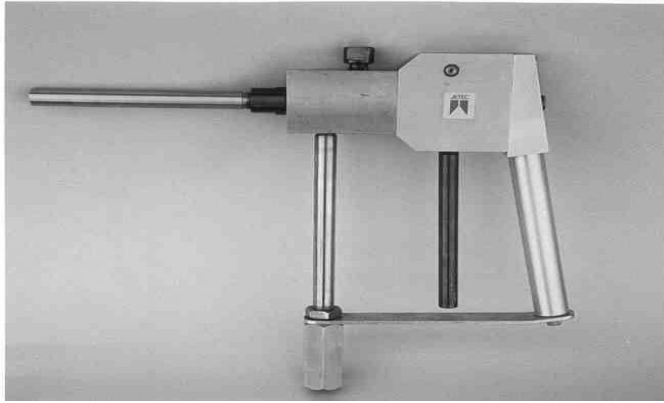


Figure 4. A Hand Operated Normally-Closed On-Off Valve

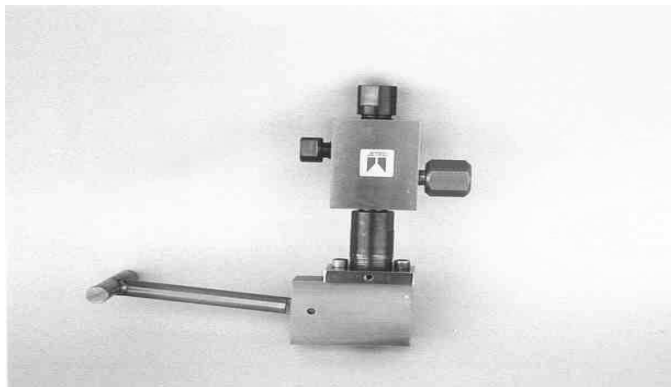


Figure 5. A Foot Operated Normally-Open On-Off Valve

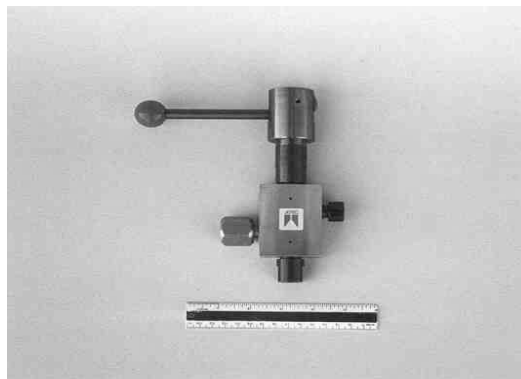


Figure 6. A Hand Operated Normally-Open On-Off Valve



Figure 7. A Spring Operated Pressure Relief Valve



Figure 8. An Air-Valve-Equipped Abrasive-Jet Cutting Nozzle Assembly

HYDRO-BALANCED PACKING SYSTEM FOR HIGH PRESSURE PUMPS

Michael T. Gracey P.E.
Weatherford ALS
Houston, Texas

ABSTRACT

A high-pressure packing system is being developed to handle the various products and fluids being moved by positive displacement pumps. The system to be described in this paper is a Hydro-Balanced Packing System designed to prevent the product being pumped from becoming exposed to the atmosphere and surrounding areas. Pressure of the product being pumped is transferred to a barrier fluid of known characteristics and good lubricating qualities. The water jetting industry generally uses water as the media for cutting, cleaning and abrading surfaces, but water is not a good lubricant. The possible benefits for the high pressure water jetting pump would be better packing life, plunger lubrication control and a decrease in environmental pollution. The technology can be built into new equipment or be retrofitted to pumps in service with the proper modifications and sealing assemblies. The technology has been tested on sucker rod pumps, hydraulic pumps and name brand positive displacement pumps. The hardware has been under development for several years and recent tests have proven its adaptability to various pump designs. The presentation is to include slides and graphics of the Hydro-Balanced Packing System and results on presently on-going tests.

1. INTRODUCTION

High-pressure pumps are used in many industries including water-jetting service. One area of development over the years has included better packing design and materials to be used at ever increasing pressures. The high cost of plungers and packing made of more exotic materials has also increased the cost of part replacement. The lubrication and cooling of the packing and plungers in these positive displacement pumps has included oil drip onto the plungers, grease in the stuffing boxes, force feed oil lubrication and water lubrication (cooling) of these components. The technology described in this paper is called the “Hydro-Balanced Packing System” and is being adapted to high-pressure pumps to improve packing life and efficiency. In a standard plunger / packing arrangement, the fluid being pumped is held by a set of packing which wears and usually destroys the plunger as part of the failure process. The Hydro-Balanced stuffing box has a transmitter / piston that sees the fluid being pumped and a primary set of packing that only sees the barrier fluid between these two seals. The barrier fluid can be chosen to accomplish the goal of lubrication or for its characteristics. Examples would be rock drill oil, food grade lubricant or biodegradable oil.

2. HISTORY

When an oil well is not flowing sufficiently, a means to pump the oil to surface that is called an “Artificial Lift System” or ALS is employed. The system may be a beam pump lift (sucker rod pump), reciprocating rod lift system, electric submersible pumping system, plunger lift system, gas lift system, progressing cavity pumping system or a hydraulic lift system. The hydraulic lift system uses a high-pressure pump in a surface power fluid unit to create a venturi effect down hole to pump the oil to the surface. The rod pump has a seal area at the surface that can leak product when the packing becomes worn, so this is where the subject of this paper was first developed. Also, the high-pressure positive displacement pumps used in the hydraulic lift systems are like the water blasting pumps used by members of the Water Jet Technology Association. Several of the manufacturers of water blasting equipment started by using oil field pumps to build their units and developed them into higher pressure pumps by replacing the fluid ends with their own designs. Later, some of the manufacturers of water blast equipment produced their own power frames to go with the high-pressure fluid ends. The next area of development of the subject of this paper was the packing in hydraulic pumps used in the hydraulic lift systems, which lead to the adaptation of the technology to higher-pressure pumps, and the present research described in this paper.

Mr. Harold Palmour started developing the idea of a balanced stuffing box back in 1994. Remote pressure transmitters were retrofitted to stuffing boxes on oil well rod pumps in eight Polk County, Texas wells to prevent pollution caused by leaking seals. The “Unitized” version (without the remote pressure transmitter) of the Hydro-Balanced Stuffing Box was first used on an oil well in Luling, Texas in 1997. The invention was marketed by Trico Industries, Inc. (later purchased by Weatherford International) to control the leakage of rod pumps at well sites in Texas, Oklahoma, Kansas and Wyoming.

3. PATENTS

The concept of hydro-balancing the pressure across the secondary seal of a stuffing box is the subject of U.S. Patent No. 5,209,495 which covers a commercial product for reciprocating sucker rod pumping systems. The patented technology features the pressure transmitter as a separate component in its own housing or cylinder. A patent is being obtained under the United States Non-provisional Application Serial Number 60/091,941 which covers the stuffing box assembly having an internal pressure transmitter piston to equalize the pressure across the secondary seal in a stuffing box. The transmitter / piston in a reciprocating high-pressure pump is used to transfer the pressure of the fluid being pumped to a sacrificial safe-lubricant of known characteristics. One advantage of the technology is that it can be retrofitted to most any make of plunger pump. The internals of the stuffing box are the main items effected and in some cases the existing stuffing box can be modified to use the Hydro-Balanced System. The tests done in recent months included a Kobe Size 3 triplex pump in methanol service and a National 100 T-4 pump used in salt-water service.

To explain the technology further, Figure 1 shows a convention high pressure stuffing box with a standard plunger / packing arrangement. The box shown is an adjustable packing type, not normally used for water jetting. The only difference would be that most water jetting pumps use spring-loaded packing instead of adjustable packing. Figure 2 shows the Hydro-Balanced stuffing box with the internal transmitter / piston toward the fluid being pumped. The barrier fluid is supplied to the area between the piston and the packing (primary seal) to balance the pressure across the transmitter / piston.

4. TESTS

In a product engineering report (ref. 7.1), test procedures were described and the finding were explained as follows. A 60 horsepower triplex pump was fitted with a version of the Hydro-Balanced Packing System and run at 2500 psi for 11 hours. The tests showed that the concept was sound and very promising for the development of the following advantages:

- Reduced operating costs and down time due to longer packing life
- Elimination of potentially contaminating fluids reaching the environment
- Improved mechanical efficiency due to lower friction losses
- Improved volumetric efficiency due to less leakage

The first paper on the development of the Hydro-Balanced Packing System was given at the Southwestern Petroleum Short Course, Lubbock, Texas in 2000 (Ref. 7.2) entitled ARTIFICIAL LIFT HYDRAULIC LIFT PUMP IMPROVEMENT. Since that time, a test facility has been planned and started to continue the development of this technology.

The second test (Ref. 7.3) was done on December 27, 1999 and included installing the technology into a Kobe high-pressure plunger pump. A methanol test loop consisting of a product tank, pressure recorder, gauges, filter, supply pump and heat exchanger were furnished by Downhole Assemblies Specialty of Louisiana. The pump used in the tests was an electric

driven, Size 3 Kobe triplex pump with 7/8" plungers to operate up to 15,000 psi. The stuffing box for the standard pump was modified for the Hydro-Balanced system test (figure 2) and a pressurized tank was used to supply rock drill oil as the barrier fluid. An air supply and regulator enabled the oil supply pressure to be varied during the tests. The first arrangement tried had the floating piston with a standard packing spring behind it. The first trial run was at 3500 psi and then the pressure was adjusted to around 5,000 psi and then to 7,000 psi. The pump ran smooth and the efficiency was measured to be around 98 per cent. After a run of about 30 minutes, methanol mist was observed around the center cylinder. The test was stopped and the stuffing box was removed for inspection. The piston was damaged in the unsupported area toward the fluid being pumped. New pistons were installed in all three stuffing boxes and a throat ring toward the fluid being pumped was added to support the piston. The test continued for about 15 minutes at 4,000 psi until the center cylinder started smoking through the drain hole in the stuffing box. The barrier fluid (rock drill oil) pressure was 70 psi and the suction pressure (methanol) was 50 psi. The temperature reached 109 degrees F and the smoking continued until the system was shutdown. The stuffing boxes were removed and a preliminary inspection revealed that there was no oil (barrier fluid) in the stuffing boxes, as was expected. The small check valves used to keep the barrier fluid in the stuffing boxes may have had a cracking pressure that was too high for the 20 psi to 30-psi differential desired for the barrier fluid. The lack of oil in the chamber caused the heating and smoking observed. The pistons and packing were in good shape and the tests suggested two changes for future tests: (1) place the spring on the pumped fluid side of the piston and (2) drill & tap for a gauge to read the barrier fluid pressure in the chamber so the presence of lubricant could be assured in future tests.

On January 5, 2000 the third test of the Hydro-Balanced System was conducted using an engine driven National brand pump in a field location. The pump used 1-3/8" plungers with conventional packing to lift salt water from the well site near Houston, Texas. A cylinder tank with a sight gauge, fill port and a fluid charging connection, was used to furnish the barrier fluid (rock drill oil). The tank was charged from the well tank and the pressure could be adjusted from 50 psi to 100 psi. The purpose of the test was to determine if a close fitted plunger & bushing could be used for salt water pumping by the installation of the Hydro-Balanced system, which separates the fluid being pumped from the primary sealing system. The metal to metal, close fitted plunger & bushing usually can not be used to pump "non lubricating" fluids. Figure 3 indicates the arrangement for the Hydro-Balanced Stuffing Box with the plunger / bushing that was installed at the field site. The original plunger & bushing were only slightly modified to adapt the Hydro-Balanced packing system into the existing pump. The pump ran smooth and a small amount of water and oil was observed dripping from around the plunger, but the plunger & bushing ran well under this condition. The stuffing box was disassembled on January 6, 2000 and the parts were found to be in good shape. The plunger had water / oil droplets on it indicating that the mixture was lubricating the bushing which eliminated the usual galling when pumping a non-lubricating fluid. A pressure gauge suggested by the former testing indicated the pressure fluctuation inside the barrier fluid chamber and a spring was used on each side of the piston. The components for the field-test included piston, liner, plunger, barrier fluid tank, stuffing box and gauges. The test showed promise for the plunger / bushing arrangement with the Hydro-Balanced system for pumping non-lubricating fluids; a concept that could be adapted to high-pressure water blasting pumps.

5. CASE STUDY

Two prototype Hydro-Balanced stuffing box units were installed on rod-pumped stripper wells in cooperation with Rocky Mountain Oilfield Testing Center (RMOTC) around August 1998. The two producing wells at the Naval Petroleum Reserve No. 3 near Casper Wyoming, have a history of packing element wear and stuffing box leaks. During the 60-day test period, performance of the stuffing box was measured by monitoring the pressure on the tubing and the inner chamber with a Barton two-pen recorder. Other parameters were recorded including polished rod temperature, ambient temperature, safe fluid pressure and fluid leakage. The test arrangement provided a better seal between the well fluids and the environment while allowing the polished rod to operate cooler. During a test by RMOTC, for example, the polished rod temperature held constant at 50 degrees F, while the well was pumping. The life of the packing elements was extended and leakage was reduced compared to the conventional stuffing box design. RMOTC reported "The tests indicate that when the Hydro-Balanced Stuffing Box is installed and adjusted properly, it is capable of significantly reducing the spillage of well fluids from the stuffing box for rod pumped wells, compared to the conventional stuffing box design." The latest progress made on the new rod pump version of the Hydro-Balanced System included an installation of a prototype kit on a Utex test pump in Weimar, Texas. This short test that lasted less than an hour, was to prove the concept of using an in-line piston on rod pumps. Mr. Rob Puckett, an engineer with Weatherford was involved in the test and he reported that the kit performed well. He suggests that the next step should be extensive testing in ALS pumps.

6. CONCLUSIONS

The primary purpose of the Hydro-Balanced Stuffing Box system, as an improvement to the high-pressure positive displacement pump, is to reduce the potential for pollution and to increase the high-pressure packing life. The invention's technical advantage over current technologies and a special feature of the system is that the primary seal is always sealing the operator's chosen fluid versus the current technology that requires a seal material that is suitable for the product being pumped.

The Hydro-Balanced Stuffing Box System will add to these advantages by increasing the life of the plungers and packing systems of the multiplex plunger pumps. Another significant advantage is it will eliminate the possibility of a fire hazard when some products leak to the atmosphere, because only a controlled safe fluid would leak when the packing wears.

Weatherford and Utex are presently discussing an agreement to develop the Hydro-Balanced Stuffing Box system for various pump brands and pressure ratings. Figure 4 shows the new test facility that is being constructed in Houston at this time for further testing of the Hydro-Balanced packing systems.

The authors want to thank the employees of Weatherford ALS and Weatherford International including Trae Rogers, Jimmy Fretwell, Gary McCann, Roger McCelvy, Jerry Kluz, Casey Birte and employees of the R&D department for the continued interest and assistance in developing the Hydro-Balanced Stuffing Box technology.

7. REFERENCES

M. Sleger, R.E. Rhodes, Progress Report on Hydro-Balanced Packing System for Triplex Pump, Product Engineering Report #122.

Michael T. Gracey, Harold H. Palmour, Artificial Lift Hydraulic Pump Improvement, Southwest Petroleum Short Course, 2000.

Michael T. Gracey, Hydro-Balanced Stuffing Box Test Report, dated December 27, 1999.

Michael T. Gracey, Hydro-Balanced Stuffing Box Test Report, dated January 5, 2000.

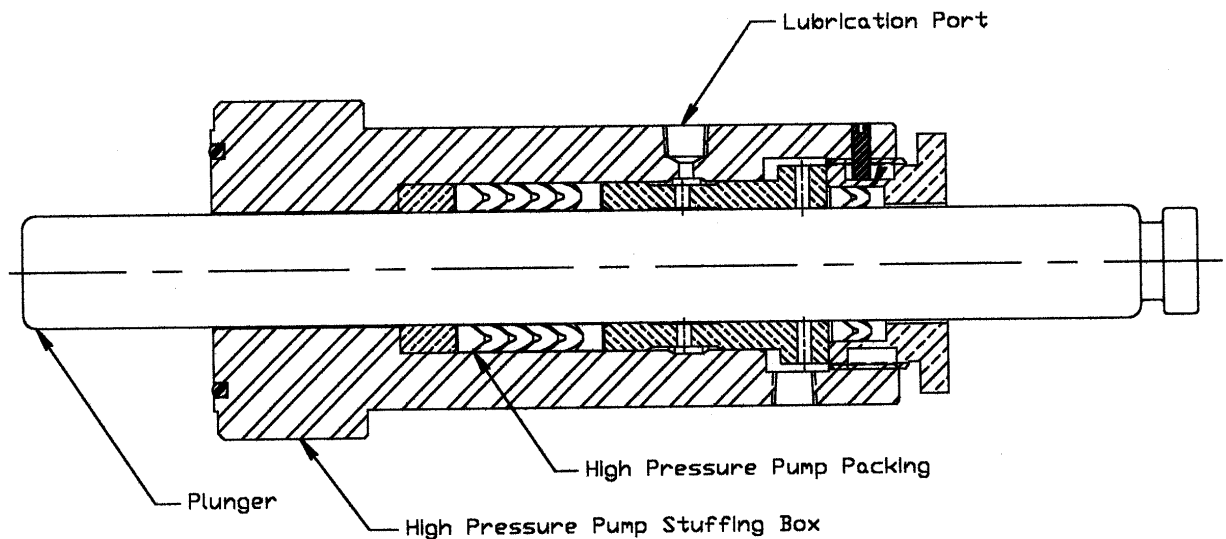


Figure 1. High Pressure Pump Stuffing Box With Plunger/Packing Arrangement

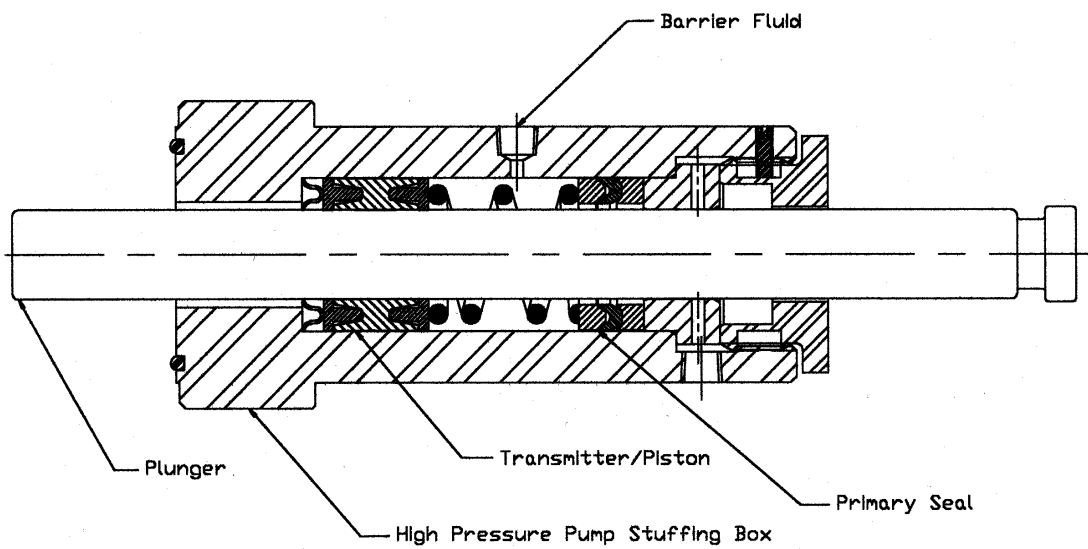


Figure 2. Hydro-Balanced Stuffing Box With Internal Transmitter/Piston

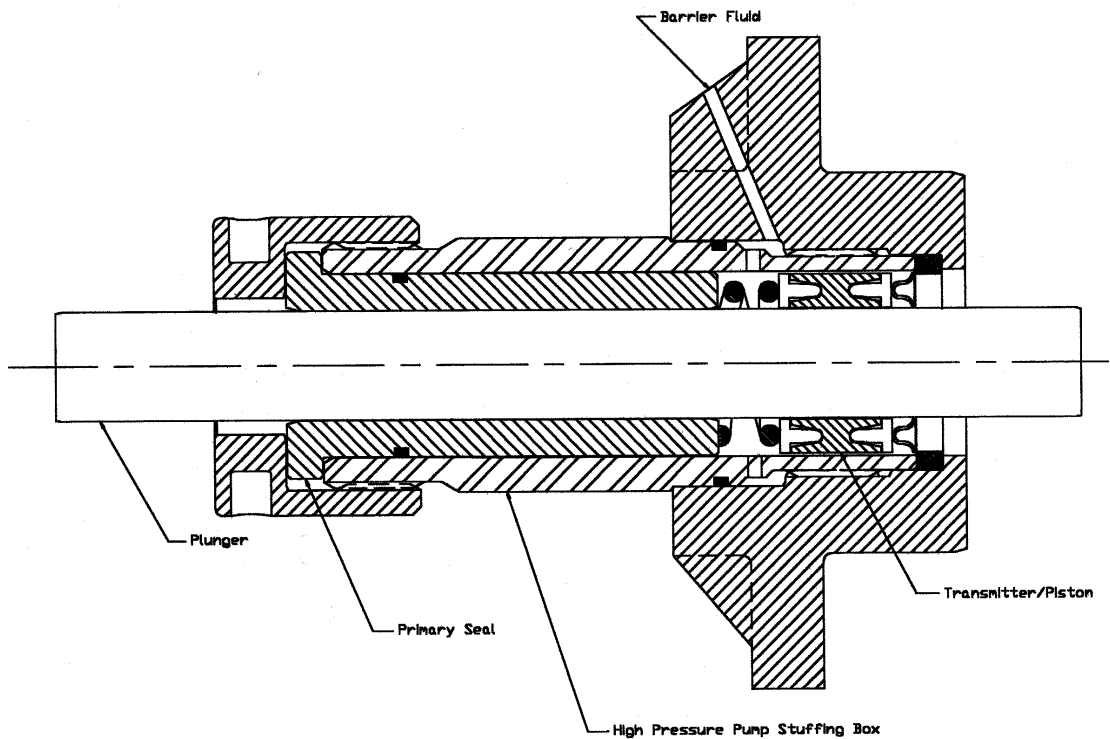


Figure 3. Hydro-Balanced Stuffing Box With Plunger and Bushing

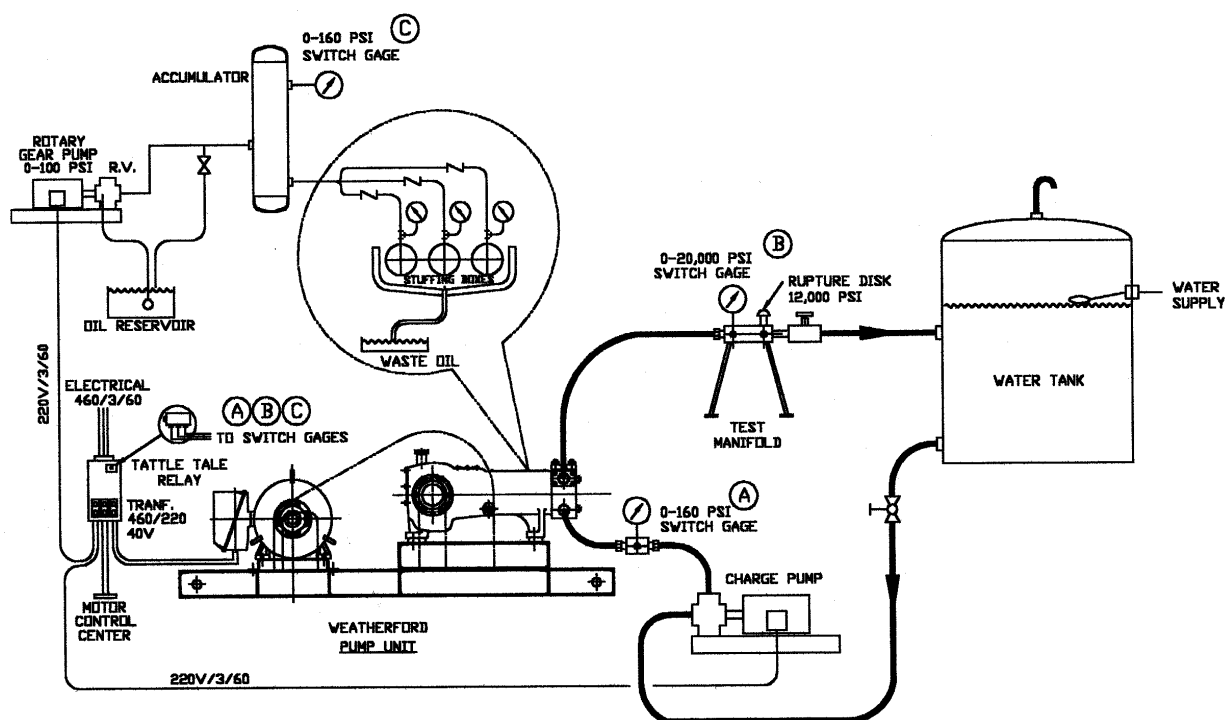


Figure 4. Test Facility to Develop Hydro-Balanced Stuffing Box for Various Pumps

**800 MPa PURE WATERJET AND
ABRASIVE WATERJET CUTTING – WHAT’S NEXT**

F. Trieb, K. Zamazal
Bohler Hochdrucktechnik GmbH
Kapfenberg, Austria

ABSTRACT

Based on the cognitions with ultra high-pressure waterjet cutting at 800 MPa this paper shows the results when adding abrasives. The effects on different materials have been investigated, especially the interdependence of operating pressures, orifice diameter, cutting speed and cut surface quality.

Pure waterjets generated at ultra high pressures are able to cut even on steel. Using abrasives in addition, either cutting depth or cutting speed will be increased tremendously. A comparison between ultra high-pressure pure waterjet and abrasive waterjet will show the competitiveness of these processes. The results give several aspects on future developments as well as new fields of application for this technology.

1. INTRODUCTION

Waterjet technology has been established for many years, but even now more and more new branches are interested in this cutting process. The specific benefits of waterjet cutting, with or without the adding of abrasives enhance the attraction.

Beside the basic advantages of waterjet and abrasive waterjet cutting - like e.g. no thermal influence on material structure, to start and to stop on every spot on the material surface and the ability of two and three dimensional machining - there are some additional aspects if the pressure is raised from 400 to 800 MPa:

- Lower required power rating
- Increased cutting speed or
- Higher cutting depth achievable

Of course the increased wearing process on high pressure sealing system and check valves have to be considered and are one of the most important economic factors when using ultra high pressure systems. Also the question whether the usage of abrasive is necessary or not becomes important in connection with ecological and economical considerations. Therefore tests with pure waterjet and abrasive waterjet at ultra high system pressure between 400 and 800 MPa have been done. The results are discussed in this paper.

2. ULTRA HIGH PRESSURE TESTING EQUIPMENT

For the aims of these experiments an ultra high-pressure pump normally used for the Autofrettage procedure has been adapted (Figure 1). At a power rating of 18.5 kW the pump generates a flow rate of 0.5 l/min at a maximum working pressure of 1,000 MPa.

In connection with waterjet cutting pressure controlled pumps are always used, the Autofrettage pump is flow controlled. Beside this the main difference between a standardized 400 MPa pump for waterjet cutting and the 800 MPa Autofrettage pump is the transmission ratio between oil and water hydraulic at the intensifier, which has been increased from about 22:1 to 50:1 by using a small plunger with 10 mm diameter.

The oscillating output pressure is harmonized by a large volume accumulator, which enables stable cutting conditions. The achieved pressure amplitudes are smaller than 20 MPa.

For pure waterjet cutting a heavy-duty nozzle holder has been designed. The orifice itself is a standard design used for cutting with 400 MPa. For abrasive waterjet cutting a conventional adjustable abrasive head has been adapted.

No valve for switching on and off the waterjet was used to avoid damages on the standard sapphire orifice. Figure 2 shows a complete pressure build-up from atmospheric pressure to the

maximum cutting pressure. Due to the large accumulator it takes about four minutes to reach the desired operating pressure value of 800 MPa.

A standard CNC cutting table has been used as a guiding system for all performed tests. The tank was not filled with water, to enable a better visibility and to monitor the generated pure and abrasive waterjet.

3. CUTTING TESTS

As material for all cutting tests aluminium AlMgSi1 and stainless steel 1.4435 (similar to AISI 316) have been used. All test cuts have been performed with a standoff distance of 3 mm between orifice respectively abrasive nozzle and workplace.

For comparable determination of flow rate sapphire orifices with 0.08 and 0.10 mm have been chosen. To get a corresponding overview for all cutting tests with pure waterjet and abrasive waterjet, an orifice of 0.1 mm has been used. The operating pressures with pure waterjet were 400 and 800 MPa, and in connection with abrasive waterjet 400, 600 and 800 MPa have been used.

3.1 Pure Waterjet Cutting

At 800 MPa the pure waterjet is coherent at a length of about 30 mm as shown in Figure 3 with the chosen orifices with diameter 0.08 mm and 0.10 mm. Therefore this is very similar to the 400 MPa waterjet discharged at the standard waterjet valve. For all cutting tests performed with pure waterjet the following parameters were used:

- Operating pressure, $p = 400$ and 800 MPa
- Orifice diameter, $d_w = 0.10$ mm
- Cutting speed, $v = 25, 50$ and 100 mm

At 800 MPa the pure waterjet with the chosen orifice of 0.10 mm is coherent to a length of about 30 mm and very similar to a jet at 400 MPa (Figure 3).

Due to the fact that the ultra high pressure pump was limited at a flow rate of 0.5 l/min it was only possible to use orifices with 0.08 and 0.10 mm. Figure 4 shows the correlation between working pressure, flow rate and orifice diameter. The observation shows that the flow rate is digressive while increasing the pressure.

3.2 Pure Waterjet - Cutting Observations

Of course even ultra high pressure cannot substitute abrasives, nevertheless an obvious improvement in cutting depth and surface finish could be ascertained. Figure 5 shows the influence of pressure regarding to cutting depth at different cutting speeds.

Test with pure waterjet at similar hydraulic power rating but only 400 MPa operating pressure and larger orifice did not result in sufficient cutting performance and have not been considered for the future observations.

Previous work (Trieb et al., 2000) where pure waterjets were used to cut different metals at 400 and 800 MPa showed that an economic way to cut abrasives was necessary. Out of experience aluminium with a thickness of 5 mm i.e. is cut with 750 mm/min in order to reach "Quality Cut", for stainless steel cutting speed has to be reduced to 300 mm/min. Cutting speed and abrasive mesh size define obviously the surface finish.

In connection with the mentioned surface finish pure waterjet cannot achieve a so called "Quality Cut", even 800 MPa and low speed of 25 mm/min generates nothing better than "Rough Cut" with R_a values between 10.5 μm and 24.2 μm . It can also be ascertained that the surface finish becomes worse while increasing the depth that is similar to abrasive waterjet.

The waterjet loses its coherence very fast, the cut width increases until kinetic energy is totally consumed. These estimations can also be seen in Figure 6, that shows pictures of the cutting result.

All samples have been kerfed with cutting speed of 25, 50 and 100 mm/min. The deepest cut of course correlates with the slowest speed. View A (top) and view B (front) show the cut itself, surface finish for both materials can be seen in view C.

3.3 Abrasive Waterjet Cutting

Similar to pure waterjet there is no big difference in jet coherency between 400 and 800 MPa. Figure 7 shows an abrasive waterjet at 800 MPa. Standard sapphire orifice and abrasive nozzle were used. In connection with all performed abrasive waterjet tests the parameters were chosen as follows:

- Operating pressure, $p = 400, 600$ and 800 MPa
- Orifice diameter, $d_w = 0.10$ mm
- Abrasive nozzle diameter, $d_a = 0.60$ mm
- Abrasive nozzle length, $l_a = 50$ mm
- Abrasive medium, Garnet, mesh 120
- Abrasive flow rate, $m_a = 100$ g/min
- Cutting speed, $v = 100$ mm

The cutting results for both aluminium and stainless steel are shown in Figure 8. As estimated there is a big difference in cutting results between pure waterjet and abrasive waterjet.

3.4 Abrasive Waterjet - Cutting Observations

Of course even ultra high pressure cannot substitute abrasives, nevertheless an obvious improvement in cutting depth and surface finish could be ascertained. Figure 8 shows the influence of pressure regarding to cutting depth.

A comparison between pure waterjet and abrasive waterjet at samples cut with 100 mm/min shows that the cutting depth at a pressure of 800 MPa can be increased at Aluminium from 3 mm to 32 mm and at stainless steel from 0.5 mm to about 15 mm.

All corresponding samples, shown in Figure 9, have been kerfed at 400, 600 and 800 MPa. The cutting speed at 100 mm/min was the same for all performed tests. On the upper area about 30% of the kerf show rather smooth surface finish. The roughness values R_a at the aluminium samples are between 4.0 μm to 4.7 μm . In the lowest area the roughness increases to a maximum of 36.6 μm .

In the upper area of the stainless steel sample the R_a values are between 3.0 μm and 4.6 μm . In the lowest area it increases to a maximum of 28.0 μm .

On both samples there seems to be a reduction of cutting quality at 600 MPa. In this connection it has to be considered that, except the pressure, for all performed tests the same parameters have been used. There has been done no adjustment on abrasive flow rate or other parameters.

4. CONCLUSION

Higher investigations, wear and reduced life time for many components in the assembly have to be noted, if materials or cutting depths require ultra high pressure. Although during the performed tests none of the components broke. One of the reasons for sure is the short testing time of only a few hours. In conclusion, for the ultra high pressures cutting tests following items can be mentioned:

- Pure waterjet cutting might have some benefits in comparison with abrasive jet; most of them can be fixed in the area of waste disposal and wear.
- In any case pure waterjet is no alternative to abrasive waterjet even if ultra high pressure is used.
- Reduced kerf width due to smaller orifice and abrasive nozzle diameter might be an advantage for future applications.
- Operating pressure of 800 MPa is not a real improvement compared to corresponding cuts with 600 MPa.
- Higher productivity, increased cutting depth and higher cutting speed are not only significant for waterjet technology. If the "Fine Tool" waterjet wants to be top also in the future machining world it has to be improved. One of the improvements could be the higher operating pressure.

So what's next? For sure there will be a slight change to pumps with higher operating pressures even if the life time of sealing and other high pressure components is lower than compared to existing pumps with about 400 MPa.

5. ACKNOWLEDGEMENTS

The described investigations are based on various discussions together with the scientists from the Institute of Material Science at the University of Hanover, Germany. Thanks for the support to BFT Fluid Technology Corp., Holland, Ohio and to the Autofrettage specialists and colleagues at the Electronic Department at Bohler Hochdrucktechnik GmbH, Kapfenberg, Austria.

6. REFERENCES

Trieb, F., Zamazal, K., "Waterjet Cutting - 300 MPa High Pressure to 800 MPa Ultra High Pressure", *6th Pacific Rim International Conference on Water Jetting Technology*, pp. 186-190, 2000

7. NOMENCLATURE

d_a	abrasive nozzle diameter
d_w	orifice diameter
h	cutting depth
l_a	abrasive nozzle length
m_a	abrasive flow rate
p	operating pressure
Q	flow rate
v	cutting speed

8. FIGURES



Figure 1. Autofrettage Pump Adapted for Waterjet Cutting at 800 MPa.

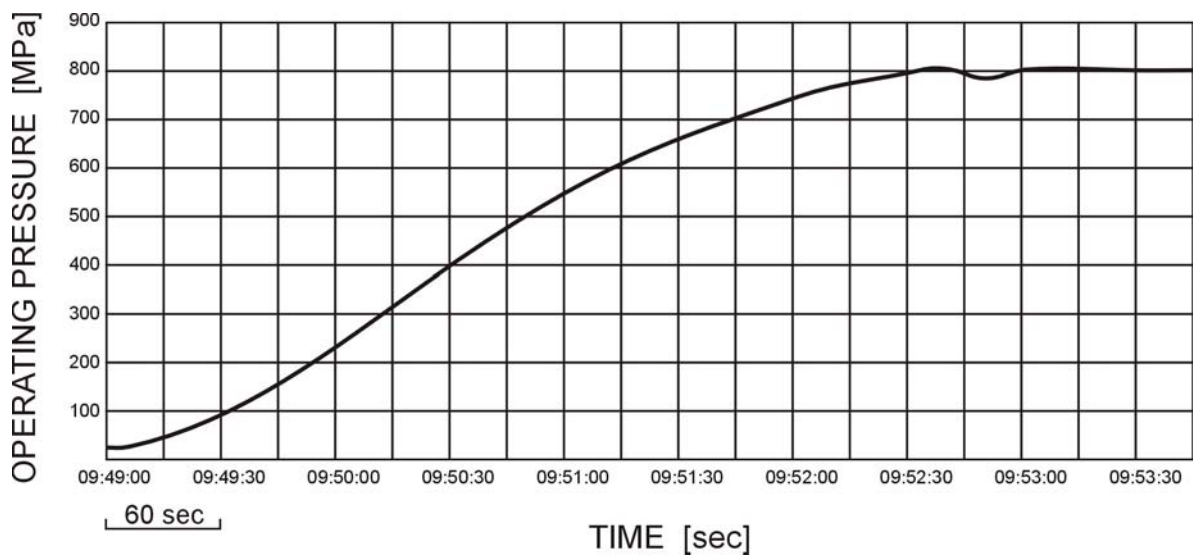


Figure 2. Harmonized Pressure Build-Up from Atmospheric Pressure to 800 MPa.

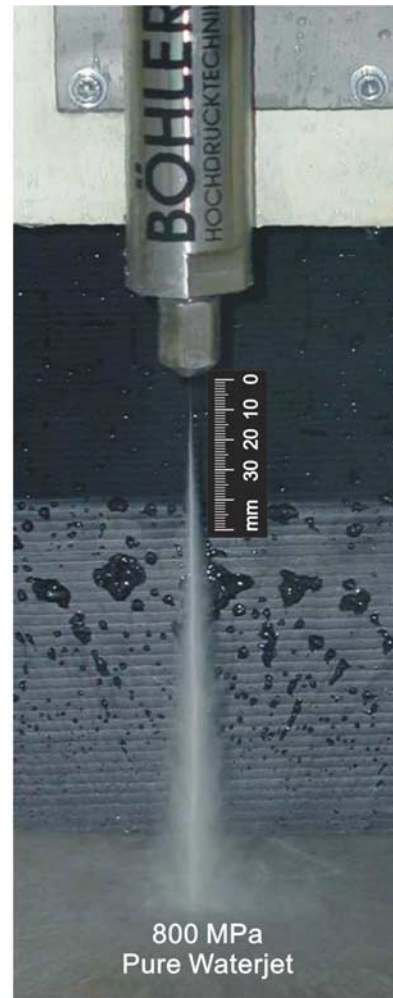
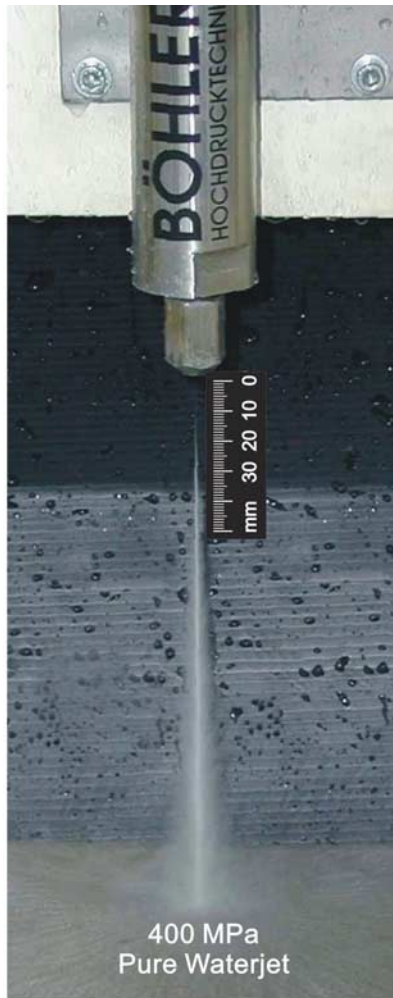


Figure 3. Pure Waterjets at 400 MPa and 800 MPa

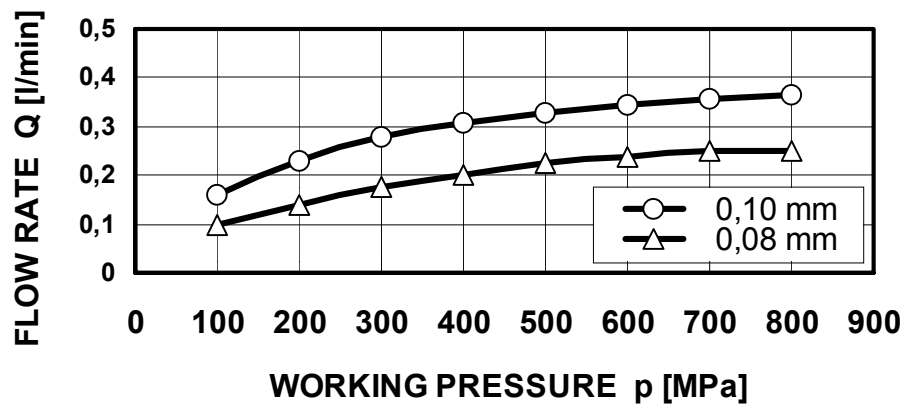


Figure 4. Correlation between Working Pressure, Flow Rate and Orifice Diameter

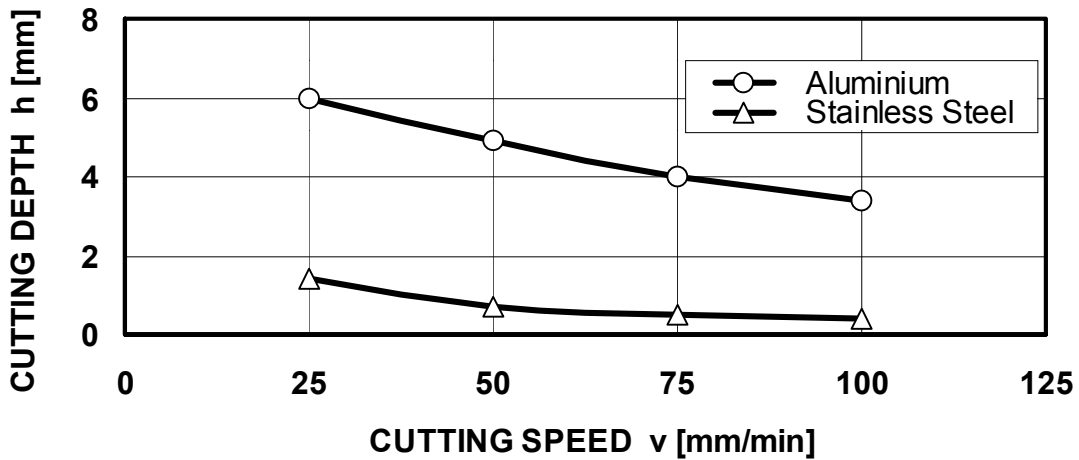
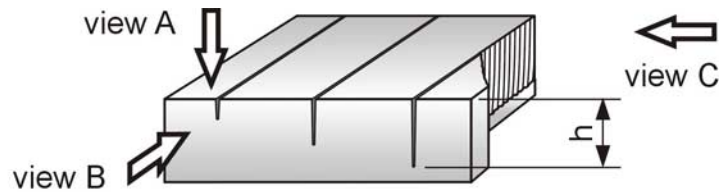
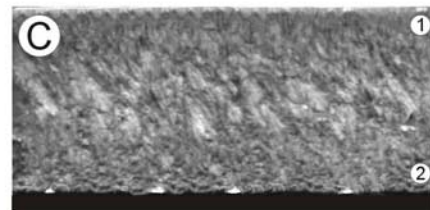


Figure 5. Cutting Depth, Aluminium and Stainless Steel, Pure Waterjet at 800 MPa



Aluminium

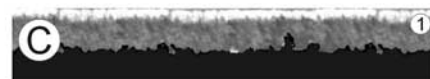
$p = 800$ MPa, $v = 100, 50, 25$ mm/min



Pos.	R_a [μm]	R_t [μm]
①	14.0	93.8
②	24.2	155.8

Stainless Steel

$p = 800$ MPa, $v = 100, 50, 25$ mm/min



Pos.	R_a [μm]	R_t [μm]
①	10.5	77.5

Figure 6. Aluminium and Stainless Steel, Cut with Pure Waterjet at 800 MPa

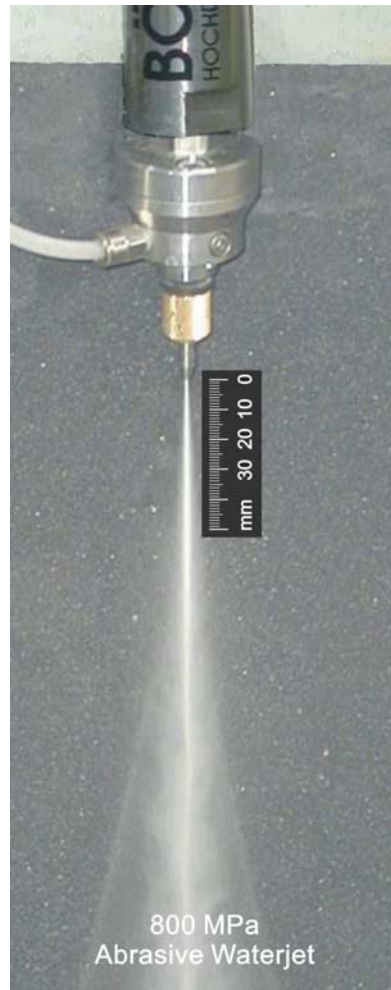


Figure 7. Abrasive Waterjet at 800 MPa

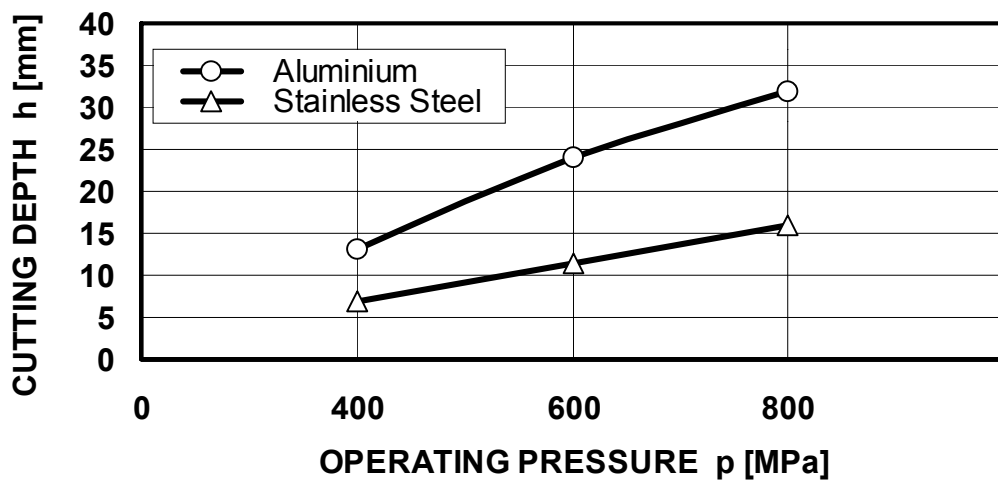
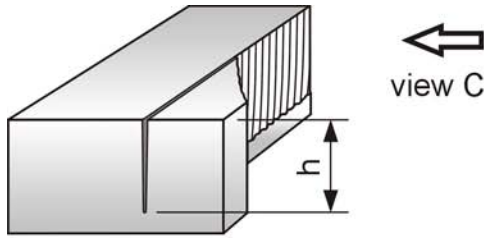
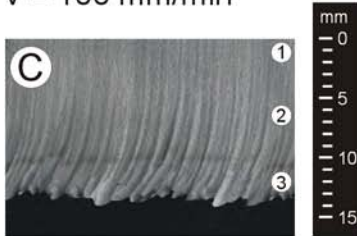


Figure 8. Cutting Depth, Aluminium and Stainless Steel, Abrasive Waterjet at 800 MPa

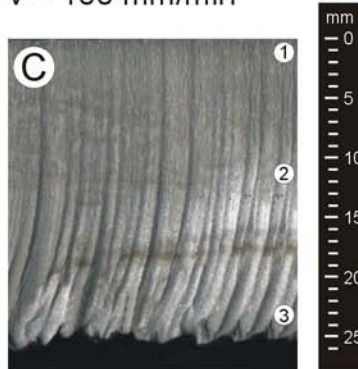


Aluminium
 $p = 400 \text{ MPa}$
 $v = 100 \text{ mm/min}$



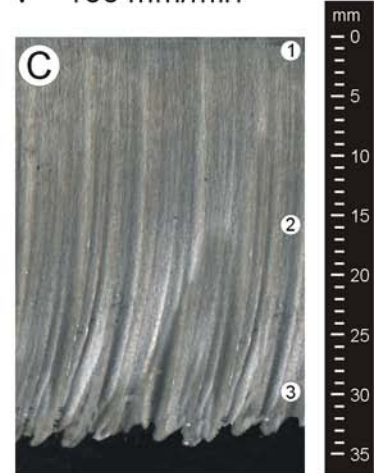
Pos.	$R_a [\mu\text{m}]$	$R_t [\mu\text{m}]$
①	4.0	27.8
②	6.5	50.0
③	23.0	198.6

Aluminium
 $p = 600 \text{ MPa}$
 $v = 100 \text{ mm/min}$



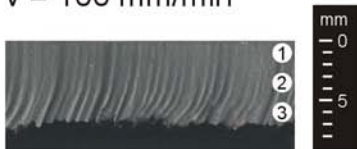
Pos.	$R_a [\mu\text{m}]$	$R_t [\mu\text{m}]$
①	4.7	36.4
②	10.8	47.3
③	32.2	276.0

Aluminium
 $p = 800 \text{ MPa}$
 $v = 100 \text{ mm/min}$



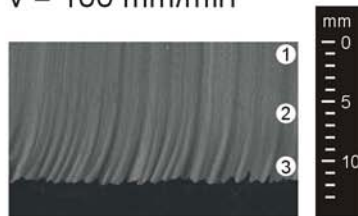
Pos.	$R_a [\mu\text{m}]$	$R_t [\mu\text{m}]$
①	4.4	30.9
②	11.9	45.2
③	36.6	282.1

Stainless Steel
 $p = 400 \text{ MPa}$
 $v = 100 \text{ mm/min}$



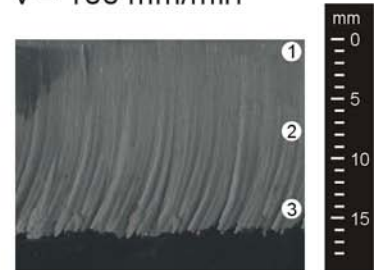
Pos.	$R_a [\mu\text{m}]$	$R_t [\mu\text{m}]$
①	3.4	27.0
②	6.2	37.9
③	12.6	91.7

Stainless Steel
 $p = 600 \text{ MPa}$
 $v = 100 \text{ mm/min}$



Pos.	$R_a [\mu\text{m}]$	$R_t [\mu\text{m}]$
①	4.6	28.8
②	6.5	32.6
③	24.4	186.2

Stainless Steel
 $p = 800 \text{ MPa}$
 $v = 100 \text{ mm/min}$



Pos.	$R_a [\mu\text{m}]$	$R_t [\mu\text{m}]$
①	3.0	37.9
②	6.4	47.3
③	28.0	252.6

Figure 9. Aluminium and Stainless Steel, Cut with Abrasive Waterjet at 400, 600 and 800 MPa